

The background of the cover is a photograph of a sunset over the ocean. The sun is a bright, glowing orb on the horizon, casting a long, shimmering reflection on the water's surface. The sky is filled with dark, heavy clouds, some of which are illuminated from below by the setting sun, creating a dramatic, high-contrast scene. In the foreground, a large, dynamic splash of water is captured mid-air, with numerous droplets frozen in time, creating a complex, crystalline structure. The water in the foreground is dark and turbulent, contrasting with the bright, golden light of the sunset.

Introduction to Graduate Fluid Mechanics

(an Electronic Text with Study Problem Solutions)

Charles R. (Chuck) Smith

**Professor Emeritus
Department of Mechanical Engineering
Lehigh University**

Fourth Edition

Self-Published

Copyright 2023

Dedication

This book has been a long labor of writing and development, and I dedicate this book to two exceptional people in my life:

My wife, Christine, who put up with my constant occupation of my retirement office to write and complete this book. She was often a writer's widow, but never complained about my continued obsession.

The other is my long-time colleague, Dr. David J. D. A. Walker, who was a consummate fluid mechanic and an outstanding teacher, and my research partner for over 30 years. He passed away too soon to collaborate on this book.

Acknowledgements

I would like to thank the many students who used the earlier versions of this book for a graduate course I taught at Lehigh University, and provided valuable feedback on clarity, errors, and suggestions for improvement. I would also like to thank Dr. Xianyang Jiang who reviewed the draft of this edition, and made several very valuable suggestions. My most humble appreciation to all those who provided input on this book, and this edition.

Objective and Scope of the book

The objective of this textbook is to provide a solid grounding in the principles of incompressible fluid mechanics for beginning graduate students. The book, and the accompanying course which would utilize it, should provide a student with the background to continue their studies into specialty areas (e.g. aerodynamics, boundary layers, turbulence, etc.), and parallel areas (e.g. heat transfer and thermodynamics). The book is relevant to students pursuing graduate degrees in mechanical, civil, chemical, aeronautical, or nuclear engineering. I have also had students with an initial degree in physics take my course, upon which this book is based, and found that their background allowed them to use the book successfully.

The book does not cover control volume fluid mechanics or hydrostatics, since these are topics that students should have covered during their undergraduate studies. It also does not cover numerical methods, since I feel that doing so distracts from the understanding of the fundamentals of fluid mechanics, and that the time is better used providing a broad theoretical background. It is my belief that students must develop a solid theoretical understanding of fluid mechanics before they can practically employ effective numerical solution techniques.

The focus of the book is on how a fluid is modeled, the development of the basic equations of fluid mechanics, the simplification of these basic equations using appropriate assumptions, the establishment of proper boundary/initial conditions, and methods of reducing the resulting equations through judicious parameter scaling. While a number of traditional and non-traditional examples are solved in the book using straight-forward analytical techniques, the solution of more complicated problems using advanced analytical (e.g. asymptotics) or numerical techniques (e.g. finite difference or finite elements) are not considered. I feel that once a student understands the process of modeling and appropriately reducing the governing equations, they can then consider solution techniques, both analytical and numerical, through advanced courses on those topics. However, as appropriate, equation-solving programs, such as [MATLAB](#) or the website [Wolfram Alpha](#), will be employed to solve problems not amenable to analytical closed-form solutions.

This book provides a student with a broad scope of the cumulative areas of incompressible fluid behavior, including the processes of modeling a fluid, the properties of importance, how properties change and modify in an Eulerian environment, and the extension to areas of practical application (boundary layers, drag, non-Newtonian flows, and the basics of turbulence). The material covered is applicable to a one-semester survey course, or could be extended to a second semester, depending on the depth to be pursued.

One practice I have tried to follow throughout the book is to assure that there is sufficient development and demonstration of key topics and examples, and not to shortcut the development of example problems. In many texts, a classic problem is presented with too few solution details, such that a student cannot follow the complete process from problem statement to solution. I have tried to provide that completeness, at the expense of added length.

I have also included a series of study problems at the end of each chapter, as appropriate. These are intended for use for further study, and to illustrate the application of the material in a chapter. In some cases, the problems will require the use of material from previous chapters as well. In

this fourth edition, each end of the chapter study problem is linked to a detailed solution via an attached solutions file. How to access the solutions is described on the following page.

In this edition of the book, I have added material on the basics of non-Newtonian boundary layers to Chapter 16, which makes the chapter a more complete introduction to the differences between Newtonian and non-Newtonian fluids. I have also added some further discussion of turbulent flow structure, and referenced some videos that describe how large turbulence computation programs model and calculate 3-D turbulence properties. Beyond that new material, I have modified and improved several graphs, and added a few more end of chapter problems. I also include a detailed appendix of the principal equations covered in the book. Finally, as mentioned above, I have electronically linked each end of chapter study problem to a detailed solution in an attached solutions file. If you have enjoyed and utilized one of my previous editions, I think you will find this fourth edition a nice upgrade, particularly the addition of study problem solutions.

As I noted in the prior editions, since this is an electronic book, I have attempted to provide electronic links to as many of the terms and references as possible. Where appropriate, I have linked references directly to bibliographic sources on the web, which hopefully avoids exhausting web searches for sources that are often hard or expensive to obtain.

How to "Read" this Book

This book contains 17 Chapters and an appendix within one hyperlinked Adobe Acrobat PDF file (download a free Adobe Acrobat Reader app [here](#); alternatively, you can download another nice PDF reader from Foxit PDF [here](#), also free). The first 12 chapters comprise Part I, which covers the basic concepts of graduate fluid mechanics; the last five chapters comprise Part II, which covers practical applications of the basic concepts to key areas of fluid mechanics (i.e. boundary layers, drag, non-Newtonian flows, and turbulence). The book begins with a Table of Chapters, with each chapter title hyperlinked to the respective chapter; left clicking on a chapter title will take you to the beginning of the selected chapter.

Each chapter begins with a Contents section, listing the key topics within the chapter. Each topic and subtopic listed in the Contents section is again hyperlinked to that topic location within the chapter, so that if you read the book electronically (as you should), you can quickly access any of the topics/subtopics by simply left clicking on the link. There are also links within the chapters, which will take you either to other portions of a chapter, or to electronic references.

To return to the location of a previous link using [Adobe Acrobat Reader](#), simultaneously hit the "Alt" and "←" keys on the keyboard, or use a "previous view" icon accessed by selecting in order: "View", then "Page Navigation", then left clicking the "Previous View" icon. However, I recommend that you make the "previous view" icon (looks like a circle with a left pointing arrow) permanently viewable in the Reader Toolbar. If you want to return to the beginning of the book, just hit the "Home" key. To return to a previous link using the [Foxit PDF Reader](#), there is a return icon at the bottom-left of the reader frame.

In this edition, I have also added bookmarks to the PDF file. Selecting the bookmark icon at the upper left of a page will expose the list of bookmarks (it is quite extensive), which will also

allow you to quickly navigate to a chapter or section of a chapter. I think you will find this a nice addition for quickly accessing particular sections of the book.

If you choose to print each chapter (or any pages of the book or solutions), you should have the book PDF file resident on your computer, and then open and print the pages you wish. Do not try to print directly from a website. This sometimes works, but it just as often creates complications.

How to view solutions to the end of chapter study problems

The end of chapter study problems are intended to be used to practice the material covered in each chapter. However, I recognize that after working on a problem you might want to see if the solution you arrived at is correct, and/or use the problem solutions to help you better understand the application of the chapter material. Thus, this fourth edition of the book includes a problem solution linked to each of the study problems.

To view the solution to a study problem, left click on the problem number at the start of the problem statement. The solution will appear in the Reader frame from a separate attached solutions file. In these solutions, the problem statement is not highlighted, while the solution is highlighted in **yellow**. You can scroll through the problem to follow the solution process. When you want to return to the book from a problem solution, scroll back to the start of the solution and again left click on the solution problem number. You will be returned to the page in the book where the problem statement appears. Additionally, the solutions file also has bookmarks for each study problem, which will let you navigate quickly to any problem within the solutions file. Remember, to return to the book, left click on the number of any study problem within the solutions file. To open the solutions file directly, you can use the paper clip icon (on the far left of the viewing frame) in either Adobe or Foxit Reader. Hopefully, access to the study problem solutions will help you further understand the material covered in the chapters.

Use this material whatever way works best for you. And enjoy it.

If you like the book, find any errors, or have suggestions for additions to the book, please send [me an email](#) and let me know your thoughts.

Note that this is a public domain document, so feel free to pass on copies electronically to all who might be interested in the topic. I am self-publishing this book, and it is open access at no charge. However, if you feel you would like to provide some compensation for the use of this book, feel free to send me a check for whatever you would like to 1209 Oxbridge Drive, Lutz, FL 33549, USA.

Chuck Smith
June 2023

Table of Chapters

<u>Chapter</u>	<u>Title</u> (left click on a chapter title to go to that chapter)	<u>Page</u>
Part I: Basic Concepts		
1	Introduction/Classification of Forces on a Fluid	1
2	Vector and Vector Operators: The Basics	18
3	Kinematics and the Substantial Derivative	40
4	Motion and Deformation of a Fluid	66
5	Differential Equations of Motion	83
6	Simple Solutions to the Navier-Stokes Equations	115
7	Equations of Motion for Inviscid Flow	192
8	The Stream Function and Vorticity	224
9	Two-Dimensional Potential Flow Theory	244
10	Changes in Circulation and Kelvin's Theorem	308
11	The Vorticity Transport Equation	332
12	More Complicated Navier-Stokes Solutions	387
Part II: Applications		
13	Boundary Layer Theory	422
14	Approximate Solutions of the Boundary Layer Equations	460
15	Flow Separation and Drag	494
16	Introduction to Non-Newtonian Fluid Behavior	528
17	Instability and Turbulence: An Introduction	609
Appendix		
	Appendix: Selected Relationships and Equations	690

Chapter 1

Basic Concepts

Contents

1.1 The Concept of a Fluid	1
1.2 A Fluid as a Continuum	2
1.3 The Concept of Viscosity	3
1.3.1 Table 1: Viscosity of Water at Standard Pressure	6
1.3.2 Table 2: Viscosity of Air at Standard Pressure	6
1.4 Types of Fluids: Newtonian and Other	7
1.5 The Differential Element	8
1.6 Body Forces	10
1.7 Surface Forces	10
1.8 Stresses	11

1.1 The Concept of a Fluid

We all inherently know what a fluid is. Most laypersons, when asked for an example of a fluid, would probably cite liquids, like water, as a fluid. However, gasses also qualify as a fluid — although most people don't readily think of gasses as a fluid, since they are generally not visible. In general, all liquids and gasses are fluids. But what properties qualify a substance as a fluid? And how does a fluid differ from a solid?

In general, a fluid is a substance that will deform continuously under an applied shearing stress (i.e. a force applied tangentially to a surface of the fluid). In solid mechanics, we learn that a solid will deform under an applied shear stress, but it will only deform a fixed amount proportional to the applied stress. In other words, a solid will deform in some proportion when a shear stress is applied, but once a balance between the stress and the amount of deformation is reached, a solid will cease to deform and will remain in a state of static deformation (unless it undergoes [creep](#), due to thermal or environmental effects). On the other hand, a fluid will continue to deform as long as a shear stress is applied.

Another way of defining a fluid is as a substance that cannot sustain a shearing stress. The key here is that the application of a shear stress causes a fluid to deform *continuously*. This implies that the applied shear stress must balance with the *rate of deformation* of the fluid. We will use this concept tying fluid shear stresses to the rate of deformation (generally termed the strain rate) to characterize different types of fluids, and

to relate shearing stresses on a fluid to the strain rates through the use of a proportionality constant known as the [coefficient of viscosity](#).

1.2 A Fluid as a Continuum

We now have a way of judge if a substance behaves as a fluid. However, to deal with a fluid mathematically, we must be able to develop ways to model the fluid behavior; and to model a fluid appropriately, we need to consider the collective behavior of all the molecules that comprise the fluid. In most macroscopic (large-scale) situations, we do not perceive the individual molecular behavior. However, from a microscopic perspective, and [statistical mechanics](#), we recognize that individual fluid molecules move in rather randomized paths, and interact with other molecules through linear and rotational collisions.

During these collisions, molecules exchange both momentum and energy, which collectively give rise to the properties we normally associate with macroscopic materials, such as pressure, temperature, internal energy, and density. However, these collective properties require that the mean-free paths of the molecules be very small, such that macroscopic property changes appear continuous. This requires that the random molecular interactions are so manifold within a given volume of the fluid that one cannot discern a change in a macroscopic property as molecules move in and out of a given volume. As pointed out by [Frank Smith \(2003\)](#), the limiting volume for a fluid to exhibit "continuous" behavior is roughly 10^{-9} mm³ of air at standard conditions. Such a volume would contain approximately 3×10^7 molecules, which is sufficient to establish the appearance of continuous properties in air. Since liquids have smaller mean free paths, liquids can also be considered continuous fluids at (and even below) this limit.

Since most engineering applications deal with volumes much larger than this lower limit, properties within essentially all fluids (with the exception of very low pressure gases, such as at the edge of outer space or in extreme vacuums) can be considered to behave in a continuous manner. The assumption of a fluid as a continuum allows the application of mathematical modeling approaches that assume continuous behavior down to infinitesimal volumes – i.e. volumes that are very small, but still larger than the molecular limit required for continuous behavior within a fluid.

Recently, the consideration of nano-scale structures containing nano-scale fluids has challenged the continuum assumption, and has required the application of alternative methods of fluid modeling. An interesting presentation on the manifold issues encountered with microfluid mechanics is found at [this Wikiversity site](#). However, for the purposes of most engineering concerns, and within this text, we will consider fluids as a continuum.

1.3 The Concept of Viscosity

There are a number of different types of fluids, each characterized by the way the fluid deforms relative to an applied shear stress. To assess the type of fluid behavior, we first must model how a shear stress applied to a fluid results in a deformation rate, i.e. strain rate, within the fluid. The simplest way to illustrate this shear stress/strain rate relationship is to consider a fluid element (a small region of fluid) sheared in one plane by a single shear stress, τ , as shown in Fig. 1.1.

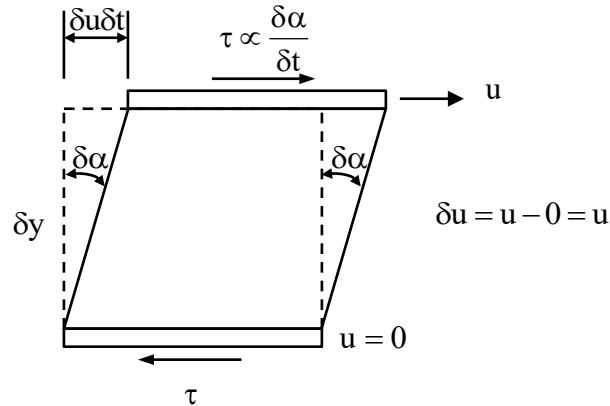


Figure 1.1 A fluid element deformed at a strain rate $\delta\alpha/\delta t$ by an applied shear stress τ .

We consider the changes here small, but continually increasing with time, such that the strain rate, $\delta\alpha/\delta t$, will be a constant value as long as the shear stress τ is maintained (which means that the shear strain angle, $\delta\alpha$, will continuously increase with time). In most common fluids, like water, air, and oil, the strain rate will be linearly proportional to the applied shear, such that:

$$\tau \propto \frac{\delta\alpha}{\delta t} \quad (1.1)$$

as indicated in figure 1.1. If the differential in velocity due to the shear stress is δu across a distance δy , then from figure 1.1 we can geometrically show that:

$$\tan(\delta\alpha) = \frac{\delta u \delta t}{\delta y} \cong \delta\alpha, \text{ if } \delta\alpha \text{ is considered small.} \quad (1.2)$$

Using Eqs. 1.1 and 1.2, we can show that:

$$\tau \propto \frac{\delta\alpha}{\delta t} = \frac{\delta u}{\delta y} \quad (1.3)$$

Now, taking the limit as δy becomes small in Eq. 1.3, mathematically we have:

$$\tau \propto \lim_{\delta y \rightarrow 0} \frac{\delta u}{\delta y} = \frac{du}{dy} \quad \text{or} \quad \tau \propto \frac{du}{dy} \quad (1.4)$$

Assuming a proportionality constant of μ in Eq. 1.4, we can write:

$$\tau = \mu \frac{du}{dy} \quad (1.5)$$

In Eq. 1.5, μ , is termed the coefficient of viscosity, often called the *absolute* or *dynamic* viscosity of the fluid. The larger the value of μ , the more viscous the fluid. The units of μ are stress-time, with units of $[FT/L^2]$ or $[M/(LT)]$, where F, M, L, and T represent respectively force, mass, length, and time in the units system being employed. Viscosity typically varies with temperature and pressure, although temperature is generally the more dominant effect, with liquids generally becoming less viscous with increasing temperature, whereas gasses become more viscous (generally) with increasing temperature.

Some typical values of absolute viscosity for various substances at standard conditions of one atmosphere pressure and 20°C are:

Air:	1.84x10 ⁻⁵	kg/(m-s)
Water:	1.0x10 ⁻³	kg/(m-s)
SAE 30 oil:	0.29	kg/(m-s)

Therefore, water is more than 50 times more viscous than air, and motor oil is 290 times more viscous than water! The following gives comparisons for other selected fluids:

Fluid	Absolute Viscosity at Room Temperature (kg/m-s)
Air	1.84 x 10 ⁻⁵
Water	1 x 10 ⁻³
Olive Oil	1 x 10 ⁻¹
Glycerol	1 x 10 ⁰
Liquid Honey	1 x 10 ¹
Golden Syrup	1 x 10 ²
Glass (Molten)	1 x 10 ⁴⁰

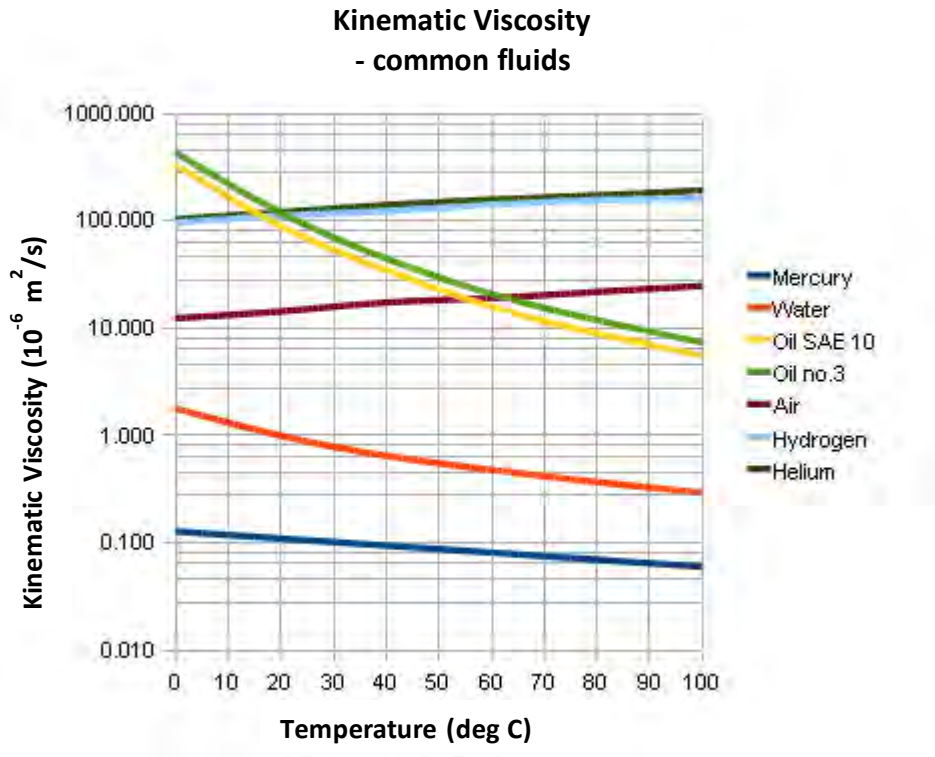
Another convenient form of viscosity that is often used in fluid mechanics is termed the *kinematic* viscosity, ν , which is defined as the ratio of the absolute viscosity to the fluid density, i.e.:

$$\nu = \frac{\mu}{\rho}, \tag{1.6}$$

where ρ is the symbol for fluid density (e.g. kg/m³). Therefore, the units of kinematic viscosity will be in [L²/T]. For the same three fluids cited previously, the kinematic viscosities are:

Air:	1.53×10^{-5}	m ² /s
Water:	1.01×10^{-6}	m ² /s
SAE 30 oil:	3.25×10^{-4}	m ² /s

Note that the kinematic viscosities of the three fluids vary much less from each other than the absolute viscosities. Since both viscosity and density vary with temperature, so will kinematic viscosity. The chart below shows the variation of the kinematic viscosity of some common fluids with temperature.



The following tables list the absolute and kinematic viscosity for water and air at atmospheric pressure, over a range of temperatures.

Table 1: Viscosity of Water at Atmospheric Pressure

Temperature - t - (°C)	Density - ρ - (kg/m ³)	Absolute Viscosity - μ - (kg/m-s) x 10 ⁻³	Kinematic Viscosity - ν - (m ² /s) x 10 ⁻⁶
0	1000.0	1.787	1.787
5	1000.0	1.519	1.519
10	1000.0	1.307	1.307
20	998.0	1.002	1.004
30	996.3	0.798	0.801
40	992.4	0.653	0.658
50	989.2	0.547	0.553
60	983.2	0.467	0.475
70	978.2	0.404	0.413
80	972.6	0.355	0.365
90	966.3	0.315	0.326
100	972.4	0.282	0.290

Table 2: Viscosity of Air at Atmospheric Pressure

Temperature - t - (°C)	Density - ρ - (kg/m ³)	Absolute Viscosity - μ - (kg/m s) x 10 ⁻⁵	Kinematic Viscosity - ν - (m ² /s) x 10 ⁻⁵
-50	1.469	0.687	0.468
0	1.295	1.736	1.341
10	1.249	1.787	1.431
20	1.206	1.837	1.523
25	1.186	1.862	1.570
30	1.166	1.886	1.617
40	1.129	1.934	1.713
50	1.094	1.982	1.812
60	1.061	2.029	1.912
70	1.030	2.075	2.014
80	1.001	2.121	2.119
90	0.974	2.166	2.225
100	0.947	2.210	2.333
150	0.835	2.423	2.900
200	0.747	2.624	3.512
300	0.617	2.994	4.854
400	0.525	3.330	6.342

You can find more information on both absolute and kinematic viscosity on the internet. Some useful sites are: [Gas viscosity calculator](#), [Viscosity-Wikipedia](#), [The Physics Hyper Textbook](#) and [The Engineering ToolBox](#)

1.4 Types of Fluids: Newtonian and Other

In section 1.3, we made the assumption that shear stress in a fluid will vary linearly with the strain rate. In the majority of fluids, such as air, water, and motor oil, this proves to be a good assumption. This linear relationship between shear stress and strain rate was first proposed by Newton in his classic "[Principia: the Mathematical Principles of Natural Philosophy](#)" in 1686 (although he did not use the same terms, but close enough). The above linked translation to English is from 1864. In honor of his observation, all fluids that display linear shear-strain rate relationships are termed a *Newtonian* fluid.

However, what about fluids that do not display such a linear relationship? They are all lumped into a category known as *non-Newtonian* fluids, which is then split into subcategories, depending on the shear–strain rate behavior. Figure 1.2 shows four possible generic behaviors (idealized) of non-Newtonian fluids, compared with a Newtonian fluid. These non-Newtonian fluids are designated as: (1) **dilatant** (shear-thickening), which increase in resistance with increasing shear stress; (2) **pseudoplastic** (shear-thinning), which decrease in resistance with increasing shear stress; (3) **plastic** (strongly shear-thinning), which show a very strong decrease in resistance with a shear stress increase; and (4) **Bingham plastic**, where the material behaves initially like a solid, until a limiting shear stress is reached, above which it continuously yields as a plastic. An *ideal* Bingham plastic (shown), would display a linear relationship after it begins to yield; however, most real Bingham plastics will generally display a plastic-type behavior after yielding.

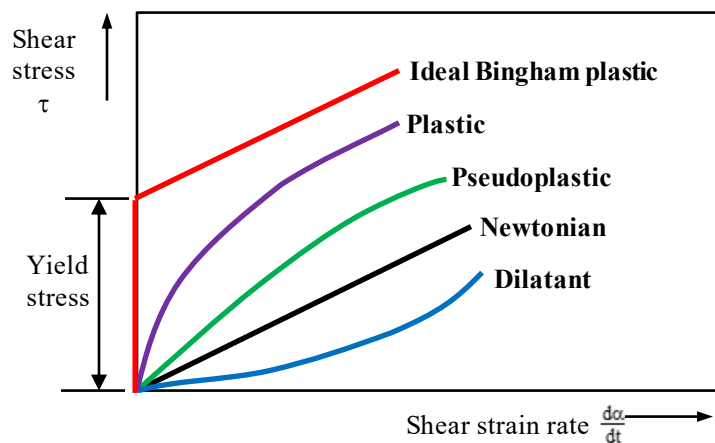


Figure 1.2 The generic behavior of various non-Newtonian fluids relative to Newtonian fluid behavior.

The modeling and assessment of non-Newtonian fluids, although of significant interest, is quite messy. Most practical engineering applications generally are concerned with fluids that behave in a Newtonian manner. Therefore, in this book, we will generally deal with Newtonian fluids. However, Chapter 16 of this text will examine some simple non-Newtonian fluids in basic flow configurations, to illustrate the variations of non-Newtonian from Newtonian fluids.

1.5 The Differential Element

Fluids, like all discrete matter, are governed by Newton's second law, where inertial accelerations/decelerations of a body are balanced by the sum of the forces applied to the body, no matter how small. As long as a fluid can be considered a continuum, and each particle of the fluid can respond independently to the applied forces, we generally find it useful and necessary to model the fluid behavior using a differential fluid element. This differential element is assumed small enough such that property changes across the element are minimal (but not negligible), but large enough to still be assumed a continuum (i.e. no discontinuities of the fluid motion within the differential element).

This approach allows us to ultimately express Newton's second law ($\vec{F} = m\vec{a}$) in terms of a very small, differential volume (i.e. an infinitesimally small control volume). The geometry of this differential volume can be expressed in terms of an appropriate reference coordinate system (generally either Cartesian, cylindrical, or spherical), such that we can describe both the differential volume and the surfaces surrounding this differential volume in terms of the coordinate directions (e.g. x, y, z for a typical Cartesian coordinate), as shown in figure 1.3

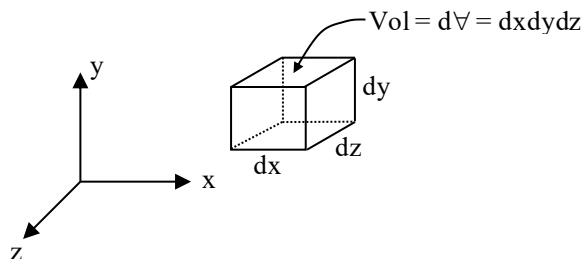


Figure 1.3 An infinitesimal differential fluid element

The volume of a differential element in a Cartesian system, as shown in figure 1.3, is defined as $dV = dx dy dz$, or the product of the three orthogonal dimensions of the differential element. Note that this element is not necessarily a cube, since no restriction is placed on the magnitude of the differential dimensions, other than the assumption that they are small enough such that second-order and higher changes (i.e. spatial derivatives) of the fluid properties (e.g. velocity) in a selected direction are negligible, relative to first-order, linear changes of the property in that same direction. This is important, since this

assumption allows us to develop differential equations modeling the property changes throughout the fluid by use of a truncated [Taylor series](#) expansion (more on this in Chapter 5).

Another important characteristic of this differential element is that it allows a systematic representation of the various bounding surfaces, which is important for establishing contact forces (such as pressure). For example, the area $dzdy$ in figure 1.3 is the area (i.e. the magnitude) of the surface bounding the right and left sides of the differential element. In order to characterize *both* the *magnitude* and the *direction of orientation* of a surface, we require a systematic method for establishing the spatial orientation of each surface relative to a selected coordinate system. Accordingly, we define the direction that a bounding surface faces by a unit vector oriented normal to that surface. By convention, this unit vector always points *outward* from the differential volume. Therefore, for the surface bounding the right side of the differential element shown in figure 1.3, the normal vector would point to the right, as shown in figure 1.4. However, for the same magnitude surface bounding the left side of the differential element, the normal vector would point in the opposite direction (i.e. to the left), as shown. As required, both of these normal vectors point outward from the differential element.

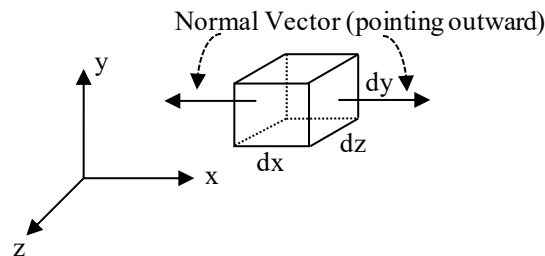


Figure 1.4 Normal vectors for the left and right faces of a differential element

Note that for the right-facing surface the normal vector points in the positive x -direction (for the coordinate system shown). However, if we were considering the outward normal for the left-facing surface of this differential element, the surface vector points to the left, in the negative x -direction, which is (of course) outward from the differential element for the left surface. The direction of the outward normal is particularly important when determining the absolute direction that a force will act when applied to a particular surface of the differential element. We will discuss this issue, and its importance, further in section 1.7 below.

We now illustrate how we make use of the differential element concept to describe the respective forces that act on a fluid. To do this, we note that the forces on a fluid are separated into two basic types: (1) Body forces, and (2) Surface forces.

1.6 Body Forces

Body forces are forces that develop within a fluid without physical contact, and are proportional to the mass of the fluid contained within a region. Particular examples are forces due to gravitational or magnetic fields. For a differential fluid element, as shown in figure 1.5, the local body force due to gravitational attraction is given by $d\vec{F}_B = \rho \vec{g} d\forall = \rho \vec{g} (dx dy dz)$, where $d\vec{F}_B$ is the differential vector body force acting on the differential fluid element, where ρ is the local fluid density, \vec{g} is the gravitational vector field, and $d\forall$ is the volume of the differential element.

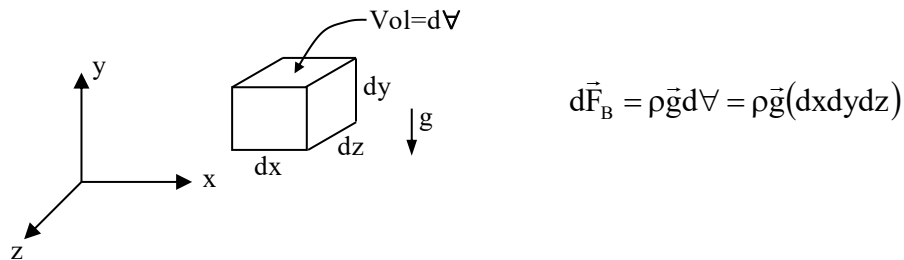


Figure 1.5 Illustration of gravitational body force generated on a differential element

In this text, we will only address gravitational effects, since it is the most common body force encountered by a fluid. However, magnetic effects can be quite important when dealing with the presence of a magnetic field within electrically conductive fluids, such as mercury, or even seawater. In fact, the field of [magnetohydrodynamics](#) is primarily concerned with the influence of magnetic fields on electrically conducting fluids.

1.7 Surface Forces

Surface forces are forces exerted by direct contact at a fluid boundary. The most common examples of such forces are normal forces generated by pressure, and shear stresses generated by fluid friction.

Surface forces, regardless of their source, are vectors that are comprised of: (a) one normal force, which acts perpendicular (normal) to a particular surface, and (b) two tangential forces, which act tangential to the surface, and perpendicular to each other. Figure 1.6 shows a general example of a surface force acting on a planar surface, and its directional components relative to a Cartesian coordinate system fixed on the surface (here, the z-direction is taken as normal to the plane).

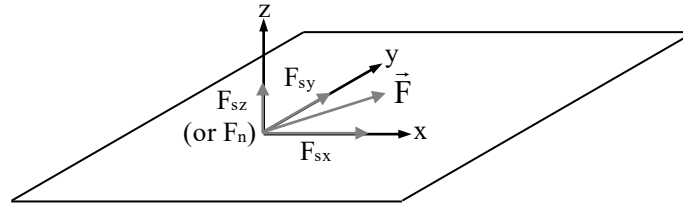


Figure 1.6 Surface forces acting on an arbitrary planar surface.

We assume that \vec{F} is an arbitrary surface force acting on the plane. We can then represent \vec{F} by its respective components, where F_{sz} is the normal component of force acting perpendicular to the surface (in the z-direction), and F_{sx} and F_{sy} act respectively in the x-direction and y-direction, where x and y are oriented at right angles within the plane.

1.8 Stresses

Although we are ultimately concerned with the total forces acting on either a body or surface (e.g. an airplane wing or the inside surface of a pipe), for the purposes of mathematically modeling the fluid behavior, it is more efficient to write the governing equations for fluid mechanics in terms of very localized stresses, where stress = force/unit area. Here we discriminate between the normal and tangential stresses as follows:

$$1) \text{ normal stress } \sigma_{ii} = \lim_{\Delta A \rightarrow 0} \frac{\Delta F_n}{\Delta A} \quad (1.7)$$

$$2) \text{ shear stress } \tau_{ij} = \lim_{\Delta A \rightarrow 0} \frac{\Delta F_s}{\Delta A} \quad (1.8)$$

Here, i and j are direction coordinates which reflect respectively the defining surface of action and the direction of the stress, according to the reference coordinate system employed. Note that a stress has both (a) a direction, and (b) a surface upon which it acts. For normal stresses, the direction of action is along the *normal* to a respective surface. However, for shear stresses, the direction of action will be *tangential to the surface* and *perpendicular to the surface normal*. Thus, we need to employ a method for defining stresses that clearly characterizes all the directional forces (i.e. one normal, and two shear forces) that act on any given surface. We do this by using a double subscript notation that characterizes both (1) the *plane*, or surface, upon which a stress acts, and (2) the *direction* in which the stress acts. This creates a higher-order type of vector description of a stress field known as a *tensor*, which is a collection of nine scalar components that describe both the direction and the surface of action for all possible stress components. For a given coordinate system, the double subscript notation is

defined as τ_{ij} , where τ is the generic stress component. Here, the first subscript (i) indicates the surface of application (defined by the direction of the normal to the surface) and the following subscript (j) indicates the direction of action of the stress. For a Cartesian coordinate system, an example is:

i.e. τ_{yx} = stress (normal or shear) (1.9)

This raises the question of which direction a calculated stress will actually act on a specified surface. One needs to recognize that a “positive” stress (as determined by an appropriate calculation) will not necessarily act in a “positive” direction relative to a specified coordinate system. While this seems strange at first, one can easily realize that for a particular geometry and flow, an imposed stress will have an *absolute* direction in which it will act (which is independent of the chosen coordinate system). For example, pressure exerted by a fluid on a surface will always act “against” the surface, and gravitational forces will always act toward the center of the earth, regardless of how we choose our coordinate system. Therefore, a stress created by a particular flow may act in a particular inherent direction (e.g. to the right of this page), but this may be construed as acting in either a positive direction (coincident with our reference coordinate) or a negative direction (in opposition to a reference coordinate), depending on how we chose to orient our coordinate system, and the particular surface of action that is selected. Confused? Let’s clarify this process further by developing a sign convention for keeping track of the direction of a positive stress.

Stress Component Sign Convention

Plane	Direction	⇒	Absolute Stress Component
+	+		+
-	-		+
+	-		-
-	+		-

Product ⇒ Component Sign

The preceding table defines all the possible signs for planes and directions of action, and the corresponding sign of the absolute stress component. Note that a surface is defined as either a “positive” or “negative” surface depending on the direction of the *outward* normal for a selected surface (relative to the coordinate system). The directions of the stress components acting on a specified surface are then established according to the sign of the

absolute value of the stress component, which is either assumed (for purposes of differential modeling and equation derivation) or calculated (if a mathematical expression is already available). The convention for defining a “positive” stress, as indicated above, depends on the *product* of the signs of: (a) the surface vector (the outward normal) and (b) the direction of the stress. If the product is positive, the absolute stress component is positive, whereas a negative product indicates a negative absolute stress component.

As an example, consider the application direction of shear stress components acting on various surfaces of a differential element volume, where all the absolute stress components are assumed to act *positively*. Here, we define the sign of all external surfaces of the differential element by their outward pointing normal relative to the Cartesian coordinate system shown. For example, the outward normal for the top surface of the differential element shown in figure 1.7 points in the positive y -direction. Thus, τ_{yz} , a z -direction shear stress, which acts in a “positive” absolute direction on this y -surface, will act in the *positive* z -direction, as shown, since the product of the sign of the surface normal (+) and the shear stress directional sign (+) must yield a *positive* (+) absolute sign.

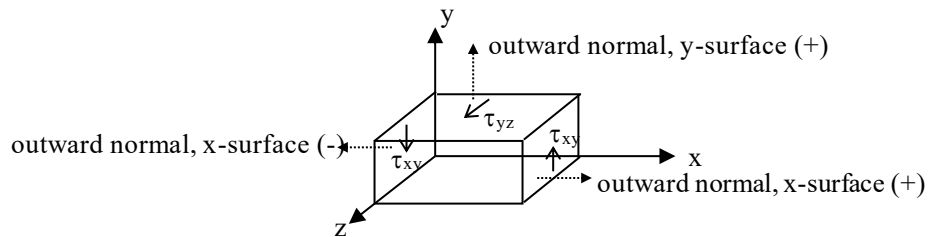


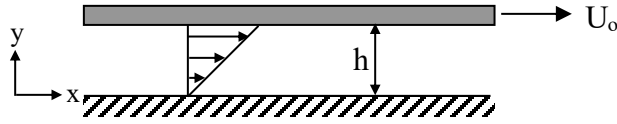
Figure 1.7 Illustration of typical orientations for “positive” stresses acting on selected surfaces of a differential fluid element

Correspondingly, for τ_{xy} , a y -directed shear stress acting on the right surface of the differential element (with outward normal in the positive x direction), the shear stress will also act in a *positive* y -direction in order to represent a positive *absolute* shear component. However, if one considers the same y -directed shear stress acting on the left surface of the differential element (with an outward normal in the *negative* x direction), the absolute direction for τ_{xy} will now act in the *negative* y -direction, as shown in figure 1.7.

Note that this sign convention is incorporated into the governing differential equations when they are derived, and is implicit in the equations when they are integrated (in either closed form or numerically) to determine the velocity field for a particular fluid flow. Thus, when the resulting velocity equations are subsequently differentiated to establish quantitative (absolute) values for the stresses, the stress sign convention provides a

logical, systematic method to establish the absolute direction that a calculated stress will act.

Example: Consider a Couette Flow ([Couette, 1890](#)), a simple viscous flow created between two infinite flat plates, where an upper plate moves at a velocity U_o parallel to a fixed lower plate, as shown.



Without going through the derivation of the velocity flow field (we do this later in Chapter 6), we will simply note here that the velocity expression for a steady, laminar flow of a fluid between the moving and fixed surfaces is given (for the coordinate system shown) by:

$$\vec{V} = u\hat{i} + v\hat{j} = U_o \left(\frac{y}{h} \right) \hat{i} \quad (1.10)$$

u and v represent the velocity components in the x and y directions, respectively, so by comparison we have:

$$u(y) = U_o \left(\frac{y}{h} \right) \quad \text{and} \quad v = 0 \quad (1.11)$$

In Eq. 1.11, $u(y)$ is the x -direction equation for the velocity as a function of y , U_o is the constant velocity of the upper plate, and h is the constant spacing between the plate surfaces (i.e. the thickness of the fluid layer). The unit vector \hat{i} indicates that the flow is in the x -direction. Now, from Eq. 1.5 the local shear stress for this one-directional flow is proportional to the local rate of deformation of the fluid, or the gradient of the velocity, given by:

$$\text{Shear Stress} \Rightarrow \tau = \mu \frac{du}{dy} = \tau_{yx} = \mu \frac{U_o}{h} > 0 \quad (1.12)$$

Here μ is the absolute fluid viscosity, which is the proportionality of the shear stress to the velocity gradient, or the rate of fluid deformation.

So, having determined the local “absolute” magnitude of the shear stress within the fluid, we can now assess in which direction the stress will act. What is not intuitively apparent is that the direction of the stress depends on which surface is of interest to us. For example, are we interested in the stress (and thus force) exerted on the fluid by the upper moving plate, or on the moving plate by the fluid? Or are we concerned with the stress exerted by the fluid on the fixed lower plate, or by the lower plate on the fluid? Just as

we did when establishing the direction of action of a specified stress component on a differential element, we must first establish our surface of interest (and thus action), and then determine the absolute direction (relative to our selected coordinate system) for our calculated stress. Figure 1.8 below illustrates several different shear stress scenarios for selected surfaces of interest.

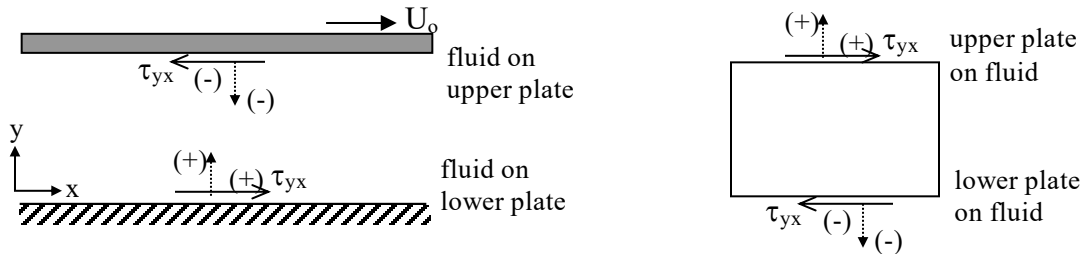


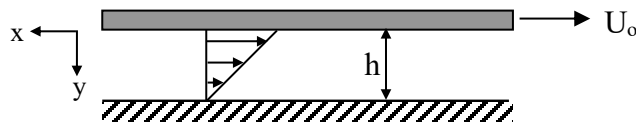
Figure 1.8 Absolute directions of the shear stress acting on selected surfaces for a Couette flow.

Consider, for example, the direction of action of the calculated shear stress, τ_{yx} , acting on the upper plate (which is proportional to how much force would have to be exerted to keep the plate moving). As shown on the left schematic of figure 1.8, the outward normal for the surface of the upper plate in contact with the fluid is in the *negative* y -direction. Since the absolute value of τ_{yx} that we calculated in Eq. 1.12 was *positive*, this means that in order for the sign product of the surface and the shear stress direction to yield a positive orientation, the shear stress must act in a *negative* x -direction, as shown. This makes physical sense when one considers the physics of the problem. As we move the upper plate to the right, the fluid resists, and we experience a force (i.e. stress) on the plate that acts in opposition to the plate movement (i.e. to the left, or negative x -direction relative to our selected coordinate system).

On the other hand, if we wish to determine the direction of action of the shear stress acting on the fluid adjacent to the upper plate, we consider the right schematic of figure 1.8, which isolates the fluid between the plates. Here the *outward* normal for the upper fluid surface points in a positive y -direction (out of the fluid). Thus, since the absolute value of τ_{yx} must still have a positive orientation, the surface-direction sign product must again be positive, which means that the shear stress on the upper fluid surface must act in the *positive* x -direction. At first, this result might seem confusing, since this is opposite to the result we obtained when considering the upper plate surface. However, if we again consider the physics of the situation, the movement of the upper plate to the right in essence “pulls” the adjacent fluid to the right, which is felt by the fluid as a stress in the positive x -direction. Clearly, the stress has the same absolute value at this location, but the direction of action depends on the surface of consideration. As Newton pointed out, every action causes an equal and opposite reaction.

Using the same approach and convention, the direction of action of the shear stress on the lower, fixed surface can also be determined as shown in figure 1.8 -- and again the “absolute” direction of application depends on whether one considers the contact surface as the plate or the fluid.

As a further exercise, consider a change of orientation of the coordinate system, to that shown below. Here the reference x-y coordinates point in the opposite directions from the original coordinate system employed, and have their origin on the surface of the upper plate, rather than on the lower plate.



While this is physically the same flow situation, using this coordinate system the velocity equation for the fluid between the plates is now given by:

$$\vec{V} = -U_0 \left(1 - \frac{y}{h}\right) \hat{i} \quad \text{or} \quad u(y) = U_0 \left(\frac{y}{h} - 1\right) \tag{1.13}$$

While this equation looks quite different, it describes the same exact linear velocity distribution, only referenced to the oppositely oriented coordinate system. Accordingly, if we calculate the corresponding shear stress we have:

$$\tau = \mu \frac{du}{dy} = \tau_{yx} = \mu \frac{U_0}{h} > 0 \tag{1.14}$$

Note that this is identical to the value determined in Eq. 1.12, using a markedly different coordinate system. However, since the coordinate system is oriented differently, we might intuitively expect that this would have a significant influence upon the “absolute” direction of the applied shear. To examine this, consider figure 1.9, which assesses the shear stress application to the same surfaces considered in figure 1.8, only with the oppositely-orientated coordinate system.

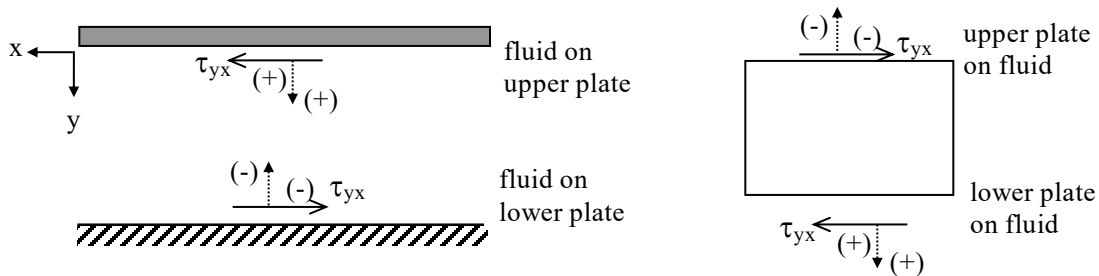


Figure 1.9 Absolute directions of the shear stress acting on selected surfaces for a Couette flow—oppositely-oriented coordinate system.

Note that although the reference coordinate directions and origin are different, when we apply our stress direction convention, the “absolute” direction of the applied shear stresses is identical, both in magnitude and absolute orientation, as they should be. So, regardless of how we define our reference coordinates, the final results of our modeling process, and the analysis of the governing equations, will yield the same absolute result, as long as we apply our convention for the action of a stress on a specified surface.

References

- Smith, F. M. (2003). *Fluid Mechanics*, McGraw-Hill, Boston
Couette, M (1890). *Ann. Chem. Phys.*, ser.6, vol. 21, pp. 433-510.

Chapter 2

Vectors and Vector Operators: The Basics

Contents

2.1	Coordinate Systems	18
2.1.1	Cartesian Coordinates	19
2.1.2	Cylindrical Coordinates	20
2.2	Vector Differentiation	21
2.2.1	Derivatives of Unit Vectors	21
2.3	Vector Operator ∇	23
2.3.1	Gradient	25
2.3.2	Divergence	26
2.3.3	Cross Product or Curl	28
2.3.4	The Laplacian and Other Useful Identities	29
2.4	Review of Line and Surface Integral Theorems	32
2.4.1	The Gauss Divergence Theorem	32
2.4.2	The Curl Theorem	33
2.4.3	The Gradient Theorem	33
2.4.4	Stokes' Theorem	34

A fluid can move and change its orientation and properties continuously in space and time. Thus, to characterize fluid behavior properly we must know both the magnitude and direction of changes at any point. This requires that we represent fluid behavior in terms of vector functions, which describe the magnitude and direction of both fluid motion and property changes throughout the extent of the fluid. Although there are excellent books that cover the details of vector calculus (e.g. [Schey, 1997](#)), and a student of fluid mechanics is expected to have had prior mathematical instruction on the basics of vector calculus, the present chapter reviews a few of the basic concepts of vector calculus that are particularly important for the derivation and utilization of the governing equations of fluid mechanics.

2.1 Coordinate Systems

To properly establish a vector representation of a fluid property (such as velocity) requires that we first establish an *appropriate* coordinate system. Note that a vector function representing a fluid property will always reflect an absolute behavior, which is inherent in the fluid behavior (e.g. water always flows downhill). However, how we choose to represent that absolute behavior mathematically depends on the coordinate

system we employ. It is to our advantage to choose a coordinate system that most easily represents the type of behavior of interest. For example, if we are concerned with flows over flat surfaces, or within rectangular tubes, a Cartesian or rectangular coordinate system (x, y, z) is best suited for representation, since all property changes will occur either along the planar boundaries or normal to them, and the Cartesian coordinate system can be easily aligned with these boundaries. Alternatively, a cylindrical or radial coordinate system (r, θ, z) can best describe, and be aligned with, flows that pass either around, along, or through geometries that are radially symmetric, such as cylinders and circular tubes, pipes, and ducts. And finally (at least for our purposes), spherical coordinates (r, θ, ϕ) provide a coordinate system that is well suited to flows over or within spherically-symmetric geometries, such as geophysical flows within the atmosphere. For the purposes of the present text, we will confine our interests to the former two coordinate systems, Cartesian and cylindrical, which have the broadest applications, and are admittedly simpler to employ. However, note that the same principles that we develop for Cartesian and cylindrical coordinate systems apply equally well in spherical coordinates, or any other coordinate system of choice, albeit yielding more complicated governing differential equations.

2.1.1 Cartesian Coordinates

A typical Cartesian coordinate system is shown in figure 2.1 below, characterized by three orthogonal coordinate axes initiating at a common origin.

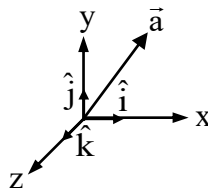


Figure 2.1 Schematic of a Cartesian coordinate system

Normally used with planar or rectangular geometries, a Cartesian coordinate system will generally be oriented such that two of the axes lie in the primary plane of interest (e.g. on the surface of a flat plate), with the other axis projecting perpendicular, or normal, to the plane of interest. As with all coordinate systems, a vector property, call it \vec{a} , when described in a Cartesian system will consist of three directional components (a_x, a_y, a_z) , which indicate the magnitude of the vector contribution in each coordinate direction. This allows the vector to be expressed in terms of the directional components as:

$$\vec{a} = \hat{i} a_x + \hat{j} a_y + \hat{k} a_z \quad (2.1)$$

Here \hat{i} , \hat{j} , and \hat{k} are unit vectors, which are each of unity magnitude and oriented in the x , y , and z directions respectively, as shown in figure 2.1. Note that a_x , a_y , and a_z can be either constants or, more likely, functions of one or more of the coordinate variables x , y , and z .

2.1.2 Cylindrical Coordinates

Similar to the Cartesian system, the cylindrical (also called radial or polar) coordinate system employs three coordinate axes: r , θ , and z . However, only two of these (r and z) originate from a common origin, as shown below.

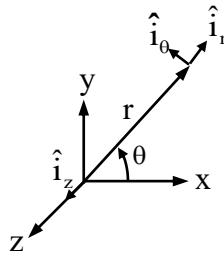


Figure 2.2 Schematic of a radial coordinate system

The third coordinate is a reference angle for the r axis, and describes the angular location of the r axis relative to a fixed reference. This coordinate system will generally be used for axisymmetric geometries, such as rods and tubes, with the z coordinate axis located along the axis of rotational symmetry (e.g. the centerline of a rod or tube). Here, we can describe a vector \vec{a} in terms of directional components a_r , a_θ , and a_z as:

$$\vec{a} = \hat{i}_r a_r + \hat{i}_\theta a_\theta + \hat{i}_z a_z, \quad (2.2)$$

In Eq. 2.2, \hat{i}_r , \hat{i}_θ , and \hat{i}_z are again unit vectors of unity magnitude, and oriented respectively in the r , θ , and z directions, as shown in figure 2.2.

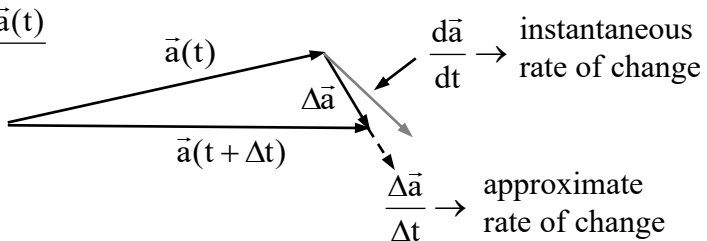
There are two things to note about the cylindrical coordinate system that make it more complicated than the Cartesian system (at least when performing vector calculus operations). The first complication is that the r and z coordinates reference spatial changes, whereas the θ coordinate references an *angular* change. This creates some complication when one takes the derivative of a vector expressed in cylindrical coordinates, since derivatives with respect to z and r yield spatial property changes, while derivatives with respect to θ indicate *angular* property changes. Consequently, it is the effect of these angular changes of the r coordinate that yields the corresponding spatial change with respect to θ . Since these angular changes are a combination of changes in

both r and θ , the terms comprising the governing differential equations will be a bit more complicated, and in some cases contain *additional* terms, relative to the Cartesian form of the governing equations.

The second complication is that the \hat{i}_r and \hat{i}_θ unit vectors within the cylindrical system change their *spatial orientation* with changes in the angular coordinate, θ . Thus, a change in the angular orientation of a vector will also result in a corresponding change in the orientation of the \hat{i}_r and \hat{i}_θ unit vectors, since these unit vectors are oriented respectively along (\hat{i}_r) and normal to (\hat{i}_θ) the r coordinate axis, and r changes its angular orientation whenever there is a change in θ . For example, if r changes its angular orientation (i.e. rotates) by 180° , the \hat{i}_r and \hat{i}_θ unit vectors will change their orientation by 180° as well. This coupling of \hat{i}_r and \hat{i}_θ with θ manifests itself when one differentiates a vector in cylindrical coordinates, which results in non-zero unit vector derivatives for \hat{i}_r and \hat{i}_θ , as we will discuss in section 2.2.1.

2.2. Vector Differentiation

Generally, vector differentiation is performed in essentially the same manner as non-vector differentiation. Going back to basics, if we let \vec{a} be a vector such that $\vec{a} = \vec{a}(t)$, we can define a derivative with respect to t as:

$$\frac{d\vec{a}}{dt} = \lim_{\Delta t \rightarrow 0} \frac{\Delta \vec{a}}{\Delta t} = \lim_{\Delta t \rightarrow 0} \frac{\vec{a}(t + \Delta t) - \vec{a}(t)}{\Delta t}$$


So, if $\vec{a}(t) = t^2 \hat{i}$, then $d\vec{a}/dt = (dt^2/dt)\hat{i} + t^2(d\hat{i}/dt) = 2t\hat{i}$, since we assume that the unit vector \hat{i} is not a function of t (which is the case for the Cartesian coordinate system). Of course, the process is the same for partial differentiation as well. However, the assumption that a unit vector is not a function of the independent coordinate variables depends on the coordinate system employed, as shown in the following.

2.2.1 Derivatives of Unit Vectors

First, let's consider the easiest situation, the Cartesian coordinate system. This is really simple, because the Cartesian unit vectors -- $\hat{i}, \hat{j}, \hat{k}$ -- are of constant magnitude (unity) and *independent* of changes in x, y, z . Thus,

$$\frac{\partial}{\partial x}, \frac{\partial}{\partial y}, \frac{\partial}{\partial z} = 0 \quad \text{for all Cartesian unit vectors.}$$

So, when performing a vector operation, whether it is the formation of a derivative or an integration, we treat Cartesian unit vectors the same as we do constants in any operation.

Now, let's consider the cylindrical coordinate system. Here, \hat{i}_z is independent of r, z, θ -- so we can treat the \hat{i}_z unit vector as a constant during differentiation. However, the unit vectors \hat{i}_r and \hat{i}_θ , while they are independent of changes in r and z , they are (as pointed out in section 2.1.2 above) *dependent* on changes in θ . Thus, when we consider the differentiation of unit vectors in the cylindrical coordinate system, we obtain the following:

$$\begin{aligned} \frac{\partial \hat{i}_r}{\partial r} &= 0 & \frac{\partial \hat{i}_\theta}{\partial r} &= 0 & \frac{\partial \hat{i}_z}{\partial r} &= 0 \\ \frac{\partial \hat{i}_r}{\partial \theta} &= \hat{i}_\theta & \frac{\partial \hat{i}_\theta}{\partial \theta} &= -\hat{i}_r & \frac{\partial \hat{i}_z}{\partial \theta} &= 0 \\ \frac{\partial \hat{i}_r}{\partial z} &= 0 & \frac{\partial \hat{i}_\theta}{\partial z} &= 0 & \frac{\partial \hat{i}_z}{\partial z} &= 0 \end{aligned} \quad (2.3)$$

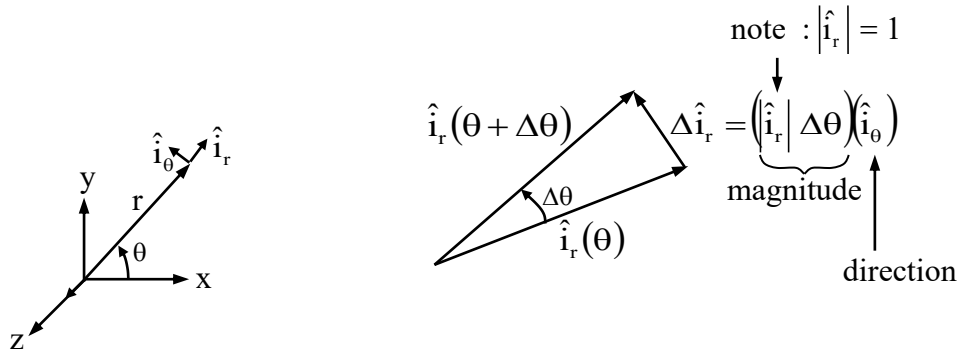
Here, differentiation of \hat{i}_r and \hat{i}_θ with respect to r and z yields zero values; however, differentiation with respect to θ yields two non-zero values, which are unit vectors themselves. This is of particular importance when dealing with vector calculus operations employing the ∇ operator, which we will discuss in section 2.3.

Example: Using the basic concept of a vector derivative, the following demonstrates how we establish the non-zero partial derivative for $\frac{\partial \hat{i}_r}{\partial \theta}$. Here, we represent \hat{i}_r as a vector of unity magnitude, oriented along the coordinate r . As shown in the figure below, we assume this vector undergoes a small angular change of $\Delta\theta$. Since the orientation of \hat{i}_r is a function of θ , this means that the change of \hat{i}_r with respect to θ is from $\hat{i}_r(\theta)$ to $\hat{i}_r(\theta + \Delta\theta)$. Thus, we can write the derivative for \hat{i}_r with respect to θ as:

$$\frac{\partial \hat{i}_r}{\partial \theta} = \lim_{\Delta\theta \rightarrow 0} \frac{\hat{i}_r(\theta + \Delta\theta) - \hat{i}_r(\theta)}{\Delta\theta} \quad (2.4)$$

Now, to approximate the difference, $\hat{i}_r(\theta + \Delta\theta) - \hat{i}_r(\theta)$ in Eq. 2.4, we examine the geometric change of these vectors, as shown below. We label this difference

$\Delta \hat{i}_r$, and note that $\Delta \hat{i}_r$ is represented by the small arc created by the rotation of the unit vector \hat{i}_r by an amount $\Delta\theta$ in the \hat{i}_θ direction. Since the magnitude of \hat{i}_r is unity, as indicated, then $\Delta \hat{i}_r = \Delta\theta \hat{i}_\theta$.



Thus, substituting our value of $\Delta \hat{i}_r$ into Eq. 2.4 yields:

$$\frac{\partial \hat{i}_r}{\partial \theta} = \lim_{\Delta\theta \rightarrow 0} \frac{\hat{i}_r(\theta + \Delta\theta) - \hat{i}_r(\theta)}{\Delta\theta} = \lim_{\Delta\theta \rightarrow 0} \frac{\Delta \hat{i}_r}{\Delta\theta} = \lim_{\Delta\theta \rightarrow 0} \frac{\Delta\theta \hat{i}_\theta}{\Delta\theta} = \hat{i}_\theta \tag{2.5}$$

As an exercise, use a similar approach to derive the result for $\frac{\partial \hat{i}_\theta}{\partial \theta}$ by considering the changes in the unit vector \hat{i}_θ for a small angular change, $\Delta\theta$.

2.3 Vector Operator ∇

To develop the governing equations of fluid mechanics, we must be able to model mathematically the changes in the various properties of a fluid, both spatially and temporally. Sometimes we are concerned with property changes from one point to another (like with the Bernoulli equation, Section 7.3), and sometimes with the local property changes with time, particularly when developing the governing differential equations of motion. These properties run the gamut from scalars (e.g. fluid density and pressure) to vectors (e.g. velocity and vorticity). To model these changes, we have several different mathematical methods to establish these property changes, described variously as the *divergence*, the *curl*, and the *gradient* of a property field. These descriptions can often get rather complicated, since we have to consider the various possible changes that can take place with respect to all the coordinate directions.

To help facilitate these “change” descriptions mathematically, we have a very convenient mathematical operator that allows us to write a bit of short hand for the various changes. This operator is designated the “del” operator, and is written as:

$$\nabla = \hat{i} \frac{\partial}{\partial x} + \hat{j} \frac{\partial}{\partial y} + \hat{k} \frac{\partial}{\partial z} \quad (\text{in Cartesian coordinates}) \quad (2.6)$$

and

$$\nabla = \hat{i}_r \frac{\partial}{\partial r} + \hat{i}_\theta \frac{1}{r} \frac{\partial}{\partial \theta} + \hat{i}_z \frac{\partial}{\partial z} \quad (\text{in cylindrical coordinates}) \quad (2.7)$$

Examination of the above definitions illustrates that the ∇ operator reflects the cumulative changes for all three respective coordinate directions. For example, the first derivative function for the Cartesian coordinate expression in Eq. 2.6 above, $\hat{i} \frac{\partial}{\partial x}$, assesses the changes in a property relative to the x-direction—the unit vector indicates that this change is an x-direction contribution to a spatial derivative vector. Applying this ∇ operator to a designated property (e.g. directly for a scalar property, and via a dot or cross product operation for a vector property), we can establish how that property is spatially “changing” at a specified point.

However, one must exercise care when using the ∇ operator in cylindrical coordinates, since, as pointed out in Section 2.2.1, the differentiation of the unit vectors \hat{i}_r and \hat{i}_θ , which change their orientation with respect to the angular coordinate θ , will yield other unit vectors. This is particularly important to understand when performing operations with the ∇ operator. The rule is that when performing operations that involve both vector differentiation and subsequent vector operations, one must *always* perform the derivative function (of *both* the magnitude function *and* the unit vectors) *first*, and then perform the prescribed vector operation. For example, if we are taking the dot product of $b\hat{i}_r$ with the angular derivative of $\vec{V} = a\theta\hat{i}_\theta$, (where a and b are constants) we would perform the operation as:

$$b\hat{i}_r \cdot \frac{\partial \vec{V}}{\partial \theta} = b\hat{i}_r \cdot \frac{\partial}{\partial \theta} (a\theta\hat{i}_\theta) = b\hat{i}_r \cdot a \left(\frac{\partial \theta}{\partial \theta} \hat{i}_\theta + \theta \frac{\partial \hat{i}_\theta}{\partial \theta} \right) = b\hat{i}_r \cdot a \left[(1)\hat{i}_\theta + \theta(-\hat{i}_r) \right] = -ab\theta$$

Note that if we didn't consider the derivatives of the unit vectors in this operation, our result would have been zero! So, the rule is: perform all derivative functions first, before performing the vector operations.

Now, let's consider the operations that can be performed using the ∇ operator: first on a scalar field, and then on a vector field. Recall that a scalar field is one for which the property has magnitude, but no direction. Pressure, fluid density, and temperature are examples of scalar properties: they will have a magnitude at a location, but do not have a

direction associated with the property. On the other hand, velocity, acceleration, and vorticity (angular rotation) are vector properties that have both a magnitude and a particular direction at any given location. The application of the ∇ operator will yield very different types of information about a property field, depending on whether the property is a scalar or a vector. And from the point of view of modeling of fluid behavior, it is important to understand what information results from the application of the ∇ operator.

2.3.1 Gradient

Consider a **scalar** field (i.e. a property like pressure or fluid density) given by $\phi = f(x, y, z)$. Such a property describes what we term a scalar field, which means that the function $f(x, y, z)$ will describe the magnitude of the property ϕ at any coordinate location within a region (the property “field” encompassed within the coordinate space). Clearly, this scalar property only has magnitude, but no direction of action. However, if the scalar property is changing with location (e.g. a change in pressure as we walk up a mountain), we can establish the *local* rate at which the property will change as we move in any direction from a specified location within the field. Clearly, these changes will have both a magnitude *and* an associated direction of that change. Taken collectively for all coordinate directions, these changes are termed the “gradient” of the property and can be mathematically determined by performing the ∇ operation directly on the scalar function ϕ , such that:

$$\nabla\phi = \hat{i} \frac{\partial\phi}{\partial x} + \hat{j} \frac{\partial\phi}{\partial y} + \hat{k} \frac{\partial\phi}{\partial z} \tag{2.8}$$

The result of this operation is a vector function, $\nabla\phi$, with magnitude and direction indicating the spatial rate of change of ϕ .

Example: Consider the static pressure field in a swimming pool given by $\phi = p(z) = p_o + \rho g z$, where ρ is a constant fluid density, g is the gravitational constant, p_o is the pressure at the surface of the pool, and z is a Cartesian coordinate pointing vertically downward from the pool surface. Accordingly, the gradient of the pressure in the swimming pool is given by:

$$\nabla\phi = \hat{i} \frac{\partial\phi}{\partial x} + \hat{j} \frac{\partial\phi}{\partial y} + \hat{k} \frac{\partial\phi}{\partial z} = +\rho g \hat{k} \quad (\text{i.e. a constant change in } z\text{-direction})$$

↑ direction
↑ magnitude

Here, the gradient indicates that the pressure is increasing at a constant magnitude in the positive z direction (i.e. as we move farther below the surface of the water). Other examples of scalar fields within a fluid where a gradient can exist include fluid density, temperature, and concentration fields. We'll show how this concept is utilized in section 2.4 below, and later in Chapter 4.

2.3.2 Divergence

Now let's consider the changes that can take place in a **vector** field (again in Cartesian coordinates), $\vec{V} = V_x \hat{i} + V_y \hat{j} + V_z \hat{k}$, which has both magnitude *and* direction. Clearly, since the ∇ operator is a vector operator, in order to operate on a vector field, one must employ an appropriate vector operation. Our options are the *dot product* of two vector functions, or the *cross product* (or curl) of two vector functions. Here we consider the dot product first, with the ∇ operator prescribed to operate (left side of the dot product) on the vector field (right side of the dot product), with the result:

$$\nabla \cdot \vec{V} = \left(\hat{i} \frac{\partial}{\partial x} + \hat{j} \frac{\partial}{\partial y} + \hat{k} \frac{\partial}{\partial z} \right) \cdot (V_x \hat{i} + V_y \hat{j} + V_z \hat{k}) = \frac{\partial V_x}{\partial x} + \frac{\partial V_y}{\partial y} + \frac{\partial V_z}{\partial z} \quad (2.9)$$

Equation 2.9 is a scalar termed the “*divergence*,” which indicates the degree of total “expansion” of a vector field at a point. Note that this expansion (of course a negative value would indicate a contraction) is the sum of the local respective changes in all three coordinate directions. The divergence is intimately related to the compressibility of a fluid – i.e. the spatial change in the local density at a point. We will show later, in Chapter 4, that for *incompressible* fluids (like water), $\nabla \cdot \vec{V} = 0$ is an expression of the conservation of mass, if the vector \vec{V} represents the velocity field of a fluid. Thus, if the density of a fluid is constant (i.e. incompressible), the local velocity changes in all coordinate directions must exactly balance each other (i.e. there can be no “expansion,” or “contraction” of the volume that an incompressible fluid occupies). However, if a fluid is compressible (like air), the local velocity changes may not balance, which indicates an expansion or contraction of the fluid. We discuss this further in Chapter 4.

Example: Divergence in Cartesian Coordinates

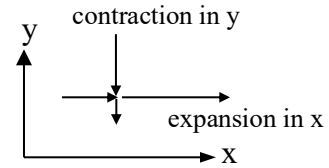
Consider a velocity field given by $\vec{V} = ax\hat{i}$ ($a = \text{constant}$). Here, there will be a non-zero divergence, indicating that the fluid is expanding at a point.

$$\nabla \cdot \vec{V} = \left(\hat{i} \frac{\partial}{\partial x} + \hat{j} \frac{\partial}{\partial y} + \hat{k} \frac{\partial}{\partial z} \right) \cdot ax\hat{i} = a \frac{\partial x}{\partial x} = a \quad \Rightarrow \quad \begin{array}{c} y \\ \uparrow \\ \text{expansion in } x \\ \text{---} \rightarrow \\ x \end{array}$$

expansion at a point

Now consider a velocity field given by $\vec{V} = x\hat{i} - y\hat{j}$.

$$\nabla \cdot \vec{V} = \left(\hat{i} \frac{\partial}{\partial x} + \hat{j} \frac{\partial}{\partial y} + \hat{k} \frac{\partial}{\partial z} \right) \cdot (x\hat{i} - y\hat{j}) = \frac{\partial x}{\partial x} - \frac{\partial y}{\partial y} = 1 - 1 = 0$$



In this latter case, the divergence is zero, indicating that the fluid is nonexpanding. Here, any expansion in the x-direction (a positive change) is balanced by a corresponding contraction (a negative change) in the y-direction. This balanced expansion/contraction is reflected by increasing or decreasing velocity components to and from a point.

Example: Divergence in Cylindrical Coordinates

As was noted in section 2.2.1, when dealing with the differentiation of a flow field described in cylindrical coordinates, one must be careful to perform any indicated differentiation (of both the vector magnitude *and* the unit vectors) *first*, and then perform the prescribed vector operation. To illustrate the importance of this process, consider the divergence of a velocity field given by $\vec{V} = V_0 \hat{i}_r$, where V_0 is a constant. Here, the divergence is given by (using Eq. 2.7)

$$\begin{aligned} \nabla \cdot \vec{V} &= \left(\hat{i}_r \frac{\partial}{\partial r} + \hat{i}_\theta \frac{1}{r} \frac{\partial}{\partial \theta} + \hat{i}_z \frac{\partial}{\partial z} \right) \cdot V_0 \hat{i}_r = \hat{i}_r \frac{\partial}{\partial r} \cdot V_0 \hat{i}_r + \hat{i}_\theta \frac{1}{r} \frac{\partial}{\partial \theta} \cdot V_0 \hat{i}_r + \hat{i}_z \frac{\partial}{\partial z} \cdot V_0 \hat{i}_r \\ &= \hat{i}_r \cdot \left(\frac{\partial V_0}{\partial r} \hat{i}_r + V_0 \frac{\partial \hat{i}_r}{\partial r} \right) + \hat{i}_\theta \frac{1}{r} \cdot \left(\frac{\partial V_0}{\partial \theta} \hat{i}_r + V_0 \frac{\partial \hat{i}_r}{\partial \theta} \right) + \hat{i}_z \cdot \left(\frac{\partial V_0}{\partial z} \hat{i}_r + V_0 \frac{\partial \hat{i}_r}{\partial z} \right) \\ &= \hat{i}_\theta \frac{1}{r} \cdot V_0 \hat{i}_\theta = \frac{V_0}{r} \end{aligned}$$

Here, the divergence of the flow field is infinite at the origin, and diminishes rapidly as the flow moves radially outward (a bit like a radially-symmetric explosion). While not a terribly realistic fluid flow, this example does illustrate the importance of completing the unit vector differentiation *before* performing the vector operation. Note that if we assumed that the derivative of the \hat{i}_r unit vector was zero, our result would also be zero, which certainly is not the case.

Note that for a general vector field of $\vec{V} = V_r \hat{i}_r + V_\theta \hat{i}_\theta + V_z \hat{i}_z$, the divergence in cylindrical coordinates can be shown to be:

$$\nabla \cdot \vec{V} = \frac{1}{r} \frac{\partial}{\partial r} (rV_r) + \frac{1}{r} \frac{\partial V_\theta}{\partial \theta} + \frac{\partial V_z}{\partial z} = \frac{\partial V_r}{\partial r} + \frac{1}{r} \frac{\partial V_\theta}{\partial \theta} + \frac{\partial V_z}{\partial z} + \frac{V_r}{r} \quad (2.10)$$

Here, the last term in Eq. 2.10 is the result of the change in the \hat{i}_r unit vector with angular displacement (i.e. a non-zero derivative of the unit vector, $\frac{\partial \hat{i}_r}{\partial \theta} = \hat{i}_\theta$).

2.3.3 Cross Product or Curl

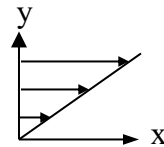
Next, we consider the cross product of a vector field, with the ∇ operator again prescribed to operate (left side of the cross product) on a vector field (right side of the cross product). The result for a velocity field (in Cartesian coordinates), $\vec{V} = V_x \hat{i} + V_y \hat{j} + V_z \hat{k}$, is:

$$\begin{aligned} \nabla \times \vec{V} &= \left(\hat{i} \frac{\partial}{\partial x} + \hat{j} \frac{\partial}{\partial y} + \hat{k} \frac{\partial}{\partial z} \right) \times (V_x \hat{i} + V_y \hat{j} + V_z \hat{k}) \\ &= \left(\frac{\partial V_z}{\partial y} - \frac{\partial V_y}{\partial z} \right) \hat{i} + \left(\frac{\partial V_x}{\partial z} - \frac{\partial V_z}{\partial x} \right) \hat{j} + \left(\frac{\partial V_y}{\partial x} - \frac{\partial V_x}{\partial y} \right) \hat{k} \end{aligned} \quad (2.11)$$

Equation 2.11 gives a resultant vector often termed the “curl” of \vec{V} . The curl indicates the amount of angular change or rotation that occurs within a vector field due to changes in the vector property in directions normal to each coordinate direction. If the vector field is a velocity field, the cross product will give the angular velocity of the fluid, which is expressed as a proportional “vorticity” in fluid mechanics. We will show later (in Chapter 7) that when $\nabla \times \vec{V} = 0$, a velocity field is said to be “irrotational” -- a condition which allows some significant simplifications to be made to the governing equations of fluid mechanics.

Example: Consider a two-dimensional velocity field given by $\vec{V} = by\hat{i} = V_x \hat{i}$ (a simple uniformly sheared flow, like a Couette flow, as shown). Eq. 2.11, the cross product for this two-dimensional flow, simplifies to:

$$\begin{aligned} \nabla \times \vec{V} &= \left(\frac{\partial V_x}{\partial z} \right) \hat{j} + \left(-\frac{\partial V_x}{\partial y} \right) \hat{k} = \frac{\partial (by)}{\partial z} \hat{j} - \frac{\partial (by)}{\partial y} \hat{k} \\ &= -b\hat{k} \end{aligned}$$



Thus, the rotation of the fluid would be like a ball rolling left to right (or clockwise around the z-coordinate, which points out of the page). In contrast, if $\vec{V} = ax\hat{i}$ (the flow field shown to have non-zero divergence in section 2.3.2), then $\nabla \times \vec{V} = 0$, indicating that although the flow is expanding, it has no rotation. This is also the case

for the second flow field we examined in section 2.3.2, $\vec{V} = x\hat{i} - y\hat{j}$. For that case, again $\nabla \cdot \vec{V} = 0$, which indicates a non-expanding field; additionally, one can show that $\nabla \times \vec{V} = 0$, which indicates that the flow field also exhibits no rotation.

Note that in cylindrical coordinates, the curl for a velocity field given by

$\vec{V} = V_r \hat{i}_r + V_\theta \hat{i}_\theta + V_z \hat{i}_z$ will be:

$$\begin{aligned} \nabla \times \vec{V} &= \left(\hat{i}_r \frac{\partial}{\partial r} + \hat{i}_\theta \frac{1}{r} \frac{\partial}{\partial \theta} + \hat{i}_z \frac{\partial}{\partial z} \right) \times (V_r \hat{i}_r + V_\theta \hat{i}_\theta + V_z \hat{i}_z) \\ &= \left(\frac{1}{r} \frac{\partial V_z}{\partial \theta} - \frac{\partial V_\theta}{\partial z} \right) \hat{i}_r + \left(\frac{\partial V_r}{\partial z} - \frac{\partial V_z}{\partial r} \right) \hat{i}_\theta + \frac{1}{r} \left(\frac{\partial}{\partial r} (rV_\theta) - \frac{\partial V_r}{\partial \theta} \right) \hat{i}_z \\ &= \left(\frac{1}{r} \frac{\partial V_z}{\partial \theta} - \frac{\partial V_\theta}{\partial z} \right) \hat{i}_r + \left(\frac{\partial V_r}{\partial z} - \frac{\partial V_z}{\partial r} \right) \hat{i}_\theta + \left(\frac{\partial V_\theta}{\partial r} - \frac{1}{r} \frac{\partial V_r}{\partial \theta} + \frac{V_\theta}{r} \right) \hat{i}_z \end{aligned} \quad (2.12)$$

Here, the last two terms in Eq. 2.12 are the result of changes in the \hat{i}_θ unit vector with angular displacement (i.e. a non-zero derivative of the unit vector, $\frac{\partial \hat{i}_\theta}{\partial \theta} = -\hat{i}_r$). Thus, taking the cross product yields an extra z-direction component.

2.3.4 The Laplacian and Other Useful identities Using the ∇ Operator

In the derivation and presentation of the various equations of fluid mechanics, it is common, and often useful, to present portions of the equations in terms of functions of the ∇ operator. This provides both a shortcut method for concisely representing manifold complex terms, and also allows equations to be represented in a more generic fashion, applicable to *all* coordinate systems. Among the ∇ operator functions that prove particularly useful is the Laplacian, ∇^2 , which evolves from equations that incorporate the divergence of the gradient of a scalar property. Examples of such scalar fields in fluid mechanics include pressure, temperature, or density fields. For example, if we consider a scalar field, ϕ , in Cartesian coordinates the divergence of the gradient of ϕ is written:

$$\nabla^2 \phi = \nabla \cdot (\nabla \phi) = \left(\hat{i} \frac{\partial}{\partial x} + \hat{j} \frac{\partial}{\partial y} + \hat{k} \frac{\partial}{\partial z} \right) \cdot \left(\hat{i} \frac{\partial \phi}{\partial x} + \hat{j} \frac{\partial \phi}{\partial y} + \hat{k} \frac{\partial \phi}{\partial z} \right) = \frac{\partial^2 \phi}{\partial x^2} + \frac{\partial^2 \phi}{\partial y^2} + \frac{\partial^2 \phi}{\partial z^2}$$

So here, the Laplacian ∇^2 (generally read as “del squared”) is:

$$\nabla^2 = \frac{\partial^2}{\partial x^2} + \frac{\partial^2}{\partial y^2} + \frac{\partial^2}{\partial z^2} \quad (2.13)$$

Equation 2.13 is a nice compact way to express the sum of the second-order derivatives of a scalar with respect to all coordinate directions. Note that an equation of the form $\nabla^2\phi = 0$ is classically termed the Laplace equation (which arises in many different areas of engineering and science), and thus the designation of ∇^2 as the Laplacian.

In cylindrical coordinates, the Laplacian is of course more complicated, due to the need to perform the unit vector derivative operations with respect to θ , and is given by:

$$\nabla^2 = \frac{1}{r} \frac{\partial}{\partial r} \left(r \frac{\partial}{\partial r} \right) + \frac{1}{r^2} \frac{\partial^2}{\partial \theta^2} + \frac{\partial^2}{\partial z^2} = \underbrace{\frac{1}{r} \frac{\partial}{\partial r} + \frac{\partial^2}{\partial r^2}}_{\text{Additional term due to unit vector differentiation}} + \frac{1}{r^2} \frac{\partial^2}{\partial \theta^2} + \frac{\partial^2}{\partial z^2} \quad (2.14)$$

Note that the Laplacian function in cylindrical coordinates is often written in the more “compact” manner on the left side of Eq. 2.14. However, writing the expanded function, to the right, illustrates the additional term that arises from unit vector differentiation

There are a number of other ∇ -based functions that are commonly employed to consolidate differential vector equations, and which are often confusing if one doesn't follow the proper order of operation (i.e. which operation you perform first). The general rule for multiple operations is that one performs the right-most operation first, and then work back to the left. For example, for $\nabla \times \nabla \times \vec{F}$ one would perform the curl of \vec{F} first, $(\nabla \times \vec{F})$, then perform the curl of that result [i.e. $\nabla \times (\nabla \times \vec{F})$]. If for $\nabla \times \nabla \times \vec{F}$ we intended the operation on the left to be performed first, we would use parentheses to indicate a variance in the order of operation. For example, if the expression was written as $(\nabla \times \nabla) \times \vec{F}$, we would perform the del cross product first, then take the cross product of the result with \vec{F} . The catch here is that sometimes certain operations don't work in the right-to-left hierarchy, and thus inherently must be performed in the only logical manner available (I'm not sure how this practice evolved, but it has). For example, consider $\vec{F} \cdot \nabla \vec{F}$. By performing the right hand operation first, this would suggest that we should have ∇ operate on \vec{F} first. However, a vector operation (dot or cross product) is not indicated for $\nabla \vec{F}$, and this can't be a gradient operation, since \vec{F} is a vector. So one must perform the only vector operation available, $\vec{F} \cdot \nabla$, first and then (since the result is a

non-vector functional operation) operate on \vec{F} . So, in essence, the proper way to write this operation should be: $(\vec{F} \cdot \nabla)\vec{F}$.

Another confusing function is the Laplacian operating on a vector, $\nabla^2\vec{F}$. Here, if we follow the origin of the Laplacian above, we would write: $\nabla^2\vec{F} = \nabla \cdot (\nabla\vec{F})$, which again doesn't make sense. So, what is generally implied by this representation is:

$$\nabla^2\vec{F} = \left(\frac{\partial^2}{\partial x^2} + \frac{\partial^2}{\partial y^2} + \frac{\partial^2}{\partial z^2} \right) \vec{F} = (\nabla \cdot \nabla)\vec{F} \quad (2.15)$$

A subtle point, but one that can be confusing when faced with manifold “compact” representations of vector equations.

One of the nice aspects of using the ∇ operator is its capability to express more voluminous governing equations in compact form (as we shall see in Chapters 4 and 5). Once an equation is written in this consolidated format (like the Laplace equation, $\nabla^2\phi = 0$), it is applicable to a flow in any general coordinate system. In addition, certain operator functions can often be expanded into sometimes more convenient identity operator functions, which may often assist in the simplification, interpretation, or metamorphosis of the original equations. Some of the most common identities employing the ∇ operator are listed below (Where f and g represent generic scalar functions, and \vec{F} and \vec{G} represent generic vector functions):

$$\begin{aligned} (a) \quad & \nabla \times \nabla f = 0 \\ (b) \quad & \nabla(fg) = f \nabla g + g \nabla f \\ (c) \quad & \nabla \cdot (\nabla \times \vec{F}) = 0 \\ (d) \quad & \nabla \times (\nabla \times \vec{F}) = \nabla(\nabla \cdot \vec{F}) - \nabla^2\vec{F} \quad [\text{i.e.} = \nabla(\nabla \cdot \vec{F}) - (\nabla \cdot \nabla)\vec{F}] \\ (e) \quad & \nabla \cdot (f\vec{F}) = f(\nabla \cdot \vec{F}) + \vec{F} \cdot \nabla f \\ (f) \quad & \nabla \times (f\vec{F}) = f(\nabla \times \vec{F}) + (\nabla f) \times \vec{F} \\ (g) \quad & \nabla(\vec{F} \cdot \vec{G}) = (\vec{G} \cdot \nabla)\vec{F} + (\vec{F} \cdot \nabla)\vec{G} + \vec{F} \times (\nabla \times \vec{G}) + \vec{G} \times (\nabla \times \vec{F}) \\ (h) \quad & \nabla \times (\vec{F} \times \vec{G}) = (\vec{G} \cdot \nabla)\vec{F} - (\vec{F} \cdot \nabla)\vec{G} + \vec{F}(\nabla \cdot \vec{G}) - \vec{G}(\nabla \cdot \vec{F}) \\ (j) \quad & \nabla \cdot (\vec{F} \times \vec{G}) = \vec{G} \cdot (\nabla \times \vec{F}) - \vec{F} \cdot (\nabla \times \vec{G}) \\ (k) \quad & \nabla \cdot \nabla f = \nabla^2 f \\ (\ell) \quad & \nabla \cdot \nabla\vec{F} = \nabla^2\vec{F} \quad [\text{i.e.} = (\nabla \cdot \nabla)\vec{F}] \\ (m) \quad & \nabla \cdot \nabla^2\vec{F} = \nabla^2(\nabla \cdot \vec{F}) \\ (n) \quad & \nabla \times \nabla^2\vec{F} = \nabla^2(\nabla \times \vec{F}) \end{aligned} \quad (2.16)$$

Although some of the expressions in Eq. 2.16 look a bit daunting, we will show in the following chapters how some of these identities can be put to good use in the derivation and evolution of the governing equations of fluid mechanics.

2.4 Review of Line and Surface Integral Theorems

There are several theorems of vector calculus that prove very useful in either developing or simplifying the equations of fluid mechanics, many of which reflect the use of the ∇ operator in some form. Most of these evolve from the [divergence theorem of Gauss](#), which demonstrates a remarkable equivalence between the integration of a vector property over a surface and the volume integral of the divergence of the property over the volume encompassed by the surface. Here, we expand the functional applications of Gauss' theorem to include not only the divergence, but also the curl of a vector field, and the gradient of a scalar field as well. Note that we will not develop a mathematical proof of these theorems, but will simply state and explain their use, and the applicability to the equations of fluid mechanics. For further background on the development, and the application of these theorems, one is referred to the very useful book by [Schey \(1997\)](#) or any good book on vector calculus.

2.4.1 The Gauss Divergence Theorem

The [Gauss Divergence Theorem](#) states that if \vec{F} is any continuously differentiable vector field, extending over a volume, \forall , which is encompassed by a surface area, A (e.g. the velocity field inside of a ball-shaped spatial volume), then:

$$\iiint_{\forall} (\nabla \cdot \vec{F}) d\forall = \oint_A \hat{n} \cdot \vec{F} dA = \oint_A \vec{F} \cdot d\vec{A} \quad (2.17)$$

(where \hat{n} is the outward normal unit vector to the surface, such that $d\vec{A} = dA \hat{n}$)

Recalling that the divergence of a vector field gives the degree of expansion (or contraction) at a point, the left side of Eq. 2.17 is the summation of the divergence of the vector field within a specified volume. In fluid mechanics one construes this as the change in the velocity field within a bounded volume (again, think of the volume enclosed by a ball-shaped region). This expansion (or contraction) is equivalent to the right side of Eq. 2.17, which represents the “flux” of a vector field across the surface surrounding the volume in question. The flux is simply the component of the vector field that crosses the bounding surface (e.g. the component of a velocity field that is normal to the surface). For example, if a fluid is flowing in or out of our envisioned ball, and thus crossing the ball's surface, then there is a flux of velocity in or out of and across the surface. On the other hand, if a fluid (or some component of the velocity vector) flows

parallel to the surface bounding the ball, there will be no flux of the velocity (or that component) across the surface.

What this divergence theorem describes is essentially the principle of conservation of mass in fluid mechanics. As we will show in Chapter 5, this theorem also proves quite useful in demonstrating the coincidence between the governing *integral* equations of fluid mechanics for a control volume, and the comparable point-wise *differential* equations.

2.4.2 The Curl Theorem

This is a variation on the divergence theorem, in essence using the same mathematical arguments that Gauss employed, but for the curl of \vec{F} instead of the divergence. This yields the following relationship, which is similar to Stokes' theorem for a bounded surface, which we will discuss below in Section 2.4.4.

$$\iiint_{\mathcal{V}} (\nabla \times \vec{F}) d\mathcal{V} = \oint_A \hat{n} \times \vec{F} dA = - \oint_A \vec{F} \times d\vec{A} \quad (2.18)$$

Equation 2.18 equates the summation of the curl of \vec{F} within a fixed volume to the negative of the surface integral of the cross product of the vector field over the bounding surface. At first glance, Eq.2.18 seems like a rather complicated expression, with unclear physical relevance. However, if one thinks in terms of a velocity vector field, the left hand term of Eq. 2.18 reflects the summation of the rotational behavior within a defined volume, which is proportional (for incompressible flows) to the angular momentum of the fluid within that volume. This equates to the right hand term of Eq. 2.18, which is the summation of the component of the velocity that acts *parallel* to the bounding surface surrounding the fluid volume (recall that $d\vec{A}$ always points out and perpendicular to the bounding surface, thus the cross product $\vec{F} \times d\vec{A}$ will only include that component of \vec{F} oriented *parallel* to the surface). Equation 2.18 proves to be a particularly useful relationship for deriving and simplifying the equations of fluid mechanics that relate to the vorticity and circulation of a fluid, which we discuss in Chapters 10 and 11.

2.4.3 The Gradient Theorem

This is yet a further variation on the divergence theorem, again using the same mathematical arguments, but for the gradient of a continuously differentiable scalar function, ϕ , giving:

$$\iiint_{\mathcal{V}} (\nabla \phi) d\mathcal{V} = \int_A \hat{n} \phi dA = \int_A \phi d\vec{A} \quad (2.19)$$

The left side of Eq. 2.19 is the summation of the gradient of ϕ over a fixed volume. Recalling that the gradient reflects the degree and direction of change of a scalar property, the left side reflects a *summation of the total spatial change of the property ϕ over a fixed volume*. The right side of Eq. 2.19 is the summation of the scalar ϕ acting *on the surface* bounding the volume \forall . As we will show in Chapter 7, Eq. 2.19 proves particularly useful for assessing the behavior of the scalar properties of height and pressure in the derivation of the Bernoulli equation for an inviscid fluid.

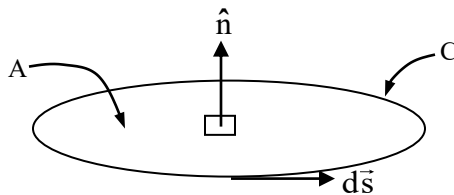
The previous three relationships are quite remarkable in that they provide vehicles for assessing the behavior of a vector field within a fixed volume by simply assessing certain characteristics of that vector field at the bounding surface of the volume. One might be tempted to envision a similar diagnostic technique that would assess the internal behavior of the human body, or a house, simply by assessing their external characteristics. However, we (humans), and our houses, are not continuously differentiable, homogeneous material, but are composed of a number of different media. So such an approach, while attractive, won't submit to the surface integral approach. One needs an identifiable, contiguous medium to apply these volume-to-surface theorems.

2.4.4 Stokes' Theorem

We often don't need to consider the behavior for a volume, but are only interested in the behavior over a two-dimensional surface bounded by a continuous curve, such as a circle. Such a situation is addressed by [Stokes' Theorem](#), which equates the integral of a continuously differentiable vector field \vec{F} around a closed curve C as *equal* to the integral of the normal component of the curl of \vec{F} over the surface bounded by C , or:

$$\int_A \hat{n} \cdot (\nabla \times \vec{F}) dA = \int_A (\nabla \times \vec{F}) \cdot d\vec{A} = \oint_C \vec{F} \cdot d\vec{s} \quad (2.20)$$

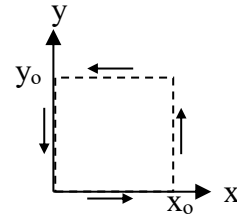
Here, $d\vec{s}$ is a differential line element lying along a curve C , and \hat{n} is a unit vector normal to the surface.



Stokes' theorem is an important relationship in fluid mechanics, and one with which we should be comfortable. The equivalency of Eq. 2.20 can be demonstrated relatively easily, as we do in the following example.

Example: Demonstration of Stokes' Theorem

Let's demonstrate how Stokes' Theorem applies to an arbitrary vector field in both Cartesian and cylindrical coordinates.



Assume an arbitrary vector field given by $\vec{F} = -y\hat{i} + x\hat{j}$. By comparison of both integrals, show that Stokes' Theorem (i.e. $\oint_C \vec{F} \cdot d\vec{s} = \iint_A (\nabla \times \vec{F}) \cdot d\vec{A}$) holds over a rectangular surface with corners at $(x, y) = (0, 0), (x_0, 0), (x_0, y_0),$ and $(0, y_0)$, as shown.

First, we examine a line integral around the rectangular surface, which must be integrated in a counter-clockwise direction (according to the right-hand rule). To perform this integration, we break the line integral into four integrals of the lines bounding the rectangle. Each of these line integrals must be integrated in the proper direction (shown on the figure), and between the appropriate starting and terminating integration limits. Finally, we note that $d\vec{s} = dx\hat{i} + dy\hat{j}$. However, when integrating in one coordinate direction, we only use the differential element corresponding to that coordinate (e.g. when integrating in the x-direction, we only use $d\vec{s} = dx\hat{i}$).

$$\begin{aligned} \oint_C \vec{F} \cdot d\vec{s} &= \int_{x=0}^{x=x_0} (-y\hat{i} + x\hat{j}) \cdot dx\hat{i} \Big|_{y=0}^{y=y_0} + \int_{y=0}^{y=y_0} (-y\hat{i} + x\hat{j}) \cdot dy\hat{j} \Big|_{x=x_0}^{x=x_0} \\ &+ \int_{x=x_0}^{x=0} (-y\hat{i} + x\hat{j}) \cdot dx\hat{i} \Big|_{y=y_0}^{y=y_0} + \int_{y=y_0}^{y=0} (-y\hat{i} + x\hat{j}) \cdot dy\hat{j} \Big|_{x=0}^{x=0} \\ &= \int_{x=0}^{x=x_0} -y dx \Big|_{y=0}^{y=y_0} + \int_{y=0}^{y=y_0} x dy \Big|_{x=x_0}^{x=x_0} + \int_{x=x_0}^{x=0} -y dx \Big|_{y=y_0}^{y=y_0} + \int_{y=y_0}^{y=0} x dy \Big|_{x=0}^{x=0} \\ &= \int_{x=0}^{x=x_0} -(0) dx + \int_{y=0}^{y=y_0} x_0 dy + \int_{x=x_0}^{x=0} -y_0 dx + \int_{y=y_0}^{y=0} (0) dy \\ &= 0 + x_0 y_0 + (-y_0)(-x_0) + 0 = 2x_0 y_0 \end{aligned}$$

Now examine the surface integral, where

$$\nabla \times \vec{F} = \left(\frac{\partial F_y}{\partial x} - \frac{\partial F_x}{\partial y} \right) \hat{k} = \left(\frac{\partial x}{\partial x} - \frac{\partial (-y)}{\partial y} \right) \hat{k} = 1 + 1 = 2$$

$$\iint_A (\nabla \times \vec{F}) \cdot d\vec{A} = \iint_A (2) \hat{k} \cdot dx dy \hat{k} = \int_{x=0}^{x=x_0} \int_{y=0}^{y=y_0} 2 dx dy = 2x \Big|_0^{x_0} y \Big|_0^{y_0} = 2x_0 y_0$$

Thus, by inspection and comparison, $\oint_C \vec{F} \cdot d\vec{s} = \oiint_A (\nabla \times \vec{F}) \cdot d\vec{A}$, and Stokes' theorem holds.

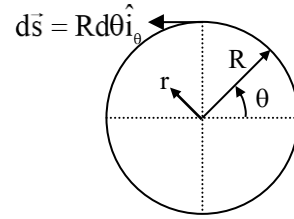
But what about demonstrating Stokes' hypothesis in cylindrical coordinates? Let's assume an arbitrary vector field given in cylindrical coordinates by:

$$\vec{F} = r \sin \theta \hat{i}_r + r \cos \theta \hat{i}_\theta = F_r \hat{i}_r + F_\theta \hat{i}_\theta$$

Again by comparison of both integrals, show that Stokes' Theorem (i.e.

$\oint_C \vec{F} \cdot d\vec{s} = \oiint_A (\nabla \times \vec{F}) \cdot d\vec{A}$) holds over a circle of radius R , centered on the origin., as shown.

Again, we first examine the line integral, which again must be integrated in a counter-clockwise direction (according to right-hand rule). Since the radius of the circle constitutes the boundary, this means that the differential element acts tangential to the circle boundary in the θ direction, or $d\vec{s} = R d\theta \hat{i}_\theta$.



$$\oint_C \vec{F} \cdot d\vec{s} = \int_{\theta=0}^{\theta=2\pi} (R \sin \theta \hat{i}_r + R \cos \theta \hat{i}_\theta) \cdot R d\theta \hat{i}_\theta = \int_{\theta=0}^{\theta=2\pi} R^2 \cos \theta d\theta = R^2 \sin \theta \Big|_{\theta=0}^{\theta=2\pi} = R^2 (0 - 0) = 0$$

Now examine the area integral, where Eq. 2.12 gives:

$$\begin{aligned} \nabla \times \vec{F} &= \left(\frac{1}{r} \frac{\partial F_\theta}{\partial z} - \frac{\partial F_r}{\partial z} \right) \hat{i}_r + \left(\frac{\partial F_r}{\partial z} - \frac{\partial F_\theta}{\partial r} \right) \hat{i}_\theta + \frac{1}{r} \left(\frac{\partial}{\partial r} (r F_\theta) - \frac{\partial F_r}{\partial \theta} \right) \hat{i}_z \\ \nabla \times \vec{F} &= \frac{1}{r} \left[\frac{\partial (r F_\theta)}{\partial r} - \frac{\partial F_r}{\partial \theta} \right] \hat{i}_\theta = \frac{1}{r} \left[\frac{\partial (r^2 \cos \theta)}{\partial r} - \frac{\partial (r \sin \theta)}{\partial \theta} \right] \hat{i}_\theta = \frac{1}{r} [2r \cos \theta - r \cos \theta] \hat{i}_\theta = \cos \theta \hat{i}_\theta \end{aligned}$$

$$\oiint_A (\nabla \times \vec{F}) \cdot d\vec{A} = \oiint_A \cos \theta \hat{i}_z \cdot r d\theta dr \hat{i}_z = \int_{r=0}^{r=R} r dr \int_{\theta=0}^{\theta=2\pi} \cos \theta d\theta = \frac{r^2}{2} \Big|_0^R \sin \theta \Big|_0^{2\pi} = \frac{R^2}{2} (0 - 0) = 0$$

Thus, again by inspection and comparison, $\oint_C \vec{F} \cdot d\vec{s} = \oiint_A (\nabla \times \vec{F}) \cdot d\vec{A}$, and Stokes' theorem holds.

Note that we might have tried a vector field like $\vec{F} = r\theta \hat{i}_r + r\theta \hat{i}_\theta = F_r \hat{i}_r + F_\theta \hat{i}_\theta$. However,

you would find (try this) that $\oint_C \vec{F} \cdot d\vec{s} = 2\pi^2 R^2$, but $\oiint_A (\nabla \times \vec{F}) \cdot d\vec{A} = 2\pi^2 R^2 - \pi R^2$.

Why aren't these the same? Because the field is not continuous (a condition for

Stokes' theorem to apply), since $\theta = 0$ and $\theta = 2\pi$ occupy the same location, but are not identical.

If one thinks of the vector field, \vec{F} , as a velocity field, \vec{V} , then the curl of \vec{V} will give the angular rotation or vorticity (see section 4.3). So Eq. 2.20 provides a method to relate the collective vorticity over an area (which we will learn in Chapter 8 is the circulation, or total rotational strength of an area of flow) to the line integral of the velocity around the periphery of that area. Equation 2.20 is again a remarkable relationship, since it implies that we can assess the rotational strength of a vortical flow by simply measuring the tangential component of velocity at the edge of a region. This allows (for example) one to assess the "strength" of a tornado or a hurricane by appropriate measurements at the edges of those huge cyclonically rotating regions (of course, measurement of those edge velocities is still no easy process). We will examine and make broad use of the Stokes' theorem when we derive various vorticity and circulation theorems in Chapters 8, 10, and 11.

References

Schey, H.M. (1997). *div grad curl and all that*, W.W. Norton & Company, New York.

Study Problems

1. Using the basic concept of a vector derivative, as done in section 2.2.1, show how the non-zero partial derivative for $\frac{\partial \hat{i}_\theta}{\partial \theta} = -\hat{i}_r$.
2. If ϕ is a scalar function, show by expansion in Cartesian coordinates that the following hold:
 - a. $\nabla \times \nabla \phi = 0$
 - b. $\nabla \phi$ is normal to a line of constant ϕ
3. For a vector function $\vec{V} = u\hat{i} + v\hat{j} + w\hat{k}$, show by expansion in Cartesian coordinates that the following hold:
 - a. $\nabla \cdot (\nabla \times \vec{V}) = 0$
 - b. $(\vec{V} \cdot \nabla) \vec{V} = (\nabla \times \vec{V}) \times \vec{V} + \nabla \left(\frac{V^2}{2} \right)$
 - c. $(\nabla \times \vec{V}) \times \vec{V}$ is normal to \vec{V}

4. In cylindrical coordinates

$$\nabla = \hat{i}_r \frac{\partial}{\partial r} + \hat{i}_\theta \frac{1}{r} \frac{\partial}{\partial \theta} + \hat{i}_z \frac{\partial}{\partial z}$$

and

$$\phi = \phi(r, \theta, z) \text{ and } \vec{V} = v_r \hat{i}_r + v_\theta \hat{i}_\theta + v_z \hat{i}_z$$

- a. Determine an expanded expression for $\nabla \cdot \nabla \phi$
 - b. Determine an expanded expression for $\nabla \cdot \vec{V}$
5. If $\vec{F} = y\hat{i} + x^2\hat{j}$ and $f = x + y^2$, by calculation of the left and right functions in the equations, show that the following are valid:

$$\text{a. } \nabla \times (\nabla \times \vec{F}) = \nabla(\nabla \cdot \vec{F}) - \nabla^2 \vec{F}$$

$$\text{b. } \nabla \times (f\vec{F}) = f(\nabla \times \vec{F}) + (\nabla f) \times \vec{F}$$

6. If $\vec{F} = r\hat{i}_r + r\theta\hat{i}_\theta$ and $f = r + r\theta$, by calculation of both the left and right functions in the equation, show that the following is valid:

$$\nabla \times (f\vec{F}) = f(\nabla \times \vec{F}) + (\nabla f) \times \vec{F}$$

7. If $\vec{F} = y\hat{i} + x^2\hat{j}$ and $\vec{G} = y^2\hat{i} + xy\hat{j}$, by calculation of both the left and right functions in the equation, show that the following is valid:

$$\nabla \cdot (\vec{F} \times \vec{G}) = \vec{G} \cdot (\nabla \times \vec{F}) - \vec{F} \cdot (\nabla \times \vec{G})$$

8. If $\vec{F} = xy\hat{i} + x^2\hat{j}$, determine $\nabla \times \vec{F}$, and then show that the following is valid:

$$\nabla \cdot (\nabla \times \vec{F}) = 0$$

9. If $\vec{F} = r\theta\hat{i}_r + r^2\hat{i}_\theta$, determine $\nabla \times \vec{F}$, and then show that the following is valid:

$$\nabla \cdot (\nabla \times \vec{F}) = 0$$

10. Let $\vec{V} = y\hat{i} + x^2\hat{j}$. By comparison of both integrals, show that Stoke's Theorem

$$\text{(i.e. } \oint_C \vec{V} \cdot d\vec{s} = \iint_A (\nabla \times \vec{V}) \cdot d\vec{A} \text{) holds over a square with corners at } (x,y) = (1,1), (1,-1), (-1,-1), \text{ and } (-1,1).$$

11. Let $\vec{V} = y^2\hat{i} + xy\hat{j}$. By comparison of both integrals, show that Stoke's Theorem

$$\text{(i.e. } \oint_C \vec{V} \cdot d\vec{s} = \iint_A (\nabla \times \vec{V}) \cdot d\vec{A} \text{) holds over a square with corners at } (x,y) = (2,2), (2,3), (3,3), \text{ and } (3,2).$$

12. Let $\vec{V} = r \cos \theta \hat{i}_r + r \sin \theta \hat{i}_\theta$. By comparison of both integrals, show that Stoke's Theorem

$$\text{(i.e. } \oint_C \vec{V} \cdot d\vec{s} = \iint_A (\nabla \times \vec{V}) \cdot d\vec{A} \text{) holds over a circle of } r = R.$$

13. Let $\vec{V} = r \sin \theta \hat{i}_r + r \cos \theta \hat{i}_\theta$. By comparison of both integrals, show that Stoke's Theorem

$$\text{(i.e. } \oint_C \vec{V} \cdot d\vec{s} = \iint_A (\nabla \times \vec{V}) \cdot d\vec{A} \text{) holds over a circle of } r = R.$$

14. Let $\vec{V} = r^2 \cos \theta \hat{i}_r + r^2 \sin \theta \hat{i}_\theta$. By comparison of both integrals, show that Stoke's Theorem

$$\text{(i.e. } \oint_C \vec{V} \cdot d\vec{s} = \iint_A (\nabla \times \vec{V}) \cdot d\vec{A} \text{) holds over a circle of } r = R.$$

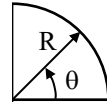
15. Let $\vec{V} = r \sin \theta \hat{i}_r + r \cos \theta \hat{i}_\theta$. By comparison of both integrals, show that Stoke's Theorem

$$\text{(i.e. } \oint_C \vec{V} \cdot d\vec{s} = \iint_A (\nabla \times \vec{V}) \cdot d\vec{A} \text{) holds over a quarter circle of } r = R$$

from $\theta = 0$ to $\theta = \frac{\pi}{2}$. Note: be sure to do you follow the boundary in

three segments correctly --- (1) $r = 0$ to R for $\theta = 0$,

(2) $\theta = 0$ to $\theta = \frac{\pi}{2}$ for $r = R$, and (3) $r = R$ to 0 for $\theta = \frac{\pi}{2}$.



Chapter 3

Kinematics, Flow Lines, and the Substantial Derivative

Contents

3.1	Acceleration of a Fluid Particle in a Velocity Field	41
3.2	Flow Lines	48
3.2.1	Flow Line Examples: Steady Flow	52
3.2.1.1	Path line: Steady Flow	52
3.2.1.2	Streak line: Steady Flow	52
3.2.1.3	Stream line: Steady Flow	54
3.2.2	Equivalence of Flow Lines in Steady Flow	54
3.2.3	Flow Line Examples: Unsteady Flow	56
3.2.3.1	Path line: Unsteady Flow	56
3.2.3.2	Streak line: Unsteady Flow	56
3.2.3.3	Stream line: Unsteady Flow	57
3.2.4	Non-Equivalence of Flow Lines in Unsteady Flow	59
3.3	The Substantial (or Material) Derivative	59
3.4	The Substantial Derivative: Cartesian and Cylindrical Coordinates	62
3.4.1	Substantial Derivative, Cartesian Coordinates	62
3.4.2	Total Acceleration, Cartesian Coordinates	63
3.4.3	Substantial Derivative, Cylindrical Coordinates	63
3.4.4	Total Acceleration, Cylindrical Coordinates	63

The assessment and prediction of the impact and consequences of fluid motion require that we develop convenient physical descriptions that allow the effective modeling, mathematical formulation, and analysis of fluid behavior. This is simplified by employing the concept of a fluid as a continuum, wherein fluid properties are considered to be distributed smoothly throughout the space of consideration. This generally implies that although a fluid is a collection of molecules, for essentially all cases of practical interest these molecular collections will behave as a continuous medium (a gas at extremely low pressures is a particular exception). Thus, when examining a fluid property (e.g. density), we assume that the property displays no discontinuous behavior within the region of consideration. Another way of putting this is that the spatial derivatives of any fluid property (i.e. the change in a property in any direction) will always have a finite value. This does not mean that a property cannot undergo large changes, but just that it cannot undergo a *discontinuous* change.

To approach the modeling and eventual analysis of fluid behavior requires that we be able to spatially describe fluid properties within a region of interest (e.g. within a pipe or over an airplane wing). We must also be able to account for changes with time (if the flow behaves in a time-dependent manner), such as the increase in the velocity of a water stream during a hard rain. Since in this book we generally focus on the behavior of incompressible fluids, the primary properties of interest will be velocity and pressure, with velocity being the more problematic property to deal with appropriately. Of particular interest is how we properly account for fluid acceleration, since acceleration is a key property in Newton's second law of motion. Our ultimate objective is to develop a form of Newton's second law that can describe the behavior of a continuously distributed fluid. However, application of Newton's second law to a fluid creates a fundamental problem, since this requires that we can somehow collectively identify and follow the acceleration/deceleration of *all* the fluid particles comprising a fluid, and likewise the collective forces acting on those particles. If we employ the Lagrangian formulations utilized for assessing the physics of discrete particles, we could end up with a particularly difficult bookkeeping process, since a *Lagrangian* approach considers the change in the spatial position of *particular* particles as a function of time alone. However, by taking a more global point of view, we can exploit what we term a *field concept*, where we view the collective motion of all particles as a continuum within a specified region, or field.

3.1 Acceleration of a Fluid Particle in a Velocity Field

The use of a field concept is generally termed an *Eulerian* description, wherein we assume that a fluid property can be described as a function of its position in space (x, y, z in Cartesian coordinates) *and* its evolution with time (t). Thus, in a Cartesian system we would describe a velocity field as $\vec{V} = \vec{V}(x, y, z, t)$, where $\vec{V}(x, y, z, t)$ is the Eulerian velocity, as illustrated in figure 3.1. This is somewhat akin to watching a river flow by through a telescope focused on a single point in the river; the speed with which the water passes across the telescope's field of view is dependent upon the location that is viewed by the telescope, and the specific time when we make our observation.

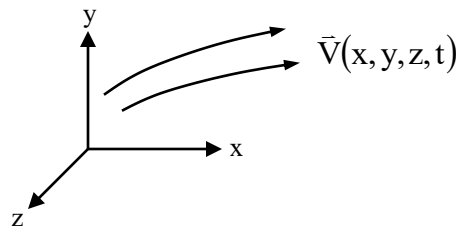


Figure 3.1 An Eulerian velocity field

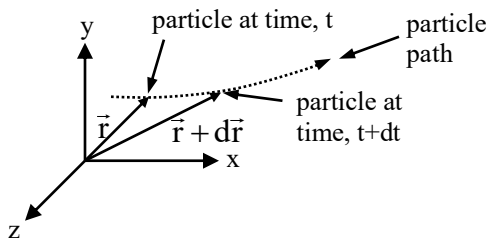
In contrast, a *Lagrangian* description focuses on the motion of one specific particle within the velocity field, and tracks the positional change of that particle as a function of time. This is like watching a small block of wood float by on that same river, and tracking the position of that block of wood from an initial instant of time onward.

So, to summarize the difference between an Eulerian and Lagrangian description:

Eulerian – Specifies the velocity field (i.e. velocity behavior in space and time). This approach specifies how particles passing through a specified location will behave (think of it as viewing a series of particles passing by a small observation window).

Lagrangian – Specifies how an individual particle will move through space as a function of time (like following a leaf in a wind storm).

Now, Newton's second law requires a balance between: (1) the forces acting on a particle, and (2) the momentum change of the particle, which is proportional to its acceleration. Our problem is how do we mathematically relate the local motion of a fluid particle to the broader velocity field, of which the particle is a part, without having to follow all of the individual particles? Let's approach this by assuming that at any instant of time, t , the location of a particle can be represented (here we use Cartesian coordinates) by a position vector, $\vec{r} = x\hat{i} + y\hat{j} + z\hat{k}$, as shown in figure 3.2. Note that although we perform this analysis in Cartesian coordinates, the result applies equally well in any coordinate system.



$$\vec{r} = \vec{r}(x, y, z)$$

$$\vec{V}(x, y, z, t) = u\hat{i} + v\hat{j} + w\hat{k} \quad (\text{Cartesian})$$

Figure 3.2 Representation of the Lagrangian change in position of a particle within an Eulerian field.

Note that for the Cartesian coordinate system shown in figure 3.2, the components of the velocity in the x , y , and z direction are generally designated u , v , and w . Now, as the particle moves within the velocity field over an infinitesimal amount of time, Δt , it attains a new position within the velocity field given by:

$$\vec{r} = \vec{r} + \Delta\vec{r} = (x + \Delta x)\hat{i} + (y + \Delta y)\hat{j} + (z + \Delta z)\hat{k}$$

where $\Delta\vec{r}$ is an infinitesimal position change that occurs over the time change Δt .

Assuming that this positional change takes place due to motion of the particle within the velocity field, then the velocity of the particle, \vec{V}_p , at the initial time t and the final time $t+\Delta t$ is given by:

$$\vec{V}_p|_t = \vec{V}(x, y, z, t) \quad \text{at time } t,$$

and

$$\vec{V}_p|_{t+\Delta t} = \vec{V}(x + \Delta x, y + \Delta y, z + \Delta z, t + \Delta t) \quad \text{at time } t + \Delta t.$$

To establish the mathematical change in \vec{V}_p over this time change, we can apply the chain rule of differential calculus, which allows us to express $\Delta\vec{V}_p$ as:

$$\Delta\vec{V}_p = \vec{V}_p|_{t+\Delta t} - \vec{V}_p|_t = \frac{\partial\vec{V}}{\partial x}\Delta x_p + \frac{\partial\vec{V}}{\partial y}\Delta y_p + \frac{\partial\vec{V}}{\partial z}\Delta z_p + \frac{\partial\vec{V}}{\partial t}\Delta t$$

where Δx_p , Δy_p , and Δz_p are the differential changes in the relative coordinate position of the particle over the differential time change, Δt . We recognize that the differential displacement components of the particle are given by the product of the local velocity component and the differential time change (i.e. $\Delta x_p = u\Delta t$, $\Delta y_p = v\Delta t$, and $\Delta z_p = w\Delta t$), since the particle will move at the local Eulerian velocity at its specified location within the velocity field. Thus, we can write the expression for $\Delta\vec{V}_p$ as:

$$\Delta\vec{V}_p = \frac{\partial\vec{V}}{\partial x}u\Delta t + \frac{\partial\vec{V}}{\partial y}v\Delta t + \frac{\partial\vec{V}}{\partial z}w\Delta t + \frac{\partial\vec{V}}{\partial t}\Delta t = \left(\frac{\partial\vec{V}}{\partial x}u + \frac{\partial\vec{V}}{\partial y}v + \frac{\partial\vec{V}}{\partial z}w + \frac{\partial\vec{V}}{\partial t} \right) \Delta t$$

Now, we divide through by Δt and take the limit of this differential velocity change, $\Delta\vec{V}_p / \Delta t$, as $\Delta t \rightarrow 0$. The result is the total acceleration for the *particle*, \vec{a}_p , moving within the Eulerian velocity field, $\vec{V}(x, y, z, t)$:

$$\vec{a}_p = \lim_{\Delta t \rightarrow 0} \frac{\Delta\vec{V}_p}{\Delta t} = \frac{\partial\vec{V}}{\partial x}u + \frac{\partial\vec{V}}{\partial y}v + \frac{\partial\vec{V}}{\partial z}w + \frac{\partial\vec{V}}{\partial t}$$

We reflect this particle acceleration by $\vec{a}_p = D\vec{V}/Dt$, where the derivative operator,

$D(\)/Dt$, is known as the “total”, “substantial”, or “material” derivative (more on this later). Thus, we write:

$$\bar{a}_p = \frac{D\bar{V}}{Dt} = \underbrace{u \frac{\partial \bar{V}}{\partial x}}_{\text{Total acceleration of a particle}} + \underbrace{v \frac{\partial \bar{V}}{\partial y} + w \frac{\partial \bar{V}}{\partial z}}_{\text{Advective acceleration}} + \underbrace{\frac{\partial \bar{V}}{\partial t}}_{\text{Local acceleration}} \quad (3.1)$$

For the present case, we are concerned with the changes in the particle velocity itself. However, this total derivative operator, $D(\)/Dt$, can also be used to mathematically establish the temporal changes in any other property associated with a material particle moving within an Eulerian velocity field, $\bar{V}(x, y, z, t)$, such as density, temperature, or position, as we will discuss in [Section 3.3](#).

Note that this particle acceleration within a velocity field is comprised of two different types of velocity change. The first of these is a *local* rate of change, which is a result of a local temporal change in velocity taking place at the point of interest. For example, if the velocity of a river increases with time at a specific point, that would cause a *local* acceleration of the flow at that point. The second type of acceleration is the result of the advection (transport) of a particle through a spatially-varying velocity field. As a particle is transported through a region of velocity change, a corresponding change in the velocity of the particle will occur. This transport-based acceleration is known as *advective* acceleration, since the velocity of the particle will change due to the *advection (movement) of the particle* through a spatially varying velocity field. Using our river example again, if the banks of a river contract inward, such that the velocity of the river increases as it flows downstream, then a particle can be viewed to be accelerating at a point due to this advective increase in velocity. Clearly, the *total acceleration* of a particle is the sum of both the local, temporal changes in velocity and the changes in velocity due to advection through a spatially-varying velocity field.

$$\begin{aligned} a_{x_p} &= \frac{Du}{Dt} = u \frac{\partial u}{\partial x} + v \frac{\partial u}{\partial y} + w \frac{\partial u}{\partial z} + \frac{\partial u}{\partial t} \\ a_{y_p} &= \frac{Dv}{Dt} = u \frac{\partial v}{\partial x} + v \frac{\partial v}{\partial y} + w \frac{\partial v}{\partial z} + \frac{\partial v}{\partial t} \\ a_{z_p} &= \frac{Dw}{Dt} = u \frac{\partial w}{\partial x} + v \frac{\partial w}{\partial y} + w \frac{\partial w}{\partial z} + \frac{\partial w}{\partial t} \end{aligned} \quad (3.2)$$

The acceleration of a particle, as derived above, is a vector derivative, comprised of three separate components of acceleration, as shown in Eq. 3.2 (for Cartesian coordinates). Equation 3.2 gives the components of acceleration for a particle at an arbitrary position within the Eulerian velocity field. This means that Eq. 3.2 must also represent the

Lagrangian acceleration of that particular particle, as determined by means of an *Eulerian* analysis. This is significant since this provides a clear connection between Newton's second law for Lagrangian particle mechanics and the acceleration of all fluid particles within a continuously distributed fluid. This connection is important in making use of Newton's second law to derive the governing differential equation of momentum for fluid motion. However, let's first assure ourselves that the acceleration reflected by the Eulerian equations derived above is truly identical to the comparable Lagrangian acceleration of an arbitrary particle.

Example: Here we examine a relatively simple Eulerian flow field, from which we will determine the Lagrangian velocity and acceleration for a specific particle moving within that flow field. We then use this information to make a comparison of: (1) the *Lagrangian* acceleration of that particular particle when it passes through a specified location within the velocity field, with (2) the general *Eulerian* acceleration at the same specified location within the velocity field.

Let's first assume a simple two-dimensional Eulerian velocity field given by $\vec{V} = (3x + t)\hat{i} + (-3y)\hat{j}$, with x and y -direction velocity components $u_E = 3x + t$ and $v_E = -3y$, respectively. Here the E subscript indicates that these are Eulerian velocity components. Now, we use this velocity field information to establish the following Lagrangian information for the movement of a particle within the velocity field:

$$\text{a) } \left. \begin{array}{l} x_L = f_1(x_{\text{init}}, y_{\text{init}}, t) \\ y_L = f_2(x_{\text{init}}, y_{\text{init}}, t) \end{array} \right\} \text{ for } \left. \begin{array}{l} x_L = x_{\text{init}} = 1 \\ y_L = y_{\text{init}} = 2 \end{array} \right\} @ t = 0;$$

$\underbrace{\hspace{10em}}$
Equation for the path
of the particle
 $\underbrace{\hspace{10em}}$
Initial starting point of
the particle

b) u_L and v_L ;

c) a_{x_L} , a_{y_L} ;

and confirm that

d) $a_{x_L} = a_{x_E}$ and $a_{y_L} = a_{y_E}$.

Here the L subscript indicates the Lagrangian expression for velocity or acceleration. Note also that $f_1(x_{\text{init}}, y_{\text{init}}, t)$ and $f_2(x_{\text{init}}, y_{\text{init}}, t)$ are the Lagrangian functions describing the x and y location of a particular particle that started at an initial position $x_{L_{\text{init}}} = x_{\text{init}}$ and $y_{L_{\text{init}}} = y_{\text{init}}$ at an initial time of $t = 0$. To derive the Lagrangian behavior of the particle within the velocity field, we assume that whenever a particle

is at a particular position within the field, it moves at the velocity for that position, as described by the velocity field, and thus $u_L = u_E$ and $v_L = v_E$.

Solution:

Part a) Let $u_L = \frac{dx_L}{dt} = u_E(x, y, t) = u_E(\overbrace{x_L, y_L, t}^{\text{Lagrangian position of a particle}}) = 3x_L + t$

Thus, $\frac{dx_L}{dt} - 3x_L = t$, which is a differential equation for x_L .

To solve this differential equation, we need to evaluate both the homogeneous and the particular solutions of the equation, since the equation is *linear* with constant coefficients, but is inhomogeneous. Therefore, we assume that the total solution is a linear combination of the homogeneous and the particular solutions of the equation, i.e.

$$x_{L\text{Total}} = x_{Lh} + x_{Lp}$$

Thus, for the homogeneous solution:

$$\frac{dx_{Lh}}{dt} - 3x_{Lh} = 0 \quad \Rightarrow \quad \frac{dx_{Lh}}{x_{Lh}} = 3dt \quad \Rightarrow \quad x_{Lh} = C_1 e^{3t}$$

Here, C_1 is an undetermined integration constant.

Considering the particular solution, we assume a general solution of the form $x_{Lp} = A + Bt$ and substitute this first-order polynomial into the differential equation to determine the coefficients A and B , which yields:

$$\frac{dx_{Lp}}{dt} - 3x_{Lp} = (B) - 3(A + Bt) = t \quad \Rightarrow \quad \underbrace{\begin{cases} B - 3A = 0 \Rightarrow A = \frac{B}{3} = -\frac{1}{9} \\ -3B = 1 \Rightarrow B = -\frac{1}{3} \end{cases}}_{\text{Equating coefficients of like powers of } t}$$

$$\text{Thus, } x_{Lp} = -\frac{1}{9} - \frac{1}{3}t$$

Now, summing x_{Lh} and x_{Lp} to get $x_{L\text{Total}}$, gives:

$$x_L = x_{L\text{Total}} = C_1 e^{3t} - \frac{1}{9} - \frac{1}{3}t$$

Applying the initial condition, $f_1 = x_{\text{init}} = 1$ at $t = 0$, we determine C_1 :

$$x_L(t=0) = x_{\text{init}} = 1 = C_1 e^{3(0)} - \frac{1}{9} - \frac{1}{3}(0) = C_1 - \frac{1}{9} \Rightarrow C_1 = \frac{10}{9}$$

Thus, the Lagrangian x -position of a particle passing through $x = 1, y = 2$, @ $t = 0$ is:

$$x_L = \frac{10}{9} e^{3t} - \frac{1}{9} - \frac{1}{3} t$$

Similarly, to determine the function f_2 , we set:

$$v_L = \frac{dy_L}{dt} = \frac{df_2}{dt} = v_E(x_L, y_L, t) = -3y_L = -3f_2 \quad (\text{a homogeneous equation})$$

$$\text{So, } \frac{df_2}{f_2} = -3dt \Rightarrow f_2 = C_2 e^{-3t}$$

Thus, for the initial condition $y_L = y_{\text{init}} = 2$ at $t = 0$:

$$y_L = 2 = C_2 e^{-3(0)} \Rightarrow C_2 = 2$$

and,

$$y_L = 2e^{-3t}$$

This is the y -location for of a particle passing through $x = 1, y = 2$, @ $t = 0$. x_L and y_L now give the Lagrangian location of that particular particle at any time $t > 0$.

Now, using the solutions for x_L and y_L , we differentiate with respect to t to obtain the Lagrangian velocity and acceleration:

$$\text{Part b): } u_L = \frac{dx_L}{dt} = \frac{10}{3} e^{3t} - \frac{1}{3} = \frac{1}{3}(10e^{3t} - 1)$$

$$v_L = \frac{dy_L}{dt} = -6e^{-3t}$$

$$\text{Part c) } a_{xL} = \frac{du_L}{dt} = 10e^{3t}$$

$$a_{yL} = \frac{dv_L}{dt} = 18e^{-3t}$$

Part d) The Eulerian acceleration we obtain from Eq. 3.2, the total acceleration, in terms of the general position of a particle within the velocity field as:

$$\begin{aligned}
 a_{xE} &= \frac{Du_E}{Dt} = u_E \frac{\partial u_E}{\partial x} + v_E \frac{\partial u_E}{\partial y} + w_E \frac{\partial u_E}{\partial z} + \frac{\partial u_E}{\partial t} \\
 &= (3x+t)(3) + (-3y)(0) + (0)(0) + 1 \\
 &= 9x + 3t + 1
 \end{aligned}$$

$$\begin{aligned}
 a_{yE} &= \frac{Dv_E}{Dt} = u_E \frac{\partial v_E}{\partial x} + v_E \frac{\partial v_E}{\partial y} + w_E \frac{\partial v_E}{\partial z} + \frac{\partial v_E}{\partial t} \\
 &= (3x+t)(0) + (-3y)(-3) + (0)(0) + (0) \\
 &= 9y
 \end{aligned}$$

Now, since x_L and y_L represent the sequence of positions of a *particular particle* as it moves through the Eulerian field, we can now substitute the functions for x_L and y_L into the Eulerian acceleration equations, to give us the comparable acceleration expressions for that *particular particle* as it passes through the velocity field.

$$\begin{aligned}
 a_{xE} &= 9 \left[\frac{10}{9} e^{3t} - \frac{1}{9} - \frac{1}{3} t \right] + 3t + 1 \\
 &= 10e^{3t} = a_{xL} \quad \text{and}
 \end{aligned}$$

$$a_{yE} = 9(2e^{-3t}) = 18e^{-3t} = a_{yL}$$

Not surprisingly, the Lagrangian and Eulerian expressions for the acceleration of the particle reduce to identical values, which illustrates that the Eulerian expressions apply not only for the particular Lagrangian particle we assessed in this example, but generically for *any* particle initiating from any position at any time. You can further demonstrate this equivalency by assuming a different initial position (e.g. $x_{init}, y_{init} = 2, 2$) and/or a different initial time (and thus a different Lagrangian particle), and show that for all particles $\vec{a}_E = \vec{a}_L$. Note that often the velocity component expressions may depend on more than one variable, creating a series of coupled differential equations. To determine the Lagrangian behavior of these sets of equations will generally require the use of Laplace transforms, or (for non-linear cases) numerical solutions.

Thus, the Total derivative of Eqs. 3.1 and 3.2 now provides us with a tool with which we can accurately assess the Lagrangian acceleration of any and all fluid particles within an Eulerian flow field. We will put this tool to good use in Chapter 5, where we derive the governing differential equations of fluid motion.

3.2 Flow Lines

In the study of fluid mechanics, we often gain important information regarding a fluid flow by experimental observation techniques involving the introduction of a visible

marker into the fluid, such as the injection of dye into water or smoke into air. We can also make good use of ad hoc observations of some natural contaminant in a flow, such as wind-blown dust or suspended dirt in a water flow. Additionally, we can develop physical insight into the voluminous results of large computational studies by establishing the behavior of a particular type of flow line, known as a stream line, which illustrates the directional flow patterns within a flow at a particular time. In this section, we examine three different types of descriptor flow lines, termed [path lines](#), [streak lines](#), and [stream lines](#), all of which can help us both visualize and assess flow behavior.

The first descriptor line we consider is a ***path line***. As the name implies, this is a line traced out by a selected particle moving within a flow over a given time interval, thus visualizing the path that the particle follows. Note that since we follow an individual particle when describing a particular path line, the Lagrangian position functions for the particle, x_L and y_L , (like we derived in the example in Section 3.1) describe the series of locations comprising a path line. A rough example of a path line would be a line connecting the temporal sequence of locations that a small piece of wood passes through as it floats along a river. We could capture such a line if we were to take a photographic time exposure of the block of wood moving with the current of a river, or of any other easily visible object moving within a velocity field.

The second descriptor line we find useful is a ***streak line***. Here, the name of this line is not as clearly descriptive of its characteristics, and it takes a bit of study to appreciate what it represents. A streak line describes the *present* position of *all* particles that initially passed through a specific point at some *earlier* point in time. So, if we can imagine coloring each fluid particle that passes through some fixed location, and then observing the trail of colored particles that emanate away from that point in space, this trail of colored particles will form a streak line. A reasonable approximation of such a line can be generated by injecting dye into water or smoke into air at a fixed point (e.g. injection of dye via a hypodermic needle into a water flow). Note, however, that to properly illustrate a true streak line, such injection processes need to be done very carefully to avoid disturbing the original flow by the injection process.

In order to obtain a mathematical description of a streak line within a given velocity field, we have to determine a series of Lagrangian functions for particles that initiate at the same position in space, but over a sequence of initiation times. Thus, we will need to generate a set of Lagrangian functions, $x_L(x_{init}, y_{init}, t_p, t_i)$ and $y_L(x_{init}, y_{init}, t_p, t_i)$. Here x_{init} and y_{init} are the initial x and y locations at particle insertion, t_i is the time of the insertion of the particle at the initial position (x_{init}, y_{init}), and t_p is the present time of interest (where $t_p > t_i$). Thus, by varying t_i , we can determine the present location of all those particles at some arbitrary later time, t_p .

Our final descriptor line is a ***streamline***. This is a line within a fluid for which the fluid particles lying along the line all have velocity vectors that are *tangent* to the line, as shown in two-dimensions in figure 3.3. This defines an interesting line of constraint. Since the velocity is always tangent to a streamline, then there can be no flow *across* (perpendicular to) a streamline. This is a very important property of a streamline --- one that we will exploit when dealing with inviscid (non-viscous) flows, and use to help simplify the governing equations of fluid mechanics.

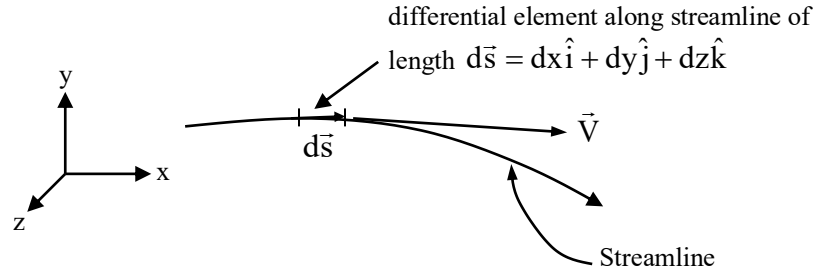


Figure 3.3 Illustration of the characteristics of a streamline

Additionally, for a two-dimensional, incompressible flow, the tangential velocity constraint implies that the flowrate between two *adjacent* streamlines must always remain constant. Thus, the *spacing* between streamlines is a general indicator of flow acceleration or deceleration, with the velocity of the flow between two adjacent streamlines increasing as the streamlines converge, and decreasing as streamlines diverge. This is a bit of a simplistic interpretation, since we will see that there can be strong velocity variations between streamlines, particularly when they are curved. However, the convergence or divergence of streamlines provides a good visual indication of strong changes in the local velocity field, and as such can be used for effective qualitative interpretation of local flow behavior.

Now, let's examine how we can develop a mathematical equation for a streamline. Figure 3.3 is a sketch of a typical streamline relative to a Cartesian coordinate system. On the line, we have indicated a velocity vector that is tangent to the stream line. Additionally, we also envision a differential element along the streamline of length $d\vec{s} = dx\hat{i} + dy\hat{j} + dz\hat{k}$, such that $d\vec{s}$ is also tangent to the streamline.

Now, if \vec{V} and $d\vec{s}$ are both tangent to the streamline, then they are also parallel to each other. Recalling that the cross product of two parallel vectors is zero, we can write:

$$\vec{V} \times d\vec{s} = 0 = \begin{bmatrix} \hat{i} & \hat{j} & \hat{k} \\ u & v & w \\ dx & dy & dz \end{bmatrix} = \hat{i}(vdz - wdy) + \hat{j}(wdx - udz) + \hat{k}(udy - vdx) = 0$$

Since each component of this vector equation must be identically zero, we reorder each component to give three governing differential equations for a streamline given by:

$$\frac{dz}{dy} = \frac{w}{v} ; \quad \frac{dx}{dz} = \frac{u}{w} ; \quad \frac{dy}{dx} = \frac{v}{u} \quad (3.3a)$$

For a three-dimensional flow, we would have to necessarily satisfy all three of these equations. However, if we consider only a two-dimensional flow field (depending only on x and y), the equation for a surface lying on the z -plane, $u dy = v dx$, is the only relevant equation, thus:

$$\frac{dy}{dx} = \frac{v}{u} \quad (3.3b)$$

Equation 3.3b is the differential equation for a two-dimensional streamline in x and y , lying on the z -plane. Note that this is also the slope of the streamline, which is the ratio of the respective velocity components.

In cylindrical coordinates, the cross product of \vec{V} and $d\vec{s}$ is given by:

$$\begin{aligned} \vec{V} \times d\vec{s} &= (v_r \hat{i}_r + v_\theta \hat{i}_\theta + v_z \hat{i}_z) \times (dr \hat{i}_r + r d\theta \hat{i}_\theta + dz \hat{i}_z) \\ &= (v_\theta dz - v_z r d\theta) \hat{i}_r + (v_z dr - v_r dz) \hat{i}_\theta + (v_r r d\theta - v_\theta dr) \hat{i}_z \end{aligned}$$

So, each component for a stream line in cylindrical coordinates can be rewritten as three differential equations:

$$\frac{dz}{r d\theta} = \frac{v_z}{v_\theta} ; \quad \frac{dr}{dz} = \frac{v_r}{v_z} ; \quad \frac{dr}{r d\theta} = \frac{v_r}{v_\theta} \quad (3.4a)$$

Again, for a three-dimensional flow, one has to satisfy all three of these equations. However, for a planar, two-dimensional flow field (depending only on r and θ), the equation for a surface on the z -plane, $v_r r d\theta - v_\theta dr$, is the only relevant equation, which can be rewritten as:

$$\frac{dr}{r d\theta} = \frac{v_r}{v_\theta} \quad (3.4b)$$

Equation 3.4b is the differential equation of a two-dimensional stream line in r and θ . Note that Eq. 3.4b is slightly different from Eq. 3.3b, since here the differential angular change, $d\theta$, must operate on r to provide a linear differential displacement.

3.2.1 Flow Line Examples: Steady Flow

For the sake of example, consider a two-dimensional velocity field given by $\vec{V} = x\hat{i} - y\hat{j}$, such that $u = x$ and $v = -y$. Here, we will derive the appropriate equations for a path line, a streak line, and a stream line, all passing through the location $x, y = 1, 1$.

3.2.1.1 Path Line: Steady Flow

To establish the path line for a particle inserted at point $x, y = x_{init}, y_{init} = 1, 1$ at $t = 0$, we determine the Lagrangian functions $x_L = x_L(x_{init}, y_{init}, t)$ and $y_L = y_L(x_{init}, y_{init}, t)$ for the velocity field $\vec{V} = x\hat{i} - y\hat{j}$. Using the same approach as employed in Section 3.1, and assuming that the velocity of a specific fluid particle at any position within the velocity field is the velocity specified for that position by the Eulerian velocity field function, we equate the following:

$$u_L = \frac{dx_L}{dt} = x_L \quad v_L = \frac{dy_L}{dt} = -y_L$$

or, rearranging and integrating gives:

$$\begin{aligned} \frac{dx_L}{x_L} &= dt & \frac{dy_L}{y_L} &= -dt \\ x_L &= C_1 e^t & y_L &= C_2 e^{-t} \end{aligned} \quad (3.5)$$

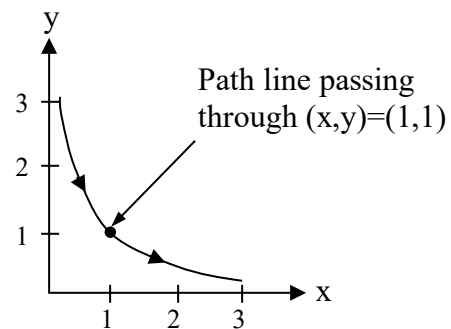
Here x_L and y_L are the general Lagrangian functions for the x and y location of any arbitrary particle moving within this velocity field. To establish the particular functions for the initial position, $x, y = x_{init}, y_{init} = 1, 1$ at $t = 0$, we substitute into our equations for x_L and y_L , and solve for the arbitrary constants C_1 and C_2 .

$$x_{init} = 1 = C_1 e^{(0)} \Rightarrow C_1 = 1 \quad y_{init} = 1 = C_2 e^{-(0)} \Rightarrow C_2 = 1$$

This gives the particular Lagrangian functions describing a path line for a fluid particle starting at position $x, y = x_{init}, y_{init} = 1, 1$ at $t = 0$ as:

$$x_L = e^t \quad \text{and} \quad y_L = e^{-t}$$

A sketch of this path line is shown at the right.



3.2.1.2 Streak line: Steady Flow

Here, we want to determine the location *at the present time*, $t = t_p$, of *all particles* that passed through point $x, y = x_{init}, y_{init}$ between a series of insertion times, $t = t_i$, and the present time, $t = t_p$, where $t_p \geq t_i$.

Using the general Lagrangian functions for a path line, Eq. 3.5, that we developed in section 3.2.1.1, we set $x, y = x_{init}, y_{init}$ at an arbitrary insertion time, t_i . Here t_i is any time prior to the present time of interest, t_p . This develops a general equation for the location of all the particles inserted before $t = t_p$. Then, by determining the present location of all those particles at $t = t_p$, we can connect all those particle locations to represent a streak line.

Thus, for a particle inserted at location $x, y = x_{init}, y_{init}$ at $t = t_i$, the Lagrangian equation for a general particle location is given by:

$$x_L = C_1 e^{t_i} = x_{init} \quad y_L = C_2 e^{-t_i} = y_{init} \quad (3.6a)$$

From Eq. 3.6a, we can solve for the constants, C_1 and C_2 as:

$$C_1 = \frac{x_{init}}{e^{t_i}} = x_{init} e^{-t_i} \quad C_2 = \frac{y_{init}}{e^{-t_i}} = y_{init} e^{t_i} \quad (3.6b)$$

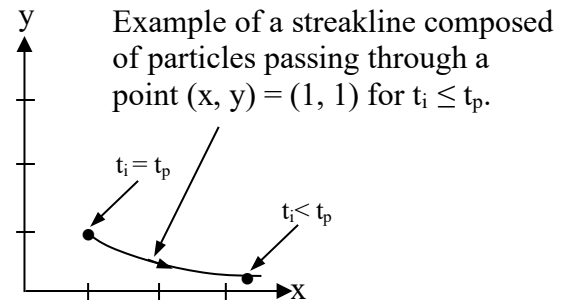
Note that C_1 and C_2 are constants for *any* arbitrary insertion time, t_i . Substituting the values of C_1 and C_2 into the equations 3.6a for x_L and y_L , gives the general equations for the *particle location at some later time, where $t > t_i$* . We will term these x_s and y_s , for the position of the streak particles. Thus:

$$\begin{aligned} x_s &= x_{init} e^{-t_i} e^t & y_s &= y_{init} e^{t_i} e^{-t} \\ &= x_{init} e^{(t-t_i)} & &= y_{init} e^{-(t-t_i)} \end{aligned} \quad (3.7)$$

In Eqs. 3.7, x_s, y_s give the x, y location of fluid particles comprising a streak line. If we now set $t = t_p$, Eq. 3.7 gives the *present position* of *all* the streak line particles, inserted at earlier times, t_i , as:

$$x_s = x_{init} e^{(t_p-t_i)} \quad \text{and} \quad y_s = y_{init} e^{-(t_p-t_i)} \quad (3.8)$$

Eqs. 3.8 now give *the present locations of all particles that passed through $x = x_{init}, y = y_{init}$ for any time $t < t_p$* . To establish a streak line at the present time, t_p , we simply plot the positions for a series of particles inserted at a series of earlier times, $t_i < t_p$. An example streak line for $(x_{init}, y_{init}) = (1, 1)$ is shown at the right.



3.2.1.3 Streamline: Steady Flow

Applying Eq. 3.4 for a two-dimensional streamline to the velocity field $\vec{V} = x\hat{i} - y\hat{j}$, we can write:

$$\frac{dy}{dx} = \frac{v}{u} = -\frac{y}{x}, \quad \text{or}$$

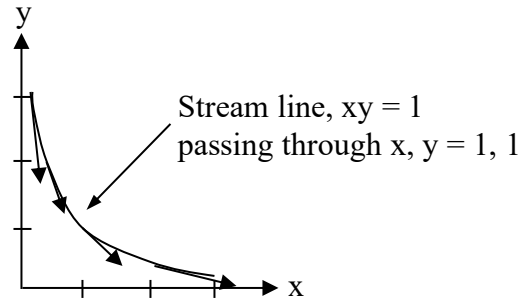
$$\frac{dy}{y} = -\frac{dx}{x}$$

Integrating gives:

$$\ln y = -\ln x + \ln C = \ln\left(\frac{C}{x}\right)$$

or

$$y = \frac{C}{x} \Rightarrow xy = C = \text{const.}$$



This is the general expression for any streamline within the specified velocity field. To determine a particular streamline, we need to specify a point that we wish that streamline to pass through. For example, if we want to identify the streamline that passes through the point $x, y = 1, 1$, we substitute those position values into the general equation and solve for the streamline constant. For this particular equation, we determine that $C = 1$. Thus, $xy = 1$ is the equation of the streamline passing through $x, y = 1, 1$, and defines all other points that will lie along that particular streamline. A sketch of this streamline is shown at the above right.

3.2.2 Equivalence of Flow Lines in Steady Flow

Note that for the example shown above, the path lines, streak lines, and streamlines are all identical lines. One can demonstrate this in several ways. For example, if the expressions determined in Section 3.2.1.1, 3.2.1.2, and 3.2.1.3 are used to determine the slope of the lines at any point along the line (e.g. at $x, y = 1, 1$), the slopes of the lines will all be identical. Alternatively, if the Lagrangian position functions for the path and streak lines are substituted into the streamline equation, they will identically satisfy the streamline equation. Figure 3.4 shows plots of the path, streak, and stream lines determined in Section 3.2.1, which illustrates the coincidence of all flow lines for steady flow.

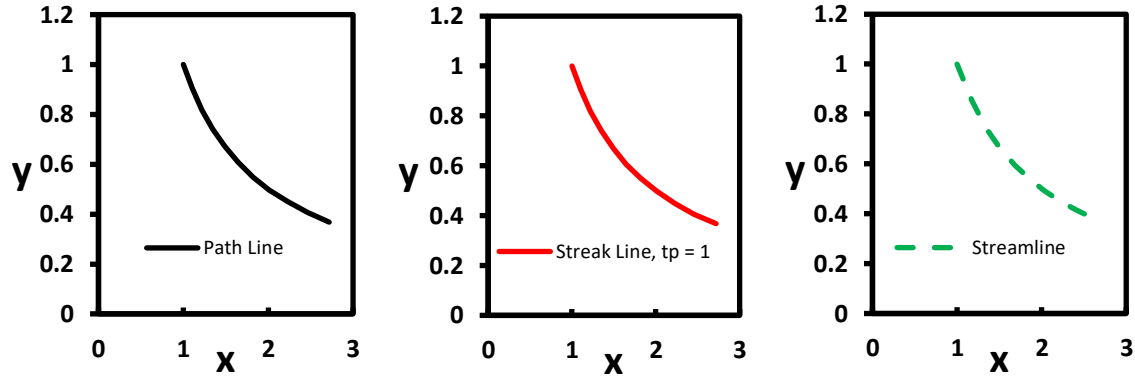


Figure 3.4 Plots of a path line, streak line (for $t_p = 1$, and $0 < t_i < 1$), and streamline passing through $x, y = 1, 1$ for velocity field $\vec{V} = x\hat{i} - y\hat{j}$.

This coincidence of path, streak, and stream lines is characteristic of *steady* velocity fields, and is quite a useful experimental tool, since a photographic image of either a set of path lines (using a time exposure of discretely added visible particles to a flow) or streak lines (using a regular photograph of continuously injected material into a flow, such as dye or smoke) will reasonably represent the behavior of the corresponding streamline. Figure 3.5 shows a photograph of the steady path/streak/stream lines visualized using smoke injection in a wind tunnel.



Figure 3.5 Smoke path/streak/streamlines in steady flow over an automobile.

Since the streamline pattern can provide valuable information regarding the pressure field of a fluid, as we will discuss in Chapter 7, such images can be quite helpful in designing and assessing geometric modifications to reduce internal energy losses in ducting or the drag on vehicles (i.e. thus the origin of the term “streamlining” of a car).

However, if the velocity field is locally *unsteady*, path lines, streak lines, and streamlines cease to be coincident, and snap-shot or time-exposure images of particle or marker behavior cannot be used to establish streamline behavior. An example of such an unsteady flow is the unsteady flow separation from the rear of a bluff body, such as a cylinder or truck traveling along a highway (which we discuss in Chapter 15). While path, streak, and streamlines can be visualized or constructed (both experimentally and

computationally) for unsteady flows, one needs to be careful not to equate one type of descriptor line with another. I illustrate the impact of unsteady flow on path, streak, and stream lines in the following section.

3.2.3 Flow Line Examples: Unsteady Flow

To illustrate the non-equivalence of flow lines in an unsteady flow, let's determine the path, streak, and stream lines for the velocity field $\vec{V} = (x + t)\hat{i} - y\hat{j}$, with x and y-direction velocity components $u_E = x + t$ and $v_E = -y$. Note that this is similar to the velocity field we considered in section 3.2.1, but with a linear time variation added to the x-direction velocity component. We again consider the flow lines for particles passing through point $x, y = x_{init}, y_{init} = 1, 1$, at an initial time, $t = 0$.

3.2.3.1 Path Line: Unsteady Flow

Writing our path line equations similar to section 3.2.1.1, we have:

$$u_L = \frac{dx_L}{dt} = x_L + t \quad v_L = \frac{dy_L}{dt} = -y_L$$

Here, our u_L equation is inhomogeneous, so we again need to use a technique similar to our example in Section 3.1. The result from the integration of these two equations is:

$$x_L = C_1 e^t - 1 - t \quad y_L = C_2 e^{-t} \quad (3.9)$$

The x_L expression of Eq. 3.9 contains additional terms due to the time variation; the y_L expression is the same as we derived in Eq. 3.5 in Section 3.2.1.1. For a particle released at $t = 0$ at location $x_{init}, y_{init} = 1, 1$, C_1 and C_2 are:

$$1 = C_1 - 1 \Rightarrow C_1 = 2 \quad \text{and} \quad C_2 = 1$$

Thus, the corresponding path line expressions are:

$$x_L = 2e^t - 1 - t \quad \text{and} \quad y_L = e^{-t} \quad (3.10)$$

3.2.3.2 Streak Line: Unsteady Flow

Here, we again determine the location *at the present time*, $t = t_p$, of *all particles* that passed through point $x_{init}, y_{init} = 1, 1$ between a series of insertion times, $t = t_i$, and the present time, $t = t_p$, where $t_p \geq t_i$.

Using our general Lagrangian functions for a path line, Eq. 3.9, from section 3.2.3.1, we set $x, y = 1, 1$ at an arbitrary insertion time, t_i , where t_i is again any time prior to the present time of interest, t_p . This develops a general equation for the location of all the particles inserted before $t = t_p$. By determining the present location of all those particles at $t = t_p$, we can connect all those particle locations to represent a streak line. Thus, for a particle inserted at location $x, y = 1, 1$ at $t = t_i$, the Lagrangian equation for a general particle location is given by:

$$x_L = C_1 e^{t_i} - 1 - t_i = 1 \quad y_L = C_2 e^{-t_i} = 1 \quad (3.11)$$

From Eq. 3.11, we can solve for the constants, C_1 and C_2 as:

$$C_1 = (2 + t_i) e^{-t_i} \quad C_2 = e^{t_i}$$

Since C_1 and C_2 are constants for *any* arbitrary insertion time, t_i , we now substitute the values of C_1 and C_2 into the equations 3.9 for f_1 and f_2 , which gives us the general equations for the *particle location at some later time, where $t > t_i$* . We again will term these locations x_s and y_s , for the position of the streak particles. Thus:

$$\begin{aligned} x_s &= (2 + t_i) e^{-t_i} e^t - 1 - t & y_s &= e^{t_i} e^{-t} \\ &= (2 + t_i) e^{-(t-t_i)} - 1 - t & &= e^{-(t-t_i)} \end{aligned} \quad \text{and} \quad (3.12)$$

In Eqs. 3.12, x_s, y_s give the x, y location of fluid particles comprising a streak line. If we now set $t = t_p$ in Eq. 3.12, this gives the *present position* of *all* the streak line particles, inserted at earlier times, t_i , as:

$$x_s = (2 + t_i) e^{-(t_p-t_i)} - 1 - t_p \quad \text{and} \quad y_s = e^{-(t_p-t_i)} \quad (3.13)$$

Eqs. 3.13 now give *the present locations of all particles that passed through $x = 1, y = 1$ for any time $t < t_p$* . To establish a streak line at the present time, t_p , we simply plot the positions for a series of particles inserted at a series of earlier times, $t_i < t_p$.

3.2.3.3 Streamline: Unsteady Flow

Applying Eq. 3.4 for a two-dimensional streamline with $\vec{V} = (x + t)\hat{i} - y\hat{j}$, we can write:

$$\frac{dy}{dx} = \frac{v}{u} = -\frac{y}{x+t}, \quad \text{or} \quad \frac{dy}{y} = -\frac{dx}{x+t}$$

Integrating gives:

$$\ln(y) = -\ln(x+t) + \ln C = \ln\left(\frac{C}{x+t}\right)$$

or

$$y = \frac{C}{x+t} \Rightarrow y(x+t) = C = \text{const.} \quad (3.14)$$

Eq. 3.14 is the general expression for any streamline within the specified velocity field. To determine a particular streamline, we need to specify a point that we wish the streamline to pass through and the time of interest. For example, if we want to identify the streamline that passes through the point $x, y = 1, 1$ at time $t = 0$, we substitute those position values into the general equation and solve for the streamline constant. For this particular streamline equation, we determine that at $t = 0$, $C = 1$. This would give an equation for that streamline as:

$$xy = 1 \quad (3.15)$$

However, the equation for a streamline passing through $x, y = 1, 1$ at time $t = 1$, would yield an equation for that streamline as:

$$y(x+1) = 2 \quad (3.16)$$

These are different streamlines, due to the time variation of the flow field, as shown in Figure 3.6.

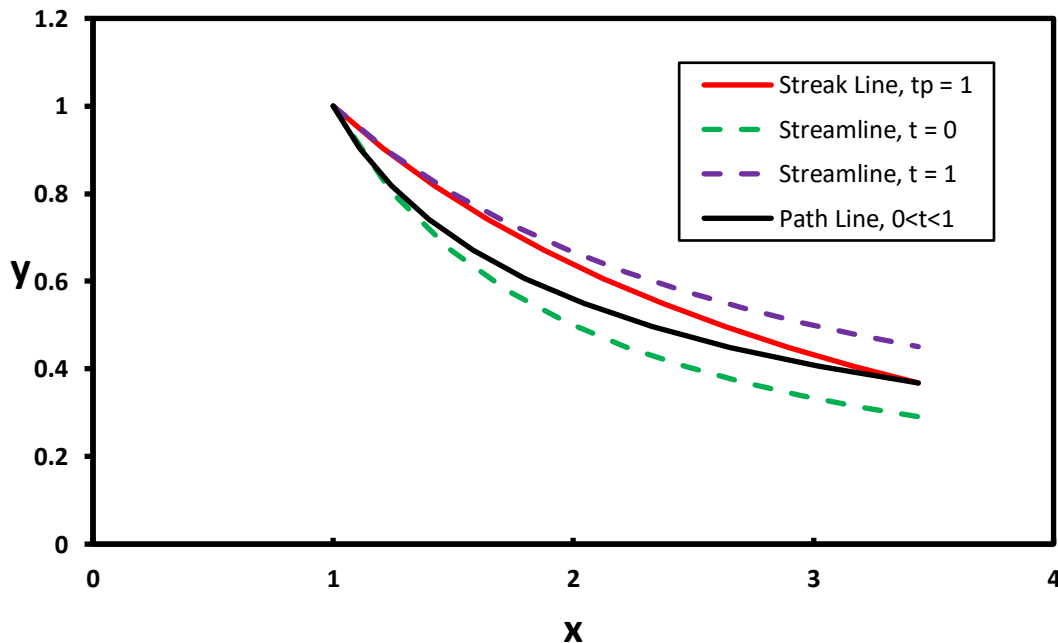


Figure 3.6 Plots of a path line, streak line (for $t_p = 1$, and $0 < t_i < 1$), and streamlines for $t=0$ and $t=1$ passing through $x, y = 1, 1$ for velocity field $\vec{V} = (x+t)\hat{i} - y\hat{j}$.

3.2.4 Non-Equivalence of Flow Lines in Unsteady Flow

Figure 3.6 shows plots of the path, streak, and streamlines determined in Section 3.2.3.

Clearly, these are all different flow lines, since the velocity field varies with time, t . Note that the path line (black) and the streak line (red) have coincident starting and termination points. This is because all particles start at $x = 1, 1$, and the particle released at $t_i = 0$ will trace the path shown (between $0 < t < 1$) in figure 3.2. So at $t = t_p = 1$, the end points (particles) of the path and streak lines shown will both occupy the same location. However, for $0 < t < 1$ the path and streak lines will describe different lines.

The variation in the velocity field is quite clearly shown by the streamlines displayed. Although the lines (Eq. 3.15 and 3.16) pass through the same initial location ($x, y = 1, 1$), because the u -velocity increases with time the streamlines will skew in a counter-clockwise manner as the flow moves more rapidly in the x -direction with increasing time.

Clearly, the various flow lines in figure 3.6 are not coincident, as they were in figure 3.4 for a steady flow. Thus, for an unsteady flow we cannot equate a path or streak line as representative of a streamline. As we will show in Chapters 7 and 8, the flow along a streamline can be directly related to the pressure field associated with a flow, and the surface pressure effects (e.g. lift and drag) on bodies within the flow field. Consequently, we must be careful in our interpretation of path and streak lines as streamlines, which is often done erroneously in experimental studies using particle, smoke, and dye visualizations (see this [link](#), which gives a good, dynamic illustration of the variations that can occur). We will discuss the characteristics and impact of unsteady behavior further in Chapters 7 and 8.

3.3 The Substantial (or Material) Derivative

In Section 3.1, we derived an expression for the acceleration of a particle in an Eulerian velocity field, which led to a derivative operator termed the total derivative. However, this derivative operator can be employed more broadly to establish the *rate of change of any property* of a material fluid particle as a result of its movement through an Eulerian velocity field. This of course assumes that we can also develop an appropriate Eulerian field description for the continuously distributed property (e.g. density, temperature, etc.) within the same spatial region as the velocity field. When such a property field exists, a particle carried through the property field by the coincident velocity field will experience changes according to the appropriate property field description.

To assess the generic property change due to the motion of a particle, let the function $F = F(x, y, z, t)$ represent the Eulerian field description of any property (either scalar or vector) coincident within the same spatial region of an Eulerian velocity field, $\vec{V}(x, y, z, t)$.

Using the same approach we employed in section 3.1 for the change of a particle velocity within a velocity field, the change in a particle property, call it F , as the particle undergoes differential displacements of Δx_p , Δy_p , and Δz_p over a differential time Δt , can be written using the chain rule as:

$$\Delta F = \frac{\partial F}{\partial x} \Delta x_p + \frac{\partial F}{\partial y} \Delta y_p + \frac{\partial F}{\partial z} \Delta z_p + \frac{\partial F}{\partial t} \Delta t$$

Again, since these displacements will be the product of the local Eulerian velocity component and the differential time change, we can write:

$$\Delta F = \frac{\partial F}{\partial x} u \Delta t + \frac{\partial F}{\partial y} v \Delta t + \frac{\partial F}{\partial z} w \Delta t + \frac{\partial F}{\partial t} \Delta t = \left(\frac{\partial F}{\partial x} u + \frac{\partial F}{\partial y} v + \frac{\partial F}{\partial z} w + \frac{\partial F}{\partial t} \right) \Delta t$$

Dividing through by the time differential, Δt , over which the property change occurs, and taking the limit as $\Delta t \rightarrow 0$, gives:

$$\lim_{\Delta t \rightarrow 0} \frac{\Delta F}{\Delta t} = \frac{DF}{Dt} = \frac{\partial F}{\partial x} u + \frac{\partial F}{\partial y} v + \frac{\partial F}{\partial z} w + \frac{\partial F}{\partial t}$$

We again define this limiting change in the property F by the derivative operator, $D(\)/Dt$, which we termed in section 3.1 as the “substantial” or “material” derivative. Here the definition of the term should be more obvious, since this operator yields the time change of F (a *substance* or *material* property of a particle) as the particle is carried through the property field, $F(x, y, z, t)$ by the Eulerian velocity field, $\vec{V}(x, y, z, t)$.

$$\text{Thus, } \underbrace{\frac{DF}{Dt}}_{\substack{\text{Total rate of} \\ \text{a change of} \\ \text{property } F}} = \underbrace{u \frac{\partial F}{\partial x} + v \frac{\partial F}{\partial y} + w \frac{\partial F}{\partial z}}_{\substack{\text{Rate of change of } F \text{ due to} \\ \text{advection through the} \\ \text{velocity field}}} + \underbrace{\frac{\partial F}{\partial t}}_{\substack{\text{Local rate of change} \\ \text{of } F \text{ at a point}}} \quad (3.17)$$

As we commented on in Section 3.1, this form of derivative operator, $D(\)/Dt$, accounts not only for the local change of a property with time, but also the changes created by the advection of a fluid particle through a medium with spatial property variations (e.g. like experiencing a decrease in temperature as you hike up a mountain).

Expressing the above equation in vector form gives:

$$\frac{DF}{Dt} = (\vec{V} \cdot \nabla)F + \frac{\partial F}{\partial t} \quad (3.18)$$

If the property under consideration is a vector, for example in Cartesian coordinates, $\vec{f} = f_x \hat{i} + f_y \hat{j} + f_z \hat{k}$, we can write:

$$\frac{D\vec{f}}{Dt} = (\vec{V} \cdot \nabla)\vec{f} + \frac{\partial \vec{f}}{\partial t} \quad (3.19)$$

A simple example of the application of the substantial derivative is an examination of the *change in a particle's position with time* as the particle passes through a velocity field.

To examine this, we define an arbitrary particle position as $\vec{r} = x\hat{i} + y\hat{j} + z\hat{k}$, where x , y , and z are the Cartesian position coordinates of the particle. Now, we seek the change in the position of the particle, $D\vec{r}/Dt$, as it passes through the velocity field. Here, equating $\vec{f} = \vec{r}$ in Eq. 3.19, we write:

$$\begin{aligned} \frac{D\vec{r}}{Dt} &= u \frac{\partial \vec{r}}{\partial x} + v \frac{\partial \vec{r}}{\partial y} + w \frac{\partial \vec{r}}{\partial z} + \frac{\partial \vec{r}}{\partial t} \\ &= u \frac{\partial(x\hat{i} + y\hat{j} + z\hat{k})}{\partial x} + v \frac{\partial(x\hat{i} + y\hat{j} + z\hat{k})}{\partial y} + w \frac{\partial(x\hat{i} + y\hat{j} + z\hat{k})}{\partial z} + \frac{\partial(x\hat{i} + y\hat{j} + z\hat{k})}{\partial t} \end{aligned}$$

Or, considering only the non-zero derivative terms,

$$\frac{D\vec{r}}{Dt} = u \frac{\partial(x\hat{i})}{\partial x} + v \frac{\partial(y\hat{j})}{\partial y} + w \frac{\partial(z\hat{k})}{\partial z} + 0 = u\hat{i} + v\hat{j} + w\hat{k} \quad (3.20)$$

So, $D\vec{r}/Dt$ is the *velocity* of the flow field itself at the point $r = x\hat{i} + y\hat{j} + z\hat{k}$, as it should be. Note that in Eq. 3.20 the term $\partial\vec{r}/\partial t$ is zero since we are dealing with an Eulerian description, and a specified point, $\vec{r} = f(x, y, z)$, and the position of that point is not a function of time.

The general form of the substantial derivative derived above can be used to express the changes of any property of a particle as the particle moves through that property field. For example, the expression for a change in density, ρ (a scalar), is given by:

$$\frac{D\rho}{Dt} = u \frac{\partial \rho}{\partial x} + v \frac{\partial \rho}{\partial y} + w \frac{\partial \rho}{\partial z} + \frac{\partial \rho}{\partial t}$$

On the other hand, a change in vorticity (i.e. fluid rotation), $\vec{\omega}$ (a vector), where $\vec{\omega} = \omega_x \hat{i} + \omega_y \hat{j} + \omega_z \hat{k}$, is given by:

$$\frac{D\vec{\omega}}{Dt} = u \frac{\partial \vec{\omega}}{\partial x} + v \frac{\partial \vec{\omega}}{\partial y} + w \frac{\partial \vec{\omega}}{\partial z} + \frac{\partial \vec{\omega}}{\partial t}$$

Note that we will use both of these expressions for density and vorticity change later, when we derive the respective differential equations for the conservation of mass, and the transport of vorticity.

Example: If we consider coincident velocity and density fields given by:

$$\vec{V} = U_o \frac{y}{h} \hat{i} \quad \text{and} \quad \rho = \rho_o(1 + ax - bt)$$

Then, the change in the density within the flow field is given by:

$$\frac{D\rho}{Dt} = u \frac{\partial \rho}{\partial x} + v \frac{\partial \rho}{\partial y} + w \frac{\partial \rho}{\partial z} + \frac{\partial \rho}{\partial t}$$

or,

$$\frac{D\rho}{Dt} = U_o \frac{y}{h} (\rho_o a) + 0 + 0 + \rho_o (-b) = \rho_o \left[\underbrace{\left(U_o \frac{y}{h} \right) a}_{\substack{\text{Changes due} \\ \text{to advective} \\ \text{motion} \\ \text{through the} \\ \text{spatially} \\ \text{varying} \\ \text{density field}}} \quad \underbrace{-b}_{\substack{\text{Changes due} \\ \text{to local time} \\ \text{variations of} \\ \text{the density} \\ \text{field}}} \right]$$

Thus, for this example, the velocity and density variations will result in the density at a point increasing both laterally and in the flow direction due to advection, but decreasing with increasing time.

3.4 The Substantial Derivative: Cartesian and Cylindrical Coordinates

3.4.1 Substantial Derivative, Cartesian Coordinates: $\vec{V} = u\hat{i} + v\hat{j} + w\hat{k}$

$$\frac{DF}{Dt} = \frac{\partial F}{\partial t} + u \frac{\partial F}{\partial x} + v \frac{\partial F}{\partial y} + w \frac{\partial F}{\partial z} \quad \text{where } F = F(x, y, z, t)$$

$$\frac{D\vec{f}}{Dt} = \frac{\partial \vec{f}}{\partial t} + u \frac{\partial \vec{f}}{\partial x} + v \frac{\partial \vec{f}}{\partial y} + w \frac{\partial \vec{f}}{\partial z} \quad \text{where } \vec{f} = \vec{f}(x, y, z, t) = f_x \hat{i} + f_y \hat{j} + f_z \hat{k}$$

$$\text{x-component:} \quad \left[\frac{D\vec{f}}{Dt} \right]_x = \frac{\partial f_x}{\partial t} + u \frac{\partial f_x}{\partial x} + v \frac{\partial f_x}{\partial y} + w \frac{\partial f_x}{\partial z}$$

$$\text{y-component:} \quad \left[\frac{D\vec{f}}{Dt} \right]_y = \frac{\partial f_y}{\partial t} + u \frac{\partial f_y}{\partial x} + v \frac{\partial f_y}{\partial y} + w \frac{\partial f_y}{\partial z}$$

$$\text{z-component:} \quad \left[\frac{D\vec{f}}{Dt} \right]_z = \frac{\partial f_z}{\partial t} + u \frac{\partial f_z}{\partial x} + v \frac{\partial f_z}{\partial y} + w \frac{\partial f_z}{\partial z}$$

3.4.2 Total Acceleration, Cartesian Coordinates

$$\begin{aligned}\bar{a} &= \frac{D\bar{V}}{Dt} = \frac{\partial\bar{V}}{\partial t} + u\frac{\partial\bar{V}}{\partial x} + v\frac{\partial\bar{V}}{\partial y} + w\frac{\partial\bar{V}}{\partial z} && \text{Total acceleration} \\ a_x &= \frac{Du}{Dt} = \frac{\partial u}{\partial t} + u\frac{\partial u}{\partial x} + v\frac{\partial u}{\partial y} + w\frac{\partial u}{\partial z} && \text{x-component of acceleration} \\ a_y &= \frac{Dv}{Dt} = \frac{\partial v}{\partial t} + u\frac{\partial v}{\partial x} + v\frac{\partial v}{\partial y} + w\frac{\partial v}{\partial z} && \text{y-component of acceleration} \\ a_z &= \frac{Dw}{Dt} = \frac{\partial w}{\partial t} + u\frac{\partial w}{\partial x} + v\frac{\partial w}{\partial y} + w\frac{\partial w}{\partial z} && \text{z-component of acceleration}\end{aligned}$$

3.4.3 Substantial Derivative, Cylindrical Coordinates: $\bar{V} = v_r\hat{i}_r + v_\theta\hat{i}_\theta + v_z\hat{i}_z$

$$\begin{aligned}\frac{DF}{Dt} &= \frac{\partial F}{\partial t} + v_r\frac{\partial F}{\partial r} + \frac{v_\theta}{r}\frac{\partial F}{\partial\theta} + v_z\frac{\partial F}{\partial z} && \text{where } F = F(r, \theta, z, t) \\ \frac{D\vec{f}}{Dt} &= \frac{\partial\vec{f}}{\partial t} + v_r\frac{\partial\vec{f}}{\partial r} + \frac{v_\theta}{r}\frac{\partial\vec{f}}{\partial\theta} + v_z\frac{\partial\vec{f}}{\partial z} && \text{where } \vec{f} = \vec{f}(r, \theta, z, t) = f_r\hat{i} + f_\theta\hat{j} + f_z\hat{k}\end{aligned}$$

$$\begin{aligned}\text{r-component: } \left[\frac{D\vec{f}}{Dt} \right]_r &= \frac{\partial f_r}{\partial t} + v_r\frac{\partial f_r}{\partial r} + \frac{v_\theta}{r} \left[\frac{\partial f_r}{\partial\theta} - f_\theta \right] + v_z\frac{\partial f_r}{\partial z} \\ \theta\text{-component: } \left[\frac{D\vec{f}}{Dt} \right]_\theta &= \frac{\partial f_\theta}{\partial t} + v_r\frac{\partial f_\theta}{\partial r} + \frac{v_\theta}{r} \left[\frac{\partial f_\theta}{\partial\theta} + f_r \right] + v_z\frac{\partial f_\theta}{\partial z} \\ z\text{-component: } \left[\frac{D\vec{f}}{Dt} \right]_z &= \frac{\partial f_z}{\partial t} + v_r\frac{\partial f_z}{\partial r} + \frac{v_\theta}{r}\frac{\partial f_z}{\partial\theta} + v_z\frac{\partial f_z}{\partial z}\end{aligned}$$

3.4.4 Total Acceleration, Cylindrical Coordinates

$$\begin{aligned}\bar{a} &= \frac{D\bar{V}}{Dt} = \frac{\partial\bar{V}}{\partial t} + v_r\frac{\partial\bar{V}}{\partial r} + \frac{v_\theta}{r}\frac{\partial\bar{V}}{\partial\theta} + v_z\frac{\partial\bar{V}}{\partial z} && \text{Total acceleration} \\ a_r &= \frac{Dv_r}{Dt} = \frac{\partial v_r}{\partial t} + v_r\frac{\partial v_r}{\partial r} + \frac{v_\theta}{r}\frac{\partial v_r}{\partial\theta} + v_z\frac{\partial v_r}{\partial z} - \frac{v_\theta^2}{r} && \text{r-component of acceleration} \\ a_\theta &= \frac{Dv_\theta}{Dt} = \frac{\partial v_\theta}{\partial t} + v_r\frac{\partial v_\theta}{\partial r} + \frac{v_\theta}{r}\frac{\partial v_\theta}{\partial\theta} + v_z\frac{\partial v_\theta}{\partial z} + \frac{v_r v_\theta}{r} && \theta\text{-component of acceleration} \\ a_z &= \frac{Dv_z}{Dt} = \frac{\partial v_z}{\partial t} + v_r\frac{\partial v_z}{\partial r} + \frac{v_\theta}{r}\frac{\partial v_z}{\partial\theta} + v_z\frac{\partial v_z}{\partial z} && \text{z-component of acceleration}\end{aligned}$$

Study Problems

1. A particular flow has the following field characteristics (assume these are non-dimensional):

velocity: $\vec{V} = x\hat{i} - (t + 2y)\hat{j} + z\hat{k}$

temperature: $T = 2x + yz$

density: $\rho = 1 - e^{-x}$

Determine (non-dimensionally) at time $t = 1$:

- a. The acceleration field
 - b. The rate of change of ρ at a point (2,1,1)
 - c. The rate of change of temperature at point (1,3,2)
2. A particular flow has the following field characteristics (assume these are non-dimensional):

velocity: $\vec{V} = (2y - y^2)\hat{i} - e^{-y}\hat{j} + 2\hat{k}$

temperature: $T = (9 - x^2 + z^2)e^{-yt}$

density: $\rho = (1 - x)e^{-y}$

Determine (non-dimensionally) at time $t=0$:

- a. The acceleration field at (0,0,0)
 - b. The rate of change of ρ at a point (1,1,1)
 - c. The rate of change of temperature at point (1,0,1)
3. Consider the plane flow field,

$$\vec{V} = 2x\hat{i} + y\hat{j}$$

Develop expressions for: a **streamline** passing through a point (a,b)=(1,2); a **path line** initiated at $t = 0$ at point (a,b)=(1,2); and **streak line** at $t = 1$ for all the particles that passed through point (a,b)=(1,2) between $t = 0$ and $t = 1$.

4. Consider the plane flow field,

$$\vec{V} = x\hat{i} + yt\hat{j}$$

Develop expressions for streamlines, pathlines, and streaklines through a point (a,b)=(1,1). Plot: **streamlines** for $t = 0, 0.5, \text{ and } 1$; a **path line** at $t=1$ for a particle introduced at $t=0$; and a **streak line** at $t = 1$ for all particles which passed through point (1,1) between $t = 0$ and $t = 1$. Show all plots on one, full-page graph..

5. Consider the plane flow field,

$$\vec{V} = \left(\frac{x}{1+t} \right) \hat{i} - [y(1+t)] \hat{j}$$

Develop expressions for streamlines, pathlines, and streaklines through a point (a,b)=(1,1).

Plot: **streamlines** for $t = 0, 0.5,$ and 1 ; a **path line** at $t=1$ for a particle introduced at $t=0$; and a **streak line** at $t = 1$ for all particles which passed through point (1,1) between $t = 0$ and $t = 1$. Show all plots on one, full-page graph..

6. A non-dimensional velocity field in cylindrical coordinates is given by:

$$\vec{V} = -\left(\frac{1}{r^2} \right) \hat{i}_r + 4r^2 \hat{i}_\theta$$

Determine:

- An expression for the acceleration of a particle anywhere within the flow field.
- The equation for a streamline passing through the point $(x,y) = (0,2)$; **plot** the streamline from $(x,y) = (0,2)$ to $(0,0)$.
- How long (in non-dimensional terms) it will take a particle to go from $(0,2)$ to $(0,0)$.

7. A non-dimensional velocity field in cylindrical coordinates is given by:

$$\vec{V} = -\left(\frac{1}{r} \right) \hat{i}_r + 4r \hat{i}_\theta$$

Determine:

- An expression for the acceleration of a particle anywhere within the flow field.
- The equation for a streamline passing through the point $(x,y) = (0,2)$; **plot** the streamline from $(x,y) = (0,2)$ to $(0,0)$.
- How long (in non-dimensional terms) it will take a particle to go from $(0,2)$ to $(0,0)$.

8. A non-dimensional velocity field in cylindrical coordinates is given by:

$$\vec{V} = -\left(\frac{1}{r^2} \right) \hat{i}_r + 4r \left(1 - \frac{r}{3} \right) \hat{i}_\theta$$

Determine:

- An expression for the acceleration of a particle anywhere within the flow field.
- The equation for a streamline passing through the point $(x,y) = (0,2)$; **plot** the streamline from $(x,y) = (0,2)$ to $(0,0)$.
- How long (in non-dimensional terms) it will take a particle to go from $(0,2)$ to $(0,0)$.

9. A non-dimensional, time-dependent velocity field in cylindrical coordinates is given by:

$$\vec{V} = -\left(\frac{t}{r} \right) \hat{i}_r + 4r \hat{i}_\theta$$

Determine:

- An expression for the acceleration of a particle anywhere within the flow field.
- The equation for a streamline passing through the point $(x,y) = (0,2)$; **plot** the streamline from $(x,y) = (0,2)$ to $(0,0)$ for times $t=1/2, 1,$ and 2 using three separate plots.

Chapter 4

Motion and Deformation of a Fluid

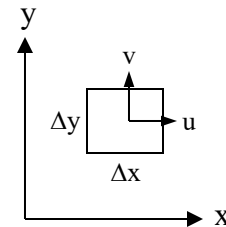
Contents

4.1	Fluid Motions	66
4.1.1	Translation	67
4.1.2	Rotation	67
4.1.3	Angular Deformation	68
4.1.4	Linear Deformation	69
4.2	Cauchy-Stokes Decomposition	70
4.2.1	Use of Tensors	73
4.2.2	Decomposition in Tensor Notation	74
4.3	Vorticity	77
4.4	Rate of Strain and Vorticity Equations: Cartesian and Cylindrical Coordinates	80
4.4.1	Rate of Strain, Cartesian Coordinates	80
4.4.2	Vorticity, Cartesian Coordinates	80
4.4.3	Rate of Strain, Cylindrical Coordinates	80
4.4.4	Vorticity, Cylindrical Coordinates	80

In order to develop differential equations of motion for a fluid, we need to understand the general types of motion we must consider. For simplicity, in this chapter we examine motion in two-dimensions, which is sufficient for our purposes of examining the types of motions that can occur, and determining how we can approach the mathematical modeling of these motions. The objective here is to provide a physical background for the development of the governing differential equations, which is done in Chapter 5.

4.1 Fluid Motions

Initially, we consider the general motions that a fluid can undergo. To do this, we examine an infinitesimal *differential element* of dimensions Δx by Δy in a Cartesian coordinate system, where the local vector velocity at the *center* of the element is assumed to be $\vec{V} = u\hat{i} + v\hat{j}$. While the dimensions of the differential element are considered infinitesimal, we accentuate the size of the element here, for the point of illustration.



Note that for all the behaviors considered, the velocity vector components u and v are assumed positive relative to the respective coordinate-axes. Basically, we recognize that a fluid element can undergo *translation, rotation, and angular and linear deformation* (i.e. distortion), depending on how the velocity components change from the center of the element to the element boundaries.

In the following sections, we examine each type of motion individually by considering the possible behavioral changes of the differential element over an infinitesimal time interval, Δt .

4.1.1 Translation

Here we assume that the velocity across the element is uniform (no changes in either coordinate direction), which will only result in a translation of the element. Assuming that Δt is so small that the velocities remain essentially constant during the time change, the magnitudes of the translation in the x and y coordinate directions are given respectively by $u\Delta t$ and $v\Delta t$, as shown in figure 4.1. This results in the differential element retaining its original geometry while translating to a new position in space.

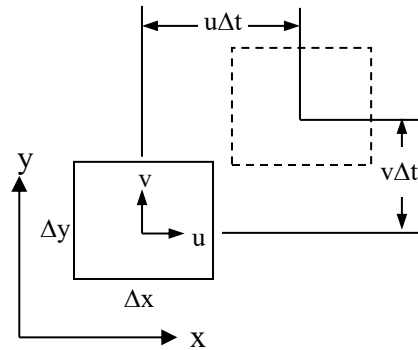


Figure 4.1 Translation of a differential element

4.1.2 Rotation

To illustrate and examine rotational motion of our differential element, we next assume that the velocities across the element change in a manner that will result in the pure rotation of the primary axes of the element (i.e. two orthogonal line segments fixed in the element, and initially aligned with the reference coordinate axes). We assume that these changes yield a positive rotation of each line segment (counter clockwise for this case, by the right-hand rule). We again assume that Δt is infinitesimal, and that the degree of rotation of the element can be characterized by the collective displacement of the two primary axes fixed in the element. We characterize the displacement of these axes by the *displacement* of their extensions at the element boundary, as shown in figure 4.2.

This displacement is the result of a change, from the center of the element to the element boundary, of the velocity *normal* to a line segment comprising a primary axis. For example, for a line segment initially oriented along the x -axis, this velocity change is given by $\Delta v/\Delta x$, or the derivative $\partial v/\partial x$ for the limit of an infinitesimal change. Thus, the

subsequent displacement of the outermost point of this line segment is $(\partial v / \partial x)(\Delta x / 2)\Delta t$, where $\Delta x / 2$ is the length of the line segment from the center of the element to the outer boundary, and Δt is the time interval of the displacement. Clearly, this change is actually assumed quite small, although it is exaggerated in figure 4.2.

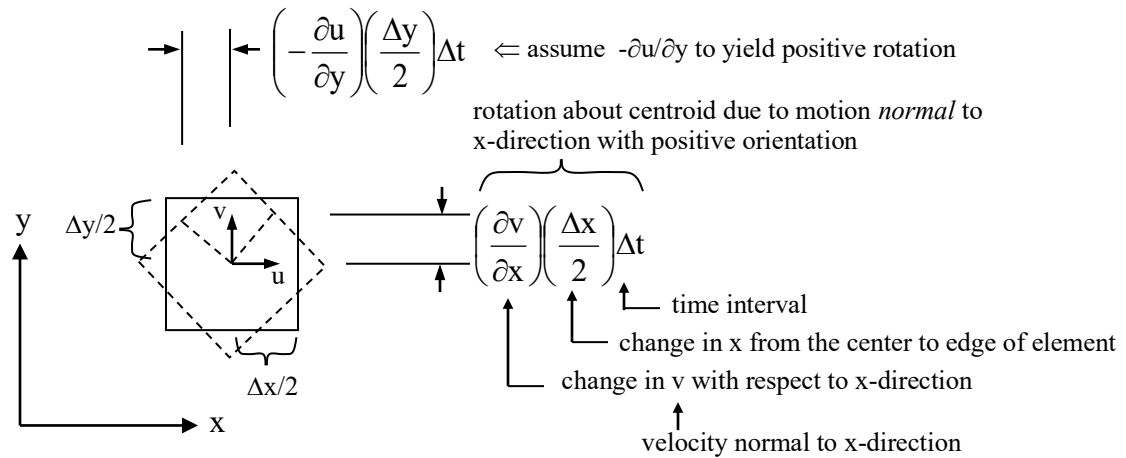


Figure 4.2 Rotation of a differential element

We recognize that rotation of the element can only occur if the two orthogonal primary axes execute identical displacements relative to the fixed coordinate axes, and remain orthogonal. Thus, a similar argument is made for the displacement of the line segment initially aligned along the y-axis, with its displacement being $(-\partial u / \partial y)(\Delta y / 2)\Delta t$, which will reflect the same magnitude of displacement as the other line segment, and yield a positive rotation of the element. Note that we need to assume $-(\partial u / \partial y)$ (where u is assumed positive) to reflect a displacement yielding a positive rotation of the element.

Also, although the displacements are relative to the centroid of the element, this does not mean that the element cannot be undergoing other simultaneous motions. Clearly, a flow can translate, rotate, and deform concurrently (as we will discuss in Section 4.2) -- here we simply illustrate how those individual motions can be envisioned geometrically, and then described mathematically.

4.1.3 Angular Deformation

To address deformation of a fluid, we first recognize that a fluid can undergo *both angular* deformation and *linear* deformation. Here, we consider angular deformation, which can be characterized by the same types of displacements that we examined in section 4.1.2 for rotation. We again assume that the change in the velocities across the element will yield a rotation of the primary axes (i.e. orthogonal line segments) of the

element about the element centroid. However, for angular deformation to occur, the primary axes of the element are assumed to move in *opposition* to each other, as shown in figure 4.3 (note that this differs from the conjunctive motion of the axes, which yielded rotation). Since we assumed u and v to be positive, angular deformation will occur when the extensions of the initially orthogonal line segments both undergo *positive differential changes*. These positive changes reflect angular motion of the line segments counter to each other, which results in a subsequent loss of orthogonality of the primary axes, as shown in figure 4.3.

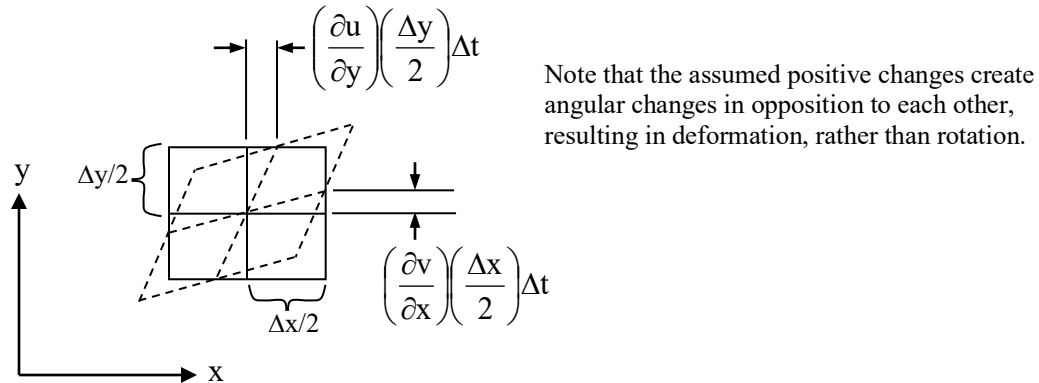


Figure 4.3 Angular deformation of a differential element

4.1.4 Linear Deformation

For linear deformation to occur, the velocity component in a specified coordinate direction must change in that direction. In such types of deformation, the extensions of the primary axes remain orthogonal, but are assumed to undergo positive differential changes in the coordinate directions as shown in figure 4.4. Thus, a positive differential change in the x -direction will be reflected by $(\partial u/\partial x)$, resulting in a corresponding displacement (lengthening) of the x -directed line segment by $(\partial u/\partial x)(\Delta x/2)\Delta t$, which reflects a linear extension of the element in the x -direction. Correspondingly, a positive change in the y -direction, reflected by $(\partial v/\partial y)$ will result in a linear extension in the y -direction of $(\partial v/\partial y)(\Delta y/2)\Delta t$.

Note that figure 4.4 illustrates positive extensions in both coordinate directions, and thus an overall expansion of the element, which might be expected for a compressible fluid, such as air. However, whereas angular deformation can only occur by rotation of the line segments in opposition to each other, linear deformation in either coordinate direction is not constrained by such a requirement, if the fluid is compressible. However, as we will show later, if a fluid is incompressible, conservation of mass requires that linear

deformations in the coordinate directions must act in opposition to each other to assure that mass is conserved.

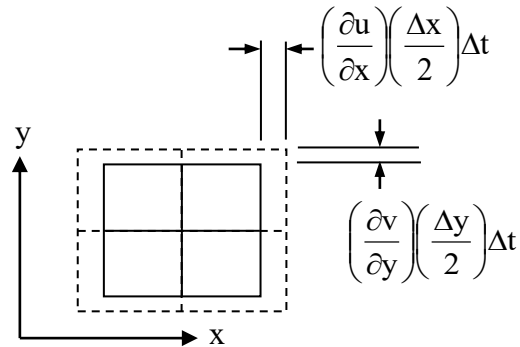


Figure 4.4 Linear deformation of a differential element

Of the described motions, which will result in stresses? Obviously, only those motions that result in a relative change in the dimensions of the line elements $\Delta x, \Delta y$ (which implies the presence of strain) can create a stress. Thus, only angular and linear deformations result in the generation of a stress within a fluid. As will be shown, angular deformation is proportional to a *shear stress*, and *linear deformation* is proportional to a *normal stress*.

Since fluid behavior is a combination of all of these four fluid motions (translation, rotation, and angular and linear deformations), we need to be able to express the cumulative motion of a fluid in a compact, mathematical manner in order to perform appropriate modeling of fluid behavior, and thus the development of the governing differential equations of fluid motion. The following discussion of the Cauchy-Stokes decomposition of fluid motion, shows how to mathematically model, represent, and examine the differential motions of a fluid.

4.2 Cauchy-Stokes Decomposition

A useful first approach to understanding the motion and deformation of a deformable medium (e.g. a fluid) is to consider an approach for “decomposing” all potential fluid behaviors mathematically using what is known as the Cauchy-Stokes Decomposition Theorem, named after the two gentlemen who developed the concept (see [Truesdale \(1954\)](#)). Although the theorem is generic to three-dimensions, we will examine a two-dimensional version here, since the two-dimensional mathematics are easier to follow and more physically instructive. And of course, what we learn from the two-dimensional approach is directly extendable to three dimensions, as will be discussed later.

direction velocity in the x-direction). However, the other derivatives are more problematic (and thus the question marks), since they reflect changes *normal* to the direction of the respective velocity component, which could reflect components of either rotation *or* angular deformation. Since these terms represent a combination of behaviors, we attempt to separate these terms further using some mathematical manipulation.

Let's first consider the x-direction term $(\partial u/\partial y)dy$ in Eq. 4.2. If we split this term in half, and both add and subtract a term $1/2(\partial v/\partial x)dy$ (this contributes nothing additional, but allows us to manipulate the initial term), we end up with an expanded expression:

$$\frac{\partial u}{\partial y} dy = \underbrace{\frac{1}{2} \frac{\partial u}{\partial y} dy + \frac{1}{2} \frac{\partial u}{\partial y} dy}_{\text{split in halves}} + \underbrace{\frac{1}{2} \frac{\partial v}{\partial x} dy - \frac{1}{2} \frac{\partial v}{\partial x} dy}_{\text{add-subtract same term}} \tag{4.3}$$

Rearranging the terms on the right side of Eq. 4.3 gives:

$$\frac{\partial u}{\partial y} dy = \frac{1}{2} \left(\frac{\partial u}{\partial y} + \frac{\partial v}{\partial x} \right) dy + \frac{1}{2} \left(\frac{\partial u}{\partial y} - \frac{\partial v}{\partial x} \right) dy \tag{4.4a}$$

Similarly, we can show that:

$$\frac{\partial v}{\partial x} dx = \frac{1}{2} \left(\frac{\partial v}{\partial x} + \frac{\partial u}{\partial y} \right) dx + \frac{1}{2} \left(\frac{\partial v}{\partial x} - \frac{\partial u}{\partial y} \right) dx \tag{4.4b}$$

Substituting Eqs. 4.4 into Eq. 4.2 for \vec{V} , and rearranging gives:

$$\therefore \vec{V} = \begin{matrix} \left[\hat{i} \left[u + \frac{\partial u}{\partial x} dx + \frac{1}{2} \left(\frac{\partial u}{\partial y} - \frac{\partial v}{\partial x} \right) dy + \frac{1}{2} \left(\frac{\partial u}{\partial y} + \frac{\partial v}{\partial x} \right) dy \right] \right. \\ \left. + \hat{j} \left[v + \frac{\partial v}{\partial y} dy + \frac{1}{2} \left(\frac{\partial v}{\partial x} - \frac{\partial u}{\partial y} \right) dx + \frac{1}{2} \left(\frac{\partial v}{\partial x} + \frac{\partial u}{\partial y} \right) dx \right] \right] \end{matrix} \tag{4.5}$$

translation linear deform. rotation angular deform.

(Compare with sketched behaviors in section 4.1)

From this expanded expression, Eq. 4.5, we can now correlate the mathematical terms with the corresponding motion they represent. Thus, we have illustrated how the motions and deformations of a fluid element moving through a velocity field can be mathematically “decomposed” into the constituent mathematical expressions reflective of translation, rotation, and angular and linear deformation.

4.2.1 Use of Tensors

A higher-order form of vector that can help generalize Eq. 4.5 is a second-order [tensor](#), which is a double-indexed mathematical expression reflecting (in this case) the *plane of application* and the *direction of action* of a tensor property relative to that plane. For example, deformation acts in directions either normal or parallel to a specified plane, while motions of rotation only act normal to a specified plane.

Note that a tensor is just a higher form of a vector. The word “tensor” is a generic term applied to mathematical functions which transform according to certain laws as a reference coordinate system is rotated about the origin. For a Cartesian coordinate system (where unit vector differentiation has no effect), we define the rank or “order” of a tensor according to the number of scalar components required to completely define it, which is equivalent to the number of coordinates comprising the reference system raised to the order power. So, for our two-dimensional example, there are two reference coordinates (x and y). Raising the coordinate number (2) to the “zero” order (i.e. $2^0=1$) yields one scalar component, which is the number of components required to specify a “zeroth-order” tensor, which is a *scalar* (of course), and is not dependent on the coordinate orientation. Two raised to “first” order ($2^1 = 2$) indicates two scalar components are required to define a “first-order” tensor in a two-dimensional system, which is of course what we commonly term a *vector*. And finally, two raised to the “second” order ($2^2 = 4$) indicates that four scalar components are required to define a “second-order” tensor in two dimensions. For example, we can write a two-dimensional tensor (let’s use the stress tensor) $\bar{\bar{\tau}}_{ab}$ in Cartesian coordinates as follows, where subscripts a and b are indices referencing coordinate directions for the components.

$$\bar{\bar{\tau}}_{ab} = \hat{i}\hat{i}\tau_{xx} + \hat{i}\hat{j}\tau_{xy} + \hat{j}\hat{i}\tau_{yx} + \hat{j}\hat{j}\tau_{yy} = \underbrace{\hat{i}(\hat{i}\tau_{xx} + \hat{j}\tau_{xy})}_{\text{tensor dyad}} + \underbrace{\hat{j}(\hat{i}\tau_{yx} + \hat{j}\tau_{yy})}_{\text{tensor dyad}} = \begin{bmatrix} \hat{i} & \hat{j} \end{bmatrix} \begin{bmatrix} \hat{i}\tau_{xx} & \hat{j}\tau_{xy} \\ \hat{i}\tau_{yx} & \hat{j}\tau_{yy} \end{bmatrix}$$

Here, the first unit vector in the dyads (the tensor components) indicates the action plane (at least for fluids), and the parenthetical vector indicates the direction of the action relative to that surface. For example, the first dyad acts on the x-plane (a plane defined by a x-direction normal). The subsequent direction of action relative to that x-plane is a vector given by $\hat{i}\tau_{xx} + \hat{j}\tau_{xy}$, where τ_{xx} acts in the x-direction, and τ_{xy} acts in the y-direction.

Tensors work well in describing multidirectional behavior, such as deformations and stresses in a fluid. In common practice, the unit vectors are implied when writing tensors in matrix format, such that we can express the above as:

$$\underline{\underline{\tau}}_{ab} = \hat{i}\hat{i}\tau_{xx} + \hat{i}\hat{j}\tau_{xy} + \hat{j}\hat{i}\tau_{yx} + \hat{j}\hat{j}\tau_{yy} = \begin{bmatrix} \tau_{xx} & \tau_{xy} \\ \tau_{yx} & \tau_{yy} \end{bmatrix}$$

For further background on tensors, and their use, you can check out a nice NASA technical memorandum by [Kolecki \(2002\)](#), for a reasonable explanation of the importance and applications of tensors.

4.2.2 Decomposition in Tensor Notation

Applying tensor notation to our decomposition expression, we now can express Eq. 4.1 as (where $d\vec{r} = dx\hat{i} + dy\hat{j}$):

$$\begin{aligned} \vec{V} &= \vec{V}_p + d\vec{V} = \vec{V}_p + \frac{\partial \vec{V}}{\partial x} dx + \frac{\partial \vec{V}}{\partial y} dy = \vec{V}_p + d\vec{r} \cdot (\nabla \vec{V})_{at\ p} = \vec{V}_p + d\vec{r} \cdot \begin{bmatrix} \frac{\partial u}{\partial x} & \frac{\partial v}{\partial x} \\ \frac{\partial u}{\partial y} & \frac{\partial v}{\partial y} \end{bmatrix} \\ &= (\mathbf{u}_p \hat{i} + \mathbf{v}_p \hat{j}) + (dx \hat{i} + dy \hat{j}) \cdot \left(\hat{i}\hat{i} \frac{\partial u}{\partial x} + \hat{i}\hat{j} \frac{\partial v}{\partial x} + \hat{j}\hat{i} \frac{\partial u}{\partial y} + \hat{j}\hat{j} \frac{\partial v}{\partial y} \right) \end{aligned}$$

2nd order tensor \Rightarrow surface of action + direction

Expansion shows this is identical to Eq. 4.5, the decomposed formulation above:

$$\vec{V} = \begin{cases} \hat{i} \left[\mathbf{u}_p + \frac{\partial u}{\partial x} dx + \frac{1}{2} \left(\frac{\partial u}{\partial y} - \frac{\partial v}{\partial x} \right) dy + \frac{1}{2} \left(\frac{\partial u}{\partial y} + \frac{\partial v}{\partial x} \right) dy \right] \\ + \hat{j} \left[\mathbf{v}_p + \frac{\partial v}{\partial y} dy + \frac{1}{2} \left(\frac{\partial v}{\partial x} - \frac{\partial u}{\partial y} \right) dx + \frac{1}{2} \left(\frac{\partial v}{\partial x} + \frac{\partial u}{\partial y} \right) dx \right] \end{cases}$$

So, rewriting Eq. 4.5 in terms of tensors, gives:

$$\vec{V} = \vec{V}_p + d\vec{r} \cdot \underbrace{\begin{bmatrix} \frac{\partial u}{\partial x} & \frac{1}{2} \left(\frac{\partial v}{\partial x} + \frac{\partial u}{\partial y} \right) \\ \frac{1}{2} \left(\frac{\partial u}{\partial y} + \frac{\partial v}{\partial x} \right) & \frac{\partial v}{\partial y} \end{bmatrix}}_{\text{Rate-of-Strain Tensor, } \vec{E}_{ab}} + d\vec{r} \cdot \underbrace{\begin{bmatrix} 0 & \frac{1}{2} \left(\frac{\partial v}{\partial x} - \frac{\partial u}{\partial y} \right) \\ \frac{1}{2} \left(\frac{\partial u}{\partial y} - \frac{\partial v}{\partial x} \right) & 0 \end{bmatrix}}_{\text{Vorticity Tensor, } \vec{\Omega}_{ab}} \quad (4.6)$$

Here, $\bar{\bar{E}}_{ab}$ is known as the rate-of-strain tensor, since it mathematically reflects all the rates of strain that can result from velocity changes. $\bar{\bar{\Omega}}_{ab}$ is termed the vorticity tensor (vorticity is discussed in section 4.3 below), since it mathematically expresses all the velocity changes that give rise to fluid rotation. Thus, we can write our final expression for the decomposed fluid motion as:

$$\bar{V} = \bar{V}_p + d\bar{r} \cdot \bar{\bar{E}}_{ab} + d\bar{r} \cdot \bar{\bar{\Omega}}_{ab} \quad (4.7)$$



Rate-of-strain
tensor



Vorticity
tensor

Note that in two dimensions these tensors are written as:

$$\bar{\bar{E}}_{ab} = \begin{bmatrix} \dot{\epsilon}_{xx} & \dot{\epsilon}_{xy} \\ \dot{\epsilon}_{yx} & \dot{\epsilon}_{yy} \end{bmatrix} = \begin{bmatrix} \frac{\partial u}{\partial x} & \frac{1}{2} \left(\frac{\partial v}{\partial x} + \frac{\partial u}{\partial y} \right) \\ \frac{1}{2} \left(\frac{\partial u}{\partial y} + \frac{\partial v}{\partial x} \right) & \frac{\partial v}{\partial y} \end{bmatrix} \quad (4.8)$$

and

$$\bar{\bar{\Omega}}_{ab} = \begin{bmatrix} \Omega_{xx} & \Omega_{xy} \\ \Omega_{yx} & \Omega_{yy} \end{bmatrix} = \begin{bmatrix} 0 & \frac{1}{2} \left(\frac{\partial v}{\partial x} - \frac{\partial u}{\partial y} \right) \\ \frac{1}{2} \left(\frac{\partial u}{\partial y} - \frac{\partial v}{\partial x} \right) & 0 \end{bmatrix} \quad (4.9)$$

Here the vorticity tensor, $\bar{\bar{\Omega}}_{ab}$, has no components in the direction of the normal to the bounding planes (or bounding line in 2-D) of application. As was shown in section 4.1.2, rotation (i.e. vorticity) requires a change in the velocity components acting perpendicular to the normal of the bounding plane. Thus, a change in the velocity component normal to a bounding plane cannot contribute to rotation (such changes only contribute to linear deformation). Additionally, since $\epsilon_{xy} = \epsilon_{yx}$ in the rate of strain matrix, this implies that the rate of strain tensor, $\bar{\bar{E}}_{ab}$, is a [symmetric tensor](#); conversely, since

$\Omega_{xy} = -\Omega_{yx}$ in the vorticity matrix, this indicates that the vorticity tensor, $\bar{\bar{\Omega}}_{ab}$, is an *antisymmetric* tensor. Confused? This YouTube [site](#) might help.

If we expand our consideration of fluid motion to three dimensions (Cartesian), we of course end up with more terms in a tensor. As was pointed out above, for a second-order tensor the number of components is equal to the number of independent coordinates raised to the second power. So for a full three-dimensional system (x, y, z), tensors will

contain nine scalar components (3^2). So, in three dimensions the rates of strain and vorticity tensors become:

$$\bar{\mathbf{E}}_{ab} = \begin{bmatrix} \dot{\varepsilon}_{xx} & \dot{\varepsilon}_{xy} & \dot{\varepsilon}_{xz} \\ \dot{\varepsilon}_{yx} & \dot{\varepsilon}_{yy} & \dot{\varepsilon}_{yz} \\ \dot{\varepsilon}_{zx} & \dot{\varepsilon}_{zy} & \dot{\varepsilon}_{zz} \end{bmatrix} = \begin{bmatrix} \frac{\partial u}{\partial x} & \frac{1}{2} \left(\frac{\partial v}{\partial x} + \frac{\partial u}{\partial y} \right) & \frac{1}{2} \left(\frac{\partial w}{\partial x} + \frac{\partial u}{\partial z} \right) \\ \frac{1}{2} \left(\frac{\partial u}{\partial y} + \frac{\partial v}{\partial x} \right) & \frac{\partial v}{\partial y} & \frac{1}{2} \left(\frac{\partial w}{\partial y} + \frac{\partial v}{\partial z} \right) \\ \frac{1}{2} \left(\frac{\partial u}{\partial z} + \frac{\partial w}{\partial x} \right) & \frac{1}{2} \left(\frac{\partial v}{\partial z} + \frac{\partial w}{\partial y} \right) & \frac{\partial w}{\partial z} \end{bmatrix} \quad (4.10)$$

and

$$\bar{\mathbf{\Omega}}_{ab} = \begin{bmatrix} \Omega_{xx} & \Omega_{xy} & \Omega_{xz} \\ \Omega_{yx} & \Omega_{yy} & \Omega_{yz} \\ \Omega_{zx} & \Omega_{zy} & \Omega_{zz} \end{bmatrix} = \begin{bmatrix} 0 & \frac{1}{2} \left(\frac{\partial v}{\partial x} - \frac{\partial u}{\partial y} \right) & \frac{1}{2} \left(\frac{\partial w}{\partial x} - \frac{\partial u}{\partial z} \right) \\ \frac{1}{2} \left(\frac{\partial u}{\partial y} - \frac{\partial v}{\partial x} \right) & 0 & \frac{1}{2} \left(\frac{\partial w}{\partial y} - \frac{\partial v}{\partial z} \right) \\ \frac{1}{2} \left(\frac{\partial u}{\partial z} - \frac{\partial w}{\partial x} \right) & \frac{1}{2} \left(\frac{\partial v}{\partial z} - \frac{\partial w}{\partial y} \right) & 0 \end{bmatrix} \quad (4.11)$$

In Eqs. 4.10 and 4.11 we include a third component of velocity in the z-direction, w , such that $\vec{V} = u\hat{i} + v\hat{j} + w\hat{k}$. Note that in three dimensions the rate-of-strain tensor remains symmetric and the vorticity tensor also remains antisymmetric.

Note also that a (3-D) symmetric tensor, like the rate of strain tensor, has six independent components, since $\varepsilon_{ij} = \varepsilon_{ji}$, where i and j represent the system coordinates (e.g. x , y , or z). For the rate of strain tensor [where $\varepsilon_{xy} = \varepsilon_{yx}$, $\varepsilon_{zy} = \varepsilon_{yz}$, and $\varepsilon_{xz} = \varepsilon_{zx}$], the six unique components account for all the types of strain rates that can be applied to the various surfaces of a fluid [we will revisit this when the differential equation of momentum is derived in Chapter 5]. Conversely, a (3-D) antisymmetric tensor, such as the vorticity tensor, has only three independent components, since $\Omega_{ij} = -\Omega_{ji}$. Note that along the diagonal the only value that can satisfy that criterion is 0, which reduces the independent components by three. Thus, the independent vorticity components (three) reflect the respective rotations in each respective coordinate direction.

Now that we have shown that we can mathematically decompose fluid motion into its component behaviors, we will make use of these elements to analyze and model fluid behavior. In Chapter 5, it is shown that the rate-of-strain tensor is used to model the stress field within a fluid, and to assess the impact of surface forces on fluid motion via Newton's second law: a critical step in the development of the governing differential equations of fluid momentum. The vorticity tensor, and the parallel concept of circulation (the summation of vorticity over a fixed area), is employed to account for the

rotational behavior of a fluid. To begin this process, in the following section we first address the concept of vorticity, and show how to assess and describe local fluid rotation.

4.3 Vorticity

Vorticity is the term applied to the angular rotation of a fluid. To develop a mathematical description of the angular rotation, we examine the behavior of two infinitesimal orthogonal line segments fixed in a fluid, as shown below. As was done in the examination of general fluid rotation in Section 4.1.2, we again assume that these line segments rotate in such a manner as to yield a positive rotation of each line segment (counter clockwise). We also again assume that Δt is infinitesimal, and that the degree of rotation of the element can be characterized by similar infinitesimal angular changes, as shown in figure 4.6.

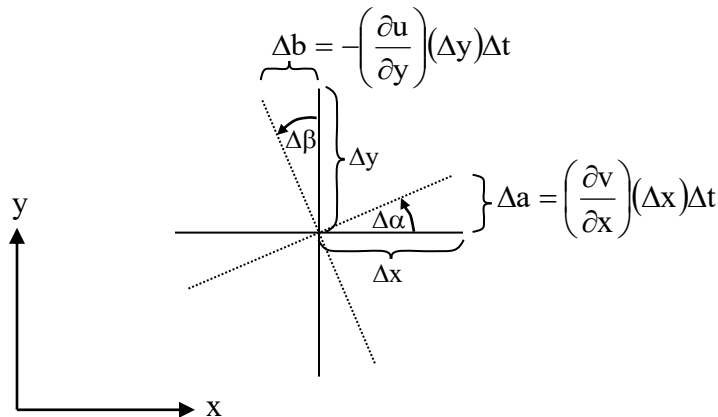


Figure 4.6 Characterization of angular rotation of two orthogonal line segments

The angular velocity of each line segment is assumed to be the differential change in angular rotation over time, Δt . However, to relate the angular rotation to characteristic changes in the velocity components, we relate the angular rotation to the arc length displacement of the line segment, identical to the process employed in our discussion of rotation in Section 4.1.2. Thus, for the rotation of the horizontal line segment shown above, this displacement is given by $\Delta a = (\partial v / \partial x)(\Delta x)\Delta t$, and thus:

$$\begin{aligned} \Omega \text{ of line } x &= \lim_{\Delta t \rightarrow 0} \frac{\Delta \alpha}{\Delta t} = \lim_{\Delta t \rightarrow 0} \frac{\Delta a / \Delta x}{\Delta t} \\ &= \lim_{\Delta t \rightarrow 0} \frac{\left(\frac{\partial v}{\partial x} \cancel{\Delta x} \cancel{\Delta t} \right) / \cancel{\Delta x}}{\cancel{\Delta t}} = \frac{\partial v}{\partial x} \end{aligned}$$

Likewise, for the angular velocity of the vertical line segment:

$$\Omega \text{ of line } y = -\frac{\partial u}{\partial y}$$

The total angular velocity is then assumed to be the *average* angular velocity of the two orthogonal line elements, with their axis of rotation about the z-axis (out of the plane of this page), i.e.

$$\Omega_z = \frac{1}{2}(\Omega \text{ of line } x + \Omega \text{ of line } y) = \frac{1}{2}\left(\frac{\partial v}{\partial x} - \frac{\partial u}{\partial y}\right)$$

↑
rotation about z-direction coordinate

The angular velocity for the other two coordinate directions can be derived similarly, giving:

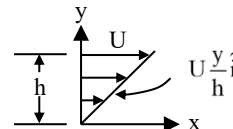
$$\Omega_x = \frac{1}{2}\left(\frac{\partial w}{\partial y} - \frac{\partial v}{\partial z}\right) \quad \text{and} \quad \Omega_y = \frac{1}{2}\left(\frac{\partial u}{\partial z} - \frac{\partial w}{\partial x}\right)$$

Thus, the total vector angular velocity for a fluid (in Cartesian coordinates) is given by:

$$\begin{aligned} \vec{\Omega} &= (\hat{i}\Omega_x + \hat{j}\Omega_y + \hat{k}\Omega_z) \\ &= \frac{1}{2}\left(\frac{\partial w}{\partial y} - \frac{\partial v}{\partial z}\right)\hat{i} + \frac{1}{2}\left(\frac{\partial u}{\partial z} - \frac{\partial w}{\partial x}\right)\hat{j} + \frac{1}{2}\left(\frac{\partial v}{\partial x} - \frac{\partial u}{\partial y}\right)\hat{k} = \frac{1}{2}\nabla \times \vec{V} \end{aligned} \quad (4.12)$$

Note that this is one half of the curl of the velocity field, which is the classical dynamical vector function relating angular velocity to the respective velocity. Since the one half is cumbersome to carry along in equations involving fluid rotation, we generally drop this coefficient and simply characterize fluid rotation by the curl of the velocity field, which we term the “vorticity,” and indicate using a lower-case omega, $\vec{\omega} = 2\vec{\Omega} = \nabla \times \vec{V}$. Note that this definition of vorticity as $\vec{\omega} = \nabla \times \vec{V}$ applies generically for all coordinate systems; however, care must be exercised in non-Cartesian coordinate systems. Additional terms will appear when determining the vorticity in cylindrical coordinates, due to the unit vector dependence upon the angular coordinate, θ (see [section 4.4.4](#) at the end of this chapter). In spherical coordinates, additional terms are generated by unit vector dependence upon *both* angular coordinates, θ and ϕ .

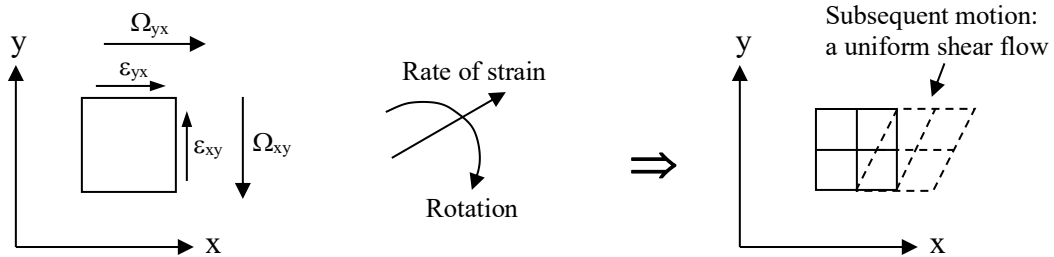
Example: Given a simple shear flow, $\vec{V} = U(y/h)\hat{i}$, determine the components of both the rate of strain and rotation tensors, and the vorticity.



Here, noting that $u = U(y/h)$ and $v = 0$, we first calculate the components of the rate of strain and vorticity tensors we developed above.

$$\begin{aligned} \varepsilon_{xx} &= \frac{\partial u}{\partial x} = 0 & \Omega_{xx} &= 0 \quad (\text{always}) \\ \varepsilon_{xy} &= \frac{1}{2} \left(\frac{\partial v}{\partial x} + \frac{\partial u}{\partial y} \right) = \frac{1}{2} \left(0 + \frac{U}{h} \right) = \frac{U}{2h} & \Omega_{xy} &= \frac{1}{2} \left(\frac{\partial v}{\partial x} - \frac{\partial u}{\partial y} \right) = \frac{1}{2} \left(0 - \frac{U}{h} \right) = -\frac{U}{2h} \\ \varepsilon_{yy} &= \frac{\partial v}{\partial y} = 0 & \Omega_{yy} &= 0 \\ \varepsilon_{yx} &= \frac{1}{2} \left(\frac{\partial u}{\partial y} + \frac{\partial v}{\partial x} \right) = \frac{U}{2h} & \Omega_{yx} &= \frac{1}{2} \left(\frac{\partial u}{\partial y} - \frac{\partial v}{\partial x} \right) = \frac{U}{2h} \end{aligned}$$

Remembering that the first index subscript indicates the plane of action, and the second index subscript indicates the direction of the action, we can qualitatively represent each of the non-zero components of strain and rotation as shown below. Here we recognize that this flow, although very simple, comprises motions of both angular deformation (opposing rotations of the primary axes) and angular rotation (like rotation of the primary axes). The result is a flow that angularly deforms at the same rate it rotates. This simultaneous, and complimentary, angular deformation and rotation maintains a non-uniform translation of the fluid parallel to the x-axis, as illustrated below.



With regard to the vorticity, the only vorticity component is in the z-direction (out of the plane of this page), such that:

$$\vec{\omega} = \nabla \times \vec{V} = \left(\frac{\partial v}{\partial x} - \frac{\partial u}{\partial y} \right) \hat{k} = -\frac{U}{h} \hat{k}$$

Here the vorticity is negative relative to the reference coordinate, or of clockwise orientation, like a ball rolling from left to right.

For some additional viewpoints on vorticity, and some further illustrations, take a look at the Wikipedia article at this [link](#).

4.4 Rate of Strain and Vorticity Equations: Cartesian and Cylindrical Coordinates

4.4.1 Rate of Strain, Cartesian Coordinates: $\vec{V} = u\hat{i} + v\hat{j} + w\hat{k}$

$$\begin{aligned}\dot{\epsilon}_{xx} &= \frac{\partial u}{\partial x} & \dot{\epsilon}_{xy} &= \frac{1}{2} \left(\frac{\partial v}{\partial x} + \frac{\partial u}{\partial y} \right) & \dot{\epsilon}_{xz} &= \frac{1}{2} \left(\frac{\partial u}{\partial z} + \frac{\partial w}{\partial x} \right) \\ \dot{\epsilon}_{yx} &= \frac{1}{2} \left(\frac{\partial v}{\partial x} + \frac{\partial u}{\partial y} \right) & \dot{\epsilon}_{yy} &= \frac{\partial v}{\partial y} & \dot{\epsilon}_{yz} &= \frac{1}{2} \left(\frac{\partial w}{\partial y} + \frac{\partial v}{\partial z} \right) \\ \dot{\epsilon}_{zx} &= \frac{1}{2} \left(\frac{\partial u}{\partial z} + \frac{\partial w}{\partial x} \right) & \dot{\epsilon}_{zy} &= \frac{1}{2} \left(\frac{\partial w}{\partial y} + \frac{\partial v}{\partial z} \right) & \dot{\epsilon}_{zz} &= \frac{\partial w}{\partial z}\end{aligned}$$

4.4.2 Vorticity, Cartesian Coordinates: $\vec{V} = u\hat{i} + v\hat{j} + w\hat{k}$

$$\vec{\omega} = \nabla \times \vec{V} = (\omega_x \hat{i} + \omega_y \hat{j} + \omega_z \hat{k}) = \left(\frac{\partial w}{\partial y} - \frac{\partial v}{\partial z} \right) \hat{i} + \left(\frac{\partial u}{\partial z} - \frac{\partial w}{\partial x} \right) \hat{j} + \left(\frac{\partial v}{\partial x} - \frac{\partial u}{\partial y} \right) \hat{k}$$

4.4.3 Rate of Strain, Cylindrical Coordinates: $\vec{V} = v_r \hat{i}_r + v_\theta \hat{i}_\theta + v_z \hat{i}_z$

$$\begin{aligned}\dot{\epsilon}_{rr} &= \frac{\partial v_r}{\partial r} & \dot{\epsilon}_{r\theta} &= \frac{1}{2} \left(r \frac{\partial}{\partial r} \left(\frac{v_\theta}{r} \right) + \frac{1}{r} \frac{\partial v_r}{\partial \theta} \right) & \dot{\epsilon}_{rz} &= \frac{1}{2} \left(\frac{\partial v_r}{\partial z} + \frac{\partial v_z}{\partial r} \right) \\ \dot{\epsilon}_{\theta r} &= \frac{1}{2} \left(r \frac{\partial}{\partial r} \left(\frac{v_\theta}{r} \right) + \frac{1}{r} \frac{\partial v_r}{\partial \theta} \right) & \dot{\epsilon}_{\theta\theta} &= \frac{1}{r} \frac{\partial v_\theta}{\partial \theta} + \frac{v_r}{r} & \dot{\epsilon}_{\theta z} &= \frac{1}{2} \left(\frac{1}{r} \frac{\partial v_z}{\partial \theta} + \frac{\partial v_\theta}{\partial z} \right) \\ \dot{\epsilon}_{zr} &= \frac{1}{2} \left(\frac{\partial v_r}{\partial z} + \frac{\partial v_z}{\partial r} \right) & \dot{\epsilon}_{z\theta} &= \frac{1}{2} \left(\frac{1}{r} \frac{\partial v_z}{\partial \theta} + \frac{\partial v_\theta}{\partial z} \right) & \dot{\epsilon}_{zz} &= \frac{\partial v_z}{\partial z}\end{aligned}$$

4.4.4 Vorticity, Cylindrical Coordinates: $\vec{V} = v_r \hat{i}_r + v_\theta \hat{i}_\theta + v_z \hat{i}_z$

$$\vec{\omega} = \nabla \times \vec{V} = (\omega_r \hat{i}_r + \omega_\theta \hat{i}_\theta + \omega_z \hat{i}_z) = \left(\frac{1}{r} \frac{\partial v_z}{\partial \theta} - \frac{\partial v_\theta}{\partial z} \right) \hat{i}_r + \left(\frac{\partial v_r}{\partial z} - \frac{\partial v_z}{\partial r} \right) \hat{i}_\theta + \frac{1}{r} \left(\frac{\partial}{\partial r} (r v_\theta) - \frac{\partial v_r}{\partial \theta} \right) \hat{i}_z$$

References

Kolecki, J. C. (2002) An Introduction to Tensors for Students of Physics and Engineering, NASA/TM—2002-211716 (link: http://www.grc.nasa.gov/WWW/k-12/Numbers/Math/documents/Tensors_TM2002211716.pdf)

Truesdell, C.A. (1954) *The Kinematics of Vorticity*. Indiana University Press, Bloomington

Study Problems

1. Consider two three-dimensional flows with velocities, $\vec{V} = c_1 x \hat{i} + c_2 y \hat{j} + c_3 z \hat{k}$, and $\vec{V} = c_1 z \hat{i} - c_2 x \hat{j} + c_3 y \hat{k}$. Determine the vorticity, the strain-rate tensor, and the rate of expansion for these flows (hint: the rate of expansion is given by the divergence).
2. A two-dimensional flow in cylindrical coordinates is given by: $\vec{V} = \left(\frac{Q}{2\pi r} \right) \hat{i}_r$. Compute the vorticity, the strain-rate tensor, and the rate of expansion for this flow (hint: the rate of expansion is given by the divergence).
3. A non-dimensional velocity field in cylindrical coordinates is given by:

$$\vec{V} = -\left(\frac{1}{r^2} \right) \hat{i}_r + 4r^2 \hat{i}_\theta$$

Determine:

- a. The components of the rate-of-strain tensor;
 - b. The vorticity of a particle at $(x,y) = (0,2)$ and $(0,0)$.
4. A non-dimensional velocity field in cylindrical coordinates is given by:

$$\vec{V} = -\left(\frac{1}{r} \right) \hat{i}_r + 4r \hat{i}_\theta$$

Determine:

- a. The components of the rate-of-strain tensor;
- b. The vorticity of a particle at $(x,y) = (0,2)$ and $(0,0)$.

5. A non-dimensional velocity field in cylindrical coordinates is given by:

$$\vec{V} = -\left(\frac{1}{r^2}\right)\hat{i}_r + 4r\left(1 - \frac{r}{3}\right)\hat{i}_\theta$$

Determine:

- The components of the rate-of-strain tensor;
 - The vorticity of a particle at $(x,y) = (0,2)$ and $(0,0)$.
6. The velocity field for a decaying, ideal line vortex is given by:

$$v_\theta = \left(\frac{\Gamma}{2\pi r}\right)\left\{1 - \exp\left(-\frac{r^2}{4\nu t}\right)\right\}$$

Where Γ is a vortex strength parameter (a constant). Let all parameters and variables be non-dimensional, and $\nu = 1$.

Determine:

- The non-zero rate-of-strain components
- The vorticity.

Plot separate graphs for $0 \leq r \leq 4$ of the normalized (1) vorticity $\left(\frac{4\omega\pi\nu}{\Gamma}\right)$, and (2) strain rate $\left(\frac{2\pi\varepsilon_{r\theta}}{\Gamma}\right)$. Show plots on each graph for $t = 0, 1, 6$ (note: you will need to use L'Hopital's Rule for r and $t \rightarrow 0$).

7. The velocity field for a decaying, ideal line vortex is given by:

$$v_\theta = \left(\frac{Hr}{8\pi\nu t^2}\right)\exp\left(-\frac{r^2}{4\nu t}\right)$$

Where H is a vortex strength parameter (a constant). Let all parameters and variables be non-dimensional, and $\nu = 1$. Determine:

- the non-zero rate-of-strain components;
- the vorticity.

Plot separate graphs for $0 \leq r \leq 4$ of non-dimensional (1) velocity $\left(\frac{8v_\theta\pi\nu}{H}\right)$, (2) vorticity $\left(\frac{16\omega\pi\nu}{H}\right)$, and (3) strain rate $\left(\frac{32\pi\nu^2\varepsilon_{r\theta}}{H}\right)$. Show 3 plots on each graph for $t = 0, 1, 3$ (note: you will need to use L'Hopital's Rule for r and $t \rightarrow 0$).

Chapter 5

Differential Equations of Motion

Contents

5.1 Background	83
5.2 The Differential Continuity Equation: Via a Differential Analysis	85
5.3 The Differential Continuity Equation: Via the Divergence Theorem	91
5.4 Special Cases of the Continuity Equation	93
5.4.1 Steady Flow	93
5.4.2 Incompressible Flow	93
5.5 Uses of the Continuity Equation	94
5.6 The Momentum Differential Equation for a Fluid: The Navier-Stokes Equation	98
5.6.1 Modeling of Differential Surface and Body Forces	100
5.6.2 The Differential Momentum Equation	103
5.6.3 Relating Stresses to Fluid Rates of Strain	103
5.6.4 Reducing the Momentum Equation to the Navier-Stokes Equation	108
5.7 Utilization of the Incompressible Continuity and Navier-Stokes Equations	111
5.8 The Governing Equations for Incompressible Flow	112
5.8.1 Stresses on an Incompressible Fluid: Cartesian Coordinates	112
5.8.2 Stresses on an Incompressible Fluid: Cylindrical Coordinates	113
5.8.3 Continuity and N-S Equations in Cartesian Coordinates	113
5.8.4 Continuity and N-S Equations in Cylindrical Coordinates	113

In this book, it is assumed that students have a basic background in undergraduate fluid mechanics, particularly the use of basic control volume equations as they apply to conservation of mass and momentum. If you feel that you don't have a reasonable grounding in the basics of control volume analysis, it is recommended that you review this material in a standard undergraduate fluid mechanics text (e.g. [Fluid Mechanics, Fox & McDonald, Chapter 4](#)), since the derivation of the differential equations of fluid motion done in this chapter will make use of several underlying control volume concepts.

5.1 Background

To understand the capabilities of a control volume analysis versus a differential analysis, let's review their respective strengths and weaknesses. In both cases, we assume that we are conducting a coupled analysis of the equations of both continuity and momentum.

Recall from your undergraduate studies that a control volume approach develops equations that assume that the velocity and property distributions are known for a flow entering and exiting a fixed region in space, such as a pipe or jet engine. In many practical cases, the velocities (and other properties, such as density and temperature) are often assumed to be uniform over the entrance and/or exit of the control volume. Given the assumed flow characteristics, the solution of the appropriate integral equations is relatively straightforward. However, the results of such calculations yield only the global characteristics of a flow system, such as the resulting force or thrust generated by the change in momentum across a control volume. Thus, the control volume equations of momentum and mass provide useful, but generally approximate, results and are reasonably easy to employ.

In contrast, a differential approach develops more sophisticated differential equations that can yield very detailed information regarding local velocity and other property information, requiring only the appropriate boundary and initial conditions to allow solution of the equations. However, the differential equations are quite complex, such that their complete solution may require sophisticated mathematical techniques or very advanced numerical/computational approaches. The solution of the differential equations provides detailed velocity and property field information, which can subsequently be: (1) employed to assess local forces on the constraining boundaries, or (2) combined with control volume approaches to assess more accurate global characteristics, such as thrust or flow-induced drag. Luckily, for our purposes, there are a number of simple flows that lend themselves to complete differential analysis, for which one can develop closed-form solutions of the governing differential equations, before branching out into more complicated flows that generally require substantial numerical analysis to achieve a solution.

In this and the following chapter, our objective is to develop systematically the basic differential equations of continuity (i.e. mass conservation) and momentum (i.e. the Navier Stokes equation). As you will see, these sets of equations are key elements for our subsequent assessment of fluid behavior. In particular, in Chapter 6, we demonstrate the application of these equations for the determination of the velocity and shear stress fields for some simple laminar flows. In addition, Chapter 12 addresses solution techniques for more complicated laminar flows. However, the differential equations of continuity and momentum are the general basis for the material we discuss throughout the rest of this book. In the present chapter, we begin our assessment of fluid dynamics by the derivation of the differential equations of both continuity and momentum.

5.2 The Differential Continuity Equation: via a Differential Analysis

Recalling our discussion in Chapter 1 of the characterization of forces acting on a differential fluid element, in this section we employ that same differential element approach for the analysis of fluid continuity, or conservation of mass. We perform our derivation in Cartesian coordinates, but similar approaches can clearly be employed using cylindrical or spherical coordinates; the resulting equations for a cylindrical coordinate system are shown in [Section 5.8.2](#). The equations for spherical coordinates can be found [here](#). As we did in Chapter 1, we start by assuming an infinitesimal differential element of volume, $d\forall = dx dy dz$, where dx , dy , and dz are the differential dimensions of the element in the respective coordinate directions, as shown in figure 5.1.

We next assume that the local density and velocity (in terms of the respective directional components) *at the center of the element* are given by ρ , u , v , and w . Our objective is to assess the changes in mass both *within* and *across* this differential volume using an integral control volume equation applied to this differential element of the form:

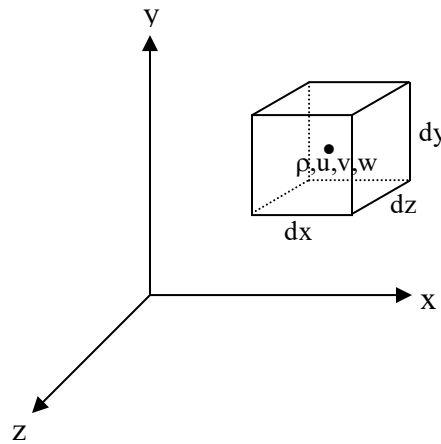


Figure 5.1 The basic differential fluid element in Cartesian coordinates.

$$\frac{\partial}{\partial t} \iiint_{C.V.} \rho d\forall + \iint_{C.S.} \rho \vec{V} \cdot d\vec{A} = 0 \quad (5.1)$$

In Eq. 5.1, C.V. implies integration across the entire control volume, and C.S. implies integration over the entire control surface bounding the control volume. The volume of the differential element is $d\forall = dx dy dz$, and the areas of the bounding control surfaces, across which the fluid can move into or out of the differential element, are given by the respective sides of the element, $dA_x = dy dz$, $dA_y = dx dz$, and $dA_z = dx dy$. To make our derivation process easier to follow, we note that we can separate the integral term reflecting the mass crossing the control surface of the differential element into the three integrals representing the mass crossing the x , y , and z surfaces respectively, such that:

$$\iint_{C.S.} \rho \vec{V} \cdot d\vec{A} = \iint_{C.S.x} \rho \vec{V} \cdot d\vec{A} + \iint_{C.S.y} \rho \vec{V} \cdot d\vec{A} + \iint_{C.S.z} \rho \vec{V} \cdot d\vec{A}$$

Using the x -direction surface integral as an example, we now determine the amount of mass crossing the two x -surfaces of the differential element, in terms of the density, ρ ,

and the x-direction velocity, u . The result is $\iint_{C.S.x} \rho \vec{V} \cdot d\vec{A} = \iint_{C.S.x} \rho u \hat{i} \cdot dA_x \hat{n}$, where u is the x-direction velocity component parallel to the *outward* normal unit vector (shown as \hat{n}) for the x-surfaces of the differential element. Note that $\hat{n} = \pm \hat{i}$, depending on the direction of the outward normal for the respective x-surface of the differential element, relative to the fixed coordinate system. Also, note that this integration only requires knowledge of the x-direction velocity, u , since the y-direction and z-direction velocities are *parallel* to the x-surfaces, and will contribute no mass flow across those surfaces. To begin, we need to establish the values of the density and the u -velocity at the point where they cross the two differential x-directed surfaces of area $dA_x = dydz$ (the magnitude of both the left and right surfaces of the differential element shown in figure 5.1).

To establish the changes of ρ and u that occur across the differential element, we start by assuming that ρ and u are the base values at the *center* of the differential element. That being the case, we can make use of a [Taylor series expansion](#) for both ρ and u to approximate the values of density and velocity at the x-surface boundaries. Recall from calculus that if we know (or we assume we know) the value of a function, call it $F(x, y, z)$, at some spatial location, x, y, z , then we can determine the value of the function at a nearby location removed by a differential amount, call it Δx , as:

$$F(x + \Delta x, y, z) = F(x, y, z) + \frac{\partial F}{\partial x} \Delta x + \frac{1}{2!} \frac{\partial^2 F}{\partial x^2} (\Delta x)^2 + \frac{1}{3!} \frac{\partial^3 F}{\partial x^3} (\Delta x)^3 + \dots (\text{higher order terms}) \quad (5.2)$$

In the mathematical sense, this expression would be termed the power series expansion of F upon x . We also note that the series must be convergent to a finite value, and not divergent. However, convergence is always the case for real fluid systems. Now, if Δx is very small, which it is since we are assuming that the differential element is infinitesimally small, then higher powers of Δx , such as Δx^2 and Δx^3 , will be much smaller--so small, that they can be considered *negligible* compared to Δx . This suggests that the higher-order terms in the Taylor series become negligible when we let $\Delta x \rightarrow 0$, such that $\Delta x \Rightarrow dx$. We thus can approximate that:

$$\lim_{\Delta x \rightarrow 0} F(x + \Delta x, y, z) = F(x + dx, y, z) \cong F(x, y, z) + \frac{\partial F}{\partial x} dx \quad (5.3)$$

This form of the Taylor series is known as a *truncated Taylor series*, and is assumed applicable in the limit of an infinitesimal differential element.

So, to establish property changes of ρ and u across the differential element in the x -direction, we apply this truncated Taylor series to model the property values at the right and left faces of the element. For example, for the density at the right face we write:

$$\rho_{\text{right face}} = \rho + \frac{\partial \rho}{\partial x} \left(+ \frac{dx}{2} \right) = \rho + \frac{\partial \rho}{\partial x} \frac{dx}{2} \tag{5.4}$$

Here ρ is the assumed value at the center of the differential element, and $+dx/2$ is the distance that the right face of the element is removed from the center of the element. Note that this is a change in *the positive x-direction*, and thus the plus sign (for emphasis of this point). In contrast, the density at the left face of the differential element will be:

$$\rho_{\text{left face}} = \rho + \frac{\partial \rho}{\partial x} \left(- \frac{dx}{2} \right) = \rho - \frac{\partial \rho}{\partial x} \frac{dx}{2} \tag{5.5}$$

Here, the change in sign is a result of the left face being removed $- dx/2$ from the center of the element *in the negative x-direction* (thus, the negative value). Similar expressions for the x -direction velocity, u , at the right and left faces of the differential element can be written as:

$$u_{\text{right face}} = u + \frac{\partial u}{\partial x} \frac{dx}{2} \quad \text{and} \quad u_{\text{left face}} = u - \frac{\partial u}{\partial x} \frac{dx}{2} \tag{5.6}$$

In Eq. 5.6, u is again the assumed value at the center of the differential element.

Using these values of density and velocity at the right and left faces of the differential element, we can now assess the mass flows across the x -surfaces of the element in figure 5.2.

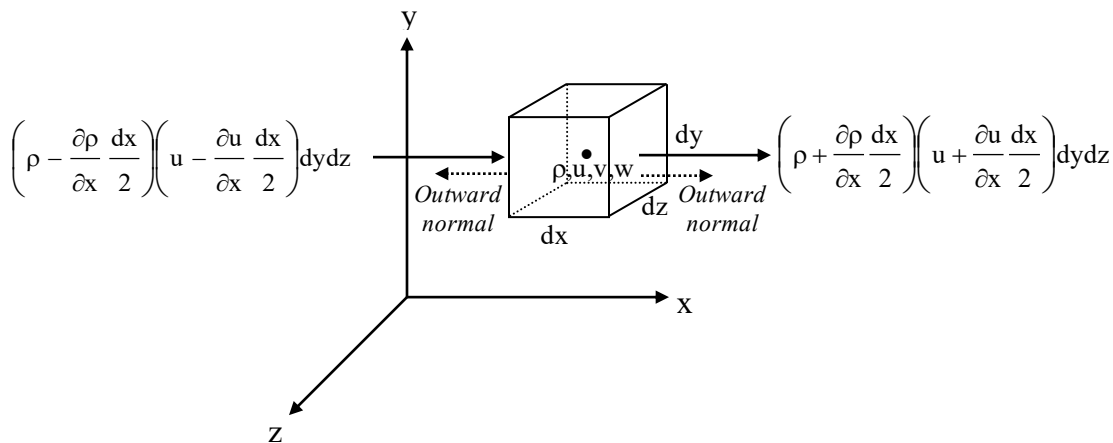


Figure 5.2 Representation of the differential mass flows across the x -surfaces of a differential fluid element.

Note that we assume that all flows (velocities) are in the positive direction relative to the coordinate direction x [density has no direction, being a scalar]. By doing this, we realize that when we later solve the differential equations, that a positive or negative result for the u -velocity will reflect the *direction of the u -velocity relative to the positive direction of the x -coordinate* we employ for the solution procedure.

We now use the respective values of density and velocity at the x -surfaces of the element to establish the mass flows across the element, for the x -direction only. Recall from above that:

$$\iint_{C.S.x} \rho \vec{V} \cdot d\vec{A} = \iint_{C.S.x} \rho u \hat{i} \cdot dA_x \hat{n}$$

Remember that the dot product of the velocity relative to the direction of the surface [defined by the direction of the outward normal ($\hat{n} = \pm \hat{i}$) from the element surface, relative to the coordinate system] determines whether the integrated mass flow is considered positive or negative. And since we have assumed all velocities (for the sake of this derivation) to be in a positive coordinate direction, the outward normal unit vector, \hat{n} , will determine whether the mass flow is considered positive or negative in the subsequent equation.

So, utilizing our expressions from Eqs. 5.4, 5.5, and 5.6, we can sum the flows of mass across the x -surfaces (defined by their outward normal relative to the x -direction, as shown in figure 5.2), as:

$$\begin{aligned} \iint_{C.S.x} \rho \vec{V} \cdot d\vec{A} &= \left(\rho + \frac{\partial \rho}{\partial x} \frac{dx}{2} \right) \left(u + \frac{\partial u}{\partial x} \frac{dx}{2} \right) \hat{i} \cdot (dydz)(+\hat{i}) + \left(\rho - \frac{\partial \rho}{\partial x} \frac{dx}{2} \right) \left(u - \frac{\partial u}{\partial x} \frac{dx}{2} \right) \hat{i} \cdot (dydz)(-\hat{i}) \\ &= \left(\rho + \frac{\partial \rho}{\partial x} \frac{dx}{2} \right) \left(u + \frac{\partial u}{\partial x} \frac{dx}{2} \right) dydz - \left(\rho - \frac{\partial \rho}{\partial x} \frac{dx}{2} \right) \left(u - \frac{\partial u}{\partial x} \frac{dx}{2} \right) dydz \end{aligned} \quad (5.7)$$

Eq. 5.7 reflects the only mass flows crossing the two x -surfaces of the differential element. Now expanding the terms on the right side of Eq.5.7, and canceling and combining like terms, we have:

$$\begin{aligned} \iint_{C.S.x} \rho \vec{V} \cdot d\vec{A} &= \left(\cancel{\rho u} + \rho \frac{\partial u}{\partial x} \frac{dx}{2} + u \frac{\partial \rho}{\partial x} \frac{dx}{2} + \frac{\partial \rho}{\partial x} \frac{\partial u}{\partial x} \frac{dx^2}{4} \right) dydz \\ &\quad - \left(\cancel{\rho u} - \rho \frac{\partial u}{\partial x} \frac{dx}{2} - u \frac{\partial \rho}{\partial x} \frac{dx}{2} + \frac{\partial \rho}{\partial x} \frac{\partial u}{\partial x} \frac{dx^2}{4} \right) dydz \end{aligned}$$

or

$$\begin{aligned}\iint_{C.S.x} \rho \vec{V} \cdot d\vec{A} &= \rho \frac{\partial u}{\partial x} dx dy dz + u \frac{\partial \rho}{\partial x} dx dy dz \\ &= \frac{\partial}{\partial x} (\rho u) dx dy dz\end{aligned}\quad (5.8)$$

If we perform similar mass flowrate balances for the y and z surfaces, conservation of mass applied to the differential control volume gives two similar expressions:

$$\iint_{C.S.y} \rho \vec{V} \cdot d\vec{A} = \frac{\partial}{\partial y} (\rho v) dx dy dz \quad (5.9)$$

$$\iint_{C.S.z} \rho \vec{V} \cdot d\vec{A} = \frac{\partial}{\partial z} (\rho w) dx dy dz \quad (5.10)$$

Combining Eqs. 5.8, 5.9, and 5.10 for the mass flow rate in each of the three coordinate directions, we obtain the *total* mass flow across the differential element as:

$$\begin{aligned}\iint_{C.S.} \rho \vec{V} \cdot d\vec{A} &= \iint_{C.S.x} \rho \vec{V} \cdot d\vec{A} + \iint_{C.S.y} \rho \vec{V} \cdot d\vec{A} + \iint_{C.S.z} \rho \vec{V} \cdot d\vec{A} \\ \iint_{C.S.} \rho \vec{V} \cdot d\vec{A} &= \frac{\partial(\rho u)}{\partial x} dx dy dz + \frac{\partial(\rho v)}{\partial y} dx dy dz + \frac{\partial(\rho w)}{\partial z} dx dy dz\end{aligned}\quad (5.11)$$

The time rate of change of mass within the differential element, $\frac{\partial}{\partial t} \iiint_{C.V.} \rho d\forall$, is modeled by

assuming that in the limit of an infinitesimal differential element ($d\forall \rightarrow 0$), the density, ρ , is relatively uniform across $d\forall$. At first this assumption of uniformity might appear inconsistent with our previous approximation of the changes across the differential element using a truncated Taylor series. However, if we assume a linear change across the element, the *average* value of the density within the differential volume will be just ρ , the assumed value at the center of the differential element. And since we will ultimately assume that $d\forall \rightarrow 0$, we approximate that $\iiint_{C.V.} \rho d\forall \cong \rho(dx dy dz)$, and thus,

$$\frac{\partial}{\partial t} \iiint_{C.V.} \rho d\forall \cong \frac{\partial(\rho dx dy dz)}{\partial t} = \frac{\partial \rho}{\partial t} dx dy dz \quad \text{since } dx dy dz \neq f(t) \quad (5.12)$$

Note in Eq. 5.12 that $\rho = \rho(x, y, z, t)$, but $dx dy dz$ is not a function of time, and thus can be factored out of the derivative, as indicated.

Substituting Eq. 5.11 and 5.12 back into Eq. 5.1, we obtain the cumulative conservation of mass balance for the differential control volume as:

$$\frac{\partial}{\partial t} \iiint_{c.v.} \rho dV + \iiint_{c.s.} \rho \vec{V} \cdot d\vec{A} = \frac{\partial \rho}{\partial t} dx dy dz + \frac{\partial(\rho u)}{\partial x} dx dy dz + \frac{\partial(\rho v)}{\partial y} dx dy dz + \frac{\partial(\rho w)}{\partial z} dx dy dz = 0$$

Since all terms are multiplied by the differential volume, $dV=dx dy dz$, we can factor this term out of the equation, leaving only the derivative functions comprising the differential equation. It would seem that this equation is independent of the size of the assumed differential element, since $dV=dx dy dz$ does not appear in the final equation. However, remember that we assumed that our differential is infinitesimal (i.e. $dV \rightarrow 0$), which allowed us to: (1) apply the approximation of a truncated Taylor series, and (2) assume that ρ varies linearly across the element.

Therefore, the differential equation for conservation of mass is:

$$\frac{\partial \rho}{\partial t} + \frac{\partial(\rho u)}{\partial x} + \frac{\partial(\rho v)}{\partial y} + \frac{\partial(\rho w)}{\partial z} \quad \text{or} \quad \frac{\partial \rho}{\partial t} + \nabla \cdot (\rho \vec{V}) = 0 \quad (5.13)$$

Equation 5.13 is also termed the *continuity* equation [a term that we employ throughout this book], emphasizing the application of mass conservation to a continuous medium. Also note this is termed a “differential” equation, since it evolves from our assumption of an infinitesimal “differential” element with continuous properties.

We can manipulate this equation further by expanding the mass flux terms to give:

$$\underbrace{\frac{\partial \rho}{\partial t} + u \frac{\partial \rho}{\partial x} + v \frac{\partial \rho}{\partial y} + w \frac{\partial \rho}{\partial z}}_{\frac{D\rho}{Dt}} + \underbrace{\rho \frac{\partial u}{\partial x} + \rho \frac{\partial v}{\partial y} + \rho \frac{\partial w}{\partial z}}_{\rho \nabla \cdot \vec{V}} = 0 \quad (5.14)$$

As we identify, the first four terms on the left of Eq. 5.14 comprise the substantial derivative of the density, and thus the changes in density that a particle experiences as it is transported through a velocity field. The remaining three terms represent the product of the density and the divergence of the velocity field, such that the resulting equation can be written in a compact form as:

$$\frac{D\rho}{Dt} + \rho \nabla \cdot \vec{V} = 0 \quad (5.15)$$

Equation 5.15 is a generic vector representation, which is applicable in any other coordinate system (i.e. cylindrical or spherical). We further explore the significance of this vector form of the continuity equation in the following section.

5.3 The Differential Continuity Equation: via the Divergence Theorem

The derivation of the differential equation of continuity that was done in section 5.2 employs the application of a control volume analysis to a differential element, using several approximations to establish the balance of the derivative changes in velocity and density that occur across and within a differential element. That approach necessitates some sweeping assumptions of behavior as the differential volume asymptotes to zero. An alternate derivation of the differential equation of continuity can be developed in a more mathematically elegant, although less physically obvious, manner using the application of the surface integral relationships reviewed in section 2.4 to the basic control volume equation (Eq. 5.1) of continuity. Consider again the general control volume equation for continuity, given by:

$$\frac{\partial}{\partial t} \iiint_{\text{c.v.}} \rho d\forall + \iint_{\text{c.s.}} \rho \vec{V} \cdot d\vec{A} = 0$$

For a fixed size control volume (i.e. the volume is constant), the time derivative can be taken inside the integral, since the limits of integration over that volume will be fixed, and thus not a function of time ([Leibnitz rule](#)), giving:

$$\iiint_{\text{c.v.}} \frac{\partial \rho}{\partial t} d\forall + \iint_{\text{c.s.}} \rho \vec{V} \cdot d\vec{A} = 0$$

or

$$\iiint_{\forall} \frac{\partial \rho}{\partial t} d\forall + \oint_S (\rho \vec{V}) \cdot d\vec{A} = 0 \quad (5.16)$$

In Eq. 5.16, \forall implies a fixed volume in space, with S indicating the bounding surface of that volume. However, the Gauss divergence theorem (Section 2.4.1, Eq. 2.15) allows us to relate the surface integral of a vector property to the volume integral of the divergence of that property, such that we can write:

$$\oint_S (\rho \vec{V}) \cdot d\vec{A} = \iiint_{\forall} \nabla \cdot (\rho \vec{V}) d\forall \quad (5.17)$$

Substituting Eq. 5.17 into Eq. 5.16 yields;

$$\iiint_{\forall} \frac{\partial \rho}{\partial t} d\forall + \iiint_{\forall} \nabla \cdot (\rho \vec{V}) d\forall = \iiint_{\forall} \left[\frac{\partial \rho}{\partial t} + \nabla \cdot (\rho \vec{V}) \right] d\forall = 0 \quad (5.18)$$

However, since there is no stipulation of the size of the control volume to which this equation applies, this means that the integrand in this equation cannot depend on the

volume of integration. The only value of the integrand that satisfies this requirement is an integrand that is everywhere equal to zero, or

$$\frac{\partial \rho}{\partial t} + \nabla \cdot (\rho \vec{V}) = 0 \quad (5.19)$$

Equation 5.19 is, of course, the same as Eq. 5.13 that we obtained previously using a differential analysis.

Another way to consider the concept of continuity is to consider a differential amount of mass, dM , which is moving through a velocity field, \vec{V} . Assuming that this arbitrary amount of mass is distributed in a continuous manner over a differential volume, $d\forall$, we can write $dM = \rho d\forall$. Now, the change in this differential mass as it moves within the velocity field is then given by the material derivative of dM , such that:

$$\frac{D}{Dt}(dM) = \frac{D}{Dt}(\rho d\forall) = 0 \quad (5.20)$$

We set the derivative in Eq. 5.20 to zero, since there can be no change in the amount of mass as it moves through the field. Expanding the right side of Eq. 5.20 gives:

$$\frac{D}{Dt}(\rho d\forall) = \rho \frac{D(d\forall)}{Dt} + d\forall \frac{D\rho}{Dt} = 0$$

or

$$\frac{1}{d\forall} \frac{D(d\forall)}{Dt} = -\frac{1}{\rho} \frac{D\rho}{Dt} \quad (5.21)$$

Equation 5.21 indicates that the relative change in volume of the fluid element is balanced by an opposite change in the density of the fluid. A substitution for $D\rho/Dt$ in Eq. 5.21 from the general continuity equation, Eq. 5.15, gives :

$$\frac{1}{d\forall} \frac{D(d\forall)}{Dt} = -\frac{1}{\rho} \frac{D\rho}{Dt} = \nabla \cdot \vec{V} \quad (5.22)$$

Equation 5.22 indicates that the divergence of the velocity field represents the *relative rate of expansion* of the fluid volume at a point. This equation provides a useful physical interpretation of the divergence of the velocity, and will prove useful in the simplifications of the continuity equation, as discussed in the following section.

5.4 Special Cases of the Continuity Equation

In its general form, the continuity equation is applicable to any fluid flow, regardless of the properties of the flow. And as such, the equation is equally valid for incompressible as well as compressible flows, and heavy viscous flows or dilute gas flows, to illustrate some extremes. Since it contains four dependent variables (ρ and three velocity components), it cannot be solved independently, and must be solved in conjunction with the other governing equations, such as the differential momentum equation [derived in section 5.6]. However, since the equation is a function of four independent variables (time and three spatial coordinates), utilization of the full equation is analytically and computationally complicated, and potentially intractable because of the degrees of freedom inherent in three-dimensional, unsteady flows. Fortunately, many flows of engineering utility can be configured or constrained to reduce the degrees of freedom, which allows the application of a simplified form of the continuity equation. Two of the constraints that are most commonly invoked are: (1) a steady flow, and (2) an incompressible fluid.

5.4.1 Steady Flow

A steady flow is one for which there is no time dependency of the flow. This assumes no local time rate of change in density at a point. All incompressible flows and many compressible flows, such as flow around high-speed aircraft in *steady* flight, are well approximated by this assumption. The subsequent continuity equation reduces to:

$$\frac{\partial(\rho u)}{\partial x} + \frac{\partial(\rho v)}{\partial y} + \frac{\partial(\rho w)}{\partial z} = \nabla \cdot (\rho \vec{V}) = 0 \quad (5.23)$$

While Eq. 5.23 is a simpler equation, it still includes four dependent variables, and can be quite complicated to solve.

5.4.2 Incompressible Flow

A further simplification is to specify the fluid as incompressible ($\rho = \text{constant}$). This is a reasonable approximation for essentially all liquids and isothermal flows of gases at low Mach numbers (roughly $M < 0.3$ for air). This incompressibility assumption is appropriate for many industrial and domestic flow systems, such as ducting and piping systems, flows around automobiles and ships, etc. For an incompressible flow, the substantial derivative of the density ($D\rho/Dt$) is zero, such that Eq. 5.15 reduces to:

$$\frac{D\rho}{Dt} + \rho \nabla \cdot \vec{V} = 0 \quad \Rightarrow \quad \nabla \cdot \vec{V} = 0 \quad (5.24)$$

or

$$\frac{\partial u}{\partial x} + \frac{\partial v}{\partial y} + \frac{\partial w}{\partial z} = 0 \quad \text{in Cartesian coordinates}$$

See section [5.8.2](#) for the continuity equation in cylindrical coordinates.

Since $\nabla \cdot \vec{V} = 0$, this implies that the velocity field for an incompressible flow is non-expanding. This means that any changes in a velocity component in its respective coordinate direction must be balanced by collective corresponding changes of each of the other coordinate velocity components, such that no local expansion or contraction of the fluid volume occurs. This is illustrated by Eq. 5.22 above, which indicates that:

$$\frac{1}{dV} \frac{D(dV)}{Dt} = -\frac{1}{\rho} \frac{D\rho}{Dt} = \nabla \cdot \vec{V}$$

Thus, when $\nabla \cdot \vec{V} = 0$, a fluid cannot undergo local expansion/contraction, the density, ρ , will remain constant everywhere, and the fluid will behave incompressibly. This will be true even if the fluid *could be compressed, but is not* for the particular flow process under consideration (e.g. low-speed flow of air through ducts or around bodies). In general, a vector field that has zero divergence is termed a [solenoidal](#) field.

5.5 Uses of the Continuity Equation

The continuity equation is a particularly powerful equation, which models the balance of changes between density and velocity. For incompressible flows, density change terms all drop out, and the equation relates the balance of velocity changes in the respective coordinate directions. This balance can be used to good effect, for example, to establish a third component of velocity when the other two components of velocity are known [e.g. if the functional behavior of two velocity components is known for a flow, then the third velocity component can be established via the continuity equation]. This same process also applies, of course, for two-dimensional flows, where only one known velocity component is necessary to establish the second. Additionally, the continuity equation is used to simplify the differential equation of momentum (the Navier-Stokes equation), as will be illustrated in Section 5.6.

Example: For an incompressible flow, $\vec{V}(x, y, z) = u\hat{i} + v\hat{j} + w\hat{k}$, the x- and y-direction velocities are given by $u = ax$ and $v = -by$, where a and b are constants. Determine the velocity component w , where $w = 0$ over the x-y plane at $z = 0$.

Here we apply Eq. 5.24 for incompressible flow, $\nabla \cdot \vec{V} = 0$, solving for the w term.

$$\nabla \cdot \vec{V} = \frac{\partial u}{\partial x} + \frac{\partial v}{\partial y} + \frac{\partial w}{\partial z} = 0 \quad \Rightarrow \quad \frac{\partial w}{\partial z} = -\frac{\partial u}{\partial x} - \frac{\partial v}{\partial y} = -a + b$$

Integrating, gives

$$w = (b-a)z + f(x, y)$$

But, $w = 0$ for all x, y at $z = 0$, thus $f(x, y) = 0$, and $w = (b-a)z$.

Note that when $a = b$, then $w = 0$ everywhere, and this is a classic inviscid solution for a flow impinging in the y -direction toward the x, y origin ($x = 0, y = 0$). We will revisit this type of flow in Chapter 9. However, if $b > a$, then w will be away from the x - y plane ($w > 0$ for $z > 0$, and $w < 0$ for $z < 0$). Likewise, if $b < a$, w will be towards the x - y plane. In both of these cases, the velocity change in the z -direction balances the collective velocity changes in the other two coordinate directions, either moving additional mass toward the x - y plane or moving mass away from it.

Example: Consider the generic flow behavior of a two-dimensional jet, which exits a nozzle into an otherwise quiescent flow as shown in figure 5.3.

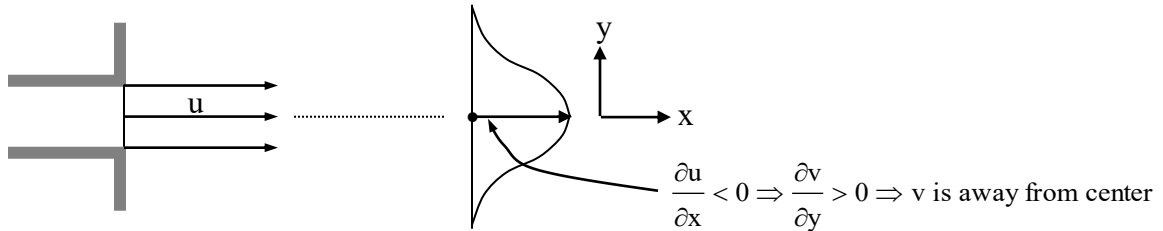


Figure 5.3 Behavior of a two-dimensional jet exiting into a quiescent flow.

As experience shows, the velocity of the jet in the streamwise x -direction, u , will decrease continuously with distance, such that along the centerline of the jet ($y = 0$), $\partial u / \partial x < 0$. Based on this observation, we want to establish how the v velocity, normal to the streamwise velocity, will behave.

Here we observe that the two-dimensional, incompressible continuity equation (in x, y) is:

$$\frac{\partial u}{\partial x} + \frac{\partial v}{\partial y} = 0 \quad \text{or rearranging,} \quad \frac{\partial v}{\partial y} = -\frac{\partial u}{\partial x} \quad (5.25)$$

Thus, if $\partial u / \partial x < 0$, this implies that $\partial v / \partial y > 0$, or that the normal velocity, v , is *away* from the axis of symmetry (in a positive y -direction for $y > 0$, and in a negative y -direction for $y < 0$). In actuality, the flow also entrains (draws in) a certain amount of flow from the quiescent fluid it is exhausting into, so that the streamline pattern for

the developing jet flow will appear approximately as shown in figure 5.4. We will show a solution for this particular type of flow later in Chapter 12.

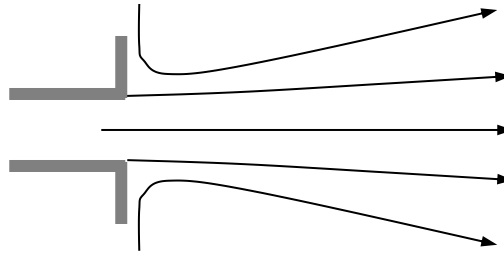


Figure 5.4 Approximate streamline pattern for a two-dimensional, steady jet.

Example: Consider a uniform, two-dimensional, incompressible flow that undergoes a change in its cross-sectional area, such as when passing through a nozzle (decreasing area) or a diffuser (increasing area). For simplicity, we will assume that u is uniform at the entrance of a nozzle, with the initial velocity and cross-sectional area given by U_o and A_o at $x = 0$, as shown in figure 5.5.

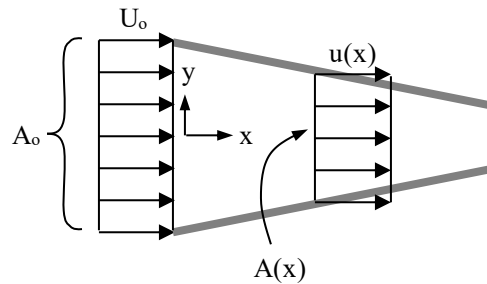


Figure 5.5 An example of uniform flow through a generic nozzle

Additionally, we assume that the streamwise velocity, $u(x)$, changes uniformly (all u -velocity components at a cross-section will be equal in magnitude). We first determine the behavior of the streamwise velocity, $u(x)$, as a function of the cross-sectional area, $A(x)$. We then determine the respective behavior of the normal velocity, $v(x)$, and the effect of the change in cross-sectional area, $dA(x)/dx$.

For a uniform flow through a constrained two-dimensional duct, as shown, using control volume considerations for an incompressible flow, we can write:

$$U_o A_o = u(x) A(x) \Rightarrow u(x) = \frac{U_o A_o}{A(x)}, \text{ and}$$

$$\frac{\partial u}{\partial x} = U_o A_o \underbrace{\left(-\frac{1}{A^2(x)} \frac{dA}{dx} \right)}_{u(x)} = -\frac{u(x)}{A(x)} \left(\frac{dA}{dx} \right) \tag{5.26}$$

Considering both a nozzle (a flow accelerator) as shown in figure 5.5, and a diffuser (a flow decelerator), from Eqs. 5.26 and 5.25 we can make the following generalizations :

$$\begin{aligned} \underline{\text{Nozzle:}} \quad A(x) \downarrow &\Rightarrow \frac{dA}{dx} < 0 \Rightarrow \frac{\partial u}{\partial x} > 0 \Rightarrow \frac{\partial v}{\partial y} < 0 \Rightarrow \text{flow toward center} \\ \underline{\text{Diffuser:}} \quad A(x) \uparrow &\Rightarrow \frac{dA}{dx} > 0 \Rightarrow \frac{\partial u}{\partial x} < 0 \Rightarrow \frac{\partial v}{\partial y} > 0 \Rightarrow \text{flow away from center} \end{aligned}$$

To establish the normal velocity behavior, $v(x,y)$, that is required to maintain a uniform streamwise velocity, $u(x)$, we write that:

$$\frac{\partial u}{\partial x} = -\frac{U_o A_o}{A(x)} \left(\frac{\frac{dA}{dx}}{A(x)} \right) = -\frac{\partial v}{\partial y} \quad \text{or} \quad \frac{\partial v}{\partial y} = \frac{U_o A_o}{A(x)} \left(\frac{\frac{dA}{dx}}{A(x)} \right) \quad (5.27)$$

Integrating Eq. 5.27 for $v(x,y)$, gives:

$$v(x,y) = U_o A_o \left(\frac{\frac{dA}{dx}}{A(x)^2} \right) \int dy = U_o A_o \left(\frac{\frac{dA}{dx}}{A(x)^2} \right) y + f(x)$$

If we assume symmetry about $x = 0$, then we surmise that $v(x,0) = 0$ on the centerline at $y = 0$, and thus $f(x) = 0$. Therefore, the general expression for $v(x,y)$ is:

$$v(x,y) = U_o A_o \left(\frac{\frac{dA}{dx}}{A(x)^2} \right) y = \frac{u(x)}{A(x)} \left(\frac{dA}{dx} \right) y \quad \text{where} \quad u(x) = \frac{U_o A_o}{A(x)} \quad (5.28)$$

To particularize this result, let a nozzle have an area distribution given by $A(x) = A_o e^{-ax}$, or an exponential nozzle. For this case we have from Eq. 5.28:

$$u(x) = \frac{U_o A_o}{A(x)} = \frac{U_o A_o}{A_o e^{-ax}} = U_o e^{ax}$$

and

$$v(x,y) = U_o A_o \left(\frac{\frac{dA}{dx}}{A(x)^2} \right) y = U_o A_o \left(\frac{-a A_o e^{-ax}}{A_o^2 e^{-2ax}} \right) y = -U_o a e^{ax} y$$

Note that if we examine the streamline equation for this flow (Eq. 3.4), we have:

$$\frac{dy}{dx} = \frac{v}{u} = \frac{-U_0 a e^{ax} y}{U_0 e^{ax}} = -ay \Rightarrow \frac{dy}{y} = -a dx$$

integrating, gives:

$$\ln y = -ax + c \Rightarrow y = C e^{-ax}$$

Here C is a constant depending on the particular streamline. For example, along the centerline, which passes through $(x,y) = (0,0)$, we get $C = 0$, and thus the streamline is the x -axis. However, for a streamline passing through $(x,y) = (0, y_0)$, $C = y_0$ and the corresponding streamline will be described by:

$$y = y_0 e^{-ax} \quad (5.29)$$

Equation 5.29 describes the family of streamlines entering at $x = 0$. Figure 5.6 shows representative streamlines for this nozzle, with various initial starting y_0 locations letting $a = 1$. Note that in this example, the streamlines that pass through $x = 0$ at $y = \pm 1$ represent the boundaries of the nozzle.

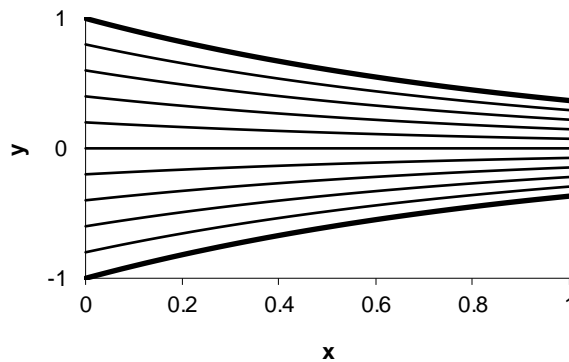


Figure 5.6 Streamlines for a two-dimensional exponential nozzle,
 $A(x) = A_0 e^{-x}$.

5.6 The Momentum Differential Equation for a Fluid: The Navier-Stokes Equation

Continuing on with our derivation of the governing equations of fluid mechanics, we now address the development of an equation that models the balance of momentum changes and forces, according to Newton's second law. Recall that Newton's second law can be

generically described as $\sum \vec{F} = \frac{\partial}{\partial t} (m\vec{V}) = m\vec{a}$, a balance of forces and changes in

momentum. Here, we will use the differential element concept to derive a differential form of Newton’s second law applicable to a fluid. There are several ways to approach this derivation, one being the use of a control volume approach, similar to what we did in the derivation of the continuity equation in section 5.3. However, a more physically appealing approach is to employ our differential element as an infinitesimal Eulerian region with fluid passing through it in a Lagrangian process.

Since we can assess the Eulerian acceleration of a fluid using the substantial derivative, as we showed in Chapter 3, this provides us with a tool to establish the acceleration of a fluid encompassed by a differential fluid element. The forces acting on the fluid can be related to: (1) surface forces acting on the respective bounding surfaces of the differential element, and (2) body forces associated with the mass contained within the differential element. We again assess these differential forces by use of a truncated Taylor series. The result of this latter process yields a stress tensor and body force vector, which we model as balancing the acceleration of the fluid, as determined from the substantial derivative of the velocity field. The figure 5.7, schematically illustrates both the generic process followed, and the desired end result, which is a single vector equation which balances velocity field momentum terms with surface and body forces.

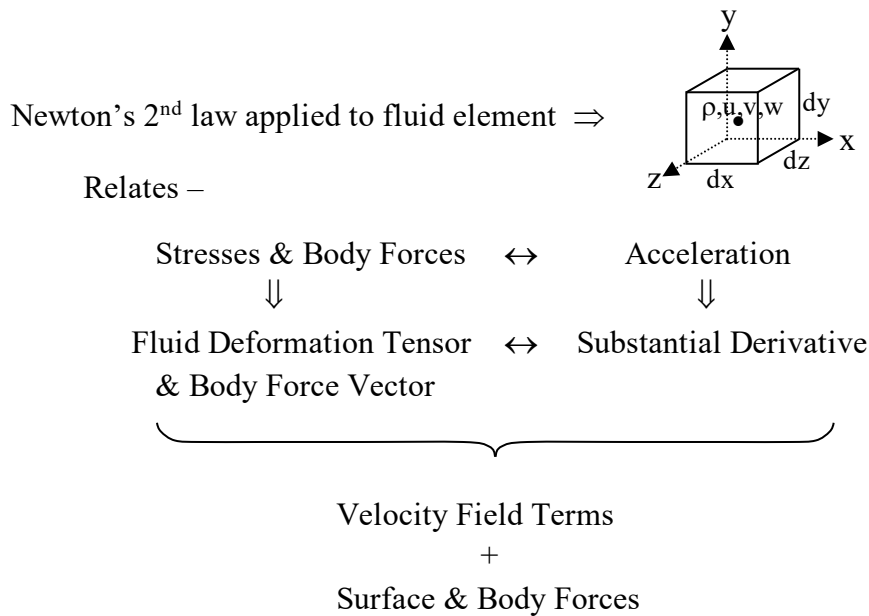


Figure 5.7 The generic process for application of Newton’s second law to a differential fluid element.

The differential equation that we will derive is termed the [Navier-Stokes equation](#), acknowledging the initial derivation of the equation, originally by [C.L. Navier](#) in 1822, with a later refinement of the derivation by [G.G. Stokes](#) in 1845. This equation is the

keystone for the science of fluid mechanics, and forms the general basis for much that follows in this text.

5.6.1 Modeling of Differential Surface and Body Forces

We begin by examining the surface forces, in the form of stresses, that exist at the surfaces of an infinitesimally small differential element of volume, $dV = dx dy dz$. Although stresses act on all surfaces of the element, to simplify our analysis, we first consider only the *x-direction stresses* that act on the six surfaces of the differential element, as shown figure 5.8. For the purposes of our differential analysis, we again use a truncated Taylor series to represent the spatial *changes* in the *x-direction stresses* across the differential element. Here one needs to recall the manner in which we define the direction of a *positive* stress acting on a surface, as discussed in Chapter 1.

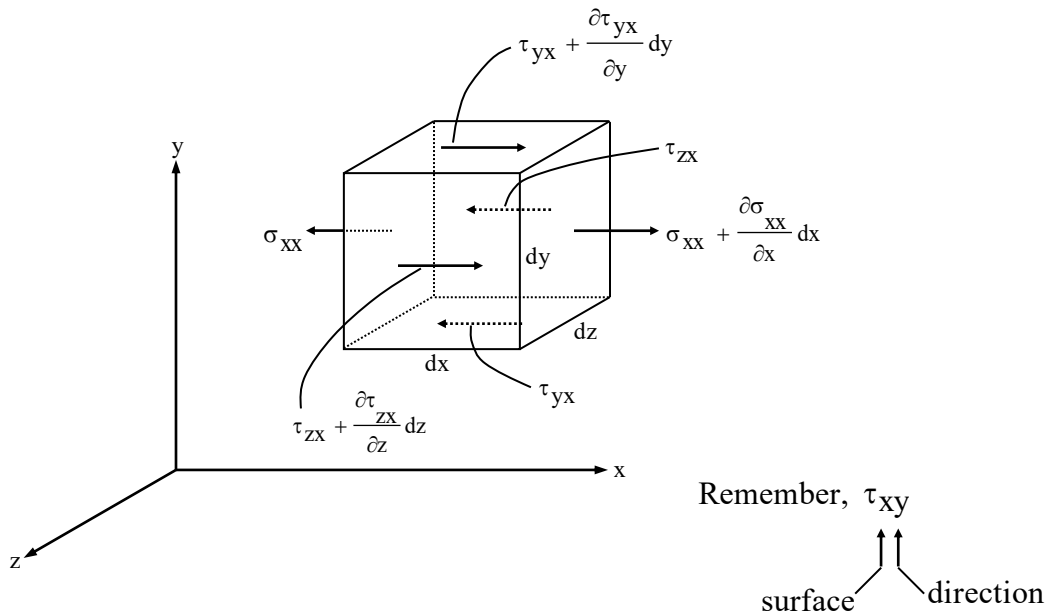


Figure 5.8 Illustration of all *x-direction stresses* acting on the bounding surfaces of a differential element. Note that we use τ to represent shear stresses, and σ to represent normal stresses.

Note that we assume that all applied stresses act with a *positive orientation* (not necessarily direction) relative to the coordinate system employed. By making this assumption during the initial derivation, when we later solve the resulting differential equation, the sign of the resultant stress will indicate whether the stress acts with a positive or negative orientation on the respective surface of interest (we will revisit this point when we engage in solutions of the Navier-Stokes equation in Chapter 6).

Recall that the direction for the positive orientation of a stress depends on the product sign of (a) the outward normal vector for a surface, and (b) the direction the stress acts on that surface. Thus, a positively-oriented stress is indicated by either: (1) a positive surface normal with a stress acting in a positive coordinate direction, or (2) a negative surface normal and a stress acting in a negative coordinate direction.

For our derivation, it is a little awkward to assume a base value for each stress at the center of the differential element, since stresses are associated with surfaces of action. Thus, we assume that all base values of the assumed stresses are those acting on the surfaces of the differential element that are closest to the origin of our coordinate system. For example, the normal stress, σ_{xx} , acting on the x-surface in the x-direction is assumed to act on the *left* face of the differential element, as shown in figure 5.8. Likewise, the shear stress, τ_{yx} , acting on the y-surface in the x-direction is assumed to act on the *bottom* face of the differential element. Note that since these respective surfaces have an outward normal that points in a negative coordinate direction, each of these assumed stresses is assumed to act in a negative x-direction to yield a positive orientation for the assumed stress, as per our convention.

As was done previously in section 5.2, a truncated Taylor series is used to characterize the changes in the respective stresses across the differential element, using the differential dimension appropriate for the direction of expansion. For example, to characterize the normal stress on the *right* facing x-surface, we expand σ_{xx} across the differential distance dx , giving a normal stress of $\sigma_{xx} + \frac{\partial \sigma_{xx}}{\partial x}(dx)$. This stress has a positive orientation in the positive x-direction since the outward normal for the right facing surface is also in the positive x-direction. Similarly, the x-directed shear stress on the top surface is

$\tau_{yx} + \frac{\partial \tau_{yx}}{\partial y}(dy)$, since we expand across dy in a positive y-direction. Likewise, this stress has its positive orientation in the positive x-direction since the outward normal for the top surface points in a positive y-direction. The other similarly modeled x-directed stresses on the differential element are as shown in figure 5.8.

Having modeled our assumed x-directed stresses on the differential element, we now apply Newton's second law, $d\vec{F} = dm\vec{a}$, using the differential stresses shown in figure 5.8 to model the resultant x-direction surface forces on each face of the differential element.

To characterize a generic differential body force, we assume that this mass-based force is characterized by some directional force field we define as $\vec{\beta}$. Such a physical field could

be a gravitational field (normally the case), a magnetic field, or even possibly an electric field (if it can cause a mass-based force on the fluid material in question). Commonly, we assume that $\vec{\beta} = \vec{g}$, where \vec{g} is a gravitational field, appropriately oriented relative to our selected coordinate system.

Having characterized all the relevant surface stresses and the body force field, we can now model the total forces acting on the differential element. Note that to establish the surface forces, we further assume that the modeled stresses act uniformly across the differential area of the respective bounding surfaces. For example, the x-directed differential force acting on the top surface of the differential element (call it $dF_{y+dy,x}$) will be a product of the x-directed shear stress times the differential area it acts on, $dA_y = dzdx$, yielding:

$$dF_{y+dy,x} = \left(\tau_{yx} + \frac{\partial \tau_{yx}}{\partial y} dy \right) (dzdx)$$

Other x-directed surface forces are modeled similarly from the assumed stresses. For the body force, we assume that both the density and the body force vector are essentially uniform across the infinitesimal differential element. Similar to the approach employed for derivation of the differential equation for continuity, the density is assumed to vary linearly across the differential element (since the element is assumed infinitesimal), and thus we use the assumed center value of density, ρ , when determining the body force. Thus, the differential mass contained within the element is assumed to be the product of the density and the differential volume, $dm = \rho(dx dy dz)$. Since the body force is proportional to the mass, the subsequent differential body force is modeled as the product of the differential mass and the body force vector field, or $d\vec{F}_{body} = \vec{\beta} \rho(dx dy dz)$.

If we now sum all x-direction forces acting on the differential element, eliminating like terms, we obtain:

body force field (e.g. gravity)
x-component
↓

$$dF_x = \rho \beta_x dx dy dz + \left(\cancel{\sigma_{xx}} + \frac{\partial \sigma_{xx}}{\partial x} dx \right) dy dz - \cancel{\sigma_{xx}} dy dz$$

$$+ \left(\cancel{\tau_{yx}} + \frac{\tau_{yx}}{\partial y} dy \right) dx dz - \cancel{\tau_{yx}} dx dz$$

$$+ \left(\cancel{\tau_{zx}} + \frac{\tau_{zx}}{\partial z} dz \right) dy dx - \cancel{\tau_{zx}} dy dx$$

or

$$dF_x = \left[\rho\beta_x + \frac{\partial\sigma_{xx}}{\partial x} + \frac{\partial\tau_{yx}}{\partial y} + \frac{\partial\tau_{zx}}{\partial z} \right] dx dy dz \quad (5.30)$$

5.6.2 The Differential Momentum Equation

Substituting Eq. 5.30 into the x-direction component of Newton's second law for the differential element, $\sum dF_x = dm a_x$, where we employ the substantial derivative of the x-direction velocity, u , to model a_x , we have:

$$\underbrace{\left[\rho\beta_x + \frac{\partial\sigma_{xx}}{\partial x} + \frac{\partial\tau_{yx}}{\partial y} + \frac{\partial\tau_{zx}}{\partial z} \right] dx dy dz}_{dF_x} = \underbrace{\rho dx dy dz}_{dm} \underbrace{\left[\frac{\partial u}{\partial t} + u \frac{\partial u}{\partial x} + v \frac{\partial u}{\partial y} + w \frac{\partial u}{\partial z} \right]}_{a_x = Du/Dt} \quad (5.31a)$$

Similarly, for the y and z directions, we obtain:

$$\rho\beta_y + \frac{\partial\tau_{xy}}{\partial x} + \frac{\partial\sigma_{yy}}{\partial y} + \frac{\partial\tau_{zy}}{\partial z} = \rho \left[\frac{\partial v}{\partial t} + u \frac{\partial v}{\partial x} + v \frac{\partial v}{\partial y} + w \frac{\partial v}{\partial z} \right] \quad (5.31b)$$

$$\rho\beta_z + \frac{\partial\tau_{xz}}{\partial x} + \frac{\partial\tau_{yz}}{\partial y} + \frac{\partial\sigma_{zz}}{\partial z} = \rho \left[\frac{\partial w}{\partial t} + u \frac{\partial w}{\partial x} + v \frac{\partial w}{\partial y} + w \frac{\partial w}{\partial z} \right] \quad (5.31c)$$

Eqs. 5.31a,b,c are the respective component equations for Newton's second law applied to a differential fluid element, and collectively they comprise the vector equation,

$\sum \vec{F} = \frac{\partial}{\partial t} (m\vec{V}) = m\vec{a}$. Note that these equations are in their most general form, and will apply to *any* fluid, regardless of its properties (i.e. viscous or visco-elastic, compressible or incompressible, etc.).

5.6.3 Relating Stresses to Fluid Rates of Strain

Since we are considering a homogeneous, continuous medium, we can reduce the stress tensor components in the above equations from nine to six by noting that the moments imparted about the center of our differential element by the shearing stresses must be in balance when the material is in equilibrium (see [Timoshenko and Goodier, 1970](#)). This

allows us to equate the shearing stresses for adjacent sides of our differential element to each other, so that:

$$\tau_{xy} = \tau_{yx}, \quad \tau_{xz} = \tau_{zx}, \quad \text{and} \quad \tau_{yz} = \tau_{zy}$$

We are still far from a satisfying set of equations, since we still have six different stresses within the governing equations. Now our objective is to represent these stresses in terms of *strain rates*, which can be directly related to the fluid deformation, and thus reflected by spatial derivatives of velocity, as was illustrated in Chapter 4. Since we are dealing with a fluid continuum, we assume that the stress tensor for a fluid is linearly related to the strain rate tensor of a fluid, in the same manner that the stress tensor for a solid material is related to the strain tensor of a solid. This assumption of a fluid with a linear stress to strain rate is termed a Newtonian fluid, after Sir Isaac Newton. Newton, in his [Principia Mathematica](#) (1687), first hypothesized that most fluids demonstrate a *linear relationship between the applied stress and the rate of strain* (although Newton expressed it a little less concisely). This concept was later adapted by [Stokes](#) (1845), who developed the mathematical model of a Newtonian fluid that is employed in modern fluid mechanics, and which we discuss below.

To develop our analogy from solid mechanics, we first review the general relation of the stress tensor to the strain tensor for a [Hookean](#) solid. Here, stresses are assumed to have a linear relationship of the form:

$$\tau_{xy} = c_1 \epsilon_{xx} + c_2 \epsilon_{xy} + c_3 \epsilon_{xz} + c_4 \epsilon_{yy} + c_5 \epsilon_{yz} + c_6 \epsilon_{zz}$$

In this most general relationship, *each* stress component is assumed to depend on all six rate-of-strain components, ϵ . Clearly this is a mess, since similar equations for the other five stress components would require 30 additional *independent* coefficients in order to define completely the state of stress in a material. However, for most solids the assumption is made of an *isotropic* medium (i.e. that the material stress vs. strain properties are independent of direction). This assumption (and simplification) reduces the number of coefficients required to define the state of stress in a solid to *two*, since many of the original coefficients are either identically zero or related to each other. Recall that these proportionality coefficients for a Hookean solid are [for normal stresses]:

E - the modulus of elasticity--a constant of proportionality of normal stress to normal strain; and

n - Poisson's ratio--which relates the lateral contraction of a material to the axial expansion (i.e. directly related to the volumetric change of a material under an applied stress).

Using these coefficients, the stress-strain relationships for a solid can be represented as:

$$\left. \begin{aligned} \varepsilon_{xx} &= \frac{1}{E} [\sigma_{xx} - n(\sigma_{yy} + \sigma_{zz})] \\ \varepsilon_{yy} &= \frac{1}{E} [\sigma_{yy} - n(\sigma_{xx} + \sigma_{zz})] \\ \varepsilon_{zz} &= \frac{1}{E} [\sigma_{zz} - n(\sigma_{xx} + \sigma_{yy})] \end{aligned} \right\} \text{Normal Stresses} \quad (5.32a)$$

$$\left. \begin{aligned} \varepsilon_{xy} &= \frac{2(1+n)}{E} \tau_{xy} = \frac{1}{G} \tau_{xy} \\ \varepsilon_{yz} &= \frac{2(1+n)}{E} \tau_{yz} = \frac{1}{G} \tau_{yz} \\ \varepsilon_{zx} &= \frac{2(1+n)}{E} \tau_{zx} = \frac{1}{G} \tau_{zx} \end{aligned} \right\} \text{Shear Stresses} \quad (5.32b)$$

In Eq. 5.32, G is termed the modulus of elasticity in shear, and is a constant of proportionality between shear stress and shear strain. Note that if we invert the shear strain equations in Eqs. 5.32, and solve the three normal strain equations simultaneously to obtain explicit expressions for each normal stress, we obtain:

$$\begin{aligned} \sigma_{xx} &= \frac{nE}{(1+n)(1-2n)} (\varepsilon_{xx} + \varepsilon_{yy} + \varepsilon_{zz}) + \frac{E}{1+n} \varepsilon_{xx} = \lambda (\varepsilon_{xx} + \varepsilon_{yy} + \varepsilon_{zz}) + 2G\varepsilon_{xx} \\ \sigma_{yy} &= \frac{nE}{(1+n)(1-2n)} (\varepsilon_{xx} + \varepsilon_{yy} + \varepsilon_{zz}) + \frac{E}{1+n} \varepsilon_{yy} = \lambda (\varepsilon_{xx} + \varepsilon_{yy} + \varepsilon_{zz}) + 2G\varepsilon_{yy} \end{aligned} \quad (5.33a)$$

$$\sigma_{zz} = \frac{nE}{(1+n)(1-2n)} (\varepsilon_{xx} + \varepsilon_{yy} + \varepsilon_{zz}) + \frac{E}{1+n} \varepsilon_{zz} = \lambda (\varepsilon_{xx} + \varepsilon_{yy} + \varepsilon_{zz}) + 2G\varepsilon_{zz}$$

$$\begin{aligned} \tau_{xy} &= G\varepsilon_{xy} \\ \tau_{yz} &= G\varepsilon_{yz} \end{aligned} \quad (5.33b)$$

$$\tau_{zx} = G\varepsilon_{zx}$$

In the three normal stress equations, Eqs. 5.33a, the first group of constants is given the designator λ , and is termed [Lame's constant](#). Since this constant modifies the collective strains, it is reflective of the volumetric expansion (or contraction) of the material. The second constant, G , is of course the modulus of elasticity in shear.

Similar arguments were made by Stokes in developing the stress-strain rate relationships for a fluid. As pointed out in Chapter 1, a fluid cannot sustain a fixed strain, but will deform continuously under an applied force or stress. This is what led Newton to the logical conclusion that any force applied to a fluid will cause it to *continuously* deform,

and that the *rate of this deformation, or strain rate*, is the appropriate response of the fluid to the applied force, or stress. What Stokes hypothesized was that a set of *stress-strain rate* equations, analogous to the *stress-strain* equations for a Hookean solid, could be developed for a Newtonian fluid, under the following set of postulates:

1. The fluid is continuous, and the components of the stress tensor vary *linearly* with the strain rate.
2. The fluid is isotropic, such that its properties are *independent of direction*.
3. When the fluid is at rest, with zero strain rates, the deformation equations must reduce to the hydrostatic pressure condition (i.e. $\sigma_{xx} = \sigma_{yy} = \sigma_{zz} = -p$).

Note that our assumptions to this point satisfy the first two postulates. The third is achieved by including a pressure term in the equations for the normal stresses.

Correspondingly, the stress equations that Stokes arrived at for a Newtonian fluid are given in the following Eq. 5.34.

$$\begin{array}{ll}
 \begin{array}{c} \text{linear strain} \\ \text{rate} \\ \downarrow \\ \sigma_{xx} = -p + 2\mu \dot{\epsilon}_{xx} + \lambda (\dot{\epsilon}_{xx} + \dot{\epsilon}_{yy} + \dot{\epsilon}_{zz}) \\ \sigma_{yy} = -p + 2\mu \dot{\epsilon}_{yy} + \lambda (\dot{\epsilon}_{xx} + \dot{\epsilon}_{yy} + \dot{\epsilon}_{zz}) \\ \sigma_{zz} = -p + 2\mu \dot{\epsilon}_{zz} + \lambda (\dot{\epsilon}_{xx} + \dot{\epsilon}_{yy} + \dot{\epsilon}_{zz}) \end{array} &
 \begin{array}{c} \text{volume rate of} \\ \text{expansion} \\ \downarrow \\ \tau_{xy} = 2\mu \dot{\epsilon}_{xy} \\ \tau_{yz} = 2\mu \dot{\epsilon}_{yz} \\ \tau_{zx} = 2\mu \dot{\epsilon}_{zx} \end{array}
 \end{array} \tag{5.34}$$

In Eqs.5.34, μ is termed the coefficient of viscosity, λ is termed the coefficient of bulk viscosity (sometimes the second coefficient of viscosity), and the $\dot{\epsilon}$ terms indicate the rate of strain components. Note that the coefficient of viscosity, μ , is analogous to G for a solid, accounting for viscous forces due to shear and incompressible deformation of a fluid. μ models the ratio of the applied stress to the local strain rate, and for Newtonian fluids will remain essentially constant over a range of local strain rates (however, it can vary, often strongly, with temperature). The coefficient of bulk viscosity, λ , performs the same function as λ for a solid, and relates the proportionality of the applied stress to the *volumetric expansion/contraction* of the fluid. This term, as we will see, only plays a significant role when variations in fluid density, or fluid compressibility, are relevant, such as for flows of high-speed gases.

The inclusion of pressure in Eqs. 5.34 satisfies Stokes' third postulate, such that if the rates of strain vanish, we still have a normal stress acting on the fluid, caused by the pressure acting inward on a fluid element. Note that the pressure term is taken as

negative since it will always act *opposite* to the outward surface normal for our differential fluid element.

Recall that in Chapter 4, Eq. 4.9, we derived the rate-of-strain tensor (in Cartesian coordinates) in terms of spatial variations of the fluid velocity field as:

$$\vec{E}_{ab} = \begin{bmatrix} \dot{\epsilon}_{xx} & \dot{\epsilon}_{xy} & \dot{\epsilon}_{xz} \\ \dot{\epsilon}_{yx} & \dot{\epsilon}_{yy} & \dot{\epsilon}_{yz} \\ \dot{\epsilon}_{zx} & \dot{\epsilon}_{zy} & \dot{\epsilon}_{zz} \end{bmatrix} = \begin{bmatrix} \frac{\partial u}{\partial x} & \frac{1}{2} \left(\frac{\partial v}{\partial x} + \frac{\partial u}{\partial y} \right) & \frac{1}{2} \left(\frac{\partial w}{\partial x} + \frac{\partial u}{\partial z} \right) \\ \frac{1}{2} \left(\frac{\partial u}{\partial y} + \frac{\partial v}{\partial x} \right) & \frac{\partial v}{\partial y} & \frac{1}{2} \left(\frac{\partial w}{\partial y} + \frac{\partial v}{\partial z} \right) \\ \frac{1}{2} \left(\frac{\partial u}{\partial z} + \frac{\partial w}{\partial x} \right) & \frac{1}{2} \left(\frac{\partial v}{\partial z} + \frac{\partial w}{\partial y} \right) & \frac{\partial w}{\partial z} \end{bmatrix}$$

So, substituting these velocity-based expressions for the rate-of-strain components into the stress-rate of strain equations, Eq. 5.34, we obtain:

$$\begin{aligned} \sigma_{xx} &= -p + 2\mu \frac{\partial u}{\partial x} + \lambda \left(\frac{\partial u}{\partial x} + \frac{\partial v}{\partial y} + \frac{\partial w}{\partial z} \right) & \tau_{xy} &= \mu \left(\frac{\partial u}{\partial y} + \frac{\partial v}{\partial x} \right) \\ \sigma_{yy} &= -p + 2\mu \frac{\partial v}{\partial y} + \lambda \left(\frac{\partial u}{\partial x} + \frac{\partial v}{\partial y} + \frac{\partial w}{\partial z} \right) & \tau_{yz} &= \mu \left(\frac{\partial v}{\partial z} + \frac{\partial w}{\partial y} \right) \\ \sigma_{zz} &= -p + 2\mu \frac{\partial w}{\partial z} + \lambda \left(\frac{\partial u}{\partial x} + \frac{\partial v}{\partial y} + \frac{\partial w}{\partial z} \right) & \tau_{zx} &= \mu \left(\frac{\partial w}{\partial x} + \frac{\partial u}{\partial z} \right) \end{aligned} \quad (5.35)$$

To further simplify these stress equations, we substitute $\frac{\partial u}{\partial x} + \frac{\partial v}{\partial y} + \frac{\partial w}{\partial z} = \nabla \cdot \vec{V}$ [the divergence of \vec{V}] into Eqs. 5.35, and have:

$$\begin{aligned} \sigma_{xx} &= -p + 2\mu \frac{\partial u}{\partial x} + \lambda \nabla \cdot \vec{V} & \tau_{xy} &= \mu \left(\frac{\partial u}{\partial y} + \frac{\partial v}{\partial x} \right) \\ \sigma_{yy} &= -p + 2\mu \frac{\partial v}{\partial y} + \lambda \nabla \cdot \vec{V} & \tau_{yz} &= \mu \left(\frac{\partial v}{\partial z} + \frac{\partial w}{\partial y} \right) \\ \sigma_{zz} &= -p + 2\mu \frac{\partial w}{\partial z} + \lambda \nabla \cdot \vec{V} & \tau_{zx} &= \mu \left(\frac{\partial w}{\partial x} + \frac{\partial u}{\partial z} \right) \end{aligned} \quad (5.36)$$

To examine the impact of Stokes' third postulate for these equations, we sum the three component *normal* stresses of Eqs. 5.36 and obtain:

$$\sigma_{xx} + \sigma_{yy} + \sigma_{zz} = -3p + 2\mu(\nabla \cdot \vec{V}) + 3\lambda(\nabla \cdot \vec{V}) = -3p + (2\mu + 3\lambda)\nabla \cdot \vec{V}$$

However, if we assume a mechanical pressure (call it \bar{p}) that is the negative *average* of the normal stresses, we can write:

$$\bar{p} = -\frac{\sigma_{xx} + \sigma_{yy} + \sigma_{zz}}{3} = p - \left(\frac{2}{3}\mu + \lambda\right) \nabla \cdot \vec{V} \quad (5.37)$$

Of course, if the fluid is at rest, and $\nabla \cdot \vec{V}$ is zero, then Eq. 5.37 yields $\bar{p} = p$, which satisfies Stokes' third postulate. However, when there is fluid motion, Eq. 5.37 is problematic, since the mean pressure in a deforming viscous fluid *may not be equivalent* to the thermodynamic pressure. This result presents a dilemma, although it is generally not a problem for incompressible flows (where $\nabla \cdot \vec{V} = 0$ always), and often has little impact for compressible flows. Stokes, faced with this dilemma (which would greatly complicate the momentum equation derivation), took the easy way out. He reasoned that $\bar{p} = p$ for all flow situations (not just static conditions), and hypothesized that $\lambda \cong -\frac{2}{3}\mu$, which is known as [Stokes' hypothesis](#). This hypothesis, although universally utilized, has been the subject of controversy [see [White, 1991](#) and the commentary by [Gad El-Hak \(1995\)](#)]. However, as White notes, for most applications Stokes' hypothesis has little impact—with the exceptions being for shock waves, and sound absorption and attenuation. For the purposes of this text, we will accept Stokes' hypothesis, since it is consistent with the types of incompressible flow problems we address here. Accepting Stokes' hypothesis further reduces Eqs. 5.36 stresses to:

$$\begin{aligned} \sigma_{xx} &= -p + 2\mu \frac{\partial u}{\partial x} - \frac{2}{3}\mu \nabla \cdot \vec{V} & \tau_{xy} &= \mu \left(\frac{\partial u}{\partial y} + \frac{\partial v}{\partial x} \right) = \tau_{yx} \\ \sigma_{yy} &= -p + 2\mu \frac{\partial v}{\partial y} - \frac{2}{3}\mu \nabla \cdot \vec{V} & \tau_{xz} &= \mu \left(\frac{\partial u}{\partial z} + \frac{\partial w}{\partial x} \right) = \tau_{zx} \\ \sigma_{zz} &= -p + 2\mu \frac{\partial w}{\partial z} - \frac{2}{3}\mu \nabla \cdot \vec{V} & \tau_{yz} &= \mu \left(\frac{\partial v}{\partial z} + \frac{\partial w}{\partial y} \right) = \tau_{zy} \end{aligned} \quad (5.38)$$

pressure

linear
strain
rate

stresses due to
compressibility

angular
deformation

5.6.4 Reducing the Momentum Equation to the Navier-Stokes Equation

Now armed with the velocity-based models of Eqs. 5.38 for the fluid stresses, we return to the differential equation for Newton's second law, and substitute our Stokes simplified stress models from Eqs. 5.38 for a Newtonian fluid into Eqs. 5.31. Considering the x-direction equation first, Eq. 5.31a, we obtain:

$$\rho \beta_x + \frac{\partial}{\partial x} \left(-p + 2\mu \frac{\partial u}{\partial x} - \frac{2}{3}\mu \nabla \cdot \vec{V} \right) + \frac{\partial}{\partial y} \left[\mu \left(\frac{\partial v}{\partial x} + \frac{\partial u}{\partial y} \right) \right] + \frac{\partial}{\partial z} \left[\mu \left(\frac{\partial u}{\partial z} + \frac{\partial w}{\partial x} \right) \right] = \rho a_x \quad (5.39)$$

If we further restrict the fluid to one of constant viscosity, $\mu = \text{constant}$, this yields:

$$\rho\beta_x - \frac{\partial p}{\partial x} + \mu \frac{\partial}{\partial x} \left(2 \frac{\partial u}{\partial x} - \frac{2}{3} \nabla \cdot \vec{V} \right) + \mu \frac{\partial}{\partial y} \left(\frac{\partial v}{\partial x} + \frac{\partial u}{\partial y} \right) + \mu \frac{\partial}{\partial z} \left(\frac{\partial u}{\partial z} + \frac{\partial w}{\partial x} \right) = \rho a_x \quad (5.40)$$

Rearranging Eq. 5.40, and numbering select terms for further simplification, we have:

$$\rho\beta_x - \frac{\partial p}{\partial x} + \underbrace{2\mu \frac{\partial^2 u}{\partial x^2}}_{\textcircled{1}} - \underbrace{\frac{2\mu}{3} \frac{\partial}{\partial x} (\nabla \cdot \vec{V})}_{\textcircled{6}} + \underbrace{\mu \frac{\partial^2 v}{\partial y \partial x}}_{\textcircled{2}} + \underbrace{\mu \frac{\partial^2 u}{\partial y^2}}_{\textcircled{3}} + \underbrace{\mu \frac{\partial^2 u}{\partial z^2}}_{\textcircled{4}} + \underbrace{\mu \frac{\partial^2 w}{\partial z \partial x}}_{\textcircled{5}} = \rho a_x \quad (5.41)$$

By judicious rearrangement of the selected terms in Eq. 5.41, as indicated below, we can make the collective identification of more compact terms that utilize the Laplacian and divergence operators, as shown:

$$\rho\beta_x - \frac{\partial p}{\partial x} + \underbrace{\mu \left[\frac{\partial^2 u}{\partial x^2} + \frac{\partial^2 u}{\partial y^2} + \frac{\partial^2 u}{\partial z^2} \right]}_{\textcircled{1}/2 \quad \textcircled{3} \quad \textcircled{4}} + \underbrace{\mu \frac{\partial}{\partial x} \left[\frac{\partial u}{\partial x} + \frac{\partial v}{\partial y} + \frac{\partial w}{\partial z} \right] - \frac{2}{3} \mu \frac{\partial}{\partial x} (\nabla \cdot \vec{V})}_{\textcircled{1}/2 \quad \textcircled{2} \quad \textcircled{5} \quad \textcircled{6}} = \rho a_x$$

$$\underbrace{\hspace{10em}}_{\nabla^2 u} \quad \underbrace{\hspace{10em}}_{\frac{1}{3} \mu \frac{\partial}{\partial x} (\nabla \cdot \vec{V})}$$

Thus, the x-direction component of the momentum equation simplifies to:

$$\rho\beta_x - \frac{\partial p}{\partial x} + \mu \nabla^2 u + \frac{1}{3} \mu \frac{\partial}{\partial x} (\nabla \cdot \vec{V}) = \rho a_x \quad (5.42a)$$

Similarly, y- and z-direction components of the momentum equation are:

$$\rho\beta_y - \frac{\partial p}{\partial y} + \mu \nabla^2 v + \frac{1}{3} \mu \frac{\partial}{\partial y} (\nabla \cdot \vec{V}) = \rho a_y \quad (5.42b)$$

$$\rho\beta_z - \frac{\partial p}{\partial z} + \mu \nabla^2 w + \frac{1}{3} \mu \frac{\partial}{\partial z} (\nabla \cdot \vec{V}) = \rho a_z \quad (5.42c)$$

So, expressing the momentum equation for a Newtonian fluid collectively as a single *vector* equation gives what is termed the Navier-Stokes equation—first derived generically by Navier, and particularized for a Newtonian fluid by Stokes:

$$\underbrace{\rho \vec{\beta}}_{\substack{\uparrow \\ \text{body} \\ \text{force}}} - \underbrace{\nabla p}_{\substack{\uparrow \\ \text{pressure} \\ \text{force}}} + \underbrace{\mu \nabla^2 \vec{V}}_{\substack{\uparrow \\ \text{deformation} \\ \text{stresses}}} + \underbrace{\frac{1}{3} \mu \nabla (\nabla \cdot \vec{V})}_{\substack{\uparrow \\ \text{compressible} \\ \text{stresses}}} = \underbrace{\rho \frac{\partial \vec{V}}{\partial t}}_{\substack{\uparrow \\ \text{local} \\ \text{acceleration}}} + \underbrace{\rho (\vec{V} \cdot \nabla) \vec{V}}_{\substack{\uparrow \\ \text{advective} \\ \text{acceleration}}} = \underbrace{\rho \frac{D\vec{V}}{Dt}}_{\substack{\uparrow \\ \text{total} \\ \text{acceleration}}} \quad \left. \vphantom{\rho \frac{D\vec{V}}{Dt}} \right\} \begin{array}{l} \text{Navier -} \\ \text{Stokes Eqn.} \end{array} \quad (5.43)$$

Now, in section 5.4.3 we showed that $\nabla \cdot \vec{V} = 0$ for an incompressible fluid. Employing this relationship in Eq. 5.43 eliminates the compressible stresses term, giving:

$$\rho \vec{\beta} - \nabla p + \mu \nabla^2 \vec{V} = \rho \frac{D\vec{V}}{Dt}$$

Since density is constant for an incompressible flow, it is often convenient to divide through by ρ , giving an equation of the form:

$$\vec{\beta} - \frac{\nabla p}{\rho} + \nu \nabla^2 \vec{V} = \frac{D\vec{V}}{Dt} \quad (5.44)$$

Here, $\nu = \frac{\mu}{\rho}$, and is termed the “kinematic” viscosity. Since ν is the ratio of two fluid properties, it is of itself also a fluid property. It is this form of the Navier-Stokes equation, Eq. 5.44, that we will make the most general use of in this text, since it provides a less cumbersome form for dealing with constant density flows.

Note that the vector form of the Navier-Stokes equation applies generically for any coordinate system. Although we developed the equation in Cartesian coordinates, the generic vector form of the equation is applicable for any coordinate system. For example, the expanded x-direction equation in Cartesian coordinates is:

$$\beta_x - \frac{1}{\rho} \frac{\partial p}{\partial x} + \nu \left[\frac{\partial^2 u}{\partial x^2} + \frac{\partial^2 u}{\partial y^2} + \frac{\partial^2 u}{\partial z^2} \right] = \left[\frac{\partial u}{\partial t} + u \frac{\partial u}{\partial x} + v \frac{\partial u}{\partial y} + w \frac{\partial u}{\partial z} \right] \quad (5.45)$$

\uparrow
 \mathbf{g}_x if $\vec{\beta} = \vec{g}$

However, note that the directional components of the Navier-Stokes equation expressed in cylindrical or spherical coordinate systems will contain additional terms that result from the dependency of selected unit vectors employed in those systems upon changes in angular position. For example the r-direction component equation in cylindrical coordinates, shown below, contains “extra” terms due to the dependence of the \hat{i}_r and \hat{i}_θ unit vectors upon changes in the angle θ .

$$\beta_r - \frac{1}{\rho} \frac{\partial p}{\partial r} + \nu \left[\frac{\partial}{\partial r} \left(\frac{1}{r} \frac{\partial}{\partial r} (r v_r) \right) + \frac{1}{r^2} \frac{\partial^2 v_r}{\partial \theta^2} + \frac{\partial^2 v_r}{\partial z^2} - \frac{2}{r^2} \frac{\partial v_\theta}{\partial \theta} \right] = \left[\frac{\partial v_r}{\partial t} + v_r \frac{\partial v_r}{\partial r} + \frac{v_\theta}{r} \frac{\partial v_r}{\partial \theta} - \frac{v_\theta^2}{r} + v_z \frac{\partial v_r}{\partial z} \right]$$

A listing of all the directional components of the incompressible Navier-Stokes equation in Cartesian and cylindrical coordinates are given in [Section 5.8](#), at the end of this chapter

and the Appendix at the end of this book. A listing of the Navier-Stokes equation, and its components, in spherical coordinates can be found [here](#).

5.7 Utilization of the Incompressible Continuity and Navier-Stokes Equations

For constant density flows, the continuity and Navier-Stokes equations are sufficient to solve for the velocity and pressure fields within an isothermal fluid. As shown in figure 5.9 below (for Cartesian coordinates), these equations provide four equations (one scalar plus three vector component equations) with four dependent unknowns (u , v , w , and p), rendering an exact solution possible.

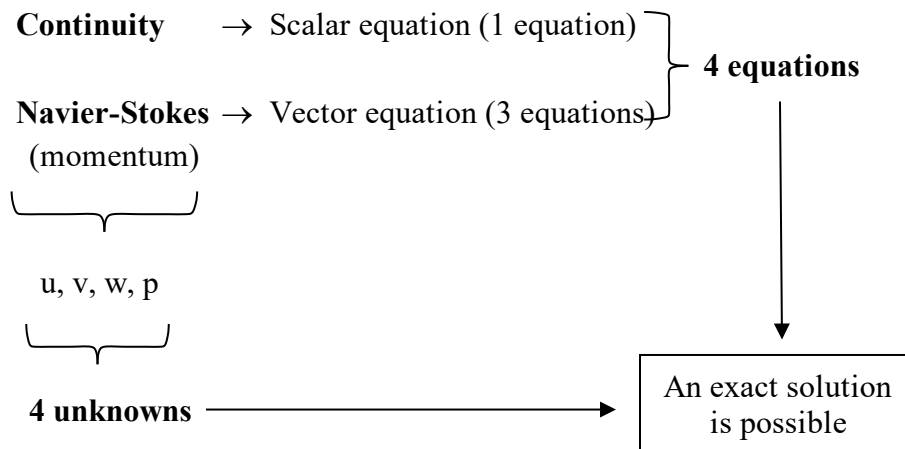


Figure 5.9 Schematic of the generic solution process for a constant density, isothermal fluid, in Cartesian coordinates.

While we now have the equations to implement exact solutions, the solution process can be quite complicated, particularly as the dimensional complexity of a flow increases. While closed-form solutions are possible for one- and some two-dimensional flows, three-dimensional flows generally necessitate the use of numerical solutions, employing sophisticated computational approaches. The addition of time dependency to a flow further compounds solution procedures, with all but the simplest of such flows requiring both numerical solution approaches, as well as possible further modeling of the unsteadiness properties, like for turbulent flows (see Chapter 17).

That being said, there is still much that can be learned about the behavior of fluid flows using closed-form solution techniques. It will be the approach in this book to exploit flow problems that lend themselves to closed-form solutions, which can then be employed to examine the implications on the physics of fluid behavior. While modern commercial computational programs can provide effective numerical solutions of many useful fluid flow geometries of significant complexity, it is important that the user of

such programs understand the interplay of the physics within a fluid that influences those solutions. In addition, it is through the solution and examination of simpler physical situations that one learns the physical trade-offs inherent in the governing equations, and develops an intuitive feel for what behavior to anticipate for a specific application, which is the hallmark of a competent fluids engineer.

Accordingly, in the following Chapter 6 we will begin to examine the application of the continuity and Navier-Stokes equations to selected physical situations, and illustrate how to utilize appropriate simplifications that allow the extraction of tractable, closed-form solutions of the velocity fields. We will do this by first considering simple solutions, which involve one-dimensional dependence. Later, in Chapter 12, we will consider more complicated solutions, which depend on two dimensions, or one dimension and time.

5.8 The Governing Equations for Incompressible Flow

5.8.1 Stresses on an Incompressible Fluid: Cartesian Cylindrical Coordinates

$$\begin{aligned}\sigma_{xx} &= -p + 2\mu \frac{\partial u}{\partial x} & \tau_{xy} &= \mu \left(\frac{\partial u}{\partial y} + \frac{\partial v}{\partial x} \right) = \tau_{yx} \\ \sigma_{yy} &= -p + 2\mu \frac{\partial v}{\partial y} & \tau_{xz} &= \mu \left(\frac{\partial u}{\partial z} + \frac{\partial w}{\partial x} \right) = \tau_{zx} \\ \sigma_{zz} &= -p + 2\mu \frac{\partial w}{\partial z} & \tau_{yz} &= \mu \left(\frac{\partial v}{\partial z} + \frac{\partial w}{\partial y} \right) = \tau_{zy}\end{aligned}$$

5.8.2 Stresses on an Incompressible Fluid: Cartesian Cylindrical Coordinates

$$\begin{aligned}\sigma_{rr} &= -p + 2\mu \frac{\partial v_r}{\partial r} & \tau_{r\theta} &= \mu \left(r \frac{\partial}{\partial r} \left(\frac{v_\theta}{r} \right) + \frac{1}{r} \frac{\partial v_r}{\partial \theta} \right) = \tau_{\theta r} \\ \sigma_{\theta\theta} &= -p + 2\mu \left(\frac{1}{r} \frac{\partial v_\theta}{\partial \theta} + \frac{v_r}{r} \right) & \tau_{\theta z} &= \mu \left(\frac{\partial v_\theta}{\partial z} + \frac{1}{r} \frac{\partial v_z}{\partial \theta} \right) = \tau_{z\theta} \\ \sigma_{zz} &= -p + 2\mu \frac{\partial v_z}{\partial z} & \tau_{rz} &= \mu \left(\frac{\partial v_z}{\partial r} + \frac{\partial v_r}{\partial z} \right) = \tau_{zr}\end{aligned}$$

5.8.3 Continuity and N-S Equations, Cartesian Coordinates (ρ, μ constant)

$$\text{Continuity: } \frac{\partial u}{\partial x} + \frac{\partial v}{\partial y} + \frac{\partial w}{\partial z} = 0 \quad (5.46a)$$

$$\text{x-direction: } \frac{\partial u}{\partial t} + u \frac{\partial u}{\partial x} + v \frac{\partial u}{\partial y} + w \frac{\partial u}{\partial z} = -\frac{1}{\rho} \frac{\partial p}{\partial x} + g_x + \nu \left[\frac{\partial^2 u}{\partial x^2} + \frac{\partial^2 u}{\partial y^2} + \frac{\partial^2 u}{\partial z^2} \right] \quad (5.46b)$$

$$\text{y-direction: } \frac{\partial v}{\partial t} + u \frac{\partial v}{\partial x} + v \frac{\partial v}{\partial y} + w \frac{\partial v}{\partial z} = -\frac{1}{\rho} \frac{\partial p}{\partial y} + g_y + \nu \left[\frac{\partial^2 v}{\partial x^2} + \frac{\partial^2 v}{\partial y^2} + \frac{\partial^2 v}{\partial z^2} \right] \quad (5.46c)$$

$$\text{z-direction: } \frac{\partial w}{\partial t} + u \frac{\partial w}{\partial x} + v \frac{\partial w}{\partial y} + w \frac{\partial w}{\partial z} = -\frac{1}{\rho} \frac{\partial p}{\partial z} + g_z + \nu \left[\frac{\partial^2 w}{\partial x^2} + \frac{\partial^2 w}{\partial y^2} + \frac{\partial^2 w}{\partial z^2} \right] \quad (5.46d)$$

5.8.4 Continuity and N-S Equations, Cylindrical Coordinates (ρ, μ constant)

$$\text{Continuity: } \frac{1}{r} \frac{\partial}{\partial r} (rv_r) + \frac{1}{r} \frac{\partial v_\theta}{\partial \theta} + \frac{\partial v_z}{\partial z} = 0 \quad (5.47a)$$

$$\begin{aligned} \text{r-direction: } & \frac{\partial v_r}{\partial t} + v_r \frac{\partial v_r}{\partial r} + \frac{v_\theta}{r} \frac{\partial v_r}{\partial \theta} + v_z \frac{\partial v_r}{\partial z} - \frac{v_\theta^2}{r} \\ & = -\frac{1}{\rho} \frac{\partial p}{\partial r} + g_r + \nu \left[\frac{\partial}{\partial r} \left(\frac{1}{r} \frac{\partial}{\partial r} (rv_r) \right) + \frac{1}{r^2} \frac{\partial^2 v_r}{\partial \theta^2} + \frac{\partial^2 v_r}{\partial z^2} - \frac{2}{r^2} \frac{\partial v_\theta}{\partial \theta} \right] \end{aligned} \quad (5.47b)$$

$$\begin{aligned} \text{\theta-direction: } & \frac{\partial v_\theta}{\partial t} + v_r \frac{\partial v_\theta}{\partial r} + \frac{v_\theta}{r} \frac{\partial v_\theta}{\partial \theta} + v_z \frac{\partial v_\theta}{\partial z} + \frac{v_r v_\theta}{r} \\ & = -\frac{1}{\rho r} \frac{\partial p}{\partial \theta} + g_\theta + \nu \left[\frac{\partial}{\partial r} \left(\frac{1}{r} \frac{\partial}{\partial r} (rv_\theta) \right) + \frac{1}{r^2} \frac{\partial^2 v_\theta}{\partial \theta^2} + \frac{\partial^2 v_\theta}{\partial z^2} + \frac{2}{r^2} \frac{\partial v_r}{\partial \theta} \right] \end{aligned} \quad (5.47c)$$

$$\begin{aligned} \text{z-direction: } & \frac{\partial v_z}{\partial t} + v_r \frac{\partial v_z}{\partial r} + \frac{v_\theta}{r} \frac{\partial v_z}{\partial \theta} + v_z \frac{\partial v_z}{\partial z} \\ & = -\frac{1}{\rho} \frac{\partial p}{\partial z} + g_z + \nu \left[\frac{1}{r} \frac{\partial}{\partial r} \left(r \frac{\partial v_z}{\partial r} \right) + \frac{1}{r^2} \frac{\partial^2 v_z}{\partial \theta^2} + \frac{\partial^2 v_z}{\partial z^2} \right] \end{aligned} \quad (5.47d)$$

References

Fox, R.W. and McDonald, A.T. , *Introduction to Fluid Mechanics* (any edition), John Wiley & Sons

[Wikipedia: Liebnitz integral rule](#); [Wikipedia: Differentiation of integral](#)

[Wikipedia: Solenoidal field](#)

Stokes, G.G. (1845) “On the Theories of Internal Friction of Fluids in Motion,”
Transactions of the Cambridge Philosophical Society, 8, pp. 287–305.

Timoshenko, S.P. and Goodier, J.N. (1970) *Theory of Elasticity*, McGraw-Hill Inc.

White, F. M. (1991) *Viscous Flow*, McGraw-Hill Inc.

Study Problems

1. Do the following:

- For a 2-D, incompressible flow, $u = Ax$. If $v = 0$ along x-axis, determine v .
- For a 3-D, incompressible flow, $u = 2x$ and $v = -y$. Determine w , if $w = 0$ in the x-y plane.
- The velocity of a flow is given by: $\vec{V} = xy\hat{i} + y^2\hat{j} + xz\hat{k}$
 - Is this an incompressible flow? Why?
 - If not, determine the rate of change of density at $(x, y, z) = (1, 2, 1)$, where $\rho = 2$.

2. Do the following:

- For a 2-D, incompressible flow, $u = Axy$. If $v = 0$ along x-axis, determine v .
- For a 3-D, incompressible flow, $u = 2y$ and $v = -x$. Determine w , if $w = 0$ in the x-y plane.
- The velocity of a flow is given by: $\vec{V} = xy\hat{i} - y^2\hat{j} + zx\hat{k}$
 - Is this an incompressible flow? Why?
 - If not, determine the rate of change of density at $(x, y, z) = (2, 1, 1)$, where $\rho = 2$.

3. Do the following:

- For a 2-D, incompressible flow, $u = Ay$. If $v = 2$ along x-axis, determine v .
- For a 3-D, incompressible flow, $u = x$ and $v = y$. Determine w , if $w = 0$ in the x-y plane.
- The velocity of a flow is given by: $\vec{V} = x^2\hat{i} + zy\hat{j} + yz\hat{k}$
 - Is this an incompressible flow? Why?
 - If not, determine the rate of change of density at $(x, y, z) = (1, 1, 1)$, where $\rho = 2$.

4. Starting from the vector equation, $\vec{\beta} - \frac{1}{\rho} \nabla p + \nu \nabla^2 \vec{V} = \frac{D\vec{V}}{Dt}$ (Eq. 5.44), derive the

The Navier-Stokes equation for cylindrical coordinates (Eqs. 5.47b-d). Remember you have to take the derivatives of the \hat{i}_r and \hat{i}_θ units vectors with respect to θ

Chapter 6

Simple Solutions to the Navier-Stokes Equations

Contents

6.1 Simplifications of the Governing Equations	116
6.1.1 Steady Flow	116
6.1.2 Dimensionality	115
6.1.3 Fully-Developed Flow	117
6.2 Boundary Conditions	118
6.2.1 Solid Boundaries and the No Slip Condition	119
6.2.2 Porous Boundaries	119
6.2.3 Boundaries within a Homogeneous Fluid	119
6.2.4 Boundaries Between Dissimilar Fluids	120
6.2.5 Laminar vs. Turbulent Flow	120
6.3 Simple One-Dimensional Solutions with Parallel Boundaries	122
6.3.1 Couette Flow	122
6.3.2 Poiseuille Flow in a Channel	127
6.3.3 Fully-Developed Flow Between Porous Plates	131
6.3.4 Two-Fluid Couette Flow	140
6.3.5 Two-Fluid Poiseuille Flow in a Channel	143
6.3.6 Falling Liquid Film on a Wall	149
6.4 Simple One-Dimensional Solutions with Radial Symmetry	152
6.4.1 Poiseuille Flow in a Pipe or a Tube	152
6.4.2 Couette Flow Between Concentric Rotating Cylinders	156
6.4.2.1 A Cylinder Rotating in an Infinite Fluid	159
6.4.2.2 Fluid Rotating within a Cylinder	159
6.4.3 Poiseuille Flow in a Duct of Annular Cross-Section	160
6.4.4 Two-Fluid Couette Flow Between Concentric Rotating Cylinders	164
6.4.5 Couette Flow Between Porous Concentric Rotating Cylinders	173
6.5 Summary	182

In this chapter, we begin to examine solutions of the Navier-Stokes equation. While the combination of the Navier-Stokes and continuity equations presents a particularly daunting set of equations, experience has shown that we can develop closed-form solutions for a number of simple flows by implementing several simplifying assumptions that reduce both the dimensionality and complexity of the governing equations. The value of these simpler solutions is that they allow one to develop accurate solutions for highly simplified physical situations, which then provide insight into the dynamics of fluid interactions, and allow examination of the behavior of associated physical properties (e.g. shear stress and vorticity). The subsequent

examination of the predicted fluid motion, and the associated properties, allows us to understand the impact of a moving fluid, and develop a physical appreciation for the expected behavior in different types of flow situations.

In its full-blown glory, the Navier-Stokes equation comprises a set of three coupled, partial differential equations of second order. As pointed out in Chapter 5, the mathematical form of these equations depends upon the specific flow conditions and geometry, which may render the equations [elliptic](#), [parabolic](#), or [hyperbolic](#) in nature. We will comment on the specific form and relevance of the simplified equations as we examine appropriate solution techniques, and illustrate the necessary conditions required to establish solutions. In the present chapter, we address only steady, one-dimensional flows, which will render the equations as ordinary [boundary-value problems](#). For such problems, we must be able to specify the conditions of the appropriate dependent variable (e.g. u , v , or w , and p in a Cartesian system) at the flow system boundary, as defined by the relevant independent coordinate (e.g. x , y , or z).

In considering appropriate solutions of the governing equations, we first discuss the types of simplifications we can invoke, and then the types of boundary conditions that we may employ. We then examine a number of simple solutions that are subject to specific simplifications and boundary conditions.

6.1 Simplifications of the Governing Equations

6.1.1 Steady Flow

Many flows of practical interest can be considered as steady (i.e. not changing with time). Examples of such flows are steady flow through a pipe, the airflow around an airplane in steady flight, or the lubricant moving between two surfaces of a continuously rotating sleeve bearing. In such cases, the time-dependent term in the Navier-Stokes equation will be negligible, leaving the advective acceleration terms as the only acceleration components in the Navier-Stokes equation. Such a condition will arise, for example, when a fluid flows steadily through a contracting nozzle. As pointed out earlier, a fluid particle will undergo advective acceleration within a contraction as the fluid particle passes through the increasing velocity field; however, when we view the flow at a fixed point, there will be no local change with time, thus the flow is steady.

6.1.2 Dimensionality

By the dimensionality of a fluid, we refer to the number of independent coordinate dimensions (e.g. x , y , z) required to specify the functional behavior of a dependent variable (e.g. u , v , w , p). Now, all real flows are three dimensional to a lesser or greater extent, depending on the initial

flow conditions and the geometry that the flow passes through or around. However, certain flow geometries lend themselves to situations where we can make a reasonable assumption of either two- or one-dimensional flow, and thus greatly simplify the governing equations. Additionally, appropriate dimensional constraints can render one or more of the dependent variables as null, thus eliminating one or more of the directional equations of motion.

The flow between parallel flat plates of infinite extent is an example of a reduced dimensional and variable type of flow. For such a flow, the sides constrain the flow to motion only in a direction parallel to the plates, which eliminates any flow normal to the plates, as we shall see in several examples we consider in this chapter. Such parallel plate flows are driven either by a pressure change parallel to the plates, or by the plate motion itself. If the driving forces are constrained to a one-dimensional direction, it is relatively easy to show that changes will only occur in the velocity component in the direction of application of the driving force(s). This will consequently reduce the Navier-Stokes equation to a one-component equation. Thus, any changes to the dependent velocity component will be constrained to changes only in the coordinate direction of, or normal to, the relevant velocity.

We will examine several of these constrained types of flows, where only one velocity component is relevant, and which undergo changes in only one coordinate direction. While such flows are highly idealized, they present quite tractable problems that lend themselves to straightforward analytical solutions, since the governing equation reduces to an ordinary differential equation (ODE). Moreover, the subsequent solutions allow for straightforward examination of the properties of the moving fluid, such as shear stress and vorticity, providing a basis to examine the behavioral tradeoffs that take place in a fluid flow. Accordingly, as we relax the constraints on a system, such as the examination of flows between converging surfaces, our more constrained solutions will provide a base of understanding that will help us assess the generally more complicated and complex flows that develop for less constrained and more geometrically complicated flow systems.

6.1.3 Fully-Developed Flow

When a steady flow passes through a constant cross-section channel or pipe, we often constrain our solution to the fully-developed flow that will exist when the flow has reached equilibrium, such that the velocity profile no longer changes with downstream position. Such conditions occur when a flow between parallel plates, or within a pipe or other constant cross-section duct, has passed far enough downstream such that the flow undergoes no further redistribution of fluid momentum. Under such a condition, the velocity distribution of the flow will remain fixed with respect to all coordinate directions. This characteristic greatly simplifies the governing equations, since all advective acceleration terms are null, which reduces the Navier-Stokes equation to a balance between viscous and pressure forces. Since the basis of the Navier-Stokes

equation is Newton's law, the presence of a fully-developed flow simply reduces the analysis of a flow field to a balance of forces, with no fluid acceleration.

Such fully-developed flows generally yield simple governing equations and solutions. These solutions are not only instructive of the flow behavior, but also form the fundamental basis for several instruments that are employed to measure fluid viscosity.

6.2 Boundary Conditions

From your calculus courses, you should recall that the complete solution of a differential equation requires that we be able to specify as many boundary conditions as the order of the derivative functions for each dependent variable relative to each independent variable. For example, consider the x-direction Navier-Stokes equation, given by:

$$\beta_x - \frac{1}{\rho} \frac{\partial p}{\partial x} + \nu \left[\frac{\partial^2 u}{\partial x^2} + \frac{\partial^2 u}{\partial y^2} + \frac{\partial^2 u}{\partial z^2} \right] = \left[\frac{\partial u}{\partial t} + u \frac{\partial u}{\partial x} + v \frac{\partial u}{\partial y} + w \frac{\partial u}{\partial z} \right] \quad (6.1)$$

Equation 6.1 contains second-order derivatives of u relative to x , y , and z . This requires two boundary conditions for each of these derivatives, providing two boundary conditions for either u or the first derivative of u at specified bounding values of x , y , and z . Thus, we require six boundary conditions for u . Note that we also require a seventh condition in x for the pressure, and an eighth for u at a specified time, t . This latter time condition is usually termed an *initial* condition, although it is still a condition for a boundary value problem. Thus, to solve the collective set of three scalar equations comprising the components of the Navier-Stokes equation would require an additional eight boundary conditions for each equation, for a total of 24 bounding conditions. Of course three of these 24 conditions will also provide the boundary conditions for the continuity equation, our fourth equation necessary for development of a complete solution.

At this point, one can be staggered by the complexity of the solution process for a fully three-dimensional, time-dependent flow, and can appreciate the need for some degree of simplification. Generally, as the governing equations are simplified (or eliminated because of non-varying dependent variables), the number of bounding conditions is reduced accordingly. In our most simplified situations, such as our first example below for a Couette flow (Section 6.3.1), which reduces to a single second-order ODE, we only require two boundary conditions. As we address more complicated flows, with either multiple equations or additional order derivatives, we will require additional boundary conditions. The most complex flow we address in this text is a boundary layer flow in two dimensions, which necessitates five boundary values: two for u with y , one for u with x , one for v with y , and one for p with x .

6.2.1 Solid Boundaries and the "No Slip" Condition

The most common boundary condition is generally specified at a solid boundary. Boundary conditions for a solid boundary will always be of the first kind, which indicates a specified value of a dependent variable (e.g. $u = 4$) that will exist at a specified spatial location (e.g. at $y = 1$). For example, the velocity of a viscous fluid adjacent to a solid boundary will always be identical to the velocity of the boundary, as a consequence of what is termed the “[no slip](#)” condition.

The no slip condition is a result of fluid-surface behavior at a molecular level. The fluid molecules immediately adjacent to a solid surface fill the molecular voids in the solid surface and mechanically bond (by [adhesion](#)) to the molecules of the solid surface. In contrast, fluid interaction away from a solid surface is due to molecular [cohesion](#), caused by individual fluid molecules being mutually attracted to other fluid molecules; the subsequent effect of molecular cohesion is reflected by the property of fluid viscosity, which was discussed in Chapter 1. Since mechanical adhesion is much stronger than molecular cohesion, a fluid adjacent to a solid surface will move at the velocity of the surface, creating the so-called no slip condition. For example, if a boundary is stationary, the bounding velocity is zero; if the boundary is moving in the x -direction at a velocity U , then the boundary condition is $u = U$. Additionally, the velocity normal to a solid boundary is always zero, unless the boundary moves in a normal direction or has fluid injected through the surface.

6.2.2 Porous Boundaries

Porous boundaries are quite interesting. Such boundaries in reality are such things as screens or (to a certain approximation) perforated plates. These boundaries differ from a solid boundary in that fluid may penetrate perpendicular to the bounding surface. For porous surfaces, we idealize that the flow parallel to the bounding surface is still subject to the no slip condition, and thus moves at the surface velocity in a direction parallel to the surface. However, the permeability of the surface allows flows to move normal to and across the surface, which requires the normal velocity to be specified at the surface. Again, these are boundary conditions of the first kind, with the velocity value specified at a particular spatial position or surface. An example of a porous surface (although the flow is not a Newtonian fluid) is a moving wire belt that is used in papermaking processes. In papermaking, fluidized paper pulp (generally 1% wood fiber in water by volume) flows tangentially onto a moving belt, where the water is rapidly removed from the pulp by suction across the moving, porous wire surface. Other quite interesting examples of porous boundaries will be addressed in this and other chapters to follow.

6.2.3 Boundaries within a Homogeneous Fluid

Boundary conditions within a homogeneous fluid may be either of the first kind or second kind (where the first derivative of an independent variable is specified at a fixed position). An

example of a boundary condition of the first kind would be if a fluid extends to infinity (or at least very far from another bounding surface), at which point the velocity asymptotes to a fixed value, such as a fluid which is at rest far from a moving surface. Another example would be where a fluid is moving at a constant value outside a region of large viscous change, such as the flow outside of the boundary layer that forms when a viscous fluid flows over a solid boundary.

Examples of a boundary condition of the second kind usually occur where the shear stress within the fluid can be considered either zero or a constant value. Since shear stress is directly proportional (for a Newtonian fluid) to the first derivatives of velocity variables, such a bounding condition would indicate a null or constant value of the appropriate velocity derivative(s). This type of boundary condition can occur where a fluid is again assumed to be either at rest or moving at a constant velocity, or where it can be surmised that the velocity has reached either a maximum or minimum (which by definition yields a null first derivative). Such an example is the flow through a pipe or tube, where by symmetry it is inferred that the velocity achieves a maximum at the centerline.

6.2.4 Boundaries between dissimilar fluids

When two fluids move adjacent to one another, this presents an interesting set of boundary conditions, since both the velocity and the shear stress at the interface between the two fluids must be identical, since the velocity in a Newtonian fluid cannot be discontinuous (by definition). This results in coupled boundary conditions of the first and second kind (via the first derivatives of velocity, related through the Stokes shear model of Chapter 5), applied at the fluid-fluid interface. These types of conditions apply for the common movement of adjacent immiscible fluids, such as water and oil.

An interesting two-fluid process is the coupled adjacent flow of water and air. Due to the significant variance in densities (approximately 1000:1), it would seem that the degree of interaction would be insignificant. And when the prime mover is water, such as a flowing river, this is to some degree true. However, when the prime mover is a high-speed airflow, as experienced in storms over the ocean, the result can be the transference of significant motion and energy to the water mass, as evidenced by the generation of ocean waves, which are essentially caused by the solar induced movement of air (i.e. “winds”). I cover an example of such an air-water flow in Chapter 12, on more complicated Navier-Stokes solutions.

6.2.5 Laminar vs. Turbulent flow

The Navier-Stokes equations for incompressible flow, with the appropriate boundary conditions discussed above, apply to all fluids, regardless of their behavior. However, to analyze a particular flow, one needs to determine the flow condition, which can either be a well-behaved

laminar flow or an unsteady, more chaotic type of flow, generally lumped under the term “turbulence.” Laminar flows move smoothly in layers, with no particular mixing. In contrast, turbulent flows, which we cover in Chapter 17, move in a more irregular manner, with significant mixing. The controlling parameter, which is indicative of whether a flow will behave as a laminar or turbulent flow is termed the [Reynolds number](#), which is a ratio of local inertia forces to viscous forces. Originally conceived by [Osborn Reynolds](#) (who first characterized turbulent flow), the Reynolds number originates from dimensional analysis, and is given by the following equation:

$$\mathbf{Re}_\delta = \frac{UL}{\nu} = \frac{UL}{\left(\frac{\mu}{\rho}\right)} = \frac{\rho UL}{\mu} = \frac{\rho U^2}{\mu \left(\frac{U}{L}\right)} \approx \frac{\rho u^2}{\mu \frac{\partial u}{\partial y}} = \frac{\text{inertia forces}}{\text{viscous forces}}$$

Where

L , is a characteristic dimension of the flow or flow geometry (e.g. a pipe diameter);
 U , is a characteristics velocity of the flow (e.g. the average velocity in a pipe); and
 ν , is the kinematic viscosity of the fluid (the ratio of absolute viscosity to density).

Each type of flow can generally be characterized by an appropriate Reynolds number, with some empirically-determined limiting value, below which one should expect laminar flow and above which turbulent flow is probable. These Reynolds number limits vary for different types of flow geometries (which also determine which characteristic length is used). For example, for a flow due to a pressure gradient between parallel plates, the characteristic length would be the distance between the plates, with the limiting Reynolds number $\mathbf{Re}_h = \frac{Uh}{\nu} \approx 1400$, where h is the distance between the plates. For flows in tubes and pipes, the limiting Reynolds number is $\mathbf{Re}_D = \frac{UD}{\nu} \approx 2300$, where D is the tube/pipe inner diameter. Other geometries will have different limiting Reynolds numbers, and be based on different characteristic lengths and velocities (see a broader discussion of the Reynolds number [here](#)).

The key point is that the Reynolds number is a parameter that helps establish whether a flow is expected to behave in a laminar or turbulent manner. We will revisit the Reynolds number, and its implications, later in Chapters 13, 15, and 17. However, for the examples that we consider in this chapter we assume that the Reynolds number is below the critical limit, and that all the flows behave as laminar flows.

6.3 Simple One-Dimensional Solutions with Parallel Boundaries

The simplest types of flows are those between closely-spaced parallel plates. Here we assume that the plates have some finite spacing, and extend to infinity in both the flow and in the cross-flow directions. In the following, we examine several classic parallel plate flows.

6.3.1 Couette Flow

The [Couette flow](#) is the simplest possible viscous flow. However, this type of flow has a variety of applications, from the development of viscometers for the measurement of fluid viscosity, to the assessment of energy dissipation in fluid bearings used in rotating machinery. The concept, as shown in figure 6.1, is quite simple. A viscous fluid is bounded between two parallel plates of infinite extent. One plate moves at a constant velocity U , while the other plate remains fixed. Here we make several simplifying assumptions, as indicated below. Key among these is that the flow is both steady and fully developed, which negates any fluid acceleration effects. Thus, we only need to consider a balance of forces—and only shear forces, since (as we will show) pressure forces are not relevant.

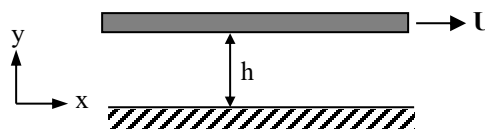


Figure 6.1 Couette flow between a lower stationary surface and an upper moving surface.

Since this configuration is rectangular (we will examine the axisymmetric version of this problem later), we utilize the Navier-Stokes equation in Cartesian coordinates to develop a solution. If we assume that the plates are infinite in extent in the z -direction, then we can further assume that there will be no flow changes in the z -direction (i.e. into the page, as drawn above). This assumption allows us to neglect the z -direction equation, and any terms in the x - and y -direction equations that contain w , the z -direction velocity.

So, writing the x and y Navier-Stokes equations in two-dimensions, we have:

$$\frac{\partial \overset{1}{u}}{\partial t} + u \frac{\partial \overset{2}{u}}{\partial x} + v \frac{\partial \overset{3}{u}}{\partial y} = \beta_x - \frac{1}{\rho} \frac{\partial p}{\partial x} + \nu \left[\frac{\partial^2 \overset{2}{u}}{\partial x^2} + \frac{\partial^2 \overset{2}{u}}{\partial y^2} \right] \quad \text{x-direction N-S} \quad (6.2a)$$

$$\frac{\partial \overset{1}{v}}{\partial t} + u \frac{\partial \overset{2,3}{v}}{\partial x} + v \frac{\partial \overset{3}{v}}{\partial y} = \beta_y - \frac{1}{\rho} \frac{\partial p}{\partial y} + \nu \left[\frac{\partial^2 \overset{3}{v}}{\partial x^2} + \frac{\partial^2 \overset{3}{v}}{\partial y^2} \right] \quad \text{y-direction N-S} \quad (6.2b)$$

Initial Assumptions

1. Steady flow
2. Fully-developed flow; no variations in x -direction
3. $\rho = \text{constant}$
4. Neglect body forces

We now delete non-relevant terms from the Eqs. 6.2 as a consequence of our simplifying assumptions. Note that the red arrows indicate the terms that we neglect in the equations, with the associated number indicating the assumption that allows us to neglect the term.

It may be initially unclear why assumption 3 results in the elimination of velocity terms in the equations. This is a consequence of the continuity equation for an incompressible flow. Recall for a constant density flow that the continuity equation reduces to $\nabla \cdot \vec{V} = 0$, which in two dimensions is:

$$\frac{\partial u}{\partial x} + \frac{\partial v}{\partial y} = 0$$

However, because of the fully-developed flow assumption, which negates any changes in the x direction, the continuity equation reduces to:

$$\frac{\partial v}{\partial y} = 0 \Rightarrow v = f(x) + \text{constant} \Rightarrow v = \text{constant}$$

Note that v will be a constant, since the fully-developed flow assumption means that the velocity characteristics will not change with x-position. To determine the constant in the equation, we note that the boundary condition for v at either solid surface is zero. So, taking $v = 0$ @ $y = 0$, then $v = 0$ everywhere (which also means that higher derivatives of v will also be null as well). Thus, continuity considerations lead to the five cancellations, noted by 3, of v-associated acceleration terms in Eqs. 6.2. Thus, by utilization of the first three assumptions, Eqs. 6.2 are reduced to:

$$\beta_x - \frac{1}{\rho} \frac{\partial p}{\partial x} + \nu \frac{\partial^2 u}{\partial y^2} = 0 \quad , \text{ and} \quad (6.3a)$$

$$\beta_y - \frac{1}{\rho} \frac{\partial p}{\partial y} = 0 \quad (6.3b)$$

Now, our fourth assumption above allows us to drop the body force terms represented by β_x and β_y . However, let's consider why this is a reasonable assumption.

If we assume that gravity acts in the y-direction (vertically, as we look at this page), then we can write:

$$\vec{\beta} = \beta_x \hat{i} + \beta_y \hat{j} = -g \hat{j}$$

This renders Eqs. 6.3 as:

$$\nu \frac{\partial^2 u}{\partial y^2} = \frac{1}{\rho} \frac{\partial p}{\partial x} \quad , \text{ and} \quad (6.4a)$$

$$\frac{\partial p}{\partial y} = -\rho g \quad (6.4b)$$

Integrating the y-equation, Eq. 6.4b, yields:

$$p = -\rho gy + f(x) + C \quad (6.5a)$$

Now, if we let the flow be quiescent, then we would have a hydrostatic condition, where $u = 0$, and Eq. 6.4a reduces to $\frac{\partial p}{\partial x} = 0$. Integrating the simplified Eq. 6.4a yields:

$$p = f(y) + C \quad (6.5b)$$

Comparing Eqs. 6.5a and 6.5b, we note that since Eq. 6.5b contains no function of x , then $f(x)$ in Eq. 6.5a must be zero. Thus, Eq. 6.5a can be reduced to $p = -\rho gy + C$, or $p_H(y) = -\rho gy + p_0$, where $C = p_0$ is the pressure at $y = 0$. $p_H(y)$ is the pressure due to hydrostatic effects, which will exist whether or not motion is imparted to the fluid. Now, when we allow the fluid to move, equation Eq. 6.5a becomes:

$$p = -\rho gy + p_0 + f(x) = p_H(y) + P(x) \quad (6.6)$$

where $p_H(y)$ reflects the hydrostatic pressure due to gravity, and $P(x)$ reflects the dynamic pressure due to the movement of the fluid. Now, substituting Eq. 6.6 back into the original Eqs. 6.4 gives:

$$v \frac{\partial^2 u}{\partial y^2} = \frac{1}{\rho} \frac{\partial P}{\partial x} \quad \text{and} \quad \frac{\partial p_H}{\partial y} + \frac{\partial P}{\partial y} = -\rho g$$

Rearranging (noting $v = \mu/\rho$) yields:

$$\frac{\partial^2 u}{\partial y^2} = \frac{1}{\mu} \frac{\partial P}{\partial x} \quad \text{and} \quad \frac{\partial P}{\partial y} = -\rho g - \frac{\partial p_H}{\partial y} = -\rho g + \rho g = 0$$

Thus, the dynamic pressure, P , can only be a function of x , the direction of fluid motion.

Now consider the assumption that the plates are infinite in the x -direction. The only way that such an assumption is realistic is if the plates were to actually circumvent the earth, and join again, making this a set of continuous parallel surfaces, one moving relative to the other. Such a situation renders the fluid region between the plates connected, and as such we could draw streamlines through the fluid, parallel to the plates. However, this also implies that when these streamlines meet after circumventing the earth, the pressure at that juncture point must be continuous, and thus identical. Moreover, since any point along a continuous streamline could be the juncture point, then the pressure at all points along the streamline must be identical. Thus, the pressure must be a constant, and the derivative of pressure with respect to x must be zero.

Thus, recognizing that $\frac{\partial P}{\partial x} = 0$, the Navier-Stokes equations for a Couette flow reduce to:

$$\frac{\partial^2 u}{\partial y^2} = 0 \quad \text{or} \quad \frac{d^2 u}{dy^2} = 0, \quad \text{since } u \text{ is only a function of } y \quad (6.7)$$

Since Eq. 6.7 is a second order equation for u with respect to y , we require two boundary conditions. Clearly the appropriate boundary conditions are:

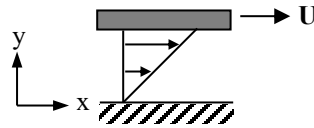
- 1) $u = 0$ @ $y = 0$ 2) $u = U$ @ $y = h$.

Integrating Eq.6.7 twice yields:

$$\begin{aligned} \frac{du}{dy} &= C_1 & \text{Applying the B.C.s} & \quad 1) \quad 0 = C_1(0) + C_2 \Rightarrow C_2 = 0 \\ u &= C_1 y + C_2 & & \quad 2) \quad U = C_1 h \Rightarrow C_1 = \frac{U}{h} \end{aligned}$$

Therefore, the general equation for flow between two parallel plates, with the lower one fixed and the upper one translating at velocity U is:

$$u = U \frac{y}{h} \quad (6.8)$$



The shear stress for this flow field is given by:

$$\tau_{yx} = \mu \left(\frac{\partial u}{\partial y} + \frac{\partial v}{\partial x} \right) = \mu \frac{du}{dy} = \mu \left(\frac{U}{h} \right) = \frac{\mu U}{h} \quad (6.9)$$

Equation 6.9 indicates that the shear is constant across the entire flow field. Additionally, the vorticity is given by:

$$\omega_{zz} = \left(\frac{\partial v}{\partial x} - \frac{\partial u}{\partial y} \right) = -\frac{du}{dy} = -\left(\frac{U}{h} \right) \quad (6.10)$$

Equation 6.10 indicates that the angular velocity is also constant, with the fluid rotating in a clockwise direction.

An additional property of interest is the total flow rate for the fluid passing across a vertical plane. If we assume the depth of the flow (into the page) to be W , we can calculate the volume flow rate, Q , crossing the region $0 \leq y \leq h$ by noting that:

$$Q = \int_{y=0}^{y=h} u W dy = \int_{y=0}^{y=h} \frac{Uy}{h} W dy = \frac{UWy^2}{2h} \Big|_0^h = \frac{UWh}{2} \quad (6.11)$$

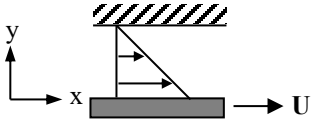
Equation 6.11 is the flow rate induced by the movement of the upper plate due to viscous interaction between the fluid and the plate surface.

Although this solution is for a set of parallel plates, to a reasonable approximation the results are representative of the behavior of a flow between two closely spaced circular surfaces with a low degree of curvature, such as in large journal bearings or any situation where two closely-spaced plates of limited curvature move relative to one another. We will assess the flow within closely adjacent surfaces with a high degree of curvature (like journal bearings) in section [6.4.2](#), when we examine simple Navier-Stokes solutions with circular symmetry.

Before we leave this Couette problem, note that the same type of solution will apply to the same geometry with different first order boundary conditions. For example, if we held the top plate fixed, and translated the lower plate, the boundary conditions would be:

$$1) \mathbf{u} = \mathbf{U} \text{ @ } y = 0 \quad \text{and} \quad 2) \mathbf{u} = \mathbf{0} \text{ @ } y = h.$$

The subsequent solution would then be:

$$\mathbf{u} = \mathbf{U} - \mathbf{U} \frac{y}{h} = \mathbf{U} \left(1 - \frac{y}{h} \right) \quad (6.12)$$


Likewise, if we translated both of the plates at different velocities, we would obtain another variation on the linear Couette flow solution.

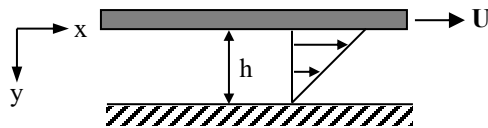


Figure 6.2 Couette flow with an alternative coordinate system.

Another consideration is the impact of the orientation of the coordinate system. Suppose we orient the coordinate system such that the origin is at the upper surface, pointing downward, as shown in figure 6.2. Here Eq. 6.7 is still valid. However, the boundary conditions are now:

$$1) \mathbf{u} = \mathbf{U} \text{ @ } y = 0 \quad 2) \mathbf{u} = \mathbf{0} \text{ @ } y = h.$$

The subsequent solution for the velocity profile will be:

$$\mathbf{u} = \mathbf{U} \left(1 - \frac{y}{h} \right) \quad (6.13)$$

Equation 6.13 describes the same flow as Eq. 6.8, but is functionally different due to the use of a different coordinate system. Note that while Eq. 6.13 and Eq. 6.12 are functionally identical,

they represent two physically different flows. This example thus illustrates the importance of understanding the particular coordinate system to which a particular solution applies.

6.3.2 Poiseuille Flow in a Channel

Whereas a Couette flow is driven by the motion of the bounding surfaces, a [Poiseuille](#) channel flow is driven by a pressure difference applied to the fluid flowing between two parallel plates. For the purposes of this problem, we assume that the pressure decreases in the x-direction, represented by the pressure gradient term, $\frac{\partial p}{\partial x}$, shown in figure 6.3.

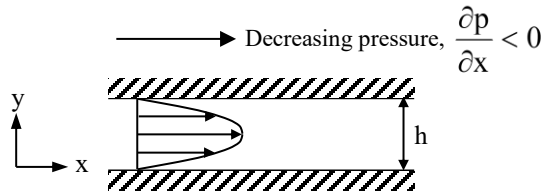


Figure 6.3 Poiseuille flow between parallel plates; fully-developed flow with a constant pressure gradient.

Again, because of the rectangular symmetry of this flow, we utilize the Navier-Stokes equation in Cartesian coordinates, and again assume that the plates are infinite in extent in the z-direction (normal to the page), such that the flow is uniform and unchanging in the z-direction. Thus, we can again neglect the z-direction equation, and terms containing w.

For the x and y Navier-Stokes equations in two-dimensions, we have:

$$\frac{\partial u}{\partial t} + u \frac{\partial u}{\partial x} + v \frac{\partial u}{\partial y} = \beta_x - \frac{1}{\rho} \frac{\partial p}{\partial x} + \nu \left[\frac{\partial^2 u}{\partial x^2} + \frac{\partial^2 u}{\partial y^2} \right] \quad \text{x-direction N-S} \quad (6.14a)$$

$$\frac{\partial v}{\partial t} + u \frac{\partial v}{\partial x} + v \frac{\partial v}{\partial y} = \beta_y - \frac{1}{\rho} \frac{\partial p}{\partial y} + \nu \left[\frac{\partial^2 v}{\partial x^2} + \frac{\partial^2 v}{\partial y^2} \right] \quad \text{y-direction N-S} \quad (6.14b)$$

Initial Assumptions

1. Steady flow
2. Fully-developed flow; no variations in x-direction
3. $\rho = \text{constant}$
4. Neglect body forces

We again employ the same simplifying assumptions employed for the Couette flow example. Note that here our assumption of fully-developed flow assumes that the flow is well downstream from any entrance effects (we will discuss entrance changes later in Chapter 12) such that we again have a flow which has no acceleration effects, and is a simple balance of shear and pressure forces.

As indicated by the red arrows, we delete the non-relevant terms from Eqs. 6.14, again noting that the incompressible continuity equation in two dimensions yields:

$$\frac{\partial u}{\partial x} + \frac{\partial v}{\partial y} = 0$$

and

$$\frac{\partial v}{\partial y} = 0 \Rightarrow v = f(x) + \text{constant} \Rightarrow v = \text{constant}$$

Again, at the plate boundaries, $v = 0$ @ $y = 0$ (or $y = h$), thus $v = 0$ everywhere. Based on this result, Eqs. 6.14 reduce to:

$$-\frac{1}{\rho} \frac{\partial P}{\partial x} + \nu \frac{\partial^2 u}{\partial y^2} = 0 \quad \text{and} \quad -\frac{1}{\rho} \frac{\partial P}{\partial y} = 0$$

Note that the rationale for dropping the body force is the same as addressed for the Couette flow, and thus the introduction of P to represent the dynamic component of pressure. Simplifying the equations gives:

$$\frac{\partial^2 u}{\partial y^2} = \frac{1}{\nu \rho} \frac{\partial P}{\partial x} = \frac{1}{\mu} \frac{\partial P}{\partial x} \quad (\text{where } \nu = \frac{\mu}{\rho}) \quad (6.15a)$$

$$\text{and} \quad \frac{\partial P}{\partial y} = 0 \quad (6.15b)$$

Integration of Eq. 6.15b indicates that $P = f(x)$. However, we don't know the functionality of P or $\frac{\partial P}{\partial x}$, which is needed if we are to solve the x-direction differential equation. We establish this functionality by taking the derivative of the x-direction differential equation, Eq. 6.15a, with respect to x , which yields:

$$\frac{\partial}{\partial x} \left(\frac{\partial^2 u}{\partial y^2} \right) = \frac{\partial}{\partial x} \left(\frac{1}{\mu} \frac{\partial P}{\partial x} \right) = \frac{1}{\mu} \frac{\partial^2 P}{\partial x^2} = 0 \quad (6.16)$$

Equation 6.16 is equal to zero, since we assumed that u is fully developed, and as such its derivatives must only be a function of y .

Equation 6.16 indicates that $\frac{\partial P}{\partial x}$ must be a constant, since $\frac{\partial^2 P}{\partial x^2} = 0$. This is reasonable since the shear stress will be a function of the derivative of the velocity profile, which will also be invariant with streamwise position. So, noting that $u = f(y)$ only, Eq. 6.15a, with appropriate boundary conditions simplifies to:

$$\frac{d^2u}{dy^2} = \frac{1}{\mu} \frac{dP}{dx} = \text{constant} \quad (6.17)$$

- B.C. 1) $u = 0$ @ $y = 0$
 2) $u = 0$ @ $y = h$.

Integrating Eq. 6.17 twice yields:

$$\frac{du}{dy} = \frac{1}{\mu} \frac{dP}{dx} y + C_1$$

$$u = \frac{1}{\mu} \frac{dP}{dx} \frac{y^2}{2} + C_1 y + C_2$$

Applying the B.C.s 1) $0 = \frac{1}{\mu} \frac{dP}{dx} \frac{(0)^2}{2} + C_1(0) + C_2 \Rightarrow C_2 = 0$

2) $0 = \frac{1}{\mu} \frac{dP}{dx} \frac{h^2}{2} + C_1 h \Rightarrow C_1 = -\frac{1}{\mu} \frac{dP}{dx} \frac{h}{2}$

This yields a general equation for a pressure driven flow between two stationary parallel plates as:

$$u = \frac{1}{\mu} \frac{dP}{dx} \frac{y^2}{2} - \frac{1}{\mu} \frac{dP}{dx} \frac{hy}{2} = \frac{1}{2\mu} \frac{dP}{dx} (y^2 - hy) = \frac{h^2}{2\mu} \frac{dP}{dx} \left(\frac{y}{h} - 1 \right) \frac{y}{h} \quad (6.18)$$

The velocity profile reflected by Eq. 6.18 is parabolic (as shown in figure 6.3 above), achieving a maximum midway between the plates, at $y = \frac{h}{2}$, or $\frac{y}{h} = \frac{1}{2}$. If we term the maximum velocity

U_{\max} , then:

$$U_{\max} = \frac{h^2}{2\mu} \frac{dP}{dx} \left(\frac{1}{2} - 1 \right) \frac{1}{2} = -\frac{h^2}{8\mu} \frac{dP}{dx} \quad (6.19)$$

Note the negative sign in Eq. 6.19. What this negative sign indicates is that in order for $U_{\max} > 0$ (i.e. flow in a positive x-direction) then $dP/dx < 0$. Since a Poiseuille flow is a pressure driven flow, Eq. 6.19 indicates that the pressure must be *decreasing* in the direction of flow (x, in this case), which is entirely logical and intuitive.

Substituting Eq. 6.19 into Eq. 6.18 gives:

$$u = 4U_{\max} \left(1 - \frac{y}{h} \right) \frac{y}{h} \quad (6.20)$$

The shear stress for this flow field is then given by:

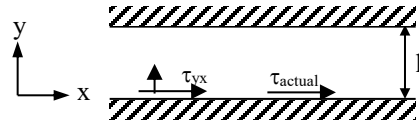
$$\tau_{yx} = \mu \frac{du}{dy} = \frac{4\mu U_{\max}}{h} \left(1 - 2\frac{y}{h}\right) \quad (6.21)$$

Equation 6.21 indicates that the shear varies linearly across the flow channel, varying uniformly from a maximum positive value at $y = 0$ to a maximum negative value at $y = h$, while passing through zero at $y = h/2$.

This shear stress result can be used to illustrate how the process used to define the positive orientation for a surface force, as discussed in Chapter 1, applies here. Recall that the *absolute* direction a stress acts, relative to the coordinate system employed, depends on: (a) the surface of application, and (b) the sign of the calculated stress. Recall also that the product of the signs of the surface normal direction and the stress direction yield the directional sign of a positive stress. Thus, if a calculated stress is positive, it will act in the direction of a positive stress; if a calculated stress is negative, it will act in opposition to the direction of a positive stress.

So, for the shear stress acting on the *lower channel surface* of the Poiseuille flow, from Eq. 6.21 we calculate:

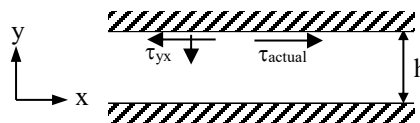
$$\tau_{yx} = \frac{4\mu U_{\max}}{h} \quad \text{at } y = 0$$



The outward normal for the lower surface is oriented in the positive y -direction. Thus, to have a positive absolute orientation, the *product* of the surface normal and the shear direction must both be *positive*. Since the calculated shear stress value is positive, the actual shear stress will act in a positive x -direction, as shown.

However, if we consider the *upper channel surface*, Eq. 6.21 gives the shear stress acting on that surface as:

$$\tau_{yx} = -\frac{4\mu U_{\max}}{h} \quad \text{at } y = h$$



Here, the outward normal for the upper surface is oriented in a negative y -direction. Thus, to have a positive absolute orientation, the *product* of the surface normal and the shear direction must both be *negative*. Since the calculated shear stress value is negative, this means that the actual shear stress acts in a positive x -direction, in opposition to the absolute orientation for that surface, as shown.

Thus, the shear stresses acting on both the upper and lower surfaces are in the *same absolute* direction (which we would anticipate by symmetry), even though the calculated shear stress

values are of different signs. As pointed out in Chapter 1, the process of assigning a “positive” orientation for forces based on the sign product of the surface normal/stress directions assures that the orientation of the force will be consistent, and independent of the particular coordinate system employed.

The vorticity for this flow is given by:

$$\omega_z = \left(\frac{\partial v}{\partial x} - \frac{\partial u}{\partial y} \right) = -\frac{du}{dy} = \frac{4 U_{\max}}{h} \left(2 \frac{y}{h} - 1 \right) \quad (6.22)$$

Equation 6.22 indicates that the vorticity varies linearly from a positive maximum at the upper surface to a negative maximum at the lower surface. As will be shown in Chapter 11, vorticity is generated at *both* channel surfaces due to the pressure gradient —positive at the upper surface and negative at the lower surface. These generated vorticities then diffuse toward the symmetry plane due to viscous effects, where they cancel each other out, thus maintaining a vorticity balance (we will demonstrate this more thoroughly in Chapter 11).

The flow rate for this channel flow (assuming again a depth into the page of W) is given by:

$$Q = \int_{y=0}^{y=h} u W dy = \frac{1}{2\mu} \frac{dP}{dx} \int_{y=0}^{y=h} (y^2 - hy) W dy = -\frac{dP}{dx} \frac{W h^3}{12\mu} = \frac{2}{3} U_{\max} W h \quad (6.23)$$

Equation 6.23 indicates that the flow rate for this viscous flow will be 2/3 of the flow rate of a uniform, inviscid flow moving at U_{\max} . Thus, the area-averaged mean velocity for a Poiseuille flow will also be 2/3 U_{\max} .

6.3.3 Fully-Developed Flow Between Porous Plates

Shown in figure 6.4 below is an interesting extension of the basic Poiseuille-type flow of Section 6.3.2, consisting of a pressure gradient driven, steady flow between two parallel porous plates with constant *transverse* flow across and through the plates. Since the plates are porous, flow can move both parallel to the plates, like a conventional Poiseuille flow, and *transverse* to the main flow, as illustrated in figure 6.4. This transverse flow results in a loss of symmetry for the x-direction velocity profile, with the cross flow skewing the u velocity profile towards the suction plate (the lower plate in figure 6.4 below).

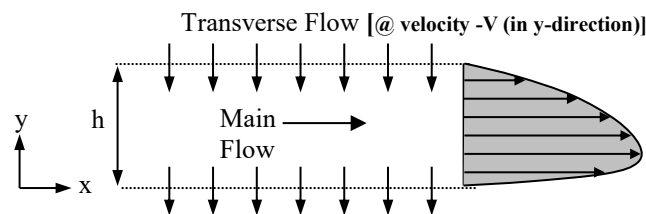


Figure 6.4 Fully-developed laminar flow between parallel plates with injection/suction.

This type of flow can be complicated if the transverse flow is allowed to vary in the x-direction, or where the flow injected through the upper surface does not equal that removed by suction from the lower surface (which would require the mass flow in the main flow to change to conserve mass). However, for the present case, we will assume that the transverse velocity is constant through both bounding surfaces, which renders this problem quite tractable.

For the coordinate system shown, we note that the boundary conditions are given by:

$$u = 0 \text{ and } v = -V \text{ @ } y = 0 \text{ and } y = h$$

Here V is a constant.

The governing two-dimensional equations (x and y directions, for constant density and no body forces) are given by:

$$\frac{\cancel{\partial u}}{\cancel{\partial t}} + u \frac{\cancel{\partial u}}{\cancel{\partial x}} + v \frac{\partial u}{\partial y} = -\frac{1}{\rho} \frac{\partial P}{\partial x} + \nu \left[\frac{\cancel{\partial^2 u}}{\cancel{\partial x^2}} + \frac{\partial^2 u}{\partial y^2} \right] \quad \text{x-direction N-S} \quad (6.24a)$$

$$\frac{\cancel{\partial v}}{\cancel{\partial t}} + u \frac{\cancel{\partial v}}{\cancel{\partial x}} + v \frac{\cancel{\partial v}}{\cancel{\partial y}} = -\frac{1}{\rho} \frac{\partial P}{\partial y} + \nu \left[\frac{\cancel{\partial^2 v}}{\cancel{\partial x^2}} + \frac{\cancel{\partial^2 v}}{\cancel{\partial y^2}} \right] \quad \text{y-direction N-S} \quad (6.24b)$$

$$\frac{\cancel{\partial u}}{\cancel{\partial x}} + \frac{\cancel{\partial v}}{\cancel{\partial y}} = 0 \quad \text{continuity} \quad (6.24c)$$

To simplify the equations, as shown by the red arrows, we assume:

- (1) steady flow
- (2) fully-developed flow $\left(\frac{\partial}{\partial x} \rightarrow 0 \right)$

To simplify the equations further, we note that we can solve the simplified continuity equation as:

$$\frac{\partial v}{\partial y} = 0 \Rightarrow v = f(x) + \text{constant}$$

Here we note that v must be a constant since we have specified that the flow is fully developed, which means that $v \neq f(x)$. Thus, from our v boundary conditions (at either boundary):

$$v = -V$$

Since v is a constant, $v = -V$ will apply everywhere within the flow field. Thus, as indicated, for Eq. 6.24b all v derivative terms drop out, leaving:

$$\frac{\partial P}{\partial y} = 0 \Rightarrow P = f(x) \text{ only}$$

Using an argument similar to that employed for the non-porous Poiseuille flow of Section 6.3.2, we can show that $\frac{\partial P}{\partial x} = \text{constant}$. Thus, since $u = u(y)$ only, we can rewrite Eq. 6.24a as:

$$\begin{aligned} \cancel{y} \frac{du}{dy} &= -\frac{1}{\rho} \frac{dP}{dx} + \nu \frac{d^2 u}{dy^2} \\ -V \frac{du}{dy} &= -\frac{1}{\rho} \frac{dP}{dx} + \nu \frac{d^2 u}{dy^2} \end{aligned}$$

or

$$\frac{d^2 u}{dy^2} + \frac{V}{\nu} \frac{du}{dy} = \frac{1}{\mu} \frac{dP}{dx} = \text{constant} \quad (6.25)$$

Equation 6.25 is a second-order, linear, inhomogeneous ordinary differential equation. To solve Eq. 6.25 we first substitute $\frac{du}{dy} = \alpha$, and rewrite the equation as:

$$\frac{d\alpha}{dy} + \frac{V}{\nu} \alpha = \frac{1}{\mu} \frac{dP}{dx} = \text{const.}$$

This reduces the equation to a first-order, linear, inhomogeneous equation, which we solve for both the homogeneous and the particular solution, where:

$$\alpha = \alpha_{\text{homo}} + \alpha_{\text{part}}$$

Assuming $\alpha_{\text{part}} = A$ (a constant) we can show that,

$$\alpha_{\text{part}} = \frac{1}{\rho V} \frac{dP}{dx}, \quad \text{and} \quad \alpha_{\text{homo}} = C_1 e^{-\frac{V}{\nu} y}$$

Such that:

$$\alpha = \frac{du}{dy} = C_1 e^{-\frac{V}{\nu} y} + \frac{1}{\rho V} \frac{dP}{dx}$$

Integrating again for u , gives;

$$u = -C_1 \frac{\nu}{V} e^{-\frac{V}{\nu} y} + \frac{1}{\rho V} \frac{dP}{dx} y + C_2$$

Now, applying the u -velocity boundary conditions at the plate surfaces, $u = 0$ @ $y = 0$ and $y = h$, yields the following solution for the x -direction velocity:

$$u = \frac{h}{\rho V} \frac{dP}{dx} \left[\frac{y}{h} - \frac{\left(1 - e^{-\frac{v}{V}y}\right)}{\left(1 - e^{-\frac{v}{V}h}\right)} \right] \quad (6.26)$$

To simplify Eq. 6.26, we let $\beta = \frac{Vh}{\nu}$ (a form of Reynolds number) and $y^* = \frac{y}{h}$, and note that $\rho = \frac{\mu}{\nu}$. The resulting expression for the velocity profile can be expressed as:

$$u = \frac{\nu h^2}{\mu V h} \frac{dP}{dx} \left[\frac{y}{h} - \frac{\left(1 - e^{-\frac{Vh}{\nu} \frac{y}{h}}\right)}{\left(1 - e^{-\frac{Vh}{\nu}}\right)} \right] = \frac{h^2}{\mu \beta} \frac{dP}{dx} \left[y^* - \frac{\left(1 - e^{-\beta y^*}\right)}{\left(1 - e^{-\beta}\right)} \right] \quad (6.27a)$$

$$\frac{u_\beta}{U_{\max \text{ at } \beta=0}} = \left[\frac{1}{\left(-\frac{h^2}{8\mu} \frac{dP}{dx}\right)} \right] \frac{h^2}{\mu \beta} \frac{dP}{dx} \left[y^* - \frac{\left(1 - e^{-\beta y^*}\right)}{\left(1 - e^{-\beta}\right)} \right] = \frac{8}{\beta} \left[\frac{\left(1 - e^{-\beta y^*}\right)}{\left(1 - e^{-\beta}\right)} - y^* \right] \quad (6.27b)$$

Figure 6.5 illustrates the effect that the transverse velocity, in terms of the parameter β , has on the velocity profile. In figure 6.5, we non-dimensionalize the stream-wise velocity on the

maximum velocity for a non-porous channel flow (Eq. 6.19), $U_{\max} = -\frac{h^2}{8\mu} \frac{dP}{dx}$, to give us Eq.

6.27b, which allows us to factor out the pressure gradient term. Note that this assumes that we maintain identical pressure gradients for both the suction and non-suction channel flows, which allows us to compare the effect of the transverse velocity on the fully-developed streamwise velocity profile under the same driving condition (i.e. the pressure gradient).

As figure 6.5 clearly shows, the impact of the transverse flow is not only to skew the velocity profile toward the suction wall ($y^* = 0$), but also to *retard* the streamwise flow.

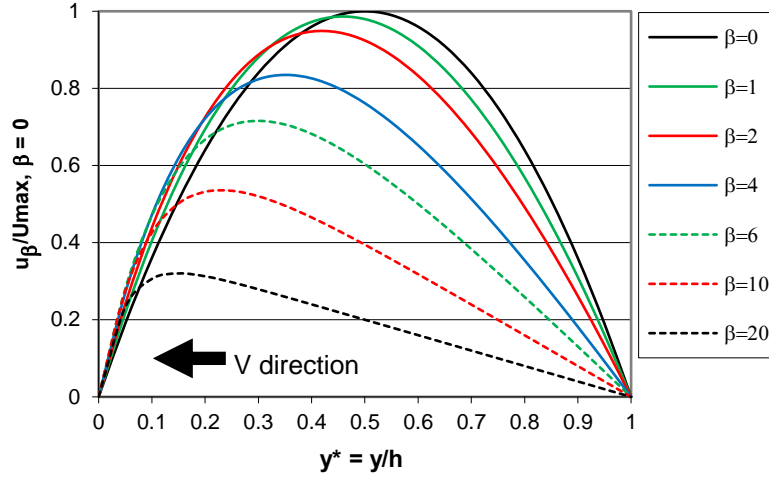


Figure 6.5 Non-dimensional channel flow velocity distributions as a function of suction parameter, $\beta = Vh/\nu$, with $dP/dx = \text{constant}$ for all β values (Eq. 6.27b).

To illustrate the magnitude of this retarding effect, we determine the volume flow rate as a function of β , as follows:

$$Q_{\beta} = \int_{y^*=0}^{y^*=1} u \, W \, h \, dy^* = \frac{h^3 W}{\mu \beta} \frac{dP}{dx} \int_{y^*=0}^{y^*=1} \left(y^* - \frac{(1 - e^{-\beta y^*})}{(1 - e^{-\beta})} \right) dy^* = \frac{h^3 W}{\mu \beta} \frac{dP}{dx} \left[\frac{y^{*2}}{2} - \frac{\left(y^* + \frac{1}{\beta} e^{-\beta y^*} \right)}{(1 - e^{-\beta})} \right]_{y^*=0}^{y^*=1}$$

$$Q_{\beta} = \frac{h^3 W}{\mu \beta} \frac{dP}{dx} \left[\frac{1}{2} - \frac{\left(1 + \frac{1}{\beta} e^{-\beta} \right)}{(1 - e^{-\beta})} + \frac{\left(\frac{1}{\beta} \right)}{(1 - e^{-\beta})} \right] = \frac{h^3 W}{\mu \beta} \frac{dP}{dx} \left[\frac{1}{2} + \frac{\frac{1}{\beta} (1 - e^{-\beta}) - 1}{(1 - e^{-\beta})} \right] \quad (6.28a)$$

To provide an appropriate reference, we non-dimensionalize the flow rate for the porous channel, Eq. 6.28a, on the flow rate for a non-porous channel, given in section 6.3.2 by Eq. 6.23 as:

$$Q_{\beta=0} = - \frac{dP}{dx} \frac{W h^3}{12 \mu}$$

This gives us:

$$\frac{Q_{\beta}}{Q_{\beta=0}} = - \frac{12}{\beta} \left[\frac{1}{2} + \frac{\frac{1}{\beta} (1 - e^{-\beta}) - 1}{(1 - e^{-\beta})} \right] \quad (6.28b)$$

Here we again we let the driving force, $\frac{dP}{dx}$, be identical for both the non-porous and porous channels. The result for Eq. 6.28b, shown in figure 6.6 as $\frac{Q_\beta}{Q_{\beta=0}}$ vs β , reveals a significant reduction of the flow rate with increasing transverse flow (note that to obtain the asymptotic value of $\frac{Q_\beta}{Q_{\beta=0}} = 1$ at $\beta = 0$, requires application of L’hopital’s rule --- 4 times!).

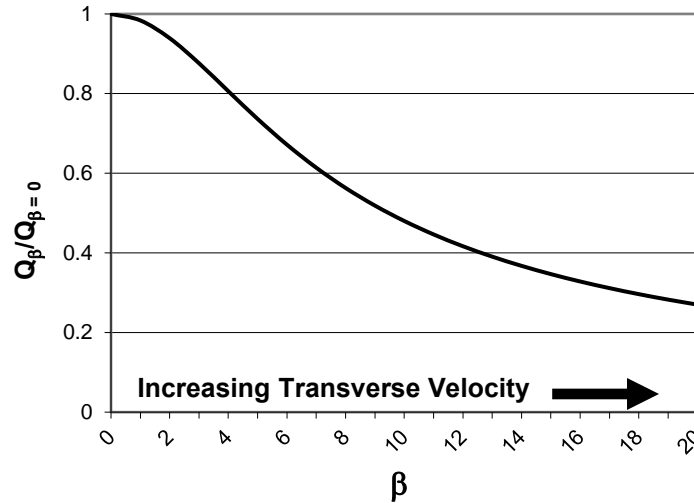


Figure 6.6 The retardation of the volume flow rate through a porous channel with increasing transverse velocity ($\beta = Vh/\nu$), Eq.6.28a.

The retardation of the main flow by transverse fluid injection/suction is clear, but it is unclear what the magnitude of the corresponding injection velocity is to a main flow velocity. To assess this, we compare the transverse velocity, V , as a function of β , again non-dimensionalized on the maximum velocity for the non-porous case, i.e. $U_{\max, \beta=0}$. To do this, we rewrite the beta parameter as:

$$\beta = \frac{Vh}{\nu} = \frac{Vh}{\nu} \left(\frac{U_{\max, \beta=0}}{U_{\max, \beta=0}} \right) = \left(\frac{V}{U_{\max, \beta=0}} \right) \left(\frac{U_{\max, \beta=0} h}{\nu} \right) = \left(\frac{V}{U_{\max, \beta=0}} \right) Re_{\beta=0}$$

We identify $Re_{\beta=0} = \frac{U_{\max, \beta=0} h}{\nu}$ as the Reynolds number of the flow for the non-porous

channel, based on the flow centerline velocity. Solving for $\frac{V}{U_{\max, \beta=0}}$, we have:

$$\frac{V}{U_{\max, \beta=0}} = \frac{\beta}{Re_{\beta=0}} \tag{6.28c}$$

For most laminar channel flows $Re_{\beta=0}$ would be on the order of 1000 to 4000. So, taking $Re_{\beta=0} = 1000$ as an example value, Eq. 6.28c indicates that:

$$\frac{V}{U_{\max, \beta=0}} \approx \frac{\beta}{1000} \approx \beta \times 10^{-3}$$

Examining Figure 6.6 indicates that for $\beta = 4$, which reflects a transverse ratio of

$\frac{V}{U_{\max, \beta=0}} = 0.004$, the volume flowrate will be reduced by 20%. Likewise, a transverse ratio of

just 0.01 ($\beta = 10$), or 1% of $U_{\max, \beta=0}$, will reduce the volume flowrate by more than 50%. These numbers indicate that a relatively small transverse velocity can have a remarkable effect on the volume flowrate of the main flow. However, transverse injection/suction at the porous boundaries may also have a destabilizing effect on the flow, and will probably cause a transition to turbulence (which we consider in Chapter 17). However, while the transition to a turbulent flow will modify the physics of the flow, transverse fluid injection/suction will still have the same retarding effect on the mainstream flow.

Since this is a fully-developed flow, we reason that the increased flow retardation may be due to a cumulative increase in the surface shear stresses. To examine this, we calculate the shear stress for this velocity profile as:

$$\tau = \mu \frac{du}{dy} = \frac{h^2}{\rho V} \frac{dP}{dx} \left[\frac{1}{h} - \frac{\frac{V}{\nu} e^{-\frac{V}{\nu} y}}{1 - e^{-\frac{V}{\nu} h}} \right] \quad \text{or} \quad \tau = \frac{h}{\beta} \frac{dP}{dx} \left[1 - \frac{\beta e^{-\beta y^*}}{1 - e^{-\beta}} \right]$$

Figure 6.7, is a plot of non-dimensionalized shear stress for the porous channel relative to the maximum wall shear stress for a non-porous Poiseuille flow determined in Section 6.2.2:

$$\tau_{\beta=0, \text{Max}} = \frac{4\mu U_{\max}}{h} = -\frac{h}{2} \frac{dP}{dx}$$

This gives the non-dimensional shear stress as:

$$\frac{\tau}{\tau_{\beta=0, \text{Max}}} = \frac{2}{\beta} \left[\frac{\beta e^{-\beta y^*}}{1 - e^{-\beta}} - 1 \right] \quad (6.29)$$

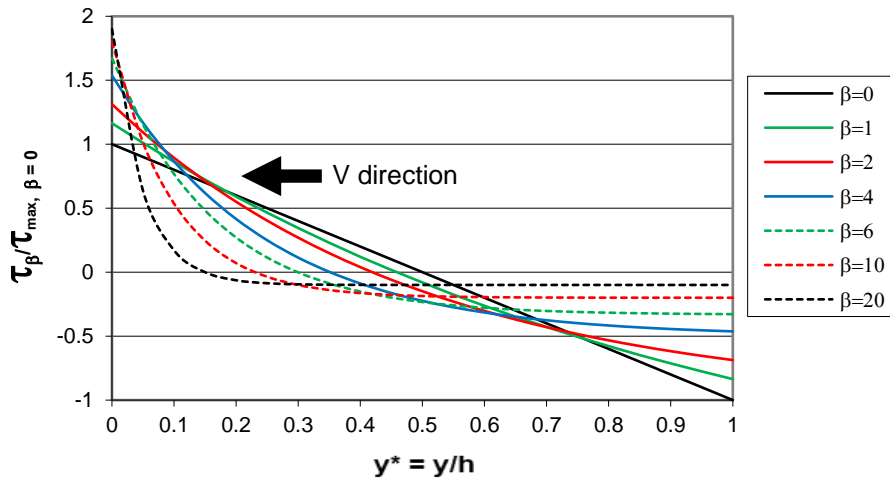


Figure 6.7 Non-dimensional channel flow shear stress distributions as a function of suction parameter, $\beta = Vh/\nu$, with $dP/dx = \text{constant}$ for all β values (Eq. 6.29).

Figure 6.7 plots $\frac{\tau_\beta}{\tau_{\max, \beta=0}}$ as a function of the suction parameter, β , and illustrates the marked

variations in shear stress that take place across the porous channel with increasing β .

Note that the shear stress adjacent to the suction surface ($y^* = 0$) increases significantly with transverse flow, whereas the shear stress is substantially reduced near the injection surface ($y^* = 1$). For higher β values the shear stress becomes almost constant over a broad region of the flow.

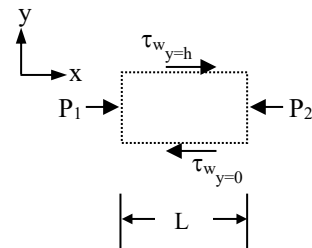
Examining Eq. 6.29 for the shear stress limits as $\beta \gg 1$ shows that $\frac{\tau_\beta}{\tau_{\max, \beta=0}} \rightarrow 2$ at the suction

surface and $\frac{\tau_\beta}{\tau_{\max, \beta=0}} \rightarrow 0$ at the injection surface, which one might surmise from the behavior of figure 6.7.

Since there is no acceleration of the fluid for a fully-developed flow, we can perform a two-dimensional, integral force balance on the fluid between the plates, for a distance L in length, obtaining:

$$\sum F = P_1 h - P_2 h + (\tau_{w, y=h} L) - (\tau_{w, y=0} L) = 0$$

$$(P_1 - P_2)h = -\frac{\mu h L}{\rho V} \frac{dP}{dx} \left[\frac{-\frac{V}{\nu} e^{-\frac{y}{h}}}{\left(1 - e^{-\frac{y}{h}}\right)} - \frac{-\frac{V}{\nu}}{\left(1 - e^{-\frac{y}{h}}\right)} \right]$$



or,

$$(P_1 - P_2)h = -\frac{\mu h L}{\rho \nu} \frac{dP}{dx} \frac{\nu}{\rho} \left[\frac{1 - e^{-\frac{\nu}{h}}}{1 - e^{-\frac{\nu}{h}}} \right] \Rightarrow \frac{P_1 - P_2}{L} = -\frac{dP}{dx} \Rightarrow \frac{dP}{dx} = -\frac{(P_1 - P_2)}{L} \quad (6.30)$$

Equation 6.30 is the same result that we would obtain for a non-porous channel Poiseuille flow. What this implies is that the sum of the shear stresses on the channel surfaces exactly balances the streamwise pressure gradient. One can see in figure 6.7 that the sum of the shear stresses on the top and bottom surfaces [note that one has to account for the “absolute” direction of the *magnitude* of the stresses---both will act in the same direction] will be the *same*, regardless of the transverse velocity (i.e. $|\tau_{y^*=h}| + |\tau_{y^*=0}| = \text{constant}$ for all β , including $\beta = 0$).

So if the cumulative shear stresses on the plate surfaces don't change, and the pressure gradient is held constant, why is the flowrate reduced with increasing β ? The answer lies in the x-direction momentum change that the transverse fluid must undergo in crossing the channel.

When a fluid particle is injected at $y^* = y/h = 1$ it has zero streamwise velocity. As it enters the channel, the collective action of the pressure gradient and viscous interaction with the faster moving streamwise fluid causes the fluid particle to *accelerate* in the x-direction as it initially proceeds across the channel. However, after the fluid particle passes the point of maximum streamwise velocity, the fluid particle encounters a *negative* velocity gradient, such that the fluid particle is now retarded in the x-direction by viscous interaction with the slower moving streamwise fluid. This retarding effect due to viscous interaction overwhelms the opposing effect of the pressure gradient, causing the particle to *decelerate* as it approaches the suction surface at $y^* = 0$, until it exits the suction surface with zero streamwise velocity. Thus, what happens physically is that the fluid particle must be accelerated by the pressure gradient, and then decelerated by viscosity as it traverses the channel. The net change in x-direction momentum is zero, since the fluid particle enters and exits with zero streamwise velocity. However, viscous effects subsequently dissipate all the x-direction momentum imparted to the fluid particle by the pressure gradient.

Thus, although there is no net increase in shear at the bounding surfaces, there is an internal dissipation of momentum that mediates the effectiveness of the driving force, $\frac{dP}{dx}$.

Consequently, the pressure gradient must not only balance the wall shear stresses, but must also provide the impetus to accelerate all of the injected fluid to steady state conditions, prior to the injected fluid being removed and that momentum “lost.” The result is a diminished flow rate, and a retarded velocity field, while experiencing the same flow resistance as a non-suction channel.

Note that for higher β values, the velocity profile adjacent to the injection surface behaves almost like a Couette flow [e.g. the $\beta = 20$ profile in figure 6.5]. If we examine the governing equation, Eq. 6.25,

$$\frac{d^2u}{dy^2} + \frac{V}{\nu} \frac{du}{dy} = \frac{1}{\mu} \frac{dP}{dx},$$

what we realize is that the change in the shear stress in this Couette-type region, reflected by the $\frac{d^2u}{dy^2}$ term in Eq.6.25, is essentially negligible. Consequently, the constant pressure gradient causes the injected particle to undergo essentially a constant streamwise acceleration as it moves across the channel, until it approaches the suction wall and experiences the significant viscous x-direction deceleration necessary to allow it to exit at zero streamwise velocity.

One of the study problems given at the end of this Chapter concerns a Couette flow with uniform transverse suction. In a boundary-driven Couette-type flow, a similar type of retardation of the induced streamwise flow rate with increasing transverse flow is also observed, reinforcing that the necessity to continually accelerate newly injected fluid particles will always reduce the effectiveness of the driving force in moving the main flow. However, for the case of a Couette flow with transverse flow, the impact of the x-direction momentum changes is experienced directly as an increase in the force required to translate the surface due to the x-direction momentum lost through the suction surface, and a consequent increase in the shear stress on the moving surface.

As a final consideration of this channel flow with transverse suction, note that if you let $V = 0$, the result should reduce to the solution for a Poiseuille flow between two non-porous parallel plates, as was derived in section 6.3.2 above. However, in order to obtain these limiting conditions from the porous plate solution you will need to apply [L'Hospital's rule](#) for $\beta \rightarrow 0$ (i.e. $V \rightarrow 0$)----often multiple times to determine the limiting values. The reader should do this as an exercise.

6.3.4 Two-Fluid Couette Flow

Consider a Couette-type flow, with two immiscible fluids (here we choose water and oil) contained within two parallel constraining plates, and driven by the steady motion of the top plate at a constant velocity U , as modeled in figure 6.8 below. For simplicity, we will assume that the two fluids are of equal thickness, h , as shown. We also assume that the upper fluid is the oil, since oils are always less dense than water (see this [link](#)). We wish to determine the velocity behavior within the two fluids, and the resulting shear stress on the moving plate. While a bit

artificial, this flow will illustrate the use of common boundary conditions when considering two mutually adjacent fluids.

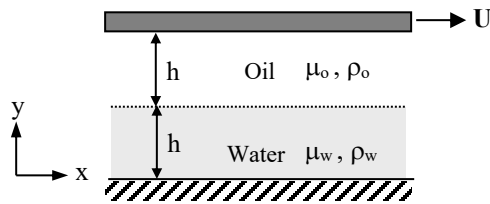


Figure 6.8 The two-fluid, Couette flow

We again utilize the two-dimensional Navier-Stokes equations, but we must apply a separate set of equations for each of the fluids. The assumptions and simplifications that apply for a single fluid Couette flow also apply here, and are:

1. Steady flow
2. Fully developed flow; no variations in x-direction
3. $\rho = \text{constant}$
4. Neglect body forces

Employing these assumptions, and noting that again that the continuity equation yields $v = 0$ throughout both fluids, we reduce the governing equations to a pair of simple second order, ordinary differential equations:

$$\frac{d^2 u_o}{dy^2} = 0 \quad (6.31a)$$

and

$$\frac{d^2 u_w}{dy^2} = 0 \quad (6.31b)$$

In Eqs. 6.31, u_o is the x-direction velocity within the oil, and u_w is the x-direction velocity within the water. Note that Eq. 6.31a and 6.31b each apply only within the region occupied by the respective fluid, and the boundary conditions at the interface between the two fluids ($y = h$) must match.

Here, the appropriate set of boundary conditions is:

- 1) $u_w = 0 @ y = 0$
- 2) $u_o = U @ y = 2h$
- 3) $u_w = u_o @ y = h$
- 4) $\tau_w = \tau_o @ y = h$ (i.e. $\mu_o \frac{du_o}{dy} = \mu_w \frac{du_w}{dy}$)

Note that we require four boundary conditions since we have two second-order differential equations, each of which will yield two constants of integration. In addition, the fourth boundary condition requires that the shear stress between the two fluids must match. Since the shear stress (for this parallel flow) is proportional to the y -derivative of the u velocities, this represents a boundary condition of the second kind.

Integrating Eqs. 6.31 twice yields two simple linear solutions:

$$u_o = C_1 y + C_2$$

and

$$u_w = C_3 y + C_4$$

Applying boundary conditions 1) and 2) yields:

$$U = C_1(2h) + C_2 \Rightarrow C_2 = U - 2hC_1 \quad \text{and} \quad 0 = C_4$$

Such that:

$$u_o = U + C_1(y - 2h) \quad \text{and} \quad u_w = C_3 y$$

Applying boundary conditions 3) and 4) at the common boundary, $y = h$, yields:

$$C_3 h = U - C_1 h \quad \text{and} \quad \mu_w C_3 = \mu_o C_1$$

Solving for C_1 and C_3 simultaneously yields velocity distributions:

$$u_o = U + \frac{U(y - 2h)}{h} \frac{\mu_w}{(\mu_w + \mu_o)} \quad (\text{for } 2h \leq y \leq h) \quad (6.32a)$$

and

$$u_w = \frac{Uy}{h} \frac{\mu_o}{(\mu_w + \mu_o)} \quad (\text{for } h \leq y \leq 0) \quad (6.32b)$$

The corresponding shear stresses within each fluid are:

$$\tau_o = \frac{\mu_o U}{h} \frac{\mu_w}{(\mu_w + \mu_o)} = \frac{\mu_o \mu_w}{(\mu_w + \mu_o)} \frac{U}{h} \quad (6.33a)$$

and

$$\tau_w = \frac{\mu_w U}{h} \frac{\mu_o}{(\mu_w + \mu_o)} = \frac{\mu_o \mu_w}{(\mu_w + \mu_o)} \frac{U}{h} \quad (6.33b)$$

Note that Eqs. 6.33 indicates that $\tau_o = \tau_w = \text{constant}$ across both fluids. This is a reasonable result, since a force balance applied to the boundaries of the fluid indicates that the shear at both the top and bottom boundaries must be equal, and thus the shear stress must be in balance throughout the fluids.

Using these results, consider a two-fluid flow of SAE 10 oil and water. At 20°C, the absolute viscosity of SAE 10 oil is about 100 times that of water, so the shear stress within the oil (and at the top surface) and the water would be:

$$\tau_o = \frac{100(\mu_w)^2}{10\mu_w} \frac{U}{h} \approx 0.99 \frac{\mu_w U}{h}$$

By comparison, if the region between the plates contained all water or all oil, the respective shear stresses would be:

$$\tau_w = \frac{\mu_w U}{2h} \quad (\text{for all water}) \quad \text{or} \quad \tau_o = \frac{\mu_o U}{2h} = \frac{50\mu_w U}{h} \quad (\text{for all SAE 10 oil})$$

So the addition of the much more viscous oil layer will only increase the shear stress of the combined fluid layers by roughly a factor of two over what would exist with only water—and much less than the 100-fold increase in shear stress that would occur from an all water flow to an all oil flow. Clearly, the layer of a much less viscous fluid in proximity to a much more viscous fluid strongly biases the wall shear stress toward the shear stress of the less viscous fluid. In fact, our analysis indicates that the shear can never reach more than twice the shear that would exist for the less viscous of the two fluids. In situations where the two fluids can be easily separated, one can conceive of using a less viscous fluid to facilitate the transport of a more viscous material at reduced power costs. However, in practice, it would be hard to maintain a laminar environment, and in a pipe flow one would have to be able to concentrate the more viscous fluid at the center, with the less viscous fluid at the boundary; not an easy thing to do.

6.3.5 Two-Fluid Poiseuille Flow in a Channel

Now, consider a pressure gradient driven Poiseuille-type flow of two immiscible fluids (fluid a and fluid b) flowing adjacent to each other, constrained by stationary flat plates. Here, we assume a channel width of h , and that fluid a is of thickness t within the channel, and fluid b fills the remainder of the channel $t < y < h$, as shown in figure 6.9.

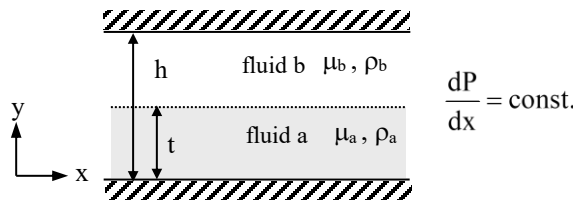


Figure 6.9 A two-fluid, Poiseuille flow

We wish to determine the velocity behavior within the two fluids, and the resulting volume flow rate. This type of flow is a bit more practical, since it can illustrate, for example, the flow interaction between two separate, but adjacent, fluids, such as air and water, or oil and water. This flow again illustrates the use of common boundary conditions when considering two

mutually adjacent fluids. However, it is a bit more complicated than the Couette flow examined in section 6.3.4.

Utilizing the two-dimensional Navier-Stokes equations, we again must apply a separate set of equations for each of the fluids. And again, the assumptions and simplifications that apply for a single fluid Poiseuille flow also apply here, and are:

1. Steady flow
2. Fully-developed flow; no variations in x-direction
3. $\rho = \text{constant}$
4. Neglect body forces

Employing these assumptions, and noting that again that the continuity equation yields $v = 0$ throughout both fluids, we reduce the governing equations to a pair of second-order ordinary differential equations similar to Eq. 6.15a:

$$\frac{d^2 u_a}{dy^2} = \frac{1}{\mu_a} \frac{dP}{dx} \quad (6.34a)$$

and

$$\frac{d^2 u_b}{dy^2} = \frac{1}{\mu_b} \frac{dP}{dx} \quad (6.34b)$$

In Eqs. 6.34, u_a is the x-direction velocity within fluid a, and u_b is the x-direction velocity within fluid b. Note that Eqs. 6.34a and 6.34b each apply only within the region occupied by the respective fluid, and the boundary conditions at the interface between the two fluids ($y = t$) must match.

Here, the appropriate set of boundary conditions is:

- 1) $u_a = 0$ @ $y = 0$
- 2) $u_b = 0$ @ $y = h$
- 3) $u_a = u_b$ @ $y = t$
- 4) $\tau_a = \tau_b$ @ $y = t$ (i.e. $\mu_a \frac{du_a}{dy} = \mu_b \frac{du_b}{dy}$)

We again require four boundary conditions, since we again have two second-order differential equations, each of which will yield two constants of integration.

Integrating Eqs. 6.34 twice yields two simple linear solutions:

$$\begin{aligned} \frac{du_a}{dy} &= \frac{1}{\mu_a} \frac{dP}{dx} y + C_{1a} \\ u_a &= \frac{1}{\mu_a} \frac{dP}{dx} \frac{y^2}{2} + C_{1a} y + C_{2a} \end{aligned} \quad (6.35)$$

and

$$\begin{aligned}\frac{du_b}{dy} &= \frac{1}{\mu_b} \frac{dP}{dx} y + C_{1b} \\ u_b &= \frac{1}{\mu_b} \frac{dP}{dx} \frac{y^2}{2} + C_{1b}y + C_{2b}\end{aligned}\quad (6.36)$$

Applying boundary condition 1) @ $y = 0$ yields:

$$u_a = 0 = \frac{1}{\mu_a} \frac{dP}{dx} \frac{(0)^2}{2} + C_{1a}(0) + C_{2a} \Rightarrow C_{2a} = 0 \quad (6.37)$$

From boundary condition 2) @ $y = h$ we have:

$$u_b = 0 = \frac{1}{\mu_b} \frac{dP}{dx} \frac{h^2}{2} + C_{1b}h + C_{2b} \quad (6.38)$$

From boundary condition 3) @ $y = t$ we get:

$$u_a = \frac{1}{\mu_a} \frac{dP}{dx} \frac{t^2}{2} + C_{1a}t = u_b = \frac{1}{\mu_b} \frac{dP}{dx} \frac{t^2}{2} + C_{1b}t + C_{2b} \quad (6.39)$$

Finally, applying boundary condition 4) @ $y = t$, yields:

$$\begin{aligned}\mu_a \frac{du_a}{dy} &= \frac{dP}{dx} t + \mu_a C_{1a} = \mu_b \frac{du_b}{dy} = \frac{dP}{dx} t + \mu_b C_{1b} \\ \mu_a C_{1a} &= \mu_b C_{1b} \Rightarrow C_{1b} = \frac{\mu_a}{\mu_b} C_{1a}\end{aligned}\quad (6.40)$$

Now, combining Eq. 6.38 and 6.40:

$$C_{2b} = -\frac{1}{\mu_b} \frac{dP}{dx} \frac{h^2}{2} - C_{1b}h = -\frac{1}{\mu_b} \frac{dP}{dx} \frac{h^2}{2} - \frac{\mu_a}{\mu_b} C_{1a}h \quad (6.41)$$

Substituting Eqns. 6.40 and 6.41 into 6.39 gives:

$$\frac{1}{\mu_a} \frac{dP}{dx} \frac{t^2}{2} + C_{1a}t = \frac{1}{\mu_b} \frac{dP}{dx} \frac{t^2}{2} + \frac{\mu_a}{\mu_b} C_{1a}t - \frac{1}{\mu_b} \frac{dP}{dx} \frac{h^2}{2} - \frac{\mu_a}{\mu_b} C_{1a}h$$

Solving for C_{1a} gives:

$$C_{1a} = \frac{\frac{h}{2\mu_b} \frac{dP}{dx} \left[\left(1 - \frac{\mu_b}{\mu_a}\right) \left(\frac{t}{h}\right)^2 - 1 \right]}{\frac{t}{h} \left(1 - \frac{\mu_a}{\mu_b}\right) + \frac{\mu_a}{\mu_b}} \quad (6.42)$$

Substituting Eq. 6.42 back into Eqs. 6.40 and 6.41, we have:

$$C_{1b} = \frac{\mu_a}{\mu_b} C_{1a} = \frac{\frac{h}{2\mu_b} \frac{dP}{dx} \left[\left(\frac{\mu_a}{\mu_b} - 1\right) \left(\frac{t}{h}\right)^2 - \frac{\mu_a}{\mu_b} \right]}{\frac{t}{h} \left(1 - \frac{\mu_a}{\mu_b}\right) + \frac{\mu_a}{\mu_b}} \quad (6.43)$$

and

$$C_{2b} = -\frac{1}{\mu_b} \frac{dP}{dx} \frac{h^2}{2} - \frac{\frac{h^2}{2\mu_b} \frac{dP}{dx} \left[\left(\frac{\mu_a}{\mu_b} - 1\right) \left(\frac{t}{h}\right)^2 - \frac{\mu_a}{\mu_b} \right]}{\frac{t}{h} \left(1 - \frac{\mu_a}{\mu_b}\right) + \frac{\mu_a}{\mu_b}} \quad (6.44)$$

Finally, substituting Eqs. 6.37, 6.42, 6.43 and 6.44 into Eqs. 6.35 and 6.36, and simplifying, we have:

$$u_a = \frac{1}{\mu_a} \frac{dP}{dx} \frac{y^2}{2} + \frac{\frac{hy}{2\mu_b} \frac{dP}{dx} \left[\left(1 - \frac{\mu_b}{\mu_a}\right) \left(\frac{t}{h}\right)^2 - 1 \right]}{\frac{t}{h} \left(1 - \frac{\mu_a}{\mu_b}\right) + \frac{\mu_a}{\mu_b}}$$

$$u_a = \frac{h^2}{2\mu_b} \frac{dP}{dx} \left\{ \frac{\mu_b}{\mu_a} \left(\frac{y}{h}\right)^2 + \left(\frac{y}{h}\right) \frac{\left[\left(1 - \frac{\mu_b}{\mu_a}\right) \left(\frac{t}{h}\right)^2 - 1 \right]}{\left[\left(1 - \frac{\mu_a}{\mu_b}\right) \frac{t}{h} + \frac{\mu_a}{\mu_b} \right]} \right\} \quad (6.45)$$

and

$$u_b = \frac{1}{\mu_b} \frac{dP}{dx} \frac{y^2}{2} + \frac{\frac{hy}{2\mu_b} \frac{dP}{dx} \left[\left(\frac{\mu_a}{\mu_b} - 1\right) \left(\frac{t}{h}\right)^2 - \frac{\mu_a}{\mu_b} \right]}{\frac{t}{h} \left(1 - \frac{\mu_a}{\mu_b}\right) + \frac{\mu_a}{\mu_b}} - \frac{1}{\mu_b} \frac{dP}{dx} \frac{h^2}{2} - \frac{\frac{h^2}{2\mu_b} \frac{dP}{dx} \left[\left(\frac{\mu_a}{\mu_b} - 1\right) \left(\frac{t}{h}\right)^2 - \frac{\mu_a}{\mu_b} \right]}{\frac{t}{h} \left(1 - \frac{\mu_a}{\mu_b}\right) + \frac{\mu_a}{\mu_b}}$$

$$u_b = \frac{h^2}{2\mu_b} \frac{dP}{dx} \left\{ \left[\left(\frac{y}{h} \right)^2 - 1 \right] + \left[\frac{y}{h} - 1 \right] \left[\frac{\left(\frac{\mu_a - 1}{\mu_b} \right) \left(\frac{t}{h} \right)^2 - \frac{\mu_a}{\mu_b}}{\left(1 - \frac{\mu_a}{\mu_b} \right) \frac{t}{h} + \frac{\mu_a}{\mu_b}} \right] \right\} \quad (6.46)$$

To make the results non-dimensional, and a bit more appropriate for plotting, we divide Eqs. 6.45 and 6.46 through by $\frac{h^2}{2\mu_b} \frac{dP}{dx}$, to give:

$$u'_a = \frac{u_a}{\frac{h^2}{2\mu_b} \frac{dP}{dx}} = \frac{\mu_b}{\mu_a} \left\{ \left(\frac{y}{h} \right)^2 + \left(\frac{y}{h} \right) \left[\frac{\left(\frac{\mu_a - 1}{\mu_b} \right) \left(\frac{t}{h} \right)^2 - \frac{\mu_a}{\mu_b}}{\left(1 - \frac{\mu_a}{\mu_b} \right) \frac{t}{h} + \frac{\mu_a}{\mu_b}} \right] \right\} \quad (6.47)$$

and

$$u'_b = \frac{u_b}{\frac{h^2}{2\mu_b} \frac{dP}{dx}} = \left\{ \left[\left(\frac{y}{h} \right)^2 - 1 \right] + \left[\frac{y}{h} - 1 \right] \left[\frac{\left(\frac{\mu_a - 1}{\mu_b} \right) \left(\frac{t}{h} \right)^2 - \frac{\mu_a}{\mu_b}}{\left(1 - \frac{\mu_a}{\mu_b} \right) \frac{t}{h} + \frac{\mu_a}{\mu_b}} \right] \right\} \quad (6.48)$$

Finally, to make Eqs. 6.47 and 6.48 less cumbersome, we define:

$$K_{ab} = \frac{\left(\frac{\mu_a - 1}{\mu_b} \right) \left(\frac{t}{h} \right)^2 - \frac{\mu_a}{\mu_b}}{\left(1 - \frac{\mu_a}{\mu_b} \right) \frac{t}{h} + \frac{\mu_a}{\mu_b}}$$

Allowing us to write:

$$u'_a = \frac{\mu_b}{\mu_a} \left[\left(\frac{y}{h} \right)^2 + \left(\frac{y}{h} \right) K_{ab} \right] \quad (6.49)$$

$$u'_b = \left[\left(\frac{y}{h} \right)^2 - 1 \right] + \left[\left(\frac{y}{h} \right) - 1 \right] K_{ab} \quad (6.50)$$

Note that if $\frac{\mu_a}{\mu_b} = 1$, then $K_{ab} = -1$, and Eqs. 6.49 and 6.50 reduce to the same equation, i.e.:

$$u'_a = u'_b = \left(\frac{y}{h} \right)^2 - \left(\frac{y}{h} \right) = \left(\frac{y}{h} - 1 \right) \frac{y}{h}$$

This is of the same form as Eq. 6.17, for a single fluid Poiseuille flow, as it should be.

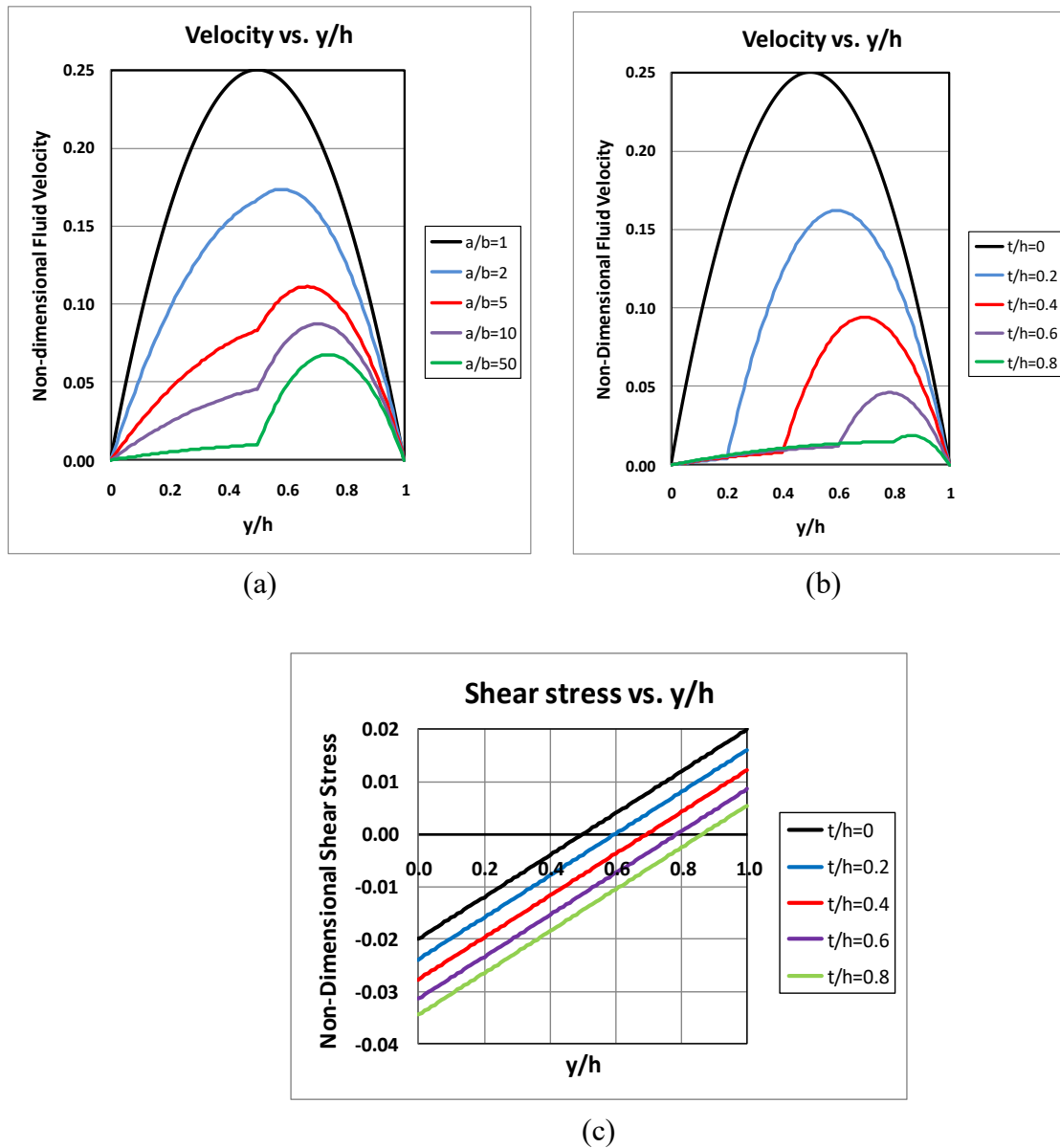


Figure 6.10 Non-dimensional velocity and shear stress for a two-fluid Poiseuille flow between parallel plates. u_a on the right, and u_b on the left.
 (a) velocity: $t/h = 0.5$, viscosity ratios $(\mu_a/\mu_b) = 1, 2, 5, 10, 50$.
 (b) velocity: $\mu_a/\mu_b = 50$, thickness ratios $(t/h) = 0, 0.2, 0.4, 0.6, 0.8$.
 (c) shear stress: $\mu_a/\mu_b = 50$, thickness ratios $(t/h) = 0, 0.2, 0.4, 0.6, 0.8$.

Figure 6.10 shows selected profiles of velocity and shear stress. Figure 6.10a (velocity) is for equal thickness fluid layers ($t = 0.5h$), for varying ratios of $\frac{\mu_a}{\mu_b}$. Figures 6.10b

(velocity) and 6.10c (shear stress) are for $\frac{\mu_a}{\mu_b} = 50$ (the ratio of the viscosities of water to air), for varying ratios of $\frac{t}{h}$.

Figure 6.10a shows that the effect of an increasing viscosity ratio is not only to retard the more viscous layer (fluid a), but also to reduce the overall flow rate of the less viscous fluid (fluid b). This retardation is reflected by the area of the cumulative velocity profiles. Note that a ratio of $\mu_a/\mu_b = 50$ is roughly that of water to air, which is probably the most common situation for a two-fluid process. Using this typical water-air viscosity ratio, figure 6.10b illustrates the effect of increasing the thickness of the more viscous fluid (fluid a), which again reduces the flow rate of the less viscous fluid, through reduction of the flow cross-section. Reduction of the flow cross-section for fluid b reduces the motive force acting on the fluid (since the pressure gradient acts over a reduced area), which means fluid b must sustain reduced fluid deformation, resulting in lower shear with the bounding surfaces, and consequently a reduced flow rate.

Figure 6.10c shows the shear stress distributions for the velocity profiles shown in figure 6.10b. While not intuitive, the shear within both fluids again varies linearly, but is biased by the ratio of the fluid thicknesses.

6.3.6 Falling Liquid Film on a Wall

Consider the motion of a viscous liquid flowing down a sloped surface due to gravitational effects, as shown in figure 6.11.

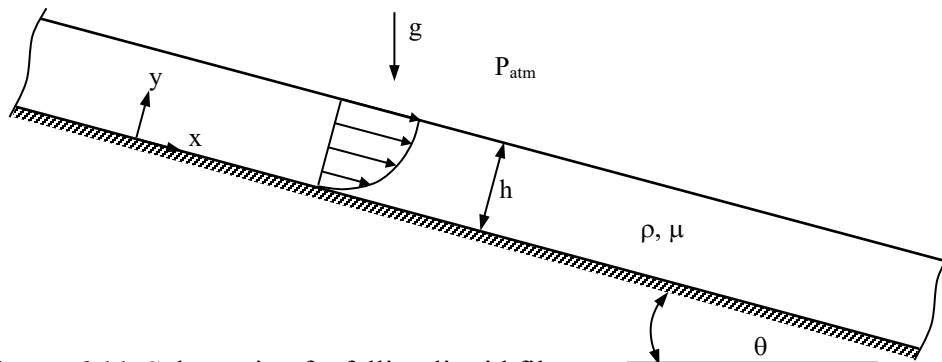


Figure 6.11 Schematic of a falling liquid film

For this problem, we align the coordinate system with the sloping surface, which is at a fixed angle to the horizontal of θ . We also assume that gravity acts vertically as shown, and that the thickness of the liquid layer is h , which remains constant as the liquid flows down the sloped surface. Here we assume governing two-dimensional N-S equations (x and y directions, constant density) given by:

$$\frac{\partial u}{\partial t} + u \frac{\partial u}{\partial x} + v \frac{\partial u}{\partial y} = \beta_x - \frac{1}{\rho} \frac{\partial p}{\partial x} + \nu \left[\frac{\partial^2 u}{\partial x^2} + \frac{\partial^2 u}{\partial y^2} \right] \quad \text{x-direction N-S} \quad (6.51a)$$

$$\frac{\partial v}{\partial t} + u \frac{\partial v}{\partial x} + v \frac{\partial v}{\partial y} = \beta_y - \frac{1}{\rho} \frac{\partial p}{\partial y} + \nu \left[\frac{\partial^2 v}{\partial x^2} + \frac{\partial^2 v}{\partial y^2} \right] \quad \text{y-direction N-S} \quad (6.51b)$$

$$\frac{\partial u}{\partial x} + \frac{\partial v}{\partial y} = 0 \quad \text{continuity} \quad (6.51c)$$

We again simplify Eqs. 6.51, as shown by the red arrows, assuming:

- (1) steady flow
- (2) fully-developed flow

Using the reduced continuity equation, Eq. 6.51c, we can again show that $v = 0$ within the liquid layer, which reduces the N-S equations to:

$$\frac{\partial^2 u}{\partial y^2} = \frac{1}{\mu} \frac{\partial p}{\partial x} - \frac{\beta_x}{\nu} \quad (6.52a)$$

and

$$\frac{\partial p}{\partial y} = \rho \beta_y \quad (6.52b)$$

Note that we have retained the total pressure in the N-S equations, since this is a gravity driven flow. For this flow, the body force vector, $\vec{\beta}$, is given by:

$$\vec{\beta} = \beta_x \hat{i} + \beta_y \hat{j} = g \sin \theta \hat{i} - g \cos \theta \hat{j}$$

So the y-direction equation, Eq. 6.52b, can be solved for the pressure as:

$$\frac{\partial p}{\partial y} = -\rho g \cos \theta \Rightarrow p = P_{\text{atm}} + \rho g \cos \theta (y - h) + f(x) \quad (6.53)$$

However, since the entire liquid layer is in contact with the atmosphere, this means that the pressure at the surface of the liquid must be atmospheric (i.e. $p = P_{\text{atm}} = \text{constant @ } y = h$). Thus, p cannot be a function of x , which means that in Eq. 6.53 $f(x) = 0$, and consequently $\frac{\partial p}{\partial x} = 0$.

Correspondingly, Eq. 6.52a reduces to:

$$\frac{d^2 u}{dy^2} = -\frac{\beta_x}{\nu} = -\frac{g \sin \theta}{\nu} \quad (6.54)$$

The boundary conditions for this flow are interesting. Clearly, at the plate surface ($y = 0$) the no slip condition requires that $u = 0$. However, at the interface between the liquid and the atmosphere ($y = h$), we do not know the boundary velocity. However, we know that the velocity and the shear stress for the liquid at the $y = h$ interface must be equivalent to that of the bounding atmosphere. However, since we assume the atmosphere to generally be at rest, this could give us some irksome boundary conditions, and require that we solve equations for the flow in the atmosphere as well. However, since we assume that the liquid moves slowly, and that both the density and the viscosity of the air are much, much less than the liquid, we ignore the boundary velocity of the atmosphere, and assume that to a good approximation there is essentially no shear stress between the liquid and the atmosphere (we will reexamine this assumption for an air-water flow in Chapter 12). Thus, we assume that at the interface $\tau_{yx} = 0$ such that $\frac{du}{dy} = 0$ at $y = h$, providing our second boundary condition (and of the second kind).

Integrating Eq. 6.54 once, and applying the boundary condition $\frac{du}{dy} = 0$ at $y = h$ gives:

$$\frac{du}{dy} = -\frac{g \sin \theta}{\nu} y + C_1 \Rightarrow C_1 = \frac{g \sin \theta}{\nu} h$$

Substituting for C_1 , integrating again, and applying the boundary condition $u = 0$ at $y = 0$ gives:

$$u = -\frac{g \sin \theta}{\nu} \frac{y^2}{2} + \frac{g \sin \theta}{\nu} hy + C_2 \Rightarrow C_2 = 0 \quad \text{for } u = 0 \text{ at } y = 0$$

Thus, the velocity profile for the liquid film is:

$$u = \frac{g \sin \theta}{\nu} \left(hy - \frac{y^2}{2} \right) = \frac{2U_{\max}}{h^2} \left(hy - \frac{y^2}{2} \right) = U_{\max} \left[2 \left(\frac{y}{h} \right) - \left(\frac{y}{h} \right)^2 \right] \quad (6.55)$$

where $U_{\max} = \frac{gh^2 \sin \theta}{2\nu}$ at $y = h$.

The corresponding shear stress within the liquid is:

$$\tau_{yx} = \mu \frac{du}{dy} = \rho g \sin \theta (h - y) \quad (6.56)$$

The volume flow rate (assuming again a depth into the page of W) is:

$$Q = \int_{y=0}^{y=h} u W dy = \frac{g \sin \theta}{\nu} \int_{y=0}^{y=h} \left(hy - \frac{y^2}{2} \right) W dy = \frac{g \sin \theta}{\nu} \frac{h^3}{3} W = \frac{2}{3} U_{\max} (Wh) \quad (6.57)$$

Dividing the volume flow rate by the cross-sectional area yields an average velocity of

$$\bar{U} = \frac{Q}{Wh} = \frac{2}{3} U_{\max}.$$

Note that the velocity, shear stress and flow rate are all a linear function of the slope angle, as we might expect. Also notice that this is the same shape velocity profile as we derived for the Poiseuille channel flow (i.e. only $\frac{1}{2}$ of the Poiseuille flow, from surface to centerline), only here the driving force is gravity, as opposed to a pressure gradient. This similar profile shape is also reflected by the average velocity, which has the same proportionality to the maximum velocity as we found for the Poiseuille channel flow of example 6.3.2.

6.4 Simple One-Dimensional Solutions with Radial Symmetry

Many practical flows have geometries with radial symmetry. Pipes, tubes, disks, annular regions are just some of these. Most of our water and air distribution systems use circular cross section pipes or ducts, and most bearing surfaces of rotating and reciprocating machinery depend on fluid lubrication via small annular regions. The following examples illustrate some of the simple fully-developed laminar flows that occur in geometries with radial symmetry.

6.4.1 Poiseuille Flow in a Pipe or Tube

In section 6.3.2 we examined a Poiseuille flow between parallel plates. In the present example, we examine the same type of pressure gradient driven flow in a pipe or tube of constant cross-section. Here we choose to use the Navier-Stokes equation in cylindrical or radial coordinates, with the z -axis aligned with the centerline of the pipe, as shown in figure 6.12.



Figure 6.12 Geometry for a Poiseuille flow in a circular cross section pipe.

We begin our analysis by assuming that there is no swirl, or flow changes in the θ or azimuthal direction, which eliminates all terms depending on θ and the velocity component, v_θ .

Consequently, the appropriate equations are the z -direction and r -direction components of the Navier-Stokes equations, and the continuity equation in cylindrical coordinates, as follows:

$$\begin{aligned}
 \text{z-N.S.: } & \frac{\partial v_z}{\partial t} + v_z \frac{\partial v_z}{\partial z} + v_r \frac{\partial v_z}{\partial r} + \frac{v_\theta}{r} \frac{\partial v_z}{\partial \theta} = -\frac{1}{\rho} \frac{\partial P}{\partial z} + \nu \left[\frac{1}{r} \frac{\partial}{\partial r} \left(r \frac{\partial v_z}{\partial r} \right) + \frac{1}{r^2} \frac{\partial^2 v_z}{\partial \theta^2} + \frac{\partial^2 v_z}{\partial z^2} \right] \\
 \text{r-N.S.: } & \frac{\partial v_r}{\partial t} + v_r \frac{\partial v_r}{\partial r} + \frac{v_\theta}{r} \frac{\partial v_r}{\partial \theta} + v_z \frac{\partial v_r}{\partial z} - \frac{v_\theta^2}{r} = -\frac{1}{\rho} \frac{\partial P}{\partial r} + \nu \left[\frac{\partial}{\partial r} \left(\frac{1}{r} \frac{\partial}{\partial r} (r v_r) \right) + \frac{1}{r^2} \frac{\partial^2 v_r}{\partial \theta^2} + \frac{\partial^2 v_r}{\partial z^2} - \frac{2}{r^2} \frac{\partial v_\theta}{\partial \theta} \right] \\
 \text{Continuity: } & \frac{1}{r} \frac{\partial}{\partial r} (r v_r) + \frac{1}{r} \frac{\partial v_\theta}{\partial \theta} + \frac{\partial v_z}{\partial z} = 0
 \end{aligned}$$

We again eliminate terms in the equations, based on the following set of assumptions:

1. steady flow
2. no v_θ motion
3. no changes in the θ -direction
4. constant density \rightarrow reduced continuity equation
5. fully-developed flow \rightarrow no z -direction changes

From the reduced continuity equation, we can write:

$$\frac{\partial}{\partial r} (r v_r) = 0 \Rightarrow r v_r = \text{constant} = C \Rightarrow v_r = \frac{C}{r}$$

However, since $v_r = 0$ at $r = R$, this implies that $C = 0$ and $v_r = 0$ throughout the pipe. Thus, the r -direction equation reduces to:

$$-\frac{1}{\rho} \frac{\partial P}{\partial r} = 0 \Rightarrow P = P(z) \text{ only}$$

Therefore, the above z -direction equation is simplified according to the above assumptions, and becomes the only relevant equation, as:

$$-\frac{1}{\rho} \frac{dP}{dz} + \frac{\nu}{r} \frac{d}{dr} \left(r \frac{dv_z}{dr} \right) = 0 \quad \text{where, } \nu = \frac{\mu}{\rho}$$

or

$$\frac{d}{dr} \left(r \frac{dv_z}{dr} \right) = \frac{r}{\mu} \frac{dP}{dz} \tag{6.58}$$

Note: if we take z -derivative of Eq. 6.58, we obtain:

$$\frac{d}{dz} \left(\frac{dP}{dz} \right) = \frac{d}{dz} \left[\frac{\mu}{r} \frac{d}{dr} \left(r \frac{dv_z}{dr} \right) \right] = 0$$

This term is not a function of z , \rightarrow thus, dP/dz must therefore, the derivative is zero. \rightarrow be a constant

The appropriate boundary conditions for this flow are:

$$(1) \quad v_z = 0 \quad @ \quad r = R$$

$$(2) \quad \frac{dv_z}{dr} = 0 \quad @ \quad r = 0$$

The first of these boundary conditions is obvious, since we require no slip at the pipe boundary. The second boundary condition is of the second kind, and reflects the expectation of symmetry for this flow about the centerline, which requires that the velocity be either a maximum or minimum at the centerline. In either case, this is expressed by a requirement that the first derivative of the streamwise velocity with respect to the radius be zero at $r = 0$.

Integrating Eq. 6.58 gives:

$$r \frac{dv_z}{dr} = \frac{r^2}{2\mu} \frac{dP}{dz} + C_1 \quad \Rightarrow \quad \frac{dv_z}{dr} = \frac{r}{2\mu} \frac{dP}{dz} + \frac{C_1}{r}$$

Applying boundary condition 2, $\frac{dv_z}{dr} = 0 \quad @ \quad r = 0$, gives:

$$0 = 0 + C_1 \Rightarrow C_1 = 0$$

Integrating again yields:

$$v_z = \frac{r^2}{4\mu} \frac{dP}{dz} + C_2$$

Now, applying boundary condition 1, $v_z = 0 \quad @ \quad r = R$:

$$0 = \frac{R^2}{4\mu} \frac{dP}{dz} + C_2 \quad \Rightarrow \quad C_2 = -\frac{R^2}{4\mu} \frac{dP}{dz}$$

Thus, the velocity for Poiseuille flow in a tube or pipe is given by:

$$v_z = -\frac{1}{4\mu} \frac{dP}{dz} (R^2 - r^2) \quad (6.59)$$

Since viscosity will cause the pressure to *decrease* in the direction of the flow, the negative sign in Eq. 6.59 indicates that the velocity will move in the positive z -direction when the pressure decreases in the positive z -direction (i.e. $\frac{dP}{dx} < 0$).

If $\frac{dP}{dx} > 0$, then the direction of flow will be reversed (i.e. moving in the negative z -direction).

Now note that the maximum velocity (as we surmised) occurs at the center of the pipe.

$$U_{\max} = v_z|_{r=0} = -\frac{1}{4\mu} \frac{dP}{dz} (R^2 - 0) = -\frac{R^2}{4\mu} \frac{dP}{dz} \quad (6.60)$$

Thus, we can rewrite Eq. 6.59 in terms of U_{\max} using Eq. 6.60 as:

$$v_z = U_{\max} \left(1 - \frac{r^2}{R^2} \right) \quad (6.61)$$

This flow distribution describes a parabola, with the maximum velocity at the center of the pipe. We obtain the volume flow rate for this pipe flow by integrating across the cross section of the pipe. This requires that we integrate both radially and azimuthally over the cross section using an appropriate differential element, dA , given by $dA = r dr d\theta$. The geometric source of this differential element is shown in figure 6.13.

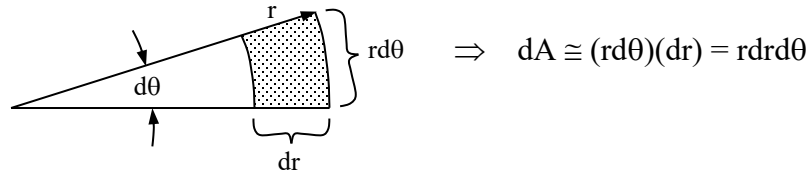


Figure 6.13 Differential area element in cylindrical coordinates.

Thus, the volume flow rate for the Poiseuille pipe flow is given by:

$$Q = \iint_A v_z dA = \int_{\theta=0}^{2\pi} \int_{r=0}^R v_z r dr d\theta = U_{\max} \int_{\theta=0}^{2\pi} d\theta \int_{r=0}^R \left(1 - \frac{r^2}{R^2} \right) r dr = U_{\max} (2\pi) \left(\frac{R^2}{4} \right)$$

$$Q = \frac{U_{\max}}{2} (\pi R^2) = -\frac{\pi R^4}{8\mu} \frac{dP}{dz} \quad (6.62)$$

Note that the average or mean velocity for this flow (the volume flow rate divided by the cross sectional area) is $\bar{U} = \frac{1}{2} U_{\max}$, as compared to the Poiseuille channel flow, where $\bar{U} = \frac{2}{3} U_{\max}$.

This difference is due to the radial symmetry of the pipe, which biases lower velocity fluid toward the region of the bounding walls, which comprises a larger component of the cross-sectional area.

The corresponding shear stress for this flow is:

$$\tau_{rz} = \mu \left(\frac{\partial v_z}{\partial r} + \frac{\partial v_r}{\partial z} \right) = \frac{r}{2} \frac{dP}{dz} = -\frac{2\mu r U_{\max}}{R^2}, \quad (6.63)$$

which is linear with the radius, r . Note however, that the shear stress at the pipe wall is:

$$\tau_{rz}|_{r=R} = \frac{R}{2} \frac{dP}{dz} = \frac{-2\mu U_{\max}}{R} \tag{6.64}$$

An interesting observation from Eq. 6.64 is that for a fixed pressure gradient the shear stress at the wall will increase linearly with the pipe radius. One might think that an increase in wall shear would reflect a corresponding decrease in the flow rate through the pipe. However, as Eq. 6.62 shows, the flow rate will increase as the fourth power of the radius. Clearly, as the pipe radius increases the effect of the pressure gradient, which is applied over the cross sectional area of the pipe, will significantly outweigh the impact of the increased wall shear which acts on only the periphery of the pipe. Eq. 6.60 further illustrates this impact of increased pipe radius, indicating that for the same applied pressure gradient the maximum velocity in the pipe will increase as the *square* of the radius. Since the fluid nearer the center of a larger pipe will be farther removed from the retarding viscous effects of the pipe boundaries, it will be less restrained and will reach higher values under the same forcing condition (i.e. pressure gradient).

6.4.2 Couette Flow between Concentric Rotating Cylinders

In section 6.3.1 we examined a Couette flow between parallel plates. In this example, we examine the same type of surface-driven flow in the annulus formed between the surfaces of concentric cylinders rotating at different angular velocities. Here we use the cylindrical Navier-Stokes equation with the z -axis aligned out of this page along the centerline of the two cylinders, as show in figure 6.14.

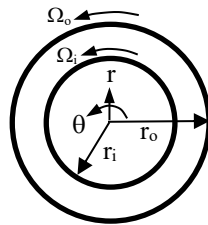


Figure 6.14 Geometry for Couette flow between concentric cylinders

We assume that there is no flow in the z -direction, which eliminates all terms depending on z and the velocity component v_z . Consequently, the appropriate set of equations is the θ -direction and r -direction components of the Navier-Stokes equations, and the continuity equation in cylindrical coordinates, as follows:

$$\theta\text{-N.S.: } \frac{\partial v_\theta}{\partial t} + v_r \frac{\partial v_\theta}{\partial r} + \frac{v_\theta}{r} \frac{\partial v_\theta}{\partial \theta} + v_z \frac{\partial v_\theta}{\partial z} + \frac{v_r v_\theta}{r} = -\frac{1}{\rho r} \frac{\partial p}{\partial \theta} + \nu \left[\frac{\partial}{\partial r} \left(\frac{1}{r} \frac{\partial}{\partial r} (r v_\theta) \right) + \frac{1}{r^2} \frac{\partial^2 v_\theta}{\partial \theta^2} + \frac{\partial^2 v_\theta}{\partial z^2} + \frac{2}{r^2} \frac{\partial v_r}{\partial \theta} \right]$$

$$\mathbf{r}\text{-N.S.: } \frac{\partial v_r}{\partial t} + v_r \frac{\partial v_r}{\partial r} + \frac{v_\theta}{r} \frac{\partial v_r}{\partial \theta} + v_z \frac{\partial v_r}{\partial z} - \frac{v_\theta^2}{r} = -\frac{1}{\rho} \frac{\partial p}{\partial r} + \nu \left[\frac{\partial}{\partial r} \left(\frac{1}{r} \frac{\partial}{\partial r} (r v_r) \right) + \frac{1}{r^2} \frac{\partial^2 v_r}{\partial \theta^2} + \frac{\partial^2 v_r}{\partial z^2} - \frac{2}{r^2} \frac{\partial v_\theta}{\partial \theta} \right]$$

$$\mathbf{Continuity: } \frac{1}{r} \frac{\partial}{\partial r} (r v_r) + \frac{1}{r} \frac{\partial v_\theta}{\partial \theta} + \frac{\partial v_z}{\partial z} = 0$$

We again eliminate terms in the equations, based on the following set of assumptions:

1. steady flow
2. no v_z motion
3. no changes in the z -direction
4. fully-developed flow \rightarrow no θ -direction changes
5. No pressure changes in θ -direction

Note that assumption 5 corresponds to the same argument we made previously in section 6.3.1 for infinite parallel plates, and applies in general for all surface-driven, Couette-type flows.

From the reduced continuity equation, we have:

$$\frac{\partial}{\partial r} (r v_r) = 0 \Rightarrow r v_r = \text{constant} = C \Rightarrow v_r = \frac{C}{r}$$

Since $v_r = 0$ at $r = r_o$ and r_i , this implies that $C = 0$ and $v_r = 0$ throughout the annulus. Thus, the Navier-Stokes equations reduce to:

$$\frac{\partial}{\partial r} \left(\frac{1}{r} \frac{\partial}{\partial r} (r v_\theta) \right) = 0 \quad (\theta\text{-direction}) \tag{6.65a}$$

$$\frac{\partial p}{\partial r} = \frac{\rho v_\theta^2}{r} \quad (r\text{-direction}) \tag{6.65b}$$

We note that $v_\theta = f(r)$ only, which also makes the pressure only a function of r .

Integrating the simplified θ -direction equation twice, Eq. 6.65a, gives:

$$\frac{d}{dr} (r v_\theta) = C_1 r$$

$$v_\theta = \frac{C_1 r}{2} + \frac{C_2}{r}$$

The appropriate boundary conditions for this flow are:

- (1) $v_\theta = \Omega_i r_i$ @ $r = r_i$
- (2) $v_\theta = \Omega_o r_o$ @ $r = r_o$

This is the most general case, where we assume that each tube rotates at a different angular (and thus tangential) velocity. Applying these boundary conditions gives us a cumbersome set of equations for C_1 and C_2 , which when solved give a velocity relationship of:

$$v_\theta = \frac{\Omega_o r_o^2 (r^2 - r_i^2) + \Omega_i r_i^2 (r_o^2 - r^2)}{r(r_o^2 - r_i^2)} \quad (6.66)$$

Using the appropriate equation for $\tau_{r\theta}$ from Section 5.8.1, the shear stress within the fluid is given as:

$$\tau_{r\theta} = \mu \left[r \frac{\partial}{\partial r} \left(\frac{v_\theta}{r} \right) + \frac{1}{r} \frac{\partial v_r}{\partial \theta} \right] = \frac{2\mu r_i^2 r_o^2 (\Omega_o - \Omega_i)}{r^2 (r_o^2 - r_i^2)} \quad (6.67)$$

The resulting torque per unit depth is given by:

$$\text{Torque} = \tau_{r\theta} (2\pi r) r = 4\pi\mu \frac{r_i^2 r_o^2}{(r_o^2 - r_i^2)} (\Omega_o - \Omega_i) \quad (6.68)$$

Therefore, the torque is constant, and equal for each cylinder, as it should be.

Thus, for a set of cylinders of known geometry and rotation, one can calculate the viscosity of the fluid by measuring the torque exerted on either cylinder. This process, first suggested by [Couette \(1890\)](#), is still a popular and practical method used in viscometry.

Consider two special cases for this type of flow. The first is for either a fixed inner cylinder ($\Omega_i = 0$), or a fixed outer cylinder ($\Omega_o = 0$). Applying these constraints to Eq. 66, gives:

$$v_\theta = \frac{\Omega_o r_o^2 (r^2 - r_i^2)}{r(r_o^2 - r_i^2)} \quad (\text{inner fixed, } \Omega_i = 0) \quad (6.69a)$$

or

$$v_\theta = \frac{\Omega_i r_i^2 (r_o^2 - r^2)}{r(r_o^2 - r_i^2)} \quad (\text{outer fixed, } \Omega_o = 0) \quad (6.69b)$$

Eq. 6.69a ($\Omega_i = 0$) is comparable to the initial parallel plate Couette solution we did in section 6.3.1, where the outer plate moved while the inner plate was held fixed. Note that if the cylinders are very close together, such that the annulus is small and the curvature large, such that we can approximate that $r \approx r_i \approx r_o$, then we can simplify Eq. 6.69a as:

$$v_\theta = \frac{\Omega_o r_o^2 (r^2 - r_i^2)}{r(r_o^2 - r_i^2)} = (\Omega_o r_o) \frac{r_o (r - r_i)(r + r_i)}{r(r_o - r_i)(r_o + r_i)} = \frac{(\Omega_o r_o)(r - r_i)}{(r_o - r_i)} \left(\frac{r_o}{r} \right) \left(\frac{r + r_i}{r_o + r_i} \right) \quad (6.70)$$

If we let $h = r_o - r_i$, and designate a variable $y = r - r_i$, then Eq.6.70 can be written as:

$$v_\theta = \frac{(\Omega_o r_o)(r - r_i)}{(r_o - r_i)} \approx \frac{(\Omega_o r_o)y}{h} = \frac{Uy}{h} \quad \text{where } U = \Omega_o r_o \quad (6.71)$$

Thus, when the curvature is quite large, the solution for the concentric cylinder Couette flow asymptotes to the solution (Eq. 6.8) for a parallel plate Couette flow in Section 6.3.1, as it should (and Eq. 6.67 for shear stress, asymptotes to Eq. 6.9 for parallel flow).

Two other variations on this type of flow are ones where we essentially remove one or the other of the cylinder surfaces. We do this by either expanding the diameter of the outer cylinder to infinity (case 1) or shrinking the diameter of the inner cylinder to zero (case 2).

6.4.2.1 A Cylinder Rotating in an Infinite Fluid

Here we let $r_o \rightarrow \infty$ and $\Omega_o \rightarrow 0$ in Eq. 6.52, and note that $(r_o^2 - r^2) \cong (r_o^2 - r_i^2)$, which yields:

$$v_\theta = \frac{\overset{=0}{\cancel{\Omega_o r_o^2}} (r^2 - r_i^2) + \Omega_i r_i^2 (r_o^2 - r^2)}{r(r_o^2 - r_i^2)} = \left(\frac{\Omega_i r_i^2}{r} \right) \frac{\overset{=1}{\cancel{r_o^2}} - r^2}{\overset{=1}{\cancel{r_o^2}} - r_i^2} \cong \frac{\Omega_i r_i^2}{r} \quad (6.72)$$

In Chapter 8, we will show that Eq. 6.72 corresponds to the behavior of an *irrotational* vortex and discuss why this profile evolves. It is of interest to note that this is the only example where a viscous flow with a bounding surface retains no vorticity within the flow field.

6.4.2.2 Fluid Rotating within a Cylinder

Alternatively, if we let $r_i \rightarrow 0$ and $\Omega_i \rightarrow 0$ in Eq. 6.66, this yields a flow with no inner cylinder:

$$v_\theta = \frac{\Omega_o r_o^2 \overset{=0}{\cancel{(r^2 - r_i^2)}} + \overset{=0}{\cancel{\Omega_i r_i^2}} (r_o^2 - r^2)}{r \overset{=0}{\cancel{(r_o^2 - r_i^2)}}} = \left(\frac{\Omega_o r_o^2}{r} \right) \frac{\overset{=0}{\cancel{r^2}}}{\overset{=0}{\cancel{r_o^2}}} = \Omega_o r \quad (6.73)$$

Equation 6.73 is simply a solid body rotation within the outer cylinder, which is to be expected. Again, we will address this flow, and its temporal development, when we discuss vorticity and vorticity transport in Chapter 11. Additionally, if the angular rotation of both cylinders is identical (e.g. $\Omega_o = \Omega_i$), Eq. 6.66 also reduces to $v_\theta = \Omega_o r$ (or $v_\theta = \Omega_i r$). Prove this to yourself.

Notice that we have not addressed the application of the simplified r-direction Navier-Stokes equation, which we derived above as Eq. 6.65b:

$$\frac{\partial p}{\partial r} = \frac{\rho v_\theta^2}{r}$$

Equation 6.65b prescribes the behavior of the pressure within to the fluid due to v_θ . This relationship indicates, as we will discuss in the following Chapter 7, that for steady circular flows pressure will only change in the radial direction. Additionally, pressure will always increase *outward* from the center of rotation, regardless of the velocity profile (since

$\frac{\partial p}{\partial r} = \frac{\rho v_\theta^2}{r} > 0$ for all possible circular velocity fields). For example, for Case 1 above, for a cylinder rotating in an infinite fluid ($r_o \rightarrow \infty$ and $\Omega_o \rightarrow 0$), we have:

$$\frac{dp}{dr} = \frac{\rho v_\theta^2}{r} = \frac{\rho \left(\frac{\Omega_i r_i^2}{r} \right)^2}{r} = \frac{\rho \Omega_i^2 r_i^4}{r^3}$$

Integrating from $r = r_i$ outward gives:

$$\int_{p=p_i}^p dp = p - p_i = \rho \Omega_i^2 r_i^4 \int_{r=r_i}^r \frac{dr}{r^3} = \frac{\rho \Omega_i^2 r_i^4}{2} \left(\frac{1}{r_i^2} - \frac{1}{r^2} \right) \quad (6.74)$$

where p_i is the pressure at the surface of the inner cylinder.

As Eq. 6.74 shows, pressure continually increases outward from the cylinder, reaching a maximum of $p = p_i + \frac{\rho \Omega_i^2 r_i^2}{2}$ as $r \rightarrow \infty$. A similar result of an outward pressure increase occurs for all other rotational variations as well.

6.4.3 Poiseuille Flow in a Duct of Annular Cross Section

This is a pressure driven flow in the annular cross section formed between two concentric cylinders. The pressure gradient acts along the axis of the cylinders, driving the flow as shown in figure 6.15 below. Such a flow is characteristic of the flow in many heat exchangers, where one fluid flows through a contained cylindrical annulus directly adjacent to a second fluid flowing in a central tube or cylinder. This is again a pressure gradient driven Poiseuille-type flow, and we again apply the Navier-Stokes equation in cylindrical coordinates, with the z-axis aligned with the centerline of the concentric cylinders, as show in figure 6.15.

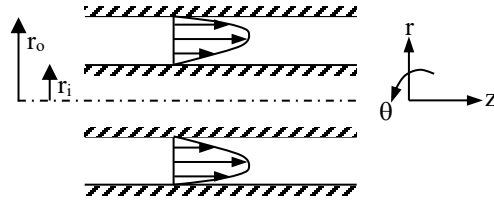


Figure 6.15 Geometry for a pressure-driven Poiseuille flow in an annular cross section

We again assume that there is no swirl, or flow changes in the θ or azimuthal direction, which eliminates all terms depending on θ and the velocity component v_θ . The appropriate set of equations is the z -direction Navier-Stokes equation, and the continuity equation in cylindrical coordinates:

$$\text{z-N.S.: } \frac{\partial v_z}{\partial t} + v_z \frac{\partial v_z}{\partial z} + v_r \frac{\partial v_z}{\partial r} + \frac{v_\theta}{r} \frac{\partial v_z}{\partial \theta} = -\frac{1}{\rho} \frac{\partial P}{\partial z} + \nu \left[\frac{1}{r} \frac{\partial}{\partial r} \left(r \frac{\partial v_z}{\partial r} \right) + \frac{1}{r^2} \frac{\partial^2 v_z}{\partial \theta^2} + \frac{\partial^2 v_z}{\partial z^2} \right]$$

$$\text{Continuity: } \frac{1}{r} \frac{\partial}{\partial r} (r v_r) + \frac{1}{r} \frac{\partial v_\theta}{\partial \theta} + \frac{\partial v_z}{\partial z} = 0$$

We eliminate terms in the equations based on the assumptions:

1. steady flow
2. no v_θ motion
3. no changes in the θ -direction
4. fully-developed flow \rightarrow no z -direction changes

The reduced continuity equation gives $v_r = 0$ throughout the pipe. Thus, the r -direction equation reduces to:

$$-\frac{1}{\rho} \frac{\partial P}{\partial r} = 0 \Rightarrow P = P(z) \text{ only}$$

Therefore, the above z -direction equation reduces to the same equation, Eq. 6.58, as Poiseuille flow in a pipe, as shown in section 6.4.1:

$$-\frac{1}{\rho} \frac{dP}{dz} + \nu \frac{d}{dr} \left(r \frac{dv_z}{dr} \right) = 0 \quad \text{where } \nu = \frac{\mu}{\rho}$$

$$\text{or } \frac{d}{dr} \left(r \frac{dv_z}{dr} \right) = \frac{r}{\mu} \frac{dP}{dz} \tag{6.75}$$

Just as with the Poiseuille flow, we can again show that $dP/dz = \text{constant}$ within the annulus. The appropriate boundary conditions for this annular flow are no slip at the two annular boundaries:

$$(1) \quad v_z = 0 \text{ @ } r = r_o$$

$$(2) \quad v_z = 0 \text{ @ } r = r_i$$

Integrating Eq. 6.75 once gives:

$$r \frac{dv_z}{dr} = \frac{r^2}{2\mu} \frac{dP}{dz} + C_1$$

$$\frac{dv_z}{dr} = \frac{r}{2\mu} \frac{dP}{dz} + \frac{C_1}{r}$$

Integrating again yields:

$$v_z = \frac{r^2}{4\mu} \frac{dP}{dz} + C_1 \ln r + C_2 \quad (6.76)$$

Applying boundary conditions 1 and 2 to Eq. 6.76:

$$0 = \frac{r_o^2}{4\mu} \frac{dP}{dz} + C_1 \ln r_o + C_2 \quad \text{and} \quad 0 = \frac{r_i^2}{4\mu} \frac{dP}{dz} + C_1 \ln r_i + C_2$$

Solving these simultaneously for C_1 and C_2 gives:

$$C_1 = -\frac{(r_o^2 - r_i^2)}{4\mu \ln\left(\frac{r_o}{r_i}\right)} \frac{dP}{dz}$$

$$C_2 = -\frac{r_i^2}{4\mu} \frac{dP}{dz} + \frac{(r_o^2 - r_i^2)}{4\mu \ln\left(\frac{r_o}{r_i}\right)} \frac{dP}{dz}$$

Substituting C_1 and C_2 into Eq. 6.76, the velocity for Poiseuille flow in an annulus is:

$$v_z = \frac{1}{4\mu} \frac{dP}{dz} \left[(r^2 - r_i^2) - (r_o^2 - r_i^2) \frac{\ln\left(\frac{r}{r_i}\right)}{\ln\left(\frac{r_o}{r_i}\right)} \right] = \frac{r_i^2}{4\mu} \frac{dP}{dz} \left[\left(\frac{r^2}{r_i^2} - 1 \right) - \left(\frac{r_o^2}{r_i^2} - 1 \right) \frac{\ln\left(\frac{r}{r_i}\right)}{\ln\left(\frac{r_o}{r_i}\right)} \right] \quad (6.77)$$

Non-dimensional velocity profiles for four radius ratios from $\frac{r_o}{r_i} = 1.25$ to 2.00 are shown in figure 6.16.

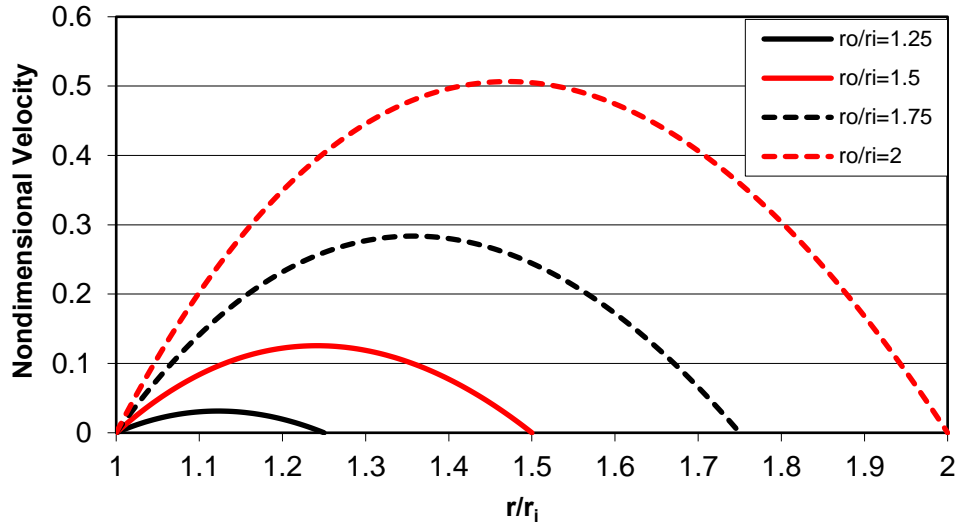


Figure 6.16 Non-dimensionalized velocity vs. r/r_i for r_o/r_i values from 1.25 to 2. Here

$$\text{Velocity} = v_z / \left(\frac{r_i^2}{4\mu} \frac{dP}{dz} \right)$$

For this flow, the maximum velocity does not occur at the center of the annulus, but is a function of the radius ratio, r_o/r_i , given by:

$$r_{@U_{max}} = \sqrt{\frac{(r_o^2 - r_i^2)}{2 \ln\left(\frac{r_o}{r_i}\right)}}$$

The expression for the maximum velocity is found by substituting the expression for $r_{@U_{max}}$ into Eq. 6.77, and is quite messy and not shown here. However, for values of r_o/r_i less than 3 the maximum velocity occurs very near to the annulus midpoint [i.e. $(r_o+r_i)/2$], so radial skewing of the profiles is minimal, as one can observe in figure 6.16. Additionally, as shown in figure 6.16, for a fixed pressure gradient, the maximum velocity and the flowrate (another messy integration) will both increase with and increase in r_o/r_i .

The corresponding shear stress for this flow is:

$$\tau_{rz} = \mu \left(\frac{\partial v_z}{\partial r} + \frac{\partial v_r}{\partial z} \right) = \frac{1}{4} \frac{dP}{dz} \left[2r - \frac{(r_o^2 - r_i^2)}{r \ln \left(\frac{r_o}{r_i} \right)} \right] = \frac{r_i}{4} \frac{dP}{dz} \left[2 \left(\frac{r}{r_i} \right) - \frac{\left(\frac{r_o^2}{r_i^2} - 1 \right)}{\left(\frac{r}{r_i} \right) \ln \left(\frac{r_o}{r_i} \right)} \right] \quad (6.78)$$

Non-dimensional shear stress profiles for four radius ratios from 1.25 to 2.00 are shown in figure 6.17.

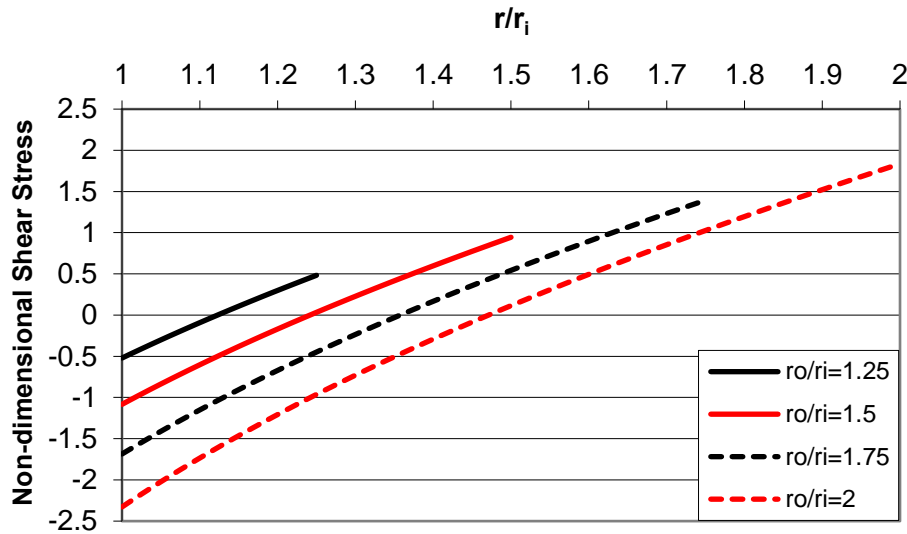


Figure 6.17 Non-dimensionalized shear stress vs. r/r_i for r_o/r_i values from 1.25 to 2.

$$\text{Here Shear Stress} = \tau_{rz} / \frac{r_i}{4} \frac{dP}{dz}$$

As figure 6.17 shows, the shear stress varies almost linearly from r_i to r_o , quite similar to the behavior for Poiseuille flow in a parallel channel, that we examined in section 6.3.2. In fact, one can show that both the velocity and shear stress equations asymptote to the parallel plate solution when $r_o/r_i \rightarrow 1$. However, notice that as the radius ratio increases, the shear stress at r_o will be correspondingly lower than the shear stress at r_i (i.e. $|\tau_{r=r_i}| > |\tau_{r=r_o}|$ for $r_o/r_i \uparrow$). Similar to Poiseuille flow in a pipe, the wall shear stress will increase with increasing annulus gap width. However, as can be seen in figure 6.16, the maximum velocity and flow rate will also increase with an increasing annulus gap, since the driving force of the pressure gradient (applied over a larger cross section area) greatly outstrips the increase in shear stress.

6.4.4 Two-Fluid Couette Flow between Concentric Rotating Cylinders

In section 6.3.4 we examined a Couette flow of two immiscible fluids between parallel plates. In the present example, we examine the same type of surface-driven flow for two immiscible fluids

in the annulus formed between the surfaces of concentric cylinders. To simplify the derivation, we hold the outer cylinder fixed, and rotate the inner cylinder at a constant velocity. In reality, to accomplish this would be a bit tricky keeping the two fluids separated, due to gravitational effects. However, if we imagine that gravity acts along the axis of the cylinders, this becomes a bit more feasible configuration. We assume we have two immiscible fluids (like oil and water), we will call them fluid a and fluid b, with respective viscosities μ_a and μ_b . Additionally, we assume that fluid b is denser than fluid a, such that $\rho_b > \rho_a$. Recall that in section 6.4.2 we discussed the radial pressure generated by a rotating flow, and showed that for any type of rotation the pressure will always increase with radius. Thus, the pressure gradient for our two fluid Couette flow will always concentrate the less dense fluid (e.g. water) adjacent to the inner cylinder wall, and force the denser fluid (e.g. oil) adjacent to the outer cylinder wall, as shown in figure 6.18.

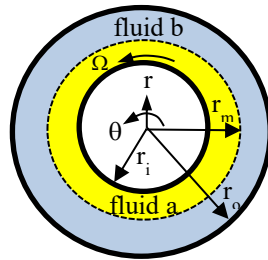


Figure 6.18 Geometry for Couette flow of two fluid layers between concentric cylinders

As we did in section 6.4.2 for a single fluid Couette flow between concentric cylinders, we assume an inner cylinder of radius r_i , and an outer cylinder of radius r_o . Additionally, we also assume that the interface between the two fluids will be at some radius r_m , where $r_i < r_m < r_o$. Here we again use the cylindrical Navier-Stokes equation with the z-axis aligned out of this page along the centerline of the two cylinders, as show in figure 6.18.

We assume that there is no flow in the z-direction, which eliminates all terms depending on z and the velocity component v_z . Consequently, the appropriate set of equations is the θ -direction and r-direction components of the Navier-Stokes equations, and the continuity equation in cylindrical coordinates, as follows:

$$\theta\text{-N.S.: } \frac{\partial v_\theta}{\partial t} + v_r \frac{\partial v_\theta}{\partial r} + \frac{v_\theta}{r} \frac{\partial v_\theta}{\partial \theta} + v_z \frac{\partial v_\theta}{\partial z} + \frac{v_r v_\theta}{r} = -\frac{1}{\rho r} \frac{\partial p}{\partial \theta} + \nu \left[\frac{\partial}{\partial r} \left(\frac{1}{r} \frac{\partial}{\partial r} (r v_\theta) \right) + \frac{1}{r^2} \frac{\partial^2 v_\theta}{\partial \theta^2} + \frac{\partial^2 v_\theta}{\partial z^2} + \frac{2}{r^2} \frac{\partial v_r}{\partial \theta} \right]$$

$$r\text{-N.S.: } \frac{\partial v_r}{\partial t} + v_r \frac{\partial v_r}{\partial r} + \frac{v_\theta}{r} \frac{\partial v_r}{\partial \theta} + v_z \frac{\partial v_r}{\partial z} - \frac{v_\theta^2}{r} = -\frac{1}{\rho} \frac{\partial p}{\partial r} + \nu \left[\frac{\partial}{\partial r} \left(\frac{1}{r} \frac{\partial}{\partial r} (r v_r) \right) + \frac{1}{r^2} \frac{\partial^2 v_r}{\partial \theta^2} + \frac{\partial^2 v_r}{\partial z^2} - \frac{2}{r^2} \frac{\partial v_\theta}{\partial \theta} \right]$$

$$\text{Continuity: } \frac{1}{r} \frac{\partial}{\partial r} (rv_r) + \frac{1}{r} \frac{\partial v_\theta}{\partial \theta} + \frac{\partial v_z}{\partial z} = 0$$

We again eliminate terms in the equations, based on the following set of assumptions:

1. steady flow
2. no v_z motion
3. no changes in the z -direction
4. fully-developed flow \rightarrow no θ -direction changes
5. No pressure changes in θ -direction

Note that assumption 5 corresponds to the same argument we made previously in sections 6.3.1 for infinite parallel plates, and applies in general for all surface-driven, Couette-type flows.

From the reduced continuity equation, we have:

$$\frac{\partial}{\partial r} (rv_r) = 0 \Rightarrow rv_r = \text{constant} = C \Rightarrow v_r = \frac{C}{r}$$

Since $v_r = 0$ at $r = r_o$ and r_i , this implies that $C = 0$ and $v_r = 0$ throughout the annulus. Thus, the Navier-Stokes equations again reduce to:

$$\frac{\partial}{\partial r} \left(\frac{1}{r} \frac{\partial}{\partial r} (rv_\theta) \right) = 0 \quad (\theta\text{-direction}) \quad (6.79a)$$

$$\frac{\partial p}{\partial r} = \frac{\rho v_\theta^2}{r} \quad (r\text{-direction}) \quad (6.79b)$$

We note that $v_\theta = f(r)$ only, which also makes the pressure only a function of r .

Integrating 6.79a twice, gives:

$$\frac{d}{dr} (rv_\theta) = C_1 r$$

$$v_\theta = \frac{C_1 r}{2} + \frac{C_2}{r}$$

This equation applies within both fluid a and fluid b, so we have two equations, Eq.6.80a and 6.80b: one for fluid a and one for fluid b, subject to different boundary conditions:

$$v_{\theta,a} = \frac{C_{1,a} r}{2} + \frac{C_{2,a}}{r} \quad \text{and} \quad v_{\theta,b} = \frac{C_{1,b} r}{2} + \frac{C_{2,b}}{r} \quad (6.80a,b)$$

The four constants of integration are determined by applying the following four boundary conditions:

$$(1) \quad v_{\theta,a} = \Omega r_i \quad @ \quad r = r_i$$

$$(3) \quad v_{\theta,a} = v_{\theta,b} \quad @ \quad r = r_m$$

$$(2) \quad v_{\theta,b} = 0 \quad @ \quad r = r_o$$

$$(4) \quad \tau_{r\theta,a} = \tau_{r\theta,b} \quad @ \quad r = r_m$$

To apply the fourth boundary condition, we note that for this flow $\tau_{r\theta}$ is given by:

$$\tau_{r\theta} = \mu \left[r \frac{\partial}{\partial r} \left(\frac{v_\theta}{r} \right) + \frac{1}{r} \frac{\partial v_r}{\partial \theta} \right] = \mu r \frac{\partial}{\partial r} \left(\frac{v_\theta}{r} \right) \quad (6.81)$$

Applying the above boundary conditions to equations 6.80 gives us four equations to solve for the constants, as follows.

$$(1) \quad C_{1,a} = 2 \left(\Omega - \frac{C_{2,a}}{r_i^2} \right) \quad (6.82a)$$

$$(2) \quad C_{2,b} = -\frac{C_{1,b} r_o^2}{2} \quad (6.82b)$$

$$(3) \quad C_{1,b} = C_{1,a} + \frac{2}{r_m^2} (C_{2,a} - C_{2,b}) \quad (6.82c)$$

(4) Note that for both fluids:

$$\tau_{r\theta} = \mu r \frac{\partial}{\partial r} \left(\frac{v_\theta}{r} \right) = \mu r \frac{\partial}{\partial r} \left(\frac{C_1}{2} + \frac{C_2}{r^2} \right) = \mu r \left(0 - 2 \frac{C_2}{r^3} \right) = -2\mu \frac{C_2}{r^2}$$

Thus, boundary condition (4) at $r = r_m$ becomes:

$$-2\mu_a \frac{C_{2,a}}{r_m^2} = -2\mu_b \frac{C_{2,b}}{r_m^2} \Rightarrow C_{2,a} = \frac{\mu_b}{\mu_a} C_{2,b} \quad (6.82d)$$

Solving Eqs. 6.82 simultaneously, which is a bit messy, yields:

$$C_{1,b} = \frac{2\Omega}{\left[1 - \frac{r_o^2}{r_m^2} + \frac{\mu_b}{\mu_a} \left(\frac{r_o^2}{r_m^2} - \frac{r_o^2}{r_i^2} \right) \right]} = \frac{2\Omega}{\beta} \quad \text{where} \quad \beta = \left[1 - \frac{r_o^2}{r_m^2} + \frac{\mu_b}{\mu_a} \left(\frac{r_o^2}{r_m^2} - \frac{r_o^2}{r_i^2} \right) \right] \quad (6.83a)$$

$$C_{2,b} = -\frac{\Omega r_o^2}{\beta} \quad (6.83b)$$

$$C_{1,a} = 2 \left(\Omega + \frac{\mu_b}{\mu_a} \frac{\Omega r_o^2}{\beta r_i^2} \right) \quad (6.83c)$$

and

$$C_{2,a} = -\frac{\mu_b}{\mu_a} \frac{\Omega r_o^2}{\beta} \quad (6.83d)$$

Substituting Eqs. 6.83 Into Eqs.6.80, yields velocity profiles for this two-layer Couette flow as:

$$v_{\theta,a} = \left(\Omega + \frac{\mu_b}{\mu_a} \frac{\Omega r_o^2}{\beta r_i^2} \right) r - \frac{\mu_b}{\mu_a} \frac{\Omega r_o^2}{\beta r} = \frac{\Omega \beta r^2 + \frac{\mu_b}{\mu_a} \Omega \frac{r_o^2}{r_i^2} (r^2 - r_i^2)}{\beta r} \quad (6.84a)$$

and

$$v_{\theta,b} = \frac{\Omega r}{\beta} - \frac{\Omega r_o^2}{\beta r} = \frac{\Omega (r^2 - r_o^2)}{\beta r} \quad (6.84b)$$

Eqs. 6.84 are a bit cumbersome, so to check their validity, we note that they should reduce to the equation for a single fluid with a stationary outer boundary, Eq. 6.69b, if we set $\frac{\mu_b}{\mu_a} = 1$.

Letting $\frac{\mu_b}{\mu_a} = 1$, the value of β is:

$$\beta = \left[1 - \frac{r_o^2}{r_m^2} + \left(\frac{r_o^2}{r_m^2} - \frac{r_o^2}{r_i^2} \right) \right] = \left[1 - \frac{r_o^2}{r_i^2} \right]$$

Substituting this relationship into Eqs. 6.84 and simplifying, gives:

$$v_{\theta,a} = \frac{\Omega \left(1 - \frac{r_o^2}{r_i^2} \right) r^2 + \Omega \frac{r_o^2}{r_i^2} (r^2 - r_i^2)}{\left(1 - \frac{r_o^2}{r_i^2} \right) r} = \frac{\Omega r_i^2 (r_o^2 - r^2)}{r (r_o^2 - r_i^2)}$$

and

$$v_{\theta,b} = \frac{\Omega (r^2 - r_o^2)}{\left(\frac{r_i^2 - r_o^2}{r_i^2} \right) r} = \frac{\Omega r_i^2 (r_o^2 - r^2)}{r (r_o^2 - r_i^2)}$$

These results show when both fluids have identical viscosities, both Eqs. 6.84 reduce to Eq.6.69b from section 6.4.2 for a single fluid with a fixed outer cylinder, as they should.

To plot the velocity behavior, we non-dimensionalize the velocities within both fluids on the inner cylinder velocity, Ωr_i , and the r values on the inner radius, r_i (e.g. $r^* = \frac{r}{r_i}$):

$$\beta = \left[1 - \frac{r_o^2}{r_m^2} + \frac{\mu_b}{\mu_a} \left(\frac{r_o^2}{r_m^2} - \frac{r_o^2}{r_i^2} \right) \right] = \left[1 - \frac{r_o^{*2}}{r_m^{*2}} + \frac{\mu_b}{\mu_a} \left(\frac{r_o^{*2}}{r_m^{*2}} - r_o^{*2} \right) \right] \quad (6.85a)$$

$$v_{\theta,a}^* = \frac{v_{\theta,a}}{\Omega r_i} = \frac{\beta \frac{r^2}{r_i^2} + \frac{\mu_b}{\mu_a} \frac{r_o^2}{r_i^2} \left(\frac{r^2}{r_i^2} - \frac{r_i^2}{r_i^2} \right)}{\beta \frac{r}{r_i}} = \frac{\beta r^{*2} + \frac{\mu_b}{\mu_a} r_o^{*2} (r^{*2} - 1)}{\beta r^*} \quad (6.85b)$$

$$v_{\theta,b}^* = \frac{v_{\theta,b}}{\Omega r_i} = \frac{\left(\frac{r^2}{r_i^2} - \frac{r_o^2}{r_i^2} \right)}{\beta \frac{r}{r_i}} = \frac{(r^{*2} - r_o^{*2})}{\beta r^*} \quad (6.85c)$$

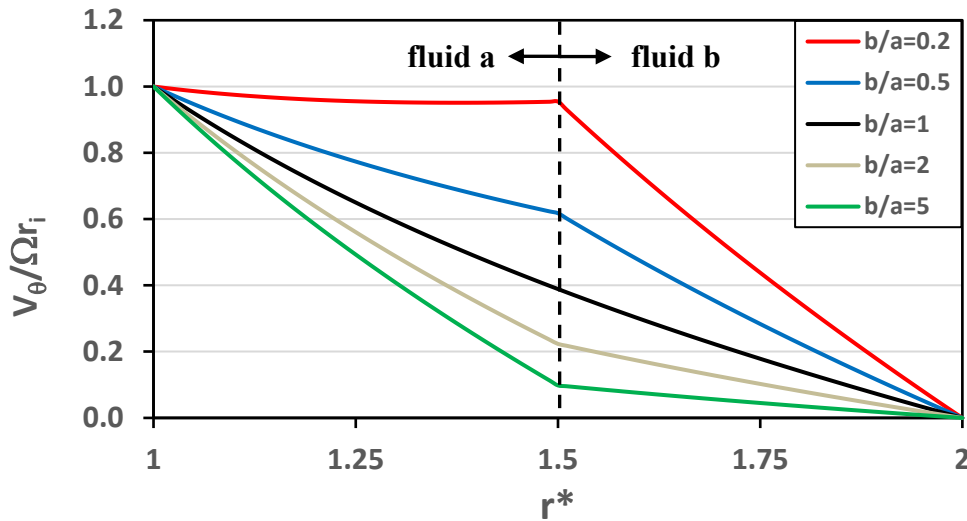


Figure 6.19 Non-dimensional velocity behavior vs. r^* (Eqs. 6.85) for five selected viscosity ratios, $0.2 \leq \frac{\mu_b}{\mu_a} \leq 5$ (b/a in the figure is $\frac{\mu_b}{\mu_a}$); $r_i^* = 1$, $r_o^* = 2$, and $r_m^* = 1.5$.

Figure 6.19 shows the non-dimensional velocity behavior within fluid a (to the left) and fluid b (to the right) for five selected viscosity ratios, $0.2 \leq \frac{\mu_b}{\mu_a} \leq 5$, and $r_i^* = 1$, $r_o^* = 2$, and $r_m^* = 1.5$.

The behavior will be different, but similar, for different bounding r^* values.

Note that when $\frac{\mu_b}{\mu_a} < 1$, fluid a experiences a lower deformation rate, whereas fluid b experiences

a higher deformation rate. Conversely, when $\frac{\mu_b}{\mu_a} > 1$, fluid a experiences a higher deformation

rate, and fluid b a lower deformation rate. The higher viscosity fluid always deforms at a lower rate, which skews the resulting velocity profiles accordingly, as shown in figure 6.19.

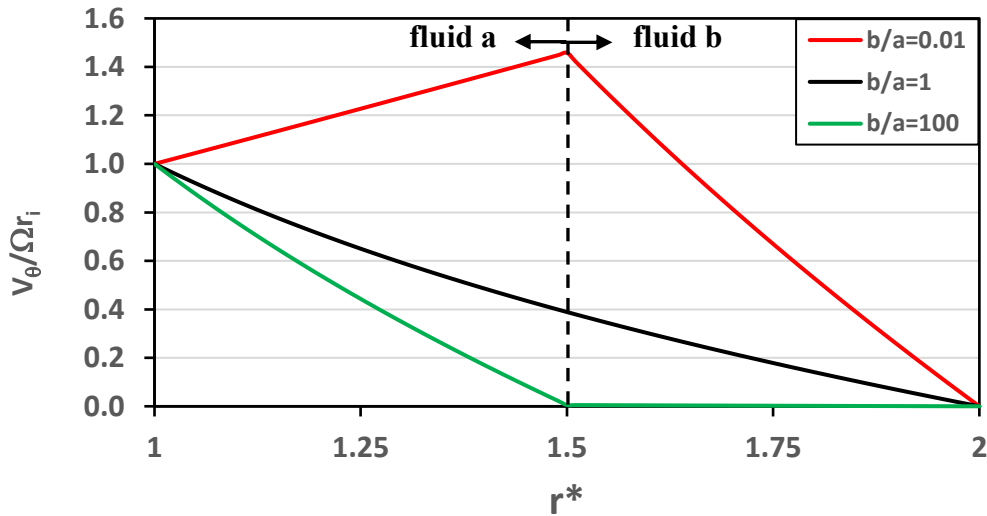


Figure 6.20 Non-dimensional velocity behavior vs. r^* (Eqs. 6.85) for extreme viscosity ratios, $\frac{\mu_b}{\mu_a} = 0.01, 1, 100$; $r_i^* = 1$, $r_o^* = 2$, and $r_m^* = 1.5$.

Figure 6.20 shows the extremes of the skewing of the velocity profiles that can take place when $\frac{\mu_b}{\mu_a} \gg 1$ and $\frac{\mu_b}{\mu_a} \ll 1$. Note that when $\frac{\mu_b}{\mu_a} = 100$ (green line), the fluid b deformation is minimal, such that fluid b behaves almost as a stationary solid, and fluid a behaves essentially like a single fluid with $v_{\theta,a} \cong 0$ at $r = r_m$. Conversely, when $\frac{\mu_b}{\mu_a} = 0.01$ (red line), fluid a moves essentially in solid body rotation (i.e. $v_{\theta,a} \cong \Omega r$) for $r_i < r < r_m$, and fluid b now behaves like a single fluid with $v_{\theta,b} \cong \Omega r_m$ at $r = r_m$.

Now consider the non-dimensional shear stresses, which are determined by substituting $r = r_i r^*$ into Eq. 6.81.

$$\begin{aligned} \tau_{r\theta} &= \mu r \frac{\partial}{\partial r} \left(\frac{v_\theta}{r} \right) = \mu r_i r^* \frac{1}{r_i} \frac{\partial}{\partial r^*} \frac{\Omega r_i}{r_i} \left(\frac{v_\theta^*}{r^*} \right) = \mu \Omega r^* \frac{\partial}{\partial r^*} \left(\frac{v_\theta^*}{r^*} \right) \\ \tau_{r\theta}^* &= \frac{\tau_{r\theta}}{\mu \Omega} = r^* \frac{\partial}{\partial r^*} \left(\frac{v_\theta^*}{r^*} \right) \end{aligned} \tag{6.86}$$

We now substitute Eqs. 6.85b and 6.85c into Eq. 6.86 to determine the shear stresses in fluids a and b. For consistency in comparing the shear stresses, $\tau_{r\theta,a}$ and $\tau_{r\theta,b}$ are both non-dimensionalized on $\mu_a\Omega$:

$$\tau_{r\theta,a}^* = \frac{\tau_{r\theta,a}}{\mu_a\Omega} = r^* \frac{\partial}{\partial r^*} \left(\frac{\beta r^{2*} + \frac{\mu_b}{\mu_a} r_o^{2*} (r^{2*} - 1)}{\beta r^{2*}} \right) = \frac{2 \frac{\mu_b}{\mu_a} r_o^{2*}}{\beta r^{2*}} \quad (6.87a)$$

$$\tau_{r\theta,b}^* = \frac{\tau_{r\theta,b}}{\mu_a\Omega} = \frac{\mu_b}{\mu_a} r^* \frac{\partial}{\partial r^*} \left(\frac{(r^{2*} - r_o^{2*})}{\beta r^{2*}} \right) = \frac{2 \frac{\mu_b}{\mu_a} r_o^{2*}}{\beta r^{2*}} \quad (6.87b)$$

Eqs. 6.87 show that the shear stress has the same functional behavior within both fluids, regardless of the viscosities.

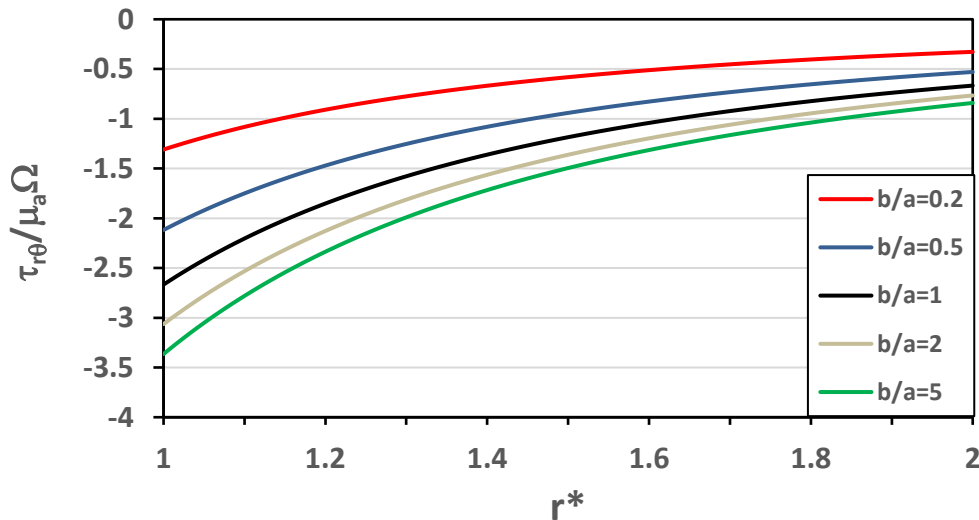


Figure 6.21 Non-dimensional shear stress vs. r^* for either fluid a or b (Eqs. 6.87).

$$0.2 \leq \frac{\mu_b}{\mu_a} \leq 5; r_i^* = 1, r_o^* = 2, \text{ and } r_m^* = 1.5.$$

Figure 6.21 is a plot of the non-dimensional shear stress, again for $0.2 \leq \frac{\mu_b}{\mu_a} \leq 5$, and $r_i^* = 1$, $r_o^* = 2$, and $r_m^* = 1.5$. Since the shear stress is of the same function within either fluid, the rate of deformation of the fluid is controlled by the fluid viscosity, which is the source of the strong variations in velocity behavior shown in figures 6.19 and 6.20. Additionally, figure 6.21 shows that increasing the viscosity ratio shifts the non-dimensional shear curve to stronger relative values; of course decreasing the viscosity ratio shifts the non-dimensional shear curve to lower

relative values. What is happening, is that when $\frac{\mu_b}{\mu_a} > 1$, the viscosity of fluid b becomes dominant, and it deforms less than fluid a. This is shown in figures 6.19 and 6.20 by the smaller velocity changes with radius for fluid b when $\mu_b > \mu_a$. However, when $\frac{\mu_b}{\mu_a} < 1$, the viscosity of fluid a is dominant, deforming less than fluid b. Again, figures 6.19 and 6.20 show these smaller velocity changes with radius for fluid a when $\mu_a > \mu_b$.

Note that figure 6.21 shows that $\tau_{r\theta}$ is negative for all $\frac{\mu_b}{\mu_a}$ and r^* values. Recall that this means for a “positive” stress orientation on a surface (determined here in cylindrical coordinates), a calculated negative shear stress for that surface will act opposite to that positive orientation.

For the rotating inner cylinder, a positive orientation would indeed be in the positive θ -direction (since the normal out of the cylinder surface would be in positive r -direction). Therefore, our calculation of a negative shear stress means the shear stress on the inner cylinder will act in opposition the direction of rotation, which is logical. Conversely, for the fixed outer cylinder, the outward normal for the surface will be negative (in a negative r -direction), such that a “positive” orientation is in the negative θ -direction. Thus, our calculated negative shear stress will actually act in the positive θ -direction on the fixed cylinder, which again is logical.

The resulting torque per unit depth is:

$$\text{Torque} = \tau_{r\theta} (2\pi r) r = \frac{2\mu_a \Omega \frac{\mu_b}{\mu_a} \frac{r_o^2}{r_i^2}}{\beta \frac{r^2}{r_i^2}} (2\pi r^2) = \frac{4\pi \mu_b \Omega r_o^2}{\beta} \quad (6.88)$$

Since the shear stress variations are identical (Eqs. 6.87), the torque is a constant value across the gap, and on each cylinder. This is consistent with the result for a single fluid. Note that Eq. 6.88 reduces to Eq. 6.68 for $\frac{\mu_b}{\mu_a} = 1$, which the reader should prove as an exercise.

Clearly, some unusual behavior takes place when there are two immiscible fluids in this rotating Couette flow. Moreover, we have examined the behavior for only one set of cylinder radii, and only equal thicknesses of the two fluids. Varying either of these will have a significant impact on the predicted results, although they will behave similarly. It would be a good exercise to replot the velocity and shear behavior for other sets of radial values. Additionally, redoing the problem assuming a rotating outer cylinder, with a fixed inner cylinder, would also be an instructive exercise.

As pointed out above, the practicality of such an annular, two-fluid flow is limited, since maintaining a consistent thickness of the fluids would be challenging, since gravity would have a buoyancy effect, which would most likely skew the behavior, so that a two-dimensional assessment would not be appropriate (perhaps an experiment for the space station, where gravity could truly be neglected!). Additionally, immiscible fluids such as oil and water generally have viscosity ratios of more than 100 (oil to water), so these would more likely reflect the extremes shown in figure 6.20. However, like the example we did in section 6.4.2, the addition of a limited amount of water to the annulus, would result in a multifold decrease in the shear and the torque required to rotate the inner cylinder (and that acts on the outer cylinder). This will be an exercise in the end of chapter problems.

6.4.5 Couette Flow between Porous Rotating Concentric Cylinders

In section 6.4.2 we examined a Couette flow between rotating cylinders with solid surfaces. Here, we examine the impact of having a cross-stream flow between the cylinders by having a constant fluid injection/suction across the bounding surfaces. For the purposes of this example, we assume a constant injection at the inner cylinder ($v_r = V @ r = r_i$), which is rotating at a constant angular velocity Ω , as shown. We again use the Navier-Stokes equation in cylindrical coordinates with the z-axis aligned out of this page on the centerline of the two cylinders, as shown in figure 6.22.

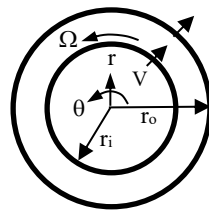


Figure 6.22 Geometry for Couette flow between concentric, porous cylinders with transverse flow in the radial direction ($v_r = V @ r = r_i$).

Also, we again assume no changes in the z-direction, which eliminates all terms depending on z and the velocity component v_z , leaving the continuity equation, and the θ -direction and r-direction component of the Navier-Stokes equations in cylindrical coordinates, as the governing equations:

$$\begin{aligned} \frac{\partial v_\theta}{\partial t} + v_r \frac{\partial v_\theta}{\partial r} + \frac{v_\theta}{r} \frac{\partial v_\theta}{\partial \theta} + v_z \frac{\partial v_\theta}{\partial z} + \frac{v_r v_\theta}{r} &= -\frac{1}{\rho r} \frac{\partial p}{\partial \theta} + \nu \left[\frac{\partial}{\partial r} \left(\frac{1}{r} \frac{\partial}{\partial r} (r v_\theta) \right) + \frac{1}{r^2} \frac{\partial^2 v_\theta}{\partial \theta^2} + \frac{\partial^2 v_\theta}{\partial z^2} + \frac{2}{r^2} \frac{\partial v_r}{\partial \theta} \right] \\ \frac{\partial v_r}{\partial t} + v_r \frac{\partial v_r}{\partial r} + \frac{v_\theta}{r} \frac{\partial v_r}{\partial \theta} + v_z \frac{\partial v_r}{\partial z} - \frac{v_\theta^2}{r} &= -\frac{1}{\rho} \frac{\partial p}{\partial r} + \nu \left[\frac{\partial}{\partial r} \left(\frac{1}{r} \frac{\partial}{\partial r} (r v_r) \right) + \frac{1}{r^2} \frac{\partial^2 v_r}{\partial \theta^2} + \frac{\partial^2 v_r}{\partial z^2} - \frac{2}{r^2} \frac{\partial v_\theta}{\partial \theta} \right] \end{aligned}$$

$$\frac{1}{r} \frac{\partial}{\partial r} (rv_r) + \frac{1}{r} \frac{\partial v_\theta}{\partial \theta} + \frac{\partial v_z}{\partial z} = 0$$

We eliminate terms in the equations, based on the following set of assumptions:

1. steady flow
2. no v_z motion
3. no changes in the z -direction
4. fully-developed flow \rightarrow no θ -direction changes
5. No pressure changes in θ -direction
6. $v_r = V$ at $r = r_i$

Assumption 5 corresponds to the same argument we made previously in sections 6.3.1 and 6.4.2.

From the reduced continuity equation, we can write:

$$\frac{d}{dr} (rv_r) = 0 \quad \Rightarrow \quad rv_r = \text{constant} = C \quad \Rightarrow \quad v_r = \frac{C}{r}$$

However, since $v_r = V$ at $r = r_i$, this implies that $C = Vr_i$ and $v_r = \frac{Vr_i}{r}$ across the annulus. Thus, the Navier-Stokes equations reduce to two ordinary differential equations for v_θ and v_r , varying only with radius, r :

$$v_r \frac{dv_\theta}{dr} + \frac{v_r v_\theta}{r} = \nu \frac{d}{dr} \left(\frac{1}{r} \frac{d}{dr} (rv_\theta) \right) \quad (\theta\text{-direction})$$

$$v_r \frac{dv_r}{dr} - \frac{v_\theta^2}{r} = -\frac{1}{\rho} \frac{dp}{dr} + \nu \frac{d}{dr} \left(\frac{1}{r} \frac{d}{dr} (rv_r) \right) \quad (r\text{-direction})$$

Here, we note that $v_r = \frac{Vr_i}{r}$, and that $\frac{d}{dr} (rv_r) = \frac{d}{dr} (Vr_i) = 0$, so we can rewrite the equations as:

$$\frac{Vr_i}{r} \frac{dv_\theta}{dr} + \frac{Vr_i v_\theta}{r^2} = \nu \frac{d}{dr} \left(\frac{1}{r} \frac{d}{dr} (rv_\theta) \right) \quad (\theta\text{-direction}) \quad (6.89a)$$

$$\frac{Vr_i}{r} \left(-\frac{Vr_i}{r^2} \right) - \frac{v_\theta^2}{r} = -\frac{1}{\rho} \frac{dp}{dr} \quad (r\text{-direction}) \quad (6.89b)$$

Note that $v_\theta = f(r)$ only, which makes the pressure only a function of r as well. Rearranging Eqs. 6.89 gives:

$$r \frac{dv_\theta}{dr} + v_\theta = \left(\frac{v}{V_{r_i}} \right) r^2 \frac{d}{dr} \left[\frac{1}{r} \frac{d}{dr} (rv_\theta) \right] \quad (\theta\text{-direction}) \quad (6.90a)$$

$$\frac{dp}{dr} = \frac{\rho V_{r_i}^2}{r^3} + \frac{\rho v_\theta^2}{r} \quad (r\text{-direction}) \quad (6.90b)$$

Here the pressure is only a function of r , and depends on knowing v_θ , but is decoupled from the differential equation for v_θ , Eq. 6.90a. So our first order of business is to determine v_θ , from which we can determine $p(r)$ from Eq. 6.90b, if we so desire.

Eq. 6.90a for v_θ looks a bit daunting and non-linear, but a solution can be found by some judicious substitution. To begin, we note that we can write:

$$r \frac{dv_\theta}{dr} + v_\theta = \frac{d(rv_\theta)}{dr} = \left(\frac{v}{V_{r_i}} \right) r^2 \frac{d}{dr} \left[\frac{1}{r} \frac{d}{dr} (rv_\theta) \right]$$

Now, we let $\alpha = rv_\theta$, and define an injection parameter $k = \frac{V_{r_i}}{v}$, so the equation becomes:

$$\frac{d\alpha}{dr} = \frac{r^2}{k} \frac{d}{dr} \left(\frac{1}{r} \frac{d\alpha}{dr} \right)$$

Dividing through by r gives:

$$\frac{1}{r} \frac{d\alpha}{dr} = \frac{r}{k} \frac{d}{dr} \left(\frac{1}{r} \frac{d\alpha}{dr} \right)$$

Finally, we let $\beta = \frac{1}{r} \frac{d\alpha}{dr}$, which gives us a final equation form of:

$$\beta = \frac{r}{k} \frac{d\beta}{dr}$$

Separating variables gives:

$$\frac{d\beta}{\beta} = k \frac{dr}{r}$$

which integrates to give:

$$\ln \beta = k(\ln r + \ln C) = \ln r^k + \ln C^k = \ln r^k + \ln C_1 = \ln(C_1 r^k)$$

or

$$\beta = C_1 r^k = \frac{1}{r} \frac{d\alpha}{dr}$$

Separating variables again, and integrating for α yields:

$$d\alpha = C_1 r^{k+1} dr$$

$$\alpha = C_1 \frac{r^{k+2}}{k+2} + C_2$$

Which from our previous substitution equates to:

$$\alpha = rv_\theta = C_1 \frac{r^{k+2}}{k+2} + C_2$$

or

$$v_\theta = C_1 \frac{r^{k+1}}{k+2} + \frac{C_2}{r}$$

(note: $k = -2$ is a special case, for which the solution is: $rv_\theta = \alpha = C_1 \ln(r) + C_2$)

The boundary conditions for the present flow are:

- (1) $v_\theta = \Omega r_i$ @ $r = r_i$
- (2) $v_\theta = 0$ @ $r = r_o$

Applying these boundary conditions gives us a set of equations for C_1 and C_2 , which when solved give a velocity relationship of:

$$v_\theta = \Omega r_i^2 \frac{(r_o^{k+2} - r^{k+2})}{r(r_o^{k+2} - r_i^{k+2})} \quad (\text{note: } k = -2 \text{ yields } v_\theta = \Omega r_i^2 \frac{\ln\left(\frac{r_o}{r_i}\right)}{r \ln\left(\frac{r_o}{r}\right)}) \quad (6.91)$$

Letting $r^* = \frac{r}{r_i}$, we can write Eq. 6.91 in non-dimensional form as:

$$\frac{v_\theta}{\Omega r_i} = \frac{(r_o^{*k+2} - r^{*k+2})}{r^* (r_o^{*k+2} - 1)} \quad (k = -2 \text{ yields } \frac{v_\theta}{\Omega r_i} = \frac{\ln\left(\frac{r_o^*}{r^*}\right)}{r^* \ln\left(\frac{r_o^*}{r^*}\right)}) \quad (6.92)$$

Note that determining the shear stress within the fluid is a bit cumbersome, and is given by:

$$\tau_{r\theta} = \mu \left[r \frac{\partial}{\partial r} \left(\frac{v_\theta}{r} \right) + \frac{1}{r} \frac{\partial v_r}{\partial \theta} \right] = - \frac{\mu \Omega r_i^2 (2r_o^{k+2} + k r^{k+2})}{r^2 (r_o^{k+2} - r_i^{k+2})} \quad (6.93)$$

Or non-dimensionally (using $r^* = \frac{r}{r_i}$ again),

$$\frac{\tau_{r\theta}}{\mu \Omega} = - \frac{(2r_o^{*k+2} + k r^{*k+2})}{r^{*2} (r_o^{*k+2} - 1)} \quad (6.94)$$

A comparison of the velocity and the shear stress for injection values of $k = \frac{Vr_i}{\nu} = 0, 2, 4,$ and -4 (the last value is a suction through the inner surface) is shown in figure 6.22.

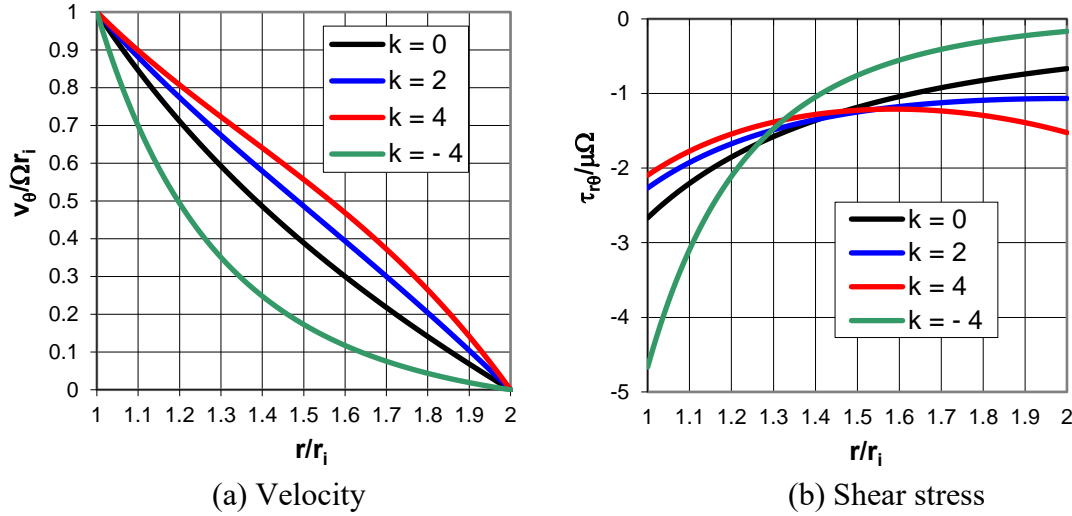


Figure 6.22 Non-dimensional velocity and shear stress vs. non-dimensional radius for a concentric annulus with cross-stream injection (V) through the inner porous boundary. The outer cylinder is fixed and inner cylinder rotates at Ω , with $r_o/r_i = 2$. Behavior is shown for injection parameters $k = Vr_i/\nu = 0, 2, 4,$ and -4 (this latter value is a suction at the inner surface).

Figure 6.22a shows that injection through the inner cylinder increases the velocity values at non-bounding radii within the annulus, whereas suction through the inner cylinder decreases the respective velocity values. This change in the velocity profile will affect the volume flow rate within the annulus accordingly.

The volume flow rate (per unit depth) within the annulus is calculated as:

$$Q_k = \int_{r_i}^{r_o} v_\theta dr = \Omega r_i^2 \int_{r_i}^{r_o} \frac{(r_o^{k+2} - r^{k+2})}{r(r_o^{k+2} - r_i^{k+2})} dr = \Omega r_i^2 \left[\frac{r_o^{k+2}}{(r_o^{k+2} - r_i^{k+2})} \ln\left(\frac{r_o}{r_i}\right) - \frac{1}{(k+2)} \right]$$

or non-dimensionally as:

$$\frac{Q_k}{\Omega r_i^2} = \left[\frac{r_o^{*k+2}}{(r_o^{*k+2} - 1)} \ln(r_o^*) - \frac{1}{(k+2)} \right] \tag{6.95}$$

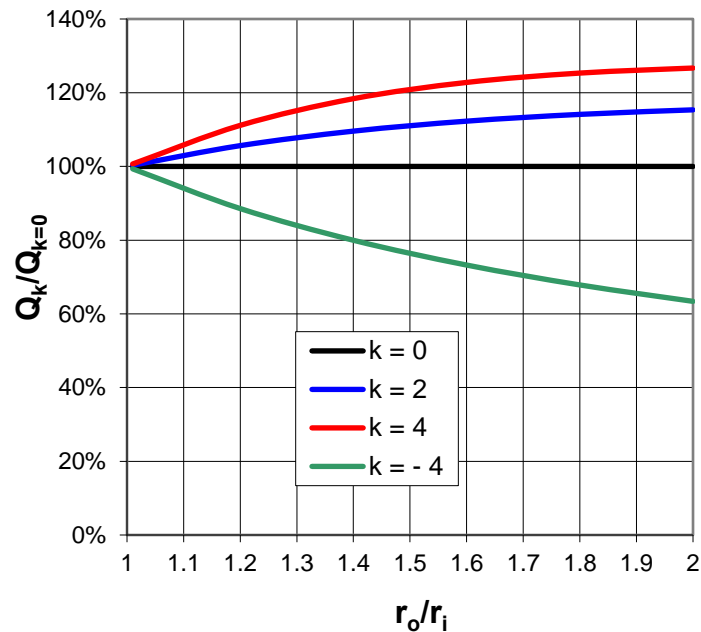


Figure 6.23 Flow Rate Ratio $= \frac{Q_k}{Q_{k=0}}$ vs. radius ratios for a concentric annulus with cross-stream injection (V) through the inner porous cylinder, and a mass balanced suction through the outer porous cylinder. The outer cylinder is fixed and the inner cylinder rotates at Ω . Behavior is shown for radii ratios $1 < r_o/r_i < 2$, and injection parameters $k = Vr_i/\nu = 0, 2, 4$, and -4 (this latter value is a suction at the inner surface).

Figure 6.23 illustrates the impact of both injection/suction and the radii ratio $r_o^* = r_o/r_i$ on the induced flow rate within the annulus. To better illustrate changes, the flow rates with suction/injection are non-dimensionalized on the flow rate for radius ratios with a non-porous surface ($k = 0$), $Q_k/Q_{k=0}$.

Figure 6.23 shows that fluid injection through the inner cylinder increases the induced flow rate, up to 27% for $k = 4$, $r_o/r_i = 2$. However, surface suction through the rotating inner cylinder has a more pronounced effect, decreasing the induced flow rate by up to 37% for $k = -4$, $r_o/r_i = 2$. Injection/suction will have differing effects, depending on which surface is rotated, the radii ratio, and the magnitude of the suction/injection, but clearly the impact of such suction, even relatively small values, can have a substantial effect. For example, if we base the Reynolds number for the fluid within the annulus on the inner cylinder surface velocity ($v_{\theta i} = \Omega r_i$), the cylinder radius (r_i), and the kinematic viscosity (ν), the Reynolds number for this flow would be $\Omega r_i^2/\nu$, and we can show that $V/v_{\theta i} = k/(\Omega r_i^2/\nu)$. Thus, for a small Reynolds number of 100, an

injection parameter of $k = 4$ would give $V/v_{0i} = 0.04$. So, a 4% injection rate results in a 27% increase in induced flow rate (and a 4% suction rate results in a 37% reduction in induced flow rate). As we showed previously in Section 6.3.3, small cross-stream flows through porous surfaces can have very significant effects on overall flow behavior.

To further illustrate the global impact of a small amount of surface injection/suction, note the effect of the injection/suction parameter k on the shear stress values shown in figure 6.22b. Figure 6.22b shows that the corresponding shear values become more uniform with injection ($k > 0$), and display larger variations with suction ($k < 0$), which suggests that suction through the inner cylinder should result in increased torque on the inner cylinder.

To examine this, we calculate the general torque (per unit depth) at a radius r , as:

$$\text{Torque}|_r = \tau_{r\theta}(2\pi r)r = \mu\Omega r_i^2 \frac{(2r_o^{k+2} + kr^{k+2})}{r^2(r_o^{k+2} - r_i^{k+2})}(2\pi r)r = 2\pi\mu\Omega r_i^2 \frac{(2r_o^{k+2} + kr^{k+2})}{(r_o^{k+2} - r_i^{k+2})}$$

Particularizing the torque to the respective cylinder surfaces, the resulting torque on the inner and outer cylinders per unit depth is given by:

$$\text{Torque}|_{r=r_i} = 2\pi\mu\Omega r_i^2 \frac{(2r_o^{k+2} + kr_i^{k+2})}{(r_o^{k+2} - r_i^{k+2})} \quad (6.96a)$$

and

$$\text{Torque}|_{r=r_o} = 2\pi\mu\Omega r_i^2 \frac{(2+k)r_o^{k+2}}{(r_o^{k+2} - r_i^{k+2})} \quad (6.96b)$$

Comparing the ratio of the torques in Eqs. 6.96, we have:

$$\text{Torque Ratio} = \frac{\text{Torque}|_{r=r_i}}{\text{Torque}|_{r=r_o}} = \frac{2r_o^{k+2} + kr_i^{k+2}}{(2+k)r_o^{k+2}} = \frac{2+k\left(\frac{r_i}{r_o}\right)^{k+2}}{(2+k)} = \frac{2+k\left(\frac{1}{r_o^*}\right)^{k+2}}{(2+k)} \quad (6.97)$$

Equation 6.97 indicates that the torque varies significantly with the injection/suction parameter k . If $k = 0$, the torques are equivalent, as we demonstrated for non-porous concentric cylinders in section 6.4.2. However, if $k > 0$ [injection from of the inner cylinder], the torque will be *lower* on the inner cylinder, whereas if $k < 0$ [suction into the inner cylinder], the torque will be *higher* on the inner cylinder. This result is again a consequence of the momentum change that the injected fluid must undergo as it passes across the gap between the cylinders, as we discussed in section 6.3.3.

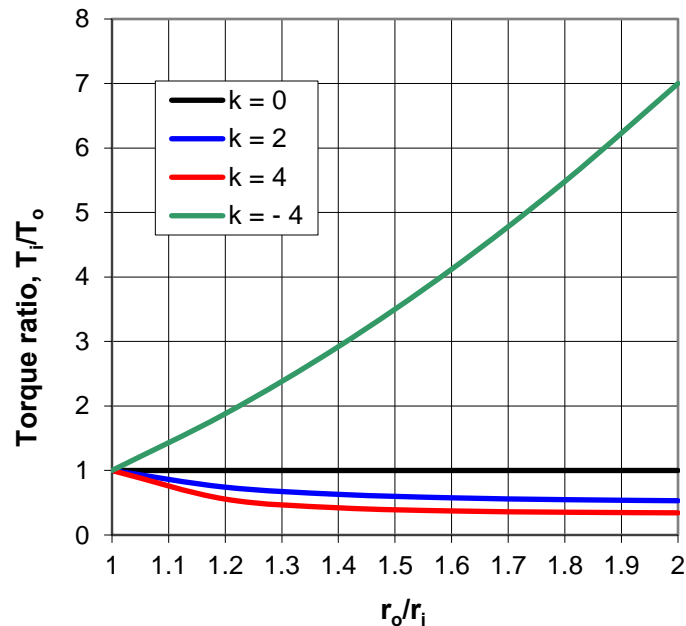


Figure 6.24 Torque Ratio = $\frac{\text{Torque}|_{r=r_i}}{\text{Torque}|_{r=r_o}}$ vs. radii ratios for a concentric annulus with cross-stream injection (V) from the inner porous cylinder, and a mass-balanced suction through the outer porous cylinder. The outer cylinder is fixed and the inner cylinder rotates at angular velocity, Ω . Behavior is shown for radii ratios $1 < r_o/r_i < 2$, and injection parameters $k = Vr_i/\nu = 0, 2, 4$, and -4 (this latter value is a suction at inner surface).

Figure 6.24 shows the variation in the torque ratio of the inner to the outer cylinder (Eq. 6.97) as a function of both the ratio of the cylinder radii and the injection/suction parameter. Note that injection reduces the torque ratio, due to a lower shear on the inner cylinder, and higher shear on the outer (figure 6.22b indicates that the shear stress, and thus the actual torque on the inner cylinder, is lower with injection). However, figure 6.24 also shows that suction significantly increases the torque ratio (seven fold for $r_o/r_i = 2$ and $k = -4$). The absolute torque on the inner cylinder also increases by 75% over that for a solid cylinder. These variations are independent of how fast the cylinder is rotated (as long as the flow in the annulus is laminar). This is a striking result, and quite illustrative of the impact of the transfer of fluid momentum across the annulus.

Now, consider the pressure behavior between the cylinders. The r -direction differential equation derived above, Eq. 6.90b, gives:

$$\frac{dp}{dr} = \frac{\rho V^2 r_i^2}{r^3} + \frac{\rho v_0^2}{r}$$

Substituting for v_θ from Eq. 6.92, we have:

$$\frac{dp}{dr} = \frac{\rho V^2 r_i^2}{r^3} + \frac{\rho \Omega^2 r_i^4 (r_o^{k+2} - r^{k+2})^2}{r^3 (r_o^{k+2} - r_i^{k+2})^2}$$

We separate variables and integrate from r_i outward, where $p = p_i$ at $r = r_i$:

$$\int_{p=p_i}^p dp = \int_{r=r_i}^r \left\{ \frac{\rho V^2 r_i^2}{r^3} + \frac{\rho \Omega^2 r_i^4 (r_o^{k+2} - r^{k+2})^2}{r^3 (r_o^{k+2} - r_i^{k+2})^2} \right\} dr$$

And after some messy integration, we get:

$$p - p_i = \frac{\rho V^2 r_i^2}{2} \left(\frac{1}{r_i^2} - \frac{1}{r^2} \right) + \frac{\rho \Omega^2 r_i^4}{2} \left\{ \frac{\left(r_o^{2k+4} + \frac{4r_o^{k+2} r_i^{k+2}}{k} - \frac{r_i^{2k+4}}{k+1} \right)}{r_i^2 (r_o^{k+2} - r_i^{k+2})^2} - \frac{\left(r_o^{2k+4} + \frac{4r_o^{k+2} r^{k+2}}{k} - \frac{r^{2k+4}}{k+1} \right)}{r^2 (r_o^{k+2} - r_i^{k+2})^2} \right\} \quad (6.98)$$

Defining a non-dimensional pressure coefficient as $C_p = \frac{p - p_i}{\frac{1}{2} \rho \Omega^2 r_i^2}$, and letting $r^* = \frac{r}{r_i}$ again, we

can rewrite Eq. 6.98 as:

$$C_p = \left(\frac{V}{\Omega r_i} \right)^2 \left(1 - \frac{1}{r^{*2}} \right) + \left\{ \frac{\left(r_o^{*2k+4} + \frac{4r_o^{*k+2}}{k} - \frac{1}{k+1} \right)}{(r_o^{*k+2} - 1)^2} - \frac{\left(r_o^{*2k+4} + \frac{4r_o^{*k+2} r^{*k+2}}{k} - \frac{r^{*2k+4}}{k+1} \right)}{r^{*2} (r_o^{*k+2} - 1)^2} \right\} \quad (6.99)$$

In most cases, we would expect $\frac{V}{\Omega r_i}$ to be very small, and thus contribute little to the pressure

change. The bulk of the change is a result of the large, bracketed terms on the right of Eq. 6.99, which reflects pressure due to variations in the angular momentum of the fluid. The behavior of the pressure coefficient from Eq. 6.99 is shown in figure 6.25.

Note that for all k values shown (and in general), the pressure increases outward, as it should, since $dp/dr > 0$ for all k values. However, as the figure shows, for $k > 0$ [injection from the inner cylinder] the pressure increases more rapidly outward; conversely, for $k < 0$ [suction into the inner cylinder] the pressure increases less rapidly, reaching a lower value at $r = r_o$.

One can understand this behavior from the velocity profiles of figure 6.22a. As the fluid particles injected through the inner surface move toward the outer surface, they retain more of their initial θ -direction momentum at the same radial location than would occur through just viscous diffusion. Since the angular velocity remains higher as it nears the outer fixed cylinder

(where the fluid must exit with zero velocity), the angular momentum of the fluid is larger, which is reflected as an increased radial pressure difference.

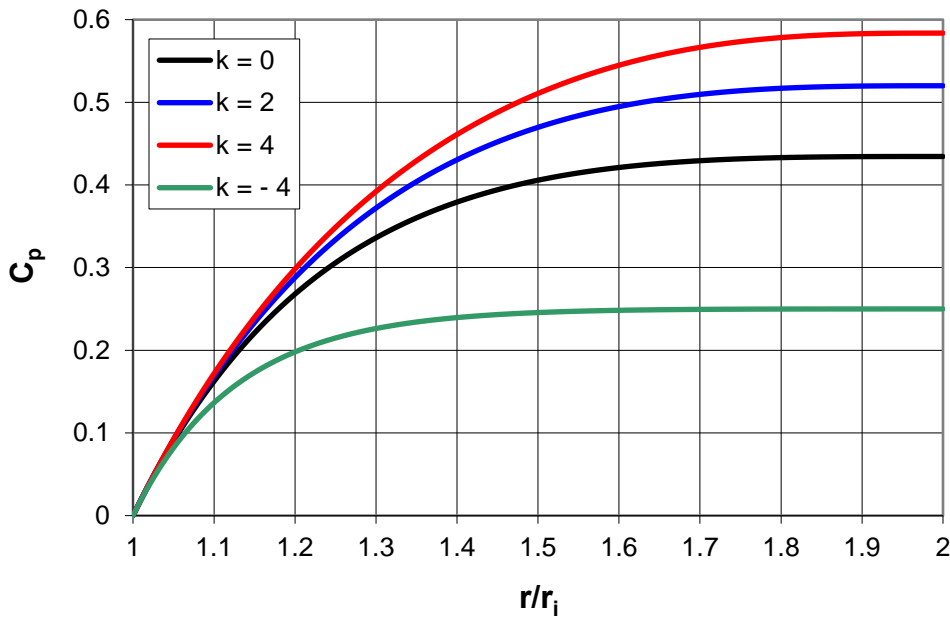


Figure 6.25 Non-dimensional pressure coefficient $C_p = \frac{p - p_i}{\frac{1}{2}\rho\Omega^2 r_i^2}$ vs. non-dimensional radius for a concentric annulus of $r_o/r_i=2$, with cross-stream injection (V) from the inner porous cylinder, and a mass balanced suction out of the outer porous cylinder. The outer cylinder is fixed and the inner cylinder rotates at Ω , with $Re_\Omega = \Omega r_i^2/\nu = 100$. Behavior is shown for injection parameters $k = Vr_i/\nu = 0, 2, 4$, and -4 (this latter value is a suction at the inner surface).

The opposite occurs if there is suction at the inner surface. In that case, the acceleration of the fluid to the inner rotation velocity as it approaches the inner cylinder occurs more slowly, thus retarding the angular momentum, which in turn reduces the radial pressure changes.

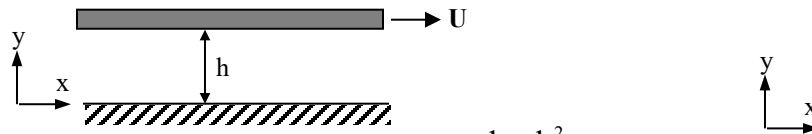
6.5 Summary

Sections 6.3 and 6.4 have presented several simple analytic, closed-form solutions to the Navier-Stokes equations. These are all one-dimensional, since they depend on only one space variable. Most of these examples reduce the Navier-Stokes to a force balance between shear stress and pressure. However, as illustrated by the examples in Sections 6.3.3 and 6.4.5, the introduction of a simple advection term due to a steady cross-stream velocity by balanced injection/suction can have a significant impact on the flow behavior, and the subsequent forces, such as wall shear and flow rates.

The inclusion of advection and time dependent acceleration term in the Navier-Stokes equation makes the solution of the resulting equations much more complicated, requiring more advanced mathematics and/or numerical solutions. In Chapter 12, we will examine more complicated, two-dimensional solutions of the Navier-Stokes equations, for which the flow is dependent on either one spatial dimension and time, or on two spatial dimensions. In either case, the number of possible closed-form solutions is limited, and the mathematics is often quite complicated.

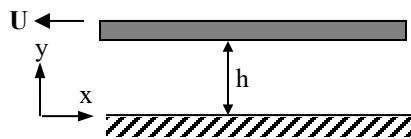
Study Problems

1. A fluid flows in the x -direction between two parallel plates, a distance h apart in the y -direction. The upper plate moves with a speed U and the lower plate is fixed.



A pressure gradient, $\frac{dp}{dx}$, is imposed on the flow. Define $P = \frac{dp}{dx} \frac{h^2}{2\mu U}$, and:

- (a) Determine the velocity profile, $u(y)$, and the shear stress, $\tau(y)$, for the flow.
 - (b) Determine the value of P which causes the shear stress on the lower plate to be zero.
 - (c) Calculate the volume flow rate, and determine the value of P which causes the volume flow rate to be zero.
 - (d) For air at 20°C , $U = 20 \text{ cm/s}$, $h = 1 \text{ cm}$, and $\frac{dp}{dx} = -0.3 \text{ N/m}^3$, calculate the value of the shear stress on the lower plate.
 - (e) If the shear stress for this flow is $\tau_{y=h} = \tau_w < 0$ at $y = h$, does this mean τ_w acts in the negative x -direction on the upper plate? Explain your answer.
 - (f) Calculate the volume flow rate (in cm^3/s per meter depth) for part (d).
2. A fluid flows in the x -direction between two parallel plates, a distance h apart in the y -direction. The upper plate moves with a speed $-U$ and the lower plate is fixed.

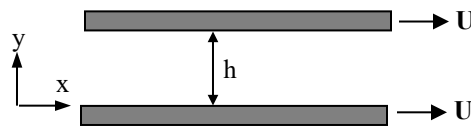


A pressure gradient, $\frac{dp}{dx}$, is imposed on the flow. Define $P = \frac{dp}{dx} \frac{h^2}{2\mu U}$, and:

- (a) Determine the velocity profile, $u(y)$, and the shear stress, $\tau(y)$, for the flow.

- (b) Determine the value of P which causes the shear stress on the lower plate to be zero.
- (c) Calculate the volume flow rate, and Determine the value of P which causes the volume flow rate to be zero.
- (d) For air at 20°C , $U = 20 \text{ cm/s}$, $h = 1 \text{ cm}$, and $\frac{dp}{dx} = -0.3 \text{ N/m}^3$, calculate the value of the shear stress on the lower plate.
- (e) If the shear stress for this flow is $\tau_{y=h} = \tau_w < 0$ at $y = h$, does this mean τ_w acts in the negative x -direction on the upper plate? Explain your answer.
- (f) Calculate the volume flow rate (in cm^3/s per meter depth) for part (d).

3. A fluid flows in the x -direction between two parallel plates, a distance h apart in the y -direction.



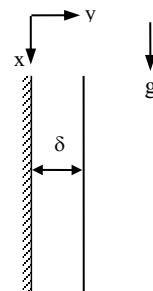
Both the upper and lower plate move with a speed U and a pressure gradient, $\frac{dp}{dx}$, is imposed on the flow.

Define $P = \frac{dp}{dx} \frac{h^2}{2\mu U}$, and:

- (a) Determine the velocity profile, $u(y)$, and the shear stress, $\tau(y)$, for the flow.
- (b) Determine the value of P which causes the shear stress on the lower plate to be zero.
- (c) Calculate the volume flow rate, and Determine the value of P which causes the volume flow rate to be zero.
- (d) For air at 20°C , $U = 20 \text{ cm/s}$, $h = 1 \text{ cm}$, and $\frac{dp}{dx} = -0.3 \text{ N/m}^3$, calculate the value of the shear stress on the lower plate.
- (e) If the shear stress for this flow is $\tau_{y=h} = \tau_w < 0$ at $y = h$, does this mean τ_w acts in the negative x -direction on the upper plate? Explain your answer.
- (f) Calculate the volume flow rate (in cm^3/s per meter depth) for part (d).

4. A vertical plate of infinite extent has a film of water flowing downward on the outside due to gravity.

- a) Determine the velocity profile in terms of gravity (g), the kinematic viscosity (ν), the volume flow rate per unit width (Q), and the distance from the surface (y).
- b) If $\nu = 10^{-2} \text{ cm}^2/\text{sec}$. for water at room temperature, determine the thickness of the water layer and the maximum velocity within the water layer if the flow rate per unit width is $Q = 0.62 \text{ cm}^2/\text{sec}$.



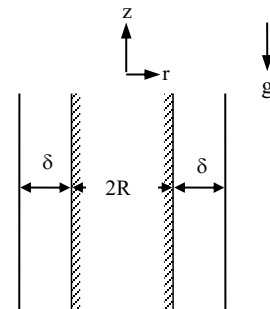
5. An intravenous feeding tube 3 mm diameter runs from a water bag $h=0.7$ M above the floor and is $L=2$ m long. Assume the water level in the bag is 10 cm above entrance to the tube, and that the flow is assumed laminar, and essentially fully developed over the length of the tube (not probable, but a reasonable estimate). If there is not restriction on the tube, and no needle at the exit, what is the maximum flowrate, in milliliters per minute ($1 \text{ ml} = 1000 \text{ mm}^3$) that could flow through the tube? Assume atmospheric pressure at the surface of the water in the bag, and at the exit of the tube. Note: the pressure gradient for this flow can be approximated as $\frac{dP}{dx} = -\rho \left(\frac{h}{L} \right) g$ and the temperature as 20°C .

Check to see if this flow would indeed be laminar (i.e. $\text{Re}_D = \frac{UD}{\nu} < 2300$).

6. A hypodermic syringe with a plunger 0.2 cm^2 in area injects 500 mm^3 of water through a 24-gauge hypodermic needle, 5 cm long and 0.311 mm diameter. Neglect the flow in the syringe, and assume that the flow is laminar and essentially fully developed within the needle during this process. In reality, there are entrance region effects for the needle. However, a fully developed assumption will give an upper limit of the flowrate that can be expected. The force exerted by the injector on the syringe is 1 N. Note that atmospheric pressure acts on all surfaces of the syringe and needle, so the pressure within the syringe will be gauge pressure (the pressure above atmospheric). How long (in seconds) will it take to inject the 500 mm^3 of water (assume temperature of 30°C) if (1) the needle exit gauge pressure is zero; (2) the needle is inserted in a portion of the body with an exit gauge pressure of 16.3 kPa.? Check to see if this latter flow would be laminar (i.e. $\text{Re}_D = \frac{UD}{\nu} < 2300$).

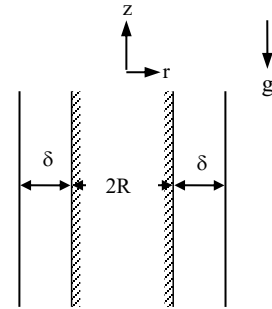
7. A thin Newtonian film of uniform thickness δ is formed on the external surface of a vertical, infinitely long, stationary rod. Assume that the flow is steady, the surface tension is zero, and the ambient air is stationary. If gravity is $g = \text{constant}$, the z -coordinate is along the rod axis in opposition to gravity, the rod diameter is R , and kinematic viscosity is ν :

- (a) Calculate the velocity within the film, $v_z(r)$, in terms of r , g , R , δ , and ν .
 (b) Determine the shear stress on the cylinder surface, τ_{rz} , in terms of ρ , g , R , and δ .



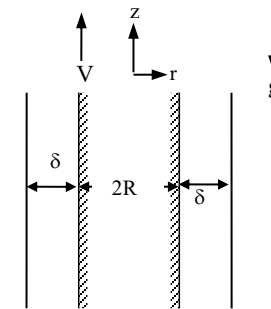
8. A thin Newtonian film of uniform thickness δ is formed on the external surface of a vertical, infinitely long, stationary rod. Assume that the flow is steady, the surface tension is zero, and the ambient air is stationary. If gravity is $g = \text{constant}$, the z -coordinate is along the rod axis in opposition to gravity, the rod diameter is R , and kinematic viscosity is ν :

- (a) Calculate the velocity within the film, $v_z(r)$, in terms of r, g, R, δ , and ν .
- (b) Determine the volume flowrate for the fluid layer, Q , in terms of g, ν, R , and δ (warning: apply the integration limits but don't attempt to simplify—it is an ugly result).



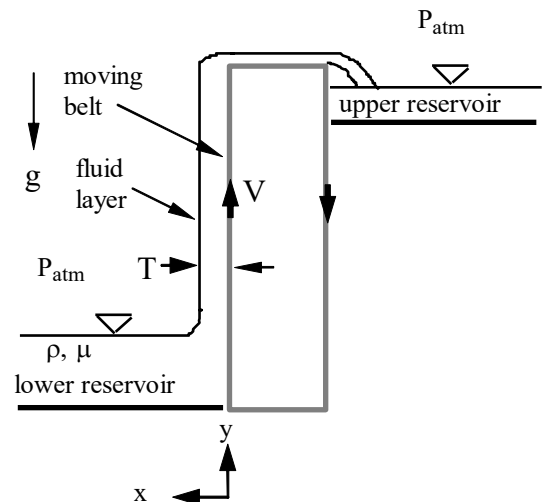
9. A thin Newtonian film of uniform thickness δ is formed on the external surface of a vertical, infinitely-long rod. The rod moves upward (against gravity) at a velocity V . Assume that the flow is steady, the surface tension is zero, and the ambient air is stationary. If gravity is $g = \text{constant}$, the z -coordinate is along the rod axis (in opposition to gravity), the rod diameter is $2R$, and kinematic viscosity is ν :

- (a) Calculate the velocity within the film, $v_z(r)$, in terms of V, r, g, R, δ , and ν .
- (b) Determine the shear stress on the cylinder surface, τ_{rz} , in terms of ρ, g, R , and δ .
- (c) If $R \gg \delta$, determine what value of rod velocity V will make $v_z = 0$ at $r = R + \delta$ in terms of g, R, δ , and ν (i.e. the outer fluid surface will be stationary relative to the z -coordinate).



10. Consider the vertically oriented moving belt shown below. The belt moves upward at velocity V out of a vat of liquid of density ρ and viscosity μ , as shown in the figure. Above a certain belt velocity, the shear stress acting on the fluid will cause the liquid to rise up the belt due to viscous effects, and to be deposited in the upper reservoir of fluid, as shown. It is assumed that the moving belt is sealed at the bottom of the two reservoirs, such that fluid will not leak out. You are to perform an analysis of the flow to determine the velocity profile and flow rate of liquid moving up the surface of the belt.

Assume that the flow is steady, the thickness of the liquid is T , atmospheric pressure acts on all surfaces of the liquid, and g acts as shown. Consider only the portion of the belt where the flow might be considered fully developed. List the remainder of your assumptions very carefully, and think hard

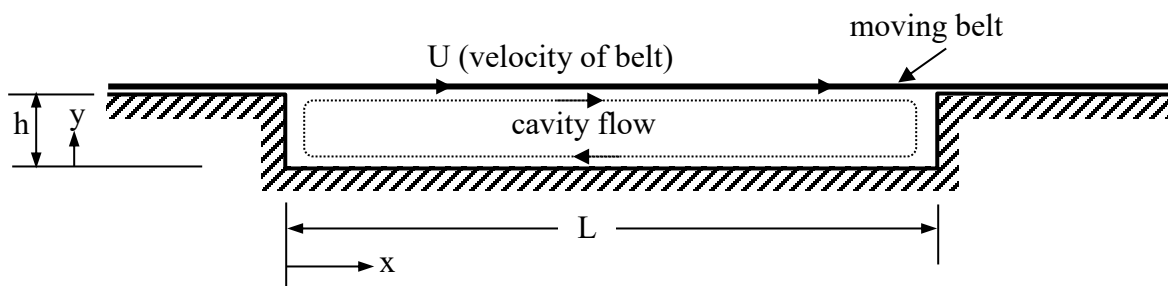


about the physics of the flow behavior since this will impact the conditions you must place on the solution.

Specifically:

- a. Starting with basic equation(s), develop a simplified differential equation to allow the determination of $v(x)$; clearly state simplifying assumptions and the boundary conditions for the problem.
 - b. Using the result of part a, establish a general solution for the velocity profile, $v(x)$, in terms of x and constants shown in the figure.
 - c. Determine the flowrate per unit depth, Q , of the liquid from the lower reservoir to the upper reservoir.
 - d. Determine (in terms of g , T , ρ and μ) the minimum velocity necessary to assure that liquid will flow upward.
 - e. Is there a limiting height to which the fluid can be pumped, and is this a function of the velocity of the belt? If so, determine the maximum pumping height as a function of velocity, V .
11. Consider the flow of a fluid of viscosity, μ , and density, ρ , in the long, rectangular cavity shown below, where $L \gg h$. The lower surface and the ends of the cavity are flat, solid surfaces. The upper surface is a flat belt that moves over the cavity from left-to-right at a constant speed U . Using the coordinates shown, determine the steady state velocity profile in the central region of the cavity, where the flow can be considered to be parallel and fully developed such that the velocity depends on y alone. Note that a constant pressure gradient, dP/dx , exists in the central region of the cavity.

Assume that the seal between the belt and the cavity corners is perfect, such that no fluid leaks from or into the cavity. List the remainder of your assumptions very carefully, and think hard about the physics of the flow behavior, since this will affect the conditions you must place on the solution.

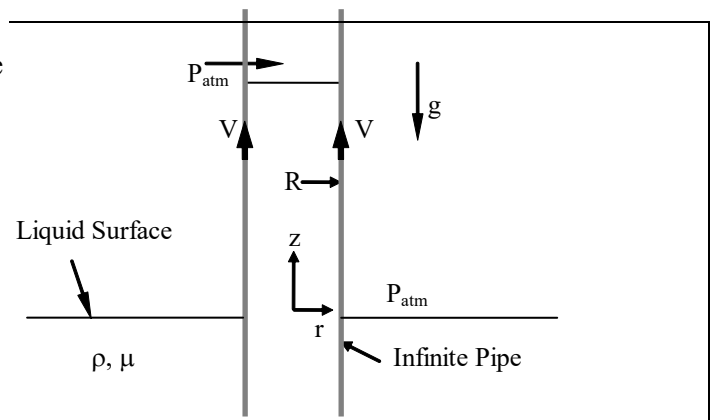


Specifically:

- a. Starting with the 2-D continuity and x -direction Navier-Stokes equations, develop a *simplified differential equation* which will allow the determination of $u(y)$; clearly state the boundary conditions for the problem.
- b. Using the result of part a, establish a *general solution* for the velocity profile, $u(y)$, in terms of defined and undefined constants and y .

- c. Determine the value(s) of the undefined constant(s) through the application of the boundary conditions to yield a *specific solution* in terms of U , h , μ , dP/dx and y .
 - d. Since dP/dx is an unknown constant, determine a way to establish the value of the pressure gradient in this central region of the cavity in terms of μ , U , and h only.
[Hint: consider the *net* flowrate, Q , at the center of the cavity]
 - e. Using the result of part d, eliminate dp/dx from your solution for $u(y)$ such that $u(y)$ is expressed as a function of U , h , and y *only*. Plot the shape of the resulting velocity profile, y/h vs. u/U .
 - f. Establish the y -location and the magnitude of the maximum and minimum velocity within the cavity.
12. Consider an infinite circular pipe of radius R , which is translating vertically upward at velocity V out of a vat of liquid of density ρ and viscosity μ , as shown in the figure. Above a certain pipe translation velocity, the shear stress acting on the fluid at the pipe inner wall will cause the liquid to rise up inside the pipe, much like a “viscous” pump (note that the liquid will also rise up on the outside of the pipe, but you are to neglect those effects). You are to perform an analysis of the flow to determine the velocity profile and flow rate of liquid inside the pipe, from $0 < r < R$.

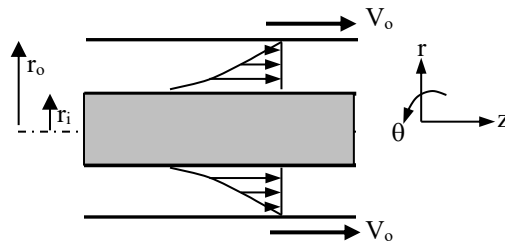
Using the coordinates shown, assume that the pipe is of infinite extent, the flow is steady, atmospheric pressure acts on all surfaces of the liquid, and g acts as shown. List the remainder of your assumptions very carefully, and think hard about the physics of the flow behavior since this will impact the conditions you must place on the solution.



Specifically:

- a. Starting with basic equations, develop a simplified differential equation which will allow the determination of $v_z(r)$; clearly state the boundary conditions for the problem.
- b. Using the result of part a, establish a general solution for the velocity profile, $v_z(r)$, in terms of r and constants shown in the figure.
- c. Determine the volume flowrate of the liquid up the pipe, Q .
- d. Determine [in terms of g , R and $\nu (= \mu/\rho)$] the *minimum pipe translation velocity* necessary to assure that liquid will flow upward.
- e. Is there a limiting height to which the fluid can rise in the pipe, and is this a function of the velocity of the pipe? If so, determine the height as a function of velocity, V .

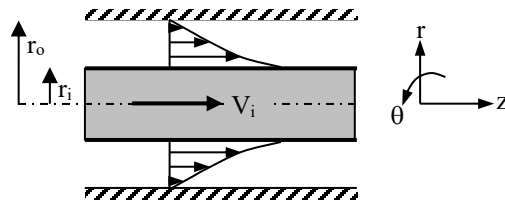
13. Consider the viscous pumping of a fluid of viscosity μ due to the axial motion of a circular tube encompassing an annulus formed between a stationary inner rod of radius r_i and a surrounding tube of r_o (assume the rod and tube are of infinite length).



Determine the velocity profile, v_z vs r/r_o , within the annulus where the outer tube is translated in the axial direction at a velocity V_o . On one graph, plot curves of v_z/V_o vs. r/r_o for $r_i/r_o = 0.9, 0.7, 0.5, 0.3,$ and 0.1 .

Also, determine the non-dimensional flow rate within the tube, $\frac{Q}{\pi r_o^2 V_o}$, as a function of $r' = \frac{r_i}{r_o}$, and on a second graph plot $\frac{Q}{\pi r_o^2 V_o}$ vs. r' for $0 < r' < 1$. What will be the force per unit length (F/L) required to keep the rod stationary?

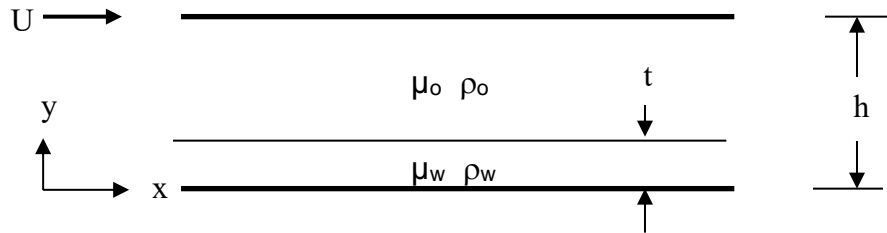
14. Consider the viscous pumping of a fluid of viscosity μ due to the axial motion of a rod within an annulus formed between the rod of radius r_i and a surrounding tube of r_o (assume the rod and tube are of infinite length).



Determine the velocity profile, v_z vs r , within the annulus where the inner rod is translated in the axial direction at a velocity V_i . On one graph, plot curves of v_z/V_i vs. r/r_o for $r_i/r_o = 0.9, 0.7, 0.5, 0.3,$ and 0.1 .

Also, determine the non-dimensional flow rate within the tube, $\frac{Q}{\pi r_o^2 V_i}$, as a function of $r'_i = \frac{r_i}{r_o}$, and on a second graph plot $\frac{Q}{\pi r_o^2 V_i}$ vs. r'_i for $0 < r'_i < 1$. Determine (mathematically, not graphically) the value of r'_i for which this viscous pump will yield the highest flow rate for a fixed value of V_i . What will be the force per unit length (F/L) required to keep the rod moving at a constant speed?

15. An upper flat plate is translated at a velocity U parallel to a lower fixed flat plate, with a spacing of h between the plates, creating a Couette flow.



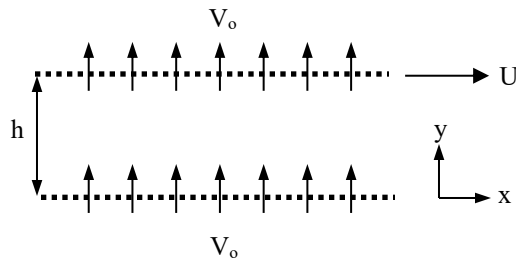
Originally the fluid between the plates is oil, which results in a shear stress within the oil, and on the bounding plates, of $\tau = \mu_o U/h$. Now, a layer of water of thickness t is introduced at the lower surface ($\rho_w > \rho_o$), as shown below. The viscosity of the water is much less than the oil, such that $\mu_o = 51\mu_w$. Again assuming a steady Couette type flow between the plates, what thickness of water, t , in terms of h , will reduce the shear stress on the translating flat plate to $1/2$ of the original shear stress with oil alone?

16. Consider the flow of a viscous fluid (viscosity = μ , density = ρ) similar to a Couette flow between two infinite, parallel, **porous** plates; fluid of the same properties is uniformly injected through the *fixed*, lower plate, and fluid is uniformly suctioned out through an upper plate, which *moves* at a velocity U . If $u = 0, v = V_o = \text{const.}$ at $y = 0$, and $u = U = \text{const.}$, and $v = V_o$ at $y = h$, with no flow in the z -direction, derive the velocity profile, $u(y)$, of the fully-developed flow between the plates, and plot $\frac{u}{U}$ vs. $\frac{y}{h}$ for

$\frac{V_o h}{\nu} = \text{Re}_{V_o} = 0, 1, \text{ and } 3$, all on one graph. Using your velocity expression, determine the shear stress

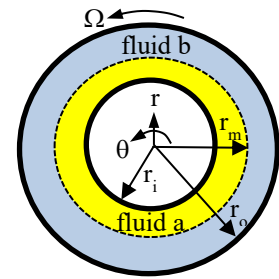
(τ) as a function of y , and on a second graph, plot $\frac{\tau h}{\mu U}$ vs. $\frac{y}{h}$, again for $\text{Re}_{V_o} = 0, 1, \text{ and } 3$. Using your

general expressions for velocity and shear stress, determine the limiting values as $V_o \rightarrow 0$, and explain the subsequent results.



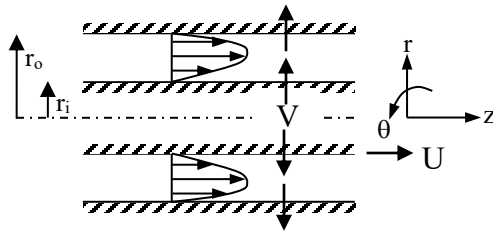
17. Using the results of section 6.4.4, assume $\mu_b = 0.01\mu_a$ and $r_i^* = 1, r_o^* = 2, \text{ and } r_m^* = 1.9$. Determine the torque on the inner cylinder in terms of $\pi, \mu_a, \text{ and } \Omega$ when: (1) fluid a fills the entire annulus (there is no fluid b), and (2) when the thin layer of fluid b is adjacent to the outer cylinder wall. By what % does adding the thin layer of much less viscous fluid b reduce the torque? What is the reduction if the fluid layers are equal thickness ($r_m^* = 1.5$)?

18. Derive the equations for velocity for the two-fluid Couette flow in section 6.4.4, with the inner cylinder fixed and the outer cylinder rotating at an angular velocity Ω . Use the radii shown in the figure at the right. Non-dimensionalize the velocities on Ωr_o , and the radii on r_i (e.g. $r^* = \frac{r}{r_i}$) $\mu_a \Omega$.



Plot the non-dimensional velocity from $1 \leq r^* \leq r_o^*$ for $\frac{\mu_b}{\mu_a} = 0.1, 1, 10$; $r_i^* = 1, r_o^* = 2$, and $r_m^* = 1.5$. Comment on the behavior.

19. Consider the flow of a viscous fluid (viscosity = μ , density = ρ) similar to a Couette-type flow between two infinite, parallel, **porous** tubes of radii r_i and r_o , where $r_i < r_o$.



The inner tube of radius r_i translates along the z -axis at a velocity U , and the outer tube of radius r_o is stationary. Fluid of the same properties is uniformly injected radially at velocity V through the inner tube of radius r_i , and fluid is uniformly suctioned out through the outer tube of radius r_o , satisfying continuity. Determine the radial velocity behavior, $v_r(r)$, and the axial velocity profile, $v_z(r)$, in the annulus between the tubes, for this fully-developed flow.

Show that the non-dimensional velocity, $v_z^* = \frac{v_z(r)}{U}$, can be determined as: $\frac{v_z(r)}{U} = \frac{1 - r^{*k}}{1 - r_i^{*k}}$, and the non-

dimensional flow rate, $\frac{Q}{2\pi r_o^2 U}$, through the annulus can be determined as:

$$Q^* = \frac{Q}{2\pi r_o^2 U} = \frac{\left[\frac{1}{2}(1 - r_i^{*k}) - \frac{1}{k+2}(1 - r_i^{*k+2}) \right]}{1 - r_i^{*k}}$$

where $k = \frac{V r_i}{U}$, and $r_i^* = \frac{r_i}{r_o}$ (note: $r_o^* = \frac{r_o}{r_o} = 1$.)

Plot two separate graphs of the results. On the first graph plot v_z^* vs. r^* for $0.5 < r^* < 1.0$, and $k = 2, 4$, and -4 (i.e. suction through the inner tube). This graph will show three separate lines—one for each k value. On the second graph plot Q^* vs. r_i^* for $0.1 < r_i^* < 0.9$, and $k = 2, 4$, and -4 (i.e. suction through the inner tube). This graph will again show three separate lines---one for each k value. What do these graphs reveal about the effect of fluid injection/suction on the velocity and flow rate?

Chapter 7

Equations of Motion for Inviscid Flow

Contents

7.1 The Euler Equation	193
7.2 Special Cases of the Euler Equation	196
7.2.1 Flow Along a Streamline	196
7.2.2 Irrotational Flow	196
7.3 The Bernoulli Equation	197
7.4 Applications of the Bernoulli Equation	198
7.4.1 Two-Dimensional Inviscid Duct Flow: Nozzles and Diffusers	198
7.4.2 Starting Flow from a Tank	201
7.4.3 Inviscid Stagnation Flow	204
7.5 Flow Curvature Effects: Euler's and n Equations	206
7.6 Applications of the Euler's and n Equations	210
7.6.1 Pressure Field Inside an Inviscid Vortex	210
7.6.2 Inviscid, Irrotational Flow Around a Bend in a Duct	212
7.6.3 The Impact of Curvature on Particulate Motion	214
7.6.3.1 Vortex-Induced Motion of Particles or Gas in a Liquid	215
7.6.3.2 Erosive Effects and River Meandering	216
7.7 Summary of Inviscid Flow Equations	218
7.7.1 Euler Equation Along a Streamline or in Irrotational Flow	218
7.7.2 Bernoulli Equation (along streamline or irrotational flow)	218
7.7.3 Euler's and n Equations (streamline coordinates, unsteady)	218
7.7.4 Euler's and n Equations (integrated, unsteady)	218

While all real flows have at least some degree of viscosity, there are many cases for which an assumption of inviscid flow ($\mu = 0$) is a reasonable approximation. The assumption of inviscid flow can greatly simplify the governing equations such that they are generally much easier to solve than the fully viscous Navier-Stokes equations, and may often yield good approximations to the true fluid behavior. These inviscid solutions can also indicate the limiting condition that is possible for a flow configuration (i.e. the “best” condition that might exist for a flow geometry). It is also often the case that an inviscid solution for one region of a flow may be selectively combined with a viscous solution within an adjacent region of the flow, in order to provide a broader global solution. Flows around airfoils are an example of this latter approach, where the

region near the surface requires use of the fully, viscous equations, but the region somewhat removed from the surface can be reasonably modeled as an inviscid flow.

7.1 The Euler Equation

In this chapter, we begin to address inviscid flows by deriving and examining the governing basic equations, which are generally known as the [Euler equations](#). To begin, consider a flow with $\mu = 0$, which we term as inviscid (i.e. lacking viscosity). However, since a real fluid can never be truly inviscid, what are situations for which the assumption of “inviscid” behavior is a close (or at least a reasonable) approximation? There are basically two situations:

1. Where shear gradients are small (i.e. the flow is relatively uniform), and
2. For high Reynolds number, where the flow is well removed from solid surfaces.

The [Reynolds number](#), which we discussed in Section 6.2.5, is defined generically as the local ratio of momentum to viscous forces. A generic momentum for a flow is characterized by: momentum = (mass flowrate)(velocity) $\approx (\rho VL^2)V = \rho V^2 L^2$. Here, ρ is the fluid density, V is a characteristic velocity, and L is a characteristic length (note that L^2 reflects a characteristic area). A generic viscous force for a flow can be characterized as: (shear stress)(area) = $\left(\mu \frac{V}{L}\right)(L^2) = \mu VL$, where μ is fluid viscosity, and V and L are again a characteristic velocity and length. Defining the Reynolds number as the ratio of the generic momentum to viscous forces gives:

$$Re = \frac{\rho V^2 L^2}{\mu VL} = \frac{\rho VL}{\mu} = \frac{VL}{\nu} \quad \text{where} \quad \nu = \frac{\mu}{\rho}$$

When the Reynolds number for a flow, Re , is very large, this implies that momentum effects dominate viscous effects, particularly if the flow is well away from a bounding surface (more on this in Chapter 13).

Given that one or both of the above situations (essentially uniform flow, or large Reynolds number) exists, we will take the liberty to assume that the viscous terms in the Navier-Stokes equation can be neglected. Thus, dropping the viscous terms from the Navier-Stokes equation (in vector form, Eq. 5.43), gives us:

$$\frac{1}{3} \mu \nabla(\nabla \cdot \vec{V}) + \mu \nabla^2 \vec{V} + \rho \vec{\beta} - \nabla P = \rho \frac{\partial \vec{V}}{\partial t} + \rho(\vec{V} \cdot \nabla)\vec{V} \tag{7.1}$$

Equation 7.1 is termed the [Euler equation](#), and applies for both compressible and incompressible flows. Note that removal of the viscous terms reduces the equation to a balance between pressure, body forces, and momentum changes.

While somewhat simplified, the remaining equation is still quite complicated. To assess possible further simplifications, we expand the velocity terms as follows, using some vector identities (determined from Eq. 2.16g — prove that for yourself) to illustrate the inherent motions involved in the equation:

$$\rho \vec{\beta} - \nabla P = \rho \frac{\partial \vec{V}}{\partial t} + \rho \left[\underbrace{\nabla \left(\frac{V^2}{2} \right) - \vec{V} \times \overbrace{\nabla \times \vec{V}}^{\text{curl } \vec{V}}}_{(\vec{v} \cdot \nabla) \vec{v}} \right] \tag{7.2}$$

Now, consider the Euler equation for any arbitrary direction in space. We will develop Eq. 7.2 in a Cartesian coordinate system by taking the dot product of the Euler equation with a differential displacement vector, given by $d\vec{s} = dx \hat{i} + dy \hat{j} + dz \hat{k}$:

$$\left\{ \rho \vec{\beta} - \nabla P = \rho \frac{\partial \vec{V}}{\partial t} + \rho \left[\nabla \left(\frac{V^2}{2} \right) - \vec{V} \times \nabla \times \vec{V} \right] \right\} \cdot d\vec{s}$$

Expanding gives:

i.e.

$$\left[\begin{aligned} & (\hat{i}\beta_x + \hat{j}\beta_y + \hat{k}\beta_z) - \frac{1}{\rho} \left(\hat{i} \frac{\partial P}{\partial x} + \hat{j} \frac{\partial P}{\partial y} + \hat{k} \frac{\partial P}{\partial z} \right) \\ & = \frac{\partial \vec{V}}{\partial t} + \hat{i} \frac{\partial \left(\frac{V^2}{2} \right)}{\partial x} + \hat{j} \frac{\partial \left(\frac{V^2}{2} \right)}{\partial y} + \hat{k} \frac{\partial \left(\frac{V^2}{2} \right)}{\partial z} - (\hat{i}u + \hat{j}v + \hat{k}w) \times \text{curl } \vec{V} \end{aligned} \right] \cdot (\hat{i}dx + \hat{j}dy + \hat{k}dz)$$

And collecting terms:

$$\begin{aligned} & (\beta_x dx + \beta_y dy + \beta_z dz) - \frac{1}{\rho} \overbrace{\left(\frac{\partial P}{\partial x} dx + \frac{\partial P}{\partial y} dy + \frac{\partial P}{\partial z} dz \right)}^{dP} = \frac{\partial \vec{V}}{\partial t} \cdot d\vec{s} + \overbrace{\left[\frac{\partial}{\partial x} \left(\frac{V^2}{2} \right) dx + \frac{\partial}{\partial y} \left(\frac{V^2}{2} \right) dy + \frac{\partial}{\partial z} \left(\frac{V^2}{2} \right) dz \right]}^{d \left(\frac{V^2}{2} \right)} \\ & - \left[\underbrace{(w dy - v dz) \left(\frac{\partial w}{\partial y} - \frac{\partial v}{\partial z} \right)}_{\omega_x} + \underbrace{(u dz - w dx) \left(\frac{\partial u}{\partial z} - \frac{\partial w}{\partial x} \right)}_{\omega_y} + \underbrace{(v dx - u dy) \left(\frac{\partial v}{\partial x} - \frac{\partial u}{\partial y} \right)}_{\omega_z} \right] \end{aligned} \tag{7.3}$$

where $\vec{\omega} = \hat{i}\omega_x + \hat{j}\omega_y + \hat{k}\omega_z \Rightarrow \text{vorticity} = \nabla \times \vec{V}$

In Eq. 7.3 we identify the gradients of pressure and V^2 (which is a scalar), as well as the components of vorticity, $\vec{\omega}$.

If we assume that gravity is the only relevant body force, and that g (as shown below) acts parallel to and always opposite to a directional displacement h , where $h = h(x, y, z)$, then we can express the body force vector in components as:

$$\vec{\beta} = \beta_x \hat{i} + \beta_y \hat{j} + \beta_z \hat{k} = -g \frac{\partial h}{\partial x} \hat{i} - g \frac{\partial h}{\partial y} \hat{j} - g \frac{\partial h}{\partial z} \hat{k} = -g \left(\frac{\partial h}{\partial x} \hat{i} + \frac{\partial h}{\partial y} \hat{j} + \frac{\partial h}{\partial z} \hat{k} \right) = -g \nabla h \quad (7.4)$$

To understand how we establish Eq. 7.4, the geometric origin of the terms in the body force vector $\vec{\beta}$ is shown in figure 7.1, for the x-direction component.

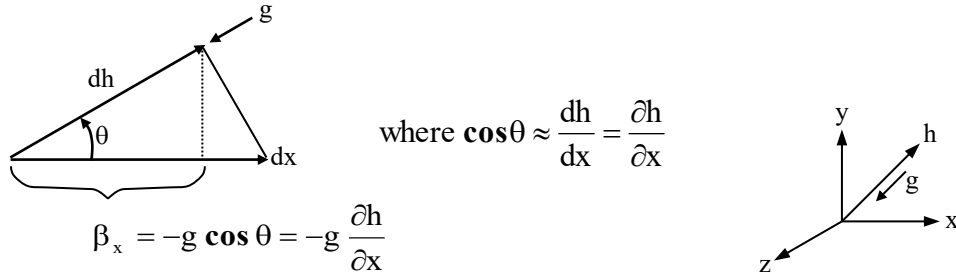


Figure 7.1 Geometric illustration of the body force component in x-direction

Using the components from Eq. 7.4, we can write the body force term in Eq. 7.3, due to a gravitational field only, as:

$$\begin{aligned} \beta_x dx + \beta_y dy + \beta_z dz &= -g \frac{\partial h}{\partial x} dx - g \frac{\partial h}{\partial y} dy - g \frac{\partial h}{\partial z} dz \\ &= -g \left(\frac{\partial h}{\partial x} dx + \frac{\partial h}{\partial y} dy + \frac{\partial h}{\partial z} dz \right) = -g dh \end{aligned} \quad (7.5)$$

Substituting Eq. 7.5 into Eq. 7.3 and rearranging gives:

$$g dh + \frac{1}{\rho} dP + d \left(\frac{V^2}{2} \right) + \frac{\partial \vec{V}}{\partial t} \cdot d\vec{s} - [(w dy - v dz)\omega_x + (u dz - w dx)\omega_y + (v dx - u dy)\omega_z] = 0 \quad (7.6)$$

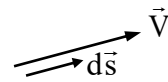
Equation 7.6 is a general equation that applies throughout the Cartesian flow field; we could of course derive a similar expression for any other coordinate system of choice, as we will show when we employ streamline coordinates in Section 7.5.

7.2 Special Cases for the Euler Equation

Clearly, the general Euler equation, Eq. 7.6, is simplified, but is still quite complicated for practical applications. However, by utilizing some further flow constraints we can simplify Eq. 7.6 even further, such that tractable solutions are possible. As we will show, these constraints require that either: (1) we are able to follow the flow along a prescribed streamline, or (2) the entire flow field is devoid of vorticity, and thus irrotational.

7.2.1 Flow along a streamline

In section 3.2 we showed that the generic equation for a streamline is given by $\vec{V} \times d\vec{s} = 0$, which mathematically represents a set of differential equations for a line that is always tangent to the velocity vectors for all particles comprising that line. Expanding this equation in Cartesian coordinates, where



$\vec{V} = u\hat{i} + v\hat{j} + w\hat{k}$, and $d\vec{s} = dx\hat{i} + dy\hat{j} + dz\hat{k}$, gives a streamline vector equation, which can be written as:

$$\vec{V} \times d\vec{s} = (w dy - v dz)\hat{i} + (u dz - w dx)\hat{j} + (v dx - u dy)\hat{k} = 0$$

Or as component equations

$$v dx - u dy = 0, \quad w dy - v dz = 0, \quad u dz - w dx = 0$$

Substitution of these component equations for a streamline into the Euler equation, Eq. 7.6, results in null coefficients for the components of vorticity in the equation, negating any influence of vorticity along a prescribed streamline, yielding:

$$g dh + \frac{1}{\rho} dP + d\left(\frac{V^2}{2}\right) + \frac{\partial \vec{V}}{\partial t} \cdot d\vec{s} = 0 \quad (7.7)$$

Equation 7.7 is [Euler's streamline equation](#) for inviscid, compressible, unsteady flow *along a streamline*, with conservative body forces (i.e. gravity only).

7.2.2 Irrotational Flow

Alternatively, we can consider Euler's equation within an *irrotational* flow field. An irrotational flow is a flow that is devoid of vorticity (more on this in Chapter 8), for which we can write:

$$\vec{\omega} = \nabla \times \vec{V} = \text{curl } \vec{V} = \omega_x \hat{i} + \omega_y \hat{j} + \omega_z \hat{k} = 0 \quad \Rightarrow \quad \omega_x = \omega_y = \omega_z = 0$$

Thus, all the vorticity components in the Euler equation, Eq. 7.6, are zero for irrotational flows, giving:

$$g dh + \frac{1}{\rho} dP + d\left(\frac{V^2}{2}\right) + \frac{\partial \vec{V}}{\partial t} \cdot d\vec{s} = 0 \quad (7.8)$$

Note that Eq. 7.8 is the same as the streamline form of the equation, Eq. 7.7. However, Eq. 7.8 may apply across streamlines (not just along them) for a flow that is inviscid, compressible, unsteady, *and irrotational* with conservative body forces. Both Eq. 7.7 and 7.8 apply throughout the flow field (assuming the respective constraints are satisfied). We will now consider the application of both equations.

7.3. The Bernoulli Equation

Consider an inviscid flow either: (1) along a streamline, or (2) within an irrotational flow field. In both cases, we can integrate Eq. 7.7 or 7.8 from a point 1 to a point 2 within the flow field, giving:

$$g(h_2 - h_1) + \int_1^2 \frac{dP}{\rho} + \left(\frac{V_2^2}{2} - \frac{V_1^2}{2}\right) + \int_1^2 \frac{\partial \vec{V}}{\partial t} \cdot d\vec{s} = 0 \quad (7.9)$$

Equation 7.9 applies for an unsteady flow of variable density, i.e. $\rho = f(P)$.

However, if the density is constant (incompressible), the equation simplifies further to:

$$g(h_2 - h_1) + \frac{1}{\rho}(P_2 - P_1) + \frac{1}{2}(V_2^2 - V_1^2) + \int_1^2 \frac{\partial \vec{V}}{\partial t} \cdot d\vec{s} = 0$$

or

$$\left(\frac{P_2}{\rho} + \frac{V_2^2}{2} + gh_2\right) - \left(\frac{P_1}{\rho} + \frac{V_1^2}{2} + gh_1\right) + \int_1^2 \frac{\partial \vec{V}}{\partial t} \cdot d\vec{s} = 0 \quad (7.10a)$$

or more generically,

$$\frac{P}{\rho} + gh + \frac{1}{2}V^2 + \int \frac{\partial \vec{V}}{\partial t} \cdot d\vec{s} = \text{constant} \quad (7.10b)$$

Equation 7.10 is termed the [“unsteady” Bernoulli equation](#), since it takes into account locally unsteady or time-varying behavior, but we clearly have to know the *path* we follow from point 1 to 2 to evaluate the time-dependent term, $\int \frac{\partial \vec{V}}{\partial t} \cdot d\vec{s}$, in Eq. 7.10. If we further require that the flow remain steady (no velocity changes with time, only spatial changes), then we obtain:

$$g(h_2 - h_1) + \frac{1}{\rho}(P_2 - P_1) + \frac{1}{2}(V_2^2 - V_1^2) = 0$$

or

$$\frac{P_2}{\rho} + gh_2 + \frac{1}{2}V_2^2 = \frac{P_1}{\rho} + gh_1 + \frac{1}{2}V_1^2 \quad (7.11)$$

Equation 7.11 is the classic [steady Bernoulli equation](#), which applies only to *steady* flows of *constant density*. This is one of the most celebrated, most useful, and most misused equations of fluid mechanics. While providing a simple relationship relating changes in pressure, gravitational effects, and velocity, the equation (as we noted) is subject to numerous restrictions. And while many flows approximately satisfy most of these restrictions, and their behavior can be assessed to a good approximation using the Bernoulli equation, many flows do not satisfy one or more of the restrictions and cannot be properly assessed using the Bernoulli equation. An example of where the Bernoulli equation cannot be used is in the analysis of real fluid flows near a solid boundary, where viscous effects are always important. Thus, while a useful tool, one must be careful to assure that the results obtained using the Bernoulli equation are appropriate to the particular type of flow situation.

7.4 Applications of the Bernoulli Equations

The following section demonstrates the application of the Bernoulli equation for several inviscid flows. Note that for all the cases discussed, viscosity will have some effect, which will influence the actual expected behavior. However, as pointed out in Section 7.3, Bernoulli solutions in many cases can provide a good *approximation* of the type of behavior that can be expected for a real flow, and provide a limiting “best case” scenario for such flows. As we illustrate, these best-case flow situations can often be used as guidelines for the real flow behavior through the use of some empirical coefficients to account for the impact of viscosity.

7.4.1 Two-Dimensional Inviscid Duct Flows: Nozzles and Diffusers

Flows through channels or pipes are frequently subject to contractions or expansions in the flow passage cross-sectional area. Here, we examine the effect of a simple contraction in area (i.e. a nozzle) and an expansion in area (i.e. a diffuser) on the fluid dynamic pressure, as predicted by the Bernoulli streamline equation, Eq. 7.10a.

For a generic, two-dimensional duct with a steady inflow, we can assess the pressure change, $P_2 - P_1$, along the duct as a function of the inlet velocity, V_1 , the inlet and outlet areas, A_1 and A_2 , and the density, ρ . Depending on the area change within the duct, the duct can act as either a nozzle (a flow accelerator) or diffuser (a flow decelerator). Here, we assume that the inlet and outlet velocities are uniform. We also establish the non-dimensional pressure rise across the duct

based on the inlet dynamic pressure (i.e. $\frac{1}{2}\rho V_1^2$) or hydraulic head (i.e. $\frac{V_1^2}{2g}$), as it is frequently termed in pipe flows.

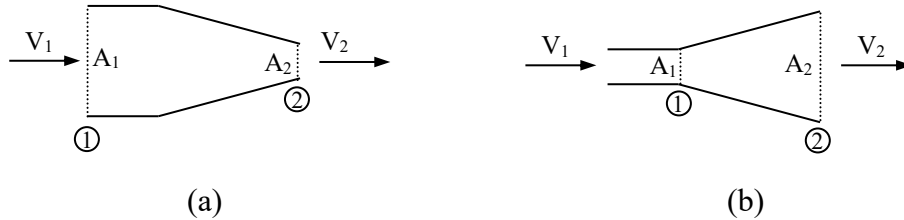


Figure 7.2 Schematic of parameters for a two-dimensional duct flow:
 (a) a nozzle (flow accelerator) and (b) a diffuser (flow decelerator)

Figure 7.2 shows the generic shape and parameters characterizing two-dimensional nozzles and diffusers. We employ the Bernoulli equation to understand the tradeoffs between velocity and pressure changes in such varying area ducts for an incompressible flow. Applying Eq. 7.10a from points 1 to 2 (we assume along any streamline), we can eliminate the terms indicated based on the listed assumptions (assumptions 1, 2, and 3 allow the use of the Bernoulli equation):

$$\left(\frac{P_2}{\rho} + \frac{V_2^2}{2} + gh_2\right) - \left(\frac{P_1}{\rho} + \frac{V_1^2}{2} + gh_1\right) + \int_1^2 \frac{\partial \bar{V}}{\partial t} ds = 0$$

$$\frac{P_2 - P_1}{\rho} = \frac{1}{2}(V_1^2 - V_2^2)$$

Assume

- 1) inviscid
- 2) $\rho = \text{const.}$
- 3) along S.L.
- 4) steady
- 5) neglect height changes
- 6) uniform flow

For constant density and uniform flow, the continuity equation gives: $V_2 = V_1 \frac{A_1}{A_2}$.

Substituting for V₂ in the Bernoulli equation gives:

$$\frac{P_2 - P_1}{\rho} = \frac{1}{2}V_1^2 \left[1 - \left(\frac{A_1}{A_2}\right)^2 \right]$$

Now, note the effect of an area change on the pressure change:

$$P_2 - P_1 = \frac{1}{2}\rho V_1^2 \left[1 - \left(\frac{A_1}{A_2}\right)^2 \right] \text{ is } \begin{cases} < 0 & \text{if } \frac{A_1}{A_2} > 1 \Rightarrow \text{nozzle} \\ > 0 & \text{if } \frac{A_1}{A_2} < 1 \Rightarrow \text{diffuser} \end{cases} \quad (7.12)$$

We apply the term “nozzle” to duct geometries that cause an *acceleration* of the flow ($V \uparrow$), and a consequent *decrease in pressure* from the inlet to the exit. Conversely, we apply the term “diffuser” to a duct geometry that causes a *deceleration* of the flow ($V \downarrow$), with a consequent *increase in pressure* from inlet to exit.

Note that the term $\frac{1}{2}\rho V_1^2$ in Eq. 7.12 above has the dimensions of pressure (Force/Area), and represents the change in pressure that would be experienced if all the entering momentum of the inlet flow were converted to pressure by bringing the flow inviscidly to rest. We term this potential pressure change the “dynamic pressure,” and utilize it to form a non-dimensional parameter, C_p , by dividing the pressure change by the dynamic pressure available at the inlet:

$$C_p = \frac{P_2 - P_1}{\frac{1}{2}\rho V_1^2} = \left[1 - \left(\frac{A_1}{A_2} \right)^2 \right] = \left[1 - \frac{1}{AR^2} \right] \quad (7.13)$$

where $AR = \frac{A_2}{A_1}$ (termed the area ratio), and C_p is termed the pressure coefficient. The pressure coefficient, which is also often termed the Euler number, is a convenient engineering relationship that removes the dimensional dependence on the actual flow velocity, and indicates the capability of a: (1) nozzle to “convert” pressure to additional momentum exiting the nozzle, or (2) diffuser to “recover” pressure from the fluid momentum entering a diffuser.

Note that for a nozzle, $AR < 1$, which means that $C_p < 0$, or that $P_1 > P_2$. A falling pressure in a duct flow creates a very stable type of flow, which assures that a nozzle flow will create an acceleration of the flow pretty much in proportion to the pressure drop from nozzle inlet to exit. However, because of viscous effects in real ducts, Eq. 7.13 will slightly under-predict C_p (i.e. a slightly higher inlet pressure will be required to achieve a desired exit velocity). Usually, this variation, known as a nozzle [discharge coefficient, \$C_D\$](#) , is taken into account by the use of an empirical correction factor. In general, because of the stability of a falling pressure, there is no limit on how small the area ratio (AR) of a nozzle may be.

Whereas, a nozzle behaves pretty much according to Eqs. 7.12 and 7.13, the flow process in a diffuser is more complicated, and subject to strong variations from Eqs. 7.12 and 7.13. For example, if $AR = 2$ for a diffuser, Eq. 7.13 indicates that $C_p = \frac{3}{4}$. This means that, ideally, $\frac{3}{4}$ of the dynamic pressure ($\frac{1}{2}\rho V_1^2$) entering the diffuser could be converted or “recovered” by the diffuser as a pressure increase. This increase in pressure could be employed productively in a fluid machine (e.g. a gas turbine) to produce more power (in the form of thermodynamic work, $\int PdV$). However, like a nozzle, viscous effects for a real fluid flow will reduce the amount of pressure actually recovered relative to this ideal amount. What is worse, if the area increase across the diffuser is too large (roughly $AR > 2.75$ to 3), the actual pressure recovery capabilities

of the diffuser will be *much less* than that predicted by the inviscid solution, Eq. 7.13. This under prediction is a result of a reduction in the effective exit area for the flow due a process of pressure-gradient induced flow separation (a process we will discuss in detail in Chapter 14).

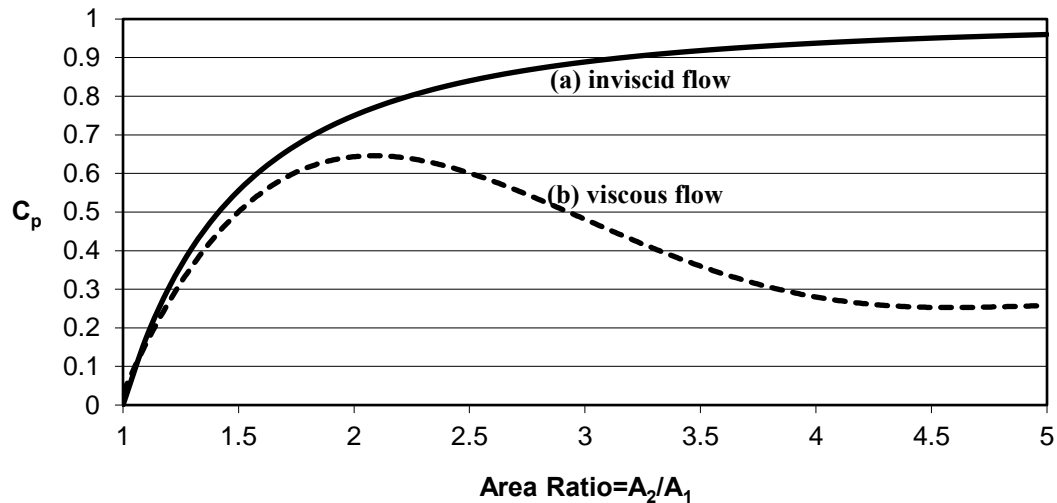


Figure 7.3 Non-dimensional pressure recovery (C_p) vs. diffuser area ratio ($AR=A_2/A_1$) for: (a) an inviscid flow, and (b) an actual viscous flow.

When flow separation develops within a diffuser, a region of stagnant or recirculating flow develops adjacent to one wall of the diffuser, which diverts the flow through the diffuser away from that wall (i.e. causing it to “separate” from the solid boundary). This process, termed diffuser separation or stall, results in a fluid blockage of a portion of the diffuser exit. This blockage thus reduces the effective exit area, A_2 , which results in a sharp reduction of the actual pressure recovery by the diffuser from the ideal recovery predicted by Eq. 7.13. Figure 7.3 is an illustration of the degree of variation the pressure coefficient can experience with increasing area ratios. Thus, when it comes to diffusers, a larger exit area is not necessarily better. More information on diffuser behavior can be found [here](#).

This example shows clearly that one must carefully assess the conditions for which the assumption of inviscid (or at least nearly inviscid) flow is an appropriate assumption.

7.4.2 Starting Flow from a Tank

Flow through channels and piping also can undergo unsteady effects due to sudden changes in the flow velocity or the driving pressure. Examples of such a situation are the sudden opening or closing of a valve or faucet in a piping system, or when a floodgate on a dam is suddenly opened or closed. To address such time-dependent behavior, we make use of the unsteady Bernoulli equation, along a streamline, Eq. 7.10a, retaining the time dependent term.

Consider a large tank, as shown in figure 7.4, filled with water to a depth D . A pipe of length L allows water to flow out of the tank. If the pipe leading from the tank is initially plugged, how will the velocity of the water leaving the tank, $V_2(t)$, behave after the tube is unplugged at $t = 0$?

To simplify this problem, we make the assumption that $A_1 \gg A_2$ such that the tank water depth, D , can be considered essentially constant. We could do the problem with h varying with time, but it makes the final differential equation non-linear, and more complicated to solve. We will also assume that we can follow a streamline from the free surface of the water in the tank (1) to the exit of the pipe at (2). Of course, we also assume an inviscid flow, which is not true if the pipe is of any modest length. However, the solution we obtain will indicate the *maximum* velocity behavior that could be expected for such a flow, and thus provides an upper bound on the velocity behavior for any real flow.

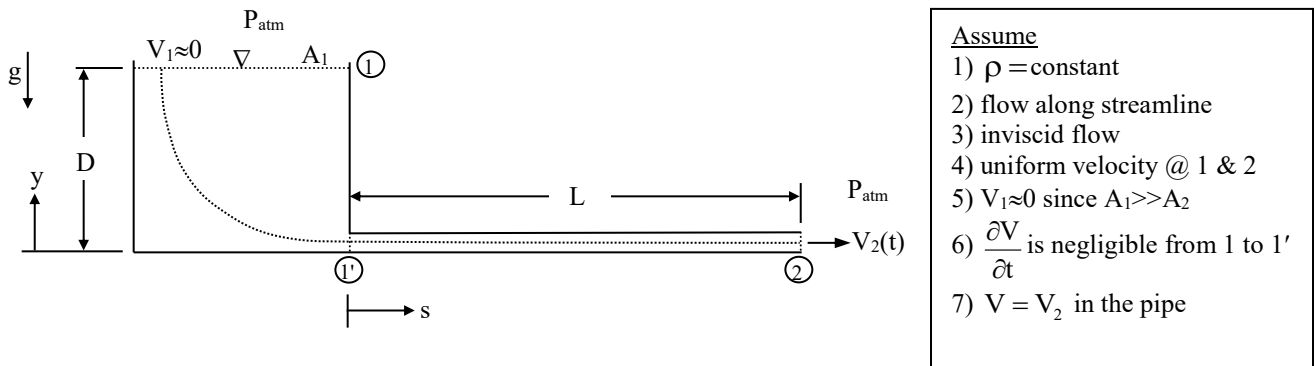


Figure 7.4 Schematic for the starting flow from a tank through a long pipe.

Applying the unsteady Bernoulli equation, Eq. 7.10, along a streamline between points 1 and 2 as shown, we have:

$$\frac{(P_2 - P_1)}{\rho} + \frac{1}{2}(V_2^2 - V_1^2) + g(h_2 - h_1) + \int_1^2 \frac{\partial V}{\partial t} ds = 0$$

$$P_{atm} - P_{atm} = 0 \quad \approx 0 \quad 0 - D$$

$$\frac{1}{2} V_2^2 - gD + \int_1^{1'} \frac{\partial V}{\partial t} ds + \int_{1'}^2 \frac{\partial V}{\partial t} ds = 0$$

$$\approx 0$$

Note that since the pressures at the beginning and end of the streamline are both atmospheric, the pressure terms cancel (we assume height effects on the surrounding atmosphere to be negligible). Also, since $A_1 \gg A_2$, the velocity V_1 will be negligible relative to V_2 . Finally, we break the integral of the flow acceleration into two parts: (a) from the tank water surface to the entrance to the pipe, and (b) from the pipe entrance [$s = 0$] to the pipe exit [$s = L$]. Since the velocity within

the tank will be quite slow, we assume that the time change within the tank will be negligible, and that within the pipe $\frac{\partial V}{\partial t} = \frac{\partial V_2}{\partial t}$, such that :

$$\frac{1}{2} V_2^2 - gD + \underbrace{\int_{s=0}^{s=L} \frac{\partial V_2}{\partial t} ds}_{\frac{dV_2}{dt}(L-0) \text{ since } \frac{dV_2}{dt} \neq f(s)} = 0$$

Rearranging terms gives:

$$\frac{dV_2}{dt} = \frac{2gD - V_2^2}{2L} \tag{7.14}$$

Separating variables and integrating Eq. 7.14:

$$\int_0^{V_2} \frac{dV_2}{2gD - V_2^2} = \int_0^t \frac{dt}{2L}$$

$$\frac{V_2}{\sqrt{2gD}} = \tanh \left(\frac{\sqrt{2gD}}{2L} t \right) \tag{7.15}$$

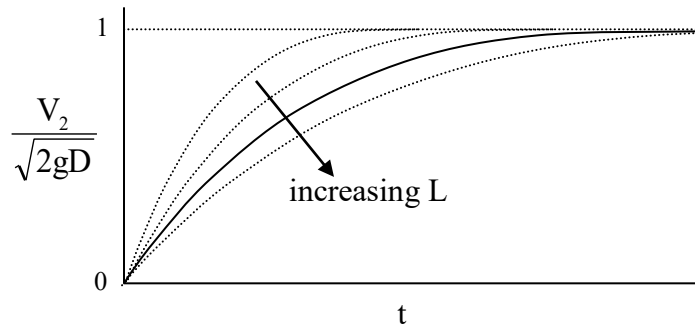


Figure 7.5 Velocity behavior of the starting flow from a tank through a pipe of length L and free surface height of D.

Equation 7.15 indicates that as t increases the pipe exit velocity will increase asymptotically toward a steady state value of $V_2 = \sqrt{2gD}$. As shown in figure 7.5, increasing the pipe length increases the time required for the velocity to reach steady state. This delay is due to the increased inertia of the water within the tube with increases in L. Clearly, as the tube length is increased, the gravitational driving force must accelerate a larger mass of water within the tube -- and since the driving force is fixed, the flow will accelerate more slowly.

Obviously, most real pipe flows will also experience viscous effects, which will both increase the time to reach steady state, and reduce the maximum flow rate that can be achieved. Therefore, Eq.7.15 represents the *upper limit* of how rapidly the water flow from the tank can accelerate, and the maximum average velocity that can be achieved at steady state.

7.4.3 Inviscid Stagnation Flow

Consider an incompressible, inviscid, two-dimensional flow toward a solid boundary as shown below. The Cartesian velocity field for this flow is given by:

$$\vec{V}(x, y) = Ax \hat{i} - By \hat{j}$$

Where A and B are constants, and the velocity components are:

$$u = Ax \quad \text{and} \quad v = -By$$

We want to establish the pressure behavior along a typical streamline for this type of flow.

As we discussed in Chapter 5, an incompressible two-dimensional flow must satisfy the reduced two-dimensional continuity equation of the form:

$$\frac{\partial u}{\partial x} + \frac{\partial v}{\partial y} = 0 = A - B \Rightarrow A = B$$

So, to have a valid incompressible flow we must have $\vec{V} = Ax \hat{i} - Ay \hat{j}$, where $u = Ax$, $v = -Ay$. To establish a streamline, we recall from section 3.2 that for a two-dimensional flow the equation for a streamline is:

$$\vec{V} \times d\vec{s} = udy - vdx = 0 \quad \text{along a streamline.}$$

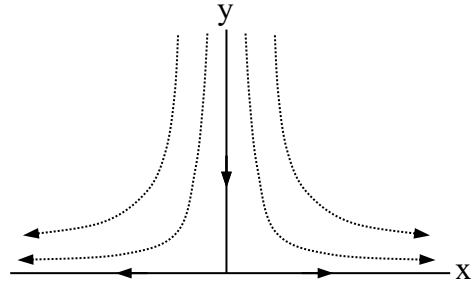
So for the present case, we have:

$$\frac{dy}{dx} = \frac{v}{u} = \frac{-Ay}{Ax} = -\frac{y}{x}$$

Separating variables and integrating gives:

$$\int \frac{dy}{y} = -\int \frac{dx}{x}$$

$\ln y = -\ln x + \ln C$, so that



$$xy = C, \text{ where } C \text{ is a constant} \quad (7.16)$$

Now, applying the steady flow Bernoulli equation, Eq. 7.11, along an inviscid streamline gives:

$$\frac{P}{\rho} + \frac{1}{2}V^2 + \overset{\text{neglect}}{gh} = \text{constant}$$

or substituting the velocity components:

$$\frac{P}{\rho} + \frac{1}{2}(A^2x^2 + A^2y^2) = \text{constant} \quad (7.17)$$

To specify a particular streamline, we select a particular point that we want the streamline to pass through. For example, if we specify that the streamline pass through the origin, $(x,y) = (0,0)$, Eq. 7.16 reduces to:

$$xy = C = 0$$

If we specify the pressure at $(x,y) = (0,0)$ to be P_o , we can solve for the constant in Eq. 7.17 as:

$$\frac{P_o}{\rho} + 0 = \text{constant} = \frac{P_o}{\rho}$$

Thus, at any other point along this streamline, $xy = 0$, we have:

$$P = P_o - \frac{\rho A^2}{2}(x^2 + y^2) \quad (7.18a)$$

Thus, the highest pressure along this streamline occurs at the point $(x,y) = (0,0)$, which happens to be the stagnation point for the flow (where $\vec{V} = 0$), and thus P_o is termed the *stagnation pressure*.

Note that there is no vorticity for this flow, $\vec{\omega} = \omega_z \hat{k} = \left(\frac{\partial v}{\partial x} - \frac{\partial u}{\partial y} \right) \hat{k} = 0$, which means that this particular flow is also *irrotational*. Thus, the pressure equation derived above will also apply at *all points* within the flow, as well as along the designated streamline. Rewriting Eq. 7.18a, as:

$$x^2 + y^2 = \frac{2}{\rho A^2}(P_o - P) \quad (7.18b)$$

Eq. 7.18b indicates that the pressure field for this flow is represented by isobaric (constant pressure) curves that are circles centered on the origin (i.e. if $P_o - P = \text{constant}$, Eq. 7.18b is the equation for a circle).

7.5 Flow Curvature Effects: Euler s and n Equations

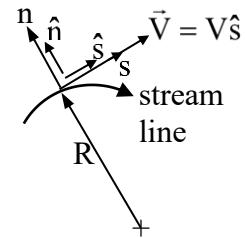
While the Bernoulli equation derived in section 7.3 provides a useful relationship between the velocity and the corresponding pressure and height changes *along* a streamline (or within an irrotational flow), it is often useful to understand how pressure varies *across* streamlines due to curvature within a flow. Many flows in nature and technical applications undergo significant curvature, which can give rise to significant pressure variations in a direction normal to the curved streamlines. For viscous fluids, the resultant cross-stream pressure variations caused by flow curvature can play a significant role in creating secondary flows of fluid near solid boundaries (note: secondary flows are localized flows, generally near a bounding surface, created by the effects of the pressure field due to the primary flow). In fact, as we discuss in Section 7.6.3, curvature-induced pressure changes are a key factor in causing the meandering of rivers and in the development of other three-dimensional flows.

To address the effects of flow curvature, and assess the impact it can have on inviscid (and viscous) flows, we will reconsider the Euler equation along a streamline, Eq. 7.7, by employing a streamline coordinate system.

Recall that along a streamline, the general Euler equation (Eq. 7.1, where $\vec{\beta} = -g\nabla h$) is given by:

$$-g\nabla h - \frac{1}{\rho}\nabla P = \frac{D\vec{V}}{Dt} = \frac{\partial\vec{V}}{\partial t} + (\vec{V} \cdot \nabla)\vec{V} \tag{7.19}$$

Now consider a two-dimensional flow along a streamline. Here we employ coordinates s and n , where s is *tangent* to the streamline and n is *normal* to the streamline, as shown in the sketch. R is the instantaneous *radius of curvature* of the streamline at the coordinate origin. Consequently, we write the velocity magnitude as a function of s and n , such that $V = f(s, n)$. Thus, the vector expression for the velocity is given by $\vec{V} = V(s, n)\hat{s}$. Here V is the magnitude of the velocity, \hat{s} is a unit vector oriented *tangent* to the streamline (along s), and \hat{n} is a unit vector oriented *normal* to the streamline (along n), as shown.

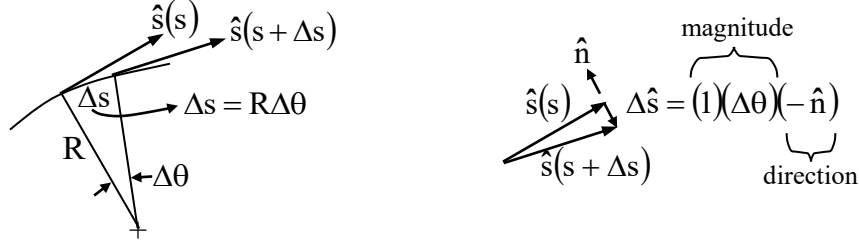


Note that we would typically write the velocity vector for such a coordinate system as $\vec{V} = V_s \hat{s} + V_n \hat{n}$. However, since the coordinates are fixed on a streamline we have $\vec{V} = V\hat{s}$ (since there is no flow across a streamline), such that $V_n = 0$, and $V_s = V$.

So, in streamline coordinates, the acceleration, given by applying the substantial derivative to $\vec{V} = V\hat{s}$, becomes:

$$\frac{D\vec{V}}{Dt} = \frac{\partial}{\partial t}(V\hat{s}) + V \frac{\partial}{\partial s}(V\hat{s}) + \overset{=0}{V_n} \frac{\partial}{\partial n}(V\hat{s}) = V \frac{\partial \hat{s}}{\partial t} + \hat{s} \frac{\partial V}{\partial t} + V^2 \frac{\partial \hat{s}}{\partial s} + \hat{s} V \frac{\partial V}{\partial s} \tag{7.20}$$

To make proper sense of Eq. 7.20 requires that we evaluate the derivatives of the unit vectors, $\frac{\partial \hat{s}}{\partial s}$ and $\frac{\partial \hat{s}}{\partial t}$, which is shown graphically below.



Thus,

$$\frac{\partial \hat{s}}{\partial s} = \lim_{\Delta s \rightarrow 0} \frac{\Delta \hat{s}}{\Delta s} = \lim_{\Delta s \rightarrow 0} \frac{-\hat{n} \Delta \theta}{R \Delta \theta} = -\frac{\hat{n}}{R} \quad \text{and} \quad (7.21a)$$

$$\frac{\partial \hat{s}}{\partial t} = \lim_{\Delta t \rightarrow 0} \frac{\Delta \hat{s}}{\Delta t} = \lim_{\Delta t \rightarrow 0} \frac{-\hat{n} \Delta \theta}{\Delta t} = -\hat{n} \frac{\partial \theta}{\partial t} \quad (7.21b)$$

Substituting Eqs. 7.21 into Eq. 7.20 we have:

$$\frac{D\vec{V}}{Dt} = \hat{s} \left(\frac{\partial V}{\partial t} + V \frac{\partial V}{\partial s} \right) - \hat{n} \left(V \frac{\partial \theta}{\partial t} + \frac{V^2}{R} \right) \quad (7.22a)$$

It is not exactly obvious how the n direction time derivative term $\frac{\partial \theta}{\partial t}$ can be handled. However,

note in the above figure that $\Delta s = R \Delta \theta$, or $\Delta \theta = \frac{\Delta s}{R}$. Thus, we can write that

$\frac{\partial \theta}{\partial t} = \lim_{\Delta t \rightarrow 0} \frac{\Delta \theta}{\Delta t} = \frac{1}{R} \lim_{\Delta t \rightarrow 0} \frac{\Delta s}{\Delta t} = \frac{1}{R} \frac{\partial s}{\partial t}$. However, a streamline is defined by its coordinate system, which is fixed on the streamline. So, s , and the unit vectors are not functions of time, such that $\frac{\partial s}{\partial t}$, and the unit vector derivative with respect to time, $\frac{\partial \hat{s}}{\partial t}$, are zero. Thus, Eq. 7.22a becomes:

$$\frac{D\vec{V}}{Dt} = \hat{s} \left(\frac{\partial V}{\partial t} + V \frac{\partial V}{\partial s} \right) - \hat{n} \left(\frac{V^2}{R} \right) \quad (7.22b)$$

Thus, the time derivative has no impact on the n-direction velocity changes, since there is no n-direction velocity across a streamline.

Using Eq. 7.22b, we rewrite Eq. 7.19 in \hat{s} and \hat{n} coordinates, where the del operator in streamline coordinates is given by $\nabla = \hat{s} \frac{\partial}{\partial s} + \hat{n} \frac{\partial}{\partial n}$. This gives us the Euler streamline equation:

$$-g\left(\frac{\partial h}{\partial s}\hat{s} + \frac{\partial h}{\partial n}\hat{n}\right) - \frac{1}{\rho}\left(\frac{\partial P}{\partial s}\hat{s} + \frac{\partial P}{\partial n}\hat{n}\right) = \left(\frac{\partial V}{\partial t} + V\frac{\partial V}{\partial s}\right)\hat{s} - \left(\frac{V^2}{R}\right)\hat{n} \quad (7.23)$$

Separating Eq. 7.23 into its vector components, and rearranging, gives:

$$g\frac{\partial h}{\partial s} + \frac{1}{\rho}\frac{\partial P}{\partial s} + V\frac{\partial V}{\partial s} + \frac{\partial V}{\partial t} = 0 \quad \text{s-direction component} \quad (7.24a)$$

$$g\frac{\partial h}{\partial n} + \frac{1}{\rho}\frac{\partial P}{\partial n} = \frac{V^2}{R} \quad \text{n-direction component} \quad (7.24b)$$

Equations 7.24a and 7.24b are known respectively as the [Euler s-equation and Euler n-equation](#).

To integrate the Euler streamline equation along a streamline, we take the dot product of Eq. 7.23 with a differential element *oriented along the streamline*, $d\vec{s} = \hat{s}ds$, and integrate the resultant equation from a point 1 to a point 2 on a streamline:

$$g\underbrace{\frac{\partial h}{\partial s}}_{dh} ds + \frac{1}{\rho}\underbrace{\frac{\partial P}{\partial s}}_{dP} ds + V\underbrace{\frac{\partial V}{\partial s}}_{dV} ds + \frac{\partial V}{\partial t} ds = 0$$

$$gdh + \frac{1}{\rho}dP + VdV + \frac{\partial V}{\partial t} ds = 0 \quad (7.25a)$$

$$\int_1^2 gdh + \int_1^2 \frac{1}{\rho}dP + \int_1^2 VdV + \int_1^2 \frac{\partial V}{\partial t} ds = 0 \quad (7.25b)$$

Note that we can associate, for example, $dh = \frac{\partial h}{\partial s}ds + \frac{\partial h}{\partial n}dn \stackrel{=0}{=} \frac{\partial h}{\partial s}ds$, since we are constraining changes to occur only along the streamline, for which $dn = 0$.

Integrating Eq. 7.25b gives:

$$g(h_2 - h_1) + \int_1^2 \frac{dP}{\rho} + \frac{1}{2}(V_2^2 - V_1^2) + \int_1^2 \frac{\partial V}{\partial t} ds = 0 \quad \text{for unsteady, } \rho = f(P) \quad (7.26)$$

or

$$g(h_2 - h_1) + \frac{1}{\rho}(P_2 - P_1) + \frac{1}{2}(V_2^2 - V_1^2) + \int_1^2 \frac{\partial V}{\partial t} ds = 0 \quad \text{for unsteady, } \rho = \text{const.} \quad (7.27)$$

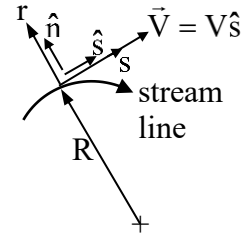
Equations 7.26 and 7.27 are the same unsteady Bernoulli equations as Eqs. 7.9 and 7.10 that we obtained in section 7.3.1 above, when we invoked the conditions of flow along a streamline for

the general Euler equation. This is of course as it should be, and illustrates that the Bernoulli equation is independent of a specific coordinate system.

To assess the effect of flow curvature, we can use the component of the Euler equation for the n -direction (Eq. 7.24b). Starting with the n -equation, we demonstrate how pressure and height vary *normal* to the direction of a streamline.

Let $d\vec{n}$ represent a differential element that is perpendicular to a streamline, where $d\vec{n} = dn \hat{n}$. We now take the dot product of $d\vec{n}$ with Eq. 7.23, giving:

$$g \underbrace{\frac{\partial h}{\partial n}}_{dh} dn + \frac{1}{\rho} \underbrace{\frac{\partial P}{\partial n}}_{dP} dn = \frac{V^2}{R} dn \tag{7.28}$$



Since we will only be integrating in the *normal direction*, n , we can associate $d(\) = \frac{\partial(\)}{\partial n} dn$, since we are constraining

the changes to only occur normal to the streamline, such that $ds = 0$. For an arbitrarily curved streamline, the integration of the velocity terms could be complicated. So, to simplify our considerations of curvature, we constrain our assessment to a set of streamlines, each of which has a circular radius of curvature R . We also let $dn = dr$, where r is a variable originating at the origin and oriented along the radii of curvature of the streamlines, so Eq.7.28 becomes:

$$g dh + \frac{1}{\rho} dP = \frac{V^2}{R} dr \tag{7.29}$$

Integrating Eq. 7.29 between two points along the radius, and letting $\rho = \text{constant}$, gives:

$$\int_1^2 g dh + \frac{1}{\rho} \int_1^2 dP = \int_1^2 \frac{V^2}{R} dr \tag{7.30}$$

$$g(h_2 - h_1) + \frac{1}{\rho} (P_2 - P_1) = \int_1^2 \frac{V^2}{R} dr$$

Note that: (1) the velocity, V , in Eqs. 7.29 and 7.30 is the *magnitude* of the velocity along the streamlines, $V=V_s=V(r,s)$, and (2) these equations only apply normal to streamlines when r is parallel to n , $\rho = \text{constant}$. Additionally, the centers of curvature must remain fixed or the equation does not apply (basically, all flow streamlines must describe a circle, or a circular arc). As we will see, generally we set $R = r$ when integrating the right hand side of Eqs. 7.29 and 7.30, since the origin of the radius of curvature, and the coordinate r will be the same for a set of circular arc streamlines.

7.6 Applications of the Euler s and n Equations

The following section demonstrates the application of the Euler s and n equations for several inviscid flows. Most real flows have some degree of curvature, which can affect the cross-stream pressure distribution. Recall that we showed this pressure variation with curvature for several of the examples we did in section 6.4. These cross-stream pressure differences can have a significant effect on what are termed [secondary flows](#), which are local flows that are not coincident with the main or primary flow. Secondary flows generally occur where viscosity retards the primary flow to such an extent that a cross-stream pressure field can cause movement of fluid normal to the primary flow direction. These secondary flows commonly develop near solid surfaces, where viscous effects are the strongest. The consequences of such secondary flows are the development of cross-stream variations in the overall velocity field, leading to significant three-dimensionality of the flow field, and often increased energy losses and flow separation. We'll discuss such losses in more detail in Chapter 15.

Euler’s n-equation, which is used to establish pressure changes across streamlines for inviscid flows, can also be used to approximate how cross-stream pressure changes result from curvature in real fluid flows.

7.6.1 Pressure Field Inside an Inviscid Vortex

One of the simplest, and most instructive, examples of curvature-induced pressure changes is a circular vortex rotating in an inviscid environment. Consider a radially symmetric vortex of radius R rotating in solid body rotation, with a velocity distribution given by $V(r) = Cr$, where C is a constant. Assuming that the flow is steady, and gravitational effects are not relevant, Euler’s n-equation, Eq. 7.29, for a fixed center of curvature, simplifies to:

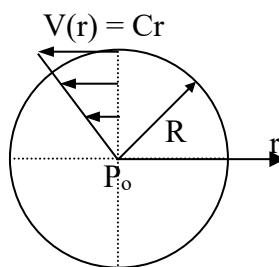
$$\frac{1}{\rho} \frac{dP}{dr} = \frac{V^2}{r}$$

Substituting the solid body velocity distribution gives:

$$\frac{dP}{dr} = \rho \frac{(Cr)^2}{r}$$

Separating variables, and integrating outward from the center of the vortex, $r = 0$, where we assume a pressure of $P = P_o$, we obtain:

$$\int_{P_o}^P dP = \int_{r=0}^r \rho C^2 r dr$$



- Assume
1. Euler n-eqn. applies
 2. $P = P(r)$
 3. $P = P_o$ at $r = 0$
 4. circular center of curvature such that $R = r$
 5. neglect h changes
 6. steady

$$P - P_o = \rho C^2 \frac{r^2}{2} \Big|_{r=0}^r = \rho C^2 \frac{r^2}{2}$$

So, the pressure distribution within the vortex is given by

$$P = P_o + \rho C^2 \frac{r^2}{2} \quad (7.31)$$

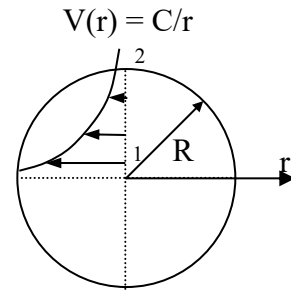
and the pressure at the outside of the vortex, $r = R$, is given by $P_R = P_o + \rho C^2 \frac{R^2}{2}$.

Thus, for a vortex with solid body rotation, the pressure *increases* with increasing radius, with the lowest pressure occurring at the *center* of the vortex.

Now, consider a vortex with a velocity profile that decreases inversely with radius, such that

$V(r) = \frac{C}{r}$ (this is a potential vortex, which we revisit in Chapter 9). Here, the same assumptions and form of Euler's n-equation apply. Substituting the velocity profile into the Euler n-equation gives:

$$\frac{dP}{dr} = \rho \frac{V^2}{r} = \frac{\left(\frac{C^2}{r^2}\right) dr}{r} = \rho \frac{C^2}{r^3}$$



Integrating from a point 1 to a point 2 along the radius, we have:

$$\int_{P_1}^{P_2} dP = P_2 - P_1 = \rho C^2 \int_{r=r_1}^{r_2} \frac{dr}{r^3} = \rho C^2 \left(-\frac{1}{2r^2} \right)_{r_1}^{r_2} = -\frac{\rho C^2}{2r_2^2} + \frac{\rho C^2}{2r_1^2} = -\rho \frac{V_2^2}{2} + \rho \frac{V_1^2}{2}$$

Where V_1 and V_2 are the velocities at the respective points, and

$$P_2 = P_1 + \rho \frac{V_1^2}{2} - \rho \frac{V_2^2}{2} \quad (7.32)$$

Note that Eq. 7.32 indicates that $\frac{(P_2 - P_1)}{\rho} + \frac{1}{2}(V_2^2 - V_1^2) = 0$, which is the same result we would

obtain integrating Euler's s-equation for an *irrotational* flow. This is because this particular type of vortical velocity profile contains no vorticity, and is thus termed an *irrotational vortex*.

However, note that there is a problem with this description of the pressure field, since if $r_1 \rightarrow 0$

this would require that $V_1 = \frac{C}{r_1} = \frac{C}{0} \rightarrow \infty$. Actually, a better way to describe this pressure field is

to let one limit of integration be the pressure at an infinite radius, such that $P = P_\infty$ as $r \rightarrow \infty$, and integrate from infinity inward, which gives:

$$\int_{P_\infty}^P dp = P - P_\infty = \rho C^2 \int_{r \rightarrow \infty}^r \frac{dr}{r^3} = -\frac{\rho C^2}{2r^2} + \frac{\rho C^2}{2(\infty)} = -\frac{\rho C^2}{2r^2} = -\rho \frac{V^2}{2}$$

or

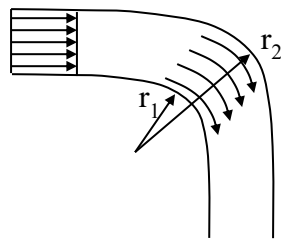
$$P = P_\infty - \frac{\rho C^2}{2r^2} = P_\infty - \rho \frac{V^2}{2} \quad (7.33)$$

Equation 7.33 indicates that the pressure will decrease from P_∞ toward the center.

Again, as $r \rightarrow 0$, the velocity will increase infinitely, and Eq. 7.33 indicates that the pressure would decrease infinitely, which is not physically possible. In a real flow of this type, viscosity would cause a “readjustment” of the velocity profile to a solid body rotation near the center of the vortex, which allows $V \rightarrow 0$ as $r \rightarrow 0$, such that the pressure at $r = 0$ will be a finite value. Such vortices, which combine an irrotational outer flow with a solid body inner rotation, are termed combined [Rankine vortices](#). These types of combined vortices provide reasonable models of the pressure behavior within actual viscous vortical flows, such as hurricanes and bathtub vortices. The analysis of such combined vortex flows is given as study problems at the end of this chapter.

Note that the two different vortical flows just examined illustrate a characteristic that is *generic for all vortical flows*, whether they are inviscid or viscous. For all vortical flows, $\frac{dP}{dr} > 0$, which implies that the pressure within a vortex will always decrease toward the center of rotation. As we discuss in the following example, cross-stream, radial pressure gradients, $\frac{dP}{dr}$, resulting from streamline curvature, can play a particularly important role in creating secondary flows near constraining solid boundaries, such as in the vicinity of bends in pipes or ducts, and even in rivers.

7.6.2 Inviscid, Irrotational Flow Around a Bend in a Duct



Assume

- 1) inviscid
- 2) $\rho = \text{constant}$
- 3) steady flow
- 4) irrotational flow
- 5) neglect height changes

Figure 7.6 Two-dimensional flow around a circular arc bend or elbow.

Consider inviscid, irrotational flow around a two-dimensional bend whose bounding surfaces are concentric, circular arcs, as shown in figure 7.6.

From the Euler s-equation for irrotational, steady flow, Eq. 7.25a, we have:

$$g dh + \frac{1}{\rho} dP + d\left(\frac{V^2}{2}\right) = 0 \tag{7.34}$$

Integrating Equation 7.34 within the bend flow field, *since the flow is assumed irrotational*, gives:

$$\frac{P}{\rho} + \frac{1}{2} V^2 = \text{constant over the flow field} \tag{7.35}$$

If we differentiate Eq. 7.35 with respect to the radius, r, we have:

$$\frac{1}{\rho} \frac{\partial P}{\partial r} + V \frac{\partial V}{\partial r} = 0 \tag{7.36}$$

Equation 7.36 will be valid anywhere for irrotational flow within the bend.

However, for any streamline passing around the bend, Euler’s n-equation, Eq. 7.29, will also apply in the form:

$$\frac{1}{\rho} \frac{\partial P}{\partial n} = \frac{V^2}{R}$$

where n is coincident with the radius, r, of the streamline, and R = r is the radius of curvature of any streamline within the bend, such that:

$$\frac{1}{\rho} \frac{\partial P}{\partial r} = \frac{V^2}{r} \tag{7.37}$$

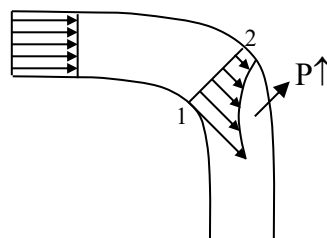
Equating the radial pressure gradients in Eq. 7.36 and 7.37 we have:

$$\frac{1}{\rho} \frac{\partial P}{\partial r} = \frac{V^2}{r} = -V \frac{\partial V}{\partial r} \approx -V \frac{dV}{dr}$$

Separating variables and integrating from the inside of the bend (V = V₁ at r = r₁) to an arbitrary point within the bend, yields,

$$\int_{V_1}^V \frac{dV}{V} = -\int_{r_1}^r \frac{dr}{r} \Rightarrow \ln \frac{V}{V_1} = -\ln \frac{r}{r_1}$$

or



$$V = V_1 \frac{r_1}{r} = \frac{C}{r} \quad \text{where } C = V_1 r_1 = \text{constant.} \quad (7.38)$$

So, the velocity is highest on the inside of the bend, diminishing toward the outside of the bend. Substituting Eq. 7.38 into Eq. 7.37 for the radial pressure gradient, indicates that

$$\frac{dP}{dr} = \rho \frac{C^2}{r^3} > 0$$

Integrating from r_1 to r_2 gives:

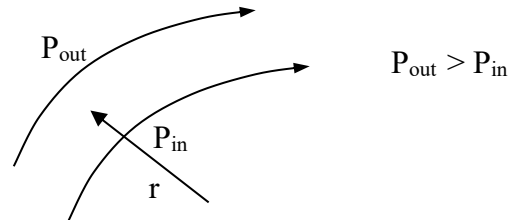
$$P_2 - P_1 = \rho \frac{C^2}{2r_1^2} - \rho \frac{C^2}{2r_2^2} = \frac{1}{2} \rho V_1^2 \left[1 - \left(\frac{r_1}{r_2} \right)^2 \right] > 0 \quad \text{since } r_1 < r_2 \quad (7.39)$$

Equation 7.39 indicates that the pressure is always higher toward the outside of a bend or elbow, and the velocity is highest near the inside of the bend. Note the similarity to the result for an irrotational vortex, Section 7.6.1.

Recalling our results for inviscid vortices in section 7.6.1, we can generalize that for curved streamlines,

$$\frac{dP}{dn} = \rho \frac{V^2}{r} > 0 \quad (7.40)$$

Equation 7.40 implies that pressure always increases in the direction of curvature, as illustrated to the right.



This characteristic of the radial pressure increasing in the direction of curvature holds true for all flows, inviscid or viscous, and for streamlines moving along non-circular paths. As discussed before, cross-stream pressure gradients that result from these curved streamline patterns are responsible for the development of secondary flows near bounding surfaces in real fluid flows.

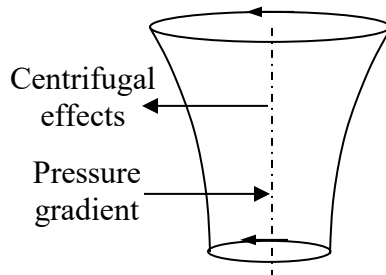
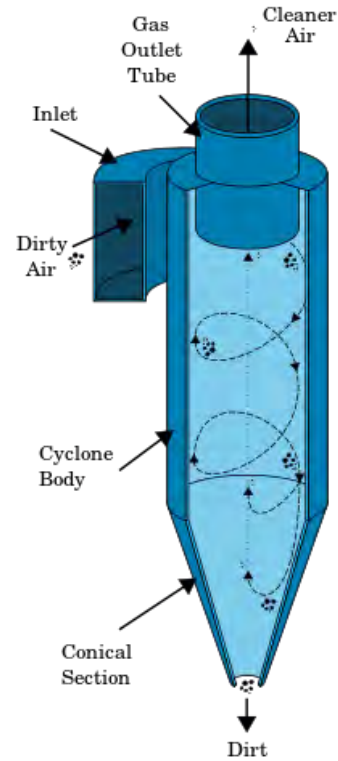
7.6.3 The Impact of Curvature on Particulate Motion

In sections 7.6.1 and 7.6.2, we illustrated how cross-stream pressure will always increase in the direction of radial curvature. The practical implications of this effect are manifold, from the creation of cross-stream secondary flows near boundaries, to the creation of swirling three-dimensional flows. Additionally, cross-stream pressure gradients due to flow curvature effects can provide a strong driving force for the motion of solid particulates or gas bubbles suspended

in a fluid. The following two qualitative examples illustrate the impact of flow curvature on particulate motion.

7.6.3.1 Vortex-Induced Motion of Particles or Gas in a Liquid.

Since pressure always increases outward from the center of fluid rotation, this pressure difference (the local magnitude reflected by the radial pressure gradient) provides a driving force toward the center of rotation. In essence, this is a driving force toward the center of curvature proportional to the local angular acceleration. The effect of the pressure gradient is to generate a surface force acting *inward*, toward the center of curvature on any particle within the flow. That surface force will be proportional to the *fluid mass displaced by the particle*. However, a particle rotating in the flow will also be subject to a [centrifugal](#) force acting *outward* from the center of curvature, but proportional to the *mass of the particle*. Consequently, for a particle that is denser than the fluid, such as most dirt particles, the centrifugal force is dominant, and the particle will move outward. This effect is the basis for the operation of [cyclone separators](#), which are used to remove heavy particulate matter from fluid and air flows. A schematic of a cyclone separator is shown at the right. Conversely, a particle that is less dense than the fluid will move inward, since the pressure gradient force will dominate. This effect can be observed, for example, by the bubbles in a carbonated beverage moving toward the center of a glass when the beverage is stirred. Of course, if the particle density is equal to that of the fluid (i.e. neutrally buoyant), the particle will maintain its position and move with the fluid.



General Particulate Behavior in Rotating Flow	
$\rho_{\text{particle}} > \rho_{\text{fluid}} \Rightarrow$	moves outward
$\rho_{\text{particle}} < \rho_{\text{fluid}} \Rightarrow$	moves inward

7.6.3.2 Erosive Effects and River Meandering

When there are substantial variations in topographical elevation, rivers and streams tend to follow the contours of the lowest points of land, or valleys. However, when a river or stream flows across a relative flat area, such as a prairie or open field, flow curvature can have a significant impact on the path of the river/stream due to the development of a secondary, cross-stream flow that carries eroded soil particles from the outside to the inside bank of a river or stream.

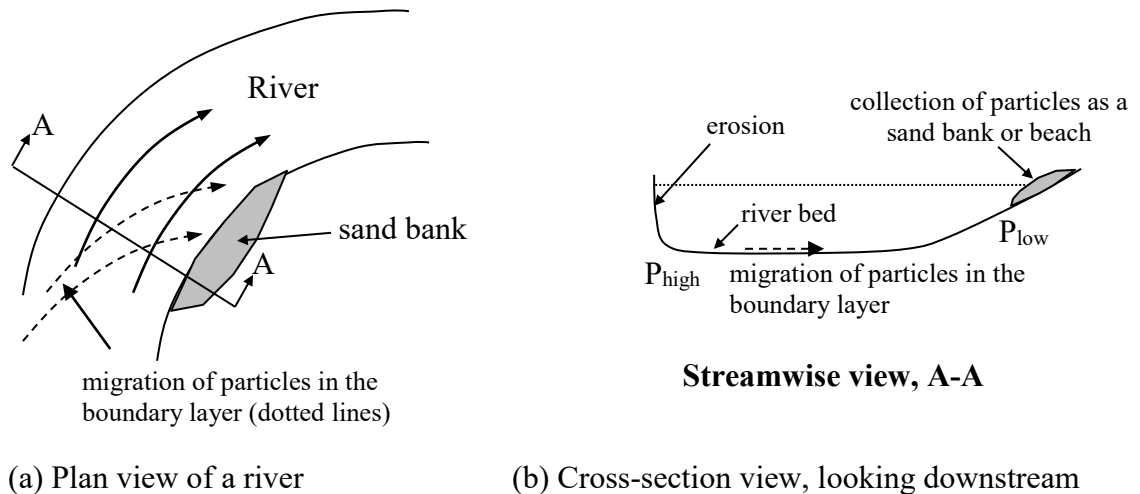


Figure 7.7 Illustration of the migration of eroded particulate material across a river or stream bed due to curvature-induced, cross-stream pressure gradients.

Consider the plan-view schematic shown in figure 7.7a of a curved river channel. The curved flow of the river causes a cross-stream pressure gradient, with pressure increasing outward from the center of curvature, such that the pressure within the main body of the flow will be higher at the outside bank of the river than the inside bank. If the flow is fast enough, this increase in pressure will also be visually evidenced by an outward increase in the cross-stream height of the river surface.

As the streamwise cross-section A-A of the river in figure 7.7b shows, the flowing water will erode the outside bank of the river, with the heavy soil particulates settling toward the riverbed. When the soil particles approach the riverbed, they will enter a viscous fluid boundary layer just above and adjacent to the riverbed (We will cover boundary layers in Chapter 13). Within this boundary layer, the flow of the water in the streamwise direction will be strongly reduced (by the no slip effect at the riverbed), and so will the associated hydrodynamic forces which drag the eroded soil particles in the streamwise direction. However, the cross-stream pressure gradient created by curvature of the main flow will be “impressed” on both the boundary layer, and the soil particles within this layer. This radial pressure gradient creates a lateral force on the particles, which pushes the particles and the local flow adjacent to the riverbed toward the inside

riverbank, causing the particles to “migrate” across the river and be deposited on the inside bank of the river. The dotted arrows in figure 7.7a roughly model the particle migration from the outer to the inner bank of the river.

As this process of cross-stream transport continues, eroded soil particles from the outer riverbank will continue to migrate and deposit on the inner riverbank, forming a beach or sand bank. This continuing erosion of the outer bank and deposition of material on the inner bank will create additional curvature of the river, which will increase the process of erosion/transport. The long-term result is the development of an increasingly curved, sinuous path for the river. This continued development of river curvature is generally termed “meandering.”



Figure 7.8 An image of river meandering, clearly showing sand bars (appearing as light yellow) formed on the inside of bends (curves) in the river.

The Mississippi River in the United States, and the Nile River in Egypt are excellent examples of meandering caused by this process of erosion and secondary flow transport, all of which can be explained by the presence of radial pressure gradients. Clearly, if a river is initially straight, this process requires some initial perturbation to start the development of curvature, but existing irregularities in the land contours are generally sufficient to initiate this natural process.

Figure 7.8 is an example of this meandering river effect, from a photograph I took from an airplane at 36,000 feet. Note how the sand bars (light yellow color) occur on the inside of the bends in the river, and in some cases form small islands at the inside of a bend in the river. Given enough time, and without interference by human engineering, these bends in the river will continue to accentuate, often causing the river to cut through these sand bars to meet upon itself and form a separate channel. The Mississippi River over time has created many of these separate islands, often modifying adjacent state boundaries, and isolating riverside homes and towns. And this is all due to the processes inferred from the Euler n -equation. For a simplistic video assessment of this process by a geologist, with some nice illustrations, go to [this link](#). It doesn't cite Euler's n -equation, but it is that process that is at work.

To illustrate the movement of heavier particulates by secondary flows due to a radial pressure gradient, try this simple experiment. Fill a circular container (any glass, coffee cup, or teacup will work) with water, and drop in some fine dirt particles (heavy enough that they settle to the bottom of the vessel—sand works well). Now stir the water until it is moving in a relatively steady circular motion. Remove your stirring implement, and watch what happens to the dirt on the bottom of the vessel. What you will observe is that as the flow slows, due to viscous effects, all the dirt particles will concentrate in the center of the vessel—proof of the presence of a secondary flow along the bottom of the vessel toward the center of curvature due to the imposed radial pressure gradient by the main flow. This is often called the "[tea leaf phenomena or paradox](#)", since it has long been observed that tea leaves within a cup of stirred tea display this central concentration behavior. Click on the above link to see a demonstration of this tea leaf concentration, which was explained originally by no other than Albert Einstein.

7.7 Summary of Inviscid flow Equations

7.7.1 Euler Equation (along a streamline or in irrotational flow)

$$g dh + \frac{1}{\rho} dP + d\left(\frac{V^2}{2}\right) + \frac{\partial \vec{V}}{\partial t} \cdot d\vec{s} = 0$$

7.7.2 Bernoulli Equation (along streamline, or irrotational flow)

$$\left(\frac{P_2}{\rho} + \frac{V_2^2}{2} + gh_2\right) - \left(\frac{P_1}{\rho} + \frac{V_1^2}{2} + gh_1\right) + \int_1^2 \frac{\partial \vec{V}}{\partial t} \cdot d\vec{s} = 0 \quad \text{Unsteady}$$

$$\left(\frac{P_2}{\rho} + \frac{V_2^2}{2} + gh_2\right) = \left(\frac{P_1}{\rho} + \frac{V_1^2}{2} + gh_1\right) \quad \text{Steady}$$

7.7.3 Euler s and n Equations (streamline coordinates, unsteady)

$$g \frac{\partial h}{\partial s} + \frac{1}{\rho} \frac{\partial P}{\partial s} + V \frac{\partial V}{\partial s} + \frac{\partial V}{\partial t} = 0 \quad \text{s-direction component}$$

$$g \frac{dh}{\partial n} + \frac{1}{\rho} \frac{\partial P}{\partial n} = \frac{V^2}{R} \quad \text{n-direction component}$$

7.7.4 Euler s and n Equations (integrated, steady)

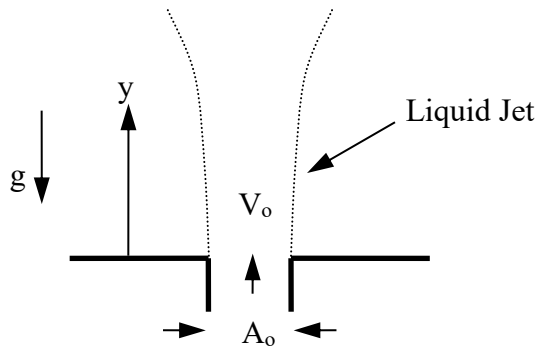
$$\left(\frac{P_2}{\rho} + \frac{V_2^2}{2} + gh_2\right) = \left(\frac{P_1}{\rho} + \frac{V_1^2}{2} + gh_1\right) \quad \text{along streamline}$$

$$g(h_2 - h_1) + \frac{1}{\rho}(P_2 - P_1) = \int_1^2 \frac{V^2}{R} dr \quad \text{normal to streamline}$$

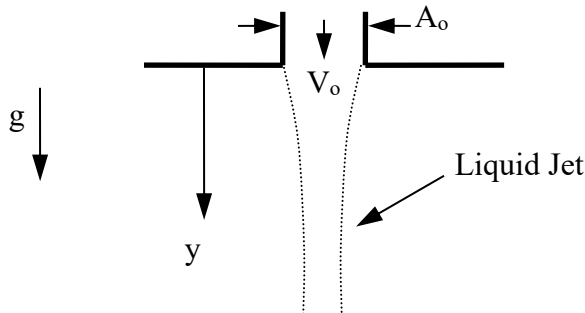
Study Problems

1. An inviscid, two-dimensional flow field is given by $\vec{V} = x^2\hat{i} - 2xy\hat{j}$. Assuming that all values are dimensionless, determine:
 - a) If this an incompressible flow; if so, let $\rho = 1$ (dimensionless)
 - b) The vorticity for the flow field;
 - c) The equation for a streamline passing through a point 1 at $x,y = 1,1$;
 - d) The value of y at a point 2 lying on the streamline of part c at $x = 2$;
From our streamline, the value of y for $x = 2$ is given by:
 - e) If the pressure at point 1, P_1 , is zero, determine the value of pressure at point 2, P_2 ;
 - f) Using point 1 in part e), could you determine the value of pressure at a point $x,y = 2,2$? If you can, determine the pressure; if you can't, explain why you can't

2. Consider a liquid jet that flows vertically upward in a gravitational field, as shown below. Assume the flow is uniform and inviscid. Determine an expression for the change in the jet cross-section with distance y from the jet orifice. What is the limiting height for this jet? Why?

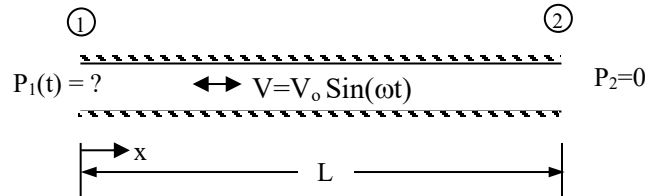


3. Consider a liquid jet that falls vertically downward in a gravitational field, as shown below. Assume the flow is uniform and inviscid. Determine an expression for the change in the jet cross-section with distance y from the jet orifice.

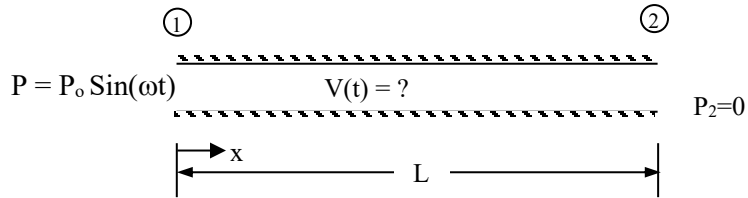


4. A home power washer generates water gage pressure of 3000 psi or 20.68 MPa. If the nozzle of the power washer has an inlet diameter of 1 cm and an exit diameter of 1 mm, assume the flow through the nozzle is inviscid, and determine: (a) the water exit velocity, and (b) the flowrate in liters/minute. Note: Assume 20 C water; gage pressure is the pressure relative to atmospheric, and the exit pressure is atmospheric.

5. A the pump of a water jet cutter generates a gage pressure of 60,000 psi or 413.7 MPa. If the nozzle of the water jet has an inlet diameter of 1 cm and an exit diameter of 1 mm, assume the flow through the nozzle is inviscid, and determine (a) the water exit velocity, and (b) the flowrate in liters/minute. Note: Assume 20 C water; gage pressure is the pressure relative to atmospheric, and the exit pressure is atmospheric.
6. An *inviscid* flow of constant density, ρ , passes through a straight pipe of length L . The pressure at the outlet of the pipe remains constant at $P_2=0$. Determine [in terms of V_0, ρ, L, ω and t] how the inlet pressure to the pipe (P_1) must vary if the velocity in the pipe is varies sinusoidally as $V=V_0 \sin(\omega t)$.

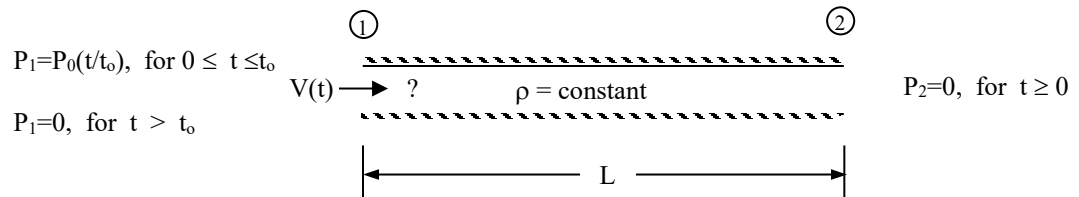


7. An *inviscid* flow of constant density, ρ , passes through a straight pipe of length L . The pressure at the outlet of the pipe remains constant at $P_2=0$. Determine [in terms of P_0, ρ, L, ω and t] how the pipe velocity, V , must vary if the inlet pressure to the pipe varies sinusoidally as $P_1=P_0 \sin(\omega t)$. Assume $V = 0$ at $t = 0$.

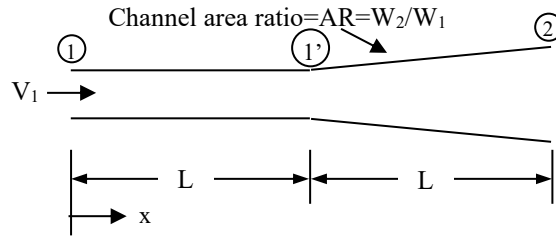


8. An *inviscid* flow of constant density, ρ , passes through a straight pipe of length L . The pressure at the outlet of the pipe (P_2) remains constant at $P_2=0$, while the inlet pressure to the pipe (P_1) varies as $P_1=P_0(t/t_0)$ for $0 \leq t \leq t_0$, after which $P_1 = 0 = \text{constant}$ for $t > t_0$. Assume $V = 0$ at $t = 0$.

- a) Determine an expression for the *velocity through the pipe* as a function of P_0, ρ, L, t_0 and t .
- b) What is the maximum velocity achieved, and when in time is it reached?
- c) Plot V/V_{\max} vs. t/t_0 from $0 < t < 2t_0$.



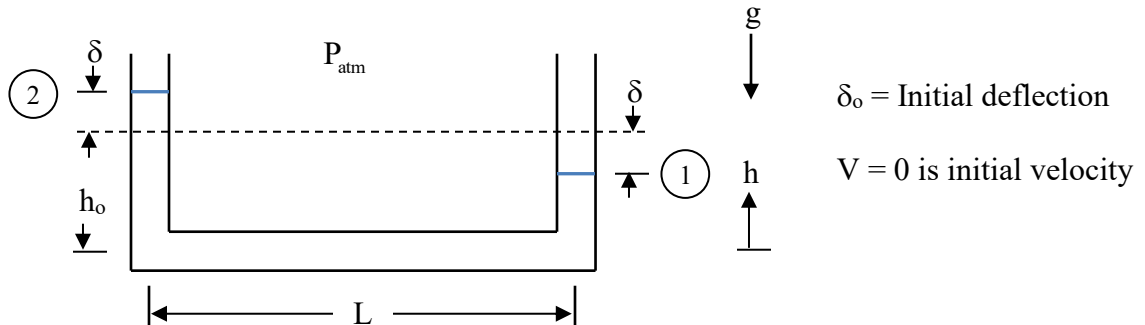
9. An inviscid flow passes through a 2-D constant area channel, followed by a 2-D channel, that undergoes an area change over the last half of the channel, as shown. Each half of the channel is L long, and the exit area ratio of the end of the channel is given by exit area (W_2) divided by the inlet area of the beginning of the channel (W_1), such that $AR=W_2/W_1$. The channel inlet velocity increases as $V_1=V_o(t/t_o)$ for $0 < t \leq t_o$, after which $V_1 = V_o = \text{constant}$ for $t > t_o$.



Determine the pressure ratio, $C_p = \frac{(P_2 - P_1)}{\frac{1}{2} \rho V_o^2}$, as a function of time, t . On a single graph, plot C_p for $AR = 2, 1,$ and 0.75 , over the time period $0 < t < 2t_o$. For purposes of dimensional correctness in plotting the behavior, assume that $t_o = 2L/V_o$.

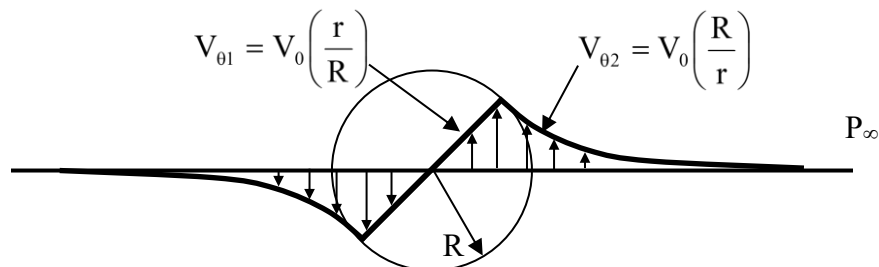
Briefly, explain what phenomena causes this unusual behavior, and what its implications are for start-up flows.

10. Apply the unsteady Bernoulli equation to an inviscid fluid in a U-tube manometer of constant diameter as shown. Assume that the manometer surface levels differ from the equilibrium level h_o by an amount δ . The initial surface deflection at $t = 0$ is $\delta = \delta_o$, and the initial surface velocity is zero. Using the unsteady Bernoulli equation, obtain a differential equation for $\delta(t)$ and, solve for δ in terms of the properties shown. Also, determine the interface velocity, $V(t)$ in terms of parameters shown.



Let the heights of the respective surfaces be $h_1 = h_o - \delta$, and $h_2 = h_o + \delta$, and the total length of the fluid column in the manometer be $S = 2h_o + L$.

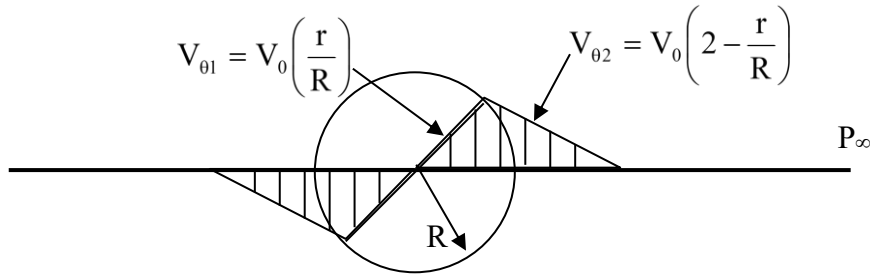
11. A circular combined Rankine vortex is present in an inviscid fluid, as shown.



The vortex consists of a core of radius R , which is in solid body rotation with velocity $V_{\theta 1} = V_0 \left(\frac{r}{R} \right)$, and a portion outside the core ($r \geq R$) that has a velocity $V_{\theta 2} = V_0 \left(\frac{R}{r} \right)$. The density of the flow is ρ , and the pressure far away from the vortex center is P_∞ . Determine the following:

- a) The vorticity for the entire flow field, as a function of r . Plot ω vs. r/R .
- b) The location of the minimum pressure, P_{\min} , and the value of that pressure in terms of ρ , V_0 , and P_∞ . Neglect any height changes.

12. A circular vortex is present in an inviscid fluid, as shown.

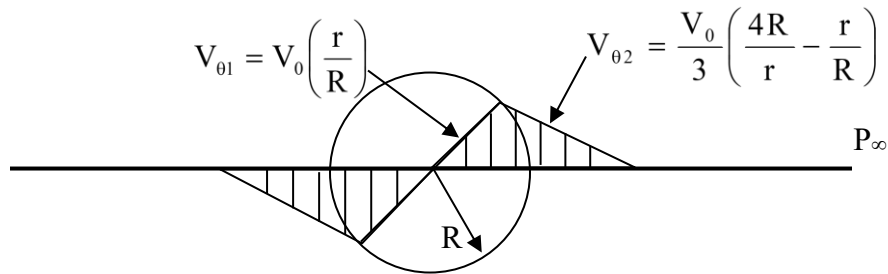


The vortex consists of a core of radius R , which is in solid body rotation with velocity $V_{\theta 1} = V_0 \left(\frac{r}{R} \right)$. The portion outside the core ($R \leq r \leq 2R$) has a velocity $V_{\theta 2} = V_0 \left(2 - \frac{r}{R} \right)$. The density of the flow is ρ , and the pressure far away from the vortex center is P_∞ , including at $r = 2R$.

Determine the following:

- a) The vorticity for the entire flow field, as a function of r . Plot or make a nice labeled sketch of ω vs. r/R .
- b) The location of the minimum pressure, P_{\min} , and the value of that pressure in terms of ρ , V_0 , and P_∞ . Neglect any height changes.

13. A circular vortex is present in an inviscid fluid, as shown.

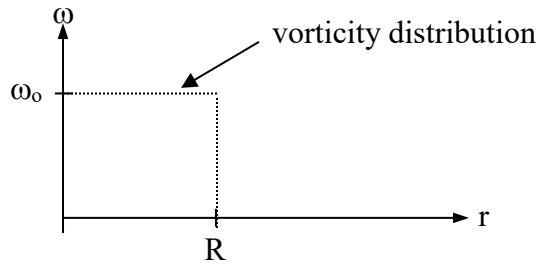


The vortex consists of a core of radius R , in solid body rotation with velocity $V_{\theta 1} = V_0 \left(\frac{r}{R} \right)$.

The portion outside the core ($R \leq r \leq 2R$) has a velocity $V_{\theta 2} = \frac{V_0}{3} \left(\frac{4R}{r} - \frac{r}{R} \right)$. The density of the flow is ρ , and the pressure far away from the vortex center is P_∞ , including at $r = 2R$. Determine the following:

- a) The vorticity for the entire flow field, as a function of r . Plot ω vs. r/R .
- b) The location of the minimum pressure, P_{\min} , and the value of that pressure in terms of ρ , V_0 , and P_∞ . Neglect any height changes.

14. A circular vortex in an inviscid fluid has the following vorticity distribution, ω vs. r , where, $\omega = \omega_0$ for $r \leq R$, and $\omega = 0$ for $r > R$.



If the velocity distribution is $\vec{V} = v_\theta \hat{i}_\theta$ only, determine the following:

- a) The velocity distribution, $v_\theta(r)$, in terms of ω_0 and r , for $r \leq R$ (assume that $v_\theta(0) = 0$).
- b) The velocity distribution, $v_\theta(r)$, in terms of ω_0 , R , and r , for $r > R$.
- c) The location of the minimum pressure, P_{\min} , and the value of that pressure in terms of ρ , ω_0 , R and P_∞ , where $P = P_\infty$ when $r \gg R$. Neglect any height changes.

Chapter 8

The Stream Function, Vorticity, and Circulation

Contents

8.1 The Stream Function	224
8.1.1 The Relation of Streamlines to Flow Rate	226
8.1.2 The Concept of a Stream Tube	227
8.2 Vorticity and Circulation	227
8.2.1 Vorticity and Circulation for a Fluid in Solid-Body Rotation	229
8.2.2 Vorticity and Circulation for an Irrotational Vortex	230
8.2.3 Vorticity and Circulation for a Fully-Developed Channel Flow	231
8.3 Vortex Lines and Vortex Tubes	234
8.3.1 Vortex Lines	234
8.3.2 Vortex Tubes	235
8.3.2.1 Solid-Body Rotation Along a Vortex Tube	237
8.3.2.2 The Tornado as a Vortex Tube	238

In previous chapters, we have developed methods to describe and visualize local fluid velocity and rotational behavior. In Chapter 2, we introduced the streamline for describing the behavior within a velocity field. In Chapter 4, we introduced vorticity, as a property reflecting fluid rotation. In this chapter, we extend those processes to assess more global behavior, in terms of both the flowrate behavior within a fluid, and a parallel method for assessment of the collective rotation within a fluid flow.

8.1 The Stream Function

In many situations, the incompressible differential continuity equation (Eq. 5.24) can be reduced to two dimensions in Cartesian coordinates (e.g. x and y) such that:

$$\frac{\partial u}{\partial x} + \frac{\partial v}{\partial y} = 0 \quad (\text{two-dimensional, } \rho = \text{constant}) \quad (8.1)$$

Equation 8.1 still leaves us with two independent velocity variables, u and v . As with most differential equations, we look for solution techniques that take advantage of constraining conditions. In the case of two-dimensional flow, we can reduce the number of dependent variables from two to one by defining a function $\psi(x,y)$, such that this function will be a solution to the two-dimensional continuity equation if u and v can be expressed as:

$$u = \frac{\partial \psi}{\partial y} \quad (8.2a)$$

and

$$v = -\frac{\partial \psi}{\partial x} \quad (8.2b)$$

If such a function $\psi(x, y)$ exists, then when we substitute Eq. 8.2 for u and v into the continuity equation, Eq. 8.1, we obtain:

$$\frac{\partial u}{\partial x} + \frac{\partial v}{\partial y} = \frac{\partial^2 \psi}{\partial x \partial y} - \frac{\partial^2 \psi}{\partial y \partial x} = 0 \quad (8.3)$$

Equation 8.3 implies that such a function, $\psi(x, y)$, is an *exact solution* of the two-dimensional continuity equation.

Now recall that the equation for a streamline is given by $\vec{V} \times d\vec{r} = 0$, which for two-dimensional flow simplifies (in Cartesian coordinates) to:

$$u dy - v dx = 0 \quad (8.4)$$

Substituting Eq. 8.2 into Eq. 8.4 gives:

$$\frac{\partial \psi}{\partial y} dy + \frac{\partial \psi}{\partial x} dx = 0 \quad (8.5)$$

Now if we also differentiate the function ψ , the chain rule gives us:

$$d\psi = \frac{\partial \psi}{\partial y} dy + \frac{\partial \psi}{\partial x} dx \quad (8.6)$$

Comparing Eq. 8.6 with Eq. 8.5, which we obtained from the streamline equation, this indicates that $d\psi = 0$ along a streamline, or that ψ must be a constant along a streamline.

We term ψ the *stream function* of the flow field, from which we can derive the velocity components, plus other useful relationships for the flow field. In Chapter 9 we will show that we can use the stream function to assess the behavior of inviscid, irrotational flows. Additionally, in Chapters 12 and 13 we will demonstrate how we can use the functionality of the stream function to reduce the order of the Navier-Stokes equations to help us solve for the behavior of two-dimensional, viscous flows (unfortunately, at the expense of generating higher-order terms).

8.1.1 The Relationship of Stream Lines to Flow Rate

Note that since $d\psi$ is an exact differential, the integral of $d\psi$ between any two points in a flow field will be independent of the path of integration (remember your calculus). Now consider the flow between two streamlines, as shown in figure 8.1.

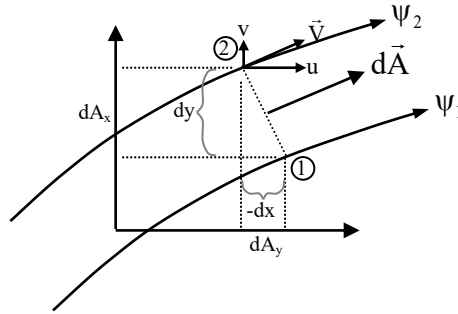


Figure 8.1 Geometric schematic of flow between two streamlines.

From control volume continuity, we know that the volume flow rate is the integral of the velocity field *normal* to the cross-sectional area spanning the streamlines, or:

$$Q = \text{flowrate} = \int_1^2 \vec{V} \cdot d\vec{A}$$

The component of the velocity crossing a surface is often termed the velocity “flux.” Thus, the flow rate is the integral of the velocity flux over a prescribed area. If we examine this flow rate integral for two-dimensional flow, using the general configuration shown in figure 8.1, we can generalize the velocity and the differential area (which in two-dimensions is really just a cross-sectional distance) as:

$$\vec{V} = u\hat{i} + v\hat{j} \quad \text{and} \quad d\vec{A} = dA_x\hat{i} + dA_y\hat{j} = dy\hat{i} + (-dx)\hat{j}$$

(note that $dA_y = -dx$, since the projection of $d\vec{A}$ is in the negative x-direction)

$$\text{Thus, } Q = \int_1^2 (u\hat{i} + v\hat{j}) \cdot (dy\hat{i} - dx\hat{j}) = \int_1^2 (udy - vdx)$$

Substituting for u and v from Eq. 8.2, we get:

$$Q = \int_1^2 \left(\frac{\partial\psi}{\partial y} dy + \frac{\partial\psi}{\partial x} dx \right) = \int_1^2 d\psi = \psi_2 - \psi_1 \tag{8.7}$$

Since the integral of Eq. 8.7 is path independent, this means that the flowrate between any two stream functions (i.e. streamlines) is a constant.

8.1.2 The Concept of a Stream Tube

Extrapolating the two-dimensional flow rate/streamline relationship to three-dimensions, we note that a collection of streamlines will form what we will term a *stream tube*, with the surface surrounding these streamlines being termed the *stream surface*. This is like closely packed glass fibers in an optical transmission cable.

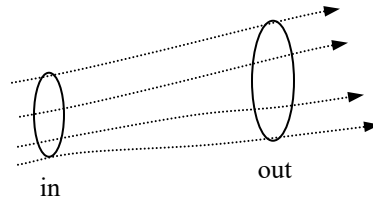


Figure 8.2 Example of a stream tube

For such a stream tube, as shown schematically in figure 8.2, we note that the velocity vector, \vec{V} , will always be *tangential* to the bounding surface of the stream tube, which means that no flow can cross the stream tube surface, except at a cross-section of the stream tube. Thus, the volume flowrate throughout a stream tube must be a constant at any area cross section,

$$\text{i.e. } Q = \iint_{A_{\text{in}}} \vec{V} \cdot d\vec{A} = \iint_{A_{\text{out}}} \vec{V} \cdot d\vec{A} = \iint_A \vec{V} \cdot d\vec{A} = \text{Constant} \quad (8.8)$$

Depending on the behavior of the streamlines comprising the stream tube, the geometry of the stream tube may change, resulting in variations of the streamwise cross-sectional area of the stream tube. Additionally, the geometry of the stream tube may vary with time, as the initial streamlines vary with time. However, regardless of how the stream tube varies geometrically with time, the instantaneous flow rate through the stream tube will always remain constant across any streamwise cross section.

8.2 Vorticity and Circulation

As discussed in Chapter 4, vorticity is the term given to the *local* rotational behavior of a fluid, which for simplicity is defined as *twice* the local angular velocity of the fluid. Given the Greek designator ω , vorticity is defined mathematically as:

$$\vec{\omega} = 2 \times \text{angular velocity} = \nabla \times \vec{V} = \text{curl } \vec{V}$$

Note that vorticity is a vector property and is expressed as derivative components of the velocity field relative to the coordinate system employed. For example, in the Cartesian coordinate system (u, v, w) , we write:

$$\vec{\omega} = \omega_x \hat{i} + \omega_y \hat{j} + \omega_z \hat{k}$$

Where, $\omega_x = \frac{\partial w}{\partial y} - \frac{\partial v}{\partial z}$, $\omega_y = \frac{\partial u}{\partial z} - \frac{\partial w}{\partial x}$, and $\omega_z = \frac{\partial v}{\partial x} - \frac{\partial u}{\partial y}$

In radial coordinates, the vorticity equations are a bit more complicated (due to non-zero derivatives of unit vectors). In radial coordinates, the equations of vorticity are:

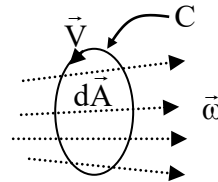
$$\vec{\omega} = \nabla \times \vec{V} = \hat{i}_r \omega_r + \hat{i}_\theta \omega_\theta + \hat{i}_z \omega_z$$

Where, $\omega_r = \left(\frac{1}{r} \frac{\partial v_z}{\partial \theta} - \frac{\partial v_\theta}{\partial z} \right)$, $\omega_\theta = \left(\frac{\partial v_r}{\partial z} - \frac{\partial v_z}{\partial r} \right)$, $\omega_z = \frac{1}{r} \left(\frac{\partial}{\partial r} (r v_\theta) - \frac{\partial v_r}{\partial \theta} \right) \hat{i}_z$

Whereas vorticity reflects the *local rotation* of a fluid at a point, we can also assess the *cumulative rotation* within a prescribed region, which we define as the *circulation strength*, Γ . We define the circulation of the fluid as the summation of the vorticity that crosses, and is enclosed by, a prescribed surface area. We first establish the flux of vorticity (i.e. the component of vorticity normal to, and thus crossing, the area in question) by taking the dot product of the vorticity with respect to the differential area vector. We then integrate the resulting vorticity flux over the prescribed area, such that:

$$\Gamma = \iint_A \vec{\omega} \cdot d\vec{A} = \underbrace{\iint_A (\nabla \times \vec{V}) \cdot d\vec{A}}_C = \oint_C \vec{V} \cdot ds \tag{8.9}$$

Stokes' Theorem



Note that by making use of Stokes' theorem (Section 2.4.4) in Eq. 8.9, we can establish a very useful relationship that relates the circulation to the velocity tangent to the boundary of the area. This relationship, which employs a line integral of the tangential velocity around a circuit bounding the prescribed area, C, bypasses the need to determine the local vorticity field, and in many cases makes the determination of the circulation mathematically much less involved.

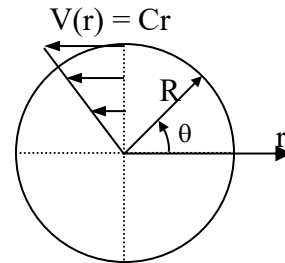
Because circulation is the summation of the vorticity flux across a designated area, it is analogous to volume flow rate, since it represents the summation of the flux of a vector property crossing a designated area or surface (defined by a bounding loop C). As such, circulation is a measure of the “strength” of the rotational behavior over a specified surface area, just as flow rate is the measure of the “volume” of fluid crossing a specified surface area. Thus, the circulation strength over a prescribed region may reflect either vorticity broadly distributed over a large region (such as a slowly rotating tropical depression over the ocean) or a strong concentration of vorticity within some portion of a larger region (e.g. a tornado). As we will discuss in Chapters 11 and 12, the effects of regions of less concentrated or more concentrated

vorticity can have comparable effects on the local velocity field, if the total circulation of both regions is also comparable.

8.2.1 Vorticity and Circulation for a Fluid in Solid Body Rotation

As we discussed in Section 7.6.1, flows with solid body rotation have a velocity field of the form:

$$\vec{V} = v_\theta \hat{i}_\theta = Cr \hat{i}_\theta \quad (\text{where } C \text{ is a constant}).$$

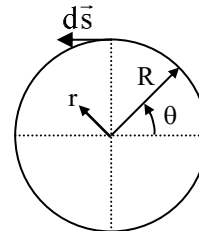


This type of flow is characteristic of the steady flow within a steadily rotating cylindrical vessel, and the flow near the core of many natural vortices (e.g. a hurricane). Since this is a cylindrically symmetric flow, we apply the equation for vorticity in cylindrical coordinates:

$$\begin{aligned} \vec{\omega} &= \nabla \times \vec{V} = \hat{i}_z \left[\frac{1}{r} \frac{\partial}{\partial r} (rv_\theta) - \frac{1}{r} \frac{\partial v_r}{\partial \theta} \right] \\ &= \hat{i}_z \left[\frac{1}{r} \frac{\partial}{\partial r} (Cr^2) \right] = \hat{i}_z \left(\frac{1}{r} 2Cr \right) = \hat{i}_z (2C) \end{aligned}$$

Thus, the vorticity for this flow is a constant across the vortex, as it should be for a solid body rotation. Now, consider the circulation strength for a vortex of radius R. Here, we apply Eq. 8.9, using an area integral,

$$\Gamma = \iint_A \vec{\omega} \cdot d\vec{A} \quad \text{where} \quad d\vec{A} = \hat{i}_z (rd\theta)dr.$$



The integration limits for a circle of radius R are $0 \leq \theta \leq 2\pi$ and $0 \leq r \leq R$, so we have:

$$\Gamma = \int_0^{2\pi} \int_0^R \hat{i}_z (2C) \cdot \hat{i}_z r dr d\theta = 2C\theta \left|_0^{2\pi} \frac{r^2}{2} \right|_0^R = 2C(2\pi) \left(\frac{R^2}{2} \right) = (2C)(\pi R^2) \tag{8.10}$$

Alternatively, we could have noted that at $r = R$, $v_\theta = CR \hat{i}_\theta$, and that a differential element at the boundary of the circle can be defined as $d\vec{s} = (Rd\theta) \hat{i}_\theta$. Thus, using the line integral approach from Eq. 8.9, we would calculate the circulation as:

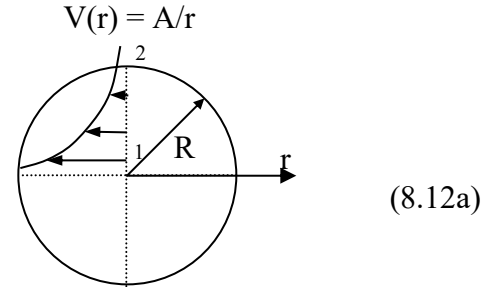
$$\Gamma = \oint_C \vec{V} \cdot d\vec{s} = \int_0^{2\pi} (CR) \hat{i}_\theta \cdot (Rd\theta) \hat{i}_\theta = \int_0^{2\pi} CR^2 d\theta = CR^2 2\pi = (2C)(\pi R^2) \tag{8.11}$$

Equation 8.11 is, of course, the same result we obtained in Eq. 8.10 using an area integral of the vorticity, and proves the validity of Stokes' theorem.

8.2.2 Vorticity and Circulation for an Irrotational Vortex

Again, as we discussed in Section 7.6.1, the velocity field for an *irrotational* vortex is given by $\vec{V} = v_\theta \hat{i}_\theta = \frac{A}{r} \hat{i}_\theta$ (where A is a constant). For this type of velocity profile, the vorticity, in cylindrical coordinates, is:

$$\vec{\omega} = \nabla \times \vec{V} = \hat{i}_z \left[\frac{1}{r} \frac{\partial}{\partial r} (r v_\theta) \right] = \hat{i}_z \left[\frac{1}{r} \frac{\partial}{\partial r} \left(r \frac{A}{r} \right) \right] = 0$$



Equation 8.12a indicates that this is a vorticity-free flow, which suggests that the flow should (logically) be irrotational, and thus have no circulation. Clearly, if we consider an area integral of the vorticity, we would have:

$$\Gamma = \iint_A \vec{\omega} \cdot d\vec{A} = \iint_A (0) \cdot d\vec{A} = 0$$
(8.12b)

However, if we consider the line integral around a circle of radius R, then at $r = R$ the velocity is $\vec{V} = \frac{A}{R} \hat{i}_\theta$, and the differential vector element along the circumference is $d\vec{s} = R d\theta \hat{i}_\theta$. Thus, the circulation can be calculated as:

$$\Gamma = \oint \vec{V} \cdot d\vec{s} = \int_0^{2\pi} \left(\frac{A}{R} \right) R d\theta = A(2\pi) \neq 0!$$
(8.13)

Equation 8.13 clearly contradicts Eq. 8.12b. Why the discrepancy? The answer is that for this irrotational-type of vortex there exists one point of vorticity: a singularity at the center of rotation, $r = 0$, where an infinite spike in vorticity exists. This illustrates that the curve surrounding the vortex distribution contains all the vorticity, regardless of how small an area the vorticity is contained within, as illustrated by figure 8.3.

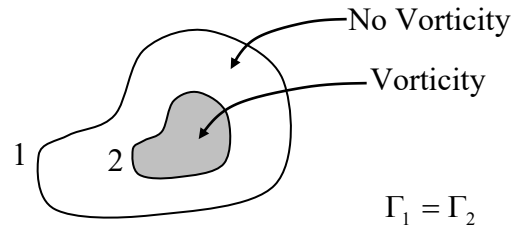


Figure 8.3 Example of two bounded regions of different area, containing the same region of vorticity, and thus having identical circulation.

This suggests that we don't have to be too exacting when choosing our boundaries from which to determine the circulation for a concentrated area of vorticity located within a region of otherwise irrotational fluid. Accordingly, we can use a boundary that encompasses not only the area containing the vorticity, but also any additional adjacent area that is devoid of vorticity. For example, if we assume that the velocity distribution within a hurricane is roughly symmetric, we could hypothetically determine the circulation strength of the hurricane by using the velocity at a boundary located well outside of the rotational core, if the additional area encompassed is reasonably irrotational.

However, if there is a concentration of vorticity within the boundaries of $r = R$, why didn't our integration of the vorticity over the area, Eq. 8.12b, give us the same answer as Eq. 8.13? Let's reexamine that integration, by using the expression for the vorticity as:

$$\bar{\omega} = \nabla \times \bar{V} = \hat{i}_z \left[\frac{1}{r} \frac{\partial}{\partial r} (r v_\theta) \right] = \hat{i}_z \left[\frac{1}{r} \frac{\partial}{\partial r} \left(r \frac{A}{r} \right) \right] = \hat{i}_z \left[\frac{1}{r} \frac{\partial}{\partial r} (A) \right] \quad (8.14)$$

Now, we integrate for the circulation over the area of a circle of radius R .

$$\Gamma = \iint_A \bar{\omega} \cdot d\bar{A} = \int_0^{2\pi} \int_0^R \hat{i}_z \left[\frac{1}{r} \frac{\partial}{\partial r} (A) \right] \cdot \hat{i}_z r dr d\theta = \int_0^{2\pi} \int_0^R \left[\frac{\partial}{\partial r} (A) \right] dr d\theta = A\theta \Big|_0^{2\pi} = A(2\pi) \quad (8.15)$$

Equation 8.15 gives the same result as Eq. 8.13 using the line integral. Since the vorticity was isolated at the origin as a discontinuity, we have to integrate the vorticity equation before taking the derivative of the velocity function. When one takes the derivative of a discontinuous function, you lose information on the discontinuity. Thus, the loss of information on circulation, as we had using our Eq. 8.12b calculation.

This reinforces the point made above that the circulation is indicative of the cumulative vorticity within the specified boundary, regardless of how it is distributed. The lesson from this? Use the line integral calculation to determine the circulation whenever possible, since it will always reveal the true circulation.

8.2.3 The Vorticity and Circulation for a Fully-Developed Channel Flow

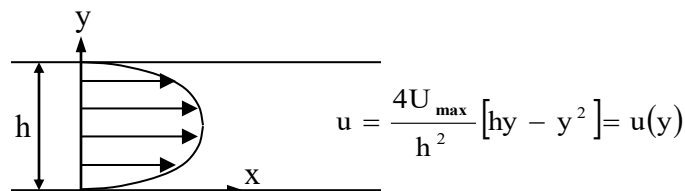


Figure 8.4 Velocity profile for a fully-developed channel flow

In Section 6.3.2, we determined the velocity profile for a Poiseuille, pressure-driven flow between the parallel surfaces of a channel. The relationship, based on the maximum centerline velocity is shown in figure 8.4. Since this is a viscous flow, we expect that this flow will contain

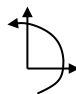
significant vorticity distributed throughout the flow, with an accompanying amount of circulation.

Here, the vorticity (in Cartesian coordinates) is given by:

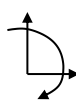
$$\vec{\omega} = \nabla \times \vec{V} = \begin{vmatrix} \hat{i} & \hat{j} & \hat{k} \\ \frac{\partial}{\partial x} & \frac{\partial}{\partial y} & \frac{\partial}{\partial z} \\ u & v & w \end{vmatrix} = \left(\frac{\partial v}{\partial x} - \frac{\partial u}{\partial y} \right) \hat{k} + (\text{zero terms}) = -\frac{\partial u}{\partial y} \hat{k}$$

$$\vec{\omega} = \omega_z \hat{k} = -\frac{4U_{\max}}{h^2} [h - 2y] \hat{k} \tag{8.16}$$

Equation 8.16 indicates a linear distribution of vorticity across the width of the channel. Examining three values of vorticity, at the two boundaries and the centerline of the flow, we have:

@ $y = h$ $\vec{\omega} = -\frac{4U_{\max}}{h^2} [h - 2h] \hat{k} = +\frac{4U_{\max}}{h} \hat{k} \Rightarrow$ 

@ $y = \frac{h}{2}$ $\vec{\omega} = 0$

@ $y = 0$ $\vec{\omega} = -\frac{4U_{\max}}{h^2} [h - 0] \hat{k} = -\frac{4U_{\max}}{h} \hat{k} \Rightarrow$ 

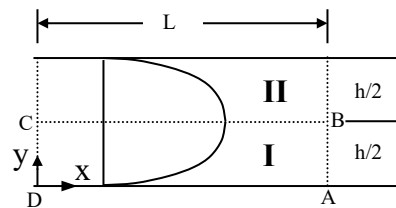
Thus, the vorticity is positive in the upper half of the channel, and negative in the lower half of the channel, and linearly distributed between these extremes, being null at the center of the channel.

To determine the circulation, we need to define a region or surface over which we want to establish the circulation strength. Since the streamwise extent of a fully-developed channel flow is indeterminate, let's examine two flow regions of an arbitrary length L: one region will lie below the centerline (region I), and the other region above the centerline (region II), as shown below. Here, we again determine the circulation strength using both (a) an integral of vorticity over a defined area, and (b) a line integral of the velocity that follows the area boundary.

For region I, using an area integral we have:

$$\Gamma_I = \int_A \vec{\omega} \cdot d\vec{A} \quad d\vec{A} = dydx \hat{k}$$

$$= \int_{x=0}^{x=L} \int_{y=0}^{y=h/2} -\frac{4U_{\max}}{h^2} [h - 2y] dydx$$



$$= -\frac{4U_{\max}}{h^2} \left[hy - y^2 \right] \Big|_0^{h/2} \Big|_0^L = -U_{\max} L$$

To determine the line integral, we employ an integration path around the region I, employing the junction points A, B, C, and D labeled above. Note that for the x-y coordinate system shown in figure 8.4, the *integration path will follow a counter-clockwise direction*, according to the right hand rule (which has the z-coordinate pointing out of the page). The direction is defined, of course, by the integration limits we impose on the sequenced integrals.

$$\begin{aligned} \Gamma_I &= \oint \vec{V} \cdot d\vec{s} = \int_A^B \vec{V}_{AB} \cdot dy\hat{j} + \int_B^C \vec{V}_{BC} \cdot dx\hat{i} + \int_C^D \vec{V}_{CD} \cdot dy\hat{j} + \int_D^A \vec{V}_{DA} \cdot dx\hat{i}, \quad \text{but } \vec{V} = u(y)\hat{i} \\ &= \underbrace{\int_{y=0}^{y=h/2} u(y)\hat{i} \cdot dy\hat{j}}_0 + \underbrace{\int_{x=L}^{x=0} U_{\max}\hat{i} \cdot dx\hat{i}}_{U_{\max}(0-L)} + \underbrace{\int_{y=h/2}^{y=0} u(y)\hat{i} \cdot dy\hat{j}}_0 + \underbrace{\int_{x=0}^{x=L} (0)\hat{i} \cdot dx\hat{i}}_0 = -U_{\max} L \\ &\qquad\qquad\qquad \underbrace{\hspace{10em}}_{-U_{\max} L} \end{aligned}$$

Thus, the area and line integral results are identical, as they should be.

Likewise, for region II, using either an area or line integral, we obtain (prove this yourself).

$$\Gamma_{II} = +U_{\max} L$$

Now if we consider the entire region between the channel walls, the total circulation of the combined regions I and II will be simply the sum of the individual circulations for both regions. Thus,

$$\Gamma_{TOT} = \Gamma_I + \Gamma_{II} = -U_{\max} L + U_{\max} L = 0 \quad \text{or no net circulation}$$

You should prove this result yourself by integrating over the collective regions I and II. This result illustrates that despite containing a significant amount of vorticity, a region can have a null amount of circulation if the total amount of positive and negative vorticity offset each other. Note that the behavior of circulation is again similar to volume flow rate, where equal amounts of positive and negative velocity flux across a specified surface would yield a null net flow rate across the surface. We will return to discuss the sources of the vorticity for this, and other viscous flows in Chapter 11.

8.3 Vortex Lines and Tubes

8.3.1 Vortex Lines

Vortex lines are lines in a flow field that are *tangent* to the vorticity vector, $\vec{\omega}$, just like a streamline is tangent to the velocity vector, \vec{V} . We define such lines in the same manner as a streamline, by setting the cross product of the vorticity with a differential element $d\vec{s}$ equal to zero, i.e.:

$$\vec{V} \times d\vec{s} = 0 \quad \Rightarrow \text{streamline equation}$$

$$\vec{\omega} \times d\vec{s} = 0 \quad \Rightarrow \text{vortex line equation}$$

For example, in Cartesian coordinates the vorticity is given by $\vec{\omega} = \omega_x \hat{i} + \omega_y \hat{j} + \omega_z \hat{k}$, and we can write an expression for a generic differential element along a vortex line as $d\vec{s} = dx \hat{i} + dy \hat{j} + dz \hat{k}$. Thus, the expanded equation for a vortex line is:

$$\vec{\omega} \times d\vec{s} = (\omega_y dz - \omega_z dy) \hat{i} + (\omega_z dx - \omega_x dz) \hat{j} + (\omega_x dy - \omega_y dx) \hat{k} \quad (8.17)$$

If we constrain a flow to two dimensions (e.g. x and y), Eq. 8.17 reduces to:

$$\vec{\omega} \times d\vec{s} = (\omega_x dy - \omega_y dx) \hat{k} \quad (8.18)$$

However, we note that for a two-dimensional flow in the x-y plane ω_x and $\omega_y = 0$, since there can be no rotation in the x or y directions. Since such a flow can only have non-zero values of ω_z , our above result implies that vortex lines (actually points) could only run perpendicular to the x-y plane in the z-direction. So for a two-dimensional flow in a plane (with no depth of flow), there can be no vortex lines, only point-wise vorticity values. Thus, unlike streamlines, a flow must be *three-dimensional* for vortex lines to have any physical relevance.

Now recall that in Chapter 2 we indicated in Eq. 2.16c that for a vector field, \vec{F} , the vector function $\nabla \cdot (\nabla \times \vec{F}) = 0$. If we now apply that relationship to a velocity field, \vec{V} , we have $\nabla \cdot (\nabla \times \vec{V}) = 0$. Since $\vec{\omega} = \nabla \times \vec{V}$, this means that $\nabla \cdot \vec{\omega} = 0$, which implies that the vorticity field is a *solenoidal* vector field --- a vector field for which the rate of expansion (i.e. divergence) of vorticity = 0. Note the similarity to the solenoidal velocity field for an *incompressible* flow, where the continuity equation reduces to $\nabla \cdot \vec{V} = 0$. This common solenoidal aspect of vorticity and an incompressible velocity field implies that vortex lines and streamlines (in incompressible flow) obey similar rules, as we will discuss in the following section.

8.3.2 Vortex Tubes

A vortex tube is like a stream tube --- i.e. a collection of vortex lines bounded by a common surface. As shown in figure 8.5, a vortex tube is similar to a stream tube, in that no vorticity will cross the surface of a vortex tube because of the requirement that the vorticity is always tangent to a vortex line.

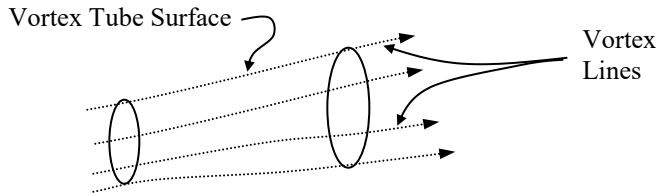
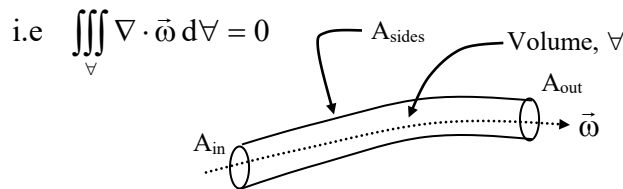


Figure 8.5 Schematic of a vortex tube

We noted in section 8.3.1 that $\nabla \cdot \vec{\omega} = 0$ everywhere within a vorticity field. Thus, if we integrate $\nabla \cdot \vec{\omega}$ over any volume of a vortex tube, \mathcal{V} , the result must also be zero. To examine how this can give us an appreciation for the circulation within a vortex tube, consider the behavior of vorticity for the model vortex tube shown in figure 8.6.



i.e. $\iiint_{\mathcal{V}} \nabla \cdot \vec{\omega} \, d\mathcal{V} = 0$

Figure 8.6 A portion of a vortex tube, with the corresponding areas bounding the tube indicated.

For a typical vortex tube shown in figure 8.6, we can employ the Gauss Divergence Theorem, Eq. 2.17, to assess the relationship of the flux of vorticity in and out of the tube. To do this, we write the volume integral of the divergence of the vorticity, $\nabla \cdot \vec{\omega}$, and use the Gauss Theorem to express the vorticity flux equivalence in terms of surface integrals over the bounding surfaces of the vortex tube as:

$$\underbrace{\iiint_{\mathcal{V}} (\nabla \cdot \vec{\omega}) \, d\mathcal{V}}_{\text{Gauss Divergence Theorem}} = \iint_{\mathcal{A}} \vec{\omega} \cdot d\vec{A} = \Gamma = \iint_{A_{in}} \vec{\omega} \cdot d\vec{A} + \iint_{A_{sides}} \vec{\omega} \cdot d\vec{A} + \iint_{A_{out}} \vec{\omega} \cdot d\vec{A} = 0 \tag{8.19}$$

$0 \Rightarrow \vec{\omega} \perp d\vec{A}_{sides}$

Recall that in the previous section, 8.3.1, we showed that vorticity is solenoidal, such that $\nabla \cdot \vec{\omega} = 0$ everywhere. Thus, it follows that the volume integral of $\nabla \cdot \vec{\omega}$ must also be zero as well.

With regard to the surface integrals of vorticity flux ($\vec{\omega} \cdot d\vec{A}$) in Eq. 8.19, only the vorticity which enters and exits a vortex tube contributes non-zero values. By our definition of a vortex tube, the side boundaries of a vortex tube are formed by vortex lines. Since the vorticity is always tangent to a vortex line, it follows that the vorticity is always tangent to the sides of the vortex tube, and thus there can be no vorticity flux across the sides of a vortex tube.

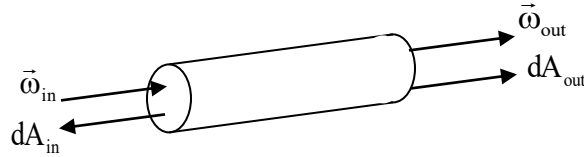


Figure 8.7 Illustration of the normal direction of the surfaces for a vortex tube relative to the vorticity entering and exiting the tube.

Noting the directional normal vectors for $d\vec{A}$ are oriented outward from the entrance and exit surfaces of a vortex tube, as shown in figure 8.7, we perform the dot products indicated in Eq. 8.19 and obtain:

$$\Gamma = -\iint_{A_{in}} \omega_{in} dA_{in} + \iint_{A_{out}} \omega_{out} dA_{out} = 0 \quad (8.20)$$

or

$$-\Gamma_{in} + \Gamma_{out} = 0$$

Equation 8.20 implies that $\Gamma_{in} = \Gamma_{out}$, or that the circulation within the vortex tube (i.e. the “strength” of the vortex tube) remains constant throughout the vortex tube. This was first proven by [Helmholtz](#), and as we will show in Chapter 10, this even extends to the temporal change for a vortex tube in an inviscid flow.

Consider the analogy of circulation to flow rate. As we know, for an incompressible velocity field, \vec{V} , the volume flow rate, Q , along a stream tube, will remain constant:

$$Q = \iint_A \vec{V} \cdot d\vec{A} = \text{constant along a stream tube}$$

Similarly, for a vorticity field, $\vec{\omega}$, the circulation strength along a vortex tube is also constant:

$$\Gamma = \iint_A \vec{\omega} \cdot d\vec{A} = \text{constant along a vortex tube}$$

Note that as the cross-sectional area of a vortex tube decreases, the average vorticity within the tube will increase; conversely, if the cross-section of a vortex tube expands, the average vorticity must correspondingly decrease. However, a vortex tube cannot shrink to zero area, since the average vorticity must remain finite. This constancy of circulation associated with a vortex tube implies that the vortex tube, or vortex filament [as we would call a vortex tube when the tube

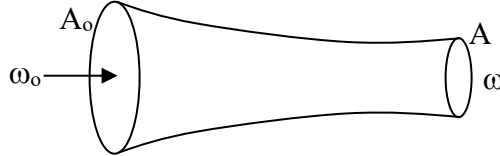
gets quite small], and by association a vortex line, cannot terminate in a fluid. For this to be true requires that a vortex tube or vortex line must either:

- (1) form a closed circuit [e.g. a vortex “ring” or loop, like a smoke ring blown by a smoker];
- (2) extend to infinity [a hypothetical circumstance];
- (3) end at a fluid-fluid boundary [e.g. at an air-water boundary, like the surface of a lake];
- (4) end at a rotating solid boundary [such that the boundary rotation matches the fluid vorticity].

Accordingly, a vortex tube cannot end at a *stationary* boundary, although one could imagine some strange form of vortical flow, with a zero vortex line at its center [and thus no velocity gradient]. This is discussed further in Section 8.3.2.2 below, and Section 10.4.

8.3.2.1 Solid-Body Rotation Along a Vortex Tube

While the assumption of solid body rotation is a bit artificial, it can be used to illustrate the process of constancy of circulation. We will examine this type of flow again later in Chapter 12 when we address the concept of vorticity transport. Here we assume that a flow enters a vortex tube with a solid body rotation, such that the *vorticity is constant* at an initial value ω_0 across a cross-section A_0 , as shown.



We designate the vorticity at any other cross-section of the vortex tube as ω , where the corresponding cross sectional area is A . The circulation strength within the vortex tube is thus established by the initial vorticity and area as $\Gamma = \omega_0 A_0$. If we assume that the flow remains in solid body rotation within the vortex tube, such that the vorticity is constant at any cross section, we have:

$$\Gamma = \omega_0 A_0 = \int_A \omega dA \approx \omega A \quad \text{or} \quad \omega \approx \frac{\omega_0 A_0}{A} = \frac{\Gamma}{A} \quad (8.21)$$

Thus, the vorticity will change inversely with the area of the vortex tube. Although Equation 8.21 was determined for a solid body rotation, the same equation applies for any vorticity distribution, and applies exactly if we consider the average vorticities at a cross-section, as indicated in Eq. 8.22.

$$\begin{aligned} A \uparrow &\Rightarrow \bar{\omega} \downarrow \\ A \downarrow &\Rightarrow \bar{\omega} \uparrow \end{aligned} \quad (8.22)$$

Equation 8.22 indicates that as a vortex tube narrows, the average vorticity will increase. This is roughly what happens when a slowly rotating fluid passes into a narrowing conduit, such as occurs when a bathtub is drained. The slowly rotating flow in the tub is constricted into a narrow exit, with a resulting marked increase in the local vorticity, reflected by a strongly rotating “bath tub vortex.” Click the following [link](#) to see such a vortex in develop at the inlet to a drain of a large lake. Note that what you see is the air core inside the vortex. Alternatively, if the vortex tube expands, the average vorticity within the vortex tube will decrease. An example here are the [trailing vortices \(i.e. vortex tubes\) from aircraft wings](#), which will undergo a decrease in vorticity as they slow and begin to expand as they trail away from the aircraft. However, the process of vortex tube expansion is a very unstable process, that degenerates very rapidly into a chaotic process termed “[vortex breakdown](#),” in which the vortex tube expands quite suddenly, rapidly dispersing and decreasing the local vorticity of the vortex tube. It should be noted, however, that this vorticity dispersion process is much more three-dimensional than the process reflected in the simple model above (as is illustrated in the video clip in the link above), and the mechanics of this break down process are still poorly understood.

8.3.2.2 The Tornado as a Vortex Tube

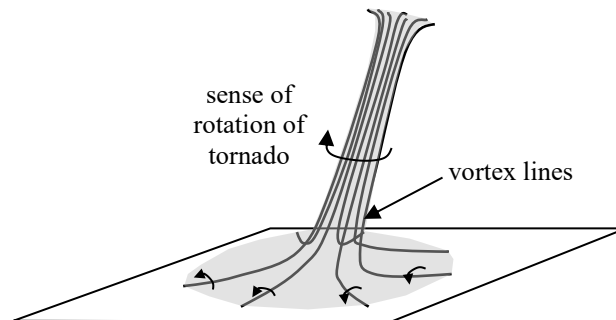


Figure 8.8 Model of a tornado as a vortex tube, comprised of vortex lines extending laterally along the earth surface. Here the vortex tube is shaded grey.

As we pointed out in section 8.3.2, a vortex tube cannot end at a *stationary* boundary, since the rotation of the boundary, and thus the vorticity would be zero. However, this raises the question of how such things as tornadoes “end”, as they impinge upon the earth. The answer is that the vortex “tube” comprising a tornado does not end at the earth’s surface, but is comprised of a collection of vortex lines that [where they appear to impinge on the earth] extend laterally away (toward infinity) from the concentrated core we view as the tornado. The general configuration of a tornado vortex tube is illustrated in Figure 8.8. Basically, this is an upward “draining” of lower density air near the earth surface into the upper atmosphere. This is also roughly the process that maintains the strength of hurricanes, which are sustained by the effects of high temperature oceans heating adjacent air layers, which becomes less dense and effectively “drain” upward, adding to the circulation of the hurricane.

Clearly, the creation of a tornado, which is a concentrated vortex tube, requires the accumulation of vorticity distributed across a broad area of land into the tornado. The source of this vorticity is due to high shearing winds, as well as strong changes in air density, which can cause both the modification and creation of vorticity. The creation and sources of vorticity is a topic we address further in Chapter 11.

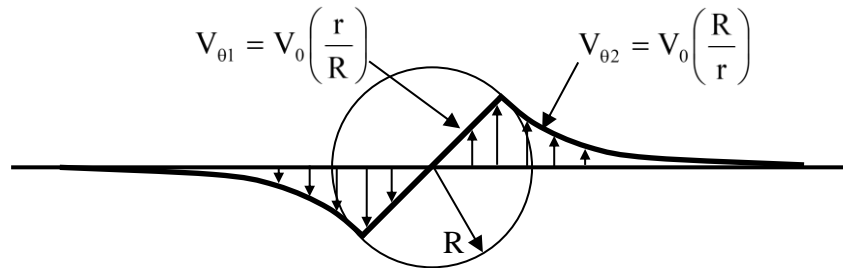
Study Problems

1. The stream function for an inviscid flow is given by

$$\psi = \left(\frac{-y}{x^2 + y^2} \right)$$

Assume all properties are dimensionless and do the following:

- a) plot the stream function $\psi = 1$ for all $y \leq 0$
 - b) determine the velocity and vorticity components for the flow field
 - c) determine the pressure differences $(P_1 - P_2)$ between P_1 at $(x,y) = (0,1)$ and P_2 at both $(x,y) = (0.5,0.5)$ and $(0,0.5)$; let $\rho = 1$.
2. If $\vec{V} = y^2\hat{i} + xz\hat{j} + x^2\hat{k}$, determine the circulation for a rectangle with vertices at $(x, y, z) = (0, 0, 0), (3, 0, 0), (3, 0, 3)$ and $(0, 0, 3)$ using both a line integral and an area integral.
3. A circular combined Rankine vortex is present in an inviscid fluid, as shown.

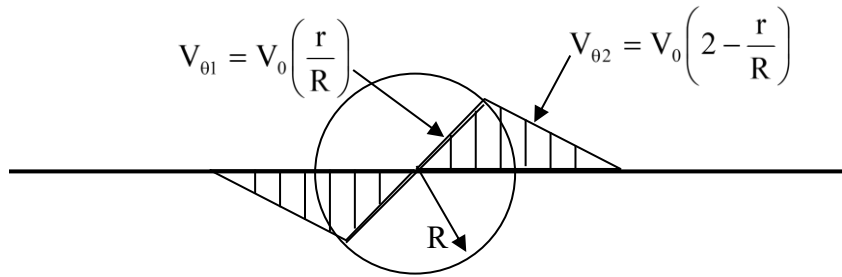


The vortex consists of a core of radius R , which is in solid body rotation with velocity $V_{\theta 1} = V_0 \left(\frac{r}{R} \right)$, and a portion outside the core ($r \geq R$) that has a velocity $V_{\theta 2} = V_0 \left(\frac{R}{r} \right)$.

Determine the following:

- a) The vorticity for the entire flow field, as a function of r . Plot or make a nice labeled sketch of ω vs. r/R .
- b) The circulation for,
 - i) a circle of radius R .
 - ii) a square of side dimensions $4R$, with the vortex in the center of the square.

4. A circular vortex is present in an inviscid fluid, as shown.



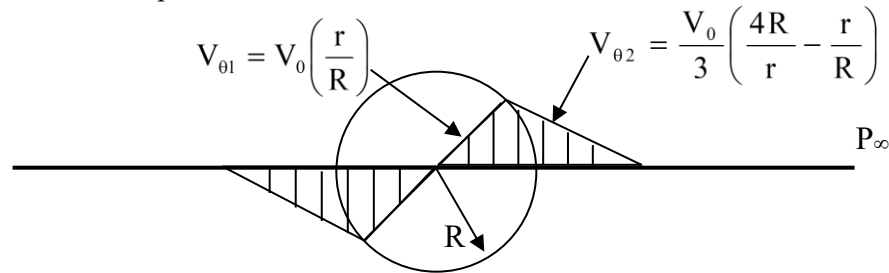
The vortex consists of a core of radius R , which is in solid body rotation with velocity

$$V_{\theta 1} = V_0 \left(\frac{r}{R} \right). \text{ The portion outside the core } (R \leq r \leq 2R) \text{ has a velocity } V_{\theta 2} = V_0 \left(2 - \frac{r}{R} \right).$$

Determine the following:

- a) The vorticity for the entire flow field, as a function of r . Plot or make a nice labeled sketch of ω vs. r/R .
- b) The circulation for,
 - i) a circle of radius R
 - ii) a square of side $4R$, with the vortex in the center of the square

5. A circular vortex is present in an inviscid fluid, as shown.



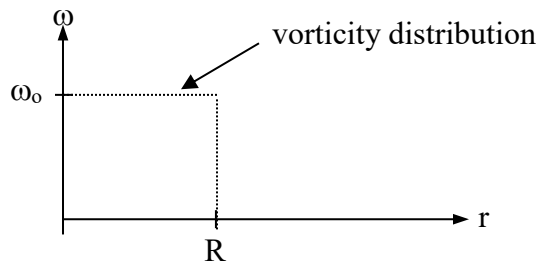
The vortex consists of a core of radius R , which is in solid body rotation with velocity

$$V_{\theta 1} = V_0 \left(\frac{r}{R} \right). \text{ The portion outside the core } (R \leq r \leq 2R) \text{ has a velocity } V_{\theta 2} = \frac{V_0}{3} \left(\frac{4R}{r} - \frac{r}{R} \right).$$

Determine the following:

- a) The vorticity for the entire flow field, as a function of r . Plot or make a nice labeled sketch of ω vs. r/R .
- b) The circulation for,
 - i) a circle of radius $r = 3R/2$
 - ii) a square of side $4R$, with the vortex is in the center of the square

6. A circular vortex in an inviscid fluid has the following vorticity distribution, ω vs. r , where, $\omega = \omega_0$ for $r \leq R_0$, and $\omega = 0$ for $r > R$.



If the velocity distribution is $\vec{V} = v_\theta \hat{i}_\theta$ only, determine the following:

- a) The velocity distribution, $v_\theta(r)$, in terms of ω_0 and r , for $r \leq R$ (assume that $v_\theta(0) = 0$).
 - b) The velocity distribution, $v_\theta(r)$, in terms of ω_0 , R , and r , for $r > R$.
 - c) The circulation for,
 - i) a circle of radius R .
 - ii) a square of side $3R$, with the vortex in the center of the square.
7. The velocity fields in a circulation preserving flow for two different vortices of radius R_1 are given by:

vortex #1: $V_\theta = 2.117V_0(r^* - r^{*4})$,

vortex #2: $V_\theta = 6.75V_0(r^{*2} - r^{*3})$,

where $r^* = r/R_1$. Determine the pressure, vorticity and circulation as a function of r^* for each vortex for $0 < r^* < 1$ (let $p = p_0$ at $r^* = 1$). On four separate graphs, comparatively plot the velocity (as $\frac{V_\theta}{V_0}$), pressure (as $\frac{p - p_0}{\rho V_0^2}$), vorticity (as $\frac{\omega_z R_1}{V_0}$), and circulation (as $\frac{\Gamma}{2\pi R_1 V_0}$) for both these vortices vs r^* , for $0 < r^* < 1$. Which vortex has: The lowest pressure? The highest circulation? The highest vorticity? How do you explain these variations?

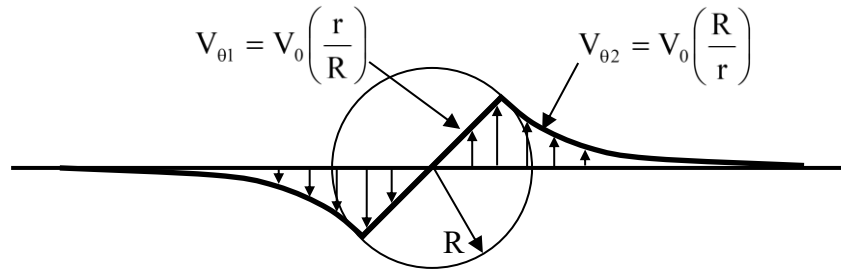
8. A solid rod of radius R rotates steadily in an infinite fluid. The surface velocity (v_0) of the rotating rod is V_0 at $r = R$ and $v_\theta = 0$ for $r \rightarrow \infty$.

Determine:

- a) The velocity of the fluid surrounding the rod, if the fluid is fully developed at steady state:
- b) The circulation Γ_C at $r = 2R$ and $r = 100R$, using a line integral of the velocity.
- c) The vorticity ω within the fluid at steady state
- d) The circulation Γ_A within the fluid by integrating the vorticity of part c) over the area encompassed from $R \leq r \leq \infty$.

Explain how parts b) and d) can both be correct.

9. A circular combined Rankine vortex is present in an inviscid fluid, as shown.



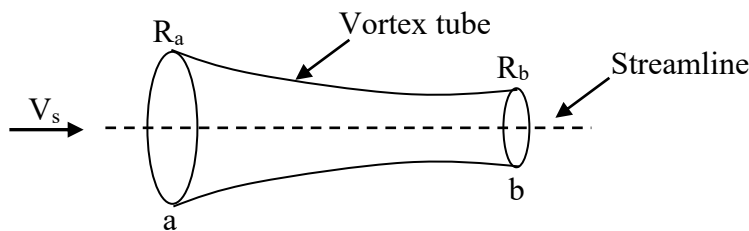
The vortex consists of a core of radius R , which is in solid body rotation with velocity $V_{\theta 1} = V_0 \left(\frac{r}{R} \right)$, and a portion outside the core ($r \geq R$) that has a velocity $V_{\theta 2} = V_0 \left(\frac{R}{r} \right)$.

Determine the following:

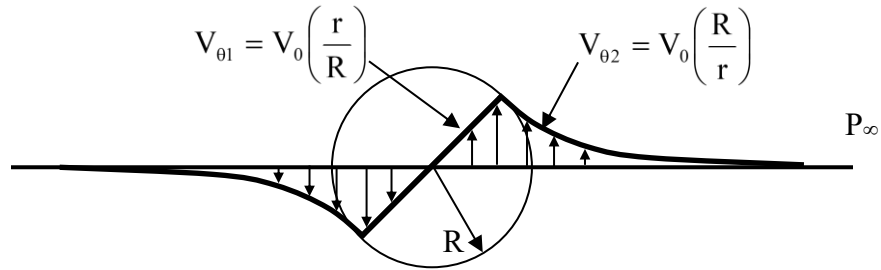
- a) The vorticity for the entire flow field, as a function of r . Plot or make a nice labeled sketch of ω vs. r/R .
- b) The circulation for,
 - i) a circle of radius R , using both an area integral of vorticity and a line integral of velocity.
 - ii) a square of side dimensions $4R$, with the vortex in the center of the square.
- c) The value of the pressure at the center of the vortex, P_o , in terms of ρ , V_0 , and P_∞ . Neglect any height changes.

This combined velocity profile exists at the beginning and end of a vortex tube in this inviscid flow, where R is the radius at any cross section of the tube (i.e. the tube contains only the solid body portion of the vortex, $V_{\theta 1}$, and the flow outside the solid body rotation is the same as $V_{\theta 2}$ above). If the center of the vortex tube is a streamline along the vortex axis, the beginning and end radii of the vortex tube are R_a and R_b , and $R_b = R_a/2$ (with corresponding velocities at the edge of the stream tube of V_{0a} and V_{0b}), will fluid flow along the axis of the vortex tube, and if so, which way and why?

Extra credit: If the velocity along the streamline at a is $V_{sa} = 0$, determine the velocity at b, V_{sb} , in terms of V_{0a} .



10. A circular combined Rankine vortex is present in an inviscid fluid, as shown.



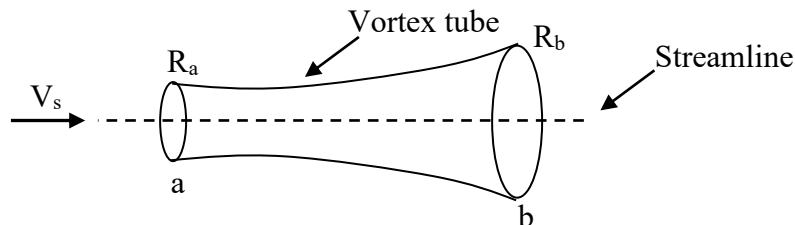
The vortex consists of a core of radius R , which is in solid body rotation with velocity $V_{\theta 1} = V_0 \left(\frac{r}{R} \right)$, and a portion outside the core ($r \geq R$) that has a velocity $V_{\theta 2} = V_0 \left(\frac{R}{r} \right)$. The density of the flow is ρ , and the pressure far away from the vortex center is P_{∞} .

Determine the following:

- a) The vorticity for the entire flow field, as a function of r . Plot or make a nice labeled sketch of ω vs. r/R .
- b) The circulation for,
 - i) a circle of radius R , using both an area integral of vorticity and a line integral of velocity.
 - ii) a square of side dimensions $4R$, with the vortex in the center of the square.
- c) The value of the pressure at the center of the vortex, P_0 , in terms of ρ , V_0 , and P_{∞} . Neglect any height changes.

This combined velocity profile exists at the beginning and end of a vortex tube in this inviscid flow, where R is the radius at any cross section of the tube (i.e. the tube contains only the solid body portion of the vortex, $V_{\theta 1}$, and the flow outside the solid body rotation is the same as $V_{\theta 2}$ above). If the center of the vortex tube is a streamline along the vortex axis, the beginning and end radii of the vortex tube are R_a and R_b , and $R_b = 2R_a$ (with corresponding velocities at the edge of the stream tube of V_{0a} and V_{0b}), will fluid flow along the axis of the vortex tube, and if so, which way and why?

Extra credit: If the velocity on the streamline at b is $V_{sb} = 0$, determine the velocity at a , V_{sa} , in terms of V_{0a} .



Chapter 9

Two-Dimensional Potential Flow Theory**Contents**

9.1	Basic Approach	246
9.2	The Stream Function, $\psi(x,y)$	246
9.3	The Potential Function, $\phi(x,y)$	247
9.4	The Pressure Field	248
9.5	The Relationship Between ψ and ϕ	250
9.6	The Complex Potential Function, $\Phi(z)$	252
9.7	Elementary Functions	253
9.7.1	Uniform, Parallel Flow	253
9.7.2	Source and Sink Flows	254
9.7.3	Point Vortices	255
9.7.4	The Doublet (dipole)	256
9.7.5	Corner and Wedge Flows	259
9.7.5.1	Concave Corner or Wedge Flow	261
9.7.5.2	Convex Corner Flow	263
9.7.6	Biasing the Origin Location for Elementary Functions	265
9.8	Superposition Flow Simulations	268
9.8.1	Flow Around a Circular Cylinder	268
9.8.2	Flow Around a Rotating Cylinder	274
9.8.3	Flow Around a Half-Body	279
9.8.4	Flow Around a Two-Dimensional Rankine Body	286
9.9	Bodies Translating in a Potential Flow	292
9.9.1	Translation of a Cylinder in a Quiescent Fluid	292
9.9.2	Pressure Field for a Translating Cylinder	296
9.10	Accelerating Bodies in a Potential Flow: Virtual/Added Mass	298
9.10.1	Acceleration of a Cylinder in a Quiescent Fluid	298
9.10.2	The Added Mass for an Accelerating Cylinder	300

In this chapter, we deal with what is variously called “ideal flow”, “irrotational flow”, and “[potential flow](#).” We consider a flow that we assume to be *incompressible*, *inviscid*, and *irrotational* (i.e. without vorticity). Obviously, no real flow truly meets these restrictions, particularly flows close to solid boundaries. However, certain types of flows come close to satisfying these assumptions, such that assessment of such idealized flows may yield reasonably

practical results. And at worst, these assumptions can often provide solutions that are good starting points, or limiting types of flows, for more complicated viscous flows.

Recall in Chapter 7 that we examined incompressible inviscid flows, which led us to the Euler and Bernoulli equations. While we were restricted in how we could apply these equations, we determined there were a number of situations for which we could effectively assess “bounding” behavior (i.e. the best-case scenarios). The same situation applies for potential flows—the solutions are restrictive, but provide the best case, limiting behavior in the absence of viscosity.

So what are some examples of where we might utilize potential flow? In regions where a uniform flow is impinging at high speed upon a solid object. In such situations, as we will discuss in Chapter 13, the Reynolds number of the flow (remember, a non-dimensional ratio of inertia to viscous forces, $Re = UL/\nu$) will generally be large, and the region of viscous behavior and deformation of the flow will be constrained to a thin region adjacent to the object, which is termed the “[boundary layer](#).” However, the flow outside this boundary layer region will behave approximately in an inviscid manner, and will be generally devoid of vorticity. So, for cases where $Re \rightarrow \infty$, the potential flow solutions can prove quite useful for flow in regions exterior to the boundary layers. As an example, consider the flow around an airfoil, as shown in figure 9.1.

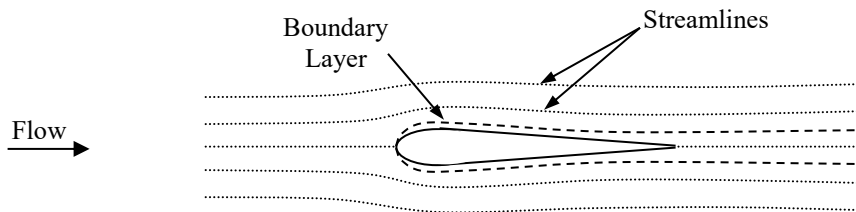


Figure 9.1 Streamline flow around an airfoil, showing a boundary layer due to viscous interaction with the airfoil surface (dotted line).

In cases where the boundary layer is minimal, the potential flow solution around the basic airfoil geometry can provide remarkably accurate information on the lift behavior for a range of airfoil shapes and angles of attack. However, the results for most practical airfoil flows is limited in application by the effects of viscosity, which will modify the resulting potential flow field due to the boundary layer development. This development of a boundary layer (shown as a dotted line in figure 9.1) will cause a displacement of the streamlines due to growth of the boundary layer. As we will discuss in Chapter 13, the developing boundary layer basically “displaces” fluid, and thus the streamlines, away from the surface.

Practical solutions for real flows over airfoils can often be determined by modeling the flow as a viscous boundary layer region adjacent to the airfoil, and an inviscid “outer” flow for the region outside the boundary layer. This two-region flow is then solved iteratively, by assuming that the velocity and pressure fields of the inviscid flow provide the boundary conditions for the velocity

and the pressure gradient at the outer edge of the boundary layer flow. The final potential flow solution can then be used to determine the resultant lift forces on the airfoil (by integrating the pressure field around the airfoil), and the boundary layer solution will yield the shear stress to help determine the drag forces on the airfoil.

Additionally, potential flow solutions indicate how an ideal flow would behave. These idealized results are then used to identify regions of the flow where we can anticipate that viscous effects will strongly modify the ideal solution (e.g. regions where strong flow deceleration is indicated). We also touch upon this in our discussion of fluid drag in Chapter 15.

9.1 Basic Approach

As we discuss above, the constraints we place upon our modeled potential flow are that it be incompressible, inviscid, and irrotational. Additionally, we require that the fluid have conservative body forces (i.e. gravity), such that the Bernoulli equation applies, which allows us to determine pressure variations based on the potential flow velocity field solutions. Since the Bernoulli equation is derived from the momentum equation (via the simplified Navier-Stokes, and subsequently the Euler equations), we need only satisfy the constraints of continuity and irrotationality ($\omega = 0$ everywhere) in order to develop a solution for the velocity field.

Recall that the incompressible continuity equation is represented by:

$$\nabla \cdot \vec{V} = 0 \quad (9.1)$$

and the irrotationality constraint is expressed by:

$$\vec{\omega} = \nabla \times \vec{V} = 0 \quad (9.2)$$

Thus, our approach will be to develop a solution technique that assures simultaneous satisfaction of both of these constraints. We will demonstrate that through the effective use of complex mathematics we can satisfy both constraint equations 9.1 and 9.2 by use of either: (a) the stream function concept we developed in Chapter 8, or (b) an alternative function termed the potential function.

9.2 The Steam Function, $\psi(x, y)$

Recall that in Chapter 8 (Section 8.1) we introduced $\psi(x, y)$ as the stream function---a function that identically satisfies the two-dimensional continuity equation, and provides a functional expression representing all streamlines for a particular flow field. In section 8.1, we showed that the velocity field is related to ψ by:

$$\mathbf{u} = \frac{\partial \psi}{\partial y} \hat{\mathbf{i}} \quad \text{and} \quad \mathbf{v} = -\frac{\partial \psi}{\partial x} \hat{\mathbf{j}}, \quad \text{or} \quad \vec{\mathbf{V}} = \frac{\partial \psi}{\partial y} \hat{\mathbf{i}} - \frac{\partial \psi}{\partial x} \hat{\mathbf{j}} \quad (9.3)$$

Substituting Eq. 9.3 into the continuity equation (Eq. 9.1), gives:

$$\nabla \cdot \vec{\mathbf{V}} = \frac{\partial u}{\partial x} + \frac{\partial v}{\partial y} = \frac{\partial^2 \psi}{\partial x \partial y} - \frac{\partial^2 \psi}{\partial x \partial y} = 0 \quad \text{thus, } \psi \text{ satisfies continuity.}$$

Now, for an irrotational flow, we know that the vorticity of the velocity field must be zero, so substituting Eq. 9.3 into Eq. 9.2 gives:

$$\nabla \times \vec{\mathbf{V}} = 0 = \frac{\partial v}{\partial x} - \frac{\partial u}{\partial y} = -\frac{\partial^2 \psi}{\partial x^2} - \frac{\partial^2 \psi}{\partial y^2}$$

or

$$\frac{\partial^2 \psi}{\partial x^2} + \frac{\partial^2 \psi}{\partial y^2} = 0 \quad (9.4)$$

We note that Eq. 9.4 is the well-known, two-dimensional [Laplace equation](#). Given the appropriate boundary conditions, the solution of Eq. 9.4 will yield the function $\psi(x,y)$, which can then be differentiated to yield the velocity field, $\vec{\mathbf{V}}$. However, the stream function can only apply in a two-dimensional plane. In order to establish a more universal function that is also applicable for three-dimensional flows, we address the solution of the two coupled equations, Eq. 9.1 and 9.2 (continuity and irrotationality), in the reverse order to derive an equation for what we term the potential function, ϕ .

9.3 The Potential Function, $\phi(x, y)$

We now stipulate a potential function, $\phi(x, y)$, for which the velocity field is given by the gradient of the potential function, $\vec{\mathbf{V}} = \nabla \phi$. In two dimensional Cartesian coordinates (x and y), the potential function is related to the velocity field components as:

$$\vec{\mathbf{V}} = u \hat{\mathbf{i}} + v \hat{\mathbf{j}} = \nabla \phi = \frac{\partial \phi}{\partial x} \hat{\mathbf{i}} + \frac{\partial \phi}{\partial y} \hat{\mathbf{j}} \quad \Rightarrow \quad u = \frac{\partial \phi}{\partial x} \quad \text{and} \quad v = \frac{\partial \phi}{\partial y} \quad (9.5)$$

Substituting the velocity functions of Eq. 9.5 into the vorticity equation, Eq. 9.2, gives:

$$\vec{\omega} = \nabla \times \vec{\mathbf{V}} = \left(\frac{\partial v}{\partial x} - \frac{\partial u}{\partial y} \right) \hat{\mathbf{k}} = \left(\frac{\partial^2 \phi}{\partial y \partial x} - \frac{\partial^2 \phi}{\partial y \partial x} \right) \hat{\mathbf{k}} = 0$$

Thus, ϕ satisfies the irrotationality condition exactly.

The potential function must also satisfy two-dimensional continuity, Eq. 9.1, which means:

$$\nabla \cdot \vec{V} = \frac{\partial u}{\partial x} + \frac{\partial v}{\partial y} = \frac{\partial^2 \phi}{\partial x^2} + \frac{\partial^2 \phi}{\partial y^2} = 0 \quad (9.6)$$

Equation 9.6 is also a Laplace equation, but now for the potential function, ϕ . Again, the solution of Eq. 9.6 will yield a function $\phi(x, y)$, from which we can also determine the velocity field via Eq. 9.5.

Note that the potential function can satisfy the irrotationality constraint in three dimensions, $\phi(x, y, z)$, not just two dimensions. To demonstrate this, consider a Cartesian system in three dimensions, such that:

$$\vec{V} = u \hat{i} + v \hat{j} + w \hat{k} = \nabla \phi = \frac{\partial \phi}{\partial x} \hat{i} + \frac{\partial \phi}{\partial y} \hat{j} + \frac{\partial \phi}{\partial z} \hat{k} \Rightarrow u = \frac{\partial \phi}{\partial x}, \quad v = \frac{\partial \phi}{\partial y}, \quad w = \frac{\partial \phi}{\partial z} \quad (9.7)$$

The vorticity in three dimensions is:

$$\vec{\omega} = \nabla \times \vec{V} = \left(\frac{\partial w}{\partial y} - \frac{\partial v}{\partial z} \right) \hat{i} + \left(\frac{\partial u}{\partial z} - \frac{\partial w}{\partial x} \right) \hat{j} + \left(\frac{\partial v}{\partial x} - \frac{\partial u}{\partial y} \right) \hat{k} \quad (9.8)$$

Substituting from Eqs. 9.7 into Eq. 9.8, we have (for a continuously differentiable function):

$$\nabla \times \vec{V} = \left(\frac{\partial^2 \phi}{\partial y \partial z} - \frac{\partial^2 \phi}{\partial z \partial y} \right) \hat{i} + \left(\frac{\partial^2 \phi}{\partial z \partial x} - \frac{\partial^2 \phi}{\partial x \partial z} \right) \hat{j} + \left(\frac{\partial^2 \phi}{\partial y \partial x} - \frac{\partial^2 \phi}{\partial x \partial y} \right) \hat{k} = 0$$

Thus, irrotationality is exactly satisfied in three-dimensions, and continuity gives us:

$$\nabla \cdot \vec{V} = \frac{\partial u}{\partial x} + \frac{\partial v}{\partial y} + \frac{\partial w}{\partial z} = \frac{\partial^2 \phi}{\partial x^2} + \frac{\partial^2 \phi}{\partial y^2} + \frac{\partial^2 \phi}{\partial z^2} = 0$$

or

$$\nabla^2 \phi = 0 \quad (9.9)$$

Equation 9.9 is again the Laplace equation, applicable in three-dimensions. The satisfaction of irrotationality and continuity in three dimensions allows the potential function to simulate flows in three dimensions, such as axisymmetric flows.

9.4 The Pressure Field

Since ψ and ϕ are both solutions to the equations for continuity and irrotationality (Eqs. 9.1 and 9.2), we could solve for either function or both. Once we have determined one or more of these functions, they can be used to establish the velocity field by the derivative functions of Eqs. 9.3

or 9.5 above. Since the flow is assumed irrotational, we can apply the incompressible form of the Bernoulli equation (7.10) everywhere to establish the pressure field.

$$\text{i.e. } \frac{P}{\rho} + gh + \frac{1}{2}V^2 + \int \frac{\partial \vec{V}}{\partial t} \cdot d\vec{s} = \text{constant} \quad (9.10)$$

Revisiting the development of Eq. 9.10 that was done in Chapter 7 (Section 7.2), we note that we can write the Euler equation for an irrotational, incompressible fluid as:

$$\frac{\nabla P}{\rho} + g\nabla h + \nabla \left(\frac{1}{2}V^2 \right) + \frac{\partial \vec{V}}{\partial t} = 0$$

or

$$\nabla \left(\frac{P}{\rho} + gh + \frac{1}{2}V^2 \right) + \frac{\partial \vec{V}}{\partial t} = 0 \quad (9.11)$$

Recall that we can write the general expression for the velocity in terms of ϕ (Eq. 9.7) as:

$$\vec{V} = u\hat{i} + v\hat{j} + w\hat{k} = \frac{\partial \phi}{\partial x}\hat{i} + \frac{\partial \phi}{\partial y}\hat{j} + \frac{\partial \phi}{\partial z}\hat{k} = \nabla \phi$$

Using this relationship, we can write:

$$\frac{\partial \vec{V}}{\partial t} = \frac{\partial (\nabla \phi)}{\partial t} = \nabla \left(\frac{\partial \phi}{\partial t} \right) \quad (9.12)$$

since x, y, z are independent variables, and not a function of time (a fourth independent variable).

Substituting Eq. 9.12 into Eq. 9.11 allows us to collect all the terms of Eq. 9.11 inside the gradient operator, such that:

$$\nabla \left(\frac{P}{\rho} + gh + \frac{1}{2}V^2 + \frac{\partial \phi}{\partial t} \right) = 0 \quad (9.13)$$

Taking a dot product of the Euler equation with $d\vec{s} = dx\hat{i} + dy\hat{j} + dz\hat{k}$, as was done in section 7.1 for an irrotational unsteady flow, Eq. 9.13 can be integrated to give:

$$\frac{P}{\rho} + gh + \frac{1}{2}V^2 + \frac{\partial \phi}{\partial t} = C(t), \quad (9.14)$$

In this modified version of the Bernoulli equation, $\frac{\partial \phi}{\partial t}$ takes care of the time dependency, and $C(t)$ is a function of time and must be determined from a known initial condition.

The key here is that we can employ the potential function *both* to determine the velocity field *and* to establish the pressure field by use of Eq. 9.14, the potential function form of the unsteady Bernoulli equation. We will show later in sections 9.9 and 9.10 that Eq. 9.14 can be used effectively (among other applications) to establish the “virtual” or “added” mass for a body accelerating through a quiescent fluid medium. The virtual/added mass is the amount of fluid mass that that moves along with a moving body, and must also be accelerated when there is a temporal change in the velocity of the moving body. This added mass can significantly affect the forces required to accelerate/decelerate the body. Added mass is minimal for heavy solid bodies, such as cars, passing through air (where air is much less dense), but is important for lighter bodies passing through a liquid medium, such as water, where the fluid is equivalent to or heavier than the body (e.g. ships, submarines, and even fish).

9.5 The Relationship Between ψ and ϕ

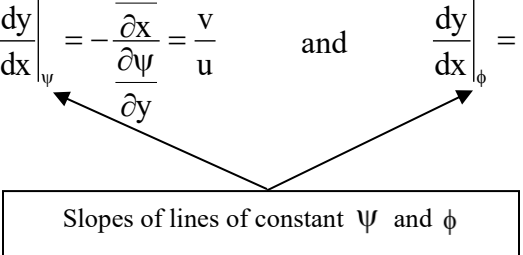
The total differentials of ψ and ϕ can be written in two-dimensions as:

$$d\psi = \frac{\partial\psi}{\partial x} dx + \frac{\partial\psi}{\partial y} dy \quad (9.15a)$$

and

$$d\phi = \frac{\partial\phi}{\partial x} dx + \frac{\partial\phi}{\partial y} dy \quad (9.15b)$$

Here we note that along a line of $\psi = \text{constant}$ we have $d\psi = 0$, and correspondingly $d\phi = 0$ along a line of $\phi = \text{constant}$. Thus, if we set $d\psi = 0$ and $d\phi = 0$ in Eqs. 9.15a and 9.15b, and solve for the slope of lines of constant ψ and ϕ , with the help of the velocity identities of Eqs. 9.3 and 9.5, we obtain:

$$\left. \frac{dy}{dx} \right|_{\psi} = - \frac{\frac{\partial\psi}{\partial x}}{\frac{\partial\psi}{\partial y}} = \frac{v}{u} \quad \text{and} \quad \left. \frac{dy}{dx} \right|_{\phi} = - \frac{\frac{\partial\phi}{\partial x}}{\frac{\partial\phi}{\partial y}} = - \frac{u}{v}$$


Slopes of lines of constant ψ and ϕ

Comparing, we have:

$$\frac{u}{v} = - \left. \frac{dy}{dx} \right|_{\phi} = \frac{1}{\left. \frac{dy}{dx} \right|_{\psi}} \quad (9.16a)$$

Recall from calculus that the relationship of the slopes shown in Eq. 9.16a is indicative of two orthogonal (perpendicular) lines. Therefore, we infer that ψ lines are orthogonal to ϕ lines.

Alternatively, we could take the dot product of the gradients (in two-dimensions) of ψ and ϕ . Recall that the gradient of ψ and ϕ will yield vectors which will always be normal to lines of constant ψ and ϕ . Substituting the relationships for the velocity components from Eqs. 9.3 and 9.5, we have:

$$\nabla\psi \cdot \nabla\phi = \left(\frac{\partial\psi}{\partial x} \hat{i} + \frac{\partial\psi}{\partial y} \hat{j} \right) \cdot \left(\frac{\partial\phi}{\partial x} \hat{i} + \frac{\partial\phi}{\partial y} \hat{j} \right) = \frac{\partial\psi}{\partial x} \frac{\partial\phi}{\partial x} + \frac{\partial\psi}{\partial y} \frac{\partial\phi}{\partial y} = -vu + uv = 0 \quad (9.16b)$$

Equation 9.16b again indicates that lines of equipotential ($\phi = \text{constant}$) and streamlines ($\psi = \text{constant}$) are *orthogonal* at all points within a flow field.

Note the similarity of potential flow theory to electric field theory, magnetic field theory, heat conduction, solid mechanics, etc., where lines of constant potential (e.g. voltage, temperature, ϕ) are normal to lines of constant flow (e.g. current, heat flow, ψ). Thus, the general solutions to Laplace's equation will satisfy all these types of similar physical phenomena.

Although we can solve for ψ or ϕ by direct solution of the Laplace equation, determining solutions for other than simple geometries can often be quite challenging. For flow in and around some simple geometries, standard closed-form solutions of the Laplace equation can be developed. However, more complicated flow geometries will generally require use of [numerical computation approaches](#). These types of analytical or numerical solutions are generally known as the *direct* method of solution (i.e. given a geometry, determine the flow field). However, by the use of complex mathematics we can develop solutions for a number of elementary flows, which can be subsequently employed in a process of linear superposition to "simulate" more complicated flows. Such a process of linear superposition is possible because both ψ and ϕ will be solutions to the Laplace equation, which is a *linear* differential equation. Recall that for linear differential equations, all solutions of the equation are directly additive [e.g. $\phi_1 + \phi_2 = \phi_{\text{total}}$, where ϕ_1 and ϕ_2 are separate solutions of the same differential equation, but subject to different boundary conditions]. Thus, we can combine any number of solutions to the Laplace equation, and their cumulative sum will also be a solution to the Laplace equation.

This process of linear superposition is generally termed the *indirect* or *inverse* method, wherein we employ judicious superposition of selected elementary solutions to create and simulate more complicated flows. Simple superposition solutions can prove quite effective in simulating the flow behavior for a number of useful flow geometries (e.g. flow around a cylinder or an ellipse). However, the simulation of the flow around a more complicated body shape using this inverse technique may require extensive numerical optimization of an array of elementary solutions. Additionally, by the use of [conformal mapping](#) techniques, simple flow geometries, such as the flow over a cylinder, can be "mapped" to simulate more geometrically complicated geometries, such as flows around airfoils. We don't cover conformal mapping techniques here, but these are fairly standard extensions of complex mathematics---see this [link](#).

9.6 The Complex Potential Function, $\Phi(z)$

Since we have shown that both ψ and ϕ are scalar point functions, satisfy the Laplace equation, and are orthogonal to each other, we can make use of [complex mathematics](#) to manipulate and solve for these functions. Using the rules of complex mathematics, we can construct in two-dimensional Cartesian coordinates a *complex potential function* defined as Φ :

$$\Phi(z) = \phi(x, y) + i\psi(x, y), \quad \text{where } z = x + iy \text{ (the complex variable)} \tag{9.17}$$

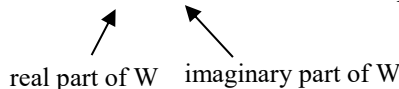
Note that Φ will be an [analytic function](#) of z since Φ and $\frac{d\Phi}{dz}$ will exist and be single-valued except at selected points. Therefore, from complex variable theory, and our previous definitions of u and v in terms of derivatives of ψ and ϕ [Eqs.9.3 and 9.5], we can write:

$$\begin{aligned} \frac{d\Phi}{dz} &= \frac{\partial\Phi}{\partial x} = -i \frac{\partial\Phi}{\partial y} \quad (\text{where } i = \sqrt{-1}) \\ &= \frac{\partial\phi}{\partial x} + i \frac{\partial\psi}{\partial x} = -i \frac{\partial\phi}{\partial y} + \frac{\partial\psi}{\partial y} = -iv + u \end{aligned} \tag{9.18a}$$

or

$$\frac{d\Phi}{dz} = u - iv \equiv \bar{W} \quad \Leftarrow \text{ the } \text{conjugate} \text{ of the complex velocity} \tag{9.18b}$$

$$\text{Thus, } W = u + iv \quad \Leftarrow \text{ the complex velocity.} \tag{9.19}$$



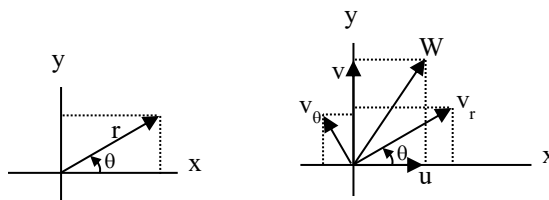
Since many flows are better suited to cylindrical symmetry (such as vortical flows), it is often more practical to express the velocity field for such flows, as well as the stream and potential functions, in cylindrical coordinates. Note that in cylindrical coordinates:

$$\Phi(z) = \phi(r, \theta) + i\psi(r, \theta), \quad \text{where } z = re^{i\theta}, \quad \text{and } r = \sqrt{x^2 + y^2}, \quad \theta = \arctan\left(\frac{y}{x}\right) \tag{9.20}$$

$$\text{Note that: } z = x + iy = r \cos \theta + ir \sin \theta = r(\cos \theta + i \sin \theta) = re^{i\theta}$$

From the velocity schematic below, we can relate u and v to the velocity components in the r, θ directions as:

$$\begin{aligned} u &= v_r \cos\theta - v_\theta \sin\theta \\ v &= v_r \sin\theta + v_\theta \cos\theta \end{aligned}$$



$$\tag{9.21}$$

Substituting Eq. 9.21 into Eq. 9.18b for the complex conjugate velocity gives:

$$\bar{W} = v_r \cos\theta - v_\theta \sin\theta - i(v_r \sin\theta + v_\theta \cos\theta) = [v_r - i v_\theta](\cos\theta - i \sin\theta)$$

or

$$\bar{W} = [v_r - i v_\theta] e^{-i\theta} \quad (9.22)$$

One could express \bar{W} in terms of cylindrical coordinates, and extract the terms for v_r and v_θ . However, a simpler alternative is to note that from complex variable theory ([Brown and Churchill, 2009](#)), the [Cauchy-Riemann conditions](#) (also see this [link](#)) in cylindrical coordinates can be shown to be:

$$\frac{\partial\phi}{\partial r} = \frac{1}{r} \frac{\partial\psi}{\partial\theta} \quad \text{and} \quad \frac{1}{r} \frac{\partial\phi}{\partial\theta} = -\frac{\partial\psi}{\partial r} \quad (9.23)$$

and

$$\frac{d\Phi}{dz} = \left[\frac{\partial\phi}{\partial r} + i \frac{\partial\psi}{\partial r} \right] (\cos\theta - i \sin\theta) = \left[\frac{\partial\phi}{\partial r} + i \frac{\partial\psi}{\partial r} \right] e^{-i\theta} = \bar{W} \quad (9.24)$$

Comparing, \bar{W} for Eq. 9.22 and 9.24, we have:

$$\bar{W} = \left[\frac{\partial\phi}{\partial r} + i \frac{\partial\psi}{\partial r} \right] e^{-i\theta} = [v_r - i v_\theta] e^{-i\theta}$$

Therefore, by comparison, and making use of the Cauchy-Riemann equations (Eq. 9.23), we obtain the cylindrical components of velocity in terms of ψ and ϕ as:

$$\begin{aligned} v_r &= \frac{\partial\phi}{\partial r} = \frac{1}{r} \frac{\partial\psi}{\partial\theta} \\ v_\theta &= -\frac{\partial\psi}{\partial r} = \frac{1}{r} \frac{\partial\phi}{\partial\theta} \end{aligned} \quad (9.25)$$

To illustrate how we incorporate the complex potential function and its component potential and stream functions, we will first examine some elementary flows that satisfy the complex potential conditions. We will then illustrate the use of these elementary flows to synthesize and simulate more complicated flows using the inverse method of superposition.

9.7 Elementary Functions

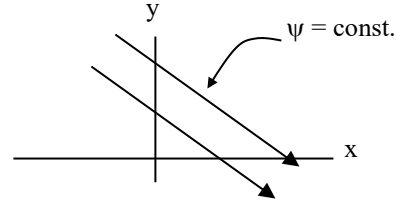
9.7.1 Uniform, Parallel Flow

The uniform flow function is a real building block of potential flow simulations, and simulates a uniform, parallel flow. This function generally provides a simulation of the *approach* flow to

various simulated bodies, such as flow around a cylinder or airfoil. Here, the complex potential function is given by:

$$\Phi(z) = (a + ib)z = \underbrace{(ax - by)}_{\phi} + i \underbrace{(ay + bx)}_{\psi} \tag{9.26}$$

Where a and b are constants. To determine the velocity of this simulated flow, we differentiate Eq. 9.26 to obtain the complex velocity.



$$\frac{d\Phi}{dz} = a + ib = \overline{W} = u - iv \quad (\text{conjugate of the complex velocity})$$

So by identity, $\left. \begin{matrix} u = a \\ v = -b \end{matrix} \right\} W = u + iv = a - ib \quad (\text{the complex velocity})$

Thus, the values of a and b determine the angle of the vector velocity relative to the coordinate system.

Special cases are:

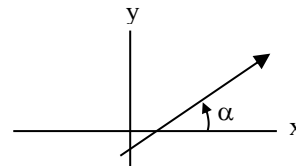
i) Flow parallel to the coordinate axis:

x-axis $\Rightarrow \Phi(z) = az \Rightarrow u = a, v = 0$ (9.27a)

y-axis $\Rightarrow \Phi(z) = -ibz \Rightarrow u = 0, v = b$ (9.27b)

ii) Flow at an angle α to the x – axis :

$$\begin{aligned} \Phi(z) &= Uze^{-i\alpha} \quad (\text{where } U \text{ is a constant}) \\ &= Uz(\cos \alpha - i \sin \alpha) \end{aligned}$$



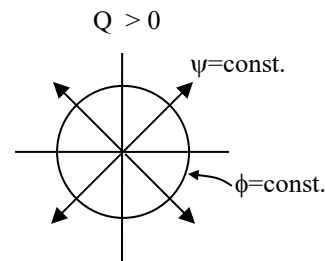
(9.27c)

9.7.2 Source and Sink Flows

These flows simulate flows that either emanate uniformly from a point (a source), or flow uniformly into a point (a sink), and are represented by a complex potential function given by:

$$\Phi(z) = \frac{Q}{2\pi} \ln(z) \tag{9.28}$$

Here, Q is a constant representing the “strength” of the function. If Q is positive (+), Eq. 9.28 represents a source; if Q is negative (-), Eq. 9.28 represents a sink.



Since source and sink flows are radially symmetric, we make use of the complex variable in cylindrical coordinates, $z = re^{i\theta}$, such that:

$$\Phi(z) = \frac{Q}{2\pi} [\mathbf{ln}r + i\theta] = \phi + i\psi$$

where,

$$\psi = \frac{Q}{2\pi} \theta \quad \text{and} \quad \phi = \frac{Q}{2\pi} \mathbf{ln}r \tag{9.29}$$

From Eq. 9.25 for cylindrical coordinates, the velocity components are given by:

$$v_r = \frac{1}{r} \frac{\partial\psi}{\partial\theta} = \frac{\partial\phi}{\partial r} \quad \text{and} \quad v_\theta = -\frac{\partial\psi}{\partial r} = \frac{1}{r} \frac{\partial\phi}{\partial\theta}$$

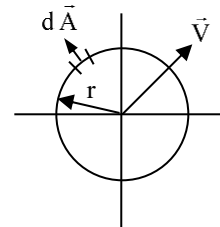
So, for a source/sink flow, the velocities in cylindrical coordinates are:

$$v_\theta = 0, \quad v_r = \frac{Q}{2\pi r} \tag{9.30}$$

Since $v_\theta = 0$, there is no azimuthal velocity (in the θ direction). Thus, this flow simulates flow radially outward or inward. If we solve for the volume flow rate (two-dimensional) for this flow, we have:

$$Q = \iint_A \vec{V} \cdot d\vec{A} \quad \text{where,} \quad \vec{V} = \frac{Q}{2\pi r} \hat{i}_r \quad \text{and} \quad d\vec{A} = r d\theta \hat{i}_r$$

$$Q = \iint_A \vec{V} \cdot d\vec{A} = \int_{\theta=0}^{2\pi} \frac{Q}{2\pi} d\theta = Q$$

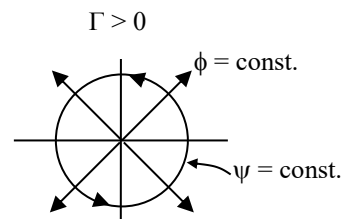


Thus, the strength of this flow, Q , is the volume flow rate (a constant).

Note that the complex potential for this flow displays a singularity and is not analytic (i.e. continuous, with a finite derivative) at the origin, $z = 0$, where the radial velocity is undefined.

9.7.3 Point Vortices

This function represents an *irrotational* vortex located at a point within the flow (nominally located at the origin, unless the position is shifted by biasing the complex variable, z — see Section 9.8.1). For a point vortex located at the origin, the complex potential function is given by:



$$\Phi(z) = -i \frac{\Gamma}{2\pi} \ln z = -i \frac{\Gamma}{2\pi} [\ln r + i\theta] = \frac{\Gamma}{2\pi} [\theta - i \ln r] = \phi + i\psi \quad (9.31)$$

So,

$$\psi = -\frac{\Gamma}{2\pi} \ln r \quad \text{and} \quad \phi = \frac{\Gamma}{2\pi} \theta \quad (9.32)$$

Here Γ is a constant reflecting the rotational “strength” of the vortex. Note that due to radial symmetry we again represent the complex variable, and its constituent stream and potential functions, in cylindrical coordinates. Here, the cylindrical velocity components are given by:

$$v_r = 0, \quad v_\theta = \frac{\Gamma}{2\pi r} \quad (9.33)$$

The rotational direction of this simulated vortex corresponds to the sign of Γ . If $\Gamma > 0$, the rotation is counter-clockwise; alternatively, if $\Gamma < 0$, the rotation is clockwise. The right-hand rule gives the sense of rotation.

Eq. 9.31 simulates an irrotational vortex with a singularity at the origin, since $\Phi(z)$ is undefined, and thus not analytic, at $z = 0$. To demonstrate this, we differentiate Eq. 9.31, giving us the conjugate complex velocity as:

$$\frac{d\Phi}{dz} = \bar{W} = -i \frac{\Gamma}{2\pi z} = -i \frac{\Gamma}{2\pi r} e^{-i\theta} = -i \frac{\Gamma}{2\pi r} (\cos\theta - i \sin\theta) = \frac{\Gamma}{2\pi r} (\sin\theta - i \cos\theta)$$

So,

$$W = u + iv = \frac{\Gamma}{2\pi r} (\sin\theta + i \cos\theta) \Rightarrow u = \frac{\Gamma}{2\pi r} \sin\theta \quad \text{and} \quad v = \frac{\Gamma}{2\pi r} \cos\theta$$

Thus, for a finite Γ , we note that \bar{W} and W are infinite at $z = 0$ ($r = 0$). Since the flow field outside of the origin ($z = 0$) is irrotational, this implies that all the vorticity for this function is concentrated at the singular point, $z = 0$, such that a point vortex violates the requirement of $\nabla \times \bar{V} = 0$ at the origin. We will discuss later how the insertion of one or more point vortices can add rotation to a simulated flow, which allows the simulation of lifting body behavior.

9.7.4 The Doublet (dipole)

The doublet is a mathematical construct that represents the linear superposition of a source of strength $+Q$ and a sink of identical, but opposite, strength, $-Q$, which are brought together at the same point (in this case, the coordinate origin). To understand how we develop this hypothetical function, consider the following schematic that shows the general streamline pattern for a source $+Q$ located at $x = -a$, and a sink $-Q$ located at $x = +a$.

The complex potential function for this superposed source/sink combination is given by (see [Section 9.7.6](#) to see how we use superposition and biasing to create this function):

$$\Phi_s(z) = \frac{Q}{2\pi} \ln(z+a) - \frac{Q}{2\pi} \ln(z-a) = \frac{Q}{2\pi} \ln\left(\frac{z+a}{z-a}\right) \quad (9.34)$$

We designate the strength of a doublet as $s = Qa/\pi$, where s is held constant while the value of a is shrunk to zero in the limit [i.e. the source and sink are brought together in such a way that they produce a new complex potential function, $\Phi(z)$]. So,

substituting $Q = \frac{s\pi}{a}$ into Eq. 9.34,

rearranging, and taking the limit as $a \rightarrow 0$, we obtain:

$$\Phi(z) = \lim_{a \rightarrow 0} \Phi_s(z) = s \lim_{a \rightarrow 0} \left[\frac{\ln(z+a) - \ln(z-a)}{2a} \right] = \frac{0}{0}$$

which is indeterminate. To establish the limit, we apply [L'Hospital's Rule](#), differentiating with respect to a :

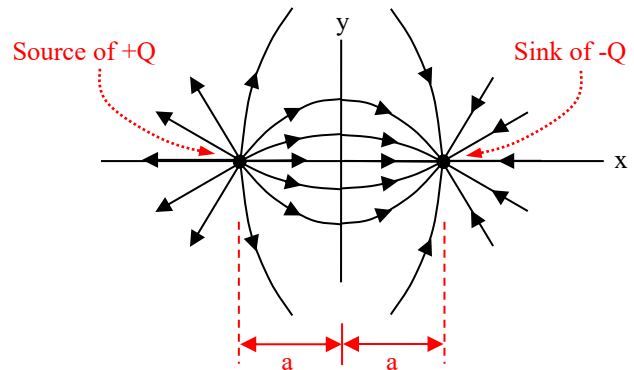
$$\Phi(z) = s \lim_{a \rightarrow 0} \left[\frac{\frac{1}{z+a} + \frac{1}{z-a}}{2} \right] = s \lim_{a \rightarrow 0} \left[\frac{(z-a) + (z+a)}{2(z+a)(z-a)} \right] = s \lim_{a \rightarrow 0} \frac{2z}{2(z^2 - a^2)} = s \frac{2z}{2z^2} = \frac{s}{z}$$

Thus, the complex potential function for a doublet (centered on the origin) in Cartesian coordinates is:

$$\begin{aligned} \Phi(z) &= \frac{s}{z} = \frac{s}{x+iy} = \frac{s}{x+iy} \left(\frac{x-iy}{x-iy} \right) = \frac{sx - isy}{x^2 + y^2} \\ \Rightarrow \phi &= \frac{sx}{x^2 + y^2} \quad \text{and} \quad \psi = \frac{-sy}{x^2 + y^2} \end{aligned} \quad (9.35)$$

or in cylindrical coordinates:

$$\begin{aligned} \Phi(z) &= \frac{s}{z} = \frac{s}{r e^{i\theta}} = \frac{s e^{-i\theta}}{r} = \frac{s}{r} (\cos\theta - i \sin\theta) \\ \Rightarrow \phi &= \frac{s}{r} \cos\theta \quad \text{and} \quad \psi = -\frac{s}{r} \sin\theta \end{aligned} \quad (9.36)$$



The streamline patterns ($\psi = \text{constant}$) for a doublet are established by noting that if we let $\psi = \text{constant}$, from Eq. 9.35 we can write:

$$\psi = \frac{-sy}{x^2 + y^2} = \text{constant} \tag{9.37}$$

Rearranging Eq. 9.37 gives:

$$x^2 + y^2 + \frac{sy}{\psi} = 0 \quad \text{or} \quad x^2 + \left(y + \frac{s}{2\psi}\right)^2 = \left(\frac{s}{2\psi}\right)^2 \tag{9.38}$$

Equation 9.38 represents a set of nested circles of diameter $D = \frac{s}{\psi}$ with their centers at

$x = 0, y = \frac{s}{2\psi}$. All the streamlines will be tangent to the x-axis at $y = 0$, as shown in figure 9.2.

Note that the $\psi > 0$ and $\psi < 0$ streamlines give reflected circle patterns about the x-axis.

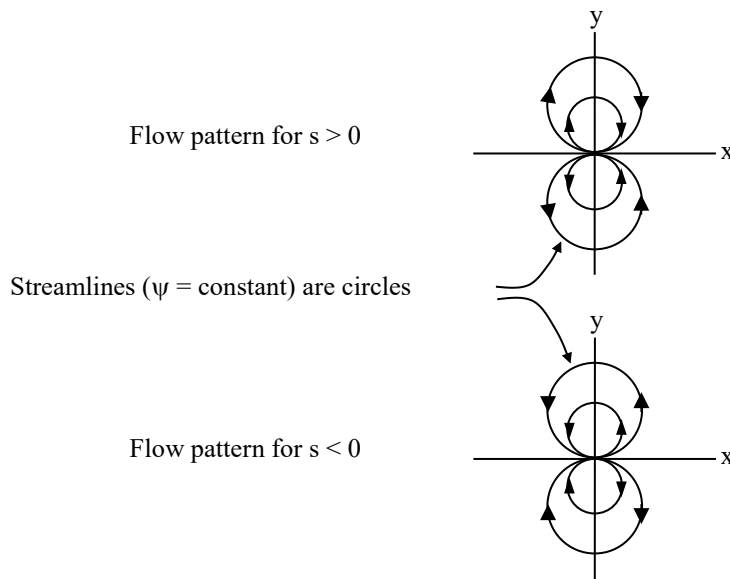


Figure 9.2 Doublet streamline patterns for $s > 0$ and $s < 0$.

Again, like the point source and point vortex, the doublet flow displays a singularity and is not analytic at the origin, with the velocity at the origin being similarly undefined.

The velocity components for a doublet flow are given by:

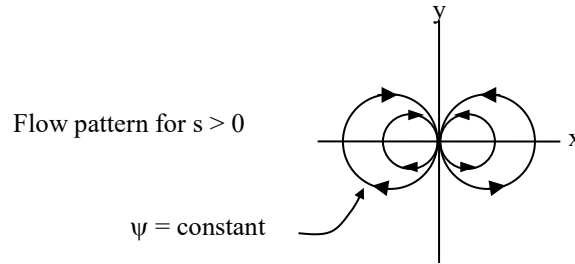
$$v_r = -\frac{s}{r^2} \cos\theta \quad \text{and} \quad v_\theta = \frac{s}{r^2} \sin\theta \quad (\text{cylindrical coordinates}) \tag{9.39}$$

$$u = -\frac{s(x^2 - y^2)}{(x^2 + y^2)^2} \quad \text{and} \quad v = -\frac{2sxy}{(x^2 + y^2)^2} \quad (\text{Cartesian coordinates}) \tag{9.40}$$

Note that since we asymptote the source/sink pair to $z = 0$ along the x-axis, the function

$\Phi(z) = \frac{S}{z}$ aligned along the x, or real axis. However, if we asymptote the source/sink pair to $z =$

0 along the y (imaginary) axis, the corresponding doublet becomes $\Phi(z) = i\frac{S}{z}$, with streamlines appearing as nested circles tangent to the y axis, as shown below.



Although a bit cumbersome, and generally not worth the effort, one can also configure the complex potential function for doublets with axes lying off the primary axes of the complex plane.

While not a particularly useful function by itself (in fluid mechanics), when the doublet is superposed with a uniform flow, the resulting pattern simulates the inviscid, two-dimensional flow over a cylinder, as we will show in [Section 9.8.2](#).

9.7.5 Corner and Wedge Flows

These are flows which simulate a flow either around a corner or impinging upon a wedge shape. The complex potential function for both of these types of flow is given by:

$$\Phi(z) = \frac{A}{n} z^n = \frac{A}{n} (x + iy)^n \quad (9.41)$$

Here, A and n are constants. The constant A controls the strength and direction of the simulated flow; the type of flow pattern that this function simulates depends on the magnitude of the exponent, n. In essence, this potential function reflects the [conformal mapping](#) of a uniform parallel flow (Section 9.7.1) onto either a larger or smaller plane.

Because explicit velocity components for u and v can only be determined in the Cartesian coordinate system for integer powers of n, it is often more functional to represent this complex potential function using cylindrical variables as:

$$\Phi(z) = \frac{A}{n} (r e^{i\theta})^n = \frac{Ar^n}{n} e^{in\theta} = \frac{Ar^n}{n} (\cos n\theta + i \sin n\theta) \quad (9.42)$$

which gives:

$$\phi = \frac{Ar^n}{n} \cos n\theta \quad \text{and} \quad \psi = \frac{Ar^n}{n} \sin n\theta \quad (9.43)$$

For these flows, streamlines are lines of constant ψ , with $\psi = 0$ representing the bounding geometric streamline. The bounding streamlines for $\psi = 0$ are simulated by straight lines passing through the origin at angles of $\theta = 0$ and $\theta = \pi/n$. Of course symmetry also dictates that lines along the angles $\theta = 2\pi/n$, $\theta = 3\pi/n$, $\theta = 4\pi/n$, can also represent a “bounding” streamline. Which of these bounding streamlines we employ depends on the particular portion of the velocity plane that is relevant to our simulation, as we will demonstrate.

Note that the complex velocity for this function is given by:

$$\frac{d\Phi}{dz} = \bar{W} = Az^{n-1} = A(x+iy)^{n-1} = Ar^{n-1}e^{i(n-1)\theta} = Ar^{n-1}[\cos(n-1)\theta + i\sin(n-1)\theta] \quad (9.44a)$$

$$\bar{W} = u - iv = Ar^{n-1}[\cos(n-1)\theta + i\sin(n-1)\theta]$$

So that

$$W = u + iv = Ar^{n-1}[\cos(n-1)\theta - i\sin(n-1)\theta] \quad (9.44b)$$

Thus, the Cartesian velocity components (in terms of cylindrical variables) are:

$$u = Ar^{n-1} \cos[(n-1)\theta] \quad \text{and} \quad v = -Ar^{n-1} \sin[(n-1)\theta] \quad (9.45)$$

However, the cylindrical velocity components are given by:

$$v_r = \frac{1}{r} \frac{\partial \psi}{\partial \theta} = Ar^{n-1} \cos(n\theta) \quad \text{and} \quad v_\theta = -\frac{\partial \psi}{\partial r} = Ar^{n-1} \sin(n\theta) \quad (9.46)$$

Examining Eqs. 9.45 and 9.46 indicates that the value of the exponent, n , markedly affects the value of the velocity, \vec{V} , at and near the origin, $r = 0$. Note that for $r = 0$, when $n > 1$, $r^{n-1} \rightarrow 0$ and $\vec{V} = 0$ at the origin, which is a stagnation type of flow. However, for $r = 0$ with $n < 1$, $r^{n-1} \rightarrow \infty$ and \vec{V} will become infinite at the origin. We will discuss and illustrate this curious variance in behavior, and the implications for the type of flow this function simulates in the following two sections.

As we mentioned above, $\Phi(z) = \frac{A}{n} z^n$ maps (termed [conformal mapping](#)) a uniform flow into a smaller or larger region of the complex flow plane. For $n > 1$, the flow is mapped into a *smaller* region of the complex plane, simulating a stagnation type flow behavior.

However, for $n < 1$, the flow is mapped into a *larger* region of the complex plane, simulating flows that have infinite velocity at the origin.

The reader should also note two further points. First, when $n = 1$, the complex potential function of course reduces to $\Phi(z) = Az$, which is just a uniform, parallel flow, as described in section 9.7.1. Secondly, the sign of the constant A dictates the direction of the simulated flow impingement. For $A > 0$ the flow will be from the left to right (depending on the value of n); for $A < 0$ the flow is reversed, and will be from the right to left.

9.7.5.1 Concave Corner or Wedge Flow (stagnation flow)

These flows are represented by exponent values $n > 1$, and simulate inviscid flow patterns characteristic of a concave corner or a wedge, as shown. Note that this can be viewed as a wedge flow because of the symmetry of the solution about the x-axis, which simulates the junction of two symmetric concave corners, as shown in figure 9.3b.

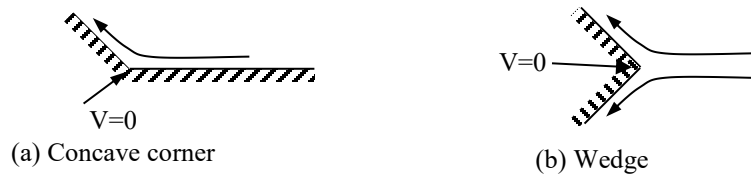


Figure 9.3 Illustration of a simulated (a) concave corner flow, and (b) wedge flow.

These types of flows have a stagnation point at the origin, and characterize a broad variety of impingement type flows.

Example: Let $n = 2$: Simulates a flow impinging on a corner or normal to a flat plate.

Using Eq. 9.41, $\Phi(z) = \frac{A}{2} z^2$, giving a stream function $\psi = A \frac{r^2}{2} \sin 2\theta$.

To establish the boundaries of the geometry, we set $\psi = 0$, which means that:

$$\sin 2\theta = 0 \Rightarrow 2\theta = 0, \pi, 2\pi, 3\pi, \dots$$

such that $\theta = 0, \frac{\pi}{2}, \pi, \frac{3\pi}{2}, \dots$ all represent four possible body boundaries, which are considered in sets of two; two possible boundary sets (hash marked) are shown in figure 9.4.

The selection of the boundaries in figure 9.4, since the flow is symmetric within each quadrant, depends on the type of flow to be simulated. Figure 9.4a represents an impinging flow in one corner, or quadrant of the flow field. Since viscosity is not an issue for these simulated flows, the combination of two adjacent 90° corners (concave corners), like that shown in figure 9.4a,

will simulate the impingement upon a semi-infinite flat plate oriented perpendicular to the impingement direction, as shown in figure 9.4b.

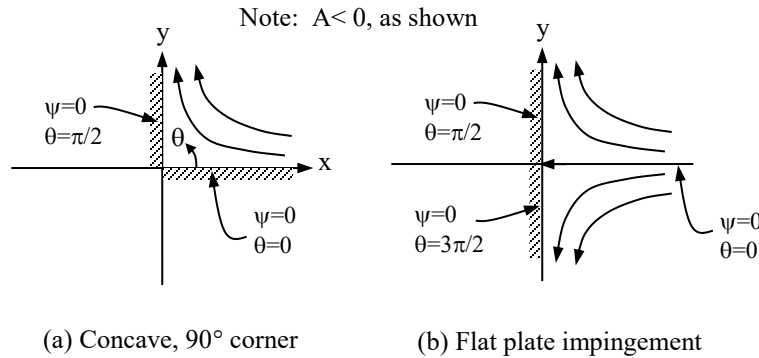


Figure 9.4 Simulated flow impinging in a 90° corner, and on a flat surface.

To establish the velocity components for the flows depicted in figure 9.4, we differentiate the complex potential function:

$$\overline{W} = \frac{d\Phi}{dz} = Az = Ax + iAy = u - iv$$

$$u = Ax$$

$$v = -Ay$$

Note that the sign of A reflects the direction of the simulated flow. If $A < 0$, the streamlines will be as shown in figure 9.4 (impinging from the right); if $A > 0$, the streamlines would be reversed, exiting to the right, as if the flows are converging from top (and bottom for figure 9.4b), and deflecting to the right (i.e. the arrows would be reversed in figure 9.4).

Example: Let $n = 3/2$, simulating an impinging flow on a shallower corner or pointed wedge.

For this flow, Eq.9.41 gives $\Phi(z) = \frac{2A}{3} z^{\frac{3}{2}}$, with a corresponding stream function,

$$\psi = \frac{2A}{3} r^{\frac{3}{2}} \sin \frac{3}{2} \theta.$$

To establish the boundaries of the geometry, we set $\psi = 0$, which means that:

$$\sin \frac{3}{2} \theta = 0 \Rightarrow \theta = 0, \frac{2\pi}{3}, \frac{4\pi}{3}, 2\pi (= 0)$$

The possible boundaries represented by this flow are shown in figure 9.5.

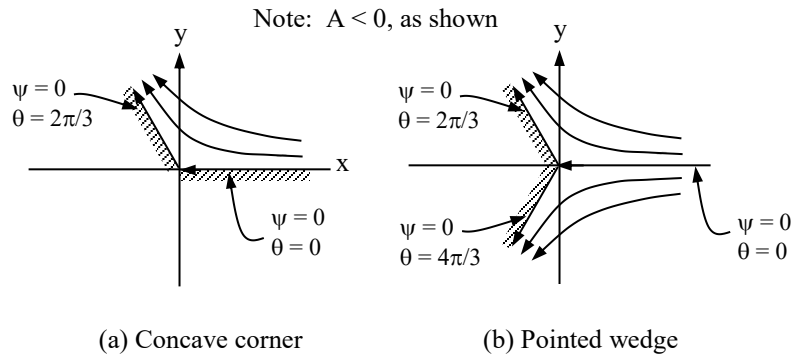


Figure 9.5 Simulated impinging flow in (a) a 120° corner, and (b) a pointed wedge.

Note that these flows are again symmetric between the upper and lower half of the complex plane. Here the flow simulated in figure 9.5a utilizes only the upper half of the plane to simulate a concave ($\theta = 120^\circ$) corner. Again, the combination of the symmetric flow patterns for both the top and bottom planes will simulate the behavior of a pointed wedge, as shown in figure 9.5b. The complex conjugate velocity for this flow in Cartesian coordinates is:

$$\bar{W} = \frac{d\Phi}{dz} = Az^{\frac{1}{2}} = A\sqrt{x+iy} = u - iv \tag{9.47}$$

Equation 9.47 is not functionally useful for establishing the velocity field, since the function is implicit. However, in cylindrical coordinates we can establish, from Eq. 9.44a:

$$\frac{d\Phi}{dz} = \bar{W} = u - iv = Ar^{\frac{1}{2}}e^{i\frac{\theta}{2}} = Ar^{\frac{1}{2}}\left[\cos\frac{\theta}{2} + i\sin\frac{\theta}{2}\right]$$

such that we can develop explicit velocity component equations:

$$u = Ar^{\frac{1}{2}}\cos\frac{\theta}{2} \quad \text{and} \quad v = -Ar^{\frac{1}{2}}\sin\frac{\theta}{2}$$

Note that for $r \rightarrow 0$, $u = 0$ and $v = 0$, so this is again a stagnation type of flow.

9.7.5.2 Convex Corner Flow (infinite corner velocity)

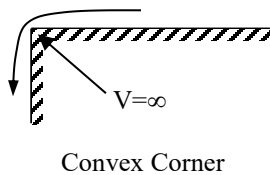


Figure 9.6 Schematic of inviscid flow over a convex corner.

For exponent values $n < 1$, the complex potential function $\Phi(z) = \frac{A}{n} z^n$ simulates flow patterns which are characteristic of what we will term a convex corner as shown in figure 9.6. These types of flows are characterized by bounding streamlines that simulate wall angles of $\theta > 180^\circ$, resulting in an infinite velocity at the origin for the simulated flow. Since real flows abhor infinite velocities, a real flow would adapt to these convex corner flows through the generation of significant viscous forces, which would significantly modify both the velocity and the pressure fields, both near and downstream of the corner region. However, examination of these inviscid flows allows one to anticipate problems that can be expected in real flow situations where rapid velocity changes occur, such as in the vicinity of sharp, convex corners. Such simulations can also assess (via modified inviscid solutions) ways that such regions might be avoided, or minimized in real flow situations. Interestingly, the flow problems encountered for sharp, convex corner geometries are similar to the [stress concentration](#) problems that accompany sharp corner geometries in the cutting or fabrication of metals and other solid materials.

Example: Let $n = 2/3$ and $n = 1/2$, respectively, simulating flows over:

- (a) a 90° step (a 270° corner), and
- (b) a 360° flow around the end of a finite plate.

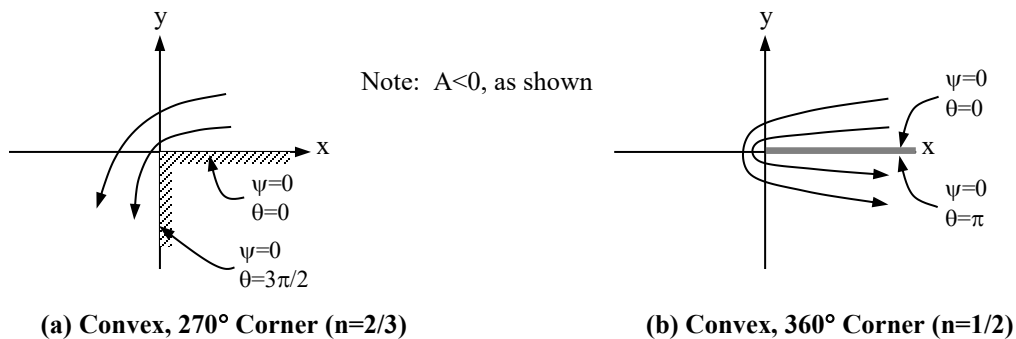


Figure 9.7 Simulated flow over (a) 270° and (b) 360° convex corners.

Again, using Eq. 9.41, these flows are simulated respectively by:

$$\Phi(z) = \frac{3A}{2} z^{\frac{2}{3}} \quad \text{and} \quad \Phi(z) = 2Az^{\frac{1}{2}}$$

with corresponding stream functions given by Eq. 9.43 as:

$$\psi = \frac{3Ar^{\frac{2}{3}}}{2} \sin \frac{2\theta}{3} \quad \text{and} \quad \psi = 2Ar^{\frac{1}{2}} \sin \frac{\theta}{2}$$

The corresponding boundaries of the geometries, for $\psi = 0$, are:

$$\sin \frac{2\theta}{3} = 0 \Rightarrow \theta = 0 \text{ and } \frac{3\pi}{2} \text{ for a } 270^\circ \text{ corner}$$

$$\sin \frac{\theta}{2} = 0 \Rightarrow \theta = 0 \text{ and } \pi \text{ for } 360^\circ \text{ flow around a finite plate}$$

Since all flows for $n < 1$ will yield implicit velocity fields in Cartesian coordinates, we again express the Cartesian velocities in cylindrical coordinates using Eq. 9.45 as:

$$u = Ar^{-\frac{1}{3}} \cos \frac{\theta}{3} \text{ and } v = Ar^{-\frac{1}{3}} \sin \frac{\theta}{3} \text{ for a } 270^\circ \text{ corner, and}$$

$$u = Ar^{-\frac{1}{2}} \cos \frac{\theta}{2} \text{ and } v = Ar^{-\frac{1}{2}} \sin \frac{\theta}{2} \text{ for } 360^\circ \text{ flow around a plate.}$$

Here, the velocity field is dominated by the inverse powers of r , which results in an infinite velocity at $r = 0$, and very high accelerations near the origin.

9.7.6 Biasing the Origin Location for Elementary Functions

Except for the uniform, parallel flow of section 9.7.1, all of the other elementary functions we examined had their origin located at $x, y = 0, 0$ ($z = 0$) in the complex plane. However, when performing a linear superposition process it is often useful, and necessary, to locate the functional origin of a superposed elementary function at a location other than the origin of the complex plane. To locate an elementary function at a position removed from the complex origin, we simply substitute a modified complex variable (z'), biased to the desired origin for the function (z_0), such that $z' = z - z_0$. For example, a source having its origin at z_0 would be written:

$$\Phi(z) = \frac{Q}{2\pi} \ln z' = \frac{Q}{2\pi} \ln(z - z_0)$$

This seems simple enough, but this can be tricky when trying to establish explicit stream and potential functions, from which to derive the velocity components. If we substitute $z = x + iy$ and $z_0 = x_0 + iy_0$ into the complex potential function for the source, we obtain:

$$\Phi(z) = \frac{Q}{2\pi} \ln z' = \frac{Q}{2\pi} \ln[(x - x_0) + i(y - y_0)]$$

for which ψ and ϕ are implicit. To allow the determination of explicit functions for ψ and ϕ , we need to again employ cylindrical coordinates biased to the origin of the function, x_0, y_0 , where

$$z' = r' e^{i\theta'}, \text{ and } r' = \sqrt{(x - x_0)^2 + (y - y_0)^2} \quad \text{and} \quad \theta' = \tan^{-1} \left[\frac{y - y_0}{x - x_0} \right].$$

Thus, the complex potential function can be written as:

$$\begin{aligned}\Phi(z) &= \frac{Q}{2\pi} \ln z' = \frac{Q}{2\pi} \ln r' e^{i\theta'} = \frac{Q}{2\pi} [\ln r' + i\theta'] \\ &= \frac{Q}{2\pi} \left[\ln \sqrt{(x-x_0)^2 + (y-y_0)^2} + i \tan^{-1} \left[\frac{y-y_0}{x-x_0} \right] \right] = \phi + i\psi\end{aligned}$$

And thus,

$$\phi = \frac{Q}{2\pi} \left[\ln \sqrt{(x-x_0)^2 + (y-y_0)^2} \right] \quad \text{and} \quad \psi = \frac{Q}{2\pi} \tan^{-1} \left[\frac{y-y_0}{x-x_0} \right]$$

Clearly, this process makes the determination of the appropriate functions a bit more cumbersome. The determination of the velocity components for these off-origin locations can be obtained either by differentiation of the complex potential function or through the appropriate differentiation of the component functions ψ and ϕ , whichever is simpler. For example, to obtain u for the above example of a two-dimensional source located at $z_0 = x_0 + iy_0$ we can write:

$$\begin{aligned}\frac{d\Phi}{dz} &= \frac{Q}{2\pi} \frac{1}{(z-z_0)} = \frac{Q}{2\pi} \frac{1}{[(x-x_0) + i(y-y_0)]} = \frac{Q}{2\pi} \frac{[(x-x_0) - i(y-y_0)]}{(x-x_0)^2 + (y-y_0)^2} \\ &= \frac{Q}{2\pi} \frac{[(x-x_0) - i(y-y_0)]}{r'^2} = u - iv \equiv \bar{W}\end{aligned}$$

thus,

$$u = \frac{Q}{2\pi} \frac{(x-x_0)}{r'^2} \quad \text{and} \quad v = \frac{Q}{2\pi} \frac{(y-y_0)}{r'^2}$$

Alternatively, we could differentiate ϕ or ψ via the Cauchy conditions:

$$\begin{aligned}u &= \frac{\partial \phi}{\partial x} = \frac{Q}{2\pi} \frac{\partial}{\partial x} \left[\ln \sqrt{(x-x_0)^2 + (y-y_0)^2} \right] \\ &= \frac{Q}{2\pi} \frac{\frac{\partial}{\partial x} [(x-x_0)^2 + (y-y_0)^2]^{\frac{1}{2}}}{[(x-x_0)^2 + (y-y_0)^2]^{\frac{1}{2}}} = \frac{Q}{2\pi} \frac{(x-x_0)}{[(x-x_0)^2 + (y-y_0)^2]} = \frac{Q}{2\pi} \frac{(x-x_0)}{r'^2}\end{aligned}$$

and similarly,

$$v = \frac{\partial \phi}{\partial y} = \frac{Q}{2\pi} \frac{(y-y_0)}{[(x-x_0)^2 + (y-y_0)^2]} = \frac{Q}{2\pi} \frac{(y-y_0)}{r'^2}$$

These yield the same functional expressions for u and v .

Note that expressions for ψ and ϕ at z_0 for point vortices are quite similar to the expressions for the source/sink flows, and thus the expressions for position-biased stream and potential functions, as well as the velocity components, will have a form similar to the point source/sink flows.

However, the doublet is a bit different. The location of a doublet at z_0 yields a complex potential function of:

$$\Phi(z) = \frac{s}{z - z_0} = \frac{s}{(x - x_0) + i(y - y_0)} = \frac{s(x - x_0) - is(y - y_0)}{(x - x_0)^2 + (y - y_0)^2} = \frac{s(x - x_0)}{r'^2} - i \frac{s(y - y_0)}{r'^2}$$

For the velocity we note:

$$\frac{d\Phi}{dz} = -\frac{s}{(z - z_0)^2} = -\frac{s}{[(x - x_0) + i(y - y_0)]^2} = -\frac{s[(x - x_0) - i(y - y_0)]^2}{[(x - x_0)^2 + (y - y_0)^2]^2} = \bar{W} = u - i v$$

From which one can show,

$$u = -\frac{s[(x - x_0)^2 - (y - y_0)^2]}{r'^4} \quad \text{and} \quad v = -\frac{2s(x - x_0)(y - y_0)}{r'^4}$$

Considering corner/wedge flows, the complex potential function for these geometries centered on z_0 is given by:

$$\Phi(z) = \frac{A}{n}(z - z_0)^n = \frac{A}{n}[(x - x_0) + i(y - y_0)]^n$$

or

$$\Phi(z) = \frac{A r'^n}{n} (\cos n\theta' + i \sin n\theta')$$

where

$$r' = \sqrt{(x - x_0)^2 + (y - y_0)^2} \quad \text{and} \quad \theta' = \tan^{-1} \left[\frac{y - y_0}{x - x_0} \right]$$

Either of these formulations is cumbersome, particularly for establishing the boundary of simulated bodies via a constant stream function, ψ . For the Cartesian form, the stream and potential functions can only be expressed as explicit algebraic functions of x and y for *integer* values of n . As we will see, establishing explicit expressions are needed to establish the bounding streamlines for a simulation, and thus the body shape. However, when dealing with fractional values of n , the cylindrical form of the complex potential function must be used, which renders the stream and potential functions trigonometric, such that positional expressions for x, y lying on bounding streamlines are generally implicit, and must be dealt with iteratively.

9.8 Superposition Flow Simulations

We have shown in sections 9.2 and 9.3 that both ψ and ϕ are solutions to the Laplace equation. Since the Laplace equation is a *linear* differential equation, that means that all solutions for ψ and ϕ are directly additive by a process of linear superposition. That is, the sum of a set of separate solutions is still a solution to the equation. As discussed in section 9.5, this process of linear superposition is termed the indirect or inverse method, since it does not allow us directly to determine the velocity field for a specified geometry. Instead, we employ this indirect approach to superpose a set of judiciously selected flow functions (ψ or ϕ), examine the velocity patterns they collectively simulate, and then associate those patterns with flows around/through geometries which approximate the bounding streamlines. Taken to its extreme, this process can be used iteratively to develop flows for somewhat complicated geometries through the optimized superposition of a large number of elementary functions. In this section, we illustrate the basic superposition approach to simulate several simple flow geometries. However, having called them “simple,” one may often find that the reduction of the superposed solutions to equations describing the respective body shape, velocity, and pressure distributions can be somewhat challenging to do in closed form, as will be demonstrated.

9.8.1 Flow Around a Circular Cylinder

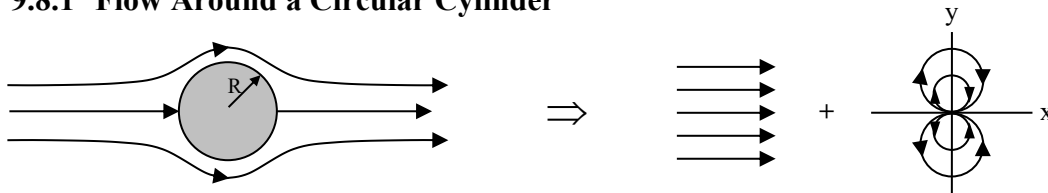


Figure 9.7 Inviscid flow over a cylinder, simulated by superposition of a uniform flow and a doublet.

A very common flow that is readily simulated using superposition techniques is a uniform flow passing around a circular cylinder (i.e. like flow around a wire or a rod). In order to simulate the inviscid flow over a cylinder, as shown in figure 9.7, we combine a uniform flow ([Section 9.7.1](#)), $\Phi(z) = Uz$, with a doublet function ([Section 9.7.4](#)), $\Phi(z) = \frac{s}{z}$, giving a combined complex potential function of:

$$\Phi(z) = Uz + \frac{s}{z} \quad (9.48)$$

As shown in figure 9.7, here we assume that: (1) $U > 0$, which gives the left-to-right uniform flow shown in figure 9.7, and (2) $s > 0$, such that the doublet flow will emanate outward, toward the left of the origin, as shown. This combination creates a simulated flow pattern where the uniform flow and the doublet impinge upon each other along the x-axis, creating a stagnation point reflecting the leading edge of a simulated cylinder.

To determine the stream and potential functions for this flow, we can use either Cartesian or cylindrical coordinates. In the following, we derive the stream and potential functions, and the velocity components in both systems. Thus, using $z = re^{i\theta}$, Eq. 9.48 becomes:

$$\begin{aligned}\Phi(z) &= Ure^{i\theta} + \frac{S}{r}e^{-i\theta} \\ &= Ur(\cos\theta + i\sin\theta) + \frac{S}{r}(\cos\theta - i\sin\theta) \\ &= \underbrace{\left(Ur + \frac{S}{r}\right)\cos\theta}_{\phi} + i \underbrace{\left(Ur - \frac{S}{r}\right)\sin\theta}_{\psi}\end{aligned}\tag{9.49}$$

Alternatively, using $z = x + iy$, we obtain:

$$\begin{aligned}\Phi(z) &= U(x + iy) + \frac{s}{(x + iy)} = U(x + iy) + \frac{s}{(x + iy)(x - iy)}(x - iy) \\ &= U(x + iy) + \frac{s}{(x^2 + y^2)}(x - iy) \\ &= x \underbrace{\left(U + \frac{s}{(x^2 + y^2)}\right)}_{\phi} + iy \underbrace{\left(U - \frac{s}{(x^2 + y^2)}\right)}_{\psi}\end{aligned}\tag{9.50}$$

For the cylindrical velocity components, we have (using the Cauchy relations):

$$v_r = \frac{1}{r} \frac{\partial \psi}{\partial \theta} = \frac{1}{r} \left[Ur - \frac{s}{r} \right] \cos\theta = \left[U - \frac{s}{r^2} \right] \cos\theta\tag{9.51a}$$

$$v_\theta = -\frac{\partial \psi}{\partial r} = -\left[U + \frac{s}{r^2} \right] \sin\theta\tag{9.51b}$$

In Cartesian coordinates, the complex velocity components are:

$$u = \frac{\partial \psi}{\partial y} = U - \frac{s}{x^2 + y^2} + \frac{2sy^2}{(x^2 + y^2)^2} = U - \frac{s}{x^2 + y^2} \left(1 - \frac{2y^2}{(x^2 + y^2)} \right)\tag{9.52a}$$

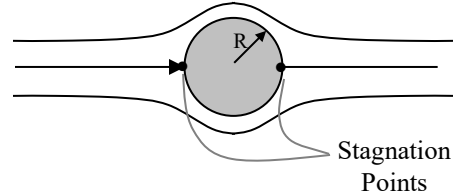
$$v = -\frac{\partial \psi}{\partial x} = -\frac{2sxy}{(x^2 + y^2)^2}\tag{9.52b}$$

A comparison of Eqs. 9.51 and 9.52 suggests that it is generally easier to perform our analysis for this configuration in cylindrical coordinates due to the radial symmetry of this flow.

Using Eqs. 9.51, we recognize that if the flow is on and around a cylinder, then at the surface of the cylinder the radius will be a constant of $r = R$, and the radial velocity, v_r , on this surface will be zero (i.e. the velocity will be tangent to the cylinder surface, with v_θ the only relevant velocity component).

Thus, we set Eq. 9.51a equal to zero, for $r = R$:

$$v_r|_{r=R} = 0 = \left(U - \frac{s}{R^2} \right) \cos\theta$$



Which indicates that:

$$U - \frac{s}{R^2} = 0 \Rightarrow R = \sqrt{\frac{s}{U}} \quad \text{or} \quad \cos\theta = 0 \Rightarrow \theta = \frac{\pi}{2}, \frac{3\pi}{2}, \dots \quad (9.53)$$

The result for θ in Eq. 9.53 is not particularly useful alone. However, Eq. 9.53 indicates that the radius of the simulated cylinder, $R = \sqrt{\frac{s}{U}}$, is a function of the respective ratio of the strengths of the doublet and the uniform flow, as might be expected. Changing the strength of either the doublet or the uniform flow will change the simulated diameter of the cylinder. However, as we will see, the dimensionless characteristics of this flow (e.g. v_θ/U , v_r/U , $C_p = (p - p_\infty)/\frac{1}{2}\rho U^2$) are invariant with changes in the flow or doublet strength.

To determine the streamline that defines the boundary of the cylinder, we assess the value of the streamline on the cylinder surface, for $r = R = \sqrt{\frac{s}{U}}$:

$$\psi = \left[Ur - \frac{s}{r} \right] \sin\theta$$

$$\psi|_{r=R} = \left[UR - \frac{s}{R} \right] \sin\theta = \left[U\sqrt{\frac{s}{U}} - \frac{s}{\sqrt{\frac{s}{U}}} \right] \sin\theta = [\sqrt{sU} - \sqrt{sU}] \sin\theta = 0$$

Thus, the bounding streamline (in this case) is $\psi = 0$. To establish the extent and shape of the bounding streamline, we now set $\psi = 0$ in Eq. 9.49, and solve for the streamline boundaries.

$$\psi = 0 = \left[Ur - \frac{s}{r} \right] \sin\theta$$

So, either $\underbrace{Ur - \frac{s}{r}} = 0$ or $\underbrace{\sin\theta} = 0$ along the $\psi = 0$ streamline.
 or $r = \sqrt{\frac{s}{U}} = R$ and $\theta = 0$ or π

Therefore, $\psi = 0$ occurs either: (1) on the cylinder surface ($r = R$), or (2) along the x-axis for $r > R$ ($\theta = 0$ or π), as shown in figure 9.8.

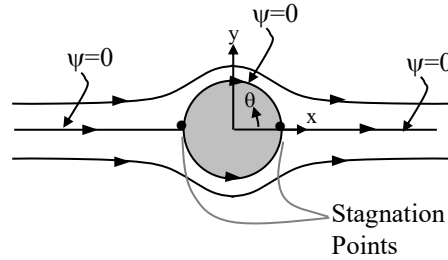


Figure 9.8 Location of the $\psi = 0$ streamline, and the respective stagnation points lying on that streamline.

The stagnation points on the cylinder will, of course, occur where $\vec{V} = 0$, or where v_r and $v_\theta = 0$. So, if we let $R = \sqrt{\frac{s}{U}}$, which assures that $v_r = 0$, we then set $v_\theta = 0$ in Eq. 9.51b and solve for the resulting angle:

$$v_\theta = - \left[U + \frac{s}{\left(\frac{s}{U}\right)} \right] \sin \theta_{\text{stag}} = -2U \sin \theta_{\text{stag}} = 0 \Rightarrow \theta_{\text{stag}} = 0 \text{ and } \pi$$

Thus, two stagnation points occur on the x-axis at both the leading and trailing edge of the cylinder (i.e. $x_{\text{stag}} = \pm R = \pm \sqrt{\frac{s}{U}}$ and $y_{\text{stag}} = 0$), as indicated in figure 9.8.

The portion of the $\psi = 0$ streamline that does not lie on the cylinder surface, lies along the x-axis, at either $\theta = \pi$ or 0 for $r > R$, or along $|x| > R$ for $y = 0$. Along the x-axis, the velocity is simply the u component of the complex velocity, Eq. 9.53a, with $y = 0$.

$$u|_{\psi=0} = U - \frac{s}{x^2} \text{ along the x-axis}$$

Note for $|x| \gg R$, we have:

$$u|_{\psi=0} \cong U$$

Therefore, the velocity is essentially constant well upstream and downstream of the cylinder, representing an impinging (and departing) uniform flow well away from the cylinder body.

To determine the maximum velocity on the cylinder surface, we note that v_θ is the velocity on the cylinder surface (since $v_r = 0$ on the cylinder). For $r = R = \sqrt{\frac{s}{U}}$, Eq. 9.51b becomes:

$$v_\theta = -2U \sin \theta \quad (9.54)$$

The maximum velocity will be where the derivative of Eq. 9.54 along the surface (with respect to θ) is zero, so

$$\frac{dv_\theta}{d\theta} = -2U \cos \theta = 0 \Rightarrow \theta = 90^\circ \text{ or } 270^\circ$$

Thus, the maximum velocity on the cylinder is $v_\theta = -2U$ (we could also have inferred this by inspection), occurring at both the top and bottom of the cylinder. Note that the negative sign in Eq. 9.54 simply indicates that the velocity moves in the negative θ direction (clockwise) for $0 < \theta < \pi$, and positive θ direction (counter clockwise) for $\pi < \theta < 2\pi$.

To establish pressure changes, both within the flow field and along the cylinder surface, we apply the Bernoulli equation, Eq. 7.11. Since the flow is inviscid and irrotational, Bernoulli applies either along a streamline or between *any* two points in the flow field.

Applying the Bernoulli equation between a point far upstream of the cylinder ($r \gg R$, where $u = U$), to any other point within the flow field, gives:

$$P + \frac{1}{2}\rho V^2 = P_\infty + \frac{1}{2}\rho U^2 \quad (9.55)$$

In Eq. 9.55, P is the local pressure and V is the local velocity at any point within the irrotational flow. P_∞ is the static press far upstream of the cylinder where the flow is uniform at velocity U .

Now, on the cylinder surface we have $V^2 = v_\theta^2 = (-2U \sin \theta)^2$. Substituting this V^2 into Eq. 9.55, and rearranging, gives:

$$\begin{aligned} P - P_\infty &= \frac{1}{2}\rho U^2 - \frac{1}{2}\rho V^2 = \frac{1}{2}\rho U^2 - \frac{1}{2}\rho(4U^2 \sin^2 \theta) = \frac{1}{2}\rho U^2(1 - 4\sin^2 \theta) \\ P &= P_\infty + \frac{1}{2}\rho U^2(1 - 4\sin^2 \theta) \end{aligned}$$

Defining a non-dimensional pressure coefficient, C_p , gives:

$$C_p = \frac{P - P_\infty}{\frac{1}{2}\rho U^2} = 1 - 4\sin^2 \theta \quad (9.56)$$

The general shape of $C_p(\theta)$ on the cylinder is shown in figure 9.9 below.

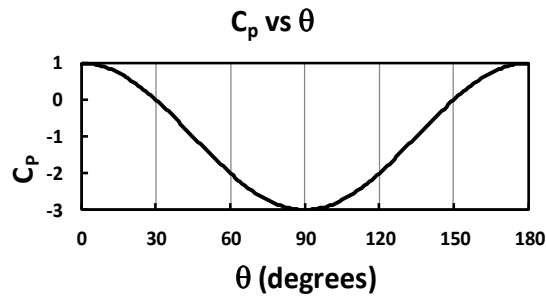
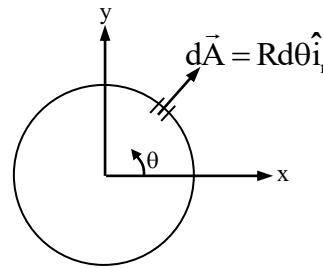


Figure 9.9 General behavior of the surface pressure coefficient versus angle (upper

surface) for inviscid flow over a cylinder, where $C_p = \frac{P - P_\infty}{\frac{1}{2}\rho U^2} = 1 - 4 \sin^2 \theta$.

Now, consider the forces that act on the cylinder due to the imposed pressure forces, where drag is a force parallel to the impinging flow (here, the x-direction), and lift will be a force normal (perpendicular) to the impinging flow direction (here the y-direction).



Thus,

$$\text{Drag} = \int dF_x = -\int P A_x$$

Where,

$$d\vec{A} = dA_x \hat{i} + dA_y \hat{j} = Rd\theta \hat{i}_r = Rd\theta(\hat{i} \cos\theta + \hat{j} \sin\theta)$$

Here, $dA_x = (Rd\theta)\cos\theta \Rightarrow$ differential area projection in x-direction

and $dA_y = (Rd\theta)\sin\theta \Rightarrow$ differential area projection in y-direction

Consequently,

$$\begin{aligned} \text{Drag} &= -\int_0^{2\pi} \left[P_\infty + \frac{1}{2}\rho U^2 (1 - 4\sin^2 \theta) \right] R \cos\theta d\theta \\ &= -\left(P_\infty + \frac{1}{2}\rho U^2 \right) R \sin\theta \Big|_0^{2\pi} + 2\rho U^2 R \frac{\sin^3 \theta}{3} \Big|_0^{2\pi} = 0 \end{aligned}$$

This curious result is known as [d'Alembert's paradox](#), and applies only for a truly inviscid flow (which, in reality, does not exist). One can observe, from the plot of C_p in figure 9.9 that the reason for the absence of pressure drag is that the pressure forces are *balanced* between the front and rear of the simulated cylinder---in a real flow there is no such balance of the pressure forces, as we will learn later in Chapters 14 and 15.

To develop a non-zero drag force on a body, which our experiences and experiments indicate must occur, requires the presence of fluid viscosity. Viscosity gives rise not only to shear forces at the body boundary, but is also responsible for the development of what is termed flow “[separation](#),” wherein a fluid flowing along a body will be brought to rest, such that the surface streamline subsequently separates from (i.e. moves away from) the body surface. Such flow separation creates a region of stagnant or recirculating fluid adjacent to the body, which strongly modifies both the velocity field around the body, and the pressure distribution imposed on the body. Thus, drag for real flows can result from *both* surface shearing forces and unbalanced pressure forces acting on the body. However, our assumption of inviscid behavior yields a fluid drag of zero on this and other (as we will see) simulated body shapes---a result that runs counter to our experiences. This discrepancy between the zero drag predicted by an inviscid analysis and the finite drag that exists for all real flows is, of course, the basis for d’Alembert’s paradox.

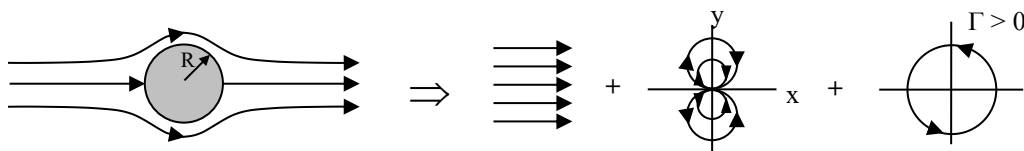
Note that the lift forces acting on the simulated cylinder (i.e. the summation of the forces acting normal to the impinging flow direction) can also be calculated for the simulated cylinder. The result, not surprisingly, is:

$$\text{Lift} = \int dF_y = -\int P dA_y = 0$$

This should not be unexpected, since the pressure forces on the simulated cylinder also are balanced top to bottom, as well as back to front, because of the symmetric pressure distribution indicated in figure 9.9. However, as we will show in the following section, the addition of rotation (circulation) to the simulated flow will modify this vertical pressure symmetry, and result in a non-zero lift force.

9.8.2 Flow Around a Rotating Cylinder

This example is similar to the analysis of a stationary cylinder in [section 9.8.1](#). However, we now simulate rotation of the cylinder by the additional superposition (addition) of a point vortex function, $\Phi(z) = -i \frac{\Gamma}{2\pi} \ln z$, to the superposed uniform flow and doublet functions employed in section 9.8.1 (i.e. uniform flow + doublet + vortex).



Here we assume $U > 0$, $s > 0$, and $\Gamma > 0$, which will simulate a cylinder rotating counter clockwise, with an impinging flow from left to right. The corresponding complex potential function for this flow is:

$$\Phi(z) = Uz + \frac{s}{z} - i \frac{\Gamma}{2\pi} \ln z \quad (9.57)$$

yielding a stream function (in cylindrical coordinates) of:

$$\psi(r, \theta) = \left(Ur - \frac{s}{r} \right) \sin \theta - \frac{\Gamma}{2\pi} \ln r \quad (9.58)$$

For this configuration, the radial velocity is the same as for a non-rotating cylinder

$$v_r = \frac{1}{r} \frac{\partial \psi}{\partial \theta} = \left[U - \frac{s}{r^2} \right] \cos \theta \quad (9.59)$$

However, the azimuthal velocity includes a new component that accounts for the magnitude of rotation,

$$v_\theta = -\frac{\partial \psi}{\partial r} = - \left[U + \frac{s}{r^2} \right] \sin \theta + \underbrace{\frac{\Gamma}{2\pi r}}_{\substack{\text{Rotation} \\ \text{Component}}} \quad (9.60)$$

Like we did for the non-rotating cylinder, we set $v_r = 0$ and solve for the radius of the simulated body. The result is $R = \sqrt{\frac{s}{U}}$, which is the same value we obtained for the non-rotating cylinder.

The bounding streamline for the body is obtained by setting $r = R = \sqrt{\frac{s}{U}}$ in Equation 9.58, which gives:

$$\begin{aligned} \psi|_{r=R} &= \left(U \sqrt{\frac{s}{U}} - \frac{s}{\sqrt{\frac{s}{U}}} \right) \sin \theta - \frac{\Gamma}{2\pi} \ln \sqrt{\frac{s}{U}} = (\sqrt{sU} - \sqrt{sU}) \sin \theta - \frac{\Gamma}{2\pi} \ln \sqrt{\frac{s}{U}} \\ \psi|_{r=R} &= -\frac{\Gamma}{2\pi} \ln \sqrt{\frac{s}{U}} \end{aligned} \quad (9.61)$$

Note that this bounding streamline varies with the respective strengths of the uniform flow, the doublet, and the rotation. That the bounding streamline is not zero is interesting, since this indicates that the streamlines above and below the real axis will *not* be symmetric, but will skew to one side of the x-axis or the other, depending on the direction of cylinder rotation.

To determine the position of the stagnation points on the rotating cylinder, we let $r = R$ (which satisfies, $v_r = 0$), set $v_\theta = 0$ (Eq. 9.60), and solve for the stagnation angles:

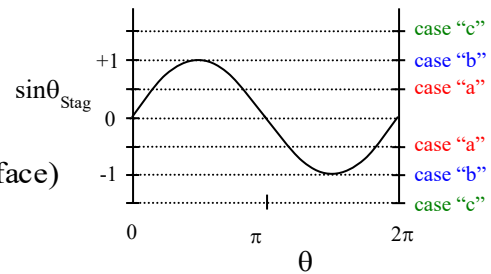
$$v_\theta|_{r=R} = -\left[U + \frac{s}{R^2}\right] \sin \theta_{\text{Stag}} + \frac{\Gamma}{2\pi R} = -[U + U] \sin \theta_{\text{Stag}} + \frac{\Gamma}{2\pi} \sqrt{\frac{U}{s}} = 0$$

or

$$\sin \theta_{\text{Stag}} = \frac{\Gamma}{4\pi\sqrt{Us}} \tag{9.62}$$

From Eq. 9.62, we can establish the angle(s), θ_{Stag} , on the cylinder where the stagnation points occur.

- (a) if $|\sin \theta_{\text{Stag}}| < 1 \Rightarrow 2$ stag. pts.
- (b) if $|\sin \theta_{\text{Stag}}| = 1 \Rightarrow 1$ stag. pt.
- (c) if $|\sin \theta_{\text{Stag}}| > 1 \Rightarrow$ No stag. pts. (on the $r = R$ surface)



Examples ($\Gamma > 0$):

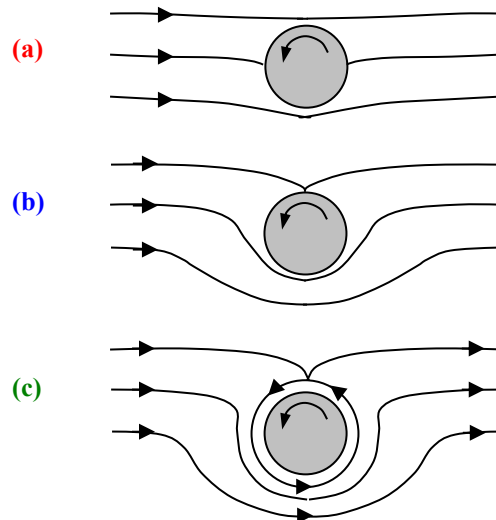


Figure 9.10 Illustration of the number of stagnation points occurring on a rotating cylinder, and the general streamline behavior, depending on the strengths of U , s , and Γ in Eq. 9.62. (a) two stagnation points, (b) one stagnation point, and (c) no stagnation points (on the cylinder surface). Here, $\Gamma > 0$, so stagnation points are in upper half of the plane. If $\Gamma < 0$, the stagnation points would occur in the lower half of the plane (and the streamlines would be mirror reflections—top to bottom—of the above patterns).

As indicated in figure 9.10, depending on the collective strengths of the uniform flow, the doublet, and the rotation, we may theoretically have two, one, or no stagnation points lying on

the cylinder. Note that the direction of the cylinder rotation dictates whether the stagnation points occur on the upper half (when $\Gamma > 0$) or lower half (when $\Gamma < 0$) of the cylinder.

Notice that for $U > 0$ and $s > 0$, the stagnation points will skew toward the upper surface ($\pi > \theta > 0$) for clockwise rotation ($\Gamma > 0$, as shown), and toward the lower surface ($2\pi > \theta > \pi$) for counter-clockwise rotation ($\Gamma < 0$). Also note that when the stagnation angle equation exceeds unity, $|\sin\theta_{\text{stag}}| > 1$, this indicates that the stagnation point *cannot occur on the body surface* ($r = R$), but must occur *outside* of the simulated body, as illustrated in figure 9.10(c) above. Such a stagnation point occurring within the fluid is a particular type of [critical point](#) termed a [saddle point](#) (with flow moving toward and then away from the point). A critical point is essentially a point within a flow field where the slope of the streamline is indeterminate. For example, a stagnation point qualifies as a critical point since the equation of the streamline intersecting a stagnation point is $dy/dx=0/0$, or indeterminate.

The velocity on the surface of the rotating cylinder, where $v_r = 0$, is given by:

$$v_{\theta}|_{R=\sqrt{\frac{s}{U}}} = - \left[U + \frac{s}{\frac{s}{U}} \right] \sin\theta + \frac{\Gamma}{2\pi R} = -2U \sin\theta + \frac{\Gamma}{2\pi R} = U \left(-2 \sin\theta + \frac{\Gamma}{2\sqrt{Us}} \right) \quad (9.63)$$

The pressure distribution on the surface, determined by substituting Eq. 9.63 into the Bernoulli equation is:

$$P - P_{\infty} = \frac{1}{2} \rho U^2 \left(1 - \frac{v_{\theta}^2}{U^2} \right) = \frac{1}{2} \rho U^2 \left[1 - \left(-2 \sin\theta + \frac{\Gamma}{2\pi R U} \right)^2 \right]$$

Here, P_{∞} is again the static press far upstream of the cylinder where the flow is uniform at velocity U . Defining a non-dimensional pressure coefficient, C_p , gives:

$$C_p = \frac{P - P_{\infty}}{\frac{1}{2} \rho U^2} = 1 - \left(-2 \sin\theta + \frac{\Gamma}{2\pi R U} \right)^2 = 1 - \left(-2 \sin\theta + \frac{\Gamma}{2\pi \sqrt{Us}} \right)^2 \quad (9.64)$$

The general shape of $C_p(\theta)$ on the upper and lower surface of the cylinder is shown in figure 9.11 for two cases of increasing rotation.

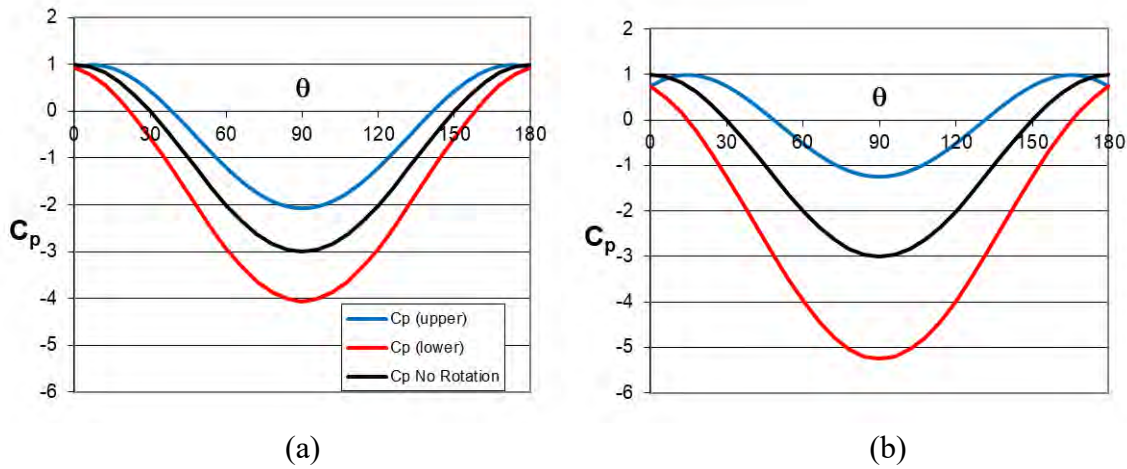


Figure 9.11 Comparison of C_p vs. θ (from Eq. 9.64) for (a) $\frac{\Gamma}{2\pi\sqrt{U_s}} = 0.25$ and (b) $\frac{\Gamma}{2\pi\sqrt{U_s}} = 0.5$. C_p with no rotation ($\Gamma = 0$) is shown for comparison.

Although the presence of rotation skews the streamlines, and creates a pressure differential between the upper and lower surfaces, as figure 9.11 shows, the pressure distribution between the front and back of the cylinder remains symmetric, so like the non-rotating cylinder there will be no drag force on the cylinder.

$$\text{Drag force} = \int dF_x = -\int P dA_x = 0$$

However, it is clear that the variance in surface pressure between the upper and lower surfaces must create an unbalanced lift force on the cylinder normal to the direction of the impinging uniform flow. This lift force can be calculated as:

$$\text{Lift force} = \int dF_y = -\int P dA_y = -\int \left(P_\infty + \frac{1}{2}\rho U^2 C_p \right) dA_y$$

where, $dA_y = (R d\theta) \sin \theta$ is the differential area projecting in the y-direction.

Thus,

$$\text{Lift Force} = -\int_0^{2\pi} \left[P_\infty + \frac{1}{2}\rho U^2 - \frac{1}{2}\rho U^2 \left(4\sin^2 \theta - \frac{2\Gamma \sin \theta}{\pi R U} + \frac{\Gamma^2}{4\pi^2 R^2 U^2} \right) \right] R \sin \theta d\theta$$

which, yields the rather simple result that:

$$\text{Lift Force} = -\frac{\rho \Gamma U \pi}{\pi} = -\rho U \Gamma \quad (9.65)$$

Equation 9.65 indicates that a counter-clockwise rotation ($\Gamma > 0$) will create a lift force in the negative y-direction (downward). From the pressure distribution shown in figure 9.11, this is clearly a result of the generation of a lower pressure on the bottom surface and a higher pressure on the upper surface of the cylinder.

Now note that the circulation around the cylinder (from Eq. 8.9) is given by :

$$\Gamma = \oint \vec{V} \cdot d\vec{s} = \int_0^{2\pi} v_\theta R d\theta = \int_0^{2\pi} \left(-2U \sin\theta + \frac{\Gamma}{2\pi R} \right) R d\theta = \Gamma \tag{9.66}$$

Since our lift result in Eq. 9.65 showed that lift = $-\rho U \Gamma$, Eq. 9.66 indicates that the lift on the cylinder is directly proportional to the circulation about the cylinder. It turns out that this result that lift is proportional to the circulation about a body, is generic, and applies for *all* inviscid flows about bodies, including airfoils, regardless of the source of the circulation.

9.8.3 Flow Around a Half-Body

One of the simpler superposition solutions would seem to be a uniform flow combined with a source, which simulates flow over what is called a half body, shown in figure 9.12.

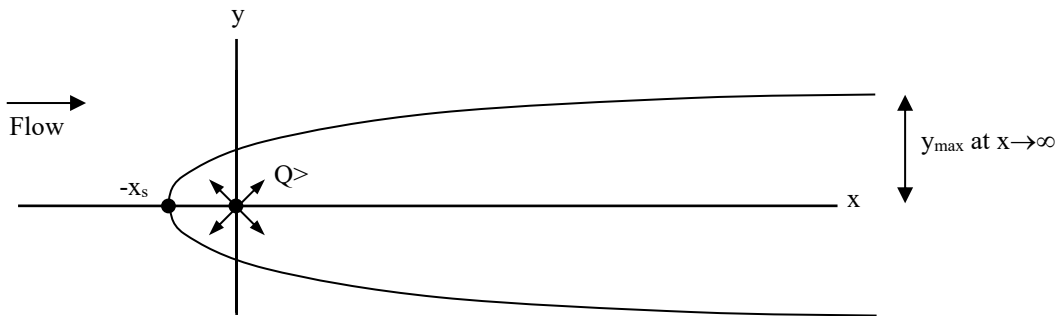


Figure 9.12 Schematic of flow over a half-body, simulated by the combination of a uniform flow and a source.

While this is a simple superposition, the calculations to establish the body shape are much less straightforward than we encountered in sections 9.8.1 and 9.8.2 using the superposition of a uniform flow and doublet to simulate flow over a cylinder. For the present simulation we superpose a uniform flow of strength $U > 0$ moving left to right, given by $\Phi(z) = Uz$, and a source of strength $Q > 0$ located at $z = 0$, given by $\Phi(z) = \frac{Q}{2\pi} \mathbf{ln}z$. Correspondingly, the superposed complex potential function is:

$$\Phi(z) = Uz + \frac{Q}{2\pi} \ln z \quad (9.67)$$

Here, we have two options: either to employ Cartesian variables or cylindrical variables—or both. We will expand Φ in both variables, and consider which better serves our purposes.

Expanding Φ using $z = re^{i\theta}$ we have:

$$\Phi(z) = Uz + \frac{Q}{2\pi} \ln z = \left[Ur \cos \theta + \frac{Q}{2\pi} \ln r \right] + i \left[Ur \sin \theta + \frac{Q}{2\pi} \theta \right] = \phi + i\psi \quad (9.68)$$

Whereas, expanding using $z = x + iy$ we have:

$$\Phi(z) = Uz + \frac{Q}{2\pi} \ln z = \left[Ux + \frac{Q}{2\pi} \ln \sqrt{x^2 + y^2} \right] + i \left[Uy + \frac{Q}{2\pi} \tan^{-1} \left(\frac{y}{x} \right) \right] = \phi + i\psi \quad (9.69)$$

Here, the complex velocity components are given by:

$$\frac{d\Phi}{dz} = U + \frac{Q}{2\pi} \frac{1}{z} = \bar{W} = u - iv$$

and

$$W = u + iv = U + \frac{Q}{2\pi} \frac{1}{\bar{z}} \quad \text{where} \quad \bar{z} = x - iy \quad (9.70)$$

The respective Cartesian velocity components can be shown, in both Cartesian and cylindrical variables, to be:

$$u = U + \frac{Q}{2\pi} \left(\frac{x}{x^2 + y^2} \right) = U + \frac{Q}{2\pi} \left(\frac{\cos \theta}{r} \right) \quad (9.71a)$$

$$v = \frac{Q}{2\pi} \left(\frac{y}{x^2 + y^2} \right) = \frac{Q}{2\pi} \left(\frac{\sin \theta}{r} \right) \quad (9.71b)$$

To establish the shape of the body, we note that a stagnation point must occur on the body, where the complex velocity, W (and so also \bar{W}), is zero. Thus, setting Eq. 9.70 to zero, we have:

$$W = U + \frac{Q}{2\pi} \frac{1}{\bar{z}} = 0 \quad \Rightarrow \quad \bar{z} = x - iy = -\frac{Q}{2U\pi}$$

Thus, $x_{\text{stag}} = -\frac{Q}{2U\pi}$, $y_{\text{stag}} = 0$ or $r_{\text{stag}} = \frac{Q}{2U\pi}$, $\theta_{\text{stag}} = \pi$ is the location of the stagnation point for the body. Correspondingly, the value of the stagnation streamline, ψ_s , which passes through the stagnation point, is given by:

$$\psi_s = Ur \overset{0}{\sin \pi} + \frac{Q}{2\pi} \overset{\cancel{\pi}}{\cancel{\pi}} = \frac{Q}{2} \quad (9.72)$$

Now, the location of the points along a streamline that describes the boundary of the body ($\psi_b = \psi_s$, since ψ_s must lie on the body boundary) is given by setting ψ from Eq. 9.68 and 9.69 equal to Eq. 9.72:

$$\psi_s = \frac{Q}{2} = \psi_b = Ur_b \sin\theta_b + \frac{Q}{2\pi} \theta_b \quad (\text{cylindrical coordinates}) \quad (9.73)$$

or

$$Uy_b + \frac{Q}{2\pi} \tan^{-1}\left(\frac{y_b}{x_b}\right) = \frac{Q}{2} \quad (\text{Cartesian coordinates}) \quad (9.74)$$

Solving Eq. 9.73 for r_b and Eq. 9.74 for x_b , we have:

$$r_b = \frac{Q}{2U\pi} \frac{(\pi - \theta_b)}{\sin\theta_b} \quad (9.75)$$

and

$$x_b = \frac{y_b}{\tan\left[\pi\left(1 - \frac{2Uy_b}{Q}\right)\right]} \quad (9.76)$$

In Eqs. 9.75 and 9.76, the subscript “b” indicates that these equations define coordinate pairs lying on the bounding streamline, and thus the surface, as shown in figure 9.13. Either of these expressions allows us to determine the boundaries of the body, although Eq. 9.75 is probably a bit more convenient.

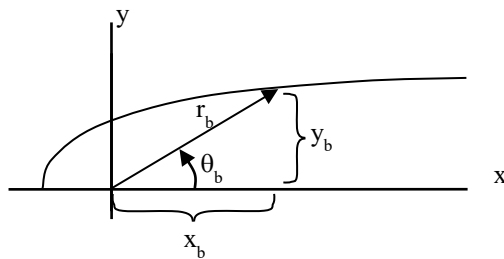


Figure 9.13 The geometric relationship of x_b and y_b to r_b and θ_b .

From the general body shape shown in figure 9.13, we infer that the maximum thickness of the half body must occur far downstream of the stagnation point, at either $x_b \rightarrow \infty$ or $\theta_b \approx 0$.

Employing r_b from Eq. 9.75 in cylindrical coordinates to obtain the half-body thickness, y_b , we have:

$$y_b = r_b \sin\theta_b = \frac{Q}{2U\pi} (\pi - \theta_b) \quad (9.77)$$

The maximum body thickness is obtained by substituting $\theta_b = 0$ into Eq. 9.77, giving:

$$y_{\max} = \frac{Q}{2U} \quad (9.78)$$

Substituting Eq. 9.78 into Eq. 9.77, and dividing through by y_{\max} , allows us to express the non-dimensional half-body thickness as:

$$\frac{y_b}{y_{\max}} = \frac{(\pi - \theta_b)}{\pi} = 1 - \frac{\theta_b}{\pi} \quad (9.79)$$

In Cartesian coordinates, the corresponding non-dimensional streamwise body coordinate from Eq. 9.76 is:

$$\frac{x_b}{y_{\max}} = \frac{\left(\frac{y_b}{y_{\max}} \right)}{\tan \left[\pi \left(1 - \frac{y_b}{y_{\max}} \right) \right]} \quad (9.80)$$

Substituting Eq. 9.79 into Eq. 9.80, yields the an expression for the corresponding non-dimensional streamwise body coordinate as a function of θ_b :

$$\frac{x_b}{y_{\max}} = \frac{(\pi - \theta_b)}{\pi \tan(\theta_b)} \quad (9.81)$$

The figure 9.14 shows the bounding streamline shape, determined by choosing selected values of θ_b , calculating y_b/y_{\max} and x_b/y_{\max} from Eqs. 9.79 and 9.81, and plotting the resulting shape.

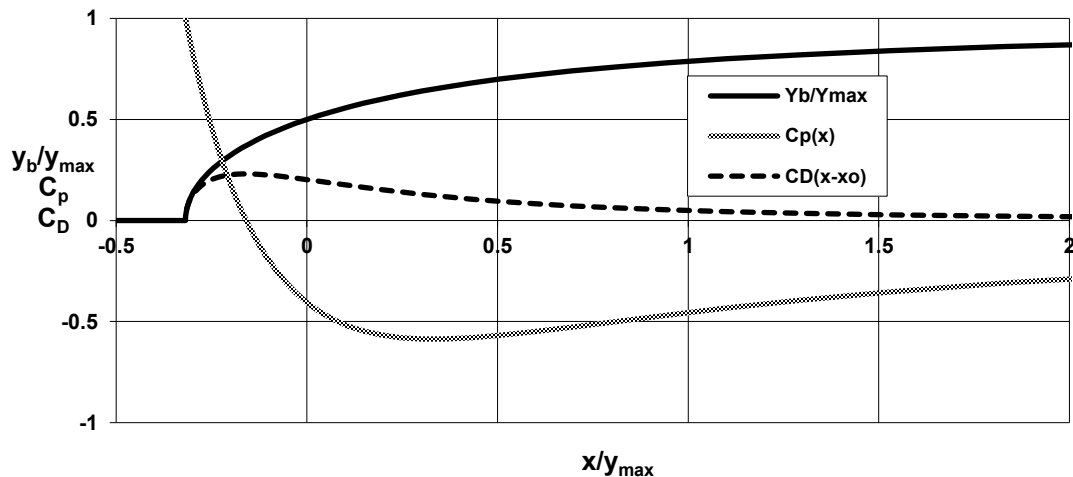


Figure 9.14 Half-body surface stream line ($\psi_b = Q/2$), pressure coefficient [$C_p(x)$], and cumulative drag coefficient [$C_D(x-x_0)$]

Alternatively, one could select a series of y_b/y_{\max} values, calculate x_b/y_{\max} from Eq. 9.80, and plot the shape directly. In either case, one has to be careful in incrementing θ_b or y_b/y_{\max} , since x_b/y_{\max} varies quite rapidly once $x_b/y_{\max} > 0.6$.

Another characteristic we can establish from this simulation is the pressure distribution or pressure coefficient (C_p) over the body. From the Bernoulli equation, we can write:

$$P + \frac{1}{2}\rho V^2 = P_\infty + \frac{1}{2}\rho U^2 \quad \text{where} \quad V^2 = \mathbf{u}^2 + \mathbf{v}^2 = \mathbf{W}\overline{\mathbf{W}} \quad (9.82)$$

Here, P_∞ is the static pressure of the upstream impinging flow ($\theta = \pi$, or $y = 0$ and $x \ll 0$), where $u = U$, $v = 0$. Rearranging Eq. 9.82, we can write the non-dimensional pressure coefficient as:

$$C_p = \frac{P - P_\infty}{\frac{1}{2}\rho U^2} = 1 - \frac{V^2}{U^2} \quad (9.83)$$

Equation 9.83 allows us to express the pressure changes along the body non-dimensionally, the way we did for the cylinder flow in [sections 9.81](#) and [9.82](#). We are again faced with which coordinate system to employ to expand this expression. Using cylindrical variables, where $z = re^{i\theta}$ and $\bar{z} = re^{-i\theta}$ we can determine V^2 as:

$$\begin{aligned} V^2 &= \mathbf{W}\overline{\mathbf{W}} = \left(U + \frac{Q}{2\pi} \frac{1}{\bar{z}} \right) \left(U + \frac{Q}{2\pi} \frac{1}{z} \right) = U^2 + \frac{QU}{2\pi} \frac{1}{\bar{z}} + \frac{QU}{2\pi} \frac{1}{z} + \left(\frac{Q}{2\pi} \right)^2 \frac{1}{z\bar{z}} \\ &= U^2 + \frac{QU}{2\pi} \frac{e^{i\theta}}{r} + \frac{QU}{2\pi} \frac{e^{-i\theta}}{r} + \left(\frac{Q}{2\pi} \right)^2 \frac{1}{r^2} \end{aligned} \quad (9.84)$$

Substituting Equation 9.75 for r_b , into Eq. 9.84 we have:

$$V^2 = U^2 + \frac{U^2 \sin \theta_b}{(\pi - \theta_b)} \overbrace{\left(e^{i\theta_b} + e^{-i\theta_b} \right)}^{\cos \theta_b} + \frac{U^2 \sin^2 \theta_b}{(\pi - \theta_b)^2} = U^2 \left(1 + \frac{2 \sin \theta_b \cos \theta_b}{(\pi - \theta_b)} + \frac{\sin^2 \theta_b}{(\pi - \theta_b)^2} \right) \quad (9.85)$$

To simplify Eq. 9.85, we let $\alpha_b = \pi - \theta_b$, and note that $\sin \theta_b = \sin(\pi - \theta_b) = \sin \alpha_b$, and $\cos \theta_b = -\cos(\pi - \theta_b) = -\cos \alpha_b$, which lets us write:

$$V^2 = U^2 \left(1 - \frac{2 \sin \alpha_b \cos \alpha_b}{\alpha_b} + \frac{\sin^2 \alpha_b}{\alpha_b^2} \right) \quad (9.86)$$

Substituting Eq. 9.86 into Eq. 9.83 for the pressure coefficient, C_p , we have:

$$C_p(\alpha_b) = \frac{P - P_\infty}{\frac{1}{2}\rho U^2} = \frac{2 \sin \alpha_b \cos \alpha_b}{\alpha_b} - \frac{\sin^2 \alpha_b}{\alpha_b^2} \quad (9.87)$$

Alternatively, we can write V^2 in Cartesian variables as:

$$V^2 = U^2 + \frac{QU}{\pi} \frac{x}{(x^2 + y^2)} + \left(\frac{Q}{2\pi}\right)^2 \frac{1}{(x^2 + y^2)} \quad (9.88)$$

Substituting into Eq. 9.88 from our expression for y_{\max} , Eq. 9.78, (rearranging as $Q = 2Uy_{\max}$) we have:

$$V^2 = U^2 + \frac{2y_{\max}U^2}{\pi} \frac{x}{(x^2 + y^2)} + \frac{y_{\max}^2U^2}{\pi^2} \frac{1}{(x^2 + y^2)} = U^2 \left\{ 1 + \frac{y_{\max}^2}{\pi(x^2 + y^2)} \left[2\frac{x}{y_{\max}} + \frac{1}{\pi} \right] \right\} \quad (9.89)$$

Substituting Eq. 9.89 into Eq. 9.83, yields a second equation for C_p on the bounding surface as:

$$C_p(x_b, y_b) = \frac{P - P_\infty}{\frac{1}{2}\rho U^2} = -\frac{y_{\max}^2}{\pi(x_b^2 + y_b^2)} \left[2\frac{x_b}{y_{\max}} + \frac{1}{\pi} \right] = -\frac{\left[2\frac{x_b}{y_{\max}} + \frac{1}{\pi} \right]}{\pi \left[\left(\frac{x_b}{y_{\max}} \right)^2 + \left(\frac{y_b}{y_{\max}} \right)^2 \right]} \quad (9.90)$$

To use Eq. 9.87, one must determine the locus of the surface using Eqs. 9.79 and 9.81 to correlate C_p with the location on the body; for Eq. 9.90, Eq. 9.80 is used to correlate the location of C_p on the body. Either approach works, but again care must be used in incrementing θ_b or y_b/y_{\max} . The previous Figure 9.14 shows C_p as a function of x_b/y_{\max} , superposed with the body shape.

Note that the pressure force per unit depth in the streamwise direction, or pressure drag, is given by:

$$F_D = \int_A (P - P_\infty) dA_x = \int_{y_b=0}^{y_b=y_{\max}} (P - P_\infty) dy_b$$

Or in terms of a non-dimensional drag coefficient, C_D :

$$C_D = \frac{F_D}{\frac{1}{2}\rho U^2 y_{\max}} = \frac{\int_{y=0}^{y=y_{\max}} (P - P_\infty) dy_b}{\frac{1}{2}\rho U^2 y_{\max}} = \int_{y_b=0}^{y_b=y_{\max}} C_p(x_b, y_b) \left(\frac{dy_b}{y_{\max}} \right) \quad (9.91)$$

To integrate Eq. 9.91 with respect to y requires that we substitute our expression above for $x_b/y_{\max} = f(y_b/y_{\max})$ in Eq. 9.80 into Eq. 9.91 for C_p , which makes the integral in Eq. 9.91 much too complicated. Accordingly, we employ our expression for $C_p(\alpha_b)$ in Eq. 9.87, and note from Eq. 9.79 that we can write $y_b = f(\alpha_b)$, where $\alpha_b = \pi - \theta_b$, along the surface as:

$$y_b = \frac{Q\alpha_b}{2U\pi} = \frac{y_{\max} \alpha_b}{\pi} \Rightarrow \frac{dy_b}{y_{\max}} = \frac{d\alpha_b}{\pi} \quad (9.92)$$

Substituting Eq. 9.92 into Eq. 9.91, and noting that the appropriate limits of integration are from $\alpha_b = 0$ ($\theta = \pi$) to $\alpha_b = \pi$ ($\theta = 0$), we have:

$$C_D = \frac{1}{\pi} \int_{\alpha_b=0}^{\alpha_b=\pi} C_p(\alpha_b) d\alpha_b = \frac{1}{\pi} \int_0^{\pi} \left(\frac{2\sin\alpha_b \cos\alpha_b}{\alpha_b} - \frac{\sin^2\alpha_b}{\alpha_b^2} \right) d\alpha_b \quad (9.93)$$

Identifying that (not quite self-evident):

$$\left(\frac{2\sin\alpha_b \cos\alpha_b}{\alpha_b} - \frac{\sin^2\alpha_b}{\alpha_b^2} \right) = \frac{d}{d\alpha_b} \left(\frac{\sin^2\alpha_b}{\alpha_b} \right)$$

We can rewrite Eq. 9.93 and integrate, giving:

$$C_D = \frac{1}{\pi} \int_0^{\pi} \frac{d}{d\alpha_b} \left(\frac{\sin^2\alpha_b}{\alpha_b} \right) d\alpha_b = \frac{1}{\pi} \left(\frac{\sin^2\alpha_b}{\alpha_b} \right) \Big|_0^{\pi} = \frac{1}{\pi} \left(\frac{0}{\pi} - \frac{0}{0} \right) = ? \quad (9.94)$$

Equation 9.94 is indeterminate at $\alpha_b = 0$. To assess the integral, we apply L'Hospital's rule to the general result of Eq. 9.94 as $\alpha_b \rightarrow 0$:

$$\lim_{\alpha_b \rightarrow 0} \left(\frac{\sin^2\alpha_b}{\alpha_b} \right) = \lim_{\alpha_b \rightarrow 0} \frac{d(\sin^2\alpha_b)}{d(\alpha_b)} = \lim_{\alpha_b \rightarrow 0} \frac{2\sin\alpha_b}{1} = 0$$

Thus, the value of Eq. 9.94 is:

$$C_D = \frac{1}{\pi} (0 - 0) = 0 \quad (9.95)$$

Now the result of no drag indicated by Eq. 9.95 might seem a bit unusual, since one would assume that the streamwise pressure force would be unbalanced for this geometry. However, recall that inviscid flow around a circular cylinder also displayed no drag. The process for the cylinder was a bit more obvious, since the pressure forces on the leading half of the cylinder were clearly balanced by the pressure forces on the trailing half. Here, the process is a bit more subtle, as shown in figure 9.14.

Note that when $C_p > 0$, a pressure drag force component is applied in the *positive* x-direction. However, such a condition only exists for a short distance after the leading edge ($-.159 \geq x_b/y_{\max} \geq -.318$). Thereafter, for $x_b/y_{\max} \geq -.159$, $C_p < 0$ on the bounding surface, which results in a *negative* drag force, or suction force, acting in the *negative* x-direction. Since $C_D \rightarrow 0$ as $x \rightarrow \infty$, this implies that the initial pressure drag forces on the leading portion of the body are identically

balanced by the suction forces over the trailing portion of the body. This is illustrated in figure 9.14 by the behavior of $C_D(x-x_0)$, which shows the cumulative drag as a function of x from the leading edge (where $x_{\text{stag}}/y_{\text{max}} = -0.318$). The velocity on the body surface reaches a maximum, and thus C_p reaches a minimum, at approximately $x_b/y_{\text{max}} = 0.33$ ($V_{\text{max}} = 1.26U$), and then decreases back to zero as $V \rightarrow U$ as $x \rightarrow \infty$. However, the deceleration of the flow is quite gradual over the remainder of the body, which ideally extends to infinity.

As we will discuss later, flow deceleration and the accompanying pressure rise (known as an “adverse” pressure gradient) are not well tolerated by real viscous flows. Real bodies, in real flows, will of course be of finite extent, which requires that at some point the body must either: (1) terminate at a finite thickness, or (2) taper back down to $y_b = 0$, such as occurs for airfoils. Such geometry changes are normally accompanied by local adverse pressure gradients in the direction of the flow. The application of an adverse pressure gradient to a real viscous flow will generally cause the flow to undergo a process of flow “separation” (a process that was referred to earlier with regard to the cylinder flow) at some point along the body. The consequence of such a flow separation is a sharp divergence from the flow pattern behavior predicted by an ideal, inviscid flow, with the consequent generation of non-zero pressure drag. We discuss the development and ramifications of flow separation on flow drag for real viscous flows later in Chapters 14 and 15.

Without offering further examples or proof here, we can comment that the general result of zero pressure drag obtained for inviscid flow over a cylinder in sections 9.8.1 and 9.8.2, and in the present section for flow over a half body, applies in general for superposition solutions incorporating any number of sources or sinks. Regardless of how many source/sink combinations we superpose to change the shape of a simulated body, the net pressure drag on any resultant “body” will always be zero. Thus, in the absence of viscosity, the flow of an ideal fluid around *any* simulated body will always satisfy the d’Alembert’s paradox of zero drag.

9.8.4 Flow Around a Two-Dimensional Rankine body

In order to simulate a closed body in a uniform flow using sources and sinks, one must assure that the total strength of the sources is *equal* to the total strength of the sinks (i.e.

$\sum_{\text{sources}} Q + \sum_{\text{sinks}} Q = 0$). When we superpose a single source and single sink of strength Q with a uniform flow, the shape of the body will be elliptical in shape, with the shape of the body dependent on both the strengths of the source/sink and the separation distance between the source and sink. Here, we superpose: (a) a uniform flow of strength U moving left to right, given by $\Phi(z) = Uz$, (b) a source located at $z = -z_0$ of strength Q , given by $\Phi(z) = \frac{Q}{2\pi} \ln(z + z_0)$, and (c) a sink located at $z = +z_0$ of strength $-Q$, given by $\Phi(z) = -\frac{Q}{2\pi} \ln(z - z_0)$, as shown in figure 9.15.

The superposed complex potential function is:

$$\Phi(z) = Uz + \frac{Q}{2\pi} \ln(z + z_0) - \frac{Q}{2\pi} \ln(z - z_0) \quad (9.96)$$

To simulate a closed body, it is clear that the source must be *upstream* of the sink, otherwise the flow will not exhibit a stagnation point at the leading edge. Additionally, to simulate a *symmetric* body, the source and sink must be located along an axis parallel to the impinging uniform flow. For the present simulation, we assume a uniform flow parallel to the real axis (x), and let $z_0 = a$, which gives:

$$\Phi(z) = Uz + \frac{Q}{2\pi} \ln(z + a) - \frac{Q}{2\pi} \ln(z - a) \quad (9.97)$$

The general configuration for this simulation is termed a Rankine body, and is shown in figure 9.15:

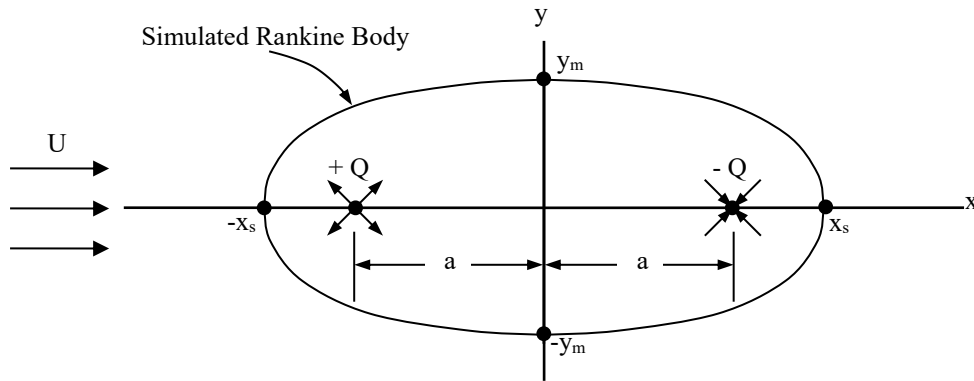


Figure 9.15 Elliptical Rankine body shape simulated by superposition of an equivalent source (+Q) and sink (-Q) with a uniform flow (U).

Since the logarithm terms in Eq. 9.97 lend themselves best to cylindrical variables, we define two new complex variables as;

$$z_1 = z + a = r_1 e^{i\theta_1} \quad (9.98a)$$

and

$$z_2 = z - a = r_2 e^{i\theta_2} \quad (9.98b)$$

where,

$$r_1 = \sqrt{(x + a)^2 + y^2} \quad \text{and} \quad \theta_1 = \tan^{-1}\left(\frac{y}{x + a}\right) \quad (9.99a)$$

and

$$r_2 = \sqrt{(x - a)^2 + y^2} \quad \text{and} \quad \theta_2 = \tan^{-1}\left(\frac{y}{x - a}\right) \quad (9.99b)$$

Substituting Eqs. 9.98 into Eq. 9.97, we have:

$$\begin{aligned}\Phi(z) &= Uz + \frac{Q}{2\pi} \ln(z_1) - \frac{Q}{2\pi} \ln(z_2) = Uz + \frac{Q}{2\pi} \ln\left(\frac{z_1}{z_2}\right) = U(x + iy) + \frac{Q}{2\pi} \ln\left(\frac{r_1 e^{i\theta_1}}{r_2 e^{i\theta_2}}\right) \\ \Phi(z) &= U(x + iy) + \frac{Q}{2\pi} \ln\left(\frac{r_1}{r_2}\right) + i \frac{Q}{2\pi} (\theta_1 - \theta_2)\end{aligned}\quad (9.100)$$

And substituting from Eq. 9.99 to express Eq.9.100 in terms of x and y yields:

$$\Phi(z) = \left\{ Ux + \frac{Q}{2\pi} \ln\left(\frac{\sqrt{(x+a)^2 + y^2}}{\sqrt{(x-a)^2 + y^2}}\right) \right\} + i \left\{ Uy + \frac{Q}{2\pi} \left[\tan^{-1}\left(\frac{y}{x+a}\right) - \tan^{-1}\left(\frac{y}{x-a}\right) \right] \right\} \quad (9.101)$$

From Eq. 9.101, we can identify the stream and potential functions for this flow as:

$$\phi(x, y) = Ux + \frac{Q}{2\pi} \ln\left(\frac{\sqrt{(x+a)^2 + y^2}}{\sqrt{(x-a)^2 + y^2}}\right) \quad (9.102)$$

$$\psi(x, y) = Uy + \frac{Q}{2\pi} \left[\tan^{-1}\left(\frac{y}{x+a}\right) - \tan^{-1}\left(\frac{y}{x-a}\right) \right] \quad (9.103)$$

We determine the velocity components by differentiating $\Phi(z)$ from Eq. 9.97 for $\bar{W} = u - iv$ (this is easier than differentiating ϕ or ψ with respect to x or y). Thus,

$$\begin{aligned}\frac{d\Phi}{dz} = \bar{W} &= U + \frac{Q}{2\pi} \left(\frac{1}{z+a} \right) - \frac{Q}{2\pi} \left(\frac{1}{z-a} \right) = U + \frac{Q}{2\pi} \left[\frac{1}{(x+a) + iy} \right] - \frac{Q}{2\pi} \left[\frac{1}{(x-a) + iy} \right] \\ \bar{W} &= U + \frac{Q}{2\pi} \left[\frac{(x+a) - iy}{(x+a)^2 + y^2} \right] - \frac{Q}{2\pi} \left[\frac{(x-a) - iy}{(x-a)^2 + y^2} \right]\end{aligned}$$

And separating the real and imaginary parts,

$$\bar{W} = \left\{ U + \frac{Q}{2\pi} \left[\frac{(x+a)}{(x+a)^2 + y^2} \right] - \frac{Q}{2\pi} \left[\frac{(x-a)}{(x-a)^2 + y^2} \right] \right\} - i \left\{ \frac{Q}{2\pi} \left[\frac{y}{(x+a)^2 + y^2} \right] - \frac{Q}{2\pi} \left[\frac{y}{(x-a)^2 + y^2} \right] \right\}$$

Thus, by identification we have the Cartesian velocity components:

$$u = U + \frac{Q}{2\pi} \left\{ \left[\frac{(x+a)}{(x+a)^2 + y^2} \right] - \left[\frac{(x-a)}{(x-a)^2 + y^2} \right] \right\} \quad (9.104a)$$

$$v = \frac{Q}{2\pi} \left\{ \left[\frac{y}{(x+a)^2 + y^2} \right] - \left[\frac{y}{(x-a)^2 + y^2} \right] \right\} \quad (9.104b)$$

The stagnation points (y_s and x_s) for the simulated body occur where $u = 0$ and $v = 0$. We note that $v = 0$ along the x axis ($y = 0$). Thus, to determine the stagnation points, we set $u = 0$ and let $y = y_s = 0$ and $x = x_s$ in Eqs.9.104. This makes $v = 0$ in Eq. 9.104b, and we can solve for the resultant x_s with $u = 0$ in Eq. 9.104a:

$$u = U + \frac{Q}{2\pi} \left\{ \left[\frac{(x_s + a)}{(x_s + a)^2} \right] - \left[\frac{(x_s - a)}{(x_s - a)^2} \right] \right\} = 0$$

After some algebra, we determine x_s as:

$$x_s = \pm a \sqrt{1 + \frac{Q}{\pi U a}} \quad (9.105)$$

At this point, it is advantageous for plotting purposes to define non-dimensional variables as $x' = \frac{x}{a}$ and $y' = \frac{y}{a}$, and a relative source strength term as $\beta = \frac{Q}{\pi U a}$. Thus, the stagnation points for the Rankine body are $x'_s = \pm \sqrt{1 + \beta}$ and $y'_s = 0$.

Now, in terms of x' and y' the stream function equation (Eq. 9.103) becomes:

$$\psi(x', y') = U a y' + \frac{Q}{2\pi} \left[\tan^{-1} \left(\frac{y'}{x' + 1} \right) - \tan^{-1} \left(\frac{y'}{x' - 1} \right) \right] \quad (9.106)$$

Since $y'_s = 0$ at the stagnation points, Eq. 9.106 indicates that the stream function equation for the body surface is $\psi(x'_s, y'_s) = 0$ (the same as for the non-rotating cylinder flow). Thus, the equation for the body shape is given by:

$$\psi(x'_b, y'_b) = \psi(x'_s, y'_s) = 0 = U a y'_b + \frac{Q}{2\pi} \left[\tan^{-1} \left(\frac{y'_b}{x'_b + 1} \right) - \tan^{-1} \left(\frac{y'_b}{x'_b - 1} \right) \right] = 0 \quad (9.107)$$

In Eq. 9.107, y'_b and x'_b are coordinates on the body surface.

Rewriting Eq. 107 in terms of β , as defined previously, gives:

$$y'_b + \frac{\beta}{2} \left[\tan^{-1} \left(\frac{y'_b}{x'_b + 1} \right) - \tan^{-1} \left(\frac{y'_b}{x'_b - 1} \right) \right] = 0 \quad (9.108)$$

The maximum thickness of the body, y'_m , occurs when $x'_b = 0$, and is (unfortunately) given implicitly by:

$$y'_m + \frac{\beta}{2} [\tan^{-1}(y'_m) - \tan^{-1}(-y'_m)] = 0 = y'_m + \frac{\beta}{2} [2 \tan^{-1}(y'_m) - \pi]$$

[Here we substitute the identity: $\tan^{-1}(-y'_m) = \pi - \tan^{-1} y'_m$]

or,

$$\beta = \left[\frac{2y'_m}{\pi - 2 \tan^{-1}(y'_m)} \right] \quad (9.109)$$

This implicit equation for y'_m must be solved either iteratively for a given value of β , or by choosing a desired value of y'_m , and solving for the required β value.

To determine the body shape from Eq. 9.108 appears to be a messy iterative process. However, we can rewrite Eq. 9.108 as:

$$\tan^{-1}\left(\frac{y'_b}{x'_b - 1}\right) = \frac{2y'_b}{\beta} + \tan^{-1}\left(\frac{y'_b}{x'_b + 1}\right)$$

or, taking the tangent of both sides of the equation:

$$\frac{y'_b}{x'_b - 1} = \tan \left[\frac{2y'_b}{\beta} + \tan^{-1}\left(\frac{y'_b}{x'_b + 1}\right) \right] = \frac{\tan\left(\frac{2y'_b}{\beta}\right) + \frac{y'_b}{x'_b + 1}}{1 - \left(\frac{y'_b}{x'_b + 1}\right) \tan\left(\frac{2y'_b}{\beta}\right)} \quad (9.110)$$

[using the trigonometric identity: $\tan(a + b) = \frac{\tan a + \tan b}{1 - \tan a \tan b}$]

Solving Eq. 9.110 for x'_b (trust me) gives:

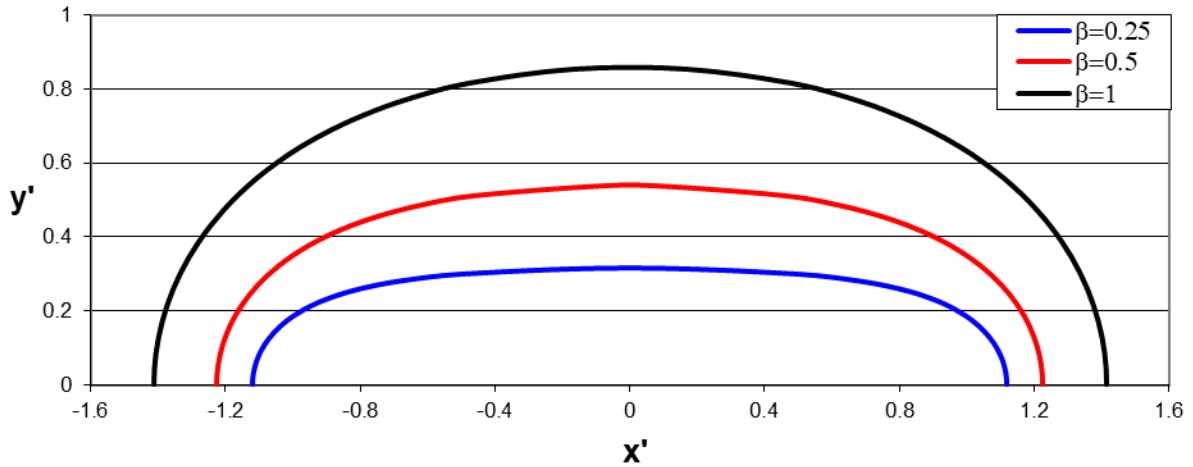
$$x'_b{}^2 = 1 - y'_b{}^2 + \frac{2y'_b}{\tan\left(\frac{2y'_b}{\beta}\right)} \quad (9.111)$$

Equation 9.111 now allows the explicit determination of the body shape. The upper half body shape determined from Eq. 9.111 is shown in figure 9.16a for $\beta=0.25$, 0.5, and 1.

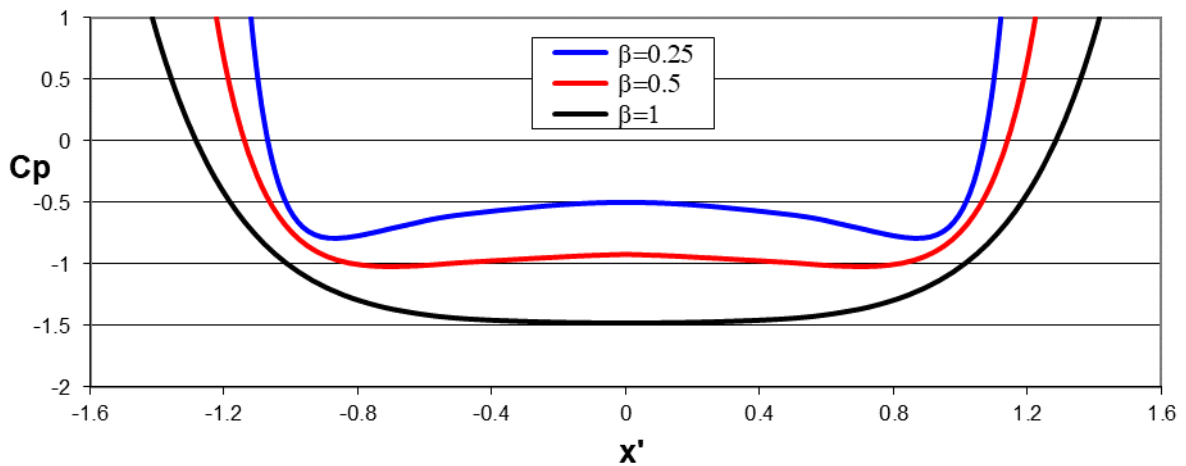
The velocity along the body surface can be determined from Eqs. 9.104, using Eq. 9.111 to specify the surface coordinates. In terms of x' and y' , we can define non-dimensional velocity components as:

$$u' = \frac{u}{U} = 1 + \frac{\beta}{2} \left\{ \left[\frac{(x'+1)}{(x'+1)^2 + y'^2} \right] - \left[\frac{(x'-1)}{(x'-1)^2 + y'^2} \right] \right\} \quad (9.112a)$$

$$v' = \frac{v}{U} = \frac{\beta}{2} \left\{ \left[\frac{y'}{(x'+1)^2 + y'^2} \right] - \left[\frac{y'}{(x'-1)^2 + y'^2} \right] \right\} \quad (9.112b)$$



(a) Non-dimensional Rankine body shape (upper half)



(b) Non-dimensional Pressure Coefficient

Figure 9.16 Body shape and pressure coefficient for inviscid flow around Rankine bodies with relative source strengths of $\beta = \frac{Q}{\pi Ua} = 0.25, 0.5, \text{ and } 1.0$.

So, knowing x'_b and y'_b from Eq. 9.111, using Eqs. 9.112 we can calculate the dimensionless velocity components on the body, u'_b, v'_b , and thus the pressure coefficient C_p , using:

$$V_b^2 = U^2(u_b'^2 + v_b'^2), \quad \text{so that: } C_p = \frac{p - p_\infty}{\frac{1}{2}\rho U^2} = 1 - \frac{V_b^2}{U^2} = 1 - (u_b'^2 + v_b'^2) \quad (9.113)$$

Figure 9.16b shows the pressure coefficient for Rankine bodies for $\beta=0.25, 0.5,$ and 1 as determined from Eq. 9.113.

Note that the shape of the body, although symmetric, varies markedly with the value of β , as does the pressure coefficient. In particular, the minimum pressure coefficient for the largest β value (1.0) occurs at the center of the body, whereas for the smallest β value (0.25), there are two minimums, occurring near the leading and trailing edges. As we pointed out earlier in this chapter, when a real flow passes a point of minimum pressure, and experiences an increasing pressure, viscous effects can cause the development of a flow separation region, a marked departure from inviscid flow simulations, and a marked increase in drag. For the present simulation of a Rankine body, we would expect our small $\beta = 0.25$ simulation to experience a flow separation sooner than the large β simulation, since the point of minimum pressure is predicted to occur much nearer the leading edge of the small $\beta = 0.25$ simulation body. We will address the sensitivity that real fluids have to pressure gradients when we discuss boundary layers in Chapter 13 and 14, and drag in Chapter 15.

9.9 Bodies Translating in a Potential Flow

In the previous section, we superposed elementary functions to create simulations of uniform flows around stationary bodies. However, what if we want to simulate the behavior of a body translating through a quiescent potential fluid? This will change the potential function of the flow field surrounding the body, although (as we will see) the pressure on the body and the relative velocity field remain the same. Basically, we take a flow that was simulated with a uniform approach velocity, and delete the uniform flow function from the initial complex potential function (this is like imposing a constant velocity of opposite sign to the superposed function). However, one must first determine how the constants for the other elementary function(s) relate to the uniform flow velocity. In the following section, we examine the translation of a cylinder through an otherwise stationary fluid.

9.9.1 Translation of a Cylinder in a Quiescent Fluid

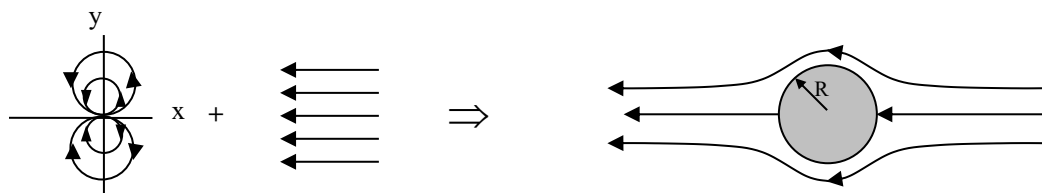


Figure 9.17 Simulated inviscid flow over a cylinder, passing right-to-left (i.e. moving in the negative x direction).

To illustrate the movement of a body through an inviscid, quiescent fluid, we will make use of our superposition of section 9.8.1, flow around a cylinder. Now, since we can make better sense

of this type of translating flow with a body moving in a positive direction, we will modify the superposed function to have the initial function simulate a flow from right-to-left (section 9.8.1 simulates the flow from left-to-right).

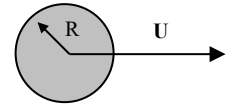
The appropriate function for this right-to-left flow, as shown in figure 9.17, is:

$$\Phi(z) = -Uz - \frac{s}{z} \quad (9.114)$$

Note that this is just the negative of Eq. 9.48, which reverses the direction of the flow field, with the cylinder stationary within the flow field. To simulate the translation of the cylinder at a positive velocity U to the right, we add $+Uz$ to the superposed function, which gives a new function:

$$\Phi(z) = -Uz - \frac{s}{z} + Uz = -\frac{s}{z} \quad (9.115)$$

Note that Eq. 9.115 is simply a doublet of strength s . This yields the flow field in a reference frame translating at a velocity U in the positive x direction, as shown at the right. However, what is the value of s for the doublet function in Eq. 9.115? Recall that we showed in section 9.8.1 that the radius of the simulated cylinder is given by:



$$R = \sqrt{\frac{s}{U}} \Rightarrow s = UR^2$$

Thus, substituting $s = UR^2$ for s into Eq. 9.115, we get:

$$\Phi(z) = -\frac{s}{z} = -\frac{UR^2}{z} \quad (9.116)$$

Expanding Eq. 9.116 in both r, θ and x, y variables, we have:

$$\begin{aligned} \Phi(z) &= -\frac{UR^2}{r}(\cos\theta - i\sin\theta) = -\frac{UR^2(x - iy)}{(x^2 + y^2)} \\ &= \left(-\frac{UR^2}{r}\cos\theta\right) + i\left(\frac{UR^2}{r}\sin\theta\right) = \left(-\frac{UR^2x}{(x^2 + y^2)}\right) + i\left(\frac{UR^2y}{(x^2 + y^2)}\right) \\ &= \phi + i\psi \end{aligned}$$

We will only need to use the potential function in this and the following section, so we note that for the translating cylinder:

$$\phi = \left(-\frac{UR^2}{r}\cos\theta\right) = \left(-\frac{UR^2x}{(x^2 + y^2)}\right) \quad (9.117)$$

Using the Cauchy relations, we can derive the velocities in both cylindrical and Cartesian as:

$$v_r = \frac{\partial\phi}{\partial r} = \frac{UR^2}{r^2} \cos\theta \quad (9.118a)$$

$$v_\theta = \frac{1}{r} \frac{\partial\phi}{\partial\theta} = \frac{UR^2}{r^2} \sin\theta \quad (9.118b)$$

and:

$$u = \frac{\partial\phi}{\partial x} = \frac{UR^2(x^2 - y^2)}{(x^2 + y^2)^2} \quad (9.119a)$$

$$v = \frac{\partial\phi}{\partial y} = \frac{2UR^2xy}{(x^2 + y^2)^2} \quad (9.119b)$$

Examining the resultant flow field is quite interesting. Let's examine the simulated velocity at three different points: (1) the leading edge of the cylinder at $(x,y) = (R,0)$, (2) the trailing edge of the cylinder at $(x,y) = (-R,0)$, and (3) the top of the cylinder $(x,y) = (0,R)$.

$$\begin{aligned} \text{Leading edge:} \quad u &= \frac{UR^2(R^2 - 0)}{(R^2 + 0)^2} = U; & v &= \frac{2UR^2(R)(0)}{(R^2 + 0)^2} = 0 \\ \text{Trailing edge:} \quad u &= \frac{UR^2((-R)^2 - 0)}{((-R)^2 + 0)^2} = U; & v &= \frac{2UR^2(-R)(0)}{(R^2 + 0)^2} = 0 \\ \text{Top of cylinder:} \quad u &= \frac{UR^2(0 - R^2)}{(0 + R^2)^2} = -U; & v &= \frac{2UR^2(0)(R)}{(R^2 + 0)^2} = 0 \end{aligned}$$

These results are shown graphically in figure 9.18.

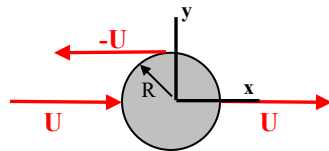


Figure 9.18 Velocity vectors at: (1) Leading edge, (2) Trailing edge, and (3) Top of a cylinder moving at velocity U left-to-right.

At the three points shown in figure 9.18, the y -direction velocity is zero, so only the u -direction velocity is relevant. Note that the velocity of the fluid at the leading and trailing edges of the cylinder are $u = U$, which is as expected, since the fluid velocity at the leading and trailing edge in a potential flow should be identical, and reflect the simulated velocity of the cylinder of U . However, at the top of the cylinder, the velocity of the fluid is $u = -U$ --- exactly the opposite of the cylinder velocity. Now consider that since the coordinates are fixed, these are the velocities

that would be observed by a fixed observer as the cylinder traveled by. Thus, a fixed observer would see a flow at the top of the cylinder in the negative x direction as the cylinder passed by. While this may seem strange, consider that for a fixed cylinder in a uniform flow of velocity U , the u velocity will increase from $u = 0$ at the leading edge to $2U$ at the top of the cylinder (in section 9.8.1 the velocity change was from 0 to $-2U$, because the flow was in the opposite direction). Thus, one might expect a total change in the velocity from the leading edge to the top of the cylinder of $|\Delta u| = 2U$, as our result shows.

This backflow behavior is not just a manifestation of potential flows, but occurs to some extent in many real fluid flows. For example, if you stand close to a passing large truck, train, or other vehicle (just not too close!) you will notice a flow of air in the opposite direction to that of the traveling vehicle. Now, a real flow is not a potential flow, but it is similar from the leading edge to the thickest point, so the same basic behavior will occur (although somewhat diminished by viscous effects).

Another example is an ocean wave---which can be roughly modeled as a translating half-cylinder. As a wave moves across the ocean on an otherwise still day, if you are floating on the ocean, you can feel a reversed flow of air as the wave passes by. This is accentuated as the wave height increases. Waves travel at velocities roughly proportional to the square root of their height, so a large wave moves faster than small waves. Consequently, a large wave has a stronger back flow of air over its face. On a calm day, if you watch a large wave just as it breaks upon approaching shore, you will see a spray of water blow backwards from the wave. This is again the result of a backflow of air created by the translating wave. The following image shows this backwards spray over a breaking wave.



This backflow of air over a wave is also put to good use by sea birds to aid in flight over water. Pelicans are the masters of harnessing these backflows of air over waves (they must have had good instruction in fluid mechanics). Next time you are at the seashore, and pelicans and modest size waves are present, notice that a pelican will often conserve energy by flying very close to the moving wave, and gliding along its face to take advantage of the backflow of air over the wave (as observed in the picture above). To see a video example of this pelican "wave" riding

behavior click this [video link](#). It is really impressive how the pelicans swoop and soar, catching the updraft off of one incoming wave after another. They are the original "surfers."

9.9.2 Pressure Field for a Translating Cylinder

It would seem that the determination of the pressure field for a translating body in a potential flow would be fairly straight forward. However, because the body is moving relative to the fixed reference frame, the calculation is a bit tricky. Recall from section 9.4 that the Bernoulli equation for an unsteady flow is given by Eq. 9.14 (neglecting the term for height changes, since we assume g is perpendicular to the flow) as:

$$\frac{P}{\rho} + \frac{1}{2}V^2 + \frac{\partial\phi}{\partial t} = C(t), \quad (9.14)$$

Now, Eq. 9.14 assumes that the flow field is stationary relative to the reference coordinates. However, the function ϕ in Eq. 9.117 for the translating cylinder is not stationary, but is translating at the cylinder velocity U . Thus, while the flow field is fixed relative to the cylinder, it is translating at a velocity U with respect to the x -coordinate. Consequently, while the flow field is fixed relative to the cylinder, it is moving relative to the fixed x - y reference frame. What this means is that we must take into account the translation relative to the reference frame when determining the pressure behavior. To do this requires that we determine $\frac{\partial\phi}{\partial t}$ in a translating reference frame. Thus, we must take into account both the temporal and the advective changes in ϕ . We do this by recalling that the substantial derivative gives the time changes for a property in a translating field. We note that we can consider ϕ as a flow field "property", since it is directly associated with the flow field (i.e. its derivatives define the flow field velocities). Thus, we realize we need to rewrite Eq. 9.14 as:

$$\frac{P}{\rho} + \frac{1}{2}V^2 + \frac{D\phi}{Dt} = C(t), \quad (9.120)$$

From Chapter 3, Eq. 3.17, we can write the substantial derivative of ϕ as:

$$\frac{D\phi}{Dt} = \mathbf{u}_{\text{rel}} \cdot \frac{\partial\phi}{\partial\mathbf{x}} + \frac{\partial\phi}{\partial t} \quad (9.121)$$

Note that in Eq. 9.121 we only include the advective acceleration term for the translation of ϕ in the x -direction, \mathbf{u}_{rel} , since ϕ does not translate relative to the y -coordinate. However, what is \mathbf{u}_{rel} ? This is the velocity observed by the cylinder relative to the flow, which is $\mathbf{u}_{\text{rel}} = -U$, since that is the velocity an observer in the cylinder would perceive relative to the coordinate system--the fluid would appear to move toward the cylinder in a negative x direction as the cylinder moves left-to-right.

Still with me? If the translation velocity U and ϕ are steady (we'll consider the case where they are not steady in section 9.11), Eq. 9.121 reduces to:

$$\frac{D\phi}{Dt} = -U \frac{\partial\phi}{\partial x} = -Uu \quad \text{since } u = \frac{\partial\phi}{\partial x} \quad (9.122)$$

Now, substituting Eq. 9.122 back into Eq. 9.120, noting $V^2 = u^2 + v^2$, gives:

$$\frac{P}{\rho} + \frac{1}{2}(u^2 + v^2) - Uu = C(t) \quad (9.123)$$

To determine $C(t)$, we note that far upstream from the translating cylinder ($x \gg R$), the flow will be quiescent and will have a pressure $P_\infty = \text{constant}$ where $u = 0$, $v = 0$. Thus, $C(t) = \frac{P_\infty}{\rho}$.

Substituting into 9.123, we do some rearranging, as shown:

$$\begin{aligned} \frac{P}{\rho} + \frac{1}{2}(u^2 + v^2) - Uu &= \frac{P_\infty}{\rho} \\ \frac{P}{\rho} + \frac{1}{2}(u^2 - 2Uu) + v^2 + \frac{1}{2}U^2 &= \frac{P_\infty}{\rho} + \frac{1}{2}U^2 \\ \frac{P}{\rho} + \frac{1}{2}(u^2 - 2Uu + U^2) + v^2 &= \frac{P_\infty}{\rho} + \frac{1}{2}U^2 \\ \frac{P}{\rho} + \frac{1}{2}(u - U)^2 + v^2 &= \frac{P_\infty}{\rho} + \frac{1}{2}U^2 \end{aligned} \quad (9.124)$$

Checking some selected points for the pressure reflected by Eq. 9.124, we showed above that $u = U$, $v = 0$ at the leading and trailing edges of the cylinder, $(x,y) = (R,0) = (-R,0)$, and $u = -U$, $v = 0$ at the top of the cylinder, $(x,y) = (0,R)$. Checking the pressures predicted by Eq. 9.124, we have:

Leading and Trailing edges: @ $(x,y) = (R,0)$ and @ $(x,y) = (-R,0)$, where $u = U$, $v = 0$:

$$\begin{aligned} \frac{P_{LE}}{\rho} + \frac{1}{2}(U - U)^2 + 0 &= \frac{P_\infty}{\rho} + \frac{1}{2}U^2 \\ \frac{P_{LE}}{\rho} &= \frac{P_\infty}{\rho} + \frac{1}{2}U^2 \quad \left(= \frac{P_{TE}}{\rho} \text{ also} \right) \end{aligned}$$

Top (and also the bottom) of cylinder: @ $(x,y) = (0,R)$, where $u = -U$, $v = 0$:

$$\frac{P_{\text{TOP}}}{\rho} + \frac{1}{2}(-U - U)^2 + 0 = \frac{P_{\infty}}{\rho} + \frac{1}{2}U^2$$

$$\frac{P_{\text{TOP}}}{\rho} = \frac{P_{\infty}}{\rho} - \frac{3}{2}U^2$$

Note that these values are identical to what we found for a flow around a stationary cylinder in section 9.8.1. Thus, the pressure field around a translating cylinder is unchanged from that for a comparable flow around a stationary cylinder. This will also be the case for any other simulated potential flow geometry translating through a quiescent potential fluid.

9.10 Accelerating Bodies in a Potential Flow: Virtual/Added Mass

Now, consider what happens if we specify that the velocity of a simulated body varies with time, such that $U(t)$. As the body accelerates or decelerates, the adjacent fluid will also undergo a commensurate acceleration or deceleration as well. The acceleration/deceleration of the adjacent fluid requires an additional force above that required to accelerate/decelerate the body alone. This additional force is reflected by a virtual or "added" mass of fluid proportional to the body displacement. In this section, we will examine how a time-changing velocity impacts the pressure field on a body, and how that is reflected in the amount of virtual or added mass. Note that fluid mechanics literature uses the terms virtual and added mass interchangeably. To simplify our discussion, we will simply use the term added mass

9.10.1 Acceleration of a Cylinder in a Quiescent Fluid

We will again consider a translating cylinder as our example of a body translating in an inviscid fluid at a velocity U in the positive x -direction, but such that U is a function of time, $U(t)$. We can revisit Eq. 9.121, the substantial derivative of ϕ .

$$\frac{D\phi}{Dt} = \mathbf{u}_{\text{rel}} \frac{\partial\phi}{\partial\mathbf{x}} + \frac{\partial\phi}{\partial t} \quad (9.121)$$

In section 9.9.2, we showed that the advective part of Eq. 9.121 was $\mathbf{u}_{\text{rel}} \frac{\partial\phi}{\partial\mathbf{x}} = -uU$. This

advective component remains the same for a time-varying velocity. And we can determine $\frac{\partial\phi}{\partial t}$

from our previous expression for ϕ , Eq. 9.117, as:

$$\frac{\partial\phi}{\partial t} = -\frac{R^2 x}{(x^2 + y^2)} \frac{dU}{dt} = -\frac{R^2}{r} \cos\theta \frac{dU}{dt}$$

Thus, Eq. 9.121 becomes:

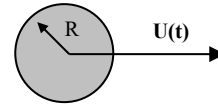
$$\frac{D\phi}{Dt} = -uU - \frac{R^2}{r} \cos\theta \frac{dU}{dt} \quad (9.125)$$

Substituting Eq. 9.125 into the unsteady Bernoulli equation, Eq. 9.120, and noting $C(t) = \frac{P_\infty}{\rho}$,

where P_∞ is the pressure in the quiescent fluid well-removed from the translating cylinder, we can rearrange the equation to give:

$$\frac{P}{\rho} + \frac{1}{2}(u-U)^2 + v^2 = \frac{P_\infty}{\rho} + \frac{1}{2}U^2 + \frac{R^2}{r} \cos\theta \frac{dU}{dt} \tag{9.126}$$

Note that this is similar to Eq. 9.124, with the addition of the last term in Eq. 9.126, which is the additional momentum change due to the acceleration of the fluid surrounding the cylinder. If we examine the pressure at the leading and trailing edge for a cylinder accelerating linearly at $U(t) = U_0(1+at)$, where U_0 and a are constants,



Eq. 9.126 gives:

Leading edge: @ $(x,y) = (R,0)$, $u = U$, $v = 0$, and $\theta = 0$

$$\frac{P_{LE}}{\rho} + \frac{1}{2}(U-U)^2 + 0 = \frac{P_\infty}{\rho} + \frac{1}{2}U^2 + R \cos(0)(U_0a)$$

$$\frac{P_{LE}}{\rho} = \frac{P_\infty}{\rho} + \frac{1}{2}U^2 + RU_0a$$

Trailing Edge: @ $(x,y) = (-R,0)$, $u = U$, $v = 0$, and $\theta = \pi$

$$\frac{P_{TE}}{\rho} + \frac{1}{2}(U-U)^2 + 0 = \frac{P_\infty}{\rho} + \frac{1}{2}U^2 + R \cos(\pi)(U_0a)$$

$$\frac{P_{TE}}{\rho} = \frac{P_\infty}{\rho} + \frac{1}{2}U^2 - RU_0a$$

These results indicate that as the cylinder accelerates, the leading and trailing sides of the cylinder are subject to significantly different pressures. This is a significant difference from the constant velocity situation we examined in section 9.9.2. For the accelerating cylinder, pressures will be higher on the leading surface, and lower on the trailing surface. This pressure difference results in an additional force on the cylinder due to acceleration or deceleration of the fluid adjacent to, and moving with, the cylinder. As we will show in the following section, this additional force can be modeled as an "added mass"--an equivalent amount of fluid mass that would have to be accelerated/decelerated to account for the force due to the unbalanced pressure difference over the cylinder surface.

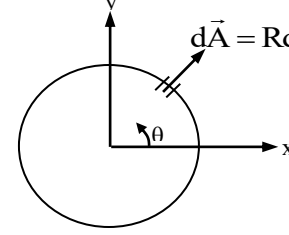
9.10.2 The Added Mass for an Accelerating Cylinder

To determine the force required to accelerate a cylinder in a quiescent flow, we note that this will just be the drag force, acting in the x-direction on the cylinder. We can determine this force by integrating the pressure field, similar to what was done in section 9.8.1. Thus, the drag force will be given by:

$$\text{Drag} = \int dF_x = -\int P A_x \quad (9.127)$$

Where,

$$d\bar{A} = dA_x \hat{i} + dA_y \hat{j} = R d\theta \hat{i}_r = R d\theta (\hat{i} \cos \theta + \hat{j} \sin \theta)$$



Thus, $dA_x = (R d\theta) \cos \theta$ is the differential area projection in the x-direction. From Eq. 9.126, we have the pressure of the surface as:

$$P|_{r=R} = P_\infty + \frac{1}{2} \rho U^2 - \frac{1}{2} \rho (u|_{r=R} - U)^2 - \frac{1}{2} \rho v|_{r=R}^2 + \rho R \cos \theta \frac{dU}{dt} \quad (9.128)$$

Now, we can most easily perform the integration along the surface of the cylinder ($r = R$, $0 < \theta < 2\pi$) in cylindrical coordinates. To do perform this integration, we must express the x and y-direction velocities in cylindrical coordinates. Using our expressions for u and v from Eq. 9.119, and noting that on the cylinder surface that $x = R \cos \theta$, and $y = R \sin \theta$, we can write u and v as:

$$u|_{r=R} = \frac{UR^2(x^2 - y^2)}{(x^2 + y^2)^2} = \frac{UR^4(\cos^2 \theta - \sin^2 \theta)}{R^4(\cos^2 \theta + \sin^2 \theta)^2} = U(\cos^2 \theta - \sin^2 \theta) = U \cos 2\theta \quad (9.129a)$$

$$v|_{r=R} = \frac{2UR^2xy}{(x^2 + y^2)^2} = \frac{2UR^4 \cos \theta \sin \theta}{R^4} = 2U \cos \theta \sin \theta = U \sin 2\theta \quad (9.129b)$$

Now, substituting Eqs.9.129 into Eq. 9.128, we get (using a few trigonometric identities along the way):

$$\begin{aligned} P|_{r=R} &= P_\infty + \frac{1}{2} \rho U^2 - \frac{1}{2} \rho U^2 (\cos 2\theta^2 - 2 \cos 2\theta + 1) - \frac{1}{2} \rho U^2 \sin^2 2\theta + \rho R \cos \theta \frac{dU}{dt} \\ &= P_\infty + \frac{1}{2} \rho U^2 - \rho U^2 (1 - \cos 2\theta) + \rho R \cos \theta \frac{dU}{dt} \\ &= P_\infty + \frac{1}{2} \rho U^2 - 2\rho U^2 (\sin^2 \theta) + \rho R \cos \theta \frac{dU}{dt} \\ &= P_\infty + \frac{1}{2} \rho U^2 (1 - 4 \sin^2 \theta) + \rho R \cos \theta \frac{dU}{dt} \end{aligned} \quad (9.130)$$

Finally substituting Eq. 9.130 into the drag equation, Eq. 9.127, and integrating from $\theta = 0$ to π :

$$\begin{aligned}
 \text{Drag} &= - \int_0^{2\pi} \left[P_\infty + \frac{1}{2} \rho U^2 (1 - 4 \sin^2 \theta) + \rho R \cos \theta \frac{dU}{dt} \right] R \cos \theta d\theta \\
 &= - \left(P_\infty + \frac{1}{2} \rho U^2 \right) R \sin \theta \Big|_0^{2\pi} + 2 \rho U^2 R \frac{\sin^3 \theta}{3} \Big|_0^{2\pi} - \rho R^2 \left(\frac{1}{2} \theta - \frac{1}{4} \sin 2\theta \right) \frac{dU}{dt} \Big|_0^{2\pi} \\
 &= \quad 0 \quad \quad \quad + \quad 0 \quad \quad \quad - \rho \pi R^2 \frac{dU}{dt} \\
 \text{Drag} &= -\rho \pi R^2 \frac{dU}{dt} = -(\rho \pi R^2) \frac{dU}{dt} \tag{9.131}
 \end{aligned}$$

Notice that the first two terms in Eq. 9.131 are identical to those in the drag calculation in section 9.8.1 for flow around a stationary cylinder, and satisfy d'Alembert's paradox. However, the last term in Eq. 9.131, that is associated with the acceleration of the cylinder, does not equate to zero, and is proportional to the mass of fluid displaced by the cylinder (per unit depth). Notice also that the Drag force is negative, indicating that it is acting in opposition to the direction of acceleration (negative if $\frac{dU}{dt} > 0$, and positive if $\frac{dU}{dt} < 0$). Thus, $m_{\text{added}} = \rho \pi R^2$ is the mass of fluid per unit depth whose acceleration must be accounted for when the cylinder is accelerated. Note that if the cylinder is much denser than the fluid (e.g. a metal rod in air), the added mass has little effect. However, if the mass of the fluid is heavier, or comparable to the mass of the cylinder, the added mass can have a significant impact (e.g. a wooden rod being moved through water).

The added mass for the cylinder is equivalent to the mass of fluid displaced by the cylinder. One might be tempted to think that all other bodies would have added masses equivalent to the mass of the fluid displaced by the body. However, that is not the case. For example, the added mass for a sphere is equivalent to $\frac{1}{2}$ the displaced fluid (i.e. $m_{\text{added}} = \frac{2}{3} \rho \pi R^3$). And the added mass for a square rod of sides w is roughly $m_{\text{added}} = 1.17 \rho w^2$, or 1.17 times the displaced mass. A good table of added mass values for a number of geometries can be found in a Naval report by [C.E. Brekken \(1982\)](#), available electronically through the Caltech library. Note that added mass is quite relevant to the U.S. Navy, and others who make use of ship and boat transport, since the mass of a ship and the water it sails in are closely equivalent, and thus added mass significantly influences the forces on a ship during acceleration/deceleration, and changes of direction.

Note that we have only considered added mass in one dimension. In reality, translating geometries can experience added mass effects in multiple directions, which can make the issue

quite complicated. [Brennen's report](#) touches on a number of the issues of added mass associated with multiple motions of a body.

The present section has considered the effects of added mass for inviscid flows. However, real flows are viscous, and bodies experience drag forces due to viscosity. Moreover, it would seem logical that the acceleration of bodies in a viscous flow should also experience some form of added mass as well. That is the case, and we will discuss how we deal with added mass in real, viscous flows when we examine flow separation and drag in Chapter 15.

Study Problems

1. The stream function for an inviscid flow is given by $\psi(x, y, t) = V_0(x+t)(y-t)$, where $V_0 = 1$.
 - a) Show that ψ represents a potential flow solution.
 - b) Determine the corresponding form of $\phi(x, y, t)$ [note: let $\phi = 0$ at $x, y = 0, 0$].
 - c) Employ ϕ to help determine a general expression for the pressure difference, $P_2 - P_1$, between any two points in the flow field, (x_1, y_1) and (x_2, y_2) .
 - d) Determine the non-dimensional pressure difference $(P_2 - P_1)/\rho V_0^2$ between:
 - Case #1: $(x_1, y_1) = (0, 0)$ and $(x_2, y_2) = (1, 0)$; and
 - Case #2: $(x_1, y_1) = (0, 0)$ and $(x_2, y_2) = (0, 1)$.
 - e) Plot $(P_2 - P_1)/\rho V_0^2$ vs. t for both cases on the same graph for $0 < t < 2$.
 - f) Plot the streamline and the potential lines passing through $(x, y) = (1, 1)$ at times $t=0$ and $t = 1$ (plot each time on separate graphs); plot over the region $0 < x < 2$ and $0 < y < 2$. What is characteristic about the behavior of the streamline and potential lines in these two graphs?

2. The stream function for an inviscid flow is given by $\psi(x, y, t) = V_0(x+t)(y+t)$, where $V_0 = 1$.
 - a) Show that ψ represents a potential flow solution.
 - b) Determine the corresponding form of $\phi(x, y, t)$ [note: let $\phi = 0$ at $x, y = 0, 0$].
 - c) Employ ϕ to help determine a general expression for the pressure difference, $P_2 - P_1$, between any two points in the flow field, (x_1, y_1) and (x_2, y_2) .
 - d) Determine the non-dimensional pressure difference $(P_2 - P_1)/\rho V_0^2$ between:
 - Case #1: $(x_1, y_1) = (0, 0)$ and $(x_2, y_2) = (1, 0)$; and
 - Case #2: $(x_1, y_1) = (0, 0)$ and $(x_2, y_2) = (0, 1)$.
 - f) Plot $(P_2 - P_1)/\rho V_0^2$ vs. t for both cases on the same graph for $0 < t < 2$.
 - g) Plot the streamline and the potential lines passing through $(x, y) = (1, 1)$ at times $t=0$ and $t = 1$ (plot each time on separate graphs); plot over the region $0 < x < 2$ and $0 < y < 2$. What is characteristic about the behavior of the streamline and potential lines in these two graphs?

3. In the section 9.8.1 example, it was shown that one could represent the flow around a cylinder by superposition of a uniform flow and a doublet, to give the complex potential function as:

$$\Phi(z) = Uz + \frac{s}{z}$$

Here the uniform velocity approaches from the left, where $x < 0$. The stream function in Cartesian variables is:

$$\psi = y \left(U - \frac{s}{x^2 + y^2} \right)$$

Assume a doublet strength $s = U$, and:

- Determine the velocity field components u and v for this stream function in terms of x and y :
 - Determine the pressure coefficient $C_p = \frac{P - P_\infty}{\frac{1}{2}\rho U^2}$ as a function of x, y variables (don't try to simplify—it's messy).
 - Simplify your expression for C_p to give $C_p = f(x)$ along the $\psi = 0$ streamline ($y=0$), for $x < -R$ (the stagnation point of the cylinder).
 - Using your result from part c, determine the non-dimensional pressure gradient coefficient, $\frac{dC_p}{dx} = \frac{\frac{dP}{dx}}{\frac{1}{2}\rho U^2} = f(x)$ along the $\psi = 0$ streamline ($y = 0$), for $x < -R$ (the stagnation point of the cylinder).
 - On one graph, plot u/U , C_p , and dC_p/dx vs. x along the $\psi = 0$ streamline ($y=0$), for $-4R < x < -R$ (use Eq. 9.53 to establish the value of R).
4. The flow field near a tornado can be approximated as the superposition of a sink and a irrotational vortex, with the steam function given by:

$$\psi = \frac{Q}{2\pi}\theta - \frac{\Gamma}{2\pi}\ln r$$

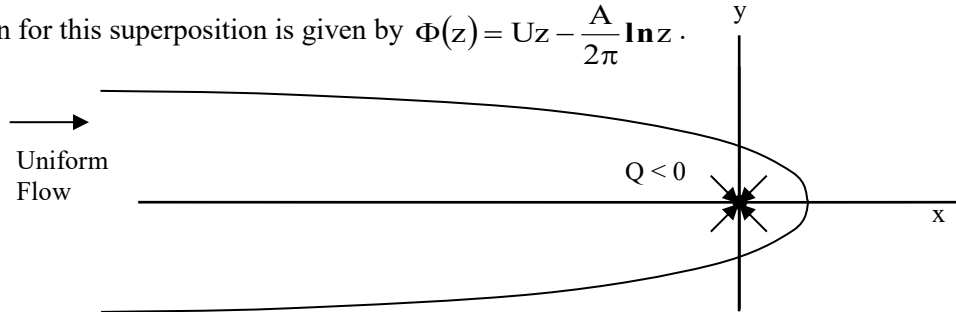
For $Q = -2\pi$ and $\Gamma = 2\pi$, determine the velocities in both radial and Cartesian coordinates, and an expression for the pressure, where $P = P_{\text{atm}}$ for $r \rightarrow \infty$. Create a plot of the streamlines that pass through $(x,y) = (2,0), (0,2), (-2,0),$ and $(0,-2)$. Show the streamlines in the region $-2 < x < 2, -2 < y < 2$.

Is this a realistic approximation as $r \rightarrow 0$? Justify your answer.

5. A point vortex with circulation strength $\Gamma = +A$ is located at $x = 0, y = 1$; a similar point vortex with $\Gamma = -A$ is located at $x = 0, y = -1$. Determine the velocity field $\vec{V} = u\hat{i} + v\hat{j}$ and the pressure coefficient C_p along the x -axis, where $C_p = \frac{p}{\frac{1}{2}\rho\left(\frac{A}{\pi}\right)^2}$.

Plot C_p for $y = 0, -3 < x < 3$. Let $p = 0$ at $x = 0, y = 0$.

6. Uniform flow U approaching from the left encounters a sink of strength $Q = -A$, located at $x, y = 0, 0$. This roughly approximates the behavior of a flow approaching a drain. The complex potential function for this superposition is given by $\Phi(z) = Uz - \frac{A}{2\pi} \ln z$.



Determine the following:

- The stream function, ψ , in terms of both r, θ and x, y ;
- The velocities u and v in terms of x, y , and r, θ ;
- The location of a stagnation point in the flow, if there is one;

Now, let $U = 1$ and $A = 1$ and make a nice engineering graph of:

- The streamlines $\psi = 0, -0.05$, and -0.30 all on one graph. Show all streamlines for the region $-0.6 < x < 0.3$ and $0 < y < 0.6$ only. Note: to plot each streamline, you will have to determine $r = f(\theta)$, calculate r for a series of θ values, then determine the corresponding series of x and y locations.

7. Consider a vertical wall with an impinging jet, as modeled by the complex potential function $\Phi(z) = (A/2)z^2$, with $A = -2$ (flow right-to-left). Determine the following, considering all quantities dimensionless (simplify all answers):

- Expressions for the stream function ψ in terms of both x, y and r, θ ;
- The velocity components v_x, v_y (in x, y) and v_r, v_θ (in r, θ);
- The location of the stagnation point for $x \geq 0$, and the value of ψ which passes through this stagnation point;
- An expression for $P - P_s$ as a function of r, θ , where P_s is the stagnation pressure (let the fluid density be $\rho = 2$);

Plot the following:

- Graphs on x, y axes of:
 - Streamlines $\psi = 0$ and -2 for the region $3 > x > 0$ and $3 > y > 0$;
 - The pressure $P - P_s$ and the pressure gradient dP/dx along $y = 0, 3 > x > 0$;
 - A line of constant pressure $p - p_s = -16$ for $x > 0$.

8. Consider a vertical wall with an impinging jet, as modeled by the complex potential function $\Phi(z) = (A/2)z^2$, with $A = -2$ (flow right-to-left) [problem 7, above]. Now, a source of strength $Q = 4\pi$ is located at the origin ($x, y = 0, 0$). Use superposition to simulate the effect of the source on the vertical wall with an impinging jet modeled in problem 7 above. For this modified flow, specify the appropriate complex potential function and determine the following:

- Expressions for the stream function ψ in terms of both x, y and r, θ ;
- The velocity components v_x, v_y (in x, y) and v_r, v_θ (in r, θ);

- c) The location of the stagnation point for $x \geq 0$, and the value of ψ which passes through this stagnation point;
- d) An expression for $P - P_s$ as a function of r, θ , where P_s is the stagnation pressure (let the fluid density be $\rho = 2$);

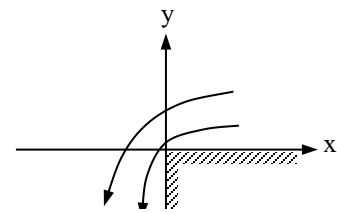
Plot the following:

- e) Graphs on x, y axes of:
 - i) Streamlines $\psi = 0$ and -2 for the region $3 > x > 0$ and $3 > y > 0$;
 - ii) The pressure $P - P_s$ and the pressure gradient dP/dx along $y = 0, 3 > x > 0$;
 - iii) A line of constant pressure $P - P_s = -16$ for $x > 0$;

9. Consider a flow over a 90° step (a convex, 270° corner), as modeled by the complex potential

function $\Phi(z) = \frac{3A}{2} z^{2/3}$, with $A = -2$ (flow right-to-left).

Note: $A < 0$, as shown



Convex, 270° Corner ($n=2/3$)

Determine the following, considering all quantities dimensionless (simplify all answers):

- a) An expressions for the stream function ψ in terms of r, θ ;
- b) Expressions for the Cartesian velocities u and v in terms of r, θ ;
- c) An expression for $P - P_\infty$ in terms of r, θ , where P_∞ is where $r \rightarrow \infty$;

Now, Create nice engineering graphs of:

- d) The streamlines $\psi = 0, -1$, and -2 all on one graph. Show all streamlines for $x < 10$ and $y > -10$ only. Note: to plot each streamline, you will have to determine $r = f(\theta)$, calculate r for a series of θ values, then determine the corresponding series of x and y locations.
- e) A plot of $P - P_\infty$ vs. x along the streamline $\psi = 0$ from $x = 10$ to $x = 0.2$. Why wouldn't you plot the pressure at $x = 0$?

10. Consider a circular cylinder of radius 1 meter and density of 500 kg/m^3 , which is moved back and forth within a vat of inviscid water ($\rho = 1000 \text{ kg/m}^3$) at a velocity $U = U_0 \sin(\omega t)$, where $U_0 = 2 \text{ m/s}$ and $\omega = \pi/2 \text{ s}^{-1}$. Determine or show the following:

- a) An expression for the displacement (in m) of the cylinder (call it x) as a function of time [let $x = 0$ at $t = 1$].
- b) An expression for the pressure difference (in N/m^2) between the leading and trailing edge of the cylinder ($P_{le} - P_{te}$) as a function of time.
- c) The force (per unit length of cylinder, in N/m) as a function of time that must be applied to the cylinder to maintain the velocity [hint: you must include both the cylinder mass and the added mass in the calculation].
- d) Three separate graphs on one sheet of: (1) the cylinder displacement, x , (2) $(P_{le} - P_{te})$, and (3) force, all for $0 < t < 4$.

11. Consider a circular cylinder of radius 1 meter and density of 1000 kg/m^3 , which is moved back and forth within a vat of inviscid water ($\rho = 1000 \text{ kg/m}^3$) by a time-dependent force (per unit length of cylinder) $F = F_0 \sin(\omega t)$, where $F_0 = 10,000 \text{ N/m}$ and $\omega = \pi/2 \text{ s}^{-1}$. Determine or show the following:
- An expression for the velocity (in m/s) of the cylinder as a function of time [let $U = 0$ at $t = 1$].
 - An expression for the displacement (in m) of the cylinder (call it x) as a function of time [let $x = 0$ at $t = 0$].
 - An expression for the pressure difference (in N/m^2) between the leading and trailing edge of the cylinder ($P_{le} - P_{te}$) as a function of time.
 - Three separate graphs on one sheet of: (1) the cylinder displacement, velocity, U , (2) displacement, x , and (3) ($P_{le} - P_{te}$), all for $0 < t < 4$.
12. A marble of density 2.5 gm/cm^3 is dropped into a vat of inviscid fluid the density of water, 1 gm/cm^3 . If gravity is constant at $g = 9.81 \frac{\text{m}}{\text{s}^2}$ (acting downward), what is the acceleration of the marble as it descends in the inviscid fluid? Take into account the buoyancy of the fluid, and the added mass of a sphere, $m_{\text{added}} = \frac{2}{3} \rho \pi R^3$. If the initial height and velocity of the marble are zero, how much less would it descend (in meters) in 3 seconds due to the added mass?
13. A six cm diameter wooden rod (density of 0.5 gm/cm^3) accelerates perpendicular to its length (sort of like rowing with the rod) through an inviscid fluid of density 2 gm/cm^3 . A one-meter length of the rod is submerged in the fluid. If a constant force of 10 N is applied normal to the rod's length, what will be the rod's velocity after 4 seconds? How far will the rod travel after 4 seconds? Assume $U = 0$ and $x = 0$ at $t = 0$.
14. A six cm diameter wooden rod (density of 0.5 gm/cm^3) accelerates perpendicular to its length (sort of like rowing with the rod) through an inviscid fluid of density 1 gm/cm^3 . A one-meter length of the rod is submerged in the fluid. If the rod is accelerated at 1 m/s^2 , determine the force applied normal to the rod's length.

What will be force on the rod after 1 second? What is the force at 4 seconds? What amount of the calculated force is due to the added mass?

Chapter 10

Changes in Circulation and Kelvin's Theorem

Contents

10.1 Circulation Changes for a Translating Fluid Region	309
10.2 Examples of Regions Showing Temporal Changes in Circulation	312
10.2.1 Diffusion of a Viscous Vortex	312
10.2.2 Regions of Baroclinic Density Variations	314
10.2.3 Baroclinic Variations in the Atmosphere	314
10.2.4 Baroclinic Variations Due to Local Heating	317
10.2.5 Baroclinic Variations Due to Density Stratification	319
10.3 Kelvin's Theorem for a Translating Fluid Region	321
10.3.1 Examples of Circulation Preserving Flows	322
10.4 Helmholtz's Theorems for Inviscid Flow	325

As we showed in Chapter 8, the circulation of a region of fluid reflects the summation of the vorticity over the area of the region, which can be shown by [Stoke's Theorem](#) to be equivalent to the integration of the tangential velocity around the bounding circuit of the region. Since both vorticity and circulation are functions of the velocity field (i.e. a property field), they are also properties of the flow field, and are subject to changes as they move within the flow field. The respective changes of circulation and vorticity due to transport through the flow field can accordingly be assessed by applying the substantial derivative to each property, and then use our previously-derived equations of momentum (i.e. Navier-Stokes) and continuity to assist in simplifying the resulting expressions. In this chapter, we address the temporal changes in circulation that take place for an initial vorticity-bearing quantity of fluid, such as a decaying vortex, as the fluid moves within a flow field. In the following Chapter 11, we will develop the vorticity transport equation, which models how vorticity can change within a flow field, and explore the different types of behavior that cause such changes in vorticity.

As we show in section 10.3, the additional assumption of inviscid flow for a flow with circulation gives rise to what is known as [Kelvin's Theorem](#). This theorem, derived initially by [Lord Kelvin](#) in the 1800's, states that for an inviscid fluid the circulation of an initial quantity of fluid will not change with time. Although limited in application, since real fluids are viscous, Kelvin's theorem allows us to consider the limiting behavior of a fluid due to changes in circulation.

10.1 Circulation Changes for a Translating Fluid Region

Consider the circulation for a region of fluid bounded by a contiguous circuit (any closed path that starts and ends at the same point within a fluid, like a circle). At any instant, from the development of the concept of circulation in Chapter 8, we know that the circulation within that circuit is given using Stokes theorem as:

$$\Gamma = \oint \vec{V} \cdot d\vec{s} \quad \text{where } d\vec{s} = dx\hat{i} + dy\hat{j} + dz\hat{k} \quad \text{where } \vec{\omega} \text{ is shown in the diagram} \quad (10.1)$$


However, what happens to the circulation within this initial region of fluid as time progresses? Is there a temporal change in Γ as the fluid particles comprising the original fluid region move within the fluid? To examine this, we take the substantial derivative of Eq. 10.1 (in Cartesian coordinates), which yields:

$$\frac{D\Gamma}{Dt} = \frac{D}{Dt} \oint \vec{V} \cdot d\vec{s} = \frac{D}{Dt} \oint (u dx + v dy + w dz) \quad \text{where } d\vec{s} = dx\hat{i} + dy\hat{j} + dz\hat{k} \quad (10.2)$$

In Eq. 10.2 we assume we can follow the original bounded region of fluid, such that the initial mass of fluid within the region remains constant (although the shape of the bounding circuit and the properties within the circuit can change). Recall that [Leibniz's rule](#) states that if the limits of integration are not a function of time [$\forall \neq f(t)$], then the derivative can be performed inside the integral. In the present case, we assume that our initial region of fluid is constant (i.e. of fixed volume), although the boundary of the volume can vary. However, since the volume of material does not change, this implies the limits of integration also do not change. Thus, by Leibniz's rule we can move the substantial derivative inside the integral, such that we perform the substantial derivative on the integrand of Eq. 10.2, which allows us to write Eq. 10.2 as:

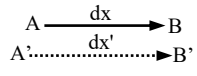
$$\frac{D\Gamma}{Dt} = \oint \frac{D}{Dt} (u dx + v dy + w dz) \quad (10.3)$$

To assess the circuit integral of Eq. 10.3, we will examine one element of the integrand, and extrapolate the resulting behavior to the other two elements. So, expanding the substantial derivative of the first term of the integrand in Eq. 10.3 (the x-direction component), we obtain:

$$\frac{D(u dx)}{Dt} = dx \frac{Du}{Dt} + u \underbrace{\frac{D(dx)}{Dt}}_{du}$$

$$\frac{D(u dx)}{Dt} = dx \frac{Du}{Dt} + u du = dx \frac{Du}{Dt} + \frac{1}{2} d(u^2)$$

Note that $\frac{D(dx)}{Dt}$ is the rate of change of the projection of dx , which is simply du , the change in the x-direction velocity, du .



$$\frac{dx - dx'}{dt} = u - u' = du \quad (10.4)$$

In Eq. 10.4, similar to what we showed in section 3.3, the substantial derivative of the differential change in the x-direction (dx) is simply the differential of the x-direction velocity (du).

We know from the x-direction component of the Navier-Stokes equation (Eqs. 5.44 and 5.46a) that:

$$\frac{Du}{Dt} = -\frac{1}{\rho} \frac{\partial P}{\partial x} + \beta_x + \nu \nabla^2 u \quad (10.5)$$

Substituting $\frac{Du}{Dt}$ from Eq. 10.5 into Eq. 10.4, we get:

$$\frac{D(udx)}{Dt} = \left(-\frac{1}{\rho} \frac{\partial P}{\partial x} + \beta_x + \nu \nabla^2 u \right) dx + \frac{1}{2} d(u^2) \quad (10.6a)$$

Similarly, the other components of the integrand in Eq. 10.3 become:

$$\frac{D(vdy)}{Dt} = \left(-\frac{1}{\rho} \frac{\partial P}{\partial y} + \beta_y + \nu \nabla^2 v \right) dy + \frac{1}{2} d(v^2) \quad (10.6b)$$

$$\frac{D(wdz)}{Dt} = \left(-\frac{1}{\rho} \frac{\partial P}{\partial z} + \beta_z + \nu \nabla^2 w \right) dz + \frac{1}{2} d(w^2) \quad (10.6c)$$

Substituting Eqs. 10.6 into Eq. 10.3 and collecting terms gives:

$$\begin{aligned} \frac{D\Gamma}{Dt} = \oint & \underbrace{-\frac{1}{\rho} \left(\frac{\partial P}{\partial x} dx + \frac{\partial P}{\partial y} dy + \frac{\partial P}{\partial z} dz \right)}_{dP} + \underbrace{(\beta_x dx + \beta_y dy + \beta_z dz)}_{d\beta} \\ & + \underbrace{\nu (\nabla^2 u dx + \nabla^2 v dy + \nabla^2 w dz)}_{\nu \nabla^2 \vec{V} \cdot d\vec{s}} + \frac{1}{2} \underbrace{d(u^2 + v^2 + w^2)}_{V^2} \end{aligned} \quad (10.7)$$

After identification of the collected terms, as indicated in Eq. 10.7, as the total differentials of pressure, body force, and V^2 , the time change in circulation can be separated into three parts as:

$$\begin{aligned} \frac{D\Gamma}{Dt} &= -\oint \frac{dP}{\rho} + \underbrace{\oint \left(d\beta + \frac{1}{2} dV^2 \right)}_{= 0, \text{ if } d\beta \text{ is a conservative body force}} + \oint \nu (\nabla^2 \vec{V} \cdot d\vec{s}) \end{aligned} \quad (10.8)$$

If we assume [conservative body forces](#) (e.g. a gravitational field), the second circuit integral in Eq. 10.8 will *not depend upon the path of integration*. Thus, the result of the second circuit integral in Eq. 10.8 must be zero, which reduces Eq. 10.8 to:

$$\begin{aligned} \frac{D\Gamma}{Dt} &= -\underbrace{\oint \frac{dP}{\rho}} + \oint \mathbf{v}(\nabla^2 \vec{V} \cdot d\vec{s}) \\ &= 0 \text{ if } \rho = f(P) \end{aligned} \quad (10.9)$$

In Eq. 10.9, the rate of change of the circulation now depends on the variation of fluid density and the viscosity. If the density of the fluid is only a function of pressure [i.e. that $\rho = f(P)$], the fluid is termed a [barotropic fluid](#), within which lines of constant pressure (i.e. isobars) are parallel, or aligned, with lines of constant density (i.e. [isopycnals](#)). If $\rho \neq f(P)$, the fluid is termed a [baroclinic fluid](#), which means that the isopycnals within the fluid are misaligned with the isobars [e.g. this often occurs when there are significant thermal variations within the fluid]. So, if a fluid is barotropic, which is true for most single, isothermal fluids in a gravity field, then the integral $\oint \frac{dP}{\rho}$ is also not dependent upon the path of integration, and also becomes zero, such that Eq. 10.9 reduces to:

$$\frac{D\Gamma}{Dt} = \oint \mathbf{v}(\nabla^2 \vec{V} \cdot d\vec{s}) \quad (10.10)$$

Equation 10.10 is generally applicable for any Newtonian fluid that is barotropic and has a body force due only to gravitation. This is the most general equation for temporal changes in circulation for a defined region of fluid moving within a broader flow field, and indicates that changes in circulation for such a fluid are due to the viscous behavior of the fluid. There are a number of practical flows that satisfy this situation, particularly single, isothermal, incompressible liquids, and [polytropic gases](#) [i.e. for which $Pv^n = P\rho^{-n} = \text{constant}$]. However, for fluids where density variations exist due to dissimilar fluids or when $\rho \neq f(P)$, we then have $\oint \frac{dP}{\rho} \neq 0$ [more on this in section 10.2.2]. For fluids with significant thermal or salinity variations, such as density stratifications within the atmosphere or the ocean, changes in the circulation of a defined material region can and will take place, as we will discuss in section 10.2.2.

Basically, circulation of an initial amount of advecting fluid can only change due to:

- 1) Viscous effects (e.g. real flows near surfaces), or
- 2) Changes in density that are not direct functions of pressure changes, $\rho \neq \rho(P)$,
- 3) Non-conservative body forces.

Generally, since the body force for most practical flows is due to gravity, circulation changes in real fluids will generally only occur due to: (1) viscous effects, and (2) density variations.

10.2 Examples of Regions Displaying Temporal Changes in Circulation

10.2.1 Diffusion of a Viscous Vortex

Consider a symmetric, viscous vortex, with its vorticity initially concentrated within a region of fluid of radius, R , as shown schematically in figure 10.1. We will assume the vortex to be stationary relative to the center of rotation, and to have only an azimuthal velocity (i.e. v_θ). Here, the effects of viscosity will cause the vorticity within the initial region of fluid to diffuse radially outward, and eventually migrate across the boundaries ($r = R$) of the fluid region. When the vorticity diffuses across the fluid boundary, there will be a corresponding loss of vorticity from the originally defined region of fluid (Area = πR^2), and thus a loss of circulation from the region.

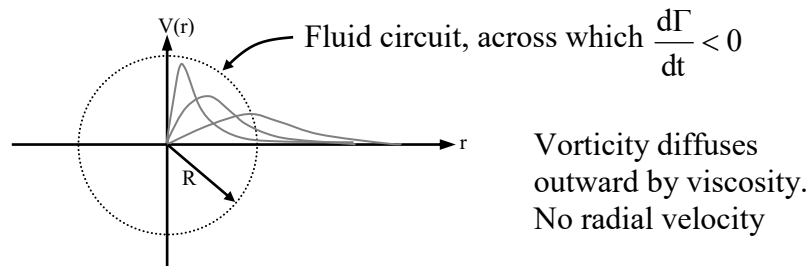


Figure 10.1 Example of the temporal diffusion of vorticity outward from an initial point vortex due to viscosity.

If the vorticity within the vortex is all concentrated into a small region such that, $r_{\text{vortex}} \ll R$, then the viscous vortex will initially be enclosed within the bounded region and Γ will initially remain constant within the region $r \leq R$. Changes will only occur when the vorticity eventually diffuses outward to and across the boundaries of the original region, R . However, given enough time, all of the vorticity will diffuse outward and across the larger bounding region, $r = R$. At that extended point in time ($t \rightarrow \infty$), $\frac{D\Gamma}{Dt} = 0$, and $\Gamma = 0$, since all of the vorticity will have diffused out of the bounded region, assuming that R is finite.

As a further example, consider an initially rotating viscous fluid inside a circular container with solid boundaries at $r = R$, as illustrated in Figure 10.2. One might think of this type of rotating flow as similar to that created within a cup of coffee or tea by the vigorous stirring of the fluid. Since the no slip condition applies at the outer solid boundary, that means that the circulation

within the confined fluid is zero, since $v_\theta = 0$ at the boundary, which gives the circulation as

$$\Gamma_{\text{total}} = \oint \vec{V} \cdot d\vec{s} = 0.$$

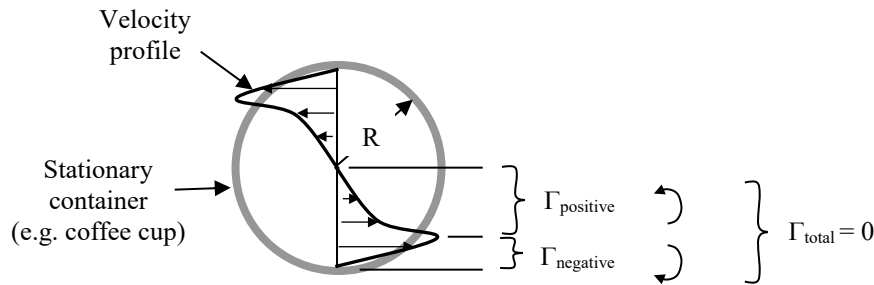


Figure 10.2 The circulation behavior of a viscous fluid contained within a circular container.

This lack of circulation and the zero velocity at the container boundary means that the total circulation within the container can never change, and that $\Gamma_{\text{total}} = 0$ for all time. Since this situation clearly involves a viscous flow, with plenty of initial vorticity, how is that possible? The key here is to recognize that such a flow contains equal amounts of *positive* and *negative* vorticity within the region $r \leq R$, and that these vorticity components diffuse and decay in such a way as to effectively cancel each other at all times. In essence, if we envision the circulation within the bounded region as the sum of: (1) the circulation associated with all elements of fluid with positive vorticity, Γ_{positive} , and (2) the circulation associated with all elements of fluid with negative vorticity, Γ_{negative} , then for any instant of time:

$$\Gamma_{\text{total}} = \Gamma_{\text{positive}} + \Gamma_{\text{negative}} = \sum_{\text{all fluid in region}} \omega dA = 0 \tag{10.11}$$

$$\text{Where } \Gamma_{\text{positive}} = \sum_{\text{all positive vorticity fluid}} \omega_{\text{positive}} dA \tag{10.12a}$$

$$\text{and, } \Gamma_{\text{negative}} = \sum_{\text{all negative vorticity fluid}} \omega_{\text{negative}} dA \tag{10.12b}$$

From Eq. 10.11 we note that:

$$\Gamma_{\text{positive}} = - \Gamma_{\text{negative}} \tag{10.13}$$

This implies $\Gamma_{\text{positive}} > 0$ and $\Gamma_{\text{negative}} < 0$, such that Γ_{positive} and Γ_{negative} always effectively offset each other, yielding a net circulation of zero. Initially, for our stirred coffee or tea, these values of Γ_{positive} and Γ_{negative} can be substantial. From consideration of Eq. 10.13 and Eqs. 10.12, we can infer that $\omega_{\text{positive}} > 0$ and $\omega_{\text{negative}} < 0$, and that these initial vorticities can also be substantial. However, after an extended period, we know that the fluid within the cup will come to rest due to

viscous effects, such that the velocity and vorticity within the cup will be zero everywhere. When the fluid is at rest, all the vorticity must have been dissipated, such that $\Gamma_{\text{positive}} = \Gamma_{\text{negative}} = 0$. What can be inferred from this assessment is that the initial distributions of positive and negative vorticity within the cup must cross-diffuse in such a manner as to continually cancel each other, eventually resulting in the dissipation of all the vorticity of both signs, as the fluid is brought to rest. We will revisit this question of cross-diffusion of vorticity in Chapter 11, as well as to examine how vorticity is initially created within such flows.

10.2.2 Regions of Baroclinic Density Variations

In Section 10.1 we discussed how circulation can change due to density variations. Assume for illustration that we have an inviscid fluid with conservative body forces. This would reduce Eq. 10.9 to:

$$\frac{D\Gamma}{Dt} = -\oint \frac{dP}{\rho} \quad (10.14)$$

As we discussed previously, if $\rho = f(P)$, or conversely $P = f(\rho)$, the result is that the circuit integral in Eq. 10.14 is independent of the path of integration, and will equal zero. These types of flows, as we discussed, are termed *barotropic*, which means is that lines of constant pressure (i.e. isobars) and lines of constant density (i.e. isopycnals) are parallel, or aligned. We can describe this process mathematically as $\nabla\rho \times \nabla P = 0$, which means that the gradients of the density and pressure are aligned. An example of such a fluid would be an isothermal body of water, or a uniformly compressible gas. Note that isobaric behavior is not necessarily constrained to isothermal flows, since it could also exist if the isotherms (i.e. lines of constant temperature) in the fluid are also parallel the isobars and isopycnals [often a difficult situation to achieve].

However, when the isobars and isopycnals *do not align* with each other, such as when there are lateral variations in temperature, then $-\oint \frac{dP}{\rho} \neq 0$, and a change in circulation will result. A flow where the isobars and isopycnals do not align is termed *baroclinic*. Examples of baroclinic flows include circulation induced by density stratifications within the world's oceans or atmosphere, where thermal gradients created by solar heating of the ocean/land can result in the generation of winds within the atmosphere or water currents in the ocean (salinity gradients within the ocean can also cause this). This is also the case for forest fires.

10.2.3 Baroclinic Variations in the Atmosphere

One of the more instructive examples of the generation of circulation by density variations is what is known as the [sea breeze](#) problem ([Green 1995](#)). Consider a simplified model of the

density variations in a coastal air layer spanning a region comprised of: (1) the sea, and (2) the land bordering the sea, as shown in Figure 10.3.

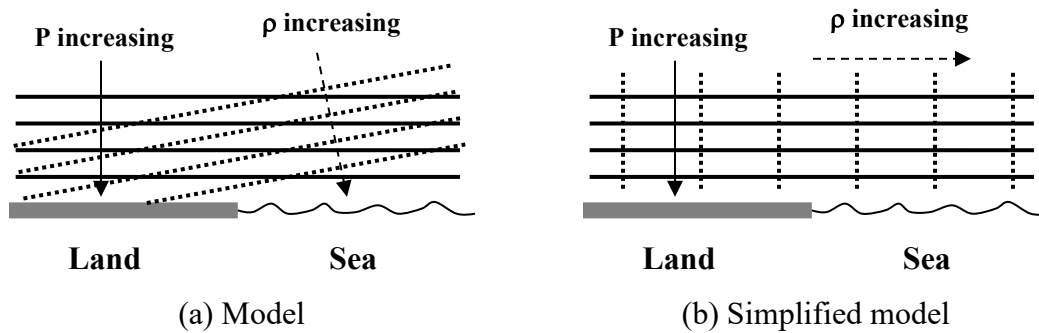


Figure 10.3 Modeling of the sea breeze problem.
 Solid lines (—) = isobars. Dotted lines (.....) = isopycnals.

Here we assume a time during mid-day, when solar radiation has had appreciable time to act upon both the land and the sea. Since land will warm more quickly than water, due to better solar absorption, a significant temperature difference will develop between the land and the sea. Consequently, the air over the sea will be cooler, and thus of higher density, whereas the air over the land will be warmer, and thus less dense. As this density variation within the air layer develops, the isopycnals (lines of constant density), will become sloped relative to the earth, and thus misaligned with the lines of constant pressure (we assume the isobars are parallel the earth), as modeled in Figure 10.3 (a). To make the calculation of circulation simpler, we will simplify the model even more, by assuming the isopycnals to be perpendicular to the isobars, as shown in Figure 10.3 (b). While this is an extreme situation, it is easy to perform the integration, and is still a reasonable, although extreme, model of the process.

Employing our simplified model, we now consider the circulation for a region one kilometer high by 20 kilometers wide, stretching equally from the land to sea, as shown in Figure 10.4.

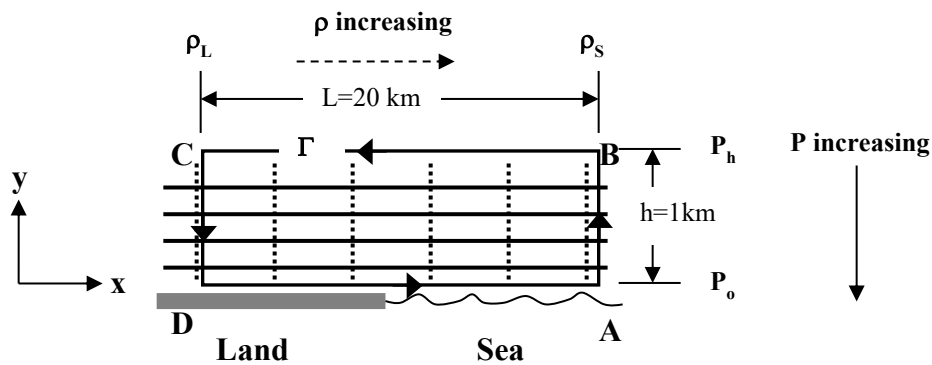


Figure 10.4 Atmospheric circulation for a region 20 km wide by 1 km high

Using Eq. 10.14, the change in circulation for the defined circulation loop can be calculated by integrating segmentally around the circuit shown in figure 10.4, starting at point A, as follows:

$$\begin{aligned}
 \frac{D\Gamma}{Dt} &= -\oint \frac{dP}{\rho} = -\int_A^B \frac{dP}{\rho_S} - \int_B^C \frac{dP}{\rho} - \int_C^D \frac{dP}{\rho_L} - \int_D^A \frac{dP}{\rho} = -\int_{P_o}^{P_h} \frac{dP}{\rho_S} - \int_{P_h}^{P_o} \frac{dP}{\rho} - \int_{P_h}^{P_o} \frac{dP}{\rho_L} - \int_{P_o}^{P_h} \frac{dP}{\rho} \\
 &= -\int_{P_o}^{P_h} \frac{dP}{\rho_S} - \int_{P_h}^{P_o} \frac{dP}{\rho_L} \\
 &= -\left[\frac{(P_h - P_o)}{\rho_S} + \frac{(P_o - P_h)}{\rho_L} \right] = (P_o - P_h) \left(\frac{1}{\rho_S} - \frac{1}{\rho_L} \right)
 \end{aligned} \tag{10.15}$$

Note that by assuming that the isopycnals are perpendicular to the isobars, only the integration of pressure in the *vertical* direction contributes to the change in circulation, since the pressure is assumed to not change laterally. If we now assume a 5 C difference in the air temperature, from 20 C (sea) to 25 C (land), this reflects air densities of approximately $\rho_S = 1.205 \text{ kg/m}^3$, and $\rho_L = 1.185 \text{ kg/m}^3$. We also assume $P_o - P_h \cong 11 \text{ kPa}$, roughly the vertical atmospheric pressure change over one kilometer, assuming a constant temperature.

Thus, Eq. 10.15 becomes:

$$\begin{aligned}
 \frac{D\Gamma}{Dt} &= (P_o - P_h) \left(\frac{1}{\rho_S} - \frac{1}{\rho_L} \right) \\
 &= (11 \text{ kPa})(1000) \frac{\text{N}}{\text{m}^2 - \text{kPa}} (1) \frac{\text{kg} - \text{m}}{\text{s}^2 - \text{N}} \left(\frac{1}{1.205} - \frac{1}{1.185} \right) \frac{\text{m}^3}{\text{kg}} \cong -154 \frac{\text{m}^2}{\text{s}^2}
 \end{aligned} \tag{10.16}$$

If we assume the average tangential velocity at the periphery of the defined circulation region is V , then the circulation for that region is approximated as: $\Gamma = \oint V \cdot ds \approx V \times 2(h + L)$. Now,

assuming that $\frac{D\Gamma}{Dt}$ is relatively constant over a period of time, we can approximate:

$$\int_0^t \frac{D\Gamma}{Dt} dt \approx \frac{D\Gamma}{Dt} t = \Gamma_t - \Gamma_0 \approx V \times 2(h + L) \tag{10.17}$$

Here we assume initially quiescent conditions, with $V_{\text{initial}} = 0$, and thus $\Gamma_0 = 0$. Solving Eq.

10.17 for the velocity, and substituting from Eq. 10.16, we can determine the wind velocity after one hour under these baroclinic conditions:

$$V \approx \frac{D\Gamma}{Dt} \frac{t}{2(h + L)} = (-154) \frac{\text{m}^2}{\text{s}^2} \left(\frac{1}{42} \right) \frac{\text{hr}}{\text{km}} (3600) \frac{\text{s}}{\text{hr}} \left(\frac{1}{1000} \right) \frac{\text{km}}{\text{m}} = -13.2 \frac{\text{m}}{\text{s}}$$

This is roughly 30 miles per hour! Since this value is negative, this implies that the velocity must move in opposition to the presumed counter-clockwise rotation (right-hand rule) for circulation. Accordingly, this means that the airflow would be toward the land at lower elevations, and toward the ocean at higher elevations. This would typically be what is known as an “on shore” wind, due to the warming of the air over land during the day. In the evening, since the land cools faster than the sea, the air over the land will cool more quickly, resulting in a reversal of the flow, with flows from the land to the sea at lower elevations, in what is termed an “off shore” wind.

Obviously, the assumed skewing of the density isopycnals is extreme, and would be much less severe. Also, for a real atmospheric flow, viscosity will mediate the wind effects. However, this example should make clear the importance of baroclinicity in generating circulation, and thus vorticity. These thermally-induced variations in atmospheric density [along with Coriolis effects] basically control the world’s wind and weather patterns, including the generation of [ocean waves](#), which are the result of prolonged wind interactions with the ocean surface.

10.2.4 Baroclinic Variations Due to Local Heating

Other examples of baroclinic generation of circulation are natural convection due to a heated vertical surface or air currents generated by a flame. In the case of a heated vertical plate, the isobars will be horizontal, but the isopycnals are essentially vertical—almost identical to the model we employed for the sea breeze problem (see study problem #6). The situation with a flame (let’s assume a candle) is also similar. Figure 10.5 illustrates (roughly), the velocity field associated with a flame. Here, we assume that the flow field is two-dimensional, but similar conclusions can be drawn for an axisymmetric flame. Note that we assume that the air adjacent to the flame is quiescent before the candle is lit, and thus has no circulation and no vorticity. However, after the candle is lit, both the air that undergoes the combustion process, and the air in proximity to the flame, become less dense, and circulation is generated.

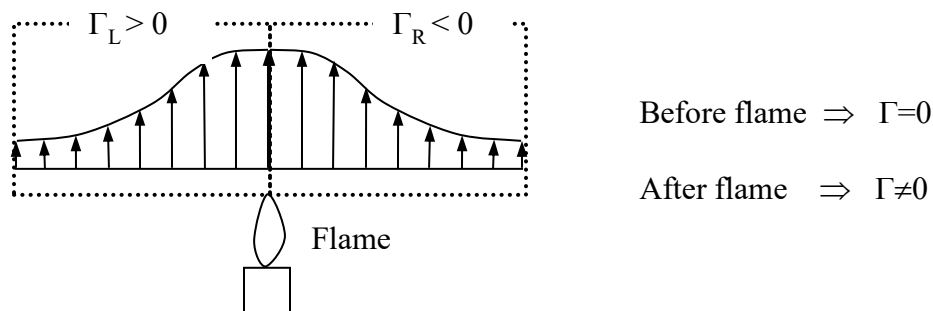


Figure 10.5 Generation of circulation by a flame.

This generation of circulation is also indicative of the accompanying generation of vorticity. However, the flow field in Figure 10.5 illustrates that the circulation for the region to the *right* of the flame, Γ_R , is *less than zero* because the vorticity generated would have a clockwise rotation (for this figure, the right-hand rule assigns counter-clockwise rotation as positive). However, the circulation for the region to the *left* of the flame, Γ_L , is *greater than zero* because the vorticity generated would have a counter-clockwise rotation. Further note that the total circulation will be the sum of both regions, i.e. $\Gamma_{\text{total}} = \Gamma_L + \Gamma_R$. If the flow is symmetric, it is obvious that $\Gamma_L = -\Gamma_R$, and $\Gamma_{\text{total}} = 0$! This is an interesting revelation, but clearly explainable. Although the flame will generate significant vorticity, it will generate equal amounts of both positive and negative vorticity, such that the cumulative positive vorticity (if one considers a large enough region surrounding the flame) will directly offset the cumulative negative vorticity. This is not dissimilar from the processes discussed in section 10.2.1 regarding the effects of viscosity in dissipating the vorticity within a contained, viscous fluid.

As a further extension of this example, consider a candle burning in air as a viscous fluid within a closed room. Here the equation that applies is: $\frac{D\Gamma}{Dt} = -\oint \frac{dP}{\rho} + \oint \mathbf{v}(\nabla^2 \vec{V} \cdot d\vec{s})$, since we must consider both baroclinic effects and viscous effects impacting the generation of circulation. However, if we note that $\Gamma_{\text{total}} = \oint \vec{V} \cdot d\vec{s} = 0$, since the boundaries of the room will be stationary, then the change in circulation within the room, $\frac{D\Gamma}{Dt} \Big|_{\text{room}} = 0$, since the circulation within the room can't change due to the no slip condition. Thus, the effects of vorticity generation by the flame due to baroclinicity, must either be: (1) balanced, due to symmetry, or (2) offset by viscous effects such that the total circulation within the room never changes. This balancing act between baroclinic effects and viscosity also assures that the velocities within the room, associated with the generation of vorticity, will never reach high values [note that without the presence of viscosity, the local velocities within the room could continually increase due to forcing by the density variations].

As a final aspect of temperature-induced circulation changes, consider the spread of a forest fire. By its very nature, a forest fire creates large local density variations, with isopycnals at sharp angles to the earth, whereas the isobars are generally aligned with the earth. As illustrated in figure 10.6, this creates strong circulation, which results in strong updrafts of high temperature gasses, flanked by strong down and side drafts that feed oxygen to the fire, thus intensifying the combustion process. Figure 10.6(a) is a balanced situation on a flat surface, with counterbalancing inflows holding the fire in place. However, when fires occur on a sloped surface, the inflows are unbalanced, such that the downhill circulation will be higher than the uphill circulation, causing such fires to migrate onto an upslope due to a skewing of the baroclinic process such that the fire creates its own uphill "wind", as depicted in figure 10.6(b). This induced uphill airflow can cause a fire to accelerate up the slope of a hill or mountain.

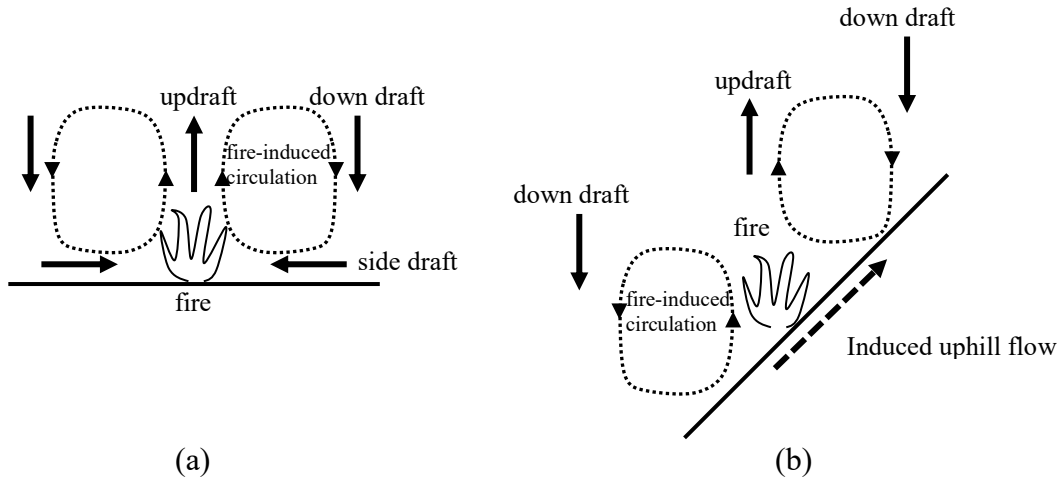


Figure 10.6 Creation of up and down drafts in proximity to fires, due to circulation created by density variations: (a) on a flat surface (b) on a sloped surface.

This generation of combustion-induced winds is extremely dangerous to fire fighters when the terrain becomes constrained, such as in a canyon, often resulting in a situation known as a “fire storm”, which usually results from a confluence of the fire with plentiful fuel on hilly terrain.

10.2.5 Baroclinic Variations Due to Density Stratification

The effects of strong density stratification (e.g. due to strong salinity variations in sea water, or dissimilar fluids) on the generation of circulation, and thus vorticity, can be illustrated by considering the behavior of two adjacent horizontal layers of inviscid, immiscible (non-mixing) fluids where $\rho_a \neq \rho_b$. If the two fluid layers are suddenly exposed to a uniform, lateral pressure difference or gradient, then Euler’s equation indicates that the acceleration of the two layers will be inversely proportional to the individual densities, such that a velocity gradient will be created across the interface, and thus vorticity and circulation must be created.

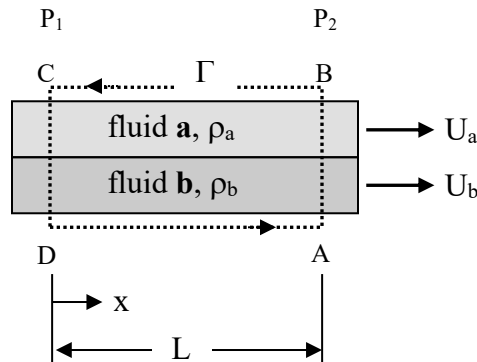


Figure 10.7 Circulation for a two layer, immiscible vertical density variation exposed to a lateral pressure gradient.

Consider the model above, and apply Euler's streamline equation (Eq. 7.7) in the x-direction :

$$\frac{1}{\rho} dP + d\left(\frac{V^2}{2}\right) + \frac{\partial \vec{V}}{\partial t} \cdot d\vec{s} = 0 \quad (10.18)$$

Here, we let $V = U$, where U is the x-direction velocity within either of the two fluids. Since the fluids are constrained to move in the x-direction, we also have $\frac{\partial \vec{V}}{\partial t} \cdot d\vec{s} = \frac{dU}{dt} dx$.

Substituting into Eq. 10.18 and rearranging, we have:

$$\frac{dU}{dt} dx = -\frac{1}{\rho} dP - d\left(\frac{U^2}{2}\right) = -\frac{1}{\rho} dP - U dU$$

$$\text{Or } \frac{dU}{dt} = -\frac{1}{\rho} \frac{dP}{dx} - U \frac{dU}{dx}$$

However, since the velocity within either fluid will increase uniformly with time, but will not vary in the x-direction, $\frac{dU}{dx} = 0$ within each fluid, and we have for either fluid:

$$\frac{dU}{dt} = -\frac{1}{\rho} \frac{dP}{dx} \quad (10.19)$$

In Eq. 10.19, the pressure difference is assumed to decrease linearly with x, and to be uniform across the two fluid layers, such that the pressure gradient is constant, and given by

$$\frac{dP}{dx} = \frac{P_2 - P_1}{L} < 0. \text{ Assuming that both fluids start from rest, we integrate Eq. 10.19 over time}$$

for fluid **a** to obtain the velocity behavior:

$$\int_{t=0}^t \frac{dU}{dt} dt = \int_{U_a=0}^{U_a} dU = -\frac{1}{\rho_a} \frac{dP}{dx} \int_{t=0}^t dt$$

$$(U_a - 0) = -\frac{1}{\rho_a} \frac{dP}{dx} (t - 0)$$

$$U_a = -\frac{t}{\rho_a} \frac{dP}{dx} = \frac{t}{\rho_a L} (P_1 - P_2) \quad \text{where } P_1 > P_2 \quad (10.20a)$$

Likewise, for fluid **b**, we get:

$$U_b = \frac{t}{\rho_b L} (P_1 - P_2) \quad (10.20b)$$

From Eqs. 10.20, we can see that if $\rho_a < \rho_b$, then $U_a > U_b$. Likewise, if $\rho_a > \rho_b$, then $U_a < U_b$. In either case, each fluid will accelerate uniformly with time, but at differential rates according to their density, such that a shear layer will be generated at the fluid interface, resulting in the generation of circulation and vorticity.

If we apply Eq. 10.14 about the circuit A-B-C-D shown in figure 10.7, we have:

$$\begin{aligned} \frac{D\Gamma}{Dt} &= -\oint \frac{dP}{\rho} = -\int_A^B \frac{dP}{\rho} - \int_B^C \frac{dP}{\rho_a} - \int_C^D \frac{dP}{\rho} - \int_D^A \frac{dP}{\rho_b} \quad \text{since } dP = 0 \text{ from A-B and C-D} \\ \frac{D\Gamma}{Dt} &= -\int_{P_2}^{P_1} \frac{dP}{\rho_a} - \int_{P_1}^{P_2} \frac{dP}{\rho_b} = -\frac{1}{\rho_a}(P_1 - P_2) - \frac{1}{\rho_b}(P_2 - P_1) \\ \frac{D\Gamma}{Dt} &= \left(\frac{1}{\rho_b} - \frac{1}{\rho_a} \right) (P_1 - P_2) \quad \text{where } P_1 > P_2 \end{aligned} \quad (10.21)$$

Equation 10.21 illustrates that if $\rho_a < \rho_b$, then $\frac{D\Gamma}{Dt} < 0$, which means that negative circulation and negative (clockwise) vorticity are generated. Conversely, if $\rho_a > \rho_b$, then $\frac{D\Gamma}{Dt} > 0$, and *positive* circulation and positive (counter-clockwise) vorticity are generated. Basically, under the same applied pressure (force) difference, the lower density fluid will accelerate faster than the higher density fluid, thus creating a velocity mismatch at the fluid interface. This velocity mismatch reflects generated vorticity, which cumulatively reflects the change in circulation.

Although not a perfect model, this example demonstrates, how vorticity can be generated within the ocean or the atmosphere when lateral pressure gradients act on a vertically stratified fluid. Examples of this situation are density stratifications near the sea surface due to strong thermal or salinity changes (although in reality these flows are a bit more complicated). As we will discuss in Chapter 11, once vorticity has been generated it can undergo a number of modifications, which can greatly change its character and complexity.

10.3 Kelvin's Theorem for a Translating Fluid Region

If we additionally restrict a material region to the flow of an ideal, inviscid fluid ($\nu = 0$), the right side of the circulation change equation, Eq. 10.10 becomes zero, due to the absence of viscosity. This further assumption of inviscid flow indicates that a region of fluid moving within an inviscid flow, and satisfying the constraints of:

- 1) barotropic fluid, with
- 2) conservative body forces, and
- 3) $\nu = 0$

will undergo no change in circulation, $\frac{D\Gamma}{Dt} = 0$, such that $\Gamma = \text{constant}$ over time. This statement is known as [Kelvin’s Theorem](#). Fluids that satisfy Kelvin’s Theorem $\left(\frac{D\Gamma}{Dt} = 0\right)$ are accordingly termed circulation-preserving fluids, since there is no change in circulation as the initial material region of fluid moves within a flow field.

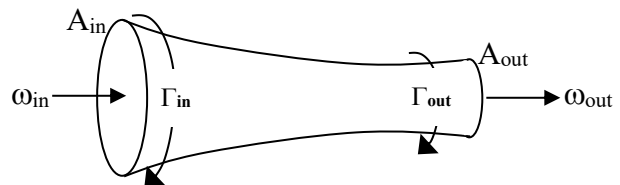
Kelvin’s theorem indicates that if a region of *inviscid* flow starts from rest, or is uniformly absent of vorticity at some initial time, then the circulation of this fluid region will remain zero as it moves through the flow field. However, if the region has some initial circulation, due to previous effects not satisfying the initial assumptions for the flow, then the circulation of the region will remain constant at its initial value.

10.3.1 Examples of Circulation Preserving Flows

Potential flows, as were discussed in Chapter 9, are examples of circulation preserving flows. For example, a material region of fluid approaching a cylinder [i.e. the potential flow process modeled in section 9.8.1], would come from a region of uniform flow (far upstream), and thus have no circulation. Since the flow is irrotational and inviscid, the material region, as it passes around the cylinder, and then departs downstream, according to Kelvin’s theorem will not change its circulation, and thus remain without circulation. This is also the case for the flow over a rotating cylinder, that we modeled by the additional superposition of a potential vortex [section 9.8.2]. Here again, the circulation within a fluid region does not change as the region passes from the upstream region of uniform flow, around the cylinder, and continues downstream. Recall that the source of vorticity in this flow, and thus the source of circulation, is confined to the origin of the superposed point vortex, which is contained within the modeled cylinder boundaries, and does not contribute circulation to the modeled material flow region. Thus, the circulation of a material fluid region, however defined, will thus remain zero as the region moves within the flow field.

Now consider the variation of circulation along a vortex tube. As we showed in section 8.3.2.1, the circulation at the entering and exiting cross-sections of a vortex tube will be constant, such that at any instant:

$$\Gamma_{in} = \iint_{A_{in}} \omega_{in} dA_{in} = \iint_{A_{out}} \omega_{out} dA_{out} = \Gamma_{out}$$



Thus, the circulation at any cross-section along a vortex tube must be constant. This relationship holds regardless of the type of fluid, as long as the boundaries of the vortex tube are comprised

of vortex lines [so this also holds if the flow is viscous or baroclinic]. However, if viscous or baroclinic effects are present, Eq. 10.9 indicates that the instantaneous circulation within the vortex tube can change within the original material region [the material volume will remain constant, but the shape of the tube may change]. However, for a circulation preserving flow, $\frac{D\Gamma}{Dt} = 0$, which means that the circulation at all cross-sections along the vortex tube will remain constant with time

A further example of the behavior of a circulation preserving fluid is illustrated by the impact of “stretching” a vortex tube (i.e. an increase in the tube length). Such stretching processes occur when a fluid with streamwise rotation passes through a nozzle, where the streamwise velocity is accelerated, and thus the fluid is “stretched” in the streamwise direction. Consider a section of a vortex tube, shown initially in Figure 10.8a below.

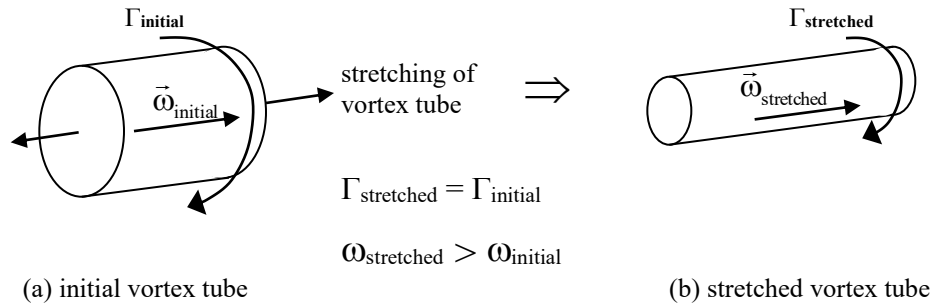


Figure 10.8 The effect of stretching on a vortex tube of constant cross-section

For simplicity, assume that the vortex tube is of constant cross-section and in solid body rotation such that, $\omega_{\text{initial}} = \text{constant}$. This vortex tube has an initial circulation at any cross-section of $\Gamma_{\text{initial}} = \omega_{\text{initial}} A_{\text{initial}}$. If this constant volume section of the vortex tube is then stretched [due to a spatial change in velocity along its axis], it will undergo an increase in length, and a commensurate decrease in cross-sectional area, as shown in Figure 10.8b.

If the fluid is circulation preserving, the circulation will not change during this stretching process, such that $\Gamma_{\text{stretched}} = \Gamma_{\text{initial}}$. Since the circulation of the stretched vortex tube will remain constant, the total vorticity encompassed at a cross-section must increase, since [assuming solid body rotation again]:

$$\omega_{\text{stretched}} A_{\text{stretched}} = \omega_{\text{initial}} A_{\text{initial}}$$

or

$$\omega_{\text{stretched}} = \omega_{\text{initial}} \left(\frac{A_{\text{initial}}}{A_{\text{stretched}}} \right) \tag{10.22}$$

From Eq. 10.22, it is clear that $\omega_{\text{stretched}} > \omega_{\text{initial}}$, since $A_{\text{stretched}} < A_{\text{initial}}$.

This is obviously a simplistic model, but it illustrates that the generic stretching of a vortex tube will result in intensification of the vorticity within the tube, due to preservation of angular momentum. In a real vortex, the vorticity will most likely not be uniform [i.e. in solid body rotation], but the vortex lines will undergo a similar intensification.

The opposite effect of stretching takes place if a vortex tube undergoes compression [i.e. a reduction in the length of the vortex tube segment]. Such a compression is accompanied by an expansion of the tube cross-section, and a reduction in the vorticity magnitude. Such processes occur when a flow undergoes a deceleration, such as in a diffuser, where the streamwise velocity is decreasing with streamwise distance. A similar analysis to Eq. 10.22 yields:

$$\omega_{\text{compressed}} = \omega_{\text{initial}} \left(\frac{A_{\text{initial}}}{A_{\text{compressed}}} \right) \quad (10.23)$$

Equation 10.23 indicates that $\omega_{\text{compressed}} < \omega_{\text{initial}}$, since $A_{\text{compressed}} > A_{\text{initial}}$. So, compression of the vortex tube results in a reduction in the local vorticity.

One caveat is that vortex compression is an *unstable* process, such that when a vortex tube undergoes more than a mild compression, the vortex tube will become unstable and “break down” or degenerate into a complicated tangle of vorticity. This process, as we discussed previously in section 8.3.2.1, is termed [vortex breakdown](#), and generally results in a loss of angular momentum, and a rapid increase in the complexity of the original vortex tube. Vortex breakdown is not well understood, and causes the rapid, and complicated, dispersion of the vorticity of the initial vortex tube over a broader cross-section. While vortex stretching is a generally stabilizing process, the viscosity of a real fluid can cause vortex breakdowns to develop in even accelerating, or stretched flows. It has been determined experimentally that vortex tubes may break down into a variety of different shapes, including closed and open bubbles, spirals and cone shapes. In general, at least seven different forms or types of breakdown have been identified. See some examples in videos shown [here](#).

It is relevant at this point to remind the reader of the analogy of circulation to flow rate, and vortex lines to streamlines. Recall that for an incompressible flow the flow rate is the area integral of the *velocity* across a material cross-section, and circulation is the area integral of the *vorticity* across a material cross-section. The flow rate within a stream tube will also be identical at any cross-section, as will the circulation at any cross-section of a vortex tube. The analogy falters for the temporal changes in flow rate and circulation, since we do not have a similar corollary to Kelvin’s theorem for flow rate. For a circulation preserving flow, the temporal flow

rate within a stream tube can change due to a temporal change in pressure, whereas circulation cannot change with time along a vortex tube.

Streamlines and vortex lines are also defined similarly [lines with their tangent parallel to the local vector property]. However, note that the velocity along a streamline can change due to pressure/height changes [Euler's equation shows us that], whereas the vorticity along a vortex line may or may not remain constant. For a circulation preserving fluid, the vortex lines are associated with a fixed set of fluid particles such that the vortex line will move with the set of fluid particles defining the vortex line. The vorticity of each fluid particle will thus be "frozen" at a constant value within the fluid. However, the influence of viscosity allows the vorticity of individual fluid particles to change, such that a vortex line will not be necessarily associated with the same fluid particles, nor will the fluid particles retain a fixed value of vorticity. Thus, if the fluid is not a circulation preserving fluid [due to viscous or baroclinic effects] the circulation *and* the vortex lines may both change with time.

10.4 Helmholtz's Theorems for Inviscid Flow

[Helmholtz \(1858\)](#) developed [three theorems](#) that govern *inviscid* flows, which preceded Kelvin's theorem. Helmholtz dealt with similar concepts for circulation preserving fluids, but also addressed some issues that Kelvin did not. These three theorems are as follows [paraphrased from Helmholtz].

- (1) An element of fluid, which is originally without rotation, will remain without rotation.
- (2) Any element of fluid on a vortex line will remain on that vortex line, regardless of the translation of the line.
- (3) The product of the area cross section and angular velocity of an infinitely thin vortex filament is constant throughout its whole length, and retains the same value during all displacements of the filament. Hence, vortex filaments must be closed curves, or must have their ends in the bounding surface of the fluid.

Since an inviscid fluid [in a gravitational, barotropic environment] will be a circulation preserving fluid, application of Kelvin's theorem to an infinitesimal element within the fluid implies that the circulation of that element will not change, from which the first theorem of Helmholtz follows directly. A corollary [from Kelvin's theorem] would be that if an element of fluid originally has initial rotation [i.e. circulation], it will retain that rotation throughout its movement within the fluid.

Helmholtz's second theorem is demonstrated by use of the result of section 8.3.2.1, where it is shown that the circulation at any cross-section along a vortex tube must remain constant. Now, imagine shrinking a vortex tube to the point where it is of infinitesimal cross-section, creating a vortex filament, which will contain: (a) a fixed line of fluid particles, and (b) a single vortex line.

From Kelvin's theorem, we know that the circulation along the inviscid filament must remain constant, and will not change as the line moves with the fluid. One can think of a linked set of symmetric fluid particles, which have both translational and angular velocities, where the angular velocities of the particles comprising the line are initially identical. If gravity or a pressure gradient acts on the flow field, the translation of the individual particles can change, but the angular velocity will remain unaffected, and the vortex line will move with the original fluid particles. One might think of a set of pearls frictionlessly rotating on a deformable string. In the absence of friction, external body or pressure forces may move the pearls about, but the rotation of each pearl, and their orientation relative to each other, will be maintained along the deformable string.

Helmholtz's third theorem is again a variation on what was shown in section 8.3.2.1, but also adds the need for a vortex tube or line to be contiguous. As discussed in section 8.3.2.2.2, vortex lines cannot summarily "end" within a fluid; there must be some aspect of closure of the line, either upon itself [e.g. a vortex ring or closed loop], or it must extend to infinity [which again actually assumes that the line must eventually close upon itself]. This is true for both inviscid and viscous fluids. A frequently cited exception to this vortex closure law is the hypothesis that a vortex line may end at the free surface of a fluid [e.g. at an air-water interface]. Such "ending" of a vortex line in water is often reflected by the dimpled swirls one sees on the surface of a stream. However, this supposed termination of the vortex line at the air-water interface only means that the water vortex line is matching the local vorticity [i.e. angular velocity] of a vortex line within the air on the opposing side of the interface. Thus, a vortex line in water "ending" at the water-air interface is contiguous to a vortex line within the air, which must somehow "close" upon itself (albeit in a complicated manner).

As a corollary, if the interface is a fluid-solid boundary, a vortex line within the fluid could only end at the boundary if the angular velocity of the solid boundary matches the angular velocity (vorticity) of the vortex line. This latter situation is relatively rare. However, this situation can occur for a fluid contained within a tank rotating about its axis. If the fluid and tank rotate in equilibrium, both the fluid and tank will be in steady, solid body rotation. The fluid will have a constant vorticity field, with vortex lines that extend from the surface of the fluid and end at the rotating surface of the tank.

Generally, when a real, viscous fluid interacts with a solid boundary, vortex lines will be generated, in the form of closed vortex "loops" either around a body [as for flow around a sphere] or within a duct [e.g. flow within a pipe]. Figure 10.8 illustrates the general orientation of several such vortex lines for flow around a sphere and through a rectangular duct.

The process of vorticity generation at a solid boundary is a topic that certainly merits further discussion. We will revisit the behavior, dynamics, and generation of vorticity, circulation, and

vortex lines further in the following Chapter 11, when we derive the governing differential equation for vorticity.

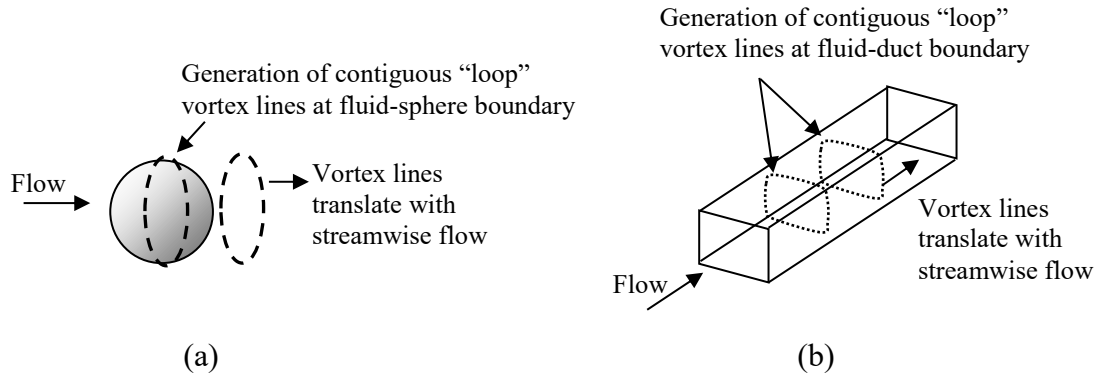


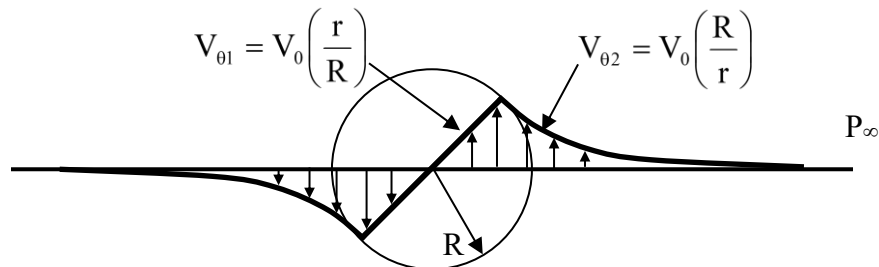
Figure 10.8 Contiguous nature of vortex lines for flow (a) around a sphere, and (b) through a rectangular duct.

References

Green, S. I. (1995). *Fluid Vortices: Fluid Mechanics and its Applications*, Kluwer Academic Publishers, Dordrecht.

Study Problems

1. A combined Rankine vortex is present in an inviscid fluid, as shown.



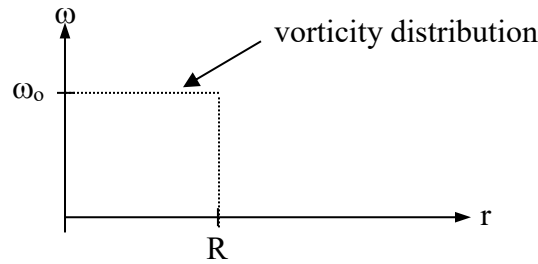
The vortex consists of a core of radius R , which is in solid body rotation with velocity $V_{\theta 1} = V_0 \left(\frac{r}{R} \right)$, and a portion outside the core ($r \geq R$) that has a velocity $V_{\theta 2} = V_0 \left(\frac{R}{r} \right)$. The

density of the flow is ρ , and the pressure far away from the vortex center is P_{∞} .

Determine the following:

- a) The vorticity, ω , for the entire flow field, as a function of r . Plot a graph of $\omega R/V_0$ vs. r/R from $0 < r/R < 2$.
- b) The circulation for,
 - i) a circle of radius R
 - ii) a square of side dimensions $4R$, with the vortex in the center of the square.
- c) The value of DI/Dt at $r = R$.

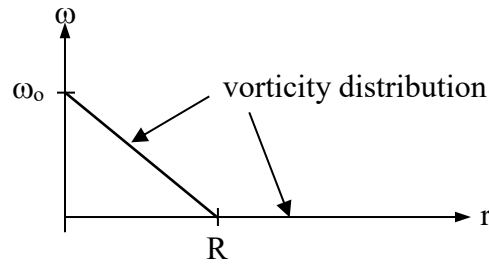
2. A vortex in an inviscid fluid has the following vorticity distribution, ω vs. r , where, $\omega = \omega_0$ for $r \leq R_0$, and $\omega = 0$ for $r > R$.



If the velocity distribution is $\vec{V} = v_\theta \hat{i}_\theta$ only, determine the following:

- The velocity distribution, $v_\theta(r)$, in terms of ω_0 and r , for $r \leq R$ (assume that $v_\theta(0) = 0$).
- The velocity distribution, $v_\theta(r)$, in terms of ω_0 , R , and r , for $r > R$.
- The circulation for,
 - a circle of radius R .
 - a square of side $3R$, with the vortex in the center of the square.
- The value of $D\Gamma/Dt$ at $r=R$.

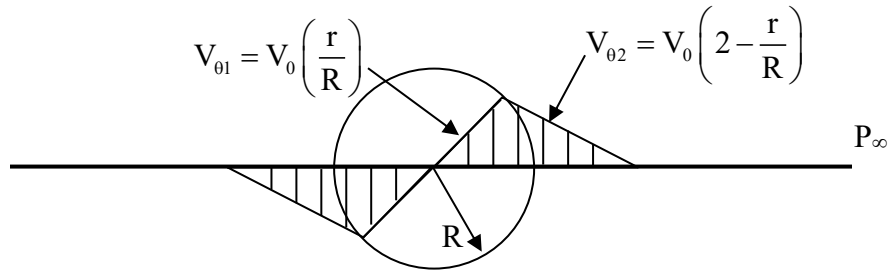
3. A vortex in an inviscid fluid has the following vorticity distribution, ω vs. r , where, $\omega = \omega_0 \left(1 - \frac{r}{R}\right)$ for $r \leq R_0$, and $\omega = 0$ for $r > R$.



If the velocity distribution is $\vec{V} = v_\theta \hat{i}_\theta$ only, do the following:

- Determine the velocity distribution, $v_\theta(r)$, in terms of ω_0 , R , and r , for $r \leq R$ (assume that $v_\theta(0) = 0$).
- Determine the velocity distribution, $v_\theta(r)$, in terms of ω_0 , R , and r , for $r > R$.
- Plot $\frac{v_\theta}{\omega_0 R}$ vs. $\frac{r}{R}$ for $0 \leq \frac{r}{R} \leq 2$
- Plot the non-dimensional circulation within a circle of radius r , $\frac{\Gamma}{2\pi\omega_0 R^2}$ vs. $\frac{r}{R}$, for $0 \leq \frac{r}{R} \leq 2$
- Explain what is happening to the circulation with increasing r , and why.

4. A vortex is present in an inviscid fluid, as shown.



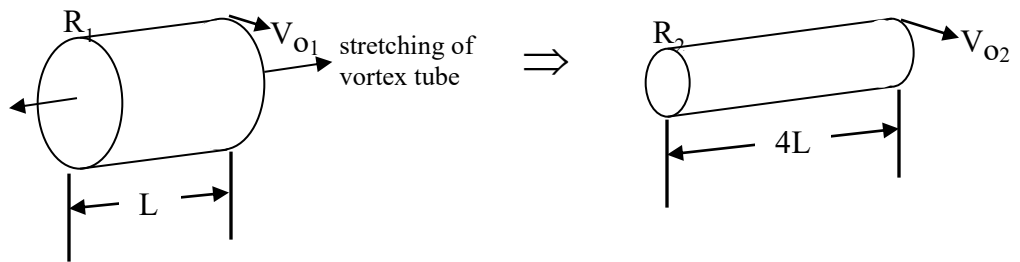
The vortex consists of a core of radius R , which is in solid body rotation with velocity

$$V_{\theta 1} = V_0 \left(\frac{r}{R} \right). \text{ The portion outside the core } (R \leq r \leq 2R) \text{ has a velocity } V_{\theta 2} = V_0 \left(2 - \frac{r}{R} \right).$$

The density of the flow is ρ , and the pressure far away from the vortex center is P_{∞} , including at $r = 2R$.

Determine the following:

- The vorticity for the entire flow field, as a function of r . Plot a graph of $\omega R/V_0$ vs. r/R from $0 < r/R < 2$.
- The circulation for,
 - a circle of radius R
 - a square of side $4R$, with the vortex in the center of the square
- The value of DI/Dt at $r=R$.
- A section of an inviscid vortex tube of length L with the velocity profile shown above, is stretched by acceleration of the fluid along the axis of the vortex tube to a length $4L$, while retaining the same rotational velocity profile. If $R = R_1$ and $V_0 = V_{O1}$ for the tube of length L , and $R = R_2$ and $V_0 = V_{O2}$ for the tube of length $4L$, determine the value of R_2 in terms of R_1 , and V_{O2} in terms of V_{O1} for the stretched tube of length $4L$.



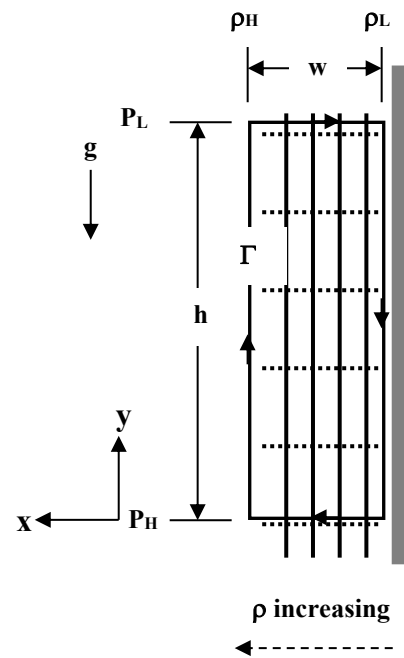
5. The velocity field for an Oseen line vortex is given by:

$$V_{\theta} = \frac{A}{2\pi r} \left[1 - \exp\left(-\frac{r^2}{4\nu t}\right) \right]$$

Let all parameters and variables be non-dimensional, and

- Determine the circulation, Γ , for curves of radius $r = R$ and $r = \infty$. For each case, determine Γ at $t = 0$, $t = R^2/4\nu$, and $t = \infty$.
- Again for curves of $r = R$ and $r = \infty$, and at $t = 0$, $t = R^2/4\nu$, and $t = \infty$, determine $D\Gamma/Dt$, both directly (by differentiation) and by using Eq. 10.10. Show that these are identical.
- Based on your results of part a and b, explain (briefly) what is physically happening to the vorticity and circulation of the flow field.

6. A vertical heated plate, 1 m in length, heats the adjacent air such that the temperature varies uniformly across a 4 cm thickness, from ambient (20 C) 4 cm from the plate surface to 30 C at the plate surface. As shown in the model at the right, assume that the isopycnals are parallel to the plate surface, and that the pressure varies with height according to $P = \rho gh$, where the density is the ambient density, and the pressure is constant perpendicular to the plate surface. Treating air as an inviscid fluid, what will be the maximum velocity within the air after 1 minute? In your opinion, is this answer reasonable? Explain your rationale for your opinion.



7. The velocity field for a viscous vortex is given by:

$$V_{\theta} = \frac{1}{2\pi r} \left[1 - \exp\left(-\frac{r}{t}\right) \right]$$

Let all parameters and variables be non-dimensional.

- Determine the circulation, Γ , for curves of radius $r = R$ and $r = \infty$. For each case, determine Γ at $t = 0$, $t = R$ and $t = \infty$.
- Again for curves of $r = R$ and $r = \infty$, and at $t = 0$, $t = R$, and $t = \infty$, determine $D\Gamma/Dt$ directly (by differentiation using the substantial derivative of Γ)
- Plot three separate graphs:
 - V_{θ} vs. r from $0 < r < 10$ for $t = 0.1, 1, \text{ and } 5$;
 - Γ vs. r from $0 < r < 10$ for $t = 0.1, 1, \text{ and } 5$; and
 - $D\Gamma/Dt$ vs. r from $0 < r < 10$ for $t = 0.1, 1, \text{ and } 5$.
- Based on your results of part a, b, and c explain (briefly) what is physically happening to the vorticity and circulation of the flow field.

8. The velocity field for a Taylor dissipating vortex is given by:

$$v_\theta = \frac{M}{16\pi \nu^2 t^2} \exp\left(-\frac{r^2}{4\nu t}\right)$$

Let all parameters and variables be non-dimensional, and

a. Determine the circulation, Γ , for curves of radius $r = R$ and $r = \infty$. For each case, determine Γ at $t = 0$, $t = R$ and $t = \infty$.

b. Again for curves of $r = R$ and $r = \infty$, and at $t = 0$, $t = R$, and $t = \infty$, determine $D\Gamma/Dt$ directly (by differentiation using the substantial derivative of Γ)

c. Plot three separate graphs:

i. $v_\theta' = \frac{16\pi\nu^2 v_\theta}{M}$ vs. r from $0 < r < 10$ for $t = 0.5, 1, \text{ and } 3$;

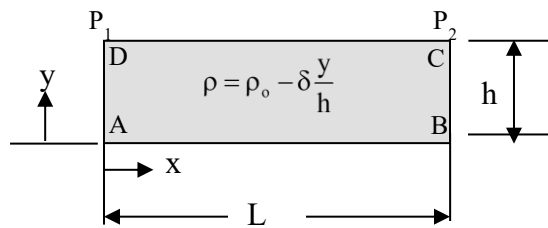
ii. $\Gamma' = \frac{8\nu^2 \Gamma}{M}$ vs. r from $0 < r < 10$ for $t = 0.5, 1, \text{ and } 3$

iii. $\frac{D\Gamma'}{Dt} = \frac{4\nu^2}{M} \frac{D\Gamma}{Dt}$ vs. r from $0 < r < 10$ for $t = 0.5, 1, \text{ and } 3$.

d. Based on your results of part a, b, and c explain (briefly) what is physically happening to the vorticity and circulation of the flow field.

9. An inviscid fluid of thickness h and length L , as shown, varies in density according to

$\rho = \rho_o - \delta \frac{y}{h}$. It is initially at rest. At time $t = 0$, a constant pressure difference is applied over the length L , with a pressure P_1 at $x = 0$, and P_2 at $x = L$, with $P_1 > P_2$.



Neglect gravity effects, and determine:

a) Using the unsteady Bernoulli equation along a streamline, an equation for the x-direction velocity within the fluid, $u = f(y, t)$, for $t > 0$ and $0 < y < h$.

b) A graph of $u(y,t)$ for $t = 1, 2, 3$ over $0 < y/h < 1$ for $(P_1 - P_2)/L = 1$, $\rho_o = 1$, and $\delta = 0.2$

c) The time rate of change in circulation, $\frac{D\Gamma}{Dt}$, for the region $0 < y < h$ and $0 < x < L$ in terms of P_1, P_2, ρ_o , and δ .

Chapter 11

The Vorticity Transport Equation

Contents

11.1 Derivation of the Vorticity Transport Equation	333
11.2 The Physical Relevance of the Terms of the Vorticity Transport Equation	335
11.2.1 Temporal Changes in Vorticity	335
11.2.2 Transport (Advection) of Vorticity by the Velocity Field	335
11.2.3 Diffusion of Vorticity	337
11.2.4 Generation of Vorticity by Stretching and Tilting	338
11.3 The Two-Dimensional Vorticity Transport Equation	342
11.4 One-Dimensional Vorticity Solutions	344
11.4.1 Flow Over a Flat Plate with Suction	345
11.4.2 Poiseuille Flow in a Parallel Channel	349
11.4.3 Steady Flow Outside a Rotating Rod	352
11.5 Sources of Vorticity	354
11.5.1 Vorticity Generation by Viscous Effects	354
11.5.2 Vorticity Generation by Acceleration	358
11.5.2.1 Acceleration of a Rotating Rod	358
11.5.2.2 Acceleration of a Circular Vessel	361
11.5.3 Vorticity Generation by a Streamwise Pressure Gradient	363
11.5.4 Vorticity Generation by Surface Transpiration	365
11.5.5 Vorticity Generation by Baroclinic Effects	368
11.6 Circulation Changes in a Fixed Reference Plane	372
11.7 Vorticity Transport Equations: Cartesian and Cylindrical Coordinates	377
11.7.1 General Vector Equation	377
11.7.2 Cartesian Equation Components (3-D)	377
11.7.3 Cartesian Equation (2-D in x, y)	378
11.7.4 Cylindrical Equation Components (3-D)	378
11.7.5 Cylindrical Equation (2-D in r, θ)	378

In Chapters 8 and 10 we dealt with vorticity and circulation, and the behavior of circulation for both viscous and inviscid fluids, as well as barotropic and baroclinic fluids. However, those considerations were primarily concerned with the behavior of either material regions or vortex tubes. In this chapter, we derive a differential equation to model the behavior of vorticity as it is *transported* within an incompressible flow field. Using this vorticity transport equation, we can assess the behavior of the vorticity field within a fluid, as well as address the processes of vorticity generation and destruction. In addition, we will employ the vorticity transport equation

to reexamine the behavior of circulation for a defined spatial region within a fluid, rather than just a material region. This will act as a springboard to begin to address the behavior of viscous flows adjacent to solid boundaries.

11.1 Derivation of the Vorticity Transport Equation

To obtain an equation for the transport of vorticity, we begin with the Navier-Stokes equation (Eq. 5.44), since we have shown that the Navier-Stokes equation models the “changes” within a velocity field. Since vorticity is defined as the curl of the velocity field, we take the curl of the Navier-Stokes equation and examine the result.

$$\begin{aligned} \nabla \times \left[\frac{D\vec{V}}{Dt} = -\frac{1}{\rho} \nabla P + \vec{B} + \nu \nabla^2 \vec{V} \right] \\ \nabla \times \frac{D\vec{V}}{Dt} = -\nabla \times \left(\frac{1}{\rho} \nabla P \right) - g(\nabla \times \nabla h) + \nu \nabla \times (\nabla^2 \vec{V}) \end{aligned} \tag{11.1}$$

0 (by Eq. 2.16a)

We expand the first term on the right hand side of Eq. 11.1:

$$\nabla \times \left(\frac{1}{\rho} \nabla P \right) = \nabla \left(\frac{1}{\rho} \right) \times \nabla P + \left(\frac{1}{\rho} \right) (\nabla \times \nabla P) = -\left(\frac{1}{\rho^2} \right) \nabla \rho \times \nabla P$$

0 (by Eq. 2.16a)

Recalling that $\nabla \times \nabla f = 0$ (see Eq. 2.16a), where f is a scalar, and noting that P and h are scalar properties, we have $\nabla \times \nabla P$ and $\nabla \times \nabla h = 0$, which reduces Eq. 11.1 to:

$$\nabla \times \frac{D\vec{V}}{Dt} = \left(\frac{1}{\rho^2} \right) \nabla \rho \times \nabla P + \nu \nabla \times \nabla^2 \vec{V} \tag{11.2}$$

Expanding the left side of Eq. 11.2 using the definition of the substantial derivative, the vector identity Eq.2.16g, and that $\nabla \times \vec{V} = \vec{\omega}$, the vorticity, we get:

$$\begin{aligned} \nabla \times \frac{D\vec{V}}{Dt} &= \nabla \times \left[\frac{\partial \vec{V}}{\partial t} + \vec{V} \cdot \nabla \vec{V} \right] = \nabla \times \left[\frac{\partial \vec{V}}{\partial t} + \frac{1}{2} \nabla (V^2) - \vec{V} \times (\nabla \times \vec{V}) \right] \\ &= \frac{\partial (\nabla \times \vec{V})}{\partial t} + \frac{1}{2} \nabla \times \nabla (V^2) - \nabla \times \underbrace{\vec{V} \times (\nabla \times \vec{V})}_{\vec{\omega}} \end{aligned}$$

0, since V^2 is a scalar

Again by Eq. 2.16a we are able to eliminate $\nabla \times \nabla (V^2)$, since V^2 is a scalar, leaving Eq. 11.3a.

$$\nabla \times \frac{D\vec{V}}{Dt} = \frac{\partial \vec{\omega}}{\partial t} - \nabla \times (\vec{V} \times \vec{\omega}) \tag{11.3a}$$

Expanding the last term in Eq. 11.3a using vector identity Eq. 2.16h, and noting that $\nabla \cdot \vec{\omega} = \nabla \cdot (\nabla \times \vec{V}) = 0$ (Eq. 2.16c) and $\nabla \cdot \vec{V} = 0$ (continuity), we end up with Eq. 11.3b.

$$\nabla \times \frac{D\vec{V}}{Dt} = \frac{\partial \vec{\omega}}{\partial t} - [(\vec{\omega} \cdot \nabla) \vec{V} - (\vec{V} \cdot \nabla) \vec{\omega} + \vec{V} (\nabla \cdot \vec{\omega}) - \vec{\omega} (\nabla \cdot \vec{V})]$$

$$\nabla \times \frac{D\vec{V}}{Dt} = \frac{\partial \vec{\omega}}{\partial t} + (\vec{V} \cdot \nabla) \vec{\omega} - (\vec{\omega} \cdot \nabla) \vec{V}$$
(11.3b)

Next, using the vector identity Eq. 2.16n, the last term on the right side of Eq. 11.2 becomes

$$\nu \nabla \times \nabla^2 \vec{V} = \nu \nabla^2 (\nabla \times \vec{V}) = \nu \nabla^2 \vec{\omega}$$
(11.4)

Finally, substituting Eqs. 11.3b and 11.4 into Eq. 11.2 gives:

$$\underbrace{\frac{\partial \vec{\omega}}{\partial t} + (\vec{V} \cdot \nabla) \vec{\omega} - (\vec{\omega} \cdot \nabla) \vec{V}}_{\frac{D\vec{\omega}}{Dt}} = \left(\frac{1}{\rho^2} \right) \nabla \rho \times \nabla P + \nu \nabla^2 \vec{\omega}$$
(11.5)

If we assume a barotropic fluid, where the gradients of density and pressure are parallel, then $\nabla \rho \times \nabla P = 0$, and our final equation becomes [moving the $(\vec{\omega} \cdot \nabla) \vec{V}$ term to the right hand side of the equation]:

$$\frac{D\vec{\omega}}{Dt} = \frac{\partial \vec{\omega}}{\partial t} + (\vec{V} \cdot \nabla) \vec{\omega} = \nu \nabla^2 \vec{\omega} + (\vec{\omega} \cdot \nabla) \vec{V}$$
(11.6)

Equation 11.6 is commonly known as the *Vorticity Transport Equation*, since it models all the processes by which vorticity can be transported and modified. The constraints on this equation are a constant density, barotropic fluid with constant viscosity. Note that a unique aspect of this equation is that by taking the curl of the Navier Stokes equation, we have eliminated any dependence of the fluid property of interest (vorticity) on pressure or height changes, as long as the only body force is conservative (i.e. gravity) and the fluid is barotropic.

The physical relevance of each of the terms Eq. 11.6 is indicated below.

$$\frac{D\vec{\omega}}{Dt} = \frac{\partial \vec{\omega}}{\partial t} + (\vec{V} \cdot \nabla) \vec{\omega} = \nu \nabla^2 \vec{\omega} + \vec{\omega} \cdot \nabla \vec{V}$$
(11.7)

\uparrow	\uparrow	\uparrow	\uparrow	\uparrow
total time rate of change of vorticity	local rate of change of vorticity	advection of vorticity by velocity field	viscous diffusion of vorticity	production of vorticity—by stretching or tilting of existing vorticity

11.2 The Physical Relevance of the Terms of the Vorticity Transport Equation

In the following section, we examine the processes modeled by the individual terms in the vorticity transport equation. As indicated in Eq. 11.7, the terms represent the: (1) local rate of change, (2) advection (transport), (3) viscous diffusion, and (4) production of vorticity. Note that production of vorticity is a process unique to the property of vorticity, since neither the continuity nor the Navier-Stokes equations include processes for “production” of either mass or momentum.

11.2.1 Temporal Changes in Vorticity, $\frac{\partial \vec{\omega}}{\partial t}$

The term $\frac{\partial \vec{\omega}}{\partial t}$ in Eq. 11.7 reflects the local temporal changes of vorticity at a point within the flow field. One might think of the decay of vorticity at a point over time in a swirling cup of coffee or tea. After the initial generation of the vorticity within the cup by stirring, the vorticity at any point within the cup will slowly decrease due to viscous effects. If we focus on a single point within the fluid, we will note temporal changes in the local vorticity as reflected by the $\frac{\partial \vec{\omega}}{\partial t}$ term. Figure 11.1 illustrates such a change in the vorticity at a point for the decay of a viscous vortex.

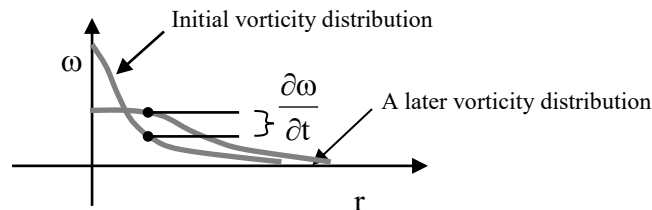


Figure 11.1 An example of the temporal change of vorticity in a viscous vortex

11.2.2 Transport (Advection) of Vorticity by the Velocity Field, $\vec{V} \cdot \nabla \vec{\omega}$

The $\vec{V} \cdot \nabla \vec{\omega}$ term in Eq. 11.7 reflects the transport (i.e. advection) of vorticity by the action of the velocity field. Note that this term is similar to the advection of momentum term $\vec{V} \cdot \nabla \vec{V}$ in the Navier-Stokes equation, and has a similar function of transporting a material (i.e. fluid) related property by physical translation of the fluid. As the material derivative [Section 3.3] illustrates, when fluid particles move within the velocity field, they also carry with them any associated property, such as mass (i.e. density), momentum (i.e. velocity itself), energy (i.e. temperature), or angular rotation (i.e. vorticity). However, since the differential equations are Eulerian-based, changes in the respective property are reflected by the spatial gradient of the property change [i.e. the spatial changes of the property with position within a non-uniform property field]. Thus,

as fluid undergoes translation within a spatial region, it will experience a change in the value of a local property due to its motion within the property field. One might think of this as similar to the change in temperature that we experience when we walk from a shaded to a sunny area. On a molecular level (i.e. using a Lagrangian view), it is of course a bit more complicated, since the cumulative distribution of a property [i.e. the property “field”] is really a reflection of the concentration of particles carrying that particular property. However, from an Eulerian viewpoint (viewing the fluid as a continuum), we perceive the local value of a fluid property as changing due to the translation of the fluid within that respective property field.

Thus, when considering the Eulerian view of a fluid as a continuum, the $\vec{V} \cdot \nabla \vec{\omega}$ term reflects changes in the vorticity at any point due to the transport of vorticity by the fluid towards or away from that point. This transport process is one means of physically redistributing *existing* vorticity within the region of interest [i.e. the “field”]. Note that since vorticity is a vector, and not a scalar, $\nabla \vec{\omega}$ is not exactly a gradient. It actually reflects three separate gradients—one for each directional component of rotation. For example, in a Cartesian coordinate system,

$$\nabla \vec{\omega} = \nabla \omega_x \hat{i} + \nabla \omega_y \hat{j} + \nabla \omega_z \hat{k} \text{]. Thus, } \nabla \omega_x = \frac{\partial \omega_x}{\partial x} \hat{i} + \frac{\partial \omega_x}{\partial y} \hat{j} + \frac{\partial \omega_x}{\partial z} \hat{k} \text{ reflects the changes in the } x\text{-}$$

direction component of vorticity, ω_x , in each respective coordinate direction. However, the actual changes in ω_x depend upon whether fluid is transported in a particular direction by the respective directional velocity component [e.g. a change of ω_x in the x-direction, $\frac{\partial \omega_x}{\partial x}$, will only occur if material is carried in the x-direction by the x-direction velocity component, u]. Thus, the product (i.e. dot product) of the directional velocity with the corresponding directional vorticity gradient gives the rate of transport of the components of vorticity.

$$\vec{V} \cdot \nabla \vec{\omega} = \underbrace{\left(u \frac{\partial \omega_x}{\partial x} + v \frac{\partial \omega_x}{\partial y} + w \frac{\partial \omega_x}{\partial z} \right)}_{\text{Transport of x-direction vorticity}} \hat{i} + \underbrace{\left(u \frac{\partial \omega_y}{\partial x} + v \frac{\partial \omega_y}{\partial y} + w \frac{\partial \omega_y}{\partial z} \right)}_{\text{Transport of y-direction vorticity}} \hat{j} + \underbrace{\left(u \frac{\partial \omega_z}{\partial x} + v \frac{\partial \omega_z}{\partial y} + w \frac{\partial \omega_z}{\partial z} \right)}_{\text{Transport of z-direction vorticity}} \hat{k}$$

Note that a change in a particular directional component of vorticity due to advection will only occur when a vorticity gradient exists in the direction of transport. In addition, even though a vorticity gradient may be present, no change in a particular component of vorticity will occur due to advection if there is no velocity component in that direction. Consider the example of the stationary, decaying vortex, as was illustrated above in Figure 11.1. Although a significant gradient of vorticity exists in the radial direction, since there is no radial velocity, there is no advection of vorticity in the radial direction.

Figure 11.2 below illustrates a simple example of vorticity transport for a vortex translating through an otherwise uniform flow in the x-direction at a velocity u . Here

$u > 0$ and $\frac{\partial \omega_z}{\partial x} < 0$ inside the vortex, and $u > 0$ and $\frac{\partial \omega_z}{\partial x} = 0$ outside of the vortex. Clearly,

vorticity transport is taking place, but only within the region where $\frac{\partial \omega_z}{\partial x} \neq 0$. Note that as the vortex moves along the x-axis, the vorticity transport at a point will change from 0 to < 0 and back to 0 at any fixed point along the x-axis.

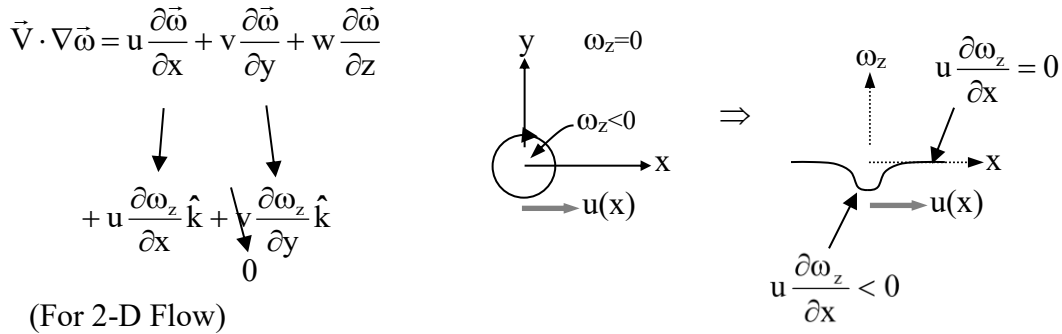


Figure 11.2 Example of the transport of vorticity along the x-axis by a compact vortex translating in an otherwise uniform x-direction flow.

11.2.3 Diffusion of Vorticity, $\nu \nabla^2 \vec{\omega}$

The $\nu \nabla^2 \vec{\omega}$ term in Eq. 11.7 models the viscous diffusion of vorticity due to fluid viscosity. This term is similar to the diffusion transport term in the Navier-Stokes equation, and is again associated with the redistribution of *existing* vorticity within the vorticity field.

The diffusion of vorticity, like the diffusion of momentum, is the result of the interaction of the fluid particles. In the case of vorticity, this interaction is reflected as fluid friction, or viscosity, which causes a reduction in the local vorticity (i.e. angular momentum). Such angular momentum losses are a result of local shear stresses created by spatial velocity gradients. The shear stresses act as a damping agent, causing a decrease in the local angular momentum, and thus a decay and redistribution of the vorticity within the fluid. Assuming a constant viscosity, the $\nu \nabla^2 \vec{\omega}$ term reflects the transport of vorticity due to viscous effects, where ν represents the diffusivity of vorticity for a given fluid (i.e. the fluid’s capacity to diffuse vorticity). Note that this term is directly proportional to the Laplacian of the vorticity, $\nabla^2 \vec{\omega}$, which deserves some assessment.

In Cartesian coordinates, we can write the Laplacian term as (see Eq.2.16ℓ):

$$\nabla^2 \vec{\omega} = \nabla \cdot \nabla (\omega_x \hat{i} + \omega_y \hat{j} + \omega_z \hat{k}) = (\nabla \cdot \nabla \omega_x) \hat{i} + (\nabla \cdot \nabla \omega_y) \hat{j} + (\nabla \cdot \nabla \omega_z) \hat{k}$$

Thus, the Laplacian represents the divergence of the gradient of each vorticity component. To assess the dynamics of this term, consider a flow with only x-direction vorticity, such that $\nabla^2 \vec{\omega} = (\nabla \cdot \nabla \omega_x) \hat{i}$, similar to that shown in Figure 11.3 for a viscous vortex tube aligned along the x-axis.

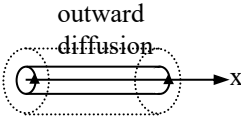
$$\nu \left[\frac{\partial^2 \omega_x}{\partial x^2} + \frac{\partial^2 \omega_x}{\partial y^2} + \frac{\partial^2 \omega_x}{\partial z^2} \right] \hat{i}$$


Figure 11.3 Example of the transport of vorticity by radial diffusion from a vortex aligned with the x-axis.

Here, $\nabla \omega_x$ reflects the gradient, or spatial variations, of the x-direction vorticity, which is given by

$$\nabla \omega_x = \frac{\partial \omega_x}{\partial x} \hat{i} + \frac{\partial \omega_x}{\partial y} \hat{j} + \frac{\partial \omega_x}{\partial z} \hat{k}. \text{ The divergence of this term gives, } \nabla \cdot \nabla \omega_x = \frac{\partial^2 \omega_x}{\partial x^2} + \frac{\partial^2 \omega_x}{\partial y^2} + \frac{\partial^2 \omega_x}{\partial z^2}.$$

Recalling that the divergence reflects the cumulative expansion of a vector field, this term is indicative of the cumulative “balance” of the spatial changes in the gradient of the vorticity field. As we discuss below in Section 11.5.1, the gradient of the vorticity can be viewed as proportional to the “flux” of vorticity within the fluid. Thus, the Laplacian of the vorticity for a “balanced” flow (i.e. one where $\nabla \cdot \nabla \omega_x = 0$) demonstrates that the flux of vorticity in one direction will be offset by changes in the other directions, similar to how the velocity field for an incompressible flow behaves (where $\nabla \cdot \vec{V} = 0$, by continuity). Thus, in the absence of other transport effects, the Laplacian indicates that viscosity will have the effect of redistributing *existing* vorticity in such a way that angular momentum is decreased, but the total (i.e. the total circulation) of each component of vorticity is conserved. Again, consider the viscous vortex shown in Figure 11.1. In the absence of advective transport, the vorticity within this vortex will redistribute, and the angular momentum will diminish, but the total vorticity, or circulation (taken over an infinite region) will be conserved.

11.2.4 Generation of Vorticity by Stretching and Tilting, $(\vec{\omega} \cdot \nabla) \vec{V}$

This last term in Eq. 11.7, $(\vec{\omega} \cdot \nabla) \vec{V}$, is unique in that it models: (1) the generation of new vorticity, and (2) the redirection of existing vorticity. This can be the result of either: (1) the generation (reduction) of vorticity by the stretching (compression) of existing vorticity in one direction, or (2) the reorientation (i.e. tilting) of existing vorticity from one direction into another direction. To illustrate how this occurs, let’s expand the $(\vec{\omega} \cdot \nabla) \vec{V}$ term in Cartesian coordinates.

$$\begin{aligned} (\vec{\omega} \cdot \nabla) \vec{V} &= \left(\omega_x \frac{\partial}{\partial x} + \omega_y \frac{\partial}{\partial y} + \omega_z \frac{\partial}{\partial z} \right) (u \hat{i} + v \hat{j} + w \hat{k}) \\ &= \left(\omega_x \frac{\partial u}{\partial x} + \omega_y \frac{\partial u}{\partial y} + \omega_z \frac{\partial u}{\partial z} \right) \hat{i} + \left(\omega_x \frac{\partial v}{\partial x} + \omega_y \frac{\partial v}{\partial y} + \omega_z \frac{\partial v}{\partial z} \right) \hat{j} + \left(\omega_x \frac{\partial w}{\partial x} + \omega_y \frac{\partial w}{\partial y} + \omega_z \frac{\partial w}{\partial z} \right) \hat{k} \end{aligned}$$

Now, if we ignore the effects of viscous diffusion, and only consider the changes for the x-direction, we can write a simplified version of Eq. 11.7 as:

$$\frac{D\omega_x}{Dt} = \omega_x \frac{\partial u}{\partial x} + \omega_y \frac{\partial u}{\partial y} + \omega_z \frac{\partial u}{\partial z} \tag{11.8}$$

Equation 11.8 indicates that as a fluid moves within a velocity field, the vorticity in the x-direction can materially change (i.e. $\frac{D\omega_x}{Dt} \neq 0$) due to the influence of gradients of the x-direction velocity (u) on existing components of vorticity [here we illustrate the x-direction changes, but the same process equally applies in the y and z directions as well]. The first term on the right-hand side of Eq. 11.8 indicates that changes in ω_x will occur when the local flow undergoes acceleration/deceleration along the x-axis. Note that an acceleration (i.e. $\frac{\partial u}{\partial x} > 0$) will result in a “stretching” of the fluid in the x-direction, with a commensurate increase in the x-direction vorticity, ω_x . However, a deceleration of the flow along the x-axis (i.e. $\frac{\partial u}{\partial x} < 0$) will result in a contraction or compression in the x-direction, which results in a reduction in the existing x-direction vorticity.

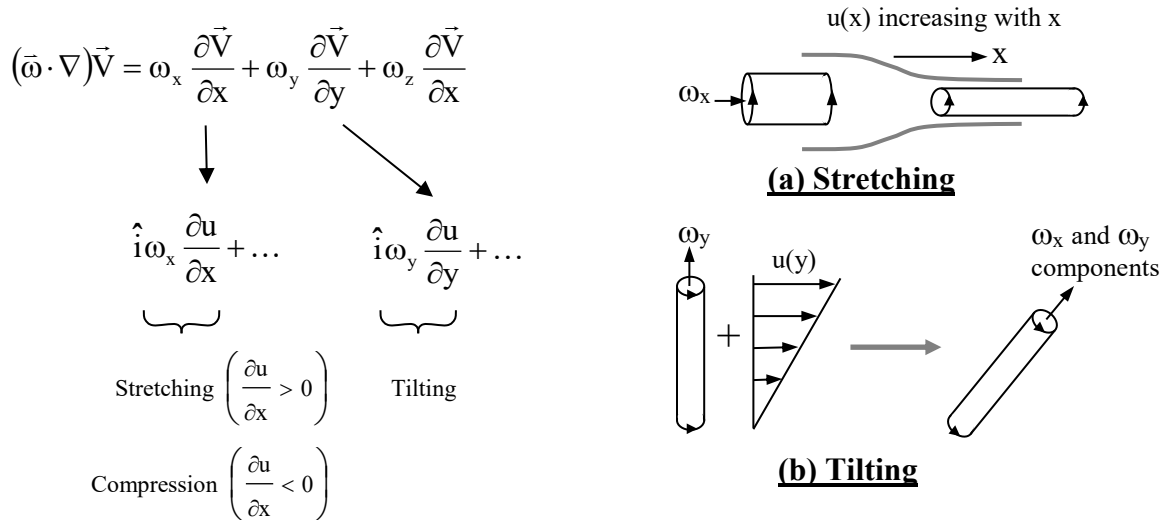


Figure 11.4 Schematic of the generation of new x-direction vorticity due to (a) “stretching”, and (b) “tilting” of existing vorticity by local velocity gradients.

The second and third terms on the right hand side of Eq. 11.8 indicate that changes in ω_x can also occur when the vorticity components orthogonal to the x-direction (ω_y or ω_z) are “tilted”

into the x-direction by a gradient of the x-velocity (u) normal to the x-direction (i.e. $\frac{\partial u}{\partial y}$ or $\frac{\partial u}{\partial z}$).

For this process, there is no generation (or reduction) of vorticity, but only a reorientation of existing vorticity components from one direction to another. Figure 11.4 shows schematically how such processes of stretching and tilting of vorticity can occur.

To illustrate that a stretching process does result in the generation of “new” vorticity, let’s consider a further simplification of Eq. 11.8, such that we only consider a fluid element with vorticity ω_x under pure stretching, such as shown in Figure 11.4a. For this situation, we can write Eq. 11.8 as:

$$\frac{D\omega_x}{Dt} = \omega_x \frac{\partial u}{\partial x} \quad (11.9)$$

We now consider that $\frac{\partial u}{\partial x}$ is the rate of x-direction stretching or straining (i.e. $\frac{d(dx)}{dx}$) of a differential material element dx lying along a vortex line of strength ω_x . Now, we can express

$\frac{\partial u}{\partial x}$ via the material derivative as:

$$\frac{\partial u}{\partial x} = \frac{du}{dx} = \frac{1}{dx} \frac{D(dx)}{Dt} \quad (11.10)$$

Here we let $\frac{\partial u}{\partial x} = \frac{du}{dx}$ for pure stretching in the x-direction only. Substituting Eq. 11.10 into Eq. 11.9 gives:

$$\frac{D\omega_x}{Dt} = \omega_x \frac{\partial u}{\partial x} = \omega_x \frac{du}{dx} = \frac{\omega_x}{dx} \frac{D(dx)}{Dt} \quad (11.11)$$

Mathematically, we note that we can write:

$$\frac{D}{Dt} \left(\frac{\omega_x}{dx} \right) = \frac{1}{dx} \frac{D\omega_x}{Dt} - \frac{\omega_x}{dx^2} \frac{Ddx}{Dt}$$

Or rearranging,

$$\frac{\omega_x}{dx} \frac{Ddx}{Dt} = \frac{D\omega_x}{Dt} - dx \frac{D}{Dt} \left(\frac{\omega_x}{dx} \right) \quad (11.12)$$

Substituting Eq. 11.12 into Eq. 11.11 gives:

$$\cancel{\frac{D\omega_x}{Dt}} = \cancel{\frac{D\omega_x}{Dt}} - dx \frac{D}{Dt} \left(\frac{\omega_x}{dx} \right) \quad \text{or} \quad \frac{D}{Dt} \left(\frac{\omega_x}{dx} \right) = 0 \quad (11.13)$$

Equation 11.13 indicates that, in a pure stretching process, the strength of the vorticity of a fluid particle increases (or decreases) proportionally to the length of dx . Thus, the generation of new vorticity, or the reduction of existing vorticity, is directly proportional to the local stretching or contraction of a fluid element with initial vorticity ω_x .

Alternatively, consider an inviscid vortex tube with its axis in the x -direction, and subjected to an accelerating flow along its axis (such as in a nozzle), such that its cross-sectional area decreases, as shown in Figure 11.5.

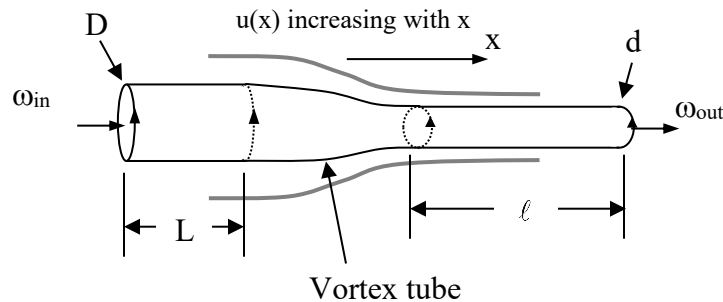


Figure 11.5 Schematic of a vortex tube undergoing stretching in a converging nozzle.

Let us assume that: (1) the stream-wise vorticity is uniform across the tube cross section at both the entrance and exit of the vortex tube, and (2) the section of the fluid within the tube of length L , as shown in Figure 11.5, will elongate during transit through the tube to a section of length ℓ , where $\ell > L$. During this transit, the diameter of the fluid section will likewise contract from diameter D to d . As we showed in Section 8.3.2.1, the circulation at any cross-section of a vortex tube will remain constant such that:

$$\Gamma_{\text{in}} = \Gamma_{\text{out}} \quad \text{or} \quad \omega_{\text{in}} \pi \frac{D^2}{4} = \omega_{\text{out}} \pi \frac{d^2}{4} \quad \text{assuming constant vorticity at each cross-section}$$

Thus,

$$\omega_{\text{out}} = \omega_{\text{in}} \left(\frac{D}{d} \right)^2 \quad \text{so} \quad \omega_{\text{out}} > \omega_{\text{in}} \quad \text{if} \quad D > d \quad (11.14)$$

Since the volume of the fluid section of length L must equal the volume of the fluid section of length ℓ , then:

$$\pi \frac{D^2}{4} L = \pi \frac{d^2}{4} \ell \quad \Rightarrow \quad \frac{D^2}{d^2} = \frac{\ell}{L}$$

and substituting into Eq.11.14 gives:

$$\omega_{\text{out}} = \omega_{\text{in}} \frac{\ell}{L} \quad (11.15)$$

Therefore, the vorticity *increases* as the fluid within the vortex tube is stretched. However, is there vorticity generated during this process? To answer this, we note that the total amount of vorticity contained within each fluid section is equal to the product of the vorticity times the fluid volume, such that:

$$\Omega_L = \text{Volume weighted vorticity for section } L = \omega_{\text{in}} \pi \frac{D^2}{4} L$$

$$\Omega_\ell = \text{Volume weighted vorticity for section } \ell = \omega_{\text{out}} \pi \frac{d^2}{4} \ell$$

However, since the volumes of the fluid sections must be equal, then a ratio of the total vorticity within the respective volumes is:

$$\frac{\Omega_\ell}{\Omega_L} = \frac{\omega_{\text{out}}}{\omega_{\text{in}}} = \frac{\ell}{L} \quad (11.16)$$

Thus, as Eq. 11.16 indicates, the *stretching* of a vortex tube ($\frac{\ell}{L} > 1$) will *generate new vorticity*, whereas the contraction of a vortex tube ($\frac{\ell}{L} < 1$) will result in an *overall decrease in the existing vorticity*.

11.3 The Two-Dimensional Vorticity Transport Equation

The vorticity transport equation, Eq. 11.7, like the Navier-Stokes equation, is a particularly complex vector equation, which requires sophisticated numerical techniques and significant computer resources to develop solutions for a three-dimensional flow. However, there are several tractable and relevant two-dimensional flow situations where the vorticity transport equation can be applied and solved in closed form. In this section, we examine the reduced two-dimensional vorticity transport equation. In Section 11.4, we consider some simple applications of this reduced equation.

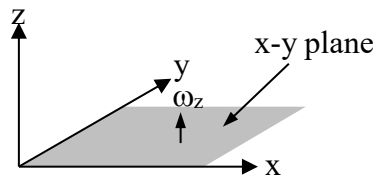


Figure 11.6 Two-dimensional vortical flow (x-y plane)

If we restrict ourselves to flows in a two-dimensional plane, we will have only one component of vorticity — that in the direction normal to the plane. For purposes of example, consider a two-dimensional flow in the x-y plane of a Cartesian coordinate system, as shown in Figure 11.6. For this case, the velocity will be given by $\vec{V} = u\hat{i} + v\hat{j}$, and the vorticity will be $\vec{\omega} = \omega_z\hat{k}$.

For this flow, note that the stretching/tilting term in Eq. 11.7, $\vec{\omega} \cdot \nabla \vec{V}$, becomes:

$$\vec{\omega} \cdot \nabla \vec{V} = \omega_z \frac{\partial u}{\partial z} \hat{i} + \omega_z \frac{\partial v}{\partial z} \hat{j} = 0 \quad \text{since } \frac{\partial u}{\partial z}, \frac{\partial v}{\partial z} = 0 \text{ for a flow in the x-y plane only.}$$

Therefore, the vorticity transport equation for this two-dimensional flow reduces to single scalar equation:

$$\frac{D\omega_z}{Dt} = \frac{\partial \omega_z}{\partial t} + u \frac{\partial \omega_z}{\partial x} + v \frac{\partial \omega_z}{\partial y} = \nu \left[\frac{\partial^2 \omega_z}{\partial x^2} + \frac{\partial^2 \omega_z}{\partial y^2} \right] \quad (11.17)$$

In a more generic vector form, applicable to all coordinate systems, the two-dimensional vorticity equation can be written as:

$$\frac{D\omega}{Dt} = \frac{\partial \omega}{\partial t} + (\vec{V} \cdot \nabla) \omega = \nu \nabla^2 \omega \quad (11.18)$$

The direction of ω , and the specific velocity components comprising Eq. 11.18 will depend upon the particular coordinate system employed. However, Eq. 11.18 will still reduce to a single, scalar equation.

The key observation from Eqs. 11.17 and 11.18 is that for a two-dimensional flow, material transport of vorticity will *balance* the diffusion of vorticity.

Two further simplifications can be made for: (1) flows where advection is irrelevant, and diffusion dominates, such as the decaying viscous vortex shown in Figure 11.1, and (2) steady flows, where there are no local temporal changes. The simplified equations for these types of flows are:

$$\text{Diffusion dominated flows: } \frac{\partial \vec{\omega}}{\partial t} = \nu \nabla^2 \vec{\omega} \quad (11.19)$$

$$\text{Steady flows: } (\vec{V} \cdot \nabla) \vec{\omega} = \nu \nabla^2 \vec{\omega} \quad (11.20)$$

Expanding Eqs. 11.19 and 11.20 in a Cartesian coordinate system (x-y plane) gives:

$$\text{Diffusion dominated flows: } \frac{\partial \omega_z}{\partial t} = \nu \left[\frac{\partial^2 \omega_z}{\partial x^2} + \frac{\partial^2 \omega_z}{\partial y^2} \right] \quad (11.21)$$

$$\text{Steady flows: } u \frac{\partial \omega_z}{\partial x} + v \frac{\partial \omega_z}{\partial y} = \nu \left[\frac{\partial^2 \omega_z}{\partial x^2} + \frac{\partial^2 \omega_z}{\partial y^2} \right] \quad (11.22)$$

Expanding Eqs. 11.19 and 11.20 in cylindrical coordinates (r- θ plane) gives:

$$\text{Diffusion dominated flows: } \frac{\partial \omega_z}{\partial t} = \nu \left[\frac{1}{r} \frac{\partial}{\partial r} \left(r \frac{\partial \omega_z}{\partial r} \right) + \frac{1}{r^2} \frac{\partial^2 \omega_z}{\partial \theta^2} \right] \quad (11.23)$$

$$\text{Steady flows: } v_r \frac{\partial \omega_z}{\partial r} + \frac{v_\theta}{r} \frac{\partial \omega_z}{\partial \theta} = \nu \left[\frac{1}{r} \frac{\partial}{\partial r} \left(r \frac{\partial \omega_z}{\partial r} \right) + \frac{1}{r^2} \frac{\partial^2 \omega_z}{\partial \theta^2} \right] \quad (11.24)$$

Since the vorticity transport equation contains both velocity and vorticity terms, the solution of a flow for which the advection terms are relevant may require that we initially substitute the velocity derivatives comprising the vorticity, which can make the resulting equation quite messy. However, there are a number of useful solutions of the vorticity equation that are independent of the advection terms, and capitalize upon the vorticity equation being decoupled from the local pressure. In the following sections, we examine several simple examples that demonstrate the application of the two-dimensional vorticity transport equation. These examples entail situations for which changes in vorticity depend upon only one independent variable (e.g. y). In Chapters 12 and 13 we will consider more complicated examples where vorticity is dependent on more than one independent variable (e.g. y and t), and thus require more sophisticated mathematical approaches.

11.4 One Dimensional Vorticity Solutions

Here we examine three simple flows: two with planar symmetry and one with radial symmetry. Two of these are flows we considered previously in Chapter 6. Similar to our solutions of the Navier-Stokes equation in Chapter 6, the key elements required to solve the vorticity transport equation for a particular flow situation are: (1) an appropriate integration technique for the differential equation, and (2) specification of the appropriate boundary/initial conditions for the flow in question. When dealing with vorticity, the appropriate boundary conditions may not be evident. Quite frequently, the boundary conditions may not be able to be specified in terms of vorticity, but may frequently be specified in terms of velocity boundary conditions (since vorticity is a derivative function of the velocity field, this generally works).

In reality, the most commonly applicable vorticity boundary condition is at certain bounding locations where there is *no vorticity*. For example, for portions of a flow well away from a solid surface, where we expect (or suspect) that a flow asymptotes to a uniform flow, we can generally specify that the vorticity (and most likely the spatial derivatives of the vorticity) within these regions far from a solid boundary will be zero. However, near solid boundaries we have no comparable condition to the velocity no-slip condition to fall back on, and thus must depend upon the use of velocity boundary conditions at those locations. We will demonstrate this process for establishing boundary conditions as we consider the following examples.

11.4.1 Flow Over a Flat Plate with Suction

As we will discuss in Chapter 13, an unconstrained flow along a solid surface results in the development of what in fluid mechanics is termed a [boundary layer](#). This is a layer of fluid adjacent to the solid surface within which viscous effects dominate, and the flow undergoes an adjustment from no slip at the surface to the velocity of the outer flow. This region is generally quite thin (relative to the surface length). Once a flow encounters a solid surface, this boundary layer thickness will generally expand continually as the flow passes along the surface. This continual expansion, due to the viscous diffusion of momentum (and vorticity) away from the surface, makes a developing boundary layer a complicated problem to solve, since changes continually take place both away from and parallel to the solid surface. However, if we consider a flow over a *porous* surface with suction through the surface, we can in essence *balance* the outward diffusion of vorticity with the advection of vorticity back toward the surface due to the suction. Once this balance develops (at some point along the surface), the thickness of the “boundary layer”, or viscous readjustment region adjacent to the surface, will remain of constant thickness, and the flow will become fully developed (such that there are no further changes in the streamwise direction). In the present example, we derive the corresponding velocity and vorticity field for this fully-developed viscous region with an external uniform flow, $u = U_\infty = \text{constant}$, passing over a flat plate with uniform suction of $v = -V$ through the surface, as shown in Figure 11.7.

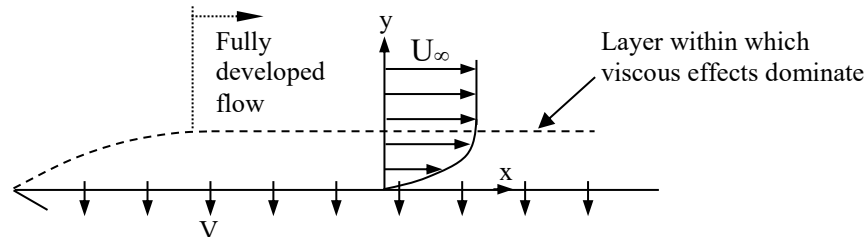


Figure 11.7 Uniform flow over a flat plate with suction.

For this flow, we employ a Cartesian coordinate system, as shown in figure 11.7. Note that since we only consider the region of fully-developed flow, the location of the x-direction origin is irrelevant (this will not be the case when we examine boundary layer growth over a non-porous surface in Chapter 13). As shown in figure 11.7, the origin of the y-axis is located at the plate surface.

From the continuity equation (in 2-D) we have:

$$\frac{\partial u}{\partial x} + \frac{\partial v}{\partial y} = 0$$

Since we assume the flow is fully developed, this means that $\frac{\partial u}{\partial x} = 0$, which gives:

$$\frac{\partial v}{\partial y} = 0 \Rightarrow v = \text{constant}$$

Since $v = -V$ at $y = 0$, then $v = -V$ everywhere.

Now, for a steady flow, Eq. 11.22 applies:

$$u \frac{\partial \omega_z}{\partial x} + v \frac{\partial \omega_z}{\partial y} = \nu \left[\frac{\partial^2 \omega_z}{\partial x^2} + \frac{\partial^2 \omega_z}{\partial y^2} \right] \tag{11.25}$$

We simplify Eq.11.25 by noting that for a fully-developed flow, all derivatives of vorticity in the streamwise (x) direction drop out, i.e. $\frac{\partial \omega_z}{\partial x}, \frac{\partial^2 \omega_z}{\partial x^2} = 0$.

Thus, Eq. 11.25 simplifies to:

$$\begin{aligned} \nu \frac{\partial \omega_z}{\partial y} &= \nu \frac{\partial^2 \omega_z}{\partial y^2} \Rightarrow \omega_z = \omega_z(y) \text{ only} \Rightarrow \frac{\partial}{\partial y} = \frac{d}{dy} \text{ and } v = -V \\ \underbrace{-V \frac{d\omega_z}{dy}}_{\text{Advection of vorticity towards plate}} &= \underbrace{\nu \frac{d^2 \omega_z}{dy^2}}_{\text{Diffusion of vorticity away from plate}} \end{aligned} \tag{11.26}$$

Rearranging Eq. 11.26, we have a second-order, linear differential equation for vorticity as a function of y:

$$\frac{d^2 \omega_z}{dy^2} = -\frac{V}{\nu} \frac{d\omega_z}{dy} \tag{11.27}$$

Integrating Eq. 11.27 once gives:

$$\int \frac{d^2 \omega_z}{dy^2} = -\frac{V}{\nu} \int \frac{d\omega_z}{dy} \Rightarrow \frac{d\omega_z}{dy} = -\frac{V}{\nu} \omega_z + C_1 \tag{11.28}$$

To determine the integration constant C_1 in Eq. 11.28, we note that the outer vorticity boundary conditions for this flow are $\omega_z = 0$ and $\frac{d\omega_z}{dy} = 0$ as $y \rightarrow \infty$ [since the velocity asymptotes to a uniform flow]. Applying these boundary conditions (simultaneously) to Eq. 11.28, gives:

$$0 = 0 + C_1 \Rightarrow C_1 = 0$$

Separating variables and integrating again:

$$\int \frac{d\omega_z}{\omega_z} = - \int \frac{V}{v} dy$$

$$\omega_z = C_2 e^{-\frac{Vy}{v}} \quad (11.29)$$

We now have a problem. If we apply our boundary condition of $\omega_z = 0$ as $y \rightarrow \infty \Rightarrow 0 = C_2(e^{-\infty}) \Rightarrow C_2 = ?$ So C_2 is indeterminate in vorticity form.

Carrying C_2 forward, we now substitute for the vorticity in Eq. 11.29 in terms of the appropriate velocity derivatives, by letting $\omega_z = \left(\frac{\partial v}{\partial x} - \frac{\partial u}{\partial y} \right) = -\frac{du}{dy}$ [since $v \neq f(x)$].

This gives:

$$\omega_z = -\frac{du}{dy} = C_2 e^{-\frac{Vy}{v}} \quad (11.30)$$

Integrating Eg. 11.30 gives:

$$u = C_2 \frac{v}{V} e^{-\frac{Vy}{v}} + C_3$$

We now apply a velocity boundary condition of $u = U_\infty$ as $y \rightarrow \infty$, which gives C_3 :

$$U_\infty = C_2 e^{-\infty} + C_3 \Rightarrow C_3 = U_\infty$$

Our final boundary condition is the no slip condition, $u = 0$ for $y = 0$, which allows us to determine C_2 .

$$0 = C_2 \frac{v}{V} e^{-0} + U_\infty \Rightarrow C_2 = -U_\infty \frac{V}{v}$$

So that the final expression for the velocity is:

$$u = U_\infty \left(1 - e^{-\frac{Vy}{v}} \right) \quad (11.31)$$

Substituting $C_2 = -U_\infty \frac{V}{v}$ into Eq. 11.30 for the vorticity, we have:

$$\omega_z = -\frac{du}{dy} = -U_\infty \frac{V}{v} e^{-\frac{Vy}{v}} \quad (11.32)$$

Figure 11.8 shows the general behavior of both the velocity and the vorticity within this boundary region

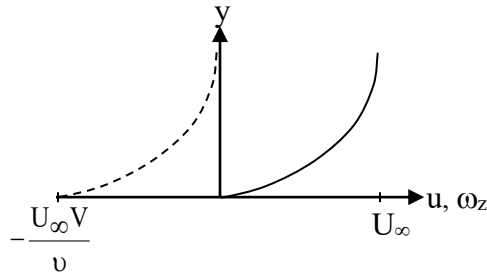


Figure 11.8 Behavior of the streamwise (u) velocity and the vorticity (ω_z) for a fully-developed flow over a flat plate with constant suction, V .

If we substitute Eq. 11.32 into the terms of the original differential equation, Eq. 11.26, we have:

$$\frac{d\omega_z}{dy} = +U_\infty \frac{V^2}{\nu^2} e^{-\frac{Vy}{\nu}}, \text{ so } -V \frac{d\omega_z}{dy} = -U_\infty \frac{V^3}{\nu^2} e^{-\frac{Vy}{\nu}} \Rightarrow \text{Advection toward plate}$$

$$\frac{d^2\omega_z}{dy^2} = -U_\infty \frac{V^3}{\nu^3} e^{-\frac{Vy}{\nu}}, \text{ and } \nu \frac{d^2\omega_z}{dy^2} = -U_\infty \frac{V^3}{\nu^2} e^{-\frac{Vy}{\nu}} \Rightarrow \text{Diffusion away from plate}$$

These are of course equivalent (as they should be), and illustrate that diffusion of vorticity away from the plate is balanced by the advection of vorticity toward the plate.

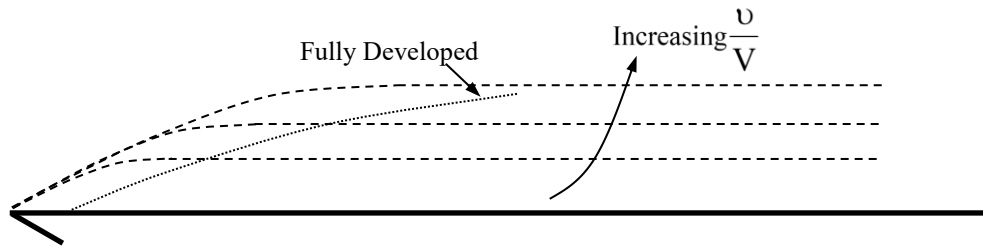


Figure 11.9 The effect of the ratio $\frac{\nu}{V}$ on the development of the vorticity-bearing layer for a flat plate with suction.

Notice that the governing parameter for this flow is the ratio of the kinematic viscosity (ν) to the suction velocity (V), as illustrated by figure 11.9. As we discussed in Section 11.2.3, the kinematic viscosity represents the diffusivity of vorticity. For this flow, V is proportional to the advection of vorticity. Note also that the ratio $\frac{\nu}{V}$ has the units of length. Thus, if the suction velocity (V) *increases* or the viscosity (ν) *decreases*, the thickness (i.e. a “length”) of the vorticity-bearing region becomes thinner, and thus moves *closer to* the porous plate. Conversely,

the vorticity-bearing region will become thicker, and extend *farther from* the plate if V decreases or ν increases. Additionally, the smaller the ratio $\frac{\nu}{V}$, the sooner the flow will become fully developed, as Figure 11.9 shows. In the limit, as $V \rightarrow 0$, diffusion of vorticity will no longer be constrained by the suction, and the vorticity bearing layer will continuously expand with distance along the plate, yielding a flat plate boundary layer—the flow behavior we address in Chapter 13.

As a final observation, note that the shear stress in this fully-developed region is given by:

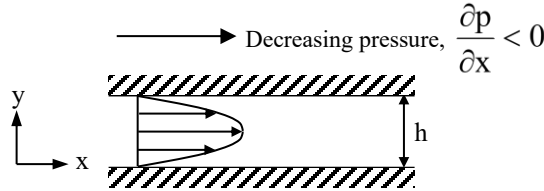
$$\tau_w = \mu \left. \frac{du}{dy} \right|_{y=0} = \mu U_\infty \frac{V}{\nu} e^{-\frac{Vy}{\nu}} \Big|_{y=0} = \mu U_\infty \frac{V}{\left(\frac{\mu}{\rho} \right)} e^{-0} = \rho U_\infty V \quad (11.33)$$

Equation 11.33 is quite interesting, since the shear stress is only a function of the suction velocity, and not the viscosity! However, this is a bit misleading. What this indicates is that the shear stress at the surface is really equivalent to the momentum “lost” from the main flow due to suction. This momentum is lost, because elements of fluid with a momentum of ρU_∞ enter the outer edge of the fully-developed region, are drawn across the region by the suction velocity V , and are removed from the region through the porous surface, having dissipated all of the original momentum due to the viscous interaction. For a more viscous fluid, the fully-developed region will be thicker, and thus the shear gradients will be smaller and this dissipation of momentum occurs more slowly (although it will take the flow longer to become fully developed). For a less viscous fluid, the fully-developed region will be thinner, with higher shear gradients, and the dissipation will occur more rapidly (with the flow becoming fully developed more rapidly). Interestingly, if the products of the density, flow velocity, and suction velocity for two different fluids are identical, then the momentum lost during the transit across the fully-developed region will also be identical, and as will the wall shear stresses, regardless of the viscosities of the two different fluids. How cool is that?

11.4.2 Poiseuille Flow in a Parallel Channel

In Section 6.3.2 we solved the problem of a pressure-gradient driven flow between two parallel plates, termed a Poiseuille flow. In this example, we demonstrate how we can solve the same problem by employing the vorticity transport equation. What is interesting here is that the vorticity transport equation has no pressure term. Therefore, the question arises as to how we incorporate the pressure into the solution. The answer, as we will show, is by use of a boundary condition that evolves from the Navier-Stokes equation.

Reconsider the basic flow behavior of a Poiseuille flow -- a fully-developed, laminar flow between parallel surfaces, with a constant, decreasing pressure gradient in the x-direction, as shown here.



We again utilize Eq. 11.22, the two-dimensional vorticity transport equation for steady flow in Cartesian coordinates.

$$u \frac{\partial \omega_z}{\partial x} + v \frac{\partial \omega_z}{\partial y} = \nu \left[\frac{\partial^2 \omega_z}{\partial x^2} + \frac{\partial^2 \omega_z}{\partial y^2} \right] \tag{11.34}$$

From our solution in Section 6.3.2, using the continuity equation we showed that $v = 0$ for this fully-developed flow. Additionally, since the flow is fully developed, all x derivatives are also zero. Applying these conditions, and noting that the vorticity is only a function of y , reduces equation 11.34 to:

$$\frac{d^2 \omega_z}{dy^2} = 0 \tag{11.35}$$

Thus, the only relevant term is the vorticity diffusion term. Integration of Eq. 11.35 is a simplistic double integration, giving:

$$\omega_z = C_1 y + C_2 \quad \text{where } C_1 \text{ and } C_2 \text{ are integration constants.} \tag{11.36}$$

The only vorticity boundary condition available to us is that on the symmetry plane, at $y = h/2$, $\omega_z = 0$ (where by symmetry, $\frac{\partial u}{\partial y} = 0$). Applying this condition gives:

$$0 = \frac{C_1 h}{2} + C_2 \Rightarrow C_2 = -\frac{C_1 h}{2}$$

And Eq. 11.36 becomes:

$$\omega_z = C_1 \left(y - \frac{h}{2} \right)$$

We also note for this flow that $\omega_z = \left(\frac{\partial v}{\partial x} - \frac{\partial u}{\partial y} \right) = -\frac{du}{dy}$, so:

$$-\frac{du}{dy} = C_1 \left(y - \frac{h}{2} \right)$$

Integrating again gives:

$$u = -C_1 \left(\frac{y^2}{2} - \frac{hy}{2} \right) + C_3 \quad (11.37)$$

Equation 11.37 requires two other boundary conditions. One of these is the no slip condition we employed for the Navier-Stokes solution in Section 6.3.2:

$$u = 0 \text{ @ } y = 0 \quad (\text{no slip})$$

which yields $C_3 = 0$.

So Eq. 11.37 becomes:

$$u = -\frac{C_1}{2}(y^2 - yh) \quad (11.38)$$

We cannot use the boundary condition on the opposing wall of:

$$u = 0 \text{ @ } y = 0 \text{ or } h \quad (\text{no slip})$$

since this would give $0 = -\frac{C_1}{2}(0-0)$ or $0 = -\frac{C_1}{2}(h^2 - h^2)$, either of which gives $\frac{C_1}{2}(0) = 0$, and makes C_1 indeterminate.

Thus, to establish C_1 requires a third boundary condition, which we obtain from the Navier-Stokes equation. Recall from Section 6.3.2 that the x-direction Navier-Stokes equation reduces to:

$$\frac{d^2u}{dy^2} = \frac{1}{\mu} \frac{\partial P}{\partial x} = \text{constant} \quad (11.39)$$

Employing equation 11.39 as a third “boundary” condition (although it applies at any point within the flow field), we differentiate Eq. 11.38 twice and equate to Eq. 11.39:

$$\frac{d^2u}{dy^2} = -C_1 = \frac{1}{\mu} \frac{\partial P}{\partial x} \Rightarrow C_1 = -\frac{1}{\mu} \frac{\partial P}{\partial x}$$

Thus, Eq. 11.38 becomes:

$$u = \frac{1}{\mu} \frac{\partial P}{\partial x} (y^2 - yh) = \frac{h^2}{\mu} \frac{\partial P}{\partial x} \left(\frac{y}{h} - 1 \right) \frac{y}{h} \quad (11.40)$$

Equation 11.40 is, of course, the same result, Eq. 6.17, that we obtained in Section 6.3.2.

Note that for this flow:

$$\omega_z = -\frac{du}{dy} = \frac{h}{\mu} \frac{\partial P}{\partial x} \left(2\frac{y}{h} - 1 \right) \tag{11.41}$$

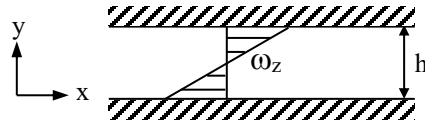


Figure 11.10 The vorticity distribution for a Poiseuille flow

Thus, although this flow clearly transports vorticity, the only “changes” in vorticity transport are due to viscous diffusion normal to the plates, in the y -direction. As Eq. 11.41 and figure 11.10 show, there must be “sources” of vorticity at either plate surface (positive at the top, negative at the bottom), with vorticity generated at the plate surfaces, and then diffusing toward the center, where the opposing sign vorticities mutually cancel each other. The processes that result in this generation of vorticity at the plate surfaces are discussed in detail in Section 11.5.

11.4.3 Steady Flow Outside of a Rotating Rod

The solutions of problems with rotational symmetry follow a similar procedure to that employed for problems with Cartesian symmetry. These flows generally vary with the radial direction, r , and possess azimuthal (angular) symmetry. These types of flows may be bounded at only one radius, or enclosed between two bounding surfaces of different radii. The simplest of these types of flows is the viscous, steady flow external to a rotating solid rod, which we examine in the following example.

Consider the 2-D flow outside a rotating circular rod. Assume that the cylinder is in a fluid of infinite extent with kinematic viscosity ν and density ρ ; the cylinder is of radius R and rotates at a constant angular velocity Ω . Note that this flow is a variation on the generic type of flow we examined in Section 6.4.2.

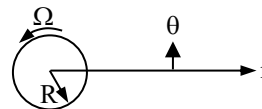
Consider a schematic of the flow, defined in cylindrical coordinates as shown below. We assume the flow is two-dimensional, steady, with no changes in the azimuthal (θ) direction.

Consequently, $\vec{V} = \vec{V}(r) = v_r \hat{i}_r + v_\theta \hat{i}_\theta$, and the 2-D continuity equation in r and θ yields:

$$\frac{1}{r} \frac{\partial}{\partial r} (rv_r) + \frac{1}{r} \frac{\partial v_\theta}{\partial \theta} = 0$$

$$\frac{d}{dr} (rv_r) = 0 \Rightarrow rv_r = \text{const}$$

but $v_r = 0$ at $r = R$, $\therefore v_r = 0$ everywhere



Eq. 11.24, the steady two-dimensional vorticity transport equation in cylindrical coordinates, can be reduced as follows:

$$\cancel{v_r} \frac{\partial \omega_z}{\partial r} + \cancel{v_\theta} \frac{\partial \omega_z}{\partial \theta} = \nu \left[\frac{1}{r} \frac{\partial}{\partial r} \left(r \frac{\partial \omega_z}{\partial r} \right) + \frac{1}{r^2} \frac{\partial^2 \omega_z}{\partial \theta^2} \right] \quad (11.42)$$

Since $v_r = 0$, derivatives in the θ -direction are zero, and $\omega_z = \omega_z(r)$, Eq. 11.42 reduces to:

$$\frac{d}{dr} \left(r \frac{d\omega_z}{dr} \right) = 0 \quad (11.43)$$

This flow is again only dependent on viscous diffusion. Integrating Eq. 11.43 twice gives:

$$\begin{aligned} r \frac{d\omega_z}{dr} &= C_1 \\ \omega_z &= C_1 \ln r + C_2 \end{aligned} \quad (11.44)$$

Since this fluid is of infinite extent, we reason that $\omega_z = 0$ as $r \rightarrow \infty$, which requires that both C_1 and C_2 must be zero [since $\ln(\infty) \rightarrow \infty$]. Thus, we have the surprising result that $\omega_z = 0$ everywhere. We now note that in cylindrical coordinates,

$$\omega_z = \frac{1}{r} \frac{\partial}{\partial r} (rv_\theta) - \frac{1}{r} \frac{\partial v_r}{\partial \theta} = \frac{1}{r} \frac{d}{dr} (rv_\theta)$$

So, for $\omega_z = 0$ we have:

$$\begin{aligned} \omega_z &= \frac{1}{r} \frac{d}{dr} (rv_\theta) = 0 \\ \frac{d}{dr} (rv_\theta) &= 0 \\ v_\theta &= \frac{C_3}{r} \end{aligned}$$

Now, since $v_\theta = \Omega R$ @ $r = R$, this yields $C_3 = \Omega R^2$, and:

$$v_\theta = \frac{\Omega R^2}{r} \quad (11.45)$$

Thus, this flow is viscous, but contains no vorticity! It also displays the same functional velocity as an irrotational point vortex we examined in Section 9.7.3 for a potential flow. However, that was for an inviscid fluid, whereas the present flow is a viscous fluid.

Consider the shear stress for this flow, which is given by (see Section 5.8.1):

$$\tau_{r\theta} = \mu \left[r \frac{\partial}{\partial r} \left(\frac{v_\theta}{r} \right) + \frac{1}{r} \frac{\partial v_r}{\partial \theta} \right] = \mu r \frac{d}{dr} \left(\frac{v_\theta}{r} \right) = \mu r \frac{d}{dr} \left(\frac{\Omega R^2}{r^2} \right) = -2\mu \left(\frac{\Omega R^2}{r^2} \right)$$

This is an interesting finding, since one might assume that if the fluid displays a shear stress, then there must also be vorticity, which is not the case here.

This absence of vorticity in a viscous flow raises the question of whether this flow ever contained vorticity (e.g. when the cylinder first started to rotate); and if vorticity was present, where did it come from and where did it go? The answers, as we will discuss in the following section, are: (1) the flow did contain vorticity when the rod initially started to rotate, (2) the vorticity was generated by the initial acceleration of the rod, and (3) the vorticity that was initially generated all diffused to infinity as the flow reached steady state. In the following section, we discuss the sources of vorticity, and mechanisms for its generation, in a viscous flow.

11.5 Sources of Vorticity

Throughout Chapters 8, 10 and the present chapter, we have developed the governing equations for and the processes by which we assess the effects of vorticity, its transport, and modification. However, the presumption in these evaluations is that vorticity is already present (or not present, in the case of irrotational flows), and that it somehow arose through the action of viscosity or baroclinic effects. Just how vorticity is generated within a fluid is the topic of this section. As we will see, there are three processes of vorticity generation that require viscous interaction with a bounding surface, and one where vorticity is created because of baroclinic behavior.

11.5.1 Vorticity Generation by Viscous Effects

Vorticity in a viscous, barotropic [$P = P(\rho)$] fluid can only be generated by fluid interaction with a bounding surface, where viscous deformation of the fluid creates gradients of vorticity. Just like the diffusion of heat in a solid or fluid is dependent on a gradient in temperature to transfer energy as heat [i.e. $q = -k\nabla T$], a vorticity gradient [actually the gradient of each directional component of vorticity, e.g. $\nabla\omega_z$] is necessary for the viscous transfer (i.e. diffusion) of vorticity. At first, this may sound a bit confusing, since there really isn't a physical property, like heat, that is proportional to the vorticity gradients. However, just as we can view the gradient of a temperature field, ∇T , as proportional to the flux of heat energy (which is reflected by the temperature within the material itself), we can view the gradient of a vorticity component (e.g. $\nabla\omega_z$) as proportional to the flux of that vorticity component. By flux, we mean the rate of transfer of a property per unit area. When this property flux, whether it is heat or vorticity, occurs adjacent to a bounding surface, this is construed as an infusion of "new" property into the fluid, which we consider an addition to the fluid. In the case of vorticity, we choose to call this

flux across the boundary a “generation” of vorticity, since no vorticity actually existed within the boundary, unlike heat.

Note that a property will diffuse in the direction of a *decreasing* property (i.e. "down" the gradient of the property). For heat transfer, heat will diffuse in the direction of decreasing temperature. Likewise, vorticity will also diffuse in the direction of decreasing vorticity.

In addition, the total vorticity flux really reflects the vector sum of the gradient of each of the directional components of vorticity. However, to demonstrate the processes that lead to viscous generation of vorticity, we will restrict our assessment to a two-dimensional flow, with only one component of vorticity.

Consider the flow of a viscous fluid parallel to a flat surface. Such flows will develop a region of viscous deformation adjacent to the surface (i.e. a boundary layer), where the velocity profile adjusts from no slip at the surface to the free stream velocity of the outer flow, as shown in Figure 11.11.

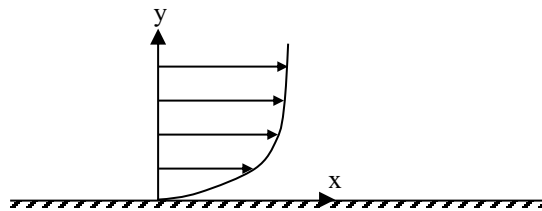


Figure 11.11 A typical velocity profile for a viscous flow adjacent to a flat surface.

To assess the behavior of the fluid at the surface boundary, we evaluate the x-direction, two-dimensional Navier-Stokes equation in Cartesian coordinates (Eq. 5.45) at the bounding surface (i.e. at $y = 0$). Therefore, at the surface, we have:

$$\left\{ \cancel{\frac{\partial u}{\partial t}} + u \cancel{\frac{\partial u}{\partial x}} + v \frac{\partial u}{\partial y} = v \left[\cancel{\frac{\partial^2 u}{\partial x^2}} + \frac{\partial^2 u}{\partial y^2} \right] - \frac{1}{\rho} \frac{\partial P}{\partial x} + g_x \right\}_{y=0} \tag{11.46}$$

Since the streamwise velocity, and its derivatives don't vary along the plate ($y = 0$), we have

$u, \frac{\partial u}{\partial x}, \frac{\partial^2 u}{\partial x^2} = 0$ at $y = 0$, allowing us to delete the terms indicated in Eq. 11.46, giving the simplified Eq. 11.47.

$$v \frac{\partial^2 u}{\partial y^2} \Big|_{y=0} = \frac{\partial u}{\partial t} \Big|_{y=0} + v \frac{\partial u}{\partial y} \Big|_{y=0} + \frac{1}{\rho} \frac{\partial P}{\partial x} - \cancel{g_x} \tag{11.47}$$

(neglect)

Note that in Eq. 11.47 we leave open the possibility for transpiration across a porous surface ($v \neq 0$). By neglecting the gravity component (assuming gravity acts in the y direction) and noting that the vorticity at the surface ($y = 0$) is:

$$\omega_z = \frac{\partial v}{\partial x} - \frac{\partial u}{\partial y},$$

we can further simplify Eq. 11.47 to yield Eq. 11.48, which describes the flux of vorticity at the surface:

$$\frac{\partial \omega_z}{\partial y} \Big|_{y=0} = \underbrace{-\frac{1}{\nu} \frac{\partial u}{\partial t}}_{\text{Acceleration}} \Big|_{y=0} - \underbrace{\frac{1}{\mu} \frac{\partial P}{\partial x}}_{\text{Pressure Gradient}} + \underbrace{\frac{v}{\nu} \omega_z}_{\substack{\text{Boundary} \\ \text{Transpiration}}} \Big|_{y=0} \tag{11.48}$$

\uparrow
 Flux of vorticity @ surface

As discussed above, at the bounding surface the flux of vorticity is indicative of vorticity generation. As Eq. 11.48 illustrates, for a *solid* boundary ($v = 0$) there are two possible sources of vorticity:

- 1) acceleration (of the surface or the adjacent fluid), and
- 2) a streamwise pressure gradient.

However, if the surface is *porous*, this also opens up the possibility for vorticity generation by transpiration at the surface ($v|_{y=0} \neq 0$).

Note that vorticity is *only generated* when $\frac{\partial \omega_z}{\partial y} \neq 0$. However, recall from the above discussion that vorticity will diffuse in the direction of a *decreasing* vorticity gradient. Consequently, the implication of the sign of $\frac{\partial \omega_z}{\partial y}$ on the type of vorticity that is generated is counter intuitive. That is:

- 1) when $\frac{\partial \omega_z}{\partial y} < 0$, *Positive* rotation vorticity will be diffused into the fluid (i.e. generated) from the boundary, whereas
- 2) when $\frac{\partial \omega_z}{\partial y} > 0$, *Negative* rotation vorticity will emanate from the boundary.

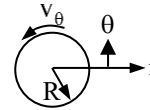
However, this generation process is relative to the direction of the normal for the generating surface. If the outward normal for the generating surface is positive (relative to the defining coordinate system), the convention is as just stated. However, if the outward normal is in a

negative coordinate direction, the sign of the vorticity generation will be reversed [e.g. if $\frac{\partial \omega_z}{\partial y} < 0$, and the surface normal is in a negative direction, the vorticity generation will be negative, relative to the coordinate system]. If we consider each of the terms on the right side of Eq. 11.48 as “sources” of vorticity, one can see that a flow could have several sources of either positive or negative vorticity, depending on the sign of each term.

We can perform a similar assessment of vorticity generation for a circular cylinder of radius R in cylindrical coordinates, starting with the two-dimensional Navier-Stokes equation in the r- θ plane. Here we consider the limiting conditions of v_θ , $\frac{\partial v_\theta}{\partial \theta}$, $\frac{\partial^2 v_\theta}{\partial \theta^2} = 0$ @ $r = R$, the cylinder surface, which yields:

$$\left\{ \frac{\partial v_\theta}{\partial t} + v_r \frac{\partial v_\theta}{\partial r} = -\frac{1}{\rho r} \frac{\partial P}{\partial \theta} + \nu \frac{\partial}{\partial r} \left(\frac{1}{r} \frac{\partial}{\partial r} (r v_\theta) \right) \right\}_{r=R}$$

ω_z



or

$$\frac{\partial \omega_z}{\partial r} \Big|_{r=R} = \underbrace{\frac{1}{\nu} \frac{\partial v_\theta}{\partial t} \Big|_{r=R}}_{\text{Acceleration}} + \frac{1}{\mu R} \frac{\partial P}{\partial \theta} + \underbrace{\frac{v_r}{\nu} \frac{\partial v_\theta}{\partial r} \Big|_{r=R}}_{\substack{\text{Boundary} \\ \text{Transpiration}}} \tag{11.49}$$

↑
Vorticity flux at cylinder surface

Eq. 11.49 is an expression for the flux of vorticity at a cylindrical surface of radius R.

Again, just as for a flat plate, the sources of vorticity are:

- 1) acceleration (of the surface or the adjacent fluid),
- 2) an azimuthal pressure gradient (in the θ direction), and
- 3) transpiration (if the boundary is porous)

Note that the sign of the first two terms on the right-hand side of equation 11.49 is positive, whereas those same terms were negative in equation 11.48. This is simply a consequence of the way that the coordinate axes in cylindrical coordinate systems are defined.

Vorticity generation by viscous processes is a quite common, since all fluid-adjacent surfaces are frequently subject to accelerations or pressure gradients. Often, the vorticity generation process is the result of the action of both localized acceleration and pressure gradients adjacent to a surface. Examples are the acceleration and movement of vehicles (e.g. cars, planes, ships), the

paddling of a canoe, and the flight of a bird. We most frequently notice this generation of vorticity as a by-product, which is the “shedding” or release of this generated vorticity into the fluid as discrete vortices (more on this in Section 15.4). Although these vortices are often not visible, their effects are often perceived by secondary effects such as pressure pulsations, noise, or deformation of the free surface of a liquid. Anyone who has driven behind a large truck has experienced the buffeting of your vehicle, which is the result of the truck shedding large, discrete vortices that are felt as oscillatory pressure changes when they impact your vehicle. The dimpling of the surface of a lake by your canoe paddle is due to vortices shed from your paddle as it both accelerates and generates a pressure gradient as it passes through the water. And if you have ever heard the thump, thump of a helicopter, or the similar (but softer) sounds of a goose, duck, or bird as they come in for a landing, or the buzzing of a bee or humming bird, then you were hearing the effects of generated vorticity as it is shed as vortices from the rotor or wings.

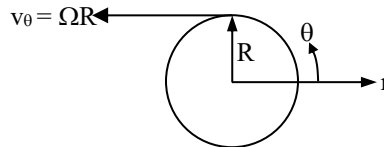
While the above processes are examples of where vorticity generation is commonly observed, they are actually quite complicated processes. To assess the processes of vorticity generation by viscous effects, we require some much simpler examples. Therefore, in the following three sections we will examine and assess some very simple examples that will illustrate more clearly the process of viscous vorticity generation by surface acceleration, streamwise pressure gradients, and transpiration.

11.5.2 Vorticity Generation by Acceleration

11.5.2.1 Acceleration of a Rotating Rod

Consider an initially stationary, solid circular rod in a viscous fluid, which at time $t = 0$ suddenly starts rotating at a constant angular velocity Ω , such that:

$$\begin{aligned}
 t < 0 &\Rightarrow v_\theta = 0 \\
 t \geq 0 &\Rightarrow v_\theta = \Omega R
 \end{aligned}$$



As we showed above, for a radially symmetric system such as this, Eq. 11.49 models the vorticity flux as:

$$\left. \frac{\partial \omega_z}{\partial r} \right|_{r=R} = \frac{1}{\nu} \left. \frac{\partial v_\theta}{\partial t} \right|_{r=R} + \frac{1}{\mu R} \frac{\partial P}{\partial \theta} + \frac{v_r}{\nu} \left. \frac{\partial v_\theta}{\partial r} \right|_{r=R}$$

Note: In the original image, the terms $\frac{1}{\mu R} \frac{\partial P}{\partial \theta}$ and $\frac{v_r}{\nu} \left. \frac{\partial v_\theta}{\partial r} \right|_{r=R}$ are crossed out with red lines and a red '0' is written above each.

For this type of flow, the flow is azimuthally symmetric such that there will be no change in pressure in the azimuthal (θ) direction, and the solid surface renders $v_r|_{r=R} = 0$. Thus, the vorticity flux for this situation is only a function of the acceleration of the rod.

$$\left. \frac{\partial \omega_z}{\partial r} \right|_{r=R} = \frac{1}{v} \left. \frac{\partial v_\theta}{\partial t} \right|_{r=R} \tag{11.50}$$

Note that Eq. 11.50 indicates that when:

$$\begin{aligned} \frac{\partial v_\theta}{\partial t} \neq 0 &\Rightarrow \text{vorticity is generated} \\ \frac{\partial v_\theta}{\partial t} = 0 &\Rightarrow \text{no vorticity is generated} \end{aligned}$$

Therefore, the generation of vorticity can only occur during the *initial acceleration* of the rod. After the rod reaches steady state, no more vorticity is generated, and the vorticity that was generated can only diffuse away from the rod.

As we showed in the example of Section 11.4.3, the steady state velocity field outside of a rod rotating at a constant speed in an infinite fluid contains no vorticity. However, vorticity was originally present, since Eq. 11.50 indicates that a finite amount of vorticity must have been generated within the fluid when the cylinder underwent its initial acceleration. However, after the cylinder reached steady state, no more vorticity was generated, and over time the vorticity generated during the initial acceleration all diffused outward to infinity, leaving the flow without vorticity.

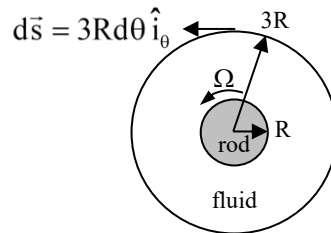


Figure 11.12 Illustration of fluid region $3R$ outside rod of radius R .

How much vorticity is generated? We can examine this question by assessing the vorticity initially present within a region of fluid extending well away from the cylinder surface. Immediately after the rod rotation is initiated, the vorticity that is generated will still remain within a region of fluid very close to the cylinder. Fluid well away from the rod (for purposes of example, let's assume a circle of radius $3R$) will not have noticed that the cylinder is rotating, since the generated vorticity will not have had sufficient time to diffuse outward, and thus the fluid at $r = 3R$ will still be quiescent ($\vec{V} = 0$).

If we calculate the circulation within the region $r = 3R$, as shown in Fig. 11.12, we have:

$$\Gamma_{\text{initial}} = \iint_A \vec{\omega} \cdot d\vec{A} = \oint_c \vec{V} \cdot d\vec{s} = \int_{\theta=0}^{\theta=2\pi} (0) 3R d\theta = 0 \tag{11.51}$$

since $\vec{V} = v_\theta \hat{i}_\theta$, $d\vec{s} = r d\theta \hat{i}_\theta = 3R d\theta \hat{i}_\theta$, and $v_\theta|_{r=3R} = 0$. However, when this flow reaches a steady state, we know from Section 11.4.3 (Eq. 11.31) that within the fluid:

$$v_\theta = \frac{\Omega R^2}{r}$$

Thus, the circulation (at any radius) for this steady state flow is:

$$\Gamma_{\text{steady state}} = \oint_c \vec{V} \cdot d\vec{s} = \int_{\theta=0}^{\theta=2\pi} \frac{\Omega R^2}{r} (r d\theta) = \int_{\theta=0}^{\theta=2\pi} \Omega R^2 d\theta = 2\pi \Omega R^2 \quad (11.52)$$

Note that $\Gamma_{\text{steady state}}$: (1) depends only on the cylinder radius, not the radius of the fluid region, and (2) is a non-zero value. However, how can $\Gamma_{\text{steady state}}$ be a non-zero value when the vorticity within this flow field was shown to be zero in Section 11.4.3? The answer is that while there is no vorticity within the steady state flow, the boundary we are integrating around *also contains the rod*, which does have “vorticity”, in the form of a solid body rotation. As we showed in Section 8.2.2, the circulation within a specified region is the sum of *all* the vorticity within that region. So, for this example, we can write that:

$$\Gamma_{\text{total}} = \Gamma_{\text{rod}} + \Gamma_{\text{fluid}} \quad (11.53)$$

Now, if we only consider the rod, the region of $r \leq R$, the circulation at any time after the rod reaches steady state is given by:

$$\Gamma_{\text{rod}} = \oint_c \vec{V} \cdot d\vec{s} = \int_{\theta=0}^{\theta=2\pi} (\Omega R) R d\theta = 2\pi \Omega R^2 \quad (11.54)$$

Substituting Eq. 11.53 back into Eq. 11.52, we have:

$$\Gamma_{\text{total}} = 2\pi \Omega R^2 + \Gamma_{\text{fluid}} \quad (11.55)$$

Thus, when the flow has reached steady state, we can set Eq. 11.52 equal to Eq. 11.55, and solve for the circulation within the fluid:

$$\Gamma_{\text{total}} = 2\pi \Omega R^2 + \Gamma_{\text{fluid}} = \Gamma_{\text{steady state}} = 2\pi \Omega R^2 \quad (11.56)$$

Equation 11.56 indicates that in the steady state flow, $\Gamma_{\text{fluid}} = 0$. This supports the fact that at steady state all the vorticity within the fluid will have diffused away to infinity, as we showed in Section 11.4.3. However, if we set the initial circulation (Eq. 11.51) within our region $r = 3R$ equal to the total circulation of Eq. 11.56, we have:

$$\Gamma_{\text{total}} = 2\pi \Omega R^2 + \Gamma_{\text{fluid}} = \Gamma_{\text{initial}} = 0 \quad (11.57)$$

Equation 11.57 indicates that $\Gamma_{\text{fluid}} = -2\pi\Omega R^2$! This represents the total amount of vorticity (i.e. circulation within the fluid) that was generated by the initial acceleration of the cylinder, and that initially resided within the fluid close to the rod. This is also the cumulative amount of vorticity that eventually diffuses out to infinity. Since the circulation for the fluid is negative, this indicates that the vorticity generated within the fluid must have a negative orientation (i.e. vorticity with a clockwise sense of rotation). As the rod accelerates in the positive θ direction, this creates a positive vorticity flux,

$$\left. \frac{\partial \omega_z}{\partial r} \right|_{r=R} = \frac{1}{\nu} \left. \frac{\partial v_\theta}{\partial t} \right|_{r=R} > 0,$$

which corresponds to the generation of negative vorticity, as discussed in Section 11.5.1.

Thus, the initial acceleration of the rod generates a finite amount of vorticity within the fluid adjacent to the rod boundary. This initial vorticity is then redistributed within the fluid according to our vorticity transport mechanisms [in this example, it eventually diffuses to infinity].

Does it make any difference how fast the rod is accelerated to ΩR ? If I accelerate the rod very slowly, or very quickly, will it influence how much total vorticity is generated? The answer is no. There will always be the same amount of vorticity generated, regardless of how the cylinder accelerates. If we expand our region of integration for the circulation outward toward infinity, the value of Γ_{initial} will remain zero for an extended period, and thus $\Gamma_{\text{fluid}} = -2\pi\Omega R^2$ for all modes of acceleration, as long as the terminal angular velocity of the rod is the same.

11.5.2.2 Acceleration of a Circular Vessel

Now, using the rotating rod example as a guide, what happens if I place a circular vessel full of quiescent water on a turntable and suddenly start it rotating at an angular velocity Ω [here we will again assume two-dimensional behavior]? For this situation, vorticity is generated at the inner boundary of the vessel, but how much? Consider the circulation within the boundaries of the vessel (i.e. @ $r = R$).

$$\Gamma = \iint \vec{\omega} \cdot d\vec{A} = \oint \vec{V} \cdot d\vec{s} = (\Omega R)2\pi R = 2\pi\Omega R^2 \quad (11.58)$$

Here, as in our previous example, vorticity is generated adjacent to the bounding surface during the acceleration of the vessel, yielding a circulation of $\Gamma = 2\pi\Omega R^2$. After the flux of new vorticity passes into the fluid adjacent to the outer boundary, the vorticity is spread by viscous diffusion uniformly throughout the fluid, eventually creating at steady state a solid body-like velocity field within the fluid, as shown in Figure 11.13.

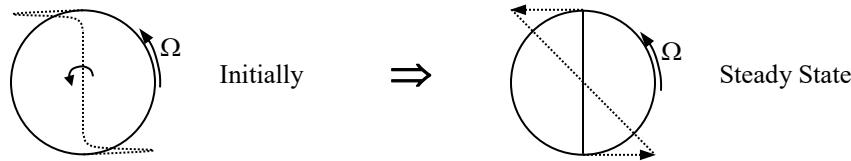


Figure 11.13 Illustration of the development of the velocity field within the fluid inside a circular vessel subjected to sudden rotation to a constant angular velocity Ω .

After reaching a steady state condition, what if we suddenly bring the vessel to rest? What happens? When the rotation terminates, $v_\theta|_{r=R}$, the velocity at the vessel surface, becomes zero, and the circulation within the vessel becomes:

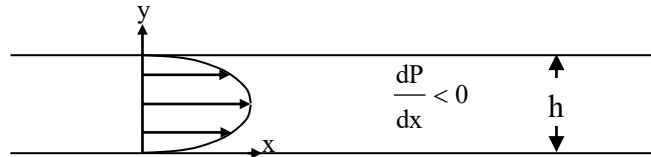
$$\Gamma = \oint \vec{V} \cdot d\vec{s} = v_\theta 2\pi R = 0! = \iint \vec{\omega} \cdot d\vec{A} \quad (11.59)$$

Equation 11.59 indicates that the *total* vorticity of the fluid within the cylinder is now zero. What happened to the original vorticity? The answer is that it was cancelled out by a new flux of vorticity of *opposite sign*, which was generated at the wall surface, and transferred to the fluid adjacent to the vessel wall when the vessel rotation was decelerated and stopped. However, while the circulation for the total fluid within the vessel will be zero at the instant of stoppage, the local response of the fluid will be quite unsteady and protracted. The original vorticity and the newly generated vorticity will interact through viscous diffusion to eventually bring the velocity field within the vessel to its new steady state of zero (vorticity, velocity, and circulation). This process is similar to what happens to the fluid in a cup of coffee or tea after it is stirred. Since the bounding surface of the cup is stationary, the circulation of the fluid within the cup must always be zero. Consequently, after stirring and removal of the stirring implement, there must be equal amounts of positive and negative vorticity contained within the cup. Over a period of time, viscous diffusion (and some advective transport and stretching/tilting) will cause the competing vorticities within the cup to cross-cancel, resulting in the eventual decay to a quiescent (but well mixed) cup of beverage.

Note that while the above examples deal with vorticity generated by the acceleration/deceleration of a surface adjacent to a fluid, the same process also holds for the acceleration of a fluid adjacent to a stationary surface. This mechanism of vorticity generation is most clearly apparent when considering a fluid that accelerates/decelerates above a flat surface, such as the interaction that occurs when gusts of wind pass in proximity to the earth. Since wind gusts (acceleration) and lulls (deceleration) occur all the time, wind interactions with the earth provide continual sources of both positive and negative vorticity, which subsequently interact in complicated vorticity transport processes that further affect local wind patterns.

11.5.3 Vorticity Generation by a Streamwise Pressure Gradient

To assess the generation of vorticity by a streamwise pressure gradient, consider a fully-developed laminar flow between parallel, bounding surfaces. This is the Poiseuille flow that we considered in Section 6.3.2, and in Section 11.4.2 above.

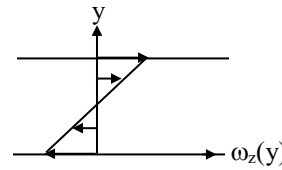


In Section 6.3.2, the velocity and vorticity for this flow were determined as:

$$u = \frac{h^2}{2\mu} \frac{dP}{dx} \left(\frac{y}{h} - 1 \right) \frac{y}{h} = 4U_{\max} \left(1 - \frac{y}{h} \right) \frac{y}{h} \tag{11.60}$$

and

$$\omega_z = \frac{4U_{\max}}{h} \left(2 \frac{y}{h} - 1 \right) \tag{11.61}$$



where $U_{\max} = -\frac{h^2}{8\mu} \frac{dP}{dx} \Rightarrow \frac{1}{\mu} \frac{dP}{dx} = -\frac{8U_{\max}}{h^2}$ (11.62)

Recall that this flow has solid boundaries, is steady, and has a constant pressure gradient that is decreasing in the x-direction (to give a positive, x-direction flow). Simplifying Eq. 11.48 for a solid boundary with a steady flow, and employing Eq. 11.62, we have for $y = 0$:

$$\left. \frac{\partial \omega_z}{\partial y} \right|_{y=0} = -\frac{1}{\nu} \frac{\partial u}{\partial t} \Big|_{y=0} - \frac{1}{\mu} \frac{\partial P}{\partial x} + \frac{v}{\nu} \omega_z \Big|_{y=0} = \frac{8U_{\max}}{h^2} \tag{11.63a}$$

Likewise, for the $y = h$ boundary, we have the same result:

$$\left. \frac{\partial \omega_z}{\partial y} \right|_{y=h} = -\frac{1}{\nu} \frac{\partial u}{\partial t} \Big|_{y=h} - \frac{1}{\mu} \frac{\partial P}{\partial x} + \frac{v}{\nu} \omega_z \Big|_{y=h} = \frac{8U_{\max}}{h^2} \tag{11.63b}$$

Thus, since the flux of vorticity is equivalent at the respective boundaries ($y = 0$ and $y = h$), equal but opposite amounts of vorticity will be generated. Since Eq. 11.63a indicates that

$$\left. \frac{\partial \omega_z}{\partial y} \right|_{y=0} > 0, \text{ this indicates that negative vorticity } \left(\omega_z \Big|_{y=0} = -\frac{4U_{\max}}{h}, \text{ from Eq. 11.61} \right) \text{ is}$$

generated at a constant rate from the lower surface. Note that the vorticity gradient at the upper

boundary, Eq. 11.63b, also gives $\left. \frac{\partial \omega_z}{\partial y} \right|_{y=h} > 0$, which we would initially anticipate indicates the generation of negative vorticity. However, Eq. 11.61 indicates that the vorticity generated at the boundary $\left(\omega_z|_{y=0} = \frac{4 U_{\max}}{h} \right)$ is *positive*. Here we note that the surface normal for the upper boundary will be in the negative y -direction. Recall from our discussion in Section 11.5.1 that a negative surface normal will reverse our convention for vorticity generation, such that a positive vorticity gradient results in the generation of positive vorticity for a negative surface.

As vorticity is generated at each of the opposing surfaces, it will diffuse toward the midline between the plates, resulting in a mutual cancellation of the respective opposing sign vorticities. Note that if there were not mutually opposing surfaces, but only one bounding surface, the presence of a pressure gradient would only generate vorticity at that bounding surface. Examples of such pressure-gradient flows are the external flow over a cylinder or an airfoil, as we discussed in Chapter 9 for inviscid potential flows. In the presence of viscosity, such external flows will result in the generation of vorticity at the body boundary due to the spatially varying pressure gradients that are created over the bodies due to their respective shapes. The subsequent transport of the generated vorticity will of course result in a modification of the associated velocity field, which will modify the external flow, and thus affect the subsequent generation of vorticity. The process, as one can imagine, can get quite interactive and complicated.

Consider the external flow over a cylinder. In Section 9.8.1 we showed that inviscid potential flow around a cylinder is subject to large spatial variations of the surface pressure (and thus pressure gradient). For a viscous flow, the variation of the pressure gradient from negative to positive, as the external flow circumvents the cylinder, will result in the generation of both positive and negative vorticity within the bounding flow. Since no opposing surface is present to generate counter-balancing vorticity, these types of flows undergo very strong modifications from the hypothetical inviscid flow, which further modify the pattern of vorticity generation. Often, a preponderance of one sign of vorticity or the other will be generated, resulting in flow field adjustments that allow the flow over the body to release or "dispose" of the continually generated and accumulating vorticity. At higher Reynolds numbers, these flow field adjustments result in very unsteady and often complicated processes of vorticity "shedding", often as discrete vortices, which pass into the departing flow field. We will discuss these types of external flows, and the processes for shedding vorticity in Chapter 15.

11.5.4 Vorticity Generation by Surface Transpiration

While transpiration through bounding surfaces is not widely encountered in many practical fluid applications, transpiration is of importance in such things as turbine blade cooling, paper making, and flow control (particularly for control of separated flows, which we discuss later in Chapters

14, 15, and 17). To examine vorticity generation due to transpiration through a porous surface, we utilize the example that we did in Section 11.4.1 for a fully developed flow over a flat plate with suction. From Eq. 11.31 and 11.32, the expressions for the velocity and vorticity were determined as:

$$u = U_\infty \left[1 - e^{-\frac{vy}{\nu}} \right] \tag{11.64}$$

and

$$\omega_z = -\frac{du}{dy} = -U_\infty \frac{V}{\nu} e^{-\frac{vy}{\nu}} \tag{11.65}$$

This flow is steady with no streamwise pressure gradient, but with a constant suction velocity through the bounding surface, $v|_{y=0} = -V$. The vorticity flux equation, 11.48, thus simplifies to:

$$\frac{\partial \omega_z}{\partial y} \Big|_{y=0} = -\frac{1}{\nu} \frac{\partial u}{\partial t} \Big|_{y=0} - \frac{1}{\mu} \frac{\partial P}{\partial x} + \frac{v}{\nu} \omega_z \Big|_{y=0} \tag{11.66}$$

Substituting $v = -V = \text{constant}$ for this flow and employing Eq. 11.65 @ $y = 0$, we have:

$$\frac{\partial \omega_z}{\partial y} \Big|_{y=0} = -\frac{V}{\nu} \omega_z \Big|_{y=0} = U_\infty \frac{V^2}{\nu^2} \tag{11.67}$$

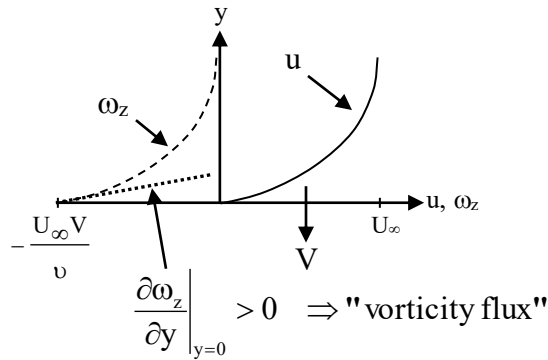


Figure 11.14 Generalized velocity and vorticity curves for flow over a porous flat plate with suction ($v|_{y=0} = -V$). The positive surface gradient of vorticity indicates a flux of *negative* vorticity across the boundary.

Since $\frac{\partial \omega_z}{\partial y} \Big|_{y=0} > 0$, this implies that vorticity is being generated at the surface (which has a positive normal) in the amount $\omega_z|_{y=0} = -U_\infty \frac{V}{\nu}$, as shown in Figure 11.14.

This negative vorticity will diffuse outward from the surface. However, as we discussed in Section 11.4.1, this vorticity is simultaneously transported (by advection) back towards and removed through the surface by the suction. Because of this balance between viscous diffusion and transpiration, the velocity profile for this flow does not change, and attains the fully developed condition shown in Figure 11.14.

However, what will happen if, as the flow passes along the flat surface, the flow leaves the porous surface with suction, and passes onto a solid boundary with $v|_{y=0} = 0$? Equation 11.66

then would give $\frac{\partial \omega_z}{\partial y} \Big|_{y=0} = 0$, which indicates that there will be no flux of vorticity from the solid

surface. Consequently, no additional vorticity will be generated, nor will the existing vorticity in the flow field be restrained by the surface suction. Therefore, the existing vorticity will diffuse outward as the fluid moves along the solid boundary, resulting in a continual increase in the thickness of the vorticity bearing layer. This process, as we will discuss in Chapter 13, results in a growing “boundary layer.” The flow for this situation is no longer fully developed, and (as we will see in Chapter 13) the analysis of the flow becomes more complicated. The general character of this flow over a solid boundary is represented in Figure 11.15.

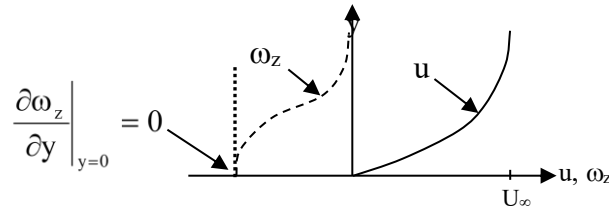


Figure 11.15 Generalized velocity and vorticity curves for flow over a solid flat plate ($v|_{y=0} = 0$). Note that there is no vorticity flux since the gradient of the vorticity at the surface is zero.

Note that although $\frac{\partial \omega_z}{\partial y} \Big|_{y=0} = 0$, at the boundary we have $\omega_z|_{y=0} \neq 0$ (from the previous developed

vorticity distribution). Since no new vorticity is generated over the solid boundary, the total vorticity that initially existed within the vorticity-bearing layer will continually redistribute as the flow advects downstream, with a non-zero vorticity value at the boundary.

Now consider what happens if we transition from a porous plate with suction, to a porous plate with *injection* of fluid through the surface and *into* the flow field. Assuming that the injection is equal, but opposite, to our suction process, this would transition from a boundary condition of $v|_{y=0} = -V$ to a boundary condition of $v|_{y=0} = +V$. Since this flow would start with an initial

distribution of negative vorticity ($\omega_z < 0$) within the vorticity-bearing region, and a non-zero vorticity at the boundary ($\omega_z|_{y=0} < 0$), the vorticity flux will now be given by:

$$\left. \frac{\partial \omega_z}{\partial y} \right|_{y=0} = \frac{V}{\nu} \omega_z \Big|_{y=0} < 0 \quad (\text{since } \omega_z < 0 \text{ initially}) \tag{11.68}$$

Equation 11.68 indicates that injection will result in the generation of positive vorticity at the surface (recall our discussion in Section 11.5.1). This positive vorticity will be both advected (by the injected fluid) and diffused away from the surface, initially modifying the vorticity and velocity profiles as shown in Figure 11.16.

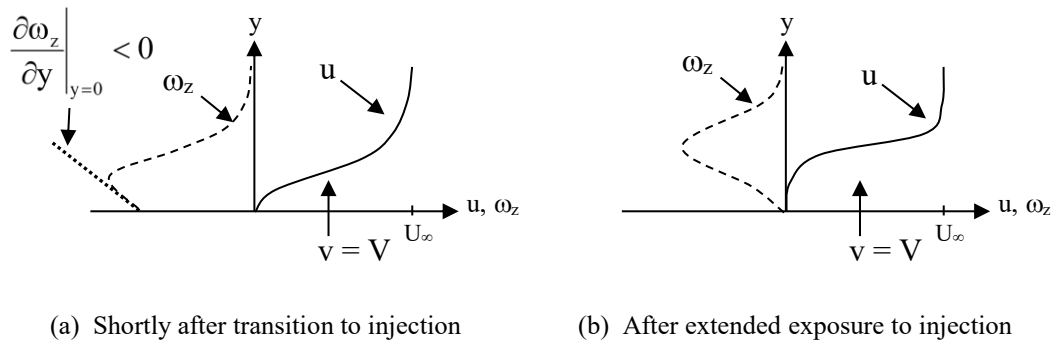


Figure 11.16 Generalized velocity and vorticity curves for flow over a porous flat plate with injection ($v|_{y=0} = +V$). Here the negative slope of the vorticity at the surface indicates a flux of *positive* vorticity across the boundary.

As shown in Figure 11.16a, the flux of positive vorticity due to injection will begin to cross-cancel with the original negative vorticity distribution within the vorticity bearing layer, such that the vorticity distribution will develop a vorticity maximum (in absolute terms) away from the plate surface. At this maximum, the slope of the vorticity is zero, $\frac{\partial \omega_z}{\partial y} = 0$. This null

vorticity gradient roughly reflects a null second derivative of streamwise velocity

$$\left(\frac{\partial \omega_z}{\partial y} \cong -\frac{\partial^2 u}{\partial y^2} = 0 \right),$$

which indicates a cross-stream inflection in the streamwise velocity. As we will discuss in Chapters 13 and 17, a cross-stream inflection in the streamwise velocity is generally an undesirable flow characteristic, since it is a precursor of unstable flow behavior, and can quickly result in a transition from laminar to turbulent flow.

Assuming that a stable flow can be maintained, as the flow proceeds along the porous plate, the fluid injection results in further generation of positive vorticity, and the vorticity profile will

skew even further, with $\omega_z|_{y=0} \rightarrow 0$. When $\omega_z|_{y=0} = 0$, as shown in Figure 11.16b, the vorticity gradient at the bounding surface becomes zero, $\frac{\partial \omega_z}{\partial y}\bigg|_{y=0} = \frac{V}{\nu} \omega_z\bigg|_{y=0} = 0$, and the flux of vorticity across the boundary will cease. Since $\omega_z|_{y=0} = 0$, this means that the slope of the velocity at the surface will be zero, $\frac{\partial u}{\partial y}\bigg|_{y=0} = 0$, such that the flow closely adjacent to the surface will become essentially stationary. Since no new vorticity is generated, the flow again grows only through a redistribution of the vorticity within the vorticity bearing layer (assuming that it remains in a stable, laminar flow--which is unlikely). Thus, as the flow moves along the boundary, and fluid injection continues, the vorticity-bearing layer will spread farther from the surface, but there will be no further addition of vorticity.

11.5.5 Vorticity Generation by Baroclinic Effects

As mentioned in Section 11.5, baroclinic effects [$P \neq P(\rho)$] also can generate vorticity. In Chapter 10 (Sections 10.2-10.5 in particular), we illustrated that when the gradients of pressure and density are not aligned, such as in buoyancy-induced flows, there will be temporal changes in circulation for a defined region of fluid. In this section, we address the generation of vorticity that gives rise to circulation changes due to baroclinic behavior. To assess this behavior, we reconsider Eq. 11.5, the equation we derived leading to the vorticity transport equation:

$$\frac{\partial \vec{\omega}}{\partial t} + (\vec{V} \cdot \nabla) \vec{\omega} - (\vec{\omega} \cdot \nabla) \vec{V} = \left(\frac{1}{\rho^2} \right) \nabla \rho \times \nabla P + \nu \nabla^2 \vec{\omega} \quad (11.5)$$

Identifying that $\frac{D\vec{\omega}}{Dt} = \frac{\partial \vec{\omega}}{\partial t} + (\vec{V} \cdot \nabla) \vec{\omega}$, and rearranging:

$$\frac{D\vec{\omega}}{Dt} = (\vec{\omega} \cdot \nabla) \vec{V} + \nu \nabla^2 \vec{\omega} + \left(\frac{1}{\rho^2} \right) \nabla \rho \times \nabla P \quad (11.69)$$

Here, we know that $\frac{D\vec{\omega}}{Dt}$ reflects the changes of the vorticity field due to material changes,

$(\vec{\omega} \cdot \nabla) \vec{V}$ models vorticity addition/removal due to stretching/compression effects, and $\nu \nabla^2 \vec{\omega}$

represents diffusion of existing vorticity due to viscous effects. The $\left(\frac{1}{\rho^2} \right) \nabla \rho \times \nabla P$ term is an

interesting term, in that it does not deal with a modification or transport of existing vorticity since it requires no action on $\vec{\omega}$, the vorticity field. Thus, this is a term that can create vorticity where none existed, and without the assistance of viscosity. For simplicity, consider a two-dimensional (Cartesian, x-y plane), inviscid flow. Eq. 11.69 then simplifies to:

$$\frac{D\vec{\omega}}{Dt} = \left(\frac{1}{\rho^2}\right) \nabla\rho \times \nabla P \tag{11.70}$$

Equation 11.70 illustrates that if the gradients of pressure and density do not align, the cross product of the gradients will be non-zero, and thus vorticity will be generated. For example, in an x-y plane the component of vorticity is $\vec{\omega} = \omega_z \hat{k}$, with $\nabla\rho = \frac{\partial\rho}{\partial x} \hat{i} + \frac{\partial\rho}{\partial y} \hat{j}$ and $\nabla P = \frac{\partial P}{\partial x} \hat{i} + \frac{\partial P}{\partial y} \hat{j}$. Thus, Eq. 11.70 reduces to a single component equation for ω_z , given by:

$$\frac{D\omega_z}{Dt} = \left(\frac{1}{\rho^2}\right) \left(\frac{\partial\rho}{\partial x} \frac{\partial P}{\partial y} - \frac{\partial\rho}{\partial y} \frac{\partial P}{\partial x} \right) \tag{11.71}$$

While Eq. 11.71 looks a little daunting, it is really quite instructive as to how baroclinic flows generate vorticity. Consider the sea breeze problem we examined previously in Section 10.2.3. For that example, we made the approximation that isobars of pressure would align with the earth, but the isopycnals of density would align vertically (due to the temperature differential between the air over land relative to the air over the ocean). This is generically illustrated in Figure 11.17 below.

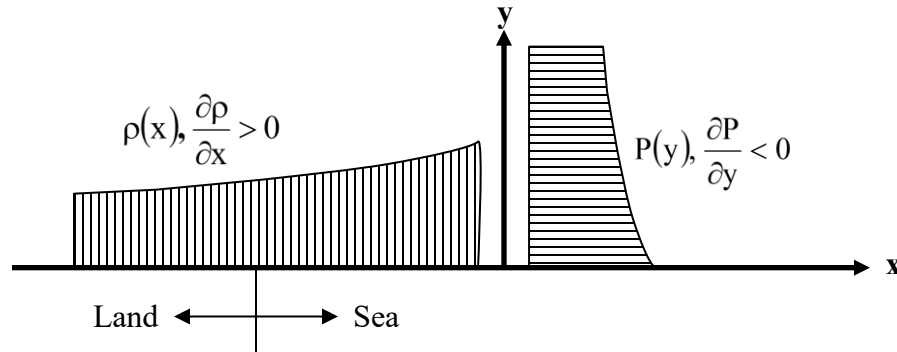


Figure 11.17 Idealized distributions of air density and pressure from land to sea.

Figure 11.17 is highly idealized, but illustrates the most extreme case. Here we assume $P = P(y)$ and $\rho = \rho(x)$, and $\frac{\partial\rho}{\partial x} > 0$, and $\frac{\partial P}{\partial y} < 0$ (since pressure will decrease with altitude). Since the gradients are orthogonal to each other, Eq. 11.71 reduces to:

$$\frac{D\omega_z}{Dt} = \left(\frac{1}{\rho^2}\right) \left(\frac{\partial\rho}{\partial x} \frac{\partial P}{\partial y} \right) < 0 \tag{11.72}$$

(+) (+) (-)

Equation 11.72 indicates that the conditions shown in figure 11.17 will generate negative vorticity. Recall in Section 10.2.3 that for these same types of conditions, we determined that the air would experience a negative change in circulation, reflecting a clockwise air flow, which is of

course consistent with the generation of negative vorticity. One might think of this as the denser air over the sea, under the influence of the pressure gradient, moving inland (on shore) to displace the lighter air, which must move upward and seaward to satisfy continuity.

Of course, in the evening, when the land cools faster than the sea, the density will be greater over the land than the sea, causing the generation of positive vorticity and a counter-clockwise circulation, such that the direction of the air flow will reverse to a seaward (off-shore) breeze.

Notice that the conditions represented in figure 11.17 could also apply to vorticity generation within the ocean, where pressure increases with depth from the ocean surface ($\frac{\partial P}{\partial y} < 0$ using the coordinates of figure 11.17). If a spanwise variation in density (e.g. $\frac{\partial \rho}{\partial x} \neq 0$ due to salinity variations) is present, vorticity will again be generated, either negative or positive depending on the value of $\frac{\partial \rho}{\partial x}$.

Now, consider the movement of a variable density fluid through a duct due to a pressure difference, as shown in Figure 11.18. Here, the density varies with y and the pressure with x . If we assume that the flow is left to right, then the pressure must decrease in the positive x -direction and $\frac{\partial P}{\partial x} < 0$.

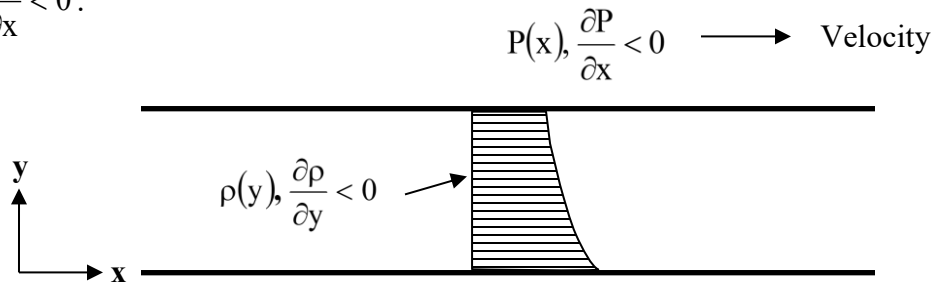


Figure 11.18 The flow of a fluid with vertical density variations in a horizontal duct.

Initially, we will assume that the density decreases in the positive y -direction, so $\frac{\partial \rho}{\partial y} < 0$. Thus,

Eq. 11.71 then reduces to:

$$\frac{D\omega_z}{Dt} = - \left(\frac{1}{\rho^2} \right) \left(\frac{\partial \rho}{\partial y} \frac{\partial P}{\partial x} \right) < 0 \tag{11.73}$$

(+) (-) (-)

Equation 11.73 indicates that negative vorticity will be generated as the flow proceeds in the x -direction. Physically, we reason that the pressure gradient will accelerate the less dense material faster than the more dense material, thus a differential in cross-stream velocity will develop.

Since we assumed the flow to be inviscid, the flow would continue to accelerate differentially, and thus continually generate negative vorticity, such that the total vorticity will continually increase (since vorticity does not dissipate in an inviscid fluid). Note that if the density increased in the y -direction (opposite to Figure 11.18), then positive vorticity would be generated.

The present discussion illustrates how baroclinic processes are another source of vorticity within a flow field. Here, the vorticity does not emanate from a boundary, nor is viscosity necessary. As pointed out in Chapter 10, such baroclinic processes are a key element in many atmospheric and oceanic flows. The particular development of rotating flows, such as [tornados](#) and [hurricanes](#), depends on strong thermal warming, and thus density variations, to generate vorticity. Such density-generated vorticity can accumulate and concentrate into tornadic flow patterns. Taken to an extreme, very strong temperature/density variations in wild fires have, under the right terrain and conditions, generated whirling flame concentrations termed “firenados”. This [link](#) shows several images of such phenomena, as well as some scary videos. Strong density gradients within the oceans can also yield strong rotational behavior, which can create/modify ocean currents, which in turn can modify the local weather patterns (e.g. such processes contribute in complicated ways to the cyclical [El Niño/La Niña](#) weather patterns).

An additional illustration of the global effects of baroclinic vorticity generation is the Gulfstream ocean current that flows north up the east coast of the United States, and then across the Atlantic ocean to Europe. The Gulfstream depends on temperature and salinity variations in sea water density to generate vorticity, and thus a large-scale circulation. With the warming of Greenland by climate change, its ice covering is rapidly melting, introducing massive amounts of fresh water into the North Atlantic ocean, which reduces the salinity (and thus density) of the surface waters of the Gulfstream. Consequently, vorticity and circulation generation are reduced, slowing the current of the Gulfstream. If Greenland, and other associated ice bound regions, continue to melt at a high rate, climate scientists predict that the Gulf stream will continue to slow, which will severely impact the climate of Europe, as well as result in substantial sea level increases along the eastern seaboard of the United States. Continued melting of the ice pack through the next century could eventually result in a collapse of the Gulfstream, and a cataclysmic change in global weather patterns.

11.6 Circulation Changes in a Fixed Reference Frame

In Section 10.1, we examined how circulation can change for a region of fluid that moves within a viscous flow field. In the present section, we examine the changes in circulation that can take place within a *fixed region* as the flow field moves through it. While in Section 10.1 we focused on a defined *material* region, which was free to move and deform, here we focus on a defined *spatial* region, through which the flow will pass. Our concern is how the circulation within this fixed region changes as vorticity-bearing fluid passes into and out of the region. Here we

consider a fixed curve in space, as shown in figure 11.19, for which the circulation is given by a line integral as $\Gamma = \oint \vec{V} \cdot d\vec{s}$.

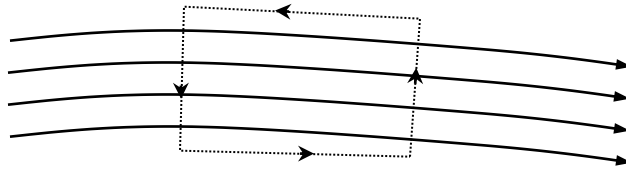


Figure 11.19 A fixed region in space, with circulation $\Gamma = \oint \vec{V} \cdot d\vec{s}$.

Now, since we consider a fixed curve, and don't follow a material region, we can write the change in Γ with time as a conventional, not a material, derivative:

$$\begin{aligned} \frac{\partial \Gamma}{\partial t} &= \frac{\partial}{\partial t} \oint \vec{V} \cdot d\vec{s} \quad (\text{note: this is not } \frac{D\Gamma}{Dt}) \\ &= \oint \frac{\partial \vec{V}}{\partial t} \cdot d\vec{s} \end{aligned} \tag{11.74}$$

Note that we can bring the time derivative inside the integral, because the region over which we integrate is of fixed dimensions (see [Liebniz rule](#) on integration limits).

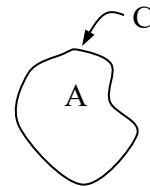
However, rearranging the Navier-Stokes equation (Eq. 5.44), we can solve for the time derivative of velocity, giving:

$$\frac{\partial \vec{V}}{\partial t} = -(\vec{V} \cdot \nabla) \vec{V} - \frac{\nabla P}{\rho} + \overset{\text{neglect}}{\vec{g}} + \nu \nabla^2 \vec{V} \tag{11.75}$$

We now substitute Eq. 11.75 into 11.74, and simplify and consolidate the terms, using a vector identity from Chapter 2 [Eq. 2.16g ---prove to yourself how we get this relationship], and then Stokes' Theorem, section 2.4.4.

$$\begin{aligned} \frac{\partial \Gamma}{\partial t} &= -\oint (\vec{V} \cdot \nabla) \vec{V} \cdot d\vec{s} - \oint \frac{\nabla P}{\rho} \cdot d\vec{s} + \oint \nu \nabla^2 \vec{V} \cdot d\vec{s} \\ &= -\oint \left[(\vec{\omega} \times \vec{V}) + \nabla \left(\frac{V^2}{2} \right) \right] \cdot d\vec{s} - \oint \frac{\nabla P}{\rho} \cdot d\vec{s} + \oint \nu \nabla^2 \vec{V} \cdot d\vec{s} \\ &= -\iint_A \left[\nabla \times (\vec{\omega} \times \vec{V}) + \nabla \times \nabla \left(\frac{V^2}{2} \right) \right] \cdot d\vec{A} - \oint \frac{\nabla P}{\rho} \cdot d\vec{s} + \oint \nu \nabla^2 \vec{V} \cdot d\vec{s} \end{aligned} \tag{11.76}$$

From Stokes' Theorem
= 0
(if P = P(ρ)
or constant)



Thus, for barotropic flows [$P = P(\rho)$], Eq. 11.76 reduces to:

$$\frac{\partial \Gamma}{\partial t} = - \iint_A [\nabla \times (\omega \times \vec{V})] \cdot d\vec{A} + \oint_C \mathbf{v} \nabla^2 \vec{V} \cdot d\vec{s} \tag{11.77}$$

Note that Eq. 11.77 is similar to Eq.10.10, with the exception of the additional first term on the right hand side of Eq. 11.77. This term, as we will illustrate in the following, represents the transport of vorticity into and out of the spatial region C.

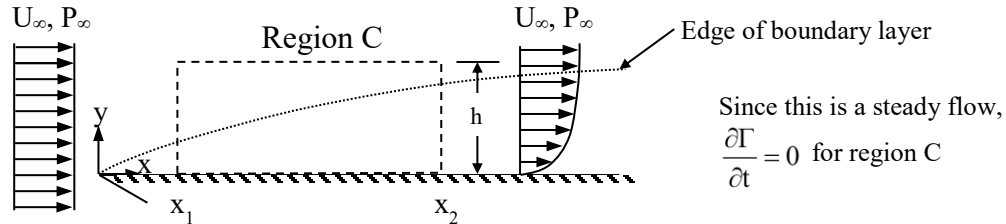


Figure 11.20 The development of a boundary layer for a viscous fluid impinging on, and passing over, a stationary flat plate.

As an illustration of how Eq. 11.77 can be employed, consider the boundary layer that develops when a viscous fluid flows over a stationary flat plate, as shown in figure 11.20. We want to examine how and why the vorticity changes as the flow passes onto and over the plate surface. To do this, we consider an arbitrary rectangular region C, as shown by the dotted line in figure 11.20, which is h high, and extends in a streamwise direction from x_1 to x_2 . Here, we assume that h is high enough that the upper extent of region C is in a region of uniform flow, such that any deformation of the passing fluid takes place only within the region C.

If this is a steady flow, then $\frac{\partial \Gamma}{\partial t} = 0$, which means that Eq. 11.77 reduces to:

$$\iint_A [\nabla \times (\omega \times \vec{V})] \cdot d\vec{A} = \oint_C \mathbf{v} \nabla^2 \vec{V} \cdot d\vec{s} \tag{11.78}$$

Now, consider the viscous term on the right of Eq. 11.78. Examining the flow in figure 11.20 within a two-dimensional x-y plane for $\vec{V} = u\hat{i} + v\hat{j}$ and $d\vec{s} = dx\hat{i} + dy\hat{j}$, we have that:

$$\begin{aligned} \mathbf{v} \nabla^2 \vec{V} \cdot d\vec{s} &= \mathbf{v} \left(\frac{\partial^2 \vec{V}}{\partial x^2} + \frac{\partial^2 \vec{V}}{\partial y^2} \right) \cdot d\vec{s} \\ &= \mathbf{v} \left(\frac{\partial^2 u}{\partial x^2} + \frac{\partial^2 u}{\partial y^2} \right) dx + \mathbf{v} \left(\frac{\partial^2 v}{\partial x^2} + \frac{\partial^2 v}{\partial y^2} \right) dy \end{aligned} \tag{11.79}$$

0 at x boundaries
0 or negligible on y boundaries

As we will show in Chapter 13, The only significant term in Eq. 11.79 is $\nu \frac{\partial^2 \mathbf{u}}{\partial y^2} dx$, since changes of u with respect to x are zero along the x -directed boundaries of region C , and since $v \ll u$, changes in v at the y -directed boundaries are either zero, or negligible. Additionally, the remaining $\frac{\partial^2 \mathbf{u}}{\partial y^2}$ term will contribute to the integral in Eq. 11.79 only along the x -boundary on the plate surface at $y = 0$, since $\frac{\partial^2 \mathbf{u}}{\partial y^2} \cong 0$ at the $y = h$ boundary, where the velocity profile is uniform. Thus, we can reduce the viscous term of Eq. 11.79 to:

$$\oint_C \nu \nabla^2 \vec{V} \cdot d\vec{s} = \oint_C \nu \left(\frac{\partial^2 \mathbf{u}}{\partial y^2} \right) dx = \int_{x=x_1}^{x=x_2} \nu \left(\frac{\partial^2 \mathbf{u}}{\partial y^2} \right) \Big|_{y=0} dx + (\text{negligible terms}) \quad (11.80)$$

Now consider the x -direction Navier-Stokes equation *at the plate surface*, which reduces to (after dropping terms that are zero at $y = 0$):

$$\nu \frac{\partial^2 \mathbf{u}}{\partial y^2} \Big|_{y=0} = \frac{1}{\rho} \frac{\partial P}{\partial x} \Big|_{y=0} \quad (11.81)$$

Substituting Eq. 11.81 into Eq. 11.80 we get:

$$\oint_C \nu \nabla^2 \vec{V} \cdot d\vec{s} = \int_{x_1}^{x_2} \nu \frac{\partial^2 \mathbf{u}}{\partial y^2} \Big|_{y=0} dx = \int_{x_1}^{x_2} \frac{1}{\rho} \frac{\partial P}{\partial x} \Big|_{y=0} dx = \frac{P_2 - P_1}{\rho} \quad (11.82)$$

Here P_1 and P_2 are the pressures at the respective x locations on the plate surface. Thus, the impact of viscosity on the circulation of region C is reflected by the change in pressure along the plate surface.

The first term on the left of Eq. 11.78 is a bit harder to assess. If we expand the integrand for a two-dimensional flow in the x - y plane, where $\vec{V} = u\hat{i} + v\hat{j}$, $\vec{\omega} = \omega_z \hat{k}$, and $d\vec{A} = dx dy \hat{k}$, we can write:

$$\iint_A [\nabla \times (\vec{\omega} \times \vec{V})] \cdot d\vec{A} = \iint_A \left[\frac{\partial}{\partial x} (\omega_z u) + \frac{\partial}{\partial y} (\omega_z v) \right] dx dy \quad (11.83)$$

Now if we integrate this term over the area encompassed by the region C , $x_1 \leq x \leq x_2$ and $0 \leq y \leq h$, we have:

$$\iint_A [\nabla \times (\vec{\omega} \times \vec{V})] \cdot d\vec{A} = \int_0^h \int_{x_1}^{x_2} \frac{\partial}{\partial x} (\omega_z u) dx dy + \int_{x_1}^{x_2} \int_0^h \frac{\partial}{\partial y} (\omega_z v) dy dx$$

$$\iint_A \left[\nabla \times (\vec{\omega} \times \vec{V}) \right] \cdot d\vec{A} = \underbrace{\int_0^h (u\omega_z)_{x=x_2} dy}_{\text{Vorticity advected out right face}} - \underbrace{\int_0^h (u\omega_z)_{x=x_1} dy}_{\text{Vorticity advected in left face}} + \int_{x_1}^{x_2} (v\omega_z)_{y=h} dx - \int_{x_1}^{x_2} (v\omega_z)_{y=0} dx \tag{11.84}$$

Here, we note that $\omega_z|_{y=h} = 0$ (since we have uniform flow at $y = h$) and $v|_{y=0} = 0$ (at the plate surface), which negates a contribution by the last two integrals of Eq. 11.84. If we now substitute Eqs. 11.82 and 11.84 back into Eq. 11.78 we obtain:

$$\underbrace{\frac{P_2 - P_1}{\rho}}_{\text{Pressure changes along plate}} = \underbrace{\int_0^h (u\omega_z)_{x=x_2} dy - \int_0^h (u\omega_z)_{x=x_1} dy}_{\text{Flux of vorticity transported across fixed region C}} \tag{11.85}$$

Equation 11.85 indicates that if $P_2 = P_1$, there is no new vorticity created inside of region C. However, if $P_2 \neq P_1$, vorticity *is created* inside of region C.

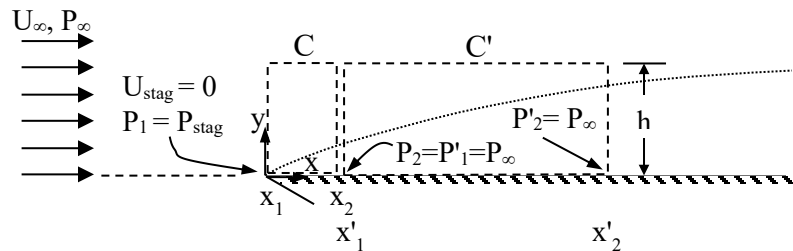


Figure 11.21 Illustration of two fixed regions encompassing the boundary layer (dotted line) created by a viscous fluid impinging on, and passing over, a stationary flat plate. Region C encompasses the leading edge of the plate; region C' encompasses a region following the leading edge region. Note that U_∞ and P_∞ are the free stream velocity and pressure.

Now, consider two different fixed regions above the plate, C and C', as shown in figure 11.21. Region C encompasses only the immediate leading edge region of the plate, whereas region C' encompasses a region that begins just after the leading edge region, and extends downstream. Using Eq. 11.85, we can assess the pressure and vorticity behavior within each of these respective regions, and the impact of pressure changes on the generation of vorticity.

For curve C, Eq. 11.85 gives,

$$\frac{P_\infty - P_{\text{stag}}}{\rho} = \underbrace{\int_0^h (u\omega_z)_{x=x_2} dy}_{\text{vorticity flux out}} - \underbrace{\int_0^h (u\omega_z)_{x=x_1} dy}_{\text{vorticity flux in}} \tag{11.86}$$

Here, we note that $\frac{P_\infty - P_{\text{stag}}}{\rho} = -\frac{U_\infty^2}{2}$ comes from applying the Bernoulli equation from the impinging free stream to the leading edge of the plate (see figure 11.21), which we surmise is a stagnation point. Since the flow undergoes little deformation prior to impacting the stagnation point, the use of the Bernoulli equation is a reasonable assumption. Additionally, since the flow will be uniform until the point of impingement, we surmise that no vorticity is transported into region C, or $\omega_z|_{x=x_1} = 0$. Thus, rewriting Eq. 11.86, we have:

$$\int_0^h (u\omega_z)_{x=x_2} dy = -\frac{U_\infty^2}{2} \tag{11.87}$$

Equation 11.87 implies that there is a flux of vorticity out of region C, so vorticity must have been generated at or in the vicinity of the leading edge of the plate.

Now, considering curve C', Eq. 11.85 yields:

$$\frac{P_\infty - P_\infty}{\rho} = \underbrace{\int_0^h (u\omega_z)_{x=x_2} dy}_{\text{vorticity flux out}} - \underbrace{\int_0^h (u\omega_z)_{x=x_1} dy}_{\text{vorticity flux in}} = 0 \tag{11.88}$$

In Eq. 11.88 we assume that the pressure at both x_1' and x_2' is P_∞ , since the streamlines along the plate will be essentially parallel, and the pressure of the outer region of uniform flow will be “impressed” across the thin boundary layer region (we confirm this at the end of section 13.2.1). Thus, rearranging Eq. 11.88, we have:

$$\underbrace{\int_0^h (u\omega_z)_{x=x_2} dy}_{\text{vorticity flux out}} = \underbrace{\int_0^h (u\omega_z)_{x=x_1} dy}_{\text{vorticity flux in}} \tag{11.89}$$

Equation 11.89 indicates that the vorticity flux into and out of C' are identical. Thus, the vorticity generated at the *leading edge of the plate* is the source of all the vorticity for a flat plate

flow (with a constant outer velocity, U_∞). Once the vorticity is generated at the leading edge, it will only redistribute laterally by viscous diffusion, as it is advected along the plate with the flow. Of course, if the external flow accelerates or decelerates due to geometry changes, this will result in pressure changes within the uniform flow external to the boundary layer. As we discussed in Chapter 9 on potential flows, these inviscid-like pressure changes within the outer flow will be impressed across the boundary layer, and reflected as changes in streamwise pressure along the plate surface. As shown in Section 11.5.3, the presence of such streamwise pressure changes along the surface will give rise to additional vorticity generation (negative or positive, depending on the change in surface pressure), and thus modification of the development of the viscous boundary layer.

In Chapter 13, we will examine how this additional vorticity is redistributed within a developing boundary layer, and how pressure gradients impact the development of boundary layers. As we will see, additional vorticity generation by changing surface pressure can either minimize boundary layer growth, or cause very rapid growth, depending on whether the pressure decreases or increases in the direction of flow.

11.7 Vorticity Transport Equations: Cartesian and Cylindrical Coordinates

11.7.1 General Vector Equation

$$\frac{D\vec{\omega}}{Dt} = \frac{\partial \vec{\omega}}{\partial t} + (\vec{V} \cdot \nabla) \vec{\omega} = (\vec{\omega} \cdot \nabla) \vec{V} + \nu \nabla^2 \vec{\omega}$$

11.7.2 Cartesian Equation Components (3-D in x,y)

x-direction:

$$\left(\frac{\partial \omega_x}{\partial t} + u \frac{\partial \omega_x}{\partial x} + v \frac{\partial \omega_x}{\partial y} + w \frac{\partial \omega_x}{\partial z} \right) = \left(\omega_x \frac{\partial u}{\partial x} + \omega_y \frac{\partial u}{\partial y} + \omega_z \frac{\partial u}{\partial z} \right) + \nu \left(\frac{\partial^2 \omega_x}{\partial x^2} + \frac{\partial^2 \omega_x}{\partial y^2} + \frac{\partial^2 \omega_x}{\partial z^2} \right)$$

y-direction:

$$\left(\frac{\partial \omega_y}{\partial t} + u \frac{\partial \omega_y}{\partial x} + v \frac{\partial \omega_y}{\partial y} + w \frac{\partial \omega_y}{\partial z} \right) = \left(\omega_x \frac{\partial v}{\partial x} + \omega_y \frac{\partial v}{\partial y} + \omega_z \frac{\partial v}{\partial z} \right) + \nu \left(\frac{\partial^2 \omega_y}{\partial x^2} + \frac{\partial^2 \omega_y}{\partial y^2} + \frac{\partial^2 \omega_y}{\partial z^2} \right)$$

z-direction:

$$\left(\frac{\partial \omega_z}{\partial t} + u \frac{\partial \omega_z}{\partial x} + v \frac{\partial \omega_z}{\partial y} + w \frac{\partial \omega_z}{\partial z} \right) = \left(\omega_x \frac{\partial w}{\partial x} + \omega_y \frac{\partial w}{\partial y} + \omega_z \frac{\partial w}{\partial z} \right) + \nu \left(\frac{\partial^2 \omega_z}{\partial x^2} + \frac{\partial^2 \omega_z}{\partial y^2} + \frac{\partial^2 \omega_z}{\partial z^2} \right)$$

11.7.3 Cartesian Equation (2-D)

$$\frac{\partial \omega_z}{\partial t} + u \frac{\partial \omega_z}{\partial x} + v \frac{\partial \omega_z}{\partial y} = \nu \left(\frac{\partial^2 \omega_z}{\partial x^2} + \frac{\partial^2 \omega_z}{\partial y^2} \right)$$

11.7.4 Cylindrical Equation Components (3-D)**r-direction:**

$$\begin{aligned} & \frac{\partial \omega_r}{\partial t} + v_r \frac{\partial \omega_r}{\partial r} + \frac{v_\theta}{r} \left[\frac{\partial \omega_r}{\partial \theta} - \omega_\theta \right] + v_z \frac{\partial \omega_r}{\partial z} \\ &= \omega_r \frac{\partial v_r}{\partial r} + \frac{\omega_\theta}{r} \left[\frac{\partial v_r}{\partial \theta} - v_\theta \right] + \omega_z \frac{\partial v_r}{\partial z} + \nu \left[\frac{\partial}{\partial r} \left(\frac{1}{r} \frac{\partial}{\partial r} (r \omega_r) \right) + \frac{1}{r^2} \frac{\partial^2 \omega_r}{\partial \theta^2} + \frac{\partial^2 \omega_r}{\partial z^2} - \frac{2}{r^2} \frac{\partial \omega_\theta}{\partial \theta} \right] \end{aligned}$$

 θ - direction:

$$\begin{aligned} & \frac{\partial \omega_\theta}{\partial t} + v_r \frac{\partial \omega_\theta}{\partial r} + \frac{v_\theta}{r} \left[\frac{\partial \omega_\theta}{\partial \theta} + \omega_r \right] + v_z \frac{\partial \omega_\theta}{\partial z} \\ &= \omega_r \frac{\partial v_\theta}{\partial r} + \frac{\omega_\theta}{r} \left[\frac{\partial v_\theta}{\partial \theta} + v_r \right] + \omega_z \frac{\partial v_\theta}{\partial z} + \nu \left[\frac{\partial}{\partial r} \left(\frac{1}{r} \frac{\partial}{\partial r} (r \omega_\theta) \right) + \frac{1}{r^2} \frac{\partial^2 \omega_\theta}{\partial \theta^2} + \frac{\partial^2 \omega_\theta}{\partial z^2} + \frac{2}{r^2} \frac{\partial \omega_r}{\partial \theta} \right] \end{aligned}$$

z- direction:

$$\begin{aligned} & \frac{\partial \omega_z}{\partial t} + v_r \frac{\partial \omega_z}{\partial r} + \frac{v_\theta}{r} \frac{\partial \omega_z}{\partial \theta} + v_z \frac{\partial \omega_z}{\partial z} \\ &= \omega_r \frac{\partial v_z}{\partial r} + \frac{\omega_\theta}{r} \frac{\partial v_z}{\partial \theta} + \omega_z \frac{\partial v_z}{\partial z} + \nu \left[\frac{1}{r} \frac{\partial}{\partial r} \left(r \frac{\partial \omega_z}{\partial r} \right) + \frac{1}{r^2} \frac{\partial^2 \omega_z}{\partial \theta^2} + \frac{\partial^2 \omega_z}{\partial z^2} \right] \end{aligned}$$

11.7.5 Cylindrical Equation (2-D in r, θ)

$$\frac{\partial \omega_z}{\partial t} + v_r \frac{\partial \omega_z}{\partial r} + \frac{v_\theta}{r} \frac{\partial \omega_z}{\partial \theta} = \nu \left[\frac{1}{r} \frac{\partial}{\partial r} \left(r \frac{\partial \omega_z}{\partial r} \right) + \frac{1}{r^2} \frac{\partial^2 \omega_z}{\partial \theta^2} \right]$$

Study Problems

- Starting with Eq. 11.2, derive Eq. 11.6, showing all the vector simplifications required in detail.
- An inviscid, three-dimensional flow is described by the velocity field:

$$\vec{V} = (5x - y)\hat{i} + (-3y + z)\hat{j} + (-2z + x)\hat{k}$$

Determine:

- If this is an incompressible flow
 - The vorticity field for this flow
 - The vortex stretching and tilting that is taking place, by calculating the value of $(\vec{\omega} \cdot \nabla)\vec{V}$.
 - Separate the $(\vec{\omega} \cdot \nabla)\vec{V}$ value of part b into the stretching components and the tilting components.
- An inviscid, three-dimensional flow is described by the velocity field:

$$\vec{V} = x^2\hat{i} + (-yx + z)\hat{j} + (y - zx)\hat{k}$$

Determine:

- If this is an incompressible flow
- The vorticity field for this flow
- The advection of vorticity
- The vortex stretching and tilting that is taking place, by calculating $(\vec{\omega} \cdot \nabla)\vec{V}$.
- Separate the $(\vec{\omega} \cdot \nabla)\vec{V}$ value of part b into the stretching components and the tilting components.

- In Chapter 9 the pressure and velocities were shown to be related by $P + \frac{1}{2}\rho V^2 = P_\infty + \frac{1}{2}\rho U^2$

for the inviscid, steady flow around a circular cylinder. If one only considers flow along the $\psi = 0$ streamline ($\theta = \pi$) approaching the cylinder ($y = 0, x < -R$), the pressure coefficient can be

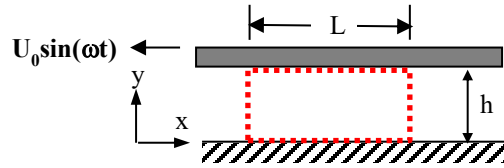
determined as: $C_p = \frac{P - P_\infty}{\frac{1}{2}\rho U^2} = \frac{2}{x^2} - \frac{1}{x^4}$, where $s = U$, and $R = 1$. Here, P is the local static

pressure, V the local velocity, and P_∞ and U are the static pressure and uniform velocity well upstream of the cylinder. If this was the pressure distribution for a flow of a real fluid adjacent to a flat plate, use Eq. 11.48 to determine the corresponding vorticity generation from the plate

as a function of x , and plot C_p and $\frac{\nu}{U^2} \frac{\partial \omega_z}{\partial y} \Big|_{y=0}$ vs. x from $x = -6$ to $x = -1$ on the same graph.

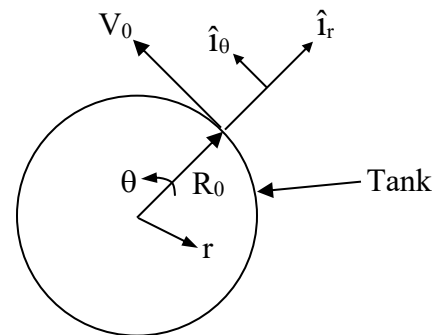
What does the graph tell you about pressure changes and vorticity generation?

5. Two parallel flat plates spaced a distance h apart contain a fluid of kinematic viscosity ν . The lower plate is fixed, and the upper plate oscillates back and forth with a velocity given by $U = U_0 \sin(\omega t)$.



- Determine the vorticity generation at both the lower plate, $y = 0$, and the upper plate, $y = h$ in terms of U_0 , ν , ω , and t . Explain what happens to the generated vorticity as the upper plate oscillates back and forth.
 - Determine the circulation for a fixed box surrounding the fluid (shown by the dotted red lines) within the two parallel plates which is L length and h in height in terms of U_0 , ω , L and t . Explain what is happening to the circulation, and why the distance between the plates does not enter into the calculation.
 - What happens to the vorticity generation and the circulation when the upper plate stops oscillating, and is fixed?
6. In Chapter 9 the surface pressure on a cylinder for an inviscid, steady flow approaching a circular cylinder was shown to be $P = P_\infty + \frac{1}{2} \rho U^2 (1 - 4 \sin^2 \theta)$. Here, P is the local static pressure, and P_∞ and U are the static pressure and uniform velocity well upstream of the cylinder. If this was the pressure distribution for a real fluid, use Eq. 11.49 to determine the corresponding vorticity generation on the cylinder as a function of θ , and plot $\frac{\partial \omega_z}{\partial r} \Big|_{r=R}$ vs. θ from $\theta = 0$ to $\theta = \pi$.

7. A circular tank filled with water rotates on its axis such that the *water in the tank is in steady state rotation*; the wall of the tank, of radius R_0 , moves with a tangential velocity of V_0 (see figure).



Do the following:

- Write an expression (do not derive) for the velocity profile of the water within the tank, $v_\theta(r)$, for the *steady state conditions*;

At $t = t_0$, the rotation of the tank is abruptly stopped. Assume that the tank is deep enough such that the flow behaves two-dimensionally (r, θ dimensions). Do the following:

- When the tank is stopped, indicate: (1) where vorticity is generated and (2) what causes the vorticity generation.
- State the steady-state solution for the velocity, $v_\theta(r)$, in the tank when $t \rightarrow \infty$
- Determine the total amount of vorticity (i.e. "new" circulation) that is generated for $t > t_0$.

8. In section 11.4.3, we considered the 2-D flow outside a circular rod of radius R , rotating at a constant angular velocity Ω in a fluid of infinite extent with kinematic viscosity ν and density ρ . The solution for the *steady-state velocity field* in the fluid external to the rod using the vorticity equation was:

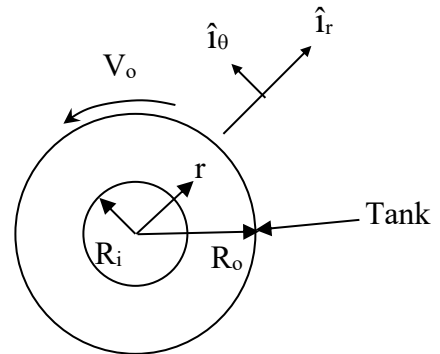
$$v_\theta = \frac{\Omega R^2}{r}.$$

- Determine the vorticity for $r > R$ and *provide a brief physical explanation of what this result implies* in one or two sentences.
- Determine the circulation for $r = 2R$ and $r = \infty$. Again, *provide a physical explanation of what this result implies* in one or two sentences.
- If I suddenly *stop* the rod rotating, assuming a viscous and laminar 2-D flow, which of the terms in the vorticity vector equation shown below would be relevant to the solution of the subsequent unsteady flow behavior? Indicate the terms that would be non-zero by indicating the identifying number in the general equation below.

$$\underbrace{\frac{\partial \vec{\omega}}{\partial t}}_1 + \underbrace{(\vec{V} \cdot \nabla) \vec{\omega}}_2 = \underbrace{(\vec{\omega} \cdot \nabla) \vec{V}}_3 + \underbrace{\nu \nabla^2 \vec{\omega}}_4$$

- Briefly explain why the terms you *did not select* are not relevant.
- After the rod rotation is stopped, is there any vorticity in the fluid? If so, where does it come from? How much is generated?

9. A circular tank of water of radius R_o rotates such that the velocity is V_o at R_o . A stationary rod of radius R_i , located at the center of the tank.(see figure below). Assume the rod and tank are infinite in the z -direction so the flow in the annulus between the rod and the tank wall is two-dimensional.



Do the following:

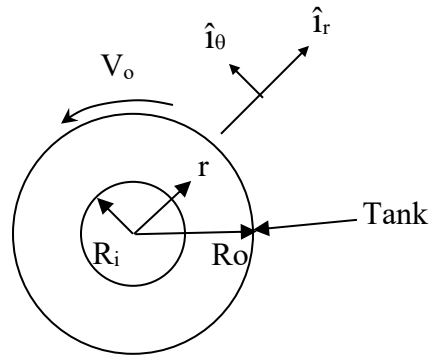
- Simplify the 2-D vorticity transport equation to allow you to calculate the vorticity distribution in the water, if the flow is at steady state conditions. Indicate the terms that can be neglected in the equation, and list the reasons that they are assumed/can be shown to be negligible.
- For one boundary condition, let the vorticity at $r = R_i$ be $\omega_z = \omega_o$. A second boundary condition is $\frac{d\omega_z}{dr} = 0$ at $r = R_o$. Explain how this second boundary condition arises.
- Using the vorticity boundary conditions in (b), solve the simplified equation from (a) to determine an expression for $\omega(r)$.

10. At a given instant of time, the vorticity, $\omega_z = \frac{\partial v}{\partial x} - \frac{\partial u}{\partial y}$, for a two-dimensional, inviscid ($\mu=0$), constant density flow field is specified at each point in the field ($\omega_z \neq 0$).

Do the following:

- Using appropriate simplifications of the vorticity transport equation, give an argument that shows that if the particle path lines are known (i.e. the velocity field, $\vec{V}(x, y, t)$, is known), one could determine ω_z for each point in the flow field at a later time.
- Show that for this flow field an equation, $\frac{\partial^2 \psi}{\partial x^2} + \frac{\partial^2 \psi}{\partial y^2} = -\omega_z$ can be developed for the stream function, ψ .
- The circulation within a marked circle of fluid in the flow field is Γ_0 at time $t = 0$. If the marked fluid moves within the flow field, such that at a later time $t = 1$ the circulation within the marked fluid is Γ_1 . What is the relationship between Γ_0 and Γ_1 and why?

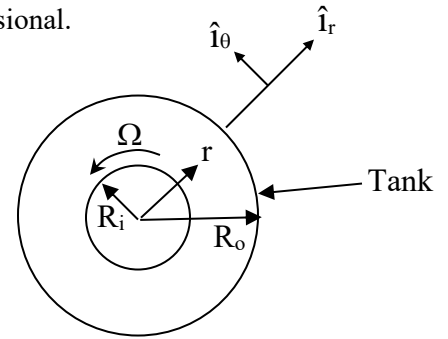
11. A circular tank of water of radius R_o rotates such that for $t < t_o$ the velocity is V_o at R_o . A stationary rod of radius R_i , located at the center of the tank. (see figure below). Assume the rod and tank are infinite in the z -direction so the flow in the annulus between the rod and the tank wall is two-dimensional. One can show (see problem 10), that at steady state, the vorticity within the annulus is $\omega_z = \omega_o = \text{constant}$.



At $t = t_o$, the rotation of the tank is abruptly stopped ($V_o = 0$ for $t > t_o$). Assume that the flow behaves two-dimensionally (r, θ dimensions). Do the following:

- Simplify, using appropriate assumptions, the 2-D vorticity transport equation to yield an equation that could be solved for the vorticity and velocity field inside the tank for $t > 0$ (**DO NOT ATTEMPT TO SOLVE THIS EQUATION!**).
- Determine the total circulation within the tank (inside $r = R_o$) for both $t < t_o$ and $t > t_o$. Briefly explain your result for both cases.
- Using your result for $t < t_o$ from part b) of this problem, determine the value of ω_o in terms of V_o, R_i , and R_o .

12. A circular rod of radius R_i rotates at an *angular* velocity, Ω , inside of a *stationary* tank of water of radius R_o (see figure below). Assume the rod and tank are infinite in the z -direction so the flow in the annulus between the rod and the tank wall is two-dimensional.



Do the following:

- a) Simplify the two-dimensional vorticity transport equation to allow you to calculate the vorticity distribution in the water, if the flow is at steady state conditions. Indicate the terms that can be neglected in the equation, and list the reasons that they are assumed/can be shown to be negligible
- b) For one boundary condition, let the vorticity at

$$r = (R_i + R_o)/2 \text{ be } \omega_z = \omega_o. \text{ A second boundary condition is } \frac{d\omega_z}{dr} = 0 \text{ at either } r = R_i \text{ or } R_o.$$

Explain how we get this second boundary condition from the concept of vorticity generation.

- c) Using the vorticity boundary conditions from b), solve the simplified equation from a) to determine an expression for $\omega(r)$.

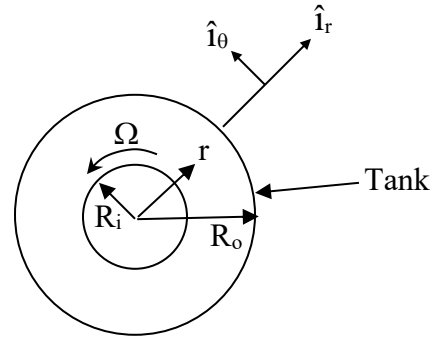
13. A circular rod of radius R_i rotates in steady state at an *angular* velocity, Ω , inside of a *stationary* tank of water of radius R_o (see figure below). Assume the rod and tank are infinite in the z -direction so the flow in the annulus between the rod and the tank wall is two-dimensional. One can show (see problem 12), that at steady state, the vorticity within the annulus is $\omega_z = \omega_o = \text{constant}$.

At $t = t_o$, the rotation of the rod is abruptly stopped. Assume that the flow behaves two-dimensionally (r, θ dimensions).

Do the following:

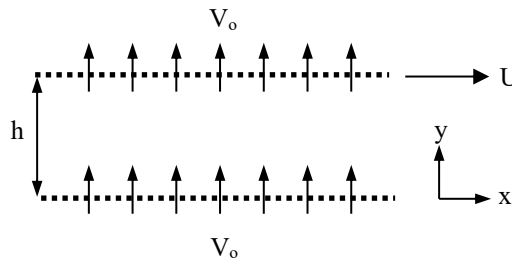
- a) Simplify, using appropriate assumptions, the 2-D vorticity transport equation to yield an equation that could be solved for the *vorticity and velocity field inside the tank for $t > t_o$* (DO NOT ATTEMPT TO SOLVE THIS EQUATION!).
- b) Determine the total circulation within the tank (inside $r = R_o$) for *both* $t < t_o$ and $t > t_o$. Briefly explain your result for both cases.
- c) Using the steady state result for your part (b) circulation, when $t < t_o$, and that $\omega_z = \omega_o = \text{constant}$, determine the value of ω_o in terms of Ω, R_i , and R_o .

14. A circular rod of radius R_i rotates at an *angular* velocity, Ω , inside of a *stationary* tank of water of radius R_o (see figure below). Assume the rod and tank are infinite in the z -direction so the flow in the annulus between the rod and the tank wall is two-dimensional.



Do the following:

- Simplify the two-dimensional vorticity transport equation to allow you to calculate the vorticity and velocity distributions in the water, if the flow is at steady state conditions. Indicate the terms that can be neglected in the equation, and list the reasons that they are assumed/can be shown to be negligible
 - Specify the necessary boundary conditions, for both ω_z and v_θ to allow you to solve this equation (you must specify at least one condition for the vorticity);
 - Solve the O.D.E. to obtain $\omega_z(r)$ and $v_\theta(r)$ in terms of Ω , r , R_i and R_o ;
 - Determine the vorticity, and circulation for $r = R_i$ and $r = R_o$. Provide a physical explanation for these results in one or two sentences.
15. In Chapter 6, problem 6.16 considers the flow of a viscous fluid (viscosity = μ , density = ρ) similar to a Couette flow between two infinite, parallel, **porous** plates; fluid of the same properties is uniformly injected through the *fixed*, lower plate, and fluid is uniformly suctioned out through an upper plate, which *moves* at a velocity U , as shown below.



Here, $u = 0$, $v = V_o = \text{const.}$ at $y = 0$, and $u = U = \text{constant}$, and $v = V_o$ at $y = h$, with no flow in the z -direction. The velocity profile, $u(y)$, for the fully-developed flow between the plates is given by:

$$u = \frac{U \left(e^{\frac{V_o}{\nu} y} - 1 \right)}{\left(e^{\frac{V_o h}{\nu}} - 1 \right)} = \frac{U \left(e^{\text{Re}_{V_o} \left(\frac{y}{h} \right)} - 1 \right)}{\left(e^{\text{Re}_{V_o}} - 1 \right)}$$

Note that by the continuity equation, $v = V_o = \text{constant}$ across the channel, and $\text{Re}_{V_o} = \frac{V_o h}{\nu}$.

(a) Make a plot of the non-dimensional velocity profile for this flow, $\frac{u}{U}$ vs. $\frac{y}{h}$, for

$$\frac{V_0 h}{\nu} = \mathbf{Re}_{V_0} = 0, 1, \text{ and } 3, \text{ all on one graph.}$$

(b) Determine the non-dimensional vorticity for this flow, $\frac{\omega_z h}{U}$. Then Plot $\frac{\omega_z h}{U}$ vs. $\frac{y}{h}$ for

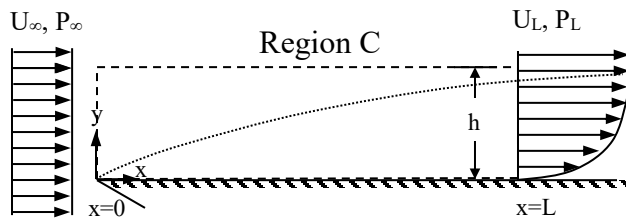
$$\frac{V_0 h}{\nu} = \mathbf{Re}_{V_0} = 0, 1, \text{ and } 3, \text{ all on one graph.}$$

(c) Calculate the non-dimensional vorticity generation at both $y = 0$ and $y = h$. Calculate both

$$\left(\frac{h^2}{U} \right) \frac{\partial \omega_z}{\partial y} \Big|_{y=0} \text{ and } \left(\frac{h^2}{U} \right) \frac{\partial \omega_z}{\partial y} \Big|_{y=h} \text{ for } \frac{V_0 h}{\nu} = \mathbf{Re}_{V_0} = 0, 1, \text{ and } 3$$

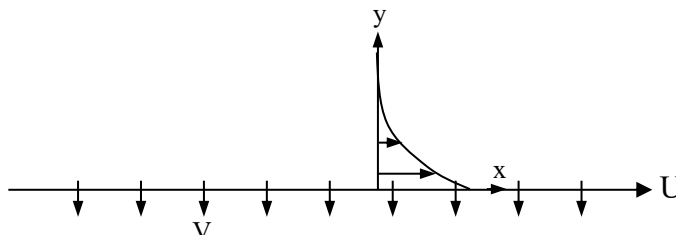
(d) Comment on what your results of part (c) show about the vorticity generation.

16. A uniform viscous flow approaches a flat plate at uniform velocity, U_∞ . After encountering the leading edge of the plate, the main outer flow velocity accelerates according to $U = U_\infty \left(1 + \frac{x}{L} \right)$, where U_∞ is the velocity approaching the plate, and P_∞ is the pressure of the approaching flow. If the flow has no vorticity, and no vorticity is transported in the flow before it encounters the plate at $x = 0$, determine the vorticity transport across the plane at $x = L$. Assume a stagnation point at the leading edge of the plate.



Since this is a steady flow,
 $\frac{\partial \Gamma}{\partial t} = 0$ for region C

17. An infinite porous flat plate translates in the x -direction at a constant velocity U beneath a quiescent fluid of kinematic viscosity ν . The fluid covers the upper surface of the plate, and is of infinite depth. Fluid is suctioned uniformly through the plate at a velocity V , as shown. If the flow is steady and fully developed, starting from the vorticity transport equation (in 2-D) determine an expression for the velocity $u(y)$ and vorticity $\omega(y)$ in terms of U , V , ν , and y . Also, determine the shear stress at the surface in terms of U , V , and ρ , the fluid density. If $V = 0$, what would the steady state velocity profile $u(y)$ become?



18. Consider the 2-D flow outside a rotating circular cylinder, at the surface of which there is an inward radial velocity, V , at the cylinder surface ($r = R$) due to suction through the wall of the cylinder. Again, assume that the cylinder is in a fluid of infinite extent with kinematic viscosity ν and density ρ ; the cylinder is of radius R and rotates at a constant angular velocity Ω . Determine the solution for the *steady-state velocity field* in the fluid external to the cylinder using the vorticity transport equation for your solution:

$$\frac{\partial \vec{\omega}}{\partial t} + (\vec{V} \cdot \nabla) \vec{\omega} = (\vec{\omega} \cdot \nabla) \vec{V} + \nu \nabla^2 \vec{\omega}$$

Let one boundary condition be $v_\theta = 0$ at $r \rightarrow \infty$; consider the other boundary conditions carefully, and perform your solution as follows:

- Simplify the vorticity transport equation to an ordinary differential equation for ω_z using the continuity equation to assist the simplification (i.e. find v_r first).
- Consider the appropriate boundary conditions for vorticity and solve the resulting O.D.E. to for $\omega = \omega(r, R, k, \text{ and } A)$, where $k = VR/\nu$ and A is an unknown constant.
- Using the results of b) solve for $v_\theta = v_\theta(r, R, k, \Omega)$, apply appropriate boundary conditions, and show that a solution exists over the flow field only if $k = VR/\nu > 2$.
- Determine the circulation, $\Gamma = \Gamma(r)$, and note its limit at $k = 2$; recalculate the value for vorticity, with A known from part c).
- If $\Omega = 2$ and $R = 1$ (both dimensionless), plot ω_z , v_θ , and Γ for $1 < r < 10$, for $k = 3$ and $k = 6$, and for the no suction case, $V = 0$, which is the solution determined in section 11.4.3. Plot separate graphs of ω_z , v_θ , and Γ , with the three curves for $k = 3$, 6 , and no suction on each plot. Interpret the results of these plots.
- Extra credit: Explain why there is the limiting behavior indicated in part c) and d), and see if you can determine what the limit of $k = 2$ implies physically.

Chapter 12

More Complicated Navier-Stokes Solutions

Contents

12.1 Fully-Developed Flow in a Rectangular Duct	388
12.2 A Suddenly Accelerated, Infinite Plate	391
12.3 Viscous Decay of a Two-Dimensional Vortex	395
12.3.1 Decay of a Line Vortex (Oseen-Lamb Vortex)	395
12.3.2 The Taylor Dissipating Eddy	401
12.4 Ekman Drift: A Wind Driven Flow	403
12.5 A Laminar Jet Issuing from a Narrow Slot	411

In Chapter 6 we examined solutions of the Navier-Stokes equation where the equation was reduced to only one dependent velocity variable and one independent spatial variable [e.g. $u = u(y)$]. These solutions were all fully-developed flows within parallel constraining boundaries of either planar or radial symmetry. In all cases, the Navier-Stokes equation reduced to an ordinary differential equation of a boundary value type.

In this chapter, we consider several flows where the velocity field is a function of more than one space parameter, or one space parameter and time. In some cases, such as fully-developed flow in a rectangular channel, the result is a [Poisson-type equation](#), which is a [boundary value problem](#) for one velocity component as a function of two spatial variables [e.g. $u = u(y,z)$].

Other types of problems are [initial value problems](#), which are unconstrained in one or more dimension. These types of problems can involve one dependent velocity variable, one independent spatial variable, and time, such as the response of a bounding fluid to the temporal motion of a boundary in one dimension [e.g. $u = u(y,t)$]. These problems can also involve the development of an unconstrained flow in two dimensions, such that $u = u(x,y)$ and $v = v(x,y)$.

All of these problems require the solution of partial differential equations. The Poisson type of equation has fairly standard solutions, which make the determination of the result relatively straight forward. The unbounded initial value problems require some creativity to develop analytical solutions. One approach that often proves very effective in solution of such problems is the use of a [similarity solution](#). Similarity solutions generally require that a flow be unconstrained by only one boundary, and that a variable can be determined that collectively collapses the two independent variables into one independent variable. Another technique that is

employed for solution of flows in which both u and v vary, is the use of the stream function to reduce the Navier-Stokes equations to one independent variable, ψ , with the penalty of increasing the order of the equation by one. In this chapter, we will explore the use of all these approaches, which will prepare us for an examination of boundary layers flows in Chapter 13.

12.1 Fully-Developed Flow in a Rectangular Duct

Consider the fully developed, steady flow within a rectangular cross-section duct, as shown in figure 12.1

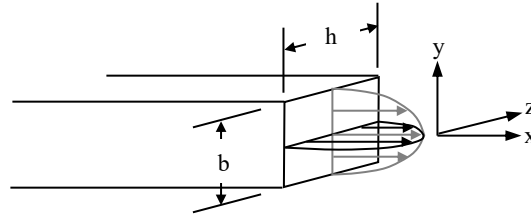


Figure 12.1 Fully-developed flow in a rectangular duct.

This is a Poiseuille type flow (Section 6.3.2) with two sets of constraining surfaces. Here we select a Cartesian coordinate system with its origin on the symmetry axis of the duct. We again invoke the assumptions of:

1. Steady flow
2. Fully developed flow; no variations in x -direction
3. $\rho = \text{constant}$
4. Neglect body forces

Since the flow is assumed incompressible, the incompressible continuity equation in three dimensions is:

$$\frac{\partial u}{\partial x} + \frac{\partial v}{\partial y} + \frac{\partial w}{\partial z} = 0 \quad (12.1)$$

If the flow is fully developed, this means that u does not change with x , thus $\frac{\partial u}{\partial x} = 0$, and Eq.

12.1 becomes:

$$\frac{\partial v}{\partial y} + \frac{\partial w}{\partial z} = 0 \quad (12.2)$$

Rearranging, Eq. 12.2, and integrating from $y = -b/2$ to $y = +b/2$, we have:

$$v_{+b/2} - v_{-b/2} = \int_{y=-b/2}^{y=+b/2} \frac{\partial v}{\partial y} dy = - \int_{y=-b/2}^{y=+b/2} \frac{\partial w}{\partial z} dy \quad (12.3)$$

Now, since $v = 0$ at $y = -b/2$ and $+b/2$ (since both limits are solid boundaries), then Eq. 12.3 becomes:

$$\int_{y=-b/2}^{y=+b/2} \frac{\partial w}{\partial z} dy = 0 \tag{12.4}$$

If we assume that $\frac{\partial w}{\partial z} = f(z, y)$, then:

$$\int_{y=-b/2}^{y=+b/2} \frac{\partial w}{\partial z} dy = g(z, y)|_{y=+b/2} - g(z, y)|_{y=-b/2} = 0$$

or

$$g(z, y)|_{y=+b/2} = g(z, y)|_{y=-b/2} \tag{12.5}$$

Since the limits on y are arbitrary, $g(z, y) = 0$ is the only solution that consistently satisfies Eq.12.5, which in turn means that $\frac{\partial w}{\partial z} = 0$ is the only value that will also consistently satisfy Eq.

12.4. Consequently, from Eq. 12.1, we have $\frac{\partial v}{\partial y} = \frac{\partial w}{\partial z} = 0$, or both v and w are constants. Since v and w are both zero at solid boundaries, we conclude that:

$$v = 0, w = 0 \text{ everywhere.} \tag{12.6}$$

Additionally, it follows that all derivatives of v and w are also zero everywhere.

$$\frac{\partial u}{\partial t} + u \frac{\partial u}{\partial x} + v \frac{\partial u}{\partial y} + w \frac{\partial u}{\partial z} = \beta_x - \frac{1}{\rho} \frac{\partial P}{\partial x} + \nu \left[\frac{\partial^2 u}{\partial x^2} + \frac{\partial^2 u}{\partial y^2} + \frac{\partial^2 u}{\partial z^2} \right] \quad \text{x-direction} \tag{12.7a}$$

$$\frac{\partial v}{\partial t} + u \frac{\partial v}{\partial x} + v \frac{\partial v}{\partial y} + w \frac{\partial v}{\partial z} = \beta_y - \frac{1}{\rho} \frac{\partial P}{\partial y} + \nu \left[\frac{\partial^2 v}{\partial x^2} + \frac{\partial^2 v}{\partial y^2} + \frac{\partial^2 v}{\partial z^2} \right] \quad \text{y-direction} \tag{12.7b}$$

$$\frac{\partial w}{\partial t} + u \frac{\partial w}{\partial x} + v \frac{\partial w}{\partial y} + w \frac{\partial w}{\partial z} = \beta_z - \frac{1}{\rho} \frac{\partial P}{\partial z} + \nu \left[\frac{\partial^2 w}{\partial x^2} + \frac{\partial^2 w}{\partial y^2} + \frac{\partial^2 w}{\partial z^2} \right] \quad \text{z-direction} \tag{12.7c}$$

Thus, Eqs. 12.7 reduce to:

$$-\frac{1}{\rho} \frac{\partial P}{\partial x} + \nu \left(\frac{\partial^2 u}{\partial y^2} + \frac{\partial^2 u}{\partial z^2} \right) = 0 \tag{12.8a}$$

$$\frac{\partial P}{\partial y} = 0 \quad (12.8b)$$

$$\frac{\partial P}{\partial z} = 0 \quad (12.8c)$$

To assess the character of $\frac{\partial P}{\partial x}$, we again establish this functionality like we did in Section 6.3.2 by taking the derivative of the x-direction differential equation, Eq. 12.8a, with respect to x, which yields:

$$\frac{\partial}{\partial x} \left(\frac{\partial^2 u}{\partial y^2} + \frac{\partial^2 u}{\partial z^2} \right) = \frac{\partial}{\partial x} \left(\frac{1}{\mu} \frac{\partial P}{\partial x} \right) = 0 \quad (12.9)$$

since u and its derivatives must be a function of y and z only (for a fully-developed flow).

Equation 12.9 again indicates that $\frac{\partial P}{\partial x}$ must be a constant, and $P=P(x)$ only. This is reasonable, since the shear stress will be a function of the derivative of the velocity profile, which will also be invariant with streamwise position. So, noting that $u = f(y, z)$ only, the x-direction differential equation, with appropriate boundary conditions simplifies to:

$$-\frac{dP}{dx} + \mu \frac{\partial^2 u}{\partial y^2} + \mu \frac{\partial^2 u}{\partial z^2} = 0$$

or

$$\underbrace{\frac{\partial^2 u}{\partial y^2} + \frac{\partial^2 u}{\partial z^2}}_{\text{Poisson type equation}} = \frac{1}{\mu} \frac{dP}{dx} = \text{constant} \quad (12.10)$$

The corresponding boundary conditions are:

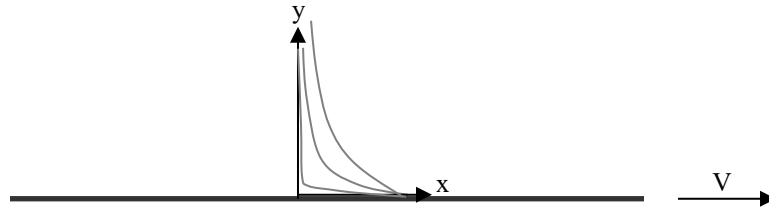
$$u = 0, \quad y = \pm \frac{b}{2}$$

$$u = 0, \quad z = \pm \frac{h}{2}$$

Note that Eq. 12.10 and the corresponding boundary conditions result in a fairly standard solution via conventional analytical solution techniques, which are available in most graduate mathematics texts on partial differential equations. To see solutions for Eq.12.10, and for a number of other common duct geometries, see [White \(1991\)](#).

12.2 A Suddenly Accelerated, Infinite Plate

This example deals with a situation where an infinite plate is instantaneously accelerated from $u = 0$ to $u = V$. This is generally known as [Stoke's first problem](#). We determine how the velocity adjacent to the plate develops as a function of time. For this situation, there is no vertical (v) velocity. Vorticity is generated instantaneously at the surface, which subsequently diffuses outward (y -direction) due to the fluid viscosity.



For this flow, the Navier-Stokes equation simplifies to:

$$\frac{\partial u}{\partial t} = \nu \frac{\partial^2 u}{\partial y^2} = \nu \frac{\partial \omega_z}{\partial y} \quad \leftarrow \text{vorticity "flux"} \quad (12.11)$$

Thus, only the local x -direction acceleration and shear forces are non-zero. Similar to a Couette flow, we can show that the pressure gradient for this flow is zero in both the x and y directions, since the plate is assumed to be infinite in x .

The appropriate initial and boundary conditions for the flow are:

$$\begin{aligned} \text{Initial condition:} \quad & u(y, t = 0) = 0 && \text{(fluid is initially quiescent)} \\ \text{Boundary conditions:} \quad & u(y = 0, t > 0) = V && \text{(plate has velocity } V \text{ after } t = 0) \\ & u(y \rightarrow \infty, t \geq 0) = 0 && \text{(fluid velocity remains quiescent far} \\ & && \text{from the plate, for all times } t > 0) \end{aligned}$$

To solve this type of equation, we employ what is termed a “similarity” solution. For this solution process, we assume that the velocity profile will expand in the y direction due to the viscous diffusion processes, and will scale on some yet to be determined universal parameter that is a function of y and t . The approach is to introduce a similarity variable that reduces the governing equation from a partial differential equation (P.D.E.) to an ordinary differential equation (O.D.E.). What we are assuming when we introduce a similarity variable is that the shape of the velocity profiles will be of the same “shape” as time progresses. It is as if we “stretch” the velocity profile in the direction normal to the plate (y) with increasing time. This approach is generally effective for flows that are unbounded, and thus have no characteristic length (unlike pipe or channel flow geometries, which have a characteristic diameter or width).

For the present solution approach, we assume a velocity form of $\frac{u}{V} = f(\eta)$, where the non-dimensional velocity is assumed to retain the same “shape” when scaled on η . Here, η is a similarity parameter, which we assume to be dependent on y and t , of the form:

$$\eta = Ay^n t^m \quad \text{where } A, n, \text{ and } m \text{ are all constants.} \quad (12.12)$$

The procedure is to substitute $f(\eta)$ and η into the original P.D.E., simplify the resulting equation, and by observation determine the appropriate values of n , m , and A that will reduce the P.D.E. of Eq. 12.11 to an O.D.E. (ordinary differential equation) in terms of f and η . Thus, we first determine the u derivative terms of Eq. 12.11 in terms of η using the chain rule, and designating

$$\frac{df}{d\eta} = f' \text{ and } \frac{d^2f}{d\eta^2} = f'' :$$

Term 1:

$$\frac{1}{V} \frac{\partial u}{\partial t} = \frac{\partial f(\eta)}{\partial t} = \frac{df}{d\eta} \frac{\partial \eta}{\partial t} = f' \frac{\partial \eta}{\partial t} = f' Ay^n m t^{m-1} = \underbrace{f'(Ay^n t^m)}_{\eta} \frac{m}{t} = f' \eta \frac{m}{t} \quad (12.13a)$$

Term 2:

$$\begin{aligned} \frac{1}{V} \frac{\partial u}{\partial y} &= \frac{\partial f(\eta)}{\partial y} = \frac{df}{d\eta} \frac{\partial \eta}{\partial y} = f' \frac{\partial \eta}{\partial y} = f' A n y^{n-1} t^m = \underbrace{f'(Ay^n t^m)}_{\eta} \frac{n}{y} = f' \eta \frac{n}{y} \\ \frac{1}{V} \frac{\partial^2 u}{\partial y^2} &= \frac{\partial^2 f(\eta)}{\partial y^2} = \frac{\partial}{\partial y} \left(f' \frac{\partial \eta}{\partial y} \right) = \left(f'' \frac{\partial \eta}{\partial y} \right) \frac{\partial \eta}{\partial y} + f' \frac{\partial}{\partial y} \left(\frac{\partial \eta}{\partial y} \right) = f'' \left(\frac{\partial \eta}{\partial y} \right)^2 + f' \frac{\partial^2 \eta}{\partial y^2} \\ &= f'' (A n y^{n-1} t^m)^2 + f' (A n (n-1) y^{n-2} t^m) \\ &= f'' \underbrace{(Ay^n t^m)^2}_{\eta^2} \frac{n^2}{y^2} + f' \underbrace{(Ay^n t^m)}_{\eta} \frac{n(n-1)}{y^2} = f'' \eta^2 \frac{n^2}{y^2} + f' \eta \frac{n(n-1)}{y^2} \end{aligned} \quad (12.13b)$$

Substituting Eqs. 12.13 into Eq. 12.11 gives:

$$f' \eta \frac{m}{t} = \nu f'' \eta^2 \frac{n^2}{y^2} + \nu f' \eta \frac{n(n-1)}{y^2} \quad \text{0 if } n=1$$

To simplify, we factor out η terms, and set $n = 1$, which eliminates one of the terms in the equation, giving:

$$f' \frac{m}{t} = \nu f'' \eta \frac{1}{y^2}$$

Rearranging gives:

$$f'' - f' \frac{my^2}{v\eta t} = 0 \tag{12.14}$$

We note that $f'' + 2\eta f' = 0$ is a tractable equation, so we work toward that form by letting:

$$2\eta = -\frac{my^2}{v\eta t} \Rightarrow \eta^2 = -\frac{my^2}{2vt} \Rightarrow \eta = \left(-\frac{my^2}{2vt}\right)^{\frac{1}{2}} = \left(-\frac{m}{2v}\right)^{\frac{1}{2}} yt^{-\frac{1}{2}}$$

Setting this relationship equal to our original assumption for the form of η from Eq. 12.12, we have:

$$\eta = Ay^n t^m = \left(-\frac{m}{2v}\right)^{\frac{1}{2}} yt^{-\frac{1}{2}} \tag{12.15}$$

By equating the constants on the left hand and right-hand sides of Eq. 12.15, we have:

$$n = 1 \text{ (from previous assumption), } m = -\frac{1}{2}, \text{ which makes } A = \left(\frac{1}{4v}\right)^{\frac{1}{2}} = \frac{1}{2\sqrt{v}}$$

So, for this case, $n = 1$, $m = -\frac{1}{2}$, and $A = \frac{1}{2\sqrt{v}} \Rightarrow \eta = \frac{y}{2\sqrt{vt}}$


Substituting these constant values into Eq. 12.12, reduces Eq. 12.14 to:

$$f'' + 2\eta f' = 0 \tag{12.16}$$

Equation 12.16 is an O.D.E. for f as a function of the similarity (stretching) parameter,

$$\eta = \frac{y}{2\sqrt{vt}}$$

For this similarity parameter, the initial and boundary conditions become:

Initial condition:	$u(y, t = 0) = 0 \Rightarrow f(\eta \rightarrow \infty) = 0$	 <p>Note that these conditions are identical, and thus represent <u>one</u> limiting condition</p>
Boundary conditions:	$u(y = 0, t > 0) = V \Rightarrow f(\eta = 0) = 1$	
	$u(y \rightarrow \infty, t \geq 0) = 0 \Rightarrow f(\eta \rightarrow \infty) = 0$	

$\tag{12.17}$

Thus, we have not only reduced the differential equation from a P.D.E. to an O.D.E., but we have reduced the limiting conditions from *three* to *two* as well (which we must, if we are to achieve a solution, since Eq. 12.16 is second order, only requiring two boundary conditions).

To solve Eq. 12.16, we let $\alpha = f'$ and substitute into Eq. 12.16, such that:

$$\alpha' = \frac{d\alpha}{d\eta} = -2\eta\alpha$$

Separating variables and integrating gives:

$$\ln \alpha = -\eta^2 + C = -\eta^2 + \ln C_1$$

$$\alpha = f' = \frac{df}{d\eta} = C_1 \exp(-\eta^2)$$

Integrating f' gives: $f = C_1 \int_0^\eta \exp(-\eta^2) d\eta + C_2 = C_1 \frac{\sqrt{\pi}}{2} \operatorname{erf}(\eta) + C_2$

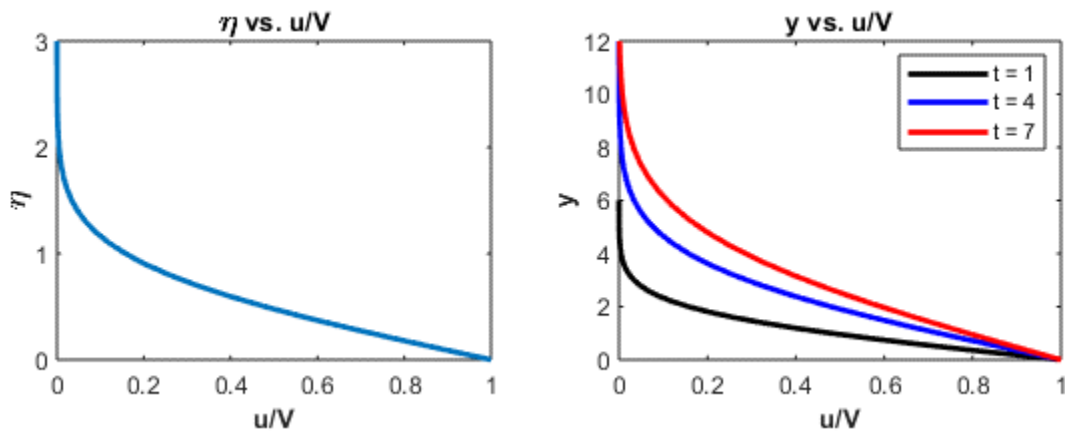


Figure 12.2 Velocity profiles for a suddenly accelerated plate using both similarity scaling and physical scaling (non-dimensional y and t , with $\nu = 1$)

The $\operatorname{erf}(\eta)$ is a tabulated function known as the [error function](#). Since this integral has no analytical solution, the function is solved numerically, and tabulated values of the function are available in most standard books of mathematical functions or from the [Wolfram Alpha](#) website. Applying the two limiting conditions from Eq. 12.17, we have:

$$f(0) = 1 = C_1 \frac{\sqrt{\pi}}{2} \overset{=0}{\operatorname{erf}(0)} + C_2 \Rightarrow C_2 = 1$$

$$f(\infty) = 0 = C_1 \frac{\sqrt{\pi}}{2} \overset{=1}{\operatorname{erf}(\infty)} + 1 \Rightarrow C_1 = -\frac{2}{\sqrt{\pi}}$$

This gives a final solution for $\frac{u}{V} = f(\eta)$, and thus $\frac{u}{V}(y, t)$, of:

$$f(\eta) = 1 - \operatorname{erf}(\eta) \quad \frac{u}{V} = 1 - \operatorname{erf}\left(\frac{y}{2\sqrt{\nu t}}\right) \quad (12.18)$$

Figure 12.2 shows plots of u/V as a function of both η , and y and t . Note how the use of η , the similarity variable, collapses the velocity profile to only one curve.

Also, note that the velocity profiles plotted with respect to y migrate outward with time, but are “similar” in shape. Thus, as time increases, the profiles are “stretched” in the y direction as the vorticity originally generated by the accelerated surface gradually diffuses outward.

12.3 Viscous Decay of a Two-Dimensional Vortex

12.3.1 Decay of a Line Vortex (Oseen-Lamb Vortex)

The velocity of an inviscid line vortex, as shown in Section 9.7.3, is described in cylindrical coordinates by the equation $v_r = 0$, $v_\theta = \frac{\Gamma}{2\pi r}$, where Γ is the total circulation, or strength, of the vortex. The shape of this velocity profile is shown in figure 12.3.

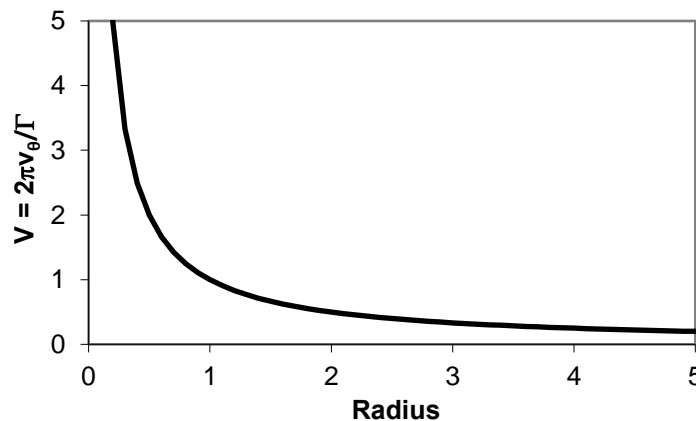


Figure 12.3 This graph shows the initial shape of an inviscid line vortex velocity profile (letting Velocity = $2\pi v_\theta / \Gamma$) as a function of radius.

Recall that this type of vortex is irrotational, except for a spike of vorticity at the origin, where the azimuthal velocity is infinite. In a viscous fluid, such a concentration of vorticity would be quickly diffused away from the origin, strongly modifying the behavior of the velocity profile as time increases.

To assess the behavior of an initially inviscid line vortex in a viscous fluid, we assume that: (1) all the initial circulation, Γ , is retained within a radius of infinite extent for all time, (2) the initial velocity distribution at $t = 0$ is that of an irrotational line vortex, given by $v_\theta = \frac{A}{2\pi r}$, where A is a constant, and (3) the azimuthal velocity is forced to be zero at $r = 0$, immediately after the initial time zero.

To solve for the velocity of a decaying line vortex, a problem originally solved by [Oseen](#), and subsequently improved by [Lamb](#), we first determine the governing equation. Since the flow will only be a function of the radius and time, the only relevant velocity component in this problem is the θ -component, v_θ , such that the continuity equation becomes:

$$\frac{1}{r} \frac{\partial}{\partial r} (rv_r) + \frac{1}{r} \frac{\partial v_\theta}{\partial \theta} = 0 \quad \text{since } v_\theta = f(r) \text{ only} \quad (12.19)$$

This gives $v_r = 0$, since $v_r = 0$ at $r = 0$ will be a boundary condition.

Subsequently, since $v_\theta = f(r)$ only, and $v_r = 0$, only the θ -direction Navier-Stokes equation (Eq. 5.47c) is relevant, and that reduces to:

$$\frac{\partial v_\theta}{\partial t} = \nu \left[\frac{\partial}{\partial r} \left(\frac{1}{r} \frac{\partial}{\partial r} (rv_\theta) \right) \right] \quad (12.20)$$

Thus, we have a balance between temporal changes and viscous diffusion. There is no momentum transport—only diffusion of vorticity—and there is no pressure change in the azimuthal direction.

Since this problem has no characteristic dimension, this is an ideal candidate for a [similarity solution](#). However, to simplify our similarity assessment, we assume a function:

$$F(\eta) = rv_\theta \quad (12.21)$$

Where rv_θ is called the reduced circulation (i.e. the circulation contained within any radius r), and η is an appropriate similarity parameter. Here we assume that $\eta = ar^n t^m$, where a , n , and m are constants to be determined. We can determine the values of a , n , and m by substituting $F(\eta)$ and η into equation 12.21, and judiciously selecting a , n , and m to develop a tractable ordinary differential equation. However, noting that $F(\eta) = rv_\theta(r, t, \nu)$, we can apply dimensional analysis to determine the appropriate non-dimensional groups for this set of parameters. For this

case, we can show that $\eta = \frac{r}{\sqrt{\nu t}}$. Thus, for our similarity parameter and velocity function we use:

$$\eta = \frac{r}{\sqrt{\nu t}}, \text{ and } v_\theta = \frac{F(\eta)}{r}. \quad (12.22)$$

The initial condition for the velocity profile is that initially it is an irrotational vortex:

$$@ t = 0, r > 0 \quad v_\theta = \frac{A}{2\pi r} \quad (12.23a)$$

The two boundary conditions that apply here are:

$$\text{for } t > 0, r = 0 \quad v_\theta = 0 \quad (12.23b)$$

and

$$\text{for } t > 0, r \rightarrow \infty \quad \Gamma = A = \text{constant} \quad (12.23c)$$

Boundary condition #2 implies that the circulation is fixed from the beginning of the decay process on, so we can calculate the circulation for $t = 0$ for any radii, as:

$$\Gamma = v_\theta (2\pi r) = \frac{A}{2\pi r} (2\pi r) = A.$$

Since the circulation will be fixed for an infinite radius (i.e. we assume the vorticity will diffuse radially, but never quite reach an infinite radius), we can solve for the velocity for $r \rightarrow \infty$ as

$$v_\theta = \frac{A}{2\pi r}.$$

Using the similarity parameters from Eq. 12.22, and designating $\frac{dF}{d\eta} = F'$ and $\frac{d^2F}{d\eta^2} = F''$, we

establish the terms for Eq. 12.20 as follows:

$$\frac{\partial v_\theta}{\partial t} = \frac{\partial}{\partial t} \left(\frac{F}{r} \right) = \frac{1}{r} \frac{\partial F}{\partial \eta} \frac{\partial \eta}{\partial t} = \frac{F'}{r} \frac{\partial \eta}{\partial t} = -\frac{F'\eta}{2rt} \quad \text{where} \quad \frac{\partial \eta}{\partial t} = -\frac{1}{2} \frac{r t^{-\frac{3}{2}}}{\sqrt{\nu}} = -\frac{1}{2t} \frac{r}{\sqrt{\nu t}} = -\frac{\eta}{2t}$$

and

$$\frac{\partial}{\partial r} (r v_\theta) = \frac{\partial}{\partial r} (F) = \frac{\partial F}{\partial \eta} \frac{\partial \eta}{\partial r} = F' \frac{\partial \eta}{\partial r} = \frac{F'}{\sqrt{\nu t}} \quad \text{where} \quad \frac{\partial \eta}{\partial r} = \frac{1}{\sqrt{\nu t}}$$

$$\text{So,} \quad \frac{\partial}{\partial r} \left(\frac{1}{r} \frac{\partial}{\partial r} (r v_\theta) \right) = \frac{\partial}{\partial r} \left(\frac{F'}{r \sqrt{\nu t}} \right) = -\frac{F'}{r^2 \sqrt{\nu t}} + \frac{F''}{r \sqrt{\nu t}} \frac{\partial \eta}{\partial r} = -\frac{F'}{r^2 \sqrt{\nu t}} + \frac{F''}{r \sqrt{\nu t}}$$

Substituting into Eq. 12.20, we have:

$$-\frac{F'\eta}{2rt} = v \left(-\frac{F'}{r^2\sqrt{vt}} + \frac{F''}{rvt} \right) = \frac{v}{r^3} \left(-\frac{F'r}{\sqrt{vt}} + \frac{F''r^2}{vt} \right) \quad (12.24)$$

Multiplying Eq. 12.24 through by rt , and noting that $\eta = \frac{r}{\sqrt{vt}}$ gives:

$$-\frac{F'\eta}{2} = \frac{vt}{r^2} \left(-\frac{F'r}{\sqrt{vt}} + \frac{F''r^2}{vt} \right) = \frac{1}{\eta^2} (-\eta F' + \eta^2 F'') = -\frac{F'}{\eta} + F''$$

Solving for F'' , we have:

$$F'' = \left(\frac{1}{\eta} - \frac{\eta}{2} \right) F' \quad (12.25)$$

Using the initial/boundary conditions from Eq. 12.23, the appropriate limiting conditions for Eq. 12.25 are:

$$@ t = 0, r > 0 \Rightarrow \eta \rightarrow \infty: \quad v_\theta = \frac{A}{2\pi r} \Rightarrow F = \frac{A}{2\pi} \quad (12.26a)$$

$$@ t > 0, r = 0 \Rightarrow \eta = 0: \quad v_\theta = 0 \Rightarrow F = 0 \quad (12.26b)$$

$$@ t > 0, r \rightarrow \infty \Rightarrow \eta \rightarrow 0: \quad v_\theta = \frac{A}{2\pi r} \Rightarrow F = \frac{A}{2\pi} \quad (12.26c)$$

Same

Since Eq. 12.26a and 12.26c are identical, we have reduced the limiting conditions on Eq. 12.25 to two, which satisfies the order of Eq. 12.25, thus yielding a tractable problem.

To solve Eq. 12.25 for F , we let $\alpha = F'$, separate variables and integrate:

$$\frac{d\alpha}{d\eta} = \left(\frac{1}{\eta} - \frac{\eta}{2} \right) \alpha \Rightarrow \frac{d\alpha}{\alpha} = \left(\frac{1}{\eta} - \frac{\eta}{2} \right) d\eta$$

$$\ln \alpha = \ln \eta - \frac{\eta^2}{4} + \ln C_1 = \ln \left[C_1 \eta \exp \left(-\frac{\eta^2}{4} \right) \right]$$

or

$$\alpha = \frac{dF}{d\eta} = C_1 \eta \exp \left(-\frac{\eta^2}{4} \right) \quad (12.27)$$

Integrating Eq. 12.27 for F , we get:

$$F = -2C_1 \exp \left(-\frac{\eta^2}{4} \right) + C_2 \quad (12.28)$$

Applying the limiting conditions of Eq. 12.26 to Eq. 12.28:

$$F(\infty) = -2C_1 \overset{0}{\exp}(-\infty) + C_2 = \frac{A}{2\pi} \Rightarrow C_2 = \frac{A}{2\pi}$$

$$F(0) = -2C_1 \overset{1}{\exp}(-0) + C_2 = 0 \Rightarrow C_1 = \frac{C_2}{2} = \frac{A}{4\pi}$$

Substituting C_1 and C_2 into Eq. 12.28 gives a final expression of:

$$F = \frac{A}{2\pi} \left[1 - \exp\left(-\frac{\eta^2}{4}\right) \right]$$

And finally,

$$v_\theta = \frac{F}{r} = \frac{A}{2\pi r} \left[1 - \exp\left(-\frac{r^2}{4\nu t}\right) \right] \quad (12.29)$$

Note that the general circulation for this flow is given by:

$$\Gamma = v_\theta (2\pi r) = \frac{A}{2\pi r} \left[1 - \exp\left(-\frac{r^2}{4\nu t}\right) \right] (2\pi r) = A \left[1 - \exp\left(-\frac{r^2}{4\nu t}\right) \right]$$

For $r \rightarrow \infty$, we have that $\Gamma_\infty = A$, so

$$\Gamma = \Gamma_\infty \left[1 - \exp\left(-\frac{r^2}{4\nu t}\right) \right] = \Gamma_\infty \left[1 - \exp\left(-\frac{\eta^2}{4}\right) \right]$$

This shows that the circulation asymptotes to $\Gamma_\infty = A = \text{constant}$ at an infinite radius.

Figure 12.4 shows the behavior of the velocity as a function of radius and time. Note the decay of the maximum velocity with time, and the movement of this maximum away from the origin due to viscous diffusion. However, the “shape” of the profile is essentially the same, only “stretched” radially.

The behavior of the vorticity is given by:

$$\omega_z = \frac{1}{r} \frac{\partial(rv_\theta)}{\partial r} = \frac{\Gamma_\infty}{4\pi\nu t} \exp\left(-\frac{r^2}{4\nu t}\right) \quad (12.30)$$

The generic shape of the vorticity profiles (letting $\nu = 1$, and Vorticity = $4\pi\omega_z/\Gamma_\infty$) is shown in Figure 12.5. Note that the vorticity is all concentrated at the origin (an infinite spike) at $t = 0$. Subsequently, the vorticity diffuses away from the center due to viscosity.

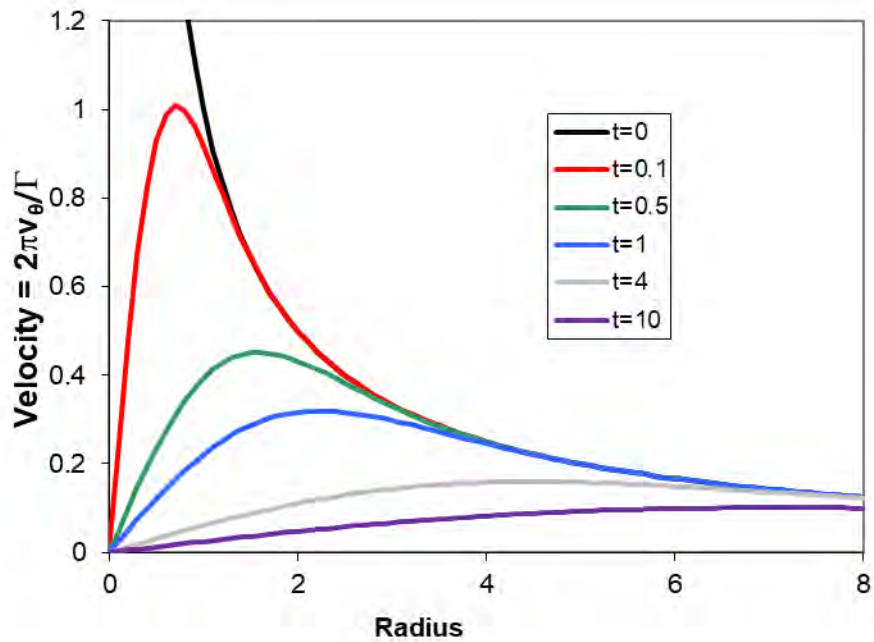


Figure 12.4 The generic shape of the Oseen velocity profiles (letting $\nu = 1$, and $\text{Velocity} = 2\pi v_\theta / \Gamma_\infty$) as a function of time and radius.

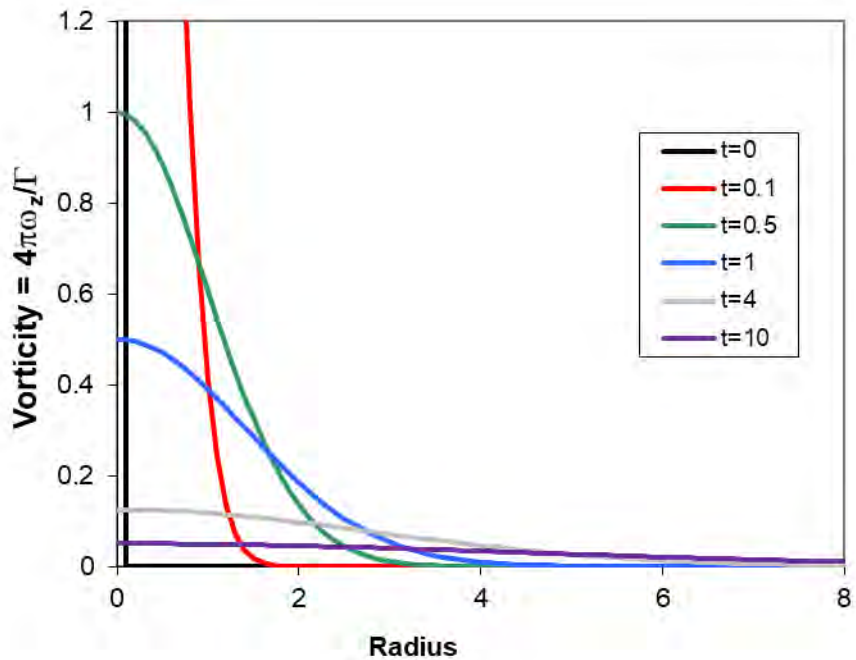


Figure 12.5 The general behavior of the vorticity for a decaying Oseen vortex (letting $\nu = 1$, and $\text{Vorticity} = 4\pi \omega_z / \Gamma_\infty$) as a function of time and radius.

12.3.2 The Taylor Dissipating Eddy

[G.I. Taylor](#) determined an additional solution to the decaying vortex problem, which he termed [dissipation of eddies](#), by employing an assumption that the angular momentum of the vortex is a constant, finite value, M . His velocity expression is:

$$v_{\theta} = \frac{M}{16\pi \nu^2 t^2} \exp\left(-\frac{r^2}{4\nu t}\right) \quad \text{where} \quad M = 2\pi \int_0^{\infty} v_{\theta} r^2 dr \quad (12.31)$$

Eq. 12.31 is similar to, but reasonably different from the Oseen expression of Eq. 12.29. Figure 12.6 shows the behavior of the velocity of this Taylor decaying vortex as a function of radius and selected times.

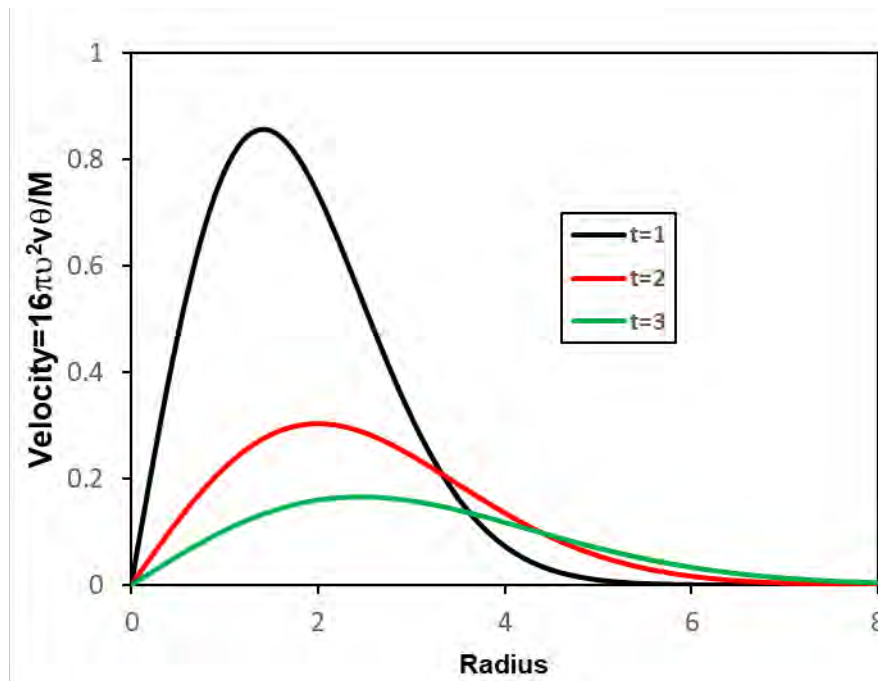


Figure 12.6 The generic shape of the Taylor vortex velocity profiles (letting $\nu = 1$, and $\text{Velocity} = 16\pi\nu^2 v_{\theta}/M$) as a function of non-dimensional time and radius.

Note that the velocity profiles for the Taylor vortex are not as skewed toward the origin, and asymptote to zero at a lower radius than the Oseen vortex, making the vortex more compact.

The differences between the two vortex models are illustrated by figures 12.7a and 12.7b, which plot the dimensionless behavior of the velocity, vorticity, and circulation versus the similarity variable $\eta = \frac{r}{\sqrt{\nu t}}$. Note that these plots have been normalized by factoring out any direct time

dependence (other than what is incorporated into the similarity variable, η). The resulting plots show the generic shape and behavior of the various properties.

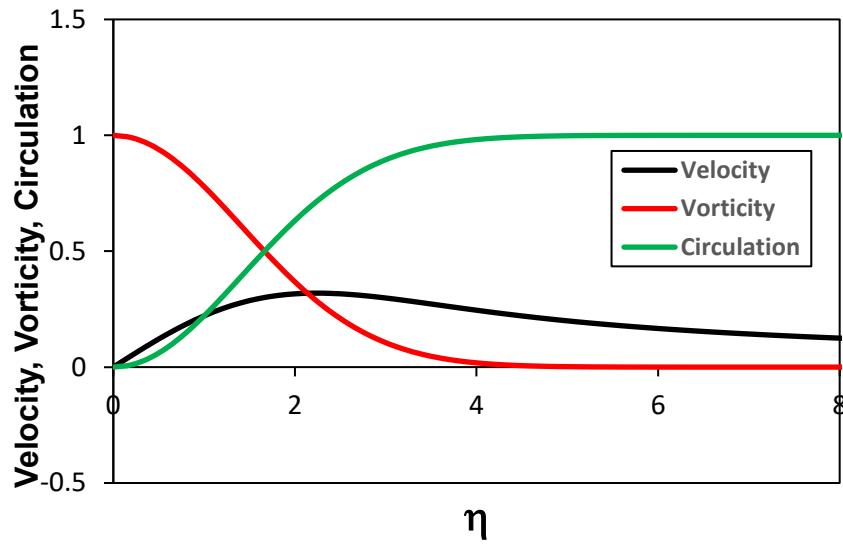


Figure 12.7a The Oseen vortex velocity, vorticity, and circulation similarity profiles

$$\text{(letting } \nu=1\text{): Velocity} = \frac{2\pi\sqrt{\nu t}v_\theta}{\Gamma_\infty}, \text{ Vorticity} = \frac{4\pi\nu t v_\theta}{\Gamma_\infty}, \text{ circulation} = \frac{\Gamma}{\Gamma_\infty} .$$

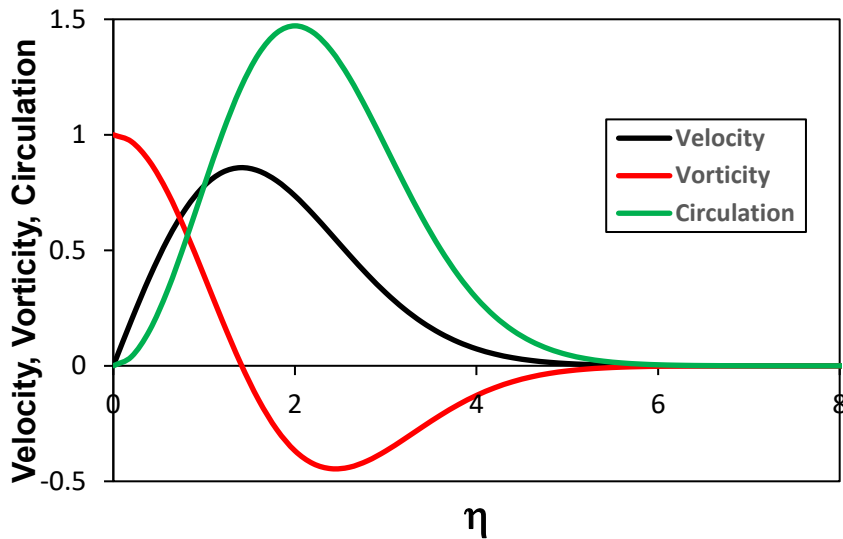


Figure 12.7b The Taylor vortex velocity, vorticity, and circulation similarity profiles

$$\text{(letting } \nu=1\text{): Velocity} = \frac{16\pi(\nu t)^{\frac{3}{2}} v_\theta}{M}, \text{ Vorticity} = \frac{8\pi(\nu t)^2 v_\theta}{M},$$

$$\text{circulation} = \frac{8\nu t \Gamma}{M} .$$

What should be obvious from figures 12.7 is that the two vortex solutions display markedly different velocity behavior, with the Oseen extending to very high similarity limits, and the Taylor reflecting a much more compact vortex. Because of these differences in velocity behavior, the circulation behavior is also remarkably different. The circulation for Oseen, because of the imposed original boundary condition at $\eta \rightarrow \infty$, reaches a constant, finite value at low η values. In contrast, the circulation for the Taylor vortex initially increases with η , reaches a peak at $\eta = 2$, and then decreases to essentially zero by $\eta \approx 7$. The reason for this marked difference is demonstrated by the differences in vorticity behavior. The Oseen vorticity is always positive, asymptoting to zero by $\eta \approx 5$, whereas the Taylor vorticity is initially positive from $\eta = 0$ to $\sqrt{2}$, and then becomes negative for $\eta > \sqrt{2}$, asymptoting to zero by $\eta \approx 7$. It is the cross-cancellation between these positive and negative vorticities that yields a zero circulation for the Taylor vortex at higher η values.

When we consider the behavior of real vortices, it would appear that the Taylor model is the more characteristic, since it does not require the effect of the vortex to have an infinite influence, and it maintains a finite angular momentum. Note that if we calculate the angular momentum of the Oseen vortex using the equation given in Eq. 12.31, the angular momentum is infinite, which does not seem a realistic model of a practical flow. However, because of its simplicity, the Oseen vortex has been widely used as a model of such things as the trailing vortices of a lifting body ([Squire, 1965](#)).

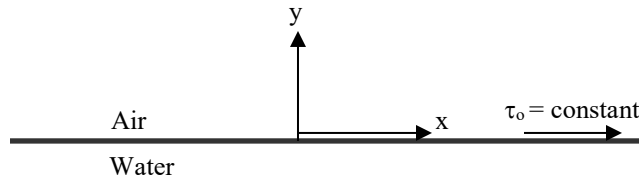
12.4 Ekman Drift: A Wind-Driven Flow

We know that much of the motion of the oceans and lakes are strongly influenced by the motion of the air above them. Let us consider the temporal development of the velocity field of an initially quiescent body of water, which is suddenly subjected to a constant surface wind shear stress of τ_0 . We know that the shear stress must be continuous at the air-water interface, as must the velocities. We could try to solve the coupled problem where surface wind shear also varies with time, but that is a much more complicated problem, requiring a coupling of Navier-Stokes solutions within both the air and the water. So, to simplify the problem, we will presume that $\tau_0 = \text{constant}$, and solve this as a similarity problem, similar to how we solved the suddenly accelerated plate problem of section 12.2.

For this wind driven flow, like the suddenly accelerated plate this is a viscous diffusion driven flow with $v = 0$, such that only the x-direction Navier-Stokes equation (Eq. 5.46b) is relevant, and within the water simplifies to:

$$\frac{\partial u}{\partial t} = \nu \frac{\partial^2 u}{\partial y^2} \quad (12.32)$$

Thus, only the local x -direction acceleration and shear forces are non-zero. Note that we assume that our coordinate system is located at the water surface, with y oriented vertically upward from the surface, as shown.



The appropriate initial and boundary conditions for the water are:

$$\begin{aligned} \text{Initial condition:} \quad & u(y < 0, t = 0) = 0 \\ \text{Boundary conditions:} \quad & \frac{\partial u}{\partial y}(y = 0, t > 0) = \frac{\tau_o}{\mu_w} = \text{constant} \\ & \frac{\partial u}{\partial y}(y \rightarrow -\infty, t > 0) = 0 \\ & u(y \rightarrow -\infty, t \geq 0) = 0 \end{aligned}$$

Since we have a second-order boundary condition that is non-zero, this means that we need to perform a solution using $\frac{\partial u}{\partial y}(y, t)$ as the similarity profile variable, and then determine $u(y, t)$ from that solution. To do this, we take the derivative of our Eq. 12.32 with respect to y , and reconfigure the equation such that:

$$\frac{\partial}{\partial y} \left(\frac{\partial u}{\partial t} \right) = \frac{\partial}{\partial y} \left(\nu \frac{\partial^2 u}{\partial y^2} \right) \Rightarrow \frac{\partial}{\partial t} \left(\frac{\partial u}{\partial y} \right) = \nu \frac{\partial^2}{\partial y^2} \left(\frac{\partial u}{\partial y} \right) \quad (12.33)$$

Note that Eq. 12.33 is an equation for $\frac{\partial u}{\partial y}(y, t)$, which can be solved for using a

“similarity” solution of the form $\frac{\partial u}{\partial y} = f(\eta)$, where the similarity parameter is $\eta = \frac{y}{2\sqrt{\nu t}}$, using a process similar to what we used in solving for the velocity in section 12.2.

To solve Eq. 12.33, we reduce the equation to an ODE in terms of $f(\eta)$, and solve to determine $f(\eta)$, and thus $\frac{\partial u}{\partial y}(y, t)$. Once we have a solution for $f(\eta)$, we can solve for $u(y, t)$ by integrating

$\frac{\partial u}{\partial y}(y, t)$, and applying the two first-order initial and boundary conditions. We first determine the derivative terms of Eq. 12.33 in terms of η , using the chain rule, and designating $\frac{df}{d\eta} = f'$ and

$$\frac{d^2f}{d\eta^2} = f'' \text{ with } \eta = \frac{y}{2\nu^{1/2}t^{1/2}} :$$

Term 1:

$$\begin{aligned} \frac{\partial}{\partial t} \left(\frac{\partial u}{\partial y} \right) &= \frac{\partial f(\eta)}{\partial t} = \frac{df}{d\eta} \frac{\partial \eta}{\partial t} = f' \frac{\partial \eta}{\partial t} \quad \text{where} \quad \frac{\partial \eta}{\partial t} = -\frac{y}{4\nu^{1/2}t^{3/2}} = -\underbrace{\left(\frac{y}{2\nu^{1/2}t^{1/2}} \right)}_{\eta} \frac{1}{2t} = -\frac{\eta}{2t} \\ &= f' \left(-\frac{\eta}{2t} \right) = -\frac{\eta f'}{2t} \end{aligned}$$

Term 2:

$$\begin{aligned} \frac{\partial}{\partial y} \left(\frac{\partial u}{\partial y} \right) &= \frac{\partial f(\eta)}{\partial y} = \frac{df}{d\eta} \frac{\partial \eta}{\partial y} = f' \frac{\partial \eta}{\partial y} \quad \text{where} \quad \frac{\partial \eta}{\partial y} = \frac{1}{2\nu^{1/2}t^{1/2}} = \underbrace{\left(\frac{y}{2\nu^{1/2}t^{1/2}} \right)}_{\eta} \frac{1}{y} = \frac{\eta}{y} \\ &= f' \frac{\eta}{y} \end{aligned}$$

$$\begin{aligned} \frac{\partial^2}{\partial y^2} \left(\frac{\partial u}{\partial y} \right) &= \frac{\partial f^2(\eta)}{\partial y^2} = \frac{\partial}{\partial y} \left(f' \frac{\partial \eta}{\partial y} \right) = \left(f'' \frac{\partial \eta}{\partial y} \right) \frac{\partial \eta}{\partial y} + f' \frac{\partial}{\partial y} \left(\frac{\partial \eta}{\partial y} \right) = f'' \left(\frac{\partial \eta}{\partial y} \right)^2 + f' \frac{\partial^2 \eta}{\partial y^2} \\ &= f'' \left(\frac{\eta}{y} \right)^2 + f'(0) \quad \text{where} \quad \frac{\partial^2 \eta}{\partial y^2} = \frac{\partial}{\partial y} \left(\frac{\partial \eta}{\partial y} \right) = \frac{\partial}{\partial y} \left(\frac{1}{2\nu^{1/2}t^{1/2}} \right) = 0 \\ &= f'' \frac{\eta^2}{y^2} \end{aligned}$$

Substituting the reduced Terms 1 and 2 into Eq.12.33 gives:

$$\begin{aligned} -\frac{\eta}{2t} f' &= \nu \frac{\eta^2}{y^2} f'' \\ -\frac{y^2}{2\nu t} f' &= \eta f'' \\ \underbrace{-2\eta^2 f'} & \\ -2\eta f' = f'' &\Rightarrow f'' + 2\eta f' = 0 \end{aligned} \tag{12.34}$$

Eq.12.34 is an O.D.E. for f as a function of the similarity (stretching) parameter, $\eta = \frac{y}{2\sqrt{\nu t}}$, and is the same equation (Eq. 12.16) we determined for the accelerated plate example, Section 12.2. For this similarity parameter, the two second-order boundary conditions shown previously become:

$$\text{Boundary conditions: } \frac{\partial u}{\partial y}(y=0, t>0) = \frac{\tau_o}{\mu_w} \Rightarrow f(\eta=0) = \frac{\tau_o}{\mu}$$

$$\frac{\partial u}{\partial y}(y \rightarrow -\infty, t>0) = 0 \Rightarrow f(\eta=-\infty) = 0$$

Thus, we have reduced the differential equation from a P.D.E. to an O.D.E., with two appropriate boundary conditions. Note that unlike the suddenly accelerated flow, we did not have to reduce three boundary conditions to two.

To solve our O.D.E, we let $\alpha = f'$ and substitute into the O.D.E., such that

$$\alpha' = -2\eta\alpha$$

Separating variables and integrating gives:

$$\ln \alpha = -\eta^2 + C$$

or

$$\alpha = f' = \frac{df}{d\eta} = C_1 \exp(-\eta^2)$$

Integrating f' gives:

$$f = C_1 \int_0^{\eta} \underbrace{\exp(-\eta^2)}_{\frac{\sqrt{\pi}}{2} \text{erf}(\eta)} d\eta + C_2 = C_1 \frac{\sqrt{\pi}}{2} \text{erf}(\eta) + C_2$$

Applying the two boundary conditions we have:

$$f(0) = \frac{\tau_o}{\mu_w} = C_1 \frac{\sqrt{\pi}}{2} \overset{=0}{\text{erf}(0)} + C_2 \Rightarrow C_2 = \frac{\tau_o}{\mu_w}$$

$$f(-\infty) = 0 = C_1 \frac{\sqrt{\pi}}{2} \overset{=-1}{\text{erf}(-\infty)} + C_2 \Rightarrow C_1 = \frac{2}{\sqrt{\pi}} C_2 = \frac{2}{\sqrt{\pi}} \left(\frac{\tau_o}{\mu_w} \right)$$

Substituting C_1 and C_2 , gives a solution for $\frac{\partial u}{\partial y} = f(\eta)$, and thus $\frac{\partial u}{\partial y} = f(y, t)$, of:

$$f(\eta) = \frac{\tau_o}{\mu_w} [1 + \text{erf}(\eta)]$$

$$\frac{\partial u}{\partial y} = \frac{\tau_o}{\mu_w} \left[1 + \operatorname{erf} \left(\frac{y}{2\sqrt{\nu t}} \right) \right] \tag{12.35}$$

Figure 12.8 is a non-dimensional plot of $\frac{\partial u}{\partial y}$ predicted by Eq. 12.35, showing the similarity shape of the shear profile in the water. Note that within the water, $\eta \leq 0$.

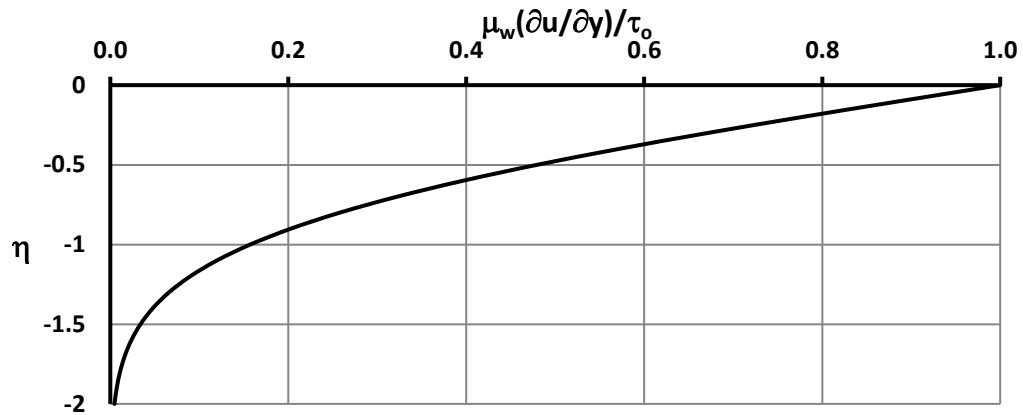


Figure 12.8 Similarity variable, $\eta = \frac{y}{2\sqrt{\nu t}}$, vs. the non-dimensional velocity gradient in water, $\mu_w(\partial u/\partial y)/\tau_o$, for a wind-driven flow with constant applied surface shear stress, τ_o .

To obtain $u(y,t)$, we integrate Eq.12.35 for $\frac{\partial u}{\partial y}$ with respect to y (I used Wolfram Alpha to do the integration), and obtain the messy:

$$u(y,t) = \frac{\tau_o}{\mu_w} \left\{ 2\sqrt{\frac{\nu t}{\pi}} \exp\left(-\frac{y^2}{4\nu t}\right) + y \left[1 + \operatorname{erf}\left(\frac{y}{2\sqrt{\nu t}}\right) \right] \right\} + g(t)$$

Applying our original first-order initial and boundary conditions:

Initial condition: $u(y < 0, t = 0) = 0$

$$u = \frac{\tau_o}{\mu_w} \left\{ (0) \overset{=0}{\exp(-\infty)} + y [1 + \overset{=-1}{\operatorname{erf}(-\infty)}] \right\} + g(0) = 0$$

$$u = \frac{\tau_o}{\mu_w} \{ 0 + y[1 - 1] \} + g(0) = g(0) = 0$$

Boundary condition: $u(y \rightarrow -\infty, t \geq 0) = 0$

$$u(-\infty, t) = \frac{\tau_o}{\mu_w} \left\{ 2\sqrt{\frac{\nu t}{\pi}} \exp(-\infty) + (-\infty)[1 + \operatorname{erf}(-\infty)] \right\} + g(t) = 0$$

$$u(-\infty, t) = \frac{\tau_o}{\mu_w} \left\{ 2\sqrt{\frac{\nu t}{\pi}} (0) + (-\infty)[1 - 1] \right\} + g(t) = 0$$

$$u(-\infty, t) = \frac{\tau_o}{\mu_w} 0\{0 + 0\} + g(t) = 0 \Rightarrow g(t) = 0$$

The term $y \left[1 + \operatorname{erf}\left(\frac{y}{2\sqrt{\nu t}}\right) \right]$ will go to zero as $y \rightarrow -\infty$. Prove this to yourself using L'Hospital's rule.

Thus:

$$u = \frac{\tau_o}{\mu_w} \left\{ 2\sqrt{\frac{\nu t}{\pi}} \exp\left(-\frac{y^2}{4\nu t}\right) + y \left[1 + \operatorname{erf}\left(\frac{y}{2\sqrt{\nu t}}\right) \right] \right\} \quad (12.36)$$

Note that in Eq.12.36 the collection of terms $\frac{2\tau_o}{\mu_w} \sqrt{\frac{\nu t}{\pi}}$ has the units of velocity, so letting:

$$u_0 = \frac{2\tau_o}{\mu_w} \sqrt{\frac{\nu t}{\pi}} \quad (12.37)$$

we can rewrite Eq.12.36 as:

$$\frac{u}{u_0} = \exp\left(-\frac{y^2}{4\nu t}\right) + \frac{y}{2} \sqrt{\frac{\pi}{\nu t}} \left[1 + \operatorname{erf}\left(\frac{y}{2\sqrt{\nu t}}\right) \right] \quad (12.38)$$

And substituting our similarity parameter, $\eta = \frac{y}{2\sqrt{\nu t}}$, into Eq. 12.38 gives:

$$\frac{u}{u_0} = \exp(-\eta^2) + \eta\sqrt{\pi}(1 + \operatorname{erf}\eta) \quad (12.39)$$

Thus, Eq. 12.39 is a "similarity" velocity profile for $\frac{u}{u_0}$.

Graphs 12.9 and 12.10 show the velocity behavior within the water, dimensionally for Eq. 12.38 and non-dimensionally for Eq.12.39. Figure 12.9 shows the dimensional effect of viscous diffusion of the applied shear within the water. Note that the thickness of the affected layer of water (that where $u > 0$) grows relatively slowly, taking 1000 seconds for the effect of the applied wind stress to be felt at a depth of 10 cm (roughly 4 inches). Even after 1 hour, the extent of the affected fluid only reaches 19 cm (about 7.5 inches).

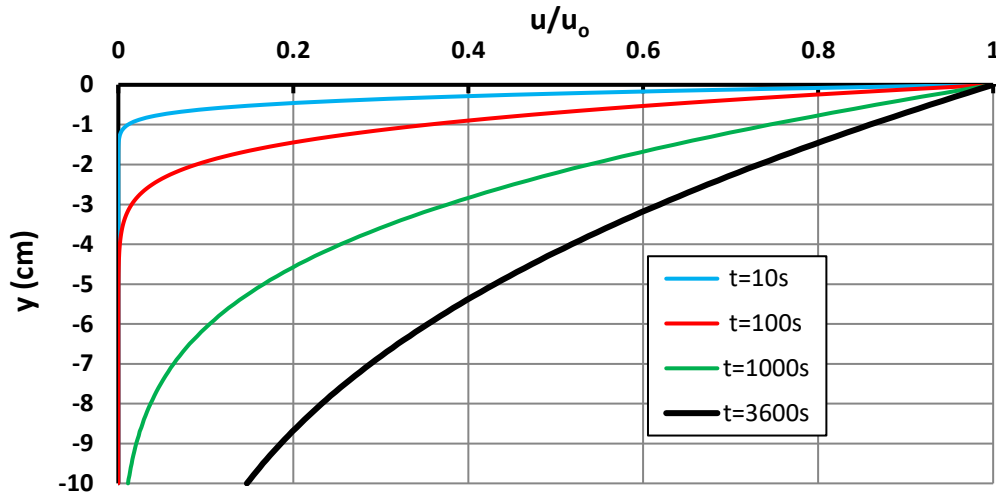


Figure 12.9 Water depth, y (cm), vs. the water velocity ratio, u/u_0 for a wind-driven flow with constant applied surface shear stress, τ_0 . Velocity profiles are shown for four increasing time increments, $t = 10, 100, 1000,$ and 3600 seconds, and $\nu = 0.01 \frac{\text{cm}^2}{\text{s}}$.

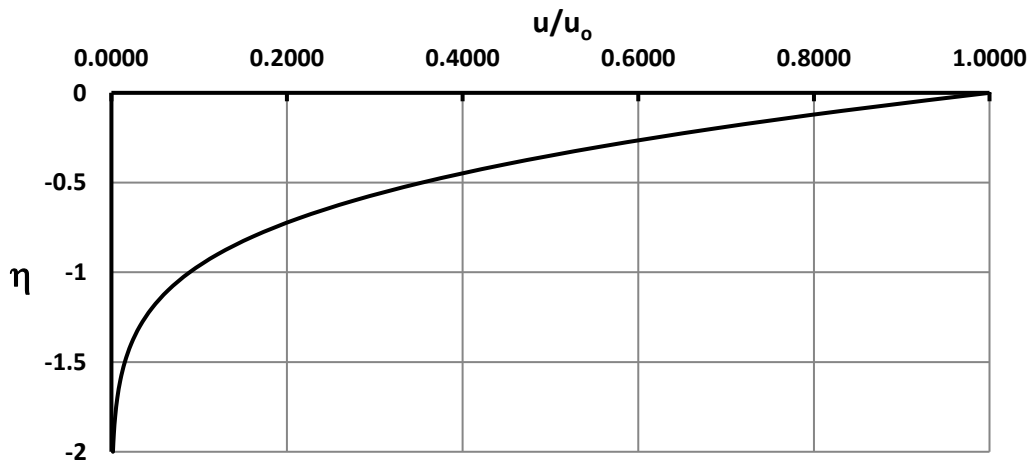


Figure 12.10 Similarity variable, $\eta = \frac{y}{2\sqrt{\nu t}}$, vs. the water velocity ratio, u/u_0 for a wind-driven flow with constant applied surface shear stress, τ_0 .

Figure 12.10 shows the shape of the velocity ratio relative to the similarity parameter, η . It is interesting that the shape of the velocity appears similar to that of the shear stress, but the functions for the shear stress and the velocity are quite different. Note that Eq. 12.38 and 12.39 indicate that u_0 is the velocity at the water surface ($y = 0$ and $\eta = 0$), which according to Eq.

12.37 increases proportional to \sqrt{t} . To examine some numbers for the movement of the water at the surface, it was pointed out by [White \(1991\)](#) that [Roll \(1965\)](#), citing several empirical studies, estimates the wind stress for airflow over a water surface to be given by the relation:

$$\tau_0 \approx 0.002\rho_{\text{air}}(V_{\text{wind}} - u_0)^2. \tag{12.40}$$

Assuming typical standard properties for water and air of $\mu_w = 10^{-3} \frac{\text{kg}}{\text{m}\cdot\text{s}}$,

$\nu_w = 10^{-6} \frac{\text{m}^2}{\text{s}}$, and $\rho_{\text{air}} = 1.2 \frac{\text{kg}}{\text{m}^3}$, we solve Eq. 12.37 for τ_0 , and substitute τ_0 into

Eq. 12.40 to give an equation for u_0 in terms of V_{wind} and t as:

$$369.3 \frac{u_0}{\sqrt{t}} - (V_{\text{wind}} - u_0)^2 = 0 \tag{12.41}$$

Note that t is in seconds, and velocities are in m/s.

Assuming a wind velocity of 2 m/s (about 4.5 mph), we solve Eq. 12.41 using a root finding program for a series of times (we could also solve using the quadratic formula, but the expression is messy). A graph of u_0 vs t is shown in Figure 12.11. Note that the water surface velocity, u_0 , initially grows quite quickly, but slows with time.

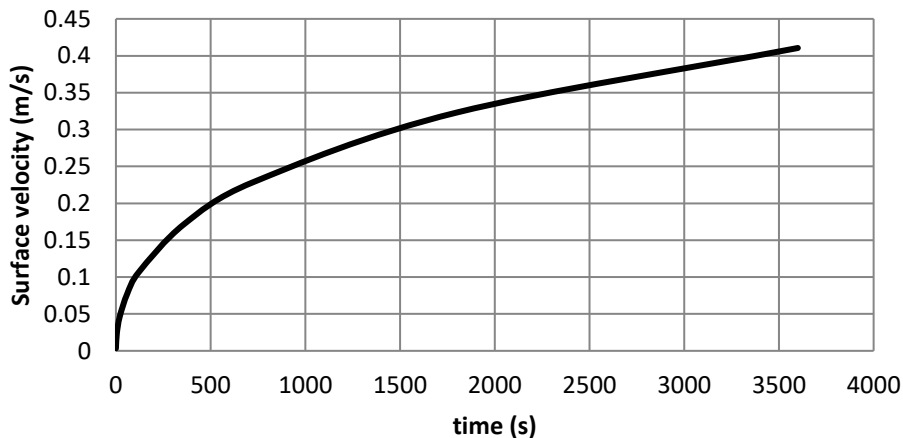


Figure 12.11 Water surface velocity, u_0 (m/s) vs. time (s) for a wind-driven flow with constant applied surface shear stress, $\frac{\tau_0}{\mu_w}$. Assumed wind velocity $V_{\text{wind}}=2$ m/s, and $\tau_0 \approx 0.002\rho_{\text{air}}(V_{\text{wind}} - u_0)^2$, from Roll (1965).

In addition, the water velocities seem somewhat unrealistic, since the water surface velocity, u_0 , is predicted to increase to 20% of the wind velocity after one hour of wind exposure. As White

points out, the water surface velocity should only grow to about 3% after an hour of wind exposure. He also notes that for such flows at higher wind velocities, both the water and air flows will be turbulent, with much higher effective turbulent viscosities (known as eddy viscosities--see Chapter 17). However, if the turbulent values of ν_w are larger, this would suggest that $u_{0\text{-turbulent}} > u_{0\text{-laminar}}$, which would result in even higher predicted values of u_0 .

So, what is the problem? This inconsistency with empirical values is most likely due to the assumption of constant shear. In reality, the shear will diminish as the water surface velocity increases. Note that Eq. 12.37 indicates that u_0 will continually increase proportional to \sqrt{t} . In reality, as time increases u_0 must reach some equilibrium value, such that $u_0 \ll V_{\text{wind}}$. Since we don't specify the wind velocity in the similarity model, and impose the actual boundary conditions that $\tau_{w,0} = \tau_{a,0}$, and $u_{w,0} = u_{a,0}$, our similarity model over simplifies, and thus over estimates the acceleration of the water. As stated previously, solution of the actual physical problem would require that we collectively solve the Navier stokes equations for both the water and the airflows. Thus, the Ekman drift problem is an interesting example of the use of similarity, but is limited in its practical applicability.

12.5 A Laminar Jet Issuing from a Narrow Slot

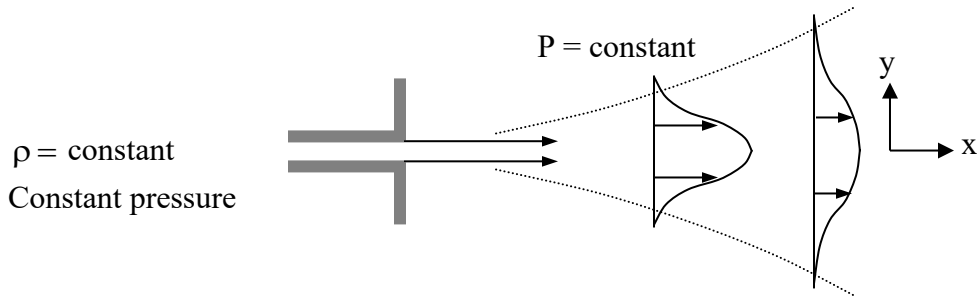
As was demonstrated in the examples of Sections 12.2, 12.3, and 12.4, the use of a similarity solution is an effective method of reducing a P.D.E. to a tractable O.D.E. This process reduces the number of independent variables by one or more (e.g. from y and t to η for the suddenly accelerated plate of Section 12.2). However, how do we approach a problem that involves more than one dependent variable? Note that our three previous examples dealt with only one non-zero velocity variable (u for the suddenly accelerated plate and Ekman drift, and v_0 for the decaying line vortex).

In the following example, we deal with a flow that requires the determination of two dependent velocity components, u and v , and thus we must develop a solution that simultaneously satisfies both the continuity and the Navier-Stokes equations. Thus, we have $u = u(x,y)$ and $v = v(x,y)$.

Here, we show how this is done making use of the stream function, as well as a similarity variable.

The problem we address here is a two-dimensional laminar jet, which issues from a slot in a wall into a region of infinite extent and constant pressure. This flow was originally solved by [Schlichting \(1933\)](#). The solution we seek will only apply for a downstream region removed from the immediate vicinity of the slot. In this downstream region, the velocity profiles are expected

to exhibit similar behavior, with the velocity profile stretching laterally in the y-direction due to viscous diffusion, and correspondingly contracting in the x-direction, as illustrated below.



An additional assumption will be that the total momentum flux in any x-plane of the jet will remain constant, and that no other external forces act on the flow. In reality, this is not exactly the case (although the momentum will not change rapidly). However, as we will see, we require four limiting conditions to solve the problem fully, and we can only identify three appropriate boundary conditions. Therefore, we use the assumption of constant momentum flux as our fallback limiting condition.

An assessment of the Navier-Stokes equation indicates that the y-direction component equation has negligible influence on the solution (we will demonstrate how we prove this for a boundary layer flow in Chapter 13), so the governing equations for this flow are the x-direction component of the Navier-Stokes equation and the continuity equation (2-D).

$$\text{Navier-Stokes (x-direction): } u \frac{\partial u}{\partial x} + v \frac{\partial u}{\partial y} = -\frac{1}{\rho} \frac{dP}{dx} + \nu \left(\frac{\partial^2 u}{\partial y^2} + \frac{\partial^2 u}{\partial x^2} \right) \quad (12.42a)$$

$\nearrow 0$ \nearrow Neglect relative to y-changes

$$\text{Continuity equation: } \frac{\partial u}{\partial x} + \frac{\partial v}{\partial y} \quad (12.42b)$$

We further assume that the pressure within the solution region is constant, which makes the pressure gradient within the flow region negligible. Additionally, we assume the viscous changes in the x-direction are minimal in comparison to viscous changes relative to the normal (y) direction (we address this assumption more closely when we assess boundary layers in Ch.13).

Finally, we identify three clear boundary conditions, all relative to y.

$$\text{Boundary Conditions: } @ y = 0: v = 0 \quad (12.43a)$$

$$@ y = 0: \frac{\partial u}{\partial y} = 0 \quad (12.43b)$$

$$@ y \rightarrow \infty: u \rightarrow 0 \quad (12.43c)$$

Because Eqs. 12.42a and 12.42b contain a first-order derivative of u with respect to x , we technically require a bounding condition for u at an appropriate x location. One possibility might be $u = 0$ as $x \rightarrow \infty$. However, such a boundary condition does not prove useful in establishing the coefficients of integration (I will illustrate). Thus, we use a fallback assumption of a constant momentum flux, which we employ after the fact to allow a (somewhat) complete solution.

To begin the solution, we note that we can reduce Eqs. 12.42a and 12.42b to one equation by the use of the stream function, $\psi(x,y)$. Recall that the stream function is an exact solution of the continuity equation (in two-dimensions; see section 9.2, Eq. 9.3). The use of the stream function reduces the two partial differential equations (P.D.E.) to one P.D.E. equation with one dependent variable (ψ), since it eliminates the continuity equation from the set of equations.

Substituting the stream function into Eq. 12.42a, where:

$$u = \frac{\partial \psi}{\partial y}, \quad v = -\frac{\partial \psi}{\partial x}, \quad \frac{\partial u}{\partial x} = \frac{\partial^2 \psi}{\partial y \partial x}, \quad \frac{\partial u}{\partial y} = \frac{\partial^2 \psi}{\partial y^2}, \quad \text{and} \quad \frac{\partial^2 u}{\partial y^2} = \frac{\partial^3 \psi}{\partial y^3}$$

yields:

$$\frac{\partial \psi}{\partial y} \frac{\partial^2 \psi}{\partial y \partial x} - \frac{\partial \psi}{\partial x} \frac{\partial^2 \psi}{\partial y^2} = \nu \frac{\partial^3 \psi}{\partial y^3} \quad (12.44)$$

Thus, by using the stream function, we have reduced two P.D.Es to one P.D.E. for $\psi = \psi(x,y)$. We now search for an independent variable, η , which will convert the partial differential equation of Eq. 12.44 to *one* ordinary differential equation for $\psi = \psi(\eta)$.

The determination of an appropriate similarity approach is not always straightforward, and requires a bit of insight, skill, and trial and error. Many approaches that work seem reasonable after the fact, but are not exactly obvious initially. For this problem, in addition to a similarity parameter, the stream function must be further scaled on the streamwise variable, x , such that we seek a functional relationship of the form:

$$\psi = \nu^a x^b f(\eta) \quad \text{and} \quad \eta = C \nu^c x^d y^e \quad (12.45)$$

Here, a , b , c , d , e , and C are all constants, to be determined. As we will see, this form of scaling reduces Eq. 12.44 to a tractable O.D.E, but the form of the scaling was probably not obvious to Schlichting who first solved this problem, and probably evolved from several different attempts at an effective scaling. Often, dimensional analysis of the governing equation may be helpful in the determination of an appropriate scaling approach, but not always.

To seek a general similarity reduction of Eq. 12.44, we could employ the general functional forms of Eq. 12.45, substitute into Eq. 12.44, and manipulate a , b , c , d , e , and C to yield a

tractable ordinary differential equation. However, this is a hard, tedious process, so we will short cut it by using the following previously established functional forms:

$$\psi = \sqrt{v}x^{1/3}f(\eta) \quad \text{and} \quad \eta = \frac{1}{3\sqrt{v}} \frac{y}{x^{2/3}} \quad (12.46)$$

Thus, we first determine the various components of Eq. 12.44 as:

$$v = -\frac{\partial\psi}{\partial x} = -\frac{\sqrt{v}}{3} \frac{f}{x^{2/3}} - \sqrt{v}x^{1/3}f' \frac{\partial\eta}{\partial x} \quad \text{Noting that} \quad \frac{\partial\eta}{\partial x} = -\frac{2}{9\sqrt{v}} \frac{y}{x^{5/3}} = -\frac{2}{3} \frac{\eta}{x}$$

$$v = -\frac{\sqrt{v}}{3x^{2/3}}(f - 2\eta f')$$

Likewise,

$$u = \frac{\partial\psi}{\partial y} = \sqrt{v}x^{1/3}f' \frac{\partial\eta}{\partial y} = \frac{f'}{3x^{1/3}} \quad \text{where} \quad \frac{\partial\eta}{\partial y} = \frac{1}{3\sqrt{v}x^{2/3}}$$

$$\frac{\partial u}{\partial y} = \frac{\partial^2\psi}{\partial y^2} = \frac{f''}{3x^{1/3}} \frac{\partial\eta}{\partial y} = \frac{f''}{9x\sqrt{v}}$$

$$\frac{\partial^2 u}{\partial y^2} = \frac{\partial^3\psi}{\partial y^3} = \frac{f'''}{9x\sqrt{v}} \frac{\partial\eta}{\partial y} = \frac{f'''}{27vx^{5/3}}$$

$$\frac{\partial u}{\partial x} = \frac{\partial^2\psi}{\partial x\partial y} = -\frac{1}{9x^{4/3}}(f' + 2\eta f'')$$

Now substituting these relationships back into Eq. 12.44 gives:

$$\left(\frac{f'}{3x^{1/3}}\right)\left(-\frac{1}{9x^{4/3}}(f' + 2\eta f'')\right) - \left(-\frac{\sqrt{v}}{3x^{2/3}}(f - 2\eta f')\right)\left(\frac{f''}{9x\sqrt{v}}\right) = v\left(\frac{f'''}{27vx^{5/3}}\right),$$

which simplifies to (trust me, or do it yourself—a good exercise).

$$\underbrace{f''' + ff'' + f'^2}_{(ff')'} = 0 \quad (12.47a)$$

Using a few mathematical identifications give a final ODE for $f(\eta)$ as:

$$f''' + (ff')' = 0 \quad \Rightarrow \quad (f'' + ff')' = 0 \quad (12.47b)$$

The modified boundary conditions from Eqs. 12.43 are:

$$\begin{aligned}
 & 1) \quad y=0 \Rightarrow \eta=0 : \quad v=0 \Rightarrow f=0 \\
 \text{Boundary Conditions:} \quad & 2) \quad y=0 \Rightarrow \eta=0 : \quad \frac{\partial u}{\partial y}=0 \Rightarrow f''=0 \\
 & 3) \quad y \rightarrow \infty \Rightarrow \eta \rightarrow \infty : \quad u \rightarrow 0 \Rightarrow f' \rightarrow 0
 \end{aligned}
 \tag{12.48}$$

Integrating Eq.12.47b for f gives:

$$f'' + ff' = C_1 \Rightarrow \text{From Eqs.12.48 for } \eta=0 \Rightarrow 0+0=C_1=0$$

Therefore,

$$f'' + ff' = 0 \tag{12.49}$$

Note that we can write, $(f^2)' = 2ff'$. This will help simplify Eq.12.49, but the coefficients are wrong to allow a closed form integration. So, we substitute further, letting:

$$f = 2F \Rightarrow f' = 2F' \Rightarrow f'' = 2F'' \tag{12.50}$$

Thus, substituting Eqs.12.50 into Eq. 12.49, with a few more mathematical identifications gives:

$$\begin{aligned}
 2F'' + (2F)(2F') &= 0 \\
 F'' + 2FF' &= 0 \\
 F'' + (F^2)' &= (F' + F^2)' = 0
 \end{aligned}
 \tag{12.51}$$

Integrating Eq. 12.51 gives:

$$F' + F^2 = \text{constant} = \alpha^2 \leftarrow \text{choose for convenience}$$

$$\text{or } \frac{dF}{d\eta} = \alpha^2 - F^2 \tag{12.52}$$

Separating variables, and integrating Eq.12.52 gives:

$$\int \frac{dF}{\alpha^2 - F^2} = \int d\eta$$

$$F = \alpha \tanh(\alpha\eta) + C_2 \Rightarrow \text{for boundary condition 1, } @\eta=0 \Rightarrow F(0) = \alpha \tanh(0) + C_2 \Rightarrow C_2 = 0$$

Thus,

$$f = 2F = 2\alpha \tanh(\alpha\eta) \tag{12.53}$$

Now, using f to solve for the velocity components gives:

$$u = \frac{\partial \psi}{\partial y} = \frac{f'}{3x^{1/3}} = \frac{2\alpha^2}{3x^{1/3}} \operatorname{sech}^2(\alpha\eta) = \frac{2}{3} \frac{\alpha^2}{x^{1/3}} (1 - \tanh^2 \alpha\eta) \quad (12.54a)$$

$$\text{where } \eta = \frac{1}{3\sqrt{v}} \frac{y}{x^{2/3}}$$

and

$$v = -\frac{\partial \psi}{\partial x} = -\frac{\sqrt{v}}{3x^{2/3}} (f - 2\eta f') = \frac{2\alpha\sqrt{v}}{3x^{2/3}} [2\alpha\eta \operatorname{sech}^2(\alpha\eta) - \tanh(\alpha\eta)] \quad (12.54b)$$

Note that we never used our third boundary condition to arrive at these expressions. However, we note that Eq. 12.54a reflects $u = 0$ ($f' = 0$) for $\eta \rightarrow \infty$, thus our third boundary condition is satisfied.

To determine the undetermined constant α , since we have no other appropriate boundary condition, Schlichting invoked the physical condition that the momentum flux for the jet must remain constant (within a reasonable distance of the orifice). Thus, if J is the momentum flux, defined by:

$$J = \int_{-\infty}^{\infty} (\rho u^2) dy \quad (12.55)$$

We determine J by substituting Eq. 12.54a for the x-direction velocity, u , into Eq. 12.55, and solving for α in terms of J , which gives:

$$\alpha = 0.8255 \left(\frac{J}{\rho\sqrt{v}} \right)^{1/3} \quad (12.56)$$

Figures 12.12a and 12.12b show the u velocity predicted by Eqs. 12.54a, illustrating the "similar" shape of the velocity profile, when scaled on η (figure 12.12a), and the spread of the velocity profile, when scaled on y (figure 12.12b), as a function of streamwise distance, x . Note that figure 12.12b also demonstrates the decrease in u_{\max} (the center line velocity, at $y = \eta = 0$) with increasing distance, x .

Figure 12.12c shows the behavior of the transverse v velocity, which appears a bit unusual. However, there is an explanation for the pattern shown. Note the change in the transverse dependence of the velocity behavior on y : when the jet is close to the wall slot ($x = 1.0$), near the centerline ($|y| < 4$) the transverse velocity, v , is away from the centerline, but well away from the centerline ($|y| > 10$), the velocity is very strongly toward the centerline. This reflects an induced flow created by the jet, which causes fluid away from the centerline to flow toward the jet. However, as the jet moves further in the x direction, this flow pattern mediates; the same outward/inward pattern is present, but much less pronounced.

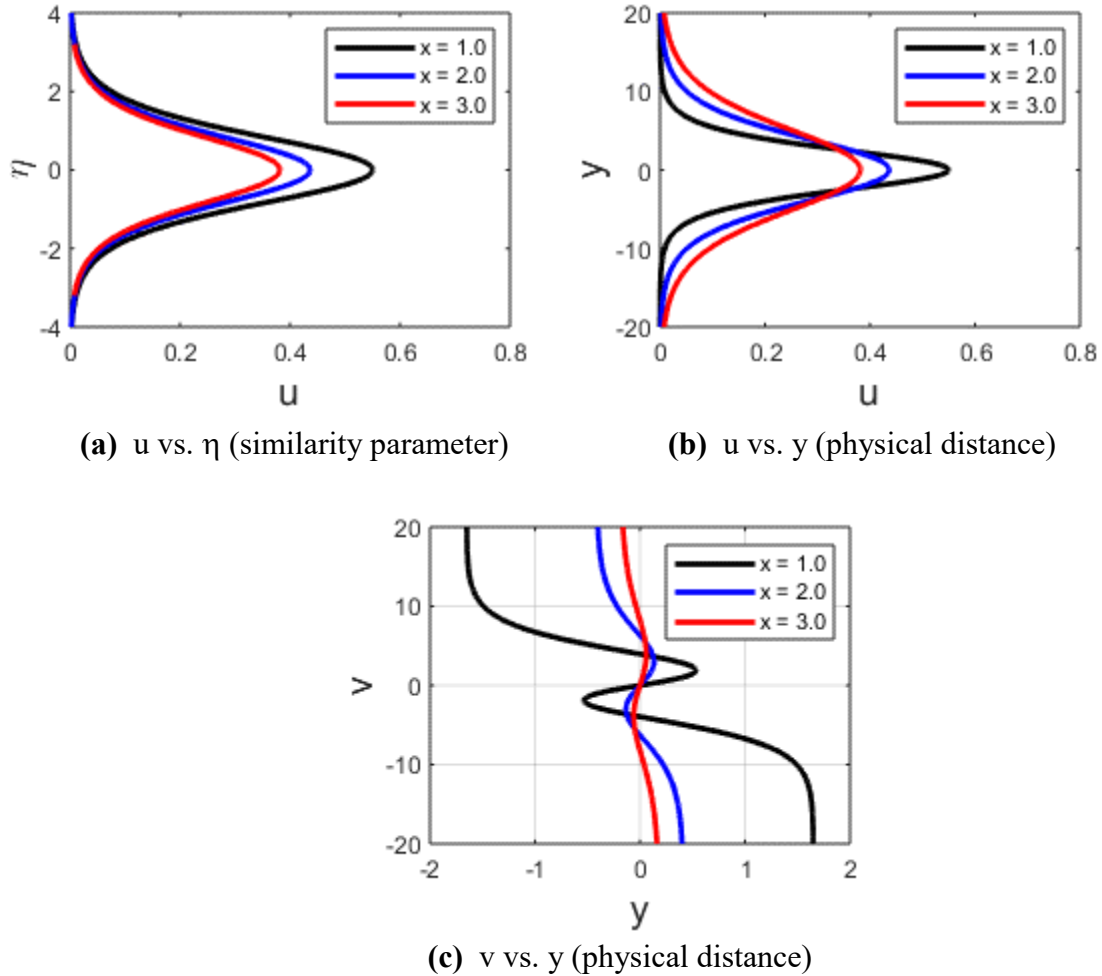


Figure 12.12 Streamwise and spanwise velocities for a laminar jet. Here we let ρ , ν , and $J = 1$, at three progressive x distances, $x=1.0$, 2.0 , and 3.0 .
 (a) u vs. η , (b) u vs. y , (c) v vs. y

To better illustrate the jet flow pattern, Figure 12.13 shows a plot of the velocity vectors for u and v calculated for the region $1 < x < 6$ and $-10 < y < 10$; overlaid on these velocity vectors are selected streamlines for the flow. These vectors and streamlines illustrate the strong inflows near the wall, the decreasing u -velocity with increasing distance from the wall, and the slow spreading of the jet as it proceeds downstream.

Equations 12.54 reflect an idealized solution, since under normal flow conditions the jet would break down due to the rapid generation of turbulence. However, Eqs. 12.54 will be a reasonable model of a low density or very viscous jet flow, at very low Reynolds number.

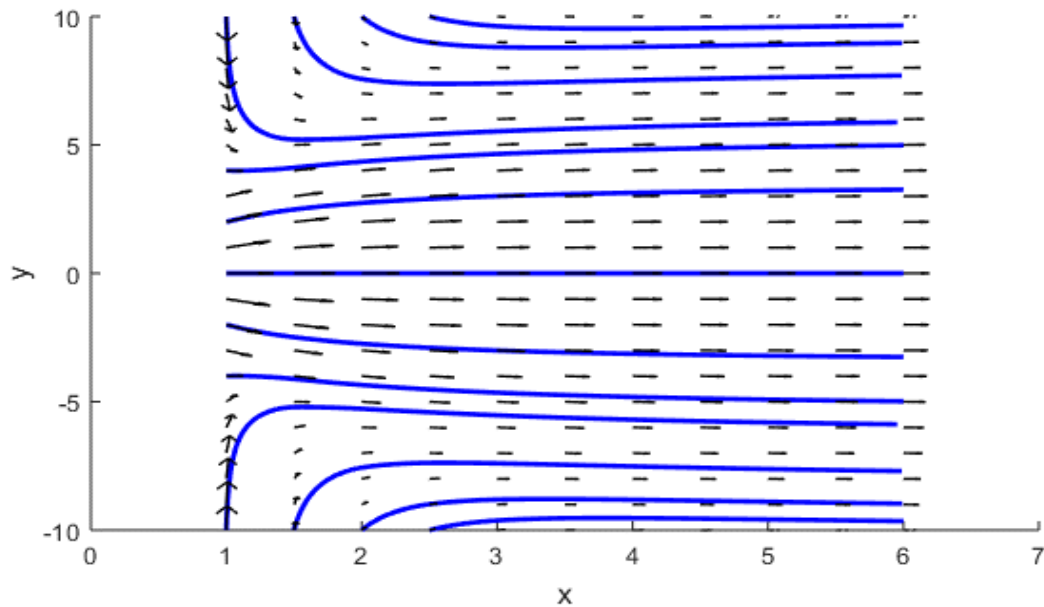


Figure 12.13 Velocity vector/streamline plot for a laminar wall jet. Here we let ρ , ν , and $J = 1$. Velocity vectors are shown in **black**, and streamlines in **blue**. Jet enters from left at $x, y = 0, 0$.

Note that if we tried to use the boundary condition $u = 0$ as $x \rightarrow \infty$, this would be indeterminate in establishing α . When $x \rightarrow \infty$, $\eta \rightarrow 0$, and Eq. 12.54a will become:

$$u = 0 = \frac{2}{3} \frac{\alpha^2}{(\infty)} (1 - \cancel{\tanh^2(0)}) = \frac{2}{3} \frac{\alpha^2}{(\infty)}$$

This result is indeterminate for α , so α cannot be determined from an assumption of $u = 0$ as $x \rightarrow \infty$. However, equation 12.54a does give the correct result or $u = 0$ as $x \rightarrow \infty$.

This approach of using similarity variables and solutions permeates fluid mechanics (as well as other scientific/engineering fields). In the next chapter, we address a very common flow behavior that again yields a similarity solution: the development of laminar boundary layers for flows over external surfaces.

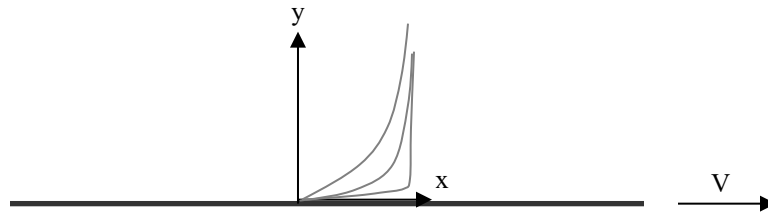
References

[White, F. M. \(1991\)](#), *Viscous Fluid Flow*, McGraw-Hill Inc., New York.
(section 3-3.3, pp. 119-122)

Roll, H. U. (1965), *Physics of the Marine Atmosphere*, International Geophysics Series, vol. 7, Academic Press, New York.

Study Problems

1. Consider the solution for a decaying Oseen-Lamb vortex solved in section 12.3.1. Using the solution for the velocity (Eq. 12.29), determine the shear stress for the vortex, and create a graph showing $\frac{\tau_{r\theta}\pi}{\mu\Gamma_\infty}$ vs. r from $0 < r < 6$ cm for water ($\nu = 10^{-2}$ cm²/s). On one graph, show 3 plots for $t = 1, 5,$ and 10 seconds. Briefly explain what is happening as time increases.
2. Consider the solution for a dissipating Taylor eddy examined in section 12.3.2. Using the solution for the velocity (Eq. 12.31), determine the shear stress for the vortex, and create a graph showing $\frac{32\pi\tau_{r\theta}}{\mu M}$ vs. r from $0 < r < 6$. Let $\nu=1$, and r and t be dimensionless. On one graph, show 3 plots for $t = 1, 2,$ and 3 . Briefly explain what is happening as time increases.
3. Consider the situation where an infinite plate and the flow above it are both moving at a constant velocity U . At $t = 0$, the plate is suddenly stopped, decelerating from $u = U$ to $u = 0$ instantaneously.



For this flow, the Navier-Stokes equation simplifies to:

$$\frac{\partial u}{\partial t} = \nu \frac{\partial^2 u}{\partial y^2}$$

Thus, only the local x -direction acceleration and shear forces are non-zero. Solve this equation for $u(y,t)$ using a “similarity” solution of the form $\frac{u}{U} = f(\eta)$, where the similarity parameter is

$\eta = \frac{y}{2\sqrt{\nu t}}$. Indicate clearly the appropriate boundary and initial conditions, reduce the equation to an ODE in terms of $f(\eta)$, and solve to determine $f(\eta)$, and thus $u(y,t)$.

Create two graphs: One of u/U vs. η for $0 < \eta < 2$; another showing three plots of u/U vs. y between $0 \text{ cm} < y < 2 \text{ cm}$, for $t = 1 \text{ s}, 10 \text{ s},$ and 100 s . Assume the fluid to be water with $\nu = 10^{-2}$ cm²/s.

4. For the Ekman Drift problem done in section 12.4, using equation 12.41, determine the value of V_{wind} (in m/s) for which u_0 will be 3% of V_{wind} after one hour of exposure.

5. For the Ekman Drift problem done in section 12.4, using equation 12.41, determine the value of V_{wind} (in m/s) required for which u_0 will be 0.5 m/s after (a) 5 minutes of exposure and (b) one hour of exposure.
6. For the Ekman Drift problem done in section 12.4, make graphs for $0 \geq y \geq -10$ cm of:
- $\frac{\mu_w}{\tau_0} \frac{\partial u}{\partial y}$ vs. y , and
 - $\frac{u \mu_w}{\tau_0}$ vs. y (let $\nu = 10^{-2} \frac{\text{cm}^2}{\text{s}}$, which will give $\frac{u \mu_w}{\tau_0}$ units of cm)

Comment on what these show about the flow.

7. For the Ekman Drift problem done in section 12.4, use a similarity method similar to that used for the water to derive the behavior of the shear stress and velocity for the air flow above the water. You will use the same reduced equation and similarity parameter, η (only for the kinematic viscosity in air), and will determine solutions for the region $y \geq 0$. Also, your initial condition will be $u(y > 0, t = 0) = U = \text{constant}$, and the boundary conditions will be

$$\frac{\partial u}{\partial y}(y = 0, t > 0) = \frac{\tau_0}{\mu} = \text{constant}, \quad \frac{\partial u}{\partial y}(y \rightarrow \infty, t > 0) = 0 \quad \text{and} \quad u(y \rightarrow \infty, t \geq 0) = U.$$

From your solutions, plot (let $\nu = 0.15 \frac{\text{cm}^2}{\text{s}}$, which will give $\frac{\mu(u-U)}{\tau_0}$ units of cm)

- η vs. $\frac{\mu_a}{\tau_0} \frac{\partial u}{\partial y}$, from $0 < \eta < 2$
- η vs. $\frac{u-U}{u_0}$, from $0 < \eta < 2$, where $u_0 = \frac{2\tau_0}{\mu} \sqrt{\nu t}$
(note that $\frac{u-U}{u_0}$ is termed a velocity "deficit")
- y vs. $\frac{\mu(u-U)}{\tau_0}$, from $0 < y < 10$ cm

Comment on the behavior of your graphs, and what they show about this flow.

8. Substitute Eq. 12.54a for the x-direction velocity, u , into Eq. 12.55, and solve for α in terms of J to show that Eq. 12.56 is correct. I would suggest you do the integration using Wolfram Alpha.
9. Using Eq. 12.54a for the x-direction velocity, u , into Eq. 12.55, determine the x-direction mass flowrate per unit depth, m , as a function of x . Let ρ , ν , and $J = 1$. Use your resulting equation to plot $\frac{m}{m_{x=1}}$ from $x = 1$ to $x = 10$. What does this show is happening in the flow?

10. Consider the velocity given by Eq. 12.31, derived by G.I. Taylor. For this velocity, the momentum is a constant, given by M .

a) Show that M is a constant by integrating for the angular momentum (massless), given by

$$M = 2\pi \int_0^{\infty} v_{\theta} r^2 dr . \text{ Hint, rewrite Eq. 12.31 in terms of } \eta = \frac{r}{\sqrt{\nu t}} .$$

b) Calculate the vorticity for this flow, and plot $\frac{8\pi\nu^2\omega_z}{M}$ vs. r for $0 < r < 8$, at $t = 1, 2$, and 3 .

Let $\nu = 1$.

c) Calculate the circulation, Γ , and plot $\frac{8\nu^2\Gamma}{M}$ vs. r for $0 < r < 8$, at $t = 1, 2$ and 3 . Let $\nu = 1$.

What is the value of Γ when $r \rightarrow \infty$? How do you explain that?

Chapter 13

Introduction to Boundary Layer Theory

Contents

13.1	Motivation	422
13.2	Development of the Boundary Layer Equations	423
13.2.1	An Order of Magnitude Reduction of N-S Equations	426
13.2.2	The Boundary Layer Equations	430
13.3	Solution of the Boundary Layer Equations for a Flat Plate Flow	431
13.4	Boundary Layer Parameters	437
13.4.1	Displacement Thickness, δ^*	437
13.4.2	Momentum Thickness, θ	438
13.4.3	Friction Coefficient, c_f	439
13.5	Boundary Layer Characteristics for a Flat Plate Flow	440
13.5.1	An Example of Boundary Layer Parameters	445
13.6	Falkner-Skan Solutions for Non-Zero Pressure Gradients	446
13.7	Conclusion	455

13.1 Motivation

Almost all practical fluid systems, from water pumps to airplanes, have fluid interacting with solid surfaces. In such real fluid flows, as opposed to “ideal” potential flows, the [“no slip” condition](#) due to the fluid viscosity constrains the fluid to adhere to, and not slip, when in contact with a solid surface. The interaction of a real fluid with a solid surface can also generate vorticity, due to the processes we discussed in sections 11.5 and 11.6. When vorticity is generated, it will diffuse away from the surface, but very slowly in comparison to its rate of transport parallel to the surface. Consequently, the interaction of a fluid with a solid boundary results in the creation of a thin layer of vorticity-bearing fluid adjacent to the solid surface. This thin region provides a transition zone from the no-slip solid boundary to the outer region fluid, where the fluid behaves in a relatively inviscid manner, like a potential flow. This transitional region is correspondingly termed the “boundary layer”, and is the region where fluid shear stresses are dominant. Consequently, we generally think of a real fluid flow in proximity to a solid surface as comprised of a thin, viscously-dominated boundary layer, with an adjoining outer region that behaves in a relatively inviscid manner. While this model is a little oversimplified, this two-region approach is a practical way to model such flows, from which to

seek practical engineering solutions. To familiarize yourself with the physical characteristics of a boundary layer, I recommend you view a video of visualized boundary layers, which can be accessed [here](#). This is a YouTube video of an old educational film (circa 1961), but one that is still quite relevant, showing the development and physical behavior of real boundary layers.

Boundary layers, as we will discuss, are subject to both viscous diffusion and to pressure gradients imposed by the outer-region flow. While viscous diffusion will cause the spread of vorticity, the presence of a pressure gradient will cause the generation of vorticity at an adjacent surface. As discussed in Section 11.5.3, depending on the direction of the pressure gradient (positive or negative), the additional vorticity generated by a pressure gradient can cause the cumulative vorticity comprising the boundary layer to either increase or decrease. For complicated geometries, the generation of vorticity, and the development of boundary layers, can be quite complex and difficult to model mathematically. However, to begin our assessment of boundary layers, we will first confine ourselves to the most elementary type of boundary layer flow—one that develops over a thin flat plate with no pressure gradient. This flow, first assessed by [Prandtl](#), and first solved mathematically by [Blasius](#), is the simplest example of a broad field of fluid mechanics known as [boundary layer theory](#).

In the present chapter, we first examine the development of what are termed the boundary layer equations, and then apply these equations to assess the behavior of the laminar boundary layer for a flat plate flow, both without and with a pressure gradient. In the following Chapter 14, we will illustrate some approximate solution techniques that allow the rapid assessment of more complicated laminar boundary layers with pressure gradients. Later, in Chapter 17, we will address some simple models and solutions for boundary layers when turbulence is present.

It should be recognized that we will only scratch the surface of this very expansive topic of boundary layer theory. We will also only address two-dimensional flows for which semi-analytical solutions are possible. In reality, most practical flows are sufficiently complicated that one must resort to numerical solutions of the complete boundary layer equations. In this text, we will not cover numerical solution techniques, which is a topic unto itself. However, upon completion of the present material, a student should be well prepared to take advanced graduate courses on numerical techniques that should allow one to solve, or at least understand the solution procedures, for more complicated boundary layer flows.

13.2 Development of the Boundary Layer Equations

As shown in the following figure 13.1, we choose the variable delta, δ , to characterize the thickness of the boundary layer. We take this thickness to be the distance away from a solid boundary where the velocity approaches that of the outer region. Since we can envision that the velocity may very slowly asymptote to the outer region streamwise velocity, U_∞ , we arbitrarily designate the boundary layer thickness as that point where $u = 0.99U_\infty$. As we will see, this is

not a particularly good designation, since if we use this criterion to determine the boundary layer thickness from experimental velocity measurements, the result will be highly dependent upon the accuracy of the measurement instrument employed. For example, a $\pm 1\%$ accurate instrument might yield values of δ with $\pm 10\%$ accuracy or worse, depending on how the velocity profile within the boundary layer asymptotes to U_∞ . We will discuss alternative ways to characterize the effects and scale of the boundary layer later in section 13.4.

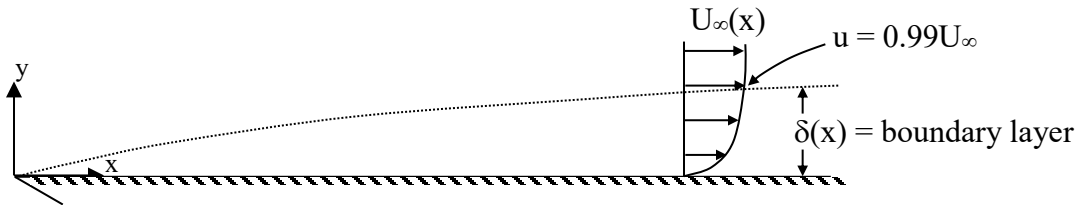


Figure 13.1 A generic model of boundary layer development (not to scale)

As figure 13.1 shows, we consider the thickness of the boundary layer, δ , to grow slowly as a function of the streamwise distance, x , such that $\delta(x) \ll x$. Note that the boundary layer growth in figure 13.1 is exaggerated for illustration purposes. In reality, a boundary layer will generally measure in height less than $1/100^{\text{th}}$ of the streamwise distance from its point of origin. In figure 13.1, we assume that the boundary layer will start at zero thickness at $x = 0$, and grow from that point onward. However, that is not necessarily the case, since δ could have some non-zero initial value, due to vorticity generated on a previous surface. Additionally, we must assume that U_∞ , the velocity of the outer region (generally known as the free stream), may also be a function of the streamwise distance.

Generally, laminar boundary layers are computed using either a combination of analysis and numerical computation, for simple flows, or purely computational techniques for more complicated flows. In contrast, calculation of turbulent boundary layer behavior, because of the tremendous complexity of turbulent flows, is done by employing significant simplifications and substantial numerical computations. As we will discuss in Chapter 17, most practical engineering solutions of turbulent boundary layer characteristics are essentially empirically-derived, requiring significant use of approximations or empirical curve fits. We will discuss the approaches for assessment of turbulent boundary layers later in Chapter 17. Here, we develop the appropriate equations to determine the characteristics of laminar boundary layers.

We first consider a model of the boundary layer, as shown in figure 13.2, which shows the relevant parameters at a point L in the direction of flow over a solid surface.

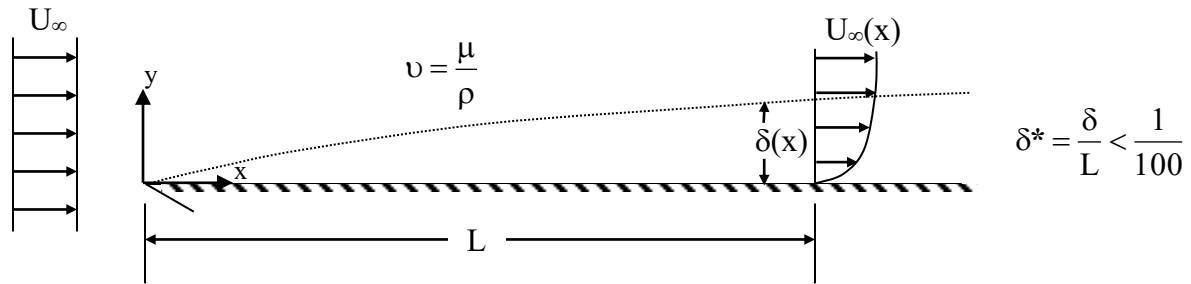


Figure 13.2 A parametric representation of boundary layer growth.

At any given distance along the surface, the relevant parameters are:

- L, the position along the surface;
- U_∞ , the local outer region velocity;
- ν , the kinematic viscosity of the fluid (the ratio of absolute viscosity to density); and
- δ , the local boundary layer thickness.

If we apply a process of [dimensional analysis](#) to this set of parameters, we can determine a set of two non-dimensional parameters:

$$\frac{\delta}{L} \tag{13.1a}$$

and

$$\frac{U_\infty L}{\nu} = \mathbf{Re}_L \quad \text{or} \quad \frac{U_\infty \delta}{\nu} = \mathbf{Re}_\delta \tag{13.1b}$$

The first parameter, Eq.13.1a, is the thickness of the boundary layer relative to the local streamwise position, L (which represents a characteristic dimension of the flow at that point). The second parameter, Eq.13.1b, is a [Reynolds number](#) (after [Osborn Reynolds](#), who first characterized turbulence), which represents the ratio of the local inertia forces to viscous forces. The Reynolds number is based on either the local position or the local boundary layer thickness, depending upon what one chooses as the repeating parameter in the non-dimensionalization process. Using the parameters of Eq. 13.1, we assume a functionality of the form:

$$\frac{\delta}{L} = f\left(\frac{U_\infty L}{\nu}\right) \quad \text{or} \quad \frac{\delta}{L} = f\left(\frac{U_\infty \delta}{\nu}\right) \tag{13.2}$$

Equation 13.2 indicates that the growth and behavior of the boundary layer is dependent upon the magnitude of the local Reynolds number.

Note that we can expand the definition of the Reynolds number, based on the boundary layer thickness, as follows:

$$\mathbf{Re}_\delta = \frac{U_\infty \delta}{\nu} = \frac{U_\infty \delta}{\left(\frac{\mu}{\rho}\right)} = \frac{\rho U_\infty \delta}{\mu} = \frac{\rho U_\infty^2}{\mu \left(\frac{U_\infty}{\delta}\right)} \approx \frac{\rho u^2}{\mu \frac{\partial u}{\partial y}} = \frac{\text{inertia forces}}{\text{viscous forces}} \quad (13.3)$$

As Eq. 13.3 illustrates, the Reynolds number represents the relative magnitude of inertia forces within the boundary layer to the comparable viscous forces (i.e. shear stresses). As we will see, when the Reynolds number is quite large this allows us to simplify the governing equations significantly, and makes the computation of boundary layers more tractable (although the solution of the resulting equations still requires the use of sophisticated analytical and numerical procedures).

13.2.1 An Order of Magnitude Reduction of the N-S Equations

To begin our assessment of the governing equations, we model the flow situation as shown in figure 13.2, and use this model to appropriately non-dimensionalize the Navier-Stokes equations. We then simplify the equations using an order-of-magnitude assessment; this lets us establish which terms within the governing equations can be considered negligible or at least very small relative to the dominant terms, and thus to a good approximation can be neglected.

Note that the terms comprising the governing equations will be non-dimensionalized and

compared relative to the non-dimensional boundary layer thickness, $\delta^* = \frac{\delta}{L}$, which we pointed out is of the order (size) of 1/100. Using this scaling on δ^* allows us to establish the order of magnitude of each term within the equations (i.e. how dominant each term is). This order of magnitude hierarchy is given by:

$$\delta^* \ll 1 \ll \frac{1}{\delta^*}, \text{ etc.}$$

We begin the non-dimensionalization process by defining the following non-dimensional ratios,

$$x^* = \frac{x}{L}, \quad y^* = \frac{y}{L}, \quad u^* = \frac{u}{U_\infty}, \quad v^* = \frac{v}{U_\infty}, \quad P^* = \frac{P}{\rho U_\infty^2} \quad (13.4)$$

as our non-dimensional variables. Considering our model of the boundary layer in figure 13.2, we use physical reasoning to establish the order (size) of the dimensionless variables in Eq.13.4 as:

$$x^* = 0(1), \quad y^* = 0(\delta^*), \quad u^* = 0(1), \quad v^* = 0(\delta^*), \quad P^* = 0(1) \quad (13.5)$$

Here, 0(1) means a variable is, or could be, a dominant variable, and 0(δ^*) indicates a variable which is an order of magnitude less dominant (roughly 100 times smaller). The rationale for this

ordering is that large changes can take place in the streamwise (x) direction and the (u) velocity component, whereas much smaller changes take place in the normal (y) direction and (v) velocity component. Since the pressure may or may not change significantly, we assume that pressure could be a potentially dominant term of $O(1)$.

The starting governing equations are the continuity and the steady-state Navier-Stokes equations in two dimensions (Note that the same process is also applied for the more complicated, three-dimensional case), which for an incompressible flow are:

$$\frac{\partial u}{\partial x} + \frac{\partial v}{\partial y} = 0 \quad \text{continuity} \quad (13.6a)$$

$$u \frac{\partial u}{\partial x} + v \frac{\partial u}{\partial y} = -\frac{1}{\rho} \frac{\partial P}{\partial x} + \nu \left(\frac{\partial^2 u}{\partial x^2} + \frac{\partial^2 u}{\partial y^2} \right) \quad \text{x-direction N.S.} \quad (13.6b)$$

$$u \frac{\partial v}{\partial x} + v \frac{\partial v}{\partial y} = -\frac{1}{\rho} \frac{\partial P}{\partial y} + \nu \left(\frac{\partial^2 v}{\partial x^2} + \frac{\partial^2 v}{\partial y^2} \right) \quad \text{y-direction N.S.} \quad (13.6c)$$

To see how this order of magnitude analysis works, consider the continuity equation, Eq. 13.6a. Using the definitions in Eq. 13.4, we can write:

$$x = Lx^*, \quad y = Ly^*, \quad u = U_\infty u^*, \quad v = U_\infty v^* \quad (13.7)$$

Substituting the variables in Eq. 13.7 into Eq. 13.6a and simplifying, we have:

$$\frac{\partial u}{\partial x} + \frac{\partial v}{\partial y} = \frac{U_\infty \partial u^*}{L \partial x^*} + \frac{U_\infty \partial v^*}{L \partial y^*} = \frac{\partial u^*}{\partial x^*} + \frac{\partial v^*}{\partial y^*} = 0 \quad (13.8)$$

Now, assessing the order of magnitude of each term in Eq. 13.8, using the relative magnitudes of each variable that were assumed in Eq. 13.5 (we assign the magnitude of each term as the ratio of the magnitude of the variables comprising the derivative), we have:

$$\frac{\partial u^*}{\partial x^*} + \frac{\partial v^*}{\partial y^*} = 0 \quad (13.9)$$

$$\frac{O(1)}{O(1)} + \frac{O(\delta^*)}{O(\delta^*)} = O(1) + O(1)$$

The order of magnitude assessment of Eq. 13.9 indicates that both terms in the continuity equation can be of comparable magnitude, and thus both must be retained. At first this may seem a bit strange, since both the v^* and y^* terms are small. However, the ratio of these terms indicates that while the values of v^* and y^* may be small, the *ratio of the changes* could be comparable to the ratio of the streamwise changes. This is logical, since for two-dimensional incompressible flow any changes in the velocity in one dimension must be balanced by

comparable changes in the velocity in the other dimension. As we will see in the following assessment of the Navier-Stokes equation, all terms in the Navier-Stokes equations are not comparable, which allows us to neglect selected terms as essentially non-contributory.

Next, we non-dimensionalize the x-direction Navier-Stokes equation, Eq.13.6b. For example, since $u = U_\infty u^*$ and $x = Lx^*$, then for the first term of Eq.13.6b we can write,

$$u \frac{\partial u}{\partial x} = (U_\infty u^*) \frac{U_\infty}{L} \frac{\partial u^*}{\partial x^*} = \left(\frac{U_\infty^2}{L} \right) \left(u^* \frac{\partial u^*}{\partial x^*} \right)$$

Performing similar non-dimensionalization of each term of Eq. 13.6b, and substituting those back into Eq.13.6b yields:

$$\left(\frac{U_\infty^2}{L} \right) u^* \frac{\partial u^*}{\partial x^*} + \left(\frac{U_\infty^2}{L} \right) v^* \frac{\partial u^*}{\partial y^*} = - \left(\frac{U_\infty^2}{L} \right) \frac{\partial P^*}{\partial x^*} + \left(\frac{U_\infty}{L^2} \right) \nu \left(\frac{\partial^2 u^*}{\partial x^{*2}} + \frac{\partial^2 u^*}{\partial y^{*2}} \right)$$

Dividing through by $\left(\frac{U_\infty^2}{L} \right)$, and simplifying yields:

$$u^* \frac{\partial u^*}{\partial x^*} + v^* \frac{\partial u^*}{\partial y^*} = - \frac{\partial P^*}{\partial x^*} + \frac{1}{\mathbf{Re}} \left(\frac{\partial^2 u^*}{\partial x^{*2}} + \frac{\partial^2 u^*}{\partial y^{*2}} \right) \quad \text{where } \mathbf{Re} = \frac{U_\infty L}{\nu} \quad (13.10)$$

Applying an order of magnitude analysis to Eq. 13.10 using Eq. 13.5 yields:

$$\underbrace{0(1) \frac{0(1)}{0(1)} + 0(\delta^*) \frac{0(1)}{0(\delta^*)}}_{\text{Both terms } 0(1)} = \frac{0(1)}{0(1)} + 0(?) \left(\frac{0(1)}{0(1)^2} + \frac{0(1)}{0(\delta^{*2})} \right) \Rightarrow \frac{1}{\mathbf{Re}} \left(\frac{\partial^2 u^*}{\partial y^{*2}} \right)$$

neglect relative to ↑ 0(1) also \Rightarrow $\mathbf{Re} \Rightarrow 0\left(\frac{1}{\delta^{*2}}\right)$

Must be because viscous terms can't be zero!

On the right side of Eq. 13.10, our order of magnitude analysis indicates that the two derivative terms arising from the viscous shear are of $0(1)$ and $0(1/\delta^{*2})$. Now, since $\delta^* \ll 1$, this means that $0(1) \ll 0(1/\delta^{*2})$, and we can effectively neglect the $\frac{\partial^2 u^*}{\partial x^{*2}}$ term relative to the $\frac{\partial^2 u^*}{\partial y^{*2}}$ term. Note

that we do not initially know the order of the reduced term, $\frac{1}{\mathbf{Re}} \left(\frac{\partial^2 u^*}{\partial y^{*2}} \right)$, relative to the other

terms in the equation. However, we reason that the viscous term must play an important role in the development of the boundary layer (it cannot be negligible, or we would have basically an inviscid flow). Thus, we further reason that the right-hand viscous term must be of $0(1)$, or of

the same magnitude as the momentum terms on the left-hand side of Eq. 13.10. In order for this to be the case, requires that the Reynolds number of the flow must be very large, or $Re_L \Rightarrow$

$0\left(\frac{1}{\delta^{*2}}\right)$. That the Reynolds number must be large was one of the key assumptions made by

[Prandtl](#), who derived the original boundary layer equations. Thus, neglecting the $\frac{\partial^2 \mathbf{u}}{\partial x^2}$ term, the x-direction Navier-Stokes equation reduces to:

$$u \frac{\partial u}{\partial x} + v \frac{\partial u}{\partial y} = -\frac{1}{\rho} \frac{\partial P}{\partial x} + \nu \left(\frac{\partial^2 u}{\partial y^2} \right) \quad (13.11)$$

Now, non-dimensionalizing the y-direction N-S equation, Eq. 13.6c, and assessing the order of magnitude of the terms gives:

$$u^* \frac{\partial v^*}{\partial x^*} + v^* \frac{\partial v^*}{\partial y^*} = -\frac{\partial P^*}{\partial y^*} + \frac{1}{Re} \left(\frac{\partial^2 v^*}{\partial x^{*2}} + \frac{\partial^2 v^*}{\partial y^{*2}} \right) \quad (13.12)$$

$$\underbrace{0(1) \frac{0(\delta^*)}{0(1)} + 0(\delta^*) \frac{0(\delta^*)}{0(\delta^*)} = \frac{0(?)}{0(\delta^*)} + 0(\delta^{*2}) \left(\frac{0(\delta^*)}{0(1)^2} + \frac{0(\delta^*)}{0(\delta^{*2})} \right)}_{\text{All } 0(\delta^*) \text{ or less}}$$

All $0(\delta^*)$ or less

Our order of magnitude analysis indicates that all terms in Eq. 13.12 must be of $0(\delta^*)$ or less, with the possible exception of the pressure term. This is particularly interesting, since it implies that all the inertia and viscous terms in the y-direction Eq. 13.12 are much, much smaller than any of the terms (except the $\frac{\partial^2 \mathbf{u}}{\partial x^2}$ term) in the x-direction Eq. 13.10. This suggests that we can neglect *all* the terms in Eq. 13.12 relative to the terms in Eq. 13.10. But this also means that the y-direction pressure gradient term, $\frac{\partial P^*}{\partial y^*}$, must also be of order $0(\delta^*)$ as well (since it must be in balance with all the other terms of Eq. 13.12).

Comparison of the order of magnitude results for Eq. 13.10 to Eq. 13.12 indicates that

$\frac{\partial P^*}{\partial y^*} \Rightarrow 0(\delta^*)$ relative to $\frac{\partial P^*}{\partial x^*} \Rightarrow 0(1)$. Thus, to a good approximation we can say that at any

streamwise location the pressure change across the boundary layer is essentially negligible, or $P \cong P(x)$. This means that the pressure at the edge of the boundary layer *is impressed across the boundary* (i.e. the pressure within the boundary layer must be $P(x)$, the pressure at the interface of the boundary layer with the outer region flow).

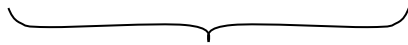
13.2.2 The Boundary Layer Equations

Since all the terms comprising the y-direction equation are of $O(\delta^*)$ or less, this means that to a good approximation we need only consider the solution of the reduced *x-direction boundary layer equation* (Eq.13.11) and *the continuity equation* (Eq.13.9) in order to determine a mathematical solution for the velocity field. Thus, the governing equations for a two-dimensional boundary layer are:

$$u \frac{\partial u}{\partial x} + v \frac{\partial u}{\partial y} = -\frac{1}{\rho} \frac{\partial P}{\partial x} + \nu \frac{\partial^2 u}{\partial y^2} \tag{13.13a}$$

and

$$\frac{\partial u}{\partial x} + \frac{\partial v}{\partial y} = 0 \tag{13.13b}$$



The Two-Dimensional
Boundary Layer Equations

Note that Eqs.13.13 require specification of four boundary conditions to allow a complete solution: Three for u (two on y , and one on x), and one for v (one on y). These are respectively (see figure 13.3):

- Boundary Conditions:
- 1) $u = 0$ @ $y = 0$
 - 2) $v = 0$ @ $y = 0$
 - 3) $u = U_\infty(x)$ @ $y \rightarrow \infty$ or δ
 - 4) $u = u(y)$ @ $x = 0$

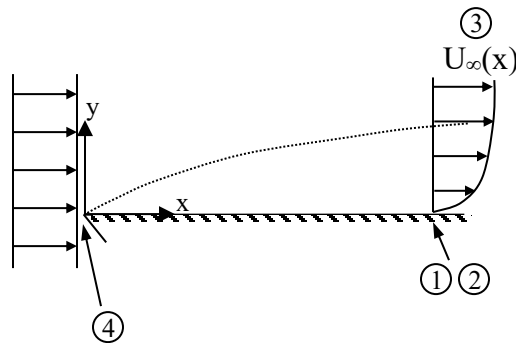


Figure 13.3 Locations of the four boundary conditions required for solution of the boundary layer equations.

Note that the boundary layer equations are parabolic. This means that the fluid can only evolve based on the imposed boundary conditions as it moves downstream, and is not influenced by *downstream* conditions (similar to a rock falling toward the ground; the rock doesn't know the

ground is approaching until it hits). Here, the only way that the downstream geometry can affect the boundary layer development is through changes in the external pressure gradient, which *will* change with geometric conditions.

Now that we have derived the governing boundary layer equations, these can be solved exactly for a few cases (the solutions, however, are not exactly simple). In addition, we can obtain some approximate solutions for other cases (we will discuss how this is done in Chapter 14). Additionally, the boundary layer equations can be solved numerically, using relatively standard numerical integration techniques. However, one caveat on numerical solutions is that under extreme changes in geometry, and thus pressure gradient behavior, the assumptions that were invoked in the order of magnitude analysis may break down (e.g. that $v^* = O(\delta^*)$), which requires that one revert to the solution of the full Navier-Stokes solution, which makes solution procedures much more complicated.

13.3 Solution of the Boundary Layer Equations for a Flat Plate Flow

Let's now use the boundary layer equations (Eqs. 13.13) to examine the simplest flow application: a steady, laminar flow over a flat plate with a uniform approach flow (i.e. $U_\infty = \text{constant}$) to the plate. This is essentially the type of flow shown in figure 13.3.

To establish the pressure gradient for this flow, we employ the Bernoulli equation for an inviscid flow, and apply it to the flow just outside of the boundary layer. We assume this external flow will be uniform (the flows outside the boundary layer are generally relatively uniform, and thus behave basically like an inviscid flow). Applying the Bernoulli equation, we have $P + \frac{1}{2}\rho U_\infty^2 = \text{constant}$ along a streamline external to the boundary layer. If we differentiate this equation with respect to x , we get:

$$\frac{dP}{dx} + \rho U_\infty \frac{dU_\infty}{dx} = 0 \Rightarrow \frac{dP}{dx} = 0 \quad (13.14)$$

Since $U_\infty = \text{constant}$, there is no pressure gradient along the flat plate. Thus, substituting Eq. 13.14 into Eq. 13.13a eliminates the pressure gradient term, such that the boundary layer equations for this flat plate flow become:

$$u \frac{\partial u}{\partial x} + v \frac{\partial u}{\partial y} = \nu \frac{\partial^2 u}{\partial y^2} \quad (13.15a)$$

And

$$\frac{\partial u}{\partial x} + \frac{\partial v}{\partial y} = 0 \quad (13.15b)$$

With the corresponding boundary conditions:

$$\begin{array}{lll}
 @ y = 0 & @ y \rightarrow \infty & @ x = 0 \\
 \mathbf{u} = \mathbf{0} & \mathbf{u} = U_\infty & \mathbf{u} = U_\infty \\
 \mathbf{v} = 0 & &
 \end{array} \quad (13.16)$$

Since we have no characteristic dimension for this flow, we will assume a similarity-type solution (like that we explored in Chapter 12), with δ assumed as a similarity (i.e. “stretching”) variable that scales all the boundary layer velocity profiles along the plate, or:

$$\text{i.e.} \quad \frac{\mathbf{u}}{U_\infty} = f\left(\frac{y}{\delta}\right)$$

Using physical reasoning, we assume that δ will be a function of (i.e. depends on) the free stream velocity, U_∞ , the distance along the plate, x , and the kinematic viscosity, ν :

$$\text{i.e.} \quad \delta = f(U_\infty, x, \nu)$$

Applying dimensional analysis, we can show that an appropriate functional relationship should be:

$$\frac{\delta}{x} = f\left(\frac{U_\infty x}{\nu}\right)$$

[Blasius](#) showed that the appropriate dimensional relationship that preserves dimensional correctness, and appropriately reduces the Eqs.13.15 is:

$$\delta \propto \sqrt{\frac{\nu x}{U_\infty}}$$

To scale changes in the y direction on changes in δ , we define a similarity variable, η , where:

$$\eta \propto \frac{y}{\delta}, \text{ so we let } \eta = y \sqrt{\frac{U_\infty}{\nu x}} \quad (13.17)$$

This gives a velocity function of the form:

$$\frac{\mathbf{u}}{U_\infty} = f(\eta) \quad (13.18)$$

However, before we can apply our similarity variable, we must reduce the two partial differential boundary layer equations to one partial differential equation. To do this, we make use of the stream function, like we did in section 12.5 for the laminar wall jet. Why? Remember that the stream function is already an exact solution of the continuity equation, and that the 2-D velocity components (in the Cartesian system) that satisfy continuity are given by:

$$u = \frac{\partial \psi}{\partial y} \quad \text{and} \quad v = -\frac{\partial \psi}{\partial x} \tag{13.19}$$

Substituting the functional relations of Eq.13.19 into the boundary layer equations of Eqs.13.15 gives:

$$\frac{\partial \psi}{\partial y} \frac{\partial^2 \psi}{\partial x \partial y} - \frac{\partial \psi}{\partial x} \frac{\partial^2 \psi}{\partial y^2} = \nu \frac{\partial^3 \psi}{\partial y^3} \quad \text{x-direction momentum} \tag{13.20a}$$

and

$$\frac{\partial^2 \psi}{\partial x \partial y} - \frac{\partial^2 \psi}{\partial y \partial x} = 0 \quad \text{continuity} \tag{13.20b}$$

Thus, Eq.13.20b is satisfied exactly, leaving us with only Eq.13.20a, which is a non-linear, partial differential equation for only *one dependent variable* (ψ), rather than u and v in the original Eqs.13.15.

While we now must solve only Eq.13.20a, the equation is a bit daunting since we have raised the order of the equation from second order to third order. To obtain a similarity solution that will reduce Eq.13.20a to an ordinary differential equation, we must relate our dependent variable in Eq.13.20a, ψ , to the velocity function, $f(\eta)$, and thus the similarity variable, η , from Eq.13.17

and 13.18. To do this, we note from Eq.13.19 that $u = \frac{\partial \psi}{\partial y}$. We use this relationship to

integrate the stream function with respect to y at a fixed streamwise (x) location, i.e.:

$$d\psi_{x=\text{fixed}} = \frac{\partial \psi}{\partial x} dx + \frac{\partial \psi}{\partial y} dy = u dy \Big|_{x=\text{fixed}} \Rightarrow \psi - \psi_0 = \int_0^y u dy \tag{13.21}$$

0
Set = 0

Equation 13.21 represents the planar volumetric flow rate of fluid over the indefinite region between the surface ($y = 0$) and an indefinite height y . Substituting 13.18 into Eq. 13.21 and utilizing Eq. 13.17, we obtain:

$$\psi = \int_0^y u dy = \int_0^y U_\infty f(\eta) dy = \int_0^\eta U_\infty f(\eta) \sqrt{\frac{\nu x}{U_\infty}} d\eta \quad (\text{note that } \int_0^y u dy \text{ reflects the planar flow rate})$$

or

$$\psi = \sqrt{U_\infty \nu x} \underbrace{\int_0^\eta f(\eta) d\eta}_{\text{Define this integral as } F(\eta)} = \sqrt{U_\infty \nu x} F(\eta) \quad \text{where} \quad \eta = y \sqrt{\frac{U_\infty}{\nu x}} \tag{13.22}$$

Note that in Eq. 13.22 we set the integral of $f(\eta)$ equal to $F(\eta)$, which is just another indefinite function of η , since η is an indefinite integration limit.

Now, using the expression for ψ from Eq. 13.22, we determine the respective terms in Eq. 13.20a, and substitute these to obtain an *ordinary differential equation* for $F(\eta)$

$$\text{e.g. } \frac{\partial \psi}{\partial x} = \frac{1}{2} \sqrt{\frac{U_\infty \nu}{x}} F + \sqrt{U_\infty \nu x} F' \frac{\partial \eta}{\partial x} \quad \frac{\partial \eta}{\partial x} = -\frac{1}{2} y \sqrt{\frac{U_\infty}{\nu x}} \frac{1}{x} = -\frac{\eta}{2x}$$

and thus,

$$\frac{\partial \psi}{\partial x} = \frac{1}{2} \sqrt{\frac{U_\infty \nu}{x}} (F - \eta F') = -v$$

Likewise, we obtain:

$$\frac{\partial \psi}{\partial y} = U_\infty F' = u \quad \frac{\partial^2 \psi}{\partial y^2} = U_\infty \sqrt{\frac{U_\infty}{\nu x}} F'' = \partial u / \partial y \quad \frac{\partial^3 \psi}{\partial y^3} = \frac{U_\infty^2}{\nu x} F''' = \partial^2 u / \partial y^2$$

and

$$\frac{\partial^2 \psi}{\partial x \partial y} = \frac{\partial}{\partial x} \left(\frac{\partial \psi}{\partial y} \right) = \frac{\partial}{\partial x} (U_\infty F') = U_\infty F'' \frac{\partial \eta}{\partial x} = U_\infty F'' \left(-\frac{\eta}{2x} \right) = -\frac{U_\infty}{2x} \eta F'' = \partial u / \partial x$$

Substituting these relationships into Eq. 13.21a,

$$\frac{\partial \psi}{\partial y} \frac{\partial^2 \psi}{\partial x \partial y} - \frac{\partial \psi}{\partial x} \frac{\partial^2 \psi}{\partial y^2} = \nu \frac{\partial^3 \psi}{\partial y^3}$$

gives,

$$(U_\infty F') \left(-\frac{U_\infty}{2x} \eta F'' \right) - \left[\frac{1}{2} \left(\frac{U_\infty \nu}{x} \right)^{1/2} (F - \eta F') \right] \left[U_\infty \left(\frac{U_\infty}{\nu x} \right)^{1/2} F'' \right] = \cancel{\nu} \frac{U_\infty^2}{\cancel{\nu x}} F''' ,$$

or

$$-\cancel{\frac{U_\infty^2}{2x}} \eta F'' F' - \frac{1}{2} \frac{U_\infty^2}{x} F'' F + \cancel{\frac{U_\infty^2}{2x}} \eta F'' F' = \frac{U_\infty^2}{x} F''' ,$$

which simplifies to what is known as the Blasius boundary layer equation:

$$F''' + \frac{1}{2} F F'' = 0 \quad (13.23)$$

Now, since $u = \frac{\partial \psi}{\partial y} = U_\infty F'$, $v = -\frac{\partial \psi}{\partial x} = \frac{1}{2} \left(\frac{U_\infty \nu}{x} \right)^{1/2} (\eta F' - F)$, and $\eta = y \sqrt{\frac{U_\infty}{\nu x}}$,

we can derive the boundary conditions for F that apply for the [Blasius equation](#) as follows:

$$\begin{array}{llll}
 y=0: & u=0 & \Rightarrow & \eta=0: & F'=0 \\
 & v=0 & \Rightarrow & \eta=0: & F=0 \\
 y \rightarrow \infty: & u=U_\infty & \Rightarrow & \eta \rightarrow \infty: & F'=1 \\
 x=0: & u=U_\infty & \Rightarrow & \eta \rightarrow \infty: & F'=1
 \end{array}
 \left. \vphantom{\begin{array}{llll} y=0: & u=0 & \Rightarrow & \eta=0: & F'=0 \\ & v=0 & \Rightarrow & \eta=0: & F=0 \\ y \rightarrow \infty: & u=U_\infty & \Rightarrow & \eta \rightarrow \infty: & F'=1 \\ x=0: & u=U_\infty & \Rightarrow & \eta \rightarrow \infty: & F'=1 \end{array}} \right\} \begin{array}{l} 3 \text{ B.C.} \\ \text{same} \end{array}$$

Table 13.1: Blasius table for F, F' and F'' vs. η

η	F	F'	F''
0	0.0000	0.0000	0.3321
0.2	0.0066	0.0664	0.3320
0.4	0.0266	0.1328	0.3315
0.6	0.0597	0.1989	0.3301
0.8	0.1061	0.2647	0.3274
1	0.1656	0.3298	0.3230
1.2	0.2380	0.3938	0.3166
1.4	0.3230	0.4563	0.3079
1.6	0.4203	0.5168	0.2967
1.8	0.5295	0.5748	0.2829
2	0.6500	0.6298	0.2668
2.2	0.7812	0.6813	0.2484
2.4	0.9223	0.7290	0.2281
2.6	1.0725	0.7725	0.2065
2.8	1.2310	0.8115	0.1840
3	1.3968	0.8461	0.1614
4	2.3058	0.9555	0.0642
5	3.2833	0.9916	0.0159
6	4.2797	0.9990	0.0024
7	5.2793	0.9999	0.0002
8	6.2793	1.0000	0.0000
9	7.2793	1.0000	0.0000

Note that the last two of the four boundary conditions for u and v in x and y reduce to one common bounding condition for F' with respect to η. Thus, we reduce the third order P.D.E. with four boundary conditions for ψ(x,y) to a third order O.D.E. for F(η) with three boundary conditions. Equation 13.23 is non-linear, and without a closed form solution. The solution of this equation is obtained using standard numerical solution techniques, generally a [Runge-Kutta](#) numerical technique. I chose to solve the equation using the MATLAB function bvp4C, which works quite quickly. The result is a set of tabulated data for F, F', and F'' , as shown in Table 13.1.

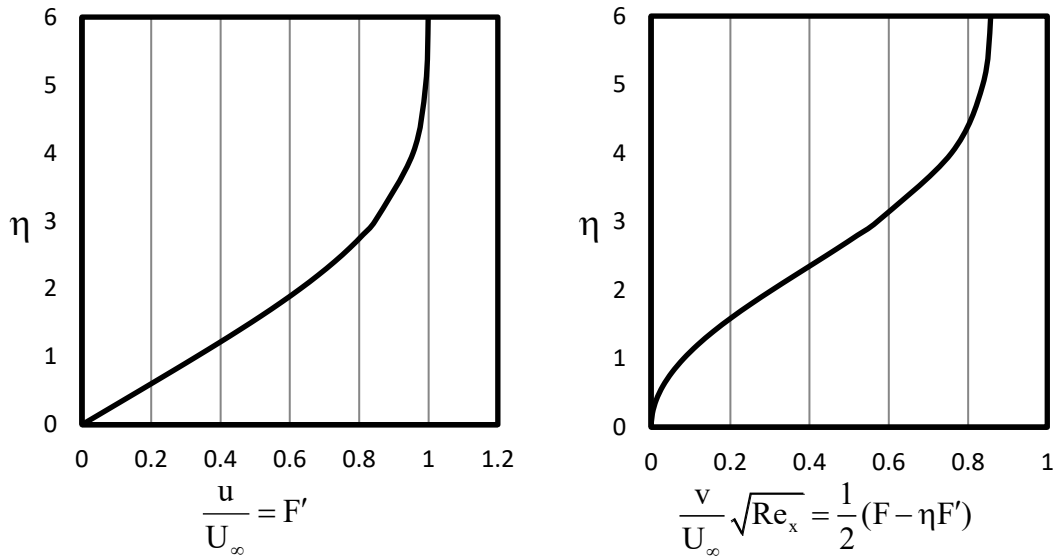


Figure 13.4 The behavior of the velocity components u and v within a Blasius flat plate boundary layer, as a function of $\eta = y \sqrt{\frac{U_\infty}{\nu x}}$.

Figure 13.4 shows the shape of the respective u and v velocity profiles, non-dimensionalized appropriately, as a function of η . Some key observations from the results of table 13.1 and figure 13.4 are as follows.

For the Blasius velocity components, note that:

$$\frac{\partial u}{\partial \eta} = U_\infty F''(0) = \text{constant}$$

$$\frac{\partial^2 u}{\partial \eta^2} = U_\infty F'''(0) = ? = -\frac{1}{2} F(0)F''(0) = 0$$

∴ this indicates an inflection point occurs at the surface (this means the velocity profile is just stable)

From Eq. 13.23

$$F''' + \frac{1}{2} FF'' = 0$$

$$@ \quad \eta \rightarrow \infty \Rightarrow \frac{v_\infty}{U_\infty} = \frac{0.865}{\sqrt{\text{Re}_x}}$$

$$\text{For } \text{Re}_x = 10^4 \Rightarrow \frac{v_\infty}{U_\infty} = 0.00865 \approx \frac{1}{100}$$

Satisfies assumption employed in simplifying the boundary layer equations. i.e. that $u \gg v$

Since $\frac{\partial^2 u}{\partial \eta^2} = 0$ at $\eta = 0$, the streamwise velocity profile is inflectional at the solid surface, which makes the profile barely stable. As we will discuss in Chapter 17, destabilization of a laminar boundary layer leads to transition from a well-behaved laminar flow (i.e. that moves in laminas, or layers) to a much more chaotically mixed flow, which is termed turbulence. Additionally, the above result shows that for a Reynolds number of 10^4 , the normal velocity, v , at the edge of the boundary layer and beyond is on the order of $1/100$ of the magnitude of the mean outer flow. This supports our previous assumption in Section 13.2 that streamwise velocity changes are the

only significant velocity changes within the boundary layer. Clearly, for larger Reynolds numbers, this v_∞/U_∞ ratio will be even smaller. However, at lower Reynolds numbers the terms we neglected in Eqs. 13.6 will play a more significant role, requiring the solution of the entire Navier-Stokes equation. The good news is that the region within which a full Navier-Stokes solution is warranted is confined to very near the initiation of the boundary layer, and neglecting this region has a minimal effect on our Blasius solution. For example, for water flow over a flat plate at 1 m/s, a Reynolds number of 10^4 will be reached after only 1 cm.

13.4 Boundary Layer Parameters

As we pointed out in section 13.2, the boundary layer thickness, δ , which characterizes the thickness of the boundary layer, is a rather arbitrary parameter. It is defined as the location above the surface where the velocity reaches 99% of the free stream velocity, which may be difficult to establish with precision. We now examine several parameters that can be derived based on more physical properties, and can more reliably characterize the physical characteristics of the boundary layer.

13.4.1 Displacement Thickness, δ^*

The displacement thickness, illustrated in figure 13.5, represents an imaginary displacement of fluid from the surface to account for the mass flow “lost” by the formation of the boundary layer, when compared to the mass flow that would exist without the boundary layer present (i.e. if the flow all the way to the boundary moved uniformly at the free stream velocity, U_∞).

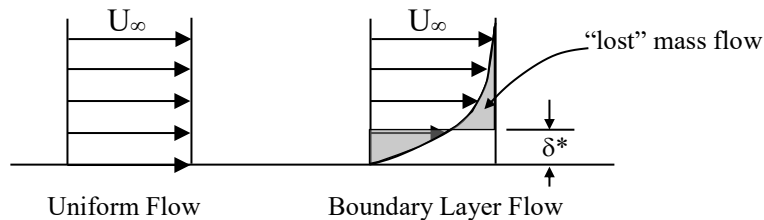


Figure 13.5 The characterization of the displacement thickness as the lost mass displaced from the surface by a distance δ^* , modeled as the displacement of a flow of uniform outer region velocity from the surface by a thickness δ^* .

To establish an equation for the displacement thickness, we use our model in figure 13.5 and equate the mass flow within the actual boundary layer to an equivalent, displaced mass moving at U_∞ as:

$$\begin{aligned}
 \dot{m}_{\text{tot}} &= \underbrace{\int_0^\infty \rho u dy}_{\text{Total flowrate within boundary layer}} = \underbrace{\int_{\delta^*}^\infty \rho U_\infty dy}_{\text{Equivalent flowrate within a displaced uniform flow}} = \int_0^\infty \rho U_\infty dy - \underbrace{\int_0^{\delta^*} \rho U_\infty dy}_{-\rho U_\infty \delta^*}
 \end{aligned}
 \tag{13.24}$$

Reorganizing Eq. 13.24 gives:

$$\rho U_\infty \delta^* = \int_0^\infty \rho U_\infty dy - \int_0^\infty \rho u dy$$

and solving for δ^* gives:

$$\delta^* = \int_0^\infty \left(1 - \frac{u}{U_\infty} \right) dy \quad \text{for } \rho = \text{constant} \quad (13.25)$$

Note that Eq. 13.25 is a very reliable measure of the degree to which the outer flow is "displaced" from the proximity of the bounding surface. In practice, such a displacement will make the effective geometry of the solid boundary appear slightly "thicker" to the outer flow, which results in a modification of the outer flow field, and consequently the associated pressure gradient. Comprehensive solution techniques generally take this boundary layer displacement into account by using an iterative procedure to converge on a combined boundary layer and outer region solution.

13.4.2 Momentum Thickness, θ

Another useful physical characterization of the boundary layer is termed the momentum thickness. The momentum thickness is a hypothetical displacement of fluid of uniform velocity, U_∞ , away from a bounding surface to account for the momentum "lost" due to the formation of the boundary layer velocity profile (and dissipated by the action of the applied shear stress). Figure 13.6 illustrates this hypothetical displacement of momentum, θ .

To establish an equation to calculate the momentum thickness, we multiply the momentum flux of a uniform flow by the lost momentum "thickness," represented by θ . We then equate this lost momentum to the difference between the maximum possible momentum (reflected by U_∞) that

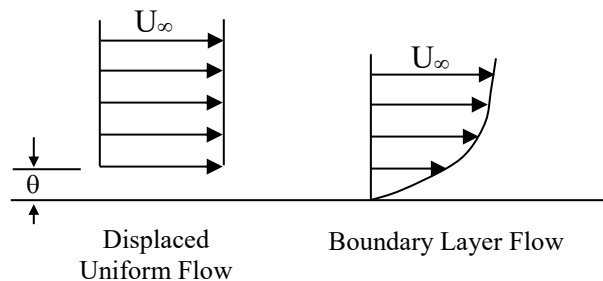


Figure 13.6 The characterization of the momentum thickness, θ , as a thickness of fluid moving at the uniform outer region velocity, U_∞ , that would have to be removed to account for the momentum "lost" due to the formation of the boundary layer.

could be carried by the actual boundary layer mass flow, *less* the actual momentum within the boundary layer, i.e.:

$$\rho U_\infty^2 \theta = \underbrace{\int_0^\infty (\rho u dy) U_\infty}_{\text{Possible Momentum}} - \underbrace{\int_0^\infty (\rho u dy) u}_{\text{Actual Momentum}} \tag{13.26}$$

Hypothetical Thickness of “Lost” Momentum
“Lost” Momentum

Solving Eq. 13.26 for θ , and assuming an incompressible flow, we have:

$$\theta = \int_0^\infty \frac{u}{U_\infty} \left(1 - \frac{u}{U_\infty} \right) dy \tag{13.27}$$

As we will see, because the momentum thickness reflects the momentum “lost” by the formation of the boundary layer due to viscous effects, it is directly related to the shear stress and the cumulative shear forces (i.e. drag) exerted by the fluid on a solid boundary.

13.4.3 Friction Coefficient, c_f

The friction coefficient is a convenient, non-dimensional parameter reflecting the *shear stress* at the surface divided by the *dynamic pressure equivalent* of the free stream flow outside the boundary layer, defined as:

$$c_f = \frac{\tau_{\text{wall}}}{\frac{1}{2} \rho U_\infty^2} = \frac{\mu \left. \frac{du}{dy} \right|_{y=0}}{\frac{1}{2} \rho U_\infty^2} \tag{13.28}$$

The friction coefficient characterizes the non-dimensional shear stress acting on the bounding wall at a specified location along the wall, and as such allows the determination of engineering shear stress data for any similar laminar flow, regardless of the flow conditions. As we will see, for a flat plate flow this coefficient is only a function of the local Reynolds number, $\mathbf{Re}_x = \frac{U_\infty x}{\nu}$, which allows effective analytical and empirical engineering correlations to be developed where $c_f = f(\mathbf{Re}_x)$. As we will discuss in Chapter 17, this functional dependence of c_f on Reynolds number also applies to turbulent flows.

13.5 Boundary Layer Characteristics for a Flat Plate Flow

Using our solution for the velocity behavior that we developed in section 13.3, we can now assess the various boundary layer properties for a laminar, flat plate flow. Examining Table 13.1, we note that $u/U_\infty \cong 0.99$ when $\eta \approx 5$, so we choose $\eta = 5$ as the hypothetical edge of the boundary layer, in similarity units. Thus, letting $y = \delta$ and $\eta = 5$ in Eq. 13.17, we obtain:

$$\begin{aligned} @ \eta = 5, \quad \frac{u}{U_\infty} = F'(5) = 0.992 &\Rightarrow \delta @ \eta = 5 \Rightarrow \delta \sqrt{\frac{U_\infty}{\nu x}} = \frac{\delta}{x} \sqrt{U_\infty x} = \frac{\delta}{x} \sqrt{\text{Re}_x} = 5 \\ \therefore \frac{\delta}{x} &\cong \frac{5}{\sqrt{\text{Re}_x}} \end{aligned} \quad (13.29)$$

Note that Eq.13.29 indicates that the ratio of the boundary layer to its streamwise location is only a function of the local Reynolds number. The use of the approximately equal symbol (\cong) in Eq.13.29 reflects the arbitrary selection of $u/U_\infty \cong 0.99$ as the edge of the boundary layer, although Eq.13.29 is generally taken as a hard value in practice.

To solve for the displacement thickness, we use Eq.13.17 to allow the integration of Eq.13.25 as a function of η (at a fixed x location):

$$\delta^* = \int_0^\delta \left(1 - \frac{u}{U_\infty}\right) dy \quad \text{note: } \eta = y \sqrt{\frac{U_\infty}{\nu x}} \Rightarrow d\eta = dy \sqrt{\frac{U_\infty}{\nu x}} \Rightarrow dy = d\eta \sqrt{\frac{\nu x}{U_\infty}}$$

Substituting for dy , $u = U_\infty F'$, integrating from $0 \leq \eta \leq 5$, and determining F from Table 13.1 gives:

$$\begin{aligned} \delta^* &= \int_0^{\eta=5} \left(1 - \frac{u}{U_\infty}\right) \sqrt{\frac{\nu x}{U_\infty}} d\eta = \sqrt{\frac{\nu x}{U_\infty}} \int_0^5 (1 - F') d\eta = \frac{x}{\sqrt{\frac{U_\infty x}{\nu}}} [\eta - F]_0^5 \\ &= \frac{x}{\sqrt{\text{Re}_x}} [(5 - 3.283) - (0 - 0)] = x \frac{1.717}{\sqrt{\text{Re}_x}} \end{aligned}$$

Solving for the ratio of displacement thickness to the streamwise location, we have:

$$\frac{\delta^*}{x} = \frac{1.717}{\sqrt{\text{Re}_x}} \quad (13.30)$$

Similarly, we can solve for the momentum thickness to give:

$$\theta = \int_0^\delta \frac{u}{U_\infty} \left(1 - \frac{u}{U_\infty}\right) dy = 0.660 \frac{x}{\sqrt{\text{Re}_x}} \Rightarrow \frac{\theta}{x} = \frac{0.660}{\sqrt{\text{Re}_x}} \quad (13.31)$$

Note that the solution for Eq.13.31 is a bit tricky, and requires the use of the original boundary layer equation, Eq.13.13, and Table 13.1 to determine the integral. This is left as an exercise for the reader in the end of chapter study problems.

One might wonder what the impact is of selecting $\eta = 5$ as the “edge” of the boundary layer when integrating for the coefficients in Eq.13.30 and 13.31. To illustrate this, we can calculate that the coefficient in Eq.13.30 changes from 1.7167 for integration over $0 < \eta < 5$, to 1.7207 for integration over $0 < \eta < 9$, or a 0.23% change. Correspondingly, the coefficient in Eq.13.31 changes from 0.6600 for $0 < \eta < 5$, to 0.6642 for $0 < \eta < 9$, or a 0.63% change. Clearly, the extension of the integration beyond $\eta = 5$ has only a minimal effect on the displacement and momentum thickness results.

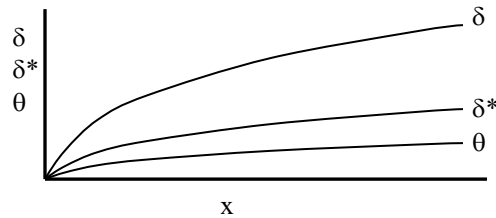


Figure 13.7 The generic behavior of the boundary layer, displacement thickness, and momentum thickness relative to the streamwise development distance, x .

The above analysis illustrates that the boundary layer, the displacement, and the momentum thicknesses all demonstrate the same functional relationship with regard to the streamwise Reynolds number. As figure 13.7 shows, each of these properties increase proportional to the square root of the streamwise distance. When considered as a ratio of each boundary layer property to the streamwise distance, x , these ratios all scale with the inverse square root of the streamwise Reynolds number.

Note that Eqns. 13.29, 13.30, and 13.31 all suggest that $\frac{\delta}{x}$, $\frac{\delta^*}{x}$, and $\frac{\theta}{x}$ become infinite for small

Reynolds numbers. As discussed previously in Section 13.3, within the region very near the leading edge of the flat plate, the assumptions employed to develop the boundary layer equations fail, since the changes in y and x will become comparable. This leading-edge region requires the use of the full Navier-Stokes equations to develop a properly exact solution. However, the amount of correction is so small, that the Blasius solution is considered essentially exact for regions immediately removed from the leading edge.

To calculate the shear stress for the flat plate boundary layer, we substitute into the wall shear stress equation, and use Table 13.1 to determine the shear stress as:

$$\begin{aligned}\tau_w &= \mu \left. \frac{du}{dy} \right|_{y=0} = \mu \left. \frac{\partial u}{\partial \eta} \frac{\partial \eta}{\partial y} \right|_{\eta=0} \Rightarrow \text{where } u = U_\infty F', \quad \eta = y \sqrt{\frac{U_\infty}{\nu x}} \\ &= \mu U_\infty \cancel{F''(0)} \sqrt{\frac{U_\infty}{\nu x}} = 0.332 \frac{\mu U_\infty^2}{\left(\frac{\mu}{\rho}\right) \sqrt{\frac{U_\infty x}{\nu}}} = \frac{0.332 \rho U_\infty^2}{\sqrt{\text{Re}_x}}\end{aligned}\quad (13.32)$$

Substituting Eq. 13.32 into Eq. 13.28 for the friction coefficient, c_f , we obtain:

$$c_f = \frac{\tau_w}{\frac{1}{2} \rho U_\infty^2} = \frac{0.664}{\sqrt{\text{Re}_x}} \quad (13.33)$$

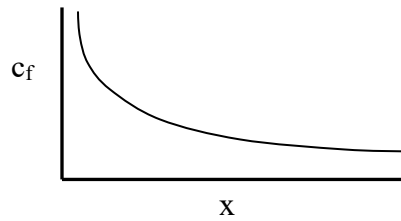


Figure 13.8 The generic behavior of the friction coefficient vs. streamwise distance, x , for a laminar, flat plate flow.

Equation 13.33 indicates that the friction coefficient behaves similar to the ratios of the boundary layer parameters (Eqns. 13.29, 13.30, and 13.31) with streamwise distance, i.e. decreasing with increasing Reynolds number. This behavior illustrates that as the Reynolds number increases, due to either increased outer region velocity or streamwise distance, or decreased kinematic viscosity, viscous forces will decrease relative to inertia forces, resulting in a consequent decrease in the friction coefficient. This behavior of c_f as a function of streamwise distance is illustrated in figure 13.8. Note that this decrease in c_f does not mean that the actual shear stress will decrease, since if U_∞ increases, this will also increase the dynamic pressure ($\frac{1}{2} \rho U_\infty^2$), such that the shear stress will actually increase (proportional to $U_\infty^{3/2}$ if x and ν remain constant).

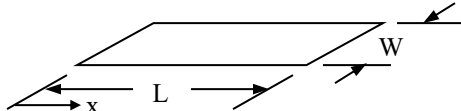
We should also note that a comparison of Eq. 13.33 for the friction coefficient and Eq. 13.31 for the momentum thickness shows that:

$$c_f = \frac{\tau_w}{\frac{1}{2} \rho U_\infty^2} = \frac{0.664}{\sqrt{\text{Re}_x}} = \frac{\theta}{x} \quad (13.34)$$

Notice that in establishing Eq. 13.34, we have used the value of 0.664 for the constant in Eq. 13.31, which is the constant one gets for an upper limit of $\eta = 9$. This is where $U = U_\infty$, which

sets the equivalency between Eqs. 13.33 and 13.31. What Eq. 13.34 illustrates is that the friction coefficient, c_f , is directly proportional to the momentum thickness, θ .

This direct relationship of the momentum thickness to shear stress is even more clearly illustrated by the calculation of the total plate drag due to shear stress. To calculate the **total drag** on a flat plate due to a developing laminar boundary layer, we integrate the shear stress, $\tau_w(x)$, over the total streamwise length of the plate, L (and width, W , although the two-dimensional boundary layer doesn't vary with width):

$$\text{Drag} = \int_0^L \tau_w W dx \quad (13.35)$$


Substituting Eq.13.32 into Eq.13.35, and simplifying yields:

$$\begin{aligned} \text{Drag} &= 0.332\rho U_\infty^2 W \int_0^L \frac{1}{\left(\frac{U_\infty x}{\nu}\right)^{1/2}} dx \\ &= 0.332 \frac{\rho U_\infty^2 W}{\left(\frac{U_\infty}{\nu}\right)^{1/2}} \left[\frac{x^{1/2}}{\frac{1}{2}} \right]_0^L = 0.664 \frac{\rho U_\infty^2 W L^{1/2}}{\left(\frac{U_\infty}{\nu}\right)^{1/2}} \\ \text{Drag} &= 0.664 \frac{\rho U_\infty^2 W L}{\left(\frac{U_\infty L}{\nu}\right)^{1/2}} = \frac{0.664}{\sqrt{\text{Re}_L}} \rho U_\infty^2 W L \end{aligned} \quad (13.36)$$

To non-dimensionalize the drag force of Eq.13.36, we divide through by the dynamic force, $\frac{1}{2}\rho U_\infty^2 (WL)$, yielding:

$$C_D = \frac{\text{Drag}}{\frac{1}{2}\rho U_\infty^2 WL} = \frac{1.328}{\sqrt{\text{Re}_L}} \quad (13.37)$$

In Eq.13.37, C_D is termed the drag coefficient, indicating the relative amount of viscous drag due to the formation of a laminar boundary layer on a flat plate. By referencing the drag to the outer region dynamic pressure ($\frac{1}{2}\rho U_\infty^2$), and the area of the plate over which the drag is generated (WL), Eq. 13.37 indicates that the relative drag decreases with increasing Reynolds number (based on the total streamwise plate length). This behavior is similar to the dependence of the friction coefficient, defined by Eq.13.33, on the *local* Reynolds number. However, the friction

coefficient is a *local* property, whereas the drag coefficient is a *cumulative* property, which takes into account the integrated effect of friction over the entire area of boundary layer development.

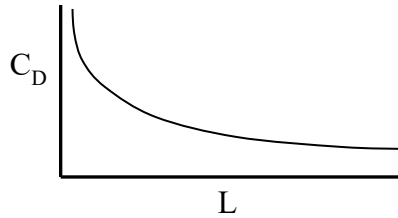


Figure 13.9 The generic behavior of the drag coefficient as a function of total plate length, L , for a laminar, flat plate flow.

Figure 13.9 shows the generic behavior for the drag coefficient as a function of total streamwise plate length. It is instructive that increasing the length of the plate results in a decrease in the drag coefficient. However, because C_D is based on the total plate area, the actual drag will *increase proportional to the square root of the plate length*, as illustrated by Eq. 13.36.

As discussed above, the friction coefficient, c_p is proportionally related to the momentum thickness along the plate. However, if we compare Eq. 13.37 for the drag coefficient and Eq. 13.31 for the momentum thickness at the end of the plate, $x = L$ (again using a constant of 0.664 for an upper limit of $\eta = 9$), we have:

$$C_D = \frac{\text{Drag}}{\frac{1}{2}\rho U_\infty^2 WL} = \frac{1.328}{\sqrt{\text{Re}_L}} \quad \text{and} \quad \frac{\theta_{x=L}}{L} = \frac{0.664}{\sqrt{\text{Re}_L}}$$

Where $\theta_{x=L}$ is the value of θ at $x = L$. Thus, we can write:

$$C_D = \frac{\text{Drag}}{\frac{1}{2}\rho U_\infty^2 WL} = \frac{2\theta_{x=L}}{L}$$

or

$$\text{Drag} = (\rho U_\infty^2) W \theta_{x=L} \quad (13.38)$$

Equation 13.38 shows that *the total drag on the plate is directly proportional to the momentum thickness at the end of the plate*. This reflects the characterization of the momentum thickness as the momentum “lost” due to the viscous shear stresses acting on the fluid as it passes over the plate. This is important, since this means that if the velocity profile at the trailing edge of the plate is known, the integrated momentum thickness for that profile is directly proportional to the viscous drag on the plate. And by extension, if the velocity profile is known at any x location along the plate, Eq. 13.34 can be used to determine the shear stress at that location.

13.5.1 An Example of Boundary Layer Parameters

Consider a thin flat plate 1 meter wide and 2 meters long that is towed through 20 °C water at 0.25 m/s. We will compute the boundary layer thickness, displacement thickness, and momentum thickness at the trailing edge of the plate in cm, and then compute the total drag due to surface shear stress on the two surfaces (top and bottom surfaces) in Newtons.

We assume that the flow is a Blasius-type flow and uniform in width. The kinematic viscosity of water at 20 °C is roughly $\nu = 10^{-6} \frac{\text{m}^2}{\text{sec}}$, and $L = 2$ m.

Thus, the Reynolds number based on the plate length is:

$$\text{Re}_L = \frac{U_\infty L}{\nu} = \frac{(0.25) \frac{\text{m}}{\text{sec}} (2) \text{m}}{(10^{-6}) \frac{\text{m}^2}{\text{sec}}} = 5 \times 10^5$$

Note that flat plate Reynolds numbers less than 5×10^5 are generally considered laminar, so this flow is at the extremes of that range. As we will discuss in Chapter 17, on smooth surfaces with little external flow disturbance, a laminar boundary layer can often be sustained for Reynolds numbers up to and slightly in excess of 10^6 .

The boundary layer, displacement, and momentum thicknesses for this flow are:

$$\frac{\delta_{x=L}}{L} \cong \frac{5}{\sqrt{\text{Re}_L}} \Rightarrow \delta_{x=L} = \frac{5L}{\sqrt{\text{Re}_L}} = \frac{5(2)\text{m}}{\sqrt{5 \times 10^5}} = 0.0141 \text{ m} = 1.41 \text{ cm}$$

$$\delta_{x=L}^* = \frac{1.717L}{\sqrt{\text{Re}_L}} = \frac{1.717(2)\text{m}}{\sqrt{5 \times 10^5}} = 0.00486 \text{ m} = 0.486 \text{ cm}$$

$$\theta_{x=L} = \frac{0.660L}{\sqrt{\text{Re}_L}} = \frac{0.660(2)\text{m}}{\sqrt{5 \times 10^5}} = 0.00187 \text{ m} = 0.187 \text{ cm}$$

At this moderate Reynolds number, these thicknesses are quite small. Note that

$$\frac{\delta_{x=L}}{L} = 0.0071 = 0.71\%$$

The total drag on one surface is given by Eq. 13.36:

$$\text{Drag} = \frac{0.664}{\sqrt{\text{Re}_L}} \rho U_\infty^2 WL$$

Here, $W = 1$ meter, $U_\infty = 0.25$ m/sec, and the density is roughly $\rho = 1000 \frac{\text{kg}}{\text{m}^3}$. Equation

13.36 predicts a drag of:

$$\text{Drag} = \frac{0.664}{\sqrt{5 \times 10^5}} (1000) \frac{\text{kg}}{\text{m}^3} (0.0625) \frac{\text{m}^2}{\text{s}^2} (1) \text{m} (2) \text{m} = 0.1174 \frac{\text{kg} \cdot \text{m}}{\text{s}^2} = 0.1174 \text{ N}$$

The drag is really quite small. However, this is characteristic of laminar drag, since it inevitably is at low velocities and Reynolds numbers. Note that if the plate length was 0.5 m and the velocity was 1 m/s, that would also give a $Re_L = 5 \times 10^5$, but the parameter thicknesses would be $\frac{1}{4}$ the thickness calculated above, and the drag would be 4 times the above drag value, but still quite small.

Alternatively, we could use Eq. 13.38 to calculate the drag using the momentum thickness, which gives drag value:

$$\text{Drag} = (\rho U_\infty^2) W \theta_{x=L} = (1000) \frac{\text{kg}}{\text{m}^3} (0.0625) \frac{\text{m}^2}{\text{s}^2} (1) \text{m} (0.00295) \text{m} = 0.1169 \frac{\text{kg} \cdot \text{m}}{\text{s}^2} = 0.1169 \text{ N}$$

Note that this latter value is slightly less than the calculation obtained using Eq. 13.36. This is due to the different coefficient value used in calculating the momentum thickness (0.66 vs. 0.664, as discussed previously in Section 13.5).

Using our first calculated values of drag, the total drag for both sides of the plate is:

$$\text{Total Drag} = 2 \times 0.1174 \text{ N} = 0.2348 \text{ N}.$$

It would not take much effort to restrain this plate.

13.6 Falkner-Skan Solutions for Non-Zero Pressure Gradients

One might ask, what happens when the pressure gradient is non-zero for a laminar boundary layer? Well, an external pressure gradient can have quite an effect on the behavior of the boundary layer. As we will discuss qualitatively in section 14.5, a favorable pressure gradient (an accelerating flow, with a decreasing streamwise pressure) will result in a boundary layer that grows slowly and remains quite stable. However, the presence of an adverse pressure gradient (a decelerating flow, with increasing stream-wise pressure) will cause a rapid growth of the boundary layer, often leading to flow separation (i.e. stagnation of the flow very near the surface, causing the boundary-layer fluid to detach and move away from the bounding surface) or rapid degeneration of the boundary layer to turbulence. In this section, we will address the simplest boundary layer flow with a pressure gradient, known as a [Falkner-Skan solution](#). We will again assume that the boundary layer velocity profile has a similarity solution, and assess what type of pressure gradient will still allow a similarity approach to be feasible.

To start our solution, we expand the solution of the boundary layer equations to flows which have a free stream velocity that varies as a function of x , or $U_\infty = U_\infty(x)$. Using the same similarity assumption that was employed by Blasius, we again assume a stream function and similarity variable as defined by Eq. 13.22:

$$\psi = \sqrt{U_\infty \nu x} F(\eta) \quad \text{where} \quad \eta = y \sqrt{\frac{U_\infty}{\nu x}}$$

However, we now assume the free stream velocity to be of the form $U_\infty = U_\infty(x)$ such that

$$\frac{dP}{dx} \neq 0. \quad \text{In the free stream, the pressure is given by the Bernoulli equation as } P + \frac{1}{2} \rho U_\infty^2 =$$

$$\text{constant, and thus the pressure gradient is given by } \frac{dP}{dx} = -\rho U_\infty \frac{dU_\infty}{dx}.$$

Since the pressure gradient for these flows is non-zero, the boundary layer equations to be addressed are Eqs. 13.13:

$$u \frac{\partial u}{\partial x} + v \frac{\partial u}{\partial y} = -\frac{1}{\rho} \frac{\partial P}{\partial x} + \nu \frac{\partial^2 u}{\partial y^2} \quad \text{or} \quad u \frac{\partial u}{\partial x} + v \frac{\partial u}{\partial y} = U_\infty \frac{dU_\infty}{dx} + \nu \frac{\partial^2 u}{\partial y^2}$$

And

$$\frac{\partial u}{\partial x} + \frac{\partial v}{\partial y} = 0$$

Here, we have again assumed that the pressure gradient within the boundary layer is again equivalent to that imposed by the adjacent free stream flow (since $\frac{dP}{dy} \cong 0$).

Using the stream function relations for u and v developed in section 13.3, Eqs. 13.13 can again be reduced to a single partial differential equation (since Eq. 13.13b, continuity, is identically satisfied by the stream function) of the form:

$$\frac{\partial \psi}{\partial y} \frac{\partial^2 \psi}{\partial x \partial y} - \frac{\partial \psi}{\partial x} \frac{\partial^2 \psi}{\partial y^2} = U_\infty \frac{dU_\infty}{dx} + \nu \frac{\partial^3 \psi}{\partial y^3} \quad (13.39)$$

Now, using the similarity variables ψ and η from Eq. 13.22, we again determine the respective derivative terms in Eq. 13.39 and simplify the resulting equation. The result is an *ordinary differential equation* for $F(\eta)$ and $U_\infty \frac{dU_\infty}{dx}$. Note that this substitution process is a bit messier than the Blasius formulation, since $U_\infty(x)$. Thus, we must consider the x -derivatives of U_∞ in calculating the terms in Eq. 13.39. The respective derivatives of ψ are:

$$\frac{\partial \psi}{\partial x} = (U_\infty \nu x)^{1/2} \left[\frac{1}{2} \frac{1}{U_\infty} \frac{dU_\infty}{dx} F + \frac{1}{2} \frac{1}{x_\infty} F + F' \frac{d\eta}{dx} \right] \quad (13.40)$$

where

$$\frac{\partial \eta}{\partial x} = \frac{y}{2} \left(\frac{v U_\infty}{x} \right) \left(-\frac{1}{x} + \frac{1}{U_\infty} \frac{dU_\infty}{dx} \right) = \frac{\eta}{2} \left(-\frac{1}{x} + \frac{1}{U_\infty} \frac{dU_\infty}{dx} \right) \quad (13.41)$$

Substituting Eq.13.41 into Eq.13.40 and simplifying, we obtain:

$$\frac{\partial \psi}{\partial x} = \frac{1}{2} \left(\frac{U_\infty v}{x} \right)^{1/2} \left[(F - \eta F') + \left(\frac{x}{U_\infty} \frac{dU_\infty}{dx} \right) (F + \eta F') \right] = -v$$

Likewise, we can show:

$$\frac{\partial \psi}{\partial y} = (U_\infty v x)^{1/2} F' \frac{d\eta}{dy} = U_\infty F' = u \quad \text{where } \frac{\partial \eta}{\partial y} = \left(\frac{U_\infty}{v x} \right)^{1/2}$$

and

$$\frac{\partial^2 \psi}{\partial y^2} = U_\infty F'' \frac{\partial \eta}{\partial y} = U_\infty \left(\frac{U_\infty}{v x} \right)^{1/2} F'' = \partial u / \partial y$$

and

$$\frac{\partial^3 \psi}{\partial y^3} = \frac{U_\infty^2}{v x} F''' = \partial^2 u / \partial y^2$$

and

$$\begin{aligned} \frac{\partial^2 \psi}{\partial x \partial y} &= \frac{\partial}{\partial y} \left(\frac{\partial \psi}{\partial x} \right) = \frac{1}{2} \left(\frac{U_\infty v}{x} \right)^{1/2} \left[\left(1 + \frac{x}{U_\infty} \frac{dU_\infty}{dx} \right) F' + \left(-1 + \frac{x}{U_\infty} \frac{dU_\infty}{dx} \right) F' + \left(-1 + \frac{x}{U_\infty} \frac{dU_\infty}{dx} \right) \eta F'' \right] \frac{d\eta}{dy} \\ \frac{\partial^2 \psi}{\partial x \partial y} &= \frac{1}{2} \frac{U_\infty}{x} \left[\frac{x}{U_\infty} \frac{dU_\infty}{dx} (2F' + \eta F'') - \eta F'' \right] = \partial u / \partial x \end{aligned}$$

Substituting these relationships into Eq. 13.39:

$$\frac{\partial \psi}{\partial y} \frac{\partial^2 \psi}{\partial x \partial y} - \frac{\partial \psi}{\partial x} \frac{\partial^2 \psi}{\partial y^2} = U_\infty \frac{dU_\infty}{dx} + v \frac{\partial^3 \psi}{\partial y^3}$$

Gives the very messy equation,

$$\begin{aligned} & (U_\infty F') \frac{1}{2} \frac{U_\infty}{x} \left[\frac{x}{U_\infty} \frac{dU_\infty}{dx} (2F' + \eta F'') - \eta F'' \right] \\ & - \frac{1}{2} \left(\frac{U_\infty v}{x} \right)^{1/2} \left[(F - \eta F') + \left(\frac{x}{U_\infty} \frac{dU_\infty}{dx} \right) (F + \eta F') \right] U_\infty \left(\frac{U_\infty}{v x} \right)^{1/2} F'' \\ & = U_\infty \frac{dU_\infty}{dx} + v \frac{U_\infty^2}{v x} F''' \end{aligned}$$

Expanding and simplifying gives:

$$\frac{U_\infty^2}{2x} \left[\left(\frac{x}{U_\infty} \frac{dU_\infty}{dx} \right) (2F'^2 + \eta F'F'') - \eta F'F'' - FF'' + \eta F'F''' - \left(\frac{x}{U_\infty} \frac{dU_\infty}{dx} \right) (FF'' + \eta F'F''') \right] = \frac{2x}{U_\infty} \frac{dU_\infty}{dx} + \nu \frac{2}{\nu} F'''$$

$$\left(\frac{x}{U_\infty} \frac{dU_\infty}{dx} \right) 2F'^2 - FF'' - \left(\frac{x}{U_\infty} \frac{dU_\infty}{dx} \right) FF'' = \frac{2x}{U_\infty} \frac{dU_\infty}{dx} + 2F'''$$

Rearranging, we finally have:

$$F''' + \frac{1}{2} FF'' - \left(\frac{x}{U_\infty} \frac{dU_\infty}{dx} \right) F'^2 + \frac{1}{2} \left(\frac{x}{U_\infty} \frac{dU_\infty}{dx} \right) FF'' + \left(\frac{x}{U_\infty} \frac{dU_\infty}{dx} \right) = 0$$

$$F''' + \frac{1}{2} FF'' + \frac{x}{U_\infty} \frac{dU_\infty}{dx} \left[1 - F'^2 + \frac{1}{2} FF'' \right] = 0 \quad (13.42)$$

Equation 13.42 is a generalized equation for an assumed similarity velocity profile within the boundary layer, which takes into account the effect of the pressure gradient on boundary layer development. Note that if $U_\infty = \text{constant}$, Eq. 13.42 reduces to Eq. 13.23, the Blasius equation, as it should. In order to be able to solve Eq. 13.42, all terms in the equation must either be derivatives of F , functions of η , or constants. Thus, Falkner and Skan realized that to be tractable, the pressure gradient term, $\left(\frac{x}{U_\infty} \frac{dU_\infty}{dx} \right)$, in Eq. 13.42 must be a constant. Thus, we set:

$$\frac{x}{U_\infty} \frac{dU_\infty}{dx} = m = \text{constant} \quad (13.43)$$

Assuming a relationship according to Eq. 13.43, we separate variables and integrate, which gives:

$$\ln \left(\frac{U_\infty}{U_0} \right) = m \ln \left(\frac{x}{x_0} \right)$$

or

$$U_\infty = U_0 \left(\frac{x}{x_0} \right)^m \quad (13.44)$$

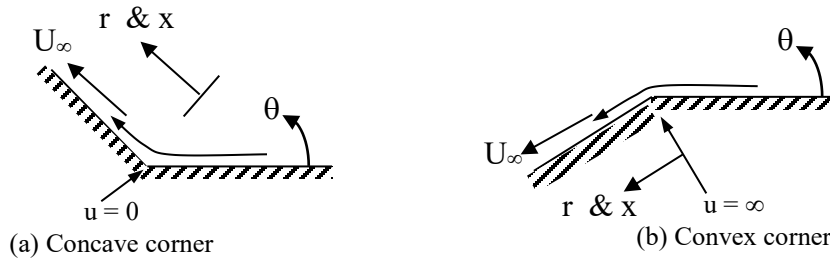
While it is not initially obvious, this velocity function represents the velocity behavior for inviscid flow over a wedge or corner. Recall from Section 9.7.5 that the complex potential function for a wedge/corner flow could be represented by (Eq. 9.41 and 9.42):

$$\Phi(z) = \frac{A}{n} z^n = \frac{Ar^n}{n} (\cos n\theta + i \sin n\theta)$$

From which we could determine the velocity along a radius r (Eq. 9.46) as:

$$v_r = \frac{1}{r} \frac{\partial \psi}{\partial \theta} = A r^{n-1} \cos(n\theta) \tag{13.45}$$

The generic configurations of the bounding shapes giving such an inviscid flow are shown below for $n > 1$ and $n < 1$.



$n > 1$ (concave corner flow)

$n < 1$ (convex corner flow)

Here, we consider that the boundary develops along a surface in the r -direction, which we equate with the x -direction in the boundary layer equations. Thus, we can rewrite equation 13.43, in terms of x , as:

$$v_r = U_\infty = A x^{n-1} \cos(n\theta) = A x_0^{n-1} \cos(n\theta) \left(\frac{x}{x_0}\right)^{n-1} = U_0 \left(\frac{x}{x_0}\right)^m$$

Where $A x_0^{n-1} \cos(n\theta) = U_0$, and $m = n - 1$. While the types of free stream velocities that Eq. 13.44 can represent are limited, it can represent the general behavior for an accelerated flow ($m > 0$) and a decelerated flow ($m < 0$) for a flow satisfying our similarity constraints.

Thus, for a free stream velocity described by Eq. 13.44, Eq. 13.42 becomes:

$$F''' + \frac{1}{2} FF'' + m \left[1 - F'^2 + \frac{1}{2} FF'' \right] = 0$$

or

$$F''' + \frac{1}{2} (1 + m) FF'' + m(1 - F'^2) = 0 \tag{13.46}$$

Equation 13.46 is similar to the classic Falkner-Skan equation, first derived by [Falkner and Skan \(1930,31\)](#). In their derivation, they used a modified similarity variable:

$$\eta_{FS} = y \sqrt{\frac{m+1}{2} \frac{U_\infty}{\nu x}}$$

This makes the reduced equation, like 13.44, a little bit simpler (but not much), and it makes the boundary layer merge with the outer region for $\eta_{FS} \cong 5$, like the Blasius boundary layer does. However, by retaining the Blasius similarity variable, this shows the reflective variation of the outer boundary layer η limit. As we will see, as m varies, not only will the shape of the velocity profile change, but also the extent of the boundary layer in η units. The choice of η does not change the results [since $(m+1)/2$ is a constant for any selected flow], but only how they scale in η units.

To set the boundary conditions, we again note that:

$$u = \frac{\partial \psi}{\partial y} = U_{\infty} F', \quad v = -\frac{\partial \psi}{\partial x} = -\frac{1}{2} \left(\frac{U_{\infty} \nu}{x} \right)^{1/2} [(F - \eta F') + m(F + \eta F')]$$

and

$$\eta = y \sqrt{\frac{U_{\infty}}{\nu x}}$$

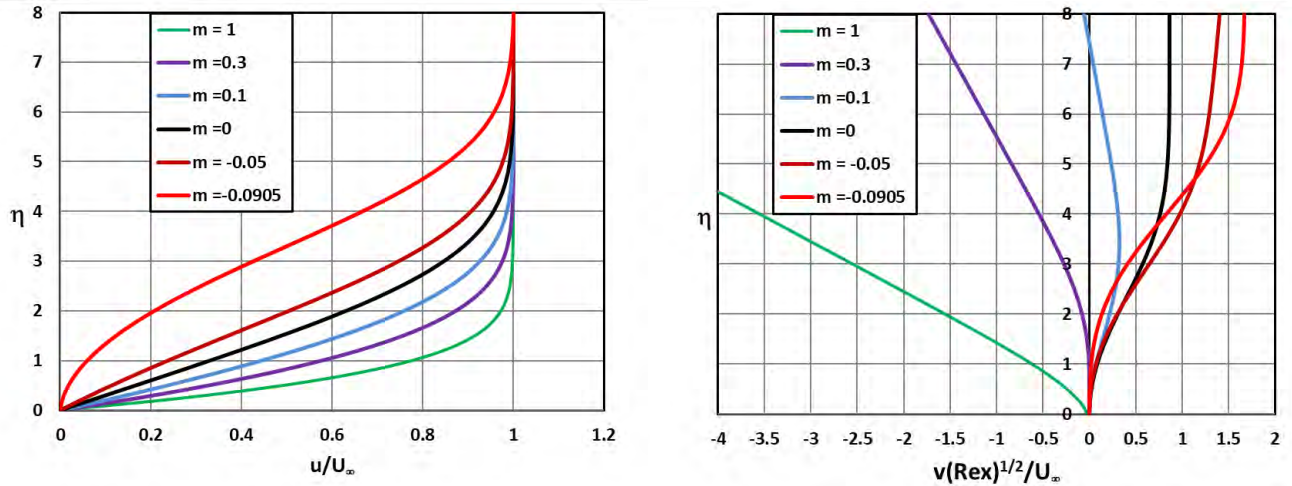
Although the velocity expressions are a bit more complicated, the boundary conditions on F and η for the Falkner-Skan equation are the same as for the Blasius equation, as follows:

$$\begin{aligned} y=0: \quad u, v=0 & \Rightarrow \eta=0: \quad F' = F = 0 \\ y \rightarrow \infty: \quad u = U_{\infty} & \Rightarrow \eta \rightarrow \infty: \quad F' = 1 \end{aligned}$$

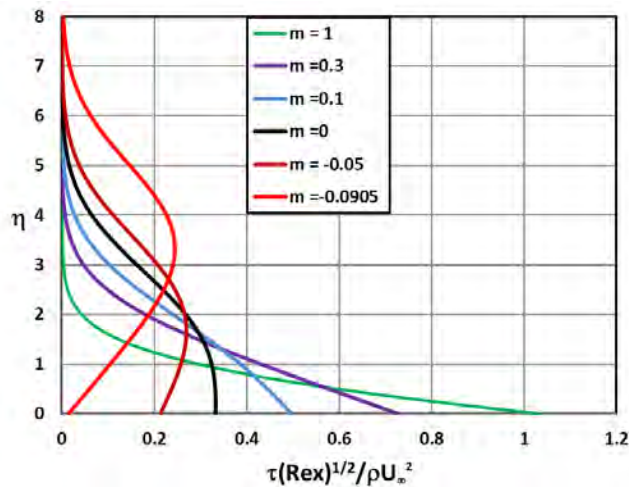
Note that we do not include an initial condition at $x = 0$, since this would over-determine the problem. Unlike the flat plate flow, the initial flow field at $x = 0$ is unrealistic, since for $m > 0$ the velocity must be zero, and for $m < 0$ the velocity is undetermined at $x = 0$. So, the free stream velocity behavior defined by Eq. 13.44 can only apply for values of $x > 0$. And for $x > 0$, the three boundary conditions listed above suffice. Thus, we have again reduced the third-order P.D.E. with four boundary conditions for $\psi(x,y)$ to a third-order O.D.E. for $F(\eta)$ with three boundary conditions.

Like the Blasius equation, Eq. 13.46 is non-linear, and doesn't lend itself to a closed-form solution. The solution of this equation is obtained numerically using a Runge-Kutta differential equation solver (I again used the MATLAB function `bvp4C`). Note that while solutions for accelerating flows exist for all values of $m > 0$, the corresponding solutions for decelerating flows can only be obtained for $-0.0905 < m < 0$. This latter result suggests how sensitive laminar boundary layers are to positive (adverse) pressure gradients. Figures illustrating u (streamwise) and v (normal) velocities and shear stress profiles for select m values from 1 to -0.0905 are shown in figure 13.10a and 13.10b.

For $m > 0$, the u -velocity profiles are much flatter, with a thinner boundary layer than the Blasius flat plate flow (represented by $m = 0$). This is a result of the assistance of the decreasing pressure gradient, which acts in the direction of flow, and helps counter the viscous forces.



(a) Nondimensional x and y-direction velocities, u and v , vs. η



(b) Nondimensional shear stress, τ , vs. η

Figure 13.10 Falkner-Skan similarity (a) velocity and (b) shear-stress profiles vs. the similarity parameter, η , for a free-stream velocity $U_\infty = U_0 \left(\frac{x}{x_0} \right)^m$.

Correspondingly, the v -velocity profiles for $m > 0$ show the development of an increasingly negative velocity normal to the wall (i.e. toward the wall) as m increases. Note that for $m = 1$, the v -velocity moves very strongly toward the surface. To understand what is happening, notice that $m = 1$ defines a free-stream flow that is impinging normal to the bounding surface (i.e. a “stagnation” flow), as represented for an inviscid flow in section 9.7.5.1, where $n = 2 \Rightarrow m = 1$ in Eq. 13.44. For a stagnation flow, the v velocity will actually be the velocity of the inviscid free stream toward the surface, and thus the reason that v increases so rapidly away from the surface.

As illustrated by figure 13.10b, the shear stress within an accelerated boundary layer flow increases quite rapidly with increasing m , which is a reflection of the increased streamwise velocity gradient at the wall, as reflected in figure 13.10a. Additionally, the slope of the shear stress (the second derivative of u) is positive for $m > 0$ flows, which is indicative of greater flow stability (we will discuss this further in Section 14.5.1). Note that solutions to the Falkner-Skan equation exist for $m > -1$. However, these flows would represent flows into a strongly concave corner (reversing the flow back on itself), which is physically unrealistic, and so of little practical interest.

If we consider the boundary layer behavior for decelerating flows, $m < 0$, the range over which flow solutions are available is limited to $-0.0905 < m < 0$. The u -velocity and shear profiles of figures 13.10a and 13.10b show that as m becomes more negative the u -velocity profile develops an obvious inflection, indicated by a maximum in the shear stress developing away from the wall. When $m = -0.0905$, the velocity near the wall essentially comes to a stop, and the wall shear stress becomes essentially zero. While zero shear stress might seem like a good thing, since this would indicate no boundary drag, this condition is problematic. Zero shear stress implies that a layer of stagnant fluid develops adjacent to the wall, around which the flow moving downstream along the wall must divert, causing what is termed a flow separation (a separation of the boundary layer from the surface). This also means that the scaling assumptions that were employed to derive the boundary layer equations will no longer be valid. Thus, beyond a point of separation, the boundary layer equations become invalid, and the flow must be assessed using the full Navier-Stokes equations---making the solution procedure much more complicated. We will discuss the onset and consequences of flow separation in detail in Section 14.6 and in Chapter 15.

For the Falkner-Skan solutions we can derive appropriate boundary layer parameters for displacement and momentum thickness. The displacement thickness is:

$$\begin{aligned}\delta^* &= \int_0^{\delta} \left(1 - \frac{u}{U_\infty}\right) dy \quad \text{where } dy = d\eta \sqrt{\frac{\nu x}{U_\infty}} \\ \delta^* &= \int_0^{\eta=8} \left(1 - \frac{u}{U_\infty}\right) \sqrt{\frac{\nu x}{U_\infty}} d\eta = \sqrt{\frac{\nu x}{U_\infty}} \int_0^8 (1 - F'_m) d\eta = \sqrt{\frac{\nu x}{U_\infty}} [\eta - F_m]_0^8 \\ \delta_m^* &= \frac{x}{\sqrt{\text{Re}_x}} [8 - F_m(8)]\end{aligned}\tag{13.47}$$

In Eq. 13.47, F_m indicates the function of $F(\eta)$ as determined from integrating Eq. 13.46 for a specified m value, and δ_m^* is the corresponding displacement thickness for the specified m value.

Note that we take $\eta = 8$ as the outer integration limit, since when $m < 0$ the point at which $u \rightarrow U_\infty$ will be beyond the $\eta = 5$ value we assumed for the Blasius solution ($m = 0$).

The momentum thickness takes a bit more work to determine, but is:

$$\theta_m = \int_0^\delta \frac{u}{U_\infty} \left(1 - \frac{u}{U_\infty}\right) dy = \sqrt{\frac{\nu x}{U_\infty}} \int_0^{n=8} F'_m (1 - F'_m) d\eta = \frac{2x}{\sqrt{\text{Re}_x}} \left\{ \frac{F''_m(0) + m[F_m(8) - 8]}{1 + 3m} \right\} \quad (13.48)$$

To show the relative changes in the displacement and momentum thickness, we normalize Eqs. 13.47 and 13.48 on the respective Blasius expressions for a zero pressure gradient from Eqs. 13.30 and 13.31 to give:

$$(\delta^*)' = \frac{\delta_m^*}{\delta_{\text{Blasius}}^*} = \frac{\delta_m^*}{\delta_{m=0}^*} = \frac{\frac{x}{\sqrt{\text{Re}_x}} [8 - F_m(8)]}{x \frac{1.717}{\sqrt{\text{Re}_x}}} = 0.5824 [8 - F_m(8)] \quad (13.49)$$

and

$$(\theta)' = \frac{\theta_m}{\theta_{\text{Blasius}}} = \frac{\theta_m}{\theta_{m=0}} = \frac{\frac{2x}{\sqrt{\text{Re}_x}} \left\{ \frac{F''_m(0) + m[F_m(8) - 8]}{1 + 3m} \right\}}{0.660 \frac{x}{\sqrt{\text{Re}_x}}} = 3.03 \left\{ \frac{F''_m(0) + m[F_m(8) - 8]}{1 + 3m} \right\} \quad (13.50)$$

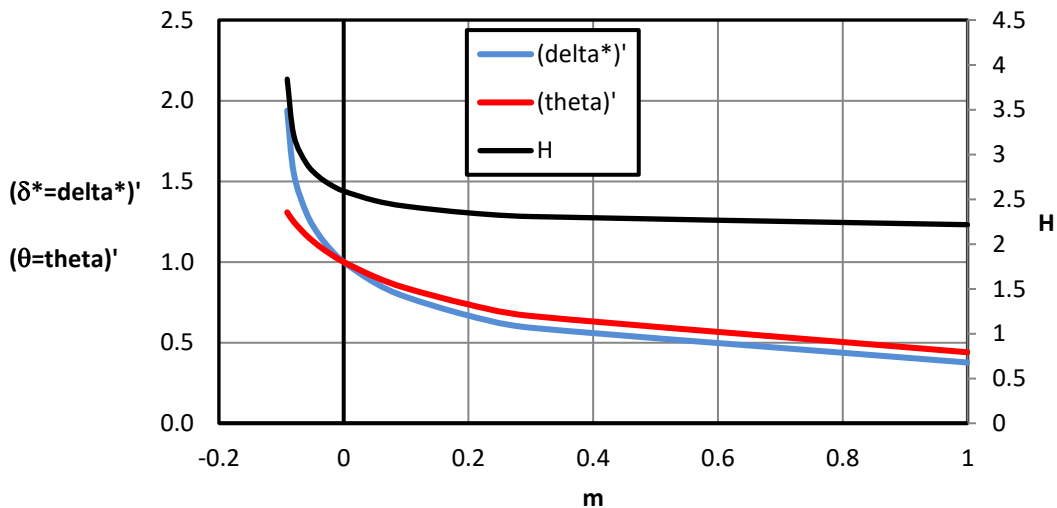


Figure 13.11 The behavior of normalized $(\delta^*)'$ and $(\theta)'$ (as per Eqs. 13.49 and 13.50), and shape factor $H = \delta^*/\theta$, as a function of the power law exponent m in Eq. 13.44.

The normalized displacement thickness and momentum thickness from Eqs. 13.49 and 13.50 are plotted for a range $-0.0905 < m < 1$ in figure 13.11. In addition, the ratio of these properties,

$H = \frac{\delta^*}{\theta}$, known as the "shape factor" of the boundary layer is also plotted in figure 13.11. This

latter property is a quantitative indication of how broadly the boundary layer extends, relative to the momentum lost to viscous friction. As figure 13.11 shows, for accelerating flows ($m > 0$), the normalized displacement and momentum thicknesses, and the shape factor, all decrease with increasing m . However, the shape factor decreases markedly slower, since the relative changes in the displacement and momentum thicknesses are quite similar. For decelerating flows ($m < 0$), all three properties grow quite rapidly with decreasing m , and essentially terminate for $m = -0.0905$, where the boundary layer essentially reaches separation.

It should be noted that when H grows beyond the Blasius value of 2.6 at $m = 0$, the boundary layer becomes quite unstable, and will usually breakdown into turbulence before it would undergo laminar separation. The process of breakdown to turbulence and the role of instabilities on fluid behavior are discussed in detail in Chapter 17.

13.7 Conclusion

In the present chapter, we developed the equations governing boundary layer development, and touched on the basics of boundary layer theory. The boundary layer equations developed in Section 13.2 can be applied to a broad variety of flow geometries, as long as the flow remains laminar, and the order of magnitude assumptions employed in Section 13.2 remain valid ($\delta/x \approx 1/100$). The laminar flat-plate solution of Blasius, developed in Section 13.3, is accepted as essentially an exact solution, and widely used to reference laminar flat-plate boundary layer growth, along with the boundary layer parameters developed in Section 13.5.

However, for more complicated flows, the solution of the boundary layer equations can be much more involved, requiring significant numerical computations, as illustrated by the Falkner-Skan solutions of section 13.6. However, as we will demonstrate in the following chapter, we can often obtain good engineering results for somewhat complicated laminar flows using approximate solution techniques, which are much more tractable than the solution of the full equations, and provide results of acceptable engineering accuracy.

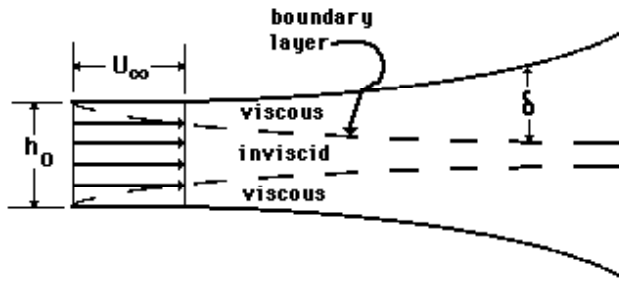
References

V. M. Falkner and S. W. Skan, (1931), "Some Approximate Solutions of the Boundary Layer Equations," *Phil. Mag.*, vol.12, no. 7, pp 865-896. [also in [*Aero. Res. Coun. Rep. and Mem.* no 1314, 1930](#)]

Study Problems

1. A thin flat plate 0.4 m. wide and 2 m. long is towed through 20 °F water at 0.5 m/s. Compute the drag due to surface resistance on the two surfaces (in Newtons)
2. For the flow described in problem 1, determine the boundary layer, displacement, and momentum thicknesses at the end of the plate.
3. A laminar, uniform air flow at 20 °C passes over a thin flat plate 1 meter wide and 4 meters long. If the Reynolds number based on the plate length is 5×10^5 , determine the flow velocity, and the boundary layer, displacement, and momentum thicknesses at the end of the plate, compute the drag due to surface resistance on the two surfaces (in Newtons.)
4. Use the tabular data from table 13.1 to calculate the shear stress, τ_{yx} , vs. η in the Blasius boundary layer for water ($\mu = 10^{-3}$ N-s/m², $\nu = 10^{-2}$ cm²/s) for a flat plate flow with $U_\infty = 10$ cm/s, at a location $x = 100$ cm. Plot a graph of τ_{yx} vs. η for $0 < \eta < 8$. Hint: copy the table from this chapter to an Excel sheet to do the plotting. Note that $\tau_{yx} = \mu \left(\frac{\partial u}{\partial y} + \frac{\partial v}{\partial x} \right)$, and you will have to determine $\frac{\partial v}{\partial x}$ from $\psi = \sqrt{U_\infty \nu x} F(\eta)$, similar to how $\frac{\partial u}{\partial y}$ is determined on page 13 in section 13.3. How much does the $\frac{\partial v}{\partial x}$ term contribute to the shear stress?
5. Using the Blasius results from section 13.3 and table 13.1, determine if the boundary layer equations should give reasonable results for $\mathbf{Re}_x = \frac{U_\infty x}{\nu} = 1000$. If not, what is the minimum value for \mathbf{Re}_x that would satisfy our initial assumption for using the boundary layer equations? Hint: consider the ratio of $\frac{v}{u}$ and $\frac{\delta}{x}$ at the edge of the boundary layer.
6. Determine how much vorticity is generated at the flat plate surface ($y = 0$) for the boundary layer. Show this using Eq. 11.48 in Chapter 11, and then confirm this by calculating $\left. \frac{\partial \omega}{\partial y} \right|_{y=0}$ directly from the Blasius solution. Note that $\omega_z = \left(\frac{\partial u}{\partial y} - \frac{\partial v}{\partial x} \right)$, and you may have to determine $\frac{\partial v}{\partial x}$ from $\psi = \sqrt{U_\infty \nu x} F(\eta)$, similar to how $\frac{\partial u}{\partial y}$ is determined in section 13.3.

7. Consider a uniform flow, $u = U_\infty$ entering a 2-D duct with sharp leading edges as shown below. The duct height is h and the flow remains laminar at all times through the duct. Assume the flow may be broken into viscous and inviscid regions as shown. Make use of the Blasius solution and determine:
- $h = h(x)$ such that $dP/dx = 0$ (let h_0 be the initial duct height). This requires that $u = U_\infty$ throughout the inviscid region.
 - the length, L , where your expression for $h(x)$ ceases to be valid.



8. For the Blasius solution, prove that $\theta/x = 0.664/(Re_x)^{0.5}$ [hint: make use of the original ODE ($FF'' = -2F'''$), and the identity that $(FF')' = F'^2 + FF''$ to assist the integration].
9. For the Falkner-Skan solution, prove that $\theta_m = \frac{2x}{\sqrt{Re_x}} \left\{ \frac{F_m''(0) + m[F_m(8) - 8]}{1 + 3m} \right\}$, where θ_m is the momentum thickness, and F_m and F_m'' are functions at a specified value of m . Make use of the original ODE, $F_m''' + \frac{1}{2}(1+m)FF_m'' + m(1-F_m'^2) = 0$, and the identity $F_m F_m'' = (F_m F_m')' - F_m'^2$ to assist the integration. Take the upper limit of the boundary layer where $\eta = 8$ (where $u = U_\infty$). Note that the values of the F_m function, and its derivative value are:
- at $\eta = 0$, $F_m = 0, F_m' = 0, F_m'' = a$ constant depending on m ;
- at $\eta = 8$, $F_m = a$ constant depending on $m, F_m' = 1, F_m'' = 0$
10. The following table (next page) is a Falkner-Skan solution for $m = -0.05$, a moderate adverse pressure gradient. Copy this table to an Excel sheet, and determine and plot y vs. u (y vertical axis, u horizontal axis) at $x = 10, 20$, and 30 cm. Assume $U_0 = 10$ cm/s at $x = 10$ cm, and $\nu = 10^{-2}$ cm²/s. All three plots should be on one graph. Hint: use the expression for u following Eq. 13.41, and note that $U_\infty = f(x)$ given by Eq. 13.44.

Falkner-Skan table
for $m = -0.05$

η	F	F'	F''
0	0	0	0.2135
0.2	0.0043	0.0437	0.2235
0.4	0.0176	0.0894	0.2332
0.6	0.0402	0.137	0.2424
0.8	0.0725	0.1863	0.2509
1	0.1148	0.2372	0.2582
1.2	0.1675	0.2895	0.264
1.4	0.2307	0.3427	0.268
1.6	0.3046	0.3965	0.2698
1.8	0.3893	0.4504	0.2691
2	0.4848	0.504	0.2658
2.2	0.5908	0.5566	0.2595
2.4	0.7073	0.6076	0.2504
2.6	0.8337	0.6566	0.2386
2.8	0.9697	0.7029	0.2241
3	1.1147	0.7461	0.2075
3.2	1.2679	0.7858	0.1892
3.4	1.4287	0.8217	0.1698
3.6	1.5963	0.8536	0.1498
3.8	1.7699	0.8816	0.13
4	1.9487	0.9057	0.1108
4.2	2.1319	0.926	0.0927
4.4	2.3189	0.9429	0.0762
4.6	2.5089	0.9566	0.0614
4.8	2.7013	0.9676	0.0486
5	2.8957	0.9762	0.0377
5.2	3.0916	0.9828	0.0287
5.4	3.2887	0.9878	0.0215
5.6	3.4867	0.9915	0.0157
5.8	3.6852	0.9942	0.0113
6	3.8843	0.9961	0.008
6.2	4.0836	0.9974	0.0055
6.4	4.2832	0.9983	0.0037
6.6	4.4829	0.9989	0.0025
6.8	4.6828	0.9993	0.0016
7	4.8827	0.9996	0.001
7.2	5.0826	0.9998	0.0007
7.4	5.2826	0.9999	0.0004
7.6	5.4826	0.9999	0.0002
7.8	5.6826	1	0.0001
8	5.8826	1	0.0001

11. The table shown in Problem 10 is a Falkner-Skan solution for $m = -0.05$, a moderate adverse pressure gradient. Using appropriate information from that table, determine general expressions for δ^* , θ , and shape factor $H = \delta^*/\theta$. On a single graph, plot U_∞ , δ^* , and θ vs. x (all on one graph) from $x = 10$ to 100 cm. Let $U_0 = 10$ cm/s and $\nu = 10^{-2}$ cm²/s. Note that $U_\infty = f(x)$ (given by Eq. 13.44) and must be taken into account when calculating Re_x . Plot δ^* and θ on the primary vertical axis, and U_∞ using a secondary vertical axis.
12. The generation of vorticity for a steady, pressure gradient flow with solid boundaries, like the Falkner-Skan flow, is given by equation 11.48 as:

$$\left. \frac{\partial \omega_z}{\partial y} \right|_{y=0} = - \left. \frac{\partial^2 u}{\partial y^2} \right|_{y=0} = - \frac{1}{\mu} \left. \frac{\partial P}{\partial x} \right|_{y=0}$$

For the Falkner-Skan flow, $-\frac{1}{\rho} \frac{dP}{dx} = U_\infty \frac{dU_\infty}{dx}$ from Bernoulli, $U_\infty = U_0 \left(\frac{x}{x_0} \right)^m$, and $\left. \frac{\partial^2 u}{\partial y^2} \right|_{y=0}$ can be determined in terms of F''' from page 447. Note that for all values of m , $F = 0$ and $F' = 0$ at $y = 0$. Show that the velocity derivative term and the pressure derivative term in the above equation are identical. Note that you will need to use Eq. 13.46 to determine F''' at $y = 0$.

13. The generation of vorticity for a steady, pressure gradient flow with solid boundaries, like the Falkner-Skan flow, is given by:

$$\left. \frac{\partial \omega_z}{\partial y} \right|_{y=0} = - \left. \frac{\partial^2 u}{\partial y^2} \right|_{y=0}$$

For the Falkner-Skan flow, $\left. \frac{\partial^2 u}{\partial y^2} \right|_{y=0}$ can be determined directly in terms of F''' from page 447.

For the table shown below, determine, the vorticity generation in terms of U_0 , x , x_0 , ν , and m . For the m values shown in the table, plot (on the same graph) the vorticity generation

$\frac{\nu x_0}{U_0^2} \left. \frac{\partial \omega_z}{\partial y} \right|_{y=0}$ vs x/x_0 , from $1 < x/x_0 < 5$. Note that you will need to use Eq. 13.46 to determine F''' at $\eta = 0$ ($y = 0$).

Values of F , F' , and F'' at $\eta=0$ ($y=0$)

m	F	F'	F''
0.3	0	0	0.726
0.1	0	0	0.497
0	0	0	0.332
-0.05	0	0	0.214
-0.0905	0	0	0.0145

What do your results indicate about the generation of vorticity for a Falkner-Skan flow?

Chapter 14

Approximate Solutions of the Boundary Layer Equations

Contents

14.1	The Approximation Concept	460
14.2	The Momentum Integral Equation for a Boundary Layer	461
14.2.1	The Simplified Momentum Integral Equation	465
14.2.2	Using Similarity Velocity Profiles with the Momentum Integral Equation	466
14.3	Approximate Solution with a Pressure Gradient: Thwaites' Method	472
14.4	Predicting Boundary Layer Characteristics with Thwaites' Method	477
14.4.1	Flat Plate Flow	477
14.4.2	Linearly Accelerating Flow	478
14.4.3	Decelerating Flow	480
14.5	The Relationship of Shear, Drag, and Momentum Thickness when $dP/dx = 0$	482
14.6	The Effect of a Pressure Gradient on Boundary Layers	483
14.6.1	Favorable Pressure Gradient—Accelerating Flow	485
14.6.2	Zero Pressure Gradient—Constant Velocity Flow	486
14.6.3	Adverse Pressure Gradient—Decelerating Flow	487
14.7	Boundary Layer Separation	488

14.1 The Approximation Concept

The exact solution of the boundary layer equations, as we saw in Chapter 13, can be mathematically quite complicated. Because of this complexity, exact solutions are possible for only a selected number of cases, such as the Blasius flat plate and Falkner-Skan solutions we covered in Sections 13.3 and 13.6. However, by relaxing the need for exactness, and using some creative approximations, we can develop some rather useful approaches that will yield approximate (but relatively accurate) solutions of the boundary layer equations. These approximation approaches are reasonably versatile, and allow consideration of a much broader variety of flow geometries and conditions.

In this chapter, we illustrate two ways to do an approximate solution:

- 1) Solve the exact equations using an approximate solution technique, or
- 2) Solve the approximate equations exactly.

Both of the approaches we discuss are relatively old techniques, but they illustrate the kind of creative thinking that can be employed to simplify the solution of the boundary layer equations, and develop relatively accurate results. As discussed previously, we will not be covering numerical solution techniques in this book, but an understanding of these approximate solution approaches can give an appreciation of how more complicated numerical approaches can be applied to either the full equations or the approximate approaches we develop in this chapter.

14.2 The Momentum Integral Equation for a Boundary Layer

This first approach was originated by [Theodore von Karman](#), and is often called the von Karman Integral Equation. This approach is based on a similarity concept, assuming that most boundary layer velocity profiles will look more or less similar at any position along a boundary (e.g. the Falkner-Skan solutions of section 13.6). Thus, we might be able to assume a mathematically simple similarity velocity profile, which satisfies the main boundary conditions, and then use this assumed velocity profile to derive the boundary layer parameters for a particular flow through the use of the integrated boundary layer equations.

The Idea:

Develop an equation that can accept “approximate” velocity profiles as input and yield accurate (close, but approximate) shear stress, δ , δ^* , θ , and c_f as outputs.

The Approach:

Integrate the boundary layer equations across the boundary layer, between $0 \leq y \leq \delta$, and use assumed similarity velocity profiles to solve the resulting integral equation, and establish the resultant boundary layer properties.

We start with the two-dimensional, steady boundary layer equations, and the appropriate boundary conditions from Eqs. 13.13. We let U_∞ be the velocity at the edge of the boundary layer, which is assumed to be a function of x and behave in an essentially inviscid manner. Thus, to a good approximation the pressure gradient is given by the Bernoulli equation as

$\frac{dP}{dx} = -\rho U_\infty \frac{dU_\infty}{dx}$. Substituting for $\frac{dP}{dx}$ in Eq. 13.13a, we have:

$$u \frac{\partial u}{\partial x} + v \frac{\partial u}{\partial y} = U_\infty \frac{dU_\infty}{dx} + \nu \frac{\partial^2 u}{\partial y^2} \quad (14.1a)$$

$$\frac{\partial u}{\partial x} + \frac{\partial v}{\partial y} = 0 \quad (14.1b)$$

$$\begin{aligned} \text{B.C. } y = 0: \quad u, v = 0 \\ y = \delta: \quad u = U_\infty(x) \end{aligned} \quad (14.1c)$$

Note that in Eq. 14.1c we do not include the initial condition $[u(y) \text{ at } x = 0]$, since this condition will be incorporated into the integral equation that will be derived here. For our purposes of integration, all we require are the three spatial boundary conditions listed.

To begin our integration process, we first separate the v -momentum transport term (second term on left) in Eq. 14.1a by parts, and use the boundary layer continuity equation, Eq. 14.1b, to rewrite one of the resulting terms, to give:

$$v \frac{\partial u}{\partial y} = \frac{\partial}{\partial y}(uv) - u \left(\frac{\partial v}{\partial y} \right) = \frac{\partial(uv)}{\partial y} + u \left(\frac{\partial u}{\partial x} \right) \tag{14.2}$$

$$\frac{\partial v}{\partial y} = -\frac{\partial u}{\partial x} \quad (\text{from continuity})$$

We now substitute Eq. 14.2 into Eq. 14.1a, collect like terms, and integrate across the boundary layer from the wall ($y = 0$) to the edge of the boundary layer ($y = \delta$):

$$\int_0^\delta 2u \frac{\partial u}{\partial x} dy + \int_0^\delta \frac{\partial(uv)}{\partial y} dy = \int_0^\delta U_\infty \frac{dU_\infty}{dx} dy + v \int_0^\delta \frac{\partial^2 u}{\partial y^2} dy \tag{14.3}$$

①
②
③
④

To facilitate the integration of Eq. 14.3, we have labeled each term of the integrated equation with a number. We now consider each of these terms in the following, and determine what they reduce to when integrated.

Consider term (2) of Eq. 14.3 first:

$$\int_0^\delta \frac{\partial(uv)}{\partial y} dy = uv \Big|_0^\delta = U_\infty v_\delta - 0 \quad \text{Note: } \int_0^\delta \frac{\partial v}{\partial y} dy = v_\delta - v_0 = -\int_0^\delta \frac{\partial u}{\partial x} dy$$

$\frac{\partial v}{\partial y} = -\frac{\partial u}{\partial x} \quad (\text{from continuity})$

$$\int_0^\delta \frac{\partial(uv)}{\partial y} dy = -U_\infty \int_0^\delta \frac{\partial u}{\partial x} dy \tag{14.4}$$

To obtain Eq. 14.4, we again make use of the continuity equation, Eq. 14.1b. By integrating the v -derivative across the boundary layer, and noting that $v = 0$ at $y = 0$, we develop a term for v_δ in terms of the integrated u -derivative, which is substituted to yield Eq. 14.4.

Term (4) in Eq. 14.3 can be integrated easily, yielding first derivative limits at the wall and the edge of the boundary layer. Since the u velocity asymptotes to the outer region velocity at the

edge of the boundary layer, this means that the derivative $\frac{\partial u}{\partial y}\Big|_{y=\delta}$ asymptotes to zero, leaving only the $\frac{\partial u}{\partial y}\Big|_{y=0}$ term.

$$\int_0^\delta \frac{\partial^2 u}{\partial y^2} dy = \int_0^\delta \frac{\partial}{\partial y} \left(\frac{\partial u}{\partial y} \right) dy = \frac{\partial u}{\partial y}\Big|_0 = \cancel{\frac{\partial u}{\partial y}\Big|_{y=\delta}} - \frac{\partial u}{\partial y}\Big|_{y=0} = -\frac{\partial u}{\partial y}\Big|_{y=0} \tag{14.5}$$

0 (because $u = U_\infty \neq f(y)$ at $y = \delta$)

Finally, we can rewrite term (1) as:

$$\int_0^\delta 2u \frac{\partial u}{\partial x} dy = \int_0^\delta \frac{\partial(u^2)}{\partial x} dy \tag{14.6}$$

Substituting Eqs. 14.4, 14.5, and 14.6 back into Eq. 14.3 gives:

$$\int_0^\delta \frac{\partial(u^2)}{\partial x} dy - U_\infty \int_0^\delta \frac{\partial u}{\partial x} dy = \int_0^\delta U_\infty \frac{dU_\infty}{dx} dy - \nu \left(\frac{\partial u}{\partial y} \right)_{y=0} \tag{14.7}$$

Since U_∞ is not a function of y , we can move U_∞ in the second term of Eq. 14.7 inside the integral, and then expand the resulting integral using integration by parts:

$$U_\infty \int_0^\delta \frac{\partial u}{\partial x} dy = \int_0^\delta U_\infty \frac{\partial u}{\partial x} dy = \int_0^\delta \left(\frac{\partial(uU_\infty)}{\partial x} - u \frac{dU_\infty}{dx} \right) dy \tag{14.8}$$

Substituting Eq. 14.8 into Eq. 14.7, and rearranging terms, we get:

$$\underbrace{\int_0^\delta \frac{\partial(u^2)}{\partial x} dy - \int_0^\delta \frac{\partial(uU_\infty)}{\partial x} dy}_{\int_0^\delta \frac{\partial}{\partial x} (u^2 - uU_\infty) dy} + \underbrace{\int_0^\delta u \frac{dU_\infty}{dx} dy - \int_0^\delta U_\infty \frac{dU_\infty}{dx} dy}_{\int_0^\delta (u - U_\infty) \frac{dU_\infty}{dx} dy} = \underbrace{-\nu \frac{\partial u}{\partial y}\Big|_{y=0}}_{-\frac{\tau_w}{\rho}} \tag{14.9}$$

by Leibnitz Rule

$$\frac{\partial}{\partial x} \int_0^\delta \underbrace{(u^2 - uU_\infty)}_{f(y, x)} dy = \int_0^{\delta(x)} \frac{\partial f}{\partial x} dy + f(\delta(x), x) \frac{\partial \delta(x)}{\partial x} - f(0, x) \frac{\partial(0)}{\partial x}$$

Note that here, $f(\delta(x)) = 0$ and $f(0) = 0$

Note that to simplify Eq. 14.9, we invoke Leibnitz rule, which considers the functional change in the limits of the integration. As the above generic Leibnitz relationship shows, while the upper

integration limit, δ , will change with x , the value of the integrand $(u^2 - uU_\infty)$ at both the limits ($y = \delta$ and $y = 0$) will be zero, thus negating any effect of moving the derivative function from outside to inside the integral. We also identify the last integrated term in Eq. 14.9 as proportional to the wall shear stress, τ_w , which illustrates its relationship to the momentum and pressure gradient changes reflected by the terms on the left side of Eq. 14.9.

Rearranging the terms on the left side of Eq. 14.9, we can rewrite the equation as:

$$\frac{\partial}{\partial x} \int_0^\delta U_\infty^2 \left(\frac{u^2}{U_\infty^2} - \frac{u}{U_\infty} \right) dy + \int_0^\delta \left(\frac{u}{U_\infty} - 1 \right) U_\infty \frac{dU_\infty}{dx} dy = -\frac{\tau_w}{\rho} \tag{14.10}$$

To simplify further, we multiply Eq. 14.10 by -1 and factor the U_∞ terms out of the integrals, since $U_\infty(x)$ does not depend on y . We then identify a set of terms in the resulting equation that represent the boundary layer properties of displacement thickness (δ^*) and momentum thickness (θ), which we defined previously in Section 13.4 (Eqs. 13.25 and 13.27):

$$\frac{\partial}{\partial x} \left[\underbrace{U_\infty^2 \int_0^\delta \frac{u}{U_\infty} \left(1 - \frac{u}{U_\infty} \right) dy}_\theta \right] + U_\infty \frac{dU_\infty}{dx} \underbrace{\int_0^\delta \left(1 - \frac{u}{U_\infty} \right) dy}_{\delta^*} = \frac{\tau_w}{\rho}$$

Rewriting Eq.14.10 in terms of these boundary layer properties, we have:

$$\underbrace{\frac{\partial}{\partial x} (U_\infty^2 \theta)} + \delta^* U_\infty \frac{dU_\infty}{dx} = \frac{\tau_w}{\rho}$$

$$U_\infty^2 \frac{\partial \theta}{\partial x} + 2\theta U_\infty \frac{dU_\infty}{dx}$$

Dividing through by U_∞^2 yields,

$$\frac{d\theta}{dx} + (\delta^* + 2\theta) \frac{1}{U_\infty} \frac{dU_\infty}{dx} = \frac{\tau_w}{\rho U_\infty^2} \tag{14.11}$$

\uparrow
 Momentum changes

\uparrow
 Pressure gradient /momentum

\uparrow
 Shear stress effects

In Eq. 14.11, we have identified the physical process that each term represents. Changes in the momentum thickness obviously reflect changes in the total x-direction momentum (i.e. the

integrated momentum within the boundary layer). The last term reflects the non-dimensional shear stress on the bounding surface. The middle term is a bit trickier, since it reflects both pressure gradient effects and momentum changes. You will notice that back in Eq. 14.9 we combined a momentum term and the pressure gradient term, which mixes the effects. However, this mixed property term is only significant when the outer flow varies with x , which results in both pressure gradient effects, and acceleration/deceleration of the boundary layer. This results in a change in the boundary layer momentum, since the outer region velocity constitutes the outer boundary condition for u . We will discuss the physical interrelationship of the terms in Eq. 14.11 later in Section 14.4.

14.2.1 The Simplified Momentum Integral Equation

We now define another boundary layer property, H , termed the boundary layer “shape factor”, defined as $H = \frac{\delta^*}{\theta}$, which we discussed at the end of section 13.6. This shape factor indicates the degree of distortion of the boundary layer velocity profile, and is a good indicator of the type of behavior reflected by the boundary layer. For example, laminar boundary layer shape factors are typically larger than 2.2, whereas shape factors for turbulent boundary layers (which we will discuss in Chapter 17), are generally less than 1.6. Variations of H also reflect whether a flow is accelerating or decelerating: for laminar flows, values of H greater than 2.6 are indicative of a decelerating outer flow ($dU_\infty/dx < 0$); H values less than 2.6 are indicative of an accelerating outer flow ($dU_\infty/dx > 0$). The Blasius flat plate boundary layer ($dU_\infty/dx = 0$) has an H value of 2.6.

Including the shape factor, and noting that $c_f = \frac{\tau_w}{\frac{1}{2}\rho U_\infty^2}$, allows Eq. 14.11 to be written as:

$$\frac{d\theta}{dx} + (H + 2) \frac{\theta}{U_\infty} \frac{dU_\infty}{dx} = \frac{c_f}{2} \quad (14.12)$$

The final result of the integration of the boundary layer equations across the boundary layer is a differential equation for $\theta(x)$. This classic equation is called the von Karman Momentum Integral Equation, after Theodore von Karman, who first derived it.

Note that the integral equation (i.e. Eqs. 14.11 and 14.12) is *exact*. That is, we have not made any approximations to bring it to its present form. However, the approximation now comes from the assumption of a particular similarity function for the velocity profile within the boundary layer. The approach is to assume a simple profile that has the proper velocity “shape” and satisfies the proper boundary conditions. We do this by writing possible similarity velocity profiles in terms of a stretching (i.e. similarity) variable, $\lambda = y/\delta$. We then apply the appropriate boundary conditions to the assumed general velocity profile in order to determine the particular form for the assumed profile. We can do this effectively for laminar flows, which we

demonstrate in the following section. We can also apply this integral approach for turbulent flow behavior, although this requires the use of some additional assumptions and empirical curve fits, as we will demonstrate in Section 17.7.

14.2.2 Using Similarity Velocity Profiles with the Momentum Integral Equation

For an approximate boundary layer velocity profile, we could choose any number of possible velocity profile shapes, such as a linear profile, a sinusoidal profile, high-order polynomials, etc. Interestingly, almost any assumed velocity profile works reasonably well, as long it matches the boundary conditions. For our first example, we consider a second-order polynomial velocity profile, where:

$$\frac{u}{U_\infty} = a + b\lambda + c\lambda^2 \quad (14.13a)$$

In Eq. 14.13a, $\lambda = y/\delta$ and a , b , c are undetermined constants.

The applicable boundary conditions for the flow are:

$$\begin{aligned} 1) \quad u &= 0 \quad @ \quad y = 0 \quad (\lambda = 0) \\ 2) \quad u &= U_\infty \quad @ \quad y = \delta \quad (\lambda = 1) \\ 3) \quad \tau &= 0 \quad @ \quad y = \delta \quad (\lambda = 1) \quad \Rightarrow \quad \frac{du}{d\lambda} = 0 \quad @ \quad \lambda = 1 \end{aligned} \quad (14.13b)$$

Note that we only require as many boundary conditions for the assumed profile as there are undetermined constants in the profile. For Eq. 14.13a, we require three: (1) no slip at the surface, (2) matching the outer region velocity at the boundary layer edge, and (3) zero shear stress at the boundary layer edge. If we assumed a higher-order polynomial, we would have to match higher order derivatives (e.g. $d^2u/dy^2 = 0$ at $\lambda = 1$, etc.). Solving for the undetermined coefficients in Eq. 14.13a using the Eq. 14.13b boundary conditions:

$$\begin{aligned} \text{B.C. \#1} &\Rightarrow 0 = a + 0 + 0 \Rightarrow a = 0 \\ \text{B.C. \#2} &\Rightarrow 1 = b + c \\ \text{B.C. \#3} &\Rightarrow 0 = b + 2c \end{aligned} \quad \left. \begin{array}{l} \\ \\ \end{array} \right\} \begin{array}{l} b = 2 \\ c = -1 \end{array}$$

Thus, the particular form of this polynomial velocity profile is:

$$\frac{u}{U_\infty} = 2\lambda - \lambda^2 = 2\left(\frac{y}{\delta}\right) - \left(\frac{y}{\delta}\right)^2 \quad (14.14)$$

Figure 14.1 shows the shape of this assumed polynomial velocity profile from Eq. 14.14.

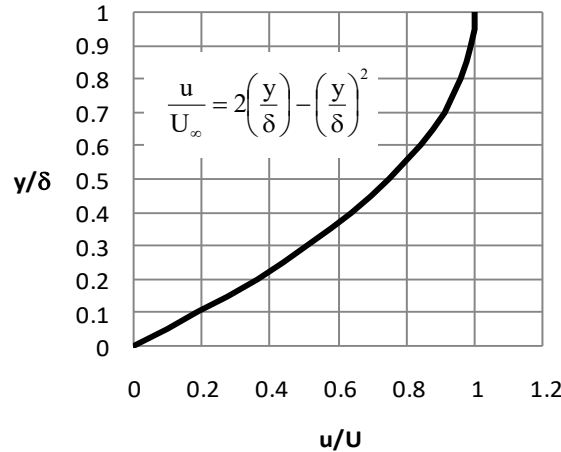


Figure 14.1 The shape of a second-order polynomial similarity velocity profile for a laminar boundary layer.

Next, we use this approximate velocity profile described by Eq. 14.14 to determine the functional relationship of the boundary layer parameters δ^* , θ , and τ_w in terms of the boundary layer thickness, δ .

$$\delta^* = \int_0^\delta \left(1 - \frac{u}{U_\infty}\right) dy \quad \text{Note that } d\lambda = \frac{dy}{\delta}, \text{ so } dy = \delta d\lambda$$

$$= \int_0^{\lambda=1} \left(1 - \frac{u}{U_\infty}\right) \delta d\lambda = \delta \int_0^1 (1 - 2\lambda + \lambda^2) d\lambda$$

$$\delta^* = \delta \left[\lambda - \lambda^2 + \frac{\lambda^3}{3} \right]_0^1 = \frac{\delta}{3} \tag{14.15a}$$

and

$$\theta = \int_0^\delta \frac{u}{U_\infty} \left(1 - \frac{u}{U_\infty}\right) dy = \delta \int_0^{\lambda=1} \frac{u}{U_\infty} \left(1 - \frac{u}{U_\infty}\right) d\lambda$$

$$= \delta \int_0^1 (2\lambda - \lambda^2)(1 - 2\lambda + \lambda^2) d\lambda = \delta \left[\lambda^2 - \frac{5}{3}\lambda^3 + \lambda^4 - \frac{1}{5}\lambda^5 \right]_0^1 = \frac{2\delta}{15} \tag{14.15b}$$

and,

$$\tau_w = \mu \left. \frac{du}{dy} \right|_{y=0} = \mu \left. \frac{du}{d\lambda} \frac{d\lambda}{dy} \right|_{\lambda=0} = \mu \underbrace{\frac{1}{\delta} \left. \frac{du}{d\lambda} \right|_{\lambda=0}}_{U_\infty(2-2\lambda)} = \frac{2\mu U_\infty}{\delta} \tag{14.15c}$$

We now substitute the boundary layer parameters from Eqs. 14.15 back into the momentum integral equation, Eq. 14.11, to obtain a differential equation for $\delta(x)$:

$$\frac{d}{dx} \left(\frac{2\delta}{15} \right) + \left(\frac{\delta}{3} + \frac{4\delta}{15} \right) \frac{1}{U_\infty} \frac{dU_\infty}{dx} = \frac{2\mu U_\infty}{\delta \rho U_\infty^2} = \frac{2\nu}{\delta U_\infty}$$

or

$$\frac{2}{15} \frac{d\delta}{dx} + \frac{3\delta}{5U_\infty} \frac{dU_\infty}{dx} = \frac{2\nu}{\delta U_\infty} \quad (14.16)$$

However, recall that for a flat plate flow, $U_\infty = \text{const.} \Rightarrow \frac{dU_\infty}{dx} = 0$

$$\therefore \frac{2}{15} \frac{d\delta}{dx} = \frac{2\nu}{\delta U_\infty} \quad \text{for a flat plate flow}$$

To solve for $\delta = \delta(x)$, we separate variables and integrate,

$$\int \delta d\delta = \frac{15\nu}{U_\infty} \int dx$$

$$\frac{\delta^2}{2} = \frac{15\nu x}{U_\infty} + C_1 \quad (14.17)$$

To determine C_1 in Eq. 14.17, we need a bounding condition on δ and x for the flow. For a flat plate flow, with the boundary layer initiating at the leading edge, we have:

$$\delta = 0 \text{ @ } x = 0 \Rightarrow C_1 = 0$$

Note that if the boundary layer had some prior initial value (e.g. δ_0 at x_0), we would have used those values as our starting conditions, and then determine the constant C_1 in Eq. 14.17.

However, for $C_1 = 0$ in Eq. 14.17, we establish the relationship for boundary layer growth with streamwise distance as:

$$\delta = \sqrt{\frac{30\nu x}{U_\infty}} = 5.477 \sqrt{\frac{\nu x}{U_\infty}}$$

or

$$\frac{\delta}{x} = \frac{5.477}{\sqrt{\text{Re}_x}} \quad \text{where} \quad \text{Re}_x = \frac{U_\infty x}{\nu} \quad (14.18)$$

Now using Eq. 14.18, and our previous Eqs. 14.15 -- the relationship of δ^* , θ , and τ_w as functions of δ -- we can write:

$$\delta^* = \frac{\delta}{3} = 1.826 \sqrt{\frac{\nu x}{U_\infty}} = \frac{1.826x}{\sqrt{\text{Re}_x}} \quad (14.19a)$$

$$\theta = \frac{2\delta}{15} = 0.730 \sqrt{\frac{\nu x}{U_\infty}} = \frac{0.730x}{\sqrt{\text{Re}_x}} \quad (14.19b)$$

$$\tau_w = \frac{2\mu U_\infty}{\delta} = \frac{2\mu U_\infty}{5.477 \sqrt{\frac{\nu x}{U_\infty}}} = \frac{2\mu U_\infty^2}{5.477 \nu \sqrt{\frac{U_\infty x}{\nu}}} = \frac{0.730 \left(\frac{1}{2} \rho U_\infty^2\right)}{\sqrt{\mathbf{Re}_x}} \quad (14.19c)$$

Comparing the results of the integral solution, Eqs. 14.18 and 14.19, to the Blasius solution of section 13.5 (Eqs. 13.29, 13.30, 13.31, and 13.32), we have:

$$\frac{\delta}{\delta_{\text{Blasius}}} = \frac{5.477}{5} = 1.095$$

$$\frac{\delta^*}{\delta_{\text{Blasius}}^*} = \frac{1.826}{1.717} = 1.063$$

$$\frac{\theta}{\theta_{\text{Blasius}}} = \frac{0.730}{0.660} = 1.106$$

$$\frac{c_f}{c_{f \text{ Blasius}}} = \frac{\tau_w}{\tau_{w \text{ Blasius}}} = \frac{0.730}{0.660} = 1.106$$

Therefore, the results from using our “approximate” velocity profile end up being approximately 10% high. Note that these results, although higher, are still relatively close to the exact Blasius solution (and a lot easier to obtain). Such results are generally quite adequate for most engineering applications.

In general, one can obtain better comparisons to the Blasius' solution by employing velocity profiles that better approximate the Blasius velocity profile. Table 14.1 shows the results obtained for the second-order polynomial profile of Eq. 14.14, compared with results for six other approximate velocity profiles, and the Blasius profile (Table 13.1). Fig. 14.2 is a graphical comparison of these approximate profiles to the Blasius profile. As Fig. 14.2 shows, the variation of the approximate profiles from the Blasius can be quite significant. However, several of the results of Table 14.1 show remarkable similarity to the Blasius results.

Table 14.1 illustrates that increasing the order of the polynomial profile does not necessarily assure a closer match to the Blasius result; for example, the four-term, fourth-order profile gives the worst results of all the approximate velocity profiles shown—even worse than the linear profile. One might also assume that a velocity profile that most closely compares to the Blasius profile would yield the best comparative boundary layer parameters. However, this is also not necessarily the case, since a comparison of the results of table 14.1 with the shape of the profiles in Fig. 14.2 illustrates that the closest approximate profile shape is the second-order polynomial (i.e. $\frac{u}{U_\infty} = 2\lambda - \lambda^2$), but this profile does not give boundary layer parameters that are the closest to the Blasius results.

Table 14.1
Comparison of predicted boundary layer characteristics
for selected approximate velocity profiles:
Flat plate flow with no pressure gradient

Assumed Velocity Profile $\frac{u}{U_\infty} = f\left(\frac{y}{\delta}\right) = f(\lambda)$	$\frac{\delta}{x} \sqrt{\text{Re}_x}$	$\frac{\delta^*}{x} \sqrt{\text{Re}_x}$	$\frac{\theta}{x} \sqrt{\text{Re}_x}$	$H = \frac{\delta^*}{\theta}$	$c_f \sqrt{\text{Re}_x}$
$f(\lambda) = \lambda$	3.464	1.732	0.577	3.00	0.577
$f(\lambda) = 2\lambda - \lambda^2$	5.447	1.826	0.730	2.50	0.730
$f(\lambda) = 1.5\lambda - 0.5\lambda^3$	4.641	1.740	0.646	2.69	0.646
$f(\lambda) = 3\lambda - 3\lambda^2 + \lambda^3$	7.483	1.871	0.801	2.34	0.801
$f(\lambda) = 4\lambda - 6\lambda^2 + 4\lambda^3 - \lambda^4$	9.486	1.897	0.843	2.25	0.843
$f(\lambda) = 2\lambda - 2\lambda^3 + \lambda^4$	5.836	1.751	0.685	2.55	0.686
$f(\lambda) = \sin\left(\frac{\pi}{2}\lambda\right)$	4.795	1.742	0.655	2.66	0.655
Blasius Solution	5	1.717	0.660	2.60	0.660

Assumed Velocity Profile $\frac{u}{U_\infty} = f\left(\frac{y}{\delta}\right) = f(\lambda)$	$\frac{\delta}{\delta_{\text{Blasius}}}$	$\frac{\delta^*}{\delta^*_{\text{Blasius}}}$	$\frac{\theta}{\theta_{\text{Blasius}}}$	$\frac{H}{H_{\text{Blasius}}}$	$\frac{c_f}{c_{f-\text{Blasius}}}$
$f(\lambda) = \lambda$	0.693	1.009	0.874	1.154	0.874
$f(\lambda) = 2\lambda - \lambda^2$	1.089	1.063	1.106	0.962	1.106
$f(\lambda) = 1.5\lambda - 0.5\lambda^3$	0.928	1.013	0.979	1.035	0.979
$f(\lambda) = 3\lambda - 3\lambda^2 + \lambda^3$	1.497	1.090	1.214	0.900	1.214
$f(\lambda) = 4\lambda - 6\lambda^2 + 4\lambda^3 - \lambda^4$	1.897	1.105	1.277	0.865	1.277
$f(\lambda) = 2\lambda - 2\lambda^3 + \lambda^4$	1.167	1.020	1.039	0.981	1.039
$f(\lambda) = \sin\left(\frac{\pi}{2}\lambda\right)$	0.959	1.014	0.992	1.023	0.992
Blasius Solution	5	1.717	0.660	2.60	0.660

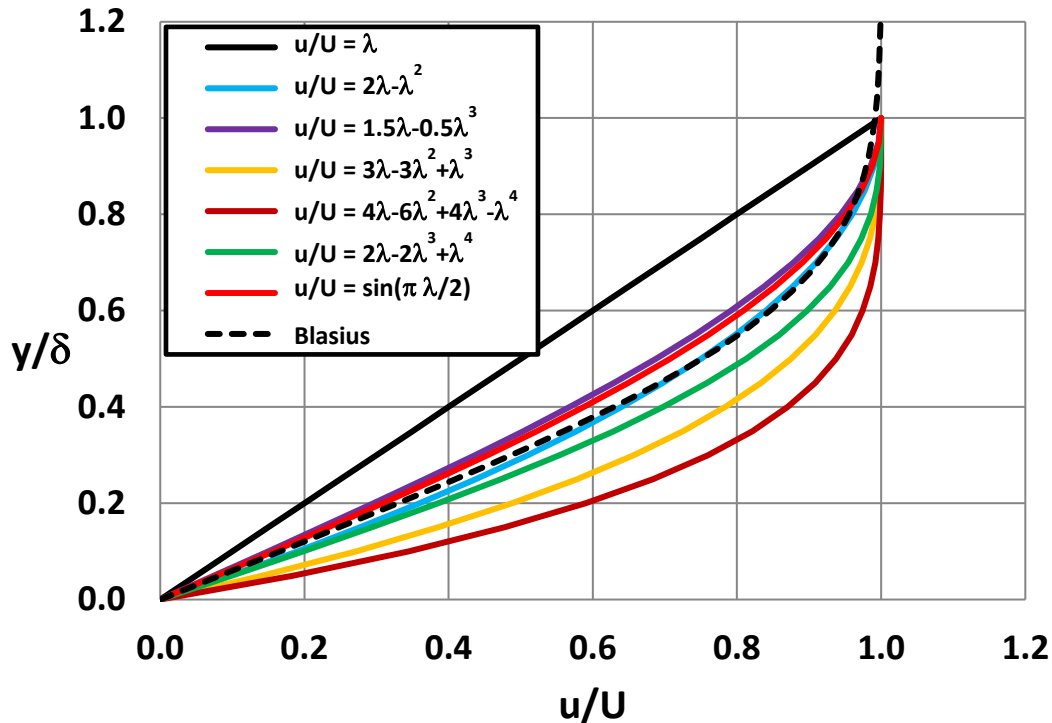


Figure 14.2 Comparison of six different approximate velocity profiles with the Blasius solution.

The best comparisons of boundary layer parameters are given by the three-term, fourth-order polynomial and the sine-shaped profile, both of which diverge further from the Blasius velocity profile than the second-order profile. Thus, while establishing the precise “shape” of the velocity profile is desirable, it is not essential in order to obtain good results for boundary layer parameters, and in particular the friction factor, c_f .

Note that Table 14.1 lists two different fourth-order velocity profiles. These are the result of using a different fifth boundary condition when developing the assumed profile. For the four-term profile, the fifth boundary condition was $\frac{d^3 u}{dy^3} = 0$ @ $y = \delta$ ($\lambda = 1$). For the three-term

profile, the fifth boundary condition was $\frac{d^2 u}{dy^2} = 0$ @ $y = 0$ ($\lambda = 0$). See problem number 5 at

the end of this chapter to see how this latter boundary condition is determined using the original boundary layer equations.

As we stated above, if the boundary layer had some prior initial value (e.g. δ_0 at x_0), we would have used those values as our starting conditions. Reassessing our Eq. 14.17 (for a second-order polynomial), we have:

$$\frac{\delta_0^2}{2} = \frac{15\nu x_0}{U_\infty} + C_1 \Rightarrow C_1 = \frac{\delta_0^2}{2} - \frac{15\nu x_0}{U_\infty}$$

Substituting C_1 back into Eq.14.17 and solving for δ gives:

$$\delta = \sqrt{\frac{30\nu(x - x_0)}{U_\infty} + \delta_0^2}$$

So, δ will grow from the original boundary layer thickness, but (show this for yourself), more slowly than it would have if it initiated at $\delta = 0$. The other boundary layer parameters will also grow more slowly.

14.3 Approximate Solution with a Pressure Gradient: Thwaites' Method

The use of similarity velocity profiles, as was done in Section 14.2, is one method of solving the momentum integral equation exactly, using approximate velocity profiles. However, the resulting equation can only be solved analytically for selected functional variations of the free stream velocity with x . Additionally, the assumed velocity profile may not be appropriate for modeling various types of free stream flows where the velocity profiles are not "similar". In this section, we will present another approximate method, which does not require an assumed velocity profile, and can be used for any type of free stream velocity, whether accelerating or decelerating.

We now consider the development of an *exact solution* of the approximated integral equation using curve fits of existing analytical and experimental data. This technique has no restrictions, and yields good, approximate answers within roughly $\pm 10\%$. The method is based on the evaluation of all existing solutions of laminar flows available at the time it was developed, and employs some judicious tabulation and curve fitting of the data to create a method that establishes key boundary layer parameters by reducing the boundary layer equations to a one-dimensional integral of the free-stream velocity behavior. Other boundary layer characteristics are then obtained by correlation with a set of tabulated data. The limitation of the method is that it is only useful for *laminar* flows. In honor of the gentleman who developed this technique, [Thwaites \(1949\)](#), this approach is termed *Thwaites' Method*.

As our starting point, consider again the momentum integral equation, Eq. 14.12. Rather than employ an approximate velocity profile, let us see how we can further manipulate the terms in the equation, to yield terms that can be related to physical aspects of the flow, and which we might be able to model approximately.

Starting with the momentum integral equation, Eq. 14.12,

$$\frac{d\theta}{dx} + \frac{1}{U_\infty} \frac{dU_\infty}{dx} (2\theta + \delta^*) = \frac{\tau_w}{\rho U_\infty^2},$$

we note that at the bounding solid surface ($y = 0$), $\tau_w = \mu \left. \frac{\partial u}{\partial y} \right|_{y=0}$. Additionally, we multiply the equation through by $2\theta U_\infty / \nu$ to give:

$$U_\infty \frac{2\theta}{\nu} \frac{d\theta}{dx} + \frac{1}{U_\infty} \frac{dU_\infty}{dx} \frac{2\theta U_\infty}{\nu} (2\theta + \delta^*) = \frac{2\theta U_\infty}{\nu} \frac{\mu}{\rho U_\infty^2} \left. \frac{\partial u}{\partial y} \right|_0 \quad (14.20)$$

Simplifying and rearranging Eq. 14.20 yields,

$$U_\infty \frac{2\theta}{\nu} \frac{d\theta}{dx} = -2 \left[\frac{\theta^2}{\nu} \frac{dU_\infty}{dx} \left(2 + \frac{\delta^*}{\theta} \right) - \frac{\theta}{U_\infty} \left. \frac{\partial u}{\partial y} \right|_0 \right] \quad (14.21)$$

Now, we introduce the following dimensionless variables,

$$\ell = \frac{\theta}{U_\infty} \left(\frac{\partial u}{\partial y} \right)_{y=0} \quad (14.22a)$$

$$H = \frac{\delta^*}{\theta} \quad (14.22b)$$

$$n = - \frac{\theta^2}{\nu} \frac{dU_\infty}{dx} \quad (14.22c)$$

Note that Eq. 14.22a reflects a shear stress parameter, Eq. 14.22b is the “shape” parameter discussed in Section 4.2.1 (reflecting the degree of deformation of the boundary layer velocity profile), and Eq. 14.22c characterizes a pressure gradient parameter. Substituting Eqs. 14.22 into Eq. 14.21 and rearranging a bit yields (prove this yourself):

$$- U_\infty \frac{d}{dx} \left(\frac{n}{dU_\infty/dx} \right) = 2[n(H + 2) + \ell] \quad (14.23)$$

Since $U_\infty(x)$ is assumed known, Eq. 14.23 is a single equation for the three unknowns n , ℓ , and H .

Thwaites collected all available analytical and experimental results for laminar boundary layers, and computed the corresponding values of the n , ℓ , and H parameters for each set of data. For example, for a flat plate (using the Blasius solution of Section 13.5):

$$\ell = \frac{\theta}{U_\infty} \left(\frac{\partial u}{\partial y} \right)_0 = \frac{0.664x}{U_\infty \sqrt{\text{Re}_x}} \frac{1}{2} \frac{U_\infty^2}{\nu} \frac{0.664}{\sqrt{\text{Re}_x}} = \frac{(0.664)^2}{2} = 0.220$$

$$H = \frac{1.726x}{\sqrt{Re_x}} \frac{\sqrt{Re_x}}{0.664x} = 2.60$$

$$n = -\frac{\theta^2}{\nu} \frac{dU_\infty}{dx} = 0$$

Table 14.2
Parametric boundary layer
data developed by Thwaites

n	ℓ	H
0.090	0.000	3.70
0.088	0.015	3.62
0.086	0.027	3.54
0.084	0.038	3.47
0.080	0.056	3.35
0.076	0.072	3.24
0.072	0.085	3.16
0.068	0.095	3.09
0.064	0.104	3.04
0.060	0.113	2.99
0.056	0.122	2.94
0.048	0.138	2.87
0.040	0.153	2.81
0.032	0.168	2.75
0.016	0.195	2.67
0.000	0.220	2.60
-0.016	0.244	2.55
-0.032	0.268	2.49
-0.048	0.291	2.44
-0.064	0.313	2.39
-0.080	0.333	2.34
-0.100	0.359	2.28
-0.120	0.382	2.23
-0.140	0.404	2.18
-0.200	0.463	2.07
-0.25	0.5	2.00

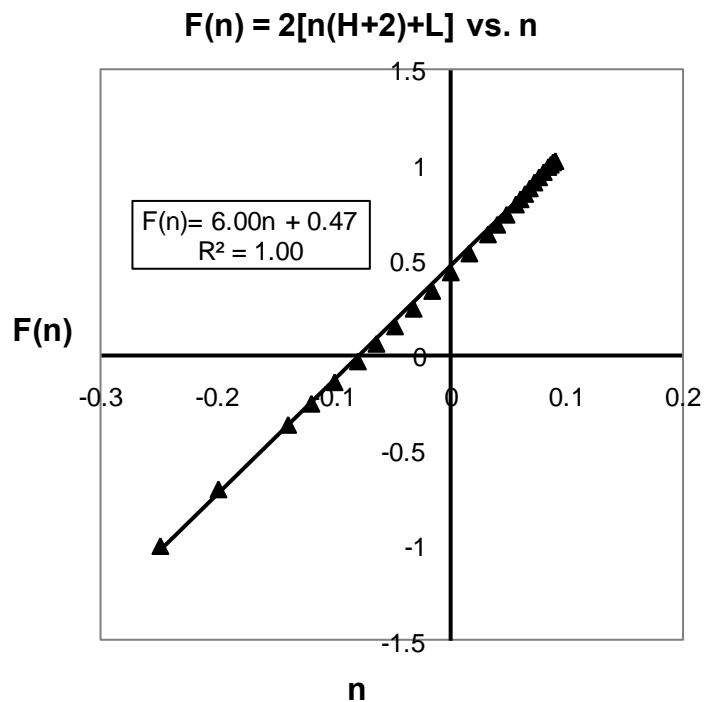


Figure 14.3 Linear regression of F(n) vs. n, reflected in Eq. 14.24.

In this way, Thwaites was able to develop a comprehensive table of n, ℓ, and H for all the available laminar boundary layer data, which is shown in Table 14.2. Using this collected data, he determined that a linear curve fit, shown in Fig. 14.3, could be developed for the parameter function $F(n) = 2[n(H + 2) + \ell]$, the right side of Eq. 14.23. Thwaites determined that the parametric fit, Eq. 14.24, is essentially only a function of the parameter n (However, it did take Thwaites a number of tries to determine this proper collection of terms for F(n)).

$$F(n) = 2[n(H + 2) + \ell] \cong 0.47 + 6n \tag{14.24}$$

Note that Eq. 14.24 is an Excel curve fit I did of Thwaites data, which yields a slightly different equation than Thwaites determined, who utilized a regression analysis that forced the curve fit to match the Blasius data exactly (his fit was $F(n) = 0.45 + 6n$). I will discuss my rationale for this variance later.

Substituting Eq.14.24 into Eq. 14.23, we obtain:

$$-U_{\infty} \frac{d}{dx} \left(\frac{n}{dU_{\infty}/dx} \right) = 0.47 + 6n = F(n) \quad (14.25)$$

Further, substituting back $n = -\frac{\theta^2}{\nu} \frac{dU_{\infty}}{dx}$ from Eq. 14.22c into Eq.14.25 gives:

$$U_{\infty} \frac{d}{dx} \left(\frac{\theta^2}{\nu} \right) = 0.47 - 6 \frac{\theta^2}{\nu} \frac{dU_{\infty}}{dx}$$

or

$$U_{\infty} \frac{d(\theta^2)}{dx} + 6\theta^2 \frac{dU_{\infty}}{dx} = 0.47\nu \quad (14.26)$$

We make the left-hand side of Eq. 14.26 a total differential by multiplying through by U_{∞}^m , and establish an integrating factor, m:

$$U_{\infty}^{m+1} \frac{d(\theta^2)}{dx} + 6\theta^2 U_{\infty}^m \frac{dU_{\infty}}{dx} = 0.47\nu U_{\infty}^m \quad (14.27)$$

Noting that we can write,

$$\frac{d(U_{\infty}^{m+1} \theta^2)}{dx} = U_{\infty}^{m+1} \frac{d(\theta^2)}{dx} + \theta^2 (m+1) U_{\infty}^m \frac{dU_{\infty}}{dx},$$

we choose $m+1 = 6$, or $m = 5$, which allows us to rewrite the left side of Eq. 14.27 as:

$$U_{\infty}^6 \frac{d(\theta^2)}{dx} + 6\theta^2 U_{\infty}^5 \frac{dU_{\infty}}{dx} = \frac{d(U_{\infty}^6 \theta^2)}{dx} = 0.47\nu U_{\infty}^5 \quad (14.28)$$

Integrating Eq. 14.28 gives:

$$U_{\infty}^6 \theta^2 \Big|_{\theta_0}^{\theta} = 0.47\nu \int_{x_0}^x U_{\infty}^5 dx \quad (14.29)$$

If we assume a starting value of $\theta_0 = 0$ at $x_0 = 0$, Eq. 14.29 becomes:

$$U_{\infty}^6 \theta^2 = 0.47\nu \int_0^x U_{\infty}^5 dx \quad (14.30)$$

Rearranging Eq. 14.30 gives an expression for the momentum thickness, θ :

$$\frac{\theta^2}{\nu} = 0.47U_\infty^{-6} \int_0^x U_\infty^5 dx \quad (14.31)$$

Substituting Eq. 14.31 into Eq. 14.22c gives an expression for n :

$$n = -0.47U_\infty^{-6} \frac{dU_\infty}{dx} \int_0^x U_\infty^5 dx \quad (14.32)$$

Thus, for a known $U_\infty(x)$, we can compute the momentum thickness, θ , from Eq. 14.31, and the pressure gradient parameter, n , from Eq. 14.32. Knowing n , the values of ℓ and H are obtained either by interpolation from Table 14.2, or from a curve fit of H vs. n and ℓ vs. n . And knowing n , ℓ , and H , all the boundary layer parameters (and τ_w) can be computed.

However, be careful using Eqs. 14.31 and 14.32. As we point out above, these are derived assuming an initial value of $\theta = 0$ at $x = 0$. If the boundary layer has had some initial development (e.g. development over a flat plate followed by an acceleration), then you will need to integrate Eq. 14.29 using an initial value of $\theta_o = \theta_{init}$ at $x_o = 0$, with the corresponding initial velocity, $U_\infty = U_{init}$ at $x_o = 0$.

Thus, reintegrating Eq. 14.29 with $\theta = \theta_{init}$ and $U_\infty = U_{init}$ at $x_o = 0$, will give:

$$U_\infty^6 \theta^2 \Big|_{\theta=\theta_{init}}^0 = U_\infty^6 \theta^2 - U_{init}^6 \theta_{init}^2 = 0.47\nu \int_0^x U_\infty^5 dx \quad (14.33)$$

or

$$\begin{aligned} \frac{\theta^2}{\nu} &= \frac{U_{init}^6}{U_\infty^6} \frac{\theta_{init}^2}{\nu} + 0.47U_\infty^{-6} \int_0^x U_\infty^5 dx \\ \theta &= \left[\frac{U_{init}^6}{U_\infty^6} \theta_{init}^2 + 0.47\nu U_\infty^{-6} \int_0^x U_\infty^5 dx \right]^{0.5} \end{aligned} \quad (14.34)$$

with the value of n being given by:

$$n = -\frac{dU_\infty}{dx} \left(\frac{U_{init}^6}{U_\infty^6} \theta_{init}^2 + 0.47\nu U_\infty^{-6} \int_0^x U_\infty^5 dx \right) \quad (14.35)$$

Equations 14.34 and 14.35 will then yield results for the behavior of a boundary layer that had some prior development. If we have $\theta_o = \theta_{init}$ at $x_o = x_{init}$, then the computation gets a bit messier, but is still a straight forward integration, starting from $x = x_{init}$, not $x = 0$.

Note that Thwaite's technique is essentially a curve fit of available data via the boundary layer equation. This is not truly a predictive technique in that all the data shown in Table 14.2 was either measured experimentally or developed from analytical data, so what we really have is a sophisticated curve fit of parametric data. That being said, Thwaites' method is a very effective technique for prediction of a wide range of laminar flows, and is still the technique of choice for engineering prediction of laminar flows, giving results that are good to $\pm 10\%$ or better.

14.4 Predicting Laminar Boundary Layer Characteristics Using Thwaites' Method

To illustrate the use of Thwaites' method, we will examine three different flows: the conventional flat plate flow, an accelerating flow, and a decelerating flow.

14.4.1 Flat Plate Flow

A flat plate flow has a constant velocity outer region flow such that $U_\infty = \text{constant}$. Thus,

$\frac{dU_\infty}{dx} = 0$, and the pressure gradient parameter, n , is calculated from Eq. 14.32 as:

$$n = -0.47U_\infty^{-6} \frac{dU_\infty}{dx} \int_0^x U_\infty^5 dx$$

$$n = 0$$

Note that $n = 0$ for all x locations, which also fixes the values of ℓ and H , as obtained from Table 14.2.

x	n	ℓ	H
	0	0.220	2.60

The value of the momentum thickness, θ , is obtained from Eq. 14.31 as:

$$\begin{aligned} \frac{\theta^2}{\nu} &= 0.47U_\infty^{-6} \int_0^x U_\infty^5 dx \\ &= 0.47U_\infty^{-6} U_\infty^5 (x - 0) \\ &= \frac{0.47x}{U_\infty} \end{aligned}$$

$$\theta = 0.685 \sqrt{\frac{\nu x}{U_\infty}} \quad \text{or} \quad \frac{\theta}{x} = \frac{0.685}{\sqrt{\text{Re}_x}} \quad (14.36)$$

Note that the value of θ determined from Eq. 14.36 is about 3% greater than that determined from the Blasius solution, Eq. 13.31. This may seem curious, since the Blasius values were incorporated into the data used to determine the function $F(n)$ in Eq. 14.25. However, $F(n)$ was a linear curve fit of the cumulative data, and as one can see in Fig. 14.3, the curve fit is slightly higher than the actual data for $n = 0$, the flat plate flow. Other versions of Thwaites' method have employed linear curve fits of the data in Table 14.2 that force the curve fit to pass through the flat plate data exactly, since it is the most reliable data value in Table 14.2. However, the present curve fit is really a more accurate reflection of the cumulative data. And a 3% variation is well within the accuracy one might expect for this technique (roughly $\pm 10\%$).

Now, if the boundary layer had some previous development, such that $\theta = \theta_i$ at $x = 0$, we would use Eqs. 14.34 and 14.35 to determine the boundary layer characteristics. So, for the momentum thickness, we would have from Eq. 14.34:

$$\frac{\theta^2}{\nu} = \frac{\theta_i^2}{\nu} + 0.47U_\infty^{-6} \int_0^x U_\infty^5 dx$$

Or solving for θ :

$$\frac{\theta^2}{\nu} = \frac{\theta_i^2}{\nu} + \frac{0.47x}{U_\infty} \Rightarrow \frac{\theta}{x} = \sqrt{\left(\frac{\theta_i}{x}\right)^2 + \frac{0.47}{\left(\frac{U_\infty x}{\nu}\right)}} = \sqrt{\left(\frac{\theta_i}{x}\right)^2 + \frac{0.47}{\text{Re}_x}}$$

And since $\frac{dU_\infty}{dx} = 0$, n is still 0. Note that if this was an accelerating or decelerating flow,

$\frac{dU_\infty}{dx} \neq 0$, and n would also be non-zero.

14.4.2 Linearly Accelerating Flow

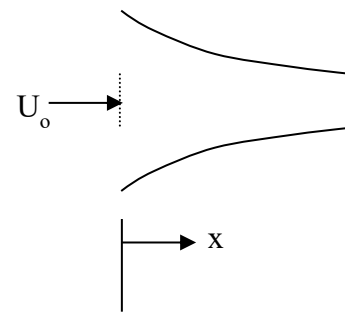
Here we examine a linearly accelerating flow given by

$$U_\infty = U_0(1 + x'), \text{ where } x' = \frac{x}{a}, \text{ and } a \text{ is a constant.}$$

Thus, $\frac{dU_\infty}{dx} = \frac{U_0}{a}$, and n is determined using Eq. 14.32

(where we note that $dx = a dx'$):

$$\begin{aligned} n &= -0.47U_0^{-6}(1+x')^{-6} \frac{U_0}{a} \int_0^{x'} U_0^5(1+x')^5 a dx' \\ &= \frac{-0.47}{(1+x')^6} \left[\frac{(1+x')^6}{6} \right]_0^{x'} \end{aligned}$$



$$n = \frac{-0.078}{(1+x')^6} [(1+x')^6 - 1] = -0.078 \left[1 - \frac{1}{(1+x')^6} \right] \tag{14.37}$$

Equation 14.37 indicates that n varies significantly with x' , which requires that one interpolate the corresponding values of ℓ and H at any x' location from Table 14.2, or by means of a curve fit of ℓ and H vs. n . The following table shows the respective values of n , ℓ , and H at $x' = 0$ and $x' = 1$. As the flow accelerates, the shear (reflected by ℓ) increases, and the shape factor, H , decreases. A decrease in H means that the velocity profile displays a stronger gradient near the wall (and thus a higher shear stress).

x'	n	ℓ	H
0	0	0.220	2.60
1	-0.077	0.329	2.35

Using Eq. 14.31, the momentum thickness for this accelerating flow is determined as:

$$\frac{\theta^2}{\nu} = \frac{0.078a}{U_0} \left[1 - \frac{1}{(1+x')^6} \right]$$

$$\theta = 0.279 \sqrt{\frac{\nu a}{U_0}} \left[1 - \frac{1}{(1+x')^6} \right]^{1/2} \tag{14.38}$$

Equation 14.38 also shows a strong initial dependence on x' . However, note that for $x' > 1$, θ becomes essentially constant. Additionally, Eq. 14.37 indicates that for $x' > 1$, n is also constant, which in turn means that ℓ and H also become constants. This means that the boundary layer basically stops growing and maintains a constant shape!

If θ and H become constant, this means that τ_o is a result of pressure gradient effects only. This can be shown from the original integral equation, Eq. 14.12, as follows:

$$\frac{d\theta}{dx} + \underbrace{\frac{1}{U_\infty} \frac{dU_\infty}{dx}}_{\text{Pressure Gradient}} (2\theta + \delta^*) = \underbrace{\frac{\tau_o}{\rho U_\infty^2}}_{\text{Shear Stress}} \tag{14.39}$$

Equation 14.38 indicates that after roughly $x' = 1$, as the flow continues to accelerate, no further momentum is lost from the flow (since θ ceases growing) and $\frac{d\theta}{dx} \cong 0$. Thus, as shown by Eq. 14.39, the changes in the pressure exactly balance the shear stress. If we rewrite Eq. 14.39 (for $\frac{d\theta}{dx} = 0$), noting that from Bernoulli,

$\frac{dP_\infty}{dx} + \rho U_\infty \frac{dU_\infty}{dx} = 0$, and $H = \frac{\delta^*}{\theta}$, we get:

$$\tau_0 = \rho U_\infty \frac{dU_\infty}{dx} (2\theta + \delta^*) = -\frac{dP_\infty}{dx} (2\theta + H\theta) = -(2 + H)\theta \frac{dP_\infty}{dx} \quad (14.40)$$

Thus, since θ and H will be constants, Eq. 14.40 indicates that the shear will be directly proportional to the pressure gradient (note that since this is an accelerating flow, the pressure is decreasing, and $\frac{dP_\infty}{dx} < 0$, such that $\tau_0 > 0$). For this particular flow, with $U_\infty = U_0(1 + x')$, Eq. 14.40 becomes:

$$\tau_0 = \rho U_0^2 (2 + H)\theta(1 + x')$$

Which indicates that when θ and H become constant, the shear stress will increase linearly with x' .

14.4.3 Decelerating Flow

Now let's examine a decelerating flow given by $U_\infty = \frac{U_0}{(1 + x')}$, where again $x' = \frac{x}{a}$, and a is a constant. Here, we first determine θ using Eq. 14.31:

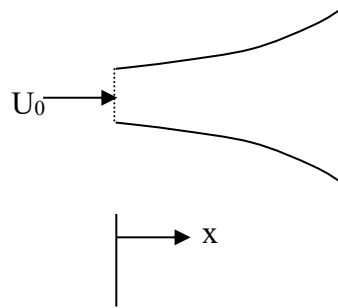
$$\frac{\theta^2}{\nu} = 0.47 U_\infty^{-6} \int_0^x U_\infty^5 dx$$

$$\frac{\theta^2}{\nu} = 0.47 U_0^{-6} (1 + x')^6 \int_0^x U_0^5 (1 + x')^{-5} a dx'$$

$$\frac{\theta^2}{\nu} = 0.47 U_0^{-1} (1 + x')^6 a \left[-\frac{(1 + x')^{-4}}{4} \right]_0^{x'}$$

$$\frac{\theta^2}{\nu} = 0.1175 \frac{a}{U_0} \left[(1 + x')^6 - (1 + x')^2 \right]$$

$$\theta = \left\{ 0.1175 \frac{\nu a}{U_0} (1 + x')^2 \left[(1 + x')^4 - 1 \right] \right\}^{1/2} \quad (14.41)$$



To get n , we note that $\frac{dU_\infty}{dx} = -\frac{U_0}{a(1 + x')^2}$, and using Eq. 14.22c we have:

$$n = -\frac{\theta^2}{\nu} \frac{dU_\infty}{dx} = -0.1175 \frac{a}{U_0} (1 + x')^2 \left[(1 + x')^4 - 1 \right] \left[-\frac{U_0}{a(1 + x')^2} \right]$$

$$n = -\frac{\theta^2}{\nu} \frac{dU_\infty}{dx} = 0.1175[(1+x')^4 - 1] \quad (14.42)$$

Equations 14.41 and 14.42 suggest that θ and n will grow quite rapidly with x' . However, for a boundary layer type flow, the limiting condition will be where the shear stress becomes zero, since at that point the flow near the wall will cease to move downstream, and the boundary layer assumptions fail. For the present decelerating flow the solution will fail when:

$$\tau_0 = \mu \left. \frac{\partial u}{\partial y} \right|_0 = 0 \Rightarrow \ell = \frac{\theta}{U_\infty} \left. \frac{\partial u}{\partial y} \right|_0 = 0$$

When $\ell = 0 \Rightarrow n = 0.090$ (from Table 14.2). Thus, the limiting condition for Eq. 14.42 is:

$$n = 0.1175[(1+x')^4 - 1] = 0.090$$

Solving for x' gives:

$$x' = \left(\frac{0.090}{0.1175} + 1 \right)^{\frac{1}{4}} - 1 \Rightarrow x' = 0.1528$$

The following table shows the initial and limiting conditions for this decelerating flow.

x'	n	ℓ	H
0	0	0.220	2.60
0.1528	0.090	0	3.70

Using this limiting value of x' , we calculate the corresponding limiting value of θ from Eq. 14.41:

$$\theta = \sqrt{0.1175 \frac{\nu a}{U_0} [(1.1528)^6 - (1.1528)^2]} = 0.346 \sqrt{\frac{\nu a}{U_0}} = \frac{0.346a}{\sqrt{\frac{U_0 a}{\nu}}}$$

As an example, consider an air flow for which $a = 1$ meter, $U_0 = 1$ m/s, $\nu = 1.6 \times 10^{-5}$ m²/s

Separation starts at 0.1528 meters

The corresponding momentum thickness: $\theta = 1.38$ mm

Thus, when $n = 0.090$, $H = 3.70 \Rightarrow \delta^* = 5.11$ mm

14.5 The Relationship of shear stress, drag, and momentum thickness when $\frac{dP}{dx} = 0$

A boundary layer flow for which the external velocity, U_∞ , remains a constant can be used to illustrate a unique relationship between shear stress and drag on a plate and the momentum thickness, θ . Consider the momentum integral equation, Eq. 14.11.

$$\frac{d\theta}{dx} + (\delta^* + 2\theta) \frac{1}{U_\infty} \frac{dU_\infty}{dx} = \frac{\tau_w}{\rho U_\infty^2}$$

If the external flow is constant, that means that $\frac{dU_\infty}{dx} = 0$, and the momentum integral equation reduces to:

$$\frac{d\theta}{dx} = \frac{\tau_w}{\rho U_\infty^2}$$

Which can be rewritten as:

$$\tau_w = \rho U_\infty^2 \frac{d\theta}{dx} \quad 14.43$$

Equation 14.43 is remarkable, since it indicates that the wall shear stress is a direct function of the change in the momentum thickness. Additionally, if we assume a plate of length L , and arbitrary width W , we can calculate the drag on that plate as:

$$\begin{aligned} \text{Drag} &= \int_{x=0}^{x=L} \tau_w W dx = \rho U_\infty^2 W \int_{x=0}^{x=L} \frac{d\theta}{dx} dx = \rho U_\infty^2 W \int_{\theta=\theta_0}^{\theta=\theta_L} d\theta \\ \text{Drag} &= \rho U_\infty^2 W (\theta_L - \theta_0) \end{aligned} \quad 14.44$$

Here, θ_0 and θ_L are the values of the momentum thickness at $x = 0$ and $x = L$ respectively.

Equation 14.44 is again remarkable, since it shows that the drag on a given plate of a length L is directly proportional to the difference in the momentum thickness at the end of the plate less the momentum thickness at the beginning of the plate. This does not just apply to a laminar flow, but also to (1) a turbulent boundary layer as well, as we will discuss in Chapter 17, and/or (2) any type of boundary layer conditions, such as transition from laminar to turbulent flow, or the effects of surface roughness and irregularities.

Thus, as long as the external flow is a constant (i.e. $\frac{dP}{dx} = 0$), a measure of the drag over a specified length of a surface (usually a flat surface) can be established using Eq. 14.44 by measurement of the velocity profiles and calculation of θ at the beginning and end locations. And if $x = 0$ is the leading edge of a plate where the boundary layer initiates (where θ is zero),

measurement of θ at any downstream location will establish the total drag up to that location. Pretty nifty.

14.6 The Effect of a Pressure Gradient on Boundary Layers

As the Thwaites solutions shown in Section 14.4 illustrate, the external pressure gradient has a strong influence on the boundary layer. Since shear effects are always working against fluid inertia (particularly near the bounding surface), the effect of the pressure gradient can either work (1) with inertia and against shear effects (for an accelerating flow, and a decreasing pressure gradient), or (2) it can work against inertia, and with the shear effects (for a decelerating flow, and an increasing pressure gradient). This latter situation, called an adverse pressure gradient, leads quickly to the termination of forward flow near the surface, resulting in reverse flow near the wall. As we have discussed before, this flow reversal causes a “separation” of the boundary layer from the surface, and the development of large energy losses in the flow. The Thwaites example done in section 14.4.3 is a particularly good illustration of the problem created by an adverse pressure gradient. For that example, the shear stress went to zero (the precursor to a flow reversal at the surface) by 15.3 cm (roughly 6 inches) from the initiation of the pressure gradient—a relatively short distance along the boundary!

This interplay between shear, inertia, and pressure is illustrated by a further manipulation of the integral equation to separate out the effects of inertia and pressure changes. Recall that Eq. 14.11 is written as:

$$\frac{d\theta}{dx} + (\delta^* + 2\theta) \frac{1}{U_\infty} \frac{dU_\infty}{dx} = \frac{\tau_w}{\rho U_\infty^2}$$

Multiplying Eq. 14.11 by ρU_∞^2 and rearranging yields:

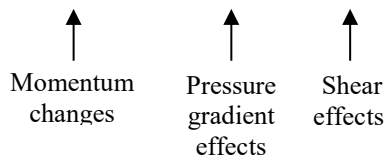
$$\rho \left(U_\infty^2 \frac{d\theta}{dx} + 2\theta U_\infty \frac{dU_\infty}{dx} \right) + \delta^* \rho U_\infty \frac{dU_\infty}{dx} = \tau_w$$

Combining the two left most terms, we have:

$$\frac{d(\rho U_\infty^2 \theta)}{dx} + \delta^* \rho U_\infty \frac{dU_\infty}{dx} = \tau_w$$

And noting that $\frac{dP}{dx} = -\rho U_\infty \frac{dU_\infty}{dx}$, and substituting, we get:

$$\frac{d(\rho U_\infty^2 \theta)}{dx} - \delta^* \frac{dP_\infty}{dx} = \tau_w \tag{14.45}$$



Equation 14.45 now clearly illustrates the interplay between shear, pressure gradient, and momentum changes. The interesting aspect of Eq. 14.45 is the impact of the pressure gradient.

Recall that for an accelerating flow, $\frac{dU_\infty}{dx} > 0$ and thus $\frac{dP}{dx} < 0$. Thus, for an accelerating flow, the changes in pressure and in momentum both contribute to an increased wall shear stress. Interestingly, even if the momentum thickness ceases growing (as was illustrated in the example in Section 14.4.2), the outer region velocity (U_∞) will continue to increase, such there will still be a positive momentum change in the boundary layer. Thus, for an accelerating flow the absolute shear will continue to increase, with the velocity profile "stretching" in the streamwise direction, since our boundary conditions require that $u = U_\infty$ at the edge of the boundary layer.

Conversely, for a decelerating flow $\frac{dU_\infty}{dx} < 0$ and thus $\frac{dP}{dx} > 0$. Consequently, the increasing pressure for a decelerating flow works in opposition to the momentum changes, and the shear will decrease. And, since U_∞ is decreasing, the momentum changes will also decrease (even as the momentum thickness grows rapidly), which further reduces the shear. As Eq. 14.45 illustrates, despite continued growth in the momentum thickness, the momentum will grow more slowly (since U_∞^2 is decreasing), and the pressure gradient will act more strongly in opposition to the flow as the displacement thickness grows. Ultimately, the momentum cannot withstand the opposing pressure force within the boundary layer, and the flow nearest the boundary will cease to move downstream, causing the boundary layer flow to separate from the surface (more on this in section 14.7).

To qualitatively examine the effect of a pressure gradient, dP/dx , on the boundary layer velocity profile, consider the two-dimensional boundary layer equation (Eq. 13.13a) evaluated at the bounding surface (i.e. at $y = 0$). By the no slip condition we have $u = 0$ at $y = 0$; and for a solid surface, we must have $v = 0$ at $y = 0$, thus:

$$\overset{0}{u} \frac{\partial u}{\partial x} + \overset{0}{v} \frac{\partial u}{\partial y} = -\frac{1}{\rho} \frac{dP}{dx} + \nu \frac{\partial^2 u}{\partial y^2} \quad \text{at } y = 0.$$

Thus, at the bounding surface we have:

$$\left. \frac{\partial^2 u}{\partial y^2} \right|_{y=0} = \frac{1}{\mu} \frac{dP}{dx} \quad (14.46)$$

Equation 14.46 indicates that the pressure gradient imposes a second-order *boundary condition* on the velocity profile at $y = 0$. Recall that in sections 11.5.1 and 11.5.3 we showed that a

streamwise pressure gradient is the source of vorticity at a bounding surface (for a steady flow).

Since at the bounding wall we have $\omega_z = -\frac{\partial u}{\partial y}$, then Eq. 14.46 can be rewritten as:

$$\left. \frac{\partial^2 u}{\partial y^2} \right|_{y=0} = \frac{1}{\mu} \frac{dP}{dx} = -\frac{\partial \omega_z}{\partial y} \tag{14.47}$$

Equation 14.47 indicates that the second order boundary condition is a vorticity source term, controlled by the pressure gradient, which will show in the following sections has a significant modifying effect on the boundary layer velocity profile.

To illustrate the impact of this pressure gradient boundary condition on the behavior of the boundary layer velocity profile, we qualitatively examine three different generic pressure gradient cases: a favorable pressure gradient ($dP/dx < 0$), no pressure gradient ($dP/dx = 0$), and an adverse pressure gradient ($dP/dx > 0$).

14.6.1 Favorable pressure gradient \Rightarrow accelerating flow ($\frac{dP}{dx} < 0$)

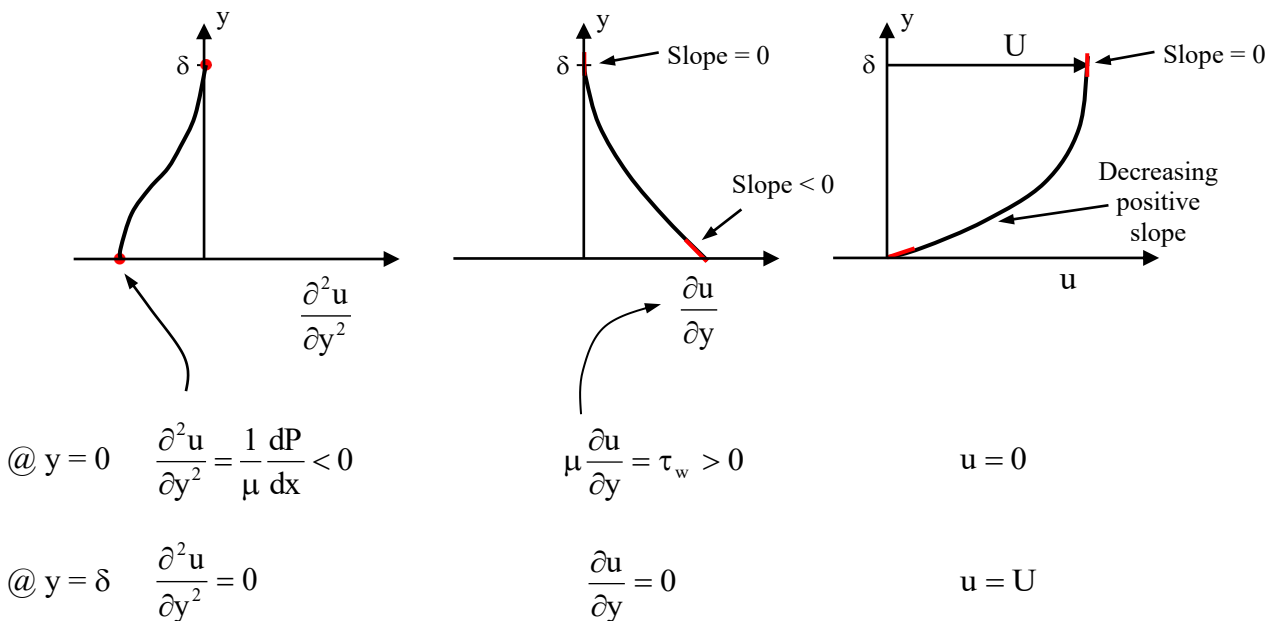


Figure 14.4 Effect of a favorable pressure gradient ($dP/dx < 0$) on the shape of the boundary layer velocity profile.

A favorable pressure gradient, as discussed above, acts in concert with the boundary layer momentum, and thus aids the flow very near the boundary to continue moving downstream. This is like having the wind at your back when running. As Fig. 14.4 illustrates, the second-order boundary condition is negative at the bounding surface ($y = 0$), and will, of course, be zero at the edge of the boundary layer ($y = \delta$). Since the second-order boundary conditions reflect the

local slope of the shear stress, the shear has a positive value, but with a negative slope at $y = 0$, and asymptotes to zero shear at $y = \delta$, with zero slope. The resulting velocity profile will maintain a full, non-inflectional shape while the pressure gradient remains favorable. Such flows are quite stable, with the boundary layer remaining attached to the surface (no reversed surface flow). Because this is a very stable type of flow, a favorable pressure gradient will help a boundary layer maintain laminar behavior, and resist transition to turbulence (we will discuss this further in Chapter 17)

14.6.2 Zero pressure gradient \Rightarrow constant velocity flow ($\frac{dP}{dx} = 0$)

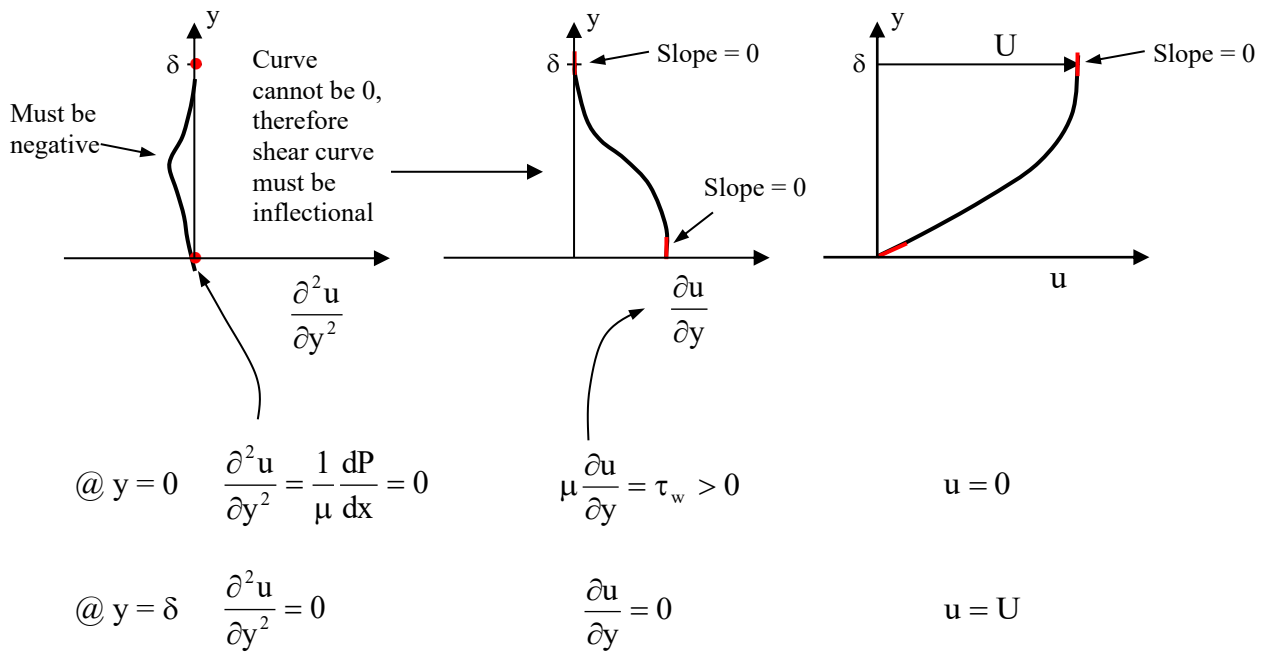


Figure 14.5 Effect of a zero pressure gradient ($dP/dx = 0$) on the shape of the boundary layer velocity profile.

For a zero pressure gradient flow, or flat plate flow, the pressure gradient has no impact on the boundary layer development. Such a flow, as was shown in the Blasius solution of Section 13.3, is a balance between inertia effects and shear effects. As is shown in Fig. 14.5, the second-order boundary condition is zero at the bounding surface ($y = 0$), and must also be zero at the edge of the boundary layer ($y = \delta$). Since the second-order boundary conditions reflect the respective local slope of the shear stress, the shear will have a positive value at $y = 0$, but with a zero slope. The shear must again asymptote to zero at $y = \delta$ with zero slope. Since the shear must experience a negative slope to connect between $y = 0$ and $y = \delta$, the shape of the shear profile will be as shown in Figure 14.5, and $\frac{\partial^2 u}{\partial y^2}$ must be negative between $y = 0$ and $y = \delta$, as shown.

The resulting velocity profile will be less full than for a favorable pressure gradient, and will

experience a point of inflection at $y = 0$. Because a [functional inflection](#) signals the possibility of unstable behavior, a flat plate laminar boundary layer is just barely stable. As such, small perturbations, such as velocity or pressure fluctuations, or surface irregularities, can cause a breakdown of the boundary layer to turbulence. In general, beyond a Reynolds number of roughly 5×10^5 , very good flow conditions (i.e. smooth surface and minimal pressure/velocity fluctuations in the outer flow) are required to maintain a laminar boundary layer over a flat plate with a zero pressure gradient. However, with ideal flow conditions laminar flows can be maintained in excess of $Re_x = 10^6$.

14.6.3 Adverse pressure gradient \Rightarrow decelerating flow ($\frac{dP}{dx} > 0$)

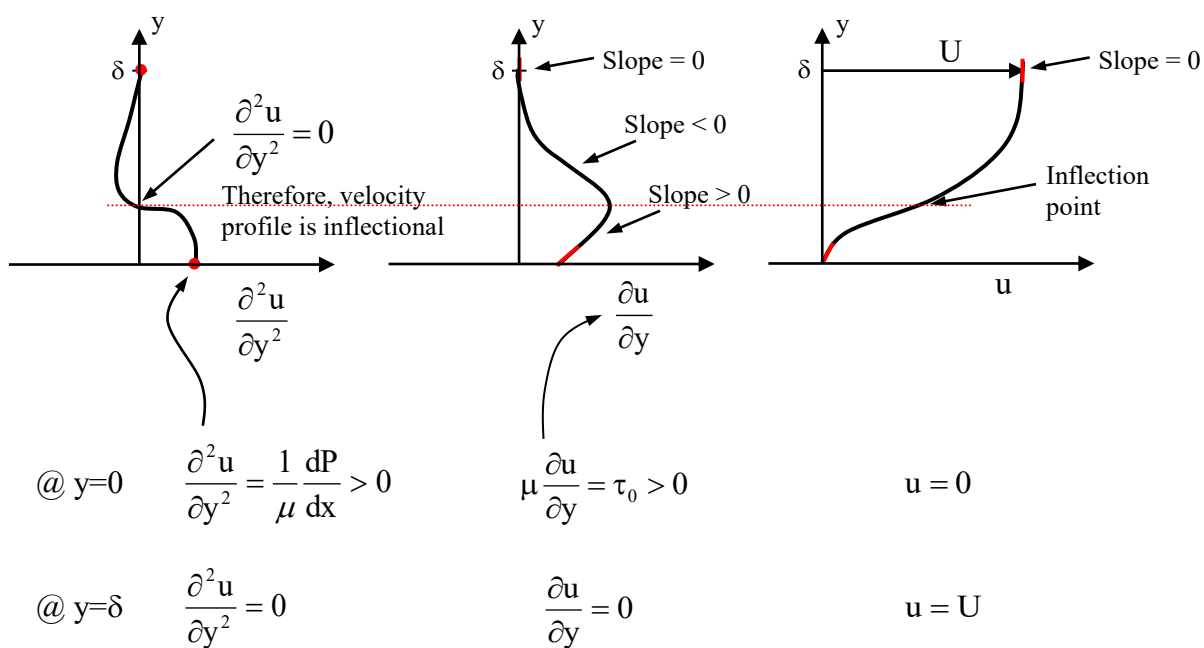


Figure 14.6 Effect of an adverse pressure gradient ($dP/dx > 0$) on the shape of the boundary layer velocity profile.

An adverse pressure gradient, as opposed to a favorable pressure gradient, will act in opposition to the boundary layer momentum, and thus further restrain the flow very near the boundary. This is like having the wind in your face while running, which makes moving forward that much harder, for both you and the boundary layer fluid. As Fig. 14.6 illustrates, the second-order boundary condition is now positive at the bounding surface ($y = 0$), while it still asymptotes to zero at the edge of the boundary layer ($y = \delta$). The shear stress still (up to a point) has a positive value, but with a positive slope at $y = 0$, and again must asymptote to zero at $y = \delta$, with zero slope. Thus, as shown in Figure 14.6, the shear stress must reach a maximum above the surface, and then develop a negative slope, which will allow it to decrease to zero at $y = \delta$. To do that,

$\frac{\partial^2 u}{\partial y^2}$ must pass through zero, which indicates that a point of inflection must occur above the boundary surface. As discussed in section 14.6.2, a point of inflection reflects a point of potential instability, which makes these adverse pressure gradient flows highly likely to a break down to turbulence. Additionally, the dual penalty of the shear stress and the pressure gradient acting in opposition to the fluid inertia can quickly reduce the velocity of the fluid very near the surface, strongly distorting the velocity profile (as shown in Fig. 14.6), which can rapidly lead to boundary layer separation, as described in the following Section 14.7.

14.7 Boundary layer separation

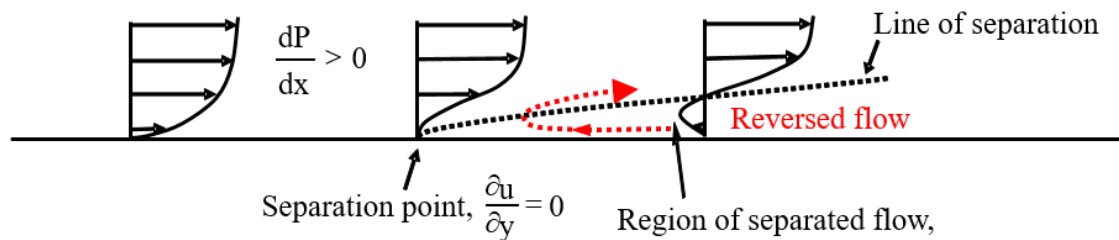


Figure 14.7 Illustration of the development of a separation point of zero shear stress, and subsequent flow separation, due to an adverse pressure gradient ($dP/dx > 0$).

When a boundary undergoes a sustained adverse pressure gradient, the flow very near the bounding surface can quickly be slowed to a halt, such that the wall shear stress becomes zero. Note that zero wall shear stress was the condition limiting the flow development for the Thwaite's method decelerating flow example in section 14.4.3. As shown in Fig. 14.7, downstream of this point of zero wall shear stress, the flow adjacent to the bounding surface will actually reverse direction, forming a stagnant or recirculating region of fluid. This recirculating fluid region will cause the impinging boundary layer flow to divert away from the surface and around this reversed flow region.

The formation of a reversed flow region, and the subsequent diversion of the impinging flow around this region of reversed flow, is termed a "flow separation." When flow separation occurs, the boundary layer ceases to be a boundary layer, and becomes a much more complicated flow, which can no longer be properly modeled using the boundary layer equations. Such separated flows must be addressed using the full Navier-Stokes equations and sophisticated numerical solution techniques.

Physically, the consequence of boundary layer separation is that the displacement thickness, which we envisioned and defined in section 13.4.1, becomes quite large, effectively displacing the outer free stream flow around the region of stagnant or reversed flow. This diversion of the outer flow will result in a significant modification of the pressure distribution within the flow.

As we will discuss in Chapter 15, the creation of these separated flow regions, and the associated modified pressure field, result in a significant net pressure force acting in the flow direction, which is termed pressure drag.

As we discussed in section 14.4.3, an additional effect of a sustained adverse pressure gradient is to move the point of inflection in the boundary layer velocity profile away from the surface, which makes the boundary layer much more sensitive to a transition to turbulence. When this happens, the inertia forces overwhelm the viscous forces in the boundary layer, and the velocity profile cannot keep its shape, subsequently breaking down into rapid, local mixing behavior known as turbulence, which in turn causes increased surface shear stress. The good news is that the mixing caused by the turbulence will feed more energy from the outer region flow into the flow very near the bounding surface, which helps maintain the downstream movement of the boundary layer. However, while a transition to turbulence may initially keep the flow attached to the bounding surface, under a continued adverse pressure gradient the now turbulent boundary layer can eventually undergo flow separation as well.

In general, adverse pressure gradients, if strong or sustained, will always lead to flow separation, and increased drag or flow resistance. In the following Chapter 15, we will examine the impact of flow separation on both the drag on external bodies, and the development of large temporal pressure fluctuations on the bodies. In addition, in Chapter 17 we will examine the basics of turbulence, and its effect on flow separation.

References

Thwaites, B. (1949). *Approximate calculation of the laminar boundary layer*. Aeronautical Quarterly, vol. 1, pp. 245-254. Also see. Thwaites, B (1960). Incompressible Aerodynamics. Oxford University Press, London. pp.62-64. ISBN 0-486-65465-6.

Study Problems

- Using the momentum integral equation, assume a velocity profile of the form $\frac{u}{U_\infty} = a + b\lambda$, where $\lambda = \frac{y}{\delta}$. Determine the constants a and b, and then the boundary layer parameters δ , δ^* , θ , and c_f for a flat plate flow. Compare your results to table 14.1 in section 14.2.2.

2. Using the momentum integral equation, assume a velocity profile of the form

$$\frac{u}{U_\infty} = a + b\lambda + c\lambda^2 + d\lambda^3, \text{ where } \lambda = \frac{y}{\delta}.$$

Determine the constants a , b , c , and d , and then the boundary layer parameters δ , δ^* , θ , and c_f for a flat plate flow. Assume that all derivatives are zero at $\lambda = 1$. Compare your results to table 14.1 in section 14.2.2.

3. Using the momentum integral equation, assume a velocity profile of the form

$$\frac{u}{U_\infty} = a + b\lambda + c\lambda^2 + d\lambda^3, \text{ where } \lambda = \frac{y}{\delta}.$$

Determine the constants a , b , c , and d , and then the boundary layer parameters δ , δ^* , θ , and c_f for a flat plate flow. Assume that the shear stress is zero

at $\lambda = 1$, but for a fourth boundary condition, assume that $\frac{d^2u}{dy^2} = 0$ at $\lambda = 0$. Note that this

boundary condition is obtained from the original boundary layer equation when $\lambda = 0$, assuming that $U_\infty = \text{constant}$ (see section 14.5, Eq. 14.42). Compare your results to table 14.1 in section 14.2.2.

4. Using the momentum integral equation, assume a velocity profile of the form

$$\frac{u}{U_\infty} = a + b\lambda + c\lambda^2 + d\lambda^3 + e\lambda^4, \text{ where } \lambda = \frac{y}{\delta}.$$

Determine the constants a , b , c , d and e , and then the boundary layer parameters δ , δ^* , θ , and c_f for a flat plate flow. Assume that all derivatives are zero at $\lambda = 1$. Compare your results to table 14.1 in section 14.2.2.

5. Using the momentum integral equation, assume a velocity profile of the form

$$\frac{u}{U_\infty} = a + b\lambda + c\lambda^2 + d\lambda^3 + e\lambda^4, \text{ where } \lambda = \frac{y}{\delta}.$$

Determine the constants a , b , c , d and e , and then the boundary layer parameters δ , δ^* , θ , and c_f for a flat plate flow. Assume that the shear stress and

$\frac{d^2u}{dy^2}$ are zero at $\lambda = 1$, but for a fifth boundary condition, assume that $\frac{d^2u}{dy^2} = 0$ at $\lambda = 0$. Note that

this boundary condition is obtained from the original boundary layer equation when $\lambda = 0$, assuming that $U_\infty = \text{constant}$ (see section 14.5, Eq. 14.42). Compare your results to table 14.1 in section 14.2.2

6. Using the momentum integral equation, assume a velocity profile of the form $\frac{u}{U_\infty} = a \sin(b\lambda)$,

where $\lambda = \frac{y}{\delta}$. Determine constants a and b , and then the boundary layer parameters δ , δ^* , θ , and c_f

for a flat plate flow. Note that you cannot use $u = 0$ at $\lambda = 0$, because the result is indeterminate in calculating the constants. Instead, use the first and second derivatives at $\lambda = 1$ as boundary conditions. Compare your results to table 14.1 in section 14.2.2. What are the problems with this

assumed velocity profile? [hint: consider the boundary condition for $\frac{d^2u}{dy^2}$ at $\lambda = 1$]

7. Using the momentum integral equation, assume a velocity profile of the form $\frac{u}{U_\infty} = a(1 - e^{-2\lambda})$, where $\lambda = \frac{y}{\delta}$, determine the constant a using $u = U_\infty$ at $\lambda = 1$, and then the boundary layer parameters δ , δ^* , θ , and c_f for a flat plate flow. Note that this function already satisfies $u = 0$ at $\lambda = 0$, but does not satisfy any of the other higher order boundary conditions. How well do the results compare with the Blasius solution? What are the problems with this assumed velocity profile?
8. Water enters a two-dimensional nozzle at free-stream velocity U_0 . The free-stream velocity accelerates exponentially according to the relationship, $U(x) = U_0 \exp(kx)$, where x is the distance from the start of the nozzle, and k is a constant. Assume that the kinematic viscosity, ν , is constant and the boundary layer thickness is $\delta = \delta_0 \neq 0$ at $x = 0$. Assuming a boundary layer profile of the form, $u/U(x) = A + By + Cy^2 + Dy^3$, use the momentum integral equation and, for a bounding surface of the nozzle, determine:
- The approximate velocity profile using appropriate no slip at $y = 0$, and appropriate other boundary conditions at $y = \delta$ to establish the values for A , B , C , D .
 - Expressions for δ^* , θ , and τ_0 as functions of δ .
 - A differential equation for δ as a function of x , with U_0 , ν , and k as constants.
 - A solution for δ in terms of U_0 , δ_0 , ν , k , and x .
 - A plot of $\delta(x)$ (in inches) for $0 \leq x \leq 2$ m, for both $\delta_0 = 0$ cm and $\delta_0 = 1$ cm, letting $k = 0.1 \text{ m}^{-1}$, $\nu = 10^{-6} \text{ m}^2/\text{sec.}$, and $U_0 = 25 \text{ cm/sec.}$
 - For the same values of k , ν , and U_0 as in part d, determine the x location (in meters) and the free-stream velocity U (in m/sec.), where δ becomes a maximum. Determine the location of the maximum for both $\delta_0 = 0$ cm and $\delta_0 = 1$ cm. Physically explain what is happening to give such significantly different maxima.
9. Assuming the same conditions as problem 8, where $U(x) = U_0 \exp(kx)$, determine an expression for $\theta(x)$ using Thwaites method, and plot $\theta(x)$ vs. x for $0 \leq x \leq 2$ ft, for $\delta_0 = 0$ inches, letting $k = 0.4 \text{ m}^{-1}$, $\nu = 10^{-6} \text{ m}^2/\text{sec.}$, and $U_0 = 25 \text{ cm/sec.}$ On the same graph, plot for comparison the $\theta(x)$ expression you derived in problem 8 using a direct solution of the momentum integral equation.
- Extra Credit:** Again, assuming the same conditions as problem 8, use Thwaites method to determine $\theta(x)$, and plot $\theta(x)$ vs. x for $0 \leq x \leq 2$ m, for $\delta_0 = 1$ cm, letting $k = 0.4 \text{ ft}^{-1}$, $\nu = 10^{-6} \text{ m}^2/\text{sec.}$, and $U_0 = 25 \text{ cm/sec.}$ On the same graph, plot for comparison the $\theta(x)$ expression you derived in problem 8 using a direct solution of the momentum integral equation.
- Note: You cannot do this directly using the original Thwaites equation, but need to employ Eqs. 14.34 and 14.35 for a non-zero momentum thickness.
10. Assume a velocity of $U(x) = U_0 \exp(-kx)$ over a surface, with $\theta = 0$ at $x = 0$. Determine an expression for $\theta(x)$ using Thwaites method, and on one graph plot both $\theta(x)$ (in cm) and n vs. x for $0 \leq x \leq 2$ m, letting $k = 0.1 \text{ m}^{-1}$, $\nu = 10^{-6} \text{ m}^2/\text{sec.}$, and $U_0 = 0.3 \text{ m/sec.}$ Determine how far along the surface (in meters) this calculation is valid.

11. A fluid entering a diffuser is decelerated according to the velocity $U(x) = U_0/(1+ax)$, where a is a constant indicating how rapidly the diffuser decelerates the flow. Assume that U_0 and ν (kinematic viscosity) are known constants. Using Thwaites method, do the following:
- Determine an expression for θ as a function of U_0 , ν , a , and x .
 - Determine an expression for the parameter n as a function of U_0 , ν , a , and x .
 - Assuming that a is inverse units to x , and determine values of θ at $x = 0.5$ for both $a = 0.1$ and $a = 0.2$ in terms of U_0 and ν .
 - Determine the values of x where $U = 0.9U_0$ for both $a = 0.1$ and $a = 0.2$; compare the respective values of θ that occur at these points, and comment on the reason for any variations.
 - For $a = 0.1$, determine the maximum value of θ and the respective x value at which this maxima occurs. Briefly explain the physical processes which result in the development of this maxima.
12. A fluid entering a diffuser is decelerated according to the velocity $U_\infty(x) = U_0(1-ax)$, where a is a constant indicating how rapidly the diffuser decelerates the flow. Assume that U_0 and ν (kinematic viscosity) are known constants. Using Thwaites method, do the following:
- Determine an expression for θ as a function of U_0 , ν , a , and x .
 - Determine an expression for the parameter n as a function of a , and x .
 - Assuming that a is in inverse units to x , determine values of θ at $x = 1$ for both $a = 0.05 \text{ ft}^{-1}$ and $a = 0.1 \text{ ft}^{-1}$ in terms of U_0 and ν .
 - Determine the values of x where $U_\infty = 0.90 U_0$ for both $a = 0.05$ and $a = 0.1$; compare the respective values of θ that occur at these points, and comment on the reason for any variations.
 - For $a = 0.1$, determine the maximum value of θ and the respective x value at which this maxima occurs. Briefly explain the physical processes that result in the development of these maxima.
13. A fluid entering a nozzle is accelerated according to the velocity $U_\infty(x) = U_0(1+ax)$ where a is a constant indicating how rapidly the nozzle accelerates the flow. Assume that U_0 and ν (kinematic viscosity) are known constants. Using Thwaites method, do the following:
- Determine an expression for θ as a function of U_0 , ν , a , and x .
 - Determine an expression for the parameter n as a function of a , and x .
 - Assuming that a is in inverse units to x , determine values of θ at $x = 1$ for both $a = 0.05$ and $a = 0.1$ in terms of U_0 and ν .
 - Determine the values of x where $U_\infty = 1.10 U_0$ for both $a = 0.05$ and $a = 0.1$; compare the respective values of θ that occur at these points, and comment on the reason for any variations.
 - For $a = 0.1$, determine the maximum value of θ and the respective x value at which this maxima occurs. Briefly explain the physical processes that result in the development of these maxima.
14. Consider the flow of air over a cylinder. Assume that the impinging velocity is $U = 1 \text{ cm/s}$, and the cylinder radius is $R = 10 \text{ cm}$. The kinematic viscosity for air is $\nu = 16 \text{ mm}^2/\text{s}$. As the flow passes around the cylinder, a laminar boundary layer develops on the cylinder surface. Assume that the velocity at the edge of the boundary layer can be approximated by the potential flow solution of $U_\infty = 2U\sin(\alpha)$, where α is the angle measured from the cylinder stagnation point around the cylinder.

(14. continued)

- a. Using Thwaites method, neglect curvature effects and determine the development of the momentum thickness (θ) as a function of x , where $x = R\alpha$, when α is in radians. You can integrate the Thwaites equation analytically (you need to review your integral tables)—do it in terms of α , and then express in terms of x .
- b. Determine the angle α_{\max} (in degrees) where the solution is no longer valid, using a parallel calculation of the parameter n . Why does the solution fail at this point?
- c. Plot θ and n on the same graph (using different axis scales) vs. x , for $0 \text{ cm} < x < 20 \text{ cm}$. Use appropriate scales for θ and n , such that the full extent of the changes in θ and n can be observed and compared to each other. I suggest you use smaller increments of α near $\alpha = 0$ to effectively resolve the curves.

15. Consider the flow of water with a Falkner-Skan type of outer region velocity $U_\infty = U_0 \left(\frac{x}{x_0} \right)^m$,

where U_0 , x_0 , and m are constants, with $U_0 = 10 \text{ cm/s}$ and $x_0 = 100 \text{ cm}$. The kinematic viscosity for water is $\nu = 0.01 \text{ cm}^2/\text{s}$. The initial momentum thickness at x_0 is $\theta_0 = 0.2 \text{ cm}$.

- a. Using Thwaites method, determine expressions for the momentum thickness (θ) and the Thwaites pressure gradient parameter (n) as a function of x , in terms of θ_0 , ν , U_0 , x_0 , x , and m . Note that you must start with your integration for the momentum thickness using Eq. 14.29 since $\theta_0 \neq 0$.
- b. Create a graph of $\frac{\theta}{\theta_0}$ (where θ_0 is the initial momentum thickness, 0.2 cm) vs. $\frac{x}{x_0}$. Show plots for $m = 0$ (Blasius), $m = 0.25$ (accelerating), and $m = -0.05$ (decelerating). For your graph, use increments of $\frac{x}{x_0}$ of 0.1 from $1 \leq \frac{x}{x_0} \leq 4$.
- c. Create a second corresponding graph of n vs. $\frac{x}{x_0}$ showing plots for $m = 0$ (Blasius), $m = 0.25$ (accelerating), and $m = -0.05$ (decelerating). For your graph, again use increments of $\frac{x}{x_0}$ of 0.1 from $1 \leq \frac{x}{x_0} \leq 4$. Is the decelerating flow likely to separate? What is your basis for judging whether or not it separates?
- d. Create a third graph of $\frac{\theta}{\theta_B}$ (where θ_B is the Blasius value for $m = 0$) vs. m , for $\frac{x}{x_0} = 4$. Plot your graph for $-0.1 \leq m \leq 1$ (use increments of 0.05). Compare your graph to the results for the Falkner-Skan solution of Figure 13.11 in Chapter 13.
- e. Using your expression for n vs. $\frac{x}{x_0}$, use a root-finding program to determine the value of m for which the Thwaites method would indicate that the flow would reach separation at $x = 400 \text{ cm}$. How does this compare with the actual Falkner-Skan solution?

Chapter 15

Flow Separation and Drag

Contents

15.1 Causes of Separation	494
15.2 Effects of Separation	498
15.3 Drag	498
15.4 Unsteady Separation/Drag Effects	510
15.4.1 Vortex Shedding by a Circular Cylinder	511
15.4.2 Vortex Shedding by Other Shapes	514
15.5 Control of Separation and Drag	515
15.5.1 Passive Control	515
15.5.1.1 Surface Effects	516
15.5.1.2 Splitter Plates	517
15.5.1.3 Sequenced Bodies	518
15.5.2 Active Control	522

15.1 Causes of Separation

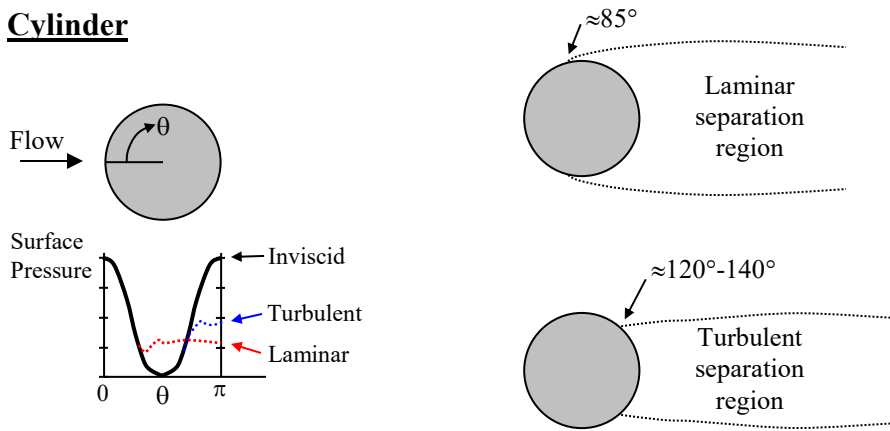
As discussed previously in Chapter 14, when a boundary layer flow comes under the influence of an adverse pressure gradient (i.e. with pressure increasing in the flow direction), both the local wall shear stress and the increasing pressure will act to retard the flow immediately adjacent to the bounding surface. In often a very short distance, the fluid adjacent to the surface will become stagnant (i.e. be brought to rest), and begin to move in opposition to the main flow. This condition results in what is known as *flow separation*, where the initially stagnated fluid will cause the following flow to divert outward, away from the surface, and around the stagnant or rearward flowing wall fluid. This process causes a substantial change of the flow field, resulting in significant losses of flow energy and pressure due to the intense mixing between the stagnant fluid and the downstream flow bounding this stagnant fluid.

The conditions necessary for such a flow separation behavior to develop are:

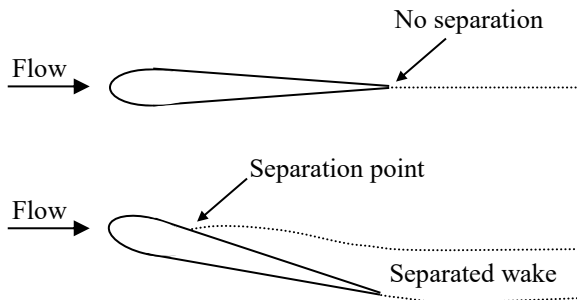
- 1) A local, adverse pressure gradient, and/or
- 2) Strong curvature or sharp corners

Figure 15.1 shows several examples of separated flows. Figure 15.1a is typical of flow separation occurring over bluff bodies. Here we show a cylinder, but the same behavior is characteristic of flows where the width and length of the body are comparable, such as

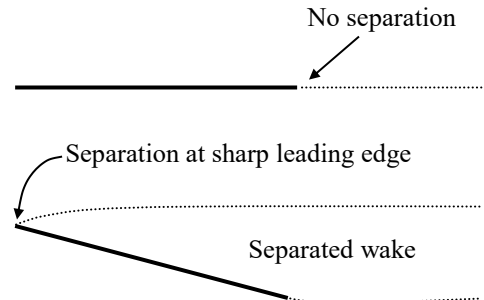
a) Cylinder



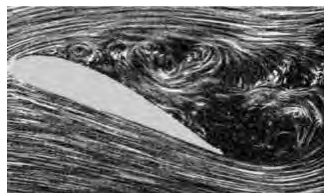
b) Airfoil



c) Flat Plate



d) Smoke flow visualization of separated flows



1. Separation for an airfoil: high angle of attack



2. Laminar separation behind a sphere



3. Turbulent separation behind a sphere

Figure 15.1 Some typical examples of separated flows: a) a circular cylinder; b) an airfoil; c) a flat plate; d) smoke visualizations of separation behind an airfoil and a sphere.

rectangular or elliptical bodies. As shown in Chapter 9, flows passing around these types of bodies will experience significant surface pressure variations. If the boundary layer that develops on these bodies encounters an adverse pressure gradient, it will be subject to possible (and often rapid) boundary layer separation. As discussed earlier in Section 14.5, once a boundary layer separates, a region of reversed flow, or a recirculating *wake*, is created downstream of the body. This wake, as shown by the pressure sketch of Figure 15.1a, will be of

relatively constant pressure, which is significantly lower than the leading edge pressures. This relatively constant trailing-edge pressure is generally characteristic of separated flow regions or wakes. The cumulative differential in pressure around the body will result in a cumulative force in the flow direction (determined by integrating the surface pressure over the body), which is termed a "drag" force. As we will discuss in section 15.3, the total drag is the sum of both pressure imbalances and surface shear stresses.

However, note that when a body is of significant thickness (i.e. not a flat plate or thin airfoil), the drag due to differences in surface pressure around the body normally exceeds the drag due to the surface shear stresses.

Additionally, the type of boundary layer on the body has a significant effect on the magnitude of the pressure drag. As we discuss in Chapter 17, a transition to turbulence results in an increase in boundary shear stresses; however, the mixing associated with turbulence will keep the boundary layer energized, so it will generally remain attached to the surface much farther around a body. As shown on the right of figure 15.1a, a laminar boundary layer will separate from a bluff body surface much sooner than a turbulent boundary layer. The result is a trailing surface pressure that is lower for a laminar separation than a turbulent separation, and consequently the pressure drag for laminar separation will exceed that for a turbulent separation, for the same impinging flow.

Figure 15.1b illustrates flow around a symmetric airfoil. When a symmetric airfoil (i.e. having the same shape above and below the centerline) is aligned with the flow, as in the upper example of Figure 15.1b, the flow will (ideally) pass around the airfoil without undergoing flow separation. Even though there will be an adverse pressure applied to the trailing portion of the airfoil (i.e. that following the thickest part of the airfoil), airfoils for aircraft applications are generally designed such that the region of adverse pressure will not result in a significant separation. Generally, to avoid a trailing edge separation, the thickness (i.e. thickest portion of the airfoil) is kept thin relative to the length of the airfoil. For a low thickness-to-length ratio, the flow will generally pass around the airfoil without separating. Note that there will still be an unbalanced pressure force on the airfoil, since the pressure at the leading edge will be the stagnation pressure of the flow, and the pressure at the trailing edge will generally be that of the local static pressure. The pressure distribution will result in a nominal amount of pressure induced drag, but much less than for a comparable body without an extended trailing edge (e.g. a circular cylinder). Additionally, surface shear stresses will more significantly contribute to the overall drag on an airfoil.

However, when an airfoil is placed at an angle of attack (the angle of the airfoil centerline to the flow direction), as shown in the lower portion of figure 15.1b, the pressure distribution over the airfoil will change significantly, creating an unbalanced pressure distribution between the top to the bottom of the airfoil. This unbalanced pressure distribution results in a lift force on the

airfoil (necessary for flight), but also increases the pressure imbalance from front-to-back of the airfoil, with a subsequent increase in the pressure-induced drag on the airfoil. If the angle of attack is increased too severely, the adverse pressure gradient over the trailing portion of the airfoil will cause the flow to separate from the upper surface, with an accompanying reduction in surface pressure over the upper surface; the result is a marked increase in pressure-induced drag. If separation occurs, it will develop quite rapidly, creating a large region of separated fluid, or wake. It also results in a significant loss in lift, which can have disastrous consequences on an aircraft, in that the aircraft will not be able to sustain flight. Such situations are known as "[stall](#)" and can develop quite rapidly; the occurrence of stall is most often the cause of aircraft accidents and associated fatalities.

Figure 15.1c represents flow over a flat plate. As we know, when a flat plate is oriented with its surface aligned with the flow direction, as in the upper portion of figure 15.1c, a boundary layer develops over the flat surfaces of the plate, resulting in frictional drag. Since the plate is aligned with the flow, the outer flow remains uniform and essentially parallel, with no variation in the bounding pressure. In addition, since no pressure gradient develops, there is no flow separation. Consequently, the plate only experiences drag due to viscous shear.

However, when a flat plate is placed at an angle of attack, as shown in the lower portion of figure 15.1c, a very large local adverse pressure gradient will develop at the sharp leading edge (even at low angles of attack). This adverse pressure gradient causes an immediate development of a flow separation, creating a large region of separated flow/wake on the upper surface of the plate, with a consequent low pressure. The result is very large pressure drag, which increases essentially proportionally to the sine of the angle of attack.

Figure 15.1d shows flow visualizations of separated flows using smoke streamers in a wind tunnel. The first visualization shows the separation developing on the upper surface of an airfoil at a high angle of attack. This degree of separation is severe, and would result in significant loss of lift and increased drag; typically such a flow would not sustain the flight of an aircraft, resulting in a "stall" referred to above. The second and third images show the difference between laminar and turbulent separation behind a sphere. Note that similar to the sketches shown on the right of figure 15.1a, the wake is smaller when the flow over the body is turbulent, and will thus have less pressure drag. Two interesting YouTube videos show a variety of flow separation behavior for real flows: [here](#) separation over a series of shapes using smoke visualization in air, and [here](#) different types of flow separation over bodies and through channels using particle visualization in water. Both of these are videos of relatively old research movies, and a bit grainy, but they show some excellent sequences of separated flow behavior for real flows.

15.2 Effects of Separation

Flow separation can have a number of deleterious effects, including:

- 1) Form or Pressure drag, and
- 2) Unsteady flow behavior

In Section 15.1 we discussed pressure drag (often called form drag, since it is a strong function of the form of the body). In Section 15.3 we will develop methods for predicting and calculating the forces due to drag over various types of bodies, and discuss the trade-off between pressure drag and drag due to shear stresses.

Unsteady flow behavior occurs when the separated flow developing over a body changes temporally, creating a time-varying pressure field, with associated time-varying pressure drag. As we will discuss in Section 15.4, such time-varying behavior can create unwanted, and often destructive, periodic loading of a body.

Finally, in Section 15.5, we will discuss several methods for controlling, minimizing, and stabilizing separation and the resultant pressure drag, and the tradeoffs between using passive or active drag control techniques.

15.3 Drag

Drag is defined as the total force exerted on a body in the direction of the fluid motion by the effects of the fluid, and is a combination of (a) unbalanced pressure forces and (b) friction forces (i.e. fluid shear stress), both acting on the body surface. Note, however, that pressure forces act *normal* to the surfaces, whereas friction forces act *parallel* to the surfaces. The total resultant force *acting in the direction of the fluid flow* comprises the *total drag on the body*. The resultant force acting *normal* to the direction of flow is termed the *lift* on the body.

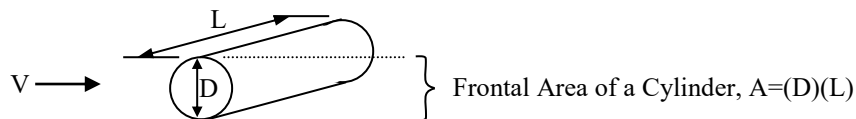


Figure 15.2 Characterization of the frontal area of a bluff body.

To quantify the drag force, we establish an equation that relates the actual drag force to the dynamic pressure (i.e. the pressure equivalent to the fluid momentum flux, $\frac{1}{2}\rho V^2$), and the frontal area of the body (i.e. the cross-sectional area of the body, as viewed from the direction of the impinging flow), as illustrated in figure 15.2.

So, we write the drag equation as:

$$\begin{array}{c}
 \text{Total Drag Force} \quad \text{Fluid Density} \quad \text{Fluid Velocity} \\
 \swarrow \quad \downarrow \quad \swarrow \\
 D = C_D \frac{1}{2} \rho V^2 A \\
 \swarrow \quad \nwarrow \\
 \text{Drag Coefficient} \quad \text{Projected Frontal Area of Body}
 \end{array} \tag{15.1}$$

In Eq. 15.1, C_D is the drag coefficient, which is proportional to the non-dimensional total drag on a body -- the combination of the shear stress drag and the form or pressure drag. We equate the total drag as proportional to the dynamic pressure ($\frac{1}{2}\rho V^2$) and the frontal area of the body. Note that the dynamic pressure is the pressure difference that would result from bringing the impinging velocity to zero, or stagnation. A drag coefficient of one or greater is considered high, with drag coefficients of 0.2 or less considered low drag values.

Analytical or computational determination of accurate drag coefficients for any but the simplest geometric body shapes has generally not been possible, although modern computational tools are making the computation of drag coefficients more feasible, but computationally time intensive. Thus, we generally rely on experimental data. However, the experiments must be done judiciously by employing dynamic [similitude techniques](#). First, we determine the non-dimensional parameters upon which the drag depends. Secondly, we determine the functional relationship of the drag coefficient to these parameters. Thirdly, we conduct experiments that cover the range of the appropriate parameters.

From dimensional analysis and similitude we can establish that:

$$C_D = C_D(\text{geometry}, \text{Re}, \text{Fr}, \text{M}), \text{ where}$$

geometry \Rightarrow scaled similarity (i.e. same geometric shape)

$$\text{Re} \Rightarrow \text{Reynolds number} = \frac{VL}{\nu} = \frac{\text{inertia forces}}{\text{viscous forces}} \quad (\text{L is a characteristic length})$$

$$\text{Fr} \Rightarrow \text{Froude number} = \frac{V^2}{gL} = \frac{\text{inertia forces}}{\text{gravity forces}} \quad (\text{for air-water interactions})$$

$$\text{Mach} \Rightarrow \text{Mach number} = \frac{V}{C} = \frac{\text{fluid velocity}}{\text{speed of sound}} \quad (\text{for compressible flows})$$

For our purposes (i.e. incompressible, single fluid), we need only consider the geometry and Reynolds number, giving:

$$C_D = C_D(\text{geometry}, \text{Re})$$

However, even this reduction in influencing parameters still requires a number of carefully controlled experiments to determine C_D for a range of geometries and Reynolds numbers. As an example, figure 15.3 shows the general behavior of the drag coefficient for a circular cylinder.

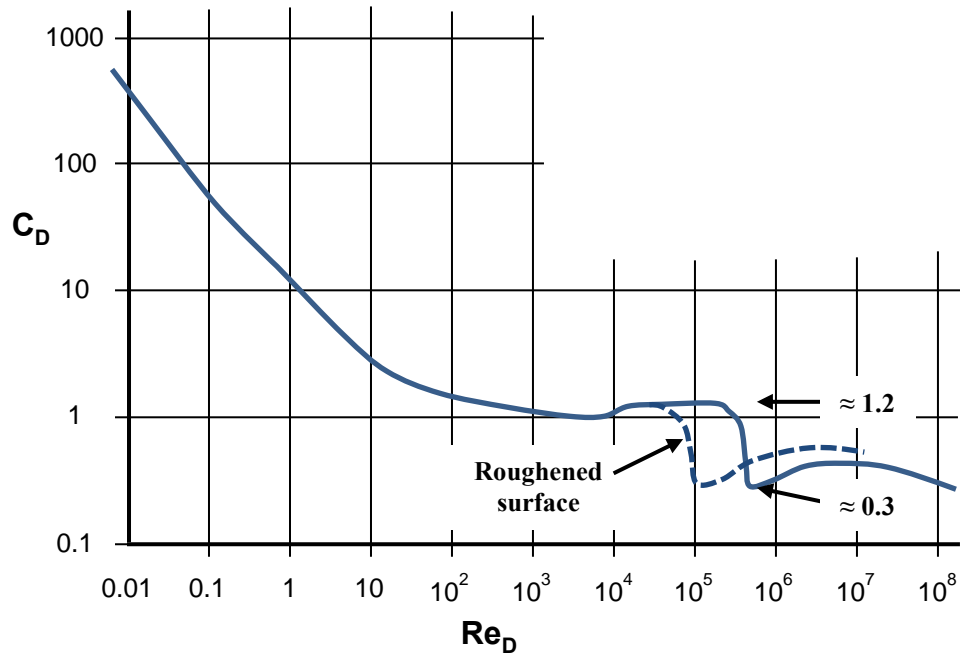


Figure 15.3 The generic behavior of the drag coefficient for a smooth circular cylinder (in blue) [after [Hoerner, 1965](#)]

The drag on a cylinder is a classic example of bluff body drag. Note that at very low Reynolds numbers ($Re_D < 10$) the flow over the cylinder is laminar, with limited flow separation, such that C_D is basically due to viscous shear, and roughly proportional to $1/Re_D$. As Re_D increases beyond 10, pressure drag starts to dominate, with C_D becoming essentially constant at ≈ 1.2 for $10^3 < Re_D < 10^5 - 10^6$, while the boundary layer over the cylinder remains laminar.

Note that the broad upper range of Re_D for laminar behavior depends on the character of the boundary layer. For a smooth cylinder, without upstream disturbances, the flow will remain laminar to a much higher Re_D (up to 10^6). However, if the cylinder surface is rough, or the external flow contains disturbances, the boundary layer on the cylinder can transition earlier to a turbulent boundary layer. This earlier transition increases local mixing, which reduces the separation behind the cylinder, as shown in figure 15.1a. When the boundary layer over the cylinder is turbulent, C_D decreases sharply to roughly 0.3, or roughly 25% of the drag with a laminar boundary layer.

Thus, in figure 15.3, the C_D vs. Re_D curve shows a region of $10^5 < Re_D < 10^6$ over which the boundary layer may become turbulent, with a consequent decrease in C_D . Note that surface

roughness, although it causes early transition to turbulence and thus a reduced C_D , also has a parasitic effect on the surface drag due to increased shear effects, which generally results in a C_D higher than that for a smooth cylinder (≈ 0.3) after transition.

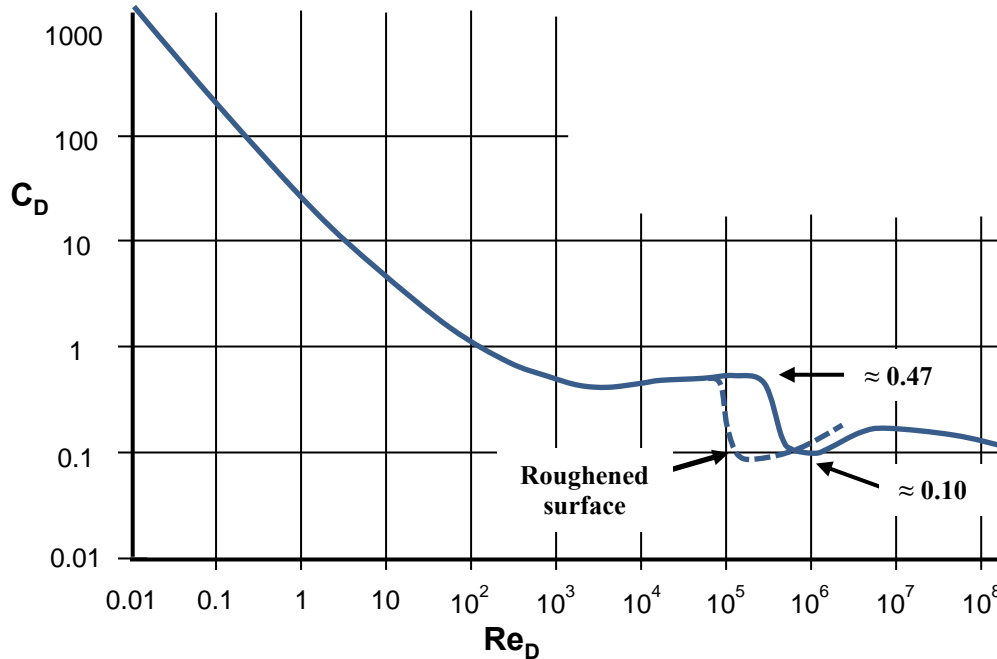


Figure 15.4 The generic behavior of the drag coefficient for a smooth sphere (in blue) [after [Hoerner, 1965](#)].

For drag on axisymmetric and three-dimensional bodies, the drag coefficient is still based on the frontal area as observed in the flow direction. For example, the frontal area of a sphere will be $\pi D^2/4$. In general, the drag coefficients for axisymmetric bodies tend to be lower than for two-dimensional bodies, such as cylinders. Figure 15.4 shows the behavior of C_D for a sphere as a function of the Reynolds number based on sphere diameter. Note that the behavior is quite similar to that for a cylinder, with a plateau in C_D of ≈ 0.47 over a range from $10^3 > Re_D > 10^5$, and transition to turbulence in the range $10^5 < Re_D < 10^6$, with a subsequent drop in C_D to ≈ 0.10 (an almost 80% reduction!). Again, roughening the sphere surface will cause an earlier transition, and a consequent decrease in C_D .

Note that both figure 15.3 and 15.4 illustrate that roughening the surface of a body will result in an earlier transition to a turbulent boundary layer over the body, and a significant reduction in C_D . Many practical flow situations take advantage of this reduction in C_D by purposely causing the boundary layer to transition to turbulence. This is done by roughening of the bounding surface, or placing irregularities (e.g. a cable or wire) on and around the surface. These surface treatments generate turbulence, which reduces the separated region, and thus the hydrodynamic drag. Another quite common technique is the roughening of the surface of a ball used in a sport.

Examples are tennis and golf balls. The "fuzz" on the exterior of the tennis ball greatly reduces both the drag and unsteadiness (more on this in Section 15.5.1), so the ball will fly faster and truer. Golfers found in the 1800's that an old, scratched-up ball would fly farther and truer than a new one. Consequently, manufacturers started putting "dimples" on golf balls, to again reduce drag and unsteadiness. Even today, golf ball manufacturers are forever tweaking the dimple pattern on their golf balls, to reduce the drag and thus increase the distance the ball will travel, assuming the same initial velocity. This [link](#) discusses the history of golf balls and drag, and this [link](#) shows an interesting simulation of the flow due to the dimpling of a golf ball.

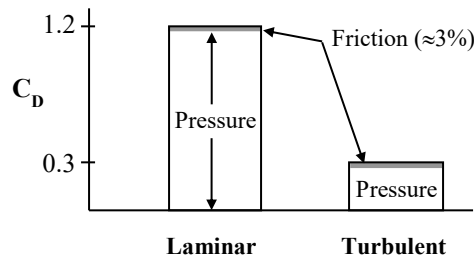


Figure 15.5 The relative contribution of fluid friction and pressure forces to cylinder drag.

Figure 15.5 shows the general difference between laminar and turbulent drag on a smooth cylinder. Note that drag due to shear stresses (i.e. friction) is a minimal contribution for both laminar and turbulent flow (although friction drag will be higher for turbulent flow—see Section 17.7.5.3). The decrease in total drag is quite remarkable, and illustrates why many practical applications want to promote turbulent flow over bluff bodies.

Figure 15.6 shows a generic characterization of the relative contribution of shear stress to the total drag on a body, using the ratio of the body thickness, t , to its length, C (known generally as the chord of the body). For a flat plate, of negligible t/C , essentially all the drag is due to surface shear, whereas for a smooth cylinder, with $t/C = 1$, the surface shear contributes roughly 3% of the total drag (note: this would increase for roughened bodies). The friction drag and pressure drag are about equal for $t/C = 0.25$, so the relative change with t/C is non-linear. Clearly, for $t/C > 1$, essentially all the drag will be due to pressure drag.

Generally, increasing t/C is accompanied by increased variations in the local pressure, resulting in local adverse pressure gradients. As discussed in Chapter 13 and 14, the presence of adverse pressure gradients almost assures the possibility/probability of a separation of the boundary layer, an increased imbalance of pressure forces, and thus more drag on the body.

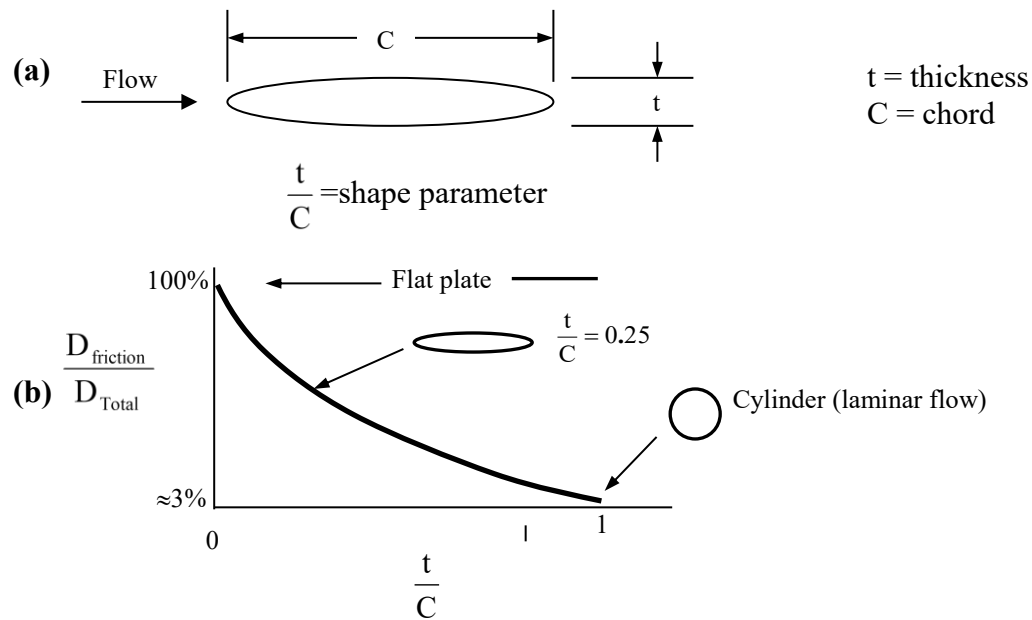


Figure 15.6 The generic effect of geometry on the contribution of surface shear drag vs. pressure drag to the total drag on a smooth body: (a) definition of a body shape parameter, (b) relative contribution of surface shear drag to total drag versus the body shape parameter, t/C .

Figure 15.7 shows C_D values for a number of common two-dimensional shapes of infinite depth into the page (e.g. long rods of different cross-sectional shapes). These values assume a laminar approach flow with $Re \geq 10^4$. The Re and cross-sectional area are based on the vertical dimension of the body normal to the flow direction. The C_D values for the smooth, more rounded bluff bodies will be reduced significantly when transition to turbulence occurs, so one needs to understand the nature of the impinging flow. The sharp-edge bodies, such as flat plates or bodies with sharp edges, will be relatively insensitive to turbulent transition, since separation will normally occur at those sharp edges, regardless of the type of boundary layer or impinging flow.

You might note that most of these bodies have drag coefficients that are larger than that for a cylinder, and often much larger. This demonstrates the drag penalty for a body with sharp corners. As we showed in Section 9.7.5.2, potential flow around a sharp corner results in an infinite local velocity at the corner, which would also reflect an infinite adverse pressure gradient. While such infinite flow singularities cannot exist in a real flow, very large pressure differences will develop at sharp edges, such that flow separation takes place immediately. Flow separation at sharp corners creates large pressure differences between the front and the back of the body, and thus large drag forces and large C_D .

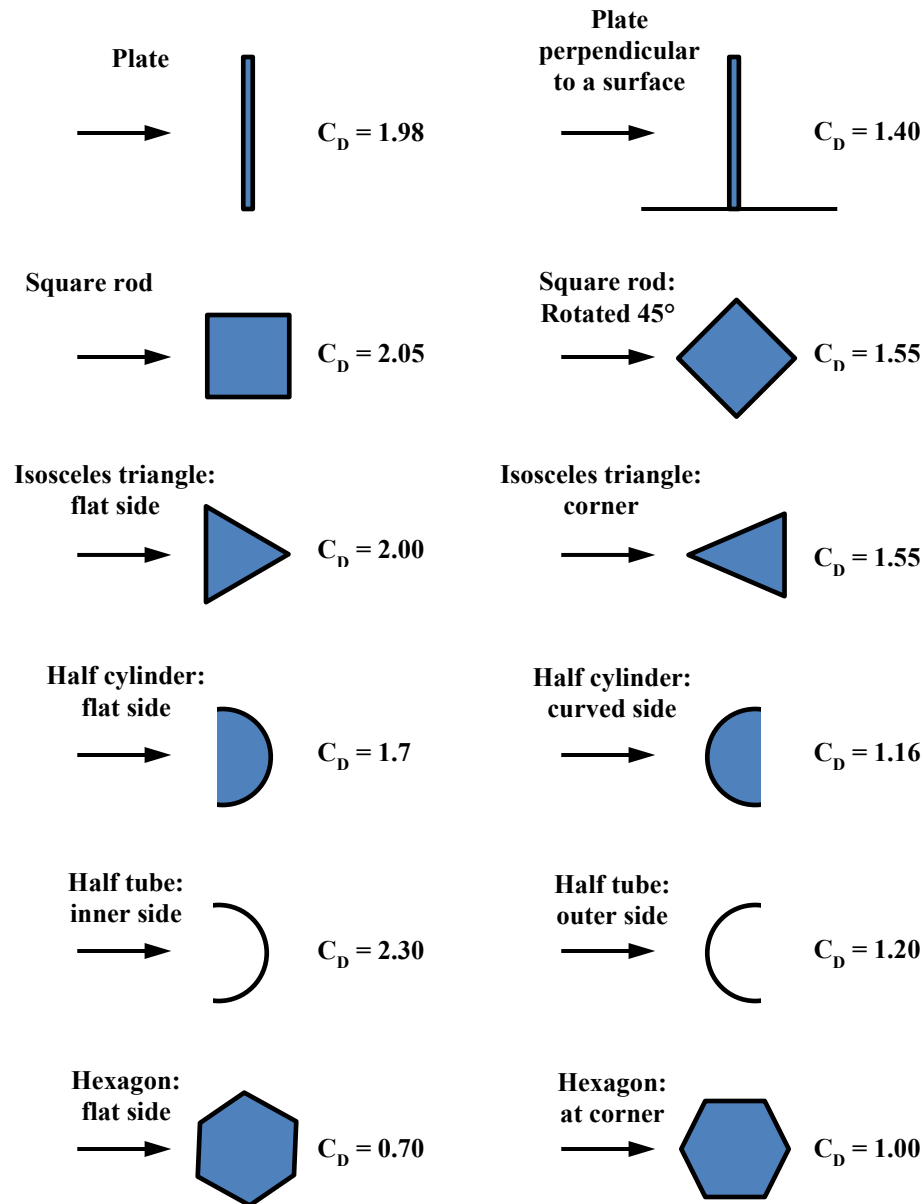


Figure 15.7 Drag coefficients for selected two-dimensional bodies of infinite extent (into the page) at $Re \geq 10^4$ (Reynolds number based on vertical dimension of the body). [after [Hoerner, 1965](#)]

Notice in figure 15.7 that bodies with more pronounced corners have higher C_D . For example, $C_D = 2.05$ for a square rod with a flat leading edge. However, rotating the rod 45° to give a pointed leading edge, which moves the corners toward the center of the body, reduces the C_D to 1.55 (a 25% reduction). A similar reduction in C_D is noted by changing the orientation of the hexagonal-shaped rod.

Note that C_D for a flat plate normal to the flow is reduced by 30% when it is located on and normal to a bounding surface, as opposed to being far removed from bounding surfaces. This is due to the presence of a boundary layer on the bounding surface, which reduces the local pressure at the leading edge of the plate, and may act to stabilize the trailing wake. This reduction in C_D is common for any bluff body mounted on a surface parallel to the flow direction. In all cases, the C_D for the bluff body will be reduced by the presence of a bounding surface. Click [here](#) to see more C_D values for a variety of two-dimensional bluff bodies.

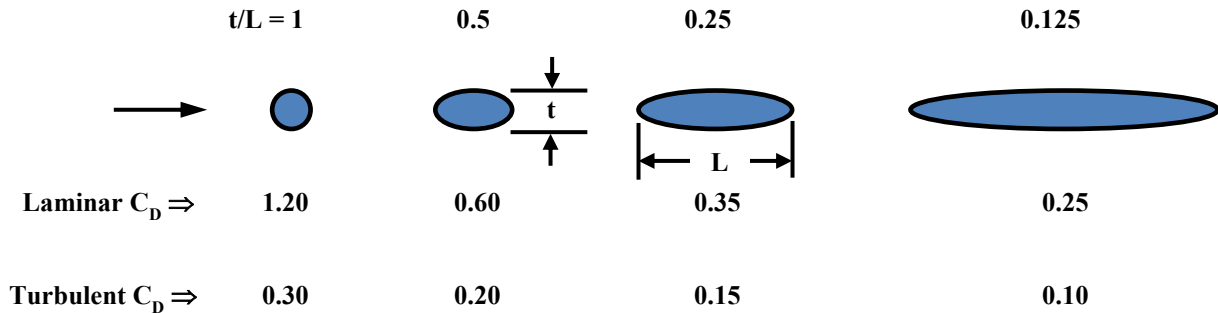


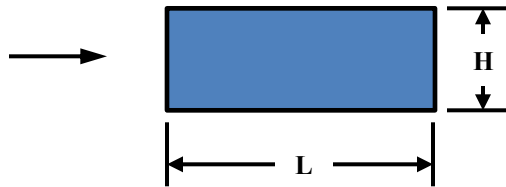
Figure 15.8 The laminar ($Re_t < 10^5$) and turbulent ($Re_t > 10^6$) drag coefficients for a series of two-dimensional oval-shaped bodies of infinite extent (into the page). [after [Hoerner, 1965](#)]

Figure 15.8 shows the effect of bluff body thickness and boundary layer characteristics on the C_D for two-dimensional elliptical rods. As pointed out above, the thicker a body is relative to its length, the greater the effect of pressure gradients on the body boundary layer and the more extensive is the flow separation. The increased separation yields correspondingly greater form drag. The change in C_D with body thickness is clearly demonstrated in figure 15.8, which shows that as t/L (termed the thickness ratio) decreases from 1 (a circular cylinder), the C_D correspondingly decreases. Note that all the bodies shown in figure 15.8 will have the same frontal area, so as the bodies become more extended the subsequent modification of the pressure gradient will strongly reduce the form drag on the body. Since the body will be longer, the shear stress drag will increase, but this is greatly exceeded by the reduction in the pressure drag due to reduced separation. As shown, extending a circular body by only one thickness (i.e. from $L = t$ to $L = 2t$), reduces the drag by 50% for a laminar flow! Moreover, extending it by seven thicknesses (to $L = 8t$) reduces the drag by 80%. This shows the benefit of a little "streamlining". Additionally, reducing t/L generally makes the flow more stable, such that time-varying separation effects are reduced as well. We will discuss this further in section 15.4.

Figure 15.8 also shows the sensitivity of C_D to the nature of the boundary layer. We noted in Figure 15.3 the significant decrease (75%) in C_D that takes place when the flow over a smooth cylinder becomes turbulent in the Reynolds number range $10^5 < Re_D < 10^6$. As one would

expect, this sensitivity to the type of boundary layer extends to $t/L < 1$, with turbulent boundary layers giving markedly lower C_D values (roughly 60% lower). One caveat is that extending the length of a body adds additional surface area, such that shear drag will begin to make more significant contributions to the total drag.

(a) Flat leading edge rod (2-D)



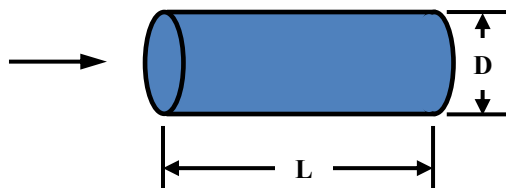
L/H	0.1	0.5	1.0	2.0	4.0	6.0
C_D	1.97	2.02	2.05	1.82	0.93	0.90

(b) Rounded leading edge rod (2-D)



L/H	0.1	0.5	1.0	2.0	4.0	6.0
C_D	-	1.16	0.90	0.70	0.58	0.54

(c) Flat-faced cylinder (3-D)



L/D	0.1	0.5	1.0	2.0	4.0	6.0
C_D	1.17	1.15	0.90	0.85	0.84	0.82

Figure 15.9 The drag coefficients for $Re \geq 10^4$ (based on H or D) as a function of body length (L): (a) a two-dimensional rod of infinite extent (into the page) with a flat leading edge; (b) a two-dimensional rod of infinite extent with a semi-circular leading edge; (c) a flat-faced cylindrical rod. [after [Hoerner, 1965](#)]

Figure 15.9 further illustrates the impact of added body length on C_D , for some generic types of smooth bodies with laminar boundary layers. Figure 15.9a is a rectangular rod with a *flat leading edge*. For this body, a very short body length (e.g. $L/H = 0.1$) is essentially a flat plate with the flow normal to the plate, as shown in figure 15.7. As body length is increased, the C_D increases slightly to 2.05 at $L/H = 1$ (the square rod of figure 15.7). Further increases in length cause C_D to decrease markedly to roughly 0.9 by $L/H = 4$, where the C_D appears to stabilize. Apparently, increasing length beyond $L/H = 1$ must have a significant impact on the separation characteristics in the wake of the body for $1 < L/H < 4$, with a corresponding reduction of C_D .

However, increasing the length beyond $L/H = 4$ appears to have minimal impact on the wake behavior and C_D .

The body shown in figure 15.9b is a rectangular rod with a *semi-circular leading edge*. Note that rounding the leading edge reduces the drag by roughly 50% from the rectangular rod with a flat leading edge (figure 15.9a). Obviously, elimination of sharp corners, which reduces the separated wake of the rod, has a marked effect on C_D . Again, there is a corresponding decrease in C_D with increased length, with increases beyond $L/H = 4$ having a limited effect on C_D .

The third body shown in figure 15.9c is a *flat-faced circular rod*, with its axis in line with the flow direction. This is considered a three-dimensional body, since it is radially symmetric in the flow direction. The behavior of C_D for this body with increases in length is similar to that for the flat leading edge rectangular rod (figure 15.9a), but with less dramatic changes in C_D . For example, for the rectangular rod, C_D decreases 53% from $L/H = 0.1$ to $L/H = 4$; for the cylindrical rod, C_D decreases only 28% from $L/D = 0.1$ to $L/D = 4$. This suggests that the wake of the circular rod is less affected by the length increases, most likely because of the closer exposure of the wake to the main flow due to the axisymmetry. This closer exposure of the wake to the main flow is also why the C_D for the cylinder does not change significantly after $L/D = 2$.

Example: Drag Force on a Suspended Telephone Cable/Smoke Stack

Consider a telephone cable of 1 cm diameter, with a wind blowing perpendicular to the cable at 10 m/s. Determine the force per unit length on the cable due to drag.

Assuming air at 20 C, the kinematic viscosity is $1.5 \times 10^{-5} \text{ m}^2/\text{s}$, and the density is $1.2 \text{ kg}/\text{m}^3$. Thus, the Reynolds number for the cable would be:

$$\text{Re}_D = \frac{VD}{\nu} = \frac{(10) \frac{\text{m}}{\text{s}} (10) \text{mm} (10^{-3}) \frac{\text{mm}}{\text{m}}}{(1.5 \times 10^{-5}) \frac{\text{m}^2}{\text{s}}} = 6.66 \times 10^3$$

From figure 15.3, at this Reynolds number the C_D for a smooth cylinder is roughly 1. The frontal area of the cable (per meter of length) is $A = (0.01) \text{m} \times (1) \text{m} = 0.01 \text{m}^2$. Thus, we calculate the drag/meter as:

$$\text{Drag} / \text{m} = C_D \rho \frac{1}{2} V^2 A = (1)(1.2) \frac{\text{kg}}{\text{m}^3} (0.5)(100) \frac{\text{m}^2}{\text{s}^2} (0.01) \text{m}^2 = 0.6 \frac{\text{kg} \cdot \text{m}}{\text{s}^2} = 0.6 \text{N}$$

Not a particularly large force. For a suspended cable 30 meters long, the total force on the cable would be 18 Newtons, or about 2.4 lbf.

Now, what if the same wind blew on a power plant smoke stack, 10 meters in diameter and 80 meters high? Here, the Reynolds number would be:

$$\text{Re}_D = \frac{VD}{\nu} = \frac{(10) \frac{\text{m}}{\text{s}} (10) \text{m}}{(1.5 \times 10^{-5}) \frac{\text{m}^2}{\text{s}}} = 6.66 \times 10^7$$

From figure 15.3, this would place the flow in the turbulent region, with a C_D of roughly 0.4. So, the drag on the smoke stack would be:

$$\text{Drag} = C_D \rho \frac{1}{2} V^2 A = (0.4)(1.2) \frac{\text{kg}}{\text{m}^3} (0.5)(100) \frac{\text{m}^2}{\text{s}^2} (800) \text{m}^2 = 19,200 \frac{\text{kg} \cdot \text{m}}{\text{s}^2} = 19,200 \text{ N}$$

A substantial force (roughly 4,300 lbf), but easily handled by such a large structure.

Note that if the wind were to blow twice as hard (i.e. 20 m/s), the force would quadruple to 76,800 N (17,300 lbf), which could begin to be worrisome for the operators. Note that 20 m/s is roughly in the range of what would be considered a gale force wind.

Figure 15.10 shows C_D values for selected smooth three-dimensional bodies with laminar approach flow and $\text{Re} \geq 10^4$. For these bodies, the Reynolds number is based on the frontal vertical dimension (i.e. diameter for bodies of revolution, like a cone, and frontal height for rectangular shapes). The behavior of these bodies is similar to that of the two-dimensional bodies shown in figure 15.7, with variations in C_D dependent upon the orientation of the body. Again, sharp corners at the leading edge create much higher C_D values. Note particularly the hemispherical cup, for which C_D varies by a factor of 375% depending on orientation. Of course this elevated drag effect is put to good use for such devices as parachutes (the last shape in figure 15.10), where high drag provides lowered terminal velocities for falling bodies (such as paratroopers), or when employed as air brakes (e.g. on aircraft or drag racers).

Example: Terminal Velocity with a Parachute

Consider an 80 kg man jumping from an airplane, and using a parachute to descend. Assume that the air (near the ground) is at 20 C, the kinematic viscosity is $1.5 \times 10^{-5} \text{ m}^2/\text{s}$, and the density is $1.2 \text{ kg}/\text{m}^3$. What should the frontal area of the parachute be to assure landing at a safe speed of 6 m/s? Let the weight of the parachute and pack be 5 kg, and neglect the drag coefficient of the man.

The drag force required at landing will be a balance of the gravitational force on the combined man + parachute:

$$\text{Drag required} = Mg = (85) \text{kg} (9.81) \frac{\text{m}}{\text{s}^2} = 833.8 \frac{\text{kg} \cdot \text{m}}{\text{s}^2} = 833.8 \text{ N}$$

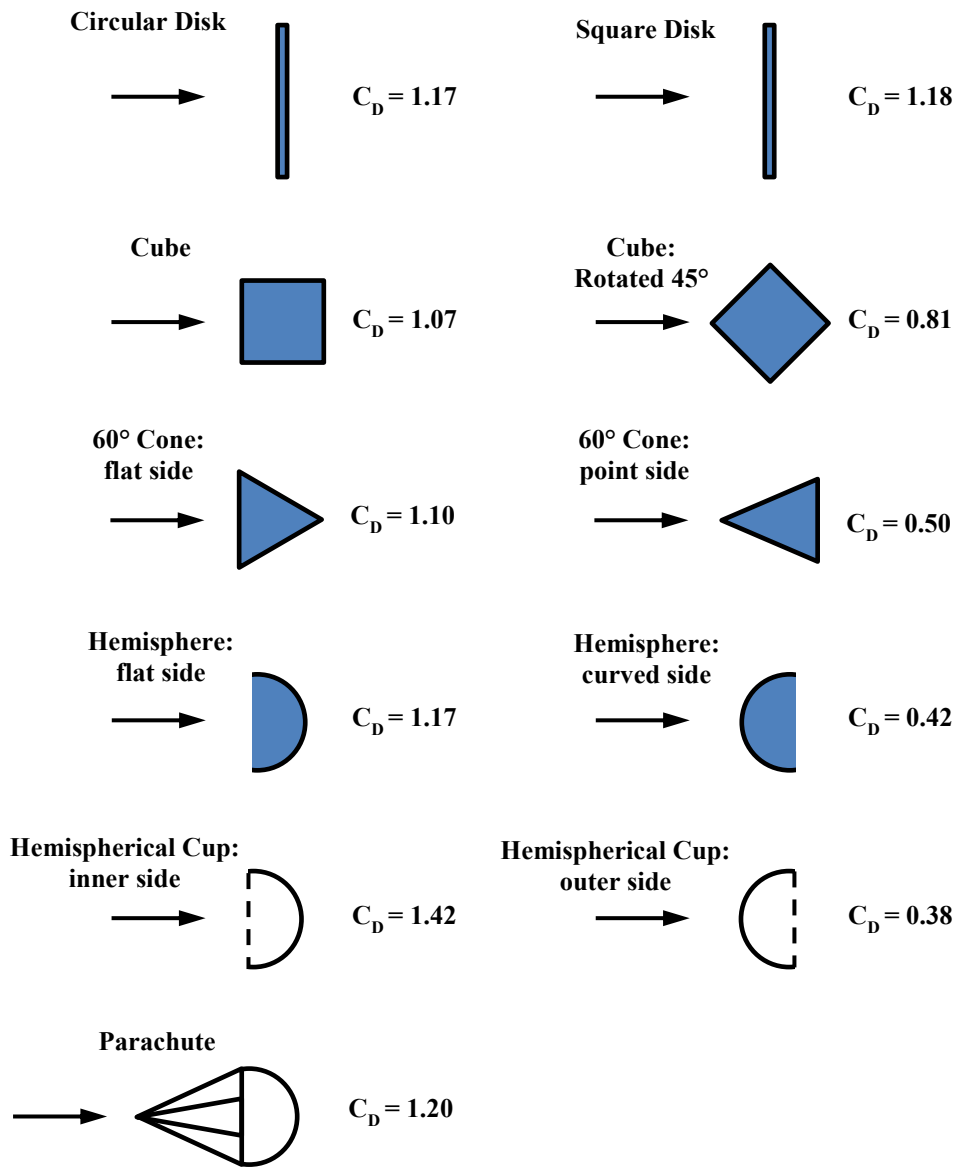


Figure 15.10 Drag coefficients for selected three-dimensional bodies at $Re \geq 10^4$ with laminar approach flow (Reynolds number based on diameter or vertical dimension of the body). [after [Hoerner, 1965](#)]

The drag equation is:

$$\text{Drag} = C_D \rho \frac{1}{2} V^2 A$$

Solving for the frontal area gives:

$$A = \frac{2 \text{ Drag}}{C_D \rho V^2}$$

From figure 15.10 $C_D = 1.2$ for a parachute, so the required frontal area is:

$$A = \frac{2(833.8) \frac{\text{kg} \cdot \text{m}}{\text{s}^2}}{(1.2)(1.2) \frac{\text{kg}}{\text{m}^3} (36) \frac{\text{m}^2}{\text{s}^2}} = 32.2 \text{m}^2$$

And since the frontal area will be $A = \pi \frac{D^2}{4}$, the parachute diameter will be 6.4 meters, or 21 feet. The amount of cloth to make the necessary parachute (assuming a hemispherical shape) would be about 64.3 m² or 692 ft²—a lot of cloth. Additionally, The Reynolds number for this chute would be 2.5×10^6 , so it easily exceeds the $Re_D > 10^4$ criteria listed in figure 15.10.

Click [here](#) to see more examples of CD values for symmetric two-dimensional, three-dimensional, and other types of common bluff bodies; this also provides a series of relevant references on bluff body drag.

15.4 Unsteady Separation/Drag Effects

As we discussed in Section 15.3, when an impinging flow encounters a bluff body, the flow will initially undergo strong acceleration toward the thickest portion of the body, followed by strong deceleration after passing the point of maximum thickness. For example, in Section 9.8.1 we showed that inviscid flow over a circular cylinder will initially accelerate to the point of maximum thickness, and then decelerate from that point to the trailing edge. Correspondingly, the pressure along the cylinder surface will decrease to the point of maximum thickness, yielding a favorable pressure gradient, followed by a pressure increase to the trailing edge of the body, reflecting an adverse pressure gradient. Figure 15.11 shows the general streamline pattern and non-dimensional pressure behavior for inviscid flow over a cylinder, from Section 9.8.1.

As was illustrated by the Falkner-Skan solutions in Section 13.6, and discussed in general in section 14.6, the boundary layer of a viscous fluid cannot be maintained under even a mild *adverse* pressure gradient, and will quickly separate from a cylinder, or other similarly bluff bodies, when an adverse pressure gradient is encountered. However, as we showed in Section 11.5.3, a region of *favorable* pressure gradient (as encountered in the leading portion of bluff bodies) will cause vorticity to be generated at the bounding surface. So, what happens to the vorticity generated by the favorable pressure gradient over the leading side of a cylinder or other bluff body when a boundary layer separates? The answer is that the vorticity is transported into the wake of the cylinder from the point of boundary layer separation (generally, shortly after reaching the maximum body thickness). In addition, because a sheet of vorticity is very unstable, the separating vorticity will generally concentrate into discrete vortices in the wake of the body. After reaching a certain strength and size (depending on the Reynolds number and type of body), these vortices periodically detach from the wake, and are carried downstream. This detachment of discrete vortices is termed "vortex shedding" since the vortices are formed near the edge of the separated wake, and then periodically "shed" from the wake and carried downstream by the flow

field. A YouTube video, [shown here](#), uses laser-illuminated dye in a water flow to visualize the type of unsteady, yet periodic, vortex shedding behavior that can develop in the wake of bluff bodies.

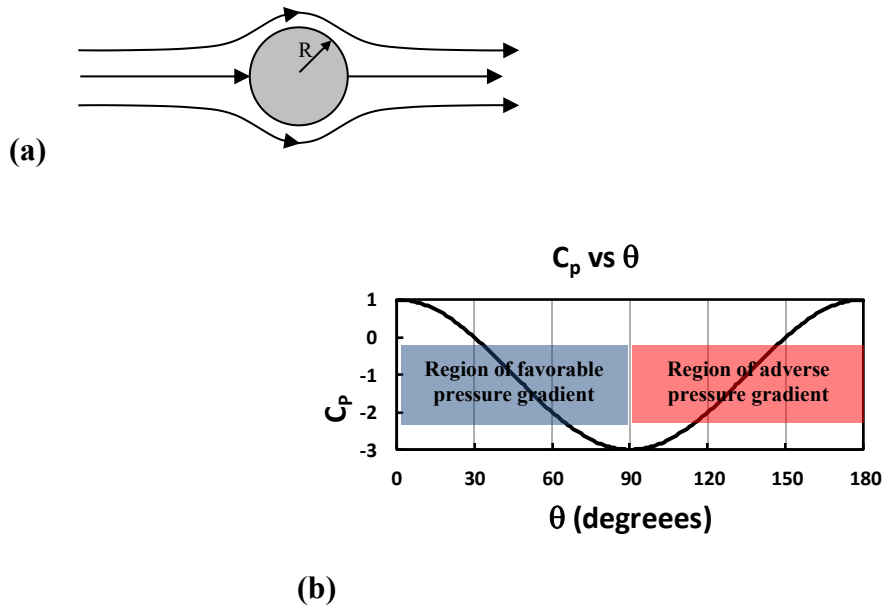


Figure 15.11 Inviscid, potential flow over a circular cylinder: (a) Streamline behavior [from figure 9.7]; (b) Surface pressure coefficient for inviscid flow over a cylinder,

$$\text{where } c_p = \frac{P - P_\infty}{\frac{1}{2}\rho U^2} = 1 - 4\sin^2\theta \text{ [from figure 9.9].}$$

As you might expect, the process of periodic vortex shedding causes an often strong oscillation of the wake of the bluff body. This wake oscillation results in a change in the trailing edge pressure on the body, which correspondingly causes a temporal change in both the drag and lift forces on the body. Depending on the size, frequency, and regularity of this vortex shedding process, these oscillations of the body wake and the associated pressure field can act as a strong forcing function on the body. A good example of periodic forcing by vortex shedding on a cylindrical pendulum can be viewed [here](#).

When this vortex-induced forcing is near the natural frequency of a solid body, it can cause the development of significant periodic movement of the body within the flow field, and under extreme cases, failure and collapse of the solid structure comprising the body. The YouTube video [shown here](#) shows the forced oscillation of a street light due to vortex shedding.

15.4.1 Vortex Shedding by a Circular Cylinder

The process of [vortex shedding](#) from a circular cylinder can display very periodic behavior, with the formation of very discrete vortices that are carried downstream by the main flow, as shown schematically in figure 15.12.

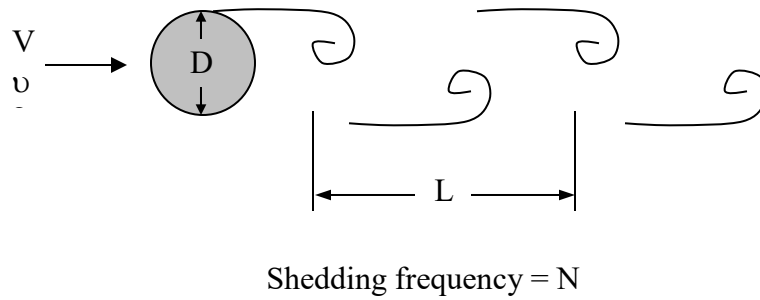


Figure 15.12 Schematic of vortex shedding from a circular cylinder of diameter D , with a shed vortex spacing L and a shedding frequency N , in an impinging fluid of velocity V and kinematic viscosity ν .

We can characterize the frequency of the shedding of the separated vortices by a non-dimensional frequency number termed the [Strouhal number](#), given by Eq. 15.2:

$$\text{Strouhal Number} = St = \frac{ND}{V} \quad \text{where } N \text{ is the shedding frequency (\#/s)} \quad (15.2)$$

Note that the Strouhal number ([Strouhal, 1878](#)) depends on the Reynolds number of the cylinder (based on the cylinder diameter, D), $Re_D = \frac{VD}{\nu}$. Figure 15.13 shows the general behavior of the Strouhal number for a cylinder as a function of Reynolds number, as determined from a number of experimental studies. The grey region in this figure indicates the spread of the data for a series of studies, with the red line indicating the general consensus for $St = f(Re_D)$.

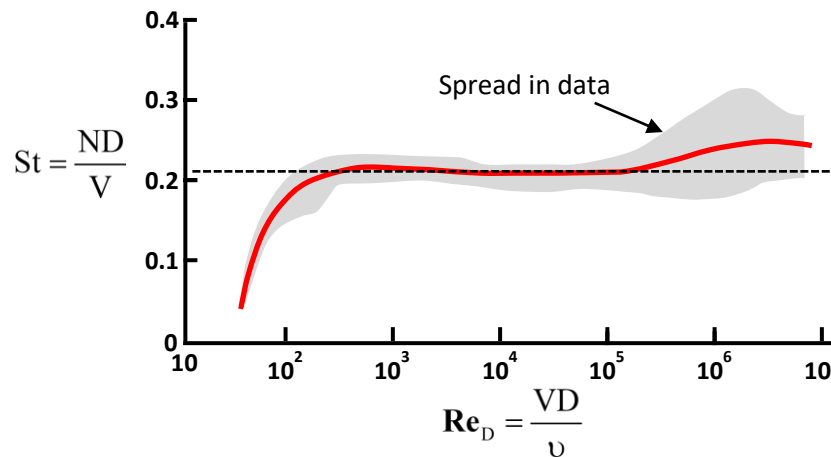


Figure 15.13 The behavior of the Strouhal number as a function of Reynolds number. The red line is the consensus behavior for a series of experimental studies, and the grey region indicates the spread in the empirical data. [after [Hoerner, 1965](#)] The dotted line indicates the accepted value of $N \approx 0.21$ for $10^3 < Re_D < 10^5$.

Generally, the separated wake behind a cylinder is relatively steady until $Re_D \approx 60$. Once $Re_D > 60$, vortex shedding initiates, and the Strouhal number increases with Re_D [i.e. $St = St(Re_D)$] up to about $Re_D \times 10^3$, where St becomes constant at ≈ 0.21 , until $Re_D \approx 10^5$. For $Re_D > 10^5$, the vortex shedding becomes less consistent and irregular, with different studies suggesting a range of behavioral changes. The red line in figure 15.13 represents a compromise, with the dotted line indicating the broadly accepted value of $N \approx 0.21$. Most studies show that when $Re_D > 10^7$ the vortex shedding becomes disorganized, and Strouhal numbers may no longer be determined.

Note that the region of constant St can be put to good use as a velocity-sensing device, by noting that for a circular cylinder we can approximate that $St \cong 0.21$ within the region $10^3 < Re_D < 5 \times 10^5$. Thus:

$$St = \frac{ND}{V} = 0.21 \quad \Rightarrow \quad V = \frac{ND}{0.21} = (4.76D)N \quad \Rightarrow \quad V \propto N$$

So, within the region of constant Strouhal number the velocity is directly proportional to the shedding frequency. Thus, by correlating the local flow velocity with the shedding frequency of a small cylinder, the shedding frequency can be used to calibrate velocity measurement devices, such as [hot-wire anemometers](#), and is the basis for certain pipe [flowmeters](#).

Example: Since each shed vortex is a source of low pressure (at the center of the vortex), the passage of a vortex will create a temporal pressure change. Since sound is created by time-varying pressure, if the vortex shedding frequency is high enough, there will be an audible sound. So, consider air at 20 m/sec (about 65 ft/s) passing across two different circular rods: a) 2 mm coat hanger, and b) a 2 cm rod.

The vortex shedding frequency will be different, due to the differing diameters, which will result in different audible frequencies. The shed vortices are sources of sound pressure, and thus we can “hear” the difference in the shedding behavior.

Here we estimate the shedding frequencies:

$$a) \text{ Coat hanger } \Rightarrow D \cong 2 \text{ mm}, V \cong 20 \text{ m/s}, \nu = 1.5 \times 10^{-5} \text{ m}^2/\text{sec}$$

$$Re_D = \frac{VD}{\nu} = \frac{(20) \frac{\text{m}}{\text{s}} (2) \text{mm} (10^{-3}) \frac{\text{m}}{\text{mm}}}{1.5 \times 10^{-5} \frac{\text{m}^2}{\text{s}}} \cong 2.66 \times 10^3 \Rightarrow St = 0.21 \text{ (from figure 15.13)}$$

$$St = 0.21 = \frac{ND}{V}$$

$$N = \frac{(0.21)(20) \frac{\text{m}}{\text{s}}}{(2)\text{mm}(10^{-3}) \frac{\text{m}}{\text{mm}}} \cong 2100 \text{ Hz}$$

$$\text{b) } 2 \text{ cm rod} \Rightarrow D \cong 2 \text{ cm}, V \cong 20 \text{ m/s}, \nu = 1.5 \times 10^{-5} \text{ m}^2/\text{sec}$$

$$\text{Re}_D \cong 2.66 \times 10^4 \quad \Rightarrow \quad \text{St} = 0.21 \quad (\text{from figure 15.13})$$

$$N \cong 210 \text{ Hz}$$

Human hearing can detect sounds in the range of 20 to 20,000 Hz (check [here](#) to see how good your hearing is). Therefore, the shedding from a coat hanger will be in the mid-higher frequency range of our hearing, and the 2 cm rod (roughly the diameter of a broomstick) will shed near the low end of our hearing. Try this as an experiment. You should be able to swing these types of rods by hand at roughly the 20 m/s speed. Note that the sounds will also be of different amplitudes, because the different diameters generate different strength and size vortices (the coat hanger sound will be harder to hear).

15.4.2 Vortex Shedding by Other Shapes

Generally, any bluff body will display similar periodic shedding, with some bodies shedding more periodically than others. [Hoerner \(1965\)](#) has shown that within $10^3 < \text{Re}_H < 10^5$ (where H is the vertical dimension of a body), the Strouhal frequency is (roughly) inversely proportional to the drag coefficient of the body, with an empirical relationship according to Eq. 15.3:

$$\text{St} = \frac{NH}{V} \cong \frac{0.21}{C_D^{0.75}} \quad (\text{H is vertical dimension of the body}) \quad (15.3)$$

So, generally a lower drag body will yield a higher Strouhal number, and a higher drag body a lower Strouhal number. However, the more streamlined a body is, the less likely it is to have organized vortex shedding. Additionally, three-dimensional bodies will generally not shed in an organized manner. Organized, periodic vortex shedding primarily occurs for flow over two-dimensional cross-section bluff bodies (e.g. long rods, wires, or poles).

So, what are common bodies that shed vortices? Almost anything that has a bluff-shaped body will shed vortices. Moreover, the bodies, and the vortices they shed, can often be quite large. For example, all the following can undergo some form of vortex shedding---periodic, or otherwise:

- girders
- buildings
- trucks & cars
- airfoils
- big ships
- dock pilings and bridge supports
- suspended pipe lines and cables

What are the consequences? Periodic pressure loading of the body, which can cause fatigue and failure of a solid body, or can act as an external forcing function that can excite large oscillations at the system natural frequency. Examples are:

- Tacoma Narrows bridge collapse (1932) (<http://www.youtube.com/watch?v=j-zczJXSxnw>)
- swaying flagpoles (<https://www.youtube.com/watch?v=ptYrbQGk6DQ>)
- buffeting of cars by shedding from large trucks
- swaying buildings
([this video](#) shows the skyline moving, while [this video](#) shows a pendulum in a room swaying as the building moves)

On a windy day, the Sears Tower in Chicago will shed large vortices, which cause it to sway slowly, with a movement of up to three feet on a windy day. Of course the higher the wind speed, the greater the movement, and the higher the frequency of the swaying motion. For example, assuming a rectangular-shaped building of the dimensions of the Sear Tower, we get following approximate frequencies

@ 10 m/s – 0.021 HZ → 48 second oscillation period.

@ 30 m/s – 0.063 HZ → 16 second oscillation period

People occupying the upper floors of the tower have been known to get "seasick" from this motion. See this video of [building sway](#) caused by vortex shedding.

15.5 Control of Separation and Drag

Since pressure/form drag is significant on bluff bodies, it is of practical advantage to employ methods to reduce pressure drag (i.e. a process generally termed “control”), and/or reduce or eliminate the pressure fluctuations due to vortex shedding. There are many different approaches to accomplish this reduction, most of which fall into two categories:

- (1) passive control, and
- (2) active control.

15.5.1 Passive Control

Passive methods of control are methods that do not require an action to effect the control process. These are methods which reduce drag and unsteady behavior by changes in surface characteristics or geometry changes, or insertion of secondary geometrical elements in the wake region.

15.5.1.1 Surface Effects

The most common passive control method is to promote mixing of the fluid passing over the body to keep the flow attached, and thus delay separation, which correspondingly reduces pressure drag and vortex shedding. Some general methods are shown in Figure 15.14. The simplest passive methods attempt to cause the boundary layer on the body to transition to turbulence as soon as possible. For these techniques, the body is either purposely roughened (e.g. the [dimples on a golf ball](#)), or fitted with a "tripping" device, such as a wire, rod, or saw-toothed blade, which generate localized disturbances. In all of these cases, artificial disturbances are generated, which promote the development of a turbulent boundary layer (see Chapter 17), which subsequently delays flow separation (see [figure 15.1a](#), and the associated visualizations in 15.1d, pictures 2 and 3).

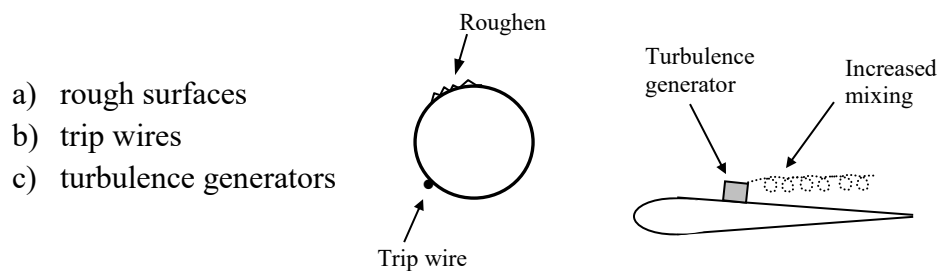


Figure 15.14 Passive methods for delaying separation by creating increased mixing. Methods causing an early transition to turbulence: (a) roughening surfaces, and (b) use of a trip wire. Methods generating vortices near the surface: (c) turbulence or vortex generators projecting from the surface.

More complicated passive methods utilize larger protrusions from the body surface (on the order of the boundary layer thickness, or larger), which generate large-scale vortices to promote strong mixing near the region of natural separation, and again delay separation. These are generally termed "[vortex](#)" or "turbulence" generators, since they promote turbulent-like behavior by generating streamwise vortices near a surface.



Vortex generators normally create stream-wise vortices of larger scale than naturally occurring turbulence. These devices range from small [protruding tabs](#) at an angle of attack, which generate trailing vortices, to the fabrication of bounding surfaces with [span-wise waviness](#), which also

promote the development of stream-wise vortices. Regardless of how the streamwise vortices are generated, their creation promotes downstream mixing, and can be very effective in delaying separation and reducing drag. Additionally, stream-wise vortices will interact with the separating vorticity layer, and interfere with the vortex shedding process, and thus reducing or eliminating the periodic pressure variations due to vortex shedding.

A variation on trip wires and vortex generators that has proven relatively successful is wrapping a [wire spirally around a cylinder](#). This is relatively easy to do, and has the combined effect of tripping the boundary layer, to make it turbulent, while generating streamwise vortices, which interfere with the periodic vortex shedding process. An additional benefit of this approach is that unlike the trip wire, it has no preferred directional orientation, and will be effective regardless of the flow direction. This spiral wrapping approach has been used successfully in a wide variety of applications, from [power plant chimneys](#) (see images [here](#)) to [large suspended cables and pipelines](#).

Passive mixing methods are generally easy to apply and implement, and do not require an additional control system to operate. However, such methods have varying degrees of effectiveness in the control of separation, depending on the type of body. The placement of trip wires and turbulence generators is sometimes a bit tricky, and may require a bit of trial and error to optimize the best location. Additionally, turbulence generators extract energy from the mean flow to generate stream-wise vortices. This energy extraction process creates additional drag on the body. However, these devices normally delay separation sufficiently, and reduce pressure drag enough, to override the added device drag of the turbulence generators.

15.5.1.2 Splitter Plates

Another passive method of drag and vortex shedding control is the use of splitter plates, several variations of which are shown in figure 15.15. The type of effect splitter plates can have on flow behavior is illustrated [here](#). Splitter plates are flat plates located in the wake of a bluff body, and extending across the span of two-dimensional geometries. Figure 15.15 shows several types of plate sizes and relative locations in the wake of a circular cylinder, from a very short plate (about $\frac{1}{4} D$ in length, known as a Thwaites flap), shown in figure 15.15a, to a long plate (about $4D$ in length), shown in figure 15.15b.

The objective of these plates is to stabilize the wake by reducing the unsteady interaction of the boundary layers separating from the top and bottom of the body. This stabilization also causes an increase in the trailing edge pressure, and thus reduces the drag on the body. It is interesting that the location of a splitter plate of roughly $1D$ length at a distance of $3D$ downstream of a cylinder, as shown in figure 15.15c, has almost the same effect on drag and unsteadiness as that of the $4D$ plate in figure 15.15b.

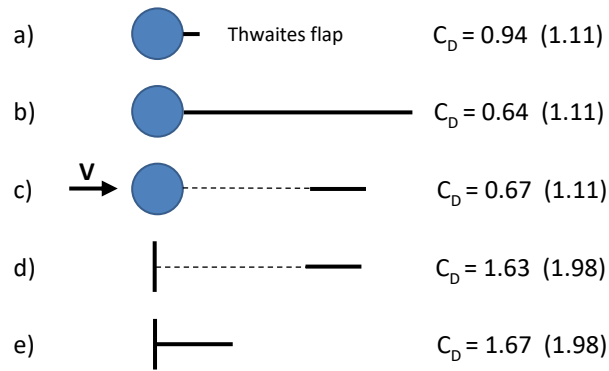
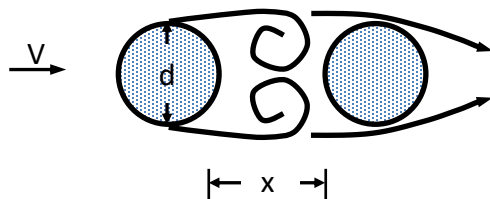


Figure 15.15 The use of splitter plates for reduction of drag and vortex shedding effects. C_D values are for the respective splitter arrangements shown (unmodified C_D values are shown in parentheses) [after [Hoerner \(1965\)](#)]

Generally, the complete elimination of vortex shedding requires a splitter plate of length $4D$ or greater. Shorter plates will cause reductions in the Strouhal number, but will not eliminate the process. The $1D$ plate was found to reduce the normal cylinder Strouhal number of $St \approx 0.21$ to $St \approx 0.19$ when the plate is in contact with the cylinder, and to roughly $St \approx 0.13$ when the plate is $3D$ removed from the cylinder (figure 15.15c). However, locating the plate farther from the cylinder ($> 3D$) results in a jump in Strouhal number back to $St \approx 0.21$ (and a return to $C_D = 1.11$, the value with no plate).

While splitter plates can reduce drag from 10 to 40%, their chief impact is to reduce or eliminate the vortex shedding. Thus, the primary application of these splitter plates would be where unsteady loading on a structure is a problem. However, fabrication of such control plates is often awkward, particularly if they are to be located away from the body, such as those in figure 15.15c and d. If the plates are not sufficiently rigid, they can be subject to forcing by the alternating vortex interactions, which can result in harmonic flexing of the plate, which can potentially exacerbate the vortex shedding. Additionally, to be effective, the direction of the flow over the body must be from a consistent direction. If a flow is an atmospheric or oceanic flow, and varies significantly in direction, the use of flaps can be quite problematic and is not recommended.

15.5.1.3 Sequenced Bodies



Another method of controlling and reducing drag for multiple bluff bodies is the process of sequencing the bodies in line with each other (i.e. having one body located in front of the other). Such an arrangement for a pair of cylinders is shown above.

As one might guess, the spacing between a sequence of bodies can have an effect on the drag of both the leading and trailing body, with the magnitude of the effect being a function of the separation distance between the bodies. In general, the closer the bodies are to each other, the greater the effect, which is to reduce the effective drag on one or more of the sequenced bodies.

Figure 15.16 shows the effects of separation distance, x/d , on the drag coefficient, C_D , for a sequence of two identical cylinders at $Re_d \approx 10^5$, such that the first cylinder is in the laminar flow regime. This figure, after [Hoerner\(1965\)](#), requires a little interpretation. C_D for both the leading edge cylinder and the trailing edge cylinder are calculated as:

$$C_D = \frac{\text{cylinder drag force}}{\frac{1}{2}\rho V^2 (dL)} \quad (15.4)$$

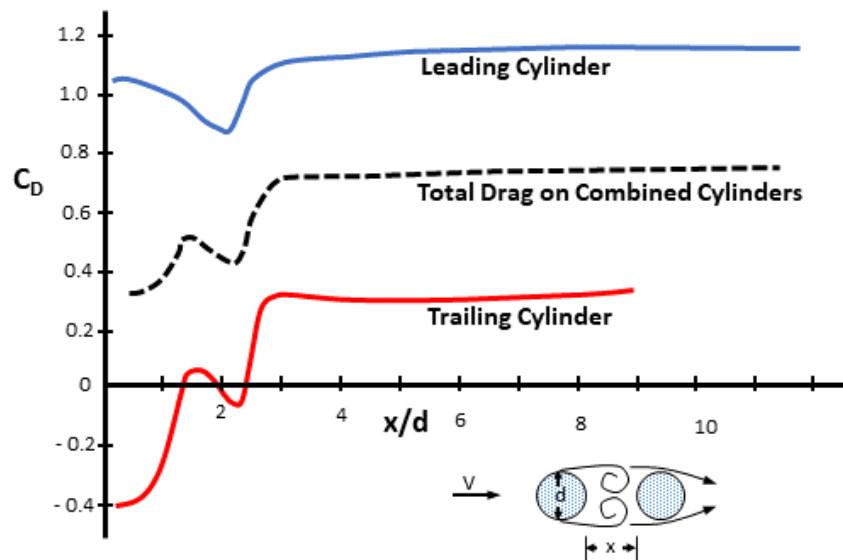


Figure 15.16 Drag coefficients for two circular cylinders, sequenced inline as a function of separation distance, x/d . $Re_d = 10^5$. [after [Hoerner, 1965](#)]

Here L is the length of the cylinder, d the cylinder diameter, and the cylinder drag force is the streamwise force acting on either the leading cylinder or the trailing cylinder. In addition, for figure 15.16, Hoerner calculates C_D for the total drag on the combined cylinders as:

$$C_{D_total} = \frac{\text{collective drag force on both cylinders}}{\frac{1}{2}\rho V^2 (2dL)} = \frac{C_{D_leading} + C_{D_trailing}}{2} \quad (15.5)$$

Thus, nondimensionalizing the total drag coefficient on the combined frontal area of the two cylinders, $2dL$.

What figure 15.16 shows is that for spacing between the cylinders of $x/d > 3$, the drag on the leading cylinder is $C_D \approx 1.2$, essentially that for a single cylinder at this Re_d (see figure 15.3). However, the drag on the trailing cylinder is significantly reduced, to roughly $C_D \approx 0.3$, which is essentially that for turbulent flow (again see figure 15.3). What is happening is that the wake of the leading cylinder is creating flow unsteadiness that behaves as a turbulent flow impinging on the trailing cylinder, thus reducing the effective drag coefficient. What this does is reduce the collective drag for the combined bodies by roughly 40% from that for two cylinders not sequenced.

However, for $x/d < 3$, the effects on the drag of each cylinder, and the collective drag is even more dramatic. As x/d decreases below 3, the trailing cylinder significantly interferes with the development of the wake of the leading cylinder, causing the wake of the leading cylinder to stabilize and merge with the outer surface of the trailing cylinder. The change in the wake flow pattern results in a modest increase in the pressure distribution on the rear of the leading edge cylinder, thus causing $C_{D_leading}$ to decrease. However, the flow field alteration also causes the pressure distribution on the front of the trailing edge cylinder to strongly decrease from stagnation levels, which causes a marked decrease in $C_{D_trailing}$. As figure 15.16 shows, by $x/d \approx 2$ the pressure distribution over the front surface of the trailing cylinder becomes equivalent to the distribution over its rear surface, which results in essentially a cancellation of drag on the trailing cylinder. Moreover, for $x/d < 1$ the pressure distribution over the front of the trailing cylinder will become less than over the rear surface, and the trailing cylinder will actually experience a significant suction, or negative drag.

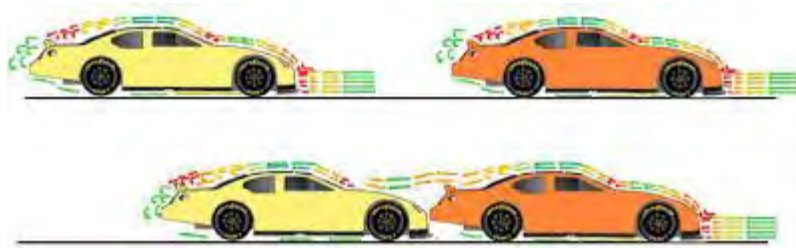
Note that when $x/d = 0$ (the cylinders touch), the C_{D_total} asymptotes to ≈ 0.3 . This is a 75% reduction in the collective drag for the combined bodies from the cumulative drag for two cylinders not sequenced. However, we could have anticipated this reduction from figure 15.8. When the cylinders are touching, the combined bodies will roughly represent a body of $t/L = 0.5$ ($d/2d$) in figure 15.8. The laminar C_D for such a tapered body is 0.6. If we now rewrite Hoerner's total drag coefficient to base it on only the frontal area of our combined body (dL), we would have:

$$\begin{aligned} C_{D_total} \Big|_{x/d=0} &= \frac{\text{collective drag force on both cylinders}}{\frac{1}{2} \rho V^2 (dL)} = C_{D_leading} + C_{D_trailing} \\ &= 1.04 - 0.4 = 0.64 \end{aligned} \quad (15.6)$$

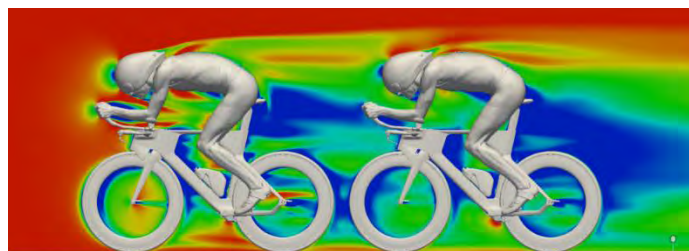
Therefore, when the two cylinders touch, they emulate the drag behavior similar to a tapered body of $2d$ in length.

We might reason that if we included more bodies in sequence, that we might experience similar reductions with increased numbers of bodies. That is true. A sequenced combination of three bodies will reduce the collective C_D further than for two sequenced bodies, and so forth, although the reductions will not be as significant.

There are a number of practical applications of sequenced body drag reduction. The aerodynamic drag of trains is one example, where the collective pressure drag on a train with multiple sequenced cars is much less than the pressure drag on a single locomotive (although long trains will have more drag due to surface shear stresses). However, some of the more common applications have to do with sports. In stock car racing, “drafting” has a big effect in improving the speed and performance of cars during a race. Two cars racing in line, and very close to one another, experience less drag than the individual cars alone. So, two cars moving in concert (with two engines powering the combination) can go much faster than one car alone. In addition, if you add more sequenced cars, that group can go even faster. In fact, it is quite common for the rear car to actually “push” on the bumper of the lead car so they share their collective engine power. While a successful strategy, it is also highly dangerous; if the rear car does not apply its push in the center of the lead car’s bumper, the lead car can become unstable and spin out, resulting in a potentially devastating crash. For a good article on the effects of car separation distance on drag, click [here](#).



Other applications of sequenced body drag reduction are in bicycle racing, cross country ski racing, and running races, to name a few. In all cases, the trailing competitors will benefit more by closely following a leading competitor who is “breaking the wind”. However, the faster the sport, the more help drafting will be to a competitor (e.g. it is much more useful in bicycle racing than distance running).



Another practical example of sequenced bodies is a variation on the principle of drafting, and can be employed to reduce one’s fuel usage on a highway trip. We can’t safely drive very closely

behind another similar vehicle, because we can't respond quickly enough if the lead vehicle brakes sharply (and you would probably sustain some angry gestures from the lead vehicle driver). However, if you are traveling at highway speeds and can drive behind a larger vehicle, such as a tractor-trailer truck, you can reasonably drive within 2-3 truck lengths. Driving at that distance, or closer, will reduce the air drag on your vehicle, require less power from your engine, and thus reduce your fuel usage. This requires strict, full-time attention so you can respond quickly should the truck brake suddenly, and again may get you nasty stares or gestures from the truck driver. Use of modern ["adaptive cruise control"](#) on newer vehicles actually helps facilitate this process, by automatically sensing and controlling the distance from the trailing vehicle to the lead vehicle. For a very good article on the manifold applications of drag reduction by multibody interactions, [click here](#).

15.5.2 Active Control

Active control of flow separation and drag is done using some form of auxiliary system to actively remove the stagnant wake fluid downstream of a flow separation or to reenergize the boundary layer fluid by some active means. As opposed to passive methods, which extract energy from the mean flow, and reenergize the boundary layer through mixing processes, active control requires the addition of energy to the local boundary layer from some external source. These approaches are generally more complicated than passive devices, but can be directed at specific regions of the flow, and can often be very effective in minimizing separation and pressure drag for flows that cannot be controlled by passive means.

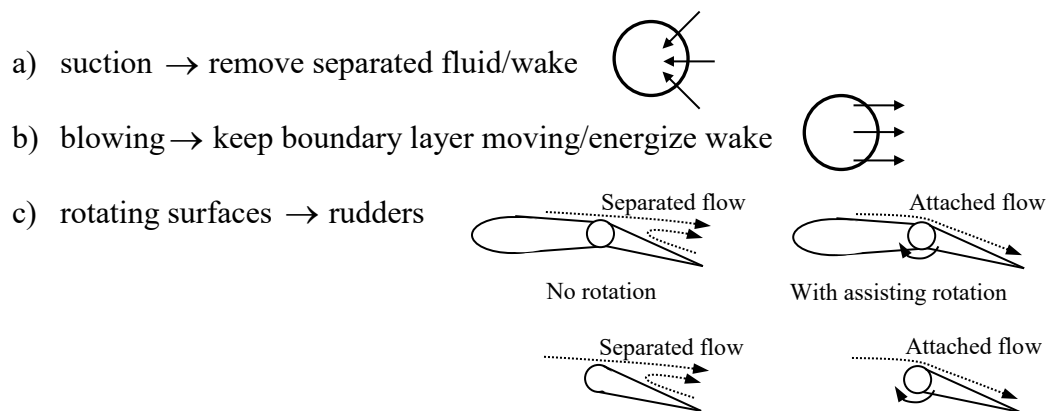


Figure 15.17 Active methods for delaying separation by removal of regions of separated fluid or reenergizing the boundary layer: (a) fluid removal by surface suction; (b) reenergizing the boundary layer/wake by injection of stream-wise fluid through the bounding surface; (c) reenergizing boundary layer fluid by use of a moving surface.

Figure 15.17 shows several general approaches to active control of separation. There are others, but those shown illustrate the most common approaches. One particularly effective technique is the use of suction (figure 15.17a) to remove boundary layer fluid that has been slowed by an adverse pressure gradient, or the stagnant wake fluid in a downstream separation region. Suctioning off of the low-speed or stagnant fluid will bring the higher-speed outer region flow into closer proximity of the bounding surface, and thus keep the boundary layer energized. Such techniques are not easy to implement, since they require a separate pump or suction device to create the suction, and a locally perforated (i.e. porous) bounding surface. In such suction systems, contamination of the porous surface, creation of the proper flow distribution through the porous surface, and proper location of the porous surface are all problems that must be addressed, usually by trial and error.

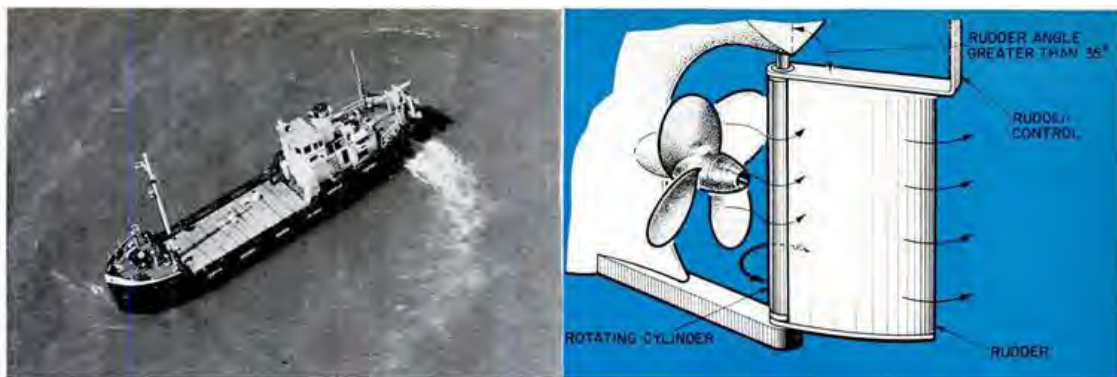
To account properly for any drag reduction due to active fluid removal, one must also account for the additional energy required to operate the suction device. The reduction in flow energy losses, reflected by the reduced total drag, is often exceeded by the energy required to run the fluid removal system. In such a situation, there is a net increase in "lost" flow energy, rather than a decrease in lost flow energy. Often suction systems are utilized when drag reduction is not the objective, but when one wants to reduce separation, and keep a flow attached and steady. If vortex shedding or unstable behavior is threatening the integrity of a structure, the penalty paid to operate the suction or injection system may be justified.

A second active technique for controlling separation/drag is fluid injection through the bounding surface (figure 15.17b), generally termed "blowing". This is usually done through surface holes or slots angled to inject the fluid in the direction of the downstream flow. Again, the objective is generally to either (1) reenergize the boundary layer fluid by the introduction of "new" high-velocity fluid, or (2) create vortices similar to a vortex generator to help control separation. This technique can be effective, if done correctly. However, it has drawbacks similar to the use of suction, such as contamination of the injection openings, proper placement of the injection ports, creation of an appropriate injection pattern, and the requirement of a separate pump or pressure device to create the flow. An additional concern is the angle of the injection openings, which cannot, due to practical considerations, be parallel to the bounding surface, but must be at some angle to the flow direction. Of course, one must again account for the added energy required to create the injection process vs. any improvement in separation/drag. In general, injection systems have proven most effective for airfoil-shaped blades used in gas turbine environments, and are generally more effective in reducing heat transfer to turbine blades, than reducing flow separation and overall drag. In such gas turbine environments, the turbine blades are essentially hollow, and receive the pressurized fluid by bleeding air from the compressor of the gas turbine system (see a discussion of turbine blade cooling [here](#)).

A third approach for active separation/drag control is to employ a moving boundary (figure 15.17c). Such an approach is only possible using a moving belt, or a circular rotor, built into the boundary of a body. The objective is to use a moving boundary to reenergize the

boundary layer fluid, such that the boundary layer does not have to work against both an adverse pressure gradient and surface shear. I am not aware of any practical applications of moving belt flows for separation control. However, rotors have been studied for improvement in airfoil lift and separation, an example study is found [here](#). While such rotors are shown to be effective, I am unaware of any practical application to aircraft, because of the weight, the high velocity of the airflows, and the complexity of operating such rotors on practical aircraft wings.

However, rotors have been put to practical use at the [junction of rudders](#) on large ships, where the flow velocities are not particularly high, and where the objective is to reduce separation downstream of the rudder junction, or pivot. This process helps the rudder retain aerodynamic "lift", and thus its effectiveness as a control surface.



She'll chase her tail without any forward motion at all. New rudder on 200-ton cargo ship uses boundary-layer control technique

used in aircraft design. Spinning cylinder diverts thrust against rudder, allowing 90-degree turns and a complete stop in seconds.

Super-Rudder Lets Super Tankers Turn on a Dime

A spinning tube on the rudder pivot could enable a 250,000-ton super-tanker steaming at 15 knots to turn on its own axis if need be to avert collisions at sea or maneuver tightly into port. It could also cut stopping time to a fraction of the usual 20 minutes needed to bring these giant vessels to a halt.

The secret is an amazing rotating-cylinder rudder developed by the National Physical Lab in England.

The trouble with a conventional rudder is that when it's turned more than 35 degrees in either direction, water turbulence and flow separation behind it cut its "bite" and reduce steering effectiveness.

NPL scientists fitted a five-foot-long, six-inch-diameter tube, rotating at 900 rpm (either right or left) to the leading edge of the rudder directly behind the propeller. Hydrodynamic action of the smooth cylinder pre-

vents flow separation and makes backwash from the prop hug the back surface of the inclined foil. The rudder can be put over to an extraordinary 90 degrees without loss of bite, and thrust is diverted at right angles to push the stern sideways.

Drive is from a reversible 3-kw motor, now hand-started. In future, the tube will automatically start spinning when the rudder reaches the critical 35 degrees.—David Scott

Figure 15.18 The use of a rotating cylinder at the leading edge of a rudder, allowing ships to turn more sharply due to elimination of rudder "stall" by the cylinder rotation. From [Popular Science, Feb. 1973, pg. 101](#).

The schematic in Figure 15.17c shows the general placement of a rotor at a rudder junction or leading edge. As shown, such configurations will keep the local boundary fluid energized such that it can remain attached under significant changes in direction. Such rotor devices have been successfully utilized on the rudders of large cargo ships, and allow them to have a much tighter turning radius when maneuvering in tight spaces, such as harbors. The figure 15.18 is an excerpt from a popular science article about such a rudder.

However, such rotor devices are not practical in aerodynamic flight systems, due to the velocities involved, and the weight of the rotor and accompanying powering system. It should be noted that such rotational devices applied in practice will reduce separation, and potentially the drag, although that is generally not their primary objective.

References

Hoerner, S. F. (1965). *Fluid-Dynamic Drag*, Hoerner Fluid Dynamics, Bricktown New Jersey.

Study Problems

1. Consider a telephone pole of circular cross section of 28 cm diameter, with a gale force wind blowing perpendicular to the pole at 20 m/s. Determine the force per unit length on the pole due to drag if the pole surface is (a) smooth, or (b) rough. Assume air at 20 C, the kinematic viscosity is $1.5 \times 10^{-5} \text{ m}^2/\text{s}$, and the density is 1.2 kg/m^3 (neglect any effect of the ground on the drag).
2. A square sign post of 28 cm on a side, with a gale force wind blowing perpendicular to the post at 20 m/s. Determine the force per unit length on the post due to drag. Assume air at 20 C, the kinematic viscosity is $1.5 \times 10^{-5} \text{ m}^2/\text{s}$, and the density is 1.2 kg/m^3 . Determine the highest drag to be expected, and the lowest drag for these conditions, and why?
3. A square sign post of 20 cm on a side, supports a thin, circular metal sign of 70 cm in diameter, with the sign attached to the post starting at 2 meters above the ground. Hurricane force winds blow perpendicular to the post at 50 m/s. Determine the Total force on the post and on the sign due to drag. Assume air at 20 C, the kinematic viscosity is $1.5 \times 10^{-5} \text{ m}^2/\text{s}$, and the density is 1.2 kg/m^3 . Neglect boundary layer effects from the ground. What is the highest drag to be expected, and what is the lowest for these conditions, and why?
4. A circular cross-section leg of an off-shore oil platform is of 3 meters in diameter, and extends down 100 meters. An ocean current of 4 meters/s flows past the leg. Determine the total force on the leg due to drag. Assume the flow velocity is uniform over the entire leg, sea water is at 10 C, the kinematic viscosity is $1.3 \times 10^{-6} \text{ m}^2/\text{s}$, and the density is 1020 kg/m^3 .
5. A two smooth spherical pieces of metal of density 3050 kg/m^3 are dropped over the side of a boat. The smaller piece is 2 cm diameter, and the larger piece is 20 cm diameter. Assume sea water is at 10 C, the kinematic viscosity is $1.3 \times 10^{-6} \text{ m}^2/\text{s}$, and the density is 1020 kg/m^3 . When the spheres reach terminal velocity (no longer accelerating), what will their descent velocities be (in m/s) and which will descend faster? What are the results if the spheres are roughened?

6. A car top carrier for a kayak has a front cross-strut that is circular in cross-section, with diameter 3 cm and 1.3 meters long. Assume the cylinder is smooth. When the car is driven, the air flows perpendicular to the strut. Assuming the flow is uniform approaching the strut, determine the total force on the strut due to drag, when the car travels at 30 m/s without the kayak on the rack. Assume air at 20 C, the kinematic viscosity is $1.5 \times 10^{-5} \text{ m}^2/\text{s}$, and the density is 1.2 kg/m^3 . How much power (in Watts) from the engine is required to maintain this force? If we change the cross-section of the rod to an oval with $t/L=0.25$, where $t = 3 \text{ cm}$, how much is the force and power requirement reduced?
7. The drag coefficient for a runner is roughly 1.2. The world record holding sprinter, Usain Bolt, can run at an average speed of about 10.6 m/s for 100 meters. The world record holder in the 1500 m run is Hicham El Guerrouj, who covered the distance in 3 minutes and 26 seconds. Your typical recreational jogger runs at a speed of about 3 m/s in running 5000 m. Assuming a cross sectional area of 0.75 m^2 for all three runners, an air density of 1.2 kg/m^3 , and that they run at a constant speed for their respective distances, determine the drag force that acts on each runner during their run, the power they must expend, and the total work they do due to overcome air drag in covering their respective distances.
8. For the conditions given in problem 1, determine the approximate vortex shedding frequency for the telephone pole.
9. For the conditions given in problem 4, determine the approximate vortex shedding frequency for the oil platform leg.
10. For the conditions given in problem 6, determine the approximate vortex shedding frequency for the circular strut. Would this be audible? How might you improve the design of this strut?
11. For the conditions given in problem 2, determine the approximate vortex shedding frequency for the square post, for both the highest drag and lowest drag configuration.
12. We want to calibrate a hot-wire anemometer (an electrically-heated wire that can measure high frequency velocity variations) by using vortex shedding from a small cylindrical rod. We want to do this in air, by measuring the vortex shedding frequency with the hot-wire anemometer, and correlating it to the respective velocity. If we need to calibrate the anemometer over a range of velocities from 1 and 20 m/s, what is the range of rod diameters that we could use to assure that the velocity will be a linear function of the shedding frequency? Assume air at 20 C with kinematic viscosity of $1.5 \times 10^{-5} \text{ m}^2/\text{s}$. What is the lowest shedding frequency we might measure with this range of rods?
13. Consider the flow of air over a cylinder. Assume that the impinging velocity is $U = 1 \text{ cm/s}$, and the cylinder radius is $R = 10 \text{ cm}$. The kinematic viscosity for air is $\nu = 16 \text{ mm}^2/\text{s}$. As the flow passes around the cylinder, a laminar boundary layer develops on the cylinder surface. Assume that the velocity at the edge of the boundary layer can be approximated by the potential flow solution of $U_\infty = 2U \sin(\alpha)$, where α is the angle measured from the cylinder stagnation point around the cylinder.

(13. continued)

- a. Using Thwaites method (from Chapter 14), neglect curvature effects and determine the development of the momentum thickness (θ) as a function of x , where $x = R\alpha$, when α is in radians. You can integrate the Thwaites equation analytically (you need to review your integral tables) or using the Seeking Alpha webpage—do it in terms of α , and then express in terms of x .
- b. Determine the angle α_{\max} (in degrees) where the solution is no longer valid, using a parallel calculation of the parameter n . Why does the solution fail at this point? [hint: consider the point of separation]
- c. Using the pressure distribution given by the potential flow solution over a cylinder (from Chapter 9), determine the drag per unit depth on the cylinder. For this real fluid flow, assume that after α_{\max} the flow is separated, and that the pressure will remain constant at the $P(\alpha_{\max})$ value until $\alpha=180^\circ$ is reached. Neglect the shear stress on the cylinder surface. Express your results in terms of the drag coefficient:

$$C_d = \frac{\text{Drag}}{\frac{1}{2}\rho U^2 (2R)}$$

How does the value you obtain compare to what you might expect for this flow (i.e. in figure 15.3)?

14. The power P to maintain a bluff body with drag of F_D at a velocity V , is given by $P = F_D V$. Consider the case of two cylinders, each of diameter d and length L , and each moving perpendicular to their length at a velocity V in a fluid of density ρ . Assume the cylinders are at $Re_d = 10^5$. Determine the power required to collectively move both the cylinders, in terms of V , d , L , and ρ if the cylinders are:
 - a) Independent of each other
 - b) In line with each other, separated by a distance $x/d = 6$
 - c) In line and touching each other ($x/d = 0$)

From your calculations, what % less power is required for b) and c) relative to a)?

Chapter 16

Introduction to Non-Newtonian Fluid Behavior

Contents

16.1	Introduction	529
16.1.1	Shear Thinning Fluids (Pseudoplastics)	529
16.1.2	Shear Thickening Fluids (Dilatants)	531
16.1.3	Viscoplastics (Bingham plastic)	532
16.2	Power-Law and Bingham Plastic Fluid Models	533
16.2.1	Ostwald-de Waele Power Law	533
16.2.2	Ideal Bingham Plastic	534
16.3	Simple Non-Newtonian Flows: Couette and Poiseuille	535
16.4	Power Law Fluid Solutions	536
16.4.1	Parallel Plate Flows	536
16.4.1.1	Couette Flow between Parallel Plates	537
16.4.1.2	Poiseuille Flow between Parallel Plates	539
16.4.2	Flows with Circular Symmetry	543
16.4.2.1	Couette Flow between Concentric, Rotating Cylinders	543
	Outer cylinder rotating at velocity V_o, Inner cylinder fixed	545
	Inner cylinder rotating at velocity V_i, Outer cylinder fixed	547
16.4.2.2	Poiseuille Flow in a Circular Duct	552
16.5	Ideal Bingham Plastic Solutions	557
16.5.1	Parallel Plate Flows	558
16.5.1.1	Couette Flow between Parallel Plates	558
16.5.1.2	Poiseuille Flow between Parallel Plates	560
16.5.2	Flows with Circular Symmetry	570
16.5.2.1	Couette Flow between Concentric, Rotating Cylinders	570
	Outer cylinder rotating at velocity V_o, Inner cylinder fixed	571
	Inner cylinder rotating at velocity V_i, Outer cylinder fixed	577
16.5.2.2	Poiseuille Flow in a Circular Duct	582
16.6	Laminar Boundary Layers	591
16.6.1	Flat-Plate Boundary Layer for a Power Law Fluid	593
16.6.2	Flat-Plate Boundary Layer for an Ideal Bingham Plastic	597
16.7	Conclusion	599
16.8	Governing Equations for Non-Newtonian Fluids	603
16.8.1	Stresses on a Non-Newtonian Fluid: Cartesian and Cylindrical Coordinates	603
16.8.2	Continuity and Momentum Differential Equations in Cartesian Coordinates ...	603
16.8.3	Continuity and Momentum Differential Equations in Cylindrical Coordinates ..	604
16.9	Table 1: Select properties of power law and ideal Bingham plastic fluids	605

16.1 Introduction

To this point, we have assumed that fluids are Newtonian, and deform linearly under an applied stress. Newtonian fluids are the most commonplace fluids, representing air and most other gasses, water, most oils, most liquid fuels, and mercury, to name a few. However, many other common materials qualify as fluids, but do not deform linearly under an applied stress. Some examples are many foodstuffs, such as peanut butter and ketchup, cosmetics such as nail polish and toothpaste, industrial materials such as freshly mixed cement and drilling mud, and biological materials like blood and mucus. Therefore, while we do not cover such non-Newtonian fluids in depth, it is appropriate that we examine some common types of non-Newtonian fluids, and understand how these behave differently than Newtonian fluids.

So, how do non-Newtonian fluids behave differently than Newtonian fluids? The key is how the shear stress is a function of the strain rate, $\dot{\epsilon}$:

$$\tau = f(\dot{\epsilon}) \quad (16.1)$$

We know that for a Newtonian fluid the shear stress changes linearly with the shear strain rate, $\dot{\epsilon}$, such that:

$$\tau = \mu(\dot{\epsilon}) \quad \left[\text{e.g., } \tau_{yx} = \mu \left(\frac{du}{dy} \right) \right],$$

where the coefficient relating shear stress and strain rate is the viscosity of the fluid, μ .

Thus, non-Newtonian fluids are those that demonstrate non-linear changes of shear stress with strain rate. Figure 16.1 shows a generic graph of several common types of non-Newtonian fluid behavior. Non-Newtonian fluids that deform continuously under an applied shear stress (the definition of a fluid, from Section 1.1), are generally categorized as either shear-thinning fluids, shear-thickening fluids, or viscoplastics.

16.1.1 Shear-Thinning Fluids (Pseudoplastics)

A shear-thinning fluid, often called a pseudoplastic fluid, will become less viscous with increasing shear stress. It turns out that many common materials display shear-thinning behavior. Two examples are peanut butter and paint. At room temperature, peanut butter is highly viscous at low shear rates. However, when one applies a high shear stress, as you do when spreading it on bread, the peanut butter flows, and can be distributed evenly (pretty much) over a piece of bread. However, once the shear is reduced, the peanut butter will recover to its more viscous nature, and will move very little, if at all. If we were to perform the same process with a Newtonian fluid, the fluid would continue to flow under very little stress (such as that applied by gravity), and flow off the bread. Note that if we were to heat the peanut butter, it would change

its characteristics. Although it would still behave as a shear thinning fluid, it would spread, and be less stable at much lower shear stresses. This explains why peanut butter sandwiches, when they are subjected to a hot environment (like leaving one in a car on a warm summer day), may result in peanut butter oozing out of the sandwich.

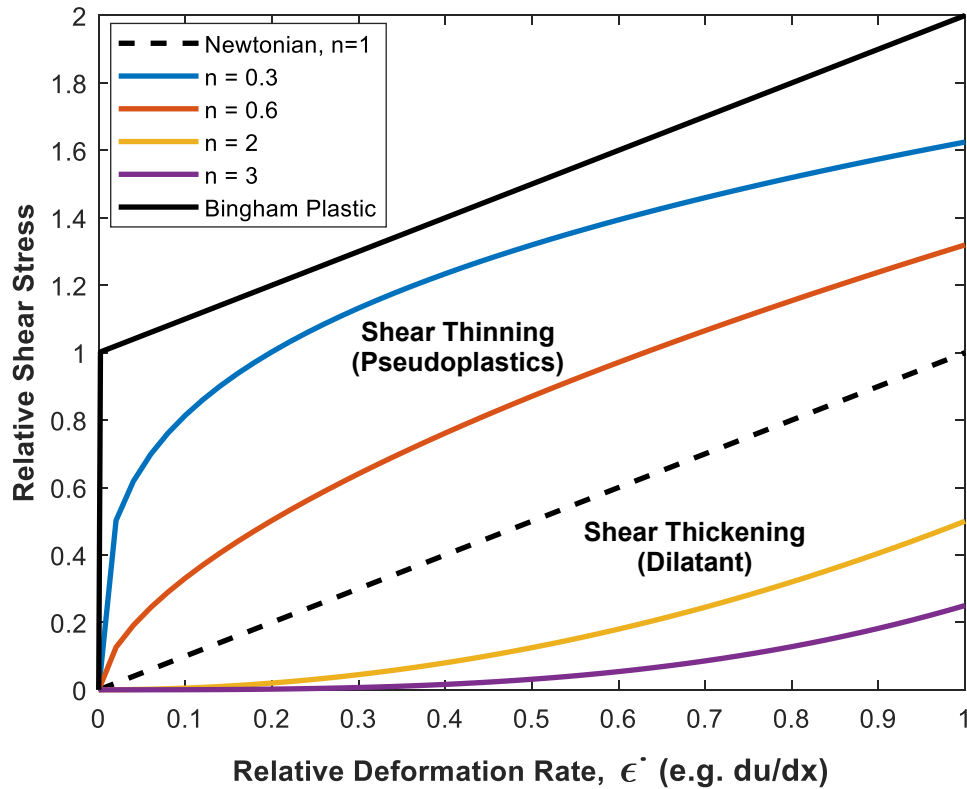


Figure 16.1 The generic behavior of power-law and Bingham plastic non-Newtonian fluids relative to Newtonian fluid behavior. The n values refer to the flow behavior index for an Ostwald-de Waele power-law model, Eq. 16.2.

Another example of a shear-thinning fluid is paint. Paint is very viscous when held within the bristles of a paintbrush. However, when we brush paint on a wall, the shear stress applied between the brush and the wall causes the paint to become less viscous, which allows it to spread evenly across the wall. Moreover, when that paintbrush shear stress is removed, the paint will return to its more viscous state. In this relaxed state, the thin paint layer will become more viscous, and behave more like a solid, maintaining an even layer on the wall while drying (however, if the paint layer is too thick, it may move under the effect of gravity, creating an undesirable irregular paint coating).

Did you ever have that age-old problem of getting ketchup out of a bottle? You open the bottle, and it just will not come out. So, you shake the bottle toward your food, and whoosh! Out comes the ketchup, often quite rapidly. That is because ketchup is a shear-thinning, pseudoplastic fluid.

It is very viscous under low stresses (when you try to pour it), but becomes less viscous (and flows more quickly) when you shake the bottle and apply a higher stress.

An interesting, and lethal, pseudoplastic is [quicksand](#). Quicksand is a suspension of loose sand saturated by water. The suspension will appear solid, but a sudden small (1 to 2%) change in pressure, or application of a shock, will cause the suspension to transform rapidly to a low viscosity fluid. If a human or animal walking on the quicksand causes the shock, they will start to sink. The good news is that due to the higher density of the quicksand, a human will only sink to about their waist. The bad news is that further agitation of the quicksand by rapid, struggling movements will further reduce the quicksand viscosity, causing one to sink further. The solution to escaping (if you are careless enough to step into quicksand) is to move your legs slowly, which causes the quicksand to remain more viscous, and slowly rotate your body to a face up floating position. Then you do a really, really slow backstroke to move your body over and out of the quicksand.

16.1.2 Shear-Thickening Fluids (Dilatants)

In contrast to shear-thinning fluids, shear-thickening fluids, many of which are termed dilatant fluids, become more viscous as the shear stress is increased (see this [link](#)). These types of fluids are generally suspensions of particulate matter in a surrounding liquid, and are less common than pseudoplastic fluids. Examples of such fluids are wet cement and synovial fluid. The explanation of why this thickening occurs with increased shear stress is speculative; it is presumed that when the fluid is at rest, or under low shear stress, the supporting liquid, which inhibits the suspended material from interacting strongly, lubricates the suspended material. However, when the dilatant material is under high shear stress, the suspension expands, reducing the liquid lubrication, and allows the suspended material to interact strongly, increasing the apparent viscous behavior. There are other speculations as to the physical reasons for shear thickening, but there is no definitive answer.

This shear thickening process within particulate suspensions, such as the cited wet cement, clearly explains our experience with these types of suspensions. For example, if one steps into wet cement, the material will allow you to move slowly, with low shear motions, to extract your foot. However, quick, high shear motions will make the material behave in a much more viscous manner, and you will have little chance of easily extracting your foot, most probably losing your shoe.

Synovial fluid, which is a suspension of biological material, is secreted by the cartilage protecting our body joints, and has a consistency like egg whites. It acts as a lubricant, becoming more viscous under strong shearing movements, such as those generated by running. This more viscous behavior acts to protect the higher loading on the joint surfaces. However, synovial fluid becomes less viscous when shear and movement are reduced, such as slow walking, where

joints are under lower loading. This lowered viscosity, of course, allows easier movement of the joint.

A truly interesting aspect of certain dilatant fluids is they will essentially solidify under a sharp impact. With certain fluids, (a highly concentrated mixture of cornstarch and water is one example), this rapid thickening allows a person to run or walk briskly across a pool of the mixture, without sinking in. However, if one just stands on the mixture, the viscous effect is diminished, and a person will slowly sink in, and have real trouble extracting themselves (see [this link](#) for a funny video example).

An unexpected practical application of shear-thickening fluids is in body armor (see this [link](#)). Tests have shown that filling Kevlar body armor with a small layer of certain shear-thickening fluids can increase the effectiveness of the armor to bullet impacts, while allowing the armor to remain relatively mobile under normal body motion. However, use of the fluid increases the weight of the armor, which may be a significant disadvantage.

16.1.3 Viscoplastics (Bingham plastic)

Fluids that do not continuously deform until a finite shearing stress is exceeded are termed a viscoplastic. These materials behave as a rigid body under low shear stresses, but flow as a fluid under high shear stresses. The fluid behavior of a viscoplastic, after reaching a minimum yield stress, can behave like either a Newtonian or a shear-thinning fluid. The simplest of these types of non-Newtonian materials is an ideal [Bingham plastic](#), named after [E. C. Bingham](#) who originally proposed the model. As shown in Figure 16.1, an ideal Bingham plastic will deform like a Newtonian fluid, after a critical yield stress is exceeded. Often these materials are composed of suspensions of particles or large molecules, which in a quiescent state interact with one another, creating a weak solid structure. However, under a critical level of applied stress the solid structure breaks down and begins to flow like a fluid. If the stress drops below the critical level, the particles/molecules reform as a weak solid. An interesting aspect of a Bingham plastic is that when it is at rest in an open container, its free surface will not even out like true fluids, but will retain peaks and valleys on the surface. For example, honey, a very viscous Newtonian fluid, will slowly relax to give a smooth free surface, but mayonnaise, a Bingham plastic, will not relax to a smooth free surface, regardless of the time allowed.

Examples of a Bingham plastic are drilling mud and toothpaste. [Drilling mud](#) is a suspension of special clays in either water or a petroleum fluid, generally resembling thick chocolate milk, or a milk shake. The mud is pumped through oil field drilling systems to lubricate and cool the drilling bit, and remove the drill cuttings. Under high pumping pressure, the fluid flows in a Newtonian-like, free-flowing fashion. However, reducing the pumping pressure below a certain level causes the mud material to transform into a “gel-like” structure, which resists flow. This solidification holds the drill cuttings in place until the flow is resumed. When the pressure is raised above a critical level, the mud will again start to flow as a fluid, carrying along the

suspended drill cuttings. However, the pressures required to cause the mud to flow are quite significant, as we will see later in Section 16.5.2.2.

You probably never paid much attention to toothpaste as a fluid, but it also behaves as a Bingham plastic. If you uncap a tube of toothpaste, the paste will remain in the tube, as a gel-like solid—even if you invert the tube with the opening facing downward. However, when you squeeze the tube, which raises the internal pressure and thus the shear stress at the wall of the outlet of the tube, the paste will flow out of the tube like a very viscous liquid; and when you stop squeezing, the tooth paste returns to a solid, or gel-like state.

16.2 Power-Law and Bingham Plastic Fluid Models

Many mathematical models have been developed to describe (or attempt to describe) non-Newtonian fluid behavior. A study of these models, and their various fluid behaviors, occupies thousands of technical papers, and numerous books on the topic (see for example, [Bird, Stewart, and Lightfoot, 2002](#), [Bird, Armstrong, and Hassager, 1987](#), and [Chhabra and Richardson, 1999](#)). However, to give you some understanding of how non-Newtonian fluids differ from Newtonian fluids, we will examine only two of these models: a simple power-law model of [Ostwald and de Waele](#), (which models both pseudoplastic and dilatant fluids) and the viscoelastic ideal [Bingham plastic](#) model. Both of these models are approximations of actual fluid behavior, but allow us to examine the generic behavior of a broad range of non-Newtonian type fluids.

Both of these models are based on curve fits of empirical data, and were hypothesized by their namesakes as reasonable curve fits of observed and measured fluid behavior. And both models recognize that, like a Newtonian fluid (Eq. 16.1), the fluid shear stress is a function of the shear strain rate, $\dot{\epsilon}$, where again $\tau = f(\dot{\epsilon})$.

16.2.1 Ostwald-de Waele Power Law

Whereas the shear stress for a Newtonian fluid is given by:

$$\tau = \mu(\dot{\epsilon}) \quad \left[\text{e.g.} \quad \tau_{yx} = \mu \left(\frac{du}{dy} \right) \right],$$

the equation for an [Ostwald-de Waele power-law fluid](#) is a variation on Newton's law, and given by:

$$\tau = K(\dot{\epsilon})^n \tag{16.2}$$

Here K is termed the flow consistency index (with SI units of Pa s^n), which is similar to (but not identical to) viscosity, and n is termed the flow behavior index ($n > 0$). Values of K and n for a range of pseudoplastic and dilatant fluids are shown at the end of this chapter in [Table 16.1](#).

Note in Figure 16.1 that fluids with flow behavior indices in the range $0 < n < 1$ are considered pseudoplastic fluids (shear thinning); the closer the value of n is to 0, the more the fluid behaves plastically. For values of $n < 0.5$, the shape of the curve will start to approximate the behavior of a Bingham plastic, with such fluids often modeled reasonably well as either a power-law or Bingham plastic fluid.

Figure 16.1 also shows that fluids with $n > 1$ are dilatant fluids (shear thickening). Such fluids are less common and often only display thickening effects over only a certain range of shear rates. Most shear-thickening fluids are suspensions, and generally don't display consistent behavior over their entire shear stress range, often displaying pseudoplastic behavior at low shear rates, transitioning to dilatant behavior at higher shear rates.

While it is a nice model for a number of non-Newtonian fluids, there are a couple of issues with the Ostwald-de Waele power law equation of Eq. 16.2. First, since the flow behavior index, n , is generally a fractional number, the equation only works for positive shear rates, since we cannot take a fractional power of a negative value. This is often circumvented by assuming absolute values of strain rate. However, for the examples shown in this chapter, coordinates and limits of integration are used that will yield positive shear rates.

Secondly, the flow consistency index K for specific fluids has units that depend upon the value of n , to yield a shear stress that is in force per area. As we point out above, the units of K will be SI units of Pa s^n . Thus, the time units are unique to the respective value of n for a specific fluid. This is quite awkward, and makes effective comparisons of one fluid to another difficult, as we will see.

Finally, if we define a relative shear viscosity for an Ostwald-de Waele fluid, we have:

$$\tau = K(\dot{\epsilon})^n = \mu_{\text{app}}\dot{\epsilon} \quad \Rightarrow \quad \mu_{\text{app}} = K(\dot{\epsilon})^{n-1},$$

where μ_{app} is the apparent viscosity of a fluid. For pseudoplastic fluids ($n < 1$), this apparent viscosity will become infinite as the shear rate approaches zero, which cannot physically happen. Other fluid models address this inconsistency, but generate expressions that are more complicated.

Despite the limitations, the Ostwald-de Waele model does a nice job of approximating the characteristics of fluids that are both shear thinning ($n < 1$) and shear thickening ($n > 1$).

16.2.2 Ideal Bingham Plastic

The equation for an ideal Bingham plastic fluid is a two-region model, and is referenced to the strain rate as:

$$\dot{\epsilon} = 0 \quad \text{when } \tau < \tau_0 \quad \text{and} \quad \tau = \tau_0 + \mu_B(\dot{\epsilon}) \quad \text{when } \tau > \tau_0 \quad (16.3)$$

Here τ_0 is termed the yield stress, and μ_b is the apparent viscosity once the material starts to flow as a fluid. In regions where $\tau < \tau_0$, the material will not deform ($\dot{\epsilon} = 0$), and simply remain static, or move in uniform motion as a solid. Values of τ_0 and μ_b are also listed in [Table 16.1](#) for a number of ideal Bingham Plastic materials.

Notice that this section is titled “Ideal Bingham Plastic.” As shown in Figure 16.1, an ideal Bingham Plastic deforms linearly, like a Newtonian fluid, after reaching the critical yield stress. In reality, Bingham fluids more often behave as pseudoplastics after reaching the yield stress. However, to make our subsequent example calculations easier, we will use the ideal plastic case.

I must note that the properties listed in Table 1 come from a wide variety of sources, and may vary widely, depending on the constituency of the material, which is often vague. For example, there are several listings for the properties of mayonnaise, which vary quite broadly, as do the listings for latex paint, the constituents of which may or may not be listed. In addition, if you solve problem 22 at the end of this text, you will note a significant difference in the calculated properties depending on whether you use the listed power-law properties or the ideal Bingham plastic properties, which are from different sources and clearly different test materials, although both are listed as the same material (25% solids tomato paste). Also, note that the cited properties are often shear dependent (i.e. they may vary with the shear value of the material). Therefore, Table 1 should be taken as exemplary, but not definitive.

16.3 Simple Non-Newtonian Flows: Couette and Poiseuille

In Sections 16.4 and 16.5, we first examine the behavior of power-law and Bingham plastic fluids in two simple flow situations that we examined previously in Chapter 6 for Newtonian fluids: Couette and Poiseuille flows. Recall that these Newtonian flows were the simplest types of flows that we modeled, and resulted in relatively simple equations modeling the respective flow behaviors. Moreover, once the controlling parameters were specified (e.g. pressure gradients, pipe diameters, viscosity, etc.), the non-dimensional flow behavior was identical for any set of parameters (e.g. the velocity profile for a Newtonian Poiseuille flow always has a parabolic shape). However, as we will discover in this chapter, flows of non-Newtonian fluids can undergo quite different flow behaviors, depending on the magnitude of the controlling parameters and the type of non-Newtonian behavior.

We will consider Couette and Poiseuille flows first in Cartesian coordinates for flows between parallel plates, then in cylindrical coordinates for flows between rotating, concentric cylinders and flows along circular ducts. We will only consider fully-developed flows, which will simplify the analysis and reduce all flows to one-dimensional flows. However, to deal with non-Newtonian flows we will have to step back from the conventional Navier-Stokes momentum equations, and consider the momentum equations in terms of stress terms, rather than the previous rate deformation equations shown in Section 5.8. The governing momentum equations

in terms of stress terms are listed at the end of the chapter in [section 16.8](#), for both Cartesian and cylindrical coordinates. Which directional equation is used to assess a particular flow depends on the geometry and the direction of motion, as we will show in the following sections.

16.4 Power Law Fluid Solutions

The Ostwald-de Waele model was indicated in Eq. 16.2 as $\tau = K(\dot{\epsilon})^n$, where $\dot{\epsilon}$ is the deformation rate. However, the relationship of $\dot{\epsilon}$ to the fluid behavior will vary depending on the geometry and coordinates considered, and the flow orientation of interest. The three model variations we will use here are:

Non-Newtonian, Cartesian:

$$\text{x-direction only: } \tau_{yx} = \mu_{\text{app}} \dot{\epsilon}_{yx} = \mu_{\text{app}} \left(\frac{\partial u}{\partial y} \right) = K \left(\frac{\partial u}{\partial y} \right)^n, \text{ and } \mu_{\text{app}} = K \left(\frac{\partial u}{\partial y} \right)^{n-1} \quad (16.4)$$

Non-Newtonian, Cylindrical

$$\begin{aligned} \theta \text{ direction only: } \tau_{r\theta} &= \mu_{\text{app}} \dot{\epsilon}_{r\theta} = \mu_{\text{app}} r \frac{\partial}{\partial r} \left(\frac{v_\theta}{r} \right) = K \left[r \frac{\partial}{\partial r} \left(\frac{v_\theta}{r} \right) \right]^n \\ \text{where } \mu_{\text{app}} &= K \left[r \frac{\partial}{\partial r} \left(\frac{v_\theta}{r} \right) \right]^{n-1} \end{aligned} \quad (16.5)$$

$$\begin{aligned} \text{z-direction only: } \tau_{rz} &= \mu_{\text{app}} \dot{\epsilon}_{rz} = \mu_{\text{app}} \left(\frac{\partial v_z}{\partial r} \right) = K \left(\frac{\partial v_z}{\partial r} \right)^n \\ \text{where } \mu_{\text{app}} &= K \left(\frac{\partial v_z}{\partial r} \right)^{n-1} \end{aligned} \quad (16.6)$$

In the above equations, μ_{app} is the apparent viscosity relative to the linear deformation rate $\dot{\epsilon}$.

16.4.1 Parallel Plate Flows

For fully-developed Couette and Poiseuille flows between infinite parallel flat plates, there is no motion in the lateral directions, but only in the streamwise, x-direction. The governing equations reduce to the x-direction momentum equation (Eq. 16.122b)

$$\frac{\partial u}{\partial t} + u \frac{\partial u}{\partial x} + v \frac{\partial u}{\partial y} + w \frac{\partial u}{\partial z} = -\frac{1}{\rho} \frac{\partial p}{\partial x} + g_x + \frac{1}{\rho} \left[\frac{\partial \sigma_{xx}}{\partial x} + \frac{\partial \tau_{yx}}{\partial y} + \frac{\partial \tau_{zx}}{\partial z} \right] \quad (16.7)$$

Simplifying Eq.16.7 for steady, fully-developed flow in the x-direction only, we get:

$$-\frac{\partial p}{\partial x} + \frac{d\tau_{yx}}{dy} = 0 \quad \text{where } \tau_{yx} = K \left(\frac{\partial u}{\partial y} \right)^n$$

Thus, for power-law flows between parallel plates, the governing equation is:

$$\frac{d}{dy} \left[K \left(\frac{du}{dy} \right)^n \right] = \frac{\partial p}{\partial x} \quad (16.8)$$

Equation 16.8 applies for both a Couette flow $\left(\frac{\partial p}{\partial x} = 0 \right)$, and a Poiseuille flow $\left(\frac{\partial p}{\partial x} = \text{constant} \right)$.

The velocity behavior for these flows is derived in the following Sections 16.4.1.1 and 16.4.1.2 respectively.

16.4.1.1 Couette Flow between Parallel Plates

Using the coordinate system in figure 16.2, we have boundary conditions of $u = 0$ at $y = 0$, and $u = U$ at $y = h$, where we consider a moving upper plate and a fixed lower plate.

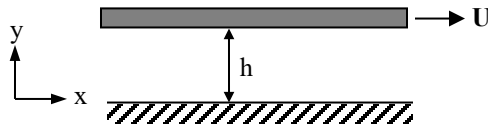


Figure 16.2 Couette flow between a lower stationary plate and an upper moving plate.

Since there is no pressure gradient for a Couette flow (see the detailed discussion of this in section 6.3.1), Eq. 16.8 reduces to:

$$\frac{d}{dy} \left[K \left(\frac{du}{dy} \right)^n \right] = 0 \quad (16.9)$$

Integrating Eq. 16.9 once we have:

$$\frac{du}{dy} = \left(\frac{C_1}{K} \right)^{\frac{1}{n}}$$

Integrating again:

$$u = \left(\frac{C_1}{K} \right)^{\frac{1}{n}} y + C_2$$

Applying the boundary condition $u = 0$ at $y = 0$, gives:

$$0 = \left(\frac{C_1}{K}\right)^{\frac{1}{n}}(0) + C_2 \Rightarrow C_2 = 0$$

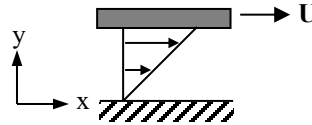
$$u = \left(\frac{C_1}{K}\right)^{\frac{1}{n}} y$$

And applying the second boundary condition $u = U$ at $y = h$:

$$U = \left(\frac{C_1}{K}\right)^{\frac{1}{n}} h \Rightarrow C_1 = K \left(\frac{U}{h}\right)^n$$

Thus,

$$u = \left(\frac{C_1}{K}\right)^{\frac{1}{n}} y = \left[\frac{K \left(\frac{U}{h}\right)^n}{K} \right]^{\frac{1}{n}} y = \frac{Uy}{h} \quad (16.10)$$



Equation 16.10 is the same result we determined for a Newtonian fluid in Section 6.3.1, Eq. 6.8, despite the non-linear relationship of shear stress to deformation rate for a power-law fluid. To examine this non-intuitive result, consider the shear stress distribution.

The shear stress is given by Eq. 16.4 as:

$$\tau_{yx} = K \left(\frac{du}{dy} \right)^n$$

Differentiating Eq. 16.10, gives: $\frac{du}{dy} = \frac{U}{h}$.

Thus,

$$\tau_{yx} = K \left(\frac{U}{h} \right)^n = \text{constant} \quad (16.11)$$

So, for a given plate gap, h , and plate velocity, U , the shear stress, Eq. 16.11, is constant across the gap (the same as for a Newtonian fluid). Since the shear stress is constant, the deformation rate, $\dot{\epsilon}$, will also be constant, and thus the velocity profile must be linear. However, note that the shear stress does not change linearly with variations in the plate velocity or the gap width, as it does for a Newtonian fluid.

It would be nice if all our other examples were so straightforward. However, as you will see in Section 16.4.2.1, Couette flow between rotating, concentric cylinders can get quite messy.

16.4.1.2 Poiseuille Flow between Parallel Plates

It might first seem that we should treat this solution the same way we did a Newtonian flow in Section 6.3.2, where we located the origin on the lower plate. However, since the integration process here deals with values of n that are generally non-integer, this creates problems with the integration process, and in developing velocity equations that can be displayed effectively. Since the flow will be symmetric about the midplane between the plates, it is the most effective to locate the coordinate system with the origin on the midplane between the two plates, as shown in figure 16.3. This allows the assessment of the flow in the upper half of the gap, recognizing that the flow in the lower half of the gap will be a mirror reflection. Using this coordinate system, the boundary conditions for the upper half of the flow are $\frac{\partial u}{\partial y} = 0$ at $y = 0$ (assuming

flow symmetry), and $u = 0$ at $y = \frac{h}{2}$.

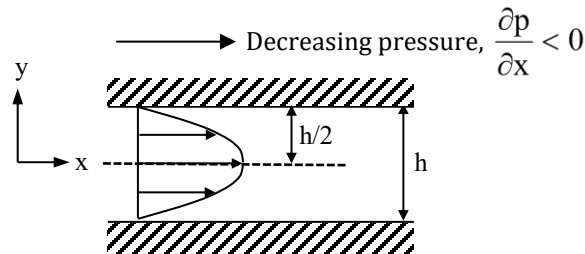


Figure 16.3 Poiseuille flow between parallel flat plates, power-law fluid.

For a Poiseuille flow, $\frac{\partial p}{\partial x} = \text{constant}$ (as was shown in section 6.3.2), and the governing equation from section 16.4.1 is Eq. 16.8

$$\frac{d}{dy} \left[K \left(\frac{du}{dy} \right)^n \right] = \frac{\partial p}{\partial x} = \text{constant},$$

with boundary conditions $u = 0$ at $y = \frac{h}{2}$, and $\frac{du}{dy} = 0$ at $y = 0$.

Integrating once gives:

$$K \left(\frac{du}{dy} \right)^n = \frac{\partial p}{\partial x} y + C_1$$

Applying boundary condition $\frac{du}{dy} = 0$ at $y = 0$:

$$0 = \frac{\partial p}{\partial x} (0) + C_1 \Rightarrow C_1 = 0$$

Thus,

$$K \left(\frac{du}{dy} \right)^n = \frac{\partial p}{\partial x} y$$

or

$$\frac{du}{dy} = \left(\frac{1}{K} \frac{\partial p}{\partial x} y \right)^{\frac{1}{n}}$$

Integrating gives:

$$u = \left(\frac{n}{n+1} \right) \left(\frac{1}{K} \frac{\partial p}{\partial x} \right)^{\frac{1}{n}} y^{\frac{n+1}{n}} + C_2$$

Applying the second boundary condition, $u = 0$ at $y = \frac{h}{2}$.

$$u = \left(\frac{n}{n+1} \right) \left(\frac{1}{K} \frac{\partial p}{\partial x} \right)^{\frac{1}{n}} \left(\frac{h}{2} \right)^{\frac{n+1}{n}} + C_2 = 0 \Rightarrow C_2 = - \left(\frac{n}{n+1} \right) \left(\frac{1}{2K} \frac{\partial p}{\partial x} \right)^{\frac{1}{n}} \left(\frac{h}{2} \right)^{\frac{n+1}{n}}$$

Thus,

$$u = \left(\frac{n}{n+1} \right) \left(\frac{h}{2K} \frac{\partial p}{\partial x} \right)^{\frac{1}{n}} \left(\frac{h}{2} \right) \left[\left(\frac{2y}{h} \right)^{\frac{n+1}{n}} - 1 \right]$$

Defining $y^* = \frac{2y}{h}$, and designating $u_n = u(n)$, since the u velocity profile will be a function of n , we have:

$$u_n = \left(\frac{n}{n+1} \right) \left(\frac{h}{2K} \frac{\partial p}{\partial x} \right)^{\frac{1}{n}} \left(\frac{h}{2} \right) \left[(y^*)^{\frac{n+1}{n}} - 1 \right] \quad (16.12)$$

At $y^* = 0 \Rightarrow u_n = u_{n,\max} = u_{n,CL}$, so from Eq. 16.12 we have:

$$u_{n,CL} = - \left(\frac{n}{n+1} \right) \left(\frac{h}{2K} \frac{\partial p}{\partial x} \right)^{\frac{1}{n}} \left(\frac{h}{2} \right) \quad (16.13)$$

Note in Eqs. 16.12 and 16.13, that the pressure gradient, $\frac{\partial p}{\partial x}$, must be positive to allow

calculation to the power of $\frac{1}{n}$, which makes u_n and $u_{n,CL}$ negative velocities (like a Newtonian fluid, a positive pressure gradient yields a negative velocity). However, we can deal with positive behavior by defining $u_n^* = \frac{u_n}{u_{n,CL}}$. Thus, dividing Eq. 16.12 by 16.13 gives:

$$u_n^* = \frac{u_n}{u_{n,CL}} = 1 - (y^*)^{\frac{n+1}{n}} \quad (16.14)$$

Equation 16.14 gives the non-dimensional velocity variation relative to the maximum centerline velocity as a function of n , the flow behavior index. A graph of Eq. 16.14 is shown for a series of n values in figure 16.4(a).

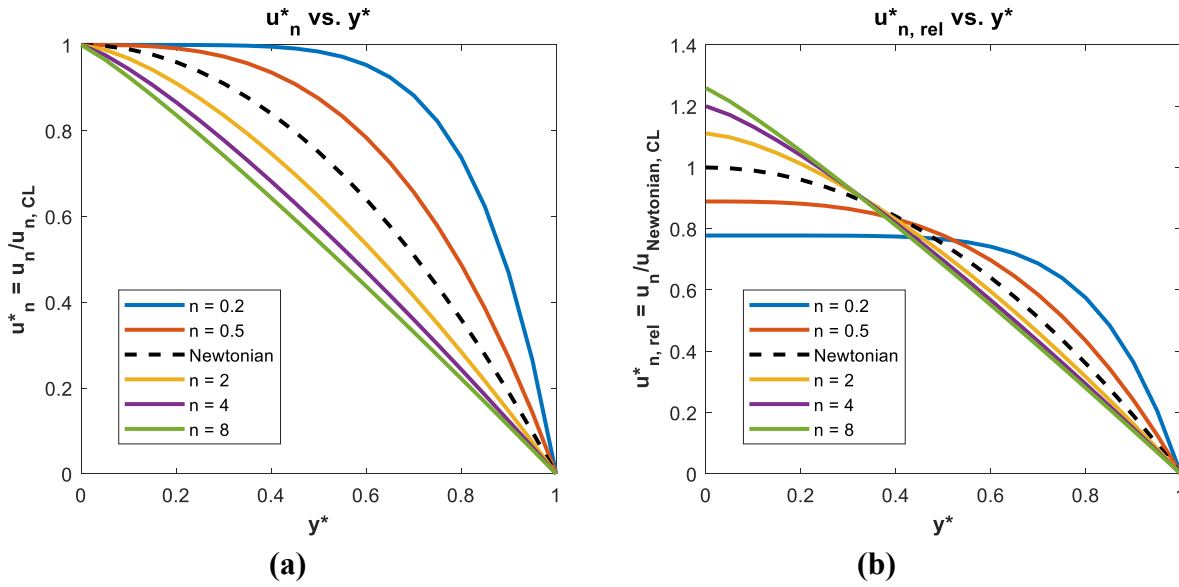


Figure 16.4 Power law velocity profiles for Poiseuille flow between parallel flat plates.
 (a) Normalized on the centerline velocity of each respective n value fluid;
 (b) Normalized on Newtonian centerline velocity; constant volume flowrate.

A limitation of Eq. 16.14 is that it does not allow a comparison of the relative velocity behavior of a power law fluid to that of a Newtonian fluid, since the K and n values will not be consistent. However, there is a way to do this for flows at equal volume flow rates.

We calculate the volume flowrate per unit depth, Q , in the upper half of the gap by integrating the velocity from $y = 0$ to $y = \frac{h}{2}$ (note that the total flowrate between plates would be twice Q):

$$Q = \int_0^{\frac{h}{2}} u_n dy = \int_0^{y^*=1} u_{n,CL} u_n^* \frac{h}{2} dy^* = u_{n,CL} \frac{h}{2} \int_0^{y^*=1} \left(1 - (y^*)^{\frac{n+1}{n}}\right) dy^*$$

$$Q = u_{n,CL} \frac{h}{2} \left(1 - \left(\frac{n}{2n+1}\right)\right) = u_{n,CL} \frac{h}{2} \left(\frac{n+1}{2n+1}\right)$$

Substituting for u_{CL} from Eq. 16.13

$$Q = -\left(\frac{n}{2n+1}\right) \left(\frac{h}{2K} \frac{\partial p}{\partial x}\right)^{\frac{1}{n}} \frac{h^2}{4} \tag{16.15}$$

Notice that the parameter $\left(\frac{h}{2K} \frac{\partial p}{\partial x}\right)^{\frac{1}{n}} \frac{h}{2}$ in Eq. 16.15 is also common to the same parameter in the velocity equation, Eq. 16.12. Solving for this parameter from Eq. 16.15 gives:

$$\left(\frac{h}{2K} \frac{\partial p}{\partial x}\right)^{\frac{1}{n}} \frac{h}{2} = \frac{-Q}{\frac{h}{2} \left(\frac{n}{2n+1}\right)} \quad (16.16)$$

Substituting Eq. 16.16 into Eq. 16.12, we have:

$$u_n = \frac{2Q}{h} \left(\frac{2n+1}{n+1}\right) \left[1 - (y^*)^{\frac{n+1}{n}}\right] \quad (16.17)$$

Using Eq. 16.17, we can now do a comparison of the velocity behavior for both pseudoplastic ($n < 1$) and dilatant ($n > 1$) fluids to a Newtonian fluid ($n = 1$) at the same volume flowrates.

Note that for Newtonian flows, $n = 1$:

$$u_{\text{Newt}} = \frac{3Q}{h} \left[1 - (y^*)^2\right],$$

with the maximum Newtonian velocity at the centerline, $y^* = 0$:

$$u_{\text{Newt, CL}} = \frac{3Q}{h} \quad (16.18)$$

Dividing Eq. 16.17 by Eq. 16.18, we calculate $u_{n,\text{rel}}^* = \frac{u_n}{u_{\text{Newt, CL}}}$, the comparative velocity profiles, for the same flowrate, Q, through a channel of width h as:

$$u_{n,\text{rel}}^* = \frac{u_n}{u_{\text{Newt, CL}}} = \frac{2}{3} \left(\frac{2n+1}{n+1}\right) \left[1 - (y^*)^{\frac{n+1}{n}}\right] \quad (16.19)$$

Figure 16.4(b) shows comparative velocity profiles, $u_{n,\text{rel}}^*$, Eq. 16.19, for a series of n values.

Figure 16.4 illustrates the comparative effect of the fluid behavior index, n , on the velocity behavior relative to a Newtonian fluid ($n = 1$). Note in figure 16.4(a) that shear-thinning pseudoplastics ($n < 1$) have flatter profiles, while shear-thickening dilatants ($n > 1$) have a more peaked profile. Figure 16.4(b), for equivalent flowrates, Q , shows that the centerline velocities for pseudoplastics will be less than Newtonian, and dilatants in excess of Newtonian. What is of real interest for pseudoplastics is that for smaller n values ($n \approx 0.5$ or less) the behavior is similar to that of a Bingham plastic, which we consider in Section 16.5.2.2, and discuss in detail in Section 16.6.

What we can't show is the general effect a power law fluid has on the pressure gradient. We might consider a relationship derived from Eq. 16.16. Solving Eq. 16.16 for the pressure gradient in terms of Q and other parameters, we have:

$$\frac{\partial p}{\partial x} = \frac{2K}{h} \left[\frac{-2Q}{h^2 \left(\frac{n}{2n+1} \right)} \right]^n \quad (16.20)$$

As Eq. 16.20 shows, if Q is assumed positive, we can't determine a value of $\frac{\partial p}{\partial x}$. However, if we assume Q is negative (i.e. flowing right to left in figure 16.3), or just assume a positive value of the numerator, a positive value of $\frac{\partial p}{\partial x}$ can be determined. However, since the K values of power-law fluids have differing units (depending on n), the only way to determine relative pressure gradients is to calculate them individually for specific fluid properties.

16.4.2 Flows with Circular Symmetry

In this section, we address Couette flow and Poiseuille flow of a power-law fluid in geometries of radial symmetry. Again, these flows will reduce to one-dimensional, fully-developed flows with no lateral cross flow. However, although each of these flows is a function of radius only, the governing momentum equation, and consequent velocity, for each of these two flows will be different. The Couette flow will depend on the azimuthal (θ) direction equation and yield $v_\theta = f(r)$, whereas the Poiseuille flow will depend on the axial (z) direction equation and yield $v_z = f(r)$. They will also depend on different constitutive equations for the shear stress, as was indicated in Section 16.4.

16.4.2.1 Couette Flow between Concentric, Rotating Cylinders

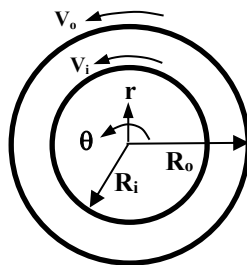


Figure 16.5 Geometry for Couette flow between concentric rotating cylinders

As shown in Section 6.4.2, the governing equation for this type of cylindrical flow reduces to the θ -direction momentum equation, 16.123c of [Section 16.7.3](#).

$$\begin{aligned} \frac{\partial v_\theta}{\partial t} + v_r \frac{\partial v_\theta}{\partial r} + \frac{v_\theta}{r} \frac{\partial v_\theta}{\partial \theta} + v_z \frac{\partial v_\theta}{\partial z} + \frac{v_r v_\theta}{r} \\ = -\frac{1}{\rho r} \frac{\partial p}{\partial \theta} + g_\theta + \frac{1}{\rho} \left[\frac{1}{r^2} \frac{\partial}{\partial r} (r^2 \tau_{r\theta}) + \frac{1}{r} \frac{\partial \sigma_{\theta\theta}}{\partial \theta} + \frac{\partial \tau_{z\theta}}{\partial z} - \frac{\tau_{\theta r} - \tau_{r\theta}}{r} \right] \end{aligned} \quad (16.123c)$$

Since this is a steady, fully-developed flow, the velocity field is given by $v_\theta = f(r)$, and Eq. 16.123c reduces to:

$$0 = -\frac{\partial p}{\partial \theta} + \frac{1}{r} \frac{d}{dr} (r^2 \tau_{r\theta}), \quad (16.21)$$

where the power-law shear stress is given by Eq. 16.5:

$$\tau_{r\theta} = K \left[r \frac{d}{dr} \left(\frac{v_\theta}{r} \right) \right]^n$$

We showed in section 6.3.1 that $\frac{\partial p}{\partial \theta} = 0$ for Couette flows, so Eq. 16.21 reduces to:

$$\frac{d}{dr} (r^2 \tau_{r\theta}) = 0$$

Integrating and substituting from Eq. 16.5 for the shear stress:

$$\tau_{r\theta} = K \left[r \frac{d}{dr} \left(\frac{v_\theta}{r} \right) \right]^n = \frac{C_1}{r^2}$$

or

$$\frac{d}{dr} \left(\frac{v_\theta}{r} \right) = \frac{1}{r} \left(\frac{C_1}{Kr^2} \right)^{\frac{1}{n}} = \frac{1}{r} \left(\frac{\alpha}{r^2} \right)^{\frac{1}{n}} = \frac{\alpha^{\frac{1}{n}}}{r^{\frac{2}{n}+1}} \quad \text{where } \alpha = \frac{C_1}{K}$$

Integrating again:

$$v_\theta = -\alpha^{\frac{1}{n}} \frac{n}{2r^{\frac{2}{n}-1}} + C_2 r \quad (16.22)$$

Equation 16.22 is a general solution, requiring boundary conditions at R_o and R_i to solve for the integration constants α and C_2 . In Section 6.4.2 we performed a general solution given independent rotations of both cylinders. However, in this case the mathematical manipulation would be quite messy, so here we will examine two simpler cases:

- (a) Rotation of the outer cylinder with the inner cylinder stationary, and
- (b) Rotation of the inner cylinder with the outer cylinder stationary.

Boundary Conditions (a): Outer cylinder rotating at velocity V_o , Inner cylinder fixed

Here the boundary conditions are:

$$(1) v_\theta = V_o \text{ at } r = R_o, \quad \text{and} \quad (2) v_\theta = 0 \text{ at } r = R_i$$

Applying boundary condition $v_\theta = V_o$ at $r = R_o$ to Eq. 16.22 gives:

$$V_o = -\alpha^n \frac{n}{2R_o^{\frac{n-1}{2}}} + C_2 R_o \quad (16.23)$$

Applying boundary condition $v_\theta = 0$ at $r = R_i$ to Eq. 16.22:

$$0 = -\alpha^n \frac{n}{2R_i^{\frac{n-1}{2}}} + C_2 R_i \Rightarrow C_2 = \alpha^n \frac{n}{2R_i^{\frac{n}{2}}}$$

Substituting for C_2 in Eq. 16.23 yields:

$$V_o = -\left(\frac{n\alpha^n}{2}\right) R_o \left(\frac{1}{R_o^{\frac{n}{2}}} - \frac{1}{R_i^{\frac{n}{2}}}\right) \Rightarrow \left(\frac{n\alpha^n}{2}\right) = -\frac{V_o}{R_o \left(\frac{1}{R_o^{\frac{n}{2}}} - \frac{1}{R_i^{\frac{n}{2}}}\right)}$$

Substituting C_2 , and $\left(\frac{n\alpha^n}{2}\right)$ back into Eq. 16.22, and simplifying gives

$$v_\theta = \frac{V_o}{R_o \left(\frac{1}{R_o^{\frac{n}{2}}} - \frac{1}{R_i^{\frac{n}{2}}}\right)} \left(\frac{1}{r^{\frac{n-1}{2}}} - \frac{r}{R_i^{\frac{n}{2}}}\right) = \frac{V_o r}{\frac{R_o^{\frac{n}{2}}}{R_o} \left(1 - \left(\frac{R_o}{R_i}\right)^{\frac{n}{2}}\right)} \left(\frac{1}{r^{\frac{n}{2}}} - \frac{1}{R_i^{\frac{n}{2}}}\right)$$

$$v_\theta = \frac{V_o \left(\frac{r}{R_o}\right)}{\left(1 - \left(\frac{R_o}{R_i}\right)^{\frac{n}{2}}\right)} \left(\frac{R_o^{\frac{n}{2}}}{r^{\frac{n}{2}}} - \frac{R_o^{\frac{n}{2}}}{R_i^{\frac{n}{2}}}\right) \quad (16.24)$$

Defining $r^* = \frac{r}{R_o}$ and $r_i^* = \frac{R_i}{R_o}$, and substituting into Eq. 16.24 we get:

$$v_{\theta} = \frac{V_o(r^*)}{\left(1 - \left(\frac{1}{r_i^*}\right)^{\frac{2}{n}}\right)} \left(\frac{1}{(r^*)^{\frac{2}{n}}} - \frac{1}{(r_i^*)^{\frac{2}{n}}} \right) = \frac{V_o}{\left(\left(r_i^*\right)^{\frac{2}{n}} - 1\right)} \left(\frac{(r_i^*)^{\frac{2}{n}} - (r^*)^{\frac{2}{n}}}{(r^*)^{\frac{2-n}{n}}} \right)$$

Rearranging terms gives:

$$v_{\theta} = V_o \left(\frac{1 - \left(\frac{r_i^*}{r^*}\right)^{\frac{2}{n}}}{1 - (r_i^*)^{\frac{2}{n}}} \right) r^*$$

Defining a non-dimensional velocity as $v_{\theta}^* = \frac{v_{\theta}}{V_o}$, our final expression is:

$$v_{\theta}^* = \frac{v_{\theta}}{V_o} = \left(\frac{1 - \left(\frac{r_i^*}{r^*}\right)^{\frac{2}{n}}}{1 - (r_i^*)^{\frac{2}{n}}} \right) r^* \quad (16.25)$$

An alternative way of writing Eq. 16.25, which is often cited, is to let $R_i = aR_o$ where

$r_i^* = \frac{R_i}{R_o} = a < 1$, and $r_o^* = 1$ then

$$v_{\theta}^* = r^* \left(\frac{1 - \left(\frac{a}{r^*}\right)^{\frac{2}{n}}}{1 - a^{\frac{2}{n}}} \right) \quad 16.26$$

Note that Eq. 16.5 gives the shear stress as (after a little work):

$$\tau_{r\theta} = K \left[r \frac{\partial}{\partial r} \left(\frac{v_{\theta}}{r} \right) \right]^n = K \left[\frac{\frac{2V_o}{nR_o}}{\left(1 - a^{\frac{2}{n}}\right)} \right]^n \left(\frac{a}{r^*} \right)^2 \quad (16.27)$$

Using Eq. 16.27, we calculate the torque on any surface between $r_i^* = a$ and $r_o^* = 1$ as:

$$T = \tau_{r\theta} (2\pi Lr)(r) = \tau_{r\theta} (2\pi LR_o^2 r^{*2}) \quad \text{where } L \text{ is the length of the cylinders}$$

$$T = 2\pi R_o^2 a^2 L K \left[\frac{\frac{2V_o}{nR_o}}{\left(1 - a^{\frac{2}{n}}\right)} \right]^n \quad (16.28)$$

Eq. 16.28 indicates that for a given V_o , R_o , and a , the torque for a given power law fluid is constant across the circular gap, and is not a function of the radius. Physically, this is as it should be since if the torque varied, there would be an acceleration of fluid layers relative to one another, which would violate the premise of a steady-state flow. Note that constant torque across a Couette flow between concentric cylinders will hold true regardless of the type of fluid within the cylinders. This constancy of torque will prove very helpful in Section 16.5.2.1 where we derive the behavior of a Couette flow for a Bingham plastic fluid.

Boundary Conditions (b): Inner cylinder rotating at velocity V_i , Outer cylinder fixed

Here the boundary conditions are reversed, with:

$$(1) v_\theta = 0 \text{ at } r = R_o \quad \text{and} \quad (2) v_\theta = V_i \text{ at } r = R_i$$

The integrated equation is again Eq. 16.22:

$$v_\theta = -\alpha^{\frac{1}{n}} \frac{n}{2r^{\frac{2-n}{n}}} + C_2 r, \quad \text{where } \alpha = \frac{C_1}{K}$$

Boundary condition $v_\theta = 0$ at $r = R_o$ gives:

$$0 = -\alpha^{\frac{1}{n}} \frac{n}{2R_o^{\frac{2-n}{n}}} + C_2 R_o \Rightarrow C_2 = \alpha^{\frac{1}{n}} \frac{n}{2R_o^{\frac{2}{n}}}$$

And boundary condition $v_\theta = V_i$ at $r = R_i$ gives:

$$V_i = -\alpha^{\frac{1}{n}} \frac{n}{2R_i^{\frac{2-n}{n}}} + C_2 R_i \quad (16.29)$$

Substituting C_2 into Eq. 16.29 and rearranging gives:

$$\left(\frac{n\alpha^{\frac{1}{n}}}{2} \right) = - \frac{V_i}{R_i \left(\frac{1}{R_i^{\frac{2}{n}}} - \frac{1}{R_o^{\frac{2}{n}}} \right)}$$

Substituting into Eq. 16.22 for C_2 and $\left(\frac{n\alpha^n}{2}\right)$, and simplifying gives:

$$v_\theta = \frac{V_i \left(\frac{r}{R_o}\right)}{\left(\frac{R_i}{R_o}\right) \left(\left(\frac{R_o}{R_i}\right)^{\frac{2}{n}} - 1\right)} \left(\frac{R_o^{\frac{2}{n}}}{r^n} - \frac{R_o^{\frac{2}{n}}}{R_o^{\frac{2}{n}}}\right)$$

Again defining $r^* = \frac{r}{R_o}$ and $r_i^* = \frac{R_i}{R_o}$, substituting and rearranging gives:

$$v_\theta = V_i \left(\frac{\left(\frac{r_i^*}{r^*}\right)^{\frac{2}{n}} - r_i^{*\frac{2}{n}}}{1 - r_i^{*\frac{2}{n}}}\right) \frac{r^*}{r_i^*}$$

With a non-dimensional velocity in terms of V_i as $v_\theta^* = \frac{v_\theta}{V_i}$, our final expression is:

$$v_\theta^* = \frac{v_\theta}{V_i} = \left(\frac{\left(\frac{r_i^*}{r^*}\right)^{\frac{2}{n}} - r_i^{*\frac{2}{n}}}{1 - r_i^{*\frac{2}{n}}}\right) \frac{r^*}{r_i^*} \quad (16.30)$$

Again, an alternative way of writing Eq. 16.30, is to let $R_i = aR_o$, where $r_i^* = \frac{R_i}{R_o} = a < 1$, and

$r_o^* = 1$ giving:

$$v_\theta^* = \frac{v_\theta}{V_i} = \left(\frac{\left(\frac{a}{r^*}\right)^{\frac{2}{n}} - a^{\frac{2}{n}}}{1 - a^{\frac{2}{n}}}\right) \frac{r^*}{a} \quad (16.31)$$

Figure 16.6 is a graph showing the comparative behavior of: (a) only the outer cylinder rotating (Eq. 16.25) and; (b) only the inner cylinder rotating (Eq. 16.30). The material behavior for three different inner cylinder radii, $r_i^* = 0.2, 0.5, \text{ and } 0.8$, and for a series of flow behavior indices, n , from 0.2 (shear thinning) to 4 (shear thickening). The behavior of a Newtonian fluid, $n = 1$, is shown for comparison. The cross-hatched bar on each figure represents the inner cylinder wall.

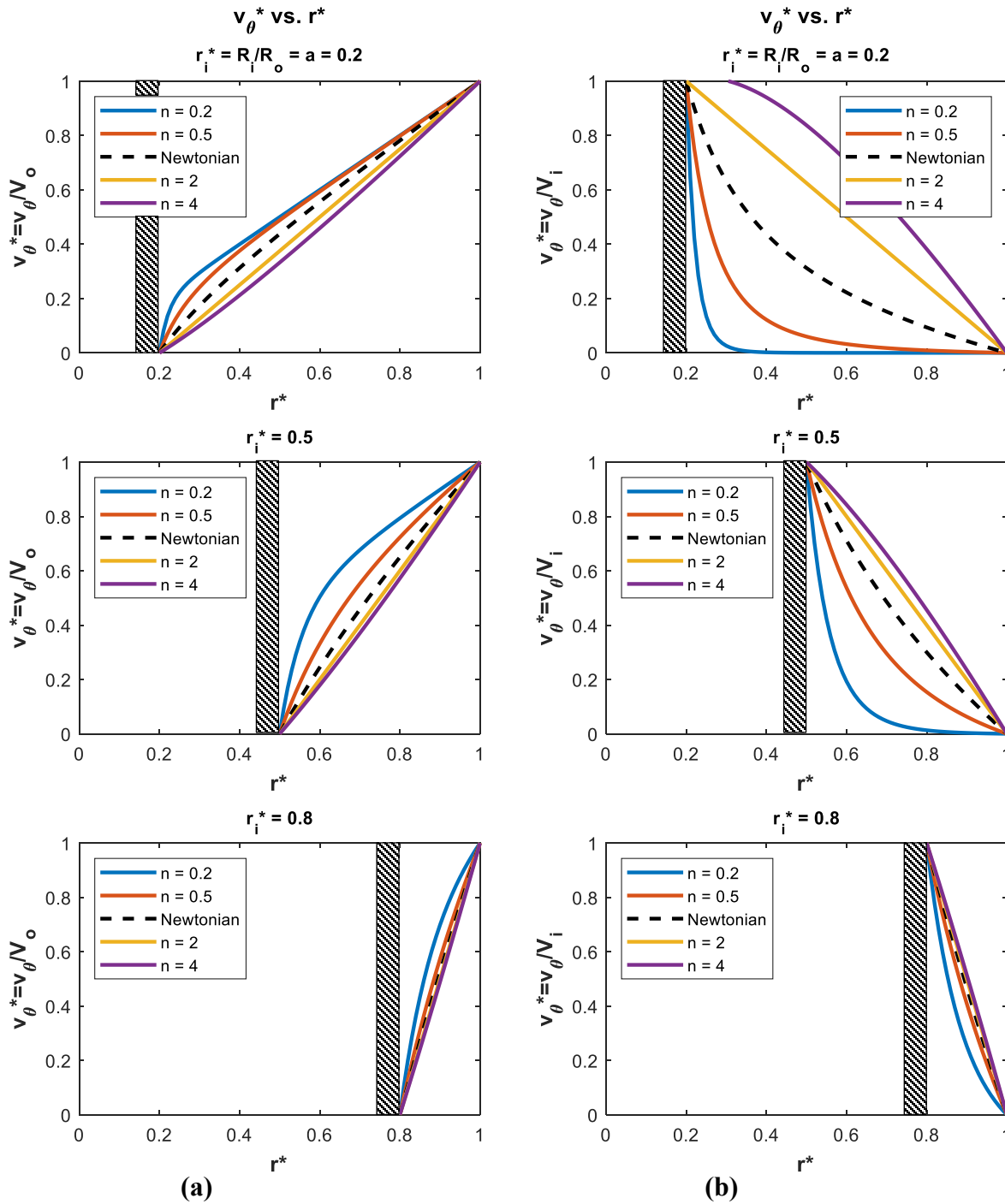


Figure 16.6 Power-law Couette flow between concentric, rotating cylinders.

(a) Outer cylinder velocity = V_o , inner cylinder fixed, $r_i^* = 0.2, 0.5, 0.8$

(b) Outer cylinder fixed, inner cylinder velocity = V_i , $r_i^* = 0.2, 0.5, 0.8$

$n = 0.2$ and 0.5 are shear thinning; $n = 2$ and 4 are shear thickening.

Figure 16.6(a) for the rotating outer cylinder is pretty much as one would assume. As Eq.16.27 indicates, the highest shear stress occurs at the inner wall. For $n < 1$, shear-thinning fluids, the fluid will be less viscous near the inner wall, and thus the velocity gradient, $\frac{dv_\theta^*}{dr}$, will be larger, and the velocity profiles will lie above the Newtonian, as shown. For $n > 1$, shear-thickening fluids, the fluid will more viscous near the inner wall, with correspondingly lower velocity gradients, with velocity profiles that lag the Newtonian.

Figure 16.6(b) for the rotating inner cylinder shows that the velocity profile behavior is reversed from figure 16.6(a). Since the shear-thinning fluids are less viscous near the inner surface, they again have correspondingly larger velocity gradients. However, since the inner cylinder is rotating, the lower viscosity results in the velocity near the inner wall lagging Newtonian behavior, yielding velocity profiles that also lag the Newtonian. The shear thickening fluids are again more viscous near the inner surface due to higher shear stress, with this more viscous region “pulling” the fluid ahead of the Newtonian behavior. This is most clearly shown for $r_i^* = 0.2$ and 0.5 , with the respective velocity profiles leading the comparable Newtonian profile.

However, note that for the rotating inner cylinder with $r_i^* = 0.2$ and $n = 4$ (figure 16.6(b), top-right), v_θ^* exceeds 1 at $r^* = 0.25$. This is unusual, since this implies that the fluid will move faster than the wall rotation! The most likely explanation is that it is a failure of the power-law model. Remember, back in sections 16.1.2 and 16.2.1 we mentioned that most shear thickening fluids often don't display consistent behavior over the entire shear stress range. Therefore, some relaxation of the shear thickening behavior at the high stress end could change this apparent unusual behavior. However, if the model holds, let's consider if such behavior is physically possible, and why.

Figure 16.7 shows a comparison of profiles of the velocity, v_θ^* , and the corresponding velocity gradient, dv_θ^*/dr^* , for inner cylinder radii $r_i^* = 0.5$ and 0.2 . Note that adjacent to the inner cylinder wall, the gradients for the shear thinning fluids are strongly negative. However, the gradients for the shear thickening fluids, are only weakly negative, and less so near the inner cylinder wall. In addition, the velocity gradient for the case of $r_i^* = 0.2$ and $n = 4$ becomes positive for $r^* < 0.25$, indicating that there is a maximum at $r^* = 0.25$, where $v_\theta^* > V_i$. If one examines the relative magnitude of the shear stress across the fluid layer for $n = 4$, the ratio of the shear stresses from the inner wall to the outer wall are $\frac{\tau_{inner}}{\tau_{outer}} = 4$ for $r_i^* = 0.5$, but $\frac{\tau_{inner}}{\tau_{outer}} = 25$ for $r_i^* = 0.2$. Therefore, it appears that the much greater shear stress differential due to shear

thickening for the smaller inner radius would cause the fluid layers closely adjacent to the inner wall to move in a somewhat solid body manner, which produces the $v_{\theta}^* > V_i$ anomaly.

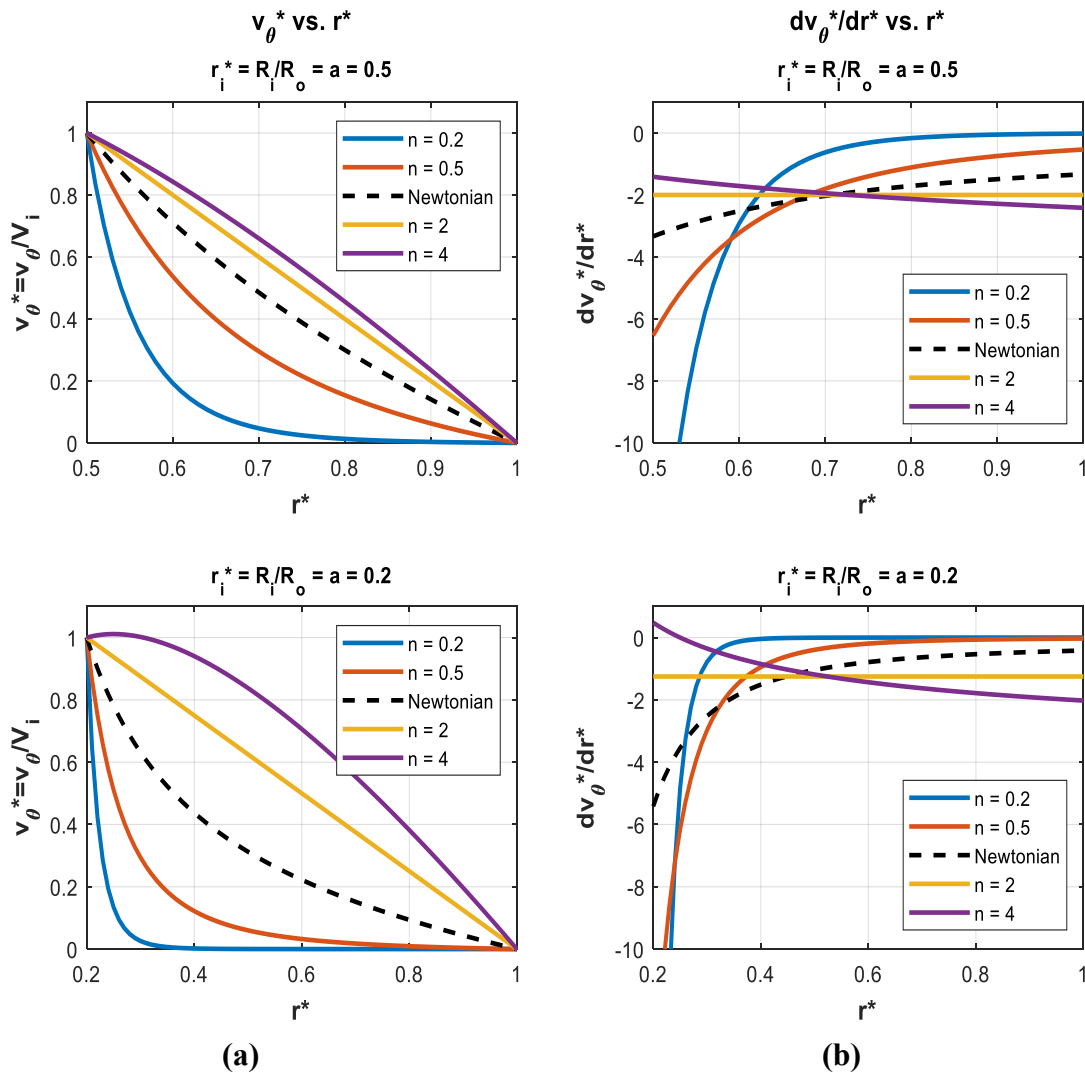


Figure 16.7 Comparative power law Couette flows with rotating inner cylinder = V_i .

(a) Velocity profiles, v_{θ}^* vs. r^* for $r_i^* = 0.5$ and 0.2 .

(b) Corresponding velocity gradients, dv_{θ}^*/dr^* vs. r^* for $r_i^* = 0.5$ and 0.2 .

$n = 0.2$ and 0.5 are shear thinning; $n = 2$ and 4 are shear thickening.

This same process, although not as accentuated for $r_i^* = 0.5$ and 0.8 in figure 16.6b is also what produces velocity profiles in excess of a Newtonian fluid as the higher shear inner region fluid pulls along the lower shear outer region fluid.

To explore this anomaly a bit more, note that the derivative of the velocity from Eq. 16.31 is:

$$\frac{dv_{\theta}^*}{dr^*} = \frac{1}{a} \left(\frac{\left(\frac{n-2}{n}\right) \left(\frac{a}{r^*}\right)^{\frac{2}{n}} - a^{\frac{2}{n}}}{1 - a^{\frac{2}{n}}} \right) \quad (16.32)$$

Setting Eq. 16.32 to zero, and solving for r^* , we have:

$$r^* = \left(\frac{n-2}{n}\right)^{\frac{n}{2}} = r_{\max}^* \quad (16.33)$$

Eq. 16.33 gives the location where v_{θ}^* will be a maximum, according to Eq. 16.31. Note that for values of $n < 2$, there is no solution for r_{\max}^* . For $n > 2$, there is a solution, but the solutions only become relevant when $r_{\max}^* > r_1^*$. Note that for $r_1^* = 0.2$, $r_{\max}^* = 0.25$, which is what is observed in figure 16.6b and 16.7.

Having made this observation, I must remind the reader that this is most likely an anomaly of the power-law assumption, which may not hold at high shear rates. This also should only occur for n values greater than 2, which are not all that common.

16.4.2.2 Poiseuille Flow in a Circular Duct

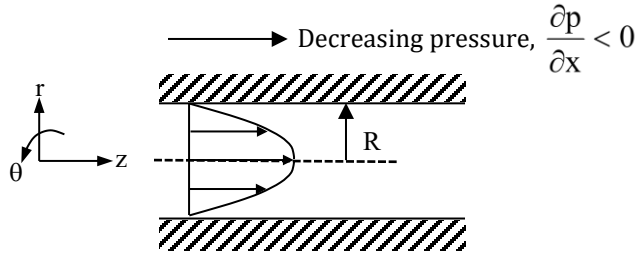


Figure 16.8 Geometry for Poiseuille flow of a power-law fluid in a circular duct

For a fully-developed Poiseuille flows in a circular duct, as shown in figure 16.8, there is no motion in the r and θ -directions, but only in the streamwise z -direction, and the governing equations reduce to the z -direction momentum equation (Eq. 16.123d of [Section 16.7.3](#)):

$$\begin{aligned} \frac{\partial v_z}{\partial t} + v_r \frac{\partial v_z}{\partial r} + \frac{v_{\theta}}{r} \frac{\partial v_z}{\partial \theta} + v_z \frac{\partial v_z}{\partial z} \\ = -\frac{1}{\rho} \frac{\partial p}{\partial z} + g_z + \frac{1}{\rho} \left[\frac{1}{r} \frac{\partial}{\partial r} (r \tau_{rz}) + \frac{1}{r} \frac{\partial \tau_{\theta z}}{\partial \theta} + \frac{\partial \sigma_{zz}}{\partial z} \right] \end{aligned} \quad (16.123d)$$

Since this is a steady, fully-developed flow, the velocity field is given by $v_z = f(r)$, and

Eq. 16.123d reduces to:

$$-\frac{\partial p}{\partial z} + \frac{1}{r} \frac{d}{dr} (r\tau_{rz}) = 0 \quad (16.34)$$

For a Poiseuille flow, $\frac{\partial p}{\partial z} = \text{constant}$ (as shown in section 6.4.1), which allows Eq. 16.34 to be rewritten as:

$$\frac{d}{dr} (r\tau_{rz}) = \frac{\partial p}{\partial z} r \quad (16.35)$$

Integrating Eq. 16.35, and equating it to the power-law shear stress from Section 16.4, Eq. 16.6, gives:

$$\tau_{rz} = \frac{\partial p}{\partial z} \frac{r}{2} + \frac{C_1}{r} = K \left(\frac{dv_z}{dr} \right)^n \Rightarrow C_1 = Kr \left(\frac{dv_z}{dr} \right)^n - \frac{\partial p}{\partial z} \frac{r^2}{2}$$

One boundary condition will be symmetry at the centerline of the tube, $\tau_{rz} = 0$, so $\frac{dv_z}{dr} = 0$ at $r = 0$, which renders $C_1 = 0$, and:

$$K \left(\frac{dv_z}{dr} \right)^n = \frac{\partial p}{\partial z} \frac{r}{2}$$

Solving for $\frac{dv_z}{dr}$:

$$\frac{dv_z}{dr} = \left(\frac{r}{2K} \frac{\partial p}{\partial z} \right)^{\frac{1}{n}}$$

Integrating again,

$$v_z = \frac{n}{n+1} \left(\frac{1}{2K} \frac{\partial p}{\partial z} \right)^{\frac{1}{n}} r^{\frac{n+1}{n}} + C_2$$

The second boundary condition is $v_z = 0$ at $r = R$,

$$0 = \frac{n}{n+1} \left(\frac{1}{2K} \frac{\partial p}{\partial z} \right)^{\frac{1}{n}} R^{\frac{n+1}{n}} + C_2 \Rightarrow C_2 = -\frac{n}{n+1} \left(\frac{1}{2K} \frac{\partial p}{\partial z} \right)^{\frac{1}{n}} R^{\frac{n+1}{n}}$$

Thus, v_z becomes:

$$v_z = \frac{nR^{\frac{n+1}{n}}}{n+1} \left(\frac{1}{2K} \frac{\partial p}{\partial z} \right)^{\frac{1}{n}} \left[\left(\frac{r}{R} \right)^{\frac{n+1}{n}} - 1 \right] \quad (16.36)$$

Defining $r^* = \frac{r}{R}$, and designating $v_{z,n} = v_z(n)$, since v_z will be a function of n , we have:

$$v_{z,n} = \frac{nR}{n+1} \left(\frac{R}{2K} \frac{\partial p}{\partial z} \right)^{\frac{1}{n}} \left[r^{*\frac{n+1}{n}} - 1 \right] \quad (16.37a)$$

From Eq. 16.37a at $r^* = 0 \Rightarrow v_{z,n} = v_{z,n,\max} = v_{z,n,CL}$:

$$v_{z,n,CL} = -\frac{nR}{n+1} \left(\frac{R}{2K} \frac{\partial p}{\partial z} \right)^{\frac{1}{n}} \quad (16.37b)$$

As I pointed out in Section 16.4.1.2, the pressure gradient, $\frac{\partial p}{\partial z}$, must be positive to allow the calculation to the power of $\frac{1}{n}$, which makes $v_{z,n}$ and $v_{z,n,CL}$ negative velocities. We again deal

with this by defining $v_{z,n}^* = \frac{v_{z,n}}{v_{z,n,CL}}$

$$v_z^* = \frac{v_{z,n}}{v_{z,n,CL}} = \left[1 - r^{*\frac{n+1}{n}} \right] \quad (16.38)$$

We obtain the shear stress by differentiating Eq. 16.36 and substituting into Eq. 16.6:

$$\frac{dv_z}{dr} = \frac{nR}{n+1} \left(\frac{1}{2K} \frac{\partial p}{\partial z} \right)^{\frac{1}{n}} \frac{\left(\frac{n+1}{n} \right) r^{\frac{1}{n}}}{R^{\frac{n+1}{n}}} = \left(\frac{r}{2K} \frac{\partial p}{\partial z} \right)^{\frac{1}{n}}$$

Thus, Eq. 16.6 gives:

$$\tau_{rz} = K \left(\frac{dv_z}{dr} \right)^n = K \left(\frac{r}{2K} \frac{\partial p}{\partial z} \right) = \frac{\partial p}{\partial z} \frac{r}{2}$$

At the tube wall, $r = R$, the shear stress is:

$$\tau_{rz,wall} = \frac{\partial p}{\partial z} \frac{R}{2}$$

So, the wall shear stress is only a function of the tube radius and the applied pressure gradient. This is the same result we obtained in section 6.4.1, Eq. 6.64, for a Newtonian fluid. Thus, this same relationship also applies for a non-Newtonian fluid at $r = R$.

Like a Poiseuille flow between flat plates, Section 16.4.1.2, we cannot compare the relative velocities for different n values based on Eqs. 16.36 or 16.37a due to the functionality of the power law. However, we can again compare different power-law fluids at the same volume

flowrate, Q , like I did in section 16.4.1.2. We determine the flowrate by integrating Eq. 16.36 (substituting for $v_{z,CL}$) for $0 \leq r \leq R$:

$$Q = \int_{r=0}^{r=R} v_z (2\pi r dr) = 2\pi v_{z,n,CL} \int_{r=0}^{r=R} \left[1 - \left(\frac{r}{R} \right)^{\frac{n+1}{n}} \right] r dr = 2\pi v_{z,n,CL} \left[\frac{r^2}{2} - \frac{n}{3n+1} \frac{r^{\frac{3n+1}{n}}}{R^{\frac{n+1}{n}}} \right]_{r=0}^{r=R}$$

$$Q = \left(\frac{n+1}{3n+1} \right) (\pi R^2) v_{z,n,CL} \quad (16.39)$$

Note that for a Newtonian fluid ($n = 1$), that:

$$Q_{\text{Newt}} = \frac{1}{2} (\pi R^2) v_{z,CL}$$

This is the same relationship of flowrate to $v_{z,CL}$ that we determined in Chapter 6 (section 6.41, Eqn. 6.62).

To allow a comparison between different power law fluids, we will use the above relationships for velocity and flowrate to show how a particular power law fluid behaves relative to a Newtonian behavior.

Substituting Eq. 16.37b into Eq. 16.39, we have:

$$Q = - \left(\frac{n}{3n+1} \right) (\pi R^2) R \left(\frac{R}{2K} \frac{\partial p}{\partial z} \right)^{\frac{1}{n}} \quad (16.40)$$

Notice that the parameter $R \left(\frac{R}{2K} \frac{\partial p}{\partial z} \right)^{\frac{1}{n}}$ in Eq. 16.40 is also common to the same parameter in the velocity equation, Eq. 16.37a. Solving for that parameter from Eq. 16.40 gives:

$$R \left(\frac{R}{2K} \frac{\partial p}{\partial z} \right)^{\frac{1}{n}} = \frac{-Q}{\left(\frac{n}{3n+1} \right) (\pi R^2)}$$

Substituting into Eq. 16.37a for $v_{z,n}$, gives:

$$v_{z,n} = \left(\frac{n}{n+1} \right) \frac{-Q}{\left(\frac{n}{3n+1} \right) (\pi R^2)} \left[r^{\frac{n+1}{n}} - 1 \right] = \frac{Q}{\pi R^2} \left(\frac{3n+1}{n+1} \right) \left[1 - r^{\frac{n+1}{n}} \right] \quad (16.41)$$

Using Eq. 16.41, we can now do a comparison of the velocity behavior for both pseudoplastic

($n < 1$) and dilatant ($n > 1$) fluids to a Newtonian fluid ($n = 1$) at the same volume flowrates. For a Newtonian flow, $n = 1$:

$$v_{z, \text{Newt}} = \frac{2Q}{\pi R^2} [1 - r^{*2}]$$

On the centerline, $r^* = 0$, we have the maximum Newtonian velocity:

$$v_{z, \text{Newt, CL}} = \frac{2Q}{\pi R^2} \quad (16.42)$$

This expression is, of course, identical to the relationship we determined in Section 6.4.1, Eq. 6.62.

Dividing Eq. 16.41 by Eq. 16.42, we calculate $v_{z, \text{n, rel}}^* = \frac{v_{z, n}}{v_{z, \text{Newt, CL}}}$, the comparative velocity

profiles, for the same flowrate, Q , through a circular duct of radius R as:

$$v_{z, \text{n, rel}}^* = \frac{v_{z, n}}{v_{z, \text{Newt, CL}}} = \frac{1}{2} \left(\frac{3n+1}{n+1} \right) \left[1 - r^{* \frac{n+1}{n}} \right] \quad (16.43)$$

Figure 16.8 shows the comparative effect of the fluid behavior index, n , on the velocity behavior relative to a Newtonian fluid ($n = 1$). Figure 16.8(a) is plots of Eq. 16.38, with each n value velocity profile normalized on its maximum centerline value. Figure 16.8(b) is plots of Eq. 16.43, with each n value velocity profile normalized on the Newtonian centerline velocity for the same flowrate. Like the Poiseuille flows between parallel plates examined in Section 16.4.1.2, figure 16.8(a) shows that shear-thinning pseudoplastics ($n < 1$) display much flatter profiles than a Newtonian flow, while shear-thickening dilatants ($n > 1$) display more peaked profiles. For equivalent flowrates, Q , figure 16.8(b) shows that the centerline velocities for pseudoplastics will lag a Newtonian fluid, and dilatants will exceed a Newtonian fluid. Moreover, as I commented on in Section 16.4.1.2 on parallel flat plate flows, the velocity behavior for smaller n values ($n \approx 0.5$ or less) often appears similar to that of a Bingham plastic.

A comparison of figure 16.8 with the similar profiles from figure 16.4 show that figures 16.8a and 16.4a are identical, since they are both are functionally the same. The relative velocity profiles of figures 16.8b and 16.4b, normalized on the Newtonian centerline velocity, are similar, but show a wider spread in the various n -profiles. This is due to a more significant difference of the centerline velocity relative to the average velocity for Poiseuille circular duct flows than for Poiseuille parallel plate flows; a result of the radial symmetry of the duct flows.

Again, like in section 16.4.1.2, because of the differing units of the K parameters we can't make a relative comparison of $\frac{\partial p}{\partial z}$ for different power law fluids without calculating the values for each specific fluid.

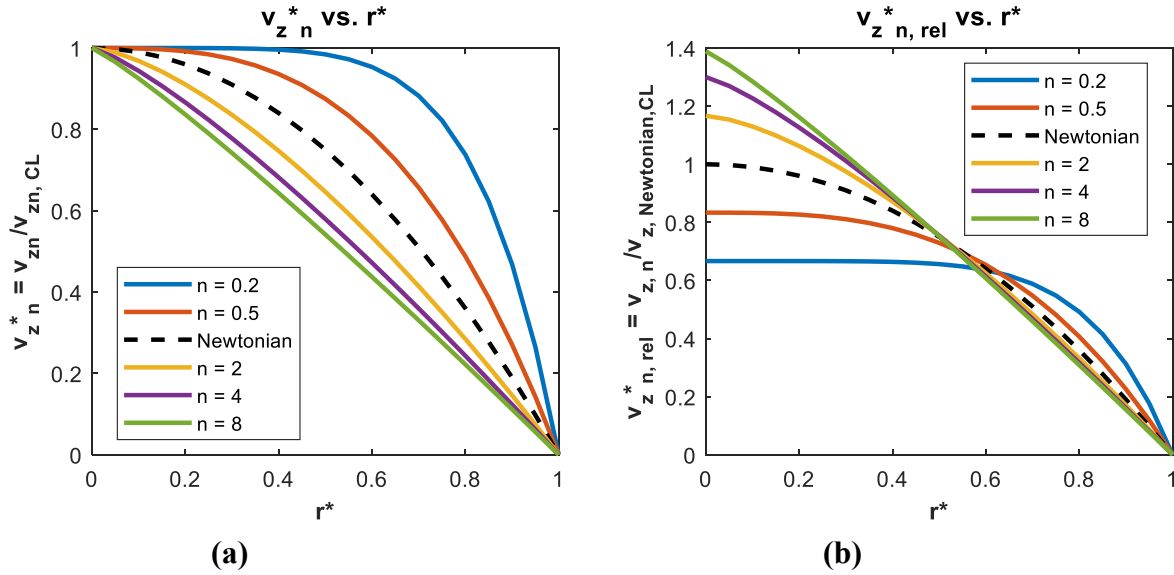


Figure 16.8 Power law velocity profiles for Poiseuille flow in a cylindrical duct.
 (a) Normalized on the centerline velocity of each respective n value fluid;
 (b) Normalized on Newtonian fluid centerline velocity for $Q = \text{constant}$.

16.5 Ideal Bingham Plastic Solutions

An ideal Bingham Plastic, as modeled by Eq. 16.3, requires that a critical stress, termed the yield stress, be reached before the material will start to flow as a fluid. Prior to reaching that yield stress, the material will act as a solid, and remain fixed, or move in unison with the surrounding material. Thus, an ideal Bingham Plastic is modeled by a two-region equation. As was indicated in Eq. 16.3, the two regions are generically related to the strain rate as:

$$\begin{aligned} \dot{\epsilon} &= 0 && \text{when } \tau < \tau_0, \text{ and} \\ \tau &= \tau_0 + \mu_B (\dot{\epsilon}) && \text{when } \tau > \tau_0 \end{aligned} \tag{16.3}$$

Here $\dot{\epsilon}$ is the generic strain rate, τ_0 is the yield shear stress, and μ_B is the apparent viscosity when the material flows as a fluid. The three particular model variations we will use in this section are:

Non-Newtonian, Cartesian

$$\text{x-direction only: } \dot{\epsilon}_{yx} = \frac{\partial u}{\partial y} = 0, \quad \text{when } \tau_{yx} < \tau_0 \text{ (assuming } \tau_0 > 0) \tag{16.44a}$$

$$\text{and } \tau_{yx} = \mu_B \left(\frac{\partial u}{\partial y} \right) + \tau_0, \quad \text{when } \tau_{yx} > \tau_0 \tag{16.44b}$$

Non-Newtonian, Cylindrical

$$\theta \text{ direction only: } \dot{\epsilon}_{r\theta} = r \frac{\partial}{\partial r} \left(\frac{v_\theta}{r} \right) = 0 \Rightarrow \frac{\partial}{\partial r} \left(\frac{v_\theta}{r} \right) = 0, \text{ when } \tau_{r\theta} < \tau_0 \quad (16.45a)$$

$$\text{and } \tau_{r\theta} = \mu_B \left[r \frac{\partial}{\partial r} \left(\frac{v_\theta}{r} \right) \right] + \tau_0, \text{ when } \tau_{r\theta} > \tau_0 \quad (16.45b)$$

$$z\text{-direction only: } \dot{\epsilon}_{rz} = \left(\frac{\partial v_z}{\partial r} \right) = 0 \Rightarrow \frac{\partial v_z}{\partial r} = 0, \text{ when } \tau_{rz} < \tau_0 \quad (16.46a)$$

$$\text{and } \tau_{rz} = \mu_B \left(\frac{\partial v_z}{\partial r} \right) + \tau_0, \text{ when } \tau_{rz} > \tau_0 \quad (16.46b)$$

16.5.1 Parallel Plate Flows

For fully-developed Couette and Poiseuille flows between infinite parallel flat plates, there is no motion in the lateral directions, but only in the streamwise direction, and (like Section 16.4.1) the governing equations again reduce to the x-direction momentum equation (Eq. 16.122b of [Section 16.7.2](#)).

$$\frac{\partial u}{\partial t} + u \frac{\partial u}{\partial x} + v \frac{\partial u}{\partial y} + w \frac{\partial u}{\partial z} = -\frac{1}{\rho} \frac{\partial p}{\partial x} + g_x + \frac{1}{\rho} \left[\frac{\partial \sigma_{xx}}{\partial x} + \frac{\partial \tau_{yx}}{\partial y} + \frac{\partial \tau_{zx}}{\partial z} \right] \quad (16.122b)$$

Again, for steady, fully-developed flow in x-direction, Eq. 16.122b simplifies to:

$$\frac{d\tau_{yx}}{dy} = \frac{\partial p}{\partial x} \quad (16.47)$$

16.5.1.1 Couette Flow between Parallel Plates

Using the coordinate system shown in figure 16.9, we again specify boundary conditions of $u = 0$ at $y = 0$, and $u = U$ at $y = h$.

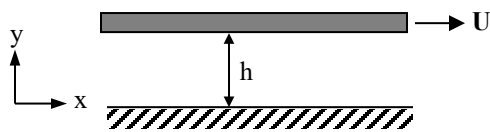


Figure 16.9 Couette flow between a lower stationary plate and an upper moving plate.

Since there is no pressure gradient for a Couette flow (see the detailed discussion of this in section 6.3.1), Eq. 16.47 further reduces to:

$$\frac{d\tau_{yx}}{dy} = \frac{\partial p}{\partial x} = 0 \quad (16.48)$$

Integrating Eq. 16.48 once:

$$\tau_{yx} = C_1$$

Now if $\tau_{yx} < \tau_0$ (assuming $\tau_0 > 0$), $\tau_{yx} = \text{constant} < \tau_0$, and thus Eq. 16.44a applies:

$$\frac{du}{dy} = 0 \Rightarrow u = C_2$$

But since $u = 0$ at $y = 0$, then $u = 0$ across the entire gap when $\tau_{yx} < \tau_0$ for $0 \leq y \leq h$.

Note that when $\tau_{yx} < \tau_0$ across the entire gap, the upper plate cannot move. So, the boundary condition of $u = U$ at $y = h$ cannot be met, and $u = 0$ across the entire channel, and the material remains fixed until $\tau_{yx} \geq \tau_0$.

When $\tau_{yx} \geq \tau_0$, Eq. 16.44b applies, $\tau_{yx} = \mu_B \left(\frac{du}{dy} \right) + \tau_0$. So, integrating Eq. 16.48 again, and equating τ_{yx} to Eq. 16.44b:

$$\tau_{yx} = \mu_B \left(\frac{du}{dy} \right) + \tau_0 = C_1$$

Rearranging,

$$\frac{du}{dy} = \frac{1}{\mu_B} (C_1 - \tau_0) \quad (16.49)$$

Integrating Eq. 16.49,

$$u = \frac{1}{\mu_B} (C_1 - \tau_0) y + C_2 \quad (16.50)$$

Applying the boundary conditions that $u = 0$ at $y = 0$, and $u = U$ at $y = h$:

$$0 = \frac{1}{\mu_B} (C_1 - \tau_0) 0 + C_2 \Rightarrow C_2 = 0$$

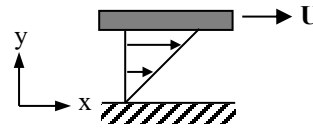
$$U = \frac{1}{\mu_B} (C_1 - \tau_0) h$$

$$C_1 = \frac{\mu_B U}{h} + \tau_0$$

Substituting C_1 and C_2 back into Eq. 16.50:

$$u = \frac{1}{\mu_B} \left(\frac{\mu_B U}{h} + \tau_0 - \tau_0 \right) y$$

$$u = \frac{Uy}{h}$$



(16.51)

Thus, as Eq.16.51 shows, the velocity profile is again linear across the gap between the plates, which is the same as for a Newtonian flow and for a power-law fluid, as shown in Section 6.4.1.1, Eq. 16.10. Note that the shear stress across the gap is:

$$\tau_{yx} = \mu_B \left(\frac{du}{dy} \right) + \tau_0 = \frac{\mu_B U}{h} + \tau_0 = \text{constant}$$

Thus, the shear stress across the gap is constant, as is the strain rate. Therefore, in parallel plate Couette flow of an ideal Bingham plastic, the material will remain static until the yield shear stress is reached, and then all the material will begin to flow with a linear velocity profile, with a constant shear stress across the material. This process is approximated by “spreading” a material like mayonaise or other stiff food product on bread. The knife acts as the moving plate, and the bread as the fixed plate.

16.5.1.2 Poiseuille Flow between Parallel Plates

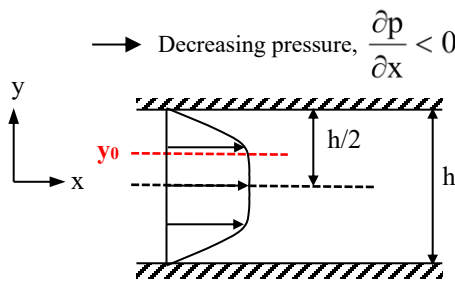


Figure 16.10 Poiseuille flow between parallel flat plates, ideal Bingham plastic.

Similar to how we approached the solution for a power law fluid in Section 16.4.1.2, here we again employ a coordinate system with the origin located on the midplane of the channel, and again recognize that the velocity profile will be symmetric about the midplane, as shown in figure 16.10. Employing this midplane coordinate system, the boundary conditions for the flow in the upper half of the flow are $\frac{\partial u}{\partial y} = 0$ for $0 \leq y \leq y_0$ (the central plug flow), and $u = 0$ at $y = \frac{h}{2}$. I discuss how we establish the first boundary condition below.

For a Poiseuille flow, $\frac{\partial p}{\partial x} = \text{constant}$ (as shown in section 6.3.2). Thus, we rearrange Eq. 16.47 to integrate for the shear stress.

$$\frac{d\tau_{yx}}{dy} = \frac{\partial p}{\partial x} = \text{constant} \tag{16.52}$$

Integrating Eq. 16.52 once gives:

$$\tau_{yx} = \frac{\partial p}{\partial x} y + C_1 \tag{16.53}$$

Note that Eq. 16.53 indicates that the shear stress will vary linearly (since $\frac{\partial p}{\partial x} = \text{constant}$), with the highest shear at the plate surface, and decreasing linearly toward the midplane. When the shear on the upper plate ($y = \frac{h}{2}$) exceeds the yield shear stress (i.e. $\tau_{yx, y=\frac{h}{2}} \geq \tau_0$), the fluid adjacent to the wall will behave as a fluid, as long as $\tau_{yx} \geq \tau_0$. However, Eq. 16.53 indicates the shear stress within the fluid region decreases as we move toward the midplane. Potentially, we will reach a location within the material where $\tau_{yx} = \tau_0$ (assuming $\tau_0 > 0$) and fluid behavior will cease. Since we don't know where that location is, we arbitrarily designate that location as the yield location, y_0 , where $0 < y_0 < \frac{h}{2}$, which I show as a red dotted line in Figure 16.10. Within the region adjacent to the wall, $y_0 < y < \frac{h}{2}$, we assume that $\tau_{yx} \geq \tau_0$, so the material will behave as a fluid. However, within the region adjacent to the midplane ($0 < y < y_0$, $\tau_{yx} \leq \tau_0$) the material will behave as solid. In this latter region, the pressure gradient will cause the material to move as a solid plug flow, with the material moving at a constant velocity equivalent to the velocity at $y = y_0$.

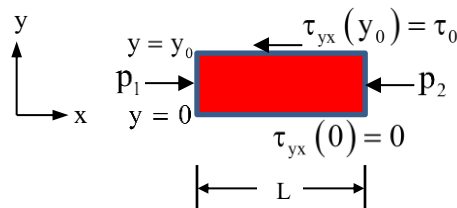


Figure 16.11 Forces acting on the solid region material, $0 < y < y_0$, of arbitrary length L .

To assess this solid region, I apply a force balance over the solid portion of the material of arbitrary length, L , as shown in figure 6.11. Note that since the solid plug will move uniformly, the shear stress within the plug, and at the centerline $y = 0$, will be zero, as indicated.

Performing a force balance on the solid material (assuming a unit depth), we have a balance between the shear stresses and pressure forces acting on the material:

$$-\tau_0 L + (0)L + p_1(y_0 - 0) - p_2(y_0 - 0) = 0$$

$$\tau_0 = \frac{(p_1 - p_2)}{L} y_0 = \frac{\partial p}{\partial x} y_0 \quad (16.54)$$

In Eq. 16.54, we note that the pressure differences, $(p_1 - p_2)$, divided by the arbitrary length, L , is simply the pressure gradient, and the shear stresses will act in a negative direction, with $\tau_{yx} = \tau_0$ at $y = y_0$, and $\tau_{yx} = 0$ at $y = 0$.

Solving Eq. 16.54 for y_0 gives:

$$y_0 = \frac{\tau_0}{\left(\frac{\partial p}{\partial x}\right)} \quad (16.55)$$

Equation 16.55 indicates that the yield location y_0 , which is the bounding location between fluid and solid behavior, is controlled by two parameters: the yield shear stress and the pressure gradient. Since y_0 cannot be greater than $\frac{h}{2}$, the pressure gradient must exceed the yield stress in order for the material to move. After the pressure gradient exceeds the yield stress, continued pressure gradient increases will cause y_0 to diminish, with the region of fluid behavior $y_0 \leq y \leq \frac{h}{2}$ expanding outward from the plate surface toward the midplane. We will see the impact of an increasing pressure gradient, and a consequent reduction in y_0 , later in this section.

Therefore, a Poiseuille flow of an ideal Bingham plastic will have two regions of behavior:

(1) for $0 < y < y_0$, $\tau_{yx} < \tau_0$, the material will behave as a solid plug flow at $u = \text{constant}$,

(2) for $y_0 < y < \frac{h}{2}$, $\tau_{yx} > \tau_0$, the material will behave as a fluid with $u = u(y)$.

Within the fluid region, $y_0 < y < \frac{h}{2}$ and $\tau_{yx} > \tau_0$, Eq. 16.53 applies:

$$\tau_{yx} = \frac{\partial p}{\partial x} y + C_1$$

Applying a boundary condition that $\tau_{yx} = \tau_0$ at $y = y_0$, we get:

$$\tau_0 = \frac{\partial p}{\partial x} y_0 + C_1 \Rightarrow C_1 = \tau_0 - \frac{\partial p}{\partial x} y_0$$

So,

$$\tau_{yx} = \frac{\partial p}{\partial x}(y - y_0) + \tau_0$$

Substituting the governing shear stress relationship for the fluid region, Eq. 16.44b:

$$\tau_{yx} = \mu_B \left(\frac{du}{dy} \right) + \tau_0 = \frac{\partial p}{\partial x}(y - y_0) + \tau_0$$

Which rearranges to:

$$\frac{du}{dy} = \frac{1}{\mu_B} \frac{\partial p}{\partial x}(y - y_0)$$

Integrating, gives:

$$u = \frac{1}{\mu_B} \frac{\partial p}{\partial x} \left(\frac{y^2}{2} - y_0 y \right) + C_2 \quad (16.56)$$

Applying the boundary condition that $u = 0$ at $y = \frac{h}{2}$, we determine C_2 as:

$$C_2 = -\frac{1}{\mu_B} \frac{\partial p}{\partial x} \left[\frac{h^2}{8} - y_0 \frac{h}{2} \right]$$

Substituting C_2 into Eq. 16.56 and rearranging gives:

$$u = \frac{1}{2\mu_B} \frac{\partial p}{\partial x} \left(y^2 - \frac{h^2}{4} \right) + \frac{y_0}{2\mu_B} \frac{\partial p}{\partial x} (h - 2y) \quad \text{for } y_0 < y < \frac{h}{2} \quad (16.57)$$

Defining a non-dimensional y variable as $y^* = \frac{2y}{h}$, and $y_0^* = \frac{2y_0}{h} = \frac{2\tau_0}{h \left(\frac{\partial p}{\partial x} \right)}$, then $u_{y_0^*} = u(y_0^*)$, since

the u velocity profile will be a function of y_0^* , as well as y^* , we rewrite Eq. 16.57 as:

$$u_{y_0^*} = \frac{h^2}{8\mu_B} \frac{\partial p}{\partial x} \left[(y^{*2} - 1) + 2y_0^*(1 - y^*) \right] \quad \text{for } y_0^* < y^* < 1 \quad (16.58a)$$

To determine the maximum velocity, which will be the velocity of the material “plug” in the center of the channel, I let $u_{y_0^*} = u_{y_0^*, \max}$ at $y^* = y_0^*$ in Eq. 16.58a:

$$u_{y_0^*, \max} = \frac{h^2}{8\mu_B} \frac{\partial p}{\partial x} \left[(y_0^{*2} - 1) + 2y_0^*(1 - y_0^*) \right]$$

Which reduces to:

$$u_{y_0^*, \max} = -\frac{h^2}{8\mu_B} \frac{\partial p}{\partial x} (y_0^* - 1)^2 \quad \text{for } 0 < y_0^* < 1 \quad (16.58b)$$

Recall that $\frac{\partial p}{\partial x} < 0$ for a flow in the positive x direction, thus Eq.16.58 will yield positive velocities for a pressure decreasing in the x direction.

Defining $u_{y_0^*}^* = \frac{u_{y_0^*}}{u_{y_0^*,\max}}$ gives:

$$u_{y_0^*}^* = \frac{u_{y_0^*}}{u_{y_0^*,\max}} = \frac{[(1 - y^{*2}) + 2y_0^*(y^* - 1)]}{(y_0^* - 1)^2} \quad \text{for } y_0^* < y^* < 1 \quad (16.59a)$$

and

$$u_{y_0^*,\max}^* = 1 \quad \text{for } 0 < y^* < y_0^* \quad (16.59b)$$

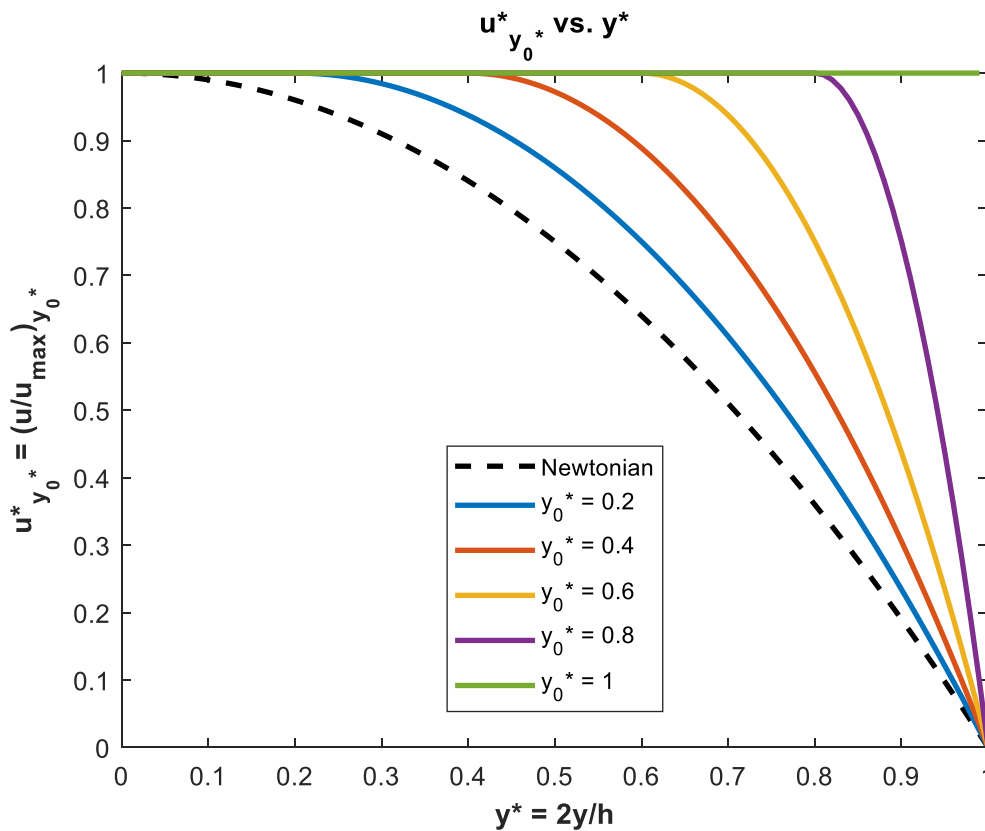


Figure 16.12 Ideal Bingham plastic Poiseuille flow between parallel flat plates. Normalized on the respective maximum velocity at the yield location, $y_0^* = \frac{2\tau_0}{h\left(\frac{\partial p}{\partial x}\right)}$.

Equation 16.59 reflects how an ideal Bingham fluid velocity profile varies relative to its maximum centerline (or plug velocity). Figure 16.12 is a series of velocity profiles of $u_{y_0^*}^*$ vs. y^* calculated from Eq. 16.59 for a range of y_0^* values, $0 \leq y_0^* \leq 1$.

As figure 16.12 shows, for a yield location near the wall ($y_0^* \approx 1$), the material profile is essentially a flat plug flow. However, as the yield location moves toward the midplane (i.e. the pressure gradient increases), the profile will display a wider region of fluid-like behavior, and the region of plug flow will decrease. Potentially, if the pressure gradient gets quite large, $\frac{\partial p}{\partial x} \gg \frac{2\tau_0}{h}$, the yield location will become quite small, and the flow will approach Newtonian behavior ($y_0^* \approx 0$).

While Figure 16.12 is instructive regarding the shape of the velocity profiles, it does not reveal the impact of the yield location on the behavior of the material relative to a comparable Newtonian fluid. Unlike the power-law fluid we examined in section 16.4.1.2, we can compare the behavior of an ideal Bingham fluid to Newtonian fluid, assuming the same pressure gradient and fluid viscosity.

A Newtonian fluid will have $\tau_0 = 0$, and thus $y_0^* = 0$. Equation 16.58b gives $u_{\text{Newt,max}} = -\frac{h^2}{8\mu} \frac{\partial p}{\partial x}$, which is the same as Eq. 6.19 we derived in Section 6.3.2. If we assume equivalent pressure gradients and fluid viscosities, $\mu_B = \mu$ (not probable, but instructive), we can determine velocity profiles for a range of Bingham fluids relative to a comparable Newtonian fluid. Thus, dividing Eq. 16.58a for $u_{y_0^*}$ by $u_{\text{Newt,max}}$, we obtain:

$$u_{\text{rel}}^* = \frac{u_{y_0^*}}{u_{\text{Newt,max}}} = \left[(1 - y^{*2}) + 2y_0^*(y^* - 1) \right] \quad \text{for } y_0^* < y^* < 1 \quad (16.60a)$$

and

$$u_{\text{rel,max}}^* = \frac{u_{y_0^*,\text{max}}}{u_{\text{Newt,max}}} = (1 - y_0^{*2}) \quad \text{for } 0 < y^* < y_0^* \quad (16.60b)$$

Equation 16.60 gives the velocity profile behavior relative to a pure Newtonian fluid, with the same pressure gradient and fluid viscosity. Figure 16.13 shows a series of velocity profiles of u_{rel}^* vs. y^* plotted for a range of y_0^* values, $0 \leq y_0^* \leq 1$.

Figure 16.13 illustrates that the flow of material does not initiate if the pressure gradient is less than the yield stress, $\frac{\partial p}{\partial x} \leq \frac{2\tau_0}{h} \Rightarrow y_0^* \geq 1$ ($y_0^* = 1$, the green line, reflects all cases for $y_0^* \geq 1$).

As the pressure gradient increases relative to the yield stress, τ_0 , the material begins to move as the yield location, y_0^* , shifts toward the midplane. As the pressure gradient is increased, this results in the expansion of the region of fluid-like behavior, with a commensurate increase in the maximum (plug) velocity. This correspondingly reduces the extent of the solid, plug-flow region, and increases the volume flowrate.

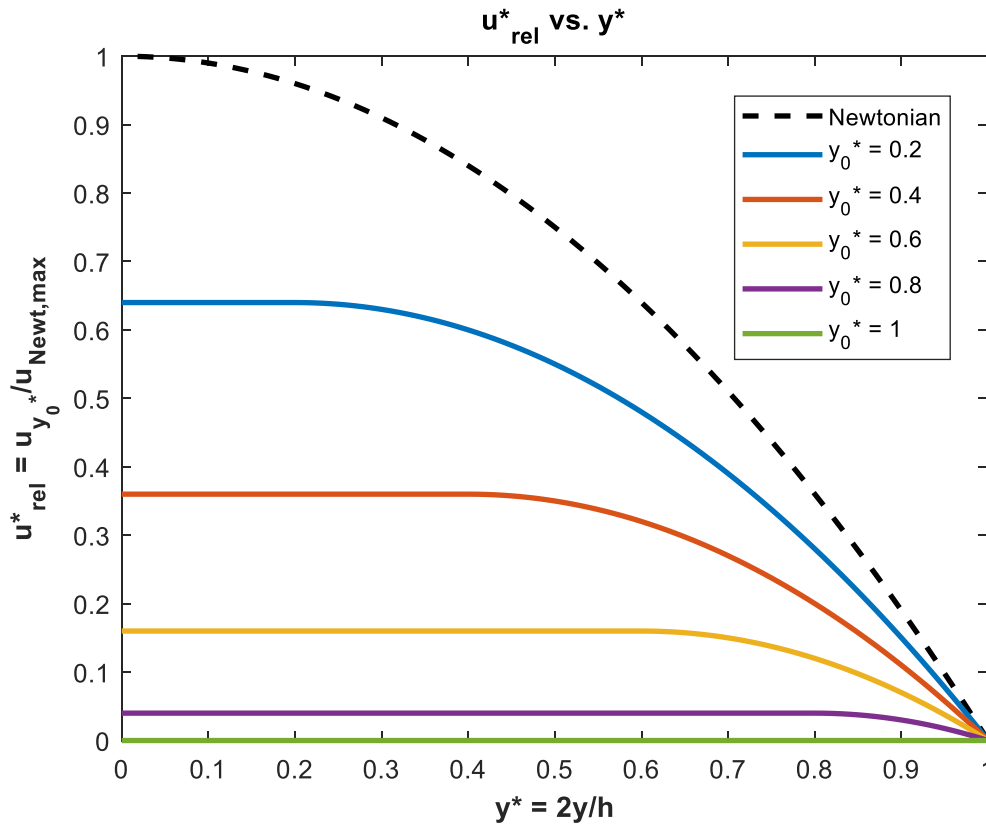


Figure 16.13 Ideal Bingham plastic Poiseuille flow between parallel flat plates for a series of yield locations, y_0^* ; normalized on the maximum (centerline) velocity for a Newtonian fluid with the same pressure gradient and fluid viscosity.

$$y_0^* = \frac{2\tau_0}{h \left(\frac{\partial p}{\partial x} \right)}$$

To understand the effect of y_0^* on both the volume flowrate and the pressure gradient, I integrate Eq. 16.58 across the duct to determine the volume flowrate, Q . Since the flow is symmetric about the x -axis, the volume flowrate for $-\frac{h}{2} < y < \frac{h}{2}$ will just be double the flowrate for $0 < y < \frac{h}{2}$.

Using $y = y^* \left(\frac{h}{2} \right)$, and an arbitrary plate width W , we have, using Eq. 16.58 (this requires a two part integral of both the fluid and solid material regions):

$$Q_{y_0^*} = 2 \int_0^{\frac{h}{2}} u_{y_0^*} W dy = 2W \int_0^{y^*=1} u_{y_0^*} \frac{h}{2} dy^* = hW \int_{y^*=0}^{y^*=y_0^*} u_{y_0^*,max} dy^* + hW \int_{y^*=y_0^*}^{y^*=1} u_{y_0^*} dy^*$$

$$Q_{y_0^*} = -\frac{Wh^3}{8\mu_B} \frac{\partial p}{\partial x} \int_{y^*=0}^{y^*=y_0^*} (y_0^* - 1)^2 dy^* + \frac{Wh^3}{8\mu_B} \frac{\partial p}{\partial x} \int_{y^*=y_0^*}^{y^*=1} [(y^{*2} - 1) + 2y_0^*(1 - y^*)] dy^*$$

$$Q_{y_0^*} = -\frac{Wh^3}{8\mu_B} \frac{\partial p}{\partial x} \left[(y_0^* - 1)^2 y^* \right]_{y^*=0}^{y^*=y_0^*} + \frac{Wh^3}{8\mu_B} \frac{\partial p}{\partial x} \left[\left(\frac{y^{*3}}{3} - y^* \right) + 2y_0^* \left(y^* - \frac{y^{*2}}{2} \right) \right]_{y^*=y_0^*}^{y^*=1}$$

Which reduces to:

$$Q_{y_0^*} = -\frac{Wh^3}{24\mu_B} \frac{\partial p}{\partial x} (y_0^{*3} - 3y_0^* + 2) \quad (16.61)$$

As a check on Eq. 16.61, we note that when $y_0^* = 0$, the fluid would behave as a Newtonian fluid, $\mu_B = \mu$, so:

$$Q_{\text{Newt}} = -\frac{Wh^3}{12\mu} \frac{\partial p}{\partial x} \quad (16.62)$$

Equation 16.62 is the same as Eqn. 6.23 for the volume flowrate of a Poiseuille flow derived in Section 6.3.2.

To compare the respective flow rates, we take the ratio of $Q_{y_0^*}$ to Q_{Newt} :

$$Q_{y_0^*, \text{rel}} = \frac{Q_{y_0^*}}{Q_{\text{Newt}}} = \frac{1}{2} (y_0^{*3} - 3y_0^* + 2) \quad (16.63)$$

Equation 16.63 gives the volume flowrate for an ideal Bingham plastic relative to a Newtonian fluid with identical pressure gradients and fluid viscosities, $\mu_B = \mu$. Figure 16.14(a) is a plot of $Q_{y_0^*, \text{rel}}$ vs. y_0^* for $0 \leq y_0^* \leq 1$.

Note that unlike the power-law solutions, the Bingham plastic solutions are linear with the pressure gradient. So, solving Eq. 16.61 for the pressure gradient, and letting $Q = Q_{y_0^*}$, we have:

$$\left. \frac{\partial p}{\partial x} \right|_{y_0^*} = -\frac{24\mu_B Q}{Wh^3} \left[\frac{1}{(y_0^{*3} - 3y_0^* + 2)} \right] \quad (16.64)$$

For a Newtonian fluid, $y_0^* = 0$, Eq. 16.64 gives:

$$\left. \frac{\partial p}{\partial x} \right|_{\text{Newt}} = -\frac{12\mu Q}{Wh^3} \quad (16.65)$$

To compare the respective pressure gradients at the same volume flowrates, we again assume identical fluid viscosities, $\mu_B = \mu$, and take the ratio of Eq. 16.64 to Eq. 16.65:

$$\left. \frac{\partial p}{\partial x} \right|_{\text{rel}} = \frac{\left. \frac{\partial p}{\partial x} \right|_{y_0^*}}{\left. \frac{\partial p}{\partial x} \right|_{\text{Newt}}} = \frac{2}{(y_0^{*3} - 3y_0^* + 2)} \quad (16.66)$$

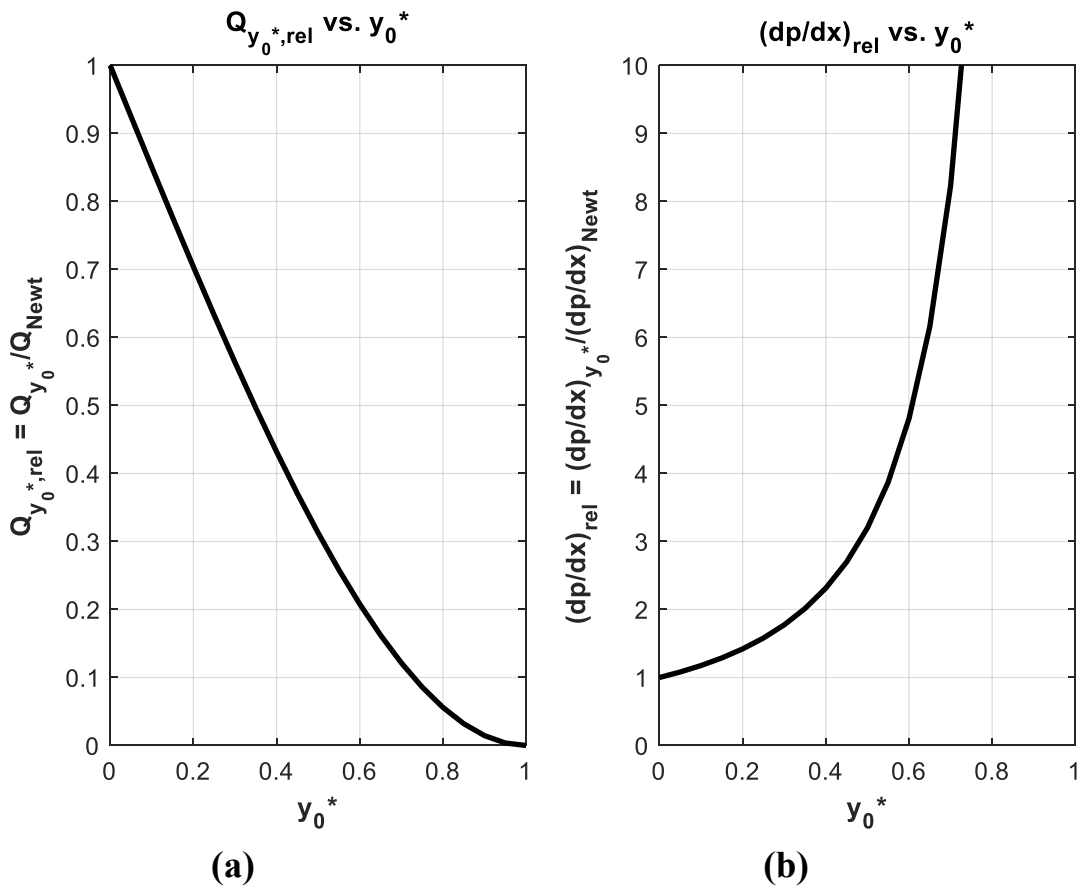


Figure 16.14 Comparisons of ideal Bingham plastic volume flowrate and pressure gradient as a function of y_0^* -- Poiseuille flat plate flow.

(a) $Q_{y_0^*,rel}$, with identical pressure gradient and fluid viscosity;

(b) $(\partial p/\partial x)_{rel}$, with identical volume flowrate and fluid viscosity.

$$y_0^* = \frac{2\tau_0}{h(\partial p/\partial x)}$$

In Eq. 16.66, $\left. \frac{\partial p}{\partial x} \right|_{rel}$ is the relative increase in pressure gradient required to maintain the same volume flowrate as a comparable Newtonian flow with the same fluid viscosity. Figure 16.14(b) is a plot of $\left. \frac{\partial p}{\partial x} \right|_{rel}$ vs. y_0^* for $0 \leq y_0^* \leq 1$.

Figure 16.14(a) shows that the flowrate of an ideal Bingham plastic will always be less than that of a comparable Newtonian fluid with the same pressure gradient and fluid viscosity. The thinner

the fluid region (larger y_0^*), the lower the flowrate. Why is this so? If we do a force balance for a control volume of length L and $0 \leq y \leq \frac{h}{2}$ we can show that the wall shear stress at $y = \frac{h}{2}$ is:

$$\tau_{\text{wall}} = \frac{\partial p}{\partial x} \frac{h}{2}$$

The governing shear stress equation for an ideal Bingham plastic, Eq. 16.44b, is:

$$\tau_{yx} = \mu_B \frac{du}{dy} + \tau_0, \quad \text{when } \tau_{yx} > \tau_0$$

So, at $y = \frac{h}{2}$

$$\tau_{\text{wall}} = \frac{\partial p}{\partial x} \frac{h}{2} = \mu_B \left. \frac{du}{dy} \right|_{\text{wall}} + \tau_0$$

Rearranging we have:

$$\left. \frac{du}{dy} \right|_{\text{wall}} = \frac{1}{\mu_B} \left(\frac{\partial p}{\partial x} \frac{h}{2} - \tau_0 \right) = \frac{\partial p}{\partial x} \frac{h}{2\mu_B} (1 - y_0^*) \quad (16.67)$$

(Note: this only holds if $\frac{\partial p}{\partial x} \frac{h}{2} > \tau_0$ and $y_0^* \leq 1$)

What Eq. 16.67 shows is that the slope of the velocity profile at the wall ($y = \frac{h}{2}$) will be

$\left. \frac{du}{dy} \right|_{\text{wall}} = 0$ (no flow) until $\frac{\partial p}{\partial x} \frac{h}{2} > \tau_0$ or $y_0^* \leq 1$. If the pressure gradient increases beyond τ_0 ,

thus reducing y_0^* , the slope of the velocity at the plate surface will increase, $\left. \frac{du}{dy} \right|_{\text{wall}} > 0$, and

the material (solid and fluid portions) will begin to move. The higher the pressure gradient relative to τ_0 , the larger the region of fluid behavior, and the faster the collective material

moves. The key is the that shear stress at the wall is always the same, $\tau_{\text{wall}} = \frac{\partial p}{\partial x} \frac{h}{2}$. So, the larger

the yield stress, τ_0 , the more the pressure gradient has to work to overcome τ_0 , and the less work it can do to move the material.

Likewise, figure 16.14(b) illustrates that the thinner the fluid region (larger y_0^*), the higher the relative pressure gradient must be to maintain the same flow rate. For example, if $y_0^* = \frac{1}{3}$, such that 66% of the material behaves as a fluid, the pressure gradient is double that of a Newtonian

fluid. By $y_0^* = 0.6$, where only 40% of the material behaves as a fluid, the required pressure gradient grows to 5 times the Newtonian. As figure 16.14(b) shows, when $y_0^* > 0.7$ the relative pressure gradient required to maintain the same flowrate is literally off the chart.

Also, since the power required to move the material will be roughly the pressure gradient times the volume flowrate (i.e. $\text{Power} \approx \frac{\partial p}{\partial x} Q$), the pumping power required to maintain a constant flowrate will behave essentially the same as the pressure gradient in figure 16.14(b).

16.5.2 Flows with Circular Symmetry

In this section, I address Couette flow and Poiseuille flow of an ideal Bingham plastic fluid in geometries with circular symmetry. Like the parallel plate flows of section 16.5.1, these flows will reduce to one-dimensional, fully-developed flows with no lateral cross flow. Also, like the power-law flows covered in section 16.4.2, different governing momentum equations apply for each of these flows. The Couette flow depending on the azimuthal (θ) direction equation and yields $v_\theta = f(r)$, whereas the Poiseuille flow depends on the axial (z) direction equation and yields $v_z = f(r)$. The two flows will also depend on different constitutive equations for the shear stress, as indicated in Section 16.5.

16.5.2.1 Couette Flow between Concentric, Rotating Cylinders

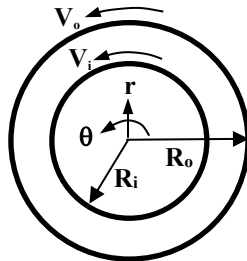


Figure 6.15 Geometry for Couette flow between concentric rotating cylinders

As discussed in Section 6.4.2, the governing equation for this type of cylindrical flow reduces to the θ -direction momentum equation, 16.123c of [Section 16.7.3](#).

$$\begin{aligned} \frac{\partial v_\theta}{\partial t} + v_r \frac{\partial v_\theta}{\partial r} + \frac{v_\theta}{r} \frac{\partial v_\theta}{\partial \theta} + v_z \frac{\partial v_\theta}{\partial z} + \frac{v_r v_\theta}{r} \\ = -\frac{1}{\rho r} \frac{\partial p}{\partial \theta} + g_\theta + \frac{1}{\rho} \left[\frac{1}{r^2} \frac{\partial}{\partial r} (r^2 \tau_{r\theta}) + \frac{1}{r} \frac{\partial \sigma_{\theta\theta}}{\partial \theta} + \frac{\partial \tau_{z\theta}}{\partial z} - \frac{\tau_{\theta r} - \tau_{r\theta}}{r} \right] \end{aligned} \tag{16.123c}$$

Since this is a steady, fully-developed flow, the velocity field is given by $v_\theta = f(r)$, and Eq. 16.123c reduces to:

$$\frac{1}{r} \frac{d}{dr} (r^2 \tau_{r\theta}) = \frac{\partial p}{\partial \theta} \quad (16.68)$$

I showed in section 6.4.4 that for Couette flow, $\frac{\partial p}{\partial \theta} = 0$, which further reduces Eq. 16.68 to:

$$\frac{d}{dr} (r^2 \tau_{r\theta}) = 0$$

Integrating, we have:

$$\tau_{r\theta} = \frac{C_1}{r^2} \quad (16.69)$$

However, in order to integrate Eq. 16.69 further, we need to assess and specify the appropriate boundary conditions.

Boundary Conditions (a): Outer Cylinder Rotating at velocity V_o , Inner Cylinder Fixed

In the case of rotating, concentric cylinders, with an ideal Bingham flow, we cannot apriori specify the velocity of rotation, V_o , since when $\tau_{r\theta} < \tau_0$ across the entire gap between the cylinders, $R_i \leq r \leq R_o$, there can be no motion, whereas when $\tau_{r\theta} > \tau_0$ over some portion of the gap, the outer cylinder can rotate. So, how do we set a boundary condition for this problem?

What we do know, from our previous examples of Couette-type flows is that the torque across the gap will always be a constant (see Sections 6.4.2, Eq. 6.68 and 16.4.2.1, Eq. 16.29). So, if we let torque = T = constant, then at any r location the torque for a depth of L is given by:

$$T = \tau_{r\theta} (2\pi r L) r = 2\pi L r^2 \tau_{r\theta}$$

Such that

$$\tau_{r\theta} = \frac{T}{2\pi L r^2} \quad (16.70)$$

For an ideal Bingham plastic, the θ -direction, two-region equations (Eq. 16.45) for the shear stress are:

$$\dot{\epsilon}_{r\theta} = r \frac{d}{dr} \left(\frac{v_\theta}{r} \right) = 0 \Rightarrow \frac{d}{dr} \left(\frac{v_\theta}{r} \right) = 0, \quad \text{when } \tau_{r\theta} < \tau_0 \quad (16.45a)$$

and

$$\tau_{r\theta} = \mu_B \left[r \frac{d}{dr} \left(\frac{v_\theta}{r} \right) \right] + \tau_0, \quad \text{when } \tau_{r\theta} > \tau_0, \quad (16.45b)$$

When $\tau_{r\theta} < \tau_0$ across the entire cylinder gap, the equation that applies is 16.45a, which integrates to:

$$\frac{v_\theta}{r} = C_1$$

However, the boundary condition for the fixed inner cylinder at $r = R_i$ is $v_\theta = 0$, which will make $v_\theta = 0$ across the gap, since the torque will be insufficient to deform the fluid, and the fluid will remain stationary.

Equation 16.70 indicates that the highest shear stress will occur at R_i (the smallest radius), so the first location that the material will reach $\tau_{r\theta} = \tau_0$ is $\tau_{r\theta} = \tau_0 = \frac{T}{2\pi L R_i^2}$ at $r = R_i$. However, as the torque is further increased, the shear stress at R_i will increase, and the location where $\tau_{r\theta} = \tau_0$ will move away from the inner surface and out into the material. We will call this location where $\tau_{r\theta} = \tau_0$ the yield radius, and designate it by r_0 . From Eq. 16.70, we can write:

$$\tau_{r\theta} = \frac{T}{2\pi L r_0^2} = \tau_0$$

Solving for r_0 in terms of the torque we have:

$$r_0 = \sqrt{\frac{T}{2\pi L \tau_0}} \quad (16.71)$$

Equation 16.71 will be the outer limit at which the Bingham plastic will behave like a fluid, with fluid behavior spanning a region $R_i < r < r_0$.

Within this region $R_i < r < r_0$, the shear stress abides by the Bingham fluid equation, Eq.16.45b, such that:

$$\tau_{r\theta} = \mu_B \left[r \frac{d}{dr} \left(\frac{v_\theta}{r} \right) \right] + \tau_0$$

or

$$\mu_B r \frac{d}{dr} \left(\frac{v_\theta}{r} \right) = \tau_{r\theta} - \tau_0$$

From Eqs. 16.70 and 16.71, we substitute for the shear stress values to give:

$$\mu_B r \frac{d}{dr} \left(\frac{v_\theta}{r} \right) = \frac{T}{2\pi L r^2} - \frac{T}{2\pi L r_0^2}$$

or

$$\frac{d}{dr} \left(\frac{v_\theta}{r} \right) = \frac{T}{2\pi \mu_B L r_0^2} \left(\frac{r_0^2}{r^3} - \frac{1}{r} \right) \quad (16.72)$$

Integrating Eq. 16.72, gives:

$$\frac{v_\theta}{r} = \frac{T}{2\pi \mu_B L r_0^2} \left(-\frac{r_0^2}{2r^2} - \ln(r) \right) + C_2$$

Employing the boundary condition that $v_\theta = 0$ at $r = R_i$, we have:

$$C_2 = \frac{T}{2\pi \mu_B L r_0^2} \left(\frac{r_0^2}{2R_i^2} + \ln(R_i) \right)$$

Substituting C_2 and simplifying:

$$\frac{v_\theta}{r} = \frac{T}{2\pi \mu_B L} \left[\frac{1}{2} \left(\frac{1}{R_i^2} - \frac{1}{r^2} \right) + \left(\frac{1}{r_0^2} \right) \ln \left(\frac{R_i}{r} \right) \right] \quad (16.73)$$

To non-dimensionalize Eq. 16.73, we first let $R_o = R$ and $R_i = aR$, where $a < 1$, then we define

$r^* = \frac{r}{R}$. Thus, substituting $r = r^*R$, $R_i = aR$, and $r_0 = r_0^*R$, into Eq. 16.73 and simplifying,

we get:

$$v_\theta = \frac{T}{2\pi \mu_B L R} \left[\frac{1}{2} \left(\frac{1}{a^2} - \frac{1}{r^{*2}} \right) + \frac{1}{r_0^{*2}} \ln \left(\frac{a}{r^*} \right) \right] r^* \quad \text{for } a < r^* < r_0^* \quad (16.74)$$

What about the region that is between r_0 and $R_o = R$, where $\tau_{r\theta} < \tau_0$? From Eq. 16.45a we have:

$$\frac{\partial}{\partial r} \left(\frac{v_\theta}{r} \right) = 0$$

Integrating gives:

$$v_\theta = C_3 r$$

For the case where at least some portion of the material behaves as a fluid adjacent to R_1 , the outer cylinder can rotate, and we have a boundary condition of $v_\theta = V_o$ at $r = R_o = R$ (even though we don't know the value of V_o). Thus, $C_3 = \frac{V_o}{R}$, and

$$v_\theta = \frac{V_o r}{R} = V_o r^* \quad \text{for } r_0^* < r^* < 1 \quad (16.75a)$$

We note that V_o , since it cannot be specified apriori (since we have specified the torque, T), is determined by equating the two velocities from the outer and inner regions (Eqs. 16.75a and 16.74) at $r^* = r_0^*$:

$$V_o r_0^* = \frac{T}{2\pi\mu_B LR} \left[\frac{1}{2} \left(\frac{1}{a^2} - \frac{1}{r_0^{*2}} \right) + \frac{1}{r_0^{*2}} \ln \left(\frac{a}{r_0^*} \right) \right] r_0^*$$

$$V_o = \frac{T}{2\pi\mu_B LR} \left[\frac{1}{2} \left(\frac{1}{a^2} - \frac{1}{r_0^{*2}} \right) + \frac{1}{r_0^{*2}} \ln \left(\frac{a}{r_0^*} \right) \right] \quad (16.75b)$$

Substituting for V_o in Eqs. 16.74 and 16.75a, the two-region velocity equations are:

$$v_\theta = V_o r^* = \frac{T}{2\pi\mu_B LR} \left[\frac{1}{2} \left(\frac{1}{a^2} - \frac{1}{r_0^{*2}} \right) + \frac{1}{r_0^{*2}} \ln \left(\frac{a}{r_0^*} \right) \right] r^* \quad \text{for } r_0^* < r^* < 1 \quad (16.76a)$$

and

$$v_\theta = \frac{T}{2\pi\mu_B LR} \left[\frac{1}{2} \left(\frac{1}{a^2} - \frac{1}{r^{*2}} \right) + \frac{1}{r^{*2}} \ln \left(\frac{a}{r^*} \right) \right] r^* \quad \text{for } a < r^* < r_0^* \quad (16.76b)$$

Notice that Eq. 16.76a is simply a solid body rotation of the solid portion of the material.

However, what if $\tau_{r\theta} > \tau_0$ all across the entire gap to $r = R$, or $r^* = 1$? Then $r_0^* = 1$, and only Eq. 16.76b applies across the whole gap from $aR < r < R$, or $a < r^* < 1$, so that:

$$v_\theta = \frac{T}{2\pi\mu_B LR} \left[\frac{1}{2} \left(\frac{1}{a^2} - \frac{1}{r^{*2}} \right) + \ln \left(\frac{a}{r^*} \right) \right] r^* \quad \text{for } a < r^* < 1, \text{ and } r_0^* = 1 \quad (16.77a)$$

and

$$V_o = \frac{T}{2\pi\mu_B LR} \left[\frac{1}{2} \left(\frac{1}{a^2} - 1 \right) + \ln(a) \right] \quad \text{at } r^* = 1 \quad (16.77b)$$

Now, what if $r_0^* = \sqrt{\frac{T}{2\pi LR^2 \tau_0}} > 1$, which can certainly happen if $T > 2\pi LR^2 \tau_0$? For this case, we need to re-examine our determination of V_o . Here, we note that r^* cannot exceed 1 ($r = R$),

but r_0^* can exceed 1. So, revisiting our boundary conditions for determining V_o , we have $v_\theta = V_o$ at $r^* = 1$, which Eq. 16.74 gives as:

$$V_o = \frac{T}{2\pi\mu_B LR} \left[\frac{1}{2} \left(\frac{1}{a^2} - 1 \right) + \frac{1}{r_0^{*2}} \ln(a) \right] \quad (16.78a)$$

Note that the value of r_0^* is a direct function of the torque, T , so V_o will increase for $r_0^* > 1$, and the equation for the velocity distribution for $a < r^* < 1$ will be:

$$v_\theta = \frac{T}{2\pi\mu_B LR} \left[\frac{1}{2} \left(\frac{1}{a^2} - \frac{1}{r^{*2}} \right) + \frac{1}{r_0^{*2}} \ln\left(\frac{a}{r^*}\right) \right] r^* \quad \text{for } (a < r^* < 1), r_0^* > 1 \quad (16.78b)$$

Since we can solve for V_o from Eqs. 16.75b, 16.77b, and 16.78a, we can non-dimensionalize v_θ as $v_\theta^* = \frac{v_\theta}{V_o}$, like we did in Section 16.4.2.1. However, here V_o is a function of r_0^* , and is not a consistent value as it was for the power-law solution. So, we reexamine our expression for r_0^* noting that from Eq. 16.71:

$$r_0^{*2} = \frac{T}{2\pi LR^2 \tau_0}$$

Substituting r_0^{*2} into Eq. 16.74, we get:

$$v_\theta = \frac{T}{4\pi\mu_B LR} \left(\frac{1}{a^2} - \frac{1}{r^{*2}} \right) r^* + \left(\frac{R\tau_0}{\mu_B} \right) \ln\left(\frac{a}{r^*}\right) r^* \quad (16.79)$$

If $\tau_0 = 0$ in Eq. 16.79 we have a Newtonian flow, with velocity:

$$v_{\theta, \text{Newt}} = \frac{T}{4\pi\mu LR} \left(\frac{1}{a^2} - \frac{1}{r^{*2}} \right) r^* \quad (16.80a)$$

At $r^* = 1$, Eq. 16.80a gives $v_{\theta, \text{Newt}}(1) = V_{o, \text{Newt}}$ of:

$$V_{o, \text{Newt}} = \frac{T}{4\pi\mu LR} \left(\frac{1-a^2}{a^2} \right) \quad (16.80b)$$

Therefore, to keep perspective on the influence of τ_0 on the outer wall velocity, I normalize our

v_θ velocities for Eqs. 16.76, 16.77, and 16.78 on $V_{o, \text{Newt}}$, i.e. $v_\theta^* = \frac{v_\theta}{V_{o, \text{Newt}}}$. This gives us

velocity profiles that compare ideal Bingham Couette behavior to comparable Newtonian

behavior (assuming $\mu_{\text{Bingham}} = \mu_{\text{Newtonian}}$ for the fluid behavior) under the same applied torque. The three possible flow cases for a rotating outer cylinder are:

Case 1(a):

When $\tau_{r\theta} < \tau_0$ across the entire Couette gap, then the material behavior across the whole gap is governed by the inner radius, $r = aR$, $r^* = a$, which is where the material will initially begin to flow. Thus, if the yield radius is less than the inner radius, i.e. $r_0 = \sqrt{\frac{T}{2\pi L \tau_0}} < aR$, the applied torque will be less than that required to initiate fluid behavior, $T < 2\pi L a^2 R^2 \tau_0$, and the material will remain stationary under the applied torque, and the outer cylinder cannot move. So,

$$\tau_{r\theta} < \tau_0, \text{ for } a < r^* < 1 \quad v_{\theta}^* = 0 \text{ and } V_o^* = 0$$

Case 2(a):

When $T > 2\pi L a^2 R^2 \tau_0$ and $\tau_{r\theta} = \tau_0$ occurs within the Couette gap at r_0 , where $aR < r_0 \leq R$ ($a < r_0^* \leq 1$), the regions of behavior will be:

$$\tau_{r\theta} > \tau_0, \text{ for } a < r^* \leq r_0^* \quad v_{\theta}^* = \frac{a^2}{(1-a^2)} \left[\left(\frac{1}{a^2} - \frac{1}{r^{*2}} \right) + \frac{2}{r_0^{*2}} \ln \left(\frac{a}{r^*} \right) \right] r^* \quad (16.81a)$$

and

$$\tau_{r\theta} < \tau_0, \text{ for } r_0^* < r^* \leq 1: \quad v_{\theta}^* = \frac{a^2}{(1-a^2)} \left[\left(\frac{1}{a^2} - \frac{1}{r_0^{*2}} \right) + \frac{2}{r_0^{*2}} \ln \left(\frac{a}{r_0^*} \right) \right] r^* \quad (16.81b)$$

with

$$V_o^* = \frac{a^2}{(1-a^2)} \left[\left(\frac{1}{a^2} - \frac{1}{r_0^{*2}} \right) + \frac{2}{r_0^{*2}} \ln \left(\frac{a}{r_0^*} \right) \right] \quad (16.81c)$$

Note that when $r_0^* = 1$, only Eq.16.81a is required across the Couette gap.

Case 3(a):

When $r_0^* = \sqrt{\frac{T}{2\pi L R^2 \tau_0}} > 1$, which occurs when $T > 2\pi L R^2 \tau_0$. Here, r^* cannot exceed 1

($r = R$), but r_0^* may exceed 1. Thus, V_o^* is the value of v_{θ}^* at $r^* = 1$, rather than at $r_0^* = 1$, which yields the equations:

$$v_{\theta}^* = \frac{a^2}{(1-a^2)} \left[\left(\frac{1}{a^2} - \frac{1}{r^{*2}} \right) + \frac{2}{r_0^{*2}} \ln \left(\frac{a}{r^*} \right) \right] r^* \quad \text{for } a < r^* < 1, \text{ and } 1 < r_0^* \quad (16.82a)$$

with

$$V_o^* = 1 + \frac{2}{r_o^{*2}} \frac{a^2}{(1-a^2)} \ln(a) \quad (16.82b)$$

Note that when $r_o^* \gg 1$, then Eqs. 16.82 collapse to the Newtonian solution, as it should.

Velocity profile behavior calculated from Eqs. 16.81 and 16.82 appear later in figure 16.16(a).

Boundary Conditions (b): Outer Cylinder Fixed, Inner Cylinder Rotating at velocity V_i

For the case of inner cylinder rotation, the derivation of the velocity behavior of an ideal Bingham plastic is similar to the case for the outer cylinder rotation.

When $\tau_{r\theta} < \tau_0$ across the entire cylinder gap, the material cannot flow and $v_\theta = 0$ across the Couette gap. The material will remain fixed, until $\tau_{r\theta} > \tau_0$, which will again initiate fluid behavior at $r = R_i$.

When $\tau_{r\theta} > \tau_0$, and a portion of the material begins to behave as a fluid, the equation derivation is the same through Eq. 16.72.

$$\frac{d}{dr} \left(\frac{v_\theta}{r} \right) = \frac{T}{2\pi\mu_B L r_o^2} \left(\frac{r_o^2}{r^3} - \frac{1}{r} \right) \quad (16.72)$$

Eq. 16.72 again integrates to:

$$\frac{v_\theta}{r} = \frac{T}{2\pi\mu_B L r_o^2} \left(-\frac{r_o^2}{2r^2} - \ln(r) \right) + C_2$$

However, here the appropriate boundary condition is again at $r = R_i$, where the material first behaves as a fluid, and where $v_\theta = V_i$. Note that we cannot use a boundary condition of $v_\theta = 0$ at $r = R_o$, since that condition will lie within the region where the material behaves as a solid. To help simplify the derivation process, we will again let $R_o = R$ and $R_i = aR$, where $a < 1$.

Employing the boundary condition that $v_\theta = V_i$ at $r = R_i = aR$, we have:

$$C_2 = \frac{T}{2\pi\mu_B L r_o^2} \left(\frac{r_o^2}{2a^2 R^2} + \ln(aR) \right) + \frac{V_i}{aR}$$

Substituting C_2 and simplifying:

$$\frac{v_\theta}{r} = \frac{T}{2\pi\mu_B L r_o^2} \left[\frac{1}{2} \left(\frac{r_o^2}{a^2 R^2} - \frac{r_o^2}{r^2} \right) + \ln \left(\frac{aR}{r} \right) \right] + \frac{V_i}{aR} \quad (16.83)$$

I non-dimensionalize Eq. 16.83, again letting $r^* = \frac{r}{R}$. Thus, substituting $r = r^* R$ and $r_0 = r_0^* R$ into Eq. 16.83 and simplifying:

$$v_\theta = \frac{T}{2\pi\mu_B LR} \left[\frac{1}{2} \left(\frac{1}{a^2} - \frac{1}{r^{*2}} \right) + \frac{1}{r_0^{*2}} \ln \left(\frac{a}{r^*} \right) \right] r^* + \frac{V_i r^*}{a} \quad \text{for } a < r^* < r_0^* \quad (16.84)$$

Again, we cannot specify V_i a priori (since we have again specified the torque, T). We determine the value of V_i by noting that within the region $r_0^* \leq r^* \leq 1$ the material behaves as a solid, with $v_\theta = 0$. Therefore, letting $v_\theta = 0$ at $r^* = r_0^*$ in Eq. 16.84 and solving for V_i :

$$V_i = -\frac{T}{2\pi\mu_B LR} \left[\frac{1}{2} \left(\frac{1}{a^2} - \frac{1}{r_0^{*2}} \right) + \frac{1}{r_0^{*2}} \ln \left(\frac{a}{r_0^*} \right) \right] a$$

Substituting V_i back into Eq. 16.84 and simplifying, we have the two-region velocity equations:

$$v_\theta = \frac{T}{2\pi\mu_B LR} \left[\frac{1}{2} \left(\frac{1}{r_0^{*2}} - \frac{1}{r^{*2}} \right) + \frac{1}{r_0^{*2}} \ln \left(\frac{r_0^*}{r^*} \right) \right] r^* \quad \text{for } a \leq r^* \leq r_0^* \quad (16.85a)$$

and

$$v_\theta = 0 \quad \text{for } r_0^* \leq r^* \leq 1 \quad (16.85b)$$

with

$$V_i = \frac{T}{2\pi\mu_B LR} \left[\frac{1}{2} \left(\frac{1}{r_0^{*2}} - \frac{1}{a^2} \right) + \frac{1}{r_0^{*2}} \ln \left(\frac{r_0^*}{a} \right) \right] a \quad \text{at } r^* = a \quad (16.85c)$$

When $r_0^* = \sqrt{\frac{T}{2\pi LR^2 \tau_0}} \geq 1$, we need to again re-examine the determination of V_i . Again, we

note that r^* cannot exceed 1, but r_0^* can exceed 1. Revisiting our boundary conditions for determining V_i , we have $v_\theta = 0$ at $r^* = 1$, rather than at $r_0^* = 1$. Substituting into Eq. 16.84 and solving for V_i :

$$V_i = \frac{T}{2\pi\mu_B LR} \left[\frac{1}{2} \left(1 - \frac{1}{a^2} \right) + \frac{1}{r_0^{*2}} \ln \left(\frac{1}{a} \right) \right] a \quad (16.86a)$$

Substituting V_i back into Eq. 16.84 and simplifying, we have the velocity equation for $r_0^* \geq 1$.

$$v_\theta = \frac{T}{2\pi\mu_B LR} \left[\frac{1}{2} \left(1 - \frac{1}{r^{*2}} \right) + \frac{1}{r_0^{*2}} \ln \left(\frac{1}{r^*} \right) \right] r^* \quad \text{for } a \leq r^* \leq 1, r_0^* \geq 1 \quad (16.86b)$$

I will now normalize v_θ on the inner wall velocity for a Newtonian flow. If we let $\tau_0 = 0$, in Eq. 16.86b this gives the equation for a Newtonian flow. When $\tau_0 = 0$, then $r_0^* \approx \infty$, and Eq. 16.86 reduces to:

$$v_{\theta, \text{Newt}} = \frac{T}{4\pi\mu LR} \left[\left(1 - \frac{1}{r^{*2}} \right) r^* \right] \quad \text{for } a \leq r^* \leq 1 \quad (16.87a)$$

with

$$V_{i, \text{Newt}} = \frac{T}{4\pi\mu LR} \left(\frac{a^2 - 1}{a} \right) \quad (16.87b)$$

Similar to the rotating outer cylinder, here I normalize the v_θ velocity from Eq. 16.85 and 16.86 on $V_{i, \text{Newt}}$, i.e. $v_\theta^* = \frac{v_\theta}{V_{i, \text{Newt}}}$. Again, this compares ideal Bingham Couette behavior to the

comparable Newtonian behavior (again letting $\mu_{\text{Bingham}} = \mu_{\text{Newtonian}}$) at the same applied torque.

The possible flow cases for a rotating inner cylinder are:

Case 1(b):

When $\tau_{r_0} < \tau_0$ across the entire Couette gap, the material behavior across the whole gap is again governed by the inner radius, $r^* = a$, which is again where the material will initially begin to

behave as a fluid. Thus, if the yield radius is less than the inner radius, i.e. $r_0 = \sqrt{\frac{T}{2\pi L \tau_0}} < aR$,

the applied torque will again be less than that required to initiate fluid behavior, $T < 2\pi L a^2 R^2 \tau_0$, and the material will remain stationary under the applied torque, and the inner cylinder cannot move. So,

$$\tau_{r_0} < \tau_0, \text{ for } a < r^* < 1 \quad v_\theta^* = 0 \text{ and } V_i^* = 0$$

Case 2(b):

When $T > 2\pi L a^2 R^2 \tau_0$ and $\tau_{r_0} = \tau_0$ occurs within the Couette gap at r_0 , where $aR < r_0 < R$ ($a < r_0^* < 1$), the regions of behavior will be:

$$\tau_{r_0} > \tau_0, \text{ for } a \leq r^* \leq r_0^* \quad v_\theta^* = \left(\frac{a}{a^2 - 1} \right) \left[\left(\frac{1}{r_0^{*2}} - \frac{1}{r^{*2}} \right) + \frac{2}{r_0^{*2}} \ln \left(\frac{r_0^*}{r^*} \right) \right] r^* \quad (16.88a)$$

and

$$\tau_{r_0} < \tau_0, \text{ for } r_0^* < r^* \leq 1 \quad v_\theta^* = 0 \quad (16.88b)$$

with

$$V_i^* = \left(\frac{a}{a^2 - 1} \right) \left[\left(\frac{1}{r_0^{*2}} - \frac{1}{a^2} \right) + \frac{2}{r_0^{*2}} \ln \left(\frac{r_0^*}{a} \right) \right] a \quad (16.88c)$$

Case 3(b):

When $r_0^* = \sqrt{\frac{T}{2\pi LR^2 \tau_0}} \geq 1$, which happens if $T \geq 2\pi LR^2 \tau_0$. In this case, r^* cannot exceed 1

($r = R$), but r_0^* can exceed 1. Therefore, we require that $v_\theta^* = 0$ at $r^* = 1$, rather than at $r_0^* = 1$, which yields the equations:

$$v_\theta^* = \left(\frac{a}{a^2 - 1} \right) \left[\left(1 - \frac{1}{r^{*2}} \right) + \frac{2}{r_0^{*2}} \ln \left(\frac{1}{r^*} \right) \right] r^* \quad \text{for } a \leq r^* \leq 1 \quad (16.89a)$$

with

$$V_i^* = 1 + \frac{2}{r_0^{*2}} \left(\frac{a^2}{1 - a^2} \right) \ln(a) \quad (16.89b)$$

Figure 16.16 shows the comparative Couette velocity profile behavior for an ideal Bingham plastic with: (a) only the outer cylinder rotating (Eqs. 16.81 and 16.82) and; (b) only the inner cylinder rotating (Eqs. 16.88 and 16.89). The material behavior is shown for three different inner cylinder radii, $r_i^* = a = 0.2, 0.5, \text{ and } 0.8$, and for a series of yield radii, r_0^* , starting at the inner cylinder radius, and extending outward to $r_0^* = 1.4$ or 1.5 .

Note that for all cases, when $r_0^* = r_i^* = a$ (or when $r_0^* < r_i^*$) there is no movement of the material (blue lines). However, once $r_0^* > r_i^*$ the fluid-like material flow begins at r_i^* and extends out to r_0^* . Figure 16.16(a) shows that if $r_0^* < 1$ the region $r_0^* < r^* < 1$ will behave as a solid, in solid body rotation. This can best be seen for $r_i^* = 0.2$ and 0.5 , where the solid portion is reflected by a linear velocity profile. However, for the case of inner cylinder rotation, figure 16.16(b), the solid portion will remain fixed for the region $r_0^* < r^* < 1$. What is clear from scaling the velocity relative to $V_{o, \text{Newt}}$ and $V_{i, \text{Newt}}$ is that for the same torque the velocity of the rotating cylinder with an ideal Bingham plastic will always be less than that for a Newtonian fluid, because of the added resistance due to the yield stress, τ_0 .

When $r_0^* \geq 1$, all of the material behaves as a fluid. Note that the larger the gap between cylinders is, the more nonlinear the velocity profiles are. And as r_0^* increases beyond 1, the more closely the velocity profiles approach the behavior of a Newtonian fluid (which would be when $r_0^* \gg 1$).

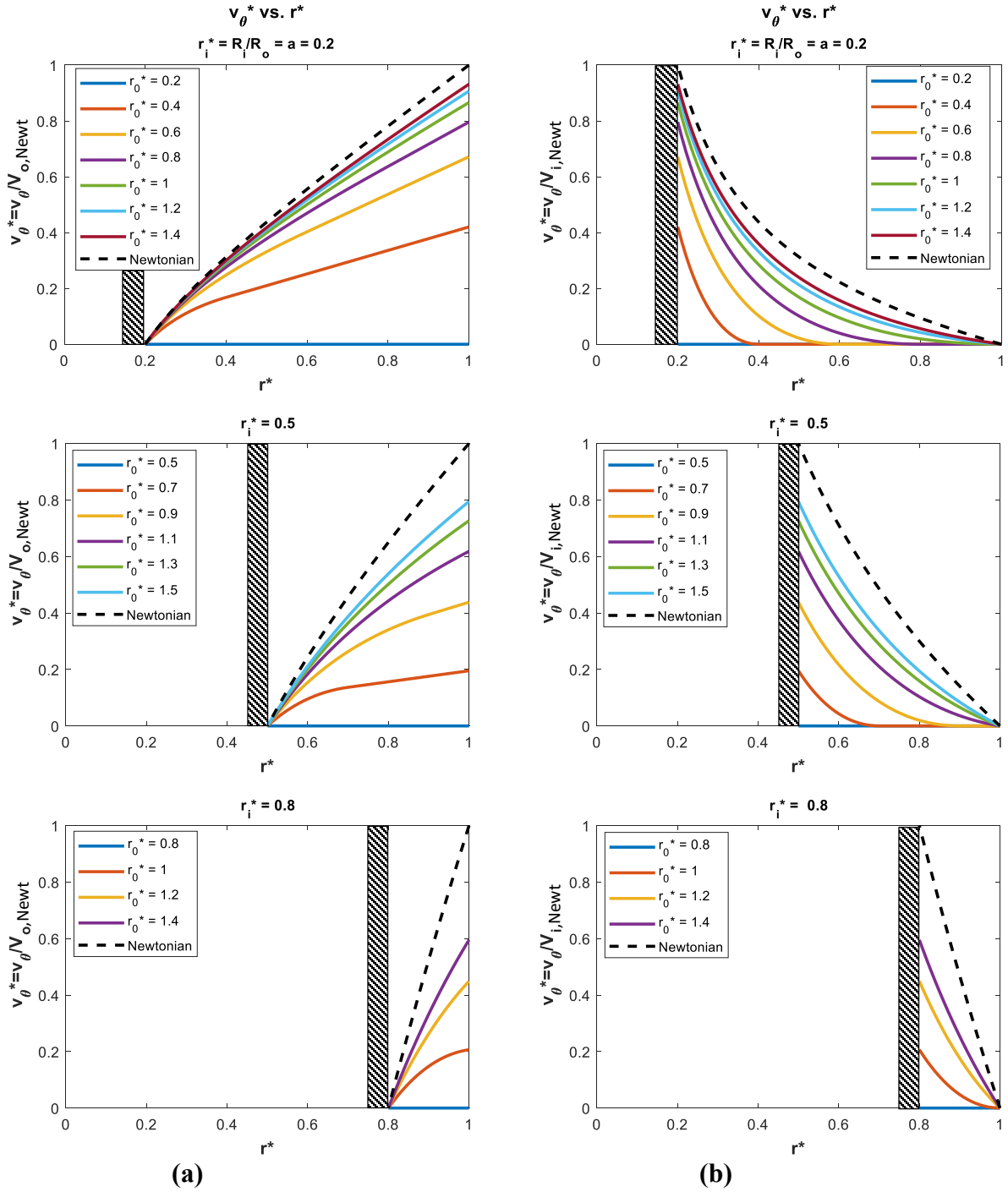


Figure 16.16 Ideal Bingham plastic Couette flow between concentric, rotating cylinders.
 (a) Outer cylinder velocity = V_o , inner cylinder fixed. $r_i^* = a = 0.2, 0.5, 0.8$
 (b) Outer cylinder fixed, inner cylinder velocity = V_i . $r_i^* = a = 0.2, 0.5, 0.8$

$$r_0^* = \sqrt{\frac{T}{2\pi LR^2\tau_0}}$$

Notice that Eq. 16.89b for V_i^* is identical to Eq. 16.82b for V_o^* , which may seem unusual. However, the Newtonian values for V_o , Eq. 16.80b, and V_i , Eq. 16.87b, which are used to normalize the velocities are quite different for the same applied torque. This is a function of the moment over which the torque is applied ($R_o = R$ for Eq. 16.80b vs. $R_i = aR$ for Eq. 16.87b). Thus, for the same applied torque, when the outer cylinder rotates (Case a), the outer wall shear stress will be less than inner wall shear stress when the inner cylinder rotates (Case b). This allows the outer cylinder to rotate at a higher velocity than the inner cylinder, under the same applied torque. Also, if we examine the angular velocity of the cylinders for a Newtonian fluid from Eq. 16.80b and 16.87b, we get:

$$V_{o, \text{Newt}} = \Omega_{o, \text{Newt}} R = \frac{T}{4\pi\mu LR} \left(\frac{1-a^2}{a^2} \right) \Rightarrow \Omega_{o, \text{Newt}} = \frac{T}{4\pi\mu LR^2} \left(\frac{1-a^2}{a^2} \right) \quad (16.90a)$$

$$V_{i, \text{Newt}} = \Omega_{i, \text{Newt}} aR = \frac{T}{4\pi\mu LR} \left(\frac{a^2-1}{a} \right) \Rightarrow \Omega_{i, \text{Newt}} = -\frac{T}{4\pi\mu LR^2} \left(\frac{1-a^2}{a^2} \right) \quad (16.90b)$$

Equation 16.90 shows that under the same applied torque, the angular velocity for both the outer rotating cylinder and the inner rotating cylinder will be equal in magnitude. The difference in the sign is a result of our assumption of a positively oriented shear stress on the material surface at the inner radius. In reality, the inner material surface has a negatively-directed normal relative to r , thus a positive orientation for the shear would point in the negative θ direction, and be considered a negative torque. Thus, the angular velocities of Eq. 16.90 will be the same.

16.5.2.2 Poiseuille Flow in Circular Duct

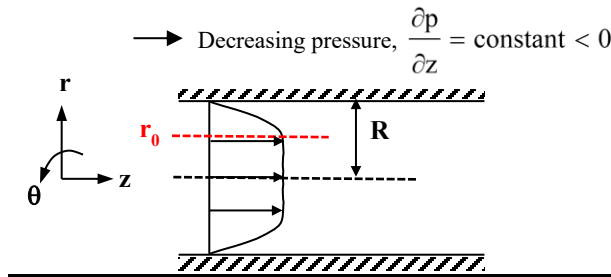


Figure 16.17 Geometry for Poiseuille flow of ideal Bingham plastic in a circular duct

For a fully-developed Poiseuille flow of an ideal Bingham fluid in a circular duct, as shown in figure 16.17, there is no motion in the r and θ -directions, but only in the streamwise z -direction, and the governing equations reduce to the z -direction momentum equation.

$$\frac{\partial v_z}{\partial t} + v_r \frac{\partial v_z}{\partial r} + \frac{v_\theta}{r} \frac{\partial v_z}{\partial \theta} + v_z \frac{\partial v_z}{\partial z} = -\frac{1}{\rho} \frac{\partial p}{\partial z} + g_z + \frac{1}{\rho} \left[\frac{1}{r} \frac{\partial}{\partial r} (r\tau_{rz}) + \frac{1}{r} \frac{\partial \tau_{\theta z}}{\partial \theta} + \frac{\partial \sigma_{zz}}{\partial z} \right] \quad (16.123d)$$

Since this is a steady, fully-developed flow, the velocity field is given by $v_z = f(r)$, Eq. 16.123d further reduces to a balance between shear stress and pressure:

$$\frac{1}{r} \frac{d}{dr} (r\tau_{rz}) = \frac{\partial p}{\partial z} \quad (16.91)$$

For a Poiseuille flow, $\frac{\partial p}{\partial z} = \text{constant}$ (as discussed in section 6.4.1), which allows Eq. 16.91 to be rewritten as:

$$\frac{d}{dr} (r\tau_{rz}) = \frac{\partial p}{\partial z} r \quad (16.92)$$

Integrating Eq. 16.92 once yields:

$$\tau_{rz} = \frac{\partial p}{\partial z} \frac{r}{2} + \frac{C_1}{r} \quad (16.93)$$

To determine the constant C_1 in Eq. 16.93, we need to consider how an ideal Bingham plastic will behave for Poiseuille flow in a duct. Like the parallel plate Poiseuille flow of Section 16.5.1.2 (and Newtonian Poiseuille flow, Section 6.4.2), the location of the highest shear stresses, and thus the location where an ideal Bingham plastic first begins to behave as a fluid will be adjacent to the cylinder wall, $r = R$, with the shear stresses decreasing away from the duct wall. The criteria for fluid behavior to occur is $\tau_{rz} > \tau_0$. Therefore, if the wall shear stress, τ_{rz} , is greater than the yield stress, τ_0 , the material in some region adjacent to the wall will behave as a fluid. The extent of this fluid region will be $r_0 \leq r \leq R$, where we designate r_0 as the yield radius, similar to the yield location, y_0 , that we employed for parallel plate flow in Section 16.5.1.2. We hypothesize r_0 as the location where $\tau_{rz} = \tau_0$, and the material ceases to behave as a fluid, and behaves as a solid.

For a Bingham fluid behaving as a solid, Eq. 16.46a specifies that:

$$\dot{\epsilon}_{rz} = \left(\frac{dv_z}{dr} \right) = 0 \quad \Rightarrow \quad , \text{ when } \tau_{rz} < \tau_0 \quad (\text{assuming } \tau_0 > 0)$$

Thus, the solid behavior region where $\tau_{rz} < \tau_0$, must behave as a solid, moving uniformly at a constant velocity as a plug flow, as shown in the central portion of figure 16.17. The extent of this plug flow region will be $0 \leq r \leq r_0$.

To determine where r_0 occurs, we perform a force balance on the region $0 \leq r \leq r_0$, similar to what we did in Section 16.5.1.2, recognizing that $\tau_{rz} = \tau_0$ at $r = r_0$, and $\tau_{rz} = 0$ at $r = 0$. The result of that force balance is:

$$\tau_0 = \frac{\partial p}{\partial z} \frac{r_0}{2}$$

Solving for r_0 gives:

$$r_0 = \frac{2\tau_0}{\left(\frac{\partial p}{\partial z}\right)} \quad (16.94)$$

Equation 16.94 indicates that the location of r_0 is a direct function of the ratio of the yield stress to the applied pressure gradient. In particular, note that r_0 must be less than R (i.e. $\frac{\partial p}{\partial z} > \frac{2\tau_0}{R}$) in order for any of the material to behave as a fluid.

Therefore, a Poiseuille flow of an ideal Bingham plastic will have two regions of behavior:

- 1) for $0 \leq r \leq r_0$, $\tau_{rx} \leq \tau_0$, the material will move as a solid at $v_z = \text{constant}$ as a plug flow, and
- 2) for $r_0 \leq r \leq R$, $\tau_{rx} > \tau_0$, the material will move as a fluid with $v_z = v_z(r)$.

Within the fluid region $r_0 \leq r \leq R$, and $\tau_{rx} > \tau_0$, Eq. 16.93 applies:

$$\tau_{rz} = \frac{\partial p}{\partial z} \frac{r}{2} + \frac{C_1}{r}$$

To determine the constant C_1 , we note that Eq. 16.46a requires that within the solid plug flow region that $\frac{dv_z}{dr} = 0$ when $\tau_{rz} < \tau_0$. And since the derivative of v_z , i.e. $\frac{dv_z}{dr}$, must be continuous within the ideal Bingham plastic, the condition that $\frac{dv_z}{dr} = 0$ for the solid material in the region $0 \leq r \leq r_0$, must also apply for the fluid behavior material at the interface $r = r_0$. To apply this condition, we substitute Eq. 16.46b, $\tau_{rz} = \mu \left(\frac{dv_z}{dr} \right) + \tau_0$, into Eq. 16.93 for the fluid region behavior, then substitute from Eq. 16.94 for τ_0 :

$$\tau_{rz} = \frac{\partial p}{\partial z} \frac{r}{2} + \frac{C_1}{r} = \mu_B \left(\frac{dv_z}{dr} \right) + \tau_0 = \mu_B \left(\frac{dv_z}{dr} \right) + \frac{\partial p}{\partial z} \frac{r_0}{2}$$

Solving for $\frac{dv_z}{dr}$:

$$\frac{dv_z}{dr} = \frac{1}{2\mu_B} \frac{\partial p}{\partial z} (r - r_0) + \frac{C_1}{\mu_B r}$$

Applying the boundary condition of $\frac{dv_z}{dr} = 0$ at $r = r_0$, we have that $C_1 = 0$, which gives;

$$\frac{dv_z}{dr} = \frac{1}{2\mu_B} \frac{\partial p}{\partial z} (r - r_0)$$

Integrating gives:

$$v_z = \frac{1}{2\mu} \frac{\partial p}{\partial z} \left[\frac{r^2}{2} - r_0 r \right] + C_2 \quad (16.95)$$

Applying the boundary condition $v_z = 0$ at $r = R$ to Eq. 16.95, and solving for C_2 :

$$C_2 = -\frac{1}{2\mu_B} \frac{\partial p}{\partial z} \left[\frac{R^2}{2} - r_0 R \right]$$

Substituting for C_2 and simplifying gives:

$$v_z = \frac{1}{2\mu_B} \frac{\partial p}{\partial z} \left[\frac{r^2}{2} - \frac{R^2}{2} \right] + \frac{1}{2\mu_B} \frac{\partial p}{\partial z} r_0 [R - r] \quad (16.96)$$

Defining $r^* = \frac{r}{R}$, and letting $v_{z,r_0^*} = v_z(r^*, r_0^*)$, since the v_z velocity profile will be a function of r_0^* as well as r^* , we rewrite Eq. 16.96 as:

$$v_{z,r_0^*} = \frac{R^2}{4\mu_B} \frac{\partial p}{\partial z} \left[(r^{*2} - 1) + 2r_0^*(1 - r^*) \right] \quad (16.97a)$$

The material velocity will reach a maximum at the interface between the fluid and solid behavior, with $v_z = v_{z,r_0^*,\max}$ at $r^* = r_0^*$, which will also be the velocity of the material “plug” in the central portion of the circular duct:

$$v_{z,r_0^*,\max} = \frac{R^2}{4\mu_B} \frac{\partial p}{\partial z} \left[(r_0^{*2} - 1) + 2r_0^*(1 - r_0^*) \right]$$

which reduces to:

$$v_{z,r_0^*,\max} = -\frac{R^2}{4\mu_B} \frac{\partial p}{\partial z} (r_0^* - 1)^2 \quad (16.97b)$$

Note that $\frac{\partial p}{\partial z} < 0$ will give a flow in the positive z direction, thus Eq. 16.97 will yield positive velocities for pressure decreasing in the z direction.

Defining $v_{z,r_0^*}^* = \frac{v_{z,r_0^*}}{v_{z,r_0^*,\max}}$ gives:

$$v_{z,r_0^*}^* = \frac{v_{z,r_0^*}}{v_{z,r_0^*,\max}} = \frac{[(1-r^{*2}) + 2r_0^*(r^*-1)]}{(r_0^*-1)^2} \quad \text{for } r_0^* < r^* < 1 \quad (16.98a)$$

And

$$v_{z,r_0^*}^* = 1 \quad \text{for } 0 < r^* < r_0^* \quad (16.98b)$$

Equation 16.98 shows how an ideal Bingham fluid velocity profile varies relative to the maximum centerline (or plug velocity) for the respective r_0^* value. Figure 16.18 is a series of velocity profiles of $v_{z,r_0^*}^*$ vs. r^* for a range of r_0^* values, $0 \leq r_0^* \leq 1$.

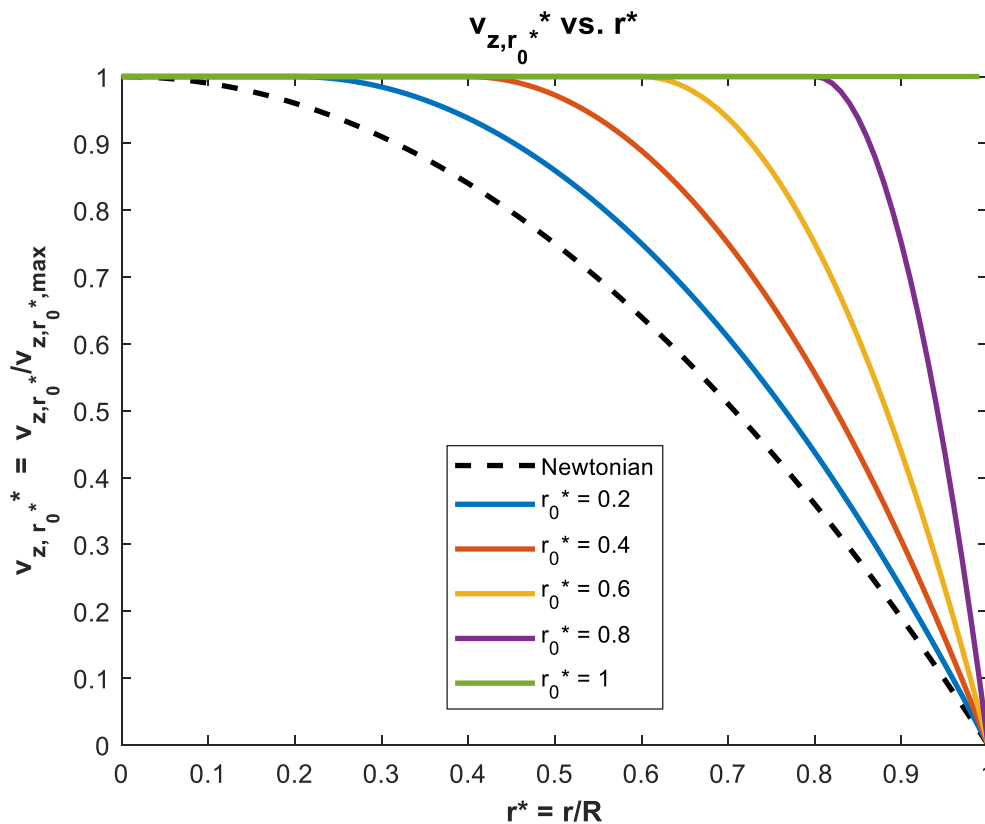


Figure 16.18 Ideal Bingham plastic flow in a circular duct. Normalized on the maximum velocity for respective values of the yield radius, $r_0^* = \frac{2\tau_0}{R \left(\frac{\partial p}{\partial x} \right)}$.

As figure 16.18 shows, for a yield location very near the wall ($r_0^* \approx 1$), the material profile is essentially a flat plug flow. However, as the yield radius decreases (i.e. the pressure gradient

increases), the profile displays a wider region of fluid-like behavior, with the extent of the plug flow region decreasing. Potentially, if the pressure gradient gets quite large, $\frac{\partial p}{\partial x} \gg \frac{2\tau_0}{R}$, the yield location will become quite small, and the flow will approach Newtonian flow behavior ($r_0^* \approx 0$).

While Figure 16.18 is instructive regarding the shape of the velocity profiles, it does not show how the yield radius affects the behavior of the material relative to a comparable Newtonian fluid. As we did in Section 16.4.2.2, we can compare the behavior of an ideal Bingham fluid to a Newtonian fluid with the same pressure gradient and fluid viscosity.

For a Newtonian fluid, $\tau_0 = 0$, which gives $r_0^* = 0$, Eq. 16.97b gives:

$$v_{z,\text{Newt,max}} = -\frac{R^2}{4\mu} \frac{\partial p}{\partial x} \quad (16.99)$$

If we again assume equivalent pressure gradients and fluid viscosities ($\mu_B = \mu$), we can compare velocity profiles for a range of ideal Bingham fluids relative to a Newtonian fluid. Thus, dividing Eq. 16.97a by Eq. 16.99, we obtain:

$$v_{z,\text{rel}}^* = \frac{v_{z,r_0^*}}{v_{z,\text{Newt,max}}} = \left[(1 - r^{*2}) + 2r_0^*(r^* - 1) \right] \quad \text{for } r_0^* < r^* < 1 \quad (16.100a)$$

and

$$v_{z,\text{rel,max}}^* = \frac{v_{z,r_0^*,\text{max}}}{v_{z,\text{Newt,max}}} = (r_0^* - 1)^2 \quad \text{for } 0 < r^* < r_0^* \quad (16.100b)$$

Equation 16.100 gives the velocity profile behavior relative to a pure Newtonian fluid, with the same pressure gradient and fluid viscosity. Figure 16.19 shows a series of velocity profiles of $v_{z,\text{rel}}^*$ vs. r^* for a range of r_0^* values, $0 \leq r_0^* \leq 1$.

Figure 16.19 illustrates that fluid behavior does not initiate if the pressure gradient is less than the yield stress, $r_0^* \geq 1$ ($r_0^* = 1$, the green line, represents all cases for $r_0^* \geq 1$). As the pressure gradient increases relative to the yield stress, τ_0 , r_0^* is reduced, expanding the region of fluid behavior. This results in an increase in the maximum velocity, a reduction in the extent of the solid plug-flow region, and a commensurate increase in the volume flowrate.

As a third comparison, we examine how the volume flowrate and pressure gradient of an ideal Bingham plastic fluid behave relative to a Newtonian flow. To do this, we calculate the volume flowrate, $Q_{r_0^*}$, by integration of Eq. 16.97 across the tube $0 \leq r^* \leq 1$.

$$Q_{r_0^*} = \int_{r=0}^{r=R} v_z 2\pi r dr = 2\pi R^2 \int_{r^*=0}^{r^*=r_0^*} v_{z,r_0^*,\text{max}} r^* dr^* + 2\pi R^2 \int_{r^*=r_0^*}^{r^*=1} v_{z,r_0^*} r^* dr^*$$

$$Q_{r_0^*} = -\frac{\pi R^4}{2\mu_B} \frac{\partial p}{\partial x} \left[\int_{r^*=0}^{r^*=r_0^*} (r_0^* - 1)^2 r^* dr^* + \int_{r^*=r_0^*}^{r^*=1} [(1 - r^{*2}) + 2r_0^*(r^* - 1)] r^* dr^* \right]$$

$$Q_{r_0^*} = -\frac{\pi R^4}{2\mu_B} \frac{\partial p}{\partial x} \left[\left[(r_0^* - 1)^2 \frac{r^{*2}}{2} \right]_{r^*=0}^{r^*=r_0^*} + \left[\left(\frac{r^{*2}}{2} - \frac{r^{*4}}{4} \right) + 2r_0^* \left(\frac{r^{*3}}{3} - \frac{r^{*2}}{2} \right) \right]_{r^*=r_0^*}^{r^*=1} \right]$$

Which yields a final solution for the volume flowrate, $Q_{r_0^*}$, as:

$$Q_{r_0^*} = -\frac{\pi R^4}{24\mu_B} \frac{\partial p}{\partial x} [r_0^{*4} - 4r_0^* + 3] \tag{16.101}$$

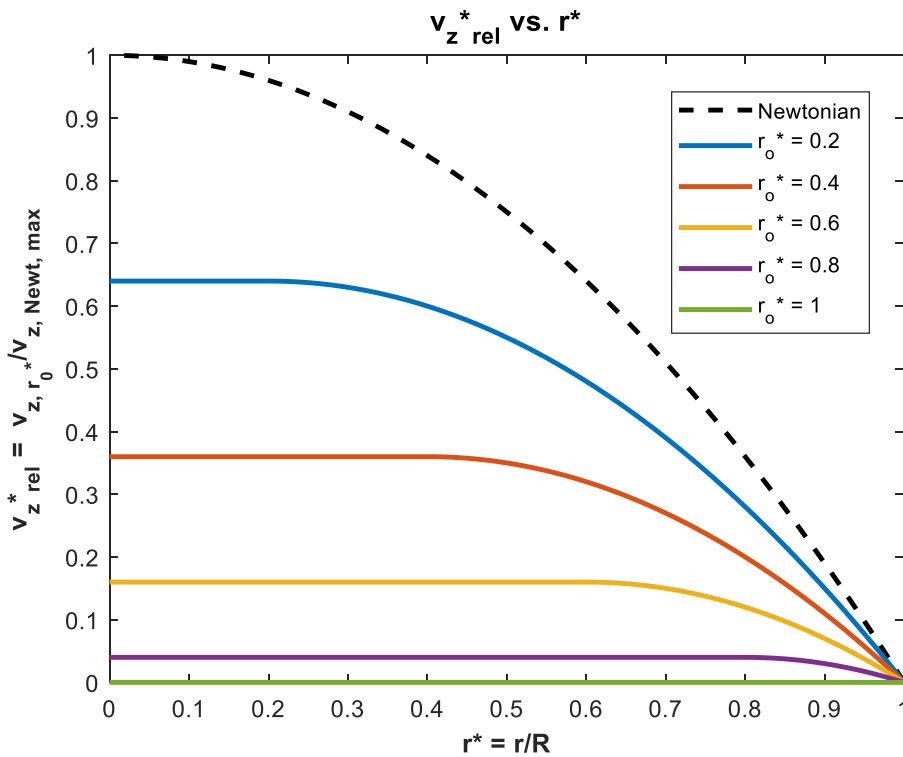


Figure 16.19 Ideal Bingham plastic Poiseuille flow in a circular duct for a series of yield radii, r_0^* ; normalized on the maximum (centerline) velocity for a Newtonian fluid with the same pressure gradient and fluid viscosity. $r_0^* = \frac{2\tau_0}{R \left(\frac{\partial p}{\partial x} \right)}$

As a check on Eq. 16.101, we note that when $r_0^* = 0$, the fluid would behave as a Newtonian fluid, so:

$$Q_{Newt} = -\frac{\pi R^4}{24\mu_B} \frac{\partial p}{\partial x} [3] = -\frac{\pi R^4}{8\mu_B} \frac{\partial p}{\partial x} \tag{16.102}$$

Equation 16.102 is the same as Eqn. 6.62 in Section 6.4.1.

To compare the respective flow rates, I take the ratio of $Q_{r_0^*}$ to Q_{Newt} :

$$Q_{r_0^*,rel} = \frac{Q_{r_0^*}}{Q_{Newt}} = \frac{1}{3}(r_0^{*4} - 4r_0^* + 3) \tag{16.103}$$

Equation 16.103 gives the volume flowrate for an ideal Bingham plastic relative to a Newtonian fluid with identical pressure gradient and fluid viscosity. A plot of $Q_{r_0^*,rel}$ vs. r_0^* for $0 \leq r_0^* \leq 1$ is shown in figure 16.20(a).

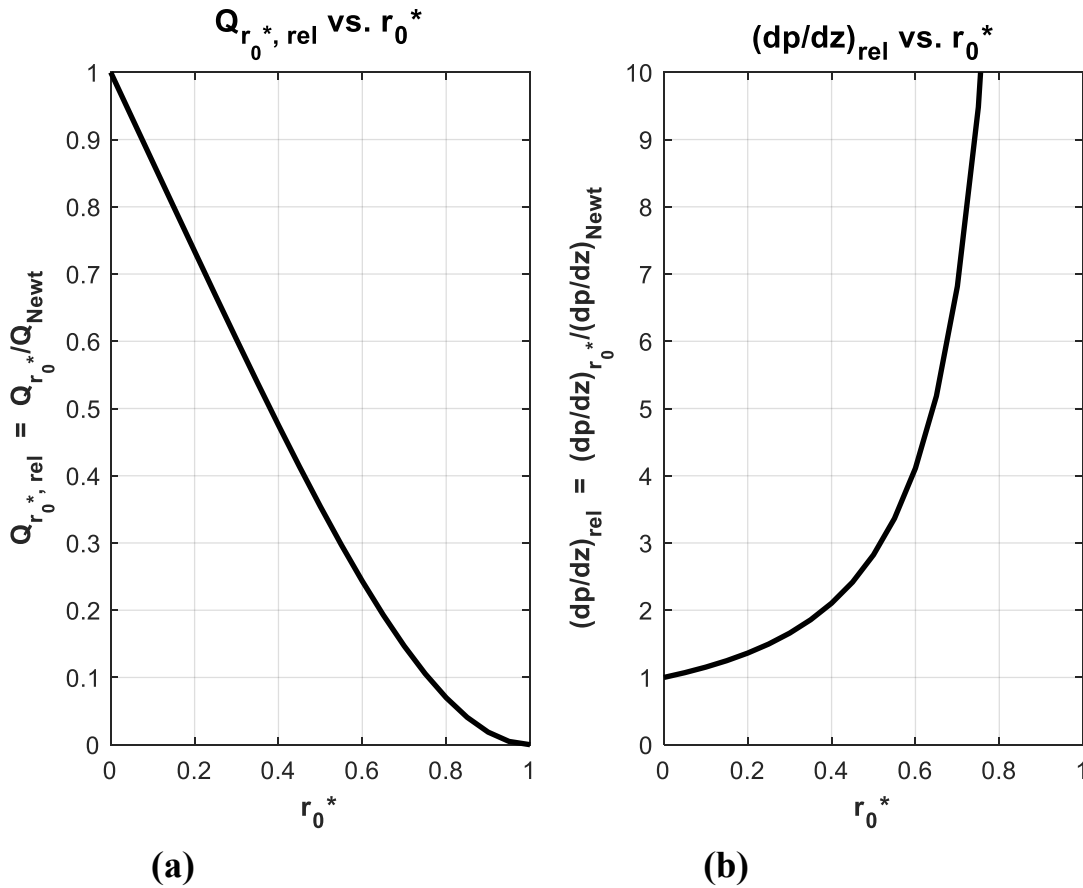


Figure 16.20 Comparisons of ideal Bingham plastic volume flowrate and pressure gradient to a comparable Newtonian fluid versus r_0^* -- Poiseuille circular duct flow.

- (a) $Q_{r_0^*,rel}$, assuming identical pressure gradient and fluid viscosity;
- (b) $(\partial p/\partial z)_{rel}$, assuming identical volume flowrate and fluid viscosity.

$$r_0^* = \frac{2\tau_0}{R(\partial p/\partial z)}$$

To examine pressure gradient variations, we solve Eq. 16.101 for the pressure gradient, and let $Q = Q_{r_0^*}$:

$$\left. \frac{\partial p}{\partial z} \right|_{r_0^*} = -\frac{24\mu_B}{\pi R^4} \frac{Q}{(r_0^{*4} - 4r_0^* + 3)} \quad (16.104)$$

For a Newtonian fluid, $r_0^* = 0$, Eq. 16.104 gives:

$$\left. \frac{\partial p}{\partial z} \right|_{\text{Newt}} = -\frac{8\mu Q}{\pi R^4} \quad (16.105)$$

To compare the respective pressure gradient at identical volume flowrates, we again assume identical fluid viscosities, and take the ratio of Eq. 16.104 to Eq. 16.105:

$$\left. \frac{\partial p}{\partial z} \right|_{\text{rel}} = \frac{\left. \frac{\partial p}{\partial z} \right|_{r_0^*}}{\left. \frac{\partial p}{\partial z} \right|_{\text{Newt}}} = \frac{3Q}{(r_0^{*4} - 4r_0^* + 3)} \quad (16.106)$$

A plot of $\left. \frac{\partial p}{\partial z} \right|_{\text{rel}}$ vs. r_0^* for $0 \leq r_0^* \leq 1$ is shown in figure 16.20b.

Figure 16.20(a) shows that the flowrate of an ideal Bingham plastic will always be less than that of a comparable Newtonian fluid with the same pressure gradient and fluid viscosity. The thinner the fluid region (larger r_0^* , and larger yield stress, τ_0), the lower the flowrate. The explanation for this behavior is the same as for the parallel plate flow of section 16.5.1.2. Applying a force balance at the wall of the duct, we can show that:

$$\left. \frac{dv_z}{dr} \right|_{\text{wall}} = \frac{1}{\mu_B} \left(\frac{\partial p}{\partial z} \frac{R}{2} - \tau_0 \right) = \frac{\partial p}{\partial z} \frac{R}{2\mu_B} (1 - r_0^*) \quad \text{for } r_0^* \leq 1 \quad (16.107)$$

Equation 16.107 shows that the slope of the velocity profile at the wall ($r = R$) will be

$\left. \frac{dv_z}{dr} \right|_{\text{wall}} = 0$ (no flow) until $\frac{\partial p}{\partial z} \frac{R}{2} > \tau_0$ or $r_0^* \leq 1$. When the pressure gradient exceeds the yield stress, which makes $r_0^* < 1$, a region of material adjacent to the cylinder wall, $r_0^* \leq r^* \leq 1$, will behave as a fluid. Eq. 16.107 indicates that the slope of the velocity at the wall will become non-zero (the sign depending on the direction of the pressure gradient), $\left. \frac{dv_z}{dr} \right|_{\text{wall}} > 0$, and the material (solid and fluid portions) will begin to move, collectively, as shown in figure 16.19. As the pressure gradient, $\frac{\partial p}{\partial z}$, increases further, the yield radius, r_0^* , will decrease accordingly. This reduction in the yield radius results in an expanded region of fluid behavior – which allows the collective material to move more rapidly, as shown by the velocity profiles of figure 16.19, and the relative flowrate of figure 16.20a.

Of course, the larger the yield stress, τ_0 , the more the pressure gradient has to work to overcome τ_0 , and the less work it can do to move the fluid. This is shown clearly in, figure 16.20b, which illustrates that the thinner the fluid region (i.e. larger r_0^* value), the larger the relative pressure gradient must be to maintain the same flow rate. For example, if $r_0^* = 0.6$, for which 64% of the material behaves as a fluid, the comparative pressure gradient is 4 times the Newtonian. And by $r_0^* = 0.8$, where only 36% of the material behaves as a fluid, the comparative pressure gradient is more than 10 times the Newtonian. Of course, as the yield radius approaches the duct wall, the pressure gradient required to maintain the same flowrate grows dramatically.

Similar to the case of Poiseuille flow between parallel plates, Section 16.5.1.2, the power required to move the material will be roughly $\text{Power} \approx \frac{\partial p}{\partial x} Q$. Therefore, the pumping power required to maintain a constant flowrate will behave essentially the same as the pressure gradient in figure 16.20b.

16.6 Flat-Plate Laminar Boundary Layers

Because of the non-linearity of the shear stress behavior in non-Newtonian fluids, computation of boundary layer behavior becomes much more involved, and exact solutions of the equations of motion require the use of advanced numerical techniques. However, we can make use of the momentum integral equation that we developed in Section 14.2, and a similarity velocity profile approximation like the one we applied in Section 14.2.2, to develop approximate solutions for the boundary characteristics for both power law and ideal Bingham plastic fluids. Moreover, while these solutions are not exact, they have been shown [[Acivios et al.\(1960\)](#)] to compare to the results of exact solutions to within $\pm 10\%$.

Applying the same order-of-magnitude analysis approach we employed in section 13.2.1 to Eqs. 16.122a (continuity), 16.122b (x-direction momentum), and 16.122c (y-direction momentum), we can reduce the equations to:

$$u \frac{\partial u}{\partial x} + v \frac{\partial u}{\partial y} = -\frac{1}{\rho} \frac{\partial P}{\partial x} + \frac{1}{\rho} \frac{\partial \tau_{yx}}{\partial y} \quad (16.109a)$$

and

$$\frac{\partial u}{\partial x} + \frac{\partial v}{\partial y} = 0 \quad (16.109b)$$

These are the boundary layer equations for a non-Newtonian fluid, but the shear stress will be a non-linear function of velocity. However, integrating Eq. 16.109a across the boundary layer, as we did in section 14.2, we can derive a momentum integral equation for a non-Newtonian fluid as:

$$\frac{d\theta}{dx} + (\delta^* + 2\theta) \frac{1}{U_\infty} \frac{dU_\infty}{dx} = \frac{\tau_w}{\rho U_\infty^2} \quad (16.110)$$

Note that Eq. 16.110 is the same as Eq. 14.11 for a Newtonian fluid. Why aren't Eqs. 16.110 and 14.11 different? Recall that in section 14.2 we integrated the momentum equation across the boundary layer from $y = 0$ to $y = \delta$. Performing the same integration for a non-Newtonian fluid yields the same results for the momentum change terms. Integrating the shear stress term, the last term in Eq. 16.120a, across the boundary layer gives:

$$\int_{y=0}^{y=\delta} \frac{\partial \tau_{yx}}{\partial y} dy = \tau_{yx} \Big|_{y=0}^{y=\delta} = \tau_{yx} \Big|_{y=\delta} - \tau_{yx} \Big|_{y=0} = 0 - \tau_w = -\tau_w$$

Since the shear stress limits of a non-Newtonian boundary layer are the same as those for a Newtonian fluid, this term integrates to the same term, the wall shear stress, τ_w , like in Section 14.2. A transposition in Eq. 14.10 makes the sign of τ_w positive in Eq. 16.110.

As we did in section 14.2.2, we will employ an approximate similarity velocity profile assuming a similarity parameter of $\lambda = \frac{y}{\delta}$, calculate the respective boundary layer parameters in term of δ , and then use the appropriate non-Newtonian relationship for τ_w to integrate Eq. 16.110 for the development of a flat-plate boundary layer thickness, $\delta = f(x)$.

Our Table 14.1 in Chapter 14 shows that for a Newtonian fluid the approximate similarity velocity profile that best compares to the exact Blasius solution was a third order equation of the form:

$$\frac{u}{U_\infty} = 1.5\lambda - 0.5\lambda^3 = 1.5\left(\frac{y}{\delta}\right) - 0.5\left(\frac{y}{\delta}\right)^3 \quad (16.111)$$

We will assume that this will be an equally good approximation for our non-Newtonian fluids as well. Employing Eq. 16.111, we calculate the relative displacement and momentum thickness as:

$$\begin{aligned} \delta^* &= \int_0^\delta \left(1 - \frac{u}{U_\infty}\right) dy = \int_0^{\lambda=1} \left(1 - \frac{u}{U_\infty}\right) \delta d\lambda \quad \text{where } d\lambda = \frac{dy}{\delta} \text{ and } dy = \delta d\lambda \\ &= \delta \int_0^1 \left(1 - \frac{3}{2}\lambda + \frac{1}{2}\lambda^3\right) d\lambda = \delta \left[\lambda - \frac{3}{4}\lambda^2 + \frac{1}{8}\lambda^4 \right]_0^1 = \frac{3\delta}{8} \end{aligned} \quad (16.112a)$$

Likewise,

$$\theta = \int_0^\delta \frac{u}{U_\infty} \left(1 - \frac{u}{U_\infty}\right) dy = \delta \int_0^{\lambda=1} \frac{u}{U_\infty} \left(1 - \frac{u}{U_\infty}\right) d\lambda$$

$$= \delta \int_0^1 \left(\frac{3}{2}\lambda - \frac{1}{2}\lambda^3 \right) \left(1 - \frac{3}{2}\lambda + \frac{1}{2}\lambda^3 \right) d\lambda = \frac{39}{280} \delta \quad (16.112b)$$

If we only consider a flat plate boundary layer, then $U_\infty = \text{constant}$, and thus $\frac{dU_\infty}{dx} = 0$, this reduces Eq. 16.110 to:

$$\frac{d\theta}{dx} = \frac{\tau_w}{\rho U_\infty^2} \quad (16.113)$$

Substituting Eq. 16.112b into Eq. 16.113 gives:

$$\frac{39}{280} \frac{d\delta}{dx} = \frac{\tau_w}{\rho U_\infty^2} \quad (16.114)$$

To integrate Eq. 16.114 for δ , we need to employ the appropriate constituent equation for τ_w , which we do in the next two sections for (1) a power-law fluid, and (2) an ideal Bingham plastic.

16.6.1 Flat Plate Boundary Layer for a Power-Law Fluid

In order to integrate Eq. 16.114, we need to have a constitutive equation for the wall shear stress in terms of the velocity behavior, which for a power-law fluid (in Cartesian coordinates) is Eq. 16.4, for $y = 0$:

$$\tau_w = \tau_{yx}|_{y=0} = K \left(\frac{\partial u}{\partial y} \Big|_{y=0} \right)^n$$

We determine the derivative, $\frac{\partial u}{\partial y} \Big|_{y=0}$, from our assumed third-order velocity profile of Eq. 16.110 as:

$$\frac{du}{dy} \Big|_{y=0} = \frac{1.5U_\infty}{\delta}$$

Thus, the wall shear stress becomes:

$$\tau_w = K \left(\frac{1.5U_\infty}{\delta} \right)^n \quad (16.115)$$

Substituting Eq. 16.115 into Eq. 16.114, we have:

$$\frac{39}{280} \frac{d\delta}{dx} = \frac{K}{\rho U_\infty^2} \left(\frac{1.5U_\infty}{\delta} \right)^n = \frac{K(1.5)^n}{\rho U_\infty^{2-n} \delta^n}$$

$$\delta^n d\delta = \frac{280K(1.5)^n}{39\rho U_\infty^{2-n}} dx$$

Letting $\delta = 0$ at $x = 0$, and integrating:

$$\frac{\delta^{n+1}}{n+1} = \frac{280K(1.5)^n}{39\rho U_\infty^{2-n}} x$$

or

$$\delta = \left[\frac{280K(n+1)(1.5)^n}{39\rho U_\infty^{2-n}} x \right]^{\frac{1}{n+1}}$$

Scaling δ on x , we have:

$$\frac{\delta}{x} = \left[\frac{7.179K(n+1)(1.5)^n}{\rho U_\infty^{2-n} x^n} \right]^{\frac{1}{n+1}} = \left[7.179(n+1)(1.5)^n \right]^{\frac{1}{n+1}} \left(\frac{K}{\rho U_\infty^{2-n} x^n} \right)^{\frac{1}{n+1}}$$

While this equation looks quite ugly, the first term is simply a function of n , and the second term is a Reynolds number for a power-law fluid. Thus, we define a relationship as:

$$\frac{\delta}{x} = \frac{F(n)}{\mathbf{Re}_{x_pl}^{\frac{1}{n+1}}} \quad \text{where } F(n) = \left[7.179(n+1)(1.5)^n \right]^{\frac{1}{n+1}} \quad \text{and } \mathbf{Re}_{x_pl} = \frac{\rho U_\infty^{2-n} x^n}{K} \quad (16.116)$$

For a given K and n , we can calculate $\frac{\delta}{x}$ for any \mathbf{Re}_{x_pl} using Eq. 16.116. Note that the form of the Reynolds number for a power-law fluid appears different from a Newtonian flow. However, this is the result of K having units of Pa s^n (i.e. $\frac{F}{L^2 t^n}$), where F = force, L = length, and t = time. So, if we consider the units of \mathbf{Re}_{x_pl} for Eq. 16.115 (noting that $F = \frac{ML}{t^2}$), we have:

$$\mathbf{Re}_{x_pl} = \frac{\rho U_\infty^{2-n} x^n}{K} \triangleq \frac{\left(\frac{M}{L^3}\right) \left(\frac{L}{t}\right)^{2-n} (L)^n}{\left(\frac{F}{L^2 t^n}\right) \left(\frac{ML}{Ft^2}\right)} = \frac{\left(\frac{M}{Lt^{2-n}}\right)}{\left(\frac{M}{Lt^{2-n}}\right)} = 1$$

So, \mathbf{Re}_{x_pl} is a dimensionless power-law Reynolds number. To verify that Eq. 16.116 is correct, if we let $n = 1$ and $K = \mu$, which is a Newtonian fluid, Eq. 16.116 becomes:

$$\frac{\delta_{\text{Newton}}}{x} = \frac{4.641}{\sqrt{\mathbf{Re}_{x_Newton}}} \quad \text{and } \mathbf{Re}_{x_Newton} = \frac{\rho U_\infty x}{\mu}$$

This is the same result we obtained for a Newtonian flow in Table 14.1 using the same similarity velocity profile of Eq. 16.110.

To determine the wall shear stress for a power-law fluid we substitute Eq. 16.116 back into Eq. 16.115:

$$\begin{aligned}\tau_w &= K \left(\frac{1.5U_\infty}{\delta} \right)^n = K \left(\frac{1.5U_\infty \text{Re}_{x_pl}^{\frac{1}{n+1}}}{F(n)x} \right)^n = \left(\frac{1.5}{F(n)} \right)^n \frac{KU_\infty^n \text{Re}_{x_pl}^{\frac{n}{n+1}}}{x^n} \frac{\rho U_\infty^2}{\rho U_\infty^2} \\ &= \rho U_\infty^2 \left(\frac{1.5}{F(n)} \right)^n \left(\frac{K}{\rho U_\infty^{2-n} x^n} \right) \text{Re}_{x_pl}^{\frac{n}{n+1}} = \rho U_\infty^2 \left(\frac{1.5}{F(n)} \right)^n \left(\frac{\text{Re}_{x_pl}^{\frac{n}{n+1}}}{\text{Re}_{x_pl}} \right) = \rho U_\infty^2 \left(\frac{1.5}{F(n)} \right)^n \left(\frac{1}{\text{Re}_{x_pl}^{\frac{1}{n+1}}} \right)\end{aligned}$$

This gives a friction coefficient, c_f , of:

$$c_f = \frac{\tau_{\text{wall}}}{\frac{1}{2}\rho U_\infty^2} = 2 \left(\frac{1.5}{F(n)} \right)^n \left(\frac{1}{\text{Re}_{x_pl}^{\frac{1}{n+1}}} \right) \quad \text{where} \quad \text{Re}_{x_pl} = \frac{\rho U_\infty^{2-n} x^n}{K} \quad (16.117)$$

To check Eq. 16.117, we again let $n = 1$ and $K = \mu$, a Newtonian fluid, and get:

$$F(n) = \left[7.179(n+1)(1.5)^n \right]^{\frac{1}{n+1}} = \left[7.179(1+1)(1.5)^1 \right]^{\frac{1}{2+1}} = 4.641$$

and,

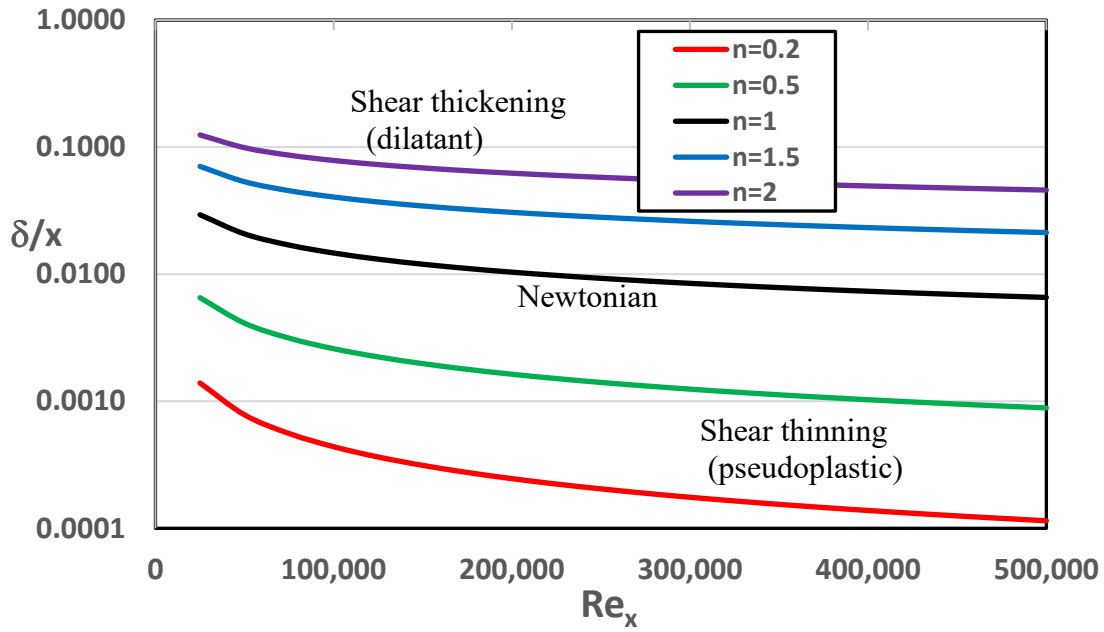
$$\text{Re}_{x_PL} = \frac{\rho U_\infty^{2-n} x^n}{K} = \frac{\rho U_\infty^{2-1} x^1}{\mu} = \frac{\rho U_\infty x}{\mu} = \text{Re}_{x_Newtonian}$$

So,

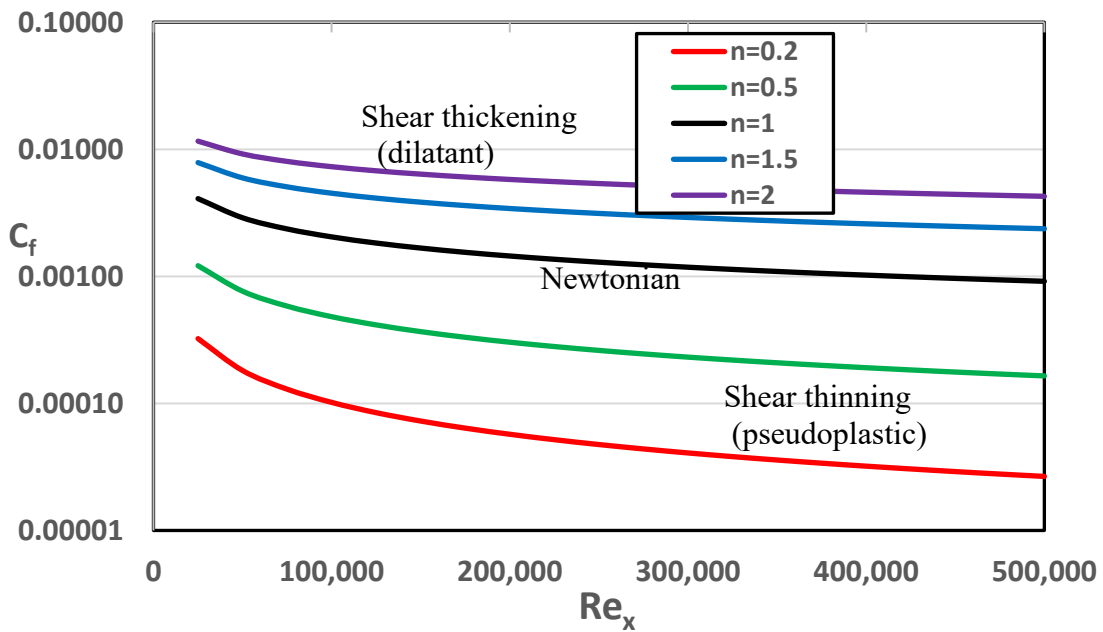
$$c_{f_Newtonian} = \frac{0.646}{\sqrt{\text{Re}_{x_Newtonian}}}$$

This is identical to the c_f shown in table 14.1 obtained for a Newtonian fluid with the same assumed similarity velocity profile, as it should be.

To examine the effect of n on the boundary layer and shear stress for power-law fluids, figure 16.21 shows plots of both $\frac{\delta}{x}$ vs. Re_{x_pl} (Eq. 16.116) and c_f vs. Re_{x_pl} (Eq. 16.117) for selected n values. While the non-dimensional property behavior shown in figure 16.21 would seem to be relatively clear, the irksome properties of power-law fluids make it a bit hard to make clear assessments of comparative behavior, since the n and K values can greatly affect dimensional properties, such as absolute shear stress and physical boundary layer thickness.



(a)



(b)

Figure 16.21 Comparisons of boundary layer characteristics of a power-law fluid as a function of Reynolds number ($Re_x = \frac{\rho U_\infty^{2-n} x^n}{K}$) for selected n values.

(a) $\frac{\delta}{x}$ vs. Re_x (b) c_f vs. Re_x .

What we can observe from figure 16.21 is that at comparable Reynolds numbers, boundary layers for shear thinning fluids ($n < 1$) are thinner and have correspondingly lower friction coefficients than a Newtonian fluid. Conversely, boundary layers for shear thickening fluids ($n > 1$) are thicker and have higher friction coefficients than a Newtonian fluid, again at comparable Reynolds numbers. However, how this relates to comparable distances along a flat plate is not intuitive, since the variations in the K and n values significantly affect the shear stress, making each fluid unique. So, figure 16.21 is suggestive, but not an ideal comparison of power-law fluids. Such comparisons, as pointed out in our examination of power law fluids in section 16.4, require the examination of the specific values of K and n .

An additional observation, is that for shear thickening fluids, δ/x remains greater than what we specified for the approximations we made to reduce the continuity/momentum equations to the boundary layer equations (i.e. $\delta/x < 0.01$), so the shear thickening fluids may not quite satisfy those approximations.

16.6.2 Flat Plate Boundary Layer for an Ideal Bingham fluid

For an ideal Bingham plastic, the constitutive equation for the wall shear stress (in Cartesian coordinates) is Eq. 16.44b, for $y = 0$:

$$\tau_w = \mu_B \left(\frac{\partial u}{\partial y} \Big|_{y=0} \right) + \tau_0$$

We again determine the derivative, $\frac{\partial u}{\partial y} \Big|_{y=0}$, from our assumed third-order velocity profile of Eq.

16.110 as:

$$\frac{du}{dy} \Big|_{y=0} = \frac{1.5U_\infty}{\delta}$$

So, the wall shear stress becomes:

$$\tau_w = \frac{1.5\mu_B U_\infty}{\delta} + \tau_0 \quad (16.118)$$

However, Eq. 16.118 is misleading. When an ideal Bingham plastic is in contact with a flat plate, the wall shear stress must exceed τ_0 in order for the fluid to move and develop a boundary layer. So, a shear stress of $\tau_w > \tau_0$ must be present in order for the outer region material to move at U_∞ . Additionally, since the shear stress away from the wall must be less than or equal to the wall shear stress, the Bingham plastic will not behave as a fluid until $\tau_w > \tau_0$. Until that criteria is met, the Bingham plastic will remain stationary over its entirety. Thus, the outer edge of the boundary layer will be where $\tau = \tau_0$, not $\tau = 0$; the latter is the case only for a

continuously deformable fluid, such as a Newtonian or a non-Newtonian power-law fluid. Thus, the simplified momentum integral equation, Eq. 16.110, must be modified by reassessing the integrated shear stress term in our Eq. 16.109a. Recall that for a fluid with $\tau = 0$ at $y = \delta$, (Newtonian or power-law fluid) we showed that:

$$\int_{y=0}^{y=\delta} \frac{\partial \tau_{yx}}{\partial y} dy = \tau_{yx} \Big|_{y=0}^{y=\delta} = \tau_{yx} \Big|_{y=\delta} - \tau_{yx} \Big|_{y=0} = 0 - \tau_w = -\tau_w$$

However, for a Bingham plastic, the upper boundary condition on the integration will be $\tau = \tau_0$ at $y = \delta$, so our integrated shear stress term will be:

$$\int_{y=0}^{y=\delta} \frac{\partial \tau_{yx}}{\partial y} dy = \tau_{yx} \Big|_{y=0}^{y=\delta} = \tau_{yx} \Big|_{y=\delta} - \tau_{yx} \Big|_{y=0} = \tau_0 - \tau_w$$

This integration makes the momentum integral equation for a Bingham plastic:

$$\frac{d\theta}{dx} + (\delta^* + 2\theta) \frac{1}{U_\infty} \frac{dU_\infty}{dx} = \frac{\tau_0 - \tau_w}{\rho U_\infty^2} \quad (16.119)$$

Thus, the simplified flat plate equation, assuming the same similarity velocity of Eq. 16.111, and substituting from the Bingham plastic constituent Eq. 16.118 into Eq. 16.119 gives:

$$\frac{39}{280} \frac{d\delta}{dx} = \frac{\tau_0 - \tau_w}{\rho U_\infty^2} = \frac{\left(\frac{1.5\mu_B U_\infty}{\delta} \right)}{\rho U_\infty^2} = \frac{1.5\mu_B}{\rho U_\infty \delta}$$

$$\delta d\delta = \frac{420\mu_B}{39\rho U_\infty} dx$$

Again, letting $\delta = 0$ at $x = 0$, integrating, and solving for $\delta(x)$:

$$\delta = 4.641 \sqrt{\frac{\mu_B x}{\rho U_\infty}} = \frac{4.641x}{\sqrt{\frac{\rho U_\infty x}{\mu_B}}} = \frac{4.641x}{\sqrt{\mathbf{Re}_{x-B}}} \quad \text{where} \quad \mathbf{Re}_{x-B} = \frac{\rho U_\infty x}{\mu_B}$$

and

$$\frac{\delta}{x} = \frac{4.641}{\sqrt{\mathbf{Re}_{x-B}}} \quad (16.120)$$

Note that Eq. 16.120 is identical to that obtained for a Newtonian fluid with the same assumed similarity velocity profile, as shown in Table 14.1. While the comparative boundary layer development will be the same as for a Newtonian fluid, as shown on the power-law graph of

figure 6.21, the behavior of the shear stress will differ quite significantly. If we substitute Eq. 16.120 back into Eq. 16.118, the wall shear stress is given by:

$$\tau_w = \frac{1.5\mu_B U_\infty}{\delta} + \tau_0 = \frac{1.5\mu_B U_\infty \sqrt{\text{Re}_{x_B}}}{4.641x} + \tau_0 = \frac{0.323\rho U_\infty^2 \sqrt{\text{Re}_{x_B}}}{\left(\frac{\rho U_\infty x}{\mu_B}\right)} + \tau_0$$

or

$$\tau_w = \frac{0.323\rho U_\infty^2}{\sqrt{\text{Re}_{x_B}}} + \tau_0$$

Which gives a friction coefficient, c_f , of:

$$c_f = \frac{\tau_{\text{wall}}}{\frac{1}{2}\rho U_\infty^2} = \frac{0.646}{\sqrt{\text{Re}_{x_B}}} + \frac{\tau_0}{\frac{1}{2}\rho U_\infty^2} \quad (16.121)$$

Note that Eq. 16.121 is the same equation for c_f as for a Newtonian flow, with the additive resistance due to the material yield stress, τ_0 , which is the wall shear stress required for the Bingham fluid adjacent to the wall to fluidize. Once the boundary layer region “fluidizes,” an ideal Bingham plastic will behave like a Newtonian fluid within the fluid region, but the actual wall shear will be that due to a combination of the fluid shear stress plus the material yield stress τ_0 .

16.7 Conclusion

As illustrated by the examples in sections 16.4, 16.5, and 16.6, non-Newtonian fluids behave markedly different than Newtonian fluids. In addition, the modeling of non-Newtonian fluids can give rise to anomalies, such as the flow consistency index, K , for power-law fluids, which has fractional property units (as a result of fractional values of the fluid behavior index n). This makes it hard to compare power-law fluids, to either a Newtonian fluid or other non-Newtonian fluids, particularly pressure gradient variations for Poiseuille flows, as was discussed at the end of Sections 16.4.1.2 and 16.4.2.2, and comparative boundary layer behavior, as discussed in Section 16.6.1.

Relative comparisons of non-Newtonian fluids to a Newtonian fluid is important, if one is to understand differences in flow behavior. What constitutes an effective presentation of relative effects is reflected by figure 16.16 in Section 16.5.2.1. In that figure, I chose to normalize the relative velocity behavior of Bingham plastic Couette flows for rotating, concentric cylinders to the Newtonian wall velocity, rather than the wall velocity for the particular Bingham plastic material. Recall that since we could not specify a common wall velocity, by necessity we had to assume a value of torque, from which we deduced the corresponding wall velocities. Since the torque was the common parameter for those flows, it seemed most logical to show how the velocity behavior varies relative to a Newtonian fluid under the same applied torque. This form

of presentation in figure 16.16 illustrates both the variation in the shape of the velocity profiles and the retardation of the wall velocity due to the presence of a Bingham plastic yield stress ($\tau_0 > 0$).

So, what if we were to normalize the velocity behavior of the Bingham plastic materials on the respective wall velocities for those materials, instead of on the wall velocity for a comparable Newtonian fluid? Would that form of presentation be as instructive? Figure 16.22 shows a comparison, for $r_i^* = 0.5$, of normalizing Bingham plastic velocity behavior on each material's moving wall velocity (i.e. $v_\theta / V_{\text{wall},r_0^*}$) versus normalizing on the moving wall velocity for a Newtonian fluid (i.e. $v_\theta / V_{\text{wall,Newtonian}}$).

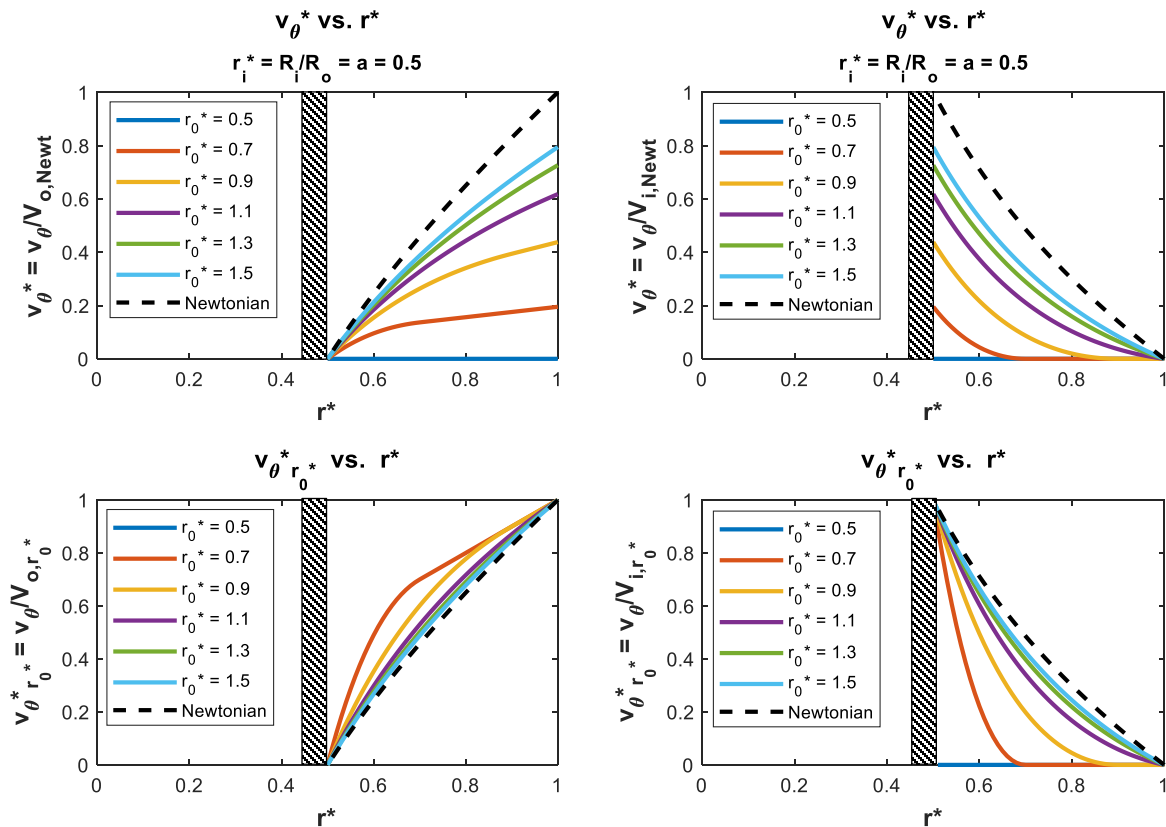


Figure 16.22 Alternative scaling for Couette flow of an ideal Bingham plastic, $r_i^* = 0.5$. Both moving outer wall (left plots) and inner wall (right plots) are shown. Upper plots scaled on $V_{\text{wall,Newtonian}}$ for a Newtonian fluid. Lower plots scaled on V_{wall,r_0^*} for each particular Bingham plastic.

The top row of figure 16.22 shows the normalization of the velocity profiles with respect to the comparable Newtonian wall velocity, as was done in figure 16.16. Using this form of normalization, it is easy to discriminate between the two regions of the flow process—fluid versus solid behavior—and to understand the degree of velocity retardation the moving wall

experiences due to the material yield stress of the Bingham plastic. In contrast, scaling on the actual material wall velocity, as is done for the bottom row of figure 16.22, does not clearly reveal the changes in the velocity behavior between solid and fluid behavior, and does not show the degree of retardation of the wall velocity under the same applied torque. Also, this latter scaling approach cannot effectively represent the stationary material behavior when $r_0^* \leq r_1^*$ (for which $V_{wall, r_0^*} = 0$). This velocity scaling issue illustrates the importance of understanding the method of presentation of relative flow behaviors in order to reveal important physical behavioral changes.

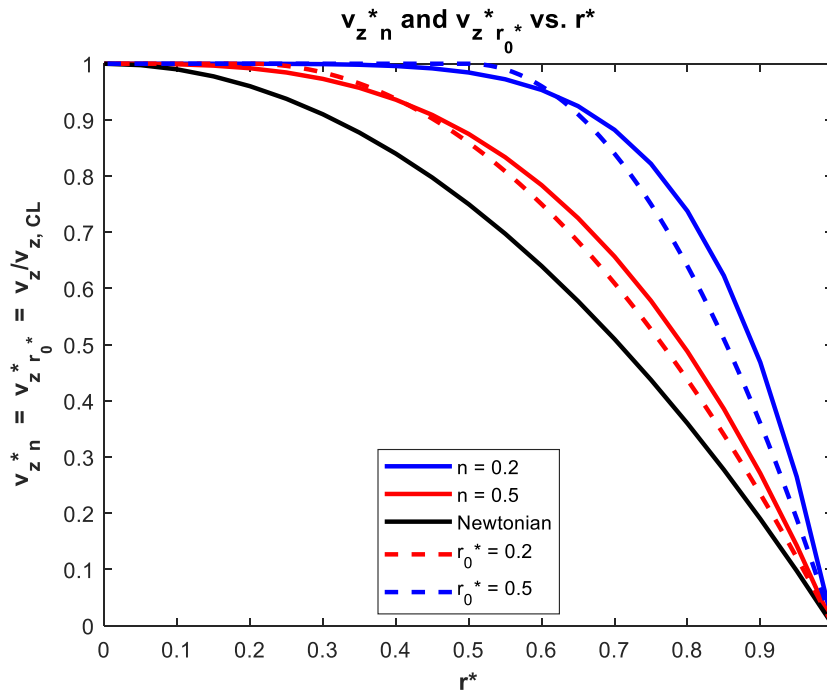


Figure 16.23 Comparison of similar Poiseuille velocity profiles for a power-law fluid and an ideal Bingham plastic flow in a circular duct. Velocities are normalized on the respective centerline velocities for selected values of the power-law fluid behavior index, n , and the Bingham plastic yield radius, $r_0^* = \frac{2\tau_0}{R \left(\frac{\partial p}{\partial x} \right)}$.

In Sections 16.4.1.2 and 16.4.2.2, I mentioned that certain non-Newtonian fluids might demonstrate behavior that could be reasonably described by either a power-law or an ideal Bingham plastic. For example, shear-thinning fluids often display Poiseuille behavior that could be approximated by either model. Figure 16.23 shows such a comparison for Poiseuille flow in a circular tube. Note how the red lines ($n = 0.5$ and $r_0^* = 0.2$) and the blue lines ($n = 0.2$ and $r_0^* = 0.5$) display similar velocity profiles, suggesting that either model might be applicable.

However, while the profiles appear similar, a shear thinning fluid ($n < 1$) will always behave as a fluid under any pressure gradient, whereas if the pressure gradient for a Bingham plastic is reduced such that:

$$r_0^* > 1 \Rightarrow \left(\frac{\partial p}{\partial x} \right) < \frac{2\tau_0}{R}$$

the Bingham plastic will behave as a solid. So, one must be careful to assess the type of behavior the fluid will assume under all conditions.

Additionally, the literature on non-Newtonian fluids is fraught with inconsistencies, due to testing of supposedly similar materials, but which give often markedly different properties, and which may be represented by significantly different models. As pointed out earlier, materials cited in the literature are often subject to variances due to the method of creating the material, the distribution of particle sizes (e.g. in food slurries, such as tomato paste), or vagueness in the constituents (e.g. the composition of particular types of paints). Therefore, caution must be exercised in using tables, such as Table 1 at the end of this chapter, or any other generic table of properties. From a practical sense, it is important to have reliable empirical test results for a particular non-Newtonian material in order to assure the accurate prediction of the material behavior in a particular flow system.

I will close this chapter by noting that we have only touched on two types of rather simple non-Newtonian fluid models, and have examined only simple types of steady state flows. You should be struck by how much more involved the “simple” solutions for a non-Newtonian fluid are than for a Newtonian fluid. Clearly, if we consider more complicated flows, such as exact boundary layer solutions, time-dependent flows, drag, and flows in multi-dimensions, solutions are generally possible only using numerical approaches. The literature is full of such solutions, as well as other manifold non-Newtonian fluid models. Hopefully, understanding the simpler examples covered in this chapter will prepare you to examine, and appreciate, more complicated non-Newtonian flows.

Speaking of complicated flows, we will now transition back to Newtonian fluids, and examine what is the most complicated type of flow behavior, turbulence, which along with the process of transition from laminar to turbulent flow will be the topic of the next, and last, chapter of this book.

16.8 The Governing Equations for Non-Newtonian Fluids

16.8.1 Stresses on a Non-Newtonian Fluid: Cartesian and Cylindrical Coordinates

Note: stresses are listed in terms of the generic deformation rate $\dot{\epsilon}$, and the effective viscosity, μ_e , which is dependent on the non-Newtonian model employed.

$$\begin{aligned}\sigma_{xx} &= -p + 2\mu_e \dot{\epsilon}_{xx} & \tau_{xy} &= \mu_e \dot{\epsilon}_{xy} = \tau_{yx} \\ \sigma_{yy} &= -p + 2\mu_e \dot{\epsilon}_{yy} & \tau_{xz} &= \mu_e \dot{\epsilon}_{xz} = \tau_{zx} \\ \sigma_{zz} &= -p + 2\mu_e \dot{\epsilon}_{zz} & \tau_{yz} &= \mu_e \dot{\epsilon}_{yz} = \tau_{zy} \\ \\ \sigma_{rr} &= -p + 2\mu_e \dot{\epsilon}_{rr} & \tau_{r\theta} &= \mu_e \dot{\epsilon}_{r\theta} = \tau_{\theta r} \\ \sigma_{\theta\theta} &= -p + 2\mu_e \dot{\epsilon}_{\theta\theta} & \tau_{\theta z} &= \mu_e \dot{\epsilon}_{\theta z} = \tau_{z\theta} \\ \sigma_{zz} &= -p + 2\mu_e \dot{\epsilon}_{zz} & \tau_{zr} &= \mu_e \dot{\epsilon}_{zr} = \tau_{rz}\end{aligned}$$

16.8.2 Continuity and Momentum Differential Equations in Cartesian Coordinates

$$\frac{\partial u}{\partial x} + \frac{\partial v}{\partial y} + \frac{\partial w}{\partial z} = 0 \quad (16.122a)$$

$$\frac{\partial u}{\partial t} + u \frac{\partial u}{\partial x} + v \frac{\partial u}{\partial y} + w \frac{\partial u}{\partial z} = -\frac{1}{\rho} \frac{\partial p}{\partial x} + g_x + \frac{1}{\rho} \left[\frac{\partial \sigma_{xx}}{\partial x} + \frac{\partial \tau_{yx}}{\partial y} + \frac{\partial \tau_{zx}}{\partial z} \right] \quad (16.122b)$$

$$\frac{\partial v}{\partial t} + u \frac{\partial v}{\partial x} + v \frac{\partial v}{\partial y} + w \frac{\partial v}{\partial z} = -\frac{1}{\rho} \frac{\partial p}{\partial y} + g_y + \frac{1}{\rho} \left[\frac{\partial \sigma_{xy}}{\partial x} + \frac{\partial \tau_{yy}}{\partial y} + \frac{\partial \tau_{zy}}{\partial z} \right] \quad (16.122c)$$

$$\frac{\partial w}{\partial t} + u \frac{\partial w}{\partial x} + v \frac{\partial w}{\partial y} + w \frac{\partial w}{\partial z} = -\frac{1}{\rho} \frac{\partial p}{\partial z} + g_z + \frac{1}{\rho} \left[\frac{\partial \sigma_{xz}}{\partial x} + \frac{\partial \tau_{yz}}{\partial y} + \frac{\partial \tau_{zz}}{\partial z} \right] \quad (16.122d)$$

16.8.3 Continuity and Momentum Differential Equations in Cylindrical Coordinates

$$\frac{1}{r} \frac{\partial}{\partial r} (r v_r) + \frac{1}{r} \frac{\partial v_\theta}{\partial \theta} + \frac{\partial v_z}{\partial z} = 0 \quad (16.123a)$$

$$\begin{aligned} \frac{\partial v_r}{\partial t} + v_r \frac{\partial v_r}{\partial r} + \frac{v_\theta}{r} \frac{\partial v_r}{\partial \theta} + v_z \frac{\partial v_r}{\partial z} - \frac{v_\theta^2}{r} \\ = -\frac{1}{\rho} \frac{\partial p}{\partial r} + g_r + \frac{1}{\rho} \left[\frac{1}{r} \frac{\partial}{\partial r} (r \sigma_{rr}) + \frac{1}{r} \frac{\partial \tau_{\theta r}}{\partial \theta} + \frac{\partial \tau_{rz}}{\partial z} - \frac{\tau_{\theta\theta}}{r} \right] \end{aligned} \quad (16.123b)$$

$$\begin{aligned} \frac{\partial v_\theta}{\partial t} + v_r \frac{\partial v_\theta}{\partial r} + \frac{v_\theta}{r} \frac{\partial v_\theta}{\partial \theta} + v_z \frac{\partial v_\theta}{\partial z} + \frac{v_r v_\theta}{r} \\ = -\frac{1}{\rho r} \frac{\partial p}{\partial \theta} + g_\theta + \frac{1}{\rho} \left[\frac{1}{r^2} \frac{\partial}{\partial r} (r^2 \tau_{r\theta}) + \frac{1}{r} \frac{\partial \sigma_{\theta\theta}}{\partial \theta} + \frac{\partial \tau_{z\theta}}{\partial z} - \frac{\tau_{\theta r} - \tau_{r\theta}}{r} \right] \end{aligned} \quad (16.123c)$$

$$\begin{aligned} \frac{\partial v_z}{\partial t} + v_r \frac{\partial v_z}{\partial r} + \frac{v_\theta}{r} \frac{\partial v_z}{\partial \theta} + v_z \frac{\partial v_z}{\partial z} \\ = -\frac{1}{\rho} \frac{\partial p}{\partial z} + g_z + \frac{1}{\rho} \left[\frac{1}{r} \frac{\partial}{\partial r} (r \tau_{rz}) + \frac{1}{r} \frac{\partial \tau_{\theta z}}{\partial \theta} + \frac{\partial \sigma_{zz}}{\partial z} \right] \end{aligned} \quad (16.123d)$$

Table 16.1
Select properties of power law and ideal Bingham plastic non-Newtonian fluids

Material	Temperature (C)	Power Law		Bingham Plastic	
		n	K (Pa s ⁿ)	τ_0 (Pa)	μ_B (Pa s)
Applesauce	27	0.45	7.3		
Chicken (minced)	23	0.1	900		
Chocolate	30	0.5	0.7	35	1
Cornstarch in water (17%)	25	1.42	6.9E-04		
Cornstarch in water (45%)	25			0.35	0.3
Human Blood	27	0.9	0.004		
Lubricating grease	25	0.1	1000		
Mayonnaise	25	0.131	100	30	0.13
Nail Polish	25	0.86	750		
Paint (latex)	25	0.6	21.5	15	0.065
Peanut Butter	30	0.07	500		
Raspberry Jam	25	0.34	12.6		
Shaving Cream	25			17.5	0.015
Sunscreen Lotions	25	0.28	75		
Synovial Fluid	37	0.4	0.5		
Tomato Juice (6% solids)	20	0.56	0.19		
Tomato Ketchup	30	0.24	33	13	0.15
Tomato Paste (25% solids)	25	0.5	1.5	104	0.3
Toothpaste	25	0.28	120	200	10
Water	25	1	0.0089		
Wheat Batter	30	0.75	110		
Whipped Butter	30	0.057	312		
49 %Fine coal slurry in water	-			1	0.005
7.5% Kaolin slurry in water	-			7.5	0.005
32% Kaolin slurry in water	-			20	0.005
14% Sewage sludge	-			3.1	0.025
39% Red mud slurry	-			23	0.030
40% Drilling mud	-	0.51	1.3	11	0.030
Fresh water mud	-	0.8	0.319		
72% Pulverized fuel ash in water	-	0.46	9.3		
Cement Slurry	-	0.36	3.0	5.4	0.029
20% Sand/Water mixture	-	1.48	0.000313		
40% Sand/Water mixture	-	1.21	0.0269		

Power law: $\tau_{PL} = \mu_{app}(\dot{\epsilon}) = K(\dot{\epsilon})^n$, $\mu_{app} = K(\dot{\epsilon})^{n-1}$ Ideal Bingham Plastic: $\tau_{BP} = \mu_B(\dot{\epsilon}) + \tau_0$

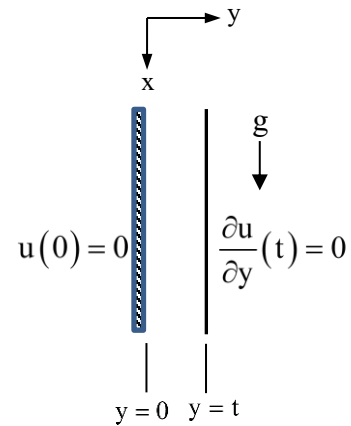
Study Problems

(note: obtain all material/fluid properties from Table 1)

1. Consider Couette flow between parallel plates, the lower plate fixed and the upper plate moving at $U=1$ m/s. If the gap between the plates is 1 mm, what are the values of shear stress for the following power law fluids: applesauce, tomato paste, and synovial fluid?
2. Consider Couette flow between parallel plates, the lower plate fixed and the upper plate moving at velocity U . If the gap between the plates is 1 mm and a shear stress of 35 Pa is applied to the upper plate, what will the velocity U be for the following Bingham plastic materials: mayonnaise, tomato ketchup, paint, and 40% drilling mud?
3. Consider Poiseuille flow between parallel plates spaced 4 cm apart. If a pressure gradient of 30 Pa/cm is applied, what are the values of flowrate per unit depth in cm^2/s for the following power law fluids: applesauce, tomato ketchup, and raspberry jam? Note: the flowrate will be negative for a positive pressure gradient.
4. Consider Poiseuille flow between parallel plates spaced 1 cm apart. If a pressure gradient of 100 Pa/cm is applied, what are the values of flowrate per unit depth in cm^2/s for the following Bingham plastic fluids: mayonnaise, tomato ketchup, paint, and 40% drilling mud?
5. Consider Couette flow between concentric circular cylinders, with diameters of 20 cm and 16 cm, and one meter long. If the inner cylinder is fixed, and the outer cylinder rotates at a velocity of 10 cm/s, determine the torque in N-cm required to rotate the outer cylinder for the following power law fluids: applesauce, tomato paste, and synovial fluid.
6. Consider Couette flow between concentric circular cylinders, both 2 m long with diameters of 20 cm and 12 cm. The inner cylinder is fixed, and a torque of 200 N-cm is applied to the outer cylinder. Determine the steady state velocity of the outer cylinder for the following Bingham plastic materials: mayonnaise and 40% drilling mud.
7. Consider Couette flow between concentric circular cylinders, both 2 m long with diameters of 20 cm and 12 cm. The inner cylinder is fixed, and a torque of 1000 N-cm is applied to the outer cylinder. Determine the steady state velocity of the outer cylinder in m/s for the following Bingham plastic materials: tomato paste and toothpaste.
8. Consider Poiseuille flow in a 4 cm diameter tube. If a pressure gradient of 10 Pa/cm is applied, what are the values of flowrate in cm^3/s for the following power law fluids: applesauce, tomato paste, and 40% drilling mud? Note: the flowrate will be negative for a positive pressure gradient.
9. Consider Poiseuille flow in a 2 cm diameter tube. If a pressure gradient of 100 Pa/cm is applied, what are the values of flowrate in cm^3/s for the following Bingham plastic materials: mayonnaise, tomato paste, and paint?
10. Mayonnaise and paint have properties that can be modeled as either a power-law fluid or a Bingham plastic. Consider Poiseuille flow between parallel plates spaced 1 cm apart. If a pressure gradient of 100 Pa/cm is applied, what are the comparative power-law vs. Bingham plastic values of flowrate per unit depth in cm^2/s for each of the fluids (i.e. what are Q_{powerlaw} vs. Q_{Bingham} for each fluid?).

11. A cement slurry can be modeled as either a power law fluid or a Bingham plastic. Consider Poiseuille flow in a 20 cm diameter tube. If a pressure gradient of 10 Pa/cm is applied, what are the comparative power-law vs. Bingham plastic values of flowrate in m^3/s (i.e. what are Q_{powerlaw} vs. Q_{Bingham} ?).
12. 40% drilling mud can be modeled as either a power-law fluid or a Bingham plastic. Consider Poiseuille flow in a 20 cm diameter tube. If a flowrate of $1 \text{ m}^3/\text{s}$ is achieved, what are the comparative power law vs. Bingham plastic values of pressure gradient in Pa/m required to achieve this flow rate (i.e. what are $\frac{\partial p}{\partial z}_{\text{powerlaw}}$ vs. $\frac{\partial p}{\partial z}_{\text{Bingham}}$?). Note that you will need to assume that $Q < 0$ for the power law model. And since $r_0 = \frac{2\tau_0}{\left(\frac{\partial p}{\partial z}\right)}$ for a Bingham plastic, you will have to iterate to determine $\frac{\partial p}{\partial z}$ and the appropriate r_0 * value.
13. Consider Couette flow of peanut butter between concentric circular cylinders, with diameters of 20 cm and 16 cm and lengths of 1 m. If the inner cylinder is fixed, and the outer cylinder rotates, determine the respective torques in N-m required to rotate the outer cylinder at velocities of 10 cm/s and 50 cm/s.
14. Peanut butter is pumped 100 m through a 12 cm diameter pipe from the processing area to the bottling area of a plant. If a pressure gradient of 200 Pa/cm is required, and Poiseuille flow is assumed, determine the flowrate in cm^3/s through the pipe, and the total power required for the pumping process in kWatts. What is the change in flowrate and power requirements if the pressure gradient is increased to 250 Pa/cm?
15. A 49% fine coal slurry in water is pumped 400 m from a mine site to a railroad tank car through a 30 cm diameter pipe as a Poiseuille flow. If we want a flowrate of $3 \text{ m}^3/\text{s}$, determine the pressure gradient required, in Pa/m, and the power required in kWatts. Since $r_0 = \frac{2\tau_0}{\frac{\partial p}{\partial z}}$ for a Bingham plastic, you will have to iterate to determine $\frac{\partial p}{\partial z}$ and the appropriate r_0 value.
16. A 40% sand in water mixture is pumped 1000 m from a mixing site to a processing plant through a 40 cm diameter pipe as a Poiseuille flow. If a flowrate of $1 \text{ m}^3/\text{s}$ is achieved, what pressure gradient in Pa/m is required to achieve this flowrate? Note that you will need to assume that $Q < 0$ for the power law model. Also, how much power will be required for this process?
17. If the sand-water mixture in problem 16 is diluted to 20% sand in water mixture, and the flowrate increased to $2 \text{ m}^3/\text{s}$ (which will keep the amount of sand delivered the same), will this reduce or increase the pressure gradient required and the power required? Again note that you will need to assume that $Q < 0$ for the power law model.
18. If latex paint behaves as a Bingham plastic, how thick can a paint layer be before it starts to run down a vertical wall? How thick would a layer of toothpaste (using its Bingham plastic properties) have to be before it would flow down the wall? Note the density of paint is $1200 \text{ kg}/\text{m}^3$, and the density of toothpaste is $1300 \text{ kg}/\text{m}^3$.

19. Using basic principles, similar to Section 16.4.1, derive an equation for $u(y)$ of a power-law fluid flowing down a vertical wall, where $\left(\frac{\partial p}{\partial x} = 0\right)$ and $g_x = g$ (where g acts in the x -direction, toward the ground, and y is oriented outward from the wall, as shown). Equation 16.7 simplifies to $\rho g + \frac{\partial \tau_{yx}}{\partial y} = 0$, where $\tau_{yx} = K \left(\frac{\partial u}{\partial y}\right)^n$, with boundary conditions $u = 0$ at $y = 0$, and $\frac{\partial u}{\partial y} = 0$ at $y = t$, where t is the fluid layer thickness. What will the velocity at $y = t$ be?



20. Using basic principles, similar to Section 16.5.1, derive an equation for $u(y)$ for a Bingham plastic material flowing down a vertical wall, where $\left(\frac{\partial p}{\partial x} = 0\right)$ and $g_x = g$ (where g acts in the positive x -direction, toward the ground, and y is oriented outward from the wall). See problem 19 schematic. Equation 16.108b simplifies to $\rho g + \frac{\partial \tau_{yx}}{\partial y} = 0$, where $\tau_{yx} = \mu_B \left(\frac{\partial u}{\partial y}\right) + \tau_0$ when $\tau_{yx} > \tau_0$ (and $\frac{\partial u}{\partial y} = 0$ when $\tau_{yx} < \tau_0$). The boundary conditions are $u = 0$ at $y = 0$, and $\frac{\partial u}{\partial y} = 0$ at $y = t$, where t is the fluid layer thickness. Here, you will have to use a variation on Eq. 16.55 as $y_0 = t - \frac{\tau_0}{\rho g}$, since gravity is the driving force, not the pressure gradient.
21. A polymer solution of density 1000 kg/m^3 flows at a free stream velocity of 1 m/s along a flat plate 30 cm long. The solution is listed as being modeled as either a power law ($K = 0.3 \text{ Pa}\cdot\text{s}^n$ and $n = 0.5$) or an ideal Bingham plastic ($\tau_0 = 2.28 \text{ Pa}$ and $\mu_B = 7.22 \text{ mPa}\cdot\text{s}$). Compare the results of these models for calculation of the boundary layer thickness and the wall shear stress at the end of the plate. Do the calculations support a preference for either model?
22. In a manufacturing plant, tomato paste at 25 C , and density of 1300 kg/m^3 , flows across a flat plate 2 meters long. Other than within the boundary layer the tomato paste flows uniformly at 1 m/s . Assume that the boundary layer thickness is zero at the leading edge of the plate. Using the properties given in Table 1, determine the boundary layer thickness and the shear stress at the trailing end of the plate if the tomato paste is modeled as (a) a power-law fluid, and (b) an ideal Bingham plastic. Compare the results of these models for calculation of the boundary layer thickness and the wall shear stress at the end of the plate. Do the calculations support a preference for either model?
23. 40% drilling mud of density of 2750 kg/m^3 , flows across a flat plate 2 meters long and develops a boundary layer. Outside the boundary layer the mud flows uniformly at 1 m/s . Assume that the boundary layer thickness is zero at the leading edge of the plate. Using the properties given in Table 1, determine the boundary layer thickness and the shear stress at the trailing end of the plate if the drilling is modeled as (a) a power-law fluid, and (b) an ideal Bingham plastic. Compare the calculated results of these models for the boundary layer thickness and the wall shear stress at the end of the plate. Do the calculations support a preference for either model?

Chapter 17

Instability and Turbulence: An Introduction**Contents**

17.1	What is Turbulence?	610
17.2	Initiation of Turbulence: Flow Instabilities	614
17.2.1	Stability of Bounded Flows	620
17.2.2	Stability of Unbounded Flows	622
17.2.3	Effect of a Pressure Gradient on Flow Stability	623
17.3	The Transition to Turbulence	624
17.3.1	Transition of Unbounded Flows	624
17.3.2	Transition of Bounded Flows: Natural	629
17.3.3	Transition of Bounded Flows: Forced	631
17.4	The Character of Turbulence	632
17.5	Mathematical Modeling of Turbulent Flow	636
17.5.1	Reynolds Averaged Equations	638
17.5.2	Turbulent Reynolds "Stresses"	643
17.5.3	Phenomenological Equations	644
17.5.3.1	Eddy Viscosity	646
17.5.3.2	Mixing Length Concepts (near a flat plate)	647
17.6	"Universal" Velocity Distribution Laws (for boundary layers)	648
17.6.1	The Inner Region	651
17.6.1.1	The Viscous Sublayer	652
17.6.1.2	Logarithmic Layer	653
17.6.1.3	Buffer Layer	655
17.6.1.4	Models of the Entire Inner Region	656
	van Driest Damping Factor	656
	Spalding's Single Inner Region Equation	658
17.6.2	The Outer Region	660
17.6.3	The Combined Universal Velocity Profile	663
17.6.4	A Shape Factor Comparison of Turbulent vs. Laminar Boundary Layers	666
17.7	A Momentum Integral Analysis of a Flat Plate Turbulent Boundary Layer	668
17.7.1	Transition to a Turbulent Boundary Layer on a Flat Plate	668
17.7.2	The Momentum Integral Equation for Turbulent Flow	670
17.7.3	The Mean Velocity Profile: Nikuradse Power Law	670
17.7.4	Assumed Shear Stress Relationship	672
17.7.5	Solution of the Momentum Integral Equation	673
17.7.5.1	Turbulent Flow from Leading Edge	675
17.7.5.2	Laminar-Turbulent Transition at Critical Reynolds Number	677
17.7.5.3	Comparison: Laminar, LE Turbulent, and Transitional Boundary Layers	679
17.8	Conclusion	683

17.1 What is Turbulence?

Anyone who has flown in a commercial aircraft has probably heard the word "turbulence" used to describe the bumpy, unsteady behavior often encountered during a flight. This unsteady flight behavior is caused by unsteady lift and drag forces, which are the result of the aircraft encountering pockets of large velocity variations in the surrounding air due to proximity to terrain variations (such as mountains) or strong thermally-induced density variations, such as those associated with thunderstorm activity. The result is generally large, somewhat random fluctuations in velocity, which in turn interact with the surfaces of the aircraft, resulting in comparable fluctuations in lift and drag. The result is a bumpy, disconcerting ride, caused by what is termed [clear-air turbulence](#).

However, turbulence occurs in most practical flows passing over, around, and through engineering systems. While the large regions of clear-air turbulence create a sometimes harrowing ride, turbulence is also always present in the boundary layer flow over the aircraft surfaces. In fact, all vehicles, whether they are cars, trucks, trains, or ships, experience and are impacted by turbulence. So are all internal fluid transport systems such as pipelines, air handling ducts, or waterways.

So, what is turbulence? The short answer is a state of seemingly random fluctuations of a flowing fluid, which results in intense mixing of mass and momentum, and dissipation of kinetic energy. There are basically two types of turbulence: non-sustaining and self-sustaining. Non-sustaining turbulence is generated by fluid-solid interactions, but then dissipates after it leaves the surface, like shedding from a cylinder, high-shear fluid interactions, or by strong density variations. However, once generated, non-sustaining turbulence will dissipate due to vortex interaction and viscous dissipation. Turbulence is always in a state of energy dissipation, and when it is removed from bounding surfaces it will gradually dissipate. Think of a jet of water entering a swimming pool—turbulence will be generated almost immediately at the boundaries of the jet, but the mixing and strong interactions of the turbulence will slowly die out as the jet flows further into the pool. On the other hand, self-sustaining turbulence is generated adjacent to solid, continuous boundaries, like flow over a flat plate or an airplane wing or fuselage. Here, the turbulence will both dissipate, and be regenerated adjacent to the bounding surface (within the boundary layer). Thus, continued regeneration balances the dissipation, creating a self-sustaining process of new turbulence generation adjacent to older turbulence dissipation. Such self-sustaining turbulent behavior, as is experienced in boundary layers, results in a continuation of turbulent behavior downstream within a boundary layer, with the strong mixing interactions near the bounding surface resulting in a significant increase in surface friction. Of course, when self-sustaining turbulence leaves a surface, such as when a boundary layer exits an airfoil, it will become non-sustaining.

Now for the hard question: where and why does turbulence occur, and how does one characterize it and its effects on the fluid and the fluid interactions with bounding surfaces? To answer this question, we will take the next multiple pages, and some admitted arm waving, to address the process even cursorily. In addition, we will again only be able to give the short answer, which, although it may seem expansive, will be somewhat incomplete. The reason for this vagueness is that next to the origin of the universe, or the establishment of a unified field theory of physics, turbulence is probably the most perplexing problem in physics. In fact, numerous giants of the fields of physics and fluid mechanics have often, in their later years, commented that turbulence remains, and will probably remain, the most difficult physical process to truly understand. Moreover, this remains true, despite a continual improvement in the tools to study turbulence (e.g. 3-D velocity measurement systems, and continually more powerful computers).

So, where to begin? First, let us review the general process by which a flow becomes turbulent. In a naturally occurring self-sustaining turbulent process, a flow will generally begin as a laminar flow. As the flow develops, either along a surface or moving within a quiescent surrounding fluid, small instabilities (think small, wave-like behavior) will develop within the flow. Under the appropriate conditions, these instabilities will begin to amplify (i.e. grow in amplitude). As the instabilities amplify and grow, they will eventually undergo a transition to a complex, three-dimensional behavior, manifested by the development of localized concentrations of time-dependent vorticity. Finally, this transitional behavior will grow into a complicated, three-dimensional distribution of vorticity of extended scales, which both (1) entrains additional mass and momentum from adjacent non-turbulent fluid, and (2) dissipates local fluid kinetic energy by intense local viscous action. Over a bounded surface, this process of entrainment, mixing, and dissipation becomes self-sustaining, continuing to entrain surrounding fluid, and dissipate local fluid energy at a much more elevated rate than a comparable laminar flow. A crude representation of this evolution from laminar to turbulent flow for a flat plate boundary layer is shown schematically in figure 17.1.

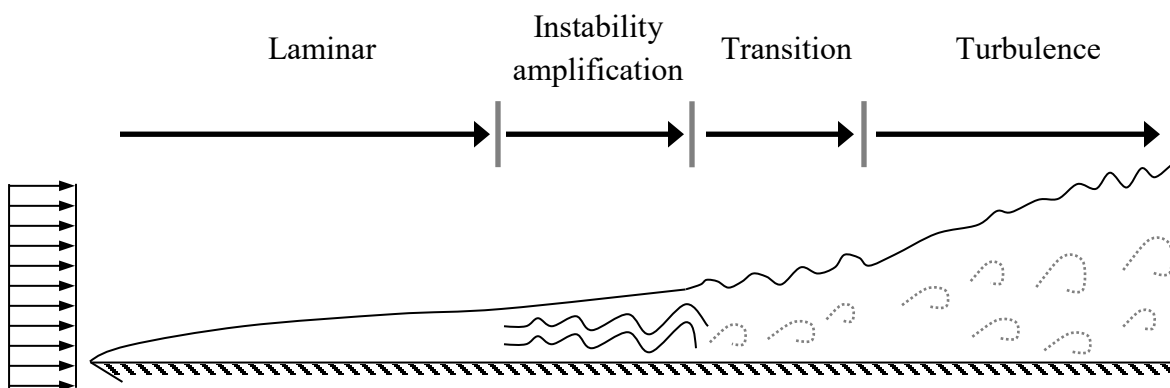


Figure 17.1 A generic schematic of the evolution of turbulence from a laminar flat plate flow (not to scale).

While turbulence is characteristic of almost all flows of practical engineering interest, a concrete description is elusive—we generally discuss generic characteristics, since it is difficult to describe the exact characteristics that will apply to all types of turbulent flows. I once paid a visit to [A.D. Young](#), a famous Queen Mary University of London fluid dynamicist, and noted on a corner of his office blackboard he had written the following statement: "When we measure a fluid behavior, and we don't know what is happening, we call it turbulence."

While there are many descriptions of turbulence, many short and many long, we will use a set of characteristics summarized by R.W. Stewart in his narration of [the educational film, "Turbulence."](#) This film (converted to a YouTube video), although old, provides a practical display of the visual characteristics of turbulence and a good, generic description of the turbulence processes. I recommend you view the video.

In the film, Stewart cites the following basic characteristics: "disorder (randomness); enhanced mixing; and three-dimensional motions involving angular momentum (i.e., vorticity)." Most researchers would agree with these, and probably add to or modify the list. However, we will use these as our basis for our discussion of turbulence. Turbulence is the epitome of a process that is described by the statement: "I don't know what it is, but I know it when I see it (or measure it)."

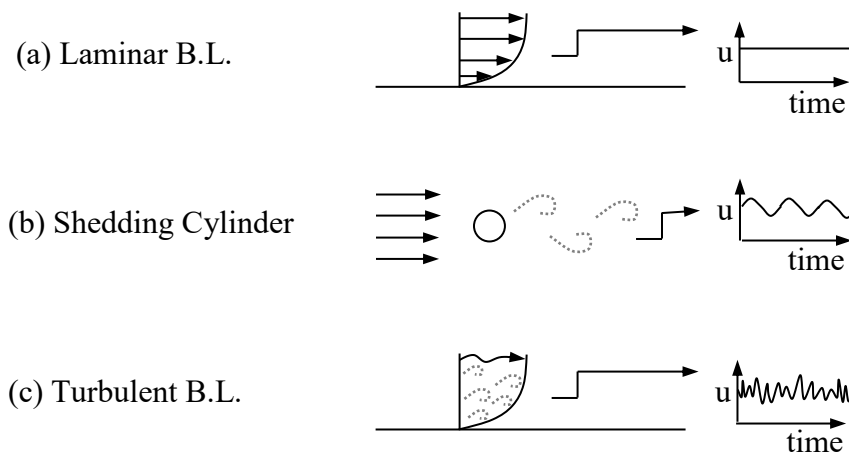


Figure 17.2 Typical hot-wire anemometer velocity measurements of the temporal velocity behavior in: (a) a laminar boundary layer, (b) the wake of a shedding cylinder, and (c) a fully-turbulent boundary layer.

As an illustration of what is and what isn't turbulence, consider the instantaneous measurement of the local velocity behavior in three different types of flow, within otherwise steady flow fields, as shown in figure 17.2. Such measurements can be made with an instrument known as a [hot-wire anemometer](#), which employs a very fine electrically heated wire, and the changes in the

wire temperature due to local velocity fluctuations, to measure changes in local velocity behavior using the relationship between electrical resistance and the temperature of the wire. The benefit of employing a hot-wire anemometer to measure turbulence is that it has a very fast response time, so it can accurately measure flows that vary very rapidly with time, such as turbulence.

The first of the measurements shown, figure 17.2a, is within a laminar boundary layer, which shows essentially no temporal changes in the velocity at a point, since laminar flows move in layers (lamina), and from an Eulerian view are steady.

The second measurement shown, figure 17.2b, is in the wake of a laminar flow over a cylinder, with the separating boundary layer forming an unsteady, but periodic, set of shedding Strouhal vortices (as we discussed in Section 15.4). As these vortices pass the velocity-sensing probe, they cause a periodic variation in the velocity. While such flows may be turbulent, such periodic variations can also occur in otherwise laminar flows, and can maintain two-dimensionality. Therefore, a lack of randomness and three-dimensionality would disqualify this flow as a turbulent flow.

The third measurement shown, figure 17.2c, represents the local velocity behavior within a turbulent boundary layer. Here, the velocity will vary in an apparently erratic, temporal manner, displaying the apparently random behavior that is characteristic of turbulence. Note that we cannot discern whether the measured velocity is three-dimensional, or is the result of vorticity variations, but a researcher encountering such a velocity behavior would presume that this is a measurement of turbulence (note the supposition that anything not reflecting laminar or pure periodicity is turbulence, as per A.D. Young's blackboard quote).

However, what conditions are necessary for a laminar flow to transition to a turbulent flow? Again, this is a debatable area, but most turbulence researchers would agree to three primary criteria:

- 1) High Reynolds number (inertia/viscous imbalance)
- 2) Velocity gradients
- 3) The presence of flow disturbances

The necessary levels or magnitudes of these criteria that are sufficient to produce a transition from a laminar to a fully-turbulent flow differ, depending on the type of initial flow (i.e. boundary layer, jet, pipe flow, etc.). For a given type of flow, there is generally a critical Reynolds number that must be reached (based on a characteristic length appropriate to the flow, such as the boundary layer thickness) before a flow will begin the process of transitioning to turbulence. Velocity gradients are also particularly important; the stronger or sharper the gradient is, the sooner turbulence will develop. In addition, to initiate the process of transition to

turbulence requires the presence of disturbances, either preexisting within the flow or created by irregularities of a bounding surface.

17.2 Initiation of Turbulence: Flow Instabilities

As was indicated in figure 17.1, the initiation of turbulence begins with the development of an instability within the flow. Now, many types of flows can undergo flow instability, and in many cases this instability is simply a transition from one stable laminar state (i.e. behavior) to another stable laminar state. In such a transition process, some effect causes a flow to change from one type of flow behavior to another. A good example is flow over a cylinder at low Reynolds numbers, as shown in figure 17.3.

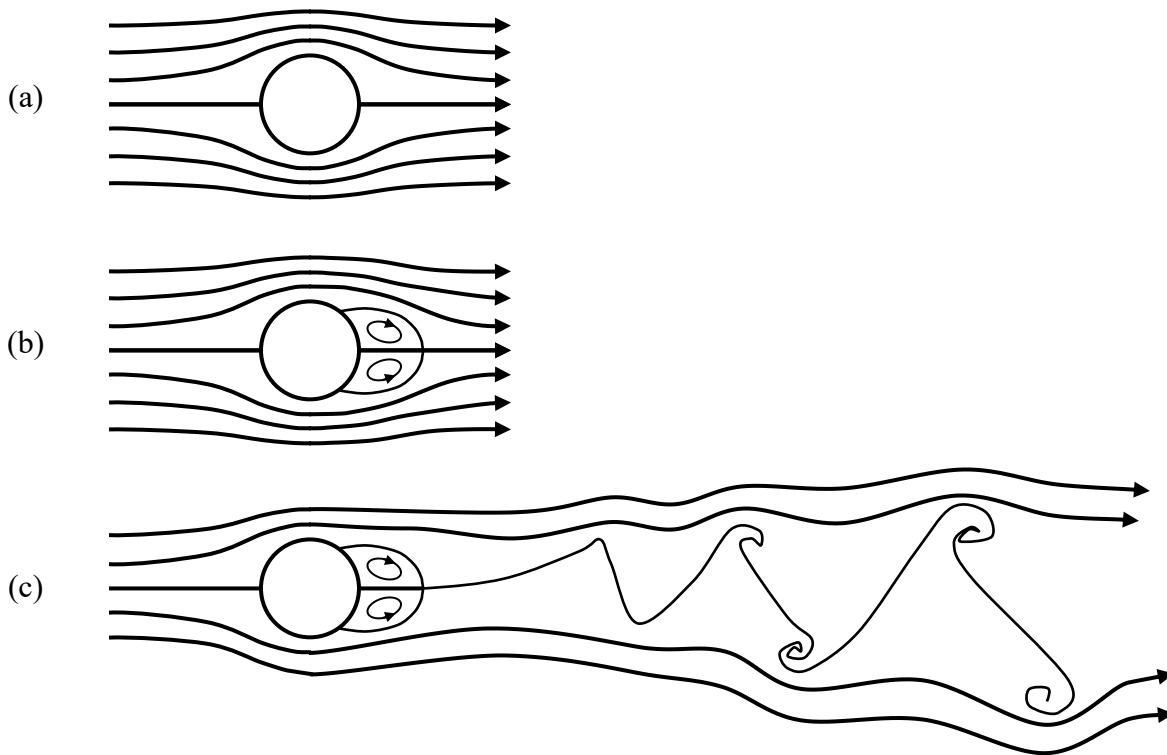


Figure 17.3 Laminar states for flow over a cylinder. (a) $0 < Re_D < 1$, symmetrical flow; (b) $4 < Re_D < 40$, attached vortices; (c) $40 < Re_D < 60-100$, laminar vortex shedding.

As pointed out in Chapter 15, at very low Reynolds numbers ($Re_D < 1$), the flow around a circular cylinder will behave very much like a potential flow (see Section 9.8.1), with the streamlines passing evenly and symmetrically around the cylinder (figure 17.3a). However, as the Reynolds number increases to $Re_D > 4$, the flow takes on a different character, where two attached, counter-rotating vortices appear adjacent to the downstream surface of the cylinder

(figure 17.3b). Then, for $Re_D > 40$, the flow transitions to an unsteady flow, with laminar vortices shed periodically from the rear of the cylinder (figure 17.3c). Thus, the flow over a circular cylinder undergoes instabilities with increasing Reynolds number, which cause a sudden, and marked change in the character of the flow field. See this [link](#) for images of the flow states for a circular cylinder.

There are many other types of flows for which a small change in the Reynolds number leads to a marked change in behavior from one stable state to another. Another example is changes in flow behavior with increased rotation. Consider a fluid contained within the annulus formed by two concentric cylinders, as shown in figure 17.4. If the inner cylinder is rotated steadily and the outer cylinder held fixed, at low rates of rotation the flow in the annulus will form a steady, Couette flow, with a two-dimensional velocity profile, as characterized by equation 6.55a:

$$v_\theta = \frac{\Omega_i r_i^2 (r_o^2 - r^2)}{r (r_o^2 - r_i^2)}$$

However, as the Reynolds number $\left[\text{given by } Re_i = \frac{\Omega_i r_i (r_o - r_i)}{\nu} \right]$ of the flow increases beyond a critical level, the flow will spontaneously undergo transition from a two-dimensional Couette flow to a [Taylor flow](#). A Taylor flow is a three-dimensional, relatively steady flow comprised of a series of steady, laminar vortices engirdling the annulus, with their axes of rotation in the azimuthal direction, as shown schematically in figure 17.4b. See also visualizations of Taylor-type flows [here](#).

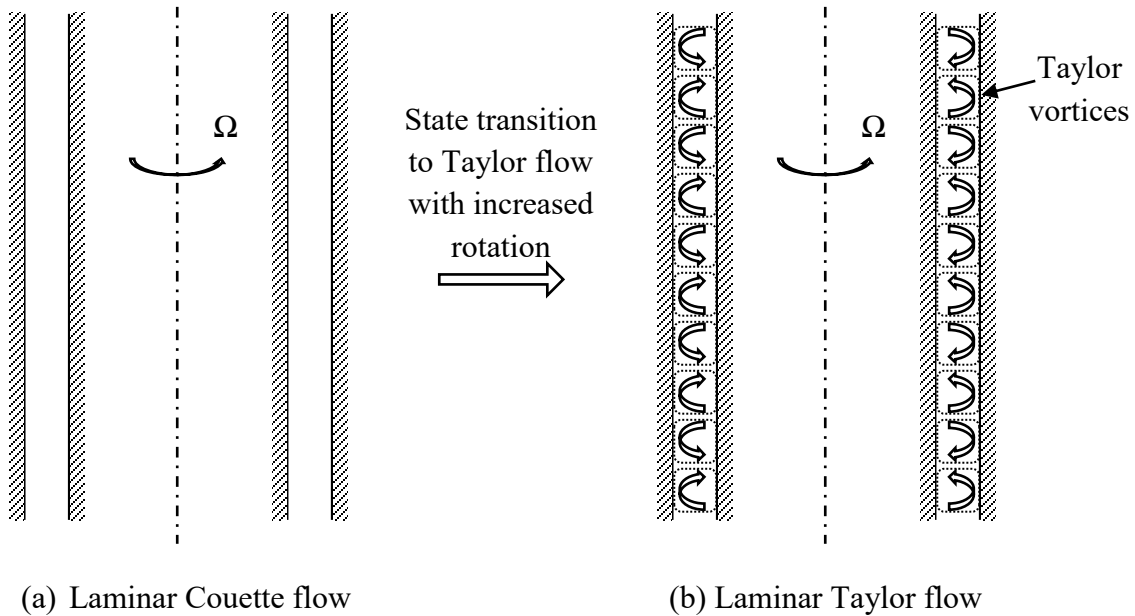


Figure 17.4 Transition from stable laminar Couette flow to stable laminar Taylor flow in the annulus of concentric cylinders due to increased rotation.

Both for flow over a cylinder and flow in a concentric cylinder annulus, a small change in the appropriate Reynolds number results in a marked change of the flow state. Recall that the Reynolds number is a measure of the ratio of inertia forces to viscous forces. So, as inertia effects increase, the less stable the original flow becomes, and the greater the probability of a change in the flow state.

To understand this loss of stability of one state, and transition to an alternative state, consider the stacking of children's blocks. If we have a set of children's wooden blocks scattered on the floor, the blocks would be in a stable state, since if they are disturbed (e.g. by giving them a push with your hand), they will not change their state (all the blocks will stay on the floor level), other than to move across the floor. However, if we stack several of the blocks, one upon the other, as shown in figure 17.5, we know from our childhood experience that a small disturbance can cause the blocks to tumble back onto the floor. Of course, if the stack of blocks is rather low (say two to three), a larger disturbance will be required to knock the stack of blocks over than if the stack of blocks is higher (say 5 to 7). Moreover, if one continues to stack the blocks to even higher heights, they eventually reach a height where the addition of another block, no matter how carefully done, will cause the stack to spontaneously collapse due to the inherent irregularities of the individual blocks.

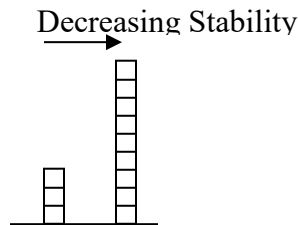


Figure 17.5 The stability of stacked blocks. The higher the stack of blocks, the more unstable the process becomes.

What is happening as we stack the blocks higher is that we are creating an unstable state, which is subject to small disturbances or perturbations from its surroundings. When the disturbance is of sufficient magnitude, the blocks will suddenly transition from one state (the stacked state) to another state (with all blocks on the floor). We might consider that the stacked state is marginally stable, which can sustain some disturbance when the stack is low, but becomes unstable as the stack grows in height, until it is unable to tolerate any level of disturbance.

The same process of stability is true for a laminar flow. In the case of a fluid, it is generally the Reynolds number that dictates the level of stability of a flow, and when a transition to another state (i.e. turbulence) can be expected. Since the Navier-Stokes equations govern all Newtonian fluids, both laminar and turbulent, an examination of the stability of a laminar flow using the Navier-Stokes equations would seem to be a reasonable approach to determine when and how

transition from a laminar to a turbulent flow occurs, and the sensitivity of the process to both Reynolds number and the type of disturbance. However, the non-linear nature of the Navier-Stokes equation makes the process of analysis not only complicated, but also necessitates some sweeping approximations. In particular, it is assumed that a flow is locally parallel, and for the simplest situation, two-dimensional.

Thus, in a two-dimensional x-y Cartesian coordinate system, we assume that we can write the equations for u and v as:

$$u = U + u' \quad \text{and} \quad v = V + v' \quad (17.1)$$

Here, U and V are the mean values of the velocity, and u' and v' represent the fluctuation or perturbation velocities (i.e. velocity components that fluctuate about the mean value). Note that the assumption of parallel flow (i.e. parallel in the x-direction) also assumes that the mean flow is fully developed, such that $U(y)$, which means (via continuity) that $V = 0$. The fluctuating velocities are, however, considered functions of x, y, and t (time).

Now, substituting Eq. 17.1 (with $V = 0$) into the two-dimensional continuity equation, Eq. 5.46a, gives:

$$\frac{\partial}{\partial x}(U + u') + \frac{\partial v'}{\partial y} = 0$$

or by the parallel flow assumption, $\frac{\partial U}{\partial x} = 0$, and thus:

$$\frac{\partial u'}{\partial x} + \frac{\partial v'}{\partial y} = 0 \quad (17.2)$$

If we now assume a stream function ψ such that Eq. 17.2 is identically satisfied, we have:

$$u' = -\frac{\partial \psi}{\partial y} \quad \text{and} \quad v' = \frac{\partial \psi}{\partial x}$$

This is very much the same process we used for potential flow theory. However, since u' and v' are functions of x, y, and t, this means that $\psi = \psi(x, y, t)$. Since we want to investigate how a disturbance develops within a flow, we further assume the perturbation can be expressed as a traveling wave with amplitude varying with y and the wavelength varying with x and t. The general form of an appropriate function for the stream function is:

$$\psi = F(y)\exp[i\alpha(x - ct)] \quad (17.3)$$

In Eq. 17.3, α is termed the wave number (proportional to 1/wave length) and c is termed the wave or phase velocity. This expression assumes the behavior of the amplitude F(y) will either grow or shrink, depending on the respective values of α and c. Since α and c are arbitrary

constants, the idea is to explore a range of values of α and c , and determine which will give rise to a growth of $F(y)$, which will damp $F(y)$, and particularly where $F(y)$ will remain constant. What we surmise is that: a growth in $F(y)$ will lead to a breakdown of the flow, leading to turbulence; a damping of $F(y)$ will result in the flow remaining in a laminar state; and the combination where $F(y)$ remains constant will be where the flow is marginally stable (i.e. the boundary of stability).

Now to complicate the matter further, we note that for a traveling wave, the wave velocity is assumed complex, such that:

$$c = c_r + ic_i, \text{ where } i = \sqrt{-1}, \quad (17.4)$$

If we substitute Eq. 17.4 into 17.3, we have:

$$\psi = F(y) \exp[i\alpha(x - c_r t - ic_i t)] = F(y) \exp[i\alpha(x - c_r t)] \exp(\alpha c_i t)$$

Clearly, the term $\exp(\alpha c_i t)$ controls whether the stream function (and thus the velocities) grows or is damped. If $\alpha c_i > 0$, the stream function grows exponentially; if $\alpha c_i < 0$ the stream function is damped exponentially. Now, since $\alpha > 0$, this means that the sign of c_i controls the stability of the flow, and that c_i can be considered as a coefficient of amplification.

Therefore, if we can develop and solve an appropriate governing equation for the stream function, we can determine which values of α and c yield stable behavior, and which yield unstable behavior, for a particular velocity profile. The appropriate governing equation is the Navier-Stokes equation, into which we substitute the derivative functions of ψ , which represent the appropriate velocity relationships. To do this properly we use non-dimensional properties to write $F(y)$ as:

$$F(y) = U_0 \delta^* f(\zeta) \quad \text{where } \zeta = y / \delta^*$$

Here, U_0 is a representative velocity of the mean flow (such as the velocity at the edge of a boundary layer, or the mean velocity in a pipe flow), δ^* is the displacement thickness for a given mean velocity, and time is non-dimensionalized as $t^* = tU_0 / \delta^*$. We also linearize the process by retaining only first-order perturbation terms (i.e. products of u' , v' , and $\partial u' / \partial x$). After substituting into the x- and y-direction Navier-Stokes equations, differentiating, and consolidating to eliminate pressure terms, we end up with (note that it is not an easy process):

$$(U - c)(f'' - \alpha^2 f) - U'' f = \frac{(f'''' - 2\alpha^2 f'' + \alpha^4 f)}{i\alpha \text{Re}_{\delta^*}} \quad (17.5)$$

In equation 17.5, $Re_{\delta^*} = \frac{U_0 \delta^*}{\nu}$, is the Reynolds number based on the boundary layer displacement thickness. Equation 17.5 is known as the [Orr-Sommerfeld equation](#), named for the two scientists, [W. Orr](#) (1907) and [A. Sommerfeld](#) (1908) who independently derived it. See [White \(1990\)](#), pp.342-345 for details of the derivation.

Equation 17.5 looks pretty complicated, and it is. Some early solutions of this equation were developed analytically by [Tollmien](#) (1929) and [Schlichting](#) (1930). By the 1950's, solutions using numerical computational approaches were possible, with recent solutions improving markedly as computational power has increased. However, the basic strategy for solving the equation has remained the same. While the mathematical details of the solution are too complicated to discuss here, and are better described elsewhere ([Wazzan, 1975](#)), the key elements are as follows.

Equation 17.5 is a homogeneous equation (all terms in the equation are functions of f and its derivatives). Additionally, the boundary conditions are that the disturbances, u' and v' , and appropriate derivatives (all of which are reflected in the function f) must vanish at infinity and bounding surfaces. This makes all the boundary conditions for $f(\zeta)$ also homogeneous. Thus, we have a homogeneous differential equation with homogeneous boundary conditions, which means this is an eigenvalue problem. What this means is that for any given mean velocity profile $U(\zeta)$ there are select combinations of the parameters α , c , and Re_{δ^*} that will be a solution for Eq. 17.5 and its boundary conditions. The sequence of α , c , and Re_{δ^*} combinations which yield valid solutions are then the eigenvalues of the eigenfunction $f(\zeta)$.

Still with me? After a lot of computations, we can determine a functional relationship for the eigenvalues of the form:

$$c = c(\alpha, Re_{\delta^*})$$

Or, since c is complex, and we are really concerned with which combination of parameters (eigenvalues) cause the disturbances to grow, damp, or remain constant, what we are really interested in is the value of c_i . Thus, we can develop a functional relationship for c_i of the form:

$$c_i = c_i(\alpha, Re_{\delta^*}) \tag{17.6}$$

So, referring back to our discussion above about c_i , if $c_i > 0$ the disturbance will grow (become unstable), and if $c_i < 0$ the disturbance will diminish (remain stable). Therefore, the key value we are interested in is $c_i = 0$, which is the demarcation between unstable and stable behavior. As Eq. 17.6 suggests, the easiest way to display this stability behavior is using a graph of α vs. Re_{δ^*} on which we plot lines of constant c_i .

17.2.1 Stability of Bounded Flows

Flows that are bounded by solid surfaces are the more stable of laminar flows, maintaining their laminar state to higher values of Reynolds number. Such flows are Poiseuille flows between plates and in pipes, and boundary layer flows over flat or curved surfaces.

Figure 17.6 is a stability graph for a Blasius flat-plate boundary layer, which displays lines of constant c_i for a laminar flat plate boundary layer flow, as determined by solution of Eq. 17.5. Of particular interest on this graph is the $c_i = 0$ line, shown as a heavier line. What this line represents is a demarcation between disturbances that will grow, and those that will be damped. Recall that α is the wave number, or the inverse of the wave length of the disturbance. So, as α increases, the wave length decreases. Note that $Re_{\delta^*} = \frac{U_0 \delta^*}{\nu}$ is fixed by the parameters of the flow.

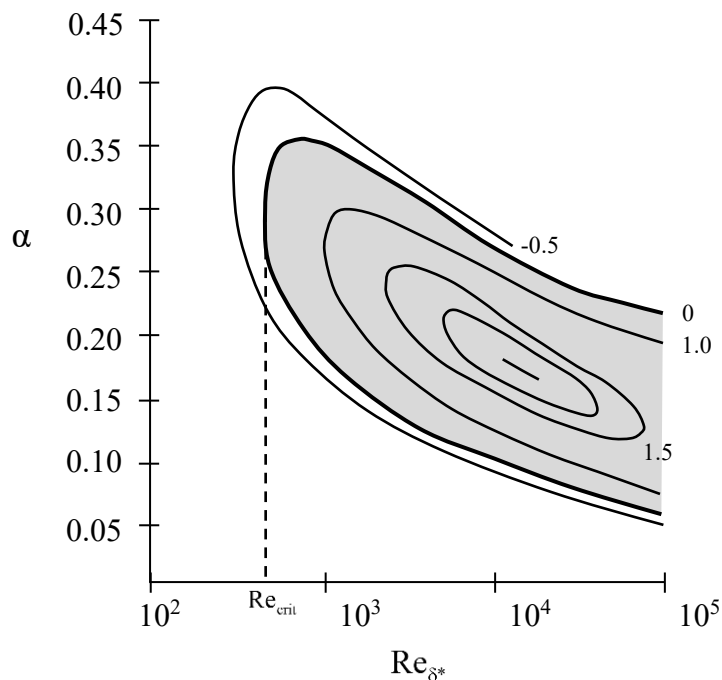


Figure 17.6 A stability graph, showing curves of constant temporal amplification rate for a Blasius laminar boundary layer. The values associated with the curves are $c_i \times 10^2$. The black line bounding the shaded area is the line of neutral stability. Values of $c_i < 0$ are in the stable regime, and $c_i > 0$ are in the unstable regime (shaded). [after Wazzen (1975)]

On figure 17.6, note that for low Re_{δ^*} the flow is stable to disturbances of all wave numbers, and thus the flow will damp out any disturbance and remain laminar. However, above a certain critical Re_{δ^*} (for a Blasius-type boundary layer profile $Re_{crit} \cong 520$) there is a certain range of disturbance wave numbers that the flow will amplify, thus producing an instability (i.e. causing the flow to transition to another state). As figure 17.6 shows, this range of amplified wave numbers is limited, and this range shifts from higher to lower α (i.e., longer wavelengths) as Re_{δ^*} increases.

Note that in Eq. 17.5 the right hand side of the equation reflects the viscous terms of the Navier-Stokes equation, and is inversely proportional to Re_{δ^*} . Thus, when Re_{δ^*} is small, viscosity has a strong damping effect on the flow. However, as Re_{δ^*} increases, the impact of viscosity is reduced, and a given flow will be more susceptible to unstable behavior. This effect of Re_{δ^*} is clearly shown in figure 17.6, which illustrates that disturbances are damped at low Re_{δ^*} , and amplified as Re_{δ^*} increases beyond Re_{crit} .

One might think that by judicious control the region of unstable growth (the shaded region in figure 17.6) might be avoided, and the flow could remain laminar to quite large Re_{δ^*} . However, while this might be possible in theory, disturbances in real flows will generally contain a broad set of wavelengths (i.e. wave numbers), and thus one or more of the wave numbers will likely be amplified as Re_{δ^*} increases. Additionally, although not shown in figure 17.6, as $Re_{\delta^*} \rightarrow \infty$, the range of unstable wave numbers tends to zero. Again, while this suggests that we might be able to finesse the flow to high Reynolds numbers by judicious control of the disturbance type, in practice a real disturbance generally will pass through a Reynolds number where at least one of its wave numbers will become unstable.

When one considers internal duct-type Poiseuille flows, similar stability graphs can be established. For a two-dimensional Poiseuille flow between parallel plates of spacing t , calculations by Nachtsheim (1964) showed that $Re_{t,crit} = 5767$, where $Re_t = \frac{U_0 t}{\nu}$. This $Re_{t,crit}$ based on linear stability theory is quite large, since experimental studies indicate transition generally occurs around $Re_t \approx 1000$. Additionally, for a Poiseuille flow in a pipe, where $Re_D = \frac{U_0 D}{\nu}$, numerous studies using linear stability theory indicate the flow should remain stable for all Re_D , and that there is no $Re_{D,crit}$ value where one should anticipate an instability. In contrast, experiments indicate transition occurring at $Re_D \approx 2000$ in practice. Although practical transition Reynolds numbers can be pushed higher (on the order of $Re_D \approx 10^5$) by

careful control of inlet disturbances and surface roughness, it is generally assumed that the stability of such ducted flows is subject to a stability process not properly modeled by linear stability theory. For an nice review of boundary layer stability and transition see ([Zaric, 1990](#)).

17.2.2 Stability of Unbounded Flows

Using Eq. 17.5, it can be shown that if a laminar velocity profile $U(\zeta)$ contains an inflection point, such that $U'' = \frac{d^2U}{dy^2} = 0$, this significantly reduces the stability of the flow. Consequently,

flows with natural inflections in their mean velocity profile, such as jets, wakes, and boundary layers with an adverse pressure gradient, will become unstable almost immediately, whereas flows without an inflection, such as boundary layers with a favorable pressure gradient will remain stable to higher Re_{δ^*} .

Unbounded flows such as jets, wakes, and shear flows (two adjacent flows moving at different mean velocities), as shown in figure 17.7, all have inflections in their respective velocity profiles, and thus are subject to an almost immediate development of instabilities. A wake, such as encountered in the flow behind a bluff body, and a jet impinging into a quiescent or lower velocity flow have $Re_{crit} \cong 4$, so these are inherently unstable for all practical flows. Moreover, linear stability theory predicts that shear flows have a $Re_{crit} \cong 0$, and are unstable under all conditions. Thus, all unbounded flows will immediately begin the process of transition to turbulence.

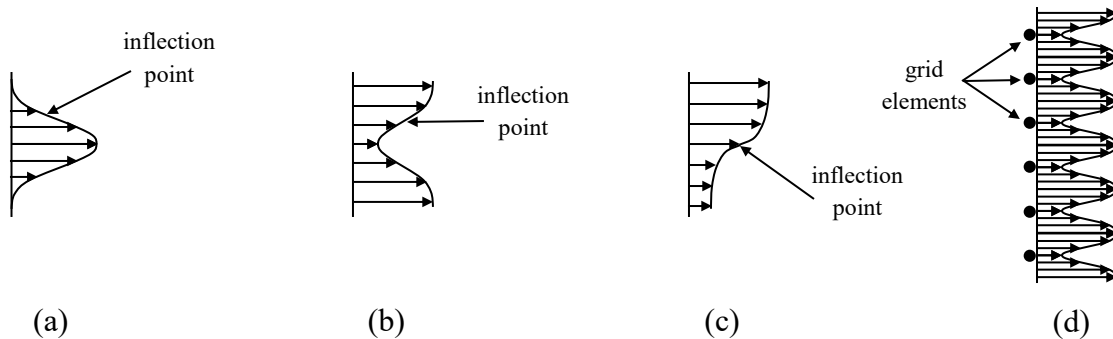


Figure 17.7 Typical unbounded laminar flow velocity profiles:
(a) jet flow, (b) wake flow, (c) shear flow, (d) grid flow

A subset of unbounded flows is the stability of flows in the wake of a grid placed normal to an impinging uniform flow. These types of flows consist of a series of transverse jets and wakes, as shown in figure 17.7d. These flows again have a $Re_{crit} \cong 4$, and again are almost immediately unstable. These types of flows, and thus cross-stream grids, are commonly employed at the

entrances of wind tunnels to actually reduce the scale of entering flow disturbances and promote lower flow disturbances in the downstream flow. More on this in Section 17.3.

17.2.3 Effect of a Pressure Gradient on Flow Stability

As mentioned in section 17.2.2, a velocity profile containing an inflection is very susceptible to instability. We noted in section 14.5.2 that a Blasius flat-plate boundary layer has an inflection point located at the boundary surface. As was illustrated in figure 17.6, a flat plate flow may become unstable starting at $Re_{crit} \cong 520$. However, as we illustrated in Section 14.6, if a boundary layer is subject to an external pressure gradient, this can strongly influence the behavior of the mean boundary layer velocity profile. For a boundary layer flow subject to an adverse pressure gradient (increasing stream-wise pressure), the inflection point will move away from the surface, which will make the flow strongly unstable. In contrast, for a boundary layer flow subject to a favorable pressure gradient (decreasing stream-wise pressure), there will be no inflection point in the velocity profile, and the flow will be more stable.

For example, consider the Falkner-Skan boundary layer flows we examined in section 13.6, which were boundary layers developing under the effect of pressure gradients ranging from strongly adverse to strongly favorable. A linear stability evaluation of Re_{crit} for the two most extreme cases [Wazzan (1975)] indicates that for $m = -0.0905$ (strongly adverse) the $Re_{crit} \cong 67$, whereas for $m = 1$ (strongly favorable) the $Re_{crit} \cong 12,500$. Thus, an adverse pressure gradient boundary layer is very unstable, and will usually break down to turbulence almost immediately; in contrast, a strong positive pressure gradient boundary layer is very stable, and is unlikely to transition to turbulence, even in the presence of strong disturbances. Thus, the stability of a boundary layer depends quite strongly on the level and the direction of the external pressure gradient.

So what do these stability concerns mean in terms of a flow degenerating to turbulence? Well, it should be clear that a laminar flow, unless it is a bounded flow either at low Reynolds number or under the influence of a favorable pressure gradient, will encounter disturbances (e.g. due to surface roughness or extraneous disturbances, such as acoustic noise, thermal gradients, etc.) that will naturally lead to an unstable change of the flow.

So, what happens when a laminar flow becomes unstable? As we discussed earlier in section 17.2, the flow will transition to another state, which eventually leads to what is known as a turbulent flow. However, how that happens is again (of course) quite complicated, and subject to significant study. In the following section we will discuss this generic process of transition from a laminar to a turbulent flow.

17.3 The Transition to Turbulence

As was illustrated in Section 17.2, as the Reynolds number increases a flow is more susceptible to amplification of disturbances, and subsequent degeneration to turbulence. However, this process of transition may be a relatively sudden process when there is an inflection point in the velocity profile; or it may be a less well-defined and more projected process, as with bounded flows. Part of the problem is that once disturbances start to grow, they give rise to additional inflections in the mean velocity, which can modify the way the original wave number amplifies, which may allow other wave numbers to amplify. As you can imagine, the process of disturbance growth becomes very complicated very quickly. The process of transition is dependent on the types of initial disturbances to the flow; even carefully designed flow systems are subject to variances in the initial disturbances due to small temporal variations in sound, vibration, density, and thermal gradients, among other external influences. Thus, the amplification of disturbances, and the transition to turbulence can occur in markedly different ways on the way to a turbulent state.

17.3.1 Transition of Unbounded Flows

The transition in unbounded flows is complicated, but is generally consistent in the way in which it occurs. In the vicinity of an inflection point in the mean velocity profile, a process known as a Kelvin-Helmholtz instability develops almost immediately. This instability is initially an inviscid process, modeled as a pressure-driven instability developing at the sharp velocity interface between two dissimilar flow streams, such as encountered at the initiation of a jet, a shear layer, or a separating wake. These types of inflectional flows are unstable to all disturbances, with instabilities initiating as transverse waves within the shear layer, and rapidly rolling up into a sequence of transverse (or azimuthal, in the case of a circular jet) vortices. Once the vortices form, viscosity begins to play a role as well, which we will discuss.

Once transverse Kelvin-Helmholtz vortices form, they will translate at roughly the average velocity between the adjacent stream velocities. So, for a jet of velocity U exiting into a quiescent environment, these vortices will initially travel at roughly $0.5 U$. As figure 17.8 schematically illustrates, once formed, a complicated process of both amalgamation and distortion of the vortices takes place, with combinations of sequential vortices rolling up (amalgamating) into larger vortical structures, while the vortices (and their associated vorticity) simultaneously undergo three-dimensional distortion due to vortex stretching by the rotation of the larger-scale vortical structures. This leads to both (a) a spatial growth in the size and complexity of the vortex structures, and (b) a stretching and concentration of the vorticity comprising the amalgamated vortices. The growth to larger scales is important, since this growth process causes the entrainment of additional fluid from bordering non-turbulent flow, which

results in both the rapid mixing of the adjacent flows, and lateral spreading of the initial disturbances. The stretching and concentration of the vorticity within the amalgamated structures accomplishes two things: (1) a transfer of kinetic energy from the motion of the larger rotating structures to smaller three-dimensional vortices contained within or adjacent to these larger structures, and (2) reduction in scale and rotational intensification of the smaller vortices. This process is again important since the smaller scale vortices will contain very large shear gradients, which will cause their kinetic energy to dissipate as heat through viscous effects.

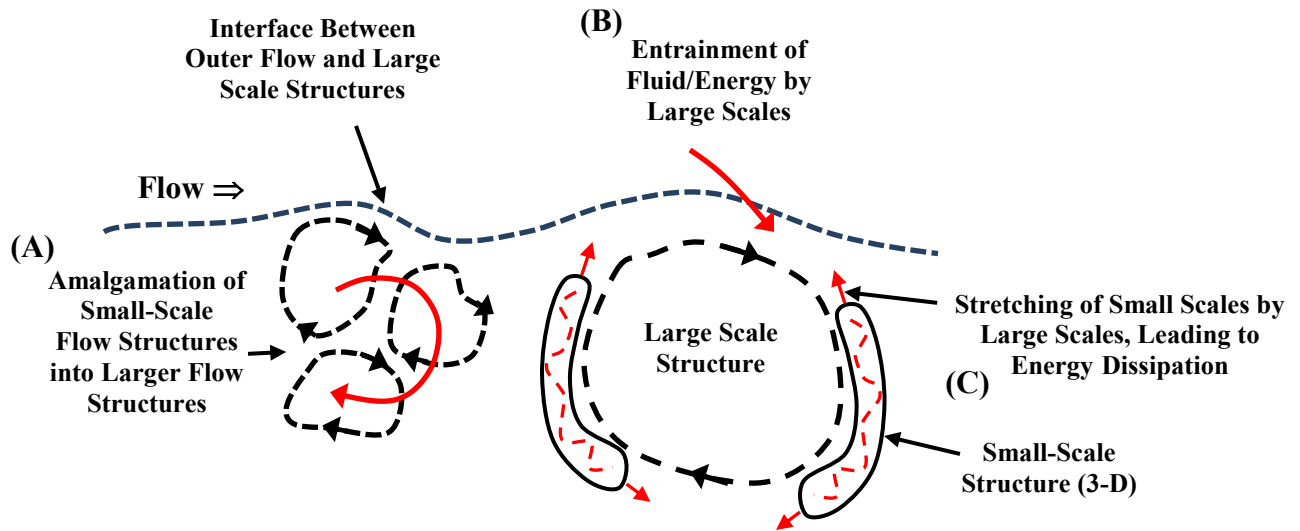


Figure 17.8 Schematic illustration of the simultaneous processes within a turbulent flow of (A) small-scale to large-scale amalgamation, (B) entrainment of outer region fluid/energy into the turbulent region by the large-scales, and (C) stretching of small-scales by large-scales leading to energy dissipation.

To illustrate how the stretching of smaller-scale vortices passes energy from larger-scale flow structures to smaller scales, consider a simple illustration. Assume that the smaller scale vortices are modeled as a vortex tube with solid body rotation, as shown in Figure 17.9.

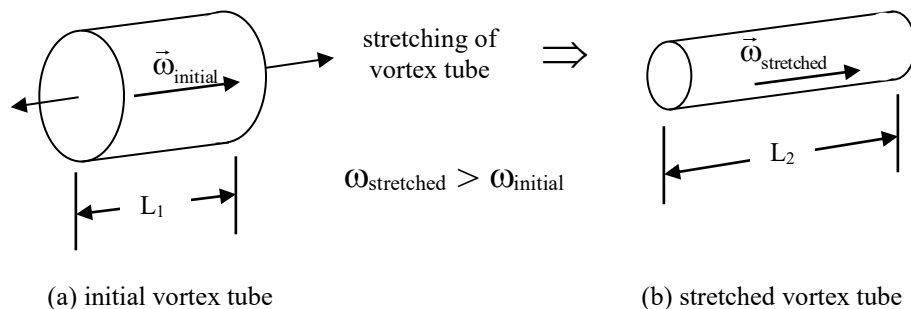


Figure 17.9 The effect of stretching on a vortex tube of constant cross-section.

For simplicity, consider the angular momentum of the vortex tube to be modeled as a rotating rod with a constant angular velocity (i.e. vorticity) throughout the tube, such that:

$$\text{Angular momentum} = I\omega$$

and

$$\text{Kinetic energy} = \frac{1}{2}I\omega^2$$

Here $I = \frac{1}{2}mr^2$ is the moment of inertia a rod rotating along its axis, and m is the rod mass, and r is the rod radius. Now, let an initial section of the rotating vortex tube of radius r_1 , and length L_1 be stretched to a length L_2 , where $L_2 > L_1$. Assume (ideally) that angular momentum is conserved during the stretching process, such that:

$$I_1\omega_1 = I_2\omega_2 \Rightarrow \frac{1}{2}m_1r_1^2\omega_1 = \frac{1}{2}m_2r_2^2\omega_2$$

Since the mass of the tube will remain constant, $m_1 = m_2$, we have:

$$r_1^2\omega_1 = r_2^2\omega_2 \Rightarrow \omega_2 = \omega_1 \frac{r_1^2}{r_2^2}$$

Note that we would also get this result assuming that circulation is constant during the process.

Since the volume of the stretched tube will remain constant, we can also write that:

$$\pi r_1^2 L_1 = \pi r_2^2 L_2 \Rightarrow r_2 = r_1 \sqrt{\frac{L_1}{L_2}}$$

Substituting into the previous equation, we have:

$$\omega_2 = \omega_1 \frac{r_1^2}{r_2^2} = \omega_1 \frac{L_2}{L_1}$$

So, as the ideal vortex tube is stretched, the vorticity is increased (we showed this previously in section 10.3.1).

Now, the angular kinetic energy of the initial vortex tube and the stretched vortex tube will be:

$$KE_1 = \frac{1}{2}mr_1^2\omega_1^2$$

$$KE_2 = \frac{1}{2}m_2r_2^2\omega_2^2 = \frac{1}{2}mr_1^2\left(\frac{L_1}{L_2}\right)\omega_1^2\left(\frac{L_2}{L_1}\right)^2 = \frac{1}{2}mr_1^2\omega_1^2\left(\frac{L_2}{L_1}\right) = KE_1\left(\frac{L_2}{L_1}\right)$$

Thus, when the vortex tube is stretched such that $L_2 > L_1$, the kinetic energy will increase proportional to the increase in length.

Since kinetic energy is fed from the larger rotational structures to these smaller vortices, the dissipation process within the small vortices provides a mechanism for the transfer and dissipation of the kinetic energy of the overall flow. Because this process is like a waterfall dissipating its energy in a cascade of scales as it plunges into a quiescent pool, the process of dissipation of the initial kinetic energy of a laminar flow by turbulence is generally known as the [energy cascade](#).

Interestingly, this process contains two divergent, but symbiotic processes: (1) the growth of larger, complex scales, which extract energy from the main flow, coupled with (2) the generation of continually smaller scales, which subsequently dissipate the extracted energy. As any turbulence expert would argue, this is an oversimplification of the process, but it does capture the essence of what nature is physically trying to achieve.

An excellent example of these processes of scale change and energy dissipation in action is the dissipation of the kinetic energy of a wall jet in a hot tub or swimming pool. If you place your hand in front of one of the jets, you will notice that when your hand is very close to the jet's origin, you will feel a pressure on your hand that is relatively uniform, with some small scale fluctuations. However, as you move your hand away from the origin, your hand will experience larger and more intermittent pulsations in the pressure (due to the growth in the larger vortical structures), but a reduction in the average pressure, as the jet kinetic energy is dissipated by the smaller vortices. As you move your hand even farther from the origin, the pulsations will become of even larger extent, but also weaker, as the large scales grow, but the total energy of the jet is dissipated. Eventually, at a distance well removed from the origin, this vortex interaction succeeds in both distributing the concentrated energy of the initial jet over a very broad area, and dissipating it via the small scales through this complicated energy cascade. At that point, it is unlikely that your hand can detect much of the previous momentum of the initial jet.

A similar type of process applies for wakes, which are generally created by flows around bluff bodies. However, wake flows are often dominated by large scale inviscid instabilities, which may initiate as periodic vortex shedding, prior to a change of state to a randomly turbulent flow. For example, the vortex shedding from a circular cylinder, as shown in figure 17.3c and discussed in Section 15.4, will develop and remain laminar well before turbulent behavior develops. And when turbulent behavior does develop (generally around $Re > 200$, where Re is based on the width of the bluff body), it will first develop within the shed vortices, rendering them subject to small-scale three-dimensional vortex stretching, leading to kinetic energy dissipation within the shed vortices. At much higher Reynolds numbers (roughly $Re > 3 \times 10^5$),

the shear layer exiting the bluff body will break down to turbulence prior to formation of the shedding vortices, and thus mediate, and eventually eliminate the periodic shedding process.

Recall that wakes, like jets, were predicted by linear stability theory to become unstable at $Re \cong 4$. As figure 17.3 illustrates, the flow over a cylinder does just that—but it transitions to a different stable state, not to turbulence. Thus, a transition from an initial laminar flow of one state can result in a different, but still laminar, state. Turbulence is not always the result of a transition of a laminar flow, but it is the most likely state.

Flow across a grid of wires presents an interesting process. One can think of this as producing a spatially periodic distribution of jets and wakes, like that shown in figure 17.7d, and thus a condition very sensitive to instability. However, unlike a jet, wake, or shear flow, the scales of this type of flow start basically at the spacing of the grid and slowly decay with distance, and do not extract additional kinetic energy from the mean flow (once passing through the grid). The reason for this is that all initial inflections and grid-created shear layers are off setting, and there are no significant velocity differences beyond the scale of the grid. Thus, the vortex structures within the flow are generated initially at the scale of the grid, and while they may expand and grow with distance, there can be no entrainment of additional kinetic energy from the mean flow. Additionally, the vorticity within this flow will quickly reorient in three-dimensions such that energy dissipation takes place in an almost isotropic manner (i.e. kinetic energy will be dissipated uniformly by vortices/vorticity oriented roughly uniformly in all three-dimensions). Since the substantive vortex stretching occurring in jets, wakes, and shear layers does not occur with grid turbulence, the initial kinetic energy imparted to the instabilities by the flow interaction with the grid will dissipate slowly with downstream distance.

A nice aspect of a grid flow is that if a flow approaching a grid contains disturbances/instabilities (e.g. large vortices) that are greater than the grid scale size, after passing through the grid these disturbances will be reduced to the scale of the grid instability, and will dissipate out of the flow at a rate corresponding to that of the grid disturbances. This process of disturbance reduction is put to good use in reducing the level of disturbances and turbulence entering wind tunnels, or any other ducted flows, where minimal flow fluctuations are required. That is the reason why all good wind tunnel facilities are built with both flow straighteners (closely-packed collections of tubes oriented in the streamwise direction), followed by a set of several screens, often of sequentially smaller grid size. This [NASA technical brief](#) discusses the use to screens to control the inlet turbulence levels in wind tunnels.

Note that jets, wakes, shear layers, and grids generate initial turbulence of some form, which (in the absence of adjacent solid surfaces) then advects with the main flow, eventually undergoing viscous dissipation. As such, these type of flows are non-sustaining turbulence, as discussed in Section 17.1. Anytime generated turbulence does not encounter subsequent solid surfaces or other dissimilar fluid streams, the turbulence is generally not sustained.

17.3.2 Transition of Bounded Flows: Natural

Although the initiation of transition for unbounded flows begins essentially at their point of formation (due to their very unstable nature), the initiation point and extent of transition for bounded flows is less well defined. Referring back to figure 17.1, the precise location of the point where transition begins and where it ends is very fuzzy, and dependent on the initial conditions of the flow, the adjacent surface roughness, and the type of disturbance(s) present. However, a remarkable observation, both experimentally, and more recently computationally, is that the end state of turbulence for most flows is quite consistent, and somewhat predictable for a wide variety of initially laminar conditions. Once a full-turbulent flow has developed, the statistics and the behavior of the flow are remarkably consistent, and in most cases ignorant of the initial conditions which precipitated the development of the turbulent flow. In other words, once a bounded flow achieves a developed state of turbulence, the method by which the flow evolved to a turbulent state is generally irrelevant.

So, what does happen during the transition process, and how does a bounded flow go from being fully laminar to fully turbulent? To understand the beginning of transition, it would help to know what actually happens as a disturbance amplifies within a laminar bounded flow. In section 17.2 we modeled the disturbances as traveling waves, with specific wave number and wave velocity. This allowed the development of a stability graph, such as figure 17.6, showing regions of damping and amplification of such waves for a specific type of flow. To test the validity of the traveling wave model, and the resultant theoretical predictions of wave growth, [Schubauer and Skramstad \(1947\)](#) performed some very meticulous experiments on laminar boundary layers in a large wind tunnel facility. Using a thin, magnetically-excited metal ribbon located close to the boundary surface, they generated periodic waves of varying wave number and amplitude, and demonstrated the validity of stability graphs like that shown in figure 17.6. The single wave number disturbances Schubauer and Skramstad generated, and tracked, are known as [Tollmien-Schlichting waves](#), after the two researchers who developed the first stability solutions of Eq. 17.5.

An important, if not more important experimental study, was that done by [Klebanoff et al. \(1962\)](#), where they showed that following the wave generation, initially two-dimensional Tollmien-Schlichting waves very rapidly develop into three-dimensional waves, developing a transverse peak-and-valley velocity profile very near the bounding surface, as shown schematically within regions 2 and 3 in Figure 17.10. It was subsequently shown that this peak-valley behavior is the result of the longitudinal (stream-wise) tilting and stretching of initially transverse boundary-layer vorticity into vortices in the stream-wise direction. This three-dimensionality is accentuated with stream-wise distance, until the stretched vortices begin to interact to form larger three-dimensional agglomerations of vorticity, while simultaneously

breaking down into smaller units of vorticity, as shown in region 4 of figure 17.10. This process is similar to that noted for the breakdown of unbounded flows, with (1) the larger structures interacting with the outer flow at the edge of the boundary layer to entrain kinetic energy, while (2) the smaller vorticity units are stretched to a small enough scale where effective viscous dissipation of the kinetic energy can take place.

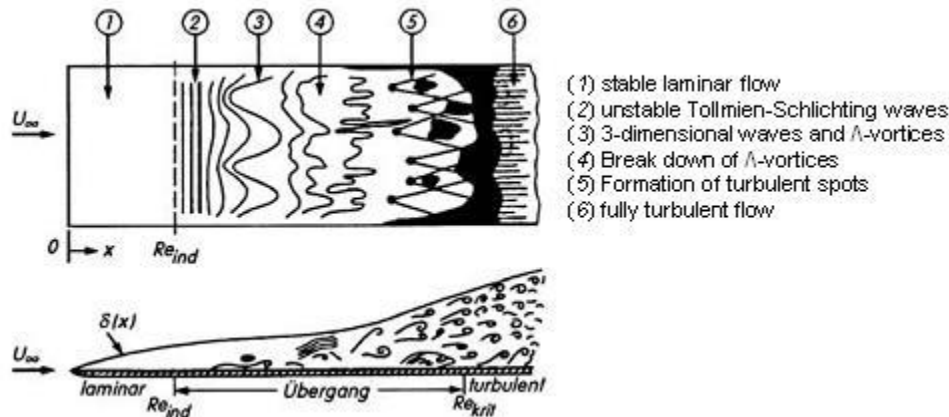


Figure 17.10 Transition mechanism on a flat plate. (Source: H. Schlichting et al, "Boundary –Layer Theory", McGraw-Hill, 2006). Note: Übergang = Transition

The experiments by [Schubauer and Skramstad \(1947\)](#) and [Klebanoff et al. \(1962\)](#) were done in extremely controlled environments, starting with two-dimensional, single wave-number disturbances. In most real systems, as we discussed, naturally occurring disturbances within a laminar flow are neither two-dimensional, nor of a single wave number. Consequently, transition does not start uniformly at a specific Re_{δ^*} . Thus, the breakdown to turbulence in a real laminar flow will begin somewhat sporadically, developing in what are termed turbulent "spots", shown schematically as region 5 of figure 17.10. Turbulent spots were first observed by [Emmons \(1951\)](#) as localized regions of turbulence, which develop naturally and apparently randomly as localized regions of turbulence. Once formed, these turbulent spots travel downstream, expanding in both the stream-wise and span-wise directions. Interestingly, the leading edge of a spot travels more rapidly ($0.9 U_\infty$, where U_∞ is the velocity of the outer edge of the boundary layer) than the trailing edge ($0.5 U_\infty$), thus expanding the stream-wise extent of the spot. A spot also acts as a moving disturbance, which entrains, disturbs, and otherwise interacts strongly with fluid adjacent to it, resulting in a transverse expansion of the spot, spreading at half angles of 8° to 12° relative to its stream-wise axis.

As turbulent spots develop and expand, both in the stream-wise and transverse directions, the manifold spots that initially develop will eventually join, or coalesce. When all regions of the flow are encompassed by turbulent behavior, the flow is considered fully turbulent, shown schematically as region 6 of figure 17.10, and transition to turbulence is considered to have been

completed. At the end of transition (a rather fuzzy demarcation), boundary layer turbulence is remarkable in that it becomes what we discussed in Section 17.1 as self-sustaining turbulence. What this means again is that once a flow becomes fully turbulent, the flow will remain turbulent, and perpetuate the complex three-dimensional generation, agglomeration, and breakdown of vorticity which is turbulence, as long as the flow remains bounded.

Now figure 17.10 may seem a bit busy, and possibly confusing. However, it is a simplification of the complicated processes of transition to turbulence. To see a simulation of the process of initial transition from turbulent spots to early turbulence, view this video by [Lee and Zaki \(2015\)](#). It is a remarkable numerical simulation that shows the manifold complexity of the transition of a flat plate boundary layer from laminar to early turbulence. Although a simulation, I am guessing that this is close to what actually happens in reality. I'm sure you will find this simulation impressive, fascinating, and very intimidating with regard to the complexity of the behavior.

17.3.3 Transition of Bounded Flows: Forced

While naturally transitioning bounded flows depend on the initial presence of disturbances to initiate the process, the point of initiation will be somewhat sporadic. However, the process of transition can be forced to occur by the use of surface roughness, either natural or artificially applied. One can generally categorize roughness into two types ([White \(1991\)](#)): (1) two-dimensional roughness, usually a wire or rod placed on the bounding surface transverse to the flow direction, and (2) three-dimensional roughness, which can consist of small spheres, hemispheres, sand grains, or similar elements, located either singly or multiply distributed on the bounding surface. These roughness elements, when artificially placed on a surface to force transition to turbulence, are typically termed "boundary layer trips." Interestingly, the effect of two- and three-dimensional roughness on transition is quite different.

Generally, small amounts of roughness of any type will not affect the transition process or location unless it is of significant height relative to the local displacement thickness, δ^* . Letting the height of the roughness be given by k , for a two-dimensional roughness, if k/δ^* is less than 0.3, the roughness will have essentially no effect on the location of transition. However, for $k/\delta^* > 0.3$, the point of transition will move upstream closer to the roughness element. It has been shown that the minimal Reynolds number based on the roughness height for "tripping" a laminar flat plate boundary layer to initiate transition is (roughly) [[White \(1991\)](#)]:

$$\text{Re}_k = \frac{Uk}{\nu} = 850$$

However, as Re_k increases, the point of transition will move back toward the trip. To have transition occur immediately following the roughness element requires $\text{Re}_k \cong 2800$. These are only rough rules of thumb, since there is no consistent agreement in the literature.

For three-dimensional roughness, little effect on transition is expected before $k/\delta^* \cong 0.6$, about twice that for two-dimensional elements.

17.4 The Character of Turbulence

As you can guess, once a flow transitions to turbulence, the behavior is, as we pointed out in section 17.1 (after R. W. Stewart), a process of "disorder, enhanced mixing, and three-dimensional motions involving angular momentum (vorticity)". The character of turbulence, often called the "structure," is such that it does satisfy these characteristics. However, as we discussed in section 17.3, there are identifiable ways that turbulence evolves which have a particular rhyme and reason. In this section, we will review a bit of this structure, which will help motivate our approach to modeling the turbulence process. Be aware, however, that the study of turbulent structure is a topic that is still widely studied and debated, and that the small amount that we discuss here is just the tip of a very complicated iceberg.

First, through hypothesis and experiment turbulence has been shown to have a flow structure that extends over a range of scales of motion. After the breakdown of a laminar flow, turbulence results in the generation of both large- and small-scale flow structures, both of which have a purpose. Following either the inviscid-type (Kelvin-Helmholtz) breakdown of unbounded shear layers, or the amplification of Tollmien-Schlichting waves in a boundary layer, the initial flow structures (usually vortical) proceed in two somewhat divergent directions: (1) amalgamation with other structures, to yield larger scale structures, and (2) stretching, tilting, and intensification, to yield progressively smaller scale vortical structures. The larger scale structures usually develop adjacent to the interface between the turbulence region and the main outer flow (which is generally non-turbulent). These larger scales interact with the outer flow to entrain more fluid into the turbulent region, which increases the extent of, and adds kinetic energy to, the turbulent region.

While the large scales are of the order of the thickness of the turbulent region (e.g. the boundary layer thickness, δ), the small dissipation scales, known as [Kolmogorov length scales](#), are of size:

$$L = \left(\frac{v^3 \delta}{U^3} \right)^{1/4} \quad \text{or} \quad \frac{L}{\delta} = \left(\frac{v^3}{U^3 \delta^3} \right)^{1/4} = \left(\frac{v}{U \delta} \right)^{3/4} = \left(\frac{1}{\text{Re}_\delta} \right)^{3/4}$$

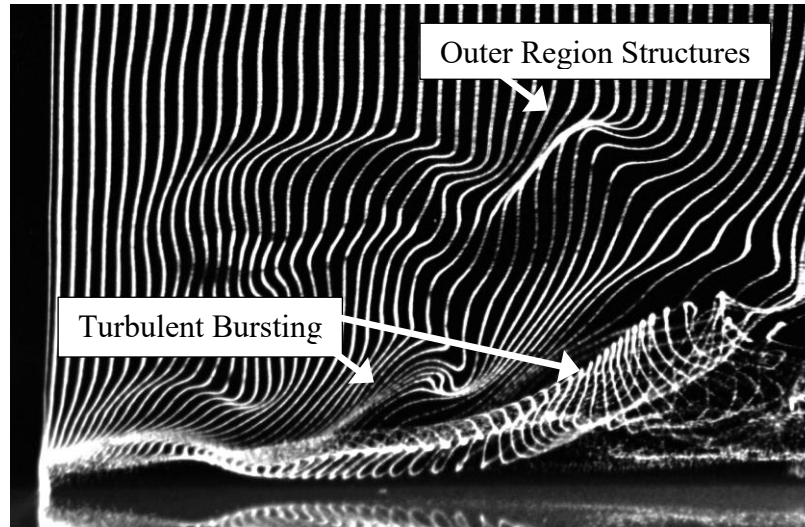
Here, δ is the thickness of the turbulent region (e.g. the boundary layer thickness for a turbulent boundary layer). To give this some perspective, a boundary layer of thickness $\delta = 3$ cm in water flowing at 1 m/s and kinematic viscosity of 10^{-6} m²/s has a $\text{Re}_\delta = 30,000$. For this flow the corresponding scale of the dissipating flow structures is $\frac{L}{\delta} = 0.00044$, or $L = 0.013$ mm. Small scales indeed!

In section 17.3.2, we mentioned that a turbulent boundary layer flow is a self-sustaining flow. What this means is once a boundary layer flow achieves a turbulent state, it not only remains turbulent, but also sustains the turbulent state, as opposed to dissipating away like an unbounded flow. We mentioned that the larger scales of boundary layer turbulence facilitate the introduction of new kinetic energy into the boundary layer from the outer flow; but while this is necessary, it is not sufficient to sustain the continuing turbulence. The sustaining mechanism of boundary layer turbulence is a process of interaction of the fluid adjacent to the solid boundary known as "bursting". Bursting is an intermittent process of fluid ejection from very near the boundary that introduces additional vorticity into the boundary layer. Note that since the total vorticity (i.e. the circulation) within the boundary layer must remain essentially constant, this bursting process introduces, on average, a balanced quantity of vorticity of both signs into the flow. This offsetting collection of discrete vorticity (1) is eventually stretched and intensified, subsequently dissipating the energy at these smaller scales, or (2) undergoes a complicated process of amalgamation with other structures of both like and opposite signs of rotation, which supports the development and growth of the larger outer-region structures. Despite the fact that these bursting processes initiate at relatively small scales, the process is so prolific near the boundary surface that collectively it becomes the source of continuing new vorticity to sustain boundary layer turbulence.

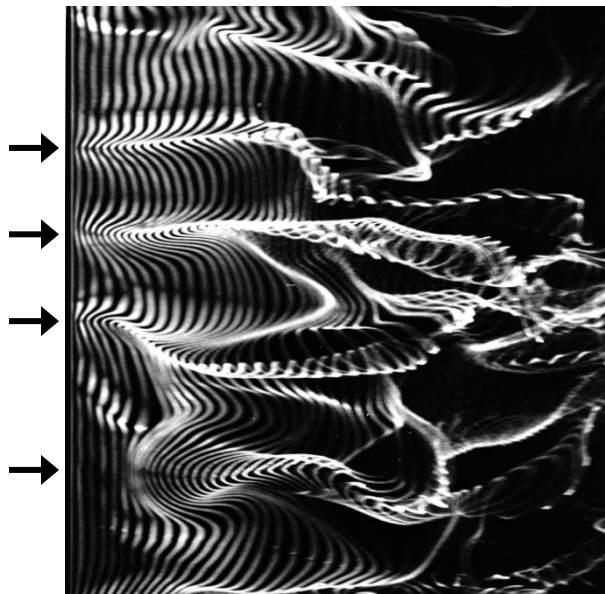
So, what causes the generation of this "new" vorticity? As we showed in section 11.5, the only source of vorticity in a flow adjacent to solid, stationary boundary is the presence of a pressure gradient. Thus, the development of new vorticity to sustain a turbulent boundary layer must come from variations in surface pressure. Since the mean pressure gradient for a flat plate flow is zero, the new vorticity must be the result of local pressure variations very near the solid boundary. What is the cause of such local pressure variations? As we showed in sections 7.5 and 7.6, flow curvature gives rise to pressure increases in the direction of the curvature. So, curvature of the streamlines near the bounding surface must be present, which will be the case when vortices are adjacent to the surface. Additionally, locally impinging flows from the outer region or local flows away from the surface will also be the result of local pressure variations, and thus sources of new vorticity.

As mentioned, the bursting process occurs intermittently, in a somewhat random, but repetitive process, with fluid appearing to erupt from very near the boundary into the boundary layer fluid. Of course, if fluid is ejected from the boundary, by conservation of mass there must be a comparable amount of fluid that moves toward the surface. The large outer region flow structures entrain high-energy fluid from the edge of the boundary layer, which penetrates down to the bounding surface, creating what is termed a high-speed "sweep". Moreover, although Stewart speaks of disorder in turbulence, the process of fluid moving toward the surface, and the bursting of fluid away from the surface, are somewhat organized processes. The turbulence production process near the surface develops as almost parallel flows both toward and away from

the surface, which gives rise to what appears to be a "streak" like pattern very near the surface, with higher-velocity regions flanked by low-velocity regions. This is not dissimilar from the three-dimensional distortion of Tollmien-Schlichting waves during the transition process, discussed in section 17.3.2.



(a) Side-view



(b) Plan-view

Figure 17.11 Hydrogen bubble flow visualization of a low Reynolds number turbulent boundary layer. Water flow: $Re_x = 2.2 \times 10^5$ and $Re_{\delta^*} = 746$. (a) Side view illustrating turbulent "bursting" near the bounding surface, and development of large outer structures. (b) Plan-view illustrating alternating low-speed "streak" like behavior [indicated by arrows \rightarrow] near the surface (visualization wire located at $y^+ = 5$ — see section 17.6.1 for discussion of y^+ scaling).

Now, since the low-velocity streak regions are adjacent to higher-velocity flows immediately above the streaks, this creates an inflection in the local mean velocity profile, which is of course unstable. The breakdown of this velocity inflection results in the "burst" of fluid and vorticity into the boundary layer. This breakdown is very sporadic, but repetitive, providing the new vorticity to sustain the boundary layer. Additionally, although the process is still widely debated, the resulting interaction adjacent to the boundary during the streak destabilization process is such that it sustains the continuing re-formation of the high- and low-velocity streak regions.

Figure 17.11 shows two hydrogen bubble visualization pictures (in a water flow) which reveal some of the flow structure of a turbulent boundary layer discussed in this section (click [here](#) to see an in depth presentation on hydrogen bubble flow visualization--a video from an older film, so a bit grainy, but informative). Very fine time-lines of hydrogen bubbles are generated at high frequency by electrolysis from a very thin (0.025 mm) wire (on the far left of each picture). Illumination of the subsequent lines of bubbles reveals the deformation of the local flow within the boundary layer. Figure 17.11(a) is a side-view, with a wire oriented vertically from the bounding wall and spanning the boundary layer. Here, the bubble time-lines reveal patterns characteristic of both bursting behavior (combined with vortex stretching) near the surface, and larger outer-region vortical structures. Figure 17.11(b) is a plan-view, with the wire stretched transverse across the plate and very near the surface. This bubble time-line image reveals the stream-wise streak-like behavior, indicative of the vertical inflow and outflow of fluid adjacent to the plate boundary.

Figure 17.12 is a simple model illustrating the basic behavior within a turbulent boundary layer that outlines the basic processes, which sustain and maintain the turbulence process.

As illustrated, the six key elements of this sustaining process are:

- (1) The bursting process occurring near the boundary, which sustains the turbulence;
- (2) Formation of wall-region vortices from the vorticity in the ejected boundary fluid;
- (3) Amalgamation of these initial burst-generated vortical structures to form larger, outer region flow structures;
- (4) Three-dimensional stretching of small-scale turbulence by the larger outer region structures, which both reduces the scales and dissipates energy;
- (5) Inward entrainment of free-stream fluid, which is manifested as a sweep of higher-speed fluid toward the boundary to replace the ejected bursting fluid.
- (6) "New" vorticity generated at boundary by local pressure gradients due to flow curvature near boundary (vortices/sweeps/ejections).

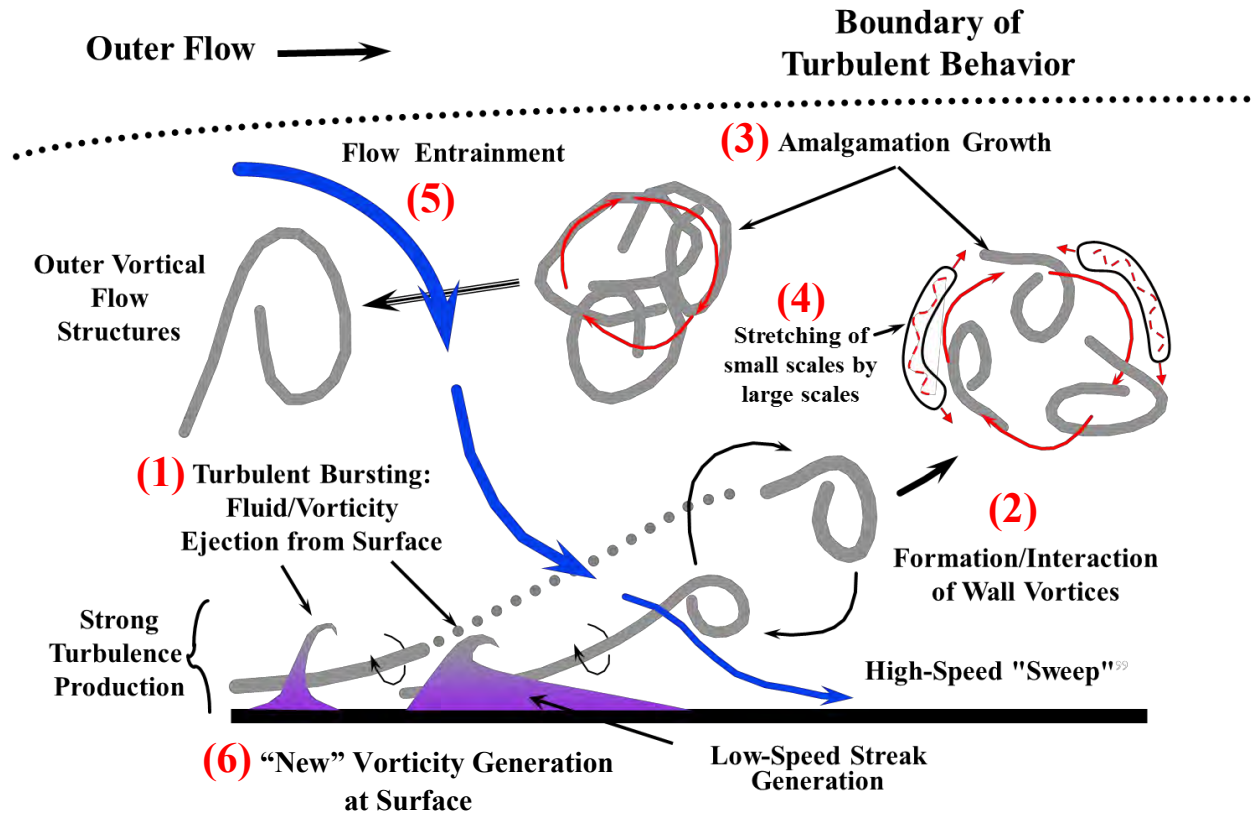


Figure 17.12 A hypothesized general model of the basis processes sustaining the development and energy dissipation within a turbulent boundary. Not to scale.

Thus, boundary layer turbulence sustains itself by creating both large- and small-scale flow structures, which respectively entrain more fluid/kinetic energy and ultimately dissipate this kinetic energy. A quasi-organized process of fluid bursting/streak formation adjacent to the bounding surface introduces new vorticity to the boundary layer, which is stretched, yielding small scales that dissipate kinetic energy, and/or amalgamate into larger flow structures that maintain the entrainment process. This is a bit of a simplistic description of a very complex process, but it captures the essence of the turbulence process in a bounded flow, and the growth/dissipation process is not dissimilar from the process for an unbounded turbulent flow. A more detailed discussion of the hypothesized processes and structure of a turbulent boundary layer can be found in [Smith and Walker \(1997\)](#).

17.5 Mathematical Modeling of Turbulent Flow

So how do we take this generic, and complicated, flow process discussed in Section 17.4, and model it such that we can predict properties of engineering interest, such as mean velocity behavior and surface shear stress? Obviously, turbulence is not a steady environment, yet it is not

exactly unsteady. Early experimental measurements of local velocities in turbulence, such as those illustrated in figure 17.2 for a turbulent boundary layer, revealed that the collective behavior of a turbulent flow created velocity behavior that appeared as somewhat random local fluctuations about some average, or mean, value. Therefore, a very simplified modeling approach that views the velocity behavior within a turbulent flow as a combination of a mean part and a fluctuating part seems promising, and reflective of the "disorder" or randomness of turbulence. Now this approach of course discounts all the flow structure we alluded to in section 17.4. However, modeling such a semi-organized process of three-dimensional vortical flow structure is quite complicated, and very computationally intensive. Therefore, we opt to make our model of turbulence as simple as possible. This approach, by the way, is the same approach suggested by [Osborne Reynolds](#) (1883), who was the first to observe and document the breakdown of turbulence (and for whom the Reynolds number is named). Reynolds did this initial research from detailed observations of dye injection into the flow of water in a pipe. To model these random fluctuations in the local velocity, we use a statistical approach, which assumes that the velocity at a point in a turbulent flow can be modeled as a set of random velocity fluctuations about a local mean value. Employing Cartesian notation, for a velocity probe measuring only the x-direction component, u , we would characterize the velocity as shown in figure 17.13.

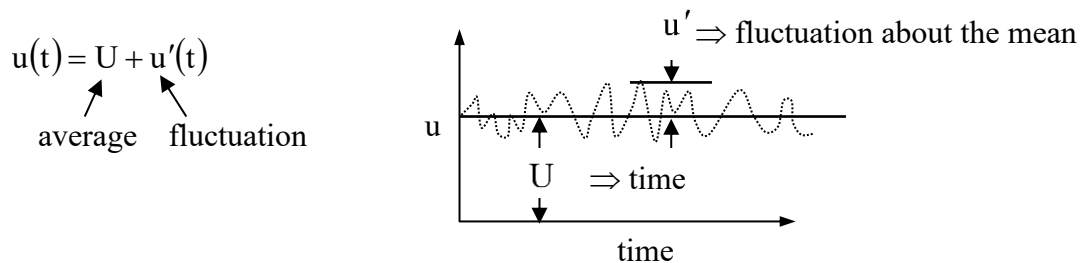


Figure 17.13 Representation of turbulent velocity as combination of a mean component, U , plus a fluctuating component, u' .

Thus, the mean component of the velocity, U , is the time average over a time period T , where T is a sufficient time for the mean to reach a constant value, given as:

$$U = \frac{1}{T} \int_0^T u dt$$

The fluctuating component of the velocity, u' , is the instantaneous velocity variation about the mean value, which can be viewed as $u'(t) = u(t) - U$. Since u' is assumed to be a random function of time, we often use the root mean square of u' to characterize the level of the unsteadiness, such that:

$$u'_{\text{rms}} = \left[\frac{1}{T} \int_0^T u'^2 dt \right]^{1/2} = \sqrt{u'^2}$$

u'_{rms} is generally termed the turbulence intensity, and is often used, particularly in experimental measurements, to characterize the magnitude of the turbulence fluctuations.

Similar to the way we chose to characterize the u velocity, we use the same approach for the y and z direction velocities, such that:

$$v = V + v' , w = W + w'$$

Recall that we applied a similar approach to the velocity behavior in section 17.2, where we considered the stability of laminar flows. For the case of stability, we made an assumption that the unsteady velocity components are periodic and subject to either damping or amplification. For turbulence, we cannot make an assumption of periodicity or amplification/damping, but only that the fluctuating velocity components are time dependent.

Since we want to determine the average mean velocity behavior of a flow, and the resultant average stresses associated with the flow, our approach is as follows:

- 1) Substitute the time-dependent velocities into the differential equations of motion (i.e. continuity and Navier-Stokes)
- 2) Time-average the equations
- 3) Drop terms which average to zero

$$\text{e.g. } \overline{u'} = \frac{1}{T} \int_0^T u' dt = 0 \quad \text{and} \quad \overline{Uu'} = \frac{1}{T} \int_0^T Uu' dt = \frac{U}{T} \int_0^T u' dt = 0$$

- 4) Solve the resulting equation.

This process of averaging is known as Reynolds averaging (often termed RANS, for Reynolds-Averaged Navier-Stokes equations), after the work by Osborne Reynolds (1895), and results in a set of equations that can *potentially* be solved for the average turbulent velocity behavior for a flow of interest (more on this later).

17.5.1 Reynolds Averaged Equations

In this section, we will develop the Reynolds averaged equations in two dimensions for a Cartesian system. This approach is, of course, generically expandable to three dimensions (see Eqs. 17.18 below), and can be done similarly in other coordinate systems (i.e., cylindrical and spherical). However, the results for two-dimensions will suffice for our purposes of

introduction. Here, we develop the x- and y-component equations, where U and V are the mean velocity components, and u' and v' are the fluctuating components. We make the same assumption for the pressure, such that we can write the total velocities and pressure for a two-dimensional turbulent flow as:

$$u = U + u', \quad v = V + v', \quad p = P + p' \tag{17.7}$$

Substituting Eqs. 17.7 into the x-direction Navier-Stokes equation, Eq. 5.46b (reduced to two dimensions, steady in the mean), gives:

$$u \frac{\partial u}{\partial x} + v \frac{\partial u}{\partial y} = -\frac{1}{\rho} \frac{\partial p}{\partial x} + \nu \frac{\partial^2 u}{\partial x^2} + \nu \frac{\partial^2 u}{\partial y^2}$$

$$(U + u') \frac{\partial(U + u')}{\partial x} + (V + v') \frac{\partial(U + u')}{\partial y} = -\frac{1}{\rho} \frac{\partial(P + p')}{\partial x} + \nu \frac{\partial^2(U + u')}{\partial x^2} + \nu \frac{\partial^2(U + u')}{\partial y^2}$$

Expanding this equation, we have:

$$U \frac{\partial U}{\partial x} + u' \frac{\partial U}{\partial x} + U \frac{\partial u'}{\partial x} + u' \frac{\partial u'}{\partial x} + V \frac{\partial U}{\partial y} + v' \frac{\partial U}{\partial y} + V \frac{\partial v'}{\partial y} + v' \frac{\partial v'}{\partial y}$$

$$= -\frac{1}{\rho} \frac{\partial P}{\partial x} - \frac{1}{\rho} \frac{\partial p'}{\partial x} + \nu \frac{\partial^2 U}{\partial x^2} + \nu \frac{\partial^2 u'}{\partial x^2} + \nu \frac{\partial^2 U}{\partial y^2} + \nu \frac{\partial^2 v'}{\partial y^2}$$

If we time average this equation -- an overbar indicating time averaging of the indicated term(s) - the time averages of fluctuating terms and the product of a mean term and a fluctuating term, will all average to zero, such that:

$$\overline{U \frac{\partial U}{\partial x}} + \overline{u' \frac{\partial U}{\partial x}} + \overline{U \frac{\partial u'}{\partial x}} + \overline{u' \frac{\partial u'}{\partial x}} + \overline{V \frac{\partial U}{\partial y}} + \overline{v' \frac{\partial U}{\partial y}} + \overline{V \frac{\partial v'}{\partial y}} + \overline{v' \frac{\partial v'}{\partial y}}$$

$$= -\frac{1}{\rho} \overline{\frac{\partial P}{\partial x}} - \frac{1}{\rho} \overline{\frac{\partial p'}{\partial x}} + \nu \overline{\frac{\partial^2 U}{\partial x^2}} + \nu \overline{\frac{\partial^2 u'}{\partial x^2}} + \nu \overline{\frac{\partial^2 U}{\partial y^2}} + \nu \overline{\frac{\partial^2 v'}{\partial y^2}}$$

Notice that the product of two fluctuating terms, since they are assumed to be unrelated, will not average to zero. Since U, V and their derivatives are time-mean terms, this means that we can drop the overbar on terms that contain only mean velocity values. Therefore, we are left with:

$$U \frac{\partial U}{\partial x} + u' \frac{\partial u'}{\partial x} + V \frac{\partial U}{\partial y} + v' \frac{\partial v'}{\partial y} = -\frac{1}{\rho} \frac{\partial P}{\partial x} + \nu \frac{\partial^2 U}{\partial x^2} + \nu \frac{\partial^2 U}{\partial y^2}$$

Moving the time-averaged fluctuation terms to the right side of the equation gives:

$$U \frac{\partial U}{\partial x} + V \frac{\partial U}{\partial y} = -\frac{1}{\rho} \frac{\partial P}{\partial x} + \nu \frac{\partial^2 U}{\partial x^2} + \nu \frac{\partial^2 U}{\partial y^2} - \overline{u' \frac{\partial u'}{\partial x}} - \overline{v' \frac{\partial u'}{\partial y}} \quad (17.8)$$

Now, substituting Eqs. 17.7 into the two-dimensional continuity equation, Eq. 5.46a (reduced to two dimensions), and expanding gives:

$$\frac{\partial u}{\partial x} + \frac{\partial v}{\partial y} = 0 = \frac{\partial(U + u')}{\partial x} + \frac{\partial(V + v')}{\partial y} = \frac{\partial U}{\partial x} + \frac{\partial V}{\partial y} + \frac{\partial u'}{\partial x} + \frac{\partial v'}{\partial y} \quad (17.9)$$

Time averaging Eq.17.9 gives:

$$\frac{\partial \overline{U}}{\partial x} + \frac{\partial \overline{V}}{\partial y} + \frac{\overset{0}{\partial u'}}{\partial x} + \frac{\overset{0}{\partial v'}}{\partial y} = 0$$

Since the time averages of the mean velocity derivatives must also satisfy continuity, we have:

$$\frac{\partial \overline{U}}{\partial x} + \frac{\partial \overline{V}}{\partial y} = \frac{\partial U}{\partial x} + \frac{\partial V}{\partial y} = 0 \quad (17.10)$$

Subtracting Eq. 17.10 From Eq. 17.9 gives:

$$\frac{\partial u'}{\partial x} + \frac{\partial v'}{\partial y} = 0 \quad (17.11)$$

Now, we rewrite the last two terms of Eq. 17.8, by adding and subtracting $\overline{u' \frac{\partial u'}{\partial x}}$

$$-\overline{u' \frac{\partial u'}{\partial x}} - \overline{v' \frac{\partial u'}{\partial y}} = -\overline{u' \frac{\partial u'}{\partial x}} - \overline{v' \frac{\partial u'}{\partial y}} - \overline{u' \frac{\partial u'}{\partial x}} + \overline{u' \frac{\partial u'}{\partial x}} = -2\overline{u' \frac{\partial u'}{\partial x}} - \overline{v' \frac{\partial u'}{\partial y}} + \overline{u' \frac{\partial u'}{\partial x}} \quad (17.12)$$

Substituting $\frac{\partial u'}{\partial x} = -\frac{\partial v'}{\partial y}$ from Eq.17.11 into Eq. 17.12, and rearranging the terms gives:

$$-2\overline{u' \frac{\partial u'}{\partial x}} - \overline{v' \frac{\partial u'}{\partial y}} - \overline{u' \frac{\partial v'}{\partial y}} = -\overline{u' \frac{\partial u'}{\partial x}} - \overline{v' \frac{\partial u'}{\partial y}} = -\frac{\partial(\overline{u'^2})}{\partial x} - \frac{\partial(\overline{u'v'})}{\partial y} \quad (17.13)$$

Substituting Eq. 17.13 back into Eq. 17.8 gives:

$$U \frac{\partial U}{\partial x} + V \frac{\partial U}{\partial y} = -\frac{1}{\rho} \frac{\partial P}{\partial x} + \nu \frac{\partial^2 U}{\partial x^2} + \nu \frac{\partial^2 U}{\partial y^2} - \frac{\partial(\overline{u'v'})}{\partial y} - \frac{\partial(\overline{u'^2})}{\partial x} \quad (17.14)$$

Similarly, if we apply the same assumptions of fluctuating properties and time averaging to the y-direction Navier-Stokes equation, Eq. 5.46c (in two-dimensions), we get:

$$U \frac{\partial V}{\partial x} + V \frac{\partial U}{\partial y} = -\frac{1}{\rho} \frac{\partial p}{\partial y} + \nu \frac{\partial^2 V}{\partial x^2} + \nu \frac{\partial^2 U}{\partial y^2} - \frac{\partial(\overline{u'v'})}{\partial x} - \frac{\partial(\overline{v'^2})}{\partial y} \quad (17.15)$$

Assuming that our fluctuation model is appropriate, Eqs. 17.14 and 17.15 are equations for the mean velocity components U and V . Note that these equations differ from those for a laminar flow by the last two terms in each equation. These last two terms account for the effects of the velocity fluctuations on the mean flow due to cross-stream momentum exchange due to the fluctuations. We learned in Section 6.3.3 and in Section 11.4.1, that the introduction of a flow normal to the direction of the mean flow, by suction through a porous surface, results in an increase in the local shear stress at the suction surface due to additional momentum changes. Recall that the shear stress developed in section 6.3.3 for a Poiseuille-type flow with transverse injection/suction, was a rather complicated term, which included both the effects of conventional shear and the effects of cross-stream momentum exchange due to the fluid suction. Also recall in section 11.4.1, Eq. 11.33 showed that the wall shear stress for a fully-developed boundary layer with wall suction could be reduced to the cross-stream momentum changes across the transpiration boundary layer. The last two terms in Eqs. 17.14 and 17.15 are of a similar origin—cross-stream momentum exchanges resulting from time-dependent variations of u and v from the local mean velocities, U and V .

Note that the first of these two terms in Eqs. 17.14 is due to cross-stream momentum exchange (since v' is normal to u'), whereas the second term is due to in-line fluctuations (e.g. $u'^2 = u' \cdot u'$), where the momentum changes are due to the fluctuations in the direction of the mean flow. Normally, cross-stream momentum changes dominate in-line momentum changes, but not always, as in the case of isotropic grid flows (i.e. flows in the wake of a crossed-wire grid). However, for most boundary layer, jet, and simple wake flows, where the u -velocity changes most strongly in the y -direction (cross stream) it can be shown that $\frac{\partial(\overline{u'v'})}{\partial y} \gg \frac{\partial(\overline{u'^2})}{\partial x}$ and likewise, $\frac{\partial(\overline{u'v'})}{\partial x} \gg \frac{\partial(\overline{v'^2})}{\partial y}$. To illustrate this, recall our order of magnitude analysis for a boundary layer (Section 13.2), where we argued that we could neglect certain negligible terms from the two-dimensional Navier-Stokes and continuity equations to yield the two-dimensional boundary layer equations:

$$u \frac{\partial u}{\partial x} + v \frac{\partial u}{\partial y} = -\frac{1}{\rho} \frac{\partial p}{\partial x} + \nu \frac{\partial^2 u}{\partial y^2} \quad (13.13a)$$

and

$$\frac{\partial u}{\partial x} + \frac{\partial v}{\partial y} = 0 \quad (13.13b)$$

Now, consider a similar order of magnitude analysis of the latter two fluctuation velocity terms of Eq. 17.14 for a boundary layer-type flow. We first assume that the velocity fluctuations in both the x and y directions are of comparable order, since the fluctuating velocity components in turbulence are somewhat isotropic. Similar to what was done in section 13.2, we now make the assumption that:

$$x = O(L), y = O(\delta), u' = O(L), v' = O(L)$$

Here L is a characteristic length of development along the boundary layer surface, and δ is the corresponding boundary layer thickness at that location, such that $O(L) \gg O(\delta)$,

Thus, we can assess that:

$$-\frac{\overline{\partial(u'v')}}{\partial y} - \frac{\overline{\partial(u'^2)}}{\partial x} = -\frac{O(L)O(L)}{O(\delta)} - \frac{O(L)O(L)}{O(L)} = -O(L) \left[\frac{O(L)}{O(\delta)} + 1 \right]$$

We note that $\frac{O(L)}{O(\delta)} \gg 1$, and by comparison $\frac{\overline{\partial(u'v')}}{\partial y} \gg \frac{\overline{\partial(u'^2)}}{\partial x}$. This assessment has been proven to be valid experimentally, with the exception of grid turbulence flows and boundary layer flows with a large adverse pressure gradient. Therefore, to a good approximation we can neglect the $\frac{\overline{\partial(u'^2)}}{\partial x}$ term, and write Eq.17.14 as:

$$U \frac{\partial U}{\partial x} + V \frac{\partial U}{\partial y} = -\frac{1}{\rho} \frac{\partial P}{\partial x} + \nu \frac{\partial^2 U}{\partial x^2} + \nu \frac{\partial^2 U}{\partial y^2} - \frac{\overline{\partial(u'v')}}{\partial y} \quad (17.16)$$

Likewise, it can be shown that $\frac{\overline{\partial(v'^2)}}{\partial y}$ in Eq. 17.15 can also be neglected, since $\frac{\overline{\partial(u'v')}}{\partial x} \gg \frac{\overline{\partial(v'^2)}}{\partial y}$.

This reduces Eq. 17.15 to:

$$U \frac{\partial V}{\partial x} + V \frac{\partial V}{\partial y} = -\frac{1}{\rho} \frac{\partial P}{\partial y} + \nu \frac{\partial^2 V}{\partial x^2} + \nu \frac{\partial^2 V}{\partial y^2} - \frac{\overline{\partial(u'v')}}{\partial x} \quad (17.17)$$

Note that when we consider all three dimensions of a turbulent flow, we must consider an additional velocity component in the z (transverse) direction, given by $w = W + w'$. For such a three-dimensional flow we have three component equations given by:

$$U \frac{\partial U}{\partial x} + V \frac{\partial U}{\partial y} + W \frac{\partial U}{\partial z} = -\frac{1}{\rho} \frac{\partial P}{\partial x} + \nu \frac{\partial^2 U}{\partial x^2} + \nu \frac{\partial^2 U}{\partial y^2} + \nu \frac{\partial^2 U}{\partial z^2} - \frac{\overline{\partial(u'^2)}}{\partial x} - \frac{\overline{\partial(u'v')}}{\partial y} - \frac{\overline{\partial(u'w')}}{\partial z} \quad (17.18a)$$

$$U \frac{\partial V}{\partial x} + V \frac{\partial V}{\partial y} + W \frac{\partial V}{\partial z} = -\frac{1}{\rho} \frac{\partial P}{\partial y} + \nu \frac{\partial^2 V}{\partial x^2} + \nu \frac{\partial^2 V}{\partial y^2} + \nu \frac{\partial^2 V}{\partial z^2} - \frac{\overline{\partial(u'v')}}{\partial x} - \frac{\overline{\partial(v'^2)}}{\partial y} - \frac{\overline{\partial(v'w')}}{\partial z} \quad (17.18b)$$

$$U \frac{\partial W}{\partial x} + V \frac{\partial W}{\partial y} + W \frac{\partial W}{\partial z} = -\frac{1}{\rho} \frac{\partial P}{\partial z} + \nu \frac{\partial^2 W}{\partial x^2} + \nu \frac{\partial^2 W}{\partial y^2} + \nu \frac{\partial^2 W}{\partial z^2} - \frac{\overline{\partial(u'w')}}{\partial x} - \frac{\overline{\partial(v'w')}}{\partial y} - \frac{\overline{\partial(w'^2)}}{\partial z} \quad (17.18c)$$

17.5.2 Turbulent Reynolds "Stresses"

Equations 17.18 are the Navier-Stokes equations with nine additional terms due to the time-averaged unsteady velocity components. Recall that these nine additional terms originate from the momentum terms in the Navier-Stokes equation. As we alluded to above, these fluctuation momentum terms result in additional forces on the fluid, which significantly modify the mean velocity profile. However, we do not know what these fluctuation terms are, so we have a quandary, with many more unknowns than we have equations. Since we only have four equations (continuity and the three Navier-Stokes components), we must find some way to solve for, or model, the nine (actually six, as we will discuss below) fluctuation terms. Trying to add higher-order equations, such as the energy equation, just makes the process more complicated, and doesn't lead to closure (i.e. a closed form solution).

So, how do we proceed with modeling the fluctuation terms? Well, moving the fluctuation terms to the right side of the Navier-Stokes equation reveals a strong similarity to stress components. To examine this, let's consider Eq. 17.16, the x-direction N-S equation applied to a boundary layer-type flow. We note that the last two terms in Eq. 17.16 can be written as:

$$\nu \frac{\partial^2 U}{\partial y^2} - \frac{\partial(\overline{u'v'})}{\partial y} = \frac{1}{\rho} \frac{\partial}{\partial y} \left[\mu \frac{\partial U}{\partial y} - \rho(\overline{u'v'}) \right] \quad (17.19)$$

Since for a laminar flow $\tau_{yx}|_{\text{lam}} = \mu \frac{\partial U}{\partial y}$, we could infer that the other component of Eq. 17.19 could be construed as a "turbulent" component of stress due to the fluctuating behavior, or:

$$\tau_{yx}|_{\text{turb}} = -\rho(\overline{u'v'}) \quad (17.20)$$

This approach was taken by early turbulence researchers, initiated by Osborne Reynolds, and thus these apparent stresses due to the fluctuating velocity components are typically known as ["Reynolds" stresses](#). Now for three-dimensional flows, the x-direction Eq. 17.18a contains three Reynolds stresses:

$$\tau_{xx}|_{\text{turb}} = -\rho(\overline{u'^2}), \quad \tau_{yx}|_{\text{turb}} = -\rho(\overline{u'v'}), \quad \text{and} \quad \tau_{zx}|_{\text{turb}} = -\rho(\overline{u'w'})$$

Collectively, in all three Eqs. 17.18, there are a total of six different Reynolds stresses:

$$\begin{aligned} \tau_{xx}|_{\text{turb}} &= -\rho(\overline{u'^2}), & \tau_{yy}|_{\text{turb}} &= -\rho(\overline{v'^2}), & \tau_{zz}|_{\text{turb}} &= -\rho(\overline{w'^2}) \\ \tau_{yx}|_{\text{turb}} &= -\rho(\overline{u'v'}) = \tau_{xy}|_{\text{turb}}, & \tau_{yz}|_{\text{turb}} &= -\rho(\overline{v'w'}) = \tau_{zy}|_{\text{turb}}, & \tau_{zx}|_{\text{turb}} &= -\rho(\overline{u'w'}) = \tau_{xz}|_{\text{turb}} \end{aligned}$$

Note that using the equilibrium argument of section 5.6 allows the equating of the shear in adjacent planes (i.e. $\tau_{yx}|_{\text{turb}} = -\rho\overline{(u'v')} = \tau_{xy}|_{\text{turb}}$), which reduces the Reynolds stresses from nine to six. However, this still leaves us far from a tractable set of equations.

Now, let's examine how fluctuations in velocity give rise to these added stresses. To do so, let's just consider a two-dimensional boundary layer-type flow, such that the x-direction stresses can be modeled as the sum of the laminar and turbulent stresses, as shown in Eq. 17.21:

$$\tau_{yx} = \tau_{yx}|_{\text{lam}} + \tau_{yx}|_{\text{turb}} = \mu \frac{\partial U}{\partial y} + \underbrace{-\rho\overline{u'v'}}_{\text{Reynolds stress}} \tag{17.21}$$

Using the simplified model of turbulent fluid motions shown in figure 17.14, we can infer how the motion of a fluid particle through a velocity gradient results in the generation of an added “stress”.

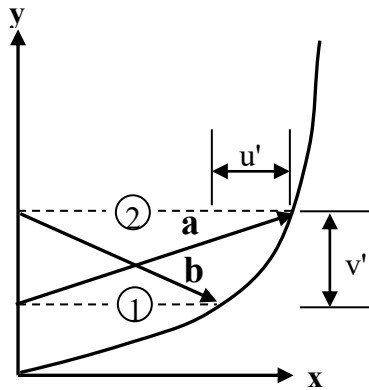


Figure 17.14 Motion of a particle: (a) upward from a region of low u-velocity (1) to a region of high u-velocity (2), or (b) downward from a region of high u-velocity (2) to a region of low u-velocity(1).

First, consider a fluid particle moving *upward* from (1) to (2). Since $v > 0$, and $u_1 < u_2$, then the fluctuating velocities for this particle would be:

$$\begin{aligned} v' &> 0 \\ u' &< 0 \quad (\text{since the arriving particle has a velocity deficit i.e. } u' = u_1 - u_2) \\ \therefore u'v' &< 0 \Rightarrow \tau_{\text{turb}} = -\rho u'v' > 0 \end{aligned}$$

Thus, a particle arriving from (1) will be accelerated to the u-velocity at (2). This requires momentum being transferred from the flow to the particle, which is the result of an applied stress equivalent to $-\rho u'v'$ on the particle by the flow at (2). Conversely, the flow at (2) will be

decelerated by the arrival of the velocity-deficit particle from (1), which is the result of an equal and opposite stress applied by the particle on the flow at (2).

Since continuity requires that every outflow must be balanced by an inflow, the upward movement of a particle from (1) to (2) must be balanced by a corresponding *downward* movement of a separate fluid particle from (2) to (1). For this downward movement, (b) in figure 17.14, we have $v < 0$, and $u_2 > u_1$, such that the fluctuating velocities for this particle would be:

$$v' < 0$$

$$u' > 0 \quad (\text{the arriving particle now has a velocity excess i.e. } u' = u_2 - u_1)$$

$$\therefore u'v' < 0 \Rightarrow \tau_{\text{turb}} = -\rho u'v' > 0$$

Thus, while the process is reversed, a positive stress again results from the arrival of the particle. In this case, the particle from (2) arrives at (1) with an excess of velocity relative to the surrounding flow, and thus will be decelerated to the velocity at (1), which is the result of an applied stress on the particle equivalent to $-\rho u'v'$ by the flow at (1). And the local flow at (1) will be accelerated by the arrival of the velocity-excess particle from (2), which is again the result of an equal and opposite stress applied by the particle on the flow.

So, what is to be inferred here? That whenever there is fluid movement normal to a shear flow (i.e. across a velocity gradient), this results in momentum exchange and resultant additional stresses within the fluid.

To exemplify this process further, consider two trucks carrying rocks, running at different speeds, and passing each other on a highway, as shown in figure 17.15. If passengers in the back of the trucks throw rocks from one truck to the other, the residual momentum in the rocks will change the overall momentum of the opposing truck. Thus, the rocks from the slow truck will cause the fast truck to decelerate, and the rocks from the fast truck will cause the slow truck to accelerate.

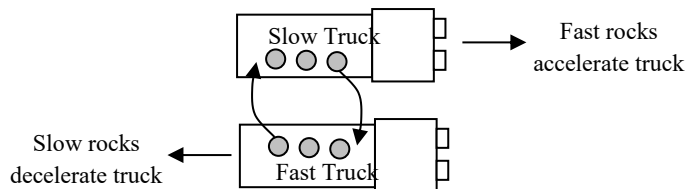


Figure 17.15 Model of momentum exchange due to the tossing rocks between a slow truck and a fast truck, resulting in the acceleration of the slow truck, and deceleration of the fast truck--an emulation of the process by which Reynolds stress is created.

17.5.3 Phenomenological Equations

As pointed out in in section 17.5.2, Reynolds stresses are pseudo-shear stress variables that arise from the Reynolds averaged Navier-Stokes equation, and are in addition to the conventional variables of mean velocity and pressure. Thus, when we include the Reynolds stresses as unknowns in the time-averaged equations, we have a mathematical dilemma:

Too few equations: 4	}	Need to determine a way to approximate the Reynolds stresses
Too many unknowns: 10		

This is of course for three-dimensional flow. For a simplified, and idealized, two-dimensional flow we would of course have three equations and seven unknowns--still too many unknowns. So, to develop solutions for the mean velocity and pressure for a turbulent flow requires that we develop other equations that provide relationships between the Reynolds stresses and the mean motion of the fluid.

Since we don't have appropriate equations for our Reynold's stress terms based on first principles, such as continuity or Newton's first law, we most commonly rely on what are termed [*phenomenological equations*](#) to allow closure (i.e. provision of enough additional equations relating mean flow variables to the required Reynolds stresses such that a solution is possible). Because of the immense complexity of turbulence, these equations are generally very simplified interpretations of the observed, or measured, characteristics of turbulent behavior. Frequently, these are little more than curve fits of particular data that relates measured stresses to mean flow behavior. In other cases, they are extrapolations of known relationships for a laminar fluid, such as the proportionality of shear stress to the velocity gradient for a laminar flow. The most sophisticated approaches utilize the Reynolds averaged differential equation of energy to provide a further degree of flexibility in calculating mean flow properties. However, despite the added complexity of this latter approach, other phenomenological relationships must still be assumed to solve the increased set of equations. Note that while there have been many attempts at developing such phenomenological equations, with varying effectiveness, we will only examine a couple of these approaches, and only for boundary layer-type flows. For further discussion of the basics of more sophisticated techniques, see [F. A. White \(1991\)](#), [W.C. Reynolds \(1976\)](#), and [G.C. Speziale \(1991\)](#) as starting points.

17.5.3.1 Eddy Viscosity

The use of an eddy viscosity is a simplistic attempt to create an artificial property, or function, that approximates the Reynolds stresses by modeling them like a laminar flow. This process, originally introduced by [Joseph Boussinesq](#), assumes a fictitious "turbulent" or "eddy" viscosity. We know that laminar shear stresses (Newtonian) are phenomenologically proportional to the local gradient of velocity, i.e. for a boundary layer type flow:

$$\tau_{\text{laminar}} = \mu \frac{\partial u}{\partial y} = \rho \nu \frac{\partial u}{\partial y}$$

Accordingly, it seems reasonable to hypothesize a “turbulent” viscosity that will relate the turbulent Reynolds stresses to the gradient of the mean velocity, such that:

$$\tau_{\text{turbulent}} = \varepsilon \frac{\partial U}{\partial y} = -\rho \overline{u'v'} \quad \text{or} \quad \varepsilon = \frac{-\rho \overline{u'v'}}{\frac{\partial U}{\partial y}} \quad (17.22)$$

Here, ε is known as the “[eddy viscosity](#)”, or sometimes “eddy” diffusivity, where the term eddy refers to the eddying interlayer mixing characteristic of turbulence. We note in general that the eddy viscosity for a turbulent flow is much larger than the comparable kinematic viscosity, with $\varepsilon \gg \nu$.

Our basic problem is how do we model ε ? For some cases, experiments reveal that $\varepsilon \propto y$ for roughly $y < 0.2$ (except very near the boundary), and $\varepsilon \cong \text{constant}$ for $y > 0.2$ (for a flat plate flow). For other types of flows, models of ε vary in myriad ways. In general, many attempts have been made to develop generic models for eddy viscosities. Several of the better models are outlined in [White \(1991\)](#). However, the models tend to be restricted to specific types of flows and geometries, and there has yet to be a generic model that works effectively over a range of flow geometries and conditions. In the following section, we examine a simple eddy viscosity model for boundary layer flows.

17.5.3.2 Mixing Length Concepts (near a flat plate)

The mixing length concept, and the subsequent phenomenological equations, was first proposed by [Ludwig Prandtl](#) [Prandtl (1925)], and was one of the early attempts at modeling an eddy viscosity for turbulent boundary layer flow. Drawing on flow visualization studies, like our previous figure 17.11, Prandtl made an analogy between the large-scale motions (that carry energy within the flow, not the dissipating scales) and molecular motion in gases, which is modeled by mean-free paths (i.e. the distance a molecule will move, before interacting with another molecule). Prandtl's idea was similar to our previous analogy of throwing rocks between trucks; i.e. a lump of fluid mixes after traveling a certain length (i.e. a normal distance from the boundary), with the distance the fluid travels dependent on its initial starting distance from a surface. The model assumes that as the fluid moves a distance, l , it conserves its momentum over that distance, and then mixes out. So, if a fluid moves from some level y to $y \pm l$, the change in the velocity, u , over l will be $u \pm l \frac{\partial u}{\partial y}$. Thus, as a crude approximation we can say

that the fluctuation velocity, similar to our model in figure 17.14 will be $u' \propto l \frac{\partial U}{\partial y}$. We additionally need a model for v' to complete the analysis. Prandtl, on a leap of faith, hypothesized that v' should be roughly proportional to u' , or $v' \propto l \frac{\partial U}{\partial y}$ as well. So, Prandtl's model of the Reynolds stress and eddy viscosity for a two-dimensional boundary layer-like flow was:

$$\tau_{\text{turbulent}} = \varepsilon \frac{\partial U}{\partial y} = -\rho \overline{u'v'} = \rho (\text{const.}) l^2 \left(\frac{\partial U}{\partial y} \right)^2 \Rightarrow \varepsilon = \rho (\text{const.}) l^2 \left(\frac{\partial U}{\partial y} \right) \quad (17.23)$$

Equation 17.23, while conceptually appealing, still leaves the modeling process in limbo, since we do not know how l varies with the mean velocity, nor the constant of proportionality. Prandtl, through an evaluation of experimental data, made some conjectures on the behavior of l , which would allow Eq. 17.23 to model the behavior of the mean velocity profile $U(y)$. However, as we will discuss in the following section, Prandtl could not determine a universal model for l , but realized that the modeling of l , and thus the eddy viscosity, depended on the specific regions of behavior within the boundary layer.

17.6 “Universal” Velocity Distribution Laws (for boundary layers)

Similar to laminar boundary layers, when one examines experimental data for turbulent flat plate boundary layers, clear characteristics of the mean velocity profiles are quite evident, as illustrated in figure 17.16. When plotted in linear form, a turbulent boundary layer velocity profile appears somewhat flat over the span of the boundary layer, with most of the change between $0 < U < U_\infty$ (with U_∞ the velocity at $y = \delta$) occurring very close to the bounding surface. This is much different than a laminar boundary layer, where the change is more distributed (see figure 13.4). The reason for this more uniform velocity profile is a result of the production and sustaining mechanisms of turbulence, as we discussed generically in Section 17.4.

Very near the bounding surface a process of turbulent "bursting" or breakdown of the local flow occurs, which generates turbulent eddies of small scale. These initially small eddies, grow quickly by amalgamation to larger scales, which subsequently entrain energy from the outer flow. What this process suggests is that flow at and very near the bounding surface will be dominated by viscosity and very high shear rates. However, the region just beyond this viscous region will be where the initiation of the bursting behavior and rapid growth in scales will take place, and where Reynolds stresses will begin to dominate laminar stresses. Further out, the growth of scales will slow, and the turbulent mixing process will become more uniform, and energy dissipation will ensue at the smallest scales. The consequent effect of these varied processes will be the rapid transition within the boundary layer from essentially laminar-like

behavior very near the boundary to a Reynolds-stress dominated behavior over the bulk of the outer region of the boundary layer.

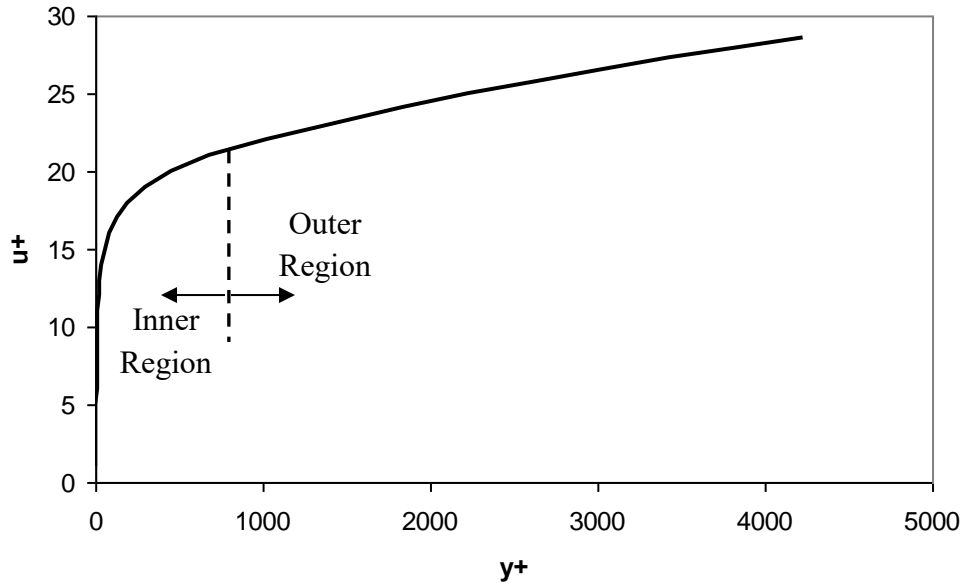
The modeling of the actual processes of the boundary layer can be quite complicated. However, by using an assumption of "regions" of behavior, and some rather simple mathematical approximations, relatively simple equations can be derived that are very effective in modeling the mean velocity behavior.

The delineation of the regions and layers of a turbulent boundary layer was first proposed by [Ludwig Prandtl](#) (1933) and [Theodore von Karmen](#) (1930), and the characterization of these regions has not significantly changed to the present day. Basically, they deduced that the velocity profile within a turbulent boundary layer consists of a thin, viscosity-dominated near-wall region, a Reynolds-stress dominated outer region, and an overlap region, where both types of stresses are important. In this way, Prandtl and von Karmen sought simple ways to model these regions, and develop "universal" mean velocity profiles, which would apply to a broad variety of boundary layer-type flows.

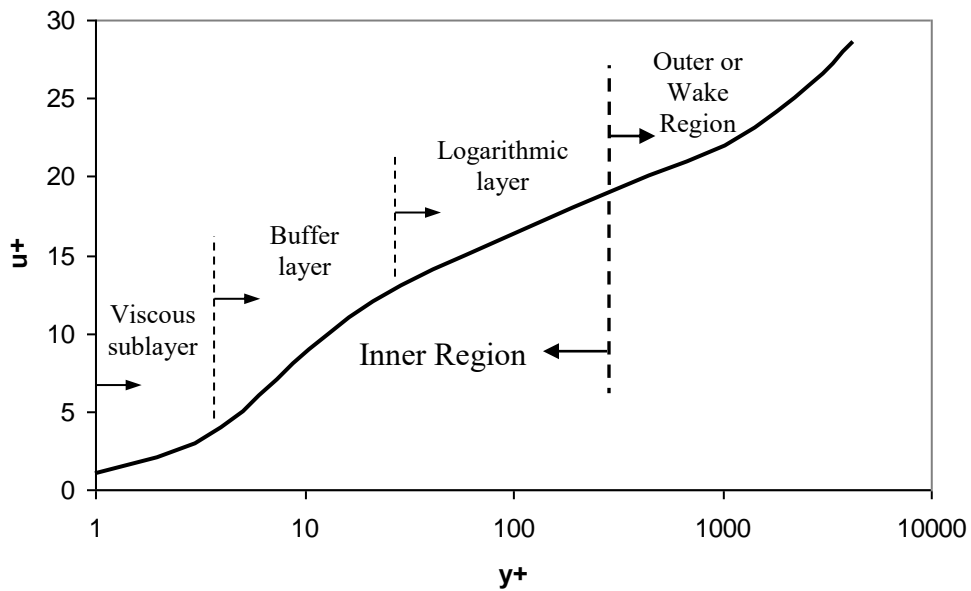
To simplify the description of the regions of behavior, Prandtl and von Karmen divided the velocity profile into several "layers" of behavior, depending on the relative dependence (based on experimental results) on viscous stresses and Reynolds stresses. They determined that a region near to the bounding surface (or wall), within $\frac{y}{\delta} \leq 0.2$, could be described by two distinct layers, with a connecting layer, all of which are dependent on the wall shear stress. The remainder of the boundary layer could be described as a single region or layer, whose behavior was modified by external conditions, such as the external pressure gradient. These two regions are generally termed the "Inner Region" and the "Outer Region" of the boundary layer, and are comprised of:

- | | | |
|-----------------------|---|--|
| a) Viscous sublayer | } | Inner Region, $\frac{y}{\delta} \leq 0.2$ |
| b) Buffer layer | | |
| c) Logarithmic layer | | |
| d) Outer (Wake) layer | | Outer Region, $0.2 < \frac{y}{\delta} < 1$ |

Figure 17.16 shows the generic shape of the mean velocity profile for a turbulent boundary layer, illustrating the respective regions and layers of behavior, plotted in both linear (17.16a) and logarithmic (17.16b) distance scales. Sections 17.6.1 through 17.6.3 discusses of each of these regions and how they are modeled.



a) Linear Plot



b) Semi-Logarithmic Plot

Figure 17.16 Typical averaged turbulent velocity profiles, plotted in non-dimensional coordinates, of $u^+ = \frac{u}{u_\tau}$ and $y^+ = \frac{u_\tau y}{\nu}$. a) plotted on linear scales. b) plotted with a logarithmic y^+ scale.

17.6.1 The Inner Region

Within a relative small region adjacent to the bounding wall, roughly $\frac{y}{\delta} \leq 0.2$, a turbulent boundary layer transitions from being dominated by purely viscous stresses very near the bounding surface to Reynolds stress dominated behavior as $\frac{y}{\delta} \Rightarrow 0.2$. This region within $\frac{y}{\delta} \leq 0.2$, is known as the "Inner Region", and is actually modeled as two distinct layers, with a transitional layer, or buffer layer, linking the two. Since this inner region is influenced most strongly by the wall shear stress, τ_w , and not the outer region free stream velocity, U_∞ , it is argued that the local mean velocity, U , has a functional relationship of the form: $U = f_{\text{inner}}(\tau_w, \rho, \mu, y)$. Dimensional analysis indicates that the functional equation for this set of parameters is:

$$\frac{U}{\sqrt{\frac{\tau_w}{\rho}}} = f_{\text{inner}} \left(\frac{\rho \sqrt{\frac{\tau_w}{\rho}} y}{\mu} \right) \quad (17.24)$$

Note that $\sqrt{\frac{\tau_w}{\rho}}$ has the dimensions of velocity. What this combination of shear stress and density represents is a characteristic velocity based on the wall shear stress. So, if τ_w is the shear stress adjacent to the wall or solid boundary, we hypothesize a velocity, u_τ , which represents a momentum flux equivalent to the local shear stress.

$$\text{i.e.} \quad \tau_w = \rho u_\tau^2 \Rightarrow u_\tau \equiv \sqrt{\frac{\tau_w}{\rho}} \quad (17.25)$$

Therefore, u_τ is a "velocity" representing the change in momentum per unit area equivalent to the shear stress τ_w . Utilizing this shear velocity, we can rewrite Eq. 17.24 as:

$$\frac{U}{u_\tau} = f_{\text{inner}} \left(\frac{\rho u_\tau y}{\mu} \right)$$

or

$$u^+ = f_{\text{inner}}(y^+) \quad (17.26)$$

where, $u^+ = \frac{U}{u_\tau}$ and $y^+ = \frac{\rho u_\tau y}{\mu} = \frac{y u_\tau}{\nu}$. Here, the plus superscript simply indicates that this is a non-dimensional property. Also note that the non-dimensional displacement, y^+ , is a positional Reynolds number based on u_τ .

The inner region has been found to scale well on the “wall” variables, u^+ and y^+ , as described by Eq. 17.26. However, to properly reflect the variations in the viscous stress and Reynolds stress across this region, this inner region is broken into three sub-regions described as the “viscous sublayer,” the “buffer layer”, and the “logarithmic layer.” As we will discuss in Section 17.6.2, the outer region scales on the actual boundary layer thickness, δ , and is comprised of both the outer portion of the logarithmic layer (an overlap region) and a layer described by a “velocity defect law,” which also displays logarithmic behavior based on the actual boundary layer thickness, δ . This probably sounds a bit confusing, and to some degree it is.

However, the use of inner variables (u^+ and y^+) for the inner region, and outer variables (U_∞ and δ) for the outer region, has proven to be a sound method to model the particular mean velocity characteristics of the regions of the boundary layer, as shown in figure 17.16 in both linear and semi-logarithmic scales. The latter semi-logarithmic presentation (figure 17.16b) is the preferred manner for representation of the velocity across a turbulent boundary layer, since it expands and emphasizes the inner region, within which the major effects of profile deformation and turbulence interaction take place. In the following, I discuss and demonstrate the modeling processes employed for each of the layers comprising the inner region.

17.6.1.1 The Viscous Sublayer

Very near the wall, viscous effects dominate such that the flow will behave in a highly-stressed, but laminar-like, manner. Within this very thin region, the shear stress across this layer is essentially constant at the boundary ($y = 0$) value, such that we can approximate that $\tau \cong \tau_w$.

Thus, we can write the equation for the shear stress as:

$$\tau = \mu \frac{dU}{dy} = \tau_w = \text{shear stress @ boundary} \Rightarrow \varepsilon = \mu$$

Rearranging, and making use of Eq. 17.25:

$$\frac{dU}{dy} = \frac{\tau_w}{\mu} = \frac{\rho \tau_w}{\mu \rho} = \frac{\tau_w}{\rho \nu} = \frac{u_\tau^2}{\nu}$$

Integrating gives:

$$U = \frac{u_\tau^2}{\nu} y + C \quad (C = 0, \text{ since } U = 0 \text{ at } y = 0)$$

Dividing through by u_τ :

$$u^+ = \frac{U}{u_\tau} = \frac{u_\tau y}{\nu} = y^+ \tag{17.27}$$

Equation 17.27 has been shown to be quite accurate for this very thin viscous sublayer, which experiments have shown to exist for roughly $y^+ < 5 - 7$. Note that this region of viscous stress is very thin. On a light aircraft traveling at about 200 miles per hour, this layer would only be about 0.025 mm (0.001 inch) thick.

17.6.1.2 Logarithmic Layer

Farther from a solid boundary, a turbulent boundary layer transitions from the viscosity dominated, laminar-like viscous sublayer, to a Reynolds stress dominated layer within the inner region. The mean velocity within this layer is observed and modeled as a layer in which the velocity scales logarithmically with distance from the boundary. This layer can extend from $y^+ \cong 30$ to 300-500, with the outer extent of this layer dependent on the maturity of the boundary layer. The maturity of a boundary layer is quantified by the Reynolds number based on either plate length or boundary layer thickness. Generally, as the Reynolds number increases, the extent of the logarithmic region expands (although non-linearly). The characterization of this logarithmic region is roughly modeled by the Prandtl mixing-length concept as described by Eq. 17.23. Since this logarithmic layer is well removed from the wall, the Reynolds stresses due to turbulent mixing are found to dominate viscous stresses, such that the stream-wise shear can be approximated as:

$$\tau = \tau_{\text{lamin}} + \tau_{\text{turb}} = \mu \frac{\partial U}{\partial y} - \rho \overline{u'v'} \approx -\rho \overline{u'v'}$$

To determine a functional form for the Reynolds stress, we employ the mixing length concept of Prandtl from Eq. 17.23:

$$\tau_{\text{turbulent}} = \varepsilon \frac{\partial U}{\partial y} = -\rho \overline{u'v'} = \rho (\text{const.}) l^2 \left(\frac{\partial U}{\partial y} \right)^2 \Rightarrow \varepsilon = \rho (\text{const.}) l^2 \left(\frac{\partial U}{\partial y} \right)$$

As we discussed in section 17.5.3.2, the modeling of the mixing length, l , is problematic, since it depends on the type of turbulent behavior present. However, for a turbulent flow adjacent to a surface, Prandtl and Von Karmen hypothesized that a lump of fluid near the wall would mix after traveling a distance proportional to its original distance from the wall, $l \propto y$, or $l = ky$, where k is an undefined constant. This was to acknowledge that Reynolds stresses appeared to increase with distance from the surface within the inner region. Thus,

$$\tau = -\rho \overline{u'v'} = \rho (\text{const.}) l^2 \left(\frac{dU}{dy} \right)^2 \cong \rho (ky)^2 \left(\frac{dU}{dy} \right)^2 = \rho k^2 y^2 \left(\frac{dU}{dy} \right)^2 \quad (17.28)$$

Note that the constant in Eq. 17.23 is assumed to be incorporated into the constant k in Eq. 17.28.

We now assume, as we did for the sublayer region, that $\tau \cong \tau_w$, i.e. that the shear stress across the inner region is equivalent to the shear stress at the wall. This has been shown to be the case experimentally, such that the inner region is often referred to as the "constant stress" region. Employing this additional assumption, we write:

$$\tau_w = \rho k^2 y^2 \left(\frac{dU}{dy} \right)^2 \Rightarrow \varepsilon = \rho k^2 y^2 \left(\frac{dU}{dy} \right)^2$$

Rearranging, to solve for the mean velocity derivative (and substituting from Eq. 17.25):

$$\left(\frac{dU}{dy} \right)^2 = \frac{\tau_w}{\rho k^2 y^2} = \frac{u_\tau^2}{k^2 y^2} = \left(\frac{u_\tau}{k y} \right)^2$$

$$\frac{dU}{dy} = \frac{u_\tau}{k y} \quad (17.29)$$

We assume that Eq. 17.29 holds from a region starting somewhere above the viscous sublayer, at y_0 , where $U = U(y_0)$. Thus, we integrate from y_0 to y :

$$\int_{U(y_0)}^U dU = \frac{u_\tau}{k} \int_{y_0}^y \frac{dy}{y}$$

$$U - U(y_0) = \frac{u_\tau}{k} [\ln(y) - \ln(y_0)] = \frac{u_\tau}{k} \ln\left(\frac{y}{y_0}\right) = \frac{u_\tau}{k} \ln\left(\frac{y u_\tau}{v} \frac{v}{y_0 u_\tau}\right)$$

$$U = \frac{u_\tau}{k} \ln\left(\frac{y u_\tau}{v}\right) + \frac{u_\tau}{k} \ln\left(\frac{v}{y_0 u_\tau}\right) + U(y_0) \quad (17.30)$$

Dividing Eq. 17.30 by u_τ , we get:

$$\frac{U}{u_\tau} = \frac{1}{k} \ln\left(\frac{y u_\tau}{v}\right) + \underbrace{\frac{1}{k} \ln\left(\frac{v}{y_0 u_\tau}\right) + \frac{U(y_0)}{u_\tau}}_{B = \text{constant}} \quad (17.31)$$

The indicated terms in Eq. 17.31 are an unidentified as an unknown constant, B , such that Eq. 17.31 becomes:

$$\frac{U}{u_\tau} = \frac{1}{k} \ln \frac{y u_\tau}{v} + B \quad \text{or} \quad u^+ = \frac{1}{k} \ln y^+ + B \quad (17.32)$$

Fitting Eq. 17.32 to experimental measurements was done originally by Prandtl based on measurements in a turbulent pipe flow by [J. Nikuradse](#), and k and B were determined to be approximately $k \cong 0.40$ and $B \cong 5.0$. Using more recent measurements, Coles and Hirst (1968) suggest values of $k \cong 0.41$ and $B \cong 5.5$. However, even more recent work at high Reynolds numbers by a group of researchers, [Marusic et al. \(2010\)](#), suggests that the Karman constant (k) may range from 0.37 to 0.42, depending on the type of flow (with corresponding variations in the constant B). Accepting the recommendations of Marusic et al., based on data which is quite comprehensive, we will assume values of $k = 0.385$ and $B = 4.2$ in this text. For more detailed assessment of the arguments for one value over another, the reader is referred to Marusic et al.

The thickness of the turbulent boundary layer that constitutes the logarithmic layer has also undergone much debate — on both its lower and upper limits. The lower limit is general accepted as roughly $y^+ \approx 30$, although limits of $y^+ \cong 50$ have been suggested. The outer limit is dependent on the Reynolds number of the flow, and increases with increasing local Reynolds number (i.e. as the flow progresses downstream). However, a range of $30 < y^+ < 300-600$ for the logarithmic layer seems to be reasonable, although arguments are also made for a narrower range. So, in general we will assume the equation for the mean velocity within the logarithmic layer, and its range of applicability, as:

$$\frac{U}{u_\tau} = \frac{1}{0.385} \ln\left(\frac{yu_\tau}{\nu}\right) + 4.2 \quad \Rightarrow \quad u^+ = 2.6 \ln y^+ + 4.2 \quad \text{for } 30 \leq y^+ \leq 300-600 \quad (17.33)$$

17.6.1.3 Buffer Layer

This layer lies roughly between $5 \leq y^+ \leq 30$, and is the transition zone between the viscous sublayer and the logarithmic layer. While this is a relatively narrow region, it is particularly important because of the high-velocity fluctuations and Reynolds stresses that develop in this region. Basically, it is within this layer that the boundary layer generates new vorticity concentrations by means of the bursting process discussed in section 17.4. It is these vorticity concentrations that subsequently propagate away from the buffer layer, create the constant Reynolds stress region of the logarithmic layer, and amalgamate to form the large, outer region structures. Modeling this layer has not been particularly successful from a physical perspective. There are models that can predict the velocity transition from the viscous sublayer to the logarithmic layer, but these are essentially hindsight relationships, which essentially use complicated curve fits to match experimental results. These approaches generally use mixing length or eddy viscosity models, or a combination of both. We will discuss two successful curve-fit models using these approaches.

17.6.1.4 Models of the Entire Inner Region

van Driest Damping Factor

First, for the inner region, we use the idea of the "viscosity" being a combination of the fluid viscosity, μ , and the turbulent, or "eddy" viscosity, ε , as defined by Eq. 17.22. Thus, for the inner region we can write:

$$\tau = (\mu + \mu_{\text{turbulent}}) \frac{dU}{dy} = (\mu + \rho\varepsilon) \frac{dU}{dy} = \left(\mu - \rho \overline{u'v'} \right) \frac{dU}{dy} \quad (17.34)$$

In Eq. 17.34, the eddy viscosity is intended to "model" the Reynolds stress, which can be related to a Prandtl-type mixing length, or other approach. To use the mixing length approach, let's reconsider Eq. 17.28, where we assumed (incorporating the constant into the mixing length l):

$$\tau = -\rho \overline{u'v'} = \rho\varepsilon \frac{dU}{dy} = \rho l^2 \left(\frac{dU}{dy} \right)^2 = \left(\rho l^2 \frac{dU}{dy} \right) \frac{dU}{dy} \quad (17.35a)$$

From Eq.17.28, we can relate the eddy viscosity to the mixing length as:

$$\varepsilon = l^2 \frac{dU}{dy} \quad (17.35b)$$

If we now substitute Eq. 17.35a into Eq. 17.34, noting that within the inner region the shear stress is essentially constant, $\tau \cong \tau_w = \rho u_\tau^2$, we get:

$$\tau = \rho u_\tau^2 = (\mu + \rho\varepsilon) \frac{dU}{dy} = \left(\mu + \rho l^2 \frac{dU}{dy} \right) \frac{dU}{dy}$$

Which we can expand and rearrange as a quadratic equation for dU/dy as:

$$l^2 \left(\frac{dU}{dy} \right)^2 + \nu \frac{dU}{dy} - u_\tau^2 = 0$$

Using the quadratic formula, we can solve for dU/dy as:

$$\frac{dU}{dy} = \frac{-\nu \pm \sqrt{\nu^2 + 4l^2 u_\tau^2}}{2l^2}$$

Retaining only the positive value of the root, and using some judicious algebraic manipulation, it can be shown that (try this as an exercise):

$$\frac{dU}{dy} = \frac{2u_\tau^2}{\nu + \sqrt{1 + \frac{4l^2 u_\tau^2}{\nu^2}}}$$

and with some more work that:

$$\frac{du^+}{dy^+} = \frac{2}{1 + \sqrt{1 + \frac{4l^2 u_\tau^2}{\nu^2}}} = \frac{2}{1 + \sqrt{1 + 4(l^+)^2}} \quad \text{where } l^+ = \frac{l u_\tau}{\nu}, \quad y^+ = \frac{l u_\tau}{\nu} \quad \text{and } u^+ = \frac{U}{u_\tau} \quad (17.36)$$

Now, within the viscous sublayer viscosity dominates, such that there is no mixing length and $l^+ \cong 0$, and Eq.17.36 reduces to:

$$\frac{du^+}{dy^+} = 1 \quad \Rightarrow \quad u^+ = y^+ \quad \text{which is Eq.17.27 for the viscous sublayer.}$$

However, within the logarithmic layer the mixing length is large such that $l^+ \gg 1$, Eq. 17.36 then reduces to:

$$\frac{du^+}{dy^+} \cong \frac{1}{l^+} \quad \Rightarrow \quad u^+ = \frac{1}{k} \ln y^+ + B \quad (\text{Eq.17.32, for a Prandtl mixing length } l = ky)$$

Clearly, one could create a model of the entire inner region if one could provide a model of the mixing length, which would make a smooth transition from the viscous sublayer to the logarithmic layer. One model that effectively did this was published by [Van Driest \(1956\)](#), who suggested an asymptotic, decaying exponential model for the transition from pure viscosity to the Prandtl mixing length, $l = ky$. His model was:

$$l^+ = ky^+ \left[1 - \exp\left(-\frac{y^+}{A}\right) \right] \quad (17.37)$$

He termed this l^+ as a "damping factor", since it gradually increased the mixing length across viscous - buffer - logarithmic layers. Substituting Eq. 17.37 into Eq.17.36 and integrating for u^+ gives:

$$u^+ = \int_0^{y^+} \frac{2dy^+}{1 + \sqrt{1 + 4(ky^+)^2 \left[1 - \exp\left(-\frac{y^+}{A}\right) \right]^2}} \quad (17.38)$$

Since there was no boundary condition to apply to determine van Driest's constant A, he basically fit Eq. 17.38 by varying the constant A until the integrated Eq.17.38 matched the logarithmic layer equation for large values of u^+ . van Driest suggested a value of $A = 26$ as the

appropriate value, but this was using the then accepted mixing length constants of $k = 0.41$ and $B = 5.5$ in Eq. 17.32. However, using our most recent values of $k = 0.385$ and $B = 4.2$, a value of $A = 21$ is a better fit. A comparison of the numerically integrated van Driest equation (there is no closed form solution) with the sublayer and logarithmic layer equations is shown in figure 17.17a, and is shown to match both equations quite well.

Spalding's Single Inner Region Equation

Another example of a model covering the entire inner region was suggested by [Spalding \(1961\)](#). His model is based indirectly on the mixing length concept, using a modification of Eq. 17.32 which will satisfy both the logarithmic behavior within the logarithmic layer, and the linear behavior within the viscous sublayer. To do this Spalding rewrote Eq.17.32 as follows:

$$u^+ = \frac{1}{k} \ln y^+ + B$$

$$ku^+ = \ln y^+ + \ln(\exp(kB))$$

$$\exp(ku^+) = \frac{y^+}{\exp(kB)}$$

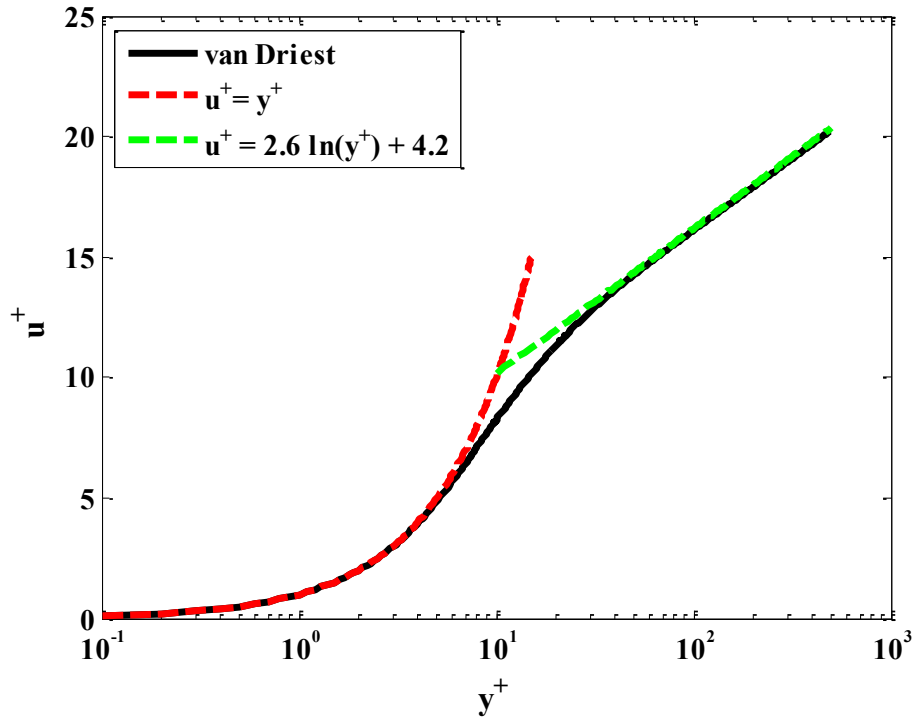
Expanding the exponential for kB as a series:

$$y^+ = \exp(-kB)\exp(ku^+) \cong \exp(-kB) \left\{ 1 + ku^+ + \frac{1}{2}(ku^+)^2 + \frac{1}{6}(ku^+)^3 + \dots \right\} \quad (17.39)$$

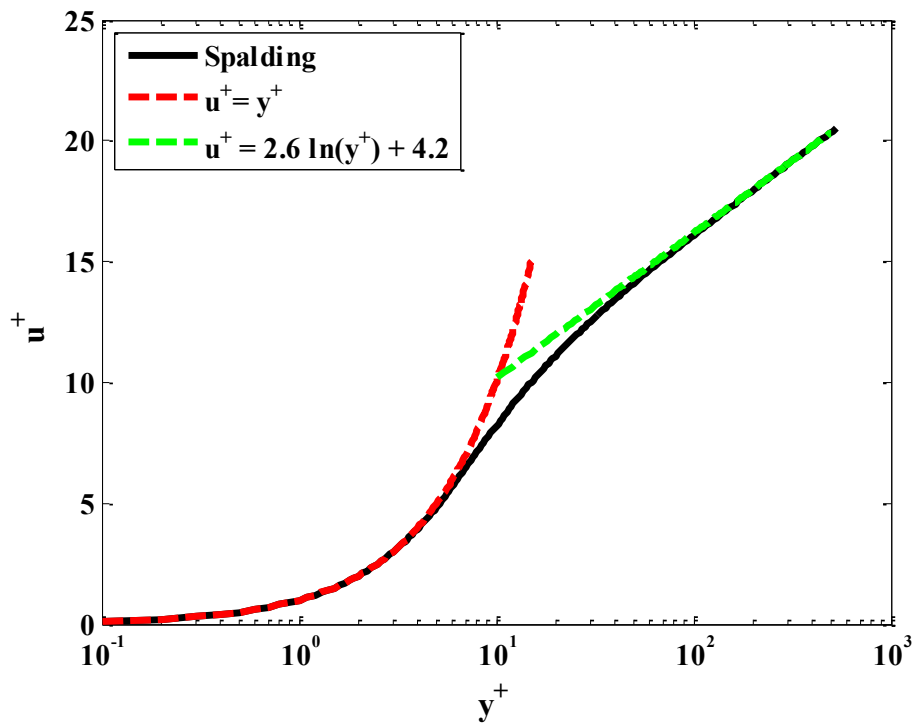
This reverses the dependency from Eq.17.32, making y^+ the dependent variable, and u^+ the independent variable in Eq.17.39. As shown on the right bracketed portion of Eq.17.39, Spalding also wrote the second exponential as a series expansion of $\exp(ku^+)$ in four terms, which is applicable when ku^+ is small. However, he noted that when ku^+ became large, greater than roughly 10, the higher order terms in the expansion (e.g. $\frac{1}{24}(ku^+)^4 + \dots$), which were neglected in the expansion, would become dominant. So, he reasoned that by adding back the $\exp(ku^+)$ inside the $\{ \}$ brackets and subtracting the four-term series expansion would create a function that was negligible when ku^+ was small, and returned to essentially the logarithmic relationship of Eq.17.32 when ku^+ exceeded roughly 20. To have the equation yield the viscous

sublayer equation for small ku^+ , Spalding also added a u^+ to the equation, which would yield the viscous sublayer equation, Eq.17.27, when $ku^+ < 7$ or so. Spalding's resulting inner region equation is:

$$y^+ = u^+ + \exp(-kB) \left\{ \exp(ku^+) - 1 - ku^+ - \frac{1}{2}(ku^+)^2 - \frac{1}{6}(ku^+)^3 \right\} \quad (17.40)$$



(a)



(b)

Figure 17.17 Comparison of: (a) van Driest and (b) Spalding inner region equations with the viscous sublayer and logarithmic layer equations.

Figure 17.17b shows Eq.17.40, Spalding's inner region equation, in comparison with the viscous sublayer and logarithmic layer equations. As shown, Spalding's inner region equation matches both equations quite well.

So, like Van Driest, Spalding used some judicious reasoning and the empirical equations for the viscous sublayer and the logarithmic layer to create a function that matches both equations in their regions of applicability. Note that Spalding did not rely on the on eddy viscosity arguments, although one can derive an eddy viscosity by taking the derivative of Eq. 17.40. One important issue with Equation 17.40 is that u^+ is implicit in this equation, as well as being quite complicated. Consequently, use of such equations is of limited utility, other than for comparison with experimental data.

To see other ways of generalizing the inner region equation, in order to account for such effects as pressure gradients and roughness, I recommend you read the NASA technical memorandum by [Shih et al.\(1999\)](#) or the assessment of various inner region models by [M. M. Gibson \(2015\)](#).

17.6.2 The Outer Region

The outer region, extends over the bulk of the boundary layer, from $0.2 < y/\delta < 1$, overlapping on the lower end with the logarithmic layer, and at the upper end with a “wake” region. This outer region is dominated by Reynolds stresses, with significant turbulent mixing. However, this vigorous mixing creates a mean velocity profile that does not change rapidly, and is somewhat uniform in appearance. The argument is that within this region viscosity is a secondary agent in establishing the mean profile. Although viscosity is the mechanism for the final energy dissipation (at very small scales), the mixing of the larger scales is what gives rise to the redistribution of momentum within this region. Within the outer layer, we view the effect of the Reynolds stresses as creating a "defect" of the mean flow from the driving velocity at the edge of the boundary layer, U_∞ . However, the level of the Reynolds stresses is still characterized by the wall shear stress, τ_w , and fluid density, ρ , which characterize the shear velocity, u_τ , as defined in Eq. 17.25. Thus, we can reason that the functional relationship for the mean velocity in the outer region should be:

$$U = f\left(U_\infty, \rho, \tau_w, y, \delta, \frac{dp}{dx}\right)$$

Here, δ is the boundary layer thickness, and $\frac{dp}{dx}$ is the pressure gradient, which is of course related to U_∞ . Von Karman in 1930 showed that the most effective functional relationship for the outer region was a modeling of the "defect" of the mean velocity, U , from the external velocity, U_∞ . Employing this defect concept (i.e. $U_\infty - U$), dimensional analysis yields a relationship for the velocity defect of the form:

$$\frac{U_\infty - U}{u_\tau} = f\left(\frac{y}{\delta}, \xi\right) \quad \text{where } \xi = \frac{\delta}{\tau_w} \frac{dp}{dx}, \text{ a dimensionless pressure gradient} \quad (17.41)$$

Equation 17.41 turns out to be a good functional relationship for the outer region. However, determining a universal relationship for this equation has proven quite challenging, since the function changes with flow geometry and history. In reality, the process has been more of an exercise in curve fitting of empirical data, rather than development by some a priori mathematical model. The simplest way to approach a model is to assume a self-preserving or equilibrium boundary layer (i.e. one where the velocity defect function of Eq. 17.41 is the same function of y/δ for all x locations). This assumption, while convenient, is not exact, and only becomes a good approximation when the Reynolds number becomes large.

The problem is to determine the functional relationship $f\left(\frac{y}{\delta}, \xi\right)$ in Eq. 17.41. The approach is a combination of empirical curve fitting, and the understanding that the inner and outer region must overlap and give identical results within that overlap region. In order for the logarithmic layer and outer layer to overlap, Eq. 17.41 must asymptote to Eq. 17.32 within this overlap region. Thus, Von Karmen suggested that the equation for the mean outer region velocity should be of the form:

$$\frac{U}{u_\tau} = \frac{1}{k} \ln\left(\frac{yu_\tau}{\nu}\right) + B + A(\xi)\phi\left(\frac{y}{\delta}\right) \quad (17.42)$$

Here we assume that $A(\xi)$ is a function of the external pressure gradient, and $\phi\left(\frac{y}{\delta}\right)$ is a function that varies with the location within the boundary layer. Now, if we set $y = \delta$, where $U = U_\infty$, Eq. 17.42 gives:

$$\frac{U_\infty}{u_\tau} = \frac{1}{k} \ln\left(\frac{\delta u_\tau}{\nu}\right) + B + A(\xi)\phi(1) \quad (17.43)$$

Subtracting Eq. 17.42 from Eq. 17.43, gives us a functional form for the velocity defect equation, Eq. 17.41, as:

$$\begin{aligned} \frac{U_\infty - U}{u_\tau} &= \frac{1}{k} \ln\left(\frac{\delta u_\tau}{\nu}\right) + A(\xi)\phi(1) - \frac{1}{k} \ln\left(\frac{yu_\tau}{\nu}\right) - A(\xi)\phi\left(\frac{y}{\delta}\right) \\ &= -\frac{1}{k} \ln\left(\frac{y}{\delta}\right) + A(\xi) \left[\phi(1) - \phi\left(\frac{y}{\delta}\right) \right] \end{aligned} \quad (17.44)$$

Now, within the overlap of the inner and outer regions, if Eq. 17.42 is to match Eq. 17.32, then $\phi\left(\frac{y}{\delta}\right) \rightarrow 0$ as $\frac{y}{\delta} \rightarrow 0$. Thus, in the overlap region, where $\frac{y}{\delta} \rightarrow 0$, Eq. 17.44 becomes:

$$\frac{U_\infty - U}{u_\tau} \cong -\frac{1}{k} \ln\left(\frac{y}{\delta}\right) + A(\xi)\phi(1) \quad (17.45)$$

Solving Eq. 17.45 for $\frac{U}{u_\tau}$, and equating it to Eq. 17.32 and rearranging, we have:

$$\begin{aligned} \frac{U}{u_\tau} &= \frac{U_\infty}{u_\tau} + \frac{1}{k} \ln\left(\frac{y}{\delta}\right) - A(\xi)\phi(1) = \frac{1}{k} \ln \frac{yu_\tau}{\nu} + B \\ &= \frac{U_\infty}{u_\tau} + \frac{1}{k} \ln\left(\frac{yu_\tau}{\nu}\right) - \frac{1}{k} \ln\left(\frac{\delta u_\tau}{\nu}\right) - A(\xi)\phi(1) = \frac{1}{k} \ln\left(\frac{yu_\tau}{\nu}\right) + B \end{aligned}$$

And solving for $A(\xi)\phi(1)$, we have:

$$A(\xi)\phi(1) = \frac{U_\infty}{u_\tau} - \left[\frac{1}{k} \ln\left(\frac{\delta u_\tau}{\nu}\right) + B \right] \quad (17.46)$$

What we have in Eq. 17.46 is the difference between the velocity at the edge of the boundary layer, and the value predicted by the logarithmic law, Eq. 17.32. If we assume that $\phi\left(\frac{y}{\delta}\right)$ is a function such that $\phi(1) = 1$ at the edge of the boundary layer, then we have:

$$A(\xi) = \frac{U_\infty}{u_\tau} - \left[\frac{1}{k} \ln\left(\frac{\delta u_\tau}{\nu}\right) + B \right] \quad (17.47)$$

So, the value of $A(\xi)$ is a measure of the difference between the actual external velocity, and that predicted by the law of the wall (the logarithmic layer). Of course, recall that the value of $A(\xi)$ is a function of the pressure gradient imposed on the boundary layer, where $\xi = \frac{\delta}{\tau_w} \frac{dp}{dx}$.

The value of $A(\xi)$ varies with the applied pressure gradient, and often the particular geometry, but in general is a fairly constant value for a given pressure gradient. Some selected values of $A(\xi)$, determined from experiment ([White, 2011](#)) are:

Pressure Gradient	ξ	$A(\xi)$ value
Strong favorable	-4.8	1.0
Flat plate	0	2.5
Mild adverse	6.3	5.6
Strong Adverse	29	13

Except for the flat plate value, these are representative of values obtained for a limited selection of experimental data. Note that a linear curve fit of this data gives an approximate relationship of:

$$A(\xi) \cong 0.36\xi + 2.8 \quad (17.48a)$$

Thus, if ξ is relatively constant, Eq. 17.48a allows the approximation of the respective value of $A(\xi)$.

The function $\phi\left(\frac{y}{\delta}\right)$ has been debated for decades, and still is undergoing scrutiny. However, Coles (1956) probably came as close as anyone to defining its functionality, in proposing what he termed the [Law of the wake](#). Here, the wake is the outer region of the boundary layer where the flow diverges from the logarithmic law of the wall. Examining a broad set of data, Coles proposed that the wake portion of Eq. 17.43 $\left[\phi\left(\frac{y}{\delta}\right)\right]$ could be approximated by an S-shaped function as:

$$\phi\left(\frac{y}{\delta}\right) \approx \mathbf{sin}^2\left(\frac{\pi y}{2\delta}\right) \quad \left(\text{sometimes approximated as } \approx 3\left(\frac{y}{\delta}\right)^2 - 2\left(\frac{y}{\delta}\right)^3\right) \quad (17.48b)$$

Thus, to a good approximation we can now rewrite the outer region mean velocity profile of Eq. 17.42 as:

$$\frac{U}{u_\tau} = \frac{1}{k} \mathbf{ln}\left(\frac{yu_\tau}{\nu}\right) + B + A(\xi) \mathbf{sin}^2\left(\frac{\pi y}{2\delta}\right) \quad (17.49)$$

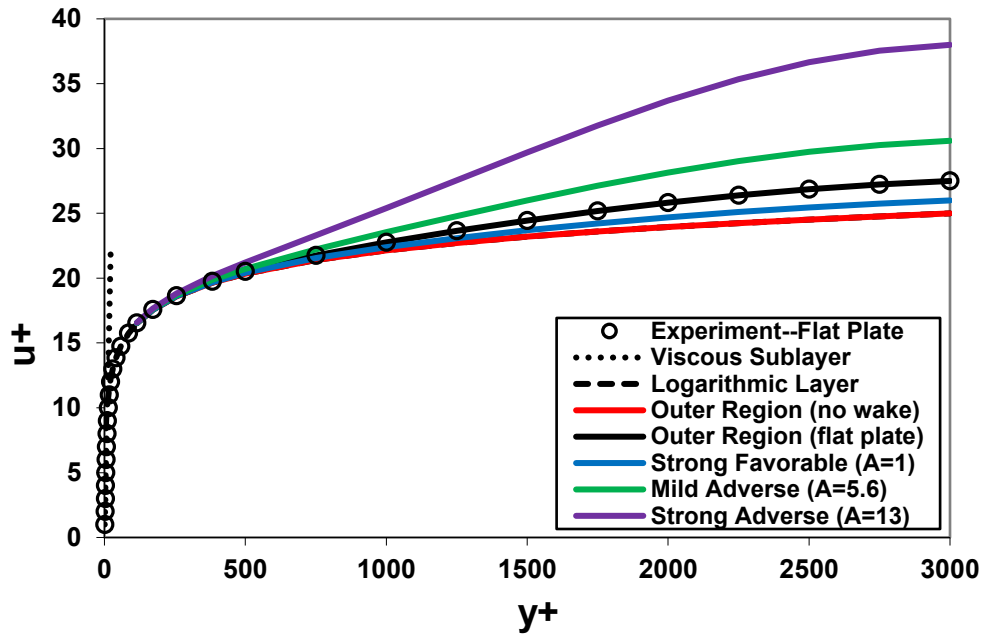
and the velocity defect form of Eq. 17.41 as:

$$\frac{U_\infty - U}{u_\tau} = -\frac{1}{k} \mathbf{ln}\left(\frac{y}{\delta}\right) + A(\xi) \left[1 - \mathbf{sin}^2\left(\frac{\pi y}{2\delta}\right)\right] \quad (17.50)$$

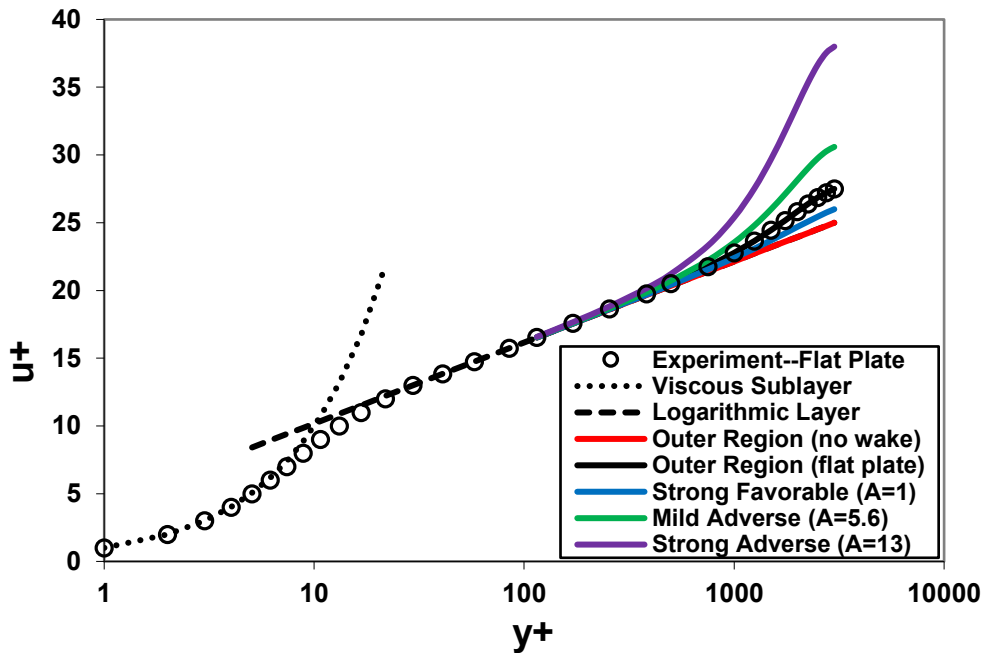
17.6.3 The Combined Universal Velocity Profile

Figure 17.18, shown in both linear and semi-logarithmic coordinates, plots the mean turbulent velocity profile predicted by Eqs. 17.27 (sublayer), 17.33 (logarithmic layer), and 17.49 (outer layer). The outer region is shown for a range of pressure gradients, from a strong favorable to a strong adverse; additionally, the outer region without a wake correction ($A = 0$) is shown for comparison. Note the significant variations in the outer region created by the application of an adverse pressure gradient.

To gain further perspective on the effect of pressure gradients on turbulent boundary layers, the velocity profiles of figure 17.18a are replotted in figure 17.19 relative to the outer flow velocity,



(a) Linear scale



(b) Logarithmic scale

Figure 17.18 Mean turbulent velocity profiles plotted using wall variables, $u^+ = \frac{U}{u_\tau}$ and

$y^+ = \frac{\rho u_\tau y}{\mu} = \frac{y u_\tau}{\nu}$, for sublayer (Eq.17.27), logarithmic (Eq.17.33), and outer

regions (Eq. 17.49). Shown for $\delta^+ = \frac{\delta u_\tau}{\nu} = 3000$.

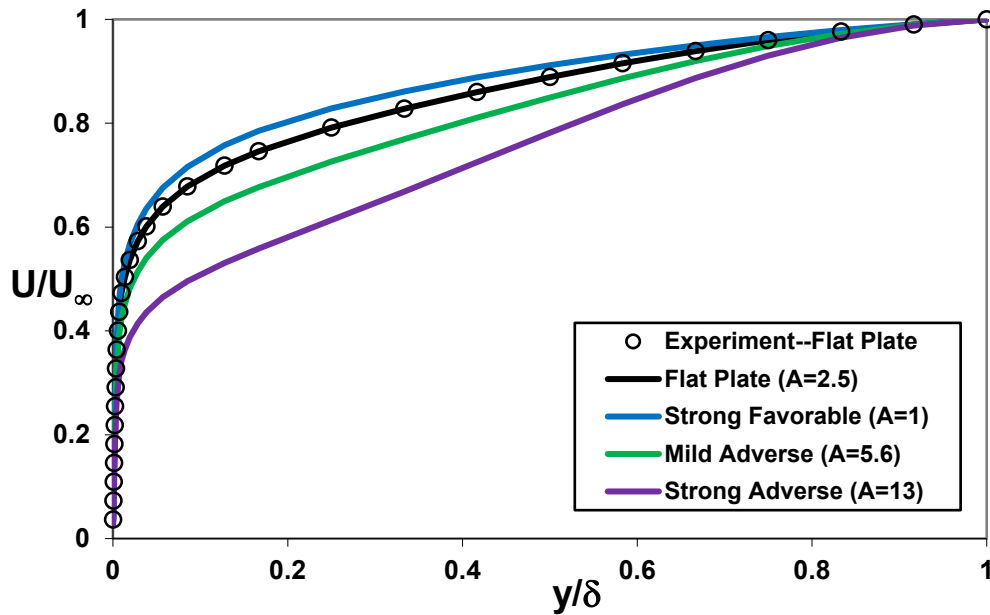


Figure 17.19 Mean turbulent velocity profiles of figure 17.18a replotted relative to U_∞ and δ .

The profiles shown assume $\delta^+ = \frac{\delta u_\tau}{\nu} = 3000$.

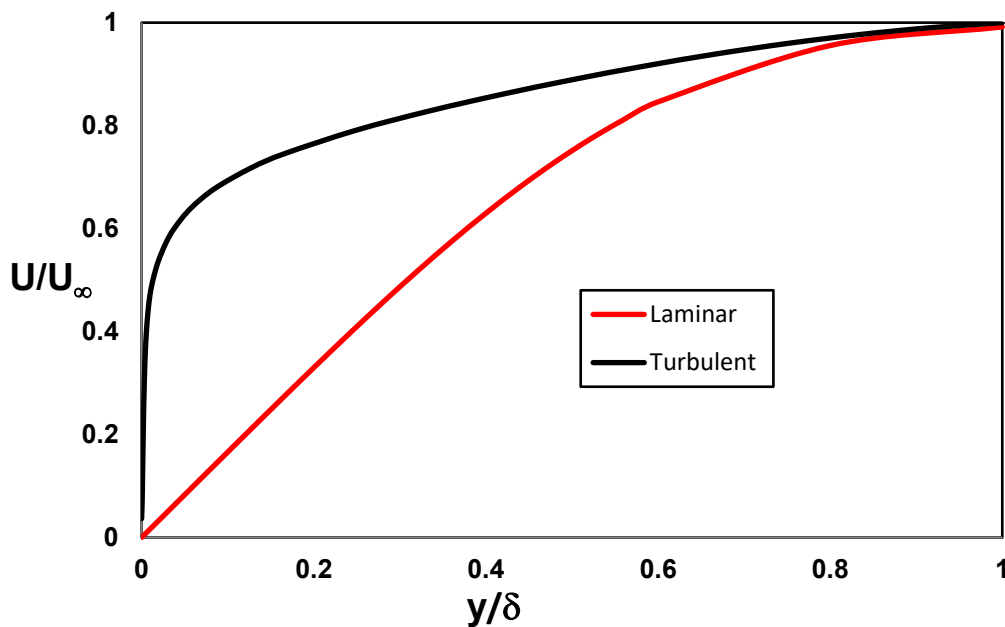


Figure 17.20 A comparison of flat plate boundary layer velocity profiles plotted relative to U_∞ and δ . The laminar boundary layer is a Blasius boundary layer, plotted from table 13.1. The turbulent boundary layer profile is plotted using a combination of Eqs.17.27, 17.33, and 17.49 assuming $\delta^+ = \frac{\delta u_\tau}{\nu} = 3000$.

U_∞ , and the boundary layer thickness, δ . As figure 17.19 shows, a favorable pressure gradient will result in a flatter velocity profile, while an adverse pressure gradient will cause a retardation of the profile. As the velocity profile for the strong adverse pressure gradient illustrates, while the outer region is strongly retarded, the near-wall region does not display as much obvious retardation (although the wall shear stress, τ_w , is reduced). For very strong adverse pressure gradients, a turbulent flow will undergo separation, although it is more robust than a laminar boundary layer, as we discuss below.

17.6.4 A Shape Factor Comparison of Turbulent vs. Laminar Boundary Layers

To illustrate how significantly the boundary layer mean velocity profile is modified by transition to turbulence, figure 17.20 shows a comparison between a turbulent boundary layer profile modeled by Eqs. 17.27, 17.33, and 17.49 for a turbulent flat plate flow, and a laminar Blasius boundary layer, as calculated from Table 13.1. Both are plotted on linear axes, and referenced to the mean outer flow, U_∞ , and assume the same boundary layer thickness, δ . Note the striking flatness of the turbulent profile versus the laminar profile. This variation is characterized by the shape factor we discussed in section 13.6, defined by $H = \frac{\delta^*}{\theta}$, the ratio of the displacement to the momentum thickness. The shape factor, H , for the laminar Blasius boundary layer is 2.6, whereas H for the turbulent boundary layer shown is 1.3, illustrating how much "flatter" a turbulent boundary layer is, which makes it much less susceptible to flow separation.

Generally, a decrease in H from the flat plate value indicates a more stable flow, whereas an increase in H indicates reduced stability. For a laminar flow, a higher H value increases the likelihood of: (a) transition to turbulence, or (b) a flow separation of the boundary layer. For a turbulent flow, since the flow is already in a turbulent state, an increase in H from the flat plate value just implies a greater likelihood of flow separation. Note that for a turbulent flow, a lower H value due to a favorable pressure gradient in some cases can result in a return of the boundary layer to a laminar state, termed "relaminarization"; for strong pressure gradients, relaminarization can occur quite quickly, in roughly 20-100 initial boundary layer thicknesses (depending on the physical situation). Relaminarization can also occur due to rotation, suction, flow curvature, and heating [[Narasimha and Sreenivasan \(1979\)](#)]. It should be noted that the relaminarization develops from the wall outward, with the acceleration of the inner region by the favorable pressure gradient causing a cessation of the bursting behavior that feeds new vorticity and vortices into the outer region [[Morkovin, \(1988\)](#)]. Thus, while the inner region may appear laminar, the residual large-scale vortical flow structures within the outer region will not decay rapidly, delaying the return to complete laminar-like behavior for some distance. Moreover, these outer region flow structures could provide sufficient disturbances to cause a retransition of the boundary layer to turbulence, should the favorable pressure gradient be relaxed.

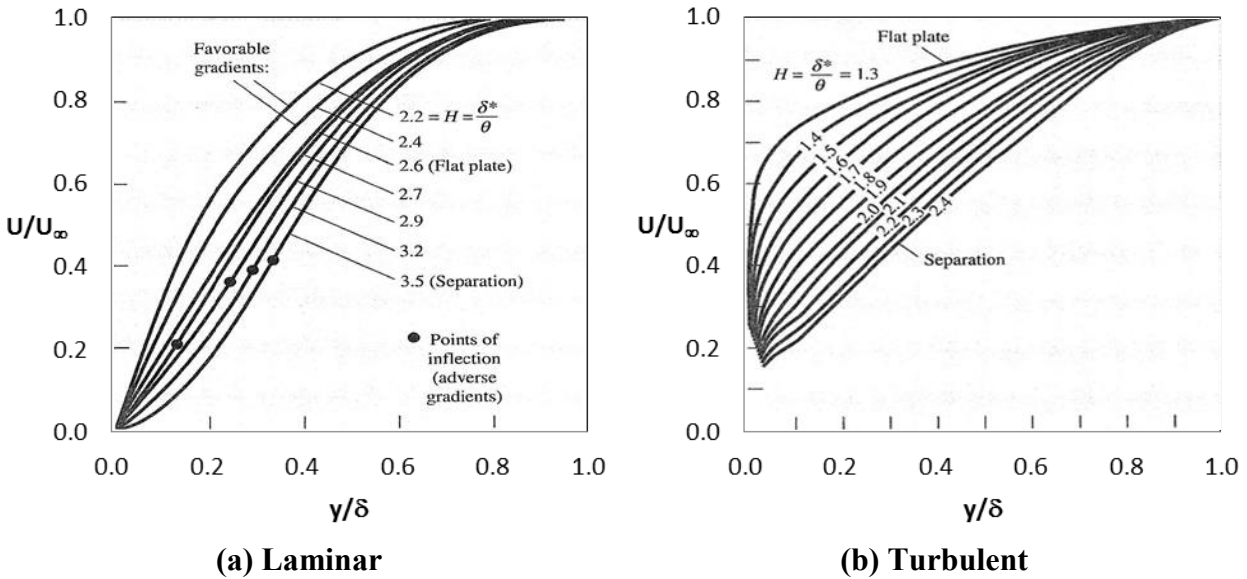


Figure 17.21 A comparison of mean flat plate boundary layer velocity profiles plotted relative to U_∞ and δ for a range of shape factors, H :
 (a) Laminar boundary layers: $2.2 < H < 3.5$ (laminar separation);
 (b) Turbulent boundary layers $1.3 < H < 2.4$ (turbulent separation).
 [from [White, 1991](#)]

Figure 17.21 shows a range of equilibrium velocity profiles for both laminar and turbulent boundary layers, due to a range of applied pressure gradients. These pressure gradients range from favorable to strong adverse pressure gradients for the laminar profiles, and from a flat plate flow to a strong adverse pressure gradient for the turbulent profiles, and illustrate the range of possible shape factors. It is interesting to note that the shape factor for a laminar flat plate flow ($H = 2.6$) is twice that of a turbulent flat plate flow ($H = 1.3$). This quantizes what is clearly shown in the comparative figure 17.20 --- that the displacement of the boundary layer fluid (δ^*) is much greater than the loss of momentum (θ) for a laminar flow as compared to a turbulent flow; and that shape factors are markedly higher for laminar vs. turbulent behavior.

In Section 13.3, it was pointed out that for a Blasius flat plate flow an inflection in the velocity profile develops at the surface, and that such an inflection point is an indication of a marginally stable flow. As figure 17.21(a) illustrates, as the pressure gradient becomes more adverse, and H correspondingly increases, the inflection in the laminar velocity profile develops away from the surface, which results in an increasingly less stable laminar boundary layer, quickly leading to rapid transition to turbulence and/or boundary layer separation. Interestingly, figure 17.21(b) shows no apparent inflection points as the adverse pressure gradient increases. This is because the resultant inflections will occur very near the boundary, within the viscous sublayer and buffer region, which are not plotted in the figure. It is worth noting that for a laminar boundary layer an increase in H by only 35% above the flat plate value will result in an immediate boundary layer

separation. In contrast, for a turbulent boundary layer H must increase by 85% before immediately separation will occur. This is another testament to the fragility of a laminar boundary layer, and the robustness of a turbulent one.

While the velocity profiles shown in figures 17.18, 17.19, and 17.21(b) are reasonably close to measured turbulent boundary layer characteristics, these reflect basically equilibrium boundary layer flows, for which the conditions, such as the pressure gradient, remain relatively constant. In most real applications, such as airfoils, a flow will generally undergo significant changes in pressure gradient over the flow surface, and thus will not be an equilibrium flow. Additionally, considerations of other effects such as surface roughness or surface transpiration require additional assumptions, and generally more sophisticated modeling [see [White \(1991\)](#)].

However, for smooth, solid boundaries with gradual streamwise changes, the collective equations reflected by figure 17.18 do a reasonable job of modeling mean turbulent velocity behavior. However, for more accurate predictions of turbulent boundary layer behavior, there is a great body of research and literature that attempts to provide more universal characteristics for turbulent boundary layers under varying conditions. In addition, many sources exist that provide ever-improving capabilities for computational prediction of turbulence in general and turbulent boundary layer characteristics in particular. Most of these prediction approaches require significant computational resources and sophisticated numerical techniques to determine significant engineering properties such as surface shear, drag, and separation behavior. Appendix B summarizes the generic way that modern turbulence computational programs model and calculate practical engineering properties.

For our present purposes, we will only consider a simple, approximate method, which employs the same momentum integral equation we applied to laminar boundary layers in Chapter 14. Here, we will adapt the momentum integral equation to predict averaged turbulent boundary layer characteristics. By utilizing a simple model of a mean turbulent velocity profile, we can approximate the basic boundary layer characteristics relevant to engineering applications, using some fairly simple calculations.

17.7 A Momentum Integral Analysis of a Flat Plate Turbulent Boundary Layer

17.7.1 Transition to a Turbulent Boundary Layer on a Flat Plate

As discussed in section 17.3.2, a laminar flow does not suddenly transition to turbulence, but does so by means of a complicated process that is still not clearly understood. What is understood is that there is a Reynolds number range over which transition may occur. The Reynolds number at which transition to turbulence initiates is known as the critical Reynolds number, or Re_{crit} . Here, Re_{crit} can be based on the x -distance along a flat plate, or on the boundary, displacement, or momentum thicknesses. This can make a discussion of the location

of Re_{crit} somewhat confusing, so for our purposes we will use $Re_{x_{crit}}$, which is based on the location from the leading edge of a flat plate, as illustrated in figure 17.22.

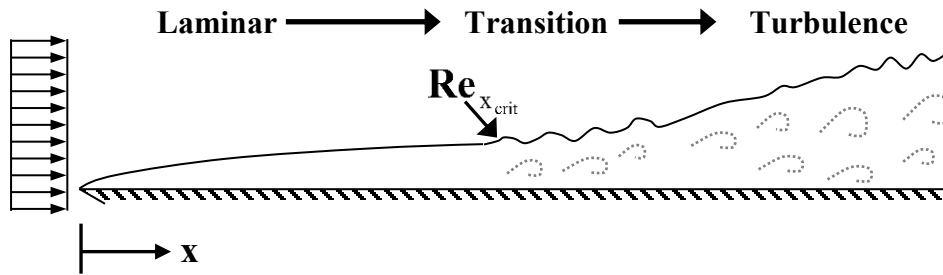


Figure 17.22 Schematic representation of transition to turbulent flow on a flat plate.

Note that the transition process will not occur immediately, but requires some distance (i.e. Reynolds number range) over which a full transition from a laminar to a fully-turbulent flow will occur. In addition, a number of things can affect the critical Reynolds number and the transition process, including surface roughness, external flow fluctuations, and pressure gradients.

In general, increasing surface roughness, or an increase in the level of external flow fluctuations (measured by the rms of the velocity fluctuations relative to the mean flow velocity) will cause a flow to begin transition to turbulence at a lower critical Reynolds number. An adverse (increasing) pressure gradient will also stimulate an early transition to turbulence; recall our discussion in Section 17.2.3 of how sensitive laminar flow stability is to an adverse pressure gradient. However, a favorable (decreasing) pressure gradient will delay the transition to turbulence to a higher critical Reynolds number. In addition, as pointed out in Section 17.6.4, strong favorable pressure gradients can actually cause turbulence to [“relaminarize”](#), or revert back to laminar behavior.

For an initially uniform flow over a flat plate, the accepted Reynolds number range for the initiation of transition is roughly $Re_{x_{crit}} = 3 \times 10^5$ to 3×10^6 , where $Re_{x_{crit}} \approx 5 \times 10^5$ is generally accepted as the critical Reynolds number for transition to turbulence under normal surface roughness and external flow conditions.

In the following analysis of a flat plate turbulent boundary layer, we will examine two situations. The first assumes that the boundary layer is turbulent from the leading edge of a flat plate. The second assumes the flow is initially laminar, and then suddenly transitions to a fully-developed and self-sustaining turbulent boundary layer. While both of these are idealized models, they provide reasonable predictions of boundary layer growth and wall shear stress, and illustrate the differences in behavior between turbulent and laminar boundary layers.

17.7.2 The Momentum Integral Equation for Turbulent Flow

As discussed in Section 17.6.4, the detailed analysis of turbulence is a complicated process requiring very complicated mathematical modeling and substantial computational resources. However, we can develop some relatively simple relationships for the characteristics of a turbulent boundary layer using a momentum integral analysis similar to that done in section 14.2.1 for a laminar flow. We will do this using an assumed velocity profile, and shear stress information obtained from the outer region equation, Eq. 17.49.

Consider the von Karman momentum integral equation, Eq. 14.11 developed in Chapter 14.

$$\frac{\tau_w}{\rho U_\infty^2} = (\delta^* + 2\theta) \frac{1}{U_\infty} \frac{dU_\infty}{dx} + \frac{d\theta}{dx}$$

For a flat plate boundary layer, with no pressure gradient and constant U_∞ , this reduces to:

$$\tau_w = \rho U_\infty^2 \frac{d\theta}{dx} \quad (17.51)$$

Here, θ is the momentum thickness, given by Eq. 13.27 as:

$$\theta = \int_0^\delta \frac{U}{U_\infty} \left(1 - \frac{U}{U_\infty} \right) dy \quad (17.52)$$

Eqs. 17.51 and 17.52 are equally applicable to turbulent boundary layers as well as laminar boundary layers, since they only require expressions for U , representing the approximation of the mean velocity profile, and τ_w , the wall shear stress. As we show in the following section, a reasonable approximation for U exists. However, determining the shear stress is problematic, since for a turbulent flow we cannot relate the shear stress to the gradient of the mean velocity, since the "stresses" in a turbulent flow must take into account the "Reynolds" stresses. Therefore, we have to seek an alternative relationship for the shear stress, which we do by employing the outer region velocity relationship from Eq. 17.49.

17.7.3 The Mean Velocity Profile: Nikuradse Power Law

Based on an extensive set of experimental studies of pipe flows, [Nikuradse](#) (1932) established that to good approximation the mean velocity profile of a turbulent flow in a fully-developed pipe flow (of radius R) can be approximated by:

$$\frac{U}{U_\infty} = \left(\frac{R-r}{R} \right)^{\frac{1}{n}} \quad \text{where } n > 6 \quad (17.53)$$

Prandtl (1921) had previously suggested the use of a power-law mean velocity profile to approximate a flat-plate turbulent boundary layer, with Eq. 17.53 being recast for a flat plate as:

$$\frac{U}{U_\infty} = \left(\frac{y}{\delta}\right)^{\frac{1}{n}} \tag{17.54}$$

Eq.17.54 presumes that since the pipe boundary layer would extend to the center of the pipe, that to a good approximation $\delta = R$, and $y = R - r$ can be substituted in Eq. 17.53 to obtain Eq.17.54. It has subsequently been shown that Eq.17.54 is a good approximate representation of a turbulent boundary layer velocity profile for use in the integral analyses of turbulent boundary layers, and we will use this relationship for our present integral analysis.

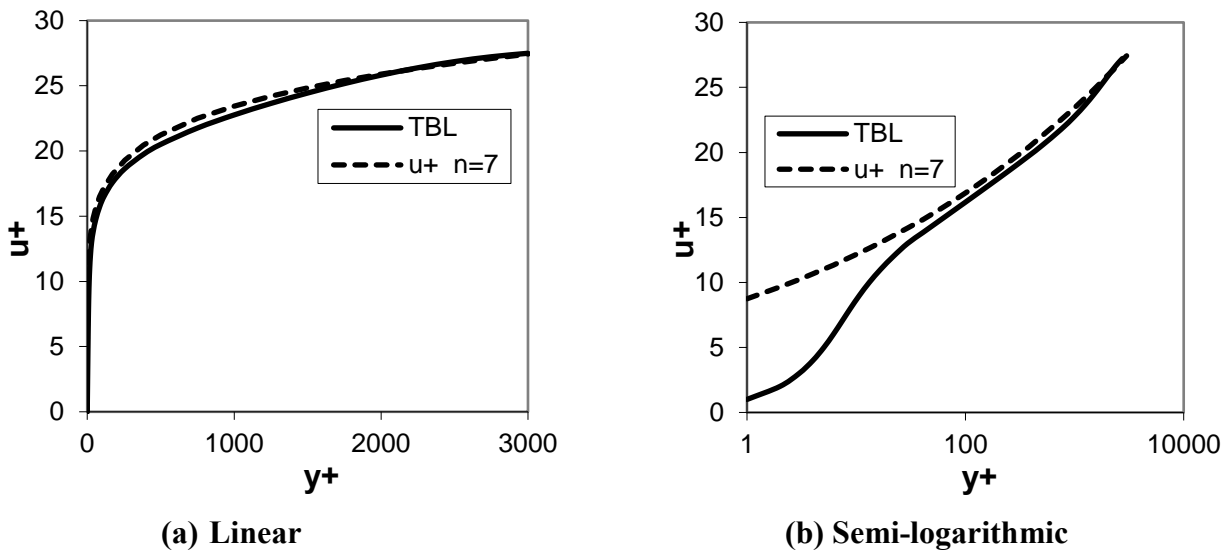


Figure 17.23 Comparison of mean turbulent boundary layer velocity and a Nikuradse $n = 7$

power law model, $\frac{U}{U_\infty} = \left(\frac{y}{\delta}\right)^{\frac{1}{n}} \Rightarrow U^+ = U_\infty^+ \left(\frac{y^+}{\delta^+}\right)^{\frac{1}{n}}$. Shown assuming

$$\delta^+ = \frac{\delta u_\tau}{\nu} = 3000.$$

Note that while Eq.17.54 is a good approximation of the mean velocity shape, it does not meet the boundary conditions exactly, as shown by figure 17.23. Although Eq.17.54 does satisfy the

first order boundary conditions $\left(\frac{U}{U_\infty} = 0 \text{ at } \frac{y}{\delta} = 0\right)$, and $\left(\frac{U}{U_\infty} = 1 \text{ at } \frac{y}{\delta} = 1\right)$, it does not satisfy

the appropriate second and higher-order derivative boundary conditions :

e.g. $\frac{dU}{dy} = \frac{U_\infty}{n\delta} \left(\frac{y}{\delta}\right)^{\frac{1-n}{n}}$ is infinite at $\frac{y}{\delta} = 0$, and non-zero at $\frac{y}{\delta} = 1$

However, because of its simplicity, Eq.17.54 has been widely employed to effectively model the approximate shape of the mean velocity behavior.

From empirical data, the value of the constant n was determined to be a function of Reynolds number, varying from roughly $7 \leq n \leq 9$ for a flat plate flow. Although there is no consensus, generally accepted values are:

$$n \cong 7 \quad 5 \times 10^5 < \text{Re}_x < 10^7$$

$$n \cong 8 \quad 10^7 < \text{Re}_x < 10^8$$

$$n \cong 9 \quad 10^8 < \text{Re}_x < 10^9$$

We shall examine the difference these respective n values have on predicted boundary layer characteristics later in section 17.7.5.

17.7.4 Assumed Shear Stress Relationship

Determining an appropriate shear stress relationship to employ with Eq. 17.51 is a bit problematic. Recall that for a laminar flow, we would simply apply the Newtonian relationship relating the viscosity to the rate of change of velocity normal to the flow direction at the wall

($y = 0$), such that $\tau_w = \mu \left. \frac{dU}{dy} \right|_{y=0}$. However, if we apply the Nikuradse-type velocity profile, we

have:

$$\tau_w = \mu \left. \frac{dU}{dy} \right|_{y=0}, \text{ with } U = U_\infty \left(\frac{y}{\delta} \right)^{\frac{1}{n}}$$

$$\tau_w = \mu \left. \frac{dU}{dy} \right|_{y=0} = \mu U_\infty \frac{1}{\delta^{\frac{1}{n}}} \frac{1}{n} (y)^{\frac{1-n}{n}} = \left(\frac{\mu U_\infty}{\delta} \right) \frac{1}{\left(\frac{y}{\delta} \right)^{\frac{n-1}{n}}} \Rightarrow \infty \text{ as } y \rightarrow 0$$

As we will see, to appropriately integrate Eq. 17.51 we will require an expression for the wall shear stress which is a function of the boundary layer thickness, δ . With this in mind, we make use of the empirical equation for the mean outer region velocity profile, Eq. 17.49, given as:

$$\frac{U}{u_\tau} = \frac{1}{k} \ln \left(\frac{y u_\tau}{\nu} \right) + B + A(\xi) \sin^2 \left(\frac{\pi y}{2 \delta} \right)$$

Letting $y = \delta$, and $U = U_\infty$, we obtain:

$$\frac{U_\infty}{u_\tau} = \frac{1}{k} \ln \left(\frac{\delta u_\tau}{\nu} \right) + B + A(\xi) \sin^2 \left(\frac{\pi \delta}{2 \delta} \right)$$

$$\text{or } \frac{U_\infty}{u_\tau} = \frac{1}{k} \ln \left(\frac{\delta u_\tau}{\nu} \right) + B + A(\xi)$$

Rearranging, we get:

$$\frac{U_\infty}{u_\tau} = \frac{1}{k} \ln \left(\frac{\delta U_\infty}{\nu} \frac{u_\tau}{U_\infty} \right) + B + A(\xi) = \frac{1}{k} \ln \left(\frac{\delta U_\infty}{\nu} \right) + \frac{1}{k} \ln \left(\frac{u_\tau}{U_\infty} \right) + B + A(\xi)$$

Noting that $\frac{\delta U_\infty}{\nu} = \text{Re}_\delta$, $u_\tau = \sqrt{\frac{\tau_0}{\rho}}$, and $\frac{u_\tau}{U_\infty} = \sqrt{\frac{\tau_0}{\rho U_\infty^2}} = \sqrt{\frac{c_f}{2}}$, we can write:

$$\sqrt{\frac{2}{c_f}} = \frac{1}{k} \ln(\text{Re}_\delta) + \frac{1}{k} \ln \left(\sqrt{\frac{c_f}{2}} \right) + B + A(\xi) \quad (17.55)$$

Equation 17.55 relates c_f directly to Re_δ , but the relationship is implicit. To develop an explicit relationship, we assume a series of c_f values from 0.0015 to 0.005, and then solve Eq.17.55 for the respective Re_δ values using a root finding program. We then use the c_f vs. Re_δ values and develop a regression power law fit for c_f as a function of Re_δ , given by (using flat plate values of $k = 0.385$, $B = 4.2$, and $A(\xi) = 2.5$):

$$c_f = \frac{\tau_w}{\frac{1}{2} \rho U_\infty^2} = 0.0195 (\text{Re}_\delta)^{-0.173} = 0.0195 \left(\frac{U_\infty \delta}{\nu} \right)^{-0.173} \quad (17.56)$$

17.7.5 Solution of the Momentum Integral Equation

Solution of Eq.17.51 requires that we first determine the momentum thickness, θ , as a function of the boundary layer thickness, δ , via Eq. 17.52. To facilitate the integration of Eq.17.52, we rewrite the Nikaradse relationship, Eq.17.54, as:

$$\frac{U}{U_\infty} = \left(\frac{y}{\delta} \right)^{\frac{1}{n}} = \alpha^{\frac{1}{n}} \quad \text{where} \quad \alpha = \frac{y}{\delta}$$

Thus, Eq.17.52 becomes:

$$\theta = \int_0^\delta \frac{U}{U_\infty} \left(1 - \frac{U}{U_\infty} \right) dy = \delta \int_{\alpha=0}^{\alpha=1} \frac{U}{U_\infty} \left(1 - \frac{U}{U_\infty} \right) d\alpha = \delta \int_0^1 \alpha^{\frac{1}{n}} \left(1 - \alpha^{\frac{1}{n}} \right) d\alpha \quad (17.57)$$

After integration of Eq.17.57, we obtain:

$$\frac{\theta}{\delta} = \frac{n}{(n+1)(n+2)} = \beta \quad (17.58)$$

Here, β is a constant, depending on the value of n . Note that we can also determine δ^* , the displacement thickness as:

$$\delta^* = \int_0^{\delta} \left(1 - \frac{U}{U_{\infty}}\right) dy = \delta \int_{\alpha=0}^{\alpha=1} \left(1 - \frac{U}{U_{\infty}}\right) d\alpha = \delta \int_0^1 \left(1 - \alpha^{\frac{1}{n}}\right) d\alpha = \frac{\delta}{n+1}$$

or

$$\frac{\delta^*}{\delta} = \frac{1}{n+1} \quad \left(\text{note that: } H = \frac{\delta^*}{\theta} = \frac{n+2}{n}\right)$$

Now, we substitute Eqs. 17.58 and 17.56 into Eq. 17.51:

$$\begin{aligned} \tau_w &= \rho U_{\infty}^2 \frac{d\theta}{dx} \\ 0.0195 \frac{1}{2} \rho U_{\infty}^2 \left(\frac{U_{\infty} \delta}{\nu}\right)^{-0.173} &= \rho U_{\infty}^2 \beta \frac{d\delta}{dx} \\ 0.00975 \left(\frac{U_{\infty} \delta}{\nu}\right)^{-0.173} &= \beta \frac{d\delta}{dx} \\ \frac{0.00975}{\beta} \left(\frac{U_{\infty}}{\nu}\right)^{-0.173} dx &= \delta^{0.173} d\delta \end{aligned} \quad (17.59)$$

To integrate Eq. 17.59 requires that we assume the state of the flow from the leading edge of the flat plate. The simplest approach is to assume that the boundary layer is turbulent from the leading edge of the plate. This is a reasonable approach if the Reynolds number is large and a boundary layer tripping mechanism (such as a rod or large sand roughness) is applied very near the leading edge. However, for the more general case, the boundary layer will be laminar from the leading edge of the plate, and then transition to a turbulent boundary layer. This can be addressed by assuming laminar behavior up to a transition location, and performing the integration in two parts: integrating the laminar equation from the leading edge to the transition point, and then integrating Eq. 17.59 from that point onward assuming turbulent flow. Here, we will examine both of these situations, and assess the difference in the predicted behavior.

17.7.5.1 Turbulent Flow from Leading Edge

First, we will assume that the flow is turbulent from the leading edge, and thus start our integration of Eq.17.59 from $\delta = 0$ at $x = 0$. Thus:

$$\frac{0.00975}{\beta} \left(\frac{U_\infty}{\nu} \right)^{-0.173} \int_{x=0}^x dx = \int_{\delta=0}^{\delta} \delta^{0.173} d\delta$$

$$\frac{0.00975}{\beta} \left(\frac{U_\infty}{\nu} \right)^{-0.173} x = \frac{\delta^{1.173}}{1.173} = 0.853 \delta^{1.173}$$

Solving for δ gives:

$$\delta = \left(\frac{0.00975}{0.853\beta} \right)^{\frac{1}{1.173}} \left(\frac{U_\infty x}{\nu} \right)^{\frac{0.173}{1.173}} x = 0.0216\beta^{-0.853} \text{Re}_x^{-0.147} x$$

or

$$\frac{\delta}{x} = \frac{0.0216\beta^{-0.853}}{\text{Re}_x^{0.147}} \quad (17.60)$$

The friction coefficient is defined as:

$$c_f = \frac{\tau_w}{\frac{1}{2}\rho U_\infty^2}$$

The wall shear stress, τ_w , is determined from the simplified integral equation, Eq. 17.51, giving:

$$c_f = \frac{\tau_w}{\frac{1}{2}\rho U_\infty^2} = 2 \frac{d\theta}{dx} \quad (17.61)$$

We obtain $\frac{d\theta}{dx}$ in Eq.17.61 from Eq. 17.58 as $\frac{d\theta}{dx} = \beta \frac{d\delta}{dx}$, so:

$$c_f = \frac{\tau_w}{\frac{1}{2}\rho U_\infty^2} = 2 \frac{d\theta}{dx} = 2\beta \frac{d\delta}{dx} \quad (17.62)$$

Finally, we determine $\frac{d\delta}{dx}$ by differentiating Eq. 17.60 and substituting into Eq. 17.62, giving the result:

$$c_f = \frac{\tau_w}{\frac{1}{2}\rho U_\infty^2} = 2 \frac{d\theta}{dx} = 2\beta \frac{d\delta}{dx} = \frac{0.0368\beta^{0.147}}{\mathbf{Re}_x^{0.147}} = .0368 \left(\frac{\beta}{\mathbf{Re}_x} \right)^{0.147} \quad (17.63)$$

For $7 \leq n \leq 9$, the values of β , $\frac{\delta^*}{\delta}$, $H = \frac{\delta^*}{\theta}$, and the corresponding equations for $\frac{\delta}{x}$ and c_f are:

$$n = 7 \quad \beta = \frac{\theta}{\delta} = 0.0972 \quad \frac{\delta^*}{\delta} = 0.125 \quad H = 1.286 \quad \frac{\delta}{x} = \frac{0.158}{\mathbf{Re}_x^{0.147}} \quad c_f = \frac{0.0261}{\mathbf{Re}_x^{0.147}} \quad (17.64a)$$

$$n = 8 \quad \beta = \frac{\theta}{\delta} = 0.0889 \quad \frac{\delta^*}{\delta} = 0.111 \quad H = 1.250 \quad \frac{\delta}{x} = \frac{0.170}{\mathbf{Re}_x^{0.147}} \quad c_f = \frac{0.0258}{\mathbf{Re}_x^{0.147}} \quad (17.64b)$$

$$n = 9 \quad \beta = \frac{\theta}{\delta} = 0.0818 \quad \frac{\delta^*}{\delta} = 0.100 \quad H = 1.222 \quad \frac{\delta}{x} = \frac{0.183}{\mathbf{Re}_x^{0.147}} \quad c_f = \frac{0.0255}{\mathbf{Re}_x^{0.147}} \quad (17.64c)$$

Note that the difference in the friction coefficient between $n = 7$ and $n = 9$ is only 2.4%, which is less than the empirical accuracy used to establish the curve fits for the velocity profile and shear stress relationships used to develop Eq. 17.63. This suggests that the selection of n for our modeling is not critically important.

The total drag on a plate is obtained by integrating the shear stress over the plate surface, such that:

$$\text{Drag} = \int_0^L \tau_w W dx \quad \text{where } W \text{ is the plate width, and } L \text{ is the plate length} \quad (17.65)$$

Note that we can perform this integration the hard way, by integrating using Eq. 17.63 for c_f , or the easier way by noting that shear stress is directly related to the change in the momentum thickness through Eq. 17.51. Therefore, substituting from the simplified integral equation, Eq. 17.51, into Eq. 17.65, we have:

$$\text{Drag} = \int_0^L \tau_w W dx = \int_0^L \rho U_\infty^2 W \frac{d\theta}{dx} dx = \rho U_\infty^2 W \int_{\theta=0}^{\theta=\theta_L} d\theta = \rho U_\infty^2 W \theta \Big|_{x=L} \quad (17.66)$$

Equation 17.66 indicates that we only need to determine the value of the momentum thickness at $x = L$ to establish the overall drag on the plate. This is because θ is a direct reflection of the momentum "lost" from the boundary layer (for a $dp/dx = 0$ flow).

From Eq. 17.58 for the momentum thickness, $\theta = \beta\delta$, which combined with Eq. 17.60 gives, for $x = L$:

$$\theta|_{x=L} = \beta \delta|_{x=L} = \frac{0.0216 \beta^{0.147} L}{\text{Re}_L^{0.147}} \quad (17.67)$$

To calculate the non-dimensional drag coefficient, C_D , we divide Eq.17.66 divide through by $\frac{1}{2} \rho U_\infty^2 (WL)$, to get a generic expression for C_D :

$$C_D = \frac{\text{Drag}}{\frac{1}{2} \rho U_\infty^2 (WL)} = \frac{\int_0^L \tau_w W dx}{\frac{1}{2} \rho U_\infty^2 WL} = \frac{\rho U_\infty^2 W \theta|_{x=L}}{\frac{1}{2} \rho U_\infty^2 WL} = \frac{2\theta|_{x=L}}{L} \quad (17.68)$$

Now, substituting Eq. 17.67 into 17.68 for θ at $x = L$, we get:

$$C_D = \frac{2\theta|_{x=L}}{L} = \frac{0.0432 \beta^{0.147}}{\text{Re}_L^{0.147}} = 0.0432 \left(\frac{\beta}{\text{Re}_L} \right)^{0.147} \quad (17.69)$$

Equation 17.69 gives the predicted flat plate drag coefficient for a boundary layer that is turbulent from the leading edge of a flat plate.

17.7.5.2 Laminar-Turbulent Transition at Critical Reynolds Number

If we now consider a boundary layer that is initially laminar, which then transitions to turbulence at some critical Reynolds number, we can derive an approximate relationship for the boundary layer growth, c_f , and C_D for the combined processes. However, we have two problems. The first is that the critical Reynolds number, Re_{crit} , at which transition from laminar to turbulent flow occurs is not a well-defined value. It may change markedly, due to variations in the impinging flow conditions, such as turbulence intensity levels, mean profile non-uniformities, and surface irregularities and roughness. The second is that transition, as we pointed out earlier, occurs over a finite length of the plate, yielding a sustaining turbulent boundary layer only after some development length. However, to facilitate a solution, we will assume that the combined laminar-turbulent flow makes an immediate transition from laminar to turbulent behavior at a specified critical Reynolds number, and that our Eq. 17.59 we derived from the integral equation, applies immediately from that critical Reynolds number onward.

We will assume that the flow over the first portion of the flat plate behaves according to the Blasius solution we developed in Chapter 13, and that the boundary layer for the laminar region develops according to Eq.13.29, given by:

$$\frac{\delta}{x} = \frac{5}{\sqrt{\text{Re}_x}} \quad \text{or} \quad \delta = \frac{5x}{\sqrt{\text{Re}_x}}$$

Equation 13.29 assumes that the boundary layer initiates at the leading edge of the plate, such that $\delta = 0$ at $x = 0$. If we assume that $\delta = \delta_{\text{crit}}$ at $x = x_{\text{crit}}$ or $\text{Re}_x = \text{Re}_{x,\text{crit}}$, we can integrate Eq. 17.59 to establish the behavior of the turbulent portion of the boundary layer, starting the integration at $\delta = \delta_{\text{crit}}$ at $x = x_{\text{crit}}$ as follows:

$$\frac{0.00975}{\beta} \left(\frac{U_\infty}{\nu} \right)^{-0.173} \int_{x_{\text{crit}}}^x dx = \int_{\delta_{\text{crit}}}^{\delta} \delta^{0.173} d\delta$$

$$\frac{0.00975}{\beta} \left(\frac{U_\infty}{\nu} \right)^{-0.173} (x - x_{\text{crit}}) = \frac{\delta^{1.173} - \delta_{\text{crit}}^{1.173}}{1.173}$$

Solving for δ gives:

$$\delta = \left[\frac{0.01144}{\beta} \left(\frac{U_\infty}{\nu} \right)^{-0.173} (x - x_{\text{crit}}) + \delta_{\text{crit}}^{1.173} \right]^{0.853}$$

With a bit of work, this can be shown to be:

$$\delta = \frac{\nu}{U_\infty} \left[\frac{0.01144}{\beta} (\text{Re}_x - \text{Re}_{x,\text{crit}}) + \text{Re}_{\delta_{\text{crit}}}^{1.173} \right]^{0.853}$$

or

$$\frac{\delta}{x} = \frac{\left[\frac{0.01144}{\beta} (\text{Re}_x - \text{Re}_{x,\text{crit}}) + \text{Re}_{\delta_{\text{crit}}}^{1.173} \right]^{0.853}}{\text{Re}_x} \quad (17.70)$$

In Eq. 17.70, $\text{Re}_x = \frac{U_\infty x}{\nu}$, $\text{Re}_{x,\text{crit}} = \frac{U_\infty x_{\text{crit}}}{\nu}$, and $\text{Re}_{\delta_{\text{crit}}} = \frac{U_\infty \delta_{\text{crit}}}{\nu}$. Equation 17.70 will give the value of δ for the turbulent portion of the boundary layer based on the respective Reynolds number, where $\text{Re}_x > \text{Re}_{x,\text{crit}}$. However, we can simplify the variables required for Eq. 17.70 by using Eq. 13.29 to show:

$$\text{Re}_{\delta_{\text{crit}}} = 5 \text{Re}_{x,\text{crit}}^{0.5} \quad (17.71)$$

So, Substituting Eq. 17.71 into Eq. 17.70 gives:

$$\frac{\delta}{x} = \frac{\left[\frac{0.01144}{\beta} (\text{Re}_x - \text{Re}_{x,\text{crit}}) + 6.61 \text{Re}_{x,\text{crit}}^{0.587} \right]^{0.853}}{\text{Re}_x} \quad (17.72)$$

To obtain the friction coefficient, we differentiate Eq. 17.72 and substitute into Eq. 17.62, which after some manipulation gives:

$$c_f = 0.0195 \left[\frac{0.01144}{\beta} (\text{Re}_x - \text{Re}_{x,\text{crit}}) + 6.61 \text{Re}_{x,\text{crit}}^{0.587} \right]^{-0.147} \quad (17.73)$$

To determine the drag coefficient, C_D , for a combined laminar-turbulent flow over a plate, we combine Eq.17.58 with Eq.17.68 and Eq. 17.72, applied at $x = L$ to obtain:

$$C_D = \frac{\text{Drag}}{\frac{1}{2} \rho U_\infty^2 WL} = \frac{2\theta|_{x=L}}{L} = \frac{2\beta\delta|_{x=L}}{L} = \frac{2\beta \left[\frac{0.01144}{\beta} (\text{Re}_L - \text{Re}_{x,\text{crit}}) + 6.61 \text{Re}_{x,\text{crit}}^{0.587} \right]^{0.853}}{\text{Re}_L} \quad (17.74)$$

17.7.5.3 Comparison: Laminar, LE Turbulent, and Transitional Boundary Layers

Figures 17.24, 17.25, and 17.26 illustrate the growth of a flat plate boundary layer with distance, x , and the consequent behavior of $c_f(x)$ and $C_D(L)$, considering the flow is either (a) turbulent from the leading edge (TLE), or (b) a combination of laminar and turbulent (L-T), with a transition at a critical Reynolds number. For the turbulent portions, a value of $n = 7$ was assumed for the power-law velocity profile ($\beta = 0.0972$).

To properly illustrate the non-dimensional change of boundary layer thickness relative to the plate length, we divide δ in Eqs.17.60 and 17.72 by the plate length, L , which gives respectively:

Turbulent from the leading edge:

$$\frac{\delta(x)}{L} = \frac{0.0216 \beta^{-0.853}}{\text{Re}_L^{0.147}} \left(\frac{x}{L} \right)^{0.853} = \frac{0.158}{\text{Re}_L^{0.147}} \left(\frac{x}{L} \right)^{0.853} \quad \text{for } n=7, \beta=0.0972 \quad (17.75)$$

Laminar-Turbulent Transition:

$$\frac{\delta(x)}{L} = \frac{5}{\sqrt{\text{Re}_L}} \left(\frac{x}{L} \right)^{0.5} \quad (\text{laminar}) \quad \text{for } \text{Re}_x \leq \text{Re}_{x,\text{crit}} \quad (17.76a)$$

$$\frac{\delta(x)}{L} = \frac{\left[\frac{0.01144}{\beta} \left(\text{Re}_L \left(\frac{x}{L} \right) - \text{Re}_{x,\text{crit}} \right) + 6.61 \text{Re}_{x,\text{crit}}^{0.587} \right]^{0.853}}{\text{Re}_L} \quad (\text{turbulent}) \quad \text{for } \text{Re}_x > \text{Re}_{x,\text{crit}}$$

$$= \frac{\left[0.1177 \left(\text{Re}_L \left(\frac{x}{L} \right) - \text{Re}_{x,\text{crit}} \right) + 6.61 \text{Re}_{x,\text{crit}}^{0.587} \right]^{0.853}}{\text{Re}_L} \quad \text{for } n = 7, \beta = 0.0972 \quad (17.76b)$$

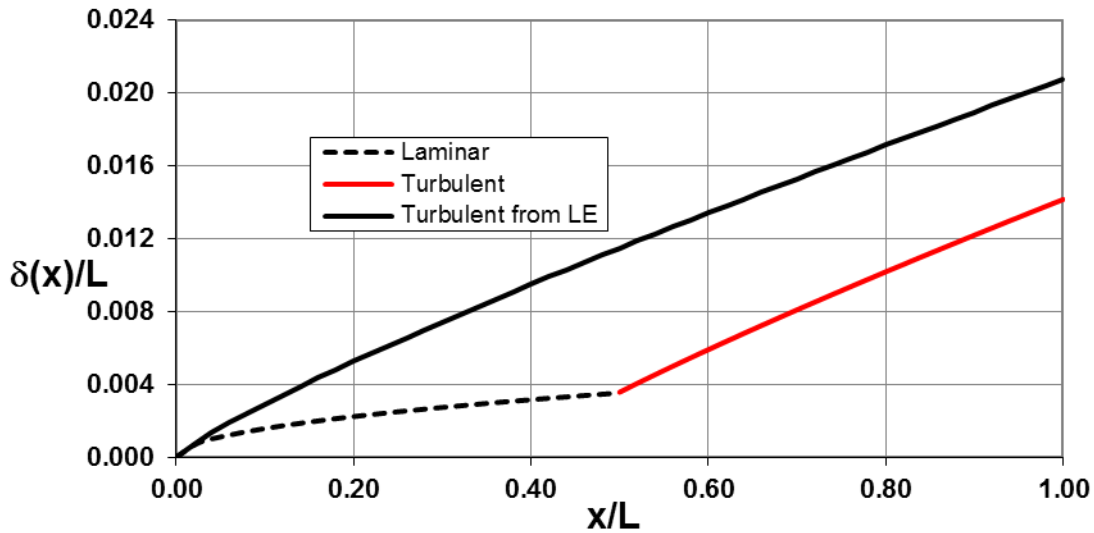
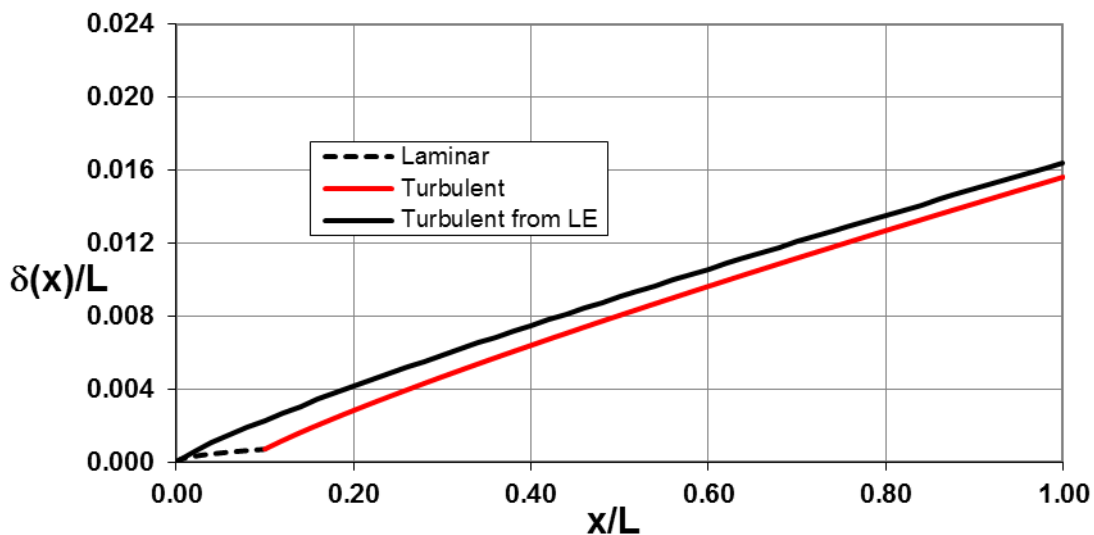
(a) $Re_L = 10^6$ (b) $Re_L = 5 \times 10^6$

Figure 17.24 Comparison of predicted flat plate boundary layer growth (for $n = 7$) assuming:
 (1) turbulent from the plate leading edge (TLE) [Eq. 17.75] and
 (2) transition from laminar to turbulent (L-T) [Eq. 17.76] at $Re_{x,crit} = 5 \times 10^5$.
 (a) $Re_L = 10^6$ (b) $Re_L = 5 \times 10^6$.

Figure 17.24 shows plots of $\delta(x)/L$ vs. x/L for (1) Eq. 17.75 (TLE), and (2) Eq. 17.76 (L-T). We assume $Re_{x,crit} = 5 \times 10^5$ for the latter equation. Results are shown for plate Reynolds numbers of both $Re_L = 10^6$ and $Re_L = 5 \times 10^6$ to illustrate the variance of the boundary layer growth over the

plate as plate length is increased. Note that the laminar boundary layer grows much more slowly than the turbulent, so for $Re_L = 10^6$ the difference in the assumed growth modes is quite pronounced, with the L-T boundary layer being 32% thinner at the end of the plate than the TLE boundary layer.

As the plate Reynolds number increases, this discrepancy in boundary layer thickness decreases, since the contribution of the laminar portion to the L-T boundary layer diminishes accordingly. So, for $Re_L = 5 \times 10^6$, the difference in the end of plate boundary layer is less than 5%. For Reynolds numbers exceeding $Re_L = 10^7$, which reflect most practical external flows, the difference drops to roughly 1%, which is essentially negligible.

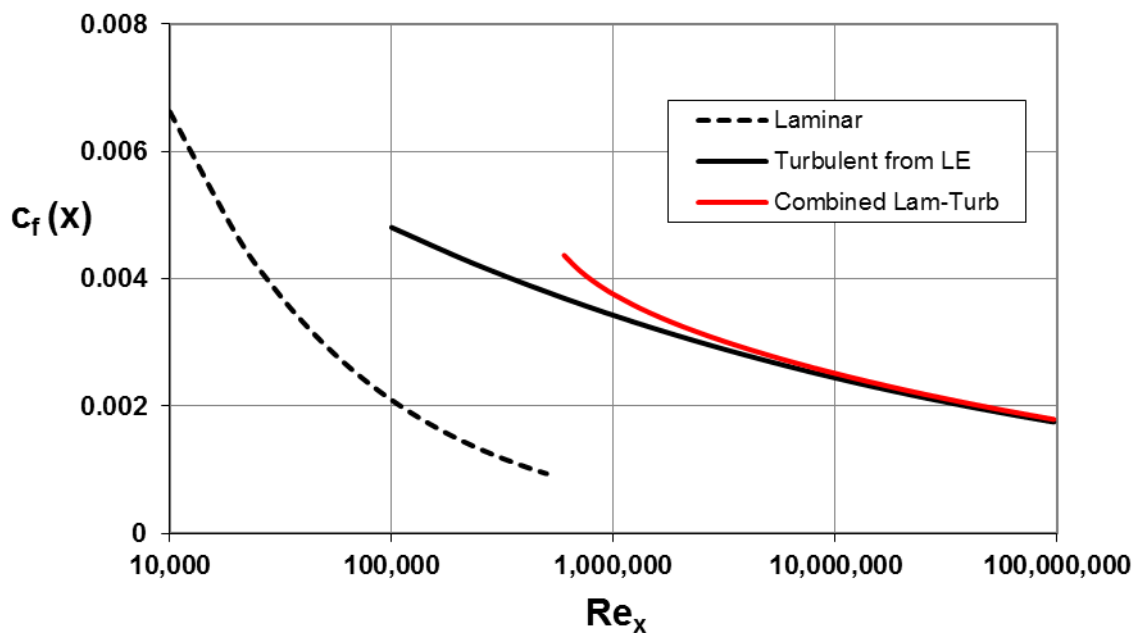


Figure 17.25 Predicted friction coefficient, $c_f(x)$ (for $n = 7$), assuming:
 (1) turbulent from the plate leading edge (TLE) [Eq. 17.64a] and
 (2) transition from laminar to turbulent (L-T) [Eq. 17.73] at $Re_{x,crit} = 5 \times 10^5$.

Figure 17.25 illustrates the behavior of the friction coefficient, c_f , as predicted by Eqs. 13.33 (laminar flow), 17.63 and 17.72. Note that c_f for a turbulent boundary is significantly greater than the c_f for a comparable laminar boundary layer at the same Reynolds number. This is a result of the more intense momentum exchange within a turbulent boundary layer, and the higher shear gradient at the surface. In fact, for $Re_x = 5 \times 10^5$ (the Re_{crit} value for the combined L-T), the c_f for the TLE turbulent boundary is roughly four times greater than the comparable c_f for a laminar boundary.

Note that the c_f predicted by Eq. 17.73 (after transition) for assumed laminar-turbulent transition (L-T) is initially in excess of that predicted by Eq. 17.64a for TLE. At first, this may seem unusual, but consider the process of boundary layer growth. At the point where the laminar portion of the L-T boundary layer transitions to turbulence, the boundary layer will be thinner than the comparable TLE boundary layer. And as figure 17.24 illustrates, the thinner the boundary layer, the faster it grows. Thus, when the boundary layer transitions from laminar to turbulent, the subsequent turbulent boundary layer will be growing faster, with a consequent higher c_f than that of the TLE boundary layer at the same Re_x . Of course, as Re_x increases, and the growth rates of the L-T and TLE become comparable, and the difference in c_f between the TLE and L-T predictions become minimal, as shown by figure 17.25.

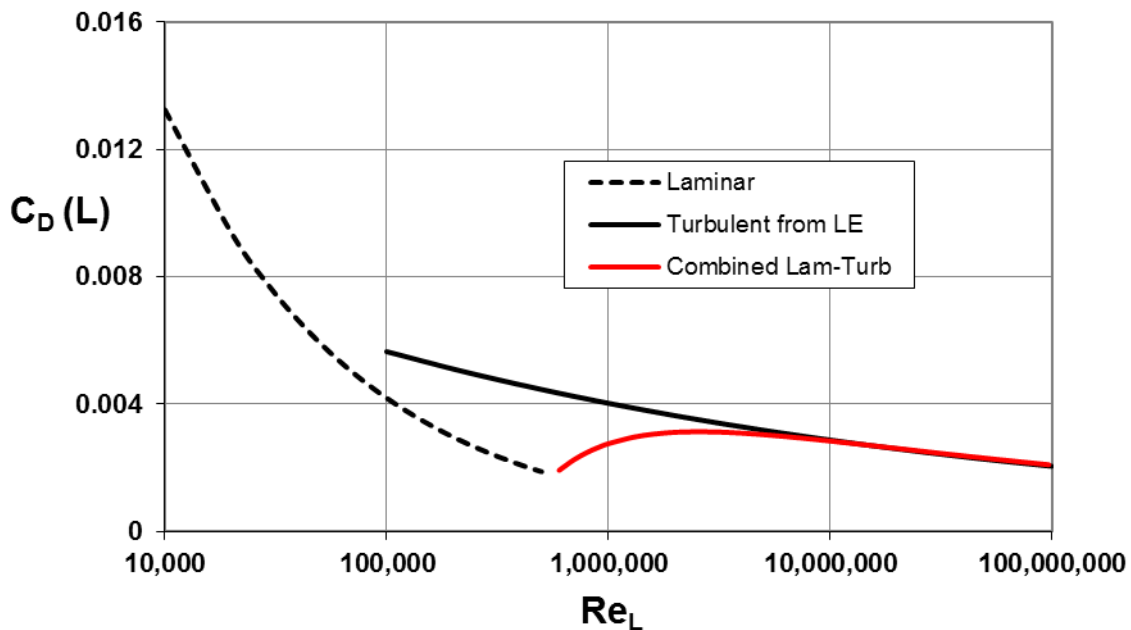


Figure 17.26 Predicted total drag coefficient, $C_D(L)$, for $n = 7$, assuming
 (1) turbulent from the plate leading edge (TLE) [Eq. 17.69] and
 (2) transition from laminar to turbulent (L-T) [Eq. 17.74] at $Re_{x,crit} = 5 \times 10^5$.

Figure 17.26 is a plot of $C_D(L)$ comparing the predictions for laminar, turbulent from the leading edge (TLE), and combined laminar-turbulent (L-T) boundary layers. Note that for $Re_L < 10^7$, a L-T boundary layer will have lower drag than the TLE boundary layer, since the initial laminar boundary layer will have significantly lower shear stress than a turbulent boundary layer. For example, if $Re_{x,crit} = 5 \times 10^5$, and $Re_L = 10^6$, the L-T drag will be roughly 30% less than for a TLE

flow. However, as Re_L increases, the difference between the L-T and the TLE drag will decrease until they are essentially equivalent at roughly $Re_L = 1.5 \times 10^7$.

As an illustration of when one should be concerned with an initial laminar region, consider that the Reynold number for the wing width (the chord) of a small private plane traveling at 150 miles per hour (220 ft/s or 67 m/s) is roughly 4 to 5×10^6 . So, from figure 17.26 there would be little reason to account for any initial laminar portion of such practical aerodynamic flows, since the C_D values for the TLE and L-T predictions are essentially identical. However, the flow over the rudder of a small boat moving at 15 ft/s or 4.5 m/s will be roughly 2×10^6 , for which the consideration of an initial portion of laminar flow could have as much as a 10-15% reduction from a flow turbulent from the rudder leading edge. The bottom line is that unless a practical flow is fairly slow, or small, adaptation for an initial laminar portion of the boundary layer is probably not warranted.

17.8 Conclusion

While this chapter is rather long, it is still a simplistic discussion of turbulence, and how it is modeled and predicted. The literature on turbulence is quite extensive, and quite contentious. Because of the complexity of turbulence, the manifold approaches for the prediction of turbulence properties, which have been suggested and pursued, have met with varying degrees of success. It was the intent of this chapter to introduce you to the generic characteristics of turbulence, and some simple and reasonably effective techniques for assessing turbulence properties for simple geometries. My hope is that having completed this chapter you have a reasonable grasp of what turbulence is, the basic methods for approaching solutions, and the difficulties that can develop when doing so. For a more thorough discussion of semi-empirical approaches to prediction of turbulence properties, I suggest reading Chapters 5 and 6 of an excellent book, "Viscous Fluid Flow," by [Frank White \(1991\)](#). However, recognize that even White's book just scratches the surface of our understanding, and does not cover the wealth of material subsequently available.

For a comprehensive overview of the modern modeling and computational approaches used to predict turbulent flow behavior in practical engineering flows, I suggest you watch three short video lectures by Professor Kevin Cassel, which start at [this link](#). These videos provide excellent descriptions of the three most common turbulence modeling approaches employed, their general effectiveness, limitations, and the differences in computational costs to make effective engineering predictions of turbulent behavior.

In closing, I note that although there have been many marvelous computational and experimental studies, which have produced incredible: (1) computational simulations of turbulence behavior through massive numerical solutions of the time-dependent, three-dimensional Navier-Stokes equations, and (2) three-dimensional experimental measurements and visualizations of real

turbulent flows. Despite these remarkable advances, we still struggle to understand the turbulence process better than it is described in this chapter. Even though studies can demonstrate a variety of vortical and wave-like structures comprising turbulence, researchers are still trying to sort out the cause and effect of these structures, and to put that understanding to the development of prediction methods that do not require hours or days on a super computer. Hopefully, there is a von Karman or Prandtl out there who can synthesize the vast amount of information that has been developed, and subsequently develop effective universal prediction methods that can be run on a personal computer in hours, not days. Time will tell.

References

[Coles, D. E. \(1956\)](#) "The Law of the Wake in the Turbulent Boundary Layer," J. Fluid Mech., vol. 1, pp. 191-226.

Coles, D. E. and Hirst, E. A. (1969) *Proceedings of Computation of Turbulent Boundary Layers, 1968*, AFOSR-IFP-Stanford Conference, vol. II. Thermosciences Division, Stanford University, California.

Emmons, H. W. (1951) "The Laminar-Turbulent Transition in a Boundary Layer: Part I," J. Fluid Mech., vol. 2, pp. 15-36.

[Klebanoff, P. S., Tidstrom, K. D., and Sargent, L. M. \(1962\)](#) "The Three-Dimensional Nature of Boundary Layer Instability," J. Fluid Mech., vol. 12, pp. 1-24.

[Marusic, I., McKeon, B. J., Mondewitz, P. A., Nagib, H. M., Smits, A. J., and Sreenivasan, K. R. \(2010\)](#) "Wall-bounded turbulent flows at high Reynolds numbers: Recent advances and key issues," Physics of Fluids, vol. 22, 065103, pp. 1-24.

Nachtsheim, P. R. (1964) "An Initial Value Method for the Numerical Treatment of the Orr-Sommerfeld Equation for the Case of Plane Poiseuille Flow," NASA Technical Note D-2414.

[Orr, W. M'F.](#) (1907). "The stability or instability of the steady motions of a liquid. Part II". *Proceedings of the Royal Irish Academy*. A **27**: 69–138{{inconsistent citations}}

Nikuradse, J. (1932) "Gesetzmässigkeit der turbulenten Stromung in glatten Rohren," Ing.-Arch. Vol. 1, pp. 306-332.

Prandtl, L. (1921) "Über den Reibungswiderstand stromender Luft," *Ergebnisse AVA Gottingen*, 1st Series, pp. 136-142.

Prandtl, L. (1925) "Über die ausgebildete Turbulenz," *Z. Angew. Math. Mech.*, vol. 5, pp. 136-139.

Prandtl, L. [with Tietjens, O. G.] (1933) In *Applied Hydro- and Aero-Mechanics*, McGraw-Hill, New York.

Reynolds O. (1883) "An experimental investigation of the circumstances which determine whether the motion of water in parallel channels shall be direct or sinuous and of the law of resistance in parallel channels," *Philos. Trans. R. Soc.*, vol. 174, pp. 935–982.

Reynolds O. (1895) "On the dynamical theory of incompressible viscous fluids and the determination of the criterion," *Philos. Trans. R. Soc.*, vol. 186, pp. 123–164.

[Reynolds, W. C. \(1976\)](#) "Computation of Turbulent Flows," *Ann. Rev. Fluid Mech.*, vol. 8, pp. 183-208.

Schlichting, H. (1933) "Laminare Strahlenausbreitung," *Z. Angew. Math. Mech.*, vol. 13, pp. 260-263.

[Schubauer, G. B. and Skramstad, H. \(1947\)](#) "Laminar Boundary Layer Oscillation and Transition on a Flat Plate," *J. Res. Nat. Bur. Standards*, vol. 38, pp. 251-292.

[Shih, T.S., Povinelli, L.A., Liu, N-S, Potapczuk, M.G., and Lumley, J.L. \(1999\)](#), "A generalized wall function," NASA/TM--1999-209398.

[Smith, C.R. and Walker, J.D.A \(1997\)](#) "Sustaining Mechanisms of Turbulent Boundary Layers: The Role of Vortex Development and Interactions," in *Self-Sustaining Mechanisms of Wall Turbulence*, R.L. Panton, ed., Computational Mechanics Publications, England England, pp. 13-47, 1997.

[Spalding, D. B. \(1961\)](#) "A Single Formula for the Law of the Wall," *J. Appl. Mech.*, vol. 28, issue 3, pp. 455-457.

[Speziale, C. G. \(1991\)](#) "Analytical Methods for the Development of Reynolds-Stress Closures in Turbulence," *Ann. Rev. Fluid Mech.*, vol. 23, pp. 107-157.

[Narashima, R. and Sreenivasan, K.R. \(1979\)](#) "Relaminarization of Fluid Flows," in *Advances in applied mechanics*. Volume 19. (A80-40840 17-31) New York, Academic Press, Inc., 1979, p. 221-309.

[Sommerfeld, A. \(1908\)](#). "Ein Beitrag zur hydrodynamische Erklärung der turbulenten Flüssigkeitsbewegungen". *Proceedings of the 4th International Congress of Mathematicians III*. Rome. pp. 116–124

Tollmien, W. (1929) "Über die Entstehung der Turbulenz," *Nachr. Ges. Wiss. Göttingen, Math. Phys. Klasse II*, pp. 21-44 [translated in NACA Technical Memo. 609].

Van Driest, E. R. (1956) "On turbulent flow near a wall," *J. Aero. Sci.*, vol. 23, pp.1007-1011.

Von Karman, T. (1930) "Mechanische Ähnlichkeit und Turbulenz," In *Proceedings of the 3rd International Congress on Applied Mechanics*.

[Wazzan, A. R. \(1975\)](#) "Spatial Stability of Tollmein-Schlicting Waves," *Prog. Aerosp. Sci.*, vol. 16, no. 2, pp. 99-127.

[White, F. M. \(1991\)](#), *Viscous Fluid Flow*, McGraw-Hill Inc., New York.

[White, F. M.\(2011\)](#), *Fluid Mechanics*, 7th Ed., McGraw-Hill, inc., New York

Study Problems

1. If $\mathbf{Re}_{\text{crit}} = \mathbf{Re}_{\delta^*} \approx 520$ for a flat plate boundary layer, determine the corresponding value for $\mathbf{Re}_{\text{crit}} = \mathbf{Re}_x$. You will need to make use of Eq. 13.30.
2. Consider a flat plate boundary layer in water with $U_\infty = 10 \frac{\text{cm}}{\text{s}}$ and $\nu = 10^{-2} \frac{\text{cm}^2}{\text{s}}$. If $\mathbf{Re}_{\text{crit}} = \mathbf{Re}_{\delta^*} \approx 520$, for a flat plate boundary layer, what will be the displacement thickness when $\mathbf{Re}_{\text{crit}}$ is reached? What will be the boundary layer thickness? At what x location will this occur along the plate? You will need to use equations for a laminar boundary layer from Chapter 13.

3. Consider a flat plate boundary layer in air with $U_\infty = 10 \frac{\text{m}}{\text{s}}$ and $\nu = 1.52 \times 10^{-5} \frac{\text{m}^2}{\text{s}}$. If $\text{Re}_{\text{crit}} = \text{Re}_{\delta^*} \approx 520$, for a flat plate boundary layer, what will be the displacement thickness when Re_{crit} is reached? What will be the boundary layer thickness? At what x location will this occur along the plate? You will need to use equations for a laminar boundary layer from Chapter 13.
4. Using Eq. 17.32 for the logarithmic layer of the inner region, determine an expression for the eddy viscosity, ε , in terms of k , y , and u_τ . Next, determine an expression for ε , in terms of k , y^+ , and the kinematic viscosity, ν . What is the value of ε/ν for $y^+ = 300$?
5. Using Eqs. 17.36 and 17.37 for the van Driest model of the entire inner region, determine an expression for the eddy viscosity, ε , in terms k , A , y^+ , and the kinematic viscosity, ν . What is the value of ε/ν for $y^+ = 5, 21$, and 300 ?
6. Consider Eq. 17.55 where $c_f = f(\text{Re}_\delta)$, but the relationship is implicit. Eq. 17.56 was determined by assuming flat plate values for k , B , and $A(\xi)$, determining Re_δ values implicitly by assuming several values of c_f from 0.0015 to 0.005 and using a root finding program to determine the corresponding Re_δ values. The resultant c_f vs. Re_δ were then fit to a power law curve to determine $c_f = f(\text{Re}_\delta)$. Repeat the curve fit process to verify Eq. 17.56 for a flat plate [$A(\xi) = 2.5$], and then determine the power law curve fit of $c_f = f(\text{Re}_\delta)$, for a strong favorable pressure gradient, with $A(\xi) = 1.0$. Assume flat plate values for k and B for both flows. It is suggested you use Excel and its function "Goal Seek" to determine c_f vs. Re_δ , and then "Trendline" on an Excel plot of c_f vs. Re_δ to establish the power law fit, giving $c_f = f(\text{Re}_\delta)$. Compare your results for $A=1.0$ to the flat plate Eq. 17.55.
7. Consider a flat plate boundary layer in water with $U_\infty = 0.2 \frac{\text{m}}{\text{s}}$, $\nu = 10^{-6} \frac{\text{m}^2}{\text{s}}$, $\rho = 1000 \frac{\text{kg}}{\text{m}^3}$, a plate length of 5 meters, and width of 2 meters.
- (a) If $\text{Re}_{\text{crit}} = \text{Re}_{\delta^*} \approx 520$, determine the corresponding value for $\text{Re}_{\text{crit}} = \text{Re}_x$.
- (b) Then determine the drag force on the plate assuming:
- (1) the flow is turbulent from the leading edge, or
 - (2) that the flow transitions at the $\text{Re}_{\text{crit}} = \text{Re}_x$ you determined.
- Assume $n = 7$ in Eq. 17.54. Is the difference between (1) and (2) substantial?
8. Consider a flat plate boundary layer in air with $U_\infty = 10 \frac{\text{m}}{\text{s}}$, $\nu = 1.52 \times 10^{-5} \frac{\text{m}^2}{\text{s}}$, $\rho = 1.2 \frac{\text{kg}}{\text{m}^3}$, a plate length of 5 meters, and width of 2 meters.
- (a) If $\text{Re}_{\text{crit}} = \text{Re}_{\delta^*} \approx 520$, determine the corresponding value for $\text{Re}_{\text{crit}} = \text{Re}_x$.
- (b) Then determine the drag force on the plate assuming:
- (1) the flow is turbulent from the leading edge, or
 - (2) that the flow transitions at the $\text{Re}_{\text{crit}} = \text{Re}_x$ you determined.
- Assume $n = 8$ in Eq. 17.54. Is the difference between (1) and (2) substantial?

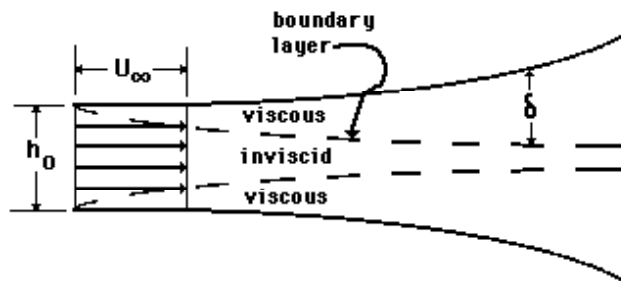
9. Consider a flat plate boundary layer in water with $U_\infty = 10 \frac{\text{cm}}{\text{s}}$, $\nu = 10^{-2} \frac{\text{cm}^2}{\text{s}}$, and a plate length of 5 meters. Assume $n = 8$ in Eq.17.54, and determine the displacement thickness (δ^*) and momentum thickness (θ) at the trailing edge if:
- (a) the flow is turbulent from the leading edge, or
 - (b) the flow transitions to turbulence at $\text{Re}_{\text{crit}} = \text{Re}_x = 3 \times 10^5$.
- Is the difference between (a) and (b) substantial?

10. Consider a flat plate boundary layer in air with $U_\infty = 10 \frac{\text{m}}{\text{s}}$, $\nu = 1.52 \times 10^{-5} \frac{\text{m}^2}{\text{s}}$, and a plate length of 5 meters. Assume $n = 8$ in Eq.17.54, and determine the displacement thickness (δ^*) and momentum thickness (θ) at the trailing edge if:
- (a) the flow is turbulent from the leading edge, or
 - (b) the flow transitions to turbulence at $\text{Re}_{\text{crit}} = \text{Re}_x = 6 \times 10^5$.
- Is the difference between (a) and (b) substantial?

11. Consider two flat plate boundary layer flows over a plate of length 5 meters. One flow is water with $U_\infty = 20 \frac{\text{cm}}{\text{s}}$, $\nu = 10^{-2} \frac{\text{cm}^2}{\text{s}}$, and the other is air with $U_\infty = 10 \frac{\text{m}}{\text{s}}$, $\nu = 1.52 \times 10^{-5} \frac{\text{m}^2}{\text{s}}$. Assume $n = 9$ in Eq.17.54, and determine the boundary layer thicknesses (δ) at the trailing edge for both flows if they both transition to turbulence at $\text{Re}_{\text{crit}} = \text{Re}_x = 3 \times 10^5$. Also, determine the Kolmogorov length scales at the trailing edge for both flows.

12. Consider the flow of air over a flat plate, which has roughly the area of one wing of a Boeing 777. The plate is of span 30 meters and chord 5 meters. The air flows at roughly a Mach number of 0.3, or $U_\infty = 100 \frac{\text{m}}{\text{s}}$ with $\nu = 1.52 \times 10^{-5} \frac{\text{m}^2}{\text{s}}$ and $\rho = 1.2 \frac{\text{kg}}{\text{m}^3}$. Assuming $n = 9$, and a flow that is turbulent from the leading edge, what is total shear drag (consider both sides) on the plate? (note the flow is across the chord of the plate, so $L = 5$ meters).

13. Consider a uniform flow, $u = U_\infty$ entering a 2-D duct, which develops a turbulent a boundary layer from the leading edges, as shown below. The duct height is h and the flow remains turbulent at all times through the duct. Assume the flow may be broken into viscous and inviscid regions as shown. Make use of the Nikuradse solution for δ^* with $n = 7$ and determine:



- a) $h = h(x)$ such that $dP/dx = 0$ (let h_0 be the initial duct height).
- b) the length, L , where your expression for $h(x)$ ceases to be valid.

14. Assuming an approximate velocity profile for a flat plate turbulent boundary layer modeled as $\frac{U}{U_\infty} = \left[1 + 0.119 \ln \left(\frac{y}{\delta} + 0.00023 \right) \right]$. First, determine δ^* and θ as functions of δ for this profile, and subsequently the shape factor H to show this is an acceptable approximation of the velocity profile. This is a pretty messy integration, so I suggest you use Wolfram Alpha to integrate for δ^* and θ . Then, following a procedure similar to Section 17.7.5, integrate the Momentum Integral Equation to determine expressions for $\delta/x = f(\text{Re}_x)$ and $c_f = f(\text{Re}_x)$. Again assume that $c_f = f(\text{Re}_\delta)$ is given by Eq. 17.56, and the flow is turbulent from the leading edge. Compare your results to the corresponding equations for $\delta/x = f(\text{Re}_x)$ and $c_f = f(\text{Re}_x)$ in

Section 17.7.5.1. Also, since $\left. \frac{dU}{dy} \right|_{y=0}$ is finite, assume laminar behavior at the wall and

calculate $\delta/x = f(\text{Re}_x)$ and compare it to that obtained using Eq. 17.56. Why doesn't this latter approach work?

Appendix I**Selected Relationships and Equations****Contents**

A.1	Viscosity Tables	691
A.2	Vector Operations and Identities	692
A.3	Vector Theorems	693
A.4	The Substantial Derivative	694
A.5	Streamlines, 2-D	695
A.6	Rate of Strain	695
A.7	Vorticity	696
A.8	The Governing Equations for Incompressible Flow	696
A.9	Inviscid Flow Equations	697
A.10	Potential Flow	698
A.11	Circulation and Circulation Theorems	699
A.12	Vorticity Transport Equations	700
A.13	Laminar Boundary Layers	701
A.14	Drag	702
A.15	Non-Newtonian Fluids	702
A.16	Turbulence: General	703
A.17	Turbulence: Approximate Boundary Layer Properties	705

A.1. Viscosity tables

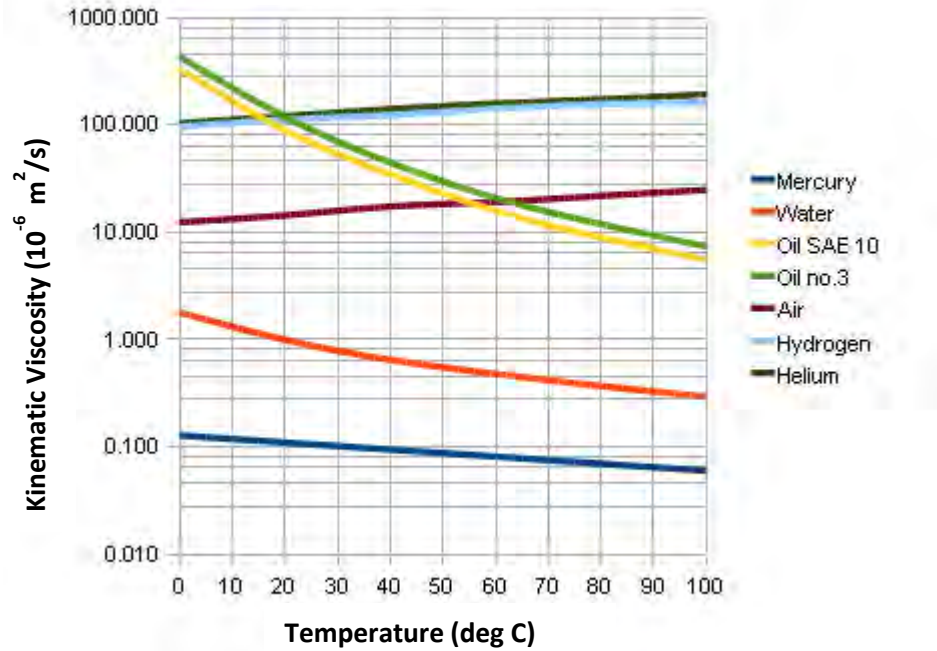
Table 1: Viscosity of Water at Atmospheric Pressure

Temperature - t - (°C)	Density - ρ - (kg/m ³)	Absolute Viscosity - μ - (kg/m-s) $\times 10^{-3}$	Kinematic Viscosity - ν - (m ² /s) $\times 10^{-6}$
0	1000.0	1.787	1.787
5	1000.0	1.519	1.519
10	1000.0	1.307	1.307
20	998.0	1.002	1.004
30	996.3	0.798	0.801
40	992.4	0.653	0.658
50	989.2	0.547	0.553
60	983.2	0.467	0.475
70	978.2	0.404	0.413
80	972.6	0.355	0.365
90	966.3	0.315	0.326
100	972.4	0.282	0.29

Table 2: Viscosity of Air at Atmospheric Pressure

Temperature - t - (°C)	Density - ρ - (kg/m ³)	Absolute Viscosity - μ - (kg/m s) $\times 10^{-5}$	Kinematic Viscosity - ν - (m ² /s) $\times 10^{-5}$
-50	1.469	0.687	0.468
0	1.295	1.736	1.341
10	1.249	1.787	1.431
20	1.206	1.837	1.523
25	1.186	1.862	1.570
30	1.166	1.886	1.617
40	1.129	1.934	1.713
50	1.094	1.982	1.812
60	1.061	2.029	1.912
70	1.030	2.075	2.014
80	1.001	2.121	2.119
90	0.974	2.166	2.225
100	0.947	2.210	2.333
150	0.835	2.423	2.900
200	0.747	2.624	3.512
300	0.617	2.994	4.854
400	0.525	3.330	6.342

Kinematic Viscosity - common fluids



A.2. Vector Operations and Identities

Derivatives of unit vectors (r, θ, z)

$$\begin{aligned} \frac{\partial \hat{i}_r}{\partial r} &= 0 & \frac{\partial \hat{i}_\theta}{\partial r} &= 0 & \frac{\partial \hat{i}_z}{\partial r} &= 0 \\ \frac{\partial \hat{i}_r}{\partial \theta} &= \hat{i}_\theta & \frac{\partial \hat{i}_\theta}{\partial \theta} &= -\hat{i}_r & \frac{\partial \hat{i}_z}{\partial \theta} &= 0 \\ \frac{\partial \hat{i}_r}{\partial z} &= 0 & \frac{\partial \hat{i}_\theta}{\partial z} &= 0 & \frac{\partial \hat{i}_z}{\partial z} &= 0 \end{aligned}$$

Vector Operator ∇

$$\nabla = \hat{i} \frac{\partial}{\partial x} + \hat{j} \frac{\partial}{\partial y} + \hat{k} \frac{\partial}{\partial z} \quad \text{Cartesian coordinates}$$

$$\nabla = \hat{i}_r \frac{\partial}{\partial r} + \hat{i}_\theta \frac{1}{r} \frac{\partial}{\partial \theta} + \hat{i}_z \frac{\partial}{\partial z} \quad \text{cylindrical coordinates}$$

Gradient

$$\nabla \phi = \hat{i} \frac{\partial \phi}{\partial x} + \hat{j} \frac{\partial \phi}{\partial y} + \hat{k} \frac{\partial \phi}{\partial z} \quad (x, y, z)$$

$$\nabla \phi = \hat{i}_r \frac{\partial \phi}{\partial r} + \hat{i}_\theta \frac{1}{r} \frac{\partial \phi}{\partial \theta} + \hat{i}_z \frac{\partial \phi}{\partial z} \quad (r, \theta, z)$$

Divergence

$$\nabla \cdot \vec{V} = \frac{\partial V_x}{\partial x} + \frac{\partial V_y}{\partial y} + \frac{\partial V_z}{\partial z} \quad (x, y, z)$$

$$\nabla \cdot \vec{V} = \frac{1}{r} \frac{\partial}{\partial r} (rV_r) + \frac{1}{r} \frac{\partial V_\theta}{\partial \theta} + \frac{\partial V_z}{\partial z} = \frac{\partial V_r}{\partial r} + \frac{1}{r} \frac{\partial V_\theta}{\partial \theta} + \frac{\partial V_z}{\partial z} + \frac{V_r}{r} \quad (r, \theta, z)$$

Curl

$$\nabla \times \vec{V} = \left(\frac{\partial V_z}{\partial y} - \frac{\partial V_y}{\partial z} \right) \hat{i} + \left(\frac{\partial V_x}{\partial z} - \frac{\partial V_z}{\partial x} \right) \hat{j} + \left(\frac{\partial V_y}{\partial x} - \frac{\partial V_x}{\partial y} \right) \hat{k} \quad (x, y, z)$$

$$\nabla \times \vec{V} = \left(\frac{1}{r} \frac{\partial V_z}{\partial \theta} - \frac{\partial V_\theta}{\partial z} \right) \hat{i}_r + \left(\frac{\partial V_r}{\partial z} - \frac{\partial V_z}{\partial r} \right) \hat{i}_\theta + \frac{1}{r} \left(\frac{\partial}{\partial r} (rV_\theta) - \frac{\partial V_r}{\partial \theta} \right) \hat{i}_z \quad (r, \theta, z)$$

Laplacian

$$\nabla^2 = \frac{\partial^2}{\partial x^2} + \frac{\partial^2}{\partial y^2} + \frac{\partial^2}{\partial z^2} \quad (x, y, z)$$

$$\nabla^2 = \frac{1}{r} \frac{\partial}{\partial r} \left(r \frac{\partial}{\partial r} \right) + \frac{1}{r^2} \frac{\partial^2}{\partial \theta^2} + \frac{\partial^2}{\partial z^2} \quad (r, \theta, z)$$

Common Identities using ∇

Where f and g are scalars, and \vec{F} and \vec{G} are vectors

- (a) $\nabla \times \nabla f = 0$
- (b) $\nabla(fg) = f \nabla g + g \nabla f$
- (c) $\nabla \cdot (\nabla \times \vec{F}) = 0$
- (d) $\nabla \times (\nabla \times \vec{F}) = \nabla(\nabla \cdot \vec{F}) - \nabla^2 \vec{F}$ [i.e. = $\nabla(\nabla \cdot \vec{F}) - (\nabla \cdot \nabla) \vec{F}$]
- (e) $\nabla \cdot (f\vec{F}) = f(\nabla \cdot \vec{F}) + \vec{F} \cdot \nabla f$
- (f) $\nabla \times (f\vec{F}) = f(\nabla \times \vec{F}) + (\nabla f) \times \vec{F}$
- (g) $\nabla(\vec{F} \cdot \vec{G}) = (\vec{G} \cdot \nabla) \vec{F} + (\vec{F} \cdot \nabla) \vec{G} + \vec{F} \times (\nabla \times \vec{G}) + \vec{G} \times (\nabla \times \vec{F})$
- (h) $\nabla \times (\vec{F} \times \vec{G}) = (\vec{G} \cdot \nabla) \vec{F} - (\vec{F} \cdot \nabla) \vec{G} + \vec{F}(\nabla \cdot \vec{G}) - \vec{G}(\nabla \cdot \vec{F})$
- (j) $\nabla \cdot (\vec{F} \times \vec{G}) = \vec{G} \cdot (\nabla \times \vec{F}) - \vec{F} \cdot (\nabla \times \vec{G})$
- (k) $\nabla \cdot \nabla f = \nabla^2 f$
- (l) $\nabla \cdot \nabla \vec{F} = \nabla^2 \vec{F}$ [i.e. = $(\nabla \cdot \nabla) \vec{F}$]
- (m) $\nabla \cdot \nabla^2 \vec{F} = \nabla^2(\nabla \cdot \vec{F})$
- (n) $\nabla \times \nabla^2 \vec{F} = \nabla^2(\nabla \times \vec{F})$

A.3. Vector Theorems

Gauss Divergence Theorem, vector field \vec{F}

$$\iiint_V (\nabla \cdot \vec{F}) dV = \oint_A \hat{n} \cdot \vec{F} dA = \oint_A \vec{F} \cdot d\vec{A}$$

Curl Theorem

$$\iiint_V (\nabla \times \vec{F}) dV = \oint_A \hat{n} \times \vec{F} dA = - \oint_A \vec{F} \times d\vec{A}$$

Gradient Theorem, scalar field ϕ

$$\iiint_V (\nabla \phi) dV = \int_A \hat{n} \phi dA = \int_A \phi d\vec{A}$$

Stokes' Theorem

$$\int_A \hat{n} \cdot (\nabla \times \vec{F}) dA = \int_A (\nabla \times \vec{F}) \cdot d\vec{A} = \oint_C \vec{F} \cdot d\vec{s}$$

A.4. The Substantial Derivative

Substantial Derivative, Cartesian Coordinates: $\vec{V} = u\hat{i} + v\hat{j} + w\hat{k}$

$$\frac{DF}{Dt} = \frac{\partial F}{\partial t} + u \frac{\partial F}{\partial x} + v \frac{\partial F}{\partial y} + w \frac{\partial F}{\partial z} \quad \text{where } F = F(x, y, z, t)$$

$$\frac{D\vec{f}}{Dt} = \frac{\partial \vec{f}}{\partial t} + u \frac{\partial \vec{f}}{\partial x} + v \frac{\partial \vec{f}}{\partial y} + w \frac{\partial \vec{f}}{\partial z} \quad \text{where } \vec{f} = \vec{f}(x, y, z, t) = f_x\hat{i} + f_y\hat{j} + f_z\hat{k}$$

$$\text{x-component:} \quad \left[\frac{D\vec{f}}{Dt} \right]_x = \frac{\partial f_x}{\partial t} + u \frac{\partial f_x}{\partial x} + v \frac{\partial f_x}{\partial y} + w \frac{\partial f_x}{\partial z}$$

$$\text{y-component:} \quad \left[\frac{D\vec{f}}{Dt} \right]_y = \frac{\partial f_y}{\partial t} + u \frac{\partial f_y}{\partial x} + v \frac{\partial f_y}{\partial y} + w \frac{\partial f_y}{\partial z}$$

$$\text{z-component:} \quad \left[\frac{D\vec{f}}{Dt} \right]_z = \frac{\partial f_z}{\partial t} + u \frac{\partial f_z}{\partial x} + v \frac{\partial f_z}{\partial y} + w \frac{\partial f_z}{\partial z}$$

Total Acceleration, Cartesian Coordinates

$$\text{Total acceleration:} \quad \vec{a} = \frac{D\vec{V}}{Dt} = \frac{\partial \vec{V}}{\partial t} + u \frac{\partial \vec{V}}{\partial x} + v \frac{\partial \vec{V}}{\partial y} + w \frac{\partial \vec{V}}{\partial z}$$

$$\text{x-component:} \quad a_x = \frac{Du}{Dt} = \frac{\partial u}{\partial t} + u \frac{\partial u}{\partial x} + v \frac{\partial u}{\partial y} + w \frac{\partial u}{\partial z}$$

$$\text{y-component:} \quad a_y = \frac{Dv}{Dt} = \frac{\partial v}{\partial t} + u \frac{\partial v}{\partial x} + v \frac{\partial v}{\partial y} + w \frac{\partial v}{\partial z}$$

$$\text{z-component:} \quad a_z = \frac{Dw}{Dt} = \frac{\partial w}{\partial t} + u \frac{\partial w}{\partial x} + v \frac{\partial w}{\partial y} + w \frac{\partial w}{\partial z}$$

Substantial Derivative, Cylindrical Coordinates: $\vec{V} = v_r\hat{i}_r + v_\theta\hat{i}_\theta + v_z\hat{i}_z$

$$\frac{DF}{Dt} = \frac{\partial F}{\partial t} + v_r \frac{\partial F}{\partial r} + \frac{v_\theta}{r} \frac{\partial F}{\partial \theta} + v_z \frac{\partial F}{\partial z} \quad \text{where } F = F(r, \theta, z, t)$$

$$\frac{D\vec{f}}{Dt} = \frac{\partial \vec{f}}{\partial t} + v_r \frac{\partial \vec{f}}{\partial r} + \frac{v_\theta}{r} \frac{\partial \vec{f}}{\partial \theta} + v_z \frac{\partial \vec{f}}{\partial z} \quad \text{where } \vec{f} = \vec{f}(r, \theta, z, t) = f_r\hat{i} + f_\theta\hat{j} + f_z\hat{k}$$

$$\text{r-component:} \quad \left[\frac{D\vec{f}}{Dt} \right]_r = \frac{\partial f_r}{\partial t} + v_r \frac{\partial f_r}{\partial r} + \frac{v_\theta}{r} \left[\frac{\partial f_r}{\partial \theta} - f_\theta \right] + v_z \frac{\partial f_r}{\partial z}$$

$$\text{\theta-component:} \quad \left[\frac{D\vec{f}}{Dt} \right]_\theta = \frac{\partial f_\theta}{\partial t} + v_r \frac{\partial f_\theta}{\partial r} + \frac{v_\theta}{r} \left[\frac{\partial f_\theta}{\partial \theta} + f_r \right] + v_z \frac{\partial f_\theta}{\partial z}$$

$$\text{z-component:} \quad \left[\frac{D\vec{f}}{Dt} \right]_z = \frac{\partial f_z}{\partial t} + v_r \frac{\partial f_z}{\partial r} + \frac{v_\theta}{r} \frac{\partial f_z}{\partial \theta} + v_z \frac{\partial f_z}{\partial z}$$

Total Acceleration, Cylindrical Coordinates

$$\begin{aligned} \text{Total acceleration: } \quad \vec{a} &= \frac{D\vec{V}}{Dt} = \frac{\partial\vec{V}}{\partial t} + v_r \frac{\partial\vec{V}}{\partial r} + \frac{v_\theta}{r} \frac{\partial\vec{V}}{\partial\theta} + v_z \frac{\partial\vec{V}}{\partial z} \\ \text{r-component: } \quad a_r &= \frac{Dv_r}{Dt} = \frac{\partial v_r}{\partial t} + v_r \frac{\partial v_r}{\partial r} + \frac{v_\theta}{r} \frac{\partial v_r}{\partial\theta} + v_z \frac{\partial v_r}{\partial z} - \frac{v_\theta^2}{r} \\ \text{\theta-component: } \quad a_\theta &= \frac{Dv_\theta}{Dt} = \frac{\partial v_\theta}{\partial t} + v_r \frac{\partial v_\theta}{\partial r} + \frac{v_\theta}{r} \frac{\partial v_\theta}{\partial\theta} + v_z \frac{\partial v_\theta}{\partial z} + \frac{v_r v_\theta}{r} \\ \text{z-component: } \quad a_z &= \frac{Dv_z}{Dt} = \frac{\partial v_z}{\partial t} + v_r \frac{\partial v_z}{\partial r} + \frac{v_\theta}{r} \frac{\partial v_z}{\partial\theta} + v_z \frac{\partial v_z}{\partial z} \end{aligned}$$

A.5. Streamlines

Cartesian: $\vec{V} \times d\vec{s} = (v dy - v dz)\hat{i} + (u dz - w dx)\hat{j} + (v dx - u dy)\hat{k} = 0$

Components: $v dx - u dy = 0, \quad w dy - v dz = 0, \quad u dz - w dx = 0$

2-D Streamline Equation: $\frac{dy}{dx} = \frac{v}{u} \quad (x, y)$

Cylindrical: $\vec{V} \times d\vec{s} = (v_\theta dz - v_z r d\theta)\hat{i}_r + (v_z dr - v_r dz)\hat{i}_\theta + (v_r r d\theta - v_\theta dr)\hat{i}_z$

Components: $v_\theta dz - v_z r d\theta = 0, \quad v_z dr - v_r dz = 0, \quad v_r r d\theta - v_\theta dr = 0$

2-D Streamline Equation: $\frac{dr}{r d\theta} = \frac{v_r}{v_\theta} \quad (r, \theta)$

A.6. Rate of Strain

Cartesian Coordinates: $\vec{V} = u\hat{i} + v\hat{j} + w\hat{k}$

$$\dot{\epsilon}_{xx} = \frac{\partial u}{\partial x} \quad \dot{\epsilon}_{xy} = \frac{1}{2} \left(\frac{\partial v}{\partial x} + \frac{\partial u}{\partial y} \right) \quad \dot{\epsilon}_{xz} = \frac{1}{2} \left(\frac{\partial u}{\partial z} + \frac{\partial w}{\partial x} \right)$$

$$\dot{\epsilon}_{yx} = \frac{1}{2} \left(\frac{\partial v}{\partial x} + \frac{\partial u}{\partial y} \right) \quad \dot{\epsilon}_{yy} = \frac{\partial v}{\partial y} \quad \dot{\epsilon}_{yz} = \frac{1}{2} \left(\frac{\partial w}{\partial y} + \frac{\partial v}{\partial z} \right)$$

$$\dot{\epsilon}_{zx} = \frac{1}{2} \left(\frac{\partial u}{\partial z} + \frac{\partial w}{\partial x} \right) \quad \dot{\epsilon}_{zy} = \frac{1}{2} \left(\frac{\partial w}{\partial y} + \frac{\partial v}{\partial z} \right) \quad \dot{\epsilon}_{zz} = \frac{\partial w}{\partial z}$$

Cylindrical Coordinates: $\vec{V} = v_r \hat{i}_r + v_\theta \hat{i}_\theta + v_z \hat{i}_z$

$$\dot{\epsilon}_{rr} = \frac{\partial v_r}{\partial r} \quad \dot{\epsilon}_{r\theta} = \frac{1}{2} \left(r \frac{\partial}{\partial r} \left(\frac{v_\theta}{r} \right) + \frac{1}{r} \frac{\partial v_r}{\partial \theta} \right) \quad \dot{\epsilon}_{rz} = \frac{1}{2} \left(\frac{\partial v_r}{\partial z} + \frac{\partial v_z}{\partial r} \right)$$

$$\dot{\epsilon}_{\theta r} = \frac{1}{2} \left(r \frac{\partial}{\partial r} \left(\frac{v_\theta}{r} \right) + \frac{1}{r} \frac{\partial v_r}{\partial \theta} \right) \quad \dot{\epsilon}_{\theta\theta} = \frac{1}{r} \frac{\partial v_\theta}{\partial \theta} + \frac{v_r}{r} \quad \dot{\epsilon}_{\theta z} = \frac{1}{2} \left(\frac{1}{r} \frac{\partial v_z}{\partial \theta} + \frac{\partial v_\theta}{\partial z} \right)$$

$$\dot{\epsilon}_{zr} = \frac{1}{2} \left(\frac{\partial v_r}{\partial z} + \frac{\partial v_z}{\partial r} \right) \quad \dot{\epsilon}_{z\theta} = \frac{1}{2} \left(\frac{1}{r} \frac{\partial v_z}{\partial \theta} + \frac{\partial v_\theta}{\partial z} \right) \quad \dot{\epsilon}_{zz} = \frac{\partial v_z}{\partial z}$$

A.7. Vorticity

Cartesian Coordinates: $\vec{V} = u\hat{i} + v\hat{j} + w\hat{k}$

$$\vec{\omega} = \nabla \times \vec{V} = (\omega_x \hat{i} + \omega_y \hat{j} + \omega_z \hat{k}) = \left(\frac{\partial w}{\partial y} - \frac{\partial v}{\partial z} \right) \hat{i} + \left(\frac{\partial u}{\partial z} - \frac{\partial w}{\partial x} \right) \hat{j} + \left(\frac{\partial v}{\partial x} - \frac{\partial u}{\partial y} \right) \hat{k}$$

$$\text{x-component: } \omega_x = \left(\frac{\partial w}{\partial y} - \frac{\partial v}{\partial z} \right)$$

$$\text{y-component: } \omega_y = \left(\frac{\partial u}{\partial z} - \frac{\partial w}{\partial x} \right)$$

$$\text{z-component: } \omega_z = \left(\frac{\partial v}{\partial x} - \frac{\partial u}{\partial y} \right)$$

Cylindrical Coordinates: $\vec{V} = v_r \hat{i}_r + v_\theta \hat{i}_\theta + v_z \hat{i}_z$

$$\vec{\omega} = \nabla \times \vec{V} = (\omega_r \hat{i}_r + \omega_\theta \hat{i}_\theta + \omega_z \hat{i}_z) = \left(\frac{1}{r} \frac{\partial v_z}{\partial \theta} - \frac{\partial v_\theta}{\partial z} \right) \hat{i}_r + \left(\frac{\partial v_r}{\partial z} - \frac{\partial v_z}{\partial r} \right) \hat{i}_\theta + \frac{1}{r} \left(\frac{\partial}{\partial r} (r v_\theta) - \frac{\partial v_r}{\partial \theta} \right) \hat{i}_z$$

$$\text{r-component: } \omega_r = \left(\frac{1}{r} \frac{\partial v_z}{\partial \theta} - \frac{\partial v_\theta}{\partial z} \right)$$

$$\text{\theta-component: } \omega_\theta = \left(\frac{\partial v_r}{\partial z} - \frac{\partial v_z}{\partial r} \right)$$

$$\text{z-component: } \omega_z = \frac{1}{r} \left(\frac{\partial}{\partial r} (r v_\theta) - \frac{\partial v_r}{\partial \theta} \right)$$

A.8. The Governing Equations for Incompressible Flow

Stresses on an Incompressible Fluid: Cartesian and Cylindrical Coordinates

$$\sigma_{xx} = -p + 2\mu \frac{\partial u}{\partial x}$$

$$\tau_{xy} = \mu \left(\frac{\partial u}{\partial y} + \frac{\partial v}{\partial x} \right) = \tau_{yx}$$

$$\sigma_{yy} = -p + 2\mu \frac{\partial v}{\partial y}$$

$$\tau_{xz} = \mu \left(\frac{\partial u}{\partial z} + \frac{\partial w}{\partial x} \right) = \tau_{zx}$$

$$\sigma_{zz} = -p + 2\mu \frac{\partial w}{\partial z}$$

$$\tau_{yz} = \mu \left(\frac{\partial v}{\partial z} + \frac{\partial w}{\partial y} \right) = \tau_{zy}$$

$$\sigma_{rr} = -p + 2\mu \frac{\partial v_r}{\partial r}$$

$$\tau_{r\theta} = \mu \left(r \frac{\partial}{\partial r} \left(\frac{v_\theta}{r} \right) + \frac{1}{r} \frac{\partial v_r}{\partial \theta} \right) = \tau_{\theta r}$$

$$\sigma_{\theta\theta} = -p + 2\mu \left(\frac{1}{r} \frac{\partial v_\theta}{\partial \theta} + \frac{v_r}{r} \right)$$

$$\tau_{\theta z} = \mu \left(\frac{\partial v_\theta}{\partial z} + \frac{1}{r} \frac{\partial v_z}{\partial \theta} \right) = \tau_{z\theta}$$

$$\sigma_{zz} = -p + 2\mu \frac{\partial v_z}{\partial z}$$

$$\tau_{rz} = \mu \left(\frac{\partial v_z}{\partial r} + \frac{\partial v_r}{\partial z} \right) = \tau_{zr}$$

Continuity and Navier-Stokes Equations (ρ, μ constant)**Cartesian Coordinates**

$$\text{continuity: } \frac{\partial u}{\partial x} + \frac{\partial v}{\partial y} + \frac{\partial w}{\partial z} = 0$$

$$\text{x-component: } \frac{\partial u}{\partial t} + u \frac{\partial u}{\partial x} + v \frac{\partial u}{\partial y} + w \frac{\partial u}{\partial z} = -\frac{1}{\rho} \frac{\partial p}{\partial x} + g_x + \nu \left[\frac{\partial^2 u}{\partial x^2} + \frac{\partial^2 u}{\partial y^2} + \frac{\partial^2 u}{\partial z^2} \right]$$

$$\text{y-component: } \frac{\partial v}{\partial t} + u \frac{\partial v}{\partial x} + v \frac{\partial v}{\partial y} + w \frac{\partial v}{\partial z} = -\frac{1}{\rho} \frac{\partial p}{\partial y} + g_y + \nu \left[\frac{\partial^2 v}{\partial x^2} + \frac{\partial^2 v}{\partial y^2} + \frac{\partial^2 v}{\partial z^2} \right]$$

$$\text{z-component: } \frac{\partial w}{\partial t} + u \frac{\partial w}{\partial x} + v \frac{\partial w}{\partial y} + w \frac{\partial w}{\partial z} = -\frac{1}{\rho} \frac{\partial p}{\partial z} + g_z + \nu \left[\frac{\partial^2 w}{\partial x^2} + \frac{\partial^2 w}{\partial y^2} + \frac{\partial^2 w}{\partial z^2} \right]$$

Cylindrical Coordinates

$$\text{continuity: } \frac{1}{r} \frac{\partial}{\partial r} (rv_r) + \frac{1}{r} \frac{\partial v_\theta}{\partial \theta} + \frac{\partial v_z}{\partial z} = 0$$

$$\begin{aligned} \text{r-component: } \frac{\partial v_r}{\partial t} + v_r \frac{\partial v_r}{\partial r} + \frac{v_\theta}{r} \frac{\partial v_r}{\partial \theta} + v_z \frac{\partial v_r}{\partial z} - \frac{v_\theta^2}{r} \\ = -\frac{1}{\rho} \frac{\partial p}{\partial r} + g_r + \nu \left[\frac{\partial}{\partial r} \left(\frac{1}{r} \frac{\partial}{\partial r} (rv_r) \right) + \frac{1}{r^2} \frac{\partial^2 v_r}{\partial \theta^2} + \frac{\partial^2 v_r}{\partial z^2} - \frac{2}{r^2} \frac{\partial v_\theta}{\partial \theta} \right] \end{aligned}$$

$$\begin{aligned} \text{\theta-component: } \frac{\partial v_\theta}{\partial t} + v_r \frac{\partial v_\theta}{\partial r} + \frac{v_\theta}{r} \frac{\partial v_\theta}{\partial \theta} + v_z \frac{\partial v_\theta}{\partial z} + \frac{v_r v_\theta}{r} \\ = -\frac{1}{\rho r} \frac{\partial p}{\partial \theta} + g_\theta + \nu \left[\frac{\partial}{\partial r} \left(\frac{1}{r} \frac{\partial}{\partial r} (rv_\theta) \right) + \frac{1}{r^2} \frac{\partial^2 v_\theta}{\partial \theta^2} + \frac{\partial^2 v_\theta}{\partial z^2} + \frac{2}{r^2} \frac{\partial v_r}{\partial \theta} \right] \end{aligned}$$

$$\begin{aligned} \text{z-component: } \frac{\partial v_z}{\partial t} + v_r \frac{\partial v_z}{\partial r} + \frac{v_\theta}{r} \frac{\partial v_z}{\partial \theta} + v_z \frac{\partial v_z}{\partial z} \\ = -\frac{1}{\rho} \frac{\partial p}{\partial z} + g_z + \nu \left[\frac{1}{r} \frac{\partial}{\partial r} \left(r \frac{\partial v_z}{\partial r} \right) + \frac{1}{r^2} \frac{\partial^2 v_z}{\partial \theta^2} + \frac{\partial^2 v_z}{\partial z^2} \right] \end{aligned}$$

A.9. Inviscid Flow Equations**Euler Equation (along a streamline or irrotational flow)**

$$g dh + \frac{1}{\rho} dP + d \left(\frac{V^2}{2} \right) + \frac{\partial \bar{V}}{\partial t} \cdot d\bar{s} = 0$$

Bernoulli Equation (along streamline, or irrotational flow)

$$\left(\frac{P_2}{\rho} + \frac{V_2^2}{2} + gh_2 \right) - \left(\frac{P_1}{\rho} + \frac{V_1^2}{2} + gh_1 \right) + \int_1^2 \frac{\partial \bar{V}}{\partial t} \cdot d\bar{s} = 0 \quad \text{Unsteady}$$

$$\frac{P}{\rho} + gh + \frac{1}{2} V^2 + \frac{\partial \phi}{\partial t} = C(t) \quad \text{Unsteady, Potential flow}$$

$$\left(\frac{P_2}{\rho} + \frac{V_2^2}{2} + gh_2 \right) = \left(\frac{P_1}{\rho} + \frac{V_1^2}{2} + gh_1 \right) \quad \text{Steady}$$

Euler s and n Equations (streamline coordinates, unsteady)

$$g \frac{\partial h}{\partial s} + \frac{1}{\rho} \frac{\partial P}{\partial s} + V \frac{\partial V}{\partial s} + \frac{\partial V}{\partial t} = 0 \quad \text{s-direction component}$$

$$g \frac{dh}{\partial n} + \frac{1}{\rho} \frac{\partial P}{\partial n} = \frac{V^2}{R} \quad \text{n-direction component}$$

Euler s and n Equations (integrated, steady)

$$\left(\frac{P_2}{\rho} + \frac{V_2^2}{2} + gh_2 \right) = \left(\frac{P_1}{\rho} + \frac{V_1^2}{2} + gh_1 \right) \quad \text{along streamline}$$

$$g(h_2 - h_1) + \frac{1}{\rho}(P_2 - P_1) = \int_1^2 \frac{V^2}{R} dr \quad \text{normal to streamline}$$

A.10. Potential Flow**Complex variable relationships**

$$\Phi(z) = \phi + i\psi$$

$$z = x + iy \quad \text{and} \quad z = re^{i\theta} \quad e^{i\theta} = \cos \theta + i \sin \theta$$

$$\text{where } r = \sqrt{x^2 + y^2} \quad \text{and} \quad \theta = \tan^{-1} \left(\frac{y}{x} \right)$$

$$\frac{d\Phi}{dz} = u - iv \equiv \bar{W}$$

$$W = u + iv$$

$$u = \frac{\partial \psi}{\partial y} = \frac{\partial \phi}{\partial x}; \quad v = -\frac{\partial \psi}{\partial x} = \frac{\partial \phi}{\partial y}$$

$$v_r = \frac{1}{r} \frac{\partial \psi}{\partial \theta} = \frac{\partial \phi}{\partial r}; \quad v_\theta = -\frac{\partial \psi}{\partial r} = \frac{1}{r} \frac{\partial \phi}{\partial \theta}$$

Elementary Functions and Relationships

$$\frac{P}{\rho} + gh + \frac{1}{2}V^2 + \frac{\partial \phi}{\partial t} = C(t) \quad : \text{ Unsteady Bernoulli }$$

$$\Phi(z) = (a + ib)z = (ax - by) + i(ay + bx) \quad : \text{ Uniform, Parallel Flow }$$

$$x\text{-axis} \Rightarrow \Phi(z) = az \Rightarrow u=a, v=0 \quad : \text{ Flow parallel to the coordinate }$$

$$y\text{-axis} \Rightarrow \Phi(z) = -ibz \Rightarrow u=0, v=b$$

$$\Phi(z) = Uze^{-i\alpha} \quad (\text{where } U \text{ is a constant}) \quad : \text{ Flow at an angle } \alpha \text{ to the } x\text{-axis} }$$

$$= Uz(\cos \alpha - i \sin \alpha)$$

$$\Phi(z) = \frac{Q}{2\pi} \ln(z) \quad : \text{ Source and Sink Flows }$$

$$\psi = \frac{Q}{2\pi} \theta \quad \text{and} \quad \phi = \frac{Q}{2\pi} \ln r$$

$$\Phi(z) = -i \frac{\Gamma}{2\pi} \ln z \quad : \text{ Point Vortex }$$

$$\psi = -\frac{\Gamma}{2\pi} \ln r \quad \text{and} \quad \phi = \frac{\Gamma}{2\pi} \theta$$

$$\Phi(z) = \frac{s}{z} \quad : \text{ Doublet }$$

$$\phi = \frac{sx}{x^2 + y^2} \quad \text{and} \quad \psi = \frac{-sy}{x^2 + y^2}$$

$$\phi = \frac{s}{r} \cos \theta \quad \text{and} \quad \psi = -\frac{s}{r} \sin \theta$$

$$\Phi(z) = \frac{A}{n} z^n \quad : \text{ Corner and Wedge Flows }$$

$$\phi = \frac{Ar^n}{n} \cos n\theta \quad \text{and} \quad \psi = \frac{Ar^n}{n} \sin n\theta$$

Added Mass

$$\text{Drag}|_{\text{Added Mass}} = -m_{\text{added}} \frac{dU}{dt}$$

$$\text{Drag}|_{\text{Added Mass Cylinder}} = -\rho\pi R^2 \frac{dU}{dt}$$

A.11. Circulation and Circulation Theorems

Circulation

$$\Gamma = \oiint_A \vec{\omega} \cdot d\vec{A} = \oiint_A (\nabla \times \vec{V}) \cdot d\vec{A} = \oint_C \vec{V} \cdot d\vec{s}$$

Circulation Theorems

$$\frac{D\Gamma}{Dt} = -\oint \frac{dP}{\rho} + \oint \mathbf{v} \cdot (\nabla^2 \vec{V} \cdot d\vec{s}) \quad \text{Conservative body forces}$$

$$\frac{D\Gamma}{Dt} = \oint \mathbf{v} \cdot (\nabla^2 \vec{V} \cdot d\vec{s}) \quad \text{Conservative body forces, } \rho = f(P)$$

$$\frac{D\Gamma}{Dt} = -\oint \frac{dP}{\rho} \quad \text{Conservative body forces, } \rho \neq f(P), \mathbf{v} = 0$$

$$\frac{D\Gamma}{Dt} = 0 \quad \text{Conservative body forces } \rho = f(P), \mathbf{v} = 0 \rightarrow \text{Kelvin's Theorem}$$

Circulation Change: Fixed Reference Frame

$$\frac{\partial \Gamma}{\partial t} = - \iint_A [\nabla \times (\omega \times \vec{V})] \cdot d\vec{A} + \oint_C \mathbf{v} \cdot \nabla^2 \vec{V} \cdot d\vec{s}$$

A.12. Vorticity Transport Equations**General Vector Equation**

$$\frac{D\vec{\omega}}{Dt} = \frac{\partial \vec{\omega}}{\partial t} + (\vec{V} \cdot \nabla \vec{\omega}) = (\vec{\omega} \cdot \nabla \vec{V}) + \mathbf{v} \nabla^2 \vec{\omega}$$

Cartesian Equation Components (3-D)

$$\text{x-dir.:} \left(\frac{\partial \omega_x}{\partial t} + u \frac{\partial \omega_x}{\partial x} + v \frac{\partial \omega_x}{\partial y} + w \frac{\partial \omega_x}{\partial z} \right) = \left(\omega_x \frac{\partial u}{\partial x} + \omega_y \frac{\partial u}{\partial y} + \omega_z \frac{\partial u}{\partial z} \right) + \mathbf{v} \left(\frac{\partial^2 \omega_x}{\partial x^2} + \frac{\partial^2 \omega_x}{\partial y^2} + \frac{\partial^2 \omega_x}{\partial z^2} \right)$$

$$\text{y-dir.:} \left(\frac{\partial \omega_y}{\partial t} + u \frac{\partial \omega_y}{\partial x} + v \frac{\partial \omega_y}{\partial y} + w \frac{\partial \omega_y}{\partial z} \right) = \left(\omega_x \frac{\partial v}{\partial x} + \omega_y \frac{\partial v}{\partial y} + \omega_z \frac{\partial v}{\partial z} \right) + \mathbf{v} \left(\frac{\partial^2 \omega_y}{\partial x^2} + \frac{\partial^2 \omega_y}{\partial y^2} + \frac{\partial^2 \omega_y}{\partial z^2} \right)$$

$$\text{z-dir.:} \left(\frac{\partial \omega_z}{\partial t} + u \frac{\partial \omega_z}{\partial x} + v \frac{\partial \omega_z}{\partial y} + w \frac{\partial \omega_z}{\partial z} \right) = \left(\omega_x \frac{\partial w}{\partial x} + \omega_y \frac{\partial w}{\partial y} + \omega_z \frac{\partial w}{\partial z} \right) + \mathbf{v} \left(\frac{\partial^2 \omega_z}{\partial x^2} + \frac{\partial^2 \omega_z}{\partial y^2} + \frac{\partial^2 \omega_z}{\partial z^2} \right)$$

Cartesian Equation (2-D)

$$\frac{\partial \omega_z}{\partial t} + u \frac{\partial \omega_z}{\partial x} + v \frac{\partial \omega_z}{\partial y} = \mathbf{v} \left(\frac{\partial^2 \omega_z}{\partial x^2} + \frac{\partial^2 \omega_z}{\partial y^2} \right)$$

Cylindrical Equation Components (3-D)

$$\begin{aligned} \text{r-dir.:} \quad & \frac{\partial \omega_r}{\partial t} + v_r \frac{\partial \omega_r}{\partial r} + \frac{v_\theta}{r} \left[\frac{\partial \omega_r}{\partial \theta} - \omega_\theta \right] + v_z \frac{\partial \omega_r}{\partial z} \\ & = \omega_r \frac{\partial v_r}{\partial r} + \frac{\omega_\theta}{r} \left[\frac{\partial v_r}{\partial \theta} - v_\theta \right] + \omega_z \frac{\partial v_r}{\partial z} + \mathbf{v} \left[\frac{\partial}{\partial r} \left(\frac{1}{r} \frac{\partial}{\partial r} (r \omega_r) \right) + \frac{1}{r^2} \frac{\partial^2 \omega_r}{\partial \theta^2} + \frac{\partial^2 \omega_r}{\partial z^2} - \frac{2}{r^2} \frac{\partial \omega_\theta}{\partial \theta} \right] \end{aligned}$$

$$\begin{aligned} \text{\theta-dir.:} \quad & \frac{\partial \omega_\theta}{\partial t} + v_r \frac{\partial \omega_\theta}{\partial r} + \frac{v_\theta}{r} \left[\frac{\partial \omega_\theta}{\partial \theta} + \omega_r \right] + v_z \frac{\partial \omega_\theta}{\partial z} \\ & = \omega_r \frac{\partial v_\theta}{\partial r} + \frac{\omega_\theta}{r} \left[\frac{\partial v_\theta}{\partial \theta} + v_r \right] + \omega_z \frac{\partial v_\theta}{\partial z} + \mathbf{v} \left[\frac{\partial}{\partial r} \left(\frac{1}{r} \frac{\partial}{\partial r} (r \omega_\theta) \right) + \frac{1}{r^2} \frac{\partial^2 \omega_\theta}{\partial \theta^2} + \frac{\partial^2 \omega_\theta}{\partial z^2} + \frac{2}{r^2} \frac{\partial \omega_r}{\partial \theta} \right] \end{aligned}$$

$$\begin{aligned} \text{z-dir.:} \quad & \frac{\partial \omega_z}{\partial t} + v_r \frac{\partial \omega_z}{\partial r} + \frac{v_\theta}{r} \frac{\partial \omega_z}{\partial \theta} + v_z \frac{\partial \omega_z}{\partial z} \\ & = \omega_r \frac{\partial v_z}{\partial r} + \frac{\omega_\theta}{r} \frac{\partial v_z}{\partial \theta} + \omega_z \frac{\partial v_z}{\partial z} + \mathbf{v} \left[\frac{1}{r} \frac{\partial}{\partial r} \left(r \frac{\partial \omega_z}{\partial r} \right) + \frac{1}{r^2} \frac{\partial^2 \omega_z}{\partial \theta^2} + \frac{\partial^2 \omega_z}{\partial z^2} \right] \end{aligned}$$

Cylindrical Equation (2-D in r, \theta)

$$\frac{\partial \omega_z}{\partial t} + v_r \frac{\partial \omega_z}{\partial r} + \frac{v_\theta}{r} \frac{\partial \omega_z}{\partial \theta} = \mathbf{v} \left[\frac{1}{r} \frac{\partial}{\partial r} \left(r \frac{\partial \omega_z}{\partial r} \right) + \frac{1}{r^2} \frac{\partial^2 \omega_z}{\partial \theta^2} \right]$$

A.13. Laminar Boundary Layers

Boundary Layer Equations

$$u \frac{\partial u}{\partial x} + v \frac{\partial u}{\partial y} = -\frac{1}{\rho} \frac{dP}{dx} + \nu \frac{\partial^2 u}{\partial y^2}$$

$$\frac{\partial u}{\partial x} + \frac{\partial v}{\partial y} = 0$$

$$\delta^* = \int_0^{\delta} \left(1 - \frac{u}{U_{\infty}}\right) dy, \quad \theta = \int_0^{\delta} \frac{u}{U_{\infty}} \left(1 - \frac{u}{U_{\infty}}\right) dy, \quad \tau_w = \mu \left. \frac{\partial u}{\partial y} \right|_{y=0}$$

Blasius Flat Plate Solution

$$\eta = y \sqrt{\frac{U_{\infty}}{\nu x}} \quad \frac{u}{U_{\infty}} = F'(\eta) \quad \frac{v}{U_{\infty}} = \frac{1}{2} \sqrt{\frac{\nu U_{\infty}}{x}} (\eta F' - F)$$

Blasius Boundary Layer Parameters

$$\frac{\delta}{x} = \frac{5}{Re_x^{1/2}} \quad \delta^* = x \frac{1.72}{\sqrt{Re_x}} \quad \frac{\theta}{x} = \frac{0.664}{\sqrt{Re_x}}$$

$$c_f = \frac{\tau_w}{\frac{1}{2} \rho U_{\infty}^2} = \frac{0.664}{\sqrt{Re_x}} \quad C_D = \frac{\text{Drag}}{\frac{1}{2} \rho U_{\infty}^2 WL} = \frac{1.328}{\sqrt{Re_L}}$$

Karman Momentum Integral Equation

$$\frac{d\theta}{dx} + (\delta^* + 2\theta) \frac{1}{U_{\infty}} \frac{dU_{\infty}}{dx} = \frac{\tau_w}{\rho U_{\infty}^2}$$

$$\frac{d\theta}{dx} + (H + 2) \frac{\theta}{U_{\infty}} \frac{dU_{\infty}}{dx} = \frac{c_f}{2}$$

Thwaites: Table, Parameters, and Equation

Thwaites Parameters

$$\ell = \frac{\theta}{U_{\infty}} \left(\frac{\partial u}{\partial y} \right)_{y=0} \quad H = \frac{\delta^*}{\theta} \quad n = -\frac{\theta^2}{\nu} \frac{dU_{\infty}}{dx}$$

Thwaites Equation

For $\theta_{init} = 0$

$$\theta = \left[0.47 \nu U_{\infty}^{-6} \int_0^x U_{\infty}^5 dx \right]^{0.5}$$

$$n = -0.47 U_{\infty}^{-6} \frac{dU_{\infty}}{dx} \int_0^x U_{\infty}^5 dx$$

Blasius table for F, F' and F'' vs. η

η	F	F'	F''
0	0.0000	0.0000	0.3321
0.2	0.0066	0.0664	0.3320
0.4	0.0266	0.1328	0.3315
0.6	0.0597	0.1989	0.3301
0.8	0.1061	0.2647	0.3274
1	0.1656	0.3298	0.3230
1.2	0.2380	0.3938	0.3166
1.4	0.3230	0.4563	0.3079
1.6	0.4203	0.5168	0.2967
1.8	0.5295	0.5748	0.2829
2	0.6500	0.6298	0.2668
2.2	0.7812	0.6813	0.2484
2.4	0.9223	0.7290	0.2281
2.6	1.0725	0.7725	0.2065
2.8	1.2310	0.8115	0.1840
3	1.3968	0.8461	0.1614
4	2.3058	0.9555	0.0642
5	3.2833	0.9916	0.0159
6	4.2797	0.9990	0.0024
7	5.2793	0.9999	0.0002
8	6.2793	1.0000	0.0000

Thwaites' Table

n	ℓ	H
0.090	0.000	3.70
0.088	0.015	3.62
0.086	0.027	3.54
0.084	0.038	3.47
0.080	0.056	3.35
0.076	0.072	3.24
0.072	0.085	3.16
0.068	0.095	3.09
0.064	0.104	3.04
0.060	0.113	2.99
0.056	0.122	2.94
0.048	0.138	2.87
0.040	0.153	2.81
0.032	0.168	2.75
0.016	0.195	2.67
0.000	0.220	2.60
-0.016	0.244	2.55
-0.032	0.268	2.49
-0.048	0.291	2.44
-0.064	0.313	2.39
-0.080	0.333	2.34
-0.100	0.359	2.28
-0.120	0.382	2.23
-0.140	0.404	2.18
-0.200	0.463	2.07
-0.25	0.5	2.00

For $\theta_{\text{init}} = \theta_{\text{init}}$

$$\theta = \left[\frac{U_{\text{init}}^6}{U_{\infty}^6} \theta_{\text{init}}^2 + 0.47 \nu U_{\infty}^{-6} \int_0^x U_{\infty}^5 dx \right]^{0.5}$$

$$n = -\frac{dU_{\infty}}{dx} \left(\frac{U_{\text{init}}^6}{U_{\infty}^6} \theta_{\text{init}}^2 + 0.47 \nu U_{\infty}^{-6} \int_0^x U_{\infty}^5 dx \right)$$

A.14. Drag

$$C_D = \frac{\text{Drag}}{\frac{1}{2} \rho U^2 A}$$

$$\text{Strouhal Number} = St = \frac{ND}{V}$$

A.15. Non-Newtonian Fluids

Continuity and Momentum Differential Equations, Cartesian Coordinates

$$\text{continuity: } \frac{\partial u}{\partial x} + \frac{\partial v}{\partial y} + \frac{\partial w}{\partial z} = 0$$

$$\text{x-component: } \frac{\partial u}{\partial t} + u \frac{\partial u}{\partial x} + v \frac{\partial u}{\partial y} + w \frac{\partial u}{\partial z} = -\frac{1}{\rho} \frac{\partial p}{\partial x} + g_x + \frac{1}{\rho} \left[\frac{\partial \sigma_{xx}}{\partial x} + \frac{\partial \tau_{yx}}{\partial y} + \frac{\partial \tau_{zx}}{\partial z} \right]$$

$$\text{y-component: } \frac{\partial v}{\partial t} + u \frac{\partial v}{\partial x} + v \frac{\partial v}{\partial y} + w \frac{\partial v}{\partial z} = -\frac{1}{\rho} \frac{\partial p}{\partial y} + g_y + \frac{1}{\rho} \left[\frac{\partial \sigma_{xy}}{\partial x} + \frac{\partial \tau_{yy}}{\partial y} + \frac{\partial \tau_{zy}}{\partial z} \right]$$

$$\text{z-component: } \frac{\partial w}{\partial t} + u \frac{\partial w}{\partial x} + v \frac{\partial w}{\partial y} + w \frac{\partial w}{\partial z} = -\frac{1}{\rho} \frac{\partial p}{\partial z} + g_z + \frac{1}{\rho} \left[\frac{\partial \sigma_{xz}}{\partial x} + \frac{\partial \tau_{yz}}{\partial y} + \frac{\partial \tau_{zz}}{\partial z} \right]$$

Continuity and Momentum Differential Equations, Cylindrical Coordinates

$$\text{continuity: } \frac{1}{r} \frac{\partial}{\partial r} (r v_r) + \frac{1}{r} \frac{\partial v_{\theta}}{\partial \theta} + \frac{\partial v_z}{\partial z} = 0$$

$$\text{r-component: } \frac{\partial v_r}{\partial t} + v_r \frac{\partial v_r}{\partial r} + \frac{v_{\theta}}{r} \frac{\partial v_r}{\partial \theta} + v_z \frac{\partial v_r}{\partial z} - \frac{v_{\theta}^2}{r}$$

$$= -\frac{1}{\rho} \frac{\partial p}{\partial r} + g_r + \frac{1}{\rho} \left[\frac{1}{r} \frac{\partial}{\partial r} (r \sigma_r) + \frac{1}{r} \frac{\partial \tau_{\theta r}}{\partial \theta} + \frac{\partial \tau_{zr}}{\partial z} - \frac{\tau_{\theta\theta}}{r} \right]$$

$$\text{\theta-component: } \frac{\partial v_{\theta}}{\partial t} + v_r \frac{\partial v_{\theta}}{\partial r} + \frac{v_{\theta}}{r} \frac{\partial v_{\theta}}{\partial \theta} + v_z \frac{\partial v_{\theta}}{\partial z} + \frac{v_r v_{\theta}}{r}$$

$$= -\frac{1}{\rho r} \frac{\partial p}{\partial \theta} + g_{\theta} + \frac{1}{\rho} \left[\frac{1}{r^2} \frac{\partial}{\partial r} (r^2 \tau_{r\theta}) + \frac{1}{r} \frac{\partial \sigma_{\theta\theta}}{\partial \theta} + \frac{\partial \tau_{z\theta}}{\partial z} - \frac{\tau_{\theta r} - \tau_{r\theta}}{r} \right]$$

$$\text{z-component: } \frac{\partial v_z}{\partial t} + v_r \frac{\partial v_z}{\partial r} + \frac{v_{\theta}}{r} \frac{\partial v_z}{\partial \theta} + v_z \frac{\partial v_z}{\partial z}$$

$$= -\frac{1}{\rho} \frac{\partial p}{\partial z} + g_z + \frac{1}{\rho} \left[\frac{1}{r} \frac{\partial}{\partial r} (r \tau_{rz}) + \frac{1}{r} \frac{\partial \tau_{\theta z}}{\partial \theta} + \frac{\partial \sigma_{zz}}{\partial z} \right]$$

Shear Stress Relationships

Power Law Fluids

Non-Newtonian, Cartesian:

$$\text{x-direction only: } \tau_{yx} = \mu_{\text{app}} \dot{\epsilon}_{yx} = \mu_{\text{app}} \left(\frac{\partial u}{\partial y} \right) = K \left(\frac{\partial u}{\partial y} \right)^n, \text{ and } \mu_{\text{app}} = K \left(\frac{\partial u}{\partial y} \right)^{n-1}$$

Non-Newtonian, Cylindrical

$$\theta \text{ direction only: } \tau_{r\theta} = \mu_{\text{app}} \dot{\epsilon}_{r\theta} = \mu_{\text{app}} r \frac{\partial}{\partial r} \left(\frac{v_\theta}{r} \right) = K \left[r \frac{\partial}{\partial r} \left(\frac{v_\theta}{r} \right) \right]^n$$

$$\text{where } \mu_{\text{app}} = K \left[r \frac{\partial}{\partial r} \left(\frac{v_\theta}{r} \right) \right]^{n-1}$$

$$\text{z-direction only: } \tau_{rz} = \mu_{\text{app}} \dot{\epsilon}_{rz} = \mu_{\text{app}} \left(\frac{\partial v_z}{\partial r} \right) = K \left(\frac{\partial v_z}{\partial r} \right)^n$$

$$\text{where } \mu_{\text{app}} = K \left(\frac{\partial v_z}{\partial r} \right)^{n-1}$$

Ideal Bingham Plastic Fluids

Non-Newtonian, Cartesian

$$\text{x-direction only: } \dot{\epsilon}_{yx} = \frac{\partial u}{\partial y} = 0, \quad \text{when } \tau_{yx} < \tau_0 \text{ (assuming } \tau_0 > 0)$$

$$\text{and } \tau_{yx} = \mu_B \left(\frac{\partial u}{\partial y} \right) + \tau_0, \quad \text{when } \tau_{yx} > \tau_0$$

Non-Newtonian, Cylindrical

$$\theta \text{ direction only: } \dot{\epsilon}_{r\theta} = r \frac{\partial}{\partial r} \left(\frac{v_\theta}{r} \right) = 0 \Rightarrow \frac{\partial}{\partial r} \left(\frac{v_\theta}{r} \right) = 0, \quad \text{when } \tau_{r\theta} < \tau_0$$

$$\text{and } \tau_{r\theta} = \mu_B \left[r \frac{\partial}{\partial r} \left(\frac{v_\theta}{r} \right) \right] + \tau_0, \quad \text{when } \tau_{r\theta} > \tau_0$$

$$\text{z-direction only: } \dot{\epsilon}_{rz} = \left(\frac{\partial v_z}{\partial r} \right) = 0 \Rightarrow \frac{\partial v_z}{\partial r} = 0, \quad \text{when } \tau_{rz} < \tau_0$$

$$\text{and } \tau_{rz} = \mu_B \left(\frac{\partial v_z}{\partial r} \right) + \tau_0, \quad \text{when}$$

A.16. Turbulence: General

Kolomogorov length scales

$$L = \left(\frac{v^3 \delta}{U^3} \right)^{1/4} \quad \text{or} \quad \frac{L}{\delta} = \left(\frac{v^3}{U^3 \delta^3} \right)^{1/4} = \left(\frac{v}{U \delta} \right)^{3/4} = \left(\frac{1}{\text{Re}_\delta} \right)^{3/4}$$

Reynolds Averaged Equations (Cartesian)

$$U \frac{\partial U}{\partial x} + V \frac{\partial U}{\partial y} + W \frac{\partial U}{\partial z} = -\frac{1}{\rho} \frac{\partial P}{\partial x} + \nu \frac{\partial^2 U}{\partial x^2} + \nu \frac{\partial^2 U}{\partial y^2} + \nu \frac{\partial^2 U}{\partial z^2} - \frac{\partial(\overline{u'^2})}{\partial x} - \frac{\partial(\overline{u'v'})}{\partial y} - \frac{\partial(\overline{u'w'})}{\partial z}$$

$$U \frac{\partial V}{\partial x} + V \frac{\partial V}{\partial y} + W \frac{\partial V}{\partial z} = -\frac{1}{\rho} \frac{\partial P}{\partial y} + \nu \frac{\partial^2 V}{\partial x^2} + \nu \frac{\partial^2 V}{\partial y^2} + \nu \frac{\partial^2 V}{\partial z^2} - \frac{\partial(\overline{u'v'})}{\partial x} - \frac{\partial(\overline{v'^2})}{\partial y} - \frac{\partial(\overline{v'w'})}{\partial z}$$

$$U \frac{\partial W}{\partial x} + V \frac{\partial W}{\partial y} + W \frac{\partial W}{\partial z} = -\frac{1}{\rho} \frac{\partial P}{\partial z} + \nu \frac{\partial^2 W}{\partial x^2} + \nu \frac{\partial^2 W}{\partial y^2} + \nu \frac{\partial^2 W}{\partial z^2} - \frac{\partial(\overline{u'w'})}{\partial x} - \frac{\partial(\overline{v'w'})}{\partial y} - \frac{\partial(\overline{w'^2})}{\partial z}$$

Reynolds stresses (Cartesian)

$$\tau_{xx}|_{\text{turb}} = -\rho \overline{u'^2}, \quad \tau_{yy}|_{\text{turb}} = -\rho \overline{v'^2}, \quad \tau_{zz}|_{\text{turb}} = -\rho \overline{w'^2}$$

$$\tau_{yx}|_{\text{turb}} = -\rho \overline{u'v'} = \tau_{xy}|_{\text{turb}}, \quad \tau_{yz}|_{\text{turb}} = -\rho \overline{v'w'} = \tau_{zy}|_{\text{turb}}, \quad \tau_{zx}|_{\text{turb}} = -\rho \overline{u'w'} = \tau_{xz}|_{\text{turb}}$$

Eddy viscosity

$$\tau_{\text{turbulent}} = \rho \varepsilon \frac{\partial U}{\partial y} = -\rho \overline{u'v'} \quad \text{or} \quad \varepsilon = \frac{-\overline{u'v'}}{\frac{\partial U}{\partial y}}$$

Universal Velocity Distribution Laws (boundary layer)

Inner Region ($0 \leq y^+ \leq 300 - 600$)

$$u_\tau \equiv \sqrt{\frac{\tau_w}{\rho}} \quad u^+ = \frac{\bar{u}}{u_\tau} \quad \text{and} \quad y^+ = \frac{yu_\tau}{\nu}$$

Viscous Sublayer

$$u^+ = \frac{U}{u_\tau} = \frac{u_\tau y}{\nu} = y^+ \quad y^+ < 5 - 7$$

Logarithmic Layer

$$u^+ = \frac{1}{k} \ln y^+ + B \quad \text{where } k = 0.385 \text{ and } B = 4.2$$

$$\frac{U}{u_\tau} = \frac{1}{0.385} \ln \left(\frac{yu_\tau}{\nu} \right) + 4.2 \Rightarrow u^+ = 2.6 \ln y^+ + 4.2 \quad \text{for } 30 \leq y^+ \leq 300 - 600$$

Outer Region ($300 - 600 \leq y^+$)

$$\frac{U_\infty - U}{u_\tau} = -\frac{1}{k} \ln \left(\frac{y}{\delta} \right) + A(\xi) \left[1 - \sin^2 \left(\frac{\pi y}{2 \delta} \right) \right]$$

Pressure Gradient	ξ	$A(\xi)$ value
Strong favorable	-4.8	1.0
Flat plate	0	2.5
Mild adverse	6.3	5.6
Strong Adverse	29	13

A.17. Turbulence: Approximate Boundary Layer Properties

Nikuradse Velocity Profile Approximation

$$\frac{U}{U_\infty} = \left(\frac{y}{\delta} \right)^{\frac{1}{n}} \quad \text{where } n > 6$$

Assumed Shear Stress Relationship

$$c_f = \frac{\tau_w}{\frac{1}{2}\rho U_\infty^2} = 0.0195 \left(\frac{U_\infty \delta}{\nu} \right)^{-0.173}$$

Turbulent from Leading Edge

$n = 7$	$\beta = \frac{\theta}{\delta} = 0.0972$	$\frac{\delta^*}{\delta} = 0.125$	$H = 1.286$	$\frac{\delta}{x} = \frac{0.158}{\text{Re}_x^{0.147}}$	$c_f = \frac{0.0261}{\text{Re}_x^{0.147}}$	$C_D = \frac{0.0307}{\text{Re}_L^{0.147}}$
$n = 8$	$\beta = \frac{\theta}{\delta} = 0.0889$	$\frac{\delta^*}{\delta} = 0.111$	$H = 1.250$	$\frac{\delta}{x} = \frac{0.170}{\text{Re}_x^{0.147}}$	$c_f = \frac{0.0258}{\text{Re}_x^{0.147}}$	$C_D = \frac{0.0303}{\text{Re}_L^{0.147}}$
$n = 9$	$\beta = \frac{\theta}{\delta} = 0.0818$	$\frac{\delta^*}{\delta} = 0.100$	$H = 1.222$	$\frac{\delta}{x} = \frac{0.183}{\text{Re}_x^{0.147}}$	$c_f = \frac{0.0255}{\text{Re}_x^{0.147}}$	$C_D = \frac{0.0299}{\text{Re}_L^{0.147}}$

Transition at Critical Re_x

$n = 7$	$\beta = \frac{\theta}{\delta} = 0.0972$	$\frac{\delta^*}{\delta} = 0.125$	$H = 1.286$
$n = 8$	$\beta = \frac{\theta}{\delta} = 0.0889$	$\frac{\delta^*}{\delta} = 0.111$	$H = 1.250$
$n = 9$	$\beta = \frac{\theta}{\delta} = 0.0818$	$\frac{\delta^*}{\delta} = 0.100$	$H = 1.222$

$$\frac{\delta}{x} = \frac{\left[\frac{0.01144}{\beta} (\text{Re}_x - \text{Re}_{\text{crit}}) + \text{Re}_{\delta_{\text{crit}}}^{1.173} \right]^{0.853}}{\text{Re}_x}$$

$$c_f = 0.0195 \left[\frac{0.01144}{\beta} (\text{Re}_x - \text{Re}_{\text{crit}}) + 6.61 \text{Re}_{\text{crit}}^{0.587} \right]^{-0.147}$$

$$C_D = \frac{\text{Drag}}{\frac{1}{2}\rho U_\infty^2 WL} = \frac{2\beta \left[\frac{0.01144}{\beta} (\text{Re}_L - \text{Re}_{\text{crit}}) + 6.61 \text{Re}_{\text{crit}}^{0.587} \right]^{0.853}}{\text{Re}_L}$$